
RECONSTRUCTING

QUATERNARY ENVIRONMENTS



Third Edition

John Lowe and Mike Walker



Reconstructing Quaternary Environments

This third edition of *Reconstructing Quaternary Environments* has been completely revised and updated to provide a new account of the history and scale of environmental changes during the Quaternary. The evidence is extremely diverse ranging from landforms and sediments to fossil assemblages and geochemistry, and includes new data from terrestrial, marine and ice-core records. Dating methods are described and evaluated, while the principles and practices of Quaternary stratigraphy are also discussed. The volume concludes with a new chapter which considers some of the key questions about the nature, causes and consequences of global climatic and environmental change over a range of temporal scales. This synthesis builds on the methods and approaches described earlier in the book to show how a number of exciting ideas that have emerged over the last two decades are providing new insights into the operation of the global earth–ocean–atmosphere system, and are now central to many areas of contemporary Quaternary research.

This comprehensive and dynamic textbook is richly illustrated throughout with full-colour figures and photographs. The book will be of interest to undergraduates, postgraduates and professionals in Earth Science, Environmental Science, Physical Geography, Geology, Botany, Zoology, Ecology, Archaeology and Anthropology.

John Lowe is former Gordon Manley Professor and now Emeritus Professor of Quaternary Science in Royal Holloway, University of London, UK.

Mike Walker is Emeritus Professor of Quaternary Science, Trinity Saint David, University of Wales, Lampeter, UK and Honorary Professor, Aberystwyth University, UK.

*For all our colleagues in the INTIMATE project
(INTegration of Ice-core, MArine and TERrestrial records)*

Reconstructing Quaternary Environments

Third Edition

**John Lowe and
Mike Walker**



First published 1984
by Longman Group Ltd

Second edition 1997
by Addison Wesley Longman Ltd

Third edition published 2015
by Routledge
2 Park Square, Milton Park, Abingdon, Oxon OX14 4RN

and by Routledge
711 Third Avenue, New York, NY 10017

Routledge is an imprint of the Taylor & Francis Group, an informa business

© 1984, 1997, 2015 John Lowe and Mike Walker

The right of John Lowe and Mike Walker to be identified as authors
of this work has been asserted in accordance with sections 77 and 78 of
the Copyright, Designs and Patents Act 1988.

All rights reserved. No part of this book may be reprinted or
reproduced or utilised in any form or by any electronic, mechanical,
or other means, now known or hereafter invented, including
photocopying and recording, or in any information storage or retrieval
system, without permission in writing from the publishers.

Trademark notice: Product or corporate names may be trademarks
or registered trademarks, and are used only for identification and
explanation without intent to infringe.

British Library Cataloguing in Publication Data
A catalogue record for this book is available from the British Library

Library of Congress Cataloging in Publication Data

Lowe, J. J. (Joseph John)

Reconstructing quaternary environments / John Lowe and
Mike Walker. — Third edition.

pages cm

Includes bibliographical references and index.

1. Geology, Stratigraphic—Quaternary. 2. Paleogeography—
Quaternary. 3. Geomorphology. I. Walker, Mike. II. Title.

QE696.L776 2014

551.7'9—dc23

2013044728

ISBN: 978-0-415-74075-3 (hbk)

ISBN: 978-0-131-27468-6 (pbk)

ISBN: 978-1-315-79749-6 (ebk)

Typeset in Minion and Univers
by Florence Production Ltd, Stoodleigh, Devon, UK

Contents

<i>List of figures and tables</i>	xv
<i>Preface to the third edition</i>	xxvii
<i>Acknowledgements</i>	xxix
<i>Cover image details</i>	xxx
1 The Quaternary record	1
1.1 Introduction	1
1.2 Interpreting the Quaternary record	2
1.3 The status of the Quaternary in the geological timescale	2
1.4 The duration of the Quaternary	3
1.5 The development of Quaternary studies	5
1.5.1 <i>Historical developments</i>	5
1.5.2 <i>Recent developments</i>	7
1.6 The framework of the Quaternary	9
1.7 The causes of climatic change	13
1.8 The scope of this book	16
Notes	17
2 Geomorphological evidence	19
2.1 Introduction	19
2.2 Methods	19
2.2.1 <i>Field methods</i>	19
2.2.1.1 Field mapping	19
2.2.1.2 Instrumental levelling	20
2.2.2 <i>Remote sensing</i>	22
2.2.2.1 Aerial photography	22
2.2.2.2 Satellite imagery	22
2.2.2.3 Radar	23
2.2.2.4 Sonar and seismic sensing	24
2.2.2.5 Digital elevation/terrain modelling	24
2.3 Glacial landforms	26
2.3.1 <i>Extent of ice cover</i>	27
2.3.2 <i>Geomorphological evidence and the extent of ice sheets and glaciers during the last cold stage</i>	30
2.3.2.1 Northern Europe	30
2.3.2.2 Britain and Ireland	33

2.3.2.3	North America	35
2.3.3	<i>Direction of ice movement</i>	39
2.3.3.1	Striations	40
2.3.3.2	Friction cracks	40
2.3.3.3	Ice-moulded (streamlined) bedrock	40
2.3.3.4	Streamlined glacial deposits	42
2.3.4	<i>Reconstruction of former ice masses</i>	43
2.3.4.1	Ice sheet modelling	43
2.3.4.2	Ice caps and glaciers	47
2.3.5	<i>Palaeoclimatic inferences using former glacier elevations</i>	50
2.3.5.1	Cirque floor altitude (CFA) and toe-to-headwall (THAR) methods	50
2.3.5.2	ELA/FLA method	51
2.4	Periglacial landforms	53
2.4.1	<i>Palaeoclimatic inferences based on periglacial evidence</i>	55
2.4.1.1	Rock glaciers	55
2.4.1.2	Pingos and palsas	56
2.4.1.3	Pronival ('protalus') ramparts	57
2.5	Sea-level change	58
2.5.1	<i>Relative and 'absolute' sea-level changes</i>	59
2.5.2	<i>Eustatic changes in sea level</i>	59
2.5.2.1	Pre-Quaternary eustatic changes	59
2.5.2.2	Quaternary eustatic changes	60
2.5.3	<i>Tectonic influences</i>	67
2.5.4	<i>Glacio- and hydro-isostasy</i>	68
2.5.5	<i>Shoreline sequences in areas affected by glacio-isostasy</i>	69
2.5.6	<i>Palaeoenvironmental significance of sea-level changes</i>	73
2.6	River terraces	73
2.6.1	<i>Origins of river terraces</i>	75
2.6.1.1	Eustatic changes in sea level	76
2.6.1.2	Climatic change	76
2.6.1.3	Glaciation	77
2.6.1.4	Tectonic changes	77
2.6.1.5	Human activity	77
2.6.2	<i>River terraces and palaeoenvironmental reconstruction</i>	78
2.6.3	<i>The terraces of the River Thames</i>	78
2.7	Quaternary landforms in low latitudes	82
2.7.1	<i>Pluvial lakes</i>	82
2.7.2	<i>Dunefields</i>	86
2.7.3	<i>Fluvial landforms</i>	89
2.7.4	<i>Weathering crusts</i>	90
2.8	Conclusions	91
	Notes	91
3	Lithological evidence	93
3.1	Introduction	93
3.2	Field and laboratory methods	93
3.2.1	<i>Sediment sections</i>	93
3.2.2	<i>Coring</i>	94
3.2.3	<i>Laboratory methods</i>	96

3.2.3.1	Particle size measurements	96
3.2.3.2	Particle shape	97
3.2.3.3	Surface textures of quartz particles	97
3.2.3.4	Organic carbon content	97
3.2.3.5	Metallic elements	98
3.2.3.6	Heavy minerals	98
3.2.3.7	Clay mineralogy	98
3.2.3.8	Mineral magnetic analysis	98
3.2.3.9	Stable isotope analysis	98
3.3.	Glacial sediments	99
3.3.1	<i>Introduction</i>	99
3.3.2	<i>The nature of glacial sediments</i>	99
3.3.2.1	Unstratified and stratified sediments	99
3.3.2.2	Glacigenic facies	100
3.3.3	<i>The classification of tills</i>	102
3.3.3.1	Lodgement, melt-out and 'flow' tills	102
3.3.3.2	Deformation tills	102
3.3.3.3	Paraglacial deposits	105
3.3.4	<i>The influence of the thermal regime of glacier ice</i>	107
3.3.5	<i>Analysis of glacigenic sequences</i>	109
3.3.5.1	Particle size and shape analysis	109
3.3.5.2	Lithofacies interpretations	109
3.3.6	<i>Ice-directional indicators</i>	111
3.3.6.1	Erratics	111
3.3.6.2	Till fabrics	113
3.3.6.3	Properties of the till matrix	115
3.4	Periglacial sediments	115
3.4.1	<i>Introduction</i>	115
3.4.2	<i>Structures associated with permafrost</i>	116
3.4.3	<i>Palaeoclimatic significance of periglacial structures</i>	118
3.5	Palaeosols	122
3.5.1	<i>Introduction</i>	122
3.5.2	<i>The nature of palaeosols</i>	122
3.5.3	<i>Analysis of palaeosols</i>	124
3.5.4	<i>Palaeosols and Quaternary environments</i>	125
3.6	Wind-blown sediments	127
3.6.1	<i>Introduction</i>	127
3.6.2	<i>Loess stratigraphy</i>	127
3.6.3	<i>Mid-latitude sand belts (coversands)</i>	130
3.6.4	<i>Low-latitude 'sand seas'</i>	131
3.6.5	<i>Wind-blown sediments and palaeoenvironmental reconstructions</i>	131
3.7	Lake-level records from low-latitude regions	132
3.7.1	<i>Introduction</i>	132
3.7.2	<i>Pluvial lake sediment sequences</i>	133
3.7.3	<i>Lake-level changes and Quaternary palaeoclimates</i>	135
3.8	Cave sediments and carbonate deposits	140
3.8.1	<i>Introduction</i>	140
3.8.2	<i>Detrital sediment in caves</i>	141
3.8.3	<i>Speleothem</i>	143
3.8.4	<i>Speleothem growth and environmental reconstruction</i>	143
3.8.4.1	Speleothem growth and climatic change	143

3.8.4.2	Stable isotope ratios in cave speleothem	145
3.8.4.3	Trace elements in cave speleothem	148
3.8.4.4	Speleothem formation and sea-level variations	149
3.8.4.5	Speleothem formation and tectonic activity	149
3.8.4.6	Speleothem formation and rates of denudation	149
3.8.5	<i>Other carbonate deposits</i>	149
3.9	Lake, mire and bog sediments	151
3.9.1	<i>Introduction</i>	151
3.9.2	<i>The nature of lake and bog sediments</i>	152
3.9.3	<i>Palaeoenvironmental evidence from lake sediments</i>	154
3.9.3.1	Lake sediments and landscape changes	155
3.9.3.2	Lake-level variations and climatic changes	159
3.9.3.3	Lake sediments and palaeotemperatures	160
3.9.4	<i>Palaeoenvironmental evidence from mire and bog sediments</i>	161
3.9.4.1	Palaeoprecipitation records from ombrotrophic peats	161
3.9.4.2	Stable isotope records from ombrotrophic peats	163
3.9.4.3	Human impact recorded in ombrotrophic peat	165
3.10	The deep-sea sediment record	165
3.10.1	<i>The nature and origin of ocean sediments</i>	165
3.10.2	<i>Oxygen isotope ratios and the ocean sediment record</i>	166
3.10.2.1	General principles	166
3.10.2.2	Glacial ice storage and the marine oxygen isotope record	167
3.10.2.3	Ice volumes, sea level and the marine oxygen isotope record	169
3.10.2.4	Sea-surface temperatures and the marine oxygen isotope record	170
3.10.3	<i>Limitations of oxygen isotope analysis</i>	170
3.10.3.1	Stratigraphic resolution	170
3.10.3.2	Sediment mixing	171
3.10.3.3	Isotopic equilibrium between test carbonate and ocean water	171
3.10.3.4	Carbonate dissolution and diagenesis	171
3.10.4	<i>Carbon isotopes in marine sediments</i>	171
3.11	Ice-core stratigraphy	172
3.11.1	<i>A brief history of deep-ice coring</i>	172
3.11.2	<i>Ice masses as palaeoenvironmental archives</i>	173
3.11.3	<i>Analysis of ice cores</i>	173
3.11.3.1	Annual ice increments	173
3.11.3.2	Dust content	175
3.11.3.3	Chemical content	175
3.11.3.4	Stable isotope records	175
3.11.3.5	Other trace substances	175
3.11.4	<i>Palaeoenvironmental significance of ice cores</i>	175
3.12	Conclusions	178
	Notes	179

4 Biological evidence

181

4.1	Introduction	181
4.1.1	<i>The nature of the Quaternary fossil record</i>	181
4.1.2	<i>The taphonomy of Quaternary fossil assemblages</i>	182
4.1.3	<i>The interpretation of Quaternary fossil assemblages</i>	182
4.2	Pollen analysis	183
4.2.1	<i>Introduction</i>	183

4.2.2	<i>The nature of pollen and spores</i>	183
4.2.3	<i>Field and laboratory work</i>	184
4.2.4	<i>Pollen diagrams</i>	185
4.2.5	<i>The interpretation of pollen diagrams</i>	190
4.2.6	<i>Applications of pollen stratigraphy</i>	194
4.2.6.1	Local vegetation reconstructions	194
4.2.6.2	Regional vegetation reconstructions	194
4.2.6.3	Space-time reconstructions	195
4.2.6.4	Human impact on vegetation cover	195
4.2.6.5	Pollen data and climatic reconstructions	197
4.3	Diatom analysis	197
4.3.1	<i>Introduction</i>	197
4.3.2	<i>The nature and ecology of diatoms</i>	198
4.3.3	<i>Field and laboratory methods</i>	200
4.3.4	<i>The interpretation of Quaternary diatom records</i>	202
4.3.5	<i>Applications of diatom analysis</i>	202
4.3.5.1	Diatoms as salinity indicators	202
4.3.5.2	Diatoms and pH	203
4.3.5.3	Diatoms and trophic status	205
4.3.5.4	Diatoms and the archaeological record	205
4.3.5.5	Other environmental applications	206
4.4	Plant macrofossil analysis	207
4.4.1	<i>Introduction</i>	207
4.4.2	<i>The nature of plant macrofossils</i>	207
4.4.3	<i>Field and laboratory work</i>	208
4.4.4	<i>Data presentation</i>	208
4.4.5	<i>The interpretation of plant macrofossil data</i>	209
4.4.6	<i>Palaeoenvironmental applications of plant macrofossil studies</i>	212
4.4.6.1	Palaeoclimatic reconstructions	212
4.4.6.2	Forest history	214
4.4.6.3	Charcoal and fire history	214
4.4.6.4	Archaeological records	215
4.5	Fossil insect remains	215
4.5.1	<i>Introduction</i>	215
4.5.2	<i>Coleoptera</i>	215
4.5.3	<i>Laboratory methods</i>	216
4.5.4	<i>Coleopteran analysis and Quaternary environments</i>	218
4.5.4.1	Habitat preferences	219
4.5.4.2	Palaeoclimatic inferences based on coleopteran assemblages	221
4.5.4.3	Insect fossils and archaeology	225
4.5.5	<i>Chironomidae</i>	225
4.6	Non-marine Mollusca	228
4.6.1	<i>Introduction</i>	228
4.6.2	<i>The nature and distribution of molluscs</i>	229
4.6.3	<i>Field and laboratory work</i>	229
4.6.4	<i>Taphonomy of non-marine molluscan assemblages</i>	231
4.6.5	<i>Interpretation of non-marine molluscan assemblages: habitat groups and indices of species diversity</i>	232
4.6.6	<i>Applications of Quaternary non-marine molluscan records</i>	233
4.6.6.1	Biostratigraphic correlation	233
4.6.6.2	Palaeoclimatic reconstructions	234

4.6.6.3	<i>Archaeological relevance</i>	234
4.7	<i>Marine Mollusca</i>	235
4.7.1	<i>Introduction</i>	235
4.7.2	<i>Analysis of marine molluscan assemblages</i>	235
4.7.3	<i>Marine Mollusca and palaeoclimatic inferences</i>	236
4.7.4	<i>Other applications of fossil marine molluscan records</i>	237
4.8	<i>Ostracod analysis</i>	238
4.8.1	<i>The nature and distribution of ostracods</i>	238
4.8.2	<i>Collection and identification</i>	238
4.8.3	<i>Ostracoda in Quaternary studies</i>	239
4.9	<i>Foraminiferal analysis</i>	241
4.9.1	<i>The nature and distribution of Foraminifera</i>	241
4.9.2	<i>Collection and identification</i>	242
4.9.3	<i>Foraminifera in Quaternary inshore and shelf sediments</i>	242
4.9.3.1	<i>Sea-level change</i>	242
4.9.3.2	<i>Shallow marine water mass and temperature variations</i>	243
4.9.3.3	<i>Other palaeoenvironmental applications</i>	244
4.10	<i>Micropalaeontology of deep-sea sediments</i>	244
4.10.1	<i>Introduction</i>	244
4.10.2	<i>Radiolaria</i>	244
4.10.3	<i>Coccolithophores</i>	245
4.10.4	<i>Dinoflagellates (dinocysts)</i>	246
4.10.5	<i>Marine microfossils in ocean sediments</i>	246
4.10.6	<i>Laboratory separation of marine microfossils</i>	248
4.10.7	<i>Marine palaeoclimatology</i>	248
4.10.8	<i>Marine palaeoproductivity and palaeocirculation</i>	253
4.11	<i>Vertebrate remains</i>	254
4.11.1	<i>Introduction</i>	254
4.11.2	<i>The structure of teeth and bones</i>	254
4.11.3	<i>Fossilization of bone material</i>	256
4.11.4	<i>Field and laboratory techniques</i>	256
4.11.5	<i>The taphonomy of fossil vertebrate assemblages</i>	257
4.11.5.1	<i>Cave and fissure deposits</i>	257
4.11.5.2	<i>Lacustrine sediments</i>	258
4.11.5.3	<i>Fluvial sediments</i>	258
4.11.6	<i>Quaternary vertebrate records</i>	258
4.11.6.1	<i>Vertebrate biostratigraphy</i>	259
4.11.6.2	<i>Vertebrate biogeography</i>	259
4.11.6.3	<i>Vertebrate fossils and Quaternary environments</i>	260
4.11.6.4	<i>Vertebrate fossils and faunal evolution</i>	262
4.12	<i>Other fossil groups</i>	263
4.12.1	<i>Chrysophytes</i>	263
4.12.2	<i>Cladocera</i>	263
4.12.3	<i>Coral polyps</i>	263
4.12.4	<i>Fungal remains</i>	264
4.12.5	<i>Testate amoebae</i>	264
4.12.6	<i>Biomarkers (ancient biomolecules)</i>	265
4.13	<i>Multi-proxy palaeoecological studies</i>	265
4.14	<i>Conclusions</i>	266
	<i>Notes</i>	266

5	Dating methods	267
5.1	Introduction	267
5.2	Precision and accuracy in Quaternary dating	267
5.3	Radiometric dating techniques	268
5.3.1	<i>The nucleus and radioactivity</i>	268
5.3.2	<i>Radiocarbon dating</i>	270
5.3.2.1	General principles	270
5.3.2.2	Measurement of ^{14}C activity	271
5.3.2.3	Quality assurance in radiocarbon dating	275
5.3.2.4	Sources of error in radiocarbon dating	275
5.3.2.5	Radiocarbon dating of soils	279
5.3.2.6	Calibration of the radiocarbon timescale	279
5.3.3	<i>Argon-isotope dating</i>	284
5.3.3.1	Potassium–argon dating	284
5.3.3.2	Argon–argon (Ar/Ar) dating	285
5.3.3.3	Problems and limitations of argon-isotope dating	285
5.3.3.4	Some applications of argon-isotope dating	285
5.3.4	<i>Uranium-series (U-series) dating</i>	286
5.3.4.1	General principles	286
5.3.4.2	Measurement, problems and age range	287
5.3.4.3	Some applications of U-series dating	288
5.3.5	<i>Fission track dating</i>	289
5.3.5.1	General principles	289
5.3.5.2	Measurement and problems	290
5.3.5.3	Some applications of fission track dating	290
5.3.6	<i>Luminescence dating</i>	291
5.3.6.1	General principles	291
5.3.6.2	Measurement and problems	291
5.3.6.3	Developments in luminescence dating	292
5.3.6.4	Age ranges and applications of luminescence dating	293
5.3.7	<i>Electron spin resonance (ESR) dating</i>	293
5.3.7.1	General principles and measurement	293
5.3.7.2	Sources of error in ESR dating	294
5.3.7.3	Some applications of ESR dating	294
5.3.8	<i>Cosmogenic radionuclide (CRN) dating</i>	294
5.3.8.1	General principles	294
5.3.8.2	Measurement and problems	295
5.3.8.3	Some applications of CRN dating	296
5.3.9	<i>Short-lived radioactive isotopes</i>	296
5.3.9.1	Lead-210	297
5.3.9.2	Caesium-137	297
5.3.9.3	Silicon-32	298
5.4	Incremental dating methods	298
5.4.1	<i>Dendrochronology</i>	298
5.4.1.1	General principles	298
5.4.1.2	Measurement and problems	298
5.4.1.3	Dendrochronological records	300
5.4.1.4	Dendroclimatology	302
5.4.2	<i>Varve chronology</i>	304
5.4.2.1	The nature of varved sediments	304

5.4.2.2	Clastic varves	304
5.4.2.3	Organic (biogenic) varves)	305
5.4.2.4	Chemical varves	306
5.4.2.5	Complex varves	306
5.4.2.6	Sources of error in varve counting	306
5.4.2.7	Applications of varve chronologies	307
5.4.3	<i>Annual layers in glacier ice</i>	310
5.4.3.1	General principles	310
5.4.3.2	Errors in ice-core chronologies	312
5.4.3.3	Ice-core chronologies	312
5.4.4	<i>Lichenometry</i>	315
5.4.4.1	General principles	315
5.4.4.2	Sources of error in lichenometric dating	315
5.4.4.3	Some applications of lichenometry	316
5.4.5	<i>Other materials dated by annual increments</i>	316
5.4.5.1	Speleothems	316
5.4.5.2	Sclerochronology	317
5.5	Age-equivalent stratigraphic markers	319
5.5.1	<i>Palaeomagnetism</i>	319
5.5.1.1	Geomagnetic field and remanent magnetism	319
5.5.1.2	Magnetostratigraphy	320
5.5.2	<i>Tephrochronology</i>	325
5.5.2.1	General principles	325
5.5.2.2	Sources of error in tephrochronology	327
5.5.2.3	Applications of tephrochronology	327
5.5.3	<i>Oxygen isotope chronology</i>	330
5.5.4	<i>Biostratigraphy and molecular clocks</i>	331
5.6	Relative chronology based on processes of chemical alteration	332
5.6.1	<i>Amino-acid geochronology</i>	332
5.6.1.1	Chemistry of proteins	332
5.6.1.2	Amino-acid diagenesis	334
5.6.1.3	Aminostratigraphy and age control	334
5.6.1.4	Problems with amino-acid geochronology	334
5.6.1.5	Recent developments in amino-acid geochronology	336
5.6.1.6	Some applications of amino-acid geochronology	336
5.6.2	<i>Fluorine, uranium and nitrogen content of fossil bones</i>	339
5.6.3	<i>Obsidian hydration dating (OHD)</i>	340
5.6.3.1	General principles	340
5.6.3.2	Problems with obsidian hydration dating	340
5.6.3.3	Some applications of obsidian hydration dating	340
5.6.4	<i>Weathering characteristics of rock surfaces</i>	340
5.6.4.1	General principles	340
5.6.4.2	Problems in using surface weathering features as indicators of relative age	341
5.6.3.4	Some applications of surface weathering dating	342
5.6.5	<i>Pedogenesis</i>	342
5.6.5.1	General principles	342
5.6.5.2	Problems in using pedogenesis as a basis for dating	342
5.6.5.3	Some applications of relative dating based on degree of pedogenesis	343
5.7	Stratigraphic and temporal resolution	343
5.8	Conclusions	344
	Notes	345

6 Approaches to Quaternary stratigraphy and correlation	347
6.1 Introduction	347
6.2 Stratigraphic subdivision	347
6.2.1 <i>Principles of Quaternary stratigraphy</i>	347
6.2.2 <i>Stratotypes</i>	349
6.2.3 <i>Elements of Quaternary stratigraphy</i>	349
6.2.3.1 Lithostratigraphy	349
6.2.3.2 Biostratigraphy	353
6.2.3.3 Morphostratigraphy	354
6.2.3.4 Soil stratigraphy	355
6.2.3.5 Oxygen isotope stratigraphy	355
6.2.3.6 Climatostratigraphy	358
6.2.3.7 Chronostratigraphy	361
6.3 Time-stratigraphic correlation	362
6.3.1 <i>Principles of Quaternary correlation</i>	362
6.3.2 <i>Bases for time-stratigraphic correlation</i>	363
6.3.2.1 Palaeomagnetic correlation	363
6.3.2.2 Correlation using tephra layers	364
6.3.2.3 Correlation using palaeosols	364
6.3.2.4 Shoreline correlation	364
6.3.2.5 Correlation on the basis of radiometric dating	365
6.3.2.6 Event stratigraphy and correlation	365
6.3.2.7 Correlation using the marine oxygen isotope record	366
6.3.3 <i>Correlation between continental, marine and ice-core records</i>	366
6.3.3.1 Long-term correlation on Milankovitch timescales	367
6.3.3.2 Correlation on sub-Milankovitch timescales	371
6.3.3.3 Synchronizing records of past environmental change	374
6.4 Conclusions	378
7 Global environmental change during the Quaternary	379
7.1 Introduction	379
7.2 Environmental simulation models (ESMs)	380
7.2.1 <i>Introduction</i>	380
7.2.2 <i>Box models</i>	380
7.2.3 <i>General circulation models (GCMs)</i>	381
7.2.4 <i>Earth system models of intermediate complexity (EMICs)</i>	383
7.2.5 <i>Transient simulations</i>	386
7.2.6 <i>Palaeodata-model comparisons</i>	387
7.2.7 <i>Limitations of ESMs</i>	388
7.2.8 <i>The importance of ESMs in Quaternary research</i>	388
7.3 Climatic change over Milankovitch timescales	389
7.3.1 <i>Introduction</i>	389
7.3.2 <i>The Mid-Pleistocene Transition (MPT)</i>	390
7.3.3 <i>The glacial-interglacial cycles of the last 800 ka</i>	394
7.3.4 <i>Overview</i>	397
7.4 Environmental change over sub-orbital (millennial) timescales	399
7.4.1 <i>Introduction</i>	399
7.4.2 <i>Ice-ocean-climate interplay in the North Atlantic</i>	400
7.4.3 <i>A bipolar teleconnection</i>	405

xiv CONTENTS

7.4.4	<i>Global teleconnections: linking mechanisms</i>	407
7.4.5	<i>Overview</i>	412
7.5	The Last Termination	413
7.5.1	<i>Introduction</i>	413
7.5.2	<i>Definition of the Last Termination</i>	413
7.5.3	<i>Onset of the Last Termination</i>	415
7.5.4	<i>Global teleconnections during the Last Termination</i>	418
7.5.5	<i>Synchronizing records of Lateglacial age</i>	419
7.5.5.1	Introduction	419
7.5.5.2	Lateglacial stratigraphy and chronology	419
7.5.5.3	Lateglacial age models and correlation procedures	420
7.5.5.4	Rapid environmental change during the Lateglacial	421
7.6.	Climate and the Holocene	427
7.6.1	<i>Introduction</i>	427
7.6.2	<i>Holocene climate trends</i>	427
7.6.3	<i>Holocene climatic events</i>	428
7.6.3.1	The Pleistocene–Holocene transition	428
7.6.3.2	The 8.2 ka event	429
7.6.3.3	The 4.2 ka event	431
7.6.3.4	The 2.8 ka event	433
7.6.3.5	The Little Ice Age	433
7.6.4	<i>Holocene climatic cycles</i>	434
7.6.4.1	Late Holocene solar cycles	434
7.6.4.2	El Niño–Southern Oscillation (ENSO)	435
7.6.4.3	Late Holocene Atlantic and Pacific Oscillations	435
7.6.5	<i>People and climate</i>	436
7.6.5.1	The greenhouse effect	437
7.6.5.2	Early human impact?	438
7.6.5.3	Delayed glaciation?	439
7.6.6	<i>The Anthropocene</i>	439
7.7	Concluding remarks	440
	Notes	443
	<i>References</i>	445
	<i>Index</i>	523

Figures and tables

FIGURES

1.1	The Quaternary relative to the geological timescale	1
1.2	The Cenozoic timescale, as defined in 2014	3
1.3	The Monte San Nicola section in southern Sicily	4
1.4	The maximum glaciation of the Northern Hemisphere during the Quaternary	6
1.5	Climatic trends during the past 3 Ma reflected in a stacked (composite) oxygen isotope record	10
1.6	The MIS record based on a composite of deep-ocean cores and the Quaternary stratigraphy of the Northern Hemisphere	11
1.7	The $\delta^{18}\text{O}$ record from the GRIP Greenland ice core showing the Lateglacial event stratigraphy and the stratigraphic subdivision of the Lateglacial in northwest Europe and the British Isles	12
1.8	The components of the Astronomical Theory of climate change	14
1.9	a) Variations in eccentricity, obliquity and the precessional index over the past 800 ka. b) Normalized and smoothed variations in the oxygen isotope signal ($\delta^{18}\text{O}$) in five deep-sea cores	14
1.10	Variations in temperature, dust flux, CO_2 and CH_4 from the EPICA Dome C ice-core record, Antarctica, over the last 800 ka	15
2.1	Geomorphological map of the West Drumochter Hills in the Scottish Highlands	21
2.2	Sonar bathymetry of the north-central English Channel shelf	25
2.3	A digital surface model showing the ice-moulded landscape of part of the Midland Valley of Scotland	26
2.4	Moraine systems in a) Bhutan-Himalaya, b) northwest Scotland and c) Antarctica	28
2.5	a) Features used to identify trimlines and other types of glacial limits in mountainous terrain. b) Nunataks bordering Liv Glacier. c) High-altitude trimline in the Grimsel Pass, Switzerland	29
2.6	a) Maximal limits of the Late Weichselian ice sheet. b) Recessional stages of the Late Weichselian ice sheet	30
2.7	a) Cross-section through ice-marginal ridges of Late Weichselian age in Denmark. b) Up-thrusted and folded Middle Weichselian lacustrine and fluvial sediments, northernmost Jutland	31
2.8	Limits of the Late Devensian British ice sheet	34
2.9	a) The Late Weichselian Laurentide, Cordilleran and Innuitian ice sheet at the LGM. b) Reconstructed ice lobes in the Great Lakes region at the LGM. c) The pattern of retreat moraines of the Michigan–Huron lobe after the LGM	36
2.10	Retreat pattern of the Laurentide ice sheet and estimated ages of major arterial flows or ice streams	37
2.11	Wisconsinan terminal moraines dating to the Tahoe series in Pine Creek Canyon, California	39
2.12	Local ice-flow direction based on mapping of lineations of striations in northern Canada	41
2.13	Mega-grooved bedrock surface showing parallel striations and gouge-marks, including crescentic fractures	42
2.14	A drumlin in the Eden Valley, northwest England, that formed beneath the last British–Irish ice sheet	42

xvi FIGURES AND TABLES

2.15	Lineation of subglacial landform suites (mostly drumlins) formed by the last Irish ice sheet	43
2.16	Examples of input and output parameters employed in a numerical model simulation of the last Laurentide ice sheet	44
2.17	Inverse models of the last (Late Devensian) British ice sheet	45
2.18	Model simulations of a) basal ice temperature and b) horizontal basal velocity of the last British Ice sheet during the LGM	46
2.19	Four numerical simulation models of the ice sheets over North America at the LGM	47
2.20	Reconstruction of the Loch Lomond (Younger Dryas) Stadial icefield in the Pass of Drumochter area, Scottish Highlands	48
2.21	ASTER images of the Chapman Glacier and adjacent piedmont glaciers, northern Canada	49
2.22	a) The relationship between mean winter snow accumulation and mean temperature during the ablation season for modern glaciers in Norway. b) Generalized contours for inferred ELAs based on reconstructed glaciers in Scotland	51
2.23	Mean equilibrium-line altitudes for reconstructed glaciers in eleven districts of the British Isles	52
2.24	Contemporary permafrost distribution in the northern hemisphere	53
2.25	a) Granite tor on the summit of Beinn Mheadhoin, Cairngorm Mountains, Scotland. b) Summit blockfield on Gros Morne Mountain, western Newfoundland, Canada	54
2.26	a) Active polygonal patterned ground, Mt Edziza, British Columbia, Canada. b) Sorted circles on the summit of Gros Morne Mountain, western Newfoundland, Canada	55
2.27	Active lobate rock glaciers near Lytton, British Columbia, Canada	56
2.28	Fossil protalus rampart and stratified scree near Cader Idris, Wales	57
2.29	Altitudes of the frontal crests of Loch Lomond (Younger Dryas) Stadial protalus ramparts in the Scottish Highlands, and reconstructed ELAs of Stadial glaciers	57
2.30	The 'High Rock Platform', northern Islay, Scottish Hebrides	58
2.31	Eustatic sea-level variations over the last 9.5 Ma based on marine oxygen isotope measurements	60
2.32	Variations in eustatic sea level over a) the past 1 Ma and b) the last 500 ka	61
2.33	Comparison of seven different eustatic sea-level records from the last glacial cycle	62
2.34	a) Rise in eustatic sea level since the LGM; b) Land elevation changes in Hudson Bay, Canada and c) in northern Sweden during the Holocene	63
2.35	River bank section in lower Strathearn, eastern Scotland showing evidence for marine regression and transgression	64
2.36	a) Chronology of isolations from, and connections to, the sea for four littoral basins in northwest Scotland. b) Relative sea-level reconstructions for selected sites in the UK, based on dated index points and sea-level tendencies	65
2.37	Relative changes in land or sea level in the UK during the late Holocene	66
2.38	Raised coral reef terraces along the coast of the Huon Peninsula, Papua New Guinea	67
2.39	Schematic diagram of the effect of an ice mass on a land surface	68
2.40	Crustal flexuring in the Pacific margin of Canada reflecting the changing mass of the last ice sheet in British Columbia	68
2.41	The development of a raised shoreline sequence reflecting isostatic recovery and eustatic rise following deglaciation	69
2.42	Height-distance diagram of measured altitudinal variations of the surfaces of shoreline fragments in Fife, eastern Scotland	70
2.43	Isobase and trend surface data reflecting patterns of uplift in a) eastern Canada, b) Scandinavia and c) Scotland	71
2.44	Sea-level changes in Atlantic Canada	72
2.45	Terraces cut into outwash gravels, Glen Roy, Scotland	74
2.46	a) Schematic representation of the staircase of river terraces preserved in the Middle Rhine area. b) Areal distribution of terrace gravels in the Lower Rhine	75
2.47	Formation of 'strath' and 'cut-and-fill' fluvial terraces	75
2.48	Schematic representation of a sequence of river terraces in the valley of the Somme, France	76

2.49	a) Average alluvial sedimentation rate for three catchments in southern Turkey over the past 6 ka. b) The number of settlements occupied in the region over the same period	78
2.50	Schematic transverse profiles through the best-preserved suite of the terrace staircase of a) the Middle Thames (<i>c.</i> 35 km west of London) and b) the Lower Thames (<i>c.</i> 15 km east of London)	79
2.51	Schematic representation of the Thames drainage system a) prior to, b) during and c) after the Anglian glaciation	80
2.52	a) Abandoned shorelines of Pluvial Lake Lahontan near Reno, Nevada, USA. b) Beach deposits and fan gravels from Pluvial Lake Lahontan	83
2.53	The maximum limits of late Pleistocene pluvial lakes in the American southwest	84
2.54	Location and surface dimensions of modern Lake Chad, Palaeolake Mega-Chad, and the Chad drainage catchment	85
2.55	a) Hydro-isostatic deformation of the Bonneville Shoreline of Pluvial Lake Bonneville. b) Chronology of water level changes in Lake Bonneville over the past 30 ka	86
2.56	Principal dune-building episodes during the last 50 ka in the deserts of Africa, Australia, Asia and North America	87
2.57	Dominant linear dune trends and present-day dust circulation in Australia	88
2.58	Linear trends of crests of sand dunes in Egypt's Western Desert	89
2.59	Remotely sensed images of the desert area of NW Sudan; a) LANDSAT ETM image of surface sands with little indication of buried palaeo-drainage features beneath. b) Radarsat-1 image that reveals the buried palaeo-drainage features below. c) Digital elevation model (DEM) that enhances the buried river channel system	90
3.1	Monolith tins (50 cm length) in a sediment exposure in the Kopanica Valley, southwest Poland	94
3.2	Examples of coring equipment used to sample Quaternary sediments	95
3.3	X-radiograph images of laminated (varved) lake sediments that accumulated in a former ice-dammed lake near Loch Lomond, Scotland	96
3.4	Schematic model of supra-, en- and subglacial 'subenvironments' within the marginal zone of a continental ice mass	100
3.5	Schematic model of modes of deposition in proximal zones associated with continental and marine ice margins	101
3.6	Examples of glaciogenic deposits that could be classified as lodgement, melt-out and possible 'flow' tills	103
3.7	Highly contorted glacial diamict (till) exposed at West Runton, Norfolk, UK	104
3.8	Range of microstructures and fabrics observed in deformed tills from micromorphological analysis of thin section samples	105
3.9	Examples of microfabrics in deformed till identified using thin-section analysis on samples obtained from tills in Ontario, Canada	106
3.10	Scanning electron photomicrographs of vertical sections through the fine matrix of tills	107
3.11	View down the Braldu Valley in the central Karakoram, northern Pakistan	108
3.12	Ternary diagram using a statistical clustering method (eigenvalues) to characterize clast fabrics obtained from diamictons	110
3.13	Particle size distributions (cumulative frequency curves) showing distinctive curves obtained from diamictons and sorted sediments	110
3.14	Schematic facies logs of glaciogenic sediments in Wales	111
3.15	Idealized lithofacies associations for glaciogenic sediment sequences developed under different thermal regimes	112
3.16	The giant quartzite erratic ('The Big Rock') near Okotoks, southwest Alberta, Canada	113
3.17	a) Distribution of some indicator erratics by ice in Britain and northwest Europe. b) The Lennoxtown boulder train in the Forth Valley, central Scotland	113
3.18	Different methods for representing till fabric data	114

xviii FIGURES AND TABLES

3.19	a) Ice-wedge cast of Anglian age (MIS 12), West Runton, Norfolk, Eastern England. b) Anglian age sand wedge, Broomfield, Essex, UK	116
3.20	Involutions/cryoturbation structures, formed in Late Weichselian fluvial sediments at the site of Bosscherheide, Netherlands	117
3.21	Classification of cryoturbation structures according to their form	118
3.22	a) Mean annual temperature in northwest Europe during the 27–20 k ¹⁴ Cyr BP interval. b) Mean annual temperature in northwest Europe during the 20–13 k ¹⁴ Cyr BP interval	120
3.23	a) Permafrost limits in northwest Europe during the Younger Dryas. b) Maximum mean annual isotherms in northwest Europe for the coldest part of the Younger Dryas Stadial	121
3.24	Examples of palaeosols	123
3.25	Photomicrographs of pedogenic structures in soil horizons within Weichselian loess deposits in southern Poland	125
3.26	a) The early Quaternary ‘Wucheng’ sequence of loess units and soil horizons exposed at the Luochuan site on the Loess Plateau, China. b) The S1 (last interglacial) soil profile exposed at the Lantian section, near Xi’an in the southern part of the Loess Plateau	128
3.27	The Loess Plateau, major deserts and mountain regions of north-central China	129
3.28	Loess–palaeosol succession at Baoji, in the southern Loess Plateau, showing thirty-two palaeosol units spanning the last 2 Ma	129
3.29	Coversands and interbedded Usselo soil of Lateglacial (late Allerød) age exposed at a site in the Netherlands	130
3.30	Magnetostratigraphy, lithology, magnetic susceptibility and grain-size variations of the Lingtai section on the Chinese Loess Plateau	132
3.31	The water-level record for Lake Lisan over the course of the last 55 ka	133
3.32	The geochemical record from a lake sequence in Tibet that developed between 9 and 4 ka	134
3.33	a) Locations of lakes for which lake-level data are lodged with the PMIP Global Lake Status Data Base. b) Lake status data for 18 ka. c) Lake status for 6 ka	136
3.34	Lake-status data for 6 ka expressed as anomalies relative to long-term status	137
3.35	Spatial patterns of inferred effective moisture for six time-slices between the Bølling-Allerød period and the present time	139
3.36	a) Carbonate δ ¹⁸ O records from eight lake sediment sequences from the Indian Monsoon region. b) A regional moisture index based on the mean of the eight curves shown in a)	140
3.37	Generalized cross-section of a cave with various types of sedimentary infill and associated biological remains	141
3.38	a) Cross-sectioned surface of a stalagmite from Akçakale Cave, northeast Turkey revealing annual growth layers spanning the last c. 500 yr. b) Cross-sectioned surface of a small stalagmite from Rukiessa Cave, southeast Ethiopia, spanning the last century	144
3.39	Compilation of c. 750 TIMS U-series speleothem dates plotted against the latitude of the relevant site	144
3.40	Composite δ ¹⁸ O curve constructed from twenty-one overlapping speleothem records for the past 185 ka from Soreq Cave, Israel	146
3.41	a) δ ¹⁸ O measurements covering the period 14 ka to the present from Höllloch Cave, Bavarian Alps, Germany. b) Timberline record from the Eastern Alps, Austria	147
3.42	δ ¹⁸ O record from Hulu Cave, China and the δ ⁸ O trace from the GISP2 Greenland ice core	148
3.43	Growth phases of ²³⁰ Th-dated portions of travertine from sites in semi-arid northeastern Brazil extending over > 600 ka	150
3.44	Tufa formations around the shore of Mono Lake, California	150
3.45	Middle Pleistocene (Cromerian Complex) organic deposits exposed beneath till at Pakefield, Suffolk, UK	152
3.46	Some sediment types deposited with increasing depth of water under oligotrophic and eutrophic conditions	154
3.47	Schematic representation of gradual infill of a small lake	155

3.48	Lateglacial and early Holocene environmental changes inferred from lithostratigraphy of a typical northwest European lake and mire sequence	156
3.49	Variations in the abundance of selected chemical elements in Lateglacial and early Holocene sediments from two sites in the Isle of Skye, Inner Hebrides, Scotland	157
3.50	Variations in rates of lake sedimentation during the Holocene in sites from the British Isles	158
3.51	The lake sediment sequence at Sevrier-Les-Charretières, Lake Annecy, France	159
3.52	a) A peat profile at Bolton Fell Moss, northern England, showing a lower dark, well-humified peat overlain by a lighter-coloured, less well-humified peat. b) A peat section from Store Vildmose, Denmark, showing both lateral and vertical alternations in darker and lighter peat layers	162
3.53	Reconstructed mire-surface wetness changes at Walton, Moss, northern England	163
3.54	Proxy climate reconstructions from Temple Hill Moss, southeast Scotland	164
3.55	Heinrich layers in deep-ocean sediments from the northwestern Labrador Sea	166
3.56	Variations in surface water oxygen isotope ratios during times of glacial maxima and interglacial high sea-level stands	168
3.57	Schematic representation of oxygen isotope variations for the past 600 ka	168
3.58	Comparison between estimates of sea-level variations for the last 140 ka based on marine isotopic and coral reef records	169
3.59	Location of some of the principal ice-core drilling stations in Greenland and Antarctica	173
3.60	Annual ice layers exposed in the Quelcayya ice cap, Peru	174
3.61	Seasonal variations in chemistry, dust content and stable oxygen isotope ratios in ice layers in a section of the NorthGRIP core	174
3.62	Continuous $\delta^{18}\text{O}$ profiles through five Greenland ice cores	176
4.1	Subsample of a pollen assemblage typical of last cold stage deposits from the site of St Front, France	184
4.2	Relative pollen diagram showing variations in abundance of principal taxa in a lake sediment sequence at Ioannina, northwest Greece	186
4.3	Pollen concentration diagram for some of the taxa represented in relative proportions in Figure 4.2	187
4.4	Pollen accumulation rate data for a sequence spanning the last 11 ka at Steel Lake, central Minnesota, USA	188
4.5	Arboreal pollen taxa and palaeotemperature inferences recorded for last interglacial deposits at Jammertal, southwest Germany	190
4.6	The changing vegetation cover of the eastern USA from 18 ka to present	195
4.7	Pollen percentage and influx diagram for <i>Abies</i> and <i>Corylus</i> , and charcoal influx record, from a site in south Switzerland spanning the period 5.1–3.1 cal. BC	196
4.8	Holocene pollen diagram from the site of An Loch Mor, the Aran Islands, western Ireland	197
4.9	Schematic representation of the procedures employed to derive quantitative lake-water pH reconstructions from fossil diatom records	198
4.10	SEM images of common northwest European diatom frustules recovered from streams and soils in southeast England	199
4.11	Late Holocene diatom stratigraphy from Beaver Lake in the Nebraska Sand Hills, USA	201
4.12	A marine incursion (positive sea-level tendency) as reflected in a diatom assemblage	202
4.13	Isolation basin studies in southeast Greenland	204
4.14	Diatom-inferred palaeosalinity through a sediment sequence in Oro Lake, Saskatchewan, Canada	205
4.15	Diatom-inferred pH history of Lysevatten Lake, southwestern Sweden, suggesting increased acidification since the 1960s	206
4.16	Scanning electron photomicrographs of terrestrial macrofossils from a 12 ka peat layer in North Dakota, USA	207
4.17	Arboreal plant macrofossils in a Lateglacial sediment sequence in Latvia, plotted against the pollen record of the same taxa	209
4.18	Influx of charcoal fragments and macrofossils of selected plant taxa in a lake sediment sequence in the North Cascade Range, Washington State, USA	210
4.19	Recruitment pathways and processes by which plant macrofossil remains are delivered to lakes	211

XX FIGURES AND TABLES

4.20	Episodes of climatic deterioration in northern Britain during the past 7.5 ka based on plant macrofossil evidence for increased bog-surface wetness	213
4.21	Subfossil coleopteran sclerites recovered by flotation from peat deposits overlying a Bronze Age occupation site near Ballyarnet Lake, Co. Derry, Northern Ireland	216
4.22	Generalized drawings of coleopteran sclerites frequently preserved as Quaternary fossils, showing a range of diagnostic features used in fossil identification	217
4.23	A coleopteran record from the Lateglacial site of Llanilid, south Wales, UK	218
4.24	Number of obligate beetle species recorded in Holocene sediment sequences from southern and central England	220
4.25	Present-day European distributions of four coleopteran species found in Lateglacial deposits at the site of Glanllynnau, north Wales	221
4.26	Schematic representation of the mutual climatic range method of quantitative temperature reconstructions	223
4.27	Test of the MCR method on assemblages of species found living today at thirty-five localities in North America	223
4.28	Generalized climatic curves of estimated T_{MAX} variations during the Lateglacial–early Holocene for different parts of Europe	224
4.29	Head capsules of common chironomid taxa recovered from late Quaternary lake sediment sequences from northwest Europe	226
4.30	Chironomid-inferred temperature variations for the Lateglacial sequence near the Majola Pass, Swiss Alps, compared with the NGRIP isotope record	227
4.31	a) Fossil shells of freshwater molluscs (principally gastropods) exposed on an abandoned beach of Pluvial Lake Lahontan, Pyramid Lake, Nevada, USA. b) <i>Valvata piscinalis</i> , a small gastropod that inhabits streams, rivers and lakes	228
4.32	Variations in relative abundance of molluscan species from the Lateglacial to mid-Holocene sequence at Holywell Coombe, southern England	230
4.33	Variations in absolute abundance of terrestrial molluscan species through a Late Quaternary loess and palaeosol succession at Weinan, China	231
4.34	Variations in species richness, abundance, diversity and habitat types in Holocene tufa sequences at Courteenhall, near Northampton, UK	232
4.35	Examples of some common marine bivalves of the North Atlantic and their water depth preferences	235
4.36	Distribution of marine zoogeographical provinces in the Northeast Atlantic	236
4.37	Variations in the dynamics of the winter North Atlantic Oscillation and of annual growth increments of the bivalve <i>Arctica islandica</i>	237
4.38	Climatically significant ostracods from the Pleistocene of the British Isles	239
4.39	Examples of planktonic foraminiferal species widely employed in Quaternary palaeocean studies	241
4.40	Relative sea-level curves for the last 12 ka for the Western Mediterranean based on benthic Foraminifera-based transfer functions	243
4.41	a) Examples of siliceous skeletons (tests) of the radiolarian groups Spumellaria and Nassellaria. b) SEM scans of coccolithophore specimens from the central Adriatic Sea	245
4.42	a) Examples of common Quaternary dinocysts. b) Structural features of some dinoflagellate cysts (dinocysts) at motile stage	247
4.43	Planktonic foraminiferal provinces in the modern ocean showing the close relationship between sea-surface temperature gradients and species abundances	249
4.44	Changes in coiling direction of tests of the high-latitude species <i>Neogloboquadrina</i>	250
4.45	Changes in ecological water masses in the Norwegian Sea and the northern North Atlantic over the past 225 ka	251
4.46	Reconstructions of surface conditions in the Northeast Atlantic during the Last Glacial Maximum based on marine microfossil records	252
4.47	Mg/Ca calibration results for several species of planktonic Foraminifera	253

4.48	Rapid changes in SST in the Alboran Sea (Mediterranean Sea) over the past 50 ka	253
4.49	a) Fossil right femur of a mammoth of Middle Pleistocene age discovered at the site of West Runton, Norfolk, UK. b) Occlusal surface and roots of the first lower molar of the ancestral water vole (<i>Mimomys savini</i>) recovered from Middle Pleistocene deposits at Pakefield, Suffolk, UK.	
	c) Reconstruction of woolly mammoth (<i>Mammuthus primigenius</i>) based on carcass remains discovered, in Yakutia, arctic Siberia	255
4.50	Age estimates of Pleistocene records of the spotted hyena (now confined to Africa) in Europe	259
4.51	Reconstructions of the large (<i>Mammuthus columbi</i>) and pygmy (<i>M. exilis</i>) mammoth species that co-inhabited Santa Rosa Island, California between c. 200 and 11 ka	260
5.1	The ranges of various dating methods discussed in the text	268
5.2	Accuracy and precision with respect to age estimates derived for a sample with a true age of 10 ka BP	269
5.3	Decay curve for radiocarbon	271
5.4	The 5 MV National Electrostatics Corporation Accelerator Mass Spectrometer at the Scottish Universities Environmental Research Centre, East Kilbride, UK	273
5.5	The exposed sample target wheel (ion source) of the AMS in Figure 5.4	273
5.6	Schematic diagram of the components of a tandem accelerator	274
5.7	Radiocarbon years versus calendar ages for the period 9.0–11.0 ka BP (10.5–12.5 cal. BP)	275
5.8	Radiocarbon calibration dating series for the period 0–50 ka	280
5.9	Age–depth plot of Cariaco Basin sediments after being tuned (matched) to the Hulu Cave record	281
5.10	The influence of the shape of the radiocarbon curve on calibration	281
5.11	The conversion of a Gaussian radiocarbon error range to a non-Gaussian, multi-modal error distribution in calibrated time	282
5.12	Wiggle-match dating of a peat sequence in the Netherlands	283
5.13	Branching decay of ^{40}K	284
5.14	Chain decay pathways and half-lives of intermediate nuclides during the decay of ^{238}U , ^{235}U and ^{232}Th to stable lead	286
5.15	Methods of measuring palaeodose (D_E) after the natural TL intensity of a sample (N) has been established	291
5.16	a) Glacial moraine in the Nubra Valley to the north of Leh, Ladakh, northern India. b) Boulders on the moraine surface dated by ^{10}Be	297
5.17	a) Cross-cut of a tree trunk showing seasonally differentiated growth rings. b) X-ray negatives of wood surfaces for analysis by a high-resolution microdensitometer, illustrated schematically in c)	299
5.18	Age profile of cross-matched tree-ring series from Finnish Lapland for the period AD 1200–160 BC	300
5.19	Standardization of ring-width measurements to generate ring-width indices	301
5.20	Ancient bristlecone pines growing in the White Mountains of California	301
5.21	a) Fossil oak trunks excavated from gravel beds of the River Danube valley. b) A section through one of the trunks of subfossil oak	302
5.22	Part of a continuous 7,519-year pine tree-ring chronology from Finnish Lapland	303
5.23	Simplified model of clastic and organic varve formation	305
5.24	The pattern and rate of ice retreat across Scandinavia based on a combination of clay-varve chronology and radiocarbon dating	308
5.25	a) Part of a varved sequence from Lake Suigetsu, Japan. b) Photomicrographs of part of the Suigetsu varve sequence in plain light and polarized light	310
5.26	Line-scan images from the NorthGRIP ice core	311
5.27	The NorthGRIP oxygen isotope record and variations in annual ice-layer thickness plotted against the GICC05 timescale	313
5.28	Lichenometric growth curves for <i>Rhizocarpon</i> spp. from West Greenland, West Spitsbergen and Baffin Island	315

xxii FIGURES AND TABLES

5.29 Radiographs of core-slabs cut from a) Pleistocene and b) modern coral reefs (<i>Montastraea</i>) in Florida Bay, Gulf of Mexico, showing seasonal growth layers. c) Cross-matching of growth layers of <i>Porites</i> coral from three locations on the central Great Barrier Reef, Australia, using UV luminescent illumination	316
5.30 A 54-year annual coral stable isotope record from the mid-Holocene	317
5.31 Annual coral $\delta^{18}\text{O}$ records from various sites in the Pacific and Indian Oceans	318
5.32 Secular changes in magnetic declination and inclination as observed in London, Rome and Boston	321
5.33 Palaeomagnetic dating of sediments from Lake Päijänne, Finland	322
5.34 The palaeomagnetic timescale of the last 3.5 Ma	323
5.35 Variations in the earth's magnetic inclination and field strength (palaeointensity) during the last 2.5 Ma	324
5.36 Magnetic susceptibility variations through a complete Quaternary loess sequence at Luochuan on the Loess Plateau, Central China	325
5.37 a) Yellow and black tephra layers exposed in a soil–peat complex in Iceland. b) The North Atlantic Ash Zone 2 tephra layer preserved in the NGRIP ice core. c) Fluted distal shards of the Campagnian Ignimbrite from Campania, Italy. d) Platy distal shards of the Vedde Ash from Katla Volcano, Iceland	326
5.38 Tephra layers exposed in sections at two sites in Montana, northwest USA	328
5.39 Widespread tephra marker horizons in marine and terrestrial sequences in the central Mediterranean and eastern Europe	329
5.40 Orbitally tuned chronostratigraphy for a composite ('stacked') deep-ocean isotopic record spanning the last 300 ka	331
5.41 Comparison of orbitally tuned age estimates based on SPECMAP and independently dated U-series coral ages	331
5.42 Chemistry of amino acids	333
5.43 Amino-acid geochronology of coastal barrier sediments (aeolinites) in the region of the Murray River mouth, South Australia	337
5.44 An aminostratigraphic framework for the Thames terraces of southeast England	338
5.45 Weathering and soil-forming indices used to establish relative age of landform surfaces	341
5.46 Stratigraphic and temporal resolution in Quaternary sediment sequences	344
6.1 Time-transgression in lithostratigraphic and biostratigraphic boundaries	349
6.2 Lithostratigraphic subdivision of a glaciogenic sequence	350
6.3 Sequence of sedimentary units deposited near continental margins during cycles of sea-level fall and rise	352
6.4 Various types of biozone used in the subdivision and correlation of strata	353
6.5 Schematic diagram showing a series of moraine ridges between which sediments have accumulated in lake basins following deglaciation	354
6.6 a) Oxygen isotope stratigraphy in a 53 m core obtained from the Indian Ocean east of the Maldives Platform. b) A stacked record of Core MD9009643 and ODP core 677 from the eastern equatorial Pacific	357
6.7 The last four terminations in different proxy records	358
6.8 A time–distance diagram showing the onset and end of glaciation at sites at increasing distance from the ice-dispersal centre	359
6.9 Different ways of defining the onset of an interglacial	360
6.10 Stratigraphic subdivision of a Quaternary sedimentary sequence and the geologic-climatic units that can be inferred	361
6.11 The Quaternary sequence in the Netherlands matched against the marine oxygen isotope record	368
6.12 Comparison of biogenic silica and diatom records from Lake Baikal with the marine oxygen isotope signal from ODP site 677	369

6.13	The sequence of loess–palaeosol units preserved at the Baoji site on the Loess Plateau, China, plotted against the marine oxygen isotope record	370
6.14	Matching of marine sediments in core ENAM93-21 from the northeast Atlantic Ocean with the GRIP $\delta^{18}\text{O}$ ice-core record using Heinrich events (H1–H5) as tie-points	371
6.15	Tentative correlations between records from the Greenland ice sheet, northern North Atlantic, Arabian Sea and Brazilian Atlantic margin	372
6.16	Comparison between colour reflectance of Cariaco Basin sediments and the GISP2 $\delta^{18}\text{O}$ record over the last glacial cycle	373
6.17	Correlation between the $\delta^{18}\text{O}$ record from Hulu Cave, China, and the $\delta^{18}\text{O}$ profile from the GISP2 Greenland ice core	374
6.18	Schematic diagram showing the principles and limitations of tuning palaeoenvironmental records from two cores	375
6.19	Synchronization of four Lateglacial and early mid-Holocene lake records from northern Germany	376
6.20	Stratigraphic framework for Quaternary marine sequences in the Mediterranean based on sapropel units, foraminiferal biozones and magnetozones	377
7.1	a) Schematic representation of coupled box model. b) Box model results simulating the 100 ka Milankovitch climatic cycle	381
7.2	Cartesian grid arrangement for a GCM	382
7.3	Comparison of GCM simulations of global temperature change since AD 1950 compared with instrumentally measured temperature variations	383
7.4	Boundary conditions for the COHMAP simulation for the last 18 ka	384
7.5	Palaeoclimatic model simulations for the last 18 ka	385
7.6	Feedback framework for the Integrated Global System Model of MIT	386
7.7	Deep Pacific records of environmental change during the past 5 Ma	390
7.8	a) Marine oxygen isotope record for the last 2.1 Ma and the spectral signal of the 41 ka and 100 ka cycles from this record. b) A measure of the strength of correlation between the stacked oxygen isotope record and Milankovitch forcing over the past 1 Ma	391
7.9	Modelled time-series of ice volume and Northern Hemisphere subarctic surface air temperatures from 1.5–0.5 Ma, encompassing the Mid-Pleistocene Transition	394
7.10	Records of deuterium (δD), dust flux and aerosols over the last 800 ka obtained from the EPICA Dome C ice core, East Antarctica, compared with sea-level changes inferred from the LR04 marine isotope record	395
7.11	Isotope time-series data for the past c. 360 ka from three East Antarctic ice-core records	396
7.12	Radiative forcing, temperature profile and the obliquity signal in the EPICA Dome C ice core over the past 800 ka	396
7.13	Milankovitch insolation record for the past 800 ka a), compared with temperature b), CO_2 c) and dust profiles d) from the EPICA Dome C ice core, Antarctica	397
7.14	Temperature anomaly record for the last 800 ka derived from the EPICA Dome C ice-core deuterium record	398
7.15	The $\delta^{18}\text{O}$ record from the NorthGRIP ice core over the last 125 ka	400
7.16	Correlation between variations in abundance of <i>N. pachyderma</i> from North Atlantic deep marine sites DSDP-609 and V23-81, and the $\delta^{18}\text{O}$ record from the GRIP Summit ice core	401
7.17	Schematic model of the main currents of the global ‘ocean conveyor’	402
7.18	Cross-section of the Atlantic Ocean basin showing thermal stratification, principal flows and surface heat exchange	402
7.19	Schematic model of three dominant types of Atlantic circulation that recurred throughout the last cold stage	403
7.20	Stable isotopic records spanning the last glacial cycle from Antarctica, aligned with the NGRIP isotopic record from Greenland	405

xxiv FIGURES AND TABLES

7.21	Synchronization of isotopic records from Antarctic and NGRIP ice cores between 10 and 52 ka using common variations in methane	406
7.22	Schematic representation of Atlantic water mass changes during DO cycles	408
7.23	Variations in concentration of terrestrial dust over the last 80 ka shown against $\delta^{18}\text{O}$ variations, a proxy for temperature fluctuations, in the NGRIP ice core	410
7.24	Terrestrial dust flux and sea-level reconstruction for the period 36–64 ka BP based on analysis of proxy records obtained from core GeoTü-KL11 in the Red Sea	411
7.25	Schematic representation of the role of dust in the earth feedback system	412
7.26	Isotopic records from Antarctica and Greenland for the Last Termination, defined here as the interval between 20 and 11.7 ka	414
7.27	Stratotype scheme for the Lateglacial–early Holocene in the North Atlantic region	415
7.28	Temperature variations in the Pacific Ocean during the Last Termination shown against ice-core CO ₂ data, ice-core temperature reconstructions and summer insolation in the Southern Hemisphere	416
7.29	a) Global temperature stack for the Last Termination based on eighty globally distributed records, compared with temperature and atmospheric CO ₂ concentration records from Antarctic ice-cores. b) Mean temperature variations for stacks of proxy records arranged in 30° latitude bands	417
7.30	Hypothesized chain of events during the Last Termination	418
7.31	Quantified palaeotemperature records for the Lateglacial and early Holocene from Scotland and Norway aligned using tephra isochrons	421
7.32	Lateglacial temperature record from Lake Suigetsu Japan, derived from a pollen-based transfer function	423
7.33	Location of the Kråkenes and Meerfelder Maar sites that contain high-resolution records of the GS-1 interval and inferred positions of the Polar Front	424
7.34	a) The end-moraine formed by a cirque glacier that blocked local drainage to create Kråkenes Lake on the western coast of Norway. b) A varved record of the YD interval which contains the Vedde Ash layer	425
7.35	Comparison of the timing of the mid-YD transitions reflected in the Kråkenes and Meerfelder Maar records	426
7.36	Temperature anomalies for the Holocene derived from seventy-three globally distributed temperature records with its 1 σ uncertainty	427
7.37	a) Visual stratigraphy of the NGRIP ice core across the Pleistocene–Holocene boundary. b) The precise location of the Pleistocene–Holocene boundary	428
7.38	a) The $\delta^{18}\text{O}$ record showing the position of the Pleistocene–Holocene boundary in the NGRIP core. b) High-resolution multiparameter record across the Pleistocene–Holocene boundary	429
7.39	Proxy records for the 8.2 ka event	430
7.40	Proxy records for the 4.2 ka event	432
7.41	Solar activity throughout the Holocene	433
7.42	Comparing historical reconstructions of near-global land temperatures ('CRUTEM4') with Callendar (1938) and Callendar (1961), using a reference period of 1880–1935	437
7.43	Atmospheric concentrations of greenhouse gases over the past 2 ka	438
7.44	Concentration of CH ₄ and CO ₂ over the last 11 ka, showing departures (increases) from the natural trace-gas trends	438
7.45	Schematic diagram showing superimposition of global climatic variations at different frequencies	441
7.46	Significant developments in human history plotted against the NGRIP climate record for the last glacial–interglacial cycle	442

TABLES

3.1	The Wentworth scale of particle size fractions and the equivalent ϕ (phi) units	97
3.2	Range of air temperature thresholds for the formation of selected periglacial features estimated by different authorities in the field	119

3.3	Classification of lakes by mode of formation	151
4.1	Estimates of the pollen production of various plant species	191
4.2	Corrosion and oxidation susceptibility of selected pollen and spores	193
5.1	Approximate $\delta^{13}\text{C}$ values for various materials	277
5.2	The effect of contamination on true age of samples selected for radiocarbon dating, a) by modern carbon, b) by inert carbon	278
5.3	Reliability of uranium-series dates for terrestrial materials due to deviations from closed system behaviour and contamination	288
5.4	Summary of characteristics and scope of nuclides used in surface exposure (CRN) dating	295
5.5	GICC05 chronology of climatic events represented in the NGRIP and GRIP ice-core records for the period <i>c.</i> 47 to <i>c.</i> 8.1 b2k (years before AD 2000)	314
5.6	Age calculations based on D/L ratios of five amino acids measured in fossil terrestrial ostracods from central and southern Spain	335
6.1	Principal descriptive criteria used in defining lithofacies in glaciogenic sequences	351
6.2	Conventional hierarchy of chronostratigraphic and geochronological units	362

This page intentionally left blank

Preface to the third edition

Looking again at the Preface to the second edition of *Reconstructing Quaternary Environments*, we get a sense of déjà vu. That book took around six years to see the light of day, and we described the gestation period as bordering on the elephantine. How therefore should we describe the time that has been spent on producing this third edition? We began work more than ten years ago, fully intending to do a ‘light touch’ revision of our 1997 text. But we should have learned our lesson. We said in 1997 that one of the principal causes of delay in delivering a final manuscript had been the enormous volume of Quaternary literature that had appeared in the previous dozen years or so. Since then, the acceleration in the rate of publication has been positively exponential, so much so in fact, that to cover the ground and digest this monumental corpus of material has almost proved to be beyond us. Having just about got away with it this time, our feeling at the moment is that we will be unlikely to take on a fourth edition!

In revising the book, we have retained the tried and tested format that we used in the earlier editions, in which we first review the various forms of evidence (geomorphological, lithological and biological) that comprise the Quaternary record, before moving on to show how we can set this evidence in the context of time (dating) and finally to consider how we can bring all of these elements together within a robust stratigraphic framework. But in Chapter 7, we have aimed for something different. In the final chapter of the second edition, we constructed a narrative of events for the last glacial–interglacial cycle in the North Atlantic region. Here we take a broader view and examine a series of themes related to patterns and causes of climate change at a range of spatial scales, and over a series of time intervals that become progressively shorter as we approach the present day. In the 1990s when the second edition of *Reconstructing Quaternary Environments* was in preparation, the Quaternary community was still coming to terms with

the implications for global palaeoceanography and palaeoclimatology of the deep-ocean marine isotope signal, and the consequent ramifications for subdividing and correlating the Quaternary record. Over the last decade or so, it has been the polar ice-core records that have taken us into new areas of Quaternary science, revealing compelling evidence of the rapidity and frequency of climate changes on millennial, centennial, decadal and, in some cases, annual timescales. In addition, like the marine isotope records before them, they offer a basis for time-stratigraphic subdivision and correlation at regional, hemispherical and global scales. When integrated with the marine records, they afford often startling new insights into the operation of the global ocean–atmosphere–cryosphere system.

A feature of Quaternary science over the past two decades or so has been the emergence of a number of multidisciplinary and interdisciplinary research groups to investigate some of these short- and long-term climatic changes. As we emphasise throughout the book, cutting-edge Quaternary research involves scientists from a range of different backgrounds, and it is now commonplace to find research collaborations in which oceanographers are involved with ice-core scientists, and isotope geochemists work hand-in-hand with palaeoecologists. And, with the rapid development and refinement of high-powered computers, a key component of these groupings is researchers from the numerical modelling community. Over the past twenty years or so, it has been our pleasure (and privilege) to coordinate two of these multidisciplinary research groups: The North Atlantic Seaboard Programme (1990–5), which was a constituent component of IGCP-253 ‘Termination of the Pleistocene’, and INTIMATE (INTegration of Ice-core, MArine, and TERrestrial Records), initially a Working Group and latterly a Focus Group of the International Union for Quaternary Research (INQUA). At the outset, the focus of INTIMATE

xxviii PREFACE TO THE THIRD EDITION

was on the North Atlantic province and specifically on events at the end of the Last Cold Stage (*c.* 8,000–15,000 years ago). More recently (2010–14), however, INTIMATE has become a research group within the European Union COST Initiative programme, with a pan-global remit and a temporal range extending back to 60,000 years ago.

Many colleagues have been active in both research groups and, while some are no longer with us (most notably Bernd Becker, Gerard Bond, Russell Coope, Sigfus Johnsen, Klaus-Felix Kaiser, Nick Shackleton and Bill Watts), happily the majority still are and, and in addition, we have brought in a steady stream of active, energetic and innovative younger scientists along the way. It would be impossible to mention all of our colleagues individually, but we would like to acknowledge the contributions of Wim Hoek, Chris

Turney, Simon Blockley and Sune Rasmussen who have followed us as the principal officers of INTIMATE, and who have taken the research group into new and exciting areas. Being involved with INTIMATE has been a stimulating experience for both of us, and has informed much of the science with which we have been involved over the past two decades. But it has also been a source of enormous pleasure, for an INTIMATE Workshop is not only about science, but it is about meeting old friends and making new ones. For all of these reasons, we would like to dedicate this book to our INTIMATE colleagues, and to INTIMATE itself – past, present and future.

John Lowe
Mike Walker

Acknowledgements

We are grateful to many friends and colleagues, as well as some new acquaintances, who have provided us with illustrative material; to our publishers (Pearson International and Routledge) for their patience and for not giving up on us; to our editorial contacts (Rufus Kurnow, Patrick Bond, Andrew Mould, Pippa Mullins, Sarah Gilkes, Lisa Salonen, and Eliza Wright) for their constant encouragement and technical advice; to our families for their continued forbearance and support while yet another book imposed on domestic routines; and most of all, to Jenny Kynaston, for her skilful adaptations of the often complex diagrams and figures, and for her undying patience. To all of you, very many thanks.

John Lowe
Mike Walker

Cover image details

The Joides Resolution trans-ocean core-drilling vessel. The Joides Resolution is a purpose-built ocean drilling vessel that can recover cores from the sea floor in water depths of up to 5,980 m. It is equipped with drilling apparatus capable of extracting cores from soft and hard sediment, as well as from rock. The core barrels employed enable single cores of 9.5 m length and 57 mm diameter to be retrieved, and sequential drilling can penetrate up to 300 m below the seabed. The vessel is used for a wide range of scientific investigations, mainly under contract to the International Ocean Drilling Program (IODP), including some of the Quaternary palaeoceanographic research described in this book. In this image the vessel is off the Osa Peninsula, Costa Rica, taking core samples for a study of earthquake and tsunami mechanisms. Photograph courtesy of Arito Sakaguchi, Yamaguchi University, Japan.

Coring in Lake Suigetsu, Japan. The photograph shows the floating drilling platform that was used in the summer of 2006 to collect a core sequence from the centre of the lake in a water depth of approximately 34 m. The coring employed a hydro-pressure, thin-walled piston sampler (diameter 7.8 cm) in four parallel bore-holes to obtain a continuous composite core (SG06) of over 73 m; this contains a palaeoenvironmental record extending back to Marine Isotope Stage 6 (*c.* 150 ka). The upper 46 m of the Lake Suigetsu sediment profile are marked by clearly-defined laminations (varves) spanning approximately the last 60 ka, and which provide a basis for calibrating the radiocarbon timescale (Chapter 5). Photograph courtesy of Takeshi Nakagawa, Ritsumeikan University, Kyoto, Japan.

The Quaternary record

1

1.1 INTRODUCTION

The **Quaternary** is the most recent major subdivision of the geological record, and it extends up to, and includes, the present day. Together with the **Neogene** and **Palaeogene** it forms the **Cenozoic**, the fourth of the great geological **eras** (Figure 1.1). The Quaternary has long been considered to be synonymous with the ‘Ice Age’ or the ‘Glacial Epoch’, a view that can be traced back to the writings of Sir Edward Forbes in 1846. One of the most distinctive features of the Quaternary has certainly been periodic glacier activity during cold periods, with the build-up of major continental ice sheets and the expansion of mountain glaciers in many parts of the world. However, these cold or **glacial** stages

were interspersed with warm episodes (**interglacials**) during which temperatures in the mid- and high-latitude regions were occasionally higher than those of the present day. During the last interglacial in Britain around 120 ka,¹ for example, hippopotamuses swam in the River Thames, while lions and elephants roamed the present site of Trafalgar Square in central London! What makes the Quaternary different, however, is not simply the occurrence of repeated warm or cold episodes, for fluctuations in global climate are apparent throughout the Cenozoic (Zachos *et al.*, 2001). Rather, it is a combination of the high amplitude and frequency of climatic oscillations, coupled with the intensity of the colder periods, that gives the Quaternary its unique character. In some parts of the world, temperatures may

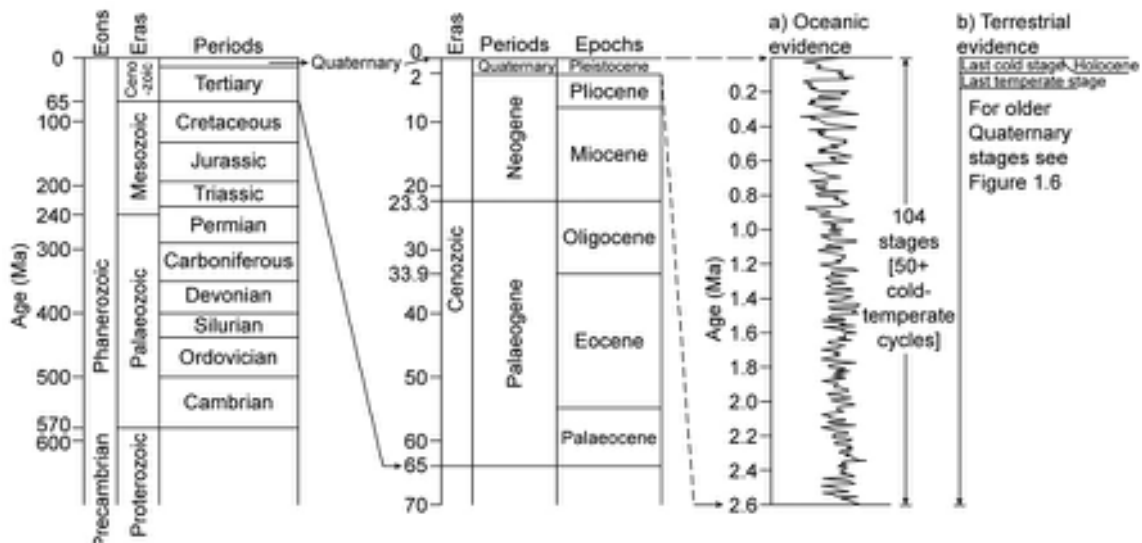


Figure 1.1 The Quaternary relative to the geological timescale. (The oxygen isotope trace (section 3.10) from deep-ocean sediments a) is after Shackleton *et al.*, 1990).

have fluctuated by more than 15°C between warm and cold episodes, temperature change was frequently rapid (measurable, in some cases, over decades), and the last 800 ka alone have witnessed ten full glacial–interglacial cycles. The deep-ocean sediment record (see section 1.6) suggests that over the course of the full range of Quaternary time, the world may have experienced more than fifty cold or glacial stages and a corresponding number of temperate or interglacial periods (Lisicki & Raymo, 2005).

The effects of these marked shifts in climate were dramatic. In the mid- and high latitudes, ice sheets and valley glaciers advanced and retreated, and the areas affected by periglacial (cold climate) processes expanded and contracted. In low-latitude regions, the desert and savannah margins shifted through several degrees of latitude as phases of aridity alternated with episodes of higher precipitation. Throughout the world, weathering rates and pedogenic processes varied with changes in temperature and precipitation, river regimes fluctuated markedly, sea levels rose and fell over a vertical range of c. 150 m, and plant and animal populations were forced to migrate and adapt in response to these environmental changes.

1.2 INTERPRETING THE QUATERNARY RECORD

The repeated climatic fluctuations that have occurred throughout this latest chapter of earth history have given rise to a highly complex record of landforms, sediments, biological (including human) remains and assemblages of human artefacts. From this legacy, it is possible to reconstruct, often with great clarity and in considerable detail, the environmental conditions and associated palaeogeography of particular intervals of Quaternary time. There are a number of separate stages in this process of palaeoenvironmental reconstruction: first, the establishment of the stratigraphy at each site in order to develop a geological framework for the investigation; second, the analysis of **proxy records**² from those stratigraphic sequences to produce the basic palaeoenvironmental information; third, the construction of a chronology of events, which involves the development of a **dating framework**; fourth, the linking of individual sequences from different locations by means of **correlation**; and finally, the integration of different lines of evidence to produce an overall palaeoenvironmental synthesis. Each one of these stages contains its own set of problems. The terrestrial stratigraphic record is often fragmented; evidence is absent from many areas, while detailed sequences are only locally preserved. Moreover, the cyclical nature of climatic

change has produced similar environmental conditions at different times and, because many records cannot be dated precisely, the process of correlation is frequently beset with difficulties. Hence, in a single exposure of Quaternary sediments, there may be much to perplex the geologist, the geomorphologist, the botanist, the zoologist or the archaeologist, and an explanation of observed geological changes will often require the combined expertise of all of these disciplines. The purpose of this book is to illustrate the very wide range of methods that are currently employed in Quaternary research, and to demonstrate that both a **multidisciplinary** and an **interdisciplinary** approach are required if a proper understanding of the complexities of the Quaternary environment is to be achieved.

1.3 THE STATUS OF THE QUATERNARY IN THE GEOLOGICAL TIMESCALE

In the terminology of the geological timescale, intervals of time that can be measured in the rock (stratigraphic) record, are referred to as **geochronological units**, and the major episodes (**eras**) are divided, respectively, into **sub-eras**, **periods**, **epochs**, **ages** and **chrons**. These are manifest in the geological record as **chronostratigraphic units**, which is the term that refers to the sequence of rocks that formed over particular time intervals; here, the hierarchy of subdivision is **erathem**, **sub-erathem**, **system**, **series** and **stage**. The distinction between geochronology on the one hand and chronostratigraphy on the other is important when the geological record is being considered, and this is discussed further in Chapter 6 (section 6.2.3.7). The Quaternary has long been considered to be a geochronological unit of **period** rank within the Cenozoic era, and to contain two separate **epochs**: the Pleistocene (originally meaning ‘most recent’), which ended around 11.7 ka, and the Holocene (‘entirely recent’), which is the present warm interval in which we live (Figure 1.2). These are represented in the stratigraphic record as the Quaternary **system** and the Pleistocene and Holocene **series**. In some quarters, there has been a tendency to regard the Holocene as simply the latest in a series of warm episodes (interglacials) forming part of a long-term climatic cycle (see below), and hence to consider this as part of the Pleistocene. However, the Holocene is now widely accepted as a separate unit because of the importance in the present interglacial of the evolution of the human environment. Indeed, it is this anthropogenic signature that is the hallmark of the Holocene, and which justifies its status as a unit of series/epoch rank within the geological timescale (Gibbard & van Kolfschoten, 2005).

Era	System	Period	Series	Epoch	Stage	Age	Age Ma	GSSP
Cenozoic	Quaternary	Pleistocene	Holocene				0.0117	←
				Upper			0.126	←
				Ionian			0.781	←
				Calabrian			1.80	←
				Gelasian			2.58	←
	Neogene	Pliocene		Piacenzian			3.600	←
				Zanclean			5.333	←
		Miocene		Messinian			7.246	←
				Tortonian			11.62	←
				Serravallian			13.82	←
				Langhian			15.97	←
				Burdigalian			20.44	←
				Aquitanian			23.03	←
		Oligocene		Chatilian			28.1	
				Rupelian			33.9	←
				Priabonian			38.0	
				Bartonian			41.3	←
				Lutetian			47.8	←
	Palaeogene	Eocene		Ypresian			56.0	←
				Thanetian			59.2	←
				Selandian			61.6	←
				Danian			66.0	←

Figure 1.2 The Cenozoic timescale, as defined in 2014. The boundary stratotypes that have been formally ratified by the International Union of Geological Sciences as global stratotype section and points (GSSPs: Section 1.4) are shown by the arrow symbols in the right-hand column. Note that some stages/ages of the Pleistocene series/epoch have yet to be formally ratified by the IUGS (after Gibbard *et al.*, 2010).

Although the term ‘Holocene’ was formally adopted by the International Geological Congress in 1885, and its lower boundary was ratified (albeit many years later) at 11.7 ka by the International Union of Geological Sciences³ (Walker *et al.*, 2009), until recently the status of the Quaternary (and also of the Pleistocene) as a geological/temporal unit remained unresolved. Indeed, the Quaternary was omitted completely from the 2004 geological

timescale (Gradstein *et al.*, 2005), despite the fact the term had been used by earth scientists for more than 150 years. However, following a protracted campaign by the Sub-commission on Quaternary Stratigraphy (SQS) and the International Union of Quaternary Research⁴ (INQUA), the body that represents Quaternary Science worldwide (e.g. Gibbard *et al.*, 2005; Bowen & Gibbard, 2007), the Quaternary was, in 2009, reinstated and recognized by the IUGS as a formal unit of system/period rank within the geological timescale (Pillans & Gibbard, 2012; Figure 1.2). Note, in passing, that the ‘Tertiary’, which formerly encompassed what are now the Palaeogene and Neogene system/periods, is no longer considered by the IUGS to be a *formal* geochronological unit, although the term continues to be used *informally* (as also is the case with ‘Precambrian’, for example), and it will be employed in this way throughout this book. Indeed, it is possible that, in due course, the Tertiary may also be reinstated along with the Quaternary as a formal period within the geological timescale (Knox *et al.*, 2012).

1.4 THE DURATION OF THE QUATERNARY

Defining the onset of the Quaternary has also been a contentious issue. For many years, it was considered that the Quaternary lasted for approximately one million years (a figure derived from extrapolations based on weathering profiles), and that it could be differentiated from the preceding Tertiary on the basis of evidence for widespread glaciation. It is now apparent, however, that many of the high-latitude regions supported glaciers long before the onset of the Quaternary. There is evidence, for example, of glacial activity during the Late Miocene (10–9 Ma) in Greenland (Lykke-Andersen, 1998) and during the Middle Miocene (16–15 Ma) in Alaska (Lagoe *et al.*, 1993), while in Antarctica the Cenozoic glacial record can be traced back to 40–35 Ma (Ingólfsson, 2004). These records of early glaciation reflect the fact that although global temperatures had oscillated, there had been a long-term high-latitude cooling that began in the Late Miocene (Maslin *et al.*, 1998). In the geological column, therefore, the Pliocene–Pleistocene (or Neogene–Quaternary) boundary cannot be drawn simply on the basis of direct terrestrial glacial evidence. Instead, the boundary has usually been located at that point in the stratigraphic record where there are the first clear indications of climatic cooling, reflected either in the fossil evidence or in some other climatic proxy.

In geology, all formal chronostratigraphic units and the boundaries between them are defined on the basis of

4 THE QUATERNARY RECORD

type/reference sections or **stratotypes**, also known as **Global Boundary Stratotype Sections and Points** or **GSSPs**, where significant changes occur in the fossil/climate record (Chapter 6). The need for an objective boundary stratotype for the base of the Quaternary (and Pleistocene) was first recognized at the International Geological Congress in London in 1948, but it was not until 1982 at the INQUA Congress in Moscow that the Vrica section in Calabria, southern Italy was formally proposed as the GSSP for the Pleistocene epoch. There the boundary was placed at the first appearance of the cold-water marine ostracod *Cytheropteron testudo*, and dated on the basis of palaeomagnetic evidence to c. 1.64 Ma (Aguirre & Pasini, 1985). Subsequent revision of the palaeomagnetic timescale using ocean-core evidence, however, suggests an older age for the Olduvai event (section 5.5.1.2), and this has been confirmed by calculations based on astronomical parameters which give a date of 1.806 Ma (Lourens *et al.*, 2005). This method, which is often referred to as **astronomical** or **orbital tuning**, employs known variations in the earth's orbit and axis (section 1.7), and is discussed more fully in Chapters 5 and 6.

Despite the fact that the Vrica section had been accepted as the internationally ratified GSSP for the Pliocene–Pleistocene boundary, there was a widespread feeling within the international Quaternary community that the boundary should be located earlier in the geological record at 2.8–2.4 Ma (Gibbard *et al.*, 2005; Head *et al.*, 2008a). This is because it was during that interval that one of the most significant transitions in the Cenozoic history of the earth occurred, notably the initiation of a pattern of glacial–interglacial cycles that have dominated global climate to the present day (Pillans, 2004). As we shall see, this major shift in the earth's climatic rhythm, centred on c. 2.6 Ma, appears to have been driven by variations in the earth's orbit and axis (section 1.6), and involved a change in pacing from 23 ka to 41 ka climatic cycles. In particular, the shape of the climate cycles, as reflected in the marine oxygen isotope ($\delta^{18}\text{O}$) records⁵ (section 3.10), becomes increasingly asymmetrical ('saw-toothed') after this time, suggesting a major change in global climate dynamics (Lisiecki & Raymo, 2007). In deep-ocean cores from the North Atlantic and North Pacific, the cooling trend that defines the onset of



Figure 1.3 The Monte San Nicola section in southern Sicily, which contains a sequence of uplifted Mediterranean marine sediments and sapropels⁶ spanning the Piacenzian, Gelasian and Calabrian. The top of the sapropelic (dark) Nicola bed marks the base of the Gelasian stage, now the boundary stratotype for the base of the Quaternary system/period and the base of the Pleistocene series/epoch (photograph by Allan Ashworth, North Dakota State University, USA).

this change in climate rhythms is marked by increased quantities of ice-rafterd detritus accompanied by significant shifts in the oxygen isotope signal, reflecting both the first major build-up of continental ice masses and major reorganizations in patterns of oceanic circulation (Kleiven *et al.*, 2002; Bartoli *et al.*, 2005). Evidence for the onset of cooling is also found in a range of continental records, particularly from mid- and high-latitude regions, including loess sediments (Ding *et al.*, 2005), pollen data (Kuhlmann *et al.*, 2006) and faunal evidence (Brugal & Croitor, 2007). However, low-latitude regions were also affected with, for example, increased regional aridity in northwest Africa between 2.8 and 2.4 Ma, and the replacement of closed canopy forest by grassland savannah (Leroy & Dupont, 1994).

The pan-global events at around 2.6 Ma therefore mark what is perhaps the most fundamental reorganization in the earth's climate system since the cooling trend associated with the glaciation of Antarctica at around 35 Ma, and appears to have been of much greater magnitude than the changes at around 1.8 Ma. This major climatic change had already been acknowledged by the geological community in the definition of a new Pliocene stage, the Gelasian (Figure 1.2), the lower boundary of which is marked by the 2.6 Ma event. The stratotype for the Gelasian is located in a section at Monte San Nicola in Sicily (Figure 1.3), and dated by orbital tuning to 2.588 Ma (Rio *et al.*, 1998; Lourens, 2008). In 2006, the SQS and INQUA formally requested the International Commission on Stratigraphy to accept the proposal that the base of the Quaternary, and also the Pleistocene, be lowered to 2.588 Ma, and that the GSSP should be that previously defined for the Gelasian stage. In other words, what had formerly been the uppermost stage of the Pliocene would now become the lowest defined stage of the Pleistocene and Quaternary, and this was accepted by the IUGS in 2009. This major reclassification of the later Cenozoic era met all of the requirements of the global Quaternary community, as well as respecting the historical precedents and established usage for the term 'Quaternary' (Gibbard *et al.*, 2010).

1.5 THE DEVELOPMENT OF QUATERNARY STUDIES

1.5.1 Historical developments

The term 'Quaternary' was first used by Giovanni Arduino in 1759 to describe the fourth stage or 'order' that he identified in the alluvial sediments of the River Po in northern Italy. It was applied in a wider context to refer to near-surface, largely unconsolidated deposits by the French

geologist Jules Desnoyers who, writing in 1829, differentiated between the strata of 'Tertiary' and 'Quaternary' age in the rocks of the Paris basin. The Quaternary was redefined by Henri Reboul in 1833 to include all strata characterized by the remains of flora and fauna whose counterparts could still be observed in the living world. The term 'Pleistocene' (most recent) was introduced by Charles Lyell some six years later to refer to all rocks and sediments in which over 70 per cent of the fossil molluscs could be recognized as living species. Only after the work of Edward Forbes in the 1840s did the term 'Pleistocene' become synonymous with the glacial period.

Quaternary studies represent one of the youngest branches of the geological sciences, with a history that goes back less than 200 years. Prior to that it was generally believed that the earth had been created in 4004 BC, a figure based on genealogical calculations from biblical sources by Archbishop James Ussher of Armagh and first published in 1658. Since early views on geological and environmental changes were constrained by the Ussher timescale of around 6,000 years, a **Catastrophist** philosophy held sway in which the form and character of the earth's surface were explained largely through the operation of great floods and other cataclysmic events. Around the turn of the eighteenth century, however, the work of the famous Edinburgh geologists James Hutton and John Playfair began to show that the features of the earth's surface could more reasonably be explained by the operation, over a protracted timescale, of processes similar to those of the present day. This significant departure in geological thinking gave rise to the principle of **Uniformitarianism**, first expounded by Hutton, but subsequently popularized by Lyell in his famous dictum 'the present is the key to the past'. Uniformitarian reasoning, in which present-day analogues are used as a basis for the interpretation of observed features within the stratigraphic record, is still fundamental to many aspects of palaeoenvironmental reconstruction (Bell & Walker, 2005).

The nineteenth century saw a number of significant advances in Quaternary studies, many of which stemmed directly from the introduction and gradual acceptance of the **Glacial Theory** (Woodward, 2014). Although for many years there had been speculation that certain Swiss and Norwegian glaciers had formerly been more extensive, it was not until the 1820s that credence was given to the notion of a glacial epoch. The work of Jens Esmark in Norway and of Albrecht Bernhardi in Germany, and particularly the investigations of the two engineers Ignaz Venetz and Jean de Charpentier in Switzerland, produced evidence for former glacier activity far beyond the limits of present-day glaciers. However, it fell to the Swiss zoologist

6 THE QUATERNARY RECORD

Louis Agassiz to expound, in 1837, the first coherent theory of ‘the great ice period’ involving worldwide climatic changes. Subsequently, Agassiz visited both Britain and North America and in both areas demonstrated that surficial deposits that had previously been interpreted as the products of marine inundation during the flood ('diluvium') could more reasonably be regarded as the results of extensive glaciation in the relatively recent past.

Although the Glacial Theory did not immediately gain widespread acceptance, its adherents rapidly refined and developed the concept. By the 1850s, evidence was beginning to emerge for two glaciations in parts of Britain and Europe and, as early as 1877, James Geikie was describing evidence for four separate glaciations in eastern England. The strata between the glacial deposits (**drift**) were referred to as ‘interglacial’, and hence the idea of oscillating warm ('interglacial') and cold ('glacial') episodes emerged. By the end of the nineteenth century, drift sheets of four separate glaciations (the Nebraskan, Kansan, Illinoian and Wisconsinan), along with deposits of three intervening interglacials (in descending order of age, the Aftonian, Yarmouthian and Sangamonian) had been identified in North America, while evidence began to emerge for multiple glaciations in different parts of Europe. Probably the most influential work in this respect, however, was that of Albrecht Penck and Eduard Brückner who, in the early years of the twentieth century, resolved the river terrace sequences in the valleys of the northern Alps into four separate series, each relating to a glacial episode. The phases of glaciation were named (from oldest to youngest) Günz, Mindel, Riss and Würm, after major rivers of southern Germany. In both Europe and North America, the maximum limits of Quaternary glaciations were first mapped around the turn of the twentieth century and have subsequently been modified only in detail (Figure 1.4; Hughes *et al.*, 2013), although views on the terminology adopted and on the number of glacial/interglacial episodes that occurred during the Quaternary have changed dramatically (see sections 1.3 and 1.6).

Other effects of glacier expansion and contraction were also recognized at a relatively early stage. The relationship between glaciers and sea level was first considered in a systematic manner by Charles MacLaren who, in 1841, reasoned that at times of glacier build-up, sea levels would fall as water was extracted from the ocean basins and locked up in the expanding ice sheets whereas, following ice melting, sea levels would rise as water was returned to the oceans. This was the first statement of the **Glacio-Eustatic Theory** of sea-level change (section 2.5.2). MacLaren suggested that sea levels would fall by 350–400 ft (c. 110–130 m) during a glacial phase, a figure that is in



Figure 1.4 The maximum glaciation of the Northern Hemisphere during the Quaternary (after Ehlers & Gibbard, 2007). (Mountain High Maps® copyright © 1993 Digital Wisdom.)

remarkably close agreement with more recent estimates. In addition to its effects on global sea levels, the results of the build-up of ice on the earth's surface were also noted. A number of geologists, including John Playfair and Charles Lyell, had described the raised shoreline sequences in Scandinavia and around the coasts of Scotland, and had inferred that in both regions crustal uplift had occurred. The mechanism involved in crustal warping, however, remained unclear. In 1865, the Scottish geologist Thomas Jamieson finally made the link between the raised shoreline evidence and the Glacial Theory when he deduced that crustal depression would result from the weight of the ice sheets and that uplift would follow deglaciation as the crust was free to rebound to its pre-glacial state. This was the first clear statement of what are now referred to as **glacio-isostatic effects** (section 2.5.4).

During the later years of the nineteenth century, evidence began to emerge for major environmental changes in areas beyond those directly affected by glacier ice. In the semi-arid southwest of the United States, for example, work by Israel Russell and Grove Karl Gilbert in particular showed that extensive lakes had existed at some time in the past, and that phases of higher rainfall (**pluvial**) had alternated with more arid (**interpluvial**) episodes. Moreover, a relationship was postulated (although not clearly

articulated) between these climatic oscillations and the glacials and interglacials at higher latitudes. Similar relict drainage features in desert and savannah regions in other parts of the world were described by Victorian explorers and provided further indications of climatic changes in the low latitudes. In the mid-latitude zones, on the other hand, it was gradually recognized that phases of glacier expansion would be accompanied by an extension of the tundra belt where cold-climate (albeit non-glacial) processes predominated. The term **periglacial** was first used to describe such regions by the Polish geomorphologist Walery von Lozinski in 1909.

Biological evidence for Quaternary environmental change also began to emerge soon after the introduction of the Glacial Theory in the middle years of the nineteenth century. The publications of Edward Forbes, in which various geographical components of the British flora and fauna were related to successive migrations into the British Isles under different climatic conditions, and of Oswald Heer wherein ecological changes in Switzerland were discussed in the context of Quaternary climatic changes, were particularly important milestones. In the later years of the nineteenth century, research by the Scandinavian botanists Axel Blytt and Rutger Sernander demonstrated the wealth of information on climatic and vegetational change that could be derived from the stratigraphy and macrofossil content of peat bogs (section 3.9). The scheme of postglacial climatic changes constructed by Blytt and Sernander from Scandinavian peat bog records was subsequently refined by the results of pollen analysis, a technique developed in Sweden by Lennart von Post and which is still one of the most widely used methods in palaeoecology (section 4.2). Systematic investigations of other forms of biological evidence also began during the last century. Important contributions in vertebrate palaeontology included the work of Richard Owen, who produced the first comprehensive volume on British fossil mammals and birds, and of his contemporary, William Buckland, who not only carried out some of the earliest detailed investigations and analyses of vertebrate assemblages in cave sites, but was one of the first British converts to the Glacial Theory. As early as 1838, James Smith ('Smith of Jordanhill') was using fossil shells to demonstrate that the seas around the coast of western Scotland had been much colder in the past, thereby laying the foundation for subsequent utilization of marine Mollusca as indicators of former marine temperatures (section 4.7). The seminal works of Alfred Kennard, often in association with Bernard Woodward, in the later part of the nineteenth and early years of the twentieth century provided a similar groundwork for the analysis of land and freshwater Mollusca (section 4.6).

1.5.2 Recent developments

The last fifty years have seen many important developments in Quaternary studies, but five in particular merit attention. The first is the methodological advances that have been made in, and the widespread application of, a range of field and laboratory techniques. Increasingly sophisticated methods of sedimentological analysis have offered new insights into the nature of Quaternary depositional environments, while the interpretation of Quaternary stratigraphy has been greatly assisted by the development of equipment for coring terrestrial, offshore and deep-ocean sequences. Analysis of both terrestrial and marine evidence has been significantly improved by the use of a range of remote sensing techniques, including airborne sensors (e.g. conventional cameras, satellite-mounted imaging systems and radar); ground-based or ship-towed sonar, radar and seismic systems; and tracer methods for the analysis of lacustrine and marine processes. Particular progress has been made in the mapping, often at very high resolution, of sea-bed topography and marine sediment architecture through the use of high-resolution sonar and seismic devices. Palaeoecological investigations have also benefited from a range of technological advances, notably in the extraction, recording and analysis of fossil assemblages, and in the fields of both light and electron microscopy. These various techniques are considered in more detail in Chapters 2–4.

The second major development has been in the dating of Quaternary events. In the nineteenth century, notions of time were founded largely on estimates of rates of operation of geological and geomorphological processes. Hence, estimated rates of delta construction, cliff retreat, stream dissection, weathering rates and degree of soil development were all used to assess the duration of Quaternary episodes. The first, and for many years the only, quantitative method for estimating the passage of time was varve chronology developed around the turn of the century by the Swedish geologist Gerard de Geer (section 5.4.2). A major breakthrough came in the years immediately following the Second World War with the discovery, by Willard Libby, of the technique of radiocarbon dating. Other radiometric methods, notably potassium/argon and uranium-series (U-series) dating, were developed in the 1950s and 1960s, along with the techniques of dendrochronology (tree-ring dating) and palaeomagnetism. The 1970s and 1980s saw the refinement of these various methods and a general increase in levels of chronological precision, particularly as a consequence of the introduction of mass spectrometry into radiometric dating. In addition, new techniques have been developed, including aminostratigraphy, fission-track dating, electron spin resonance,

luminescence dating, and the use of long-lived cosmogenic radioisotopes such as ^{10}Be and ^{36}Cl (Walker, 2005). Recent research on ancient DNA involving, in particular, the timing of genetic mutations ('molecular clock analysis': Bromham & Penny, 2003) offers an exciting and potentially valuable addition to the Quaternary dating portfolio. The principles and applications of the range of dating methods now available to the Quaternary scientist are discussed in Chapter 5.

The third important development in Quaternary studies during the second half of the twentieth century has been the stratigraphic investigation of sedimentary sequences on the deep-ocean floors. Indeed, it would not be overstating the case to suggest that the results of research into ocean sediments have revolutionized our view of the Quaternary (Imbrie & Imbrie, 1979). In one sense, trying to reconstruct environmental changes from terrestrial evidence is like trying to assemble a jigsaw puzzle and then make sense of the picture when more than 90 per cent of the pieces are missing. This is because much of the evidence has been removed by subaerial weathering and erosional processes and, in mid- and high latitudes, by glacial erosion. In parts of the deep oceans of the world, however, sediments have been accumulating in a relatively undisturbed manner for thousands, or even millions, of years, and therefore frequently span the entire range of Quaternary time.

Although the investigation of deep-sea sediments actually began in the nineteenth century with the voyage of the British government research vessel HMS *Challenger* in 1872, it was not until the 1930s that the German palaeontologist Wolfgang Schott began the first detailed work on the fossil content of core samples from the ocean. Prior to the Second World War, only short sediment cores (less than 1 m in length) could be raised from the sea bed. The development of a piston corer by the Swedish oceanographer Börje Kullenberg heralded the modern phase of deep-sea research, for with the Kullenberg corer and specially equipped research ships, it became possible to take undisturbed sediment cores of more than 10 m in length. The changing fossil content of these cores has provided a remarkable record of changes in ocean water temperatures and, by implication, in global atmospheric temperatures during the course of the Quaternary (section 4.10). Many fossils, however, contain other indices of environmental change, most notably variations in oxygen isotope content. Pioneered by Cesare Emiliani, oxygen isotope analysis is now regarded as one of the most powerful tools in Quaternary stratigraphy and palaeoenvironmental reconstruction (section 3.10), and continuous isotopic records are now available extending back into the Pliocene (e.g. Lisiecki & Raymo, 2005).

A fourth major development over recent decades has been the coring of polar ice sheets and glaciers. Ice-core drilling began on the Greenland ice sheet in the late 1950s, and was followed in the 1960s by the drilling of the first deep polar ice core to bedrock at Camp Century, Greenland (Dansgaard *et al.*, 1969). Subsequently, long continuous cores have been recovered from other sites in Greenland, from Antarctica, and from other polar ice caps and mountain glaciers. The ice layers revealed in the cores represent annual increments of frozen precipitation, and contain a range of proxy indicators (oxygen isotopes, trace gases, chemical compounds, particulate matter) of past atmospheric and climatic conditions. Ice-core data not only provide a temporal framework for Late Quaternary climatic change (section 3.11), but the upper levels of the ice cores also record the effects of recent industrial activity. The most recent phase of this research has involved the drilling to bedrock of cores near the thickest part (3 km) of the Greenland ice sheet by the European Greenland Ice-core Project (GRIP, NGRIP), the American Greenland Ice Sheet Project (GISP2) and the European North Greenland Eemian Project (NEEM). The data have provided startling evidence not only of the magnitude of climatic change over the last interglacial–glacial cycle (Hammer *et al.*, 1997; North Greenland Ice Core Project Members, 2004), but also of the extraordinary rapidity of climate change (Steffensen *et al.*, 2008). Perhaps even more impressive, given the remote location, has been the deep drilling of the Antarctic ice sheet where the Vostok core has produced a record of climate and atmospheric history for the last four glacial cycles (Petit *et al.*, 1999), while the European Project for Ice Coring in Antarctica (EPICA) at Concordia Station, Dome C, has generated a palaeoclimatic record extending back over 800 ka (EPICA Community Members, 2004; Fischer *et al.*, 2010a).

The fifth significant advance in Quaternary science, particularly during the second half of the twentieth century, has been in the development of increasingly sophisticated computer-based models which simulate a range of aspects of Quaternary environments. This type of work began in the late 1960s with the development of **general circulation models (GCMs)**, numerical models that were initially designed to reconstruct patterns of atmospheric circulation during the last cold stage, and possible linkages between terrestrial and atmospheric environments (section 7.2). A range of increasingly sophisticated models has since been developed to explore, in addition to atmospheric circulation, such diverse phenomena as ice sheet behaviour (Siegent & Dowdeswell, 2004), glacio-isostatic effects (Peltier, 2002), oceanographical changes (Weber *et al.*, 2007), past vegetation dynamics (Claussen, 2009) and

human migrations (Mithen & Reed, 2002). Some of the most impressive results have been achieved, however, where scientists from a range of disciplines have collaborated to integrate data on Quaternary environmental change from a variety of different sources, and to use those data as a basis for both descriptive and predictive modelling of Quaternary environments and environmental change. Such an approach is typified by the Climate/Long Range Investigation Mapping and Prediction (CLIMAP) group (CLIMAP Project Members, 1976, 1981) and by the Co-operative Holocene Mapping Project (COHMAP) programme (COHMAP Members, 1988; Wright *et al.*, 1993). These interdisciplinary and multidisciplinary projects are considered in more detail in section 4.10.7.

1.6 THE FRAMEWORK OF THE QUATERNARY

The conventional subdivision of the Quaternary is into **glacial** and **interglacial** stages, with further subdivision into **stadial** and **interstadial** episodes. Glacial stages have traditionally been regarded as protracted cold phases when the major expansions of ice sheets and glaciers took place, whereas stadials have been viewed as shorter cold episodes during which local ice advances occurred. Interglacials are usually recognized as warm intervals when temperatures at the thermal maximum were as high as, or even higher than, those experienced during the Holocene, and which were characterized in the mid-latitudes by the development of mixed woodland. Interstadials, by contrast, are traditionally regarded as relatively short-lived periods of thermal improvement during a glacial phase, when temperatures did not reach those of the present day and, in lowland mid-latitude regions, the climax vegetation was boreal woodland.

These terms are still widely used in Quaternary science, although they clearly lack precision and, as a consequence, are often difficult to apply. Take, for example, the problem of recognizing an interglacial as opposed to an interstadial episode on the basis of degree of vegetation development. In northwest Europe, both the interglacials and interstadials of the Late Quaternary were characterized by a range of vegetation types (mixed woodland, boreal woodland, open grassland) depending on latitude, altitude, duration of the warm stage, etc. In more northerly regions, the ‘vegetational signature’ of an interglacial might be boreal woodland; further south, this type of forest development would be more indicative of an interstadial. Hence, the palaeobotanical distinction between ‘interglacial’ and ‘interstadial’ becomes blurred by geographical province. Moreover, this terminology may even be misleading. In the British Isles,

for instance, there is only fragmentary evidence for glacier activity during the early Quaternary cold stages (Lee *et al.*, 2011), and, indeed, this is also the case for many other parts of the world (Ehlers *et al.*, 2011a). It is also apparent that during the last cold stage, Southern Hemisphere ice contributed less than 3 per cent to the overall increase in global ice volume, prompting the observation that ‘the growth of ice in the Quaternary was essentially a Northern Hemisphere phenomenon’ (Williams *et al.*, 1998). The term ‘glacial’ therefore may have a different connotation in the two hemispheres.

Because of these difficulties, the terms ‘temperate stage’ and ‘cold stage’ might be considered more appropriate to describe the major climatic episodes of the Quaternary. However, these terms contain their own sets of problems (defining acceptable thresholds between ‘warm’ and ‘cold’ episodes; quantifying climatic change; conflicting proxy records for former climate; etc.) and, as a consequence, are equally arbitrary. Moreover, for historical reasons, it is not always possible to avoid the traditional terminology when referring to certain named Quaternary stages. For convenience, therefore, we have opted for the lesser of the evils and have retained the terms ‘glacial’ and ‘interglacial’ but, where appropriate, have used these interchangeably with ‘cold’ and ‘temperate’ stages. This type of categorization, based on inferred climatic characteristics, is known as **climatostratigraphy**, and is considered further in Chapter 6.

Attempts to subdivide the stratigraphic record from the land areas of the Northern Hemisphere into a coherent scheme of glacial and interglacial stages that has regional or inter-regional application have hitherto proved to be extremely difficult, principally because of the fragmented nature of most terrestrial sedimentary sequences. Over the past two decades, therefore, reference has increasingly been made to the relatively undisturbed sedimentary sequence in the deep ocean, and particularly to the **oxygen isotope record** in the marine microfossils contained within those sediments. As will be shown in Chapter 3, the oxygen isotope trace (or ‘signal’) obtained from these microfossils reflects the changing isotopic composition of ocean waters over time. Insofar as the marine oxygen isotope balance is largely controlled by fluctuations in volume of land ice (section 3.10), variations in the isotopic signal in fossils from deep-ocean sediment profiles can be read as a record of glacial/interglacial fluctuations (Figure 1.5). Working from the top of the sequence, each **isotopic stage** has been assigned a number, with even numbers denoting ‘glacial’ (cold) episodes while the ‘interglacial’ (warmer) phases are denoted by odd numbers. One of the most impressive features of the deep-sea **MIS (marine isotope stage)** record

10 THE QUATERNARY RECORD

is that the isotopic signal is geographically consistent, and can be replicated in cores taken from different parts of the world's oceans. Hence, the marine oxygen isotope sequence provides a climatic signal of global significance.

Twenty-two isotopic stages can be recognized in the past 880 ka or so (Lisiecki & Raymo, 2005), indicating that around ten or eleven glacials and a similar number of interglacials (or near-interglacials) occurred during that time period, and the total number of isotopic stages formally identified in the deep-ocean record of the past 2.5 Ma now exceeds 100. In the Monte San Nicola type section (Figure 1.3), for example, the base of the Gelasian stage which marks the Pliocene–Quaternary boundary corresponds to MIS stage 103 (Gibbard *et al.*, 2010). This means that over the course of the Quaternary more than fifty cold/temperate cycles have occurred, which is many more temperate and cold stages than have been formally recognized and named on the basis of the terrestrial evidence. Hence, the deep-sea sequence provides an independent, continuous and unique climatostratigraphic template against which the often fragmented terrestrial sequences can be compared (Figure 1.6). Correlations

between the marine isotope record and terrestrial sequences are discussed more fully in Chapter 6.

The most complete system of designated glacial and interglacial episodes is that for northern Europe, the British Isles and European Russia, with a less detailed formal scheme for North America (Figure 1.6). There is general agreement that the **Flandrian** of the British sequence can be equated with the **Holocene** of the European and North American sequences, and that the last cold stage identified in Britain (**Devensian**), northern Europe (**Weichselian**), the Alpine region of Europe (**Würmian**) and North America (**Wisconsinan**) can be considered as broad correlatives. The **Ipswichian**, **Eemian**, **Riss–Würmian** and **Sangamonian** ‘temperate’ records from each of these regions are also believed to be essentially coeval and are assigned to the last interglacial, despite the fact that identification is often based on quite different types of proxy evidence. In Europe, a number of *stadials* and *interstadials* are evident in stratigraphic records from areas that lay beyond the limits of the Weichselian ice sheets.

Throughout northern Europe there is a broad measure of agreement over the brief climatic oscillation that

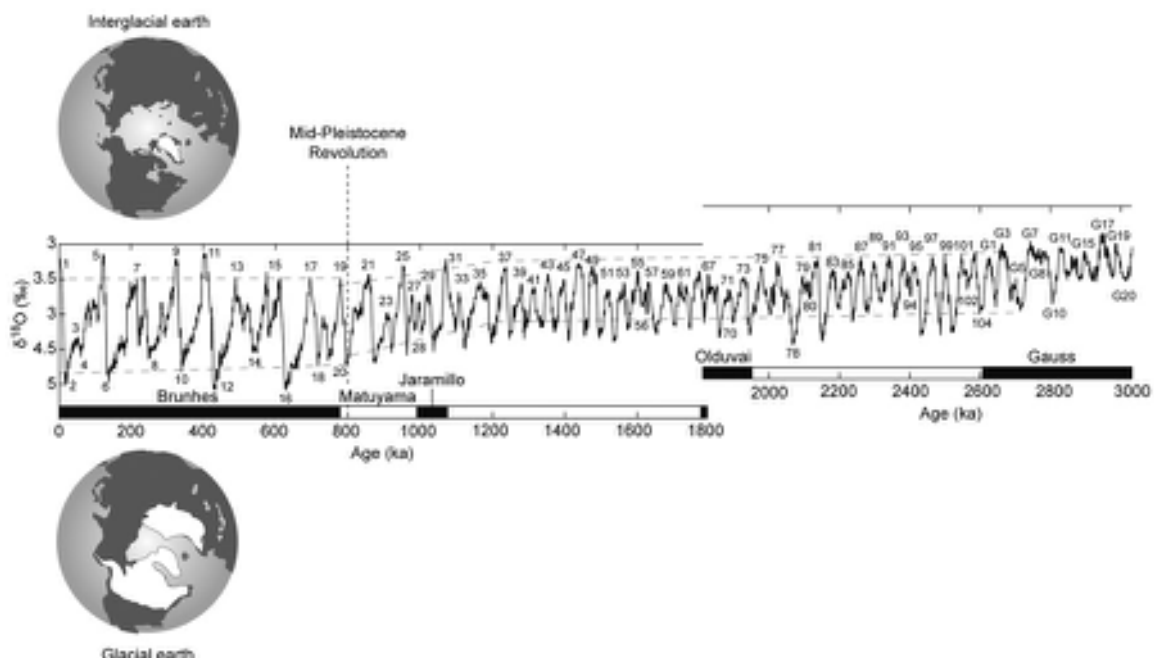


Figure 1.5 Climatic trends during the past 3 Ma reflected in a stacked (composite) oxygen isotope record (after Lisiecki & Raymo, 2005). The isotopic trace can be read as a proxy climate record with ‘peaks’ marking warmer (interglacial) intervals and ‘troughs’ colder (glacial) episodes (section 3.10). The astronomically driven millennial-scale climatic oscillations are present throughout, but their frequency and amplitude changes over time, and especially after the Mid-Pleistocene Revolution (MPR: sections 1.7 and 7.3) at c. 800 ka when climatic extremes increased and Northern Hemisphere ice sheets reached their greatest extents.



Figure 1.6 The MIS record based on a composite of deep-ocean cores (V19-30, ODP-677 and ODP-846) (left) and the Quaternary stratigraphy of the Northern Hemisphere set against this record (right). The marine isotope signal shows the oxygen isotope stages back to 2.6 Ma. In the correlation table, temperate (interglacial) stages are shown in upper case, while cold (glacial) stages are in lower case. Complexes which include both temperate and cold stages are in italics (based on Cohen & Gibbard, 2011).

occurred towards the close of the last cold stage (termed the **Devensian Lateglacial** in Britain and the **Weichselian Lateglacial** in northern Europe), for this period can be more precisely dated than older parts of the sequence. However, opinions differ over the extent to which the 'Lateglacial' can be subdivided; in Britain, most scientists accept a twofold division into a **Lateglacial** (or **Windermere**) **Interstadial** and a **Loch Lomond Stadial**, whereas a more complex sequence with two interstadial episodes, **Bølling** and **Allerød**, separated by a brief cold episode (**Older Dryas**) and followed by the **Younger Dryas Stadial** has been recognized in records from the European mainland (Figure 1.7). A climatic oscillation that appears to be the correlative

of the Younger Dryas cold episode has been identified in eastern North America, and also in Arctic Alaska (Elias, 2007b). An alternative stratigraphic scheme for the Lateglacial, based on the oxygen isotope signal in the GRIP Greenland ice core, has two cold events, **Greenland Stadial 2 (GS-2)** and **Greenland Stadial 1 (GS-1)**, the latter broadly correlating with the Younger Dryas; and an intervening warmer episode, **Greenland Interstadial 1 (GI-1)**, which equates with the Lateglacial Interstadial. Two short-lived colder episodes (GI-1b and GI-1d) are apparent during Greenland Interstadial 1 (Björck *et al.*, 1998; Walker *et al.*, 1999). The Lateglacial record is considered further in section 7.5.5.

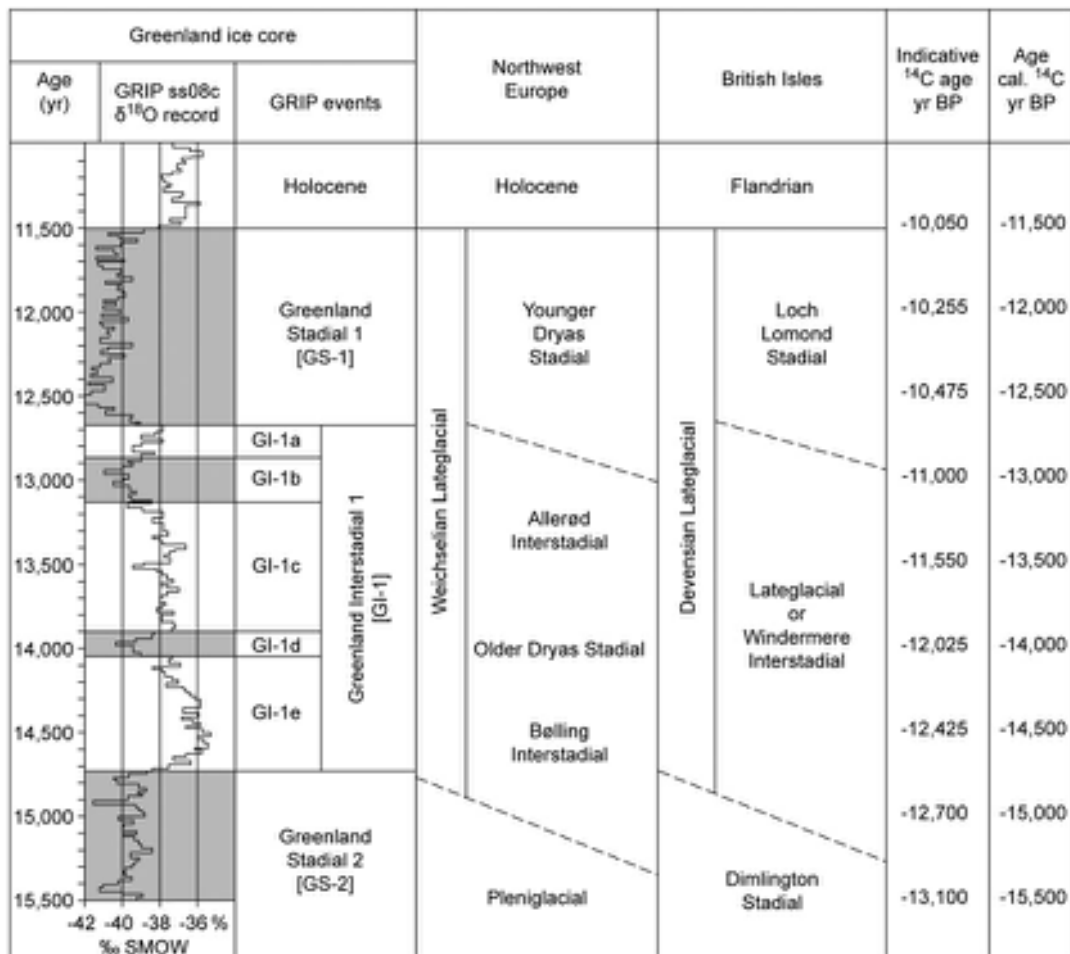


Figure 1.7 The $\delta^{18}\text{O}$ record from the GRIP Greenland ice core showing the Lateglacial event stratigraphy (left) and the stratigraphic subdivision of the Lateglacial in northwest Europe and the British Isles. The isotopic record is based on the GRIP ss08c ice-core chronology, and the colder stadial episodes are indicated by dark shading. The radiocarbon timescales (right) are shown as 'indicative' (or 'average') radiocarbon (^{14}C) ages and their 'calibrated' (cal.) equivalents (partly after Lowe *et al.*, 2001).

Prior to the last interglacial, however, the Quaternary records are much more difficult to resolve and, although inter-regional correlations have been attempted (Figure 1.6), these are frequently speculative, and become increasingly so as the age of the depositional record increases. In the European Alpine area, the sequence of glacial sediments and 'interglacial' soils now appears to be far more complicated than in the classical Alpine model, and hence the standard nomenclature of Günz, Mindel and Riss glacials can be used only in a very general sense. Similarly in North America, the terms 'Kansan' and 'Nebraskan' glacial periods and 'Yarmouthian' and 'Aftonian' interglacials have been largely abandoned in favour of a series of stages prior to the Illinoian Glacial that are designated simply by letter. In Britain and northern Europe, it is now generally accepted that several of the established named stages must contain a number of separate episodes of cold or temperate character (Figure 1.6). Hence, the Cromerian Complex in the Netherlands is believed to encompass four warm (interglacial?) episodes, while in Britain at least five interglacial episodes may be represented in the 'Cromerian' of the Middle Pleistocene (Preece & Parfitt, 2012). In northern Continental Europe, two or maybe three glacial events may have occurred during the classical Saalian Glacial (Ehlers *et al.*, 2011b). A further problem concerns gaps in the terrestrial stratigraphic records. Comparison between the Dutch and British Early and Middle Pleistocene sequences, for example, suggests that as much as a million years of sedimentary history may be missing from the stratigraphic record in southeastern England between the Pastonian and Cromerian (Gibbard *et al.*, 1991), with other major hiatuses elsewhere (Figure 1.6). Overall, therefore, the individual stages and suggested correlations between those stages shown in Figure 1.6 must be regarded as no more than a provisional approximation of the Quaternary climastratigraphic sequence in Europe and North America.

1.7 THE CAUSES OF CLIMATIC CHANGE

It is now apparent that the climatic fluctuations of the past 2.5 Ma or so have followed a series of distinctive patterns, and hence contemporary explanations of long-term climatic change have tended to focus on the factors that have given rise to both the regularity and frequency of climatic fluctuations. The hypothesis that has attracted the greatest attention is undoubtedly the **Astronomical Theory**, developed by James Croll a little over 100 years ago and subsequently elaborated by the Serbian geophysicist

Milutin Milankovitch. The theory is based on the assumption that surface temperatures of the earth would vary in response to regular and predictable changes in the earth's orbit and axis. Due to planetary gravitational influences, the shape of the earth's orbit is known to change from almost circular to elliptical and back again (Figure 1.8a), a process referred to as the **eccentricity of the orbit**. The timing varies between 95 and 136 ka, although this is generally referred to as the 100 ka eccentricity cycle. Over a longer time-scale, however, a 413 ka eccentricity cycle is also apparent. In addition, the tilt of the earth's axis varies from $21^{\circ}39'$ to $24^{\circ}36'$ and back over the space of c. 41 ka (Figure 1.8b). Because the angle of tilt is measured relative to an imaginary line representing the plane of the ecliptic (the plane described by the earth's elliptical path around the sun), this phenomenon is known as the **obliquity of the ecliptic**. The third variable arises because the gravitational pull exerted by the sun and the moon causes the earth to wobble on its axis like a top (Figure 1.8c). The consequence of this is that the seasons (or the equinoxes) seem to move around the sun in a regular fashion, hence the term **precession of the equinoxes** or **precession of the solstices**. In effect this means that the season during which the earth is nearest to the sun (**perihelion**) varies. At present, the Northern Hemisphere winter occurs in perihelion (Figure 1.8c-i) while the summer occurs at the furthest point on the orbit (aphelion). In c. 10.5 ka time, the position will be reversed (Figure 1.8c-iii), while c. 21 ka hence the cycle will be complete. In fact, it now appears that there are two separate interlocked cycles, a major one averaging around 23 ka and a minor one at c. 19 ka.

These variables, in combination, exert a profound effect on global temperatures. The total amount of radiation received is determined largely by the eccentricity of the earth's orbit, while the other astronomical variables affect the way in which that heat energy is distributed at different latitudes. In general it seems that solar radiation receipt in the low- and middle-latitude regions is governed mainly by precession and eccentricity variations, while in higher latitudes the obliquity cycle predominates. Patterns of change through time can be calculated from astronomical data (Figure 1.9a), and Milankovitch was therefore able to obtain estimates for radiation inputs at different latitudes, and from these to reconstruct long-term temperature changes.

The theory was first published in 1924 and initially found favour with many European geologists, for the sequence of warm and cold stages predicted by the radiation curves appeared to match the record of glacials and interglacials in the classical Alpine region of Penck and Brückner. Increasingly, however, it became apparent

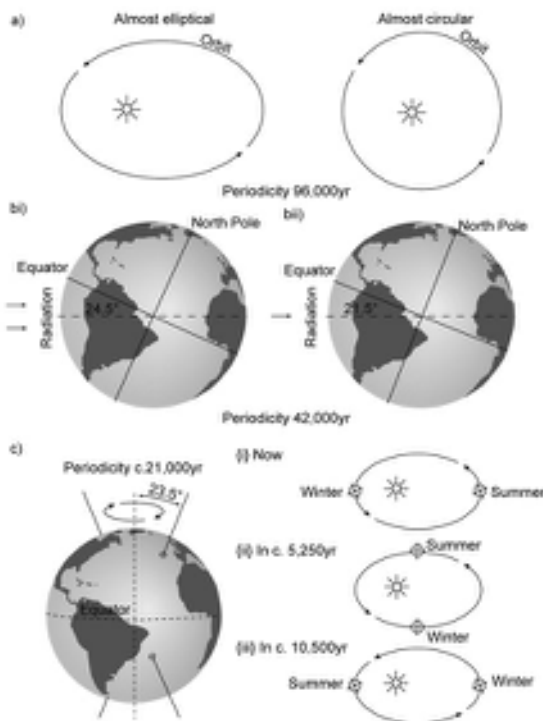


Figure 1.8 The components of the Astronomical Theory of climate change: a) eccentricity of the orbit; b) obliquity of the ecliptic; c) precession of the equinoxes.

that the timing and frequency of glacial episodes during the Late Quaternary did not seem to accord with the pattern of climatic changes predicted by the astronomical variables. This was thrown into sharp relief in the 1940s and 1950s with the development of radiocarbon dating which provided, for the first time, an independent chronology for the Late Quaternary glacial sequence. By the mid-1950s, the Milankovitch hypothesis as an explanation of climatic change had been almost universally rejected. Writing in 1957, for example, Richard Foster Flint discussed ‘geometric variation in elements of the earth’s orbit’ as a factor in global climate change, but concluded that ‘the geometric scheme of distribution of insolation heating must be considered inadequate in itself to explain the Pleistocene climatic changes’. He accepted that ‘geometric factors are present’ and ‘must have influenced climate to some degree’, but ‘opinions differ as to how closely the insolation curve matches the Pleistocene record. Presumably the geometric factors are superposed on some other cause of climatic fluctuation’ (Flint, 1957, p. 509).

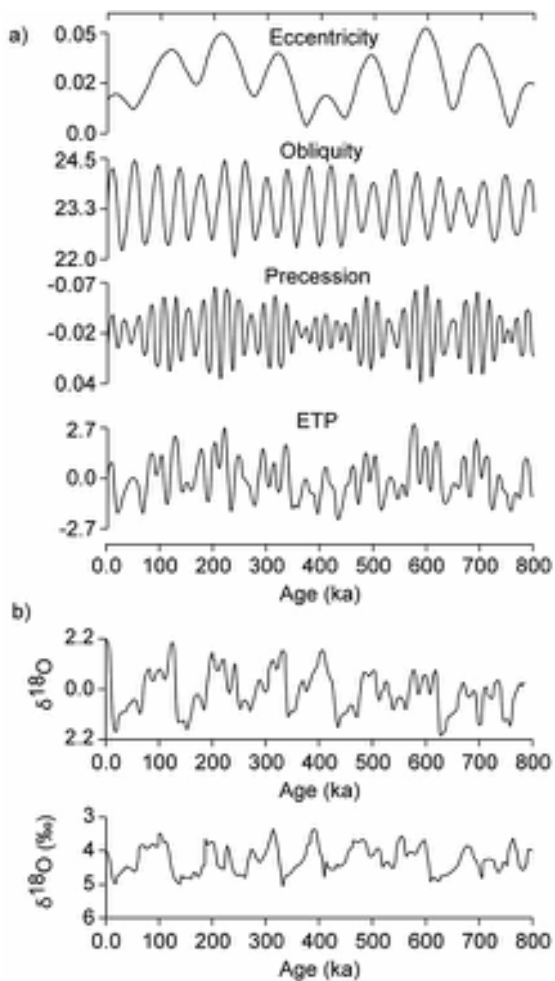


Figure 1.9 a) Variations in eccentricity, obliquity and the precessional index over the past 800 ka. The three time series have been normalized and added to form the composite eccentricity-tilt-precession curve (ETP). The scale for obliquity is in degrees and for the ETP is in standard deviation units. b) Normalized and smoothed variations in the oxygen isotope signal ($\delta^{18}\text{O}$) in five deep-sea cores. Note the similarity between this record and the ETP curve above (after Imbrie *et al.*, 1984).

In the late 1960s and early 1970s, however, work initially on sea-level changes and subsequently on deep-ocean sediments reawakened interest in the Milankovitch hypothesis (Imbrie & Imbrie, 1979). The first clue came from the dating of coral reefs around the island of Barbados, which showed high sea-level stands (reflecting warmer episodes) at around 82 ka, 105 ka and 125 ka, which coincide closely with the phasing of the precessional

cycle (Mesolella *et al.*, 1969). More significant, however, were oxygen isotope variations found in marine micro-fossils which provided a long-term proxy record of environmental and climatic change (section 3.10; Figure 1.9b). Spectral analysis⁷ of ocean-core sequences revealed evidence of cycles of 100 ka, 43 ka, 24 ka and 19 ka in the isotopic signal, with the longest cycle driving the glacial/interglacial oscillations of the past 700 ka or so while the others, in combination, modulate or amplify the effects of longer-term changes (Hays *et al.*, 1976). These data provided the first unequivocal evidence of the Milankovitch cycles in the recent geological record, and were an impressive demonstration of the potential role of the astronomical variables in determining patterns of long-term climatic change – hence the title of the seminal paper of Hays *et al.* (1976), ‘Variations in the earth’s orbit: pacemaker of the Ice Ages’. Subsequently, Milankovitch cycles have been detected in a wide range of proxy records including ice cores (Petit *et al.*, 1999), lake sediments (Trauth *et al.*, 2001), loess sequences (Sun *et al.*, 2006b) and pollen records (Torres *et al.*, 2013). Collectively these data confirm the hypothesis that changes in the earth’s orbit and axis, what is often referred to as **orbital forcing**, are the primary driving mechanisms in Quaternary climatic change (Imbrie *et al.*, 1993).

Although the Astronomical Theory offers a basis for understanding the sequence of major Quaternary climatic oscillations, it is now apparent that factors other than orbital forcing have influenced the course of global climatic change. Furthermore, a number of outstanding problems relating to the Astronomical Theory still need to be resolved. For example, although the onset of Northern Hemisphere glaciation, as reflected in the build-up of large ice sheets in North America and Europe, dates from around 2.7 Ma (Haug *et al.*, 2005), proxy data from deep-ocean cores suggest that global climate had cooled, albeit in an oscillatory manner, from around 3.6 Ma (Mudelsee & Raymo, 2005). In addition, the climatic cycles of the Quaternary have not been constant, but have shifted from a periodicity of around 41 ka prior to 900–800 ka to a prevailing rhythm of c. 100 ka over the course of the last c. 800 ka, a phenomenon often referred to as the **Middle Pleistocene Revolution** (Maslin & Ridgwell, 2005) or the **Middle Pleistocene Transition (MPT)**. This, in turn, was accompanied by an apparent intensification of glaciation, with the growth of Northern Hemisphere ice sheets to volumes very much larger than those attained over the course of the previous 1.7–1.6 Ma. Neither the onset of Northern Hemisphere glaciation at around 2.7 Ma, nor the shift in climatic phasing around the MPT, can be accounted for solely by Milankovitch forcing, which suggests that some

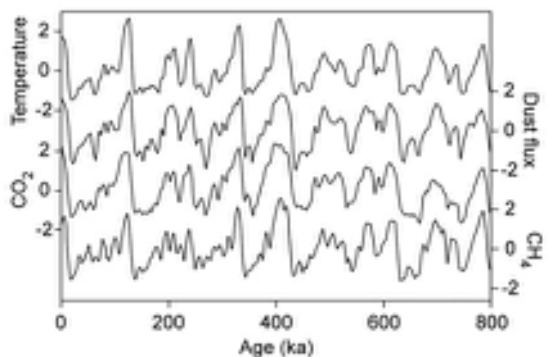


Figure 1.10 Variations in temperature, dust flux, CO₂ and CH₄ from the EPICA Dome C ice-core record, Antarctica, over the last 800 ka (based on Masson-Delmotte *et al.*, 2010).

change (or changes) internal to the global climate system must have been responsible (see section 7.3).

The major elements in the climatic equation that serve to modulate or amplify the effects of the astronomical variables appear to be changes in the disposition of the continental land masses, tectonic activity, feedback mechanisms caused by oceanic circulation and changes in the extent of continental ice cover (Denton, 2000). A further influential factor may have been variations in the constituents of the atmosphere including, for example, aeolian dust (Rea *et al.*, 1998) and particularly atmospheric trace gases such as CO₂ and methane (CH₄) (Ruddiman 2003a, 2006; Figure 1.10). Although the long-term cooling trend during the late Pliocene has been attributed, in part, to the influence of obliquity minima between 3.2 and 2.5 Ma (Maslin *et al.*, 1998), other factors may have contributed to the cooling and to the onset of continental glaciation. A necessary precursor was the closing of the Isthmus of Panama which was completed around 2.75 Ma (Schneider & Schmittner, 2006), and which led to an intensification of North Atlantic circulation and enhanced moisture flux into high-latitude regions (Bartoli *et al.*, 2005); in the western Pacific, the restriction of the Indonesian Seaway at about the same time (4–3 Ma) could have reduced heat transport to the high northern latitudes (Cane & Molnar, 2001). Tectonic activity in Tibet may also have contributed to the long-term cooling trend, as land uplift could alter the wave structure in the airstreams of the upper atmosphere, the effects of which would have been to cool the Eurasian and American land masses and hence increase their sensitivity to orbitally driven insolation changes (Ruddiman & Kutzbach, 1990). In addition, a more intense monsoonal circulation and increased rainfall following uplift may

have led to accelerated rates of chemical weathering of silicate minerals. The latter involves CO₂ from the atmosphere, and the products are ultimately deposited on the ocean floor where they are removed from the global geochemical carbon cycle. As a consequence, the atmosphere becomes depleted in CO₂, a process which may have contributed to the long-term Plio-Pleistocene global cooling trend (Raymo & Ruddiman, 1992).

In addition to these long-term variations in climate during the Quaternary, high-resolution proxy records provide evidence of rapid climatic variations, frequently of large amplitude, which are superimposed on the orbitally driven cycles. These short-lived '**sub-Milankovitch**' events occur over timescales varying from centuries to millennia and have been found, *inter alia*, in ice-core records from Greenland (North Greenland Ice Core Project Members, 2004), in Chinese cave speleothems (Wang *et al.*, 2008), in vegetational records from the last glacial stage from Africa and South America (Hessler *et al.*, 2010) and in marine records from the northwest Pacific (Khim *et al.*, 2012). Energy transfer in the world's oceans, driven by salt-density variations (**thermohaline circulation**), along with chemical changes resulting from biological activity, appear to be major causal factors underlying these events. For example, the abrupt climatic changes that have occurred during the Late Quaternary in many low-latitude regions may be related to changes in the nature and rate of North Atlantic ocean circulation, with fluctuations in sea-surface temperatures (**SSTs**) influencing the pattern and timing of tropical monsoons, in turn leading to marked spatial and temporal variations in precipitation over tropical Africa. Other causal factors of decadal to millennial-scale climatic changes include short-term fluctuations in radiatively active atmospheric trace gases (**greenhouse gases**), most notably CO₂, CH₄, N₂O; variations in solar output (as reflected, for example, in sunspot cycles) and in the intensity of the solar wind (the stream of protons and electrons emitted by the sun); and volcanic eruptions during which both particulate matter and sulphur volatiles were injected into the atmosphere, and which might lead to short-term temperature reductions on the earth's surface through the screening out of incoming radiation. All of these, singly or in combination, could, through a complex series of feedback loops, serve to modulate or amplify the effects of climate change resulting from orbital forcing or from oceanographical changes. We return to the factors driving Quaternary climate change, on both long- and short-term timescales, in Chapter 7, while further discussion can be found in Bradley (1999), Bell & Walker (2005) and Cronin (2009).

1.8 THE SCOPE OF THIS BOOK

The aim of this book is to describe and evaluate the methods and approaches that are currently employed in the reconstruction of Quaternary environments. The work does not, however, claim to be exhaustive. Indeed, in view of the wide range of disciplines involved in Quaternary research and, particularly, the 'information explosion' that has occurred over the past two decades, a comprehensive treatment would run far beyond the scope of a single volume. Some aspects are, therefore, considered only briefly, while others (which some will no doubt believe to be important) are omitted altogether. Nevertheless, an attempt has been made to present a balanced view of the various methods employed in, and sources of evidence that form the basis for, Quaternary environmental reconstructions. Some temporal bias is inevitable, as far more is known about the later Quaternary than about the earlier parts of the period, and therefore the majority of examples are drawn from the last interglacial and last glacial stages. The methods, approaches and principles are, however, equally applicable to the analysis of Early and Middle Quaternary environments. In addition, although there is an emphasis on evidence from the Northern Hemisphere mid-latitude regions, particularly from Europe and North America, it is hoped that readers in other parts of the world will find material here that is of interest to them as well.

The book falls naturally into three parts. In Chapters 2, 3 and 4, the geomorphological, lithological and biological evidence that forms the basis for environmental reconstruction is outlined. Although these are useful general categories within which to describe particular techniques and approaches, they are, to some extent, artificial and there are considerable overlaps between them. Hence, in Chapter 2, where the emphasis is on geomorphology (i.e. surface architecture), certain aspects of the stratigraphy of river terraces and raised shoreline sequences need to be considered also, while in Chapter 3, where sedimentological evidence is being discussed, reference is frequently made to landform evidence as, for example, in the analysis of sand dunes formed in loess and coversand deposits. In all three chapters, field and laboratory techniques are introduced in order to give an indication of the procedures that are involved in generating the basic data.

Chapters 5 and 6 make up the second part of the book. The various dating methods that are currently employed in Quaternary science are described and evaluated in Chapter 5, while the principles of stratigraphy and correlation which enable the researcher to construct meaningful spatial and temporal sequences from often fragmentary

evidence are outlined in Chapter 6. The final part, Chapter 7, illustrates how insights into the timing, rate and impacts of past climate change can be gained by synthesizing evidence obtained using the various methods and approaches outlined in Chapters 1–6. The aim here is to highlight recent advances in understanding of the processes that drive climatic change over different timescales (Milankovitch to decadal), and of their environmental consequences.

NOTES

- 1 A number of conventions are currently employed for abbreviating geological ages. In this book we use the shorthand form 'ka' to refer to ages in thousands of years (e.g. 3 ka = 3,000 years ago). Similarly, 'Ma' refers to ages in millions of years. When radiocarbon dating (^{14}C dating) is used to determine age, however, the dates are expressed in years BP (before present), the reference or baseline year being AD 1950 (e.g. 3 ka BP). As we shall see in Chapter 5, radiocarbon dates do not equate precisely to calendar years, but can be 'calibrated' to these, in which case they are expressed as 'cal. BP' (section 5.3.2.6). In ice-core chronologies, the reference year is AD 2000 (section 5.4.3.3). Although other age estimates (based on both radio-metric and incremental methods: Chapter 5) are often expressed in years BP, the baseline year is the actual year in which the measurement was made.
- 2 The term 'proxy' or 'proxy record' is used to refer to any line of evidence that provides an indirect measure of former climates or environments. It can include materials as diverse as pollen grains, isotopic records, glacial sediments, tree rings or animal bones.
- 3 The International Union of Geological Sciences (IUGS) is the body that oversees and arbitrates on all matters relating to geological nomenclature. It operates through a series of Commissions (the International Commission on Stratigraphy [ICS], for example, deals with issues relating to stratigraphy and correlation), and is responsible for the production of the international geological timescale and associated stratigraphic charts (e.g. Gradstein *et al.*, 2012). Within the ICS are a number of subcommissions, each responsible for a particular interval of geological time, such as the Subcommission on Quaternary Stratigraphy (SQS).
- 4 INQUA is the International Union for Quaternary Research, established in 1928 to encourage and facilitate the research of Quaternary scientists in all disciplines (<http://www.inqua.org/>). It holds a major international congress every four years.
- 5 Isotopes are atoms of an element that are chemically similar, but have different atomic weights (section 5.3.1). Oxygen, for example, consists principally of two isotopes, the 'heavier' ^{18}O isotope and the 'lighter' ^{16}O . $^{18}\text{O}/^{16}\text{O}$ ratios (termed $\delta^{18}\text{O}$) in the atmosphere, seas, groundwater and ice are often controlled by oceanographic or climatic conditions.
- 6 Sapropels are dark-coloured marine sediments rich in organic matter that develop during periods of reduced oxygen availability in bottom waters. For further details, see sections 5.5.4 and 6.3.3.3.
- 7 Spectral analysis is a statistical technique which aims to identify cycles in time-series data. Cycles may be characterized in two ways: the *period* of a cycle is the length of time between consecutive repeats, while the *frequency* is the number of cycles (i.e. repeats) that occur per unit of time (Green, 1995).

This page intentionally left blank

Geomorphological evidence



2.1 INTRODUCTION

The marked oscillations in global climate that occurred during the Quaternary led to major changes in modes and rates of operation of geomorphological processes. Undoubtedly the most spectacular manifestations of climatic change were the great continental ice sheets whose passage resulted in widespread modification of the land surface of mid- and high-latitude regions. The growth and decay of the ice sheets were accompanied by the expansion and contraction of areas affected by periglacial activity, there were major changes in the regimes of many river systems, and the nature and effectiveness of geomorphological processes were strongly influenced by changes in the distribution and type of vegetation cover. In low-latitude regions, phases of aridity alternated with periods of wetter climatic conditions leading to migration of desert, savannah and rainforest margins, lake levels rose and fell, and fluvial and colluvial processes varied both spatially and temporally. On the global scale, sea level during the glacial phases was frequently more than 100 m lower but rose to positions above present levels during some of the interglacial stages.

Landforms that developed under a previous climatic regime have often survived, albeit sometimes in a much modified form, as ‘relic’ or ‘fossil’ features. Analysis of these can often provide valuable information about the nature of the climatic regime under which they evolved, as well as about other environmental parameters such as glacial and fluvial processes, slope stability, groundwater movement and tectonic activity. However, the use of geomorphological evidence for this purpose requires a proper understanding of the relationships between geomorphological processes and landforms. Moreover, it must be emphasized that there is frequently a close relationship between geomorphological evidence and lithological evi-

dence (Chapter 3) and that, wherever possible, the two should be used in conjunction in the reconstruction of Quaternary environments.

2.2 METHODS

2.2.1 Field methods

2.2.1.1 Field mapping

The production of a map illustrating the type and distribution of the principal landforms is often the first stage in the investigation of the Quaternary history of an area, and a wide range of automated survey, mapping and imaging tools, as well as user-friendly software for their manipulation, is now available (Pike, 2000). Because these enable large tracts of the earth’s surface to be mapped and analysed very rapidly, they are often now preferred to the more time-consuming process of ground survey using manually operated instruments. The latter have not yet been entirely superseded, however, because they can resolve features too fine in scale to be detected by remote methods (e.g. Hubbard & Glasser, 2005), and they also provide data for the ‘ground-truthing’ of remotely captured images (Lane & Chandler, 2003).

Morphological mapping, using either remote or manual techniques, is the recording and depiction of individual slope elements in the landscape, and the nature of the junctions between them (Griffiths, 2002). A simple hand-held instrument such as an Abney Level or a clinometer can be used for slope measurement. Typical morphological maps are produced at scales of 1:10,000 or larger, on which even the most subtle changes in the shape of the land can be recorded (Griffiths *et al.*, 1995). This approach has been widely employed in land survey, but because it is not specifically concerned with landscape evolution,

it has found less favour with Quaternary scientists. **Geomorphological mapping**, on the other hand, is one of the most important techniques in Quaternary research, for the maps produced contain information not only on morphology but also on the genesis and, in some cases, on the age of the landforms. This type of mapping can be carried out at different scales ranging from very detailed maps of small areas (typically 1:10,000) to maps at the national scale (e.g. IGS Quaternary Map of the British Isles 1977, scale 1:625,000; see also the regional compilations in Ehlers & Gibbard, 2003, and Ehlers *et al.*, 2011a). Geomorphological mapping is essentially interpretative and therefore requires both an appreciation of the complexity of landform assemblages and a detailed knowledge of their genesis. It also needs an eye for detail, some training in field mapping and surveying techniques, and a knowledge of aerial photographs and satellite images, as the mapping of landforms can be greatly aided by comparison with high-quality optical images of the field area. Geomorphological mapping, particularly at scales of 1:10,000 or greater, has been most effectively employed in the analysis of glacial landscapes, including those resulting from the passage of the last ice sheets and, in particular, from more recent phases of glacier activity (Figure 2.1).

2.2.1.2 Instrumental levelling

In reconstructing the Quaternary history of an area, it is often essential to determine the precise altitude of, and differences in altitude between, particular landforms and landform assemblages. The same applies equally to lithological units (Chapter 3). Altitudinal data can aid in the interpretation of landforms, and may also enable landforms of different age to be identified. For example, only fragments of former river terraces may be preserved in a particular area, and it may be impossible to identify and correlate fragments of similar age, and to establish a chronology of terrace development on the basis of field mapping alone. By obtaining precise altitudinal measurements on each terrace fragment, however, formerly continuous features can be reconstructed, gradients can be measured and altitudinal relationships between individual terraces can be established (section 2.6). This, in turn, may enable the relative order of age of the features within a terrace sequence to be deduced. Similar principles can be applied in the investigation of abandoned shoreline remnants (section 2.5). Where only a general impression of altitude is required, and where the mapping is being carried out at a relatively small scale, it may be sufficient to obtain the altitudinal data from spot heights and contours on the relevant base maps. However, where a

more detailed investigation is being conducted, the altitudes and surface gradients of landforms must be obtained by instrumental measurements in the field.

The comparison of altitudes of landforms or stratigraphic horizons, especially from widely separated localities, requires a common **geodetic datum**,¹ a plane or point of precisely fixed altitude to which all subsequent measurements can be referred (e.g. North American Datum NAD83; the European Datum of 1950, with its origin at Potsdam, Germany; and the UK's Ordnance Datum (OD), measured at Newlyn, Cornwall). A frequently employed regional datum has been sea level, but as this varies both spatially and temporally, altitudinal data are more reliable when related to precisely surveyed surface altitudes of fixed geodetic coordinates; in the UK, these are known as **Ordnance Survey Bench Marks** and are marked on the ground surface by a symbol cast in metal.

In many parts of the world, however, only low-quality maps and limited geodetic information are available, but the surface altitudes and spatial relationships of landforms in these regions can be estimated using a range of instruments. These include **aneroid barometers**, hand-held (e.g. **Abney** levels, **surveyor's levels**, **theodolites** and **electronic distance measures (EDMs)**), the more sophisticated versions of which are commonly termed '**total stations**' (Bannister *et al.*, 1998). Aneroid barometers are affected by variations in barometric pressure, while the other instruments, although providing positional data of increasing degrees of precision, also have operational and technical limitations (Ghilani & Wolf, 2008). For example, hand-held levels are useful for rapid surveys, but tend to produce variable results due principally to operator errors. In most geomorphological fieldwork in the mid-latitude regions, therefore, particularly where precise altitudinal data are required, surveyor's levels, theodolites and EDMs are most frequently used and traverses opened and closed at national survey benchmarks in order to provide an estimate of accuracy. However, in those parts of the world where no such benchmarks are available, such as Arctic Canada, Greenland, and parts of Africa and Antarctica, the local marine tidal level or some prominent landmark may be selected to provide an arbitrary temporary datum. While these may provide a reasonable basis for determining the relative heights of features within the survey area, the 'absolute' geodetic position of the temporary datum cannot be established, and this limits the potential for altitudinal correlation with features in other areas.

An important innovation in geomorphological studies, especially in remote locations, is the **Global Positioning System (GPS)**. This is a method of triangulation based on automated computation of distances between points on the

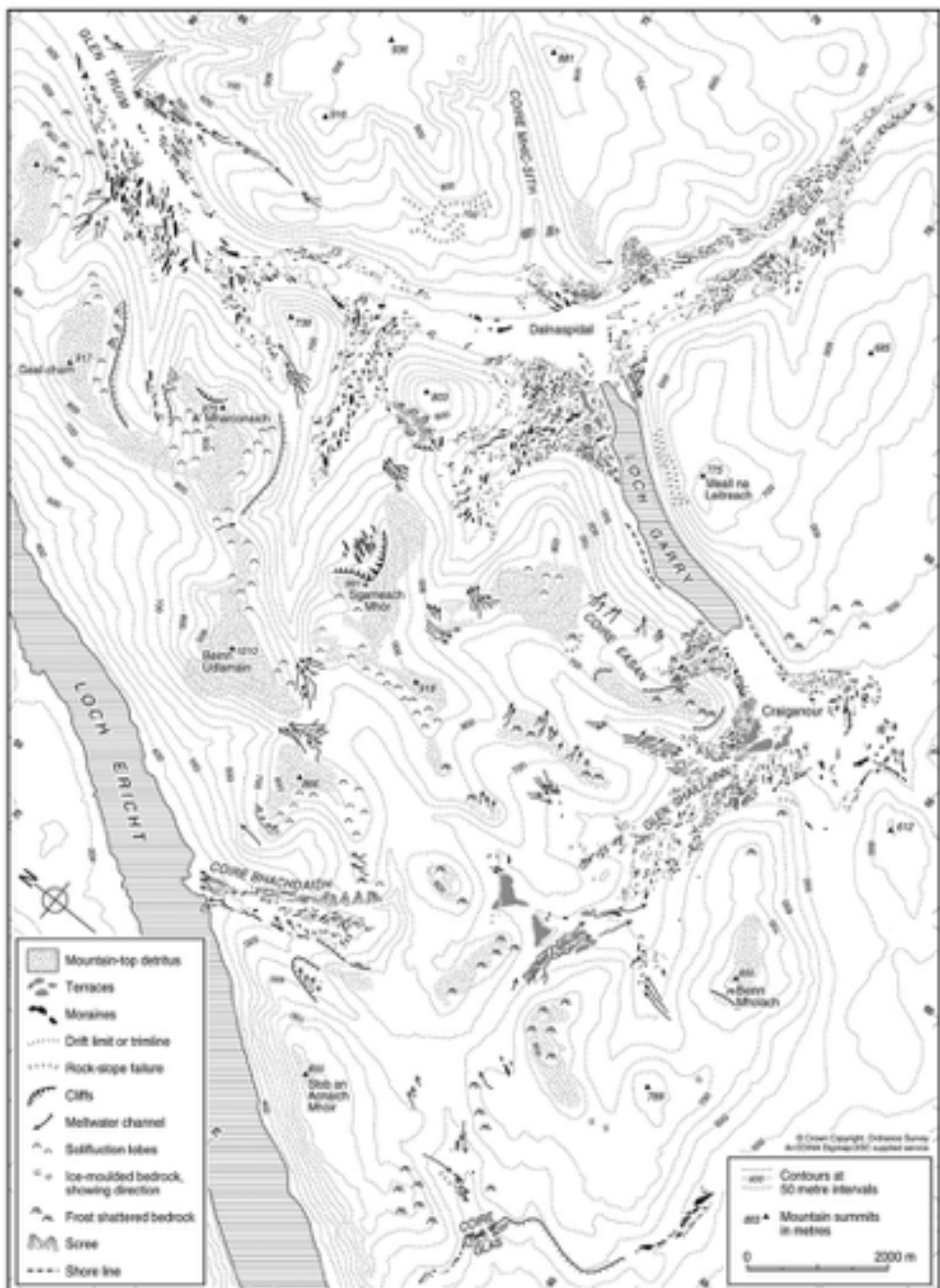


Figure 2.1 Geomorphological map of the West Drumochter Hills in the Scottish Highlands (from Benn & Ballantyne, 2005). The nature and distribution of glacial landforms enable the areal extent and thickness of the former ice mass to be determined (copyright © 2005 John Wiley & Sons, Ltd).

earth's surface and a number of earth-orbiting satellites. It was developed initially for military purposes by the USA in the 1970s, and civilian access to the network was granted for the first time in the early 1990s. A range of affordable hand-held receivers is now available which can achieve remarkable precision. At the lower end of the price range, 'recreational' GPS receivers enable the position and altitude of the ground at any point to be determined to within a few metres, depending on the receiver model, the nature of the local terrain, the number of satellites that the receiver is able to track and the positioning correction factors that can be applied (Spencer *et al.*, 2003a). More sophisticated '[differential receivers](#)'² (Trimble Navigation, 1989) are able to pinpoint locations to within a few centimetres.

2.2.2 Remote sensing

'[Remote sensing](#)' refers to the acquisition of images or scans of the earth's surface and subsurface by instruments that can detect elements of the electromagnetic spectrum reflected or emitted by different surface materials. A range of devices can be mounted on aircraft, satellites and boats to capture signals of selected wavelength in order to 'sense' and record spatial and temporal variations in the earth's surface albedo, roughness, lithology, sediment architecture or other physical attributes. Remote sensing includes conventional [photography](#) using visible and non-visible (e.g. infra-red) light spectra, [multispectral](#) (multi-wavelength) [scanning systems](#), [radar sensing](#), [sonar signals](#) (echo-sounding) and, more recently, [laser technology](#) (Lillesand *et al.*, 2004; Jensen, 2007).

2.2.2.1 Aerial photography

Since the First World War, aerial photographic reconnaissance has increased both in frequency of use and in degree of sophistication. Good-quality aerial photographs are now available even for some of the most inaccessible parts of the world, allowing at least preliminary maps to be made of landforms and landform assemblages (Poole *et al.*, 2002). A system of grid corrections using ground control points can be used to transfer details from photographs to maps where scales differ, or where the photographs contain serious distortions (Baily *et al.*, 2002). Aerial photographs are especially useful in the mapping of landforms in that they (a) direct attention to areas where landforms are most evident or abundant, thereby avoiding wasted ground reconnaissance; (b) reveal larger-scale landform patterns that may go undetected in ground mapping, such as the shorelines of lakes in semi-arid regions or streamlined patterning in glacial bedforms; (c) record morphological

features subsequently obscured by afforestation, the products of catastrophic events such as landslips or tsunamis, or urbanization; and (d) allow the monitoring of changing landscapes and landform assemblages, or changes in other features, such as glacier and ice sheet margins (Khan *et al.*, 2012).

Disadvantages of aerial photographs include distortions due to camera tilt or variations in camera altitude, loss of detail due to cloud cover or shadow effects, poor tonal contrasts so that, for example, unconsolidated surface sediments sometimes cannot be distinguished from bedrock, and difficulty in the detection of small-scale landforms. Field mapping, therefore, remains essential, and even where mapping is based on large-scale, good-quality aerial photographs, the results must be viewed as no more than a *provisional* map of the Quaternary geomorphology of a region until the interpretations can be checked in the field. For areas where good topographic maps are unavailable, aerial photographs or satellite images provide the only realistic basis for the mapping of landforms, and enlargements can be made specifically for this purpose.

2.2.2.2 Satellite imagery

Satellite imagery offers great advantages over aerial photography as distortions are minimized, the process is much more rapid, and repetitive images of large parts of the earth's surface can be obtained. In terms of image generation, conventional photographs are produced by the simultaneous recording on film of all features viewed through the lens of the camera. Satellites, on the other hand, carry a wide range of sensors and filters that receive and process images in various light-wave bands, and hence are considerably more versatile.

The development of non-military satellite earth monitoring began in the late 1960s when the National Aeronautics and Space Administration (NASA), with the cooperation of the US Department of the Interior, initiated a programme to place in orbit a series of [Earth Resource Technology Satellites \(ERTS\)](#), the first of which, [ERTS-1](#), was launched in 1972. Just before the launch of the second ERTS satellite in January 1975, it was renamed [Landsat](#), and all subsequent satellites in the series have carried the Landsat designation. In January 1983, NASA transferred Landsat to the National Oceanic and Atmospheric Administration (NOAA), but in October 1985, the whole operation was commercialized. Space Imaging, Inc. of Colorado, USA, obtained exclusive sales rights to all Landsat images, although the U.S. Geological Survey (USGS) retained primary responsibility as the government's long-term archive of Landsat data. In 2001, Space Imaging relin-

quished their commercial rights and Landsat data are now jointly owned by the USGS and NASA (<http://landsat.usgs.gov/>). Seven Landsats have been launched since 1972, current data being supplied mostly by Landsat-5 (1984) and Landsat-7 (1999).

All seven Landsats have been equipped with two types of sensor: a set of **return beam vidicon (RBV) cameras** and a **multispectral scanning system (MSS)**. While RBVs do not contain film, images are received and stored on a photosensitive surface in each camera. This is then scanned by an internal electron beam to produce a video signal, which is similar to that in a conventional television camera (Lillesand *et al.*, 2004). In MSS systems, a scanner produces a set of corresponding digital images of terrain in four different wavelength bands of the electromagnetic spectrum. Digital images comprise a grid of cells (picture elements or **pixels**), each of which is assigned a value that corresponds to the intensity of electromagnetic radiation measured by the sensor from a portion of the terrain in the sensor's instantaneous field of view (IFOV). The satellites orbit at a height of *c.* 700 km above the earth's surface, and the MSS sequentially scans sectors of the surface measuring 185 km by 170 km, recording radiance from an IFOV of approximately 80 m by 80 m. A second sensor, the **thematic mapper (TM)**, was added to Landsats launched after 1982. This records electromagnetic reflectance of sunlight from the earth's surface in seven spectral bands ranging from the visible to infra-red, and at a higher spatial resolution (IFOV of 30 m by 30 m). Landsat-7 carries an **enhanced thematic mapper** that provides images with a spatial resolution of 15 m, greatly improving the definition of scanned surface features.

A number of other satellites specifically designed for terrain monitoring have been placed in orbit during the past thirty years. These include the French **SPOT** (Système Pour l'Observation de la Terre) constellation of five satellites, the first of which was launched in 1986 and the most recent (SPOT-5) in 2002. SPOT-5 carries **high-resolution visible (HRV) multi-spectral linear array (MLA)** sensors which sequentially scan surface areas of 60 km by 60 km, from which stereo-pair images can be generated enabling accurate topographic mapping at a resolution of 10 m. Three satellites have been launched by the European Space Agency (ESA), the latest of which, **Envisat** (2002), carries an array of nine instruments which capture a wide range of information from land, water and ice surfaces, as well as from the atmosphere. Perhaps the most advanced earth observation programme, however, is NASA's **Earth Observing System (EOS)**, which comprises three main artificial satellites: **Terra (EOS AM-1: 1999)** monitors environment and climate; **Aqua (EOS PM-1: 2002)**,

generates precipitation, evaporation and water cycle data; and **Aura (EOS CH-1: 2004)** studies ozone, air quality and climatic variables.

Several satellites carry instruments that focus on particular earth surface or atmospheric properties. These include the **TOPEX/Poseidon** satellite (1995), a French–USA collaboration for monitoring the oceans, and its successor **Jason-1** (2001) which has provided measurements of the surface altitude of the world's oceans to an accuracy of 3.5 cm; **GEOSAT** (Geodetic Satellite: 1985), a US Navy observation satellite which can determine sea-surface altitude with a precision of *c.* 5 cm; and NASA's **ICESat** (Ice, Cloud, and Land Elevation Satellite: 2003), which measures ice sheet, cloud and aerosol properties, as well as surface topography and vegetation.

The potential of satellite imagery in Quaternary research is clearly considerable, not only for detecting and mapping ancient landforms, but also for monitoring modern earth surface processes. Satellite images have been employed to map, *inter alia*, desert landforms (Al-juaidi *et al.*, 2003), glacial moraines and streamlined glacial bedforms (Stokes *et al.*, 2005), ancient lake shorelines (Leblanc *et al.*, 2006) and a range of periglacial landforms (Walsh *et al.*, 2003). Examples of modern geomorphic processes that can be observed using satellite imagery include the evolution of alluvial channels (Gupta *et al.*, 2002), mountain mega-fan development (Leier *et al.*, 2005), glacier outburst floods (Worni *et al.*, 2012) and formation of thermokarst (permafrost) features (Grosse *et al.*, 2005). Satellite imagery has also been used to measure the changing positions of the margins of glaciers and ice caps (Berthier *et al.*, 2010), and also to monitor variations in sea-ice cover (Laxon *et al.*, 2013).

2.2.2.3 Radar

Radio detection and ranging (**radar**) is based on the emission of pulsed signals from a transmitter, usually in the microwave and higher radio frequencies, and the recording of the 'echoes' of these signals as they bounce back from the ground surface. The returning 'back-scattered' signals are affected by ground surface roughness, by the orientation of upstanding features, and by the density and electrical properties of ground materials. Back-scattered radiation is recorded in pixels and, as a general rule, the rougher the terrain, the more back-scattered energy is returned, and the brighter the resulting images. In dry sediments or cold ice, boundaries between stratigraphic units or ice layers can often be detected.

Airborne radar equipment ('**echo sounders**') have been developed that automatically transform received signals

into images (**imaging radar**), usually referred to as **side-looking airborne radar (SLAR)** because the radar antenna fixed below the aircraft is pointed to the side. As in satellite scanners, the pulsed signals scan the terrain and the received signals are subsequently converted into electrical impulses that are digitized or transformed into a photographic image. In practice, however, SLAR systems are limited by resolution problems to relatively short-range and low-altitude operations (Lillesand *et al.*, 2004). They have now been largely replaced by more sophisticated systems known as **synthetic aperture radar (SAR)**, which combines the echo signals through the radar instrument's aperture as it moves along the flight track, thereby significantly enhancing signal resolution. SAR systems have been mounted on aircraft and on many earth-observing satellites, for example on Seasat and the ERS satellites (see above). A new phase in SAR began in 2007 with the launch of the **TerraSAR-X** satellite, a joint project between the German Aerospace Centre and EADS Astrium, an aerospace subsidiary of the European Aeronautic Defence and Space Company (EADS). This earth observation satellite uses an X-band SAR (the X band is a part of the microwave sector of the electromagnetic spectrum) to provide very high-quality topographic images for both commercial and scientific applications.

As with other remote sensing systems, the great advantages of radar imaging are that micro- and radiowaves can penetrate thick clouds and are unaffected by adverse weather conditions, while the reflections received are frequently more sensitive to ground surface textural variations than is visible light. Radar has proved to be a useful and versatile technique for geomorphological mapping and terrain evaluation, for example in the analysis of mass movement phenomena (Catani *et al.*, 2004), palaeodrainage features (Robinson *et al.*, 2006) and the movement of rock glaciers (Rignot *et al.*, 2002). It also has a range of glaciological (Gao & Liu, 2001; Rémy & Parouty, 2009) and geoarchaeological applications (Wiseman & El-Baz, 2007).

A specialized aspect of radar imaging is **ground penetrating radar (GPR)**, a geophysical investigative procedure that employs radar signals to image subsurface phenomena. It offers a non-destructive and rapid method for analysing subsurface objects and structures in a variety of materials, including rock, sediments, soil, ice and water. Penetration is limited by a number of factors, including the electrical conductivity of the medium through which the signals are transmitted, and the maximum depth of penetration (*c.* 15 m) is only achievable in dry, sandy media. GPR has been widely employed in archaeology, for example to detect and record shallow burials (Cheetham, 2005) and to map subsurface archaeological structures

(Piro & Campana, 2012), but it also has applications in sedimentology (Neal, 2004), in investigations of periglacial landforms, such as pingos (Ross *et al.*, 2005) and rock glaciers (Degenhardt, 2009), and in the measurement of soil and debris mantle thickness (Sucre *et al.*, 2011).

2.2.2.4 Sonar and seismic sensing

Several techniques have been developed that are based on the gravitational, magnetic or electrical properties of the earth. Transmission of **acoustic** or **sonic waves** through the ground is affected by the density and other characteristics of different materials, and these form the basis for **seismic surveys** that have been extensively used in geophysical exploration. The sonic or seismic waves are created by controlled, minor explosions or induced vibrations at the ground surface, the returning reflections being captured by specialized receivers ('**geophones**' on land, '**hydrophones**' in water). Various devices are employed to emit short, compressional seismic waves, one of the most common being a spark chamber, or '**Sparker**'. In studies of submarine geomorphology, **side-scan sonar** rapidly surveys and images large sectors (swathes) of the sea floor to establish bathymetry (**swathe bathymetry**) and bottom sediment architecture (**acoustic profiling**). Side-scan is a device that transmits acoustic signals in a wide arc or fan towards the seabed, and the apparatus can be towed behind a boat or attached to a ship's hull. The vessel surveys the sea floor along parallel tracks, and the continuous sonic reflections are integrated to provide 2-D and 3-D bathymetric images (Figure 2.2). Definition depends upon the sonar frequencies used, with higher frequencies delivering better resolution, but possessing a more limited range.

High-resolution acoustic profiling is used in studies of seabed processes and stratigraphy (Sacchetti *et al.*, 2013), in the mapping of submerged landforms (Dowdeswell *et al.*, 2010) and in investigations of sedimentary sequences beneath polar ice shelves (Johnson & Smith, 1997). Other applications include investigations of lake-bed sediments (Eyles *et al.*, 2003), calculation of suspended sediment loads (Thorne & Hanes, 2002) and offshore palaeoseismicity (Hutri & Kotilainen, 2007). Further details on geophysical exploration can be found in Kearey *et al.* (2002).

2.2.2.5 Digital elevation/terrain modelling

Remote sensing methods enable accurate topographic models of the earth's surface, known as **digital elevation models (DEM)** or **digital terrain models (DTM)**, to be

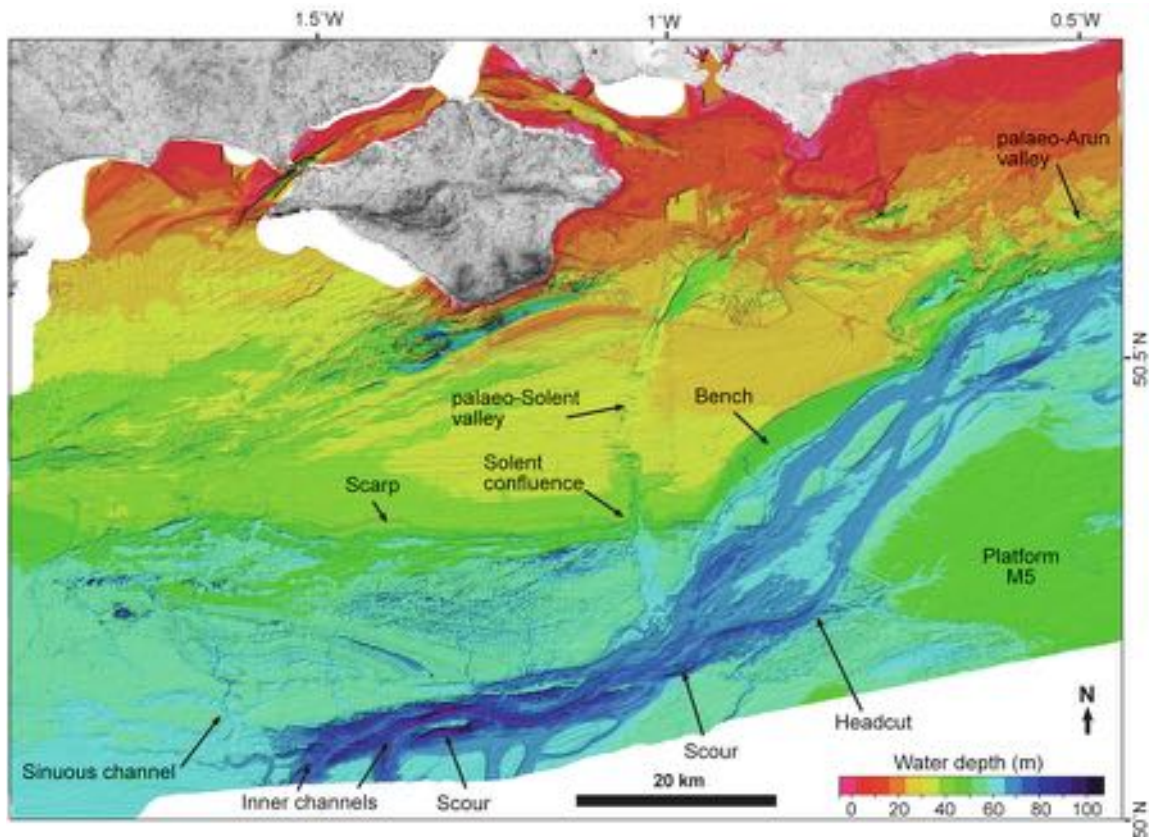


Figure 2.2 Sonar bathymetry of the north-central English Channel shelf showing (in blue) the deeply incised channel of a major river which was cut following the confluence of the Thames, Rhine, Seine and other major European rivers at a time when sea level was >100 m lower than today (from Gupta *et al.*, 2007). Onshore topography is shown as black and white relief (Isle of Wight and southern shores of England) (image provided by Sanjeev Gupta, Imperial College, London, UK. Reprinted by permission from Macmillan Publishers Ltd: *Nature*, Gupta *et al.*, copyright 2007).

constructed. DEMs/DTMs are created from regularly spaced grids of elevation data which are referenced to a common geographic coordinate system. These can then be used to create 2-D and 3-D topographic representations of the area of ground surface that they cover. DEMs show all the features captured by the survey process, including woodland and buildings for example, whereas the superficial features are filtered out in a DTM to show the ground surface only ('bald-earth' elevation mapping). A number of different types of remotely sensed data can be used for terrain modelling, but one of the more important is **interferometric synthetic aperture radar (IFSAR)**, which can generate DEMs with a resolution of less than 10 m.

DEM s have revolutionized the study of landforms as the images often show ground surface detail that is not

obvious on maps or generated by ground-based surveying. The azimuth of light incidence can be rotated through 360° in DTMs to vary the length and direction of shadows cast by surface features; this can greatly enhance the 3-D appearance of individual landforms and also reveal patterns in the landscape that may be less obvious under high incident light or overcast conditions (Figure 2.3). The data can also be linked into GIS software such as ARC/INFO, which enables other data to be overlain on the terrain surface.

A number of companies offer access to DEM/DTM data-sets. InterMap Technologies, for example, provides **NEXTMap**, a DEM program that covers most of Europe and the USA, and selected areas such as some Pacific islands. It is now widely used to generate base surfaces for

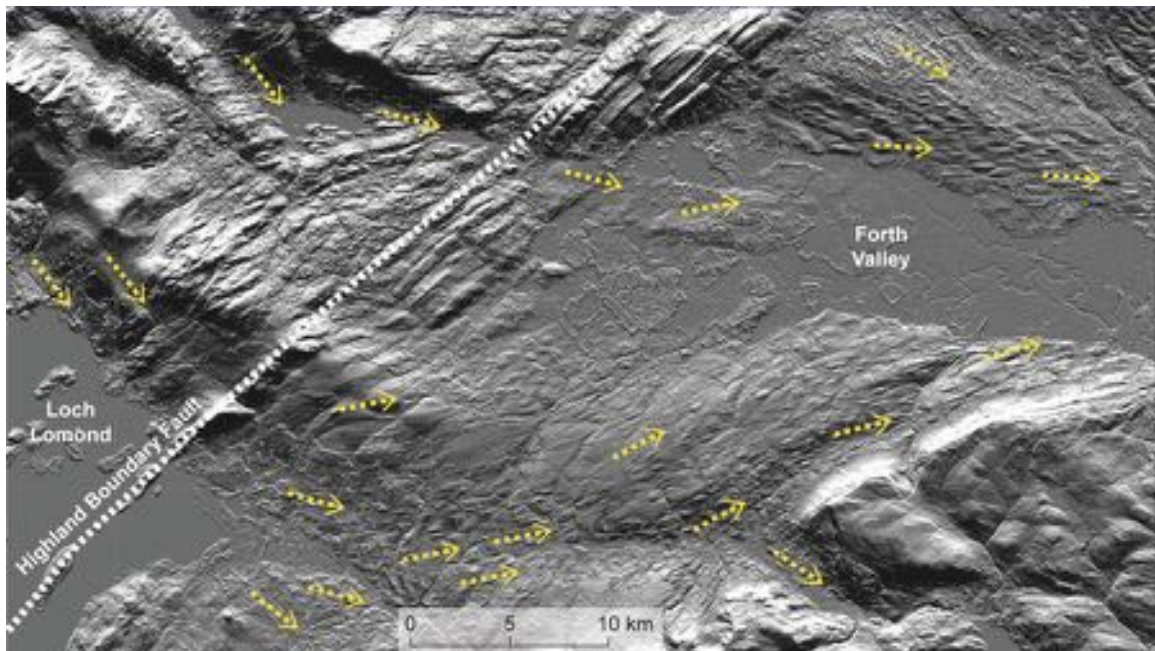


Figure 2.3 A digital surface model (DSM) based on NEXTMap showing the ice-moulded landscape of part of the Midland Valley of Scotland to the northeast of Glasgow. The Highland Boundary Fault marks the southern margin of the Grampian Highlands. Ice-moulded bedrock and drumlin orientations show that ice flowed from the Highland valleys along the Forth Valley towards the North Sea (arrows indicate inferred ice-flow directions) (DSM model generated by Chaoyuan Chen, Royal Holloway, University of London, UK using interferometric synthetic aperture radar [InSAR] data obtained by Internet Technologies, Inc. and provided courtesy of the British Geological Survey).

geomorphological mapping. The spatial resolution and accuracy of DEMs and DTMs depends on a number of factors, including the type of sensing device employed and the algorithms used to convert the raw data into elevation data. Remotely sensed images have to be corrected (a process known as **orthorectification**) to remove distortions caused by topographic slope, lens distortion (parallax), camera tilt and other influences. This process can improve the spatial resolution of the resulting images to 1 m or less.

A recent development in digital elevation/terrain modelling is **light detection and ranging (LIDAR)** technology. This operates on the same basis as radar, except that it employs laser beams rather than radiowaves for detection. LIDAR supports **airborne laser swath mapping (ALSM)** and **laser altimetry** which can scan ground surfaces at a much higher density of beam points than radar, and hence can generate elevational data and images with, potentially, a centimetre-scale resolution. LIDAR mapping is therefore rapidly becoming the new generation DEM. Further details can be found in Hatzopoulos (2008).

2.3 GLACIAL LANDFORMS

Ever since the acceptance of the ‘Glacial Theory’ by the geological community in the middle years of the nineteenth century, it has been recognized that landforms of glacial erosion and deposition are important palaeoenvironmental indicators. When mapped systematically, they reveal a great deal about the extent, thickness and behaviour of former ice masses, the direction of ice movement at both local and regional scales, and the nature and pattern of glacier retreat. In certain circumstances, the evidence may be used to reconstruct the configuration of former ice sheet or glacier surfaces, and to allow former ice volumes to be estimated. Comparisons with present-day glaciers, particularly those where a close relationship has been established between glacier behaviour and climatic parameters, enable inferences to be made about former climatic regimes. Glacial geomorphological evidence is also key to the development of computer models that simulate the geometry and behaviour of former ice sheets and glaciers. Global ice volume co-varies with changes in

sea level, ocean circulation and hemispherical climate (Chapter 7), and an understanding of these complex interrelationships is an important element of contemporary environmental science. The first stage in this process, however, is the production of an accurate map of the extent of Quaternary ice masses for different times in the past.

2.3.1 Extent of ice cover

Establishing the extent of former ice sheets and glaciers has long been regarded as one of the most challenging objectives of Quaternary research. In North America, the systematic field mapping of the outer limit of Pleistocene glaciation began soon after 1860. The maximal extent of ice cover was based largely on the evidence of conspicuous 'end moraines' or on the limits of glaciogenic deposits ('Drift Border'), and by 1878, a map had been produced of the southern margin of the glaciated area between Cape Cod and North Dakota. Similar investigations of glacial drift cover and end moraines were underway in Europe, Asia and parts of the Southern Hemisphere, so that by 1894 James Geikie was able to compile maps of the worldwide distribution of glaciers during what he referred to as the 'Great Ice Age'.

The principal types of geomorphological evidence used in the reconstruction of former ice-marginal positions are lateral, terminal, end and retreat moraines, outwash spreads and sandar,³ ice contact features such as kame terraces, and valley-side or down-valley limits of stagnation moraine, boulder spreads (boulder limits) or drift limits (Bennett & Glasser, 2009; Benn & Evans, 2010). Lateral and terminal moraines (and, in some cases, marginal meltwater channels) mark the maximal positions of glacier margins, whereas within those limits, linear moraine ridges will reflect subsequent **recessional stages** as the ice becomes temporarily stabilized during deglaciation (Figure 2.4), while widespread moundy topography ('dump' or **hummocky moraine**) may result from glacier stagnation in situ (section 3.3). Kame terraces, which reflect glaciofluvial deposition along a decaying ice margin, may also preserve a record of ice-marginal positions during glacier wastage (Bitinas *et al.*, 2004). The types of deposits and landform assemblages produced during deglaciation will be determined by a range of often interconnected factors, including manner and rate of glacier retreat, debris content of the ice, position of entrainment of debris within the ice, and topographical influences (Glasser and Hambrey, 2001; Benn & Lukas, 2006). In general, however, the overall distribution of a range of glacial landforms will broadly define the extent of the formerly glaciated area, with both lateral (ice-marginal) and vertical (valley-side) limits.

The land lying beyond or above the area directly affected by glacier ice will have been affected by periglacial activity, with the shattering of exposed rocks by freeze-thaw processes, the development of gelifluction features (lobes, terraces, etc.) and the formation of structures associated with the action of ground ice (wedges, patterned ground, etc.). The distribution of these periglacial features can, in certain cases, provide further evidence of the former extent of glacier ice. In upland areas, for example, the boundary (or, more commonly, the zone of transition) between glacially scoured and frost-shattered bedrock is referred to as the **trimline**, and indicates the approximate positions of the former ice margins (Figure 2.5). Careful measurement of the trimline altitude on different mountain peaks enables the upper limit of glaciers and ice sheets to be established at the regional scale (Ballantyne *et al.*, 2008). The lateral extent of the area affected by frost action can be used in a similar manner to delimit formerly glacierized areas.

A number of difficulties arise in mapping the former extent of Pleistocene glaciers on the basis of geomorphological evidence. First, at the height of the last glaciation in both Europe and North America, ice masses submerged many of the upland areas. Hence, although geomorphological evidence marking the lateral extent of the ice sheets and glaciers is widespread, the vertical extent of the ice mass is much more difficult to establish from field evidence alone. In order to obtain estimates of ice thickness, therefore, recourse may have to be made to models of former ice sheets (section 2.3.4). Second, successive ice sheets covered broadly the same areas, except towards the outer margins (Figure 1.4 and section 2.3.2), so that geomorphological evidence from earlier glacial episodes has usually been destroyed by later ice advances. Consequently, in many areas of the mid-latitudes that were affected by Pleistocene glaciers, the majority of the landforms that have been preserved date only from the later stages of the last glaciation. Third, many glacial landforms have been considerably modified by periglacial and paraglacial activity (section 3.3.3.3) both during and after regional deglaciation, and this often poses problems in field mapping and interpretation. Fourth, some glacial landforms may resemble ice-marginal features, but may not, in fact, be so. Glaciofluvial landforms (e.g. kames and eskers) often display linear trends and have, on occasion, been interpreted erroneously as evidence for former ice limits. In the majority of cases, the lineations displayed by such features reflect local patterns of ice disintegration rather than the retreating margins of active ice masses. Hence, a proper understanding of the nature and origin of glacial landforms is necessary if this type of evidence is to be used to determine

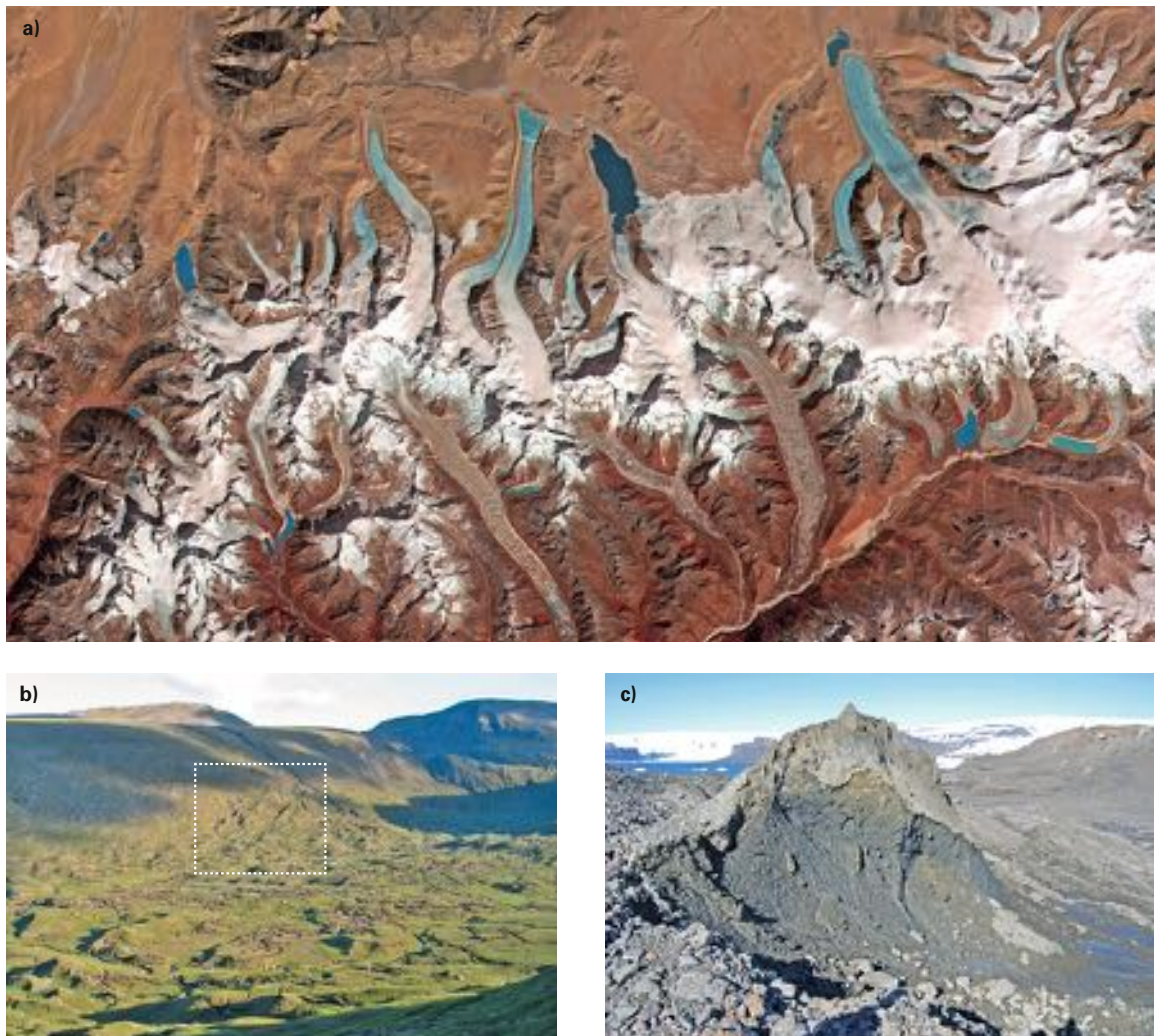
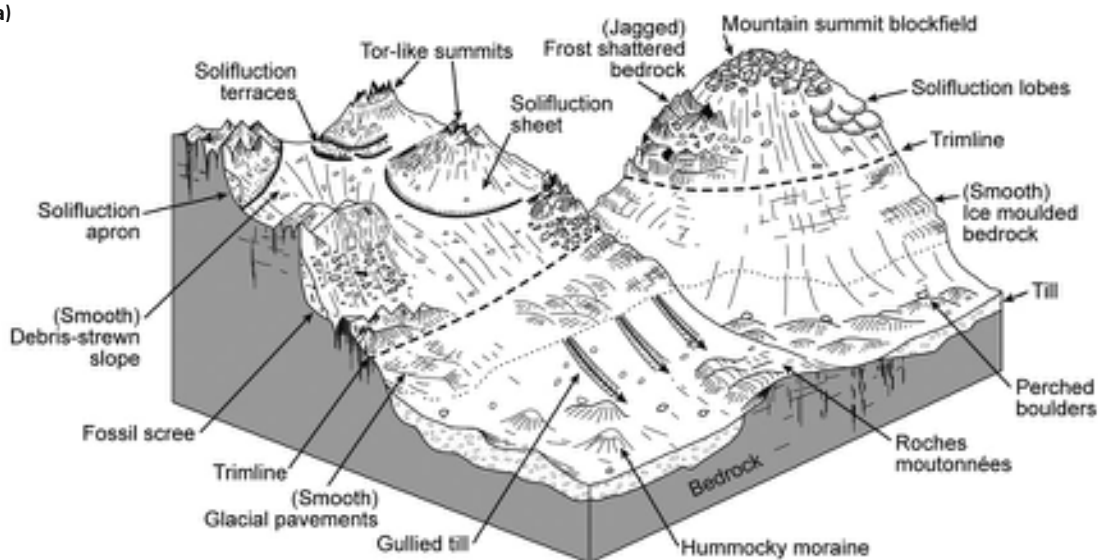


Figure 2.4 Moraine systems. a) NASA satellite image of the glacier icefield in Bhutan-Himalaya. Note the glaciers are receding, leaving a series of arcuate ('horse-shoe') moraines and lakes near their termini. b) Marginal lateral moraines (dotted box) and 'hummocky' or 'dump' moraines of Loch Lomond Stadial age (c. 12.9–11.7 ka) in Coire na Phris, northwest Scotland (from Lukas & Benn, 2006; photograph by Sven Lukas, Queen Mary University of London, UK. © Royal Scottish Geographic Society, reprinted by permission of Taylor & Francis Ltd, <http://www.tandfonline.com> on behalf of The Royal Society Geographic Society). c) Moraine-mound comprising diamictite and sandy gravel melting out of glacier ice at Alpha Glacier on James Ross Island, Antarctica – a possible modern analogue for 'hummocky moraine' (photograph by Neil Glasser, Aberystwyth University).

the former extent of Pleistocene glacier ice. Fifth, mapping of the upper limits of glaciers and ice sheets on the basis of trimline evidence may be problematical, for high-level trimlines may not always reflect former periglacial weathering limits, but rather the position of a thermal boundary separating wet-based ice at pressure-melting point from cold-based ice on summit plateaux (Fabel *et al.*, 2012).

Sixth, the outer margins of large areas of the last great ice sheets lay beyond the present coastline on the continental shelves, and accurate determination of the ice limits has only recently become possible through the application of remote sensing techniques (Bradwell *et al.*, 2008a). Finally, it should be noted that the outer margins of drift sheets often have no distinctive geomorphological expression,

a)



b)



c)



Figure 2.5 a) Features used to identify trimlines and other types of glacial limits in mountainous terrain (from Thorp, 1981). b) Nunataks bordering Liv Glacier in the 3,000 m high Queen Maud Mountains, a major outlet glacier from the East Antarctic Ice Sheet to the Ross Ice Shelf. Flow is from right to left (photograph © Mike Hambrey, Aberystwyth University, from <http://www.glaciers-online.net>). c) High-altitude trimline (dashed line) marking the maximum late Würm ice surface at c. 2,670 m in the Grimsel Pass, Switzerland, this is marked by the upper limit of ice-polished bedrock above which the rock surfaces show evidence of prolonged frost shattering (photograph by Sven Lukas, Queen Mary University of London, UK).

and end moraines in particular are absent. In some cases, the evidence has been destroyed, either by meltwater activity during deglaciation, or by postglacial erosion or subaerial weathering. In other situations, the glaciers either did not carry sufficient debris, or did not maintain a steady-state⁴ position for the length of time required for the construction of an end moraine.

Where end moraines are found within areas formerly covered by glacier ice, further problems of interpretation are encountered. There has been considerable debate over whether such moraines are, strictly speaking, recessional, in that they formed during the still-stand of the ice margin during a phase of overall glacier retreat, or whether they have been produced by a renewed episode of glacier

expansion, and therefore reflect a **glacier readvance**. Where prominent end moraines occur, the latter interpretation has usually been adopted, as it has been considered unlikely that large constructional forms would have been produced during a still-stand of the ice margin. The geomorphological evidence, however, is frequently equivocal, and it must be emphasized that conclusive proof of a glacier withdrawal and a subsequent readvance can only be obtained from stratigraphic evidence (where organic sediments are found interbedded with two glaciogenic units, for example) or, in some instances, from other geomorphological features, such as indicators of changing directions of ice flow between successive glacial episodes (Clark, 1997). An additional complication in the interpretation of end-moraine evidence is that it is frequently very difficult to distinguish between those landforms that reflect a glacier readvance induced by a deterioration in climate, and constructional forms that have been produced by a **glacier surge**⁵ resulting from short-lived instability within the former glacier system which may, or may not, have been climatically determined (Lingle & Fatland, 2003). Despite these difficulties, however, there is now a broad consensus about the positions of the maximal limits and general patterns of decay of the last ice sheets that occupied North America and northern Eurasia, although in some areas local details remain contentious (Ehlers *et al.*, 2011a; Hughes *et al.*, 2013).

2.3.2 Geomorphological evidence and the extent of ice sheets and glaciers during the last cold stage

2.3.2.1 Northern Europe

In northern Europe, conspicuous ‘end moraines’ mark the maximal limits (Figure 2.6a) and initial recessional stages of the last (Weichselian) Fennoscandian ice sheet (Böse, 2005). These extend over considerable distances from northern Denmark through Germany into Poland, and then northwards through the Baltic states and into European Russia (Figure 2.6b). In places they are discrete narrow ridges, while elsewhere they comprise broad tracts of hummocky ground a kilometre or more wide; sometimes the ridges fade into flat, almost featureless ground and cannot be traced continuously (Rinterknecht *et al.*, 2005). Moreover, the term ‘moraine’ that is widely applied to these features may not always be appropriate, since some segments comprise glaciofluvial or outwash sediments, while others have been formed by the bulldozing action of the ice margin, which has thrust and deformed superficial deposits or pre-Quaternary strata (Figure 2.7).

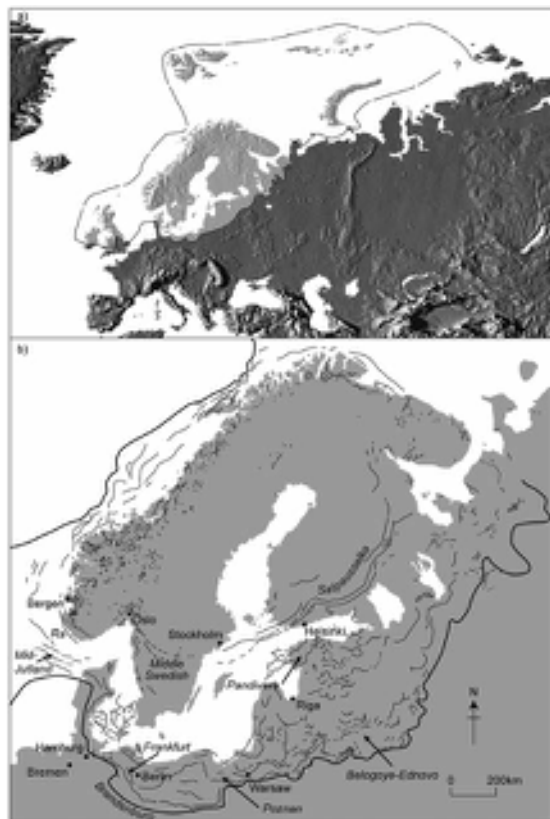


Figure 2.6 a) Maximal limits of the Late Weichselian ice sheet in MIS 2 (after Svendsen *et al.*, 2004). b) Recessional stages of the Late Weichselian ice sheet (after Böse, 2005).

The southern ice-marginal zone on the north German plain is characterized by three prominent moraine belts named (from south to north) the **Brandenburg**, **Frankfurt** and **Pomeranian Moraines**. These are not single structures, however, for each comprises a narrow band of subparallel, sometimes branching and occasionally linked ridges. In between lie flatter till plains with minor moraine mounds and kames, incised through which are large abandoned fluvial channels (**Urströmtaler**) which were the principal meltwater conduits along the receding ice margin (Böse, 2005). The geomorphological evidence points to episodic retreat of the last ice sheet from its most southerly position marked by the Brandenburg Moraine (Figure 2.6b).

Radiocarbon dating of organic material beneath the moraine suggests a maximal age for the feature of c. 21 ka ¹⁴C BP (c. 24 ka cal. BP: Chapter 5), which is very similar to the age estimate (23.2 ka) inferred for the Brandenburg Moraines from an annually laminated lake sediment record

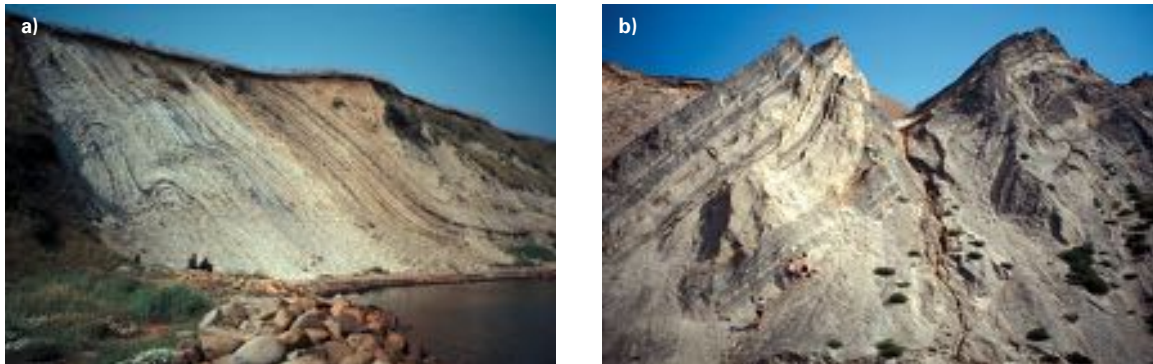


Figure 2.7 a) Cross-section through ice-marginal ridges (push moraines) of Late Weichselian age in the Limfjord Area, Jutland, Denmark, exposing a series of glaciectonally displaced slabs of Eocene diatomite (white cliff faces) with volcanic ash layers (black) overlain by Quaternary diamictites (ice-push from north-east [right to left], cliff height 25 m). b) Up-thrusted and folded Middle Weichselian lacustrine and fluvial sediments exposed on the North Sea coast of northernmost Jutland; deformation is from north to south (left to right) (photographs by Michael Houmark-Nielsen, University of Copenhagen, Denmark).

in the Eifel district of Germany (Zolitschka *et al.*, 2000). The lake sediment data suggest maximal ages for the Frankfurt and Pomeranian stages of 19.7 ka and 16.5 ka, respectively. Cosmogenic radionuclide dating (CRN dating: Chapter 5) of boulders on these moraines implies ice retreat northward from the Brandenburg Moraine around 19 ka, with retreat from the Frankfurt and Pomeranian Moraines c. 18 ka and c. 16 ka, respectively (Heine *et al.*, 2009). These ages are broadly confirmed by more recent CRN of Pomeranian stage deposits which show a tightly clustered distribution of ages between 17.2 and 16.4 ka (Rinterknecht *et al.*, 2012).

Correlations between the north German moraines and those in other parts of Europe have proved problematical. In Denmark the maximum extent of Weichselian ice is marked by the **Mid Jutland** (Figure 2.6b) or **Main Stationary Line**: this is not, however, correlated with the Brandenburg, but with the Frankfurt Moraine, while the more northerly **East Jutland Line** is considered to be a continuation of the Pomeranian Moraine (Lundqvist, 1986; Houmark-Nielsen, 1989). In Poland, the Frankfurt Moraine has been correlated with the **Poznan Moraine** and the Pomeranian with the **Pomorze Moraine**, because more southerly ridges (the **Leszno Moraine** in Poland and the **Belogoye Moraine** in Russia) have been judged to be extensions of the Brandenburg Moraine. Attempts have also been made to link prominent linear ridges in the eastern Baltic region to the Brandenburg–Frankfurt–Pomeranian model, although this frequently rests on visual matching of linear trends and often equivocal stratigraphic evidence. Where CRN dates are available, however, these offer a basis for construction of glacial chronologies and inter-

regional correlation. In the eastern Baltic lowlands, for example, the CRN evidence suggests that the last ice sheet advanced after c. 25 ka, reached its maximal extent by c. 21 ka and began to retreat c. 19 ka, a chronology that is broadly comparable with that obtained for the north German Plain (Rinterknecht *et al.*, 2006). In Poland the **Lezno** phase is CRN-dated to around 24 ka, the **Poznan** phase to c. 19 ka and the **Pomeranian** phase to 17–16 ka BP (Marks, 2012). Further east in Belarus, the maximal extent of the last ice sheet is indicated by the **Orsha Moraine**, with ice retreat from that position dated at 17.7 ka (Rinterknecht *et al.*, 2007). However, subsequent ice wastage of this south-eastern flank of the Scandinavian ice sheet may have been largely through surface thinning rather than marginal retreat (Bitinas, 2012). In the far north, the situation is less clear, for it is only recently that geomorphological evidence from around the Barents Shelf has become available to scientists outside the former USSR, while interpretation of marine records from the Barents Sea is far from straightforward (Svendsen *et al.*, 2004). It does appear, however, that during the Late Weichselian, an extensive and dynamic, possibly multi-domed ice sheet formed over the Svalbard–Barents Sea (Ingólfsson & Landvik, 2013). This extended to Svalbard in the far north and to the edge of the Barents Shelf, and was confluent with the northern margins of the Fennoscandian ice sheet (Figure 2.6a).

More is known about the limits of the last Fennoscandian ice sheet along its western margin due largely to several decades of exploration of submarine deposits for oil and gas. A combination of remote-sensing and marine core data has revealed submarine ridges close to the edge

of the continental shelf with large fans of glaciogenic sediment along the continental slope (Sejrup *et al.*, 2005). These were produced by major ice streams from the mountains of Norway that reached the shelf margin on at least three occasions during the Weichselian, the last being between 28 and 22 ka. Off the northwest coast of Norway, the limit of the last ice advance is marked by the **Egga Moraines**, the oldest of which is dated to > 25 ka (Vorren & Plassen, 2008). Further south, data from exploration activities in the northern North Sea have also helped to settle a long dispute about whether or not the Late Weichselian Fennoscandian ice sheet was confluent with the Late Devensian British ice sheet (section 2.3.2.2), the evidence now suggesting coalescence between the two ice masses in the central North Sea between 29 and 25 ka (Sejrup *et al.*, 2009; Figure 2.6a).

Following the Pomeranian stage, episodic retreat of the last Fennoscandian ice sheet is marked by a series of sub-parallel moraines across northern Denmark and southwest Sweden. From south to north these are the **Halland** (18–16 ka), **Göteborg** (15.4–14.5 ka), **Berghem** (14.4–14.2 ka), **Trollhättan** (14.2 ka) and **Levene Moraines** (13.4 ka) (Lundqvist & Wohlfarth, 2001). The Trollhättan Moraine is correlated with the prominent **Hvaler Moraine** in the outer Oslofjord of southern Norway (Andersen *et al.*, 1995) and possibly with the **Little Fiskebank Moraine** of Denmark (Nesje & Sejrup, 1988). It is not clear, however, whether the linear moraine systems of Germany, Poland and the eastern Baltic are the temporal equivalents of those in Denmark and southern Sweden. Indeed, it seems likely that retreat of the southern ice margin was a time-transgressive process, which was interrupted by both local and regional readvances (Lagerlund & Houmark-Nielsen, 2008).

The best-known and most prominent moraines of the Fennoscandian ice sheet formed as a result of a readvance during the **Younger Dryas Stadial** (c. 12.9–11.7 ka). These have been mapped as almost continuous belts across southern Norway (**Ra Moraines**), Sweden (**Middle Swedish Moraines**) and Finland (**Salpausselkä Moraines**). Along or close to the west coast of Norway, distinctive terminal moraines dated to this period can be traced within a narrow belt stretching from the Russian border in the north to the Swedish border in the south, a distance of some 2,500 km (Andersen *et al.*, 1995). They include the **Herdla Moraines** of the Bergen area and the **Tromsø–Lyngen Moraines** of northwest Norway. Morphologically and genetically, however, the Younger Dryas terminal moraines are very different. In the west of Norway, they frequently comprise single or paired subparallel ridges, while those that terminated in the sea are occasionally associated with prominent ice-front deltas. By contrast, the **Salpausselkä Moraines**

of the northern Baltic consist of three prominent moraine belts commonly over 60 m in height, with the two outermost moraines extending almost continuously for almost 600 km from the coast of southwestern Finland to North Karelia in eastern Finland (Rainio *et al.*, 1995). All were once considered to be true end moraines, but the Salpausselkä consist largely of deltas and smaller till ridges which appear to have formed in the Baltic Ice Lake, the extensive water body that was impounded to the south of the Fennoscandian ice sheet during deglaciation (Björck, 1995). The composition of the Salpausselkä Moraines in eastern Finland was largely determined by the nature of the ice-marginal environment; where the ice terminated in water, massive glaciofluvial sediment sequences accumulated, whereas discontinuous and narrow moraine ridges formed where the ice-front stabilized on dry land. The form of the Salpausselkä Moraines indicates a lobate ice margin, with the outermost of the Salpausselkä ridges possibly marking the most advanced position during the Younger Dryas (Rainio *et al.*, 1995). CRN dating indicates that retreat from the outermost moraine occurred at c. 12.5 ka, which is consistent with an age of 12.3 ka based on varve chronology (Rinterknecht *et al.*, 2004). However, it appears that the Salpausselkä may not be synchronous features throughout southern Finland, but could represent re-advances by different ice lobes at slightly different times.

The same situation obtains in Norway, for new dating evidence indicates that the Younger Dryas maximum occurred significantly later in western Norway than elsewhere in Scandinavia, whereas small glaciers in the north expanded to their maximal positions very early during the Younger Dryas (Bondevik & Mangerud, 2002). These contrasts reflect differing glaciological responses to topographic and climatic factors at different locations around the ice sheet margin and suggest that, on the continental scale at least, former ice limits as shown by geomorphological evidence are more likely to have been metachronous than synchronous. This has implications for ice sheet models derived from such data (section 2.3.4).

During the Holocene, the last ice sheet over Scandinavia retreated from its Younger Dryas limits, although episodic readvances formed moraines some distance beyond younger ('Neoglacial') maxima. These included the **Erdalen Event** between 10.1 and 9.7 ka (Dahl *et al.*, 2002), and the **Finse Event** c. 8.3 ka (Nesje *et al.*, 2000). Between c. 8 and 4 ka, however, most glaciers in Norway had melted completely due to a combination of high summer temperatures and reduced precipitation (Nesje *et al.*, 2008). But throughout the high mountain areas of Norway and Sweden, there is abundant evidence for renewed glacier activity after that time. This consists of 'fresh' and relatively

unvegetated terminal and lateral moraines down-valley from present-day active glaciers (Nesje *et al.*, 2001). In some areas, as many as seven readvances occurred during the late Holocene or ‘Neoglacial’ period (Matthews & Dresser, 2008), the youngest of which occurred during the ‘Little Ice Age’, the period of widespread cooling that lasted from the fourteenth to the eighteenth centuries (section 7.6.3.5).

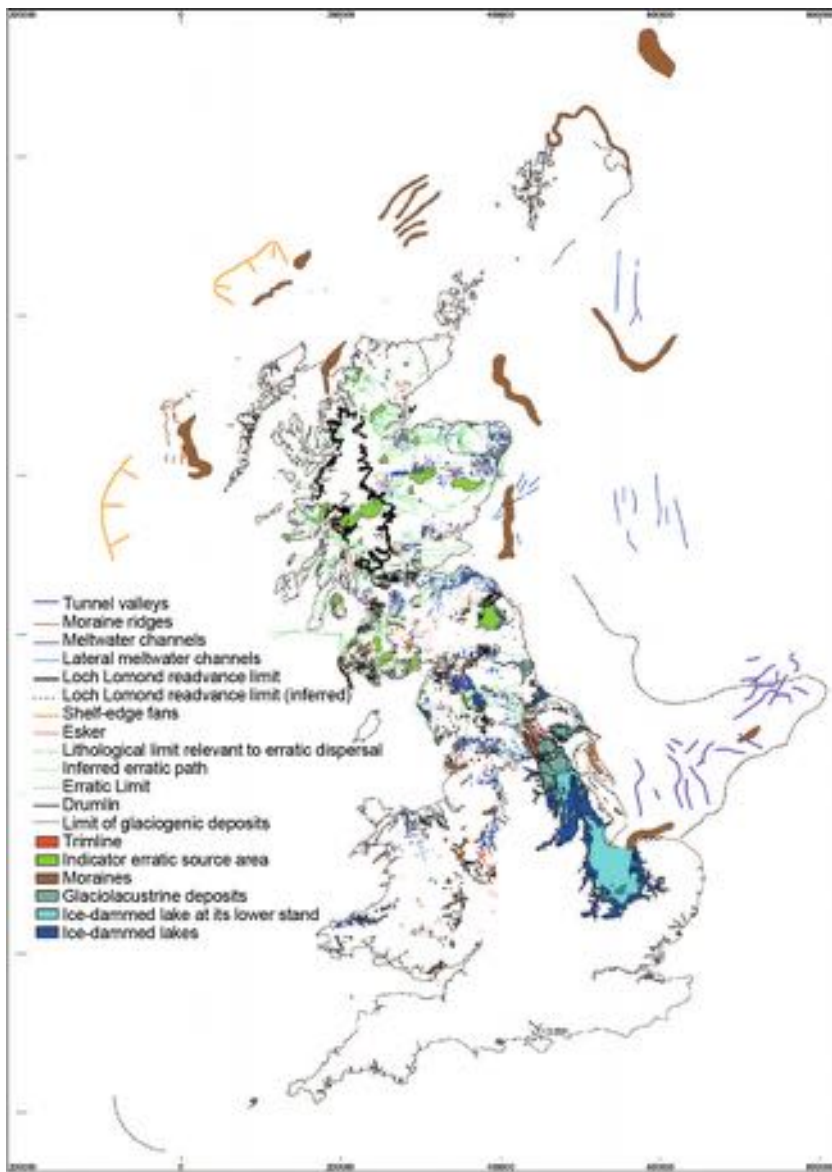
2.3.2.2 Britain and Ireland

In Britain, the maximum expansion of the last ice sheet occurred towards the end of the Devensian cold stage, during the Dimlington Stadial (Rose, 1985). The limits (Figure 2.8) were initially inferred from geomorphological evidence, with products of the Late Devensian ice sheet (‘Newer Drift’) in England and Wales being differentiated from those of earlier glaciations (‘Older Drift’) on the basis of contrasts in degree of dissection and relative preservation of ‘constructional’ glacial topography (Bowen *et al.*, 2002). In Ireland, the ‘South Irish End Moraine’ has long been considered to delimit the maximum extent of Late Midlandian (cf. Late Devensian) ice. In many places, however, the geomorphological evidence is equivocal, and it is clear from more recent stratigraphic records and from other data that the geomorphic features that have traditionally been regarded as marking the maximal limits of the ‘Newer Drift’ may not, in fact, do so. In southwest Wales, for example, it has long been known that the ice maximum lay to the south of the mapped position of the ‘South Wales End Moraine’ (Bowen, 1981), while in Ireland, it is now apparent that the Late Midlandian ice sheet extended well beyond the ‘South Irish End Moraine’ (Ó Cofaigh & Evans, 2007), with a major lobe of ice spreading southwards down the Irish Sea basin to reach the Scilly Isles where it is marked by a well-defined terminal moraine (Hiemstra *et al.*, 2006). Indeed, most of southern Ireland was glaciated at the Last Glacial Maximum (LGM), and hence the morainic belts which have traditionally been interpreted as marking the last glacial limits, such as the South Irish End Moraine, are now considered as recessional features during ice sheet retreat (Ó Cofaigh *et al.*, 2012a). In the Vale of York, it remains uncertain whether the Escrick and York Moraines mark the maximal extent of the Late Devensian ice sheet (as has long been considered to be the case) or whether the ice extended c. 50 km further south into a large ice-dammed lake (Glacial Lake Humber), possibly accompanied by a glacier surge (Evans *et al.*, 2005). In Scotland, the long-held view that areas of northeast Scotland (‘moraineless Buchan’) remained free from glacier ice during the Late Devensian has now been

falsified by CRN dating (Phillips *et al.*, 2008b). Indeed, evidence from offshore (Figure 2.8) shows that ice covered the whole of the Scottish mainland at the Late Devensian maximum (Chiverrell & Thomas, 2010).

As in other areas of Europe (section 2.3.2.1), CRN dating is one of a number of important recent developments that have provided new insights into the dimensions and behaviour of the last British–Irish ice sheet (Ballantyne, 2010). A second is digital elevation mapping based on high-quality satellite imagery by the BRITICE project,⁶ and which provides high-resolution data on glacial landform assemblages that can be viewed at both regional and national scales (Clark *et al.*, 2004; Evans *et al.*, 2005). Landform patterns that reflect ice-marginal or subglacial contexts can be readily distinguished, providing a first approximation of the dimensions and flow patterns of the last British–Irish ice sheet at its maximum extent (Figure 2.8). Third, considerable advances have been made in the mapping of submarine landforms and deposits on the continental shelf (Bradwell *et al.*, 2007) and in the North Sea (Graham *et al.*, 2007). Fourth, the recognition of trimlines in some upland regions has enabled the vertical dimension of the ice sheet to be established and hence regional ice-surface gradients of the last ice sheet to be delimited (McCarroll & Ballantyne, 2000). CRN dating provides the essential chronological control on these landform features (Ballantyne *et al.*, 2008).

Bathymetric data from the seabed around northern Britain has revealed remarkable geomorphological evidence in the form of moraines and tunnel valleys⁷ of the dimensions and behaviour of the former British–Irish and Fennoscandian ice sheets (Bradwell *et al.*, 2008a). At its maximum, a grounded ice sheet flowed southeast to northwest across the northern North Sea basin and terminated at the continental shelf edge, the northwestern part of the ice sheet being most extensive between c. 27 and 25 ka (Everest *et al.*, 2013). The zone of confluence with the much larger Fennoscandian ice sheet was probably across the northern Orkney Islands. The period of maximum confluent glaciation (c. 29–25 ka) was followed by the opening of a marine embayment in the northern North Sea, the decoupling of the two ice sheets and stabilization at new margins marked by a second distinct set of moraines (24–18 ka). The lobate, over-printed morphology of these moraines, particularly on the mid-continental shelf west of Orkney and Shetland, indicates that this reorganization of the British ice sheet was extremely dynamic and punctuated by a series of readvances. To the west of the British Isles, numerous large moraines along the continental shelf record an extensive pattern of retreat stretching from southwest Ireland to the Shetland Isles (Clark *et al.*, 2012).

**Figure 2.8**

Limits of the Late Devensian British ice sheet and principal geomorphological lines of evidence (generalized) on which they are based (from Clark *et al.*, 2004. Copyright © 2008, John Wiley and Sons).

Geochronological data from the Irish Sea basin indicates that the ice maximum in the Celtic Sea to the southeast of Ireland was reached around 25.3–24.5 ka (Chiverrell *et al.*, 2013).

Elsewhere, readvances of the British–Irish ice sheet during deglaciation from the LGM are reflected in both geomorphological and stratigraphic evidence. Prominent moraine complexes up-glacier from the maximal ice limits, such as the Wrexham–Ellesmere–Whitchurch Moraine of

the Cheshire–Shropshire lowlands, have long been regarded as marking readvances of the ice sheet margin. In other areas, a combination of glacial geomorphology and stratigraphy provide firm evidence for readvances, as in the Solway Lowlands of Cumbria (Livingstone *et al.*, 2010) and on the Isle of Man where the stratigraphic succession associated with the major constructional form of the Bride Moraine indicates a readvance episode between 22 and 18 ka (Thomas *et al.*, 2004).

In the Irish Sea Basin, the interdigitation of glaciomarine muds and glacial diamictites also provides compelling evidence for ice-margin readvances, particularly where marine fossils contained within the glaciomarine sediments have been radiocarbon dated. In Dundalk Bay on the northeast coast of Ireland, for example, moraines record two readvances of the ice sheet into the northern Irish Sea basin, the **Clogher Head Readvance** (*c.* 18.3–17.3 ka) and the **Killard Point Readvance** (*c.* 17.1–15.2 ka) (McCabe *et al.*, 2007). In western Ireland, CRN dating of moraines to *c.* 15.6 ka suggests that these also formed during the latter glacial event (Clark *et al.*, 2009a). In western Scotland, glacial erosional and depositional landform assemblages revealed in high-resolution remote sensing datasets indicate renewed ice sheet thickening in the Firth of Clyde during the Killard Point Stadial (Finlayson *et al.*, 2010). Further north, the prominent **Wester Ross Moraine**, a distinctive boulder-strewn linear ridge which extends across the peninsulas of Wester Ross, has been CRN-dated to *c.* 16.3 ka (Everest *et al.*, 2006) and, more recently, to *c.* 14–15.5 ka (Ballantyne *et al.*, 2009), the latter age estimate being very similar to those obtained on major readvance moraines elsewhere in northwest Scotland (Bradwell *et al.*, 2008b).

The most convincing evidence for a renewed period of glacial activity following retreat from the Late Devensian maximum can be found in the uplands of Scotland, northern England, Wales and southern Ireland, where terminal and lateral moraines, spreads of hummocky recessional moraine (Figure 2.4b), well-developed trim-lines on mountain sides (Figure 2.5), intricate meltwater channel systems and the distribution of periglacial features define the limits of the **Loch Lomond Readvance**. This is broadly equivalent to the Younger Dryas readvance of Scandinavia, and is dated to between 12.9 and 11.7 ka (Golledge, 2010). Confirmation of a readvance of ice is provided by radiocarbon dates of *>11.0* ka BP on marine shells which subsequently became incorporated into terminal deposits as ice invaded estuarine localities (Sissons, 1979), and on organic debris buried beneath till (MacLeod *et al.*, 2011).

The freshness and relatively unweathered nature of the landforms have enabled the extent of the readvance to be mapped in great detail (Benn & Ballantyne, 2005; Ballantyne, 2007a). This has not only allowed the ice limits to be established accurately, but has also made possible the reconstruction of individual cirque and valley glaciers (section 2.3.4.2). In many upland areas of Britain, glaciers formed anew during the Loch Lomond Stadial, but in Scotland, where a substantial ice sheet existed across the west-central highlands (Figure 2.8), the episode of renewed

glacier activity now appears to reflect a short-lived re-advance of the downwasting residual mass of the Late Devensian ice sheet (Bradwell *et al.*, 2008b). Some Scottish glaciers seem to have reached their maximum extent during the early part of the Stadial (Golledge, 2010), while others attained maximal positions towards the end of the cold phase (MacLeod *et al.*, 2010). At the onset of the Holocene, glacier ice wasted rapidly and has not reappeared since in the British Isles.

2.3.2.3 North America

There were three major ice sheets in North America during the Wisconsinan: the **Laurentide**, which covered the Canadian Shield and northern USA as far south as the Great Lakes; the **Cordilleran**, in the mountains of Alaska, Yukon and British Columbia; and the **Innuitian** over Ellesmere and the Queen Elizabeth Islands (Figure 2.9a). Smaller mountain glacier complexes also developed over the Rockies in the western USA (Hughes *et al.*, 2013).

The Laurentide ice sheet formed from three ice centres located in Quebec–Labrador, Keewatin and Foxe Basin, near Baffin Island (Dyke *et al.*, 2002), and reached its maximum towards the end of the Wisconsinan (28–25 ka) when it was more extensive than in any previous glacial stage (Andrews & Dyke, 2007). For more than half its length, the outer limit of the ice sheet between the Atlantic Ocean and the Rocky Mountains is marked by prominent terminal moraines, although there are large areas where no geomorphological distinction can be made between Late Wisconsinan and older deposits, and where mapping of the last ice limit rests largely on stratigraphic evidence. Within the Late Wisconsinan limits of the Laurentide ice sheet, end moraines marking possible stillstands or readvances of the ice margin occur (Figure 2.10), and in many areas the deglacial chronology of the last ice sheet can be reconstructed (Dyke, 2004). Unlike western Europe, CRN dating has not been as widely used on moraines around much of the former Laurentide ice sheet margin, but it has been employed to date landforms and exposed bedrock surfaces in the western mountains and Alaska (e.g. Owen *et al.*, 2003; Refsnider *et al.*, 2008; Badding *et al.*, 2013).

In the Great Lakes region, where different ice lobes formed during ice wastage from 15 ka onwards, there are large numbers of end moraines, some of which can be traced over considerable distances and which appear to reflect broadly synchronous regional readvances of the ice margin in both the western and eastern parts of the Great Lakes basin. These include the **Port Huron Advance** in the Erie–Ontario region (*c.* 14.5 ka), the **Greatlakean**

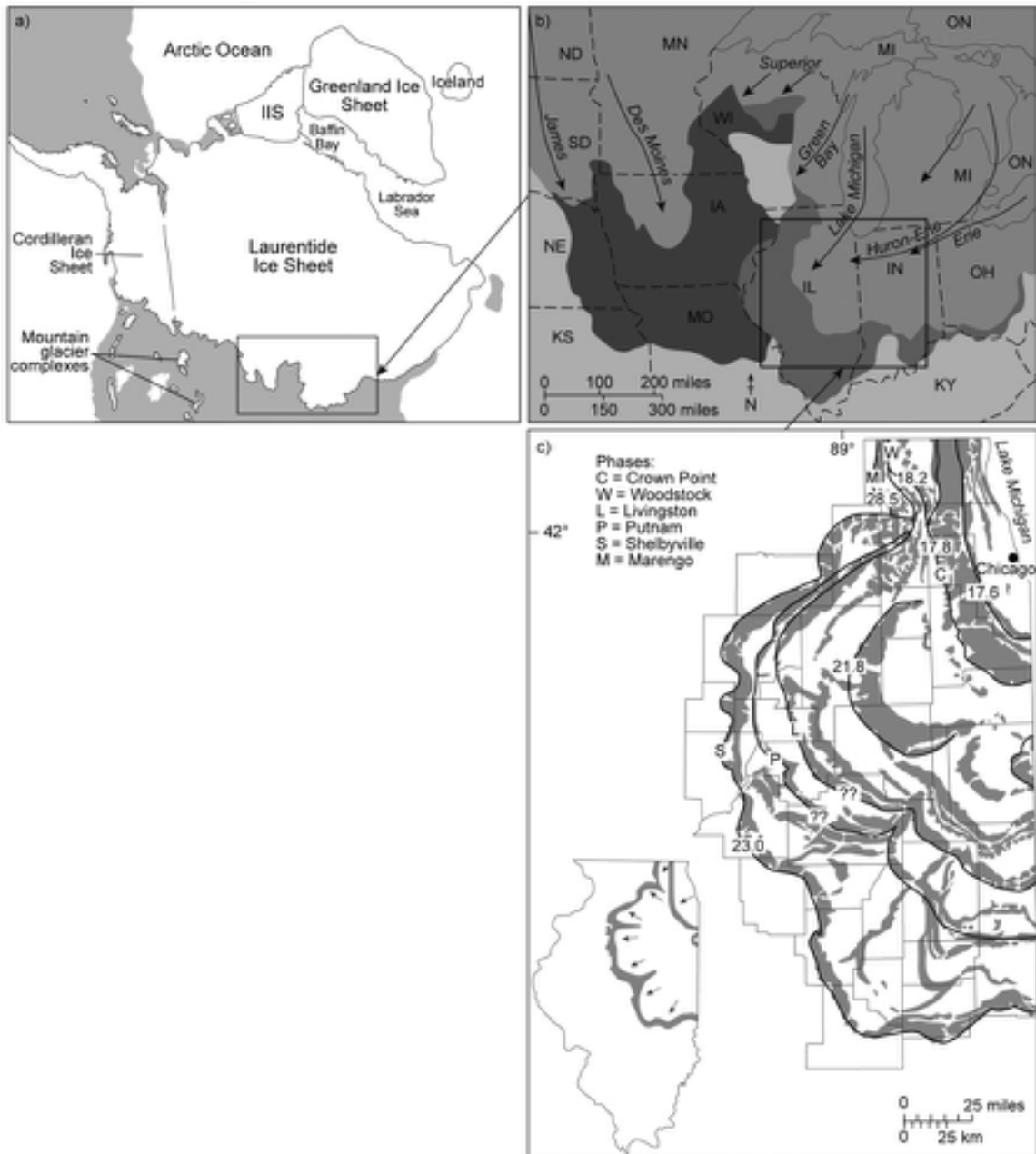
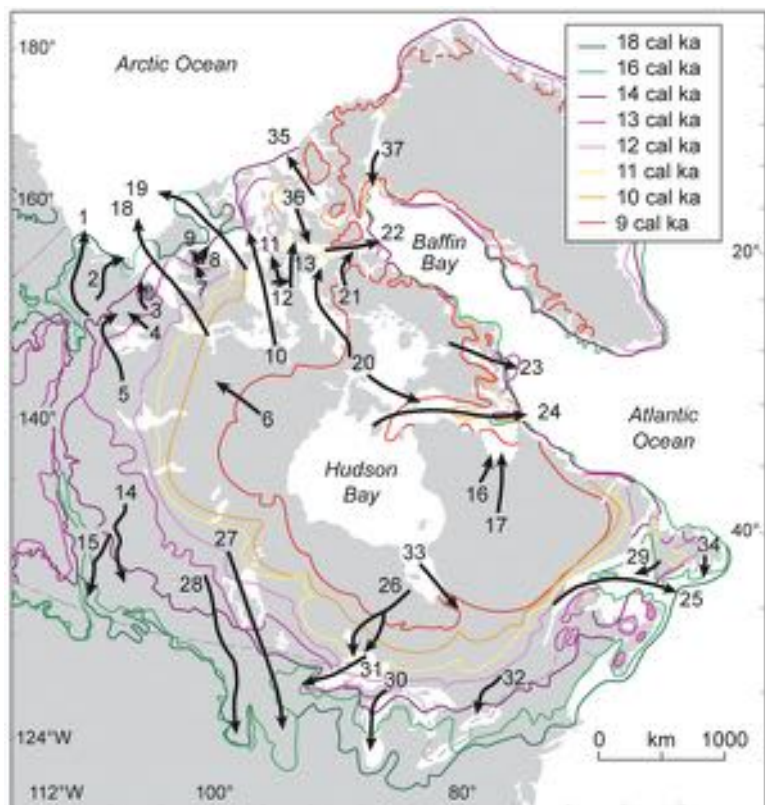


Figure 2.9 a) The Late Weichselian Laurentide, Cordilleran and Innuitian ice sheet (IIS) at the LGM (after Andrews & Dyke, 2007). b) Reconstructed ice lobes in the Great Lakes region at the LGM. c) The pattern of retreat moraines of the Michigan–Huron lobe after the LGM (b) and c) are from Curry *et al.*, 2011).

Figure 2.10

Retreat pattern of the Laurentide ice sheet and estimated ages of major arterial flows or ice streams. The ages are in calibrated radiocarbon years BP (after Stokes & Tarasov, 2010).



Advance in the Michigan, Huron and Green Bay areas (*c.* 13.5–13.2 ka), and the **Marquette Advance** into areas presently occupied by Lake Superior and northern Michigan culminating around 11.7 ka (Larson, 2011). This last-named readvance has been traced along a broad front from the prairies (**Cree Lake Moraine**) to Ontario (**Dog Lake** and **Hartman Moraines**), and along the northern shore of the St Lawrence. There, the prominent **Narcisse** (12.8–12.2 ka) and **Mars Batican Moraines** (12.2–11.5 ka) have been equated with the early and later stages of the Younger Dryas cooling of northwest Europe (Occiatti, 2007).

In many parts of the Great Lakes region, however, the moraine pattern is complex and younger moraines are frequently found overlapping or cross-cutting older landforms. These reflect rapid and irregular changes in the position of the ice margin, driven largely by instabilities within the ice sheet, and which led to repeated glacier surges. These may have been caused by deforming sediments at the glacier bed, as high pore-water pressures in the low-permeability tills of the Great Lakes region created conditions conducive to surging of individual ice lobes

(Hooyer & Iverson, 2002). Surging appears to have been less widespread after *c.* 11.5 ka, by which time the ice sheet margin had retreated northwards onto the more permeable substrates of the Canadian Shield. Further factors promoting surging may have been the degradation of permafrost prior to ice advance, which reduced the shear strength of subglacial materials (Cutler *et al.*, 2000), and the termination of many ice lobes in proglacial lakes that developed around the southern margin of the ice sheet (Cutler *et al.*, 2001). Although extensive, therefore, landform evidence for ice-marginal positions in the Great Lakes region is often difficult to interpret, and recourse must be made to lithostratigraphic and biostratigraphic evidence in order to reconstruct the deglacial sequence of events.

To the west and southwest of the Great Lakes, a range of geomorphological features, including end moraines, outwash fans, meltwater channels and hummocky glacial topography, has been used to infer former ice-marginal positions, while readvances are indicated by truncating and overlapping patterns of end moraines and disintegration features, cross-cutting and overriding relationships of meltwater channels and glacial spillways, and superposed till

units (Fullerton & Clayton, 1986). The landform pattern is complicated by ice advances from different directions that reflect shifting ice divides in the Laurentide ice sheet (Figure 2.9b). In the Dakota–Minnesota–Iowa region, for example, moraines of the earliest glacial advance (>20 ka) from the Hudson Bay/Labrador area are truncated by the [Bemis Moraine](#) (c. 16.25 ka) formed by ice moving south from Keewatin (Lowell *et al.*, 1999). Subsequent fluctuations of the ice margin, possibly reflecting repeated surging, produced a series of cross-cutting moraines (e.g. the [Altamont](#) and [St Croix Moraines](#)) that extend throughout northern Minnesota and northwest Wisconsin. In much of Minnesota, the former ice margins are not marked by single-crested moraine ridges, but more commonly are reflected in broad complexes of hummocky topography (Jennings, 2004; Jennings & Johnson, 2011). These include the [Alexandria Moraine Complex](#) near the centre of the state, which may have been formed by the interaction between four different ice lobes. In southern Wisconsin and Illinois, the sequence is even more complicated with the Lake Michigan ice lobe forming numerous distinctive curvilinear moraines with gently hummocky topography, the morainic pattern delimiting five distinctive sublobes (Figure 2.9c). The maximum southwesterly extent of ice, marked by the extensive [Shelbyville Moraine](#), occurred around 23 ka, after which ice retreated in an irregular fashion, marked by numerous recessional moraines (Curry *et al.*, 2011).

On the Canadian Prairies, the distribution of hummocky drift and patterns of meltwater channels delimit the extent of Late Wisconsinan ice, although geomorphological evidence is absent in many areas and the limits of the last ice sheet can only be established on stratigraphic grounds. Large expanses of hummocky moraine suggest widespread stagnation following the Late Wisconsinan glacial maximum (Eyles *et al.*, 1999), while till lineations and subglacial bedform assemblages revealed by remotely sensed data provide evidence of ice streaming and major changes in ice-flow configuration (Ó Cofaigh *et al.*, 2009; Ross *et al.*, 2009). On the eastern flank of the Laurentide ice sheet, the extensive lateral moraines of the [Saglek](#) system, CRN-dated to c. 13.4 ka (Clark *et al.*, 2003), define the upper limits of the Wisconsinan ice in northern Labrador. Numerous end moraine sequences, dated to between 10 and 9 ka (the [Cockburn Event](#)) and marking recessional stages of the last ice sheet, have been mapped throughout the Canadian Arctic and sub-Arctic. These include moraines of the [Cochrane Advances](#) of the eastern Canadian Arctic, the Hudson Bay region and the James Bay lowlands. This reactivation of the Laurentide ice sheet, which resulted in advances and retreats of up to 75 km from

residual ice over Hudson Bay, has again been attributed to repeated surging of the ice margin (Clark, 1994). Subsequently, two episodes of catastrophic collapse of the ice sheet (at c. 9 ka and 7.5 ka) led to rapid deglaciation. The decaying ice sheet split into three residual masses, those in Keewatin and Labrador Ungava having virtually disappeared by c. 7 ka, leaving only the Barnes Ice cap on Baffin Island as the last vestige of the Laurentide ice sheet.

In the mountains of western North America, the Late Wisconsinan Cordilleran ice sheet covered British Columbia, the southern Yukon Territory, parts of Alaska, and northern areas of Washington, Idaho and Montana. In its major source areas, the high mountain ranges of the Canadian Cordillera, the ice sheet began to develop c. 33–28 ka, and achieved its maximum extent c. 18 ka. Ice sheet decay was rapid and was characterized by complex frontal retreat at the periphery, accompanied locally by brief readvances, and by downwasting and stagnation (Clague & James, 2002). Further south, valley and piedmont glaciers left abundant evidence in the form of lateral and terminal moraines, outwash terraces and trimlines which mark the maximal extent of Wisconsinan ice, and also recessional stages and readvances during deglaciation. In the southern and central cordillera, for example, nested moraines of Wisconsinan age show that ice descended from the eastern flanks of the mountains into the Great Basin of the western USA, sourced from up to forty individual ranges, plateaux or massifs (Osborn & Bevis, 2001). In California, the CRN-dated [Tahoe Moraines](#) (Figure 2.11) show that many valley glaciers in the Sierra Nevada reached their maximum extent in the Early and Middle Wisconsinan, while later ice advances, which terminated further up-valley, are marked by the [Tioga Moraines](#) (Sampson & Smith, 2006). Although an Early Wisconsinan glacial advance may have occurred further north in the Rocky Mountains of Idaho, Colorado and Wyoming, there are few surviving moraines that date to this period, in contrast to the widely developed [Pinedale Moraines](#) of the Late Wisconsinan (Pierce, 2003). Moraines resulting from glacier readvances that may equate with the Younger Dryas of Europe include those of the [Crowfoot Advance](#) in Glacier National Park, Montana (MacLeod *et al.*, 2006), the [Titcomb Lakes Moraine](#) in the Wind River Mountains, Wyoming (Gosse *et al.*, 1995), the multiple moraines of the [Sumas Drift](#) in the Fraser Lowland of Washington and British Columbia (Kovanen & Easterbrook, 2002), and the [Finlay Moraines](#) of northern British Columbia (Lakeman *et al.*, 2008).

Some of the most prominent moraine sequences formed during glacier readvances in the [Neoglacial period](#) of the mid- and late-Holocene. In the southern Coast Mountains of British Columbia, the earliest of these

**Figure 2.11**

Wisconsinan terminal moraines dating to the Tahoe series in Pine Creek Canyon on the eastern flank of the Sierra Nevada, near Bishop, California (photograph by Ron Wolf, EyeOnNature.com).

date to *c.* 8.6–8.0 ka (Osborn *et al.*, 2007), while readvances from *c.* 7.5 ka have been reported in the Canadian Rockies (Luckman *et al.*, 1993) and from *c.* 9.5–8.4 ka further south in Washington state (Thomas *et al.*, 2000). In Alaska, the earliest Neoglacial advances appear to have occurred much later, around 4 ka (Barclay *et al.*, 2009). Subsequent readvances, many marked by well-developed moraines, include the **Tiedemann–Peyto Advance** of the Canadian Rockies which are dated to *c.* 3.5–1.9 ka (Clague *et al.*, 2009). Radiocarbon dates and lichen-dated moraines suggest that a widespread advance occurred in many regions of the Pacific North American cordillera between AD 400 and 700 (Reyes *et al.*, 2006), but the most widespread late Holocene advances appear to have occurred during the **Little Ice Age**, with a number of glaciers achieving their maximal Holocene extent at that time (Luckman, 2000; Barclay *et al.*, 2009). In the Coast Mountains of British Columbia, ten separate moraine-building episodes have been identified from around AD 1450, with glacier readvances occurring, on average, every 65 years (Larocque & Smith, 2003).

The third of the great ice masses of North America, the Innuitian ice sheet, reached its maximum after *c.* 22 ka, at which time ice caps that had formed over the mountains of eastern Ellesmere Island were confluent with the western margins of the Greenland ice sheet, the configuration of the Ellesmere Island and Greenland ice being based on moraine and meltwater channel patterns and on erratic distributions (England, 1999). To the south, the ice sheet was confluent with the northern sector of the Laurentide ice sheet (Figure 2.9a). Retreat of the Innuitian ice sheet began along the southwestern margins around 13 ka, considerably later

than in the Laurentide ice sheet to the south, with the absence of deglacial landforms in some areas prior to 11 ka BP suggesting that the majority of the retreat post-dates the Younger Dryas (England *et al.*, 2006). By contrast, retreat of the Greenland ice sheet from the West Greenland shelf bordering Baffin Bay (Figure 2.9a) began much earlier (*c.* 14.9 ka), and there is evidence for an extensive readvance of outlet glaciers during the Younger Dryas Stadial (Ó Cofaigh *et al.*, 2012b).

Glacial landforms therefore continue to act as a cornerstone in establishing the extent of former glacier ice. They are of greatest value in the investigation of recent (i.e. Lateglacial and Neoglacial) patterns of glacier activity, especially in highland regions where the features are often well preserved and relatively easily mapped, and from which the vertical and lateral extent of ice can often be reconstructed. For earlier glacial episodes, morainic landforms in particular can still be used to delimit the glacierized area, and as a basis for mapping of readvances, although it is clear that a proper appreciation of glacial and deglacial sequences rests as much on stratigraphic verification as on geomorphological evidence. This is considered further in Chapter 3. Meanwhile, one further line of evidence is required before ice sheets and glaciers can be reconstructed, namely the former directions of ice movement, and it is to this aspect of glacial landforms that we now turn our attention.

2.3.3 Direction of ice movement

In many formerly glaciated areas, a ‘grain’ or streamlined sculpture is evident in the landscape (Figure 2.3) reflecting

the former direction of ice movement. At a small scale, bedrock protuberances are scratched (striated), fractured, polished and grooved, and at larger scales, whalebacks, *roches moutonnées*⁸ and glaciated valleys (troughs) are fashioned by overriding ice. This preferred alignment of erosional forms in a glaciated landscape is often best seen where ice has emphasized local bedrock contrasts, particularly when exploiting the trend of geological weaknesses such as relatively incompetent strata and joint and fault lines (Bennett & Glasser, 2009; Benn & Evans, 2010). Certain glacial depositional landforms, such as drumlins and fluted moraines (section 2.3.3.4), may also be aligned in the direction of glacier flow. Careful field mapping and remote sensing of landforms that are ice-directed, therefore, allows the dominant patterns of ice movement to be reconstructed.

2.3.3.1 *Striations*

Striations (or **striae**) form where stones entrained within the basal layers of the ice are dragged across bedrock surfaces, the size of the indentation being determined by the load and relative hardness of the stone and the substrate across which it is dragged. The plotting of striation trends is a relatively straightforward field exercise and, given the availability of exposed striated bedrock, regional directions of ice movement can often be ascertained fairly rapidly. Where the evidence is abundant and has been mapped over a sufficiently large area (e.g. Catto, 1998), the dominant directions of ice movement become apparent, and the results may reveal local deflections of ice flow caused by topographic obstructions and interference between competing ice streams (Figure 2.12).

In practice, however, the interpretation of striation data is seldom straightforward. Not all ‘scratch marks’ on bedrock surfaces in formerly glaciated regions have resulted from the passage of ice. Many may simply reflect lines of weaknesses in the rock, accentuated perhaps by subaerial weathering, while others may have resulted from fluvial, glaciofluvial, snowcreep or avalanche activity. Where striations are of glacial origin, they may indicate basal ice movements determined by local bedrock irregularities. They can frequently be seen, for example, to follow the curvature of the face of bedrock protuberances, and on the lee sides (with respect to ice movement) of rock obstacles are often oblique to the dominant or regional direction of glacier flow. In some areas, diverging sets of striae can reflect more than one direction of ice movement, while on certain rock outcrops striations with significantly different trends may be found crossing or superimposed upon one another. **Crossing striae** can arise where

glaciological conditions have changed over time, or when ice has readvanced into a region. If the later ice advance has a different direction of flow and the striations resulting from the initial ice advance have not been completely erased, a second set of striations will become superimposed upon the earlier ones (Figure 2.12). In some instances, it may be possible to distinguish between sets of cross-striations of different age; for example, in Snowdonia in North Wales, striae produced by the last ice sheet can be differentiated from those superimposed upon them by ice of the later Loch Lomond (Younger Dryas) Stadial (Sharp *et al.*, 1989). In most areas, however, such distinctions are difficult to make. Overall, therefore, it would seem that striations are best used in conjunction with other lines of evidence in the reconstruction of regional patterns of ice movement.

2.3.3.2 *Friction cracks*

A range of bedrock fractures or arcuate ‘**friction cracks**’ results from stones in basal ice being forced against underlying bedrock (Glasser & Bennett, 2004). The best known are ‘**crescentic gouges**’ and ‘**crescentic fractures**’. Crescentic gouges are believed to form concave down-ice and crescentic fractures concave up-ice, the direction of concavity reflecting the former direction of ice movement (Figure 2.13). Consistent patterns do not always emerge, however, and the use of friction cracks in isolation as ice-directional indicators now seems a doubtful procedure, although friction-crack data often lend useful support to the reconstruction of regional ice-flow patterns and past glacier activity based on other lines of evidence (Kelly *et al.*, 2004).

2.3.3.3 *Ice-moulded (streamlined) bedrock*

An irregular bedrock surface presents numerous obstacles to the passage of ice. This leads to compression of the ice and erosion of the upstream (stoss) sides of the obstruction, whereas plucked and shattered craggy surfaces tend to characterize the downstream (lee) sides. A series of bedrock ridges running at right angles to the direction of basal ice flow will, after prolonged glaciation, be smoothed only on the up-ice side to form **stoss-and-lee** landforms, and if a consistent pattern is evident in the landscape, this can be used to infer ice-flow directions. Where a bedrock ridge runs parallel to the direction of ice flow, the bedrock will become smoothed on the up-ice side and also along the flanks to produce the landforms known as **roches moutonnées** or ‘**whalebacks**’. The process of smoothing operates at a range of scales, from micro-features etched on

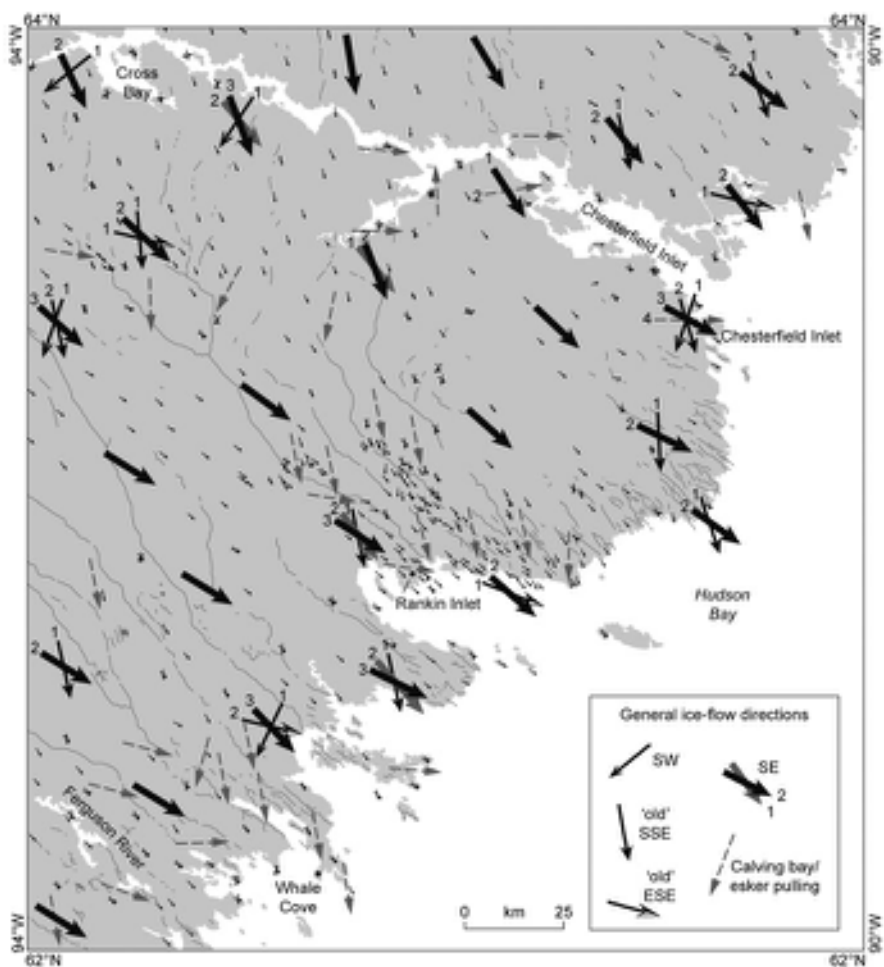


Figure 2.12 Local ice-flow direction based on mapping of lineations of striations in the Keewatin district of Nunavut, northern Canada. Crossing striation patterns are indicative of changing ice dynamics, with the older sets reflecting ice advance, while younger striations result from ice-divide migration and diversion of flow towards melting ice margins in Hudson Bay (after McMartin & Henderson, 2004).

polished bedrock surfaces, visible only by close observation, through ‘**mega-grooved**’ terrain composed of linear, parallel bedrock undulations of a few metres in vertical amplitude (Figure 2.13), to whole mountain sides worn by the passage of ice (Bradwell *et al.*, 2008c). Where localized outcrops of particularly resistant bedrock occur, such as volcanic plugs, these serve to protect the bedrock on the lee side and glacial erosion results in the development of a **crag-and-tail** feature, the orientation of the often drift-veneered ‘tail’ indicating the former direction of ice movement. The overall directional ‘grain’ imposed on the landscape is commonly described as **glacially sculpted** or

glacially moulded terrain (Figure 2.13) and, where strongly developed, may indicate the courses of **palaeo-ice streams**, the former arterial pathways of fast-flowing ice moving from source areas towards the ice sheet margins. Ice streams may also be reflected in patterns of **glacial troughs**, for while over-deepening of pre-existing valleys commonly occurs during ice-sheet build-up, troughs continue to constitute the principal avenues of flow within the resulting ice sheet. By plotting the trends of glacial troughs, therefore, the major routes taken not only by valley glaciers but also ice streams beneath the former ice sheets can be established, and centres of ice accumulation and dispersal can

**Figure 2.13**

Mega-grooved bedrock surface showing parallel striations and gouge-marks, including crescentic fractures, located in the vicinity of the present-day terminus of the Findelengletscher, near Zermatt and the Matterhorn, Switzerland (photograph by John Lowe).

be identified. The mapping and analysis of ice-moulded landforms, in conjunction with other ice-directional indicators such as striations and friction cracks, can therefore provide important insights into former directions of ice flow and positions of ice divides, although the fact that some large-scale ice-moulded features can survive more than one phase of glaciation can lead to problems of interpretation where the direction of ice movement has changed between successive glacial episodes.

2.3.3.4 Streamlined glacial deposits

Subglacial debris deposited beneath moving ice is frequently streamlined in the direction of ice movement (Figure 2.3). Streamlined glacial deposits are often found in glaciated landscapes and range in size from small-scale **fluted moraine** with heights of a metre or less (Glasser & Hambrey, 2001) to larger flutes and **drumlins** (see below) sometimes comprising drift accumulations some tens of metres in thickness (Clark *et al.*, 2009b). These depositional landforms invariably record the basal movements of the last ice mass to have affected an area, for any subsequent glacier with a different direction of movement would have erased or at least substantially modified such features. Almost all of the detailed work that has been published on drumlins and fluted moraines relates to forms that have developed in drift of the last glaciation.

Drumlins are among the most intensively studied of all glacial landforms, with at least 1,300 contributions in the literature and more than 400 scientific papers since 1980 alone (Clark *et al.*, 2009a). They are low hills with an oval

outline, usually less than 60 m in height, and are composed mainly of till, although some contain stratified material and have a bedrock core (Figure 2.14). They frequently occur in ‘fields’ or ‘swarms’ in lowland areas where there was little obstruction to the passage of ice, or in piedmont zones where flow was radiative or dispersive. Most possess a prominent stoss end with a trailing distal slope. It is generally agreed that the direction of the drumlin long axis reflects local direction of ice movement with the stoss end pointing up-glacier, and hence they have been particularly widely used as ice-directional indicators (e.g. Greenwood & Clark, 2009). Detailed field mapping of drumlins reveals the dominant local ice-flow paths that prevailed over a



Figure 2.14 A drumlin in the Eden Valley, northwest England, that formed beneath the last British–Irish ice sheet; ice flowed from right to left across the photograph (photograph by Mike Walker).

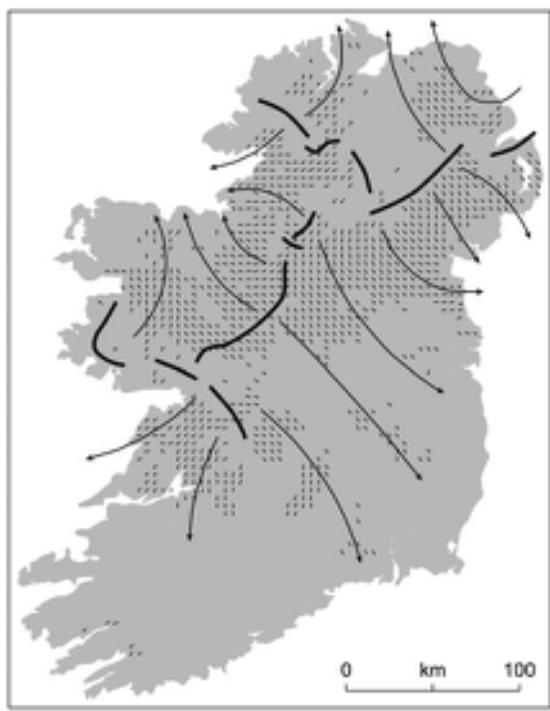


Figure 2.15 Lineation of subglacial landform suites (mostly drumlins) formed by the last (Late Midlandian) Irish ice sheet. These enable regional flow-lines (arrows) and principal ice divides (thick black lines) to be inferred (after Greenwood & Clark, 2009).

particular region and, when the evidence is viewed collectively, macro-scale patterns of ice movement frequently become apparent (Figure 2.15). More than any other line of evidence, perhaps, maps based on drumlins and other streamlined deposits have provided the most striking images of the major arterial flow systems of the last great ice sheets. However, drumlins remain enigmatic features, for while it is generally agreed that they form in the subglacial environment as a response to fluctuating stress and strain conditions within a deforming sediment layer trapped between a rigid bed and overlying mobile ice (Hart, 1997), precisely how they develop continues to be the subject of considerable debate (Benn & Evans, 2010).

In addition to the regional ice flow trends displayed by their long axes, the overall shape and distribution of drumlins can provide information on former glacier dynamics, such as basal ice pressure, rate and type of ice flow, and basal shear stress variations (Mooers, 1989). Numerous shape indices have been developed using axial and outline ratios (Briner, 2007; Hess & Briner, 2009) that

enable comparisons to be made between drumlins in different areas. These studies frequently equate elongation ratios with relative speed of ice flow during drumlin formation, a notion that is supported by remotely sensed images of bedforms beneath the present-day polar ice sheets (King *et al.*, 2009a). Although most measurements of drumlin shapes have been made from maps and aerial photographs, detailed field mapping is essential, for subtleties in form are not always expressed on topographic maps, or may not always be clearly identifiable on aerial photographs.

2.3.4 Reconstruction of former ice masses

2.3.4.1 Ice-sheet modelling

Glacial landforms provide empirical evidence for determining the margins, upper limits and, to an extent, the internal architecture of former ice sheets. For example, ice-directional indicators such as drumlins, fluted moraines, drift lineations and striations, in association with evidence from glacial erratics and till provenance studies (section 3.3), enable the principal flow lines of the ice to be established, from which major ice-dispersal centres, ice domes and ice divides can be inferred. Such reconstructions have improved substantially in recent years with the development of remote sensing techniques, for these enable many more features and much larger areas to be surveyed than is possible by mapping on the ground. The flow paths of the last ice sheet in Ireland (Figure 2.15), for example, have been reconstructed by mapping more than 39,000 individual landforms from satellite images (Greenwood & Clark, 2009). Large data-sets such as these provide important baseline information for modelling former glaciers and ice sheets.

Models of glacier and ice sheet behaviour are based on established physical parameters that govern ice flow rate and surface form. As glaciers increase in thickness, the ice deforms and flows, the rate and direction of which is determined, *inter alia*, by ice volume, glacier length/thickness ratio, inclination of underlying topography and ice temperature (Ng *et al.*, 2010). Ice will flow from high surface points (e.g. ice domes) to lower areas (e.g. ice margins), but if the ice is sufficiently thick, the basal layers can be forced to flow uphill, for example over saddles between adjacent valleys or up-gradient into ice-free valleys. The rate of build-up of the ice, and hence of migration of ice margins, will depend on the **mass balance** of the ice, the ratio between the total amount of snow added to the glacier system and the amount lost through melting and other processes (Paterson, 1994; Knight, 1999).

Simulations of the growth and behaviour of glacial ice masses can be developed from empirically tested mass balance and ice-flow equations (Carr & Coleman, 2007), and for individual cirque or valley glaciers, a simple Excel spreadsheet model is available (Benn & Hulton, 2010). Numerical simulations of ice sheets are more complicated, however, since these have multiple ice centres with complex flow paths, and they take much longer to achieve equilibrium states (Siegent, 2001). Nevertheless, steady-state models of the last great ice sheets have been developed (Marshall *et al.*, 2002) that integrate the physical behaviour of ice, the underlying topography and assumed climatic variables (e.g. Figure 2.16). In addition, dynamic numerical models that are calibrated against geomorphological and geophysical data (relative sea level, marine limits, present-day rates of uplift, etc.), enable the inception and growth of ice sheets, and their behaviour over time, to be simulated (Stokes *et al.*, 2012). In some instances, models can simulate ice sheet behaviour over very long timescales, such as the growth and collapse of the West Antarctic ice sheet over several million years (Pollard & DeConto, 2009). In these cases, outputs of the models can be tested against reconstructions based on empirical data (e.g. Stokes & Tarasov, 2010), and compared with the behaviour of modern ice sheets.

Where ice sheet models are prescribed to yield outputs that approximate empirically based (field-based) reconstructions, they are referred to as **inverse models**. In the models shown in Figure 2.17, the southern and western margins of the Late Devensian ice sheet (cf. Figure 2.8) were predetermined by the geomorphological evidence for the positions of the ice margins, and the input parameters were varied to influence simulation outputs. For example, by altering basal shear stress values, the resulting simulated ice

sheet might be independent from (Figure 2.17b) or confluent with (Figure 2.17a) the Scandinavian ice sheet. But simply using ice-marginal evidence to constrain the models may not be sufficient to generate simulations that explain all aspects of the geological evidence for former ice masses. For example, as we have seen above, the last British ice sheet appears to have been confluent with Scandinavian ice at least during the early stages of the last cold stage, and hence the eastern ice margin cannot be clearly delimited. In addition, geomorphological and geophysical evidence suggest that the ice sheet had a relatively low profile, low summit elevation, and extensive elongated lobes at the ice margin (Figure 2.17). In order to explain these characteristics, Boulton and Hagdorn (2006) developed a dynamic thermo-mechanically coupled ice sheet model, driven by proxy climate, which simulated the behaviour of the British ice sheet throughout the last glacial cycle. This showed that the ice sheet may indeed have been confluent with the Scandinavian ice sheet during parts of its history, and that unforced periodic and asynchronous oscillations could have occurred in different areas of the ice marginal zones creating the distinctive ice lobes. These are indicative of streaming within the ice which drew down ice from the ice sheet interior (Figure 2.18). The interior ice on upland surfaces thinned as a result and was largely cold-based or immobile, while the ice streams were warm-based and flowed at rates of up to 500–1,000 m yr⁻¹ compared with a surface velocity of 10–50 m yr⁻¹ in interstream zones. The simulations suggest that 60–84 per cent of the ice flux was delivered to the margins via the ice streams.

In northern Europe, ice-sheet numerical modelling was used to reconstruct a history of the Eurasian ice sheet during the last glacial cycle that again was compatible with

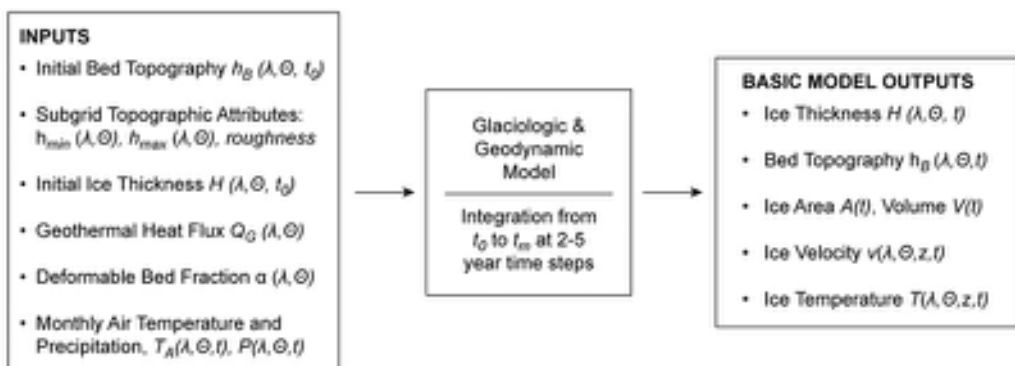


Figure 2.16 Examples of input and output parameters employed in a numerical model simulation of the last Laurentide ice sheet (from Marshall *et al.*, 2002).

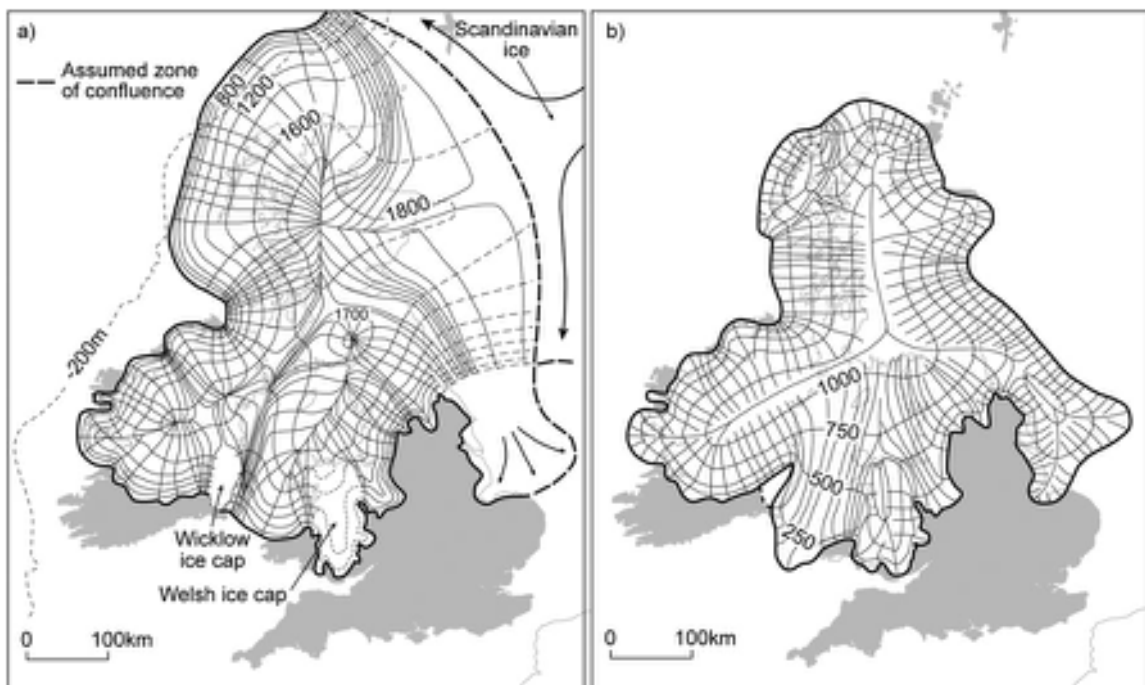


Figure 2.17 Inverse models of the last (Late Devensian) British ice sheet. For a) the basal shear stress is assumed to be 100 kPa⁹ throughout, while in b) the basal shear stress is 70 kPa on the modern land and 30 kPa outside the modern coastline (from Boulton & Haggard, 2006).

a range of geological datasets, including evidence for ice-sheet limits, sedimentary records of palaeo-ice streams and uplift information relating to ice-sheet configuration and the overall pattern of deglaciation. The result was a quantitative assessment of the behaviour of the ice sheet, its mass balance and climate, and predictions of glaciological outputs, including sediments, icebergs and meltwater (Siegert & Dowdeswell, 2004). In North America, a modelling exercise of the Laurentide ice sheet by Marshall *et al.* (2002) generated 190 different simulations for a range of combinations of input variables (Figure 2.16), and run over a model period of 17 ka, which is the approximate time taken for the last ice sheet to reach its greatest extent at the LGM. Of these, thirty-three simulations closely resemble the geomorphologically determined LGM limits (Figure 2.19), when the ice volume is estimated to have been between 28.5 and $38.9 \times 10^{15} \text{ m}^3$ (Marshall *et al.*, 2002). Both empirically based and simulated models confirm the locations of maximum ice thickness at the LGM. For the Laurentide ice sheet, this was over Hudson Bay, with a surface altitude in excess of 3.5 km (Figure 2.19), while the Fennoscandian ice sheet was thickest in the western part of

the Gulf of Bothnia, where the surface altitude was around 2,000 m (Arnold & Sharp, 2002).

Models such as these not only provide insights into the dynamic nature of ice sheets, but also the scale of their environmental impacts. As ice sheets grow in size, they influence local wind patterns, changing the supply routes for snow, and ultimately leading to migration of ice divides. In the case of the Laurentide ice sheet, for example, the ice domes were sufficiently large to prevent snow-bearing winds from reaching the original source areas. Moisture-bearing air masses would have been forced to rise over the expanding ice on lower ground, depositing more snow than previously, before reaching the mountains. A positive feedback mechanism accentuates this situation, creating a '**snow shadow**' (equivalent to rain shadow) effect that increasingly isolates the original snow gathering grounds. Ice-sheet models also provide insights into past sea-level changes resulting from ice-sheet melting. For example, a model simulation of the Greenland ice sheet, forced by data from an independent climatic model, and constrained by empirical evidence from Greenland ice cores, indicates that Greenland ice melt contributed at least 0.6 m to

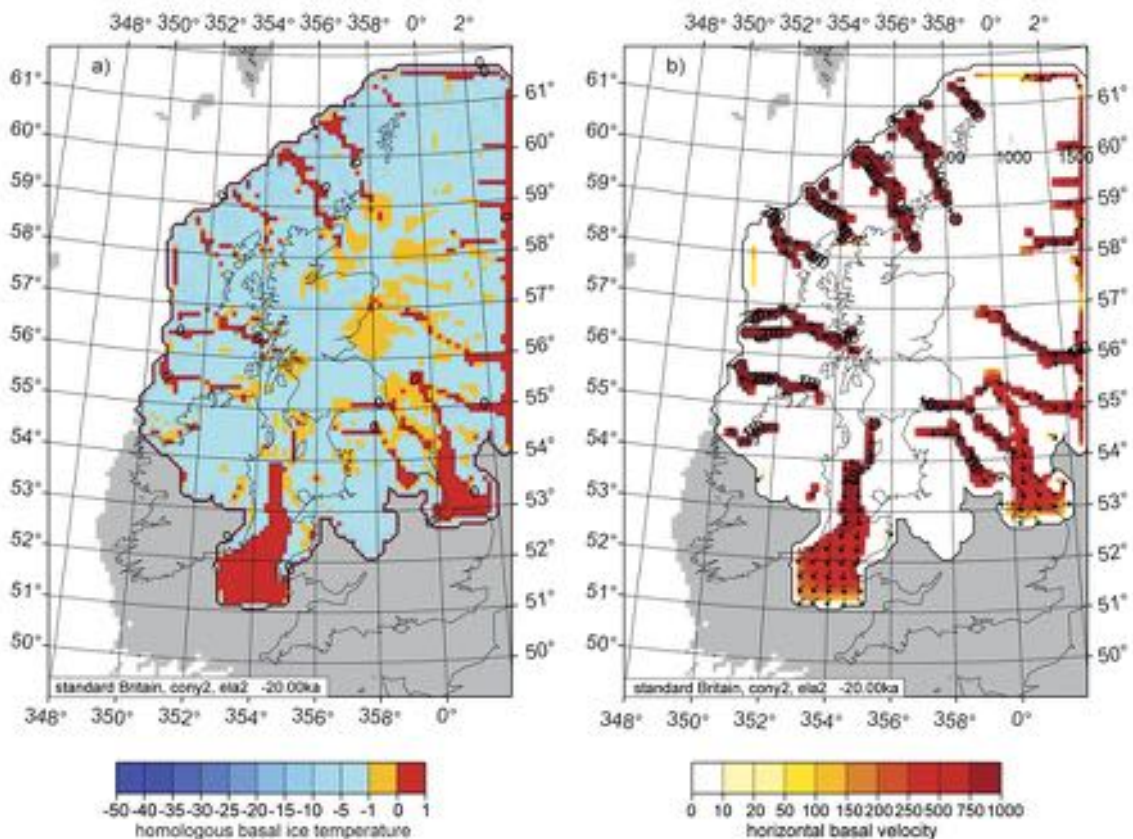


Figure 2.18 a) Simulated basal ice temperature and b) horizontal basal velocity of an ice sheet generated by proxy climate inputs over a model-equivalent period of 17 ka, considered equivalent to LGM conditions. See text for further explanation (from Boulton & Hagdorn, 2006).

sea-level rise during the Last Interglacial (Stone *et al.*, 2013).

Numerical reconstructions of ice sheets may also help explain many of the observed geomorphological characteristics of glaciated landscapes. Of particular significance are **ice divides**, those parts of a former ice mass where flow was radiative or dispersive. Erosion is believed to be minimal in such areas, and hence ancient land surface features, such as tors, may be preserved despite the fact that they were covered by considerable thicknesses of ice (Phillips *et al.*, 2006; Goodfellow, 2007). However, non-eroded pre-glacial features tend to be preserved only in those areas where ice divides remained fixed throughout a glacial cycle. Where ice divide migration occurred, as the ice sheet models predict for parts of the Laurentide ice sheet, no areas seem to have escaped the effects of erosion. In Keewatin, for example, crossing striations and super-

imposed streamlined landforms suggest migrations of the main ice divide by up to 500 km (McMartin & Henderson, 2004).

In addition to reconstructing the Quaternary ice sheets, models have been developed that simulate the behaviour of the present Antarctic and Greenland ice sheets (Payne, 1999; Denton & Hughes, 2002). Climatic and glaciological data from contemporary glaciated regions provide modern analogues for the last great ice sheets at the LGM. Such models of the polar ice sheets can help clarify the location of ice streams (Bamber & Rivera, 2007), the processes leading to the development of subglacial lakes (Siegent, 2005) and the transient positions of **grounding lines** (where the ice margin remains in contact with the substrate beneath, rather than floating), an important consideration for mass balance calculations (e.g. Conway *et al.*, 1999). The models also provide a basis for estimating future glacio-

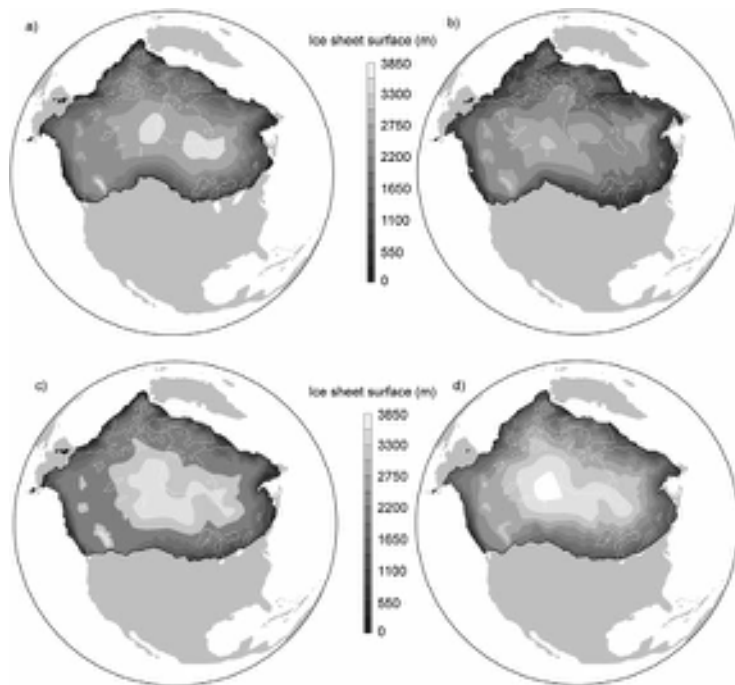


Figure 2.19 Four numerical simulation models of the ice sheets over North America at the LGM based on different combinations of input variables. In each case, the ice margin is fixed, but different model parameters generate different ice-sheet configurations reflected, for example, in the number and locations of the main ice domes (after Marshall *et al.*, 2002).

logical changes, particularly under scenarios of human-induced global warming (Huybrechts, 2006). Modelling results suggest that the ice sheets are more sensitive to warming than previously thought (Alley *et al.*, 2005), inducing fears of accelerated sea-level rise (Overpeck *et al.*, 2006). The modelling results can be compared with data from satellite measurements. In the period 1992–2002, for example, these show that the Greenland ice sheet thinned at its margins, the West Antarctic ice sheet also lost mass, while the East Antarctic ice mass gained a small amount (Zwally *et al.*, 2005). Subsequent measurements between 2002 and 2005 by the Gravity Recovery and Climate Experiment (GRACE) satellite monitoring system have confirmed these trends, the data suggesting an overall ice loss equivalent to a sea-level rise of $0.47 \text{ mm} \pm 0.1 \text{ mm a}^{-1}$ (Ramillien *et al.*, 2006). These and other data suggest that ice sheets are more dynamic than previously believed, and that, valuable as they are, numerical models do not at present capture this dynamism adequately (Bamber *et al.*, 2007). It is important that improvements continue to be made in glaciological modelling, for ice sheets play crucial roles in the global environmental system, as we shall see again in Chapter 7.

2.3.4.2 Ice caps and glaciers

More detailed reconstructions are possible for smaller ice caps and for glaciers that were restricted to cirque and valley situations. These include many of the Loch Lomond Readvance glaciers of Britain (Benn & Ballantyne, 2005), the Younger Dryas and early Holocene glaciers and ice caps of Scandinavia (Bakke *et al.*, 2005) and the Neoglacial glaciers that developed in the mountains of both the Northern and Southern Hemispheres (Klok & Oerlemans, 2004; Thompson Davis *et al.*, 2009). The shape of the former glacier margin can be traced by joining those points or areas where clear ice-marginal evidence (e.g. terminal or lateral moraines, trimlines or valley side drift-limits) is preserved (Figure 2.4b). However, while glaciers often leave abundant depositional evidence in the lower ablation zones, there is little in the higher accumulation zones, and if trimline evidence is unavailable, then extrapolation between scattered ice-marginal indicators becomes necessary in order to delimit the former glacier. When the glacier outline has been reconstructed, ice-surface contours can be inferred by analogy with typical contour patterns on present-day glaciers (Figure 2.20). These are commonly

**Figure 2.20**

Reconstruction of the Loch Lomond (Younger Dryas) Stadial icefield in the Pass of Drumochter area, Scottish Highlands, based on the type and distribution of the glacial geomorphological features shown in Figure 2.1 (from Benn & Ballantyne, 2005).

normal to valley walls near the median altitude of a valley glacier, and become progressively more convex towards the glacier terminus and more concave towards the upper reaches (glacier source). In practice, contour drawing is constrained by features indicating direction of ice movement, such as striae and fluted moraines, for contours tend to be normal to direction of ice movement.

Once the ice-surface contours have been drawn, the altitude of the **equilibrium line** can be estimated. The equilibrium line is the line on a glacier separating the **accumulation area**, the area where the glacier gains in mass, from the **ablation area** where a net loss of mass occurs. A term that is often used synonymously with equilibrium line is **firn line**, which is the altitude on a glacier surface to which

consolidated granular snow (**firn**) recedes on surviving a full summer season's melt (Figure 2.21). In fact, the two are not quite the same¹⁰ but for the purposes of the present discussion, the **equilibrium line altitude (ELA)** and **firn line altitude (FLA)** can be taken to be synonymous. Once the ELA/FLA has been established for individual glaciers, the regional firn line (or snowline) can then be reconstructed either by averaging the altitudes from individual glaciers, or by means of trend-surface analysis.

A range of approaches has been employed to estimate the altitude of the ELA or FLA on reconstructed glaciers. These include the balance ratio (BR), accumulation area ratio (AAR), maximum elevation of lateral moraines (MELM), toe-to-headwall altitude ratio (THAR), toe-



Figure 2.21 ASTER images (north to right) of the Chapman Glacier (left) and adjacent piedmont glaciers, Nunavut Territory, Ellesmere Island, northern Canada. During the summer months, the positions of glacier firn lines (FLAs) are shown by marked contrast between debris-laden ice in the lower ablation zones (darker ice surfaces) and the snow-covered accumulation zones in the upper areas of the glaciers. The FLAs approximate the positions of the equilibrium-line altitudes (ELAs) of the glaciers. Note how the lines of debris (medial moraines) reflect flow patterns within the ice (NASA image dated 29 July 2000 from NASA web site, <http://www.jpl.nasa.gov/news/news/2009-059>, reproduced with permission of NASA/GSFC/METI/ERSDAC/Japan Space Systems, and U.S./Japan ASTER Science Team).

to-summit altitude (TSA), cirque floor altitude (CFA) and area-altitude balance ratio (AABR). Some incorporate an aspect of glacier mass balance assessment (BR, AABR, AAR, MELM), while others approximate the elevation of an attribute of the glacier catchment, because the size of the glacier itself is not known (THAR, TSA, CFA; Benn & Lemkuhl, 2000). The latter are less precise and are referred to as 'glacier elevation indices'.

The most widely employed and easily accomplished is the calculation of an AAR, which is the ratio between the accumulation area and the total area of the glacier. The AARs of modern steady-state glaciers in the mid- to high latitudes can range between 0.5 and 0.8, but most commonly lie between 0.55 and 0.65; by contrast, the AARs of glaciers in the humid tropics tend towards the upper part of that range, whereas debris-covered glaciers in the Himalayas can have AARs as low as 0.2–0.4 (Benn *et al.*,

2005). A typical AAR value of between 0.60 and 0.65 is normally assumed when estimating the ELAs of former glaciers in mid- to high-latitude regions, that is, the accumulation area accounted for 60–65 per cent of the total glacier area. ELAs can be computed from maps or from photographs where the altitudinal distribution of the former glacier surface can be measured, and this approach has been employed to establish the ELA of Late Pleistocene and Holocene glaciers in many parts of the world (e.g. Porter, 2000). On present-day glaciers, the colour contrast in late summer between the ablation and accumulation surfaces (Figure 2.21) enables the AARs and ELAs to be monitored by remote sensing (Bamber & Rivera, 2007), and the links to contemporary climatic parameters provide the necessary modern analogue for palaeoclimatic reconstruction (section 2.3.5.2).

Although the AAR method provides a useful first

approximation, it is limited because it takes into account only the plan dimensions and not the three-dimensional geometry of the (inferred) glacier. Sissons (1974) introduced a procedure for taking glacier hypsometry into account, based on the area-weighted mean altitude distribution of the reconstructed glacier surface, using the following formula:

$$x = \frac{\sum_{i=0}^n A_i h_i}{\sum_{i=0}^n A_i}$$

where x = the altitude of the firn line in metres; A_i = the area of the glacier surface at contour interval i in km^2 ; h_i = the altitude of the mid-point of contour interval i ; and n = the number of contour intervals. This formula has since been widely employed to calculate equilibrium ELAs of reconstructed Loch Lomond (Younger Dryas) Stadial glaciers in many parts of the British Isles (section 2.3.5). However, the method assumes a linear correspondence between the accumulation and ablation gradients, whereas studies of modern glaciers have shown that the ablation gradient usually tends to be steeper than the accumulation gradient (Oerlemans, 2001). The AABR method overcomes this problem by allowing variable mass balance gradients to be used in the computation of the ELA (Rea, 2009). Ballantyne (2007a) used the AABR method to calculate the ELAs of ten reconstructed Loch Lomond Stadial glaciers on the Island of Harris, Scottish Hebrides (location 3 in Figure 2.23b) and found that the Sissons's (1974) equation tended to over-estimate the ELA by c. 25–30 m.

2.3.5 Palaeoclimatic inferences using former glacier elevations

Expansion of the ice masses in mid-latitude regions resulted from a combination of reduction in temperatures and increased snowfall which, in turn, caused widespread lowering of regional ELAs. If regional ELAs can be estimated for times in the past, then by studying the relationships between present-day climatic parameters and ELAs of contemporary ice masses, former temperature regimes and, in some cases, seasonal or annual precipitation values can be inferred.

2.3.5.1 Cirque floor altitude (CFA) and toe-to-headwall (THAR) methods

As mentioned above, the CFA and THAR methods provide relatively imprecise estimates of ELAs, because the mass

balance of the glaciers that occupied the cirques is not known. However, they offer first-order estimates of the average ELA reduction in formerly glaciated regions and hence are still widely employed (Munroe & Mickelson, 2002; Lachnić & Vazquez-Selem, 2005). The precise relationship between the ELA of a small cirque glacier and the altitude of the cirque is difficult to determine, though a close correspondence is generally assumed. Since the regional snowline approximates the ELA of cirque glaciers (the exact relationship can be measured for any particular area), the latter can be estimated for times in the past from measurements of the average altitude of cirque floors. The alternative index, THAR, is based on the premise that ELAs are located a certain fraction (normally 0.4) of the vertical distance between the headwall and the palaeoglacier 'toe' or inferred terminus. Where the average annual temperature is known for the altitude of the present snowline, the temperature reduction required to lower the snowline to the altitude of cirque floors presently devoid of glaciers can be calculated from regional temperature lapse rates. This approach suggests that, at the LGM, regional ELAs and mean temperatures, respectively, were depressed by 900 ± 135 m and $5.4 \pm 0.8^\circ\text{C}$ in tropical alpine regions (Porter, 2000), 1,100 m and c. $8\text{--}9^\circ\text{C}$ in Northern Baikal, Russia (Osipov, 2004) and 1,100 m and c. $7\text{--}8^\circ\text{C}$ in Tasmania (Mackintosh *et al.*, 2006).

There are, however, a number of problems in the use of cirque floor altitudes as a basis for palaeoclimatic reconstruction. First, the snowline associated with cirque and valley glaciers is normally lower than the average altitude on exposed summits and slopes, since wind-drifting and low insolation protect accumulated snow and ice within cirque basins. Second, the method can only provide a means of estimating the snowline elevation, and hence palaeotemperatures, for the time when the glaciers were confined to cirques or individual valleys and it is not suitable for calculating temperatures during periods of more extensive ice cover. Third, not all cirques in an area were occupied by ice at the same time, and since some variation in the altitude of cirque glaciers can be expected, contemporaneity of cirque glacier development may be difficult to establish. Finally, it is an implicit assumption in the lapse-rate calculations that the same annual accumulation at the ELA of a modern glacier in a mountain region occurred at the ELA of Late Pleistocene glaciers, which may have been several hundred metres lower. However, empirical data show that precipitation in mountain regions typically decreases with decreasing altitude, and hence the precipitation on the lower-altitude Pleistocene glaciers would also have been lower.

2.3.5.2 ELA/FLA method

An alternative, and possibly more accurate, approach for deriving temperature estimates from reconstructed glaciers involves the use of present or recent glacier mass balance/climate relationships as an analogue for past glacier/climate conditions. The ELA on a glacier is determined by both seasonal precipitation and temperature regimes within the glacier catchment. The mean summer ablation season temperature (t) on modern glaciers is closely related to accumulation at the equilibrium line (Figure 2.22a) which, in turn, approximates average accumulation (A) over the whole glacier (Sutherland, 1984). For ten Norwegian glaciers, Ballantyne (1989) found that this relationship corresponds to the regression equation

$$A = 0.915e^{0.339t} \quad (r^2 = 0.989, P = 0.0001)$$

The ELA is also linearly related to temperature, which Sutherland (1984) calculated to be 0.58°C per 100 m. Hence, a rise or fall in ELA can be directly related to a change in temperature, or precipitation, or some combination of the two. If either former precipitation values or former temperatures are known or can be estimated within

reasonable limits, the appropriate value for the other variable can be calculated. Similar relationships have been calculated for modern glaciers elsewhere, which demonstrates that glaciers worldwide are restricted to a relatively narrow range of combined mean accumulation and mean summer temperature conditions (Ohmura *et al.*, 1992). For reconstructed Quaternary glaciers, therefore, reference to such data allows summer temperature values to be estimated where the altitude of the former equilibrium line and associated accumulation data are known. On the Isle of Mull in western Scotland, for example (locality 6 in Figure 2.23b), geomorphological mapping of former Loch Lomond Stadial glaciers and subsequent application of the AABR indicated a former regional ELA of 250 m (Ballantyne, 2002b). A combination of modern meteorological data and the application of the equation above suggested a mean temperature for July at the ELA of $2.5 \pm 0.5^\circ\text{C}$ ($5.7 \pm 0.5^\circ\text{C}$ at sea level) and annual precipitation values of between *c.* 2,700 and 3,800 mm (Figure 2.22). In some instances, it may be possible to use independent proxy data to infer either former temperature or precipitation values. For example, on reconstructed Loch Lomond Stadial glaciers on the island of Arran in western Scotland (locality 7 in Figure 2.23b), mean July–August

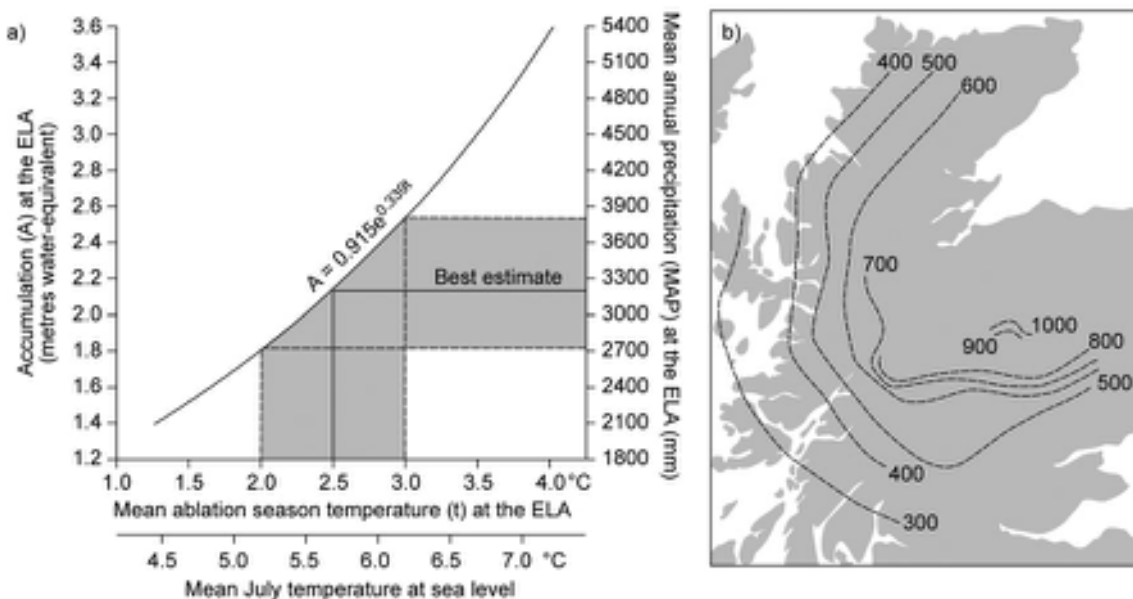


Figure 2.22 a) The relationship between mean winter snow accumulation (defined as October–April period) and mean temperature during the ablation season (May–September) for modern glaciers in Norway. This curve has been used to estimate the temperature and precipitation values for former glaciers in Scotland. b) Generalized contours (m) for inferred ELAs based on reconstructed Loch Lomond Readvance (Younger Dryas) glaciers in Scotland (from Sissons, 1980).

temperatures at the regional climate ELA estimated from fossil chironomid (non-biting midge) records (section 4.5.5) in southeast Scotland lay between $5.7 \pm 0.1^\circ\text{C}$ and $4.1 \pm 0.2^\circ\text{C}$ (Ballantyne, 2007b). Empirical relationships between temperature and precipitation at modern glacier ELAs indicates equivalent mean annual precipitation at the ELA on Arran lay between $2,002 \pm 409$ mm and $2,615 \pm 449$ mm.

There are a number of potential difficulties in the application of this method, however. First, precipitation/temperature ELA graphs have to be employed that are applicable to the area under investigation, and in the case of the British Isles, for example, it has been assumed that the curves calculated for Norwegian glaciers provide the closest analogues for the last glaciers in northern Britain. This may not necessarily be the case. Second, the method depends on the establishment of a sound statistical relationship between ELA/FLA and regional climatic data, but glaciers in many mountain glaciers have been shrinking in recent decades and may not be in phase with prevailing climatic conditions (Solomina *et al.*, 2008), while not all glaciers in a particular area respond to climatic shifts in exactly the same way (Pelto & Hedlund, 2001). Third, the approach rests on the assumption that the 'palaeoglaciers' reconstructed from the geomorphological evidence were themselves in equilibrium with the prevailing climatic

conditions. This is almost impossible to establish for individual 'palaeoglaciers' but if, as seems likely, lags have occurred between recent climatic change and glacier response, cirque and valley glaciers must frequently have been out of synchrony with climate during the cold stages of the Quaternary. Finally, some reconstructed glaciers have been found to have anomalously low long-profile gradients due largely, it appears, to the effects of deformation of subglacial sediment. Where this has occurred, it may undermine the assumption of a linear relationship between accumulation and ablation in the calculation of former ELAs (Ballantyne, 1989).

Despite these limitations, this approach offers the potential for deriving quantitative palaeoclimatic data from, in the first instance, glacial geomorphological evidence. It is encouraging that in areas such as the British Isles, ELA-based reconstructions exhibit consistent regional glacier-climate trends. From the time that Sissons (1980) first demonstrated a strong SW-NE gradient across Scotland for Loch Lomond Stadial ELAs (Figure 2.22b), subsequent research has tended to reinforce this pattern (Benn, 1997). For example, ELA reconstructions from sites extending along the western seaboard of the British Isles show a clear latitudinal gradient (Figure 2.23a), equivalent to a northward temperature decrease of $0.42^\circ\text{C}/100$ km (Ballantyne, 2007b). This is remarkably close to the present

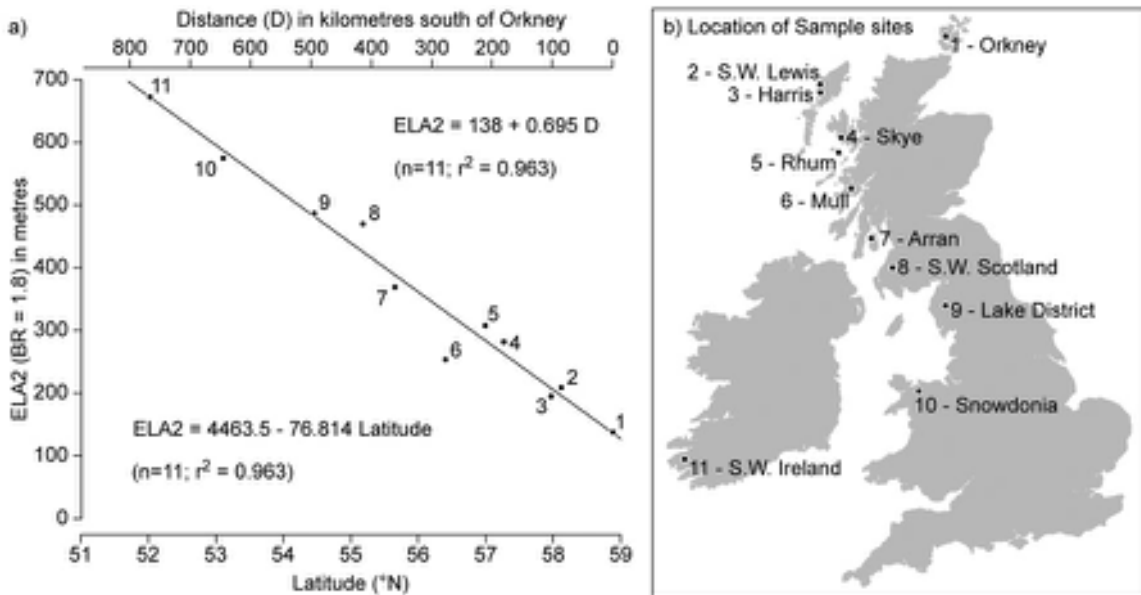


Figure 2.23 Mean equilibrium-line altitudes for reconstructed Loch Lomond (Younger Dryas) Stadial glaciers in eleven districts of the British Isles shown on the right (from Ballantyne, 2007a).

summer temperature gradient ($0.45^{\circ}\text{C}/100\text{ km}$) between the Outer Hebrides and Snowdonia, which lends credence to the method and to its underlying assumptions.

In addition to providing evidence of past temperature and precipitation, former ELAs offer insights into other aspects of Late Quaternary palaeoclimate. In western North America, for example, where precipitation patterns during the LGM varied due to the influence of continental ice sheets, there has been a degree of uncertainty as to the moisture sources for many mountain glaciers. In the Sangre de Cristo mountains of southern Colorado, however, the observed ELA pattern is very similar to modern precipitation patterns, suggesting that southeasterly derived precipitation had a significant influence on the mass balances of LGM glaciers (Refsnider *et al.*, 2009). Likewise, in the Brooks Range of Alaska, the regional west-to-east gradient in reconstructed ELAs on LGM glaciers is comparable to that of contemporary glaciers, suggesting the same primary moisture source in the North Pacific as today. However, a reduction in ELAs in the northeastern part of the range may point to a secondary source of moisture in the Beaufort Sea (Balascio *et al.*, 2005). In the European Alps, analysis of ELAs during the Younger Dryas period shows the greatest depression relative to modern in the west and northwest. This points to a more zonal type of atmospheric circulation than that which characterizes the region today, an inference that accords with data from other proxies, as well as with atmospheric circulation models (Kerschner *et al.*, 2000). In western Norway, variations in glacier ELAs during the Holocene suggest a close correspondence between glacier size and storm-track variability over the North Atlantic, which regulates winter precipitation levels (Bakke *et al.*, 2008).

Spatial patterns and altitudinal trends exhibited by past ELAs therefore provide a basis for palaeoclimatic reconstructions. Inferred palaeotemperatures often show a broad measure of agreement with estimates from other proxy data (section 4.5 and Chapter 7), as well as with contemporary climatic records. They may also offer a basis for distinguishing between those changes in mass balance of modern glaciers that are due to natural climate variability, and those that reflect more pervasive, anthropogenically forced climatic warming (Owen *et al.*, 2009).

2.4 PERIGLACIAL LANDFORMS

The term ‘periglacial’ was first used by the Polish geologist Walery von Lozinski in the early years of the twentieth century to describe both the climate and characteristic cold-climate features (landforms and sediments) found in areas adjacent to the Pleistocene ice sheets. Since then,

however, it has been used in a much broader sense to refer to non-glacial processes and features of cold climates, irrespective of age or proximity to glacier ice (André, 2009). Periglacial processes and features are generally associated with zones of continuous or discontinuous **permafrost** (Figure 2.24), that is, ground that is permanently or seasonally frozen. Today continuous permafrost exists where mean annual air temperature (MAAT) is about or below -6 to -8°C (Smith & Riseborough, 2002). Those areas that are characterized by cold-climate processes where frost action predominates constitute the **periglacial domain** (French, 2007) and are found in both high-altitude and high-latitude regions of the world. They currently cover c. 25 per cent of the earth’s land surface (Anisimov & Nelson, 1996), but tracts of permafrost also lie beneath the Arctic Ocean and on the northern continental shelves of North America and Eurasia. The occurrence of fossil or relict periglacial landforms and deposits throughout the temperate mid-latitude regions suggests that perhaps a further fifth of the earth’s land surface was affected by cold-climate processes on occasions during the Quaternary (French, 2008).

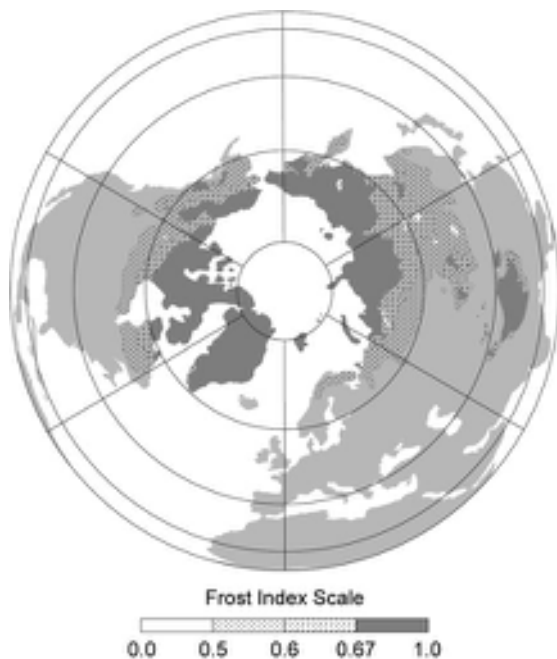


Figure 2.24 Contemporary permafrost distribution in the northern hemisphere based on modern climatic data and computed ‘frost index’ values (FIVs) which define the southern limits of permafrost zones, as follows: continuous permafrost – FIV of 0.67; extensive – FIV of 0.60; sporadic – FIV of 0.50 (from Anisimov & Nelson, 1996).

54 GEOMORPHOLOGICAL EVIDENCE

The periglacial domain is characterized by an extremely active geomorphological environment in which processes operating on the ground surface include:

- (a) frost-shattering of bedrock and of particles within unconsolidated sediments;
- (b) the growth of ground ice, leading to upheaval of the ground surface, and the lateral displacement of surface materials;
- (c) accelerated wind erosion and transport in environments where vegetation cover is sporadic and unconsolidated materials are exposed over wide areas;
- (d) thermal erosion by fluvial activity;
- (e) accelerated downslope movement of materials (**gelifluction**) where near-surface thawing results in a saturated surface layer overlying a still-frozen substrate, resulting in mass flow on slopes with angles as low as 2°.

Some of these processes are unique to periglacial environments, most notably those associated with the growth of ground ice, while others, including fluvial, aeolian and gelifluction processes, are particularly effective in high-latitude and high-altitude regions of the world. Collectively, they give rise to a suite of landforms that is highly distinctive and that is characteristic of a periglacial landscape (Ballantyne & Harris, 1994; French, 2007).

On upper slopes, exposed bedrock is highly fractured, angular and craggy in appearance as a result of frost action, with upstanding masses of bedrock (**tors**: Figure 2.25a) and frost-weathered mountain-top debris (**block-fields**: Figure 2.25b). A characteristic step-like, hillslope profile typically evolves in which a process of excavation of

bedrock by frost action and the transport of frost-riven material by gelifluction produce **alтиplanation** or **cryoplanation terraces** (Thorn & Hall, 2002). Footslopes, by contrast, tend to develop smooth, low-angled profiles, with the accumulation of **gelifluction sheets** and **terraces** (Kneisel, 2010). The latter are typically lobate in form and evolve through the combination of creep induced by frost heave and the downslope movement of saturated surficial debris. Modern lobes are most active under high pore-water pressures in spring, when snow melts over frozen substrates (Harris *et al.*, 2008), inducing down-slope movements of up to 63 mm a⁻¹ (Ridefelt *et al.*, 2009).

On valley floors, on hillside benches, and on plateau surfaces, a number of features occur in geometric patterns, referred to generally as **patterned ground** (Ballantyne & Harris, 1994). This term covers landform assemblages that have been produced by a variety of processes. Perhaps the best known is that of the **ice-wedge polygon** (Figure 2.26a), which can develop either through ground cracking at very low ground temperatures (Christiansen, 2005), or by sorting processes, where coarser materials are selectively separated from finer particles. More common, however, are **sorted nets** and **circles** (Figure 2.26b). **Sorted stripes** tend to form where sorting processes operate on gentle to moderate slopes up to about 25°. Patterned ground may also be found, however, on mountain summits, on gelifluction terraces and on alтиplanation terraces. Regular depressions reflect the original locations of ground ice lenses (**palsas**), which accumulate in substrates where groundwater is preferentially diverted under high pore-water pressure during ground freezing. Following thaw, subsidence occurs and, in present-day arctic environments, the resulting hollows are normally filled with water (**thaw**



Figure 2.25 a) Granite tor on the summit of Beinn Mheadhoin, Cairngorm Mountains, Scotland. Also included is Colin Ballantyne, University of St Andrews, UK, who provided the photograph. b) Summit blockfield on Gros Morne Mountain, western Newfoundland, Canada (photograph by Mike Walker).

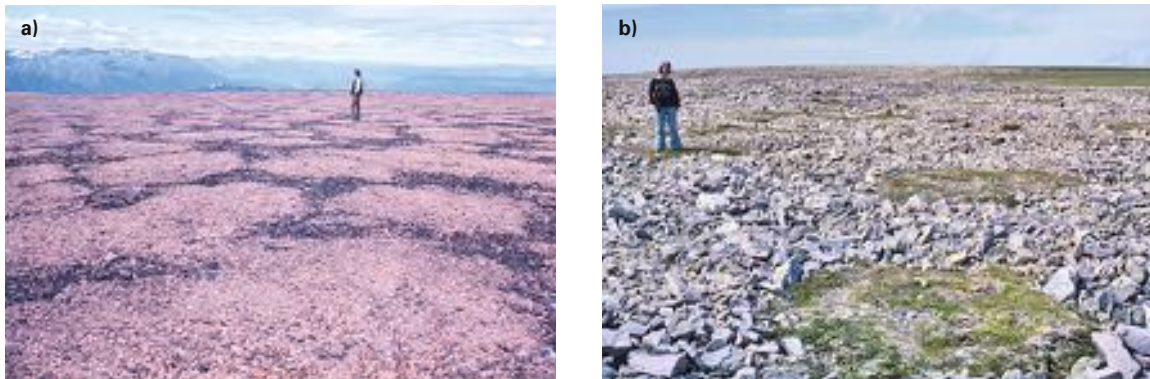


Figure 2.26 a) Active polygonal patterned ground, Mt Edziza, British Columbia, Canada (photograph by Neville Alley, University of Adelaide, Australia). b) Sorted circles on the summit of Gros Morne Mountain, western Newfoundland, Canada (photograph by Mike Walker).

[lakes](#)). The landscape is commonly described as [thermo-karst](#) (Luoto & Seppälä, 2003), from a visual analogy with karst regions, which are often marked by numerous sink-holes. Thermokarst is normally associated with the degradation of continuously frozen ground. Finally, there are the [polar deserts](#), which occupy the driest parts of the periglacial domain, such as in the McMurdo Dry Valleys of Antarctica today, where extensive sand sheets and dune systems occur (Speirs *et al.*, 2008).

Many of these features of the periglacial landscape have been recognized in relict form in Eurasia and North America, either through field mapping or through the use of remote sensing techniques (Grosse *et al.*, 2005), and reflect the extensive areas of continuous and discontinuous permafrost that developed during the cold stages of the Quaternary. Patterned ground forms, for example, can frequently be identified on aerial photographs, for the geometrical patterns tend to be emphasized by differences in crop growth resulting from drainage variations. They are particularly clear on flat alluvial plains or on the coastal terraces of northwest Europe (Svensson, 2005), and on the Late Wisconsinan drift plains of North America (Lusch *et al.*, 2009). The tracts of former polar deserts are marked by the extensive dune fields and ‘sand belts’ that stretch across the northern European plains, the northern belt of the Great Plains of North America, and large parts of northern China and Mongolia (Yang *et al.*, 2004). Relict desert landforms often enable wind patterns at their time of formation to be inferred. Patterned ground and polar desert features therefore provide good evidence for the former existence of periglacial conditions, although in most cases they only allow the most generalized of climatic inferences to be made (Humlum & Christiansen, 2008).

Some landforms, however, may form the basis for more detailed palaeoclimatic reconstructions, and these are considered in the next section.

2.4.1 Palaeoclimatic inferences based on periglacial landforms

Certain periglacial landforms are unique to present-day arctic and alpine environments, and aspects of the prevailing climate under which they have evolved can sometimes be quantified. Where comparable relict features can be identified, therefore, they can be used as a basis for estimating climatic parameters for earlier times during the Quaternary. Examples of periglacial landforms that have been employed in this way are rock glaciers, pingos and palsas, and protalus ramparts. The potential of periglacial deposits for palaeoclimatic reconstruction is discussed in section 3.4.3.

2.4.1.1 Rock glaciers

These are active tongue-shaped or lobate accumulations of rock debris (Figure 2.27) that move slowly downslope as a result of deformation of interstitial ice or frozen sediment, with rates of movement ranging from 1 cm a^{-1} to greater than 130 cm a^{-1} (Giardino & Vitek, 1988). Two main types can be distinguished on the basis of their characteristic length/breadth ratios (Hamilton & Whalley, 1995). [Rock glaciers](#) *sensu stricto* (also termed [morainic rock glaciers](#)), are formed through the burial and subsequent incorporation of a core of glacier ice under a thick cover of morainic debris. These are frequently found spreading down-valley from a cirque glacier, but might also



Figure 2.27 Active lobate rock glaciers near Lytton, British Columbia, Canada (photograph by Neville Alley, University of Adelaide, Australia).

be initiated by avalanches which concentrate large amounts of rock debris (Humlum *et al.*, 2007). **Protalus lobes**, sometimes referred to as '**protalus rock glaciers**', develop through the deformation of thick accumulations of talus in ice-rich permafrost regions, and are nearly always found at the foot of steep cliffs, where they form step-like or lobate extensions of the lower parts of talus slopes (Harrison *et al.*, 2008). Protalus lobes and rock glaciers are characteristic features of the discontinuous permafrost zone in mountain regions, and their formation appears to be governed by a threshold MAAT of -2°C (Brazier *et al.*, 1998). Hence, in a mountain region where relict protalus rock glaciers are found at lower elevations than modern ones, the degree of cooling required to generate the relict features can be estimated from regional temperature lapse rates. This line of reasoning suggests a reduction of mean annual temperature by $2\text{--}4^{\circ}\text{C}$ in the Swiss Alps during the Late-glacial period (Frauenfelder *et al.*, 2001) and by $8\text{--}9^{\circ}\text{C}$ in northwest Greece during the LGM (Hughes *et al.*, 2003), while shorter episodes of climate cooling during the Neoglacial period have also been inferred from relict rock glaciers in the Front Range mountains of Colorado (Refsnider & Brugger, 2007). However, this type of evidence often needs to be supported by independent proxy records, as climate is not the only variable that directly affects rock glacier formation and dynamics (Harrison *et al.*, 2008; Janke & Frauenfelder, 2008). Moreover, attribution of debris accumulations in upland areas to relict rock glaciers is often contentious, as many such features can be explained without recourse to forward movement controlled or facilitated by incorporated ice as it deforms and melts out (Jarman *et al.*, 2013).

2.4.1.2 Pingos and palsas

Pingos are dome-shaped mounds or hills that occur in permafrost regions as a result of the uplift of frozen ground by the growth of a large mass of ground ice in the substratum, and are prominent periglacial landforms in vast regions of the Arctic and Subarctic (Grosse & Jones, 2011). Two broad types of pingos have been recognized: the '**closed-system**' (hydrostatic) or **Mackenzie Delta** type that form by groundwater expulsion during permafrost aggradation; and the '**open-system**' (hydraulic) or **East Greenland** type, in which the ice core is fed by subsurface groundwater seepage from unfrozen parts of discontinuous permafrost. Smaller cryogenic mounds also occur in the discontinuous and sporadic permafrost zones, the most common of which are **palsas** and **mineral palsas**, the former developing in peat while the latter form in mineral soils. Mineral palsas are also known as **lithalsas** (Pissart, 2002). Melting of the ice core within a pingo or palsa leads to ground collapse, forming a central depression or crater, with a characteristic ring-shaped rampart around the depression (Mollard, 2000).

Relict pingo ramparts have been recognized in many mid-latitude regions where periglacial conditions once obtained and, by using prevailing climatic conditions in areas where pingos are currently forming as an analogue, MAATs at times of former pingo growth may be inferred (Ballantyne & Harris, 1994; French, 2007). For example, relict pingo scars and other periglacial indicators suggest MAATs at sea level of around or below -8°C in Fennoscandia, northern Britain and Ireland during the Younger Dryas Stadial, while in the Netherlands, upland Belgium, northern Germany and Poland, MAATs are estimated to be in the range $-8\text{ to }-1^{\circ}\text{C}$ (Isarin, 1997). The presence of lithalsas in upland Belgium, Wales and Ireland adds support to these reconstructions, as the features are found today in northern Quebec where MAATs are in the range $-4\text{ to }-6^{\circ}\text{C}$ (Pissart, 2001). Modelling of palsa distribution in northern Europe suggests the optimum areas for their development are those with a MAAT of $-3\text{ to }-5^{\circ}\text{C}$ and with low levels of precipitation ($< 450 \text{ mm}$) (Luoto *et al.*, 2004).

There are two important limitations to the use of this approach, however. First, while both pingos and palsas occur in areas of discontinuous permafrost (MAAT $\leq -3^{\circ}\text{C}$), pingos are also features of the continuous permafrost zone ($\leq -7^{\circ}\text{C}$), while palsas are found in regions of sporadic permafrost ($\leq -1^{\circ}\text{C}$). Hence, appropriate contemporary analogues for relict features may be difficult to determine (Gurney, 2003). This problem may be compounded by the difficulty of classifying relict ramparted depressions in former periglacial regions as either pingos or palsas. Second, the remains of these ground-ice features

display a variety of forms, from isolated ridges to clustered collectives of ramparts, the often complex structures of the latter suggesting not only polygenetic origins (Mollard, 2000), but that factors other than climate may have influenced their development.

2.4.1.3 Pronival ('protalus') ramparts

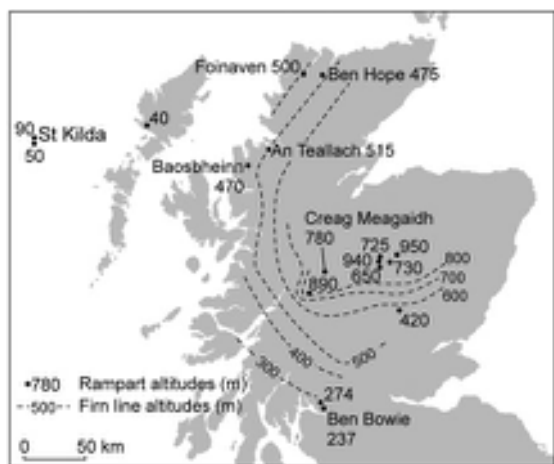
A pronival (protalus) rampart, also termed a **nivation ridge**, is a lobe, ridge or ramp formed of debris that accumulates along the downslope margins of a perennial snow patch. The term 'pronival' is now generally preferred to 'protalus', because the presence of a snow patch is essential to ridge formation. Originally it was assumed that the ridge was largely composed of frost-riven bedrock from above the snow patch, and that build-up of debris occurred mainly over the distal slope of the ridge. However, analysis of both active and fossil features has shown that rounded as well as angular clasts occur within ramparts, suggesting a variety of transport processes (Shakesby, 1997), while debris also accumulates on both proximal slopes and rampart crests (Hedding *et al.*, 2007). Perennial snow patches develop in sheltered situations on mountainsides

where snow survives the ablation season but where accumulation is insufficient to promote the development of glacier ice, the snowbed being partly nourished by direct precipitation input, but also often by redistribution of snow from surrounding mountain and plateau areas (Brook & Williams, 2012). Their survival is governed partly by local temperature regime, but the primary control on their development appears to be precipitation, since the accumulation of too much snow would result in rapid snow patch growth and the transition to glacier ice (Ballantyne & Benn, 1994). Fossil protalus ramparts (Figure 2.28), therefore, mark the positions of former snow patches that accumulated under colder temperatures than today, but in conditions marginal for glaciation. In the uplands of the British Isles, for example, such features appear to be mostly of Loch Lomond/Younger Dryas Stadial in age, and in Scotland their altitudinal range is very similar to that of reconstructed glacier ELAs (section 2.3.4.2), with protalus ramparts increasing in altitude from west to east (Ballantyne & Kirkbride, 1986). This appears to reflect heavier snowfall in western Scotland by comparison with the mountains in the east, a pattern that is also apparent in the ELA reconstructions (Figure 2.29).



Figure 2.28 (left) Fossil protalus rampart (middle distance) and stratified scree (foreground; see section 3.4.1) near Cader Idris, Wales (photograph by Mike Walker).

Figure 2.29 (below) Altitudes in metres of the frontal crests of Loch Lomond (Younger Dryas) Stadial protalus ramparts in the Scottish Highlands, and reconstructed ELAs of Stadial glaciers at their maximal extent (see also Figure 2.22) (after Ballantyne & Kirkbride, 1986).



The distribution of fossil periglacial landforms, therefore, not only provides evidence for the former extent of the periglacial domain, but in certain cases their occurrence can be used to derive palaeoclimatic data for times during the Quaternary. In addition to the three examples discussed above, other periglacial landforms used as a basis for palaeoclimatic reconstruction include **blockfields** (Nelson *et al.*, 2007) and small cryogenic mounds known as **earth hummocks** or **thúfur** (Grab, 2005). Care must be exercised in the use of this type of evidence, however, for the occurrence of fossil periglacial landforms indicates only that certain critical temperature thresholds were transgressed. It is possible, and in many cases likely, that temperatures were lower than the threshold values, and hence the derived palaeotemperatures must be regarded as maximal values only. The influences of non-climatic variables on the development and distribution of periglacial landforms poses further difficulties (Harris *et al.*, 2009). These and other problems associated with the use of fossil periglacial evidence in palaeoenvironmental reconstruction are considered further in section 3.4.

2.5 SEA-LEVEL CHANGE

There is abundant geomorphological evidence in many parts of the world for fluctuations in sea level during the course of the Quaternary (Murray-Wallace & Woodroffe, 2014). This includes former coastal landforms now standing above present sea level, such as rock platforms sometimes with prominent backing cliffs (Figure 2.30), ‘raised beaches’ consisting of estuarine or littoral sand and gravel deposits, deltas, spits, shingle ridges, stacks, caves and coral reefs. Evidence for sea-level change can also be found offshore in the form of submerged landforms, including caves, platforms, beaches, reefs and river valleys. Mapping and altitudinal measurement of such features enables the positions of former coastlines to be established and the vertical range of sea-level variations to be determined. In many situations, however, a complete picture of sea-level change can only be obtained using both geomorphological and lithostratigraphic data. Not only do marine deposits form a more continuous record of sea-level change than the fragmentary geomorphological evidence, many littoral



Figure 2.30 The ‘High Rock Platform’, northern Islay, Scottish Hebrides: this raised marine platform that is cut into quartzite dominates the picture. Its surface altitude varies between 32 and 35 m above present mean tide level and it extends for between 400 and 600 m from seaward edge to backing cliff. It is locally covered by marine gravels, indicating that it was covered by a higher marine level after it was formed. It has been etched into by a lower and younger platform of Younger Dryas age (the ‘Main Lateglacial Platform’) that in this locality is between c. 3 and 5 m above present mean tide level. It has formed the backing cliff and caves seen in the foreground (a figure in the foreground provides scale) while isolated stacks can be seen closer to the present shore. A gravel ridge that covers the lower platform (lower right of photo) was formed during the Holocene. This sequence of shorelines reflects the complex interplay between glacio-isostatic rebound and eustatic sea-level variations during the waning stages of the last British ice sheet (photograph from <http://www.islay.org.uk/tag/mala-bholsa/>).

sedimentary sequences contain fossils that provide an additional source of information for the reconstruction of sea-level histories. In addition, sedimentological and biological evidence offers a basis for the dating and correlation of sea-level changes, whereas geomorphological features (platforms, beaches, etc.) are usually more difficult to date precisely. By combining landform evidence with sedimentary and fossil records from boreholes or exposures, therefore, the sea-level history of a particular locality can be established, often in considerable detail. In this section, therefore, the geomorphological evidence and the lithostratigraphic evidence for changes in sea level are considered together. The biological evidence for sea-level change is discussed in Chapter 4.

2.5.1 Relative and 'absolute' sea-level changes

The level of the sea relative to the land can vary through the vertical change of *either* the sea *or* the land surface *& both* of these. Where subsidence of the land takes place at a time of stable ocean levels, there will be a local rise in sea level; conversely, land uplift will lead to the elevation of littoral features, and an apparent fall in sea level. Where changes in sea level take place either through land or through sea-level movements, they are referred to as **relative sea-level changes**, that is, a change in the position of the sea relative to the land. Such changes are essentially local in effect. Worldwide sea-level changes, on the other hand, that result from fluctuations in the volume of water in the ocean basins, are termed **eustatic**. At one time it was assumed that the extent of any eustatic change would be uniform worldwide, but it is now acknowledged that local gravitational effects can influence the rates and magnitudes of sea-level rise or fall in different coastal regions (Milne & Mitrovica, 2008). In effect, this means that while eustatic changes may be broadly similar at the local or regional scale, this cannot be assumed when comparing records at the continental or global scale (section 2.5.2). Moreover, even where the amplitude of eustatic change has been the same in two coastal regions, this need not result in the same geomorphological response. For example, a eustatic rise of 50 m over a 1,000 year period will result in a relative rise in sea level of 50 m in areas where the land surface is stable, but a 50 m *fall* in relative sea level (RSL) along coastlines being uplifted at a rate of 10 cm per year.

Some land movements are long term and result from tectonic activity associated with the migration of the great lithospheric plates across the surface of the globe. Others may be of shorter duration and are generally more localized in their effects; these are known as **isostatic**

movements. The term '**isostasy**' refers to the state of balance that exists within the earth's crust so that a depression of the crust by the addition of a load (sediment, lava, ice, water, etc.) in one locality will be compensated for by a rise in the crust elsewhere (Teixell *et al.*, 2009). The state of isostatic equilibrium is considered to be maintained by viscous flow of the mantle, although the precise nature of the processes involved is still a matter of debate (Thorson, 2000). In order to understand Quaternary sea-level variations, therefore, it is first necessary to establish how the separate effects of isostatic and eustatic changes have affected a region. In more tectonically stable areas (such as the islands of Bermuda and the Bahamas, for example), where the eustatic effect appears to have been the major factor influencing sea levels, it may be possible to reconstruct a sequence of what have been termed '**absolute**' as opposed to relative sea-level changes. **Absolute sea levels** cannot easily be discerned in areas where crustal movements have occurred, however, as it is often difficult to discriminate between the isostatic and eustatic components jointly responsible for movements of the sea surface relative to land. One way to resolve this problem is to compile records of sea-level change for tectonically 'stable' coastlines, for these (in theory) should reflect eustatic variations only, and these data should then enable the magnitude of land movement to be calculated for tectonically active regions. However, as discussed in the following sections, there are important methodological limitations to this approach. An alternative strategy is to use an independent measure of sea-level change, such as the oxygen isotope record from marine microfossils in deep-ocean cores (Figure 2.31). This type of evidence is considered in the following section and is discussed in more detail in section 3.10.

2.5.2 Eustatic changes in sea level

2.5.2.1 Pre-Quaternary eustatic changes

Major changes in global sea level have occurred throughout the Phanerozoic.¹¹ Most reconstructions suggest much higher stands of the sea during pre-Quaternary periods (e.g. Figure 2.31), although estimates of the magnitude and timing of high sea levels vary considerably (Miller *et al.*, 2005; Müller *et al.*, 2008). The discrepancies arise because long-term sea-level trends are difficult to establish, as they reflect, *inter alia*, continental-scale and localized tectonic effects; changes in mass distribution and shape of the earth; changes in the volume and mass of the hydrosphere through the addition of juvenile water;¹² and temporal variations in the rate of rotation or in the axial (angular)

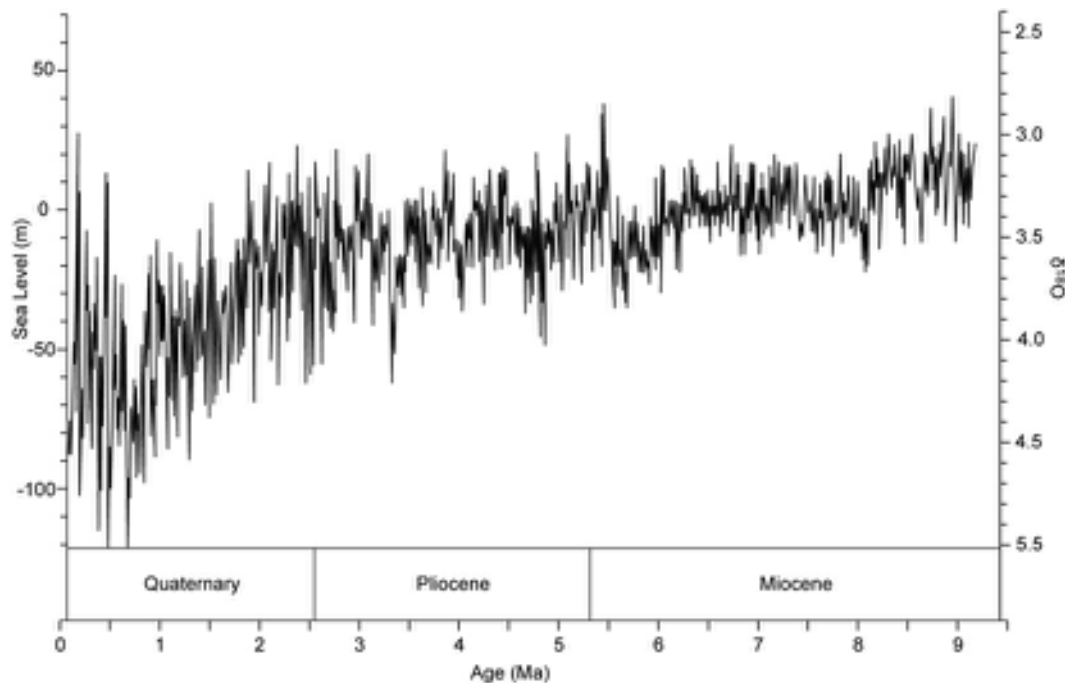


Figure 2.31 Eustatic sea-level variations over the last 9.5 Ma based on marine oxygen isotope measurements (modified from Miller *et al.*, 2005). Note the distinct cooling trend reflected in the oxygen isotope record that begins c. 2.6 Ma.

momentum of the earth (Johnston & Lambeck, 2002; Gross *et al.*, 2005). In addition, temperature and chemical variations within the water column can lead to ‘steric’ (density) changes that affect ocean water volume and thus sea level (Chambers, 2006). Fluctuations in volume and mass of sea water will also influence the hydro-isostatic load (section 2.5.4) on the underlying seabed, a process that may explain the emergence of coral atolls from the Pacific Ocean during the late Holocene, when eustatic sea-level rise was reversed by hydro-isostatic depression (Dickinson, 2004). In addition, long-term changes in sea level can result from changes in the configuration of ocean basins caused either by sediment infill and the consequent displacement of ocean water, or by the lateral movement of lithospheric plates and associated vertical displacements of crust and mantle in the vicinity of subduction zones. Accelerated rates of sea-floor spreading lead to an increase in volume of the mid-ocean ridges, resulting in a sea-level rise; conversely, slower rates of spreading reduce both ridge volume and sea level. Reconstructing changes in ocean bathymetry over long geological timescales is therefore a complicated exercise which is compounded further by chronological uncertainties (Müller *et al.*, 2008),

and by the lack of fixed stable reference points from which to determine the height of eustatic sea level for specific times in the past (Moucha *et al.*, 2008).

2.5.2.2 Quaternary eustatic changes

More is known about sea-level variations during the late Pliocene and the Quaternary. The Pliocene was generally warmer than the Quaternary by approximately 3°C (annual average) and, with less polar ice cover, eustatic sea level has been estimated to have been between 10 and 25 m higher than present (Haywood & Valdes, 2004). Global sea-levels show progressive lowering towards the end of the Pliocene, and this pattern appears to have continued throughout the Quaternary (Figure 2.31). Superimposed on this long-term trend, however, is a cyclical pattern of shorter-term oscillations in eustatic sea level related to the expansion and contraction of the great ice sheets. During glacial episodes, ice sheets grow by storing water abstracted from the oceans (section 3.10), while melting of ice during warmer episodes returns water to the oceans. Sea-level changes controlled by the growth and contraction of the ice sheets are termed **glacio-eustatic**. During the Late

Quaternary, sea levels were lowered glacio-eustatically by as much as 130 m at glacial maxima, but returned to levels similar to, or higher than, those of the present during interglacials.

This link between changes in global ice volume and sea level is reflected in oxygen isotope profiles from deep-ocean cores where the isotopic ‘signal’ can be read as a proxy sea-level record, and a chronology of long-term sea-level change can be established (Shackleton, 1987). While it is now recognized that oxygen isotope ratios in marine microfossils are not governed solely by ice-ocean volumetric changes (section 3.10), the fragmented nature of empirical evidence from coastal localities means that the marine oxygen isotope curve remains the only basis for establishing a long-term continuous eustatic record (Figure 2.32). Initially, sea-level reconstructions based on the oxygen isotope approach used simple inversions of the isotopic data

(Lourens & Hilgen, 1997), but more sophisticated models are now available that can isolate the ice-volume component from other influences affecting marine isotope ratios (Lea *et al.*, 2002; Bintanja *et al.*, 2005).

Chronologies of Quaternary sea-level change can also be obtained from the direct dating of shoreline features and deposits, most notably in those areas considered to be tectonically stable. Of particular importance are coral reefs found, for example, around Caribbean or Pacific islands and atolls, for some reef-forming corals occur only within the intertidal zone, and hence submerged or raised inactive reefs provide direct evidence for changes in sea level. Reef carbonate can be dated by U-series and amino-acid racemization methods (sections 5.3.4 and 5.6.1) to provide chronologies of sea-level change, for instance around the islands of Bermuda (Peltier & Fairbanks, 2006) and Mururoa (Camoin *et al.*, 2001). In Tunisia interglacial

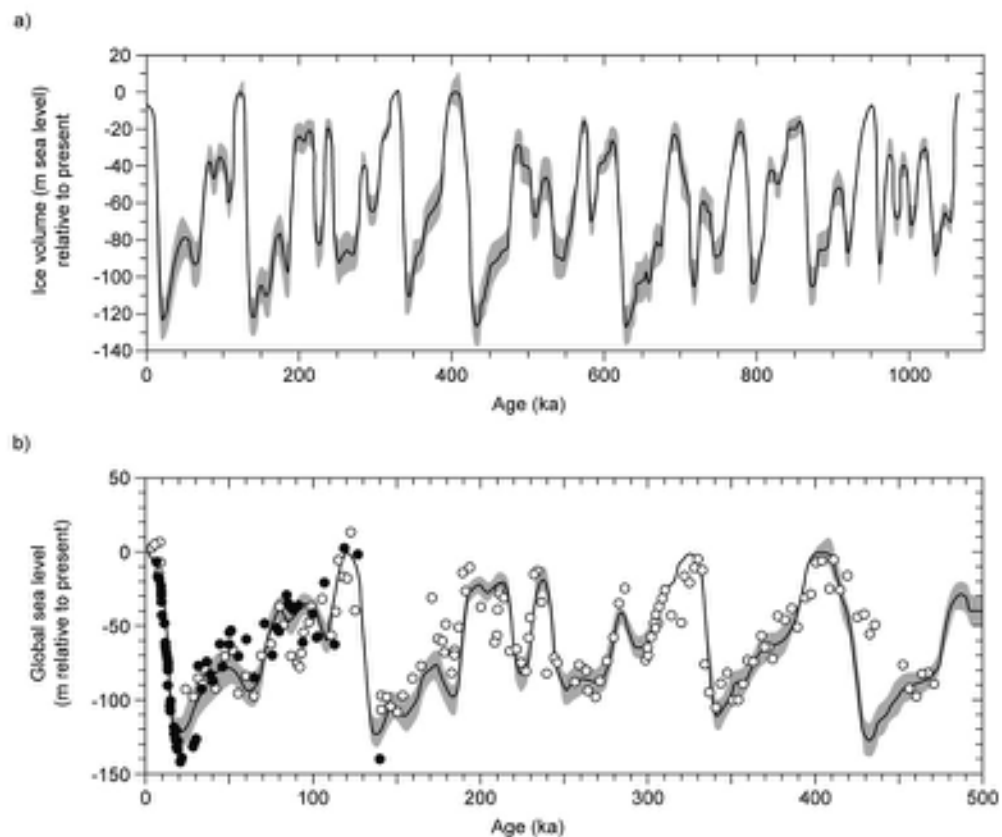


Figure 2.32 a) Variations in eustatic sea level (with 1σ confidence limits shown in grey shading) over the past 1 Ma based on ice-volume changes reflected in marine oxygen isotope records. b) The sea-level record for the last 500 ka compared with independent isotopic measurements from the Red Sea basin (white circles) and from coral reef data from New Guinea and Barbados (black circles) (from Bintanja *et al.*, 2005).

highstands of sea level have also been dated by U-series, although in this case using marine Mollusca associated with the shorelines (Jedouï *et al.*, 2003). Luminescence dating (section 5.3.6) has also been used to establish chronologies of sea-level change, for example on interglacial shorelines on the northeast coast of Brazil (Barreto *et al.*, 2002), and on Holocene marine sequences in southeast India (Thomas, 2009). Another approach employs evidence from submerged caves that contain cave speleothems (section 3.8.4.4). Since these only develop under subaerial conditions, speleothem evidence provides constraints on maximum heights of sea level, while the termination of speleothem formation reflects the time when caves were submerged beneath the sea. Dating of speleothem carbonate, again using U-series, has been employed to reconstruct sea-level histories in many coastal limestone regions, such as along the coastlines of Italy (Antonioli *et al.*, 2004) and Croatia (Surić *et al.*, 2009). Other features that enable a chronology of sea-level change to be established include carbonate aeolianite beach ridges on some coastal fringes as, for example, in western Australia (Hearty & O'Leary, 2007).

In some coastal localities, there is evidence for several glacial–interglacial sea-level cycles. In Bermuda and the Bahamas, interglacial highstand positions are represented by coral limestone while low sea levels during cooler periods are marked by palaeosols (section 3.5). The record extends over 1.2 Ma and includes evidence for at least seven interglacial highstands between 2.5 and >20 m above present sea level, and dated to MOI stages 11–5e (Hearty & Kindler, 1995; Kindler & Hearty, 2000). In the Mediterranean region, ‘staircases’ of raised marine terraces are widespread, and while some of these reflect episodic tectonic uplift (section 2.5.3), a number mark eustatic sea-level highstands. The oldest pre-date MIS 11, while up to three highstand positions have been recognized for the last interglacial stage (MIS 5e) alone (Zazo *et al.*, 2003).

Some of the most detailed records of eustatic sea-level change are available for the last glacial–interglacial cycle (the last c. 120 ka), for not only is the evidence better preserved, but shoreline sequences are often less disturbed than is the case for earlier periods. Reconstructions are based on a variety of approaches, but frequently use dated coral reef records combined with marine oxygen isotope data (Lambeck & Chappell, 2001; Siddall *et al.*, 2003). Records from different regions are remarkably similar (Figure 2.33), and reflect changes in global ice volume as the principal controlling factor in overall sea-level trends. Superimposed on this pattern, however, are more subtle influences. Thompson and Goldstein (2005), for example, found evidence for persistent short-term oscillations in sea level

that are too frequent to be explained solely by reference to ice volume changes, while Chappell (2002) concluded that temporary reversals of the general downward trend of sea level during the last glacial are connected with ‘Heinrich events’, extremely cold climatic pulses recorded in North Atlantic marine records (section 3.10.1). It has also been suggested that the separate influences of the polar ice sheets can be detected in sea-level cycles, with the Antarctic ice sheet dominating during cooling phases, but the Greenland ice sheet becoming the more important driver during warming events (Siddall *et al.*, 2010b).

At the Last Glacial Maximum (LGM) around 21 ka (Mix *et al.*, 2001) when the Laurentide, Fennoscandian, British–Irish and Antarctic ice sheets were at their greatest extent, global sea levels may have been 130 and 135 m below those of the present (Yokoyama *et al.*, 2000). The sea-level rise that accompanied the wastage of these ice sheets is reflected in records from **far field locations**, coastal regions

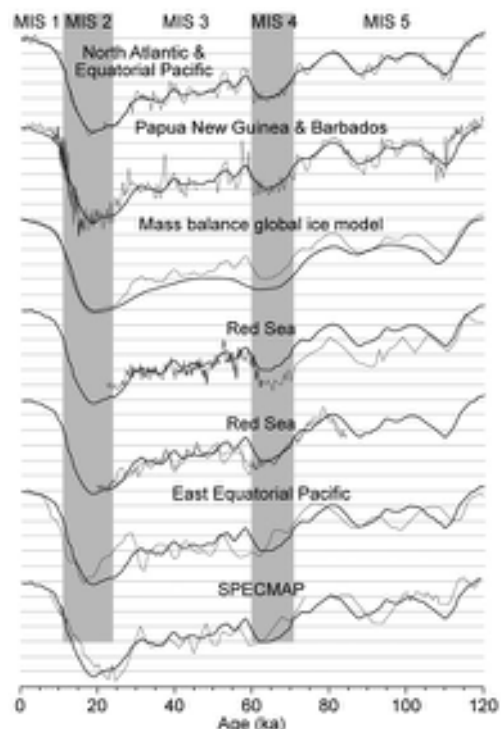


Figure 2.33 Comparison of seven different eustatic sea-level records from the last glacial cycle. The interval between horizontal lines represents 20 m vertical depth, and each curve ranges between modern sea level (zero datum) at the top and c. -120 to -130 m at the bottom (adapted from Siddall *et al.*, 2010b).

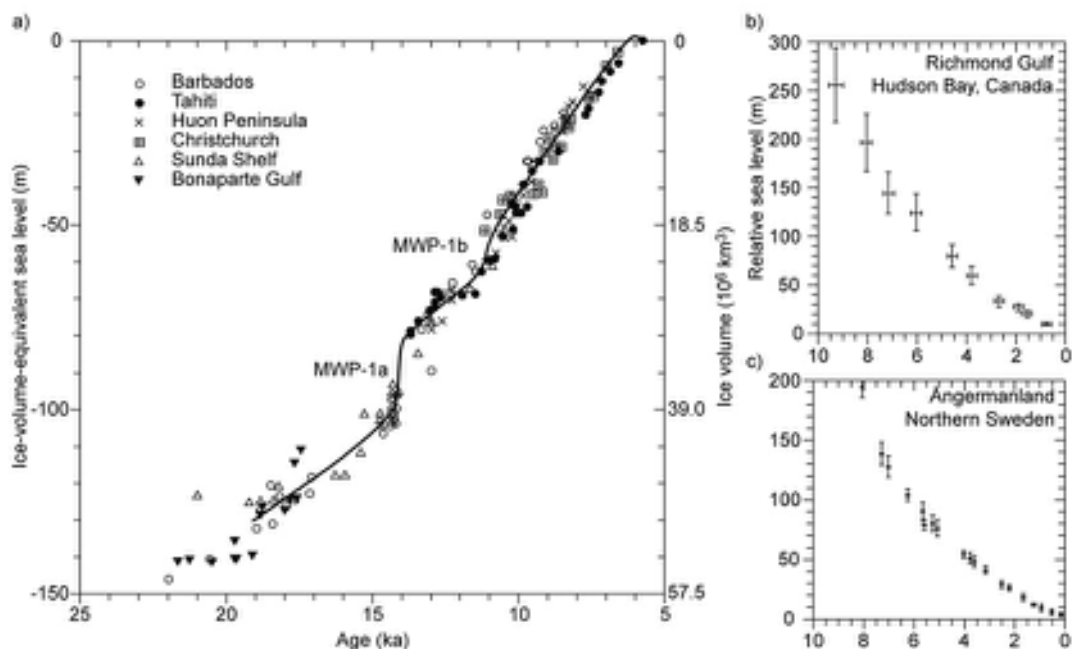


Figure 2.34 a) Rise in eustatic sea level since the LGM based on evidence from several independent studies; the mean sea-level curve has been interpolated between the data points. b) Land elevation changes in Hudson Bay, Canada and c) in northern Sweden during the Holocene (modified from Lambeck & Chappell, 2001). Vertical and horizontal bars represent errors of altitudinal and age estimates respectively; MWP – meltwater pulse. For further explanation, see text.

that were unaffected by glacier activity (Fleming *et al.*, 1998). Six such records are shown in Figure 2.34a, and show a rapid rate of sea-level rise, with two episodes of further acceleration at around 14 and 11.5 ka that are assumed to reflect increased rates of global ice melt (Alley *et al.*, 2005). **Meltwater pulse (MWP) 1a** (14 ka), the earlier and most pronounced of the two, was originally considered to be the signature of rapid retreat of the Northern Hemisphere ice sheets, although contributions from Southern Hemisphere ice cannot now be excluded (Peltier, 2005). The less pronounced **MWP 1b** (11.5 ka) has proved to be more enigmatic, for while it seems to be clearly represented in some records, for example from the Sea of Japan (Tanabe *et al.*, 2009), it is absent or very poorly defined in others, such as in the Indian Ocean (Camoin *et al.*, 2004) and around Tahiti (Bard *et al.*, 2010).

Eustatic sea-level rise during the Holocene is most clearly reflected in estuarine sediments and in stratigraphic records from coastal lakes. Sedimentation in estuaries is usually rapid and the deposits tend to be protected from erosional processes. Relatively shallow waters are often found in estuaries, so that even minor falls in sea level can lead to the exposure of marine and brackish water

sediments, while a slight rise can result in the submergence of terrestrial or freshwater deposits. As a consequence, in estuarine contexts there is often a stacked sequence of marine, estuarine, freshwater and terrestrial sediments, from which a detailed history of sea-level change can be reconstructed. Figure 2.35, for example, shows a terrestrial peat interbedded between two layers of estuarine marine sediment. The boundary between the lower marine unit and the base of the peat marks the emergence of mud-flats above local high-tide level, the surface of which was subsequently colonized by land plants whose remains make up the peat. If dated, this horizon would provide a **sea-level index point**, from which not only the age and altitude of RSL could be established, but also the **tendency** of relative sea-level change could be deduced (Shennan *et al.*, 2006a). The ‘tendency’ of an index point refers to the **trend** of RSL, in other words whether there is an increase or decrease in marine influence at that locality. This can be inferred not only from changes in the nature of the sediments (from terrestrial to marine or vice versa), but also from pollen, diatom or other microfossil evidence (sections 4.3.5 and 4.9.3). In this particular case, the transition from marine to terrestrial deposits indicates a decrease in marine

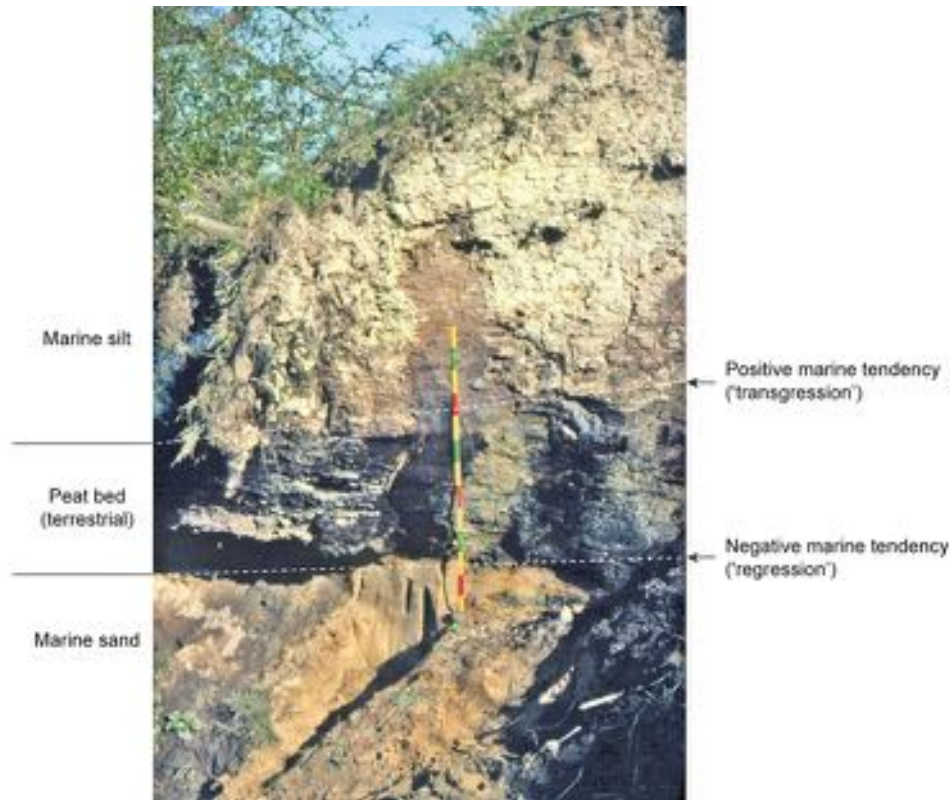
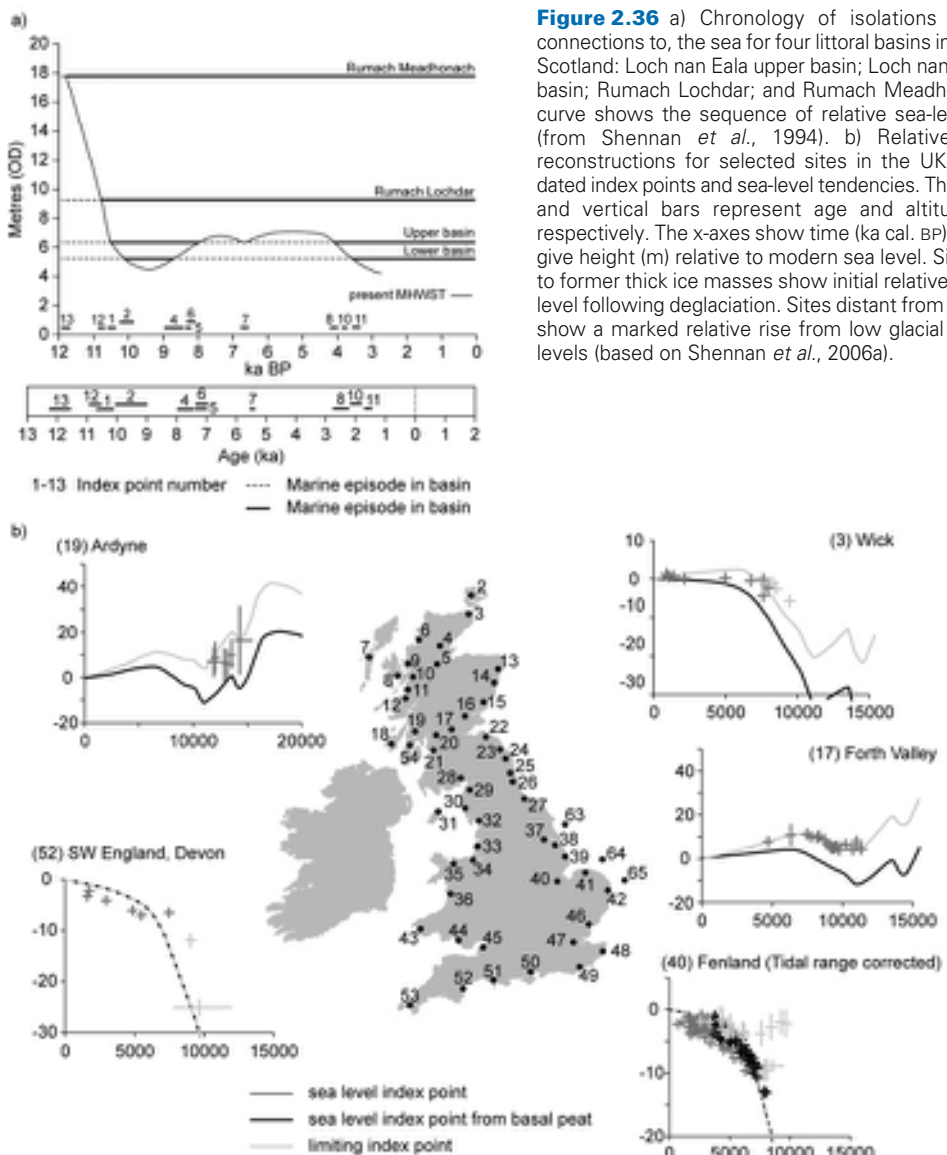


Figure 2.35 River bank section in lower Strathearn, eastern Scotland, showing Holocene marine sands overlain by a peat layer which in turn is overlain by up to 6 m of marine silts and clay. All the deposits lie above present sea level. Radiocarbon dating of the bottom and top of the peat bed indicates a relative sea-level fall (marine regression) at c. 9.6 ka cal. BP and a relative sea-level rise (marine transgression) at c. 7.5 ka cal. BP (Cullingford *et al.*, 1980; photo by John Lowe).

influence and hence a *negative sea-level tendency*. In Figure 2.35, the boundary between the top of the peat and the base of the overlying marine deposits reflects the re-submergence of the estuary, and provides a sea-level index point for an increase in marine influence, in other words a *positive sea-level tendency*. In the older literature, such evidence was often interpreted in terms of **marine regressions** and **transgressions** (falls and rises in sea level), although these terms are now less widely used as they imply absolute changes in sea level, whereas only relative sea-level tendencies can really be inferred from such evidence.

Lake basins that lie near the coast may also preserve sea-level index points where, for example, such basins have been raised above the sea and subsequently begin to accumulate freshwater sediment. These are referred to as **isolation basins**. In some instances, a rise in RSL may lead to the re-submergence of these basins, in which case brackish or marine deposits accumulate over freshwater sediments.

In northwest Scotland, for example, analysis of sedimentary sequences from a number of littoral basins shows that these had once been flooded by the sea (Figure 2.36a). In each basin, sea-level index points and tendencies suggest that, relative to the land, sea level fell by about 14 m between 12 and 10 ka as a result of isostatic recovery following deglaciation. Subsequently, sea level rose by 2–3 m relative to the land so that between 9 and 4 ka sea waters reoccupied some of the basins, while all had re-emerged from the sea by c. 3 ka (Figure 2.36a). In parts of southern England, by contrast, sea level appears to have risen relative to the land by c. 30 m or more between 10 and 4 ka (Figure 2.36b). The difference in sea-level tendencies between the English and Scottish records reflects the glacio-isostatic effects of the last ice sheet, which depressed the northern parts of the country, while southern areas lay beyond its impact. There is still a small, residual reflex movement today (Figure 2.37), for northern Britain has



been rising during the late Holocene by rates up to 2.0 mm yr^{-1} , while southern England has been subsiding by rates of up to 1.2 mm yr^{-1} (Shennan & Horton, 2002). It must be emphasized, however, that unlike the curves in Figures 2.31–2.33, those in Figure 2.36b are *relative* sea-level curves, as they are derived from localities where crustal warping has occurred. They therefore provide an indication of local trends in sea level only.

The rate of Holocene eustatic sea-level rise slowed markedly after c. 5 ka, reflecting contraction of the great

continental ice sheets to small residual remnants, and broadly stabilized between 3 and 2 ka (Intergovernmental Panel on Climate Change, 2007). Indeed, sea levels may have fallen slightly during the late Holocene as ocean water was transferred from equatorial to high-latitude regions to fill space in the ocean basins caused by the subsidence of glacial forebulges (section 2.5.4). This process has been reversed in recent centuries, however, as both tide gauge records and empirical evidence from, for example, salt marsh contexts (Gehrels *et al.* 2004, 2006), show evidence

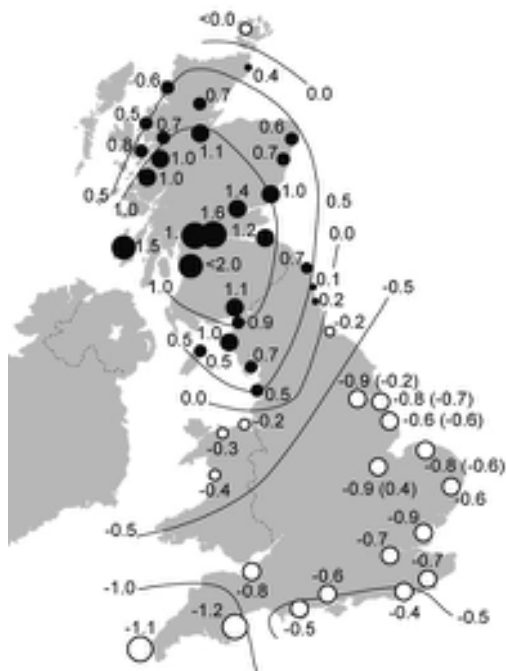


Figure 2.37 Relative changes in land or sea level in the UK during the late Holocene (mm yr^{-1}). Positive values (filled circles) indicate relative land elevation or sea-level fall; open circles indicate land subsidence or sea-level rise. Figures in parentheses are model-adjusted (from Shennan & Horton, 2002).

of rising sea levels from the early 1800s onwards. Indeed, data from the east coast of the USA suggest a rise of around 1.7 mm yr^{-1} during the twentieth century (Engelhart *et al.*, 2011). Modelling studies confirm the sea-level acceleration from the nineteenth to the twentieth century and point to anthropogenic forcing as a partial cause (Gregory *et al.*, 2006), although discrepancies between model simulations and observed sea-level rise mean that further work is required to reconcile observations from tide-gauge and proxy data with the modelling studies (Gehrels, 2010). This is an important research area because concern over possible future sea-level rise caused by anthropogenically forced climate change is leading to greater demands for better baseline data from which to predict future sea-level scenarios (Church *et al.*, 2008; Woodroffe & Murray-Wallace, 2012).

Despite the advances that have been made over recent years in understanding long-term eustatic changes, quantifying the eustatic element in Quaternary sea-level records on the basis of empirical evidence remains extremely problematical. Attempts have repeatedly been made to separate the isostatic from the eustatic component by using

eustatic sea-level data from ‘stable’ coastlines, but it is now acknowledged that few parts of the world have been unaffected by some form of tectonic activity and hence can be considered as ‘stable’. In southern Australia, for example, which occupies a passive enclave within a **craton** (the stable core of a lithospheric plate) and is located far from the isostatic impacts of Quaternary ice sheets, interglacial shorelines have, nevertheless, been tectonically deformed (Murray-Wallace, 2002). Similarly in the Caribbean region, again often considered to be relatively stable, a *c.* 80 ka raised shoreline that can be traced from Barbados, through the Bahamas, Florida and Bermuda, to the Atlantic coast of the USA, has clearly been disrupted, partly by differential hydro-isostatic effects (section 2.5.3.), and partly by glacio-isostatic influences of the last North American ice sheet (Potter & Lambeck, 2003). A clearer differentiation of the eustatic component in long-term Quaternary glacial–interglacial sea-level oscillations will therefore require the improved definition of palaeo sea-level indicators, more secure chronologies, and the development of geophysical models that integrate eustatic and tectonic data (Mastronuzzi *et al.*, 2005).

A second major difficulty is posed by **geoidal eustasy**. The earth is not spherical, but is flattened at the poles and bulging at the equator, and it has generally been assumed that the free ocean surface or **geoid**, which is the averaged elevational surface that is everywhere perpendicular to the direction of gravity, is smooth and regular and parallels the shape of the earth. However, satellite measurements have shown that this is not the case: the real geoid is highly irregular, even over the ocean surface, and varies by as much as 200 m between elevational highs and lows (<http://earthobservatory.nasa.gov/Features/GRACE/>; Tapley *et al.*, 2004). Furthermore, its shape is constantly changing. Some of the geoidal irregularity is caused by gravitational deformities resulting from the earth’s rotation or from the spatial complexity of its internal density structure. But there are also glacio-isostatic effects caused by the transfer of mass from the oceans to the higher latitudes during build-up of ice sheets, and the reversal of this process during phases of ice melt. Furthermore, oscillations in sea level lead to variations in hydro-isostatic pressure on the beds of the ocean basins. The result is that there is unlikely to be any part of the geoid that remains unaffected (Milne & Mitrovica, 2008). Not only does the geoidal ocean surface intersect different land masses simultaneously at different altitudes, but the overall pattern of gravitational deformation of the geoid changes over time. While this may not affect the construction of sea-level curves for individual localities, it does mean that realistic eustatic sea-level curves can only be constructed for individual regions, and that



Figure 2.38 Raised coral reef terraces extend for over 80 km along the coast of the Huon Peninsula, Papua New Guinea, reflecting tectonic uplift rates of up to c. 5.0 m ka^{-1} . In the part of the sequence shown here, the Holocene (MIS-1) platform is now at 18 m and the last interglacial (MIS-5e) terrace at 350 m above present sea level, indicating a mean uplift rate of c. 2.8 m ka^{-1} (from Esat *et al.*, 1999; photograph by Tezer Esat, Australian National University, Canberra; reprinted with permission from AAAS).

those curves remain area-specific. The corollary, of course, is that a single, globally valid eustatic sea-level curve based on shoreline evidence, so long regarded as the holy grail of sea-surface studies, is effectively unattainable (PALSEA, 2010).

2.5.3 Tectonic influences

Shoreline displacement and deformation resulting from long-term earth movements is apparent in many parts of the world and provides important evidence for the rates of operation of tectonic processes. In New Guinea, for example, the spectacular flights of raised coral terraces that extend for almost 80 km along the emergent coastline of the Huon Peninsula (Figure 2.38) have been uplifted at rates of $0.5\text{--}4 \text{ m ka}^{-1}$ over a period of $>300 \text{ ka}$, the oldest and highest terrace now lying at c. 400 m above present sea level (Esat *et al.*, 1999). Similar 'staircases' of raised marine terraces occur near other active plate boundaries, including New Zealand (Claessens *et al.*, 2009), eastern Patagonia (Pedoja *et al.*, 2011) and the Aegean (Vött, 2007). At a

number of sites around the western margin of the Pacific Rim, similar numbers of Holocene terraces with typical maximum uplift rates of 4 m ka^{-1} have been observed, although much higher rates of uplift (15 m ka^{-1}) are evident along the east coast of Taiwan (Ota & Yamaguchi, 2004).

While raised shorelines provide evidence of long-term activity and recurrence intervals of major faults and earthquakes in tectonically active regions (e.g. Gardner *et al.*, 2008), they may also be indicative of rates of tectonic activity in less active areas. For example, beach ridges of Last Interglacial age (MIS 5e, c. 125 ka) confirm the long-term stability of the Carmel coastal plain of Israel, for they are all no higher than 9 m above present sea level, implying a maximum possible uplift of 48 mm ka^{-1} (Galili *et al.*, 2007). By contrast, on the coast of northeastern Brazil, there is clear evidence of down-faulting of the MIS 7c marine terrace and uplift of the MIS 5c terrace, the latter being locally c. 12 m higher than features of similar age some 1,000 km to the south (Barreto *et al.*, 2002). In this case, the shoreline evidence suggests that this passive plate margin

region, formerly considered to be relatively stable, is far more tectonically active than hitherto believed (Barreto *et al.*, 2002).

2.5.4 Glacio- and hydro-isostasy

Crustal deformation resulting from the expansion and contraction of the great ice sheets has been, and continues to be, a major cause of relative sea-level change during the Quaternary (Milne *et al.*, 2009). An increase in ice mass leads to increased loading on, and depression in, the underlying crust, while the reverse occurs during ice sheet wastage. This process of crustal warping is referred to as **glacio-isostasy**. The oceans also have a loading effect on the crust, which also varies as the ice sheets expand and contract, and the deformation of the crust that results is known as **hydro-isostasy**.

The consequences of glacial loading will vary with the rigidity of the crust, although it is clear that the earth's crust does not behave as a solid block when under stress, but rather in a malleable, visco-elastic manner, and this enables it to respond flexibly to differential ice loads (Plag *et al.*, 1998). In general, maximum loading and crustal depression occur near the centre of an ice sheet and there is a gradual rise in crustal surface towards the ice sheet margins (Figure 2.39). However, crustal depression at one point must be compensated for elsewhere, one result being an upward bulging of the crust (**forebulge**) beyond the margins of the ice mass (Figure 2.39). The areal extent of former glacial forebulges can be inferred from RSL index points, regional variations in which display complex patterns of differential crustal movement in areas that lay beyond (in some instances well beyond) the margins of the last ice sheets. In western Europe, RSL data suggest that the zone of maximum forebulge subsidence extends from Lower

Saxony in Germany, westwards through the Netherlands to the Dogger Bank area of the southern North Sea basin (Vink *et al.*, 2007), while RSL evidence from the Gulf of Mexico shows that although this area is far removed from the maximal limits of glaciation, the region is still responding glacio-isostatically, by means of forebulge collapse, to the melting of the Laurentide ice sheet (Törnqvist *et al.*, 2004). In other areas, ice sheet forebulge collapse is superimposed on regional isostatic influences, for example in west Greenland, where the RSL history of the Late Holocene reflects a combination of local and non-Greenland RSL processes, notably the reloading of the earth's crust caused by Neoglacial expansion of the Greenland ice sheet, and continued subsidence associated with the collapse of the Laurentide ice sheet forebulge (Long *et al.*, 2009). The vertical extent of crustal displacement associated with forebulge development is often considerable. In western Canada, for example, evidence from the coast of British Columbia indicates land uplift from the forebulge of the Cordilleran ice sheet of the order of 85 m, which exposed parts of the currently submerged coastal shelf close to Queen Charlotte Island (Figure 2.40).

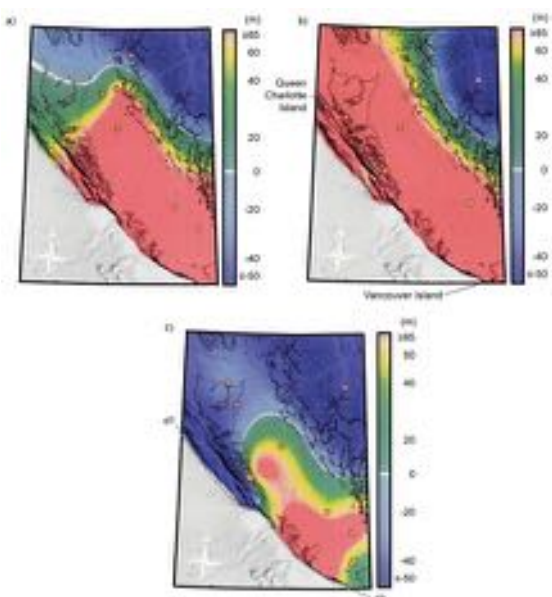


Figure 2.40 Crustal flexuring in the Pacific margin of Canada reflecting the changing mass of the last ice sheet in British Columbia at a) 13.2–12.7 ka, b) 11.7–11.2 ka and c) 10.2–9.7 ka. Areas in shades of blue/purple are depressed, while those in green, yellow and pink are elevated, relative to the present. The latter represent a transient glacial forebulge situated beyond the perimeter of the ice mass (from Hetherington & Barrie, 2004, reprinted with permission from Elsevier).

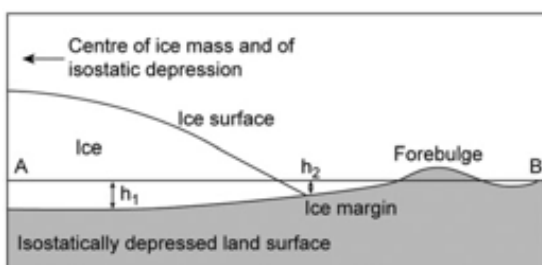


Figure 2.39 Schematic diagram of the effect of an ice mass on a land surface. In general terms, the amount of isostatic depression of the land surface A-B increases proportionately with ice load, so that greater depression occurs towards the centre of an ice mass than around its margin (cf. h_1 and h_2).

In a now classic work on the Canadian Arctic, Andrews (1970) proposed three developmental stages in the process of isostatic recovery after ice-sheet melt. The rapid crustal adjustment that occurs at a site between initial ice sheet contraction and subsequent deglaciation is referred to as **restrained rebound**. Following ice wastage, more gradual **postglacial rebound** takes place, which continues up to the present day. The relatively small amount of uplift still required to re-establish crustal equilibrium is termed **residual rebound**. Isostatic recovery can therefore be seen as a process that accelerates rapidly at first, but which then slows down gradually as the pre-glacial state of crustal equilibrium is approached. In many areas, isostatic uplift is not yet complete (Figure 2.37). Parts of Norway and the Gulf of Bothnia, for example, are presently rising at a rate of c. 1.0 mm yr⁻¹ (Fjeldskaar *et al.*, 2000), while in North America, GPS measurements show the most rapid current rate of land uplift to be c. 10 mm yr⁻¹ in the Hudson Bay area, where ice cover was thickest at the LGM. The computed uplift rates decline with distance from Hudson Bay and, further south, change to subsidence by c. 1–2 mm yr⁻¹ in the region of the southern Great Lakes (Sella *et al.*, 2007).

The magnitude and regional impacts of hydro-isostatic effects are more difficult to estimate. The problem is that both the sea surface and seabed have been subject to differential flexuring, the former by geoidal variations, and the latter by glacio-isostatic effects which, as we have seen, extended far beyond the ice sheet margins. Moreover, spatial variations in the rheological behaviour of the crust and in ocean density mean calculation of past hydro-isostatic effects is not straightforward (Lambeck *et al.*, 2003; Mitrovica, 2003) and, moreover, it is particularly difficult to separate the impacts of the hydro-isostatic component from those of other flexural stresses. A particular problem arises from the process of **ocean siphoning** (Mitrovica & Peltier, 1991). As the ice sheets melted and forebulges collapsed, the continental shelves were tilted towards the oceans, partly by continental isostatic recovery and partly by the increased mass of the oceans from meltwater input. Sea water could therefore encroach across previously glaciated and up-tilted shelf areas, progressively drawing (siphoning) water away from the open oceans. Some regions may therefore have experienced rapid rise in sea level during the early Holocene, followed by a relative fall in sea level as a consequence of the siphoning effect (section 2.5.2). Indeed, marked Holocene shorelines traceable throughout the central Pacific between New Zealand and Japan are considered to reflect this process (Dickinson, 2000), while variations in the timing and elevation of the Holocene high sea-level stand around the coast of Australia are attributed largely to ocean siphoning

(Lewis *et al.*, 2012). In smaller ocean basins, the interaction between deglacial sea-level rise and local flexuring of the crust can result in **continental levering**. In the Mediterranean region, for example, subsidence caused by increased weight of water resulting from sea-level rise is pronounced in the central, deeper parts of the basin, leading to uplift and hence emergence of strandlines around the periphery (Stocchi & Spada, 2007). A combination of hydro-isostatic effects and crustal warping from sedimentary loading may also occur close to large deltas, such as in the Gulf of Mexico (Simms *et al.*, 2007).

2.5.5 Shoreline sequences in areas affected by glacio-isostasy

During glacial episodes, eustatic sea levels were low, but because the crust was also depressed beneath the weight of

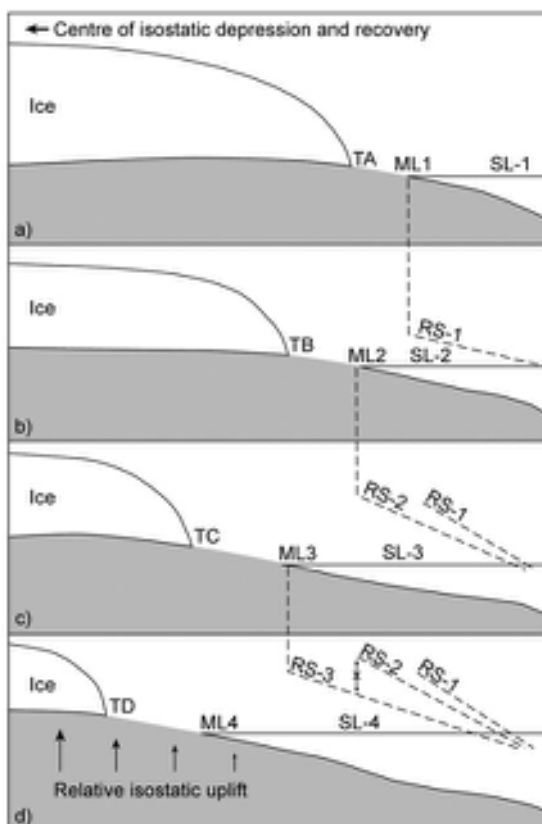


Figure 2.41 The development of a raised shoreline sequence reflecting isostatic recovery and eustatic rise following deglaciation. ML – marine limit; SL – sea level; RS – raised shoreline. The effects of the forebulge (Figure 2.39) have been omitted from this diagram. See text for further explanation.

ice, shorelines may have formed in some localities close to the margins of the ice sheets. This is indicated by the fact that in many areas, raised shorelines terminate inland in glacial outwash and related deposits. Following deglaciation, both land uplift and sea-level rise occurred and hence sequences of raised shorelines have developed that reflect the interplay of isostatic and eustatic factors.

Figure 2.41 shows the type of shoreline sequence that might be found in an area undergoing isostatic recovery. As the ice front recedes from terminus TA to TB, uplift occurs so that the shoreline formed when the sea level stood at SL-1 is raised above the new sea level, SL-2. Because isostatic recovery decreases with distance from the centre of an ice sheet, the shoreline RS-1 will be tilted away from the ice-sheet centre. During glacier retreat from TB to TC, the shoreline that developed while the sea stood at SL-2 is raised and tilted (RS-2), but it will be less steeply inclined than RS-1, which has now been even further deformed. However, because the rate of isostatic recovery at that time was accelerating due to rapid ice wastage, the marine limit (ML2) of RS-2 has been raised to a higher altitude than the marine limit ML1 of shoreline RS-1. Subsequently, a third raised shoreline (RS-3) develops, but by this time isostatic recovery has slowed down, so that the marine limit ML3 is found at a lower altitude than either ML1 or ML2. Moreover, a combination of decreased uplift and an increase in the rate of eustatic sea-level rise means

that the RSL in the area is rising and therefore later shorelines will progressively truncate the older and more steeply inclined features (Figure 2.41d). In general, therefore, the oldest and most steeply tilted shorelines will form at the greatest distance from the ice centre, younger shorelines will be less steeply inclined and more extensively developed, and older features will have been destroyed or partly destroyed during the formation of younger shorelines or, in certain cases, will either be buried beneath later sediments or will be found below present sea level. The vertical interval between individual shorelines at particular localities shows the amount of isostatic uplift that has occurred between the times of shoreline formation ('x' in Figure 2.41d).

Raised shorelines can be both depositional and erosional forms, and the extent to which a clear geomorphological feature develops depends on a range of factors including the length of time that sea level remained constant relative to the land, and on the operation of local glacial, fluvial and marine processes. Continuous shoreline features will have evolved in some areas, while in others the geomorphological expression of relative sea-level change may be more sporadic. However, postglacial subaerial and marine activity may have destroyed or extensively modified much of the evidence, even in those localities where coastal landforms were originally well developed. Consequently, only shoreline fragments remain in most areas, and careful mapping

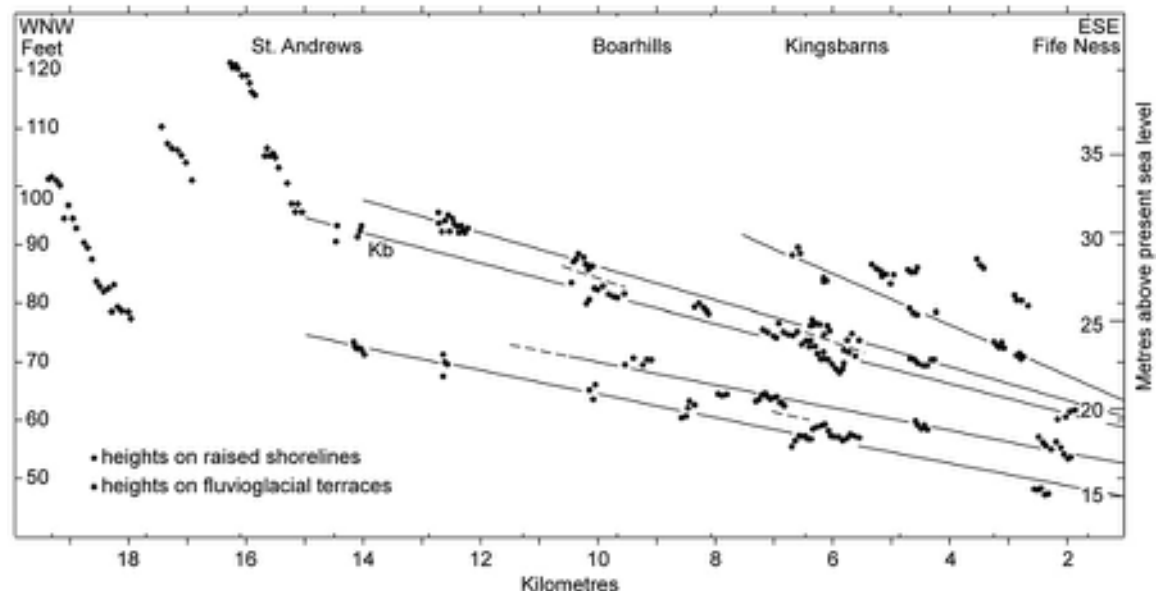


Figure 2.42 Height-distance diagram of measured altitudinal variations of the surfaces of shoreline fragments in Fife, eastern Scotland (modified after Cullingford & Smith, 1966). For further explanation see text.

and instrumental levelling of each shoreline remnant is necessary before individual shorelines can be reconstructed and inferences made about former sea levels (Smith *et al.*, 2006), a procedure that has become easier to conduct in more remote regions by using airborne LIDAR data and digital terrain modelling (Kovanen & Slaymaker, 2004). In some sheltered localities, however, because of the complex interplay between land uplift and eustatic sea-level rise, some shorelines may become buried by younger marine sediment. Further isostatic recovery may raise these above present sea level to produce **raised buried shorelines** (Gray, 1984). In order to reconstruct the complete history of isostatic and eustatic changes in such areas, therefore, subsurface stratigraphic information obtained from boreholes needs to be integrated with the results of detailed mapping of visible shoreline fragments.

Raised shoreline data are usually presented in the form of a height-distance diagram (Figure 2.42), which is a plot of all the individual data points in a vertical plane running parallel to a line towards the assumed ice centre. Shoreline fragments are resolved into a series of inferred shorelines, and the gradients of the features can then be calculated, usually by means of regression analysis. Where prominent shorelines of the same age are found in different areas, **isobases** can be constructed for these shorelines. Isobases join points of equal altitude (or uplift) on shorelines of the same age. The pattern of isobases, reconstructed either manually or using trend surface analysis, gives a three-dimensional image of the deformation of the land surface by the weight of glacier ice (Figure 2.43). It is important to appreciate, however, that while the isobase patterns may indicate in a very general way those areas that experienced maximum glacio-isostatic depression, the values of the isobases themselves bear no relation to the amount of depression (or subsequent rebound) that has actually occurred. Hence, isobase maps such as Figure 2.43 show only uplift *relative to present sea level*, and not *absolute* uplift following deglaciation. Moreover, large-scale isobase maps tend to be generalized, and fail to represent the complex deformational effects that arise when there was more than one ice accumulation centre, or the consequences of local crustal flexuring that only become apparent when there is sufficient evidence to reveal isobase trends at the regional scale (e.g. Figure 2.43).

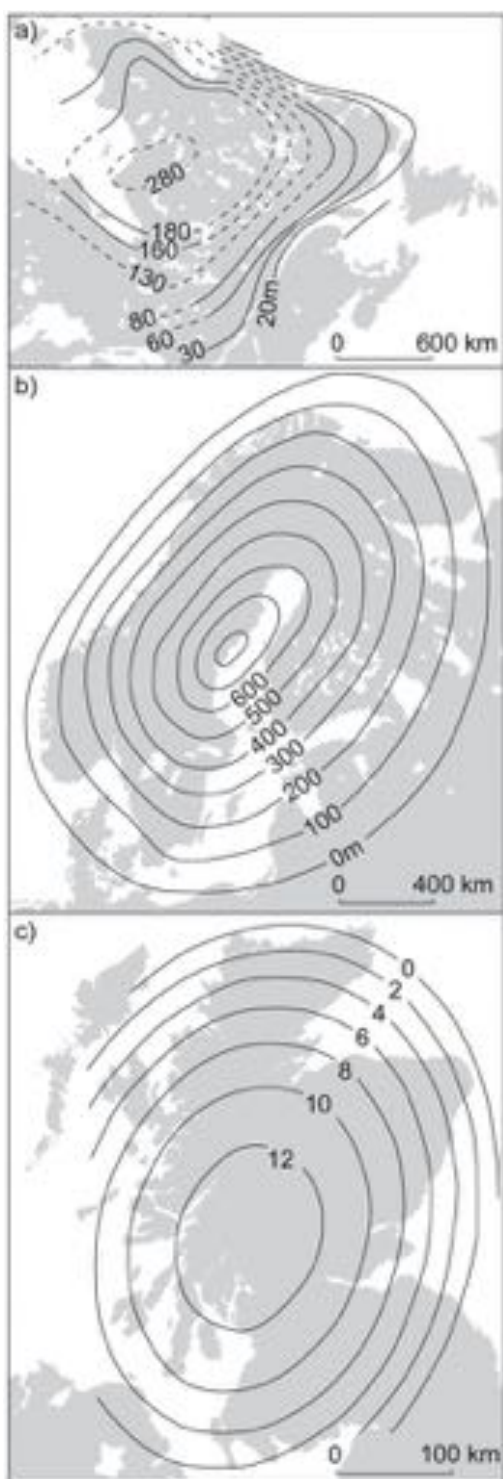


Figure 2.43 a) Isobase map showing uplift (in metres) in eastern Canada since 7.5 ka (Hillaire-Marcel & Ochietti, 1980). b) Isobases (in metres) showing absolute uplift of Scandinavia during the Holocene (Mörner, 1980). c) Quadratic trend surface showing isobases (in metres) on the Main Postglacial Shoreline (c. 6.5 ka) in Scotland (Firth *et al.*, 1993).

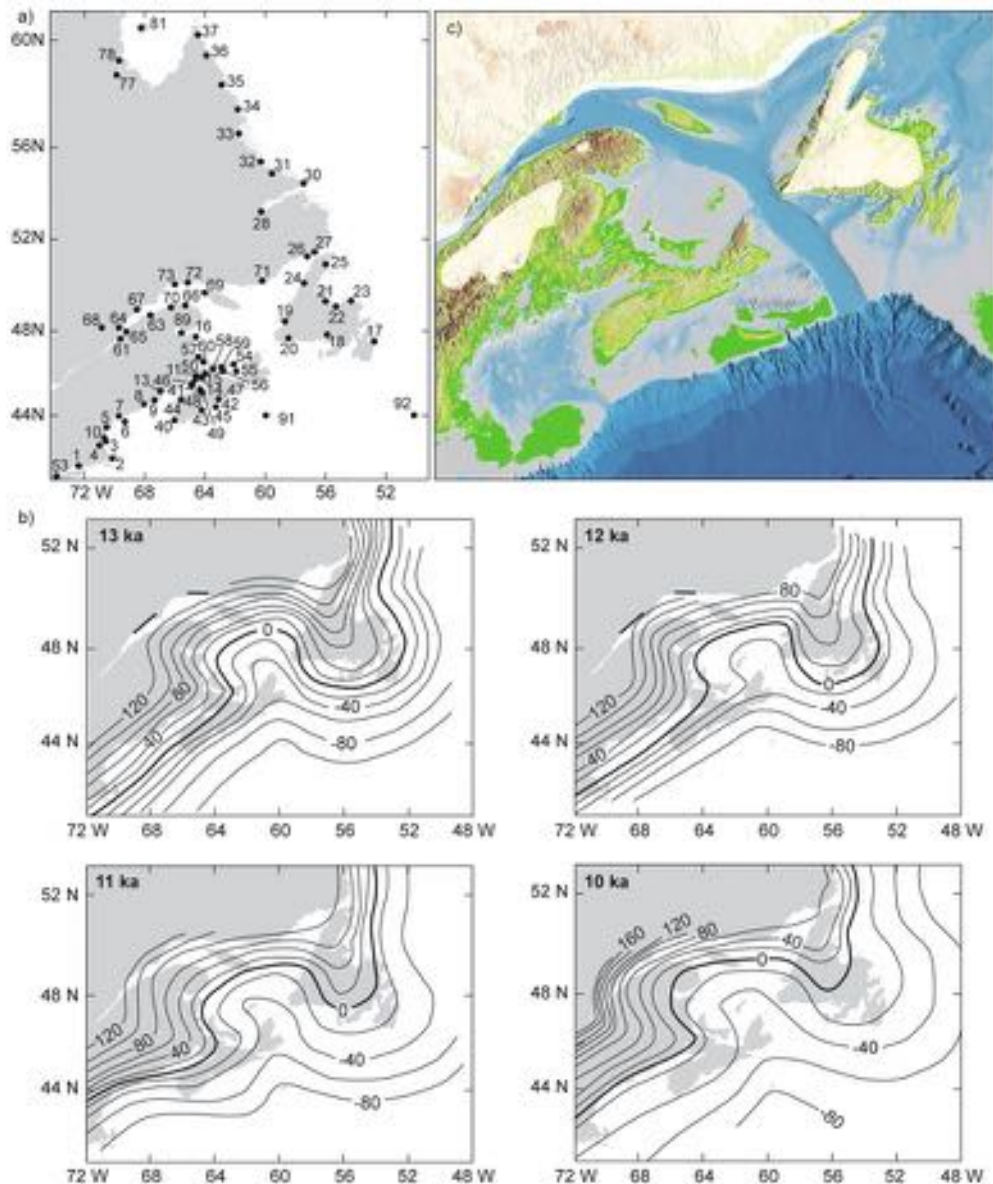


Figure 2.44 Sea-level changes in Atlantic Canada. a) Location of sites from which relative sea-level data have been obtained. b) Isobases (in m) for shoreline uplift for 13, 12, 11 and 10 ka. c) Palaeogeographic map for 12 ka based on isobase data: green and yellow are land areas, grey is shallow littoral zone, blue is sea and white is glacial ice cover (from Shaw *et al.*, 2002).

Recent years have seen the development of more sophisticated numerical models of glacio-isostatic rebound and associated sea-level fluctuations. Such models provide information on, *inter alia*, the earth's response to surface loading; on ice-sheet dimensions and behaviour (section

2.3.4); on the ages of raised shorelines where dating by direct means (e.g. radiometric dating) is not possible; on the palaeogeography of the changing coastline (e.g. Figure 2.44); and on the extent to which sea-level measurements from different sites can be combined to form representative

sea-level curves for a given region (Shennan *et al.*, 2006b; Smith *et al.*, 2012). The models combine glaciological evidence, empirical data relating to sea-level change, and geophysical parameters relating to the rheological¹³ properties of the upper mantle (Peltier, 2002; Shennan *et al.*, 2006a). In northern Ireland, for example, RSL evidence combined with glacial isostatic adjustment modelling have been used to constrain the evolution of the last Irish ice sheet, the ‘best-fit’ ice model pointing to the development of a spatially extensive ice sheet of around 700 m thickness over much of northern and central Ireland at the LGM, with very rapid deglaciation after 21 ka (Brooks *et al.*, 2007a). In the high Arctic to the north of Norway, outputs from a fully integrated ice-mass and glacio-isostatic model of the Late Weichselian ice sheet suggest that initial ice growth over Scandinavia and adjacent island archipelagos caused uplift of the central Barents Sea, and subsequent growth of ice across the entire Barents Shelf (Howell *et al.*, 2000), a reconstruction that could not have been made from empirical evidence alone. Elsewhere, geophysical modelling and empirical data on sea-level variations have been used to reconstruct patterns of crustal tilting and uplift at the north Cascadia subduction zone of western Canada during the retreat of the Cordilleran ice sheet (James *et al.*, 2000), while empirical evidence of RSL and ice extent were employed to calibrate a glaciological model of the behaviour of the Greenland ice sheet between the LGM and the present day (Simpson *et al.*, 2009). Isostatic rebound models, combined with empirical data of sea-level change, therefore provide a basis for assessing the rheological behaviour of the earth’s crust, and also for testing glaciological reconstructions.

2.5.6 Palaeoenvironmental significance of sea-level changes

Understanding the causes and effects of sea-level change is of fundamental importance in the analysis of Quaternary environments, for not only do they enable sea-level histories to be reconstructed, but as we have seen in the foregoing sections, they provide additional insights into glacier and ice sheet behaviour, into deglacial chronologies and into the tectonic history of littoral zones. Changing levels of land and sea impact on other aspects of Quaternary research, however. For example, lowered sea levels in the past have provided migration corridors and access routes to new territories for plants and animals, while shorter sea passages may have encouraged movements of humans by boat. Land bridges formed at times of lower sea level, such as that across the Bering Strait (Dixon, 2001); the Indonesian islands were joined together to form the now submerged

Sundaland; and Australia and New Guinea were connected by the Sahul Shelf (Bird *et al.*, 2005). It was across these land bridges that the peopling of the Americas and Australia took place (Davidson, 2013). By contrast, rising sea levels submerged former land-links, a process that may have encouraged the spread of early farmers into Europe during the Neolithic after previously occupied fertile lowlands were lost to the sea (Turney & Brown, 2007). The reconstruction of former coastlines can therefore provide an important aid to understanding human history, not least because of the resource potential of littoral zones for prehistoric communities (Smith *et al.*, 2010). Finally, there are indirect effects of the crustal stresses caused by glacio- and hydro-isostatic change, for these may have caused increased eruptive activity in major volcanic centres, such as the Campanian region in Italy (D’Argenio *et al.*, 2004), and perhaps more widely in the Mediterranean area (McGuire *et al.*, 1997). These crustal stresses may have also influenced (and continue to influence) the rates of release of fluids and gas, such as methane, from sea-bed repositories, and thus affect the greenhouse gas content of the atmosphere (Boles *et al.*, 2001).

2.6 RIVER TERRACES

River valleys throughout the world contain abundant evidence for changes in fluvial activity. Short-term adjustments in river regime and channel course lead to the erosion of floodplain deposits, especially during peak discharge (flood) events. If the river permanently changes course, former channels may be marked by distinctive erosional scars or remnant meander loops, and abandoned flood-plain levels by inactive sand or gravel (braid) bars and overbank, finer-grained deposits (Blum and Törnqvist, 2000). The dominant factor governing these hydrological changes is precipitation, although the impact of rainfall variations on fluvial systems is modulated by other components of the landscape, notably soil and vegetation cover, which are themselves influenced by changes in climate (Törnqvist, 2007). To a large extent, therefore, relict fluvial landforms reflect the impacts of regional climatic variations, although during the Late Quaternary, the increasing influence of people on hydrological processes adds a further dimension to the interpretation of river histories (Hoffmann *et al.*, 2010).

In many river valleys, long-term changes in river regime are reflected in **river terraces** preserved on valley sides or alongside the present river channel on the floodplain (Figure 2.45). Sometimes these exist as single features, but on occasions they are arranged in vertical succession forming a flight or ‘staircase’, and, in major river valleys such as the



Figure 2.45 Terraces cut into outwash gravels, Glen Roy, Scotland (photograph by John Lowe).

Rhine (Figure 2.46), Somme or Danube, these represent episodes of alluviation and incision over a considerable part of the Quaternary period (Bridgland & Westaway, 2008a). Fluvial terraces may be erosional, with bedrock being planated to form a low-gradient **strath** which is often covered by a thin veneer of alluvium, or they may represent the upper levels of aggradation (alluvial sediment accumulation) on the valley floor before subsequent downcutting, that is, the surfaces of former floodplains (Figure 2.46). River terraces occur in all geomorphological and climatic environments and may be preserved as either ‘paired’ or ‘unpaired’ features. Where there has been an episode of rapid incision by the river, then ‘paired terraces’ may form on both sides of the valley. During times of slow downcutting or land surface stability, however, lateral migration of the stream channel leads to erosion of floodplain gravels on the outer edges of meanders. If prolonged, this may lead to complete removal of former floodplain gravels from one flank of the valley, leaving a single or **unpaired terrace** on the other (protected) side. Terrace formation and preservation therefore reflects the rate and magnitude of incision and

lateral migration of the river channel, while episodes of fluvial downcutting are usually interspersed with aggradational phases, a process referred to as ‘**cut and fill**’ (Figure 2.47).

Because river terraces are most frequently developed on unconsolidated alluvial sediments, they are easily destroyed by subsequent fluvial action, and hence a previous floodplain surface will usually only be preserved in the form of individual, sometimes isolated, terrace fragments. Instrumental levelling of the terrace remnants and collation of the data by means of height–distance diagrams enables down-valley gradients of former floodplain levels to be reconstructed. It has usually been assumed that the highest (and generally the most fragmented) forms in a terrace series represent the oldest river levels, and lower terraces reflect successively younger stages. In broad outline, this relationship seems to hold, but it is now apparent that the sequences in many river valleys is more complicated than this, and stratigraphic evidence is usually required if a complete fluvial history of a river valley is to be reconstructed. Older terrace surfaces can be buried beneath

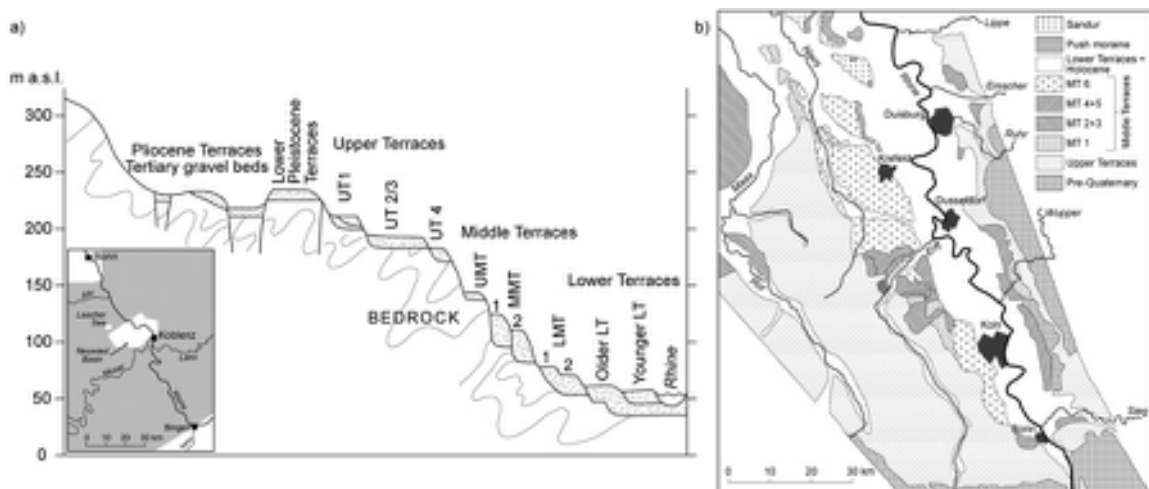


Figure 2.46 a) Schematic representation of the staircase of river terraces preserved in the Middle Rhine area, which spans the Pliocene to Late Quaternary. b) Areal distribution of terrace gravels in the Lower Rhine, reflecting long-term lateral migration of the river's course (after Boenigk & Frechen, 2006).

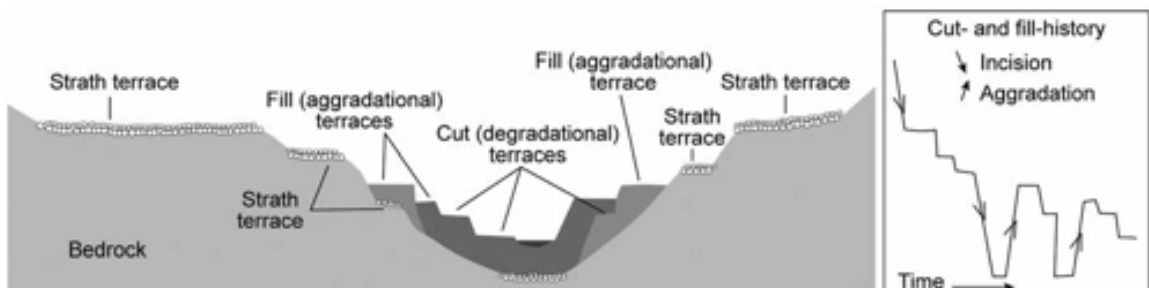


Figure 2.47 Formation of 'strath' and 'cut-and-fill' fluvial terraces. Strath terraces are formed by lateral fluvial erosion of bedrock, while cut-and fill terraces are composed of fluvial deposits (from Merritt, 2007).

younger alluvial fills or other deposits, and might only be discovered where exposed by erosion or through systematic borehole survey, the former terrace surfaces being indicated by buried soils, weathering profiles, peat layers, fossiliferous beds or archaeological features. In the Somme valley of northern France, for example, a 700 ka terrace sequence has been buried by aeolian sediments (loess) with intercalated palaeosols (Figure 2.48). Where exposures are not available, therefore, and river terraces are recognized purely on the basis of observable geomorphological characteristics, a greatly over-simplified history of fluvial activity could be inferred. In the study of river terrace sequences, therefore, recourse is increasingly being made to sedimentary, biological and archaeological evidence, both in the recon-

struction of palaeoenvironments associated with alluvial deposition and also in the dating and correlation of individual terrace remnants (Bridgland, 2000; Gibbard & Lewin, 2009). Hence, geomorphological evidence for past fluvial activity represents only one aspect of these wider palaeohydrological investigations.

2.6.1 Origins of river terraces

River incision into a valley floor leading to the abandonment of floodplain levels, or to renewed aggradation along the river's course, may result from a number of factors. These include the following.

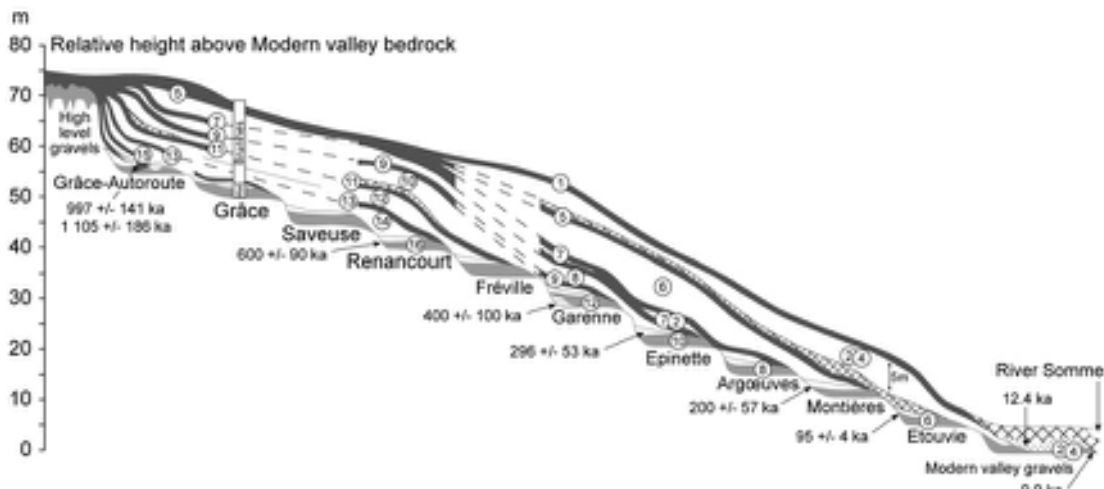


Figure 2.48 Schematic representation of a sequence of river terraces in the valley of the Somme, France, which extends over the last c. 1 Ma. The terraces can be dated by a variety of means and assigned to oxygen isotope stages (numbers in circles). The terrace surfaces have subsequently become buried beneath a thick accumulation of windblown silt (loess) and intercalated soils (from Antoine *et al.*, 2000).

2.6.1.1 Eustatic changes in sea level

Changes in sea level (base level) have long been considered to be a major variable governing river terrace development. Eustatic sea levels appear to have fluctuated through a range of perhaps 150 m during the glacial and interglacial cycles of the Quaternary (section 2.5.2). Traditional models envisage a situation in which active downcutting and river incision accompanied falling sea levels (i.e. during cold stages), while increased aggradation was associated with high sea-level stands, particularly in the lower reaches of river valleys inundated by the rising sea. Reconstructions of the long profiles of former floodplains should therefore show convergent grading to these interglacial sea-level positions. Terraces related to sea level in this way have been referred to as **thalassostatic terraces** ('thalassa' is Greek for sea). However, this paradigm is not well supported by empirical evidence for past river behaviour, as reflected in the geomorphological and stratigraphical archives preserved in major river valleys. Rather, aggradation appears to have dominated in the lower reaches of fluvial valleys during cold stages, while alternation between phases of incision and aggradation has clearly been a driving force behind river terrace formation in river reaches well-upstream of any marine influence (Bridgland & Westaway, 2008a). Moreover, spatial and temporal variations in geomorphic activity within a river system make it extremely difficult to isolate those changes in fluvial activity induced by base-level changes from those caused by other environmental variables, such as river discharge and sediment yield from the catchment, or tectonic influences (Hancock & Anderson, 2002).

2.6.1.2 Climatic change

The influence of climatic change on river valley evolution has long been recognized, and is still regarded as a major influence on river terrace development (Starkel, 2003; Bridgland & Westaway, 2008a). The relationship between river behaviour and climate depends on the nature of climatic change and on the effects of such changes on discharge and sediment load. In semi-arid and arid regions, river incision occurred primarily during pluvial episodes (section 2.7.1), when discharge was more constant and sediment yield was reduced by an expansion in regional vegetation cover. Phases of aggradation, on the other hand, were more characteristic of arid periods, when discharge was reduced and sediment yield from more sparsely vegetated catchments was enhanced. In the northwest Himalayas, for example, phases of fluvial aggradation have been correlated with intensification of the Indian summer monsoon, while downcutting coincided with weaker monsoonal activity (Brookhaven *et al.*, 2006). In temperate regions, increased aggradation occurred during colder periods when rivers were more heavily debris-laden. Present arctic nival discharge regimes are marked by a major flood event during the spring resulting from the rapid melt of winter snow (Syvitski, 2002). Hence, areas

affected by periglacial conditions in the past would have experienced seasonal flooding due to snowmelt, and increases in sediment yield due to a combination of a relatively sparse vegetation cover and ground disturbance by periglacial processes (Vandenbergh & Woo, 2002). During warmer periods, sediment yield would have been reduced and discharge variations less marked. Terraces related primarily to climatic changes have been referred to as '[climatic terraces](#)', but clearly some geographical variation in the relationship of terrace formation to climatic factors is to be expected. Moreover, it must be stressed that climate is only one of a number of variables affecting discharge, sediment load and sedimentation (Vandenbergh, 2003).

2.6.1.3 Glaciation

In areas formerly covered by glacier ice, deglaciation was typically associated with the accumulation of glaciofluvial sediments (mainly outwash gravels), followed by alternating periods of incision and aggradation or channel stability, which resulted in the formation of terrace sequences in river valleys (Evans & Twigg, 2002). These are usually described as [outwash terraces](#), and are frequently preserved as complex terrace systems comprising several surface levels along the margins of upland river valleys (Figure 2.45). In some areas, catastrophic release of water from glacier-dammed lakes ([jökulhlaps](#)) may have been a further factor in the formation of outwash terraces (Alho *et al.*, 2005). Throughout the mid-latitudes, moreover, many major drainage basins may not have been directly affected by glacier ice, but were sufficiently close to the ice margins to be indirectly influenced by glaciofluvial processes. Consequently, the geomorphology of these proglacial drainage basins may have been affected not only by an increase in river discharge, but also by higher sediment loads as debris was released from melting ice margins. During cold stages, therefore, considerable aggradation might be expected in the upper reaches of such rivers, and terraces would remain as evidence of these aggraded surfaces following river incision during the subsequent warmer phase (Bridgland & Westaway, 2008a, 2008b). In some river catchments affected by glaciation in their upper reaches, there are complex terrace suites that reflect the impact of several episodes of enhanced bedload supply during successive glacial cycles (Boenigk & Frechen, 2006; Tyrácek & Havlíček, 2009).

2.6.1.4 Tectonic changes

In general terms, tectonic uplift leads to rejuvenation of rivers and therefore to accelerated incision. These effects

are best seen in the highly active orogenic areas of, for example, southeast Asia and New Zealand, where rapid uplift has produced flights of widely separated terrace levels in many river valleys (Tsai *et al.*, 2007; Claessens *et al.*, 2009). River long profiles frequently show abrupt changes in gradient that are thought to reflect variations in uplift rates ('[knickpoints](#)'), while more subtle deformation reflecting epeirogenic influences¹⁴ can sometimes be detected (Brocklehurst, 2010). River terraces that have clearly been warped by tectonic activity enable rates and patterns of folding and faulting (Yang *et al.*, 2011). River valleys affected by glacio-isostasy would also have experienced gradient changes as a result of differential land uplift as, for example, in the Rhine–Meuse system in northwest Europe and rivers draining the Sudeten Mountains in southwest Poland (Busschers *et al.*, 2007). Even in small alpine glacier systems, ice loading can influence river terrace gradients (Pazzaglia & Brandon, 2001). In some large river valleys, however, only part of the basin may have been affected by uplift or tectonic down-warping, so that the original river long profiles traced by contemporaneous terrace fragments have become deformed or differentially displaced. This complicates the interpretation of river terrace records in valleys such as the Rhine and Danube, where the lower reaches of the rivers have been affected by downwarping, while uplift has occurred in the higher parts of the drainage systems (Ruszkinzay-Rüdiger *et al.*, 2005; Nivière *et al.*, 2008). A compilation of river terrace sequences in a number of major river catchments has revealed not only a wide variation in the extent of tectonic deformation, but also that tectonic uplift has affected some areas previously considered to have been tectonically stable (Westaway *et al.*, 2009). The possibility of crustal warping should therefore always be considered when interpreting and comparing height-distance diagrams of river terrace sequences.

2.6.1.5 Human activity

It is now apparent that in many river basins, hydrological regimes, sediment yield and consequent changes in floodplain levels have been affected by anthropogenic activity. Throughout the Mediterranean region, for example, early Holocene palaeoenvironmental records show increases in alluvial sedimentation immediately after the expansion of agriculture and settlement (Figure 2.49), while archaeological evidence points to a further acceleration in sediment yields during the Hellenic and Roman periods (Hooke, 2006). Forest clearance and cultivation practices remove the natural vegetation cover, which reduces the water-retentive

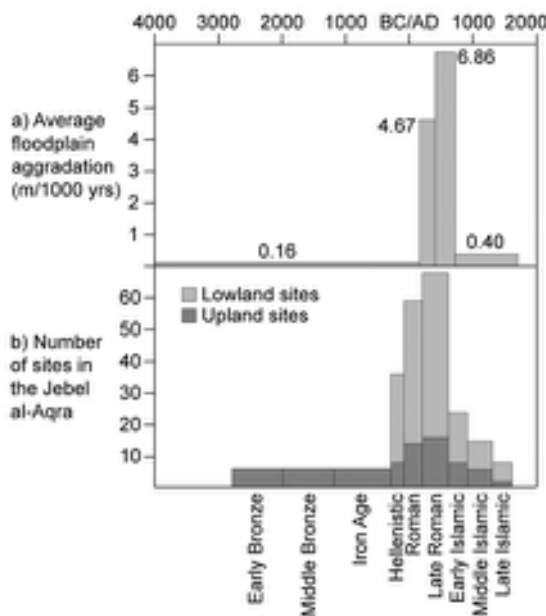


Figure 2.49 a) Average alluvial sedimentation rate calculated for three catchments in southern Turkey over the past 6 ka. b) The number of settlements occupied in the region over the same period; lowland sites are those on valley bottoms, and upland sites were located on hill-slopes or hilltops (from Casana, 2008).

capacity of the soil and leads to increased runoff. Overgrazing and over-cultivation also result in substantially increased erosion and therefore higher river sediment loads. In the Po valley in northern Italy, it has been estimated that during the Roman period, at least 60 per cent of the area was deforested and converted to cultivation, commencing in the second century BC and continuing for about 400 years. During this period, topsoils were removed from valley sides and the field systems on the Po plain became buried beneath extensive spreads of alluvial deposits, leading eventually to abandonment of the area (Marchetti, 2002). Similar episodes of alluviation associated with prehistoric woodland clearance, and with prehistoric and historic farming activity, have been recorded in Britain and Ireland (Foulds & Macklin, 2006) and throughout much of mainland Europe (Notebaert & Verstraeten, 2010). In many areas of the world, therefore, Late Holocene alluviation and associated terrace development is as likely to have been the product of human activity as of natural processes (Syvitski *et al.*, 2005).

2.6.2 River terraces and palaeo-environmental reconstruction

River terraces and their underlying sediments have long attracted the interest of those concerned with Quaternary environments. Not only do they provide evidence of former river regimes, which can offer insights into aspects of both environmental change and human history (Mishra *et al.*, 2007), but they often contain sediments with floral and faunal remains (Schreve *et al.*, 2007). Fossils are preserved, for example, in abandoned meander scrolls, in oxbow lakes or in overbank and ‘backswamp’ deposits, and from these the nature of the environment under which the terraces evolved can often be established. In some subsiding basins, fluvial deposits appear to have accumulated continuously over long timescales, such as the stacked alluvial sediments of the River Danube in the Pannonian Basin in Hungary, which contain a record of glacial–interglacial cycles spanning the whole of the Quaternary (Nádor *et al.*, 2003). In the majority of river catchments, however, the palaeoenvironmental record is much more fragmentary, due to the intermittent formation and erosion of terraces, and piecing together the fluvial historical record requires the combined efforts of geomorphologists, sedimentologists, palaeoecologists, archaeologists and geochronologists. Such reconstructions include important reference horizons for linking sedimentary sequences in different areas, while also providing a time-stratigraphic framework for Quaternary environmental changes (Bridgland, 2010). In addition, both short- and long-term climate signals can be recognized in river terrace records. For example, the Dansgaard–Oeschger oscillations (section 3.11.4) and centennial events like the Little Ice Age (section 7.6.3.5) have been detected in fluvial sequences (Macklin & Lewin, 2008), while in many areas there are indications that downcutting and terrace formation occurred close to glacial–interglacial transitions (Pan *et al.*, 2003). On longer timescales, links have been inferred between terrace formation and Milankovitch cycles. In Turkey, for instance, a 41 ka obliquity signal is reflected in river terrace sequences (Maddy *et al.*, 2005), while in the Thames basin of south-east England, a distinct aggradational terrace formed in each of the last five 100 ka eccentricity cycles (see below). Quaternary fluvial records may therefore provide important baseline data for predictive modelling of the relationships between long-term river behaviour and climate change (Macklin & Woodward, 2009).

2.6.3 The terraces of the River Thames

One of the most intensively studied river terrace sequences is that of the River Thames in southern England. The

Thames basin contains a long record of fluvial activity and river terrace genesis that reflects the influence of a number of the factors discussed above. Research on the terraces of the River Thames has a long history extending back well over a hundred years (Gibbard, 1994; Bridgland, 1994). Work during the first half of the twentieth century focused primarily on the geomorphology of the Thames Valley, and on the discrimination of different terraces (Wooldridge & Linton, 1955). Over the past two decades, a more comprehensive approach involving not only geomorphological mapping, but also lithostratigraphic and biostratigraphic investigations of the terrace gravels and their included organic deposits and associated archaeology, has provided new insights into the temporal and

spatial relationships of the Thames terrace sequence (e.g. Bridgland *et al.*, 2013). This new work has demonstrated that the terrace sequence and associated sediment stratigraphy of the Thames Valley are considerably more complicated than previously envisaged. However, many of the terrace names introduced by Wooldridge and Linton have been retained, as these refer to features that represent important stratigraphic marker horizons throughout the Thames Valley, although the terrace fragments are now named after the sedimentary units of which they are predominantly composed (e.g. Boyn Hill Gravel; Lynch Hill Gravel; see Figure 2.50) rather than after the particular terrace levels (i.e. Boyn Hill Terrace; Lynch Hill Terrace).

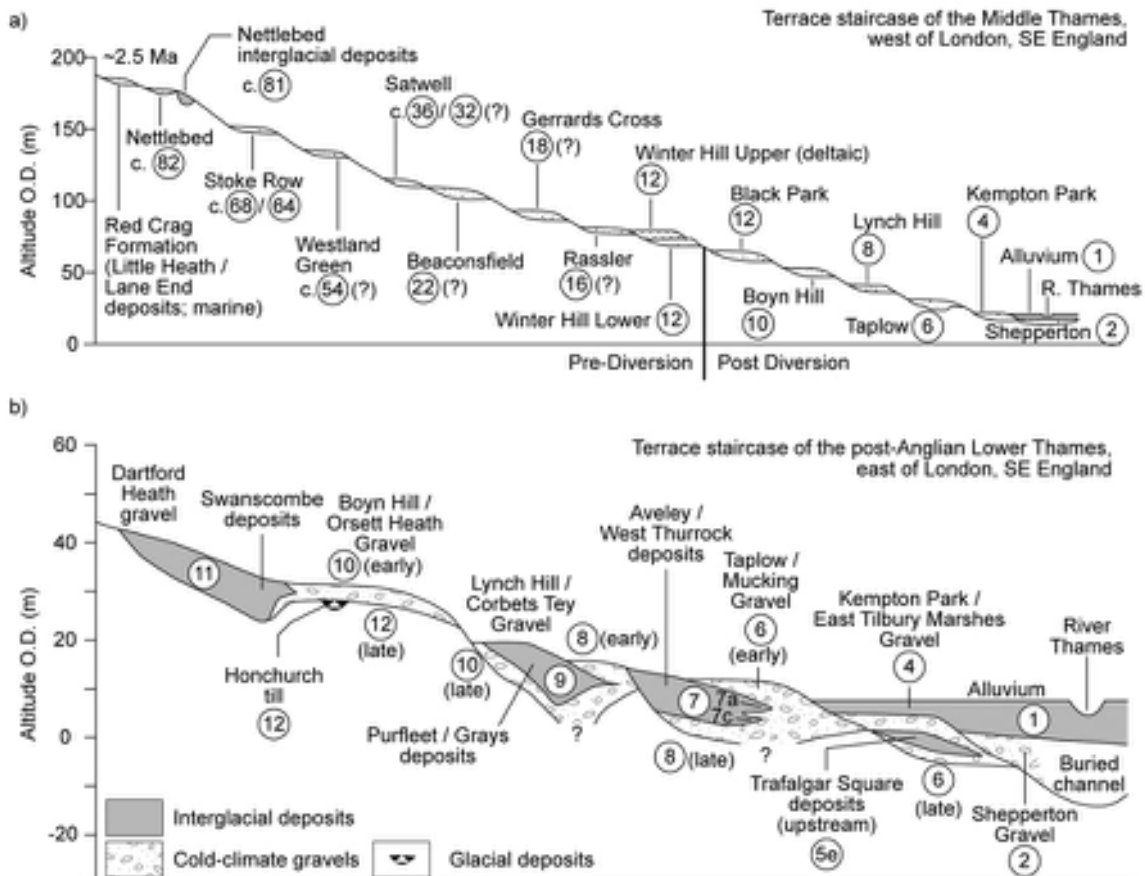


Figure 2.50 Schematic transverse profiles through the best-preserved suite of the terrace staircase of a) the Middle Thames (c. 35 km west of London) and b) the Lower Thames (c. 15 km east of London). Note that the higher and older terraces of the upper Thames are not included, and the sequence has been simplified. The circled numbers refer to the marine isotope stage (MIS) to which each terrace fragment has been assigned (from Bridgland & Westaway, 2008b).

Despite the fact that much has been learned about the history of the Thames from these recent studies, difficulties continue to be encountered in the interpretation of the record. One reason for this is that the period of time represented by preserved deposits may be relatively short, with evidence from the Devensian part of the sequence suggesting accumulation within a timespan of no more than 35–30 ka, that is, around 30 per cent of the time range of

the Devensian stage. In fact, much less time is actually represented in the sedimentary record at any one locality, for there are numerous non-sequences and minor unconformities within sequences that arise from the complex nature of the depositional processes. Downcutting between aggradations must account for a substantial part of the missing record, but the consequence is that many terraces are locally poorly defined or fragmented and hence



Figure 2.51 a) Schematic representation of the drainage system prior to the advance of the Anglian ice, c. 450 ka. b) Diverted drainage pattern and limits of the Anglian ice in eastern England during MIS 12. c) Distribution of gravel terraces in the lower Thames Valley and adjacent parts of southeast England that post-date the Anglian glaciation (after Bridgland, 2006, and Bridgland & Shreve, 2009).

correlation between individual terrace remnants and their contained sediments is seldom straightforward.

A further complication is that the River Thames has changed its course over the course of the Quaternary, principally as a result of ice sheets advancing into the drainage basin from the north. Buried valleys, spreads of fluvial gravels, and the distribution and gradient of certain terraces show that the river originally flowed out to sea on the present-day Norfolk coast some 100 km to the north of its present outlet. On at least two occasions prior to MIS 12 (before c. 450 ka), however, southward-moving ice sheets deflected the river into a new course that turned northeastwards immediately downstream from Reading, through the Vale of St Albans and across the present-day coastline near Colchester in Essex (Figure 2.51a and b). The river finally gained its present course after the Anglian glaciation (MIS 12). The consequence of these changes in river direction is that terraces of different age have diverging surface gradients, which adds a further complication to the correlation of terrace remnants. In addition, glacial encroachment into the Thames basin affected sediment input to the river, with higher sediment yields in areas adjacent to the ice margins, while glacio-isostatic loading depressed the crust beneath the ice, and compensatory forebulge effects (section 2.5.4) raised ground level beyond the ice margins. It has been estimated, for example, that glacio-isostatic adjustments have raised the terraces of Anglian age in the Middle reaches of the Thames some 55 m higher than corresponding terraces in the Upper Thames, as a result of glacio-isostatic adjustments (Bridgland & Schreve, 2009).

It was implicit in early interpretations of the Thames terrace system that the sequence, particularly in its lower reaches, reflected primarily the influence of sea-level changes, and hence terrace remnants standing above sea level were generally regarded as thalassostatic features. It is now apparent, however, that the majority of the terrace deposits aggraded under cold conditions, when sea levels were well below those of the present. In the upper parts of the drainage system, most terrace forms relate to increased aggradation during deglaciation, when meltwaters were feeding large quantities of debris into the Thames system from the northwest. Moreover, these cold-stage terraces that lie above present sea level would have been some distance from the sea at the time of their formation. At the LGM, for example, the Thames flowed over exposed parts of the English Channel to join the Rhine, Seine and other major European rivers, forming a large fluvial system that eventually drained southwards to join the sea near the edge of a wide continental shelf (Figure 2.2; Gupta *et al.*, 2007). Hence, terraces formed at that time in the lower Thames

basin were far removed from the coast, and are therefore highly unlikely to be thalassostatic. The influence of sea-level changes on the formation of the Thames terrace system has therefore been over-estimated (Bridgland, 2000).

This view has been further reinforced by evidence which shows that the Thames terraces, particularly in the lower reaches, form a well-ordered ‘staircase’, with the oldest terraces highest and younger lowest. Given that eustatic sea levels were close to (or slightly higher than) the present level during interglacials, and were lower (>100 m) during glacial periods, terraces related to former sea levels should be confined within a narrow altitudinal range, and should also show evidence of repeated reworking of sediments. That this is evidently not the case suggests the operation of another mechanism, namely crustal uplift, induced by repeated loading and unloading of the crust by glacier ice over successive glacial-interglacial cycles (Maddy, 1997; Westaway, 2002). Glacial advance would have led to the removal of surface mass by erosion and transfer to the adjacent North Sea basin, and that would have led to a compensatory net inflow of the more mobile lower crust after the ice load is removed. The overall result is incision of the River Thames to ever lower valley floor levels in response to this background of regional uplift (Bridgland, 2006).

An equally important development in understanding the evolution of the Thames terrace sequence, particularly in the lower reaches of the drainage system where post-Anglian diversion terraces are preserved (Figure 2.51c), has been the emergence of evidence for climatic forcing of terrace formation. A combination of biostratigraphy, notably mammalian and molluscan records, artefact assemblages and amino-acid geochronology (Bridgland & Schreve, 2009; Penkman *et al.*, 2013), has enabled the interglacial deposits associated with individual terrace fragments to be assigned to different warm stages, which can be correlated with marine oxygen isotope stages (Figure 2.50). The evidence demonstrates that a separate aggradational terrace formed in each of the last five 100 ka Milankovitch cycles, and that downcutting took place close to warming transitions (Bridgland, 2006, 2010). During the preceding cold phase, sediment transfer to the river channel from poorly vegetated slopes led to aggradation on the braided river floodplain. As the climate warmed and vegetation developed, sediment supply diminished and river flow was confined to single channels, where erosion could be focused and incision accelerated, while interglacial deposits accumulated in pools and areas of impeded drainage. Renewed onset of cold conditions initiated a further aggradational episode, which buried and

preserved remnants of these interglacial sediments. A much longer record of terrace deposits is preserved in the pre-diversion section of the Middle Thames, although here correlations with the MIS sequence are more speculative.

After more than a century of research, a coherent account of the evolution of the complex sedimentary archive preserved within the Thames terrace sequence is now beginning to emerge. The current view is that the river terrace staircase is generated by long-term crustal uplift, while the internal stratigraphical detail of individual terraces is determined primarily by long-term climatic variations, with the 100 ka eccentricity cycle proving to be an important driving mechanism. The Thames terrace sequence therefore provides a highly complex record of Quaternary environmental change, and the multi-disciplinary approach that has been employed to reconstruct the history of this river system constitutes a template for the analysis of fluvial sequences in other areas of the world.

2.7 QUATERNARY LANDFORMS IN LOW LATITUDES

There is abundant geomorphological and lithological evidence to show that major climatic changes have affected the tropical, subtropical and warm temperate regions of the world during the Quaternary. The periodic expansions and contractions of the great ice sheets in the high and mid-latitudes were accompanied by shifts in the climatic zones of the low latitudes, leading to marked spatial and temporal variations in regional rainfall values, seasonal distribution of rainfall, annual temperatures, and wind directions and strengths. The effects were most pronounced in the desert and savannah margins of, for example, the Sahara (LeBlanc *et al.*, 2006), northwest India (Juyal *et al.*, 2006), China (Zhang *et al.*, 2004b) and Australia (DeVogel *et al.*, 2004), although fluctuations between humid and more arid periods also affected some mid-latitude regions, such as parts of western USA (Sack, 2009) and southern Eurasia (Dogan, 2010). In many of these regions, fossil landforms and deposits are preserved that can be used to infer climatic changes during the Late Quaternary. Of particular importance are lacustrine features that provide evidence for wetter conditions at times in the past, and sand-dune complexes (or ‘sand seas’) indicating former episodes of increased aridity.

2.7.1 Pluvial lakes

In many arid and semi-arid regions of the world, **saline lakes** and ephemeral water bodies (**playa lakes**) experienced

phases of expansion and contraction during the Quaternary, while levels of present-day lakes in tropical and subtropical regions also rose and fell. Abandoned lake shorelines (Figure 2.52a) and associated littoral deposits (Figure 2.52b) are often found around large structural basins and surface depressions in which drainage is predominantly internal (**endoreic**). Lakes that show evidence of expansion and contraction unrelated to worldwide changes in base level have been termed **pluvial lakes**, as their high-water stages have been attributed to wetter climatic phases, termed ‘**pluvials**’ or **pluvial episodes**. Low water levels or periods of complete desiccation are, in turn, assumed to reflect ‘**interpluvials**’ or **interpluvial episodes**. Because of the close correspondence that appears to exist in closed-basin catchments between the status of a lake (i.e. its volume, depth, surface area, etc.) and the balance between seasonal precipitation and evaporation, temporal variations in lake surface level provide a proxy record of continental climatic change, particularly during the Late Quaternary.

Geomorphological evidence for the existence of pluvial lakes and for oscillations in water level includes former cliff-lines, shorelines, beaches, bars, spits and deltas, as well as abandoned watercourses that acted as overflows at times of high lake-level stands (Jewell, 2007). Frequently associated with these landforms are freshwater evaporates, such as marls and tufas (sections 3.7 and 3.8). The landforms and their associated deposits are not only distinctive in the field (Figure 2.52), but often appear as prominent features on aerial photographs and satellite images (e.g. Maxwell *et al.*, 2010). Strandline evidence in particular enables the former extent of Quaternary pluvial lakes, some of which occupied considerable areas, to be established. In the southwest United States, for example, where one of the greatest concentrations of pluvial lake features in the world is to be found (Figure 2.53), Lake Bonneville, a precursor of the Great Salt Lake, had a maximum surface area of 51,300 km² (the present-day Great Salt Lake is c. 4,000 km²), a volume of c. 9,500 km³ and a depth of 370 m, making it the largest known pluvial lake in North America. The second largest, Lake Lahontan in Nevada, covered an area of 23,000 km², more than fourteen times larger than the existing lake (Adams, 2010). In North Africa, Lake Chad (Figure 2.54) had a surface area of c. 350,000 km² at its maximum during the Late Quaternary (the present lake fluctuates between 10,000 and 25,000 km²), although its depth may have been no more than 50 m (Schuster *et al.*, 2005). Other large Late Quaternary pluvial lake systems include Palaeolake Makgadikgadi in the Kalahari Desert (Burrough *et al.*, 2009), Palaeolake Suguta in the African Rift Valley of northern Kenya (Garcin *et al.*, 2009) and Lake Mega-



Figure 2.52

a) Abandoned shorelines of Pluvial Lake Lahontan near the northern end of Pyramid Lake, near Reno, Nevada, USA. b) Beach deposits (lower) and fan gravels (upper) from Pluvial Lake Lahontan (Mike Walker for scale; photographs by Allan Ashworth, North Dakota State University, USA).

Frome in the Lake Eyre Basin, which contains Australia's largest endoreic drainage network (Cohen *et al.*, 2011).

The most extensive Late Quaternary palaeolake so far recorded, however, is the Caspian and Aral Sea systems of central Eurasia which reached maximum dimensions around 16–15 ka (Chepalyga, 2007). At that time, the lake covered an area in excess of 1.5 million km², stood more than 75 m above the level of the present Caspian Sea, and extended some 3,000 km up the Volga River valley. The lake was different from other pluvial lakes, however, as it was fed by waters from the Yenisei, Ob and Pechora rivers which had been diverted southwards by the Eurasian ice sheet (Mangerud *et al.*, 2004), while spring flooding and permafrost melt during warmer periods were additional

factors contributing to lake-level fluctuations (Chepalyga, 2007).

Abandoned lake shorelines in many low-latitude regions of the world therefore provide clear evidence of both the former extent of palaeolakes and of fluctuations in lake water level, and where these primarily reflect changes in atmospheric moisture balance, they can provide a basis for reconstructing past changes in precipitation regimes. However, as is evident in the case of the Caspian–Aral Sea palaeolake, lake basins may be affected in complex ways by climate change, especially those with catchments periodically fed by meltwaters from glaciers or permafrost. Moreover, as enclosed lakes expand, their surface levels may reach new overspill cols, with the result that lake volume



Figure 2.53 The maximum limits of late Pleistocene pluvial lakes in the American southwest (from Orme, 2008).

is no longer solely controlled by precipitation/evaporation ratios, which further complicates the links between lake volume and rainfall regime. An additional difficulty may be the modification of lake drainage systems by humans, notably during the Holocene, as appears to have been the case around the Aral Sea (Boomer *et al.*, 2009). One final problem arises from the use of geomorphological evidence alone to infer past lake volume changes and their palaeoclimatic significance. Although the majority of former lake

shorelines appear as horizontal features and can readily be correlated across the lake basin, in certain cases the differential effects of hydro-isostatic loading and unloading can lead to shorelines of a similar age being found at different altitudes. In the Great Basin of Utah, for example, the weight of the waters of Lake Bonneville caused isostatic depression of the crust, especially towards the middle of the lake where it was deepest (Godsey *et al.*, 2005; Sack, 2009). Following the disappearance of the lake around 10 ka,

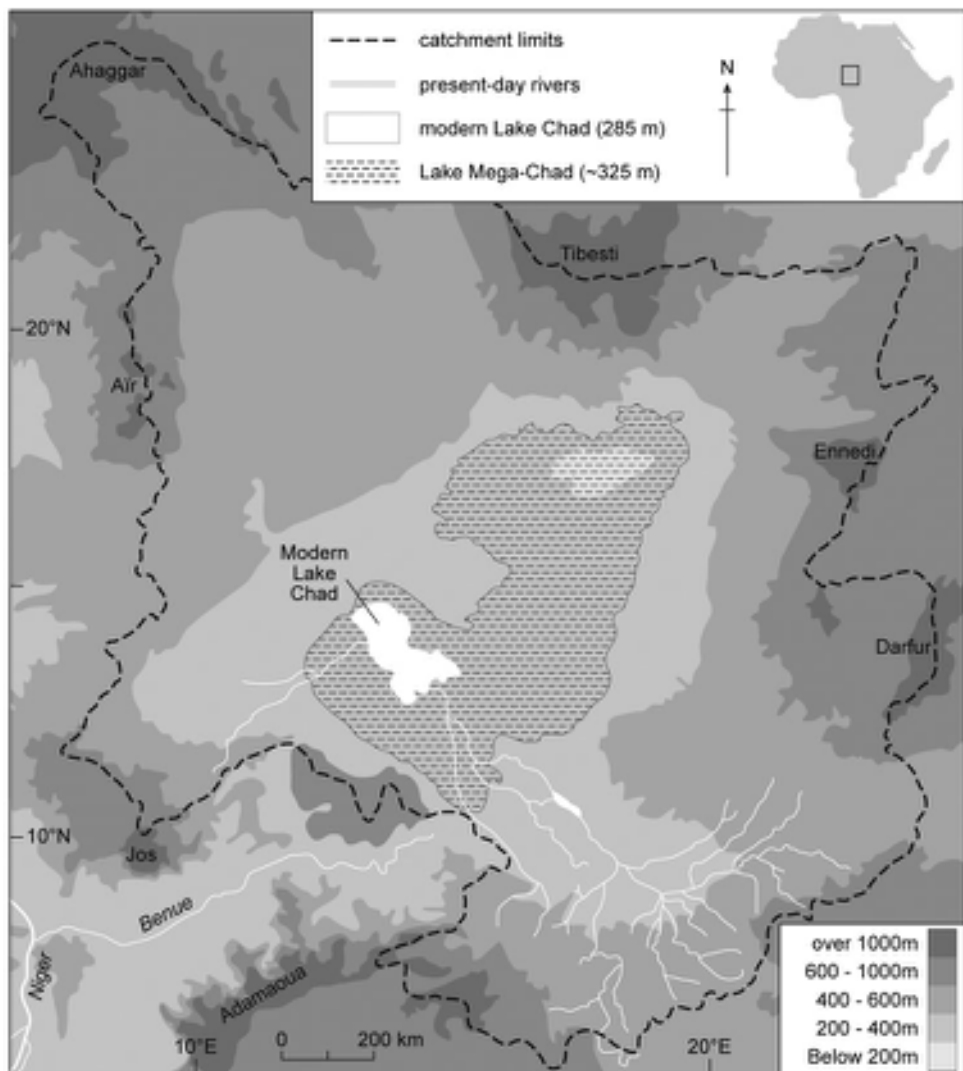


Figure 2.54 Location and surface dimensions of modern Lake Chad, Palaeolake Mega-Chad, and the Chad drainage catchment (from Schuster *et al.*, 2005).

isostatic recovery led to warping of the shorelines so that the main Bonneville Shoreline is now c. 74 m above the former lake margins (Figure 2.55a).

The reconstruction of histories of lake-level variations, therefore, requires not only detailed mapping of the preserved palaeolake features, but also a reliable chronology of shoreline formation, as well as a knowledge of the wider palaeoenvironmental context in which the lake system has evolved (Bohacs *et al.*, 2003). In these circumstances, it may

be possible to construct a record (a **hydrograph**) of pluvial lake-level fluctuations through time. In Lake Bonneville, for example, dated strandline evidence indicates at least six major water-level fluctuations with amplitudes of up to 50 m between 21 and 10 ka (Figure 2.55b), and it has been suggested that these may reflect the millennial-scale climatic fluctuations that affected the North Atlantic region during that time interval (Oviatt, 1997; Orme, 2008). More detailed palaeoclimatic reconstructions based on data from closed-

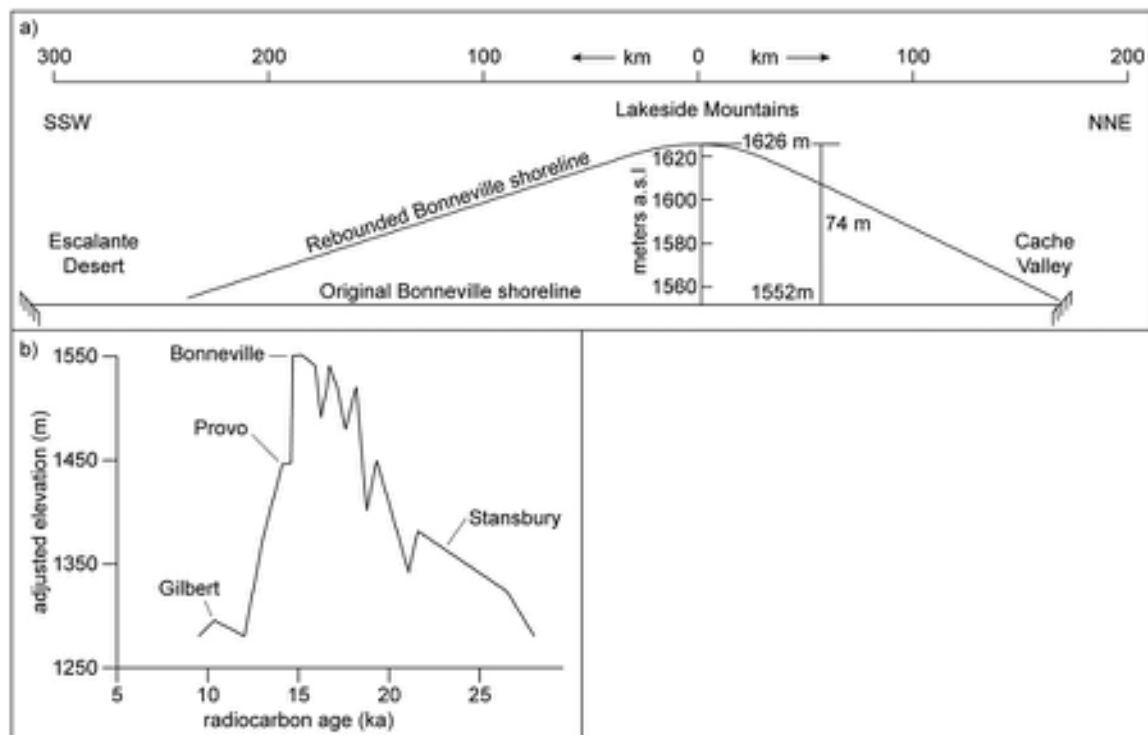


Figure 2.55 a) Post-drainage hydro-isostatic deformation of the Bonneville Shoreline that formed during the maximal extent of Pluvial Lake Bonneville (from Sack, 2009). b) Chronology of water level changes in Lake Bonneville over the past 30 ka. Note the catastrophic drop in lake level of around 100 m from the Bonneville to the Provo Shorelines. This was caused by a major flood event and is reflected in a distinctive marker bed in deep-water sediments (after Oviatt, 1997).

basin lakes can be made where the geomorphological evidence is supported by stratigraphic records, and these aspects of pluvial lake sequences are discussed further in section 3.7.

2.7.2 Dunefields

Increased aridity at times in the past can be demonstrated by the existence of desert landforms, especially sand dunes, in areas where such features are no longer forming. Even when heavily vegetated, dunefields often stand out clearly on aerial photographs and satellite images (Brookes, 2003), so that mapping is possible of inactive dune systems beyond the margins of the present desert regions. Such evidence shows, for example, that the Sahara once extended south into the Sahel to latitude 10–12°N over a distance of some 5,000 km, while fossilized dune systems occur throughout southwest Africa, northwest India and around the margins of the Australian arid zone (Figure 2.56). Stabilized dunes have also been found in present-day humid forest zones of

Amazonia and the Gulf of Mexico coast plain (Latrubesse & Nelson, 2001; Otvos, 2004), and on the pampas of Argentina (Tripaldi & Forman, 2007). The geomorphological evidence in all of these regions indicates phases of significantly increased aridity or ‘megadroughts’ in the past, and particularly around the time of the Last Glacial Maximum (LGM) (Hanson *et al.*, 2010).

In some areas it may be difficult to make a clear distinction between active and fossil dunes, particularly where sand has been remobilized and secondary dune patterns have become superimposed on an older primary set. Most fossil dunes have been distinguished on the basis of features indicative of a period of stability under humid climatic conditions. These include evidence of gullying and truncation by fluvial activity, and features produced by pedogenesis and chemical weathering, including chemical alteration of clay minerals, decalcification and staining by iron oxide. In hyper-arid regions, these usually take the form of calcrete or gypsum concentrations (section 2.7.4), sometimes associated with illuviated clay coatings that

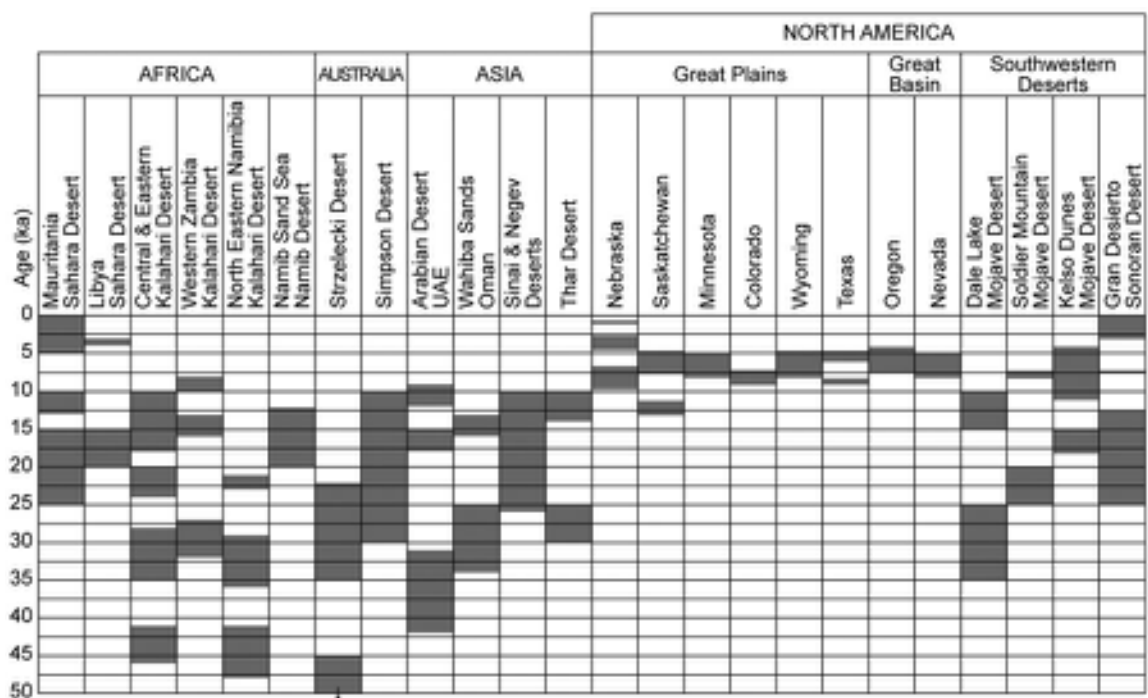


Figure 2.56 Principal dune-building episodes (shaded) during the last 50 ka in the deserts of Africa, Australia, Asia and North America (from Tchakerian, 2009).

have formed around pedogenically altered sand grains (Fitzsimmons *et al.*, 2009). Former dune surfaces may also be indicated by archaeological evidence, for example concentrations of human or other animal bones, indicating a sufficient degree of sand stabilization and moisture availability to permit humans to occupy previously hyper-arid regions (Nicoll, 2001). Vegetated dunes may indicate relict features, although as some dunes may be preferential sites for plant growth in arid environments, vegetation cover may simply reflect better water-retaining properties and deep-rooting opportunities offered in such areas. Chronologies of dune formation can be obtained using luminescence dating of sand grains (Lancaster, 2008; section 5.3.6.) and, in less extreme environments, by radiocarbon dating of organic carbon residues in palaeosols (Goble *et al.*, 2004). In addition, CRN dating (section 5.3.8) enables ages to be obtained on eroded rocks and on desert pavement surfaces (Fujioka *et al.*, 2009).

In some areas, fossil dunefields have been found on the beds of former pluvial lakes, with shorelines either

truncating older dunes or being buried by later sand-dune expansion (Drake & Bristow, 2006). Such geomorphological relationships provide convincing evidence for the alternation of arid and pluvial phases. In the Erg of Bilma in eastern Nigeria, for example, dune formation in the period 23–19 ka was followed by a more humid episode that culminated during the early Holocene (*c.* 10–9 ka) in the development of an extensive pluvial lake system. Drier conditions around 6 ka led to a second phase of dune construction and, following disappearance of the lakes, a third episode of dune expansion began after *c.* 3 ka. The first two generations of dunes show evidence of weathering, but the third is still active at the present day (Völkel & Grunert, 1990). Dunefields may also occur in conjunction with fluvial landforms and deposits, with erosion of dunes by streams during humid periods and the avulsion of stream channels by dunes during more arid episodes. In the eastern MacDonnell Ranges of central Australia, for example (Figure 2.57), fluvial erosion prior to the LGM created desert surfaces of different ages on which successive

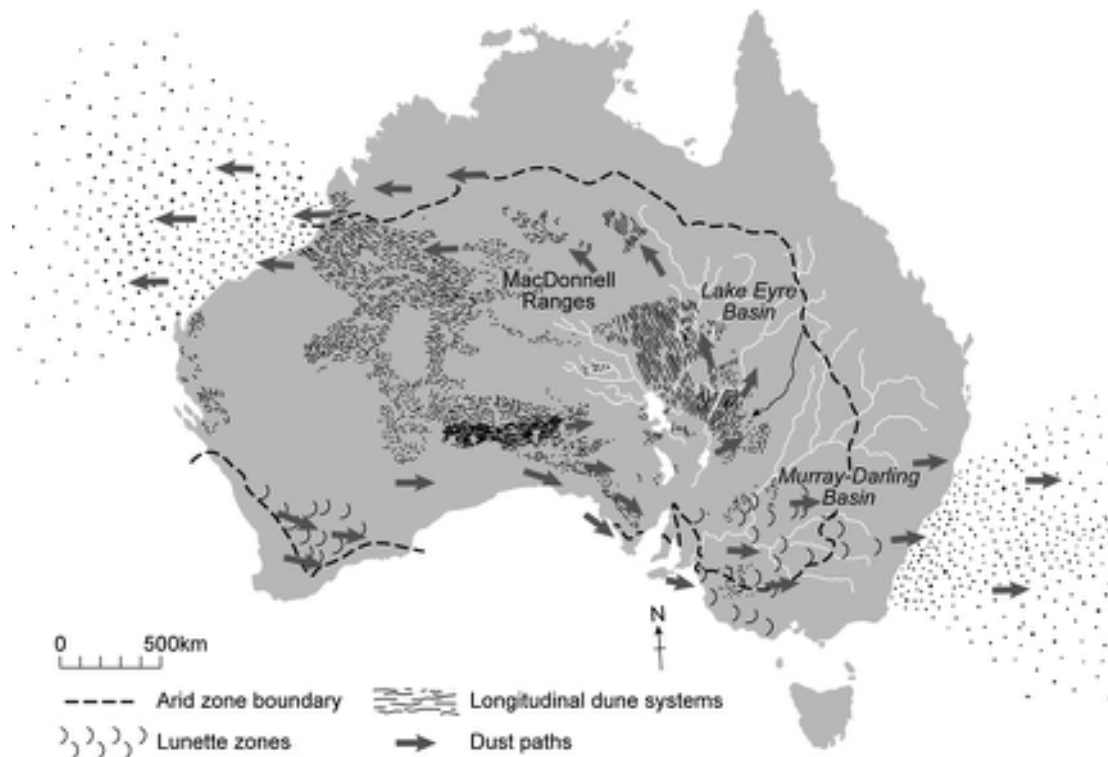


Figure 2.57 Dominant linear dune trends and present-day dust circulation in Australia (from Hesse & McTainsh, 2003).

generations of dunes developed, with an earlier generation (75–65 ka) preceding the main fluvial phase and a later set of dunes forming on abandoned river floodplains during the LGM and Holocene.

Fossil dunefields also provide valuable data on past wind directions and strengths, thereby permitting former synoptic atmospheric circulation patterns to be inferred. In the example from central Australia referred to above, contrasts in alignment and distribution of the two dune sets suggests that the circular Australian wind system shifted southwards by some 160 km (1.5°) after the LGM (Hollands *et al.*, 2006). In the Western Desert of Egypt, north- and northeast-trending dune crests cross-cut older west- and northwest-trending ones (Figure 2.58). The latter are of early Holocene age and were formed by ‘palaeo-westerly’ winds that steered moist Atlantic/Mediterranean air masses across Egypt towards the Red Sea. The younger dunes, orientated along a north–south axis, developed later than 4–3 ka, at about the time the north African savannah boundary stabilized at its present position (Brookes, 2003). In Mauritania, three generations of dune formation have

been identified, the oldest emplaced during the LGM (25–15 ka), a second set during the Younger Dryas (13–10 ka) and the youngest after c. 5 ka. The trends of the dune crests suggest that the pre-Holocene features reflect easterly, northerly and northwesterly winds, resulting from the intensification of the seasonal high-pressure air cell over North Africa (Lancaster *et al.*, 2002).

Dune patterns also provide valuable input data for, as well as independent tests of, numerical simulations of past atmospheric circulation. For example, the mapped pattern of parabolic dune crests and other aeolian indicators in northern Europe, dating to between 20 and 15 ka, accord closely with model-based simulations of the prevailing wind pattern for that period. Both the empirical evidence and modelling outputs suggest winds that were generally more westerly-to-northwesterly and significantly stronger than those of the southwesterly air stream that dominates the region today, the former being attributed to a stronger circulation regime induced by the northern ice sheets and a colder North Atlantic Ocean at the end of the last cold stage (Renssen *et al.*, 2007a). Finally, there is evidence in

some palaeo-dune records of cyclical variations in aeolian deposition, for instance a possible precessional-forced cycle of dune accretion in the Thar Desert in India over the last 200 ka (Singhvi *et al.*, 2010) and a 2.6 ka cycle in dust delivery to the Gulf of Carpenteria in northern Australia over the last 40 ka (De Deckker, 2001).

Although fossil dunefields are therefore potentially valuable indicators of the former extent of arid environments, again care must be exercised in their use as palaeoclimatic indicators. Desert conditions result from a variety of climatic factors, the most important being temperature, precipitation and wind. A change in any of these variables may be sufficient to alter the balance between adequate groundwater retention for plant growth and excessive evaporation leading to drought. Hence, a change towards an episode of dune construction may result from higher temperatures, lower precipitation levels, increased wind strength, or a combination of all three. Similarly, it cannot be assumed that higher precipitation levels constitute the only environmental factor leading to sand-dune stability, as this is partly dependent on a balance between sediment availability, supply and mobility (Lancaster, 2008). There is also evidence to suggest that stabilization of dunes following a major climatic shift can be time-transgressive over large areas (Werner *et al.*, 2011). For transitional periods, therefore, additional lithological, biological and chronological evidence may be required

if correct inferences are to be made about the nature and timing of periods of dune formation, and their links to climatic change. A further problem arises from the activities of human groups on the desert and savannah margins. It is clear that, over recent millennia, people have played an increasingly important role in the expansion of the desert margins, and human-induced desertification has to be considered when palaeoenvironmental inferences are being made on the basis of dunefield evidence, particularly for the late Holocene (Nicoll, 2004).

2.7.3 Fluvial landforms

Relict fluvial features are found throughout the tropics and subtropics, and are clearly revealed in remote sensing surveys (Ori *et al.*, 2009). For example, Landsat and SLAR imagery has identified integrated fluvial channel networks around oases in the eastern Sahara (Robinson *et al.*, 2006), in the Lake Chad basin of the southwestern Sahara (Leblanc *et al.*, 2006), and in the arid region of Rajasthan in northwest India (Rathore *et al.*, 2010). In parts of interior Australia, complex systems of palaeochannels and palaeofloodplains, many of which contrast markedly with the form of contemporary alluvial channels, appear to have developed under climatic regimes very different from those of the present day (Nanson *et al.*, 2008). Fluvial response to climatic fluctuations is also reflected in river sediment

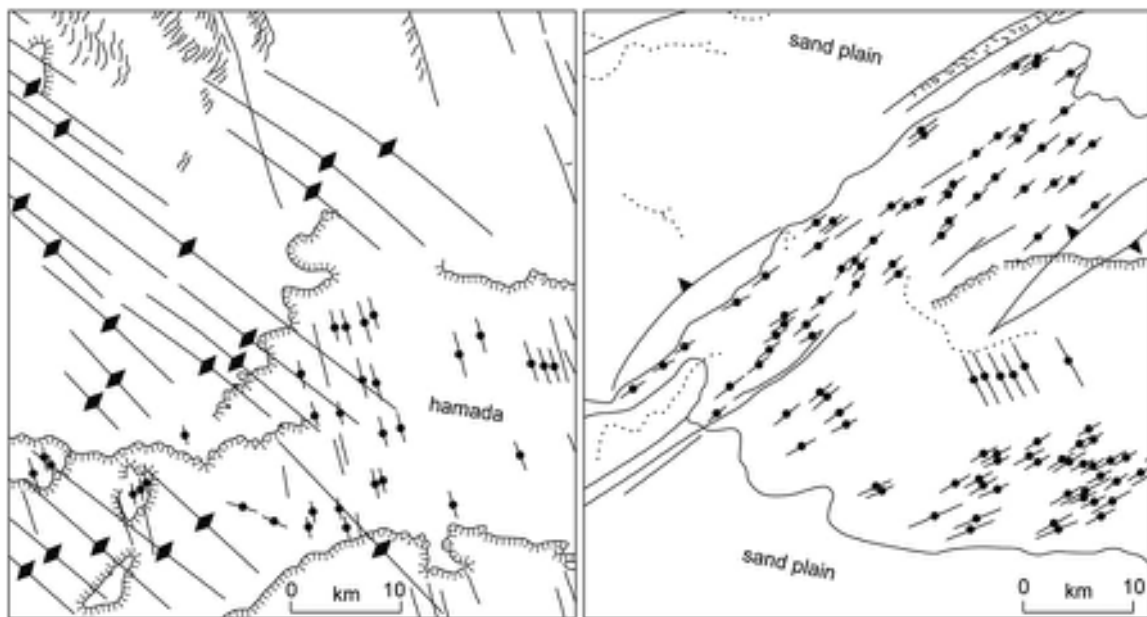


Figure 2.58 Linear trends of crests of sand dunes in Egypt's Western Desert (from Brookes, 2003).

records, for example on the Deccan Plateau in India where alternations between episodes of alluviation during wetter periods and fluvial incision during drier phases are attributed to centennial or millennial variations in the strength of the Indian monsoon (Kale, 2007).

The identification of palaeo-drainage channels in semi-arid areas is not always straightforward, however, because modern rivers in these areas are prone to seasonal flooding and frequent channel shifts, making it difficult to distinguish between degraded modern and much older, permanently abandoned, features (Tooth, 2000). Moreover, palaeo-channels often tend to become obscured by shifting aeolian and alluvially deposited sands. To some extent, the latter problem can be overcome by the use of synthetic aperture radar (SAR), which can penetrate surface sands to reveal buried fluvial channel networks (Figure 2.59). SAR also enables groundwater aquifers to be detected beneath sand sheets and dune systems, and it has also revealed archaeological sites in close proximity to palaeo-drainage networks in what are currently hyper-arid and inhospitable regions (Kindermann *et al.*, 2006).

In reconstructing palaeoenvironments of the arid and semi-arid zone from relict fluvial landforms, however, a range of non-climatic factors must be taken into account (Tooth, 2000). Fluvial processes are governed by a range of environmental variables that include, in addition to climate, geology, relief, soil, vegetation cover and the influence of people. All of these, in combination, will affect the rate at which fluvial activity proceeds as well as the geomorphological response, and again climate may not always be the dominant factor. For example, in highly arid regions, increased sediment load in rivers may result from increased rainfall, whereas in the semi-arid zone, lower rainfall levels may lead to higher sediment yields as a result of reduced vegetation cover. Moreover, where large rivers drain into arid areas, changes in flow regime may not necessarily reflect the ambient climatic conditions in the desert, but may have been caused by changes in precipitation in the region beyond the desert margins (Lancaster, 2000).

2.7.4 Weathering crusts

Weathering crusts, or **duricrusts**, are resistant ground surface mantles or cappings commonly found as protective layers at the surface of eroded bedrock or sediments in low latitudes (Dixon & McLaren, 2009). They originate through the concentration of chemical elements in soils, sediments or permeable rocks, either by accumulation of residual compounds following the removal of more mobile elements by solution or translocation, or by the reprecipitation of soluble compounds from groundwaters. These

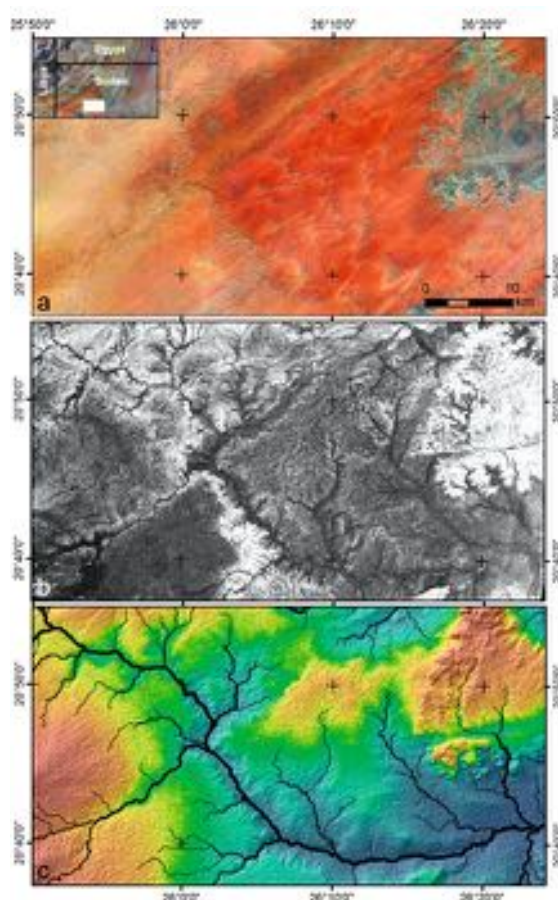


Figure 2.59 a) LANDSAT ETM image of part of the desert area of northwest Sudan, showing the dominance of surface sands, with little indication of the palaeo-drainage forms buried beneath. b) Radarsat-1 image of same area which uses synthetic aperture radar (SAR) to penetrate dry sand deposits to reveal buried palaeo-drainage features below. c) Digital elevation model (DEM) of the same area based on 90 m spatial resolution Shuttle Radar Topography Mission (SRTM) data to enhance the buried river channel system (from Ghoneim & El-Baz, 2007, reprinted with permission from Elsevier).

concentrations develop as hardpans and, when exposed, form cemented (**indurated**) layers which are more durable than adjacent sedimentary horizons (Nanson *et al.*, 2005). There is a wide range of weathering crusts of different chemical constituents but, in general, they can be divided into those that originate as weathering layers in humid tropical environments, and those that develop under arid or semi-arid conditions. **Laterites**, for example, evolve through the accumulation of residual hydroxides of

aluminium and iron in humid tropical soils which, when exposed, form cemented surface layers. Laterite or **ferricrete** (iron-rich) crusts are typically found as caprocks in desert and savannah regions where their presence on plateau surfaces reflects inversion of relief (Ollier & Sheth, 2008). Their occurrence also indicates a major change in climate, for they are believed to form where both temperature and precipitation levels are high, although the precise climatic parameters governing the formation of laterites are difficult to establish. Moreover, as deep-weathering profiles and ferricretes are usually polygenetic in origin and of considerable antiquity, they tend to be of relatively limited value in inferring former climatic conditions during the course of the Quaternary (Widdowson, 2007).

Weathering crusts that formed under more arid conditions include **calcrete** (sometimes termed **caliche**), which is composed of cemented calcareous horizons and often forms the hard rim of exposed escarpments in deserts and savannah regions (Alonso-Zarza & Wright, 2010), **gypcrete** or gypsum cement (Aref, 2003) and siliceous crusts known as **silcrete** (Nash *et al.*, 1994). These weathering crusts and related structures in soils have been found in many low-latitude regions and have been interpreted as reflecting Quaternary climatic change; they are often degraded, however, which suggests that some may be relict forms from previous arid phases (Hirmas & Allen, 2007). Again, the climatic conditions governing their formation are difficult to quantify, partly because they are highly variable in composition, frequently intergrading between different duricrust types (Ringrose *et al.*, 2009). Other factors also contribute to their formation, especially in the case of pedogenic carbonate, which appears to be largely biologically produced (Alonso-Zarza & Wright, 2010). The ages of different phases of carbonate production can be determined by uranium-series dating (section 5.3.4), and when the results are compared with independent palaeoclimatic estimates, climatic control over carbonate production seems to be implied. For example, data from Spain spanning the last 120 ka suggest that pedogenic carbonate has formed predominantly under warmer and more arid climatic conditions (Candy & Black, 2009), while in Chinese loess sequences, carbonate nodules in soil horizons appear to have developed during colder and more arid phases (Rowe & Maher, 2000). Where a chronology of carbonate production can be established, therefore, calcrete–climate relationships may prove to be useful as generalized palaeoclimatic indicators. In many cases, however, establishing the age of weathering crusts is seldom straightforward for, as with laterites, not only do many have polygenetic origins, but they may have been forming since early or even pre-Quaternary times.

2.8 CONCLUSIONS

Geomorphological evidence provides a valuable starting point in the investigation of Quaternary environments. By using modern landforms as analogues, aspects of former glacial, periglacial, fluvial, marine and aeolian environments can be inferred. In many cases, only relatively general conclusions are possible, but in certain instances, specific climatic parameters can be deduced. Throughout this chapter, however, it has been stressed that geomorphology is but one of the lines of evidence used in the reconstruction of Quaternary environments and that, wherever possible, landform records should be employed in conjunction with other forms of evidence. A second major data source lies immediately beneath the earth's surface, and it is to the stratigraphic record that we now turn our attention.

NOTES

- 1 For survey purposes, small sectors of the earth's surface can be considered flat, and no account need be taken of surface curvature. For larger areas, however, the earth's curvature needs to be accounted for and appropriate corrections applied. This is the study of **geodesy**, and the determination and application of fixed positional reference points is known as **geodetic survey**.
- 2 A differential global positioning system (**DGPS**) provides more accurate measurements of ground position than the less expensive 'recreational' GPS instruments. It involves the use of at least two receivers, one of which is left stationery (the 'reference station') at a point which has been accurately surveyed for position and altitude; the second ('roving') receiver can then measure the location and altitude of other points relative to the position of the reference station using more accurate computations of coordinate error (see http://www.trimble.com/gps_tutorial/dgps or Spencer *et al.*, 2003a).
- 3 'Sandar' is an Icelandic term to describe the outwash plains that form in lowland areas in front of valley glaciers and ice sheets. The singular is sandur.
- 4 In glaciology, the term 'steady-state' refers to the condition whereby a glacier or ice sheet maintains equilibrium over time as a result of a balance between the major controlling variables such as seasonal climatic variations, albedo, rate of flow, etc.
- 5 Glacier surges are short-lived, often substantial, advances of an ice sheet or glacier over timescales ranging from a few years to several centuries (Benn & Evans, 2010).
- 6 BRITICE is a GIS-based compilation of glacial and associated landforms in and adjacent to the British Isles (see <http://www.shef.ac.uk/geography/staff/clarkchris/britice.html>).
- 7 Tunnel valleys are large over-deepened channels cut into bedrock or sediment near the margins of continental ice sheets, and they often terminate abruptly at major moraines (Benn & Evans, 2010).

92 GEOMORPHOLOGICAL EVIDENCE

- 8 A *roche moutonnée* is a form of ice-moulded and polished bedrock, elongated in the direction of ice flow, with a distinct shallow gradient on the up-glacier (stoss) surface and a steeper irregular surface (caused by ice plucking of rock fragments) on the down-glacier (lee) surface. The term was coined by the Alpine geologist Horace-Bénédict de Saussure, who saw a resemblance between a land surface with well-developed *roches moutonnées* and the curled ornamentation of wigs worn by French gentry in the eighteenth century.
- 9 The Pascal (Pa) is the SI unit for pressure, and is the measure of force per unit area. In glaciology, pressure of ice is usually measured in kilopascals (kPa), in other words $1\text{ kPa} = 1,000\text{ Pa}$.
- 10 In some glaciers, particularly in the High Arctic, there may be a complex zone of transition between accumulation and ablation areas. This is usually referred to as the **superimposed ice zone**, in which ice will have formed from the refreezing of meltwater runoff or avalanche material from up-glacier. The lower boundary of the superimposed ice zone is the **equilibrium line** (up-glacier from which there is a gain in mass), whereas the **firn line**, that is, the line dividing fresh snow from ice, forms the upper boundary. On most maritime temperate glaciers, where snowfall is heavy, there is frequently no superimposed ice zone, and therefore the firn line and the equilibrium line coincide (Paterson, 1994).
- 11 The **Phanerozoic** is the period of time during which sediments have accumulated that contain remains of plants and animals. It refers to the geological systems from the Cambrian to the Quaternary and covers approximately 540 Ma of the geological timescale.
- 12 **Juvenile water** originates deep in the earth, possibly from processes associated with degasification of mantle material during metamorphism and magmatism. Juvenile water reaching the crust mixes with water derived from precipitation (meteoric water). Higher levels of carbon dioxide, helium and oxygen in groundwater are indicative of the presence of juvenile water.
- 13 **Rheology** is the branch of Newtonian mechanics that deals with the deformation and flow of materials that are neither solid nor completely liquid, such as semi-molten (ductile) rock or glacier ice. The term **deformation** refers to the process by which a substance changes shape without breaching continuity.
- 14 **Epeirogenic** movements of the earth's crust and surface are those that involve gentle uplift or subsidence over very large areas, with little folding or other localized deformation of rock formations.

Lithological evidence

3.1 INTRODUCTION

Although geomorphological evidence can provide useful insights into former climatic regimes and environmental conditions, a more detailed impression of events during the Quaternary can often be gained from the sedimentary record. Not only can valuable data on Quaternary environments be obtained from the sediments themselves, by relating observations on present depositional environments to features preserved in the recent stratigraphic record, but since many deposits are fossiliferous, inferences based on lithological changes can often be supported directly by those based on fossil evidence. Furthermore, because sedimentary sequences frequently reflect sediment accumulation over an extended time period, some appreciation can be gained of both spatial and temporal aspects of environmental change. Finally, while geomorphological evidence is restricted largely (although not wholly) to the terrestrial environment, sedimentary data can be obtained from beneath the waters of present-day lakes, from the world's ice caps and, perhaps most important of all, from the deep-ocean floors where lengthy sequences of virtually undisturbed deposits are preserved.

Quaternary sediments are generally unconsolidated and are of two principal types: inorganic (**clastic**) deposits, consisting of mineral particles (termed **clasts**) ranging in size from large boulders to very fine clays; and **biogenic** sediments, consisting of the remains of plants and animals. Biogenic sediments can, in turn, be divided into an organic component of humus and the decayed remains of plants and animals, and an inorganic component of such elements as mollusc shells and diatom frustules. In this chapter, we are concerned primarily with inorganic sediments such as tills, aeolian and cave sediments, and fossil soils, although some of the properties of biogenic sediments are also considered. A full discussion of the fossil record contained in Quaternary sediments can be found in Chapter 4.

3.2 FIELD AND LABORATORY METHODS

3.2.1 Sediment sections

Wherever possible, lithological investigations should be carried out on open sections so that variations in stratigraphy, both vertically and horizontally, can be carefully recorded. Before commencing fieldwork, the section should be cleaned of slumped material, and a 'fresh' face revealed by cutting back into the exposure. On large sections, steps can be cut on slumped material or directly into the face to provide temporary working surfaces, but a ladder may be necessary to reach the less accessible parts. Careful drawing of the exposure is the first stage in analysis, and this should be supported wherever possible by a photographic record. It may be useful to grid the face with measuring tapes as this will provide an accurate scale for section drawing. Detailed notes should be taken on all aspects of exposed stratigraphy, using Munsell colour charts to obtain a relatively precise description of colour changes between and within lithostratigraphic units. Where a mixture of organic and inorganic sediments is under examination, descriptive schemes can be used to classify the different sediment types (e.g. Schnurrenberger *et al.*, 2003). Instrumental levelling from a benchmark will enable the various stratigraphic features to be related to a common datum, for purposes of altitudinal comparison both within and between sites. A detailed guide to the description of Quaternary stratigraphic field sections is provided by Jones *et al.* (1999).

The type of sampling framework employed will depend on the nature and purpose of the investigation. For certain types of study, for example the analysis of soil or loess profiles (both discussed in this chapter), a sequence of samples may be required from a representative vertical section of the exposure. Depending on the aims of the

investigation, these might vary from relatively small samples (perhaps no more than 1 cm³) to larger bulk samples weighing several kilograms, both taken at a set vertical interval. In other circumstances, it might be necessary to remove a complete sequence of samples, either in the form of monoliths (perhaps 20–30 cm³) cut from the section with a spade, or in metal boxes (monolith tins) which can be hammered into the face (Figure 3.1). In each of these cases, sampling horizons should be carefully related to a measuring tape attached to the free face at the side of the sampling line; the trowels, spades, knives and spatulas should be cleaned between the extraction of individual samples; and care must be taken over the packaging, sealing and labelling of the sediment samples. Detailed notes should be made throughout the sampling process. In other types of investigation, it may be necessary to take a number of samples from points scattered across the face of the

section. These can be selected subjectively, but random sampling of a face that has been gridded will provide a more objective sampling framework. The same approach can be applied where measurement of sedimentary properties needs to be undertaken in the field, such as the recording of the orientation and dip of pebbles or other clasts (termed ‘sediment fabrics’: see section 3.3.6.2).

3.2.2 Coring

Although section work is preferable to coring, relatively few natural sections are to be found, and there are many situations where it is impossible to excavate exposures because of, *inter alia*, problems of time, expense, sediment thickness or the likelihood of waterlogging. Hence, recourse must be made to coring. A range of coring equipment is now available, with different operating mechanisms and different levels of success in core recovery. Hand-operated corers of either the side-sampling (e.g. ‘Russian’) or piston (e.g. ‘Livingstone’) type are widely used for sampling peat and lake sediments, although motor-driven equipment (e.g. ‘rotary’ or ‘percussion’ corers) is required for more cohesive sediment such as gravels and tills (Figure 3.2). Specialized motor-driven or hydraulically operated corers are also used to sample sediments in deep lakes or on the seabed, and are also employed to obtain cores from glaciers and ice sheets.

Numerous problems are encountered in coring operations, including the facts that (1) cores may be distorted during recovery or extrusion from the sampling chamber, a problem that becomes particularly acute when cores are being taken from poorly consolidated sediments, such as certain types of peat and lake muds; (2) unless overlapping cores are taken, stratigraphic units that are either thin or of limited lateral extent may be missed during sampling; and (3) it is often difficult to transport heavy coring equipment to remote areas where other logistical problems may also be encountered, such as a lack of water for hydraulic coring operations. Despite such difficulties, however, the development of increasingly sophisticated coring machinery in recent years has enabled the successful drilling of marine sediments, of the polar ice sheets and of deep lake sequences, all of which have revolutionized our understanding of the Quaternary environmental record (section 1.5).

Since most Quaternary sedimentary sequences, when traced laterally, vary in both thickness and complexity, the sedimentary history of a site is often difficult to ascertain when only a single core is taken. It is common practice, therefore, to obtain several borehole records, usually arranged in transects, so that a two-dimensional, or even

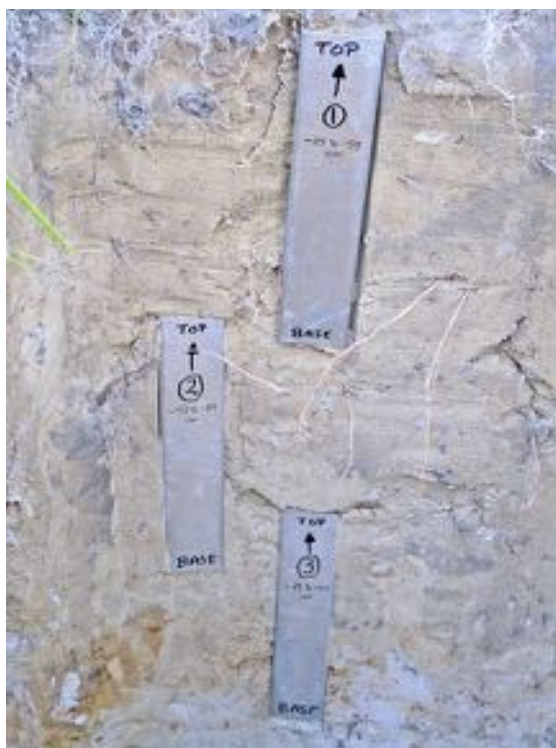


Figure 3.1 Monolith tins (50 cm length) in a sediment exposure in the Kopanica Valley, southwest Poland. The monolith tins were used to collect contiguous sediment samples for tephrochronological analysis (section 5.5.2); overlapping samples between adjacent tins ensured the complete sequence was sampled (photograph by Alison MacLeod, Royal Holloway, University of London, UK).

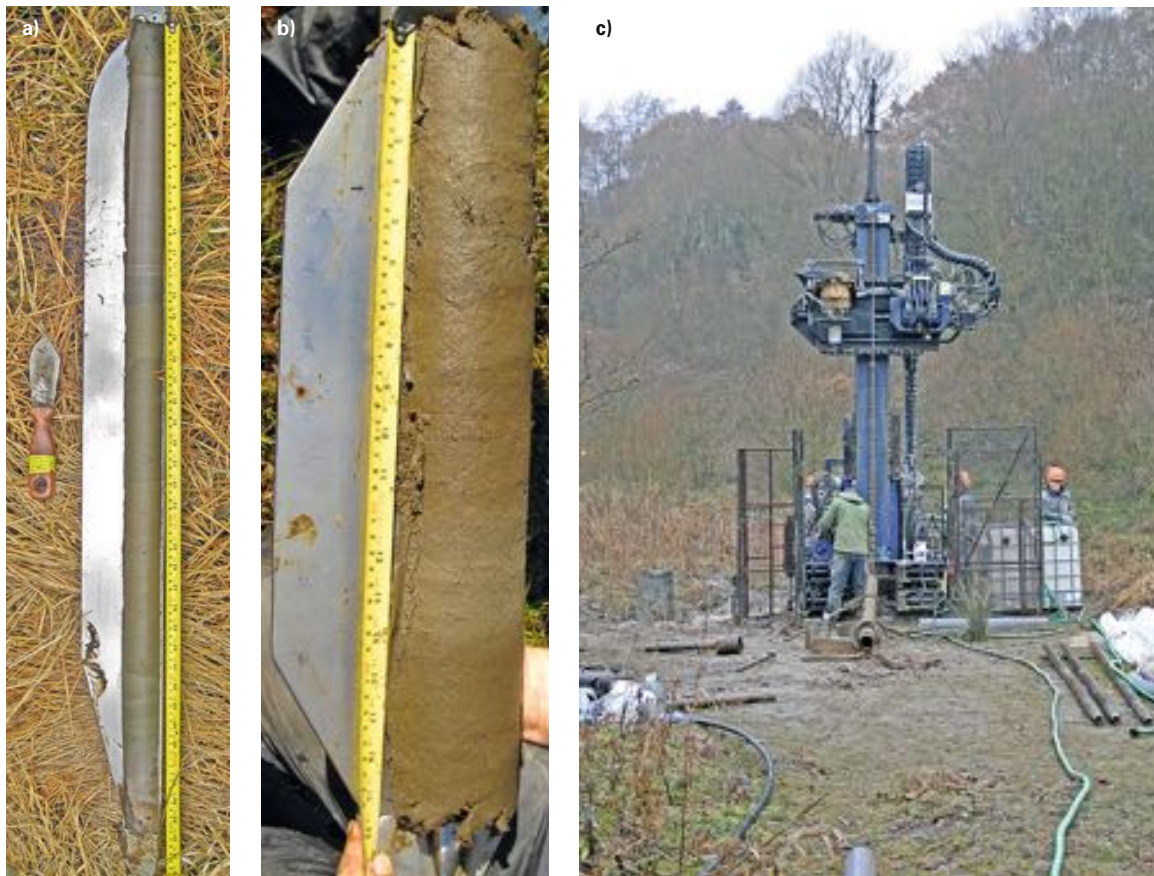


Figure 3.2 Examples of coring equipment used to sample Quaternary sediments. a) The hand-operated 'Russian' sampler with internal chamber of 1 m length and 5 cm internal diameter, employed mainly to sample soft, Late Quaternary lake sediment and peat. These can be manufactured to suit different purposes, for example b) a wide-diameter (10 cm) version is suitable for plant macrofossil studies, as much larger samples can be recovered. c) An Ecologia Joy-4 rotary drilling machine recovering cores from an 18.5 m thick sequence of resistant bedded sands, silts and laminated clays at the Middle Pleistocene site of Marks Tey, Essex, UK, where sediments spanning MIS 12 to MIS 10 are preserved. Overlapping cores of 3 m length and 10 cm diameter were obtained from two adjacent boreholes to ensure that the complete sequence was sampled (photographs by Alison MacLeod and Adrian Palmer, Royal Holloway, University of London, UK).

three-dimensional, schematic model of lithological variability can be constructed. The number of boreholes employed in such an exercise will depend upon the area to be surveyed, the complexity of the lithological sequence, the time available for fieldwork and other logistical considerations, such as costs. Remote sensing techniques, particularly seismic and sonar sounding methods, may also be used in conjunction with coring (section 2.2.2).

Once recovered, the surfaces of the cores should be cleaned and then analysed using a range of rapid, non-destructive, down-core scanning methods that are now becoming routine. The first step is photo-imaging, which

provides a detailed and precise record of the lithological variations represented in the cores before destructive sampling procedures are applied. Enhanced imaging using, for example, X-radiography, often reveals important lithological variations that are not clear to the naked eye or shown by standard photography (Figure 3.3). A number of scanning methods are also available that can measure down-core variations in abundance of chemical elements in sediment, such as X-ray fluorescence (XRF), with a potential scanning resolution of c. 100 µm (Rothwell, 2006). Figure 3.3 shows how relative variations in the ratio of Fe (iron) to Ca (calcium), measured using an ITRX core

scanner, reflect alternations between silt and clay layers (varved deposits: section 5.4.2) in a former lake basin, and which enables lithological boundaries between layers to be clearly identified. The images and comprehensive suites of analytical data can be visualized and integrated using software developed specifically for the analysis of core material (marine, terrestrial and polar ice cores), such as CoreWall (<http://www.corewall.org/>).

3.2.3 Laboratory methods

Laboratory analysis of Quaternary sediments is an integral part of palaeoenvironmental investigations. Both the physical and chemical properties of sediments can provide valuable data on the nature of former depositional environments, and are often useful indices of climatic and other environmental changes. A very wide range of laboratory methods is now available, and a detailed account is beyond the scope of this book. In this section, however, we provide a brief introduction to the methods that are most commonly used in the description and analysis of Quaternary sediments. For further details the reader is referred to Gale & Hoare (2011), Evans & Benn (2004), and to the Technical Guides produced by the Quaternary Research Association of Great Britain (e.g. Jones *et al.*, 1999; <http://www.qra.org.uk>).

3.2.3.1 Particle size measurements

Particle size distribution is a most important diagnostic property of a body of sediment, for even very subtle variations in average grain size or in the range of sizes of clasts may reflect important changes in sedimentary environment. The particle size distribution of coarser grades of sediment (sand size and above: Table 3.1) can be established by sieve analysis, but sedimentation methods are required for finer materials. Different grades of sediment suspended in a liquid will settle under gravity at different rates and these can be established either by using a hydrometer to record changes in the density of the suspension over time, or by extracting subsamples from the suspension using a pipette and then measuring the changing concentrations of suspended matter over time by successive weighings (Gale & Hoare, 2011). More sophisticated approaches to particle size analysis include the use of **X-radiography** (Andrews & Principato, 2002), **pulse counters** (such as the Coulter counter) and **laser diffraction** (Blott *et al.*, 2004). In pulse counters, sediments are suspended in an electrolyte and passed through an electrode-flanked aperture; voltage pulses proportional to the volumetric size of the particles are counted and the particle size distribution established (Molinaroli *et al.*, 2000). Laser diffraction uses the forward scattering of a laser

Glacial Lake Blane: Varve Analysis

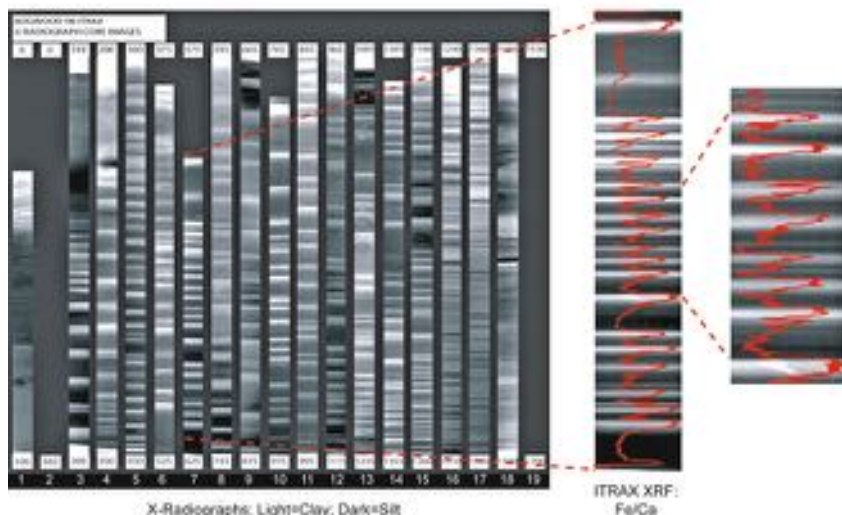


Figure 3.3 X-radiograph images of laminated (varved) lake sediments that accumulated in a former ice-dammed lake near Loch Lomond, Scotland. On the right is a graph showing variations in Fe/Ca as measured by an ITRAX core scanner (see text) based at the National Oceanography Centre, Southampton, UK (images provided by Alison MacLeod, Royal Holloway, University of London, UK).

Table 3.1 The Wentworth scale of particle size fractions and the equivalent ϕ (phi) units. Phi units are obtained by conversion from the millimetre scale, where phi is $-\log_2$ of the diameter in millimetres. The phi scale has the advantage of using integer numbers only, making the statistical description of sediments more straightforward.

Name	mm scale	ϕ unit
Boulder	> 256	> -8
Cobble	256–64	-8 to -6
Pebble	64–4	-6 to -2
Granule	4–2	-2 to -1
Very coarse sand	2–1	-1 to 0
Coarse sand	1–0.5	0–1
Medium sand	0.5–0.25	1–2
Fine sand	0.25–0.125	2–3
Very fine sand	0.125–0.0625	3–4
Coarse silt	0.0625–0.0312	4–5
Medium silt	0.0312–0.0156	5–6
Fine silt	0.0156–0.0078	6–7
Very fine silt	0.0078–0.0039	7–8
Coarse clay	0.0039–0.00195	8–9
Medium clay	0.00195–0.00098	9–10

beam by particles passing through it, and back-calculation of the sizes of these particles from the properties of the diffraction pattern produced (Hoey, 2004). Comparison of the results obtained using these different methods suggests that measurement of particle settling velocities by **sedigraph** is the most reliable for fine-grained deposits, as other approaches over-estimate the significance of platy-shaped particles (McCave *et al.*, 2006). An alternative approach to the derivation of grain-size data is to make measurements from digital images, which can be scanned and analysed using image analysis software (Sime & Ferguson, 2003). Particle-size data are usually presented in the form of sigmoidal curves on probability graph paper (section 3.3.5.1; Figure 3.13) or in ternary diagrams (triangular graphs: section 3.3.5.1; Figure 3.12) or histograms.

3.2.3.2 Particle shape

Particle shape has been used to distinguish between sediments that have accumulated in different depositional environments, and has been employed particularly effectively in the analysis of glacial, glaciofluvial and fluvial sediments. Techniques include the purely visual assessment of particle shape, the use of prepared charts as a basis for

the division of pebbles into classes ranging from angular to rounded, and the direct measurement of particles themselves. Shape measurements are then based on the axial ratios of the particles and include a variety of indices of elongation, roundness, flatness and sphericity (to derive classes of blades, rods, spheres and discs, for example). These methods are described in Gale & Hoare (2011) and Evans & Benn (2004). Automated methods of particle form analysis (e.g. image analysis) are discussed in Blott & Pye (2008).

In recent years, micro-scale features and structures of sediments have been increasingly widely used as diagnostic properties of different depositional environments. **Micro-morphological analysis** of samples is typically undertaken either at low magnification (10–100 \times), using **thin sections** of sediment and petrographic microscopes, or at higher magnification (100 \times and greater) using a scanning electron microscope¹ (Carr, 2004). Micromorphology was initially most widely used in Quaternary soil science (section 3.5.3), but is now being employed in other sedimentary contexts, most notably in the analysis of glaciogenic deposits (e.g. van der Meer *et al.*, 2003; Kilfeather *et al.*, 2010).

3.2.3.3 Surface textures of quartz particles

Different sedimentary environments (e.g. glacial, marine, aeolian) give rise to particular textural features on the surfaces of quartz and sand grains, and these can be analysed using an electron microscope. Characteristic textural features on quartz grains that can be detected by scanning electron microscopy (SEM) include fracture patterns, scratches, grooves, chatter marks, solution pits and cleavage flakes (Fuller & Murray, 2002). Moreover, it is often possible to identify superimposed features and hence more than one palaeoenvironment of modification can sometimes be inferred. A recent innovation is the use of **atomic force microscopy (AFM)**, a technique that enables 3-D representations of microscopic surface textures to be determined, and these can be quantified to derive empirical measures and indices of surface texture that corroborate the qualitative data derived from SEM analysis (Konopinski *et al.*, 2012).

3.2.3.4 Organic carbon content

The determination of organic carbon content is of considerable importance in palaeolimnology where it provides an index of biological productivity in former lake basins. It is also useful for establishing the amount of organic material that is likely to be required for the radiocarbon dating of a sample (section 5.3.2). The most widely used

method is **loss on ignition**, in which the amount of carbon in a sample is indicated by the weight loss following combustion in a furnace, and which can be used for estimating both organic carbon and carbonate in sediments (Heiri *et al.*, 2001). More accurate results can usually be obtained using standard titration methods or colorimetry techniques (Meyers & Teranes, 2001).

3.2.3.5 Metallic elements

The variations in proportions of metallic ions, such as calcium, potassium, sodium or magnesium, in Late Quaternary lake sediments are now regarded as important indicators of the changing erosional history of lake catchments (see section 3.9.3.1). The concentration of such elements in a sediment sample can be determined using either a **flame photometer** or an **atomic absorption spectrophotometer (AAS)**. The former operates on the principle that a metallic salt drawn into a non-luminous flame ionizes and emits light of a characteristic wavelength, while the AAS measures the concentration of an element by its capacity to absorb light of its characteristic resonance while in an atomic state. In both cases, the light emissions are recorded photoelectrically. More rapid methods, which measure the proportions of metallic ions present in minute quantities of sediment, use mass spectrometers to analyse atomic emissions with a high degree of precision. The **inductively coupled plasma atomic emission spectrometry (ICP-AES)** method, for example, involves the creation of an aerosol (or plasma) of ionized gas from a homogenized sediment sample, which is then analysed for elemental content using mass (ICP-MS), atomic emission (ICP-AES) or atomic fluorescence (ICP-AFS) spectrometry. Applications of ICP-MS in archaeology are described by Pollard & Heron (1996) and Ciliberto & Spoto (2000).

3.2.3.6 Heavy minerals

Heavy-mineral assemblages often reflect the derivation or provenance of Quaternary deposits. They have been used in a number of Quaternary studies including the investigation of weathering profiles, the differentiation of tills (section 3.3.6.3), and the analysis of aeolian and marine deposits (e.g. Eitel *et al.*, 2001; Schüttenhelm & Laban, 2005). Heavy minerals are those with a specific gravity (SG) greater than 2.85, and are usually separated from the lighter mineral fraction in a sample by settling in a heavy liquid such as bromoform (SG 2.89). The heavy mineral assemblage is then dried and mounted on a slide, and the percentage of individual types can be determined using a petrological microscope.

3.2.3.7 Clay mineralogy

The clay mineralogy of a sediment can provide information on both the origins of the material and on any chemical changes that have resulted from the effects of different weathering processes since deposition. Examples of the use of clay mineral analysis in Quaternary studies include the provenancing of glaciogenic sediments (Hillebrand *et al.*, 2009), and the verification of trimlines (section 2.3.1) in mountain regions where differences in lengths of time over which surfaces above and below the former ice limit have been exposed are reflected in contrasts in clay fraction mineralogy (McCarroll & Ballantyne, 2000). The most widely applied method in clay mineral analysis is **X-ray diffraction (XRD)**, which involves the rotation of a sample in a stream of directed electrons. The clay minerals present (e.g. illite, chlorite, montmorillonite) are identified by observing and comparing the spacing and intensity of peaks on diffractometer traces: this approach enables clay mineral ratios and inferred environmental changes to be reconstructed at high stratigraphic and temporal resolution (e.g. Fagel & Boës, 2008).

3.2.3.8 Mineral magnetic analysis

Because sediments vary enormously in the quantity, size and type of magnetic minerals that they contain, they can often be readily characterized on the basis of their magnetic properties. A range of magnetic signals can be measured rapidly, both in the field and in the laboratory, and these enable the concentration and types of magnetic minerals present in sediments to be determined (Walden *et al.*, 1999; Evans & Heller, 2003). Variations in the magnetic properties of sediments can then be used to establish changes in rates of sedimentation and to correlate sediment units (Maher & Hallam, 2005). In lake sediment records, environmental changes around the catchments can be inferred on the basis of mineral magnetic properties (e.g. Oldfield *et al.*, 2003). The application of magnetic measurements in the analysis of sediment sequences is discussed in more detail in section 5.5.1. Wider applications of mineral magnetic analysis in the field of Quaternary climatic and environmental reconstruction can be found in Maher & Thompson (1999).

3.2.3.9 Stable isotope analysis

Several common elements (e.g. oxygen, carbon and hydrogen) exist in nature in different isotopic states, reflecting variations in the number of neutrons in the nuclei (see section 5.3). This results in slight, but very important, differences in their physico-chemical behaviour, and a

selective separation between molecules of different atomic mass (see e.g. sections 3.8.4.2 and 3.10.2) often occurs as a result of crystallization, evaporation, precipitation, osmosis, metabolism, etc. Changes in the ratios of isotopes of different atomic mass can subsequently become locked into fossils or precipitates, and hence into the sedimentary record. For example, where lake water levels fall during drought conditions, the ‘environmental stress’ that results may be reflected in a shift in isotopic ratios, and this will be registered in the tissues and skeletons of biota inhabiting the lake as well as in chemical precipitates. The isotopic composition of meteoric water may also change due to climatic variations, and these may also be reflected in isotopic ratios in lake sediments, ice sheets and cave speleothem. Variations in isotope ratios in sediments are measured using mass spectrometers, and the results not only provide insights into the environmental conditions under which the sediments accumulated, but also constitute a proxy record of regional and, in some cases, global climatic change (Leng, 2004). Stable isotope data from lake sediments, speleothems, deep-sea sediments and ice cores are described in more detail later in this chapter.

3.3 GLACIAL SEDIMENTS

3.3.1 Introduction

Glacial sediments of Quaternary age cover large areas of the earth’s surface, particularly in the mid-latitude regions. In Europe, for example, glacially derived **diamicton**² forms an intermittent blanket over at least one-third of the land area, while in North America, such deposits are spread over half the continent. It has already been shown (section 2.3.3) that the moulding of these deposits into characteristic glacial landforms can be used to establish former glacier extent and direction of ice movement, and such data form the basis for glacier modelling and climatic reconstruction. However, equally important palaeoenvironmental evidence can be derived from an analysis of the deposits themselves, for the distinctive properties of many glacial sediments allow inferences to be made about former glacier types, the mode of sediment deposition, ice-flow directions and the sources of sediment supply. An understanding of these properties can also have economic benefits as, for example, in tracing the sources of ore bodies or modelling ground-water flow in glacigenic deposits. Indeed, in view of the widespread nature of glacial deposits by contrast with well-defined landforms, such as moraines and drumlins, it could be argued that lithological evidence has a more important role to play in the reconstruction of Quaternary environments although, as in many other instances, the

most secure palaeoenvironmental inferences are likely to be drawn from situations where geomorphological and sedimentological evidence are employed together. Good accounts of Quaternary glacial sediments can be found in Evans & Benn (2004), Bennett & Glasser (2009) and Benn & Evans (2010).

3.3.2 The nature of glacial sediments

3.3.2.1 Unstratified and stratified sediments

The nomenclature of glacial deposits can be very confusing reflecting, at least in part, the bewildering variety and complexity of sediment sequences in glacial environments (Benn & Evans, 2010). The superficial sediments that blanket the landscape in many parts of Europe were originally believed to have been derived from a great flood and were termed **diluvium**, although Sir Charles Lyell referred to them as **drift** because, along with many of his contemporaries in the early years of the nineteenth century, he believed that the deposits had been derived primarily from the melting of icebergs that had drifted in during a marine inundation. Curiously, the latter term has survived in the literature to the present day and is still used to refer to deposits formed by, or in association with, glacier ice or by ice-melt. Glacial ‘drift’ has long been divided into **stratified** and **unstratified** sediment, and although more recent work has tended to blur the distinction between these two categories (section 3.3.3), it remains a useful first step in classification of glacial deposits. Unstratified drift is usually referred to as **till** or (inappropriately) ‘**boulder clay**’. The former term was first used by Archibald Geikie in 1863 to describe coarse stony soil commonly found on the glacigenic deposits of northern Britain. It is preferable to, and now more widely used than, the term ‘boulder clay’ since many non-glacigenic diamictons contain boulders and clay whereas till frequently does not. The term ‘till’ is also more satisfactory than ‘**ground moraine**’, which has often been employed to describe glacigenic deposits. ‘Moraine’ is a geomorphological term and hence should not be used for lithological classification. Diamictons that have been transported and deposited by or from glacier ice with little or no sorting by water should be termed **till** (Menzies *et al.*, 2006).

Stratified drift is characterized by sorting of material by the action of glacial meltwater. These deposits show many affinities with fluvial sediments and are therefore referred to as **glaciofluvial** (or **glacifluvial**). The term covers a range of sedimentary environments, including **ice-contact deposits** (sediments formed adjacent to, or in contact with, glacier ice), **proglacial** or **outwash deposits** (sediments

accumulating close to the frontal margin of an ice sheet or terminus of a glacier) and **glaciolacustrine deposits** (sediments accumulating in lakes or located on, within, or adjacent to, glacier ice, or fed directly by glacial meltwaters). The sediments found in these various contexts range from coarse gravels and sands formed in braided streams on land to laminated clays and silts formed in lakes. Where the latter are seasonally frozen, **varves** (section 5.4.2) may develop. In the marine environment, distinctive, mostly stratified, **glacimarine deposits** accumulate around the margins of grounded tide-water glaciers or floating ice shelves, while ice-raftered debris may be deposited by icebergs and can be carried some considerable distance from the ice margins (Ó Cofaigh, 2007).

3.3.2.2 Glacigenic facies

The nature and composition of glacigenic sediment depend on a number of factors, including the thickness of the ice, the rate of melting, the topographic context (e.g. whether

the ice is confined within a narrow valley, or spreads out into a piedmont lobe), the concentration and type of clasts contained within the ice, and the zone or part of the ice in which the sediments were initially entrained (Figure 3.4). Sediments may accumulate in a **subglacial** (at the base of the ice), **englacial** (within the ice body) or **supraglacial** (on the ice surface) position. The supraglacial environment is especially complex with a mixture of glacially derived and subaerially derived sediments often forming debris flows (section 3.3.3). Short-term oscillations of the ice margin may lead to the superimposition of sediments from each of these contexts, as well as the incorporation of materials (including glaciofluvial sediments) deposited either prior to glacial advance or during ice wastage. As a consequence, glacigenic sequences frequently reveal intercalations of tills, flow materials and stratified sediments with complex vertical and spatial **facies** variations (Evans & Benn, 2004). The term ‘facies’ (from the Latin word meaning ‘external form’ or ‘appearance’) refers to a body of sediment that is characterized by a combination of lithological, physical or

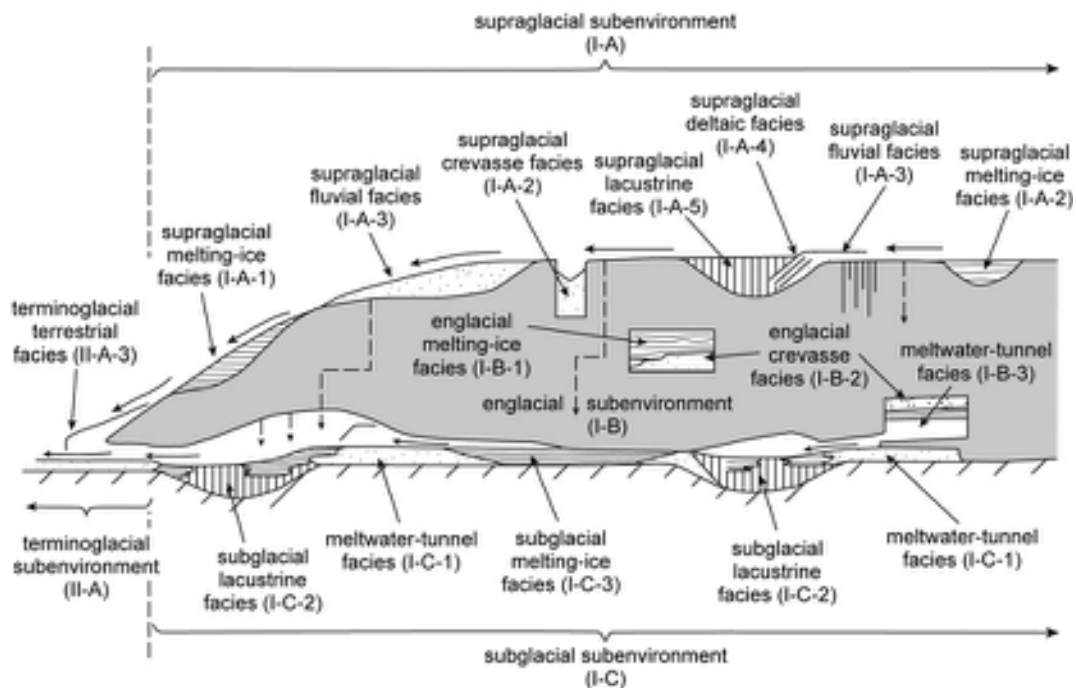


Figure 3.4 Schematic model of supra-, en- and subglacial ‘subenvironments’ within the marginal zone of a continental ice mass. Characteristic sediment facies are associated with each ‘subenvironment’, and classified according to the dominant mode(s) of sedimentation, with the following main facies types recognized: in the supraglacial subenvironment (I-A), melting-ice (I-A-1), crevasse (I-A-2), fluvial (I-A-3), deltaic (I-A-4) and lacustrine (I-A-5) facies; in the englacial subenvironment (I-B), melting-ice (I-B-1), crevasse (I-B-2) and meltwater-tunnel (I-B-3) facies; in the subglacial subenvironment (I-C), meltwater-tunnel (I-C-1), lacustrine (I-C-2) and melting-ice (I-C-3) facies (after Brodzikowski & Van Loon, 1987 reprinted with permission from Elsevier).

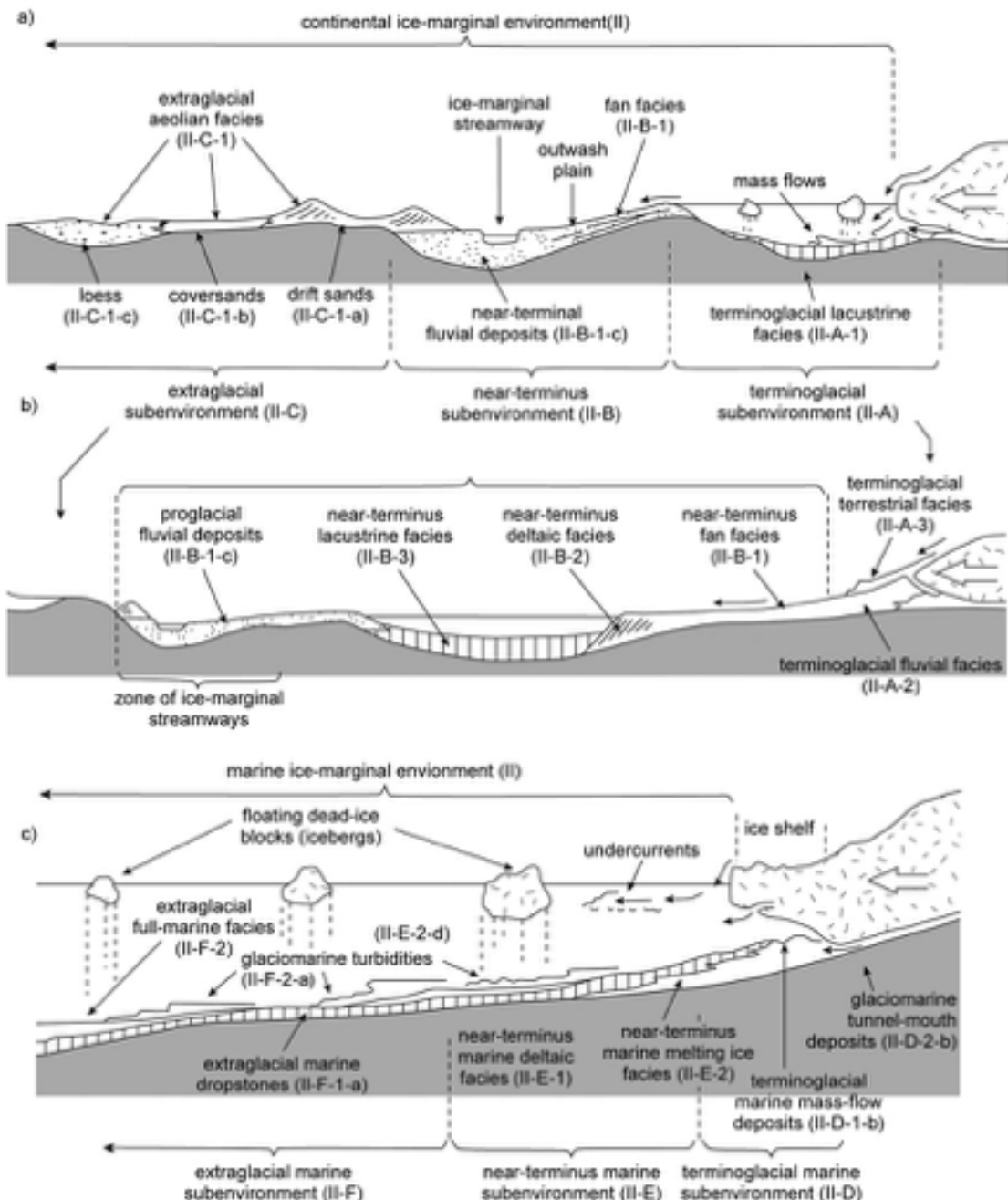


Figure 3.5 Schematic model of modes of deposition in proximal zones associated with continental a) b) and marine c) ice margins. Characteristic facies in the continental proximal ice-marginal zone include: in the terminoglacial subenvironment (II-A), lacustrine (II-A-1), fluvial (II-A-2) and terrestrial (II-A-3) facies; in the near-terminus subenvironment (II-B), fan (II-B-1), deltaic (II-B-2) and lacustrine (II-B-3) facies; and in the extraglacial subenvironment (II-C), aeolian facies (II-C). In the marine ice-marginal zone, a range of facies typifies each of the terminological (II-D), near-terminus (II-E) and extraglacial (II-F) marine subenvironments (after Brodzikowski & Van Loon, 1987, reprinted with permission from Elsevier).

biological properties, and which can be distinguished from adjacent bodies of sediment by a well-defined geometry and structure. Facies, or combinations of facies, reflect certain types of sedimentary process or a particular sedimentary environment. Facies that are defined solely on the basis of their physical properties are termed **lithofacies**; by contrast, **genetic facies** are defined using descriptive terms that imply a mode of formation, e.g. ‘varved deposit’ or ‘debris flow’.

The analysis of glacigenic facies in contemporary ice-marginal environments reveals diagnostic features that can be employed in the interpretation of older Quaternary sequences (the ‘analogue’ approach). A number of classificatory schemes of glacigenic sediment sequences have now been developed, but all are simplifications of the complex range of facies associations that form within and adjacent to glacial ice (Benn & Evans, 2010). Figure 3.5 illustrates the range of ‘subenvironments’ encountered in ice-marginal areas, and the lithofacies sequences that characterize them. For each subenvironment, a number of distinctive facies types and associations can be identified, depending on the local style of ice melting, as well as on whether the sediments accumulate against, above or beneath active or inactive ice. In the continental ice-marginal environment (Figure 3.5a,b), for example, the type of sediment deposited is determined by distance from the ice margin and position of the material within the ice mass. Both of these factors influence hydrological conditions as well as the physical and mechanical properties of the accumulating sediment which, in turn, will determine the rate of sedimentation and the extent of sediment **deformation**³ (section 3.3.3.2). A characteristic range of facies can also be found in marine ice-marginal zones (Figure 3.5c).

3.3.3 The classification of tills

3.3.3.1 *Lodgement, melt-out and ‘flow’ tills*

Prior to the 1970s, till classification and genesis were based mainly on the analysis of glacigenic sequences that accumulated during the last, or earlier, glacial stages in Europe and North America. It was not until the later 1960s and the early 1970s that detailed observations of the active processes operating today in ice-marginal zones began to appear regularly in the literature. A number of important new approaches to the study of glacigenic sequences emerged in publications from this period. One example was the classification of tills and of the factors influencing their formation introduced by Geoffrey Boulton (e.g. Boulton & Eyles, 1979).

On the basis of observations of deposits associated with contemporary glaciers in Spitsbergen, three main types of

till were recognized: lodgement till, melt-out till and flow till. Lodgement till (Figure 3.6a) is deposited at the ice base and accumulates on the subglacial floor either through pressure against bedrock protuberances or against patches of stagnant ice underneath the moving glacier body. Melt-out till (Figure 3.6b) consists of englacial debris released from melting ice either above the glacier sole or at the glacier surface. In the former situation, it is confined beneath the overlying ice body and the glacier bed, while at the surface it is trapped beneath the overburden of surface debris. Hence, melt-out till can be either subglacial or supraglacial in origin (Boulton, 1980), although the latter may be indistinguishable from the overlying surface debris. Indeed, there have been few studies of tills in modern environments where till genesis by melt-out can be clearly demonstrated (Benn & Evans, 2010). In dry arid regions, such as parts of Antarctica, ice may vaporize directly without passing through the liquid phase, a process that is a form of freeze-drying. This is known as **sublimation** and the material that is released from the ice is **sublimation till** (Marchant *et al.*, 2002). Material that has been termed **flow till** (Figure 3.6c) is thought to be released as a water-saturated fluid mass from the downwasting glacier surface, and to be augmented by material from subaerial sources, such as avalanches and rockfalls. This debris tends to be highly unstable resulting in flowage, a process that is especially common near the snouts of receding or stagnating glaciers (Menzies & Zaniewski, 2003). However, because processes and products of debris flow can be identical in both glacial and non-glacial environments, many glacial sedimentologists now prefer to use the terms ‘debris flow deposit’ or ‘**mass flow diamict**’ (Figure 3.6c) in preference to ‘flow till’, although the prefix ‘glacigenic’ may be added where direct associations with glacier ice can be demonstrated (Benn & Evans, 2010). Flowage of successive generations of material leads to interbedding of flow deposits, not only with outwash and lacustrine sediments deposited on the ice surface, but also with spreads of outwash beyond the glacier terminus. As a consequence, complex stratigraphic sequences of till, debris flow, outwash and lacustrine sediments can result from a single phase of ice wastage.

3.3.3.2 *Deformation tills*

In recent years, a considerable amount of attention has been focused on the subglacial environment, where the recognition of the importance of coupling between the glacier and its bed has resulted in a paradigm shift in glacial geological studies. This emphasizes the importance of **subglacial deformation** as opposed simply to subglacial



Figure 3.6 Examples of glacigenic deposits that could be classified as: a) lodgement till (subglacial traction till *sensu* Evans *et al.*, 2006) from Isle of Skye, Scotland (reprinted with permission from Elsevier); b) melt-out till, showing water-lain sediments interbedded with diamictite, from Alberta, Canada; and c) possible ‘flow till’, showing partial alignment of large clasts suggesting mass flow, and hence now more typically classified as a mass flow deposit (photographs by Dave Evans, Durham University, UK).

deposition and sliding (Evans *et al.*, 2006). The principal product of this process is what has become known as **deformation till** (Figure 3.7), a rock or sediment that has been disaggregated completely or largely homogenized by shearing in the deforming layer at the base of the ice (Benn & Evans, 2010). It now appears that many subglacial tills are not, as previously thought, built up gradually in layers by the release of material from the base of the ice (sometimes referred to as a ‘plastering-on’ process), but rather that a body of soft sediment, transported en masse at the base of the ice, is continuously subjected to shear stresses and remoulding by deformation. The concept of a ‘deforming bed’ is based on observations of modern glaciers which indicate that most of the movement of glaciers is achieved by continuous deformation of the subglacial debris (Boulton *et al.*, 2001). The confining, compressional stresses generate a range of deformational features, including, for example, isoclinal recumbent folds, shears, boudins (Figure 3.7), hook folds, diapirs, tension fractures, sediment wedges, brecciated beds and conjugate fracture patterns (Roberts & Hart, 2005). However, deformational structures, mainly folds, can also form in flow tills, as a

result of sliding or slumping under saturated conditions, while it may be difficult to distinguish between intraformational deformation structures (those generated during the initial settling of the till) and those resulting from post-depositional deformation, by the readvance of ice over older, unconsolidated glacigenic sediments (Phillips *et al.*, 2008a).

An important innovation in the analysis of glacigenic deposits has been the use of micromorphology, which has revealed a remarkable array of microstructures within subglacially deformed deposits (Menzies *et al.*, 2006). These include various forms of foliation, rotational structures, shear lines and zones, water escape structures and a range of microfabrics (Figures 3.8, 3.9). Scanning electron micrographs also reveal these microstructures (Figure 3.10). The characteristic micromorphological features that can be observed in deformed tills are partly dependent on grain size. At the microscopic level, sediment dominated by particles $< 20 \mu\text{m}$ in size is termed **plasma** (formerly termed ‘groundmass’ or sediment ‘matrix’), while larger individual mineral or organic particles are termed **skeleton grains**. During deformation, micro-



Figure 3.7 Highly contorted glacial diamictite (till) exposed at West Runton, Norfolk, UK (from Roberts & Hart, 2005, reprinted with permission from Elsevier). a) Folded layers of till and chalk wrapped around large 'pods' of rafted chalk. b) A layer of chalk that has been compressed and strained under high subglacial pressures, leading to formation of boudins, which are bead- or lozenge-shaped moulded remnants of the original layer; boudins are common features along faults and compressional stresses, where a competent bed (in this case a chalk layer) is moulded and stretched by lateral stress, while less competent adjacent material (in this case the grey till) migrates into any resulting voids. c) Recumbent fold structures displayed by light-grey silt layers within deformed subglacial till (photographs by Dave Roberts, Durham University, UK).

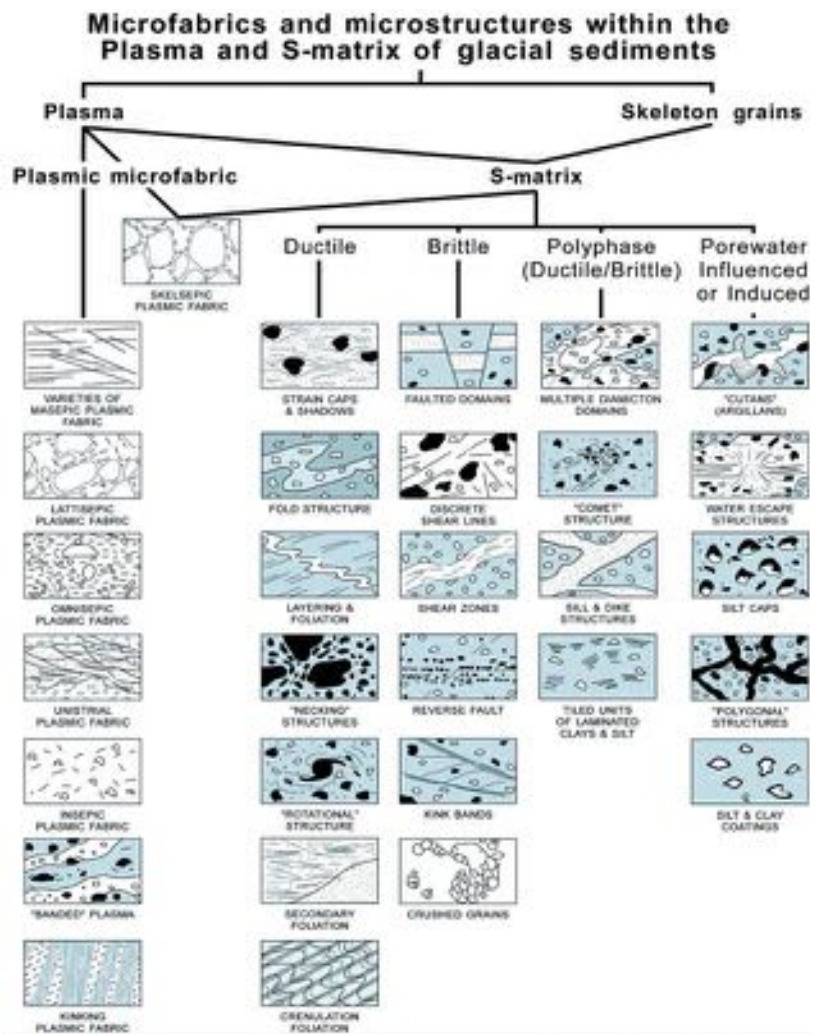
structures and fabrics that form in plasma can be distinguished from those that form where plasma and skeletal components are combined (**S-matrix structures**). These can be divided into those characteristic of ductile or brittle deformation, and those associated with high pore-water content. Analysis of the type and distribution of these features can reveal the processes of till formation (Menzies *et al.*, 2006). One important advantage of the thin-section micromorphological approach is that it can be employed to analyse small samples obtained from boreholes drilled into unexposed sediments, including submarine strata, to discriminate between subglacial till and other sediments (Carr *et al.*, 2006).

Macro- and micro-deformational features are commonly encountered in subglacial tills, so much so that there is growing support for recognizing deformational stress as probably the most important mechanism affecting till formation during the Pleistocene (van der Meer *et al.*, 2003). While this view has been contested (e.g. Piotrowski *et al.*, 2004), some geologists argue that since all basal or lodgement tills show evidence of subglacial deformation, they should be described in tectonic rather than sedimentary terms (e.g. Menzies *et al.*, 2006; Evans *et al.*, 2006). Hence, many researchers now use the term '**glacitectonite**' or '**tectomicts**' to refer to subglacially deformed material in general, while some maintain a distinction between glacitectonite, materials that have undergone subglacial shear but retain some of the structural characteristics of the parent material, and **subglacial traction till**, sediment deposited by basal melting and subsequently disaggregated and perhaps homogenized by shearing (Evans *et al.*, 2006). Some have gone further, with Menzies *et al.* (2006) suggesting that all subglacial tills are effectively deforming glacier beds and hence the terms 'lodgement till' and 'melt-out till' are effectively redundant. Future work on the subglacial environment and its deposits will show whether or not this is indeed the case.

The presence of a deforming or mobile bed at the base of an ice sheet has important palaeoenvironmental implications. It has generally been considered, for example, that climate change has been the primary driver of glacier behaviour, with a direct relationship between temperature and precipitation on the one hand, and glacier advance and retreat on the other. However, if the majority of glacier movement takes place in the basal sediment, then changes in the deforming layer, such as drainage of the sediment and changes in sediment texture, may have a more significant impact on glacier behaviour than climate (Hart & Rose, 2001). Similarly, deforming bed processes may help to explain a continuing problem in glaciology, namely discontinuous fast ice flow in surging valley glaciers. Indeed,

Figure 3.8

Range of microstructures and fabrics observed in deformed tills from micromorphological analysis of thin section samples (from Menzies *et al.*, 2006, reprinted with permission from Elsevier).

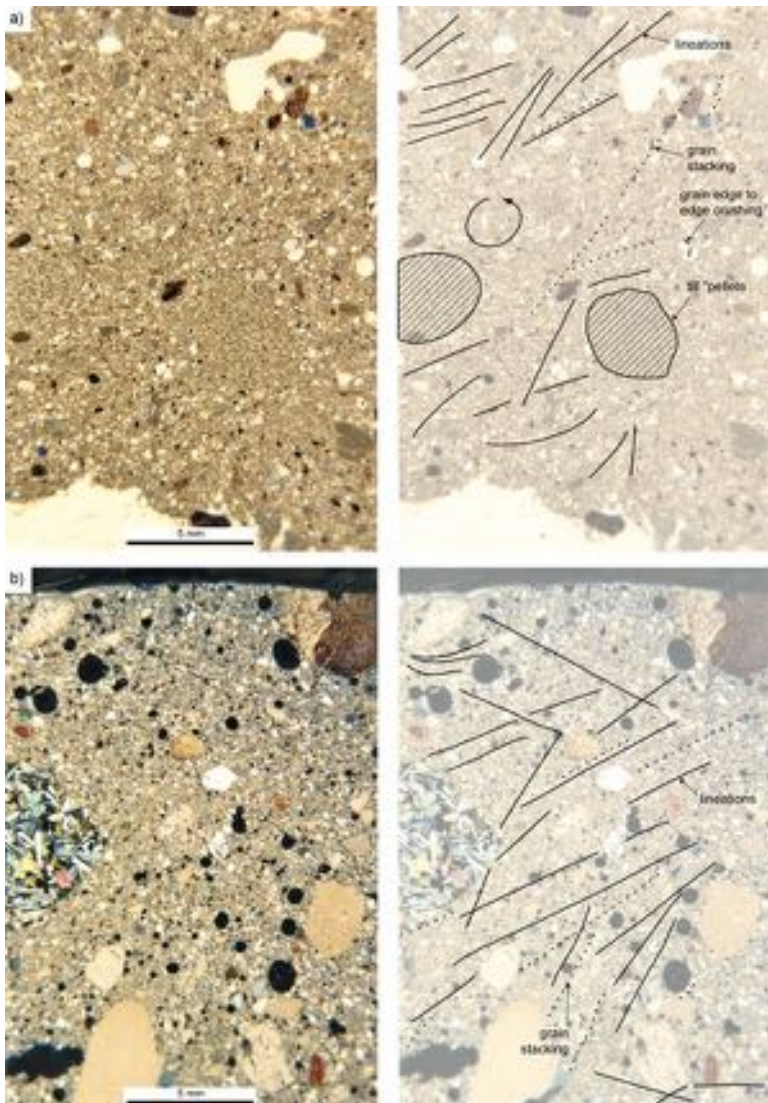


deformation of subglacial till is now thought to be one of the primary mechanisms maintaining the high rates of ice movement associated with ice streams in Antarctica, and may also be responsible for the generation of glacier surges (Dowdeswell *et al.*, 2004; Winsborrow *et al.*, 2010). Episodes of fast flow over a mobile glacier bed may also explain the massive discharges of the Laurentide ice sheet into the North Atlantic ocean (**Heinrich events**: section 3.10.1). While simulation modelling of palaeo-ice sheets (e.g. Bremer *et al.*, 2002) and modern observational studies of Antarctic fast-flow (e.g. Smith *et al.*, 2007) appear to support these ideas, there is still uncertainty as to whether soft-bed deformation is more important than basal sliding in the promotion of fast-flowing ice. Water, which is

concentrated under high pressure at the base of modern ice streams, saturates basal sediment reducing its friction and increasing its plasticity and mobility; it is therefore difficult to distinguish between the mechanical effects of sediment deformation and lubrication as agents of basal sliding (Marshall, 2005).

3.3.3.3 Paraglacial deposits

The retreat or withdrawal of glacier ice exposes landscapes that are inherently unstable and which are liable to modification, erosion and sediment release at rates greatly exceeding background denudation rates. Such accelerated geomorphological activity has been described as

**Figure 3.9**

Examples of microfabrics in deformed till identified using thin-section analysis on samples obtained from tills in Ontario, Canada (from Menzies *et al.*, 2006, reprinted with permission from Elsevier). The images on the right are annotated versions of those on the left, with characteristic microstructures outlined and labelled (images provided by John Menzies, Brock University, Ontario, Canada).

paraglacial. The term was introduced by Ryder (1971) but subsequently defined by Church & Ryder (1972, p. 3059) to refer to ‘nonglacial processes that are directly conditioned by glaciation’ and both to ‘proglacial processes, and to those occurring around and within the margins of a former glacier that are the direct result of the former presence of ice’. The essence of the concept is that of *glacially conditioned sediment availability* (Ballantyne, 2002a). Recently deglaciated terrain is often initially in an unstable or metastable state, and is therefore vulnerable to modification by subaerial processes including, for

example, slope failure, debris flow and fluvial reworking of materials. All of these are characterized by high rates of sediment delivery from slopes into fluvial and aeolian systems, and while they are not unique to the **paraglacial landscape**, they are especially effective during the adjustment of newly deglaciated landscapes to non-glacial conditions (Figure 3.11). The temporal operation of these processes (the **paraglacial period**) will vary because different elements of the paraglacial landscape will relax at different rates: steep, debris-mantled hillslopes may achieve stability within a few centuries of ice retreat, whereas large fluvial



Figure 3.10 Scanning electron photomicrographs of vertical sections through the fine matrix of tills. a) Slate-rich till, showing anisotropy with elongated clasts dipping towards the right, indicating ice movement direction towards the left. b) Shears in silty, deformation till indicating movement of ice towards the right (SEM Images provided by Lewis Owen, University of Cincinnati, USA).

systems may still be reworking glaciogenic sediment more than 10 ka after deglaciation (Ballantyne, 2002a). It is also possible for external factors (e.g. climate change and sea-level change) to induce sediment release millennia after termination of the initial (deglacial) period of paraglacial activity (Ballantyne, 2002b). It is important, however, to note the key distinction between paraglacial and *periglacial* processes, with the latter being characteristic of all cold, non-glacial environments, irrespective of whether glacier ice is or was present in the catchment (Knight & Harrison, 2009).

In the last two decades increasing attention has focused on paraglacial geomorphology and, in particular, on paraglacial facies represented in Quaternary stratigraphic sequences. In many parts of the British Isles, for example, landscapes that were previously interpreted in terms of more conventional glacial or periglacial models have been re-evaluated in the context of the paraglacial concept. In coastal areas of Wales, exposures of diamictons hitherto considered to be of glacial or periglacial derivation are now considered to reflect widespread redistribution of glacial sediments during and after deglaciation (e.g. McCarroll & Rijssdijk, 2003). Remobilization of valley-side tills and other glaciogenic deposits by debris flow and erosional processes is increasingly being recognized and reflected in the mapping of sediment–landform associations in other regions as well, for example in studies of recently deglaciated terrain in Patagonia (Glasser *et al.*, 2009), the Himalayas (Iturriaga, 2008) and the Alps (Curry *et al.*, 2006). The identification of paraglacial facies within Quaternary sequences is not always straightforward, however, and in some cases it may be impossible to distinguish paraglacial diamictons from, for example, flow or deformation tills. Paraglacial sediments therefore constitute a source of continuing ambiguity in the Quaternary stratigraphic record (Ballantyne, 2002a).

3.3.4 The influence of the thermal regime of glacier ice

A fundamental factor in determining the type of till that will be deposited at any one locality is the position at which debris is transported within the ice and this, in turn, is governed largely by the thermal regime of the glacier (Benn & Evans, 2010). The thermal regime is determined by ice thickness, mass balance and, above all, climate, and can be used to define four boundary conditions at the glacier sole. These are:

- A. a zone of net basal melting where more heat is provided to the glacier sole than can be conducted through the glacier;



Figure 3.11 View down the Braldu Valley in the central Karakoram, northern Pakistan (photograph by Lewis Owen, University of Cincinnati, USA). In the foreground is a large moraine ridge, while in the background is a series of massive fans, created by paraglacial mass movement of glacigenic sediments that took place soon after the ice retreated from the valley slopes (see Seong *et al.*, 2009).

- B. a zone in which a balance exists between melting and freezing where the heat provided at the glacier sole is approximately equal to the amount that can be conducted through the glacier per unit time;
- C. a zone of net basal freezing but where sufficient meltwater may still be present to raise the temperature and maintain parts of the sole at the melting point;
- D. a zone in which the amount of heat provided at the sole is insufficient to prevent freezing throughout.

In zone A, the glacier slips over its bed and material entrained in the basal ice layers will subsequently be deposited where frictional retardation against the bed is high. Similar processes operate in zone B, although lodgement (and deformation) of material will tend to be greater with lower amounts of meltwater present. In zone C, plucking of subglacial material occurs as the glacier slides over its bed, little lodgement/deformation till is deposited and material tends to be carried up into the ice

through shearing action. Subsequent deposition may therefore be in the form of mass flow deposits. In zone D, the bed is frozen, no basal sliding occurs and glacier movement is entirely a result of internal shearing. Again, mass flow diamictons may be the dominant depositional types. Zones A and B tend to be associated with 'warm-based' or temperate glaciers, while zones C and D are found principally in 'cold-based' or polar glaciers. It is important to appreciate that within a single ice sheet, some or all of these zones may be present, and that during the course of an ice sheet cycle (ice growth, ice maximum, ice wastage), the various boundary conditions will vary in both space and time (e.g. Boulton *et al.*, 2001). Changing dynamic and thermal regimes have also been noted in valley glaciers ('polythermal glaciers') leading to contrasting styles of sedimentation (Glasser & Hambrey, 2001).

The importance of this concept for the interpretation of glacigenic sediments and sequences is that it explains why in some areas subglacial tills tend to be the dominant

depositional type, while in others supraglacially derived debris is more common. It also explains why, in regions where cold-based conditions occurred in ice-marginal zones, stacked multiple-depositional sequences including a range of interbedded glacigenic facies (lodgement/deformation till, mass flow diamictons and glaciofluvial sediments) can be the product of a single wasting ice mass (McCarroll & Rijssdijk, 2003; Lukas *et al.*, 2005). This is a significant departure from earlier thinking where, for many years, multiple-till sequences were commonly interpreted as reflecting two or more glacial advances. Equally important has been the recognition that glacigenic sediments are spatially complex as a consequence of variations in basal thermal regime. Research on the beds of modern glaciers has shown that subglacial conditions vary between cold-based and warm-based ice over short distances leading, in some areas, to a highly complex mosaic of glacigenic deposits (Evans *et al.*, 2006). The local topographic context will also influence the basal thermal regime, and thus the type and complexity of glacigenic sequences that develop in ice-marginal zones. This is particularly the case where proglacial and subglacial lakes develop, for not only does this result in interdigitation of outwash sediments with diamictons, but it can also induce instability in the ice margin, leading to glaciectonic disturbance of the sedimentary facies (e.g. Knight, 2012). Complex sedimentary facies are also characteristic of ice-marginal zones that extend into the sea, reflecting local variations in basal thermal regime, especially where the ice front oscillates across the grounding line (Ó Cofaigh, 2013).

3.3.5 Analysis of glacigenic sequences

In view of the complexities of till genesis, the analysis of glacigenic sequences requires the application of a range of field and laboratory techniques in order to distinguish between different types of glacigenic sediment and to establish their field relationships (Hubbard & Glasser, 2005). The aim should be to gain an understanding of both the internal structure and constituents of each sedimentary unit, as well as the three-dimensional geometry of the glacigenic sequence under investigation. A detailed description should be obtained of each lithological unit, including changes in grain size, shapes of particles, and the presence or absence of bedding and deformational structures such as shears and folds (Chapter 6, Table 6.1). Evidence of flowage of material, for example current bedding or ripple structures in stratified sediments or clast fabrics (section 3.3.6.2) in unstratified deposits, should also be recorded. It is particularly important to note the facies relationships between lithological units, including details

of the nature of the contacts between them, any lateral variations both within and between beds, and any evidence for superimposition of sediments as well as the degree of deformation or of other post-depositional modifications. The analysis of facies relationships and facies variations can provide greater insights into the nature of the former depositional environment than the more traditional analysis of individual sedimentary units (Thomas & Chiverrell, 2007). Some of these aspects of glacial sediment analysis are now considered in more detail.

3.3.5.1 Particle size and shape analysis

Individual till units often have characteristic grain-size variations and particle shapes. Particle size distributions are a function of a number of factors, including rock and mineral types of which the clasts are composed, transportation processes, transport distance and mode of deposition. In lodgement/deformation tills, for example, the particles tend to be closely packed and little winnowing by drainage takes place, so that if the sediment has a high clay content, this will tend to be preserved. Mass flow diamictons, on the other hand, may lose much of the finer matrix through rapid drainage which removes clay and silt particles, a process known as **illuviation**. If the depositional process is passive, however, much of the fine matrix can be preserved, whereas active slides followed by free water escape may reduce the amount of fine particles during settling. Laboratory measurement of particle size distributions, in the form of ternary plots (Figure 3.12) or cumulative frequency curves (Figure 3.13) can sometimes discriminate till units of different genesis, or isolate tills from other diamictons, and can even reveal subtle differences in lithology between tills of similar origin (Curry *et al.*, 2009). An analysis of particle shape and surface textures, along with signs of micro-wear, may also be important for establishing the mode of formation of tills. There will be a tendency for particles to be more strongly affected by abrasion, faceting and crushing in lodgement/deformation than in supraglacial tills, for example, and so this evidence, in combination with particle size data, may help to differentiate between tills of different genesis (e.g. Evans *et al.*, 2012).

3.3.5.2 Lithofacies interpretations

Most interpretations of glacigenic sequences are based on the synthesis of a range of lithological data, involving detailed vertical logs of sediment exposures, and the analysis of clast lithology, fabric (section 3.3.6.2) and grain-size variations from as many beds as possible. These are plotted to provide an overview of the three-dimensional geometry

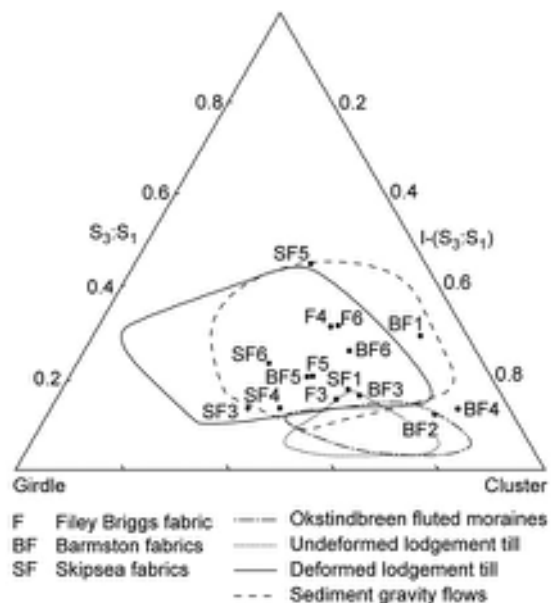


Figure 3.12 Ternary diagram using a statistical clustering method (eigenvalues) to characterize clast fabrics obtained from different types of diamicton in eastern England (from Evans *et al.*, 1995).

of lithofacies represented at a site, and this forms the basis for the correlation of beds and reconstructions of their genesis (e.g. Figure 3.14). The number of logs and associated field measurements depends on the local stratigraphic complexity. The more sedimentary characteristics that can be established for each bed, the more confidently can the mode of deposition be inferred. Examples of the sort of characteristics that can be logged, and how the combined information may help to differentiate between particular types of till and between tills and other diamictons can be found in Pawley *et al.* (2004) and Thomas & Chiverrell (2007).

Despite the meticulous and painstaking nature of this type of work, the evidence often remains frustratingly equivocal. This can be exemplified by the differences of view that currently exist over the interpretation of the sedimentary record of ice wastage in the Irish Sea basin in western Britain. Some have interpreted the stratigraphic evidence as indicating deposition within a glaciomarine

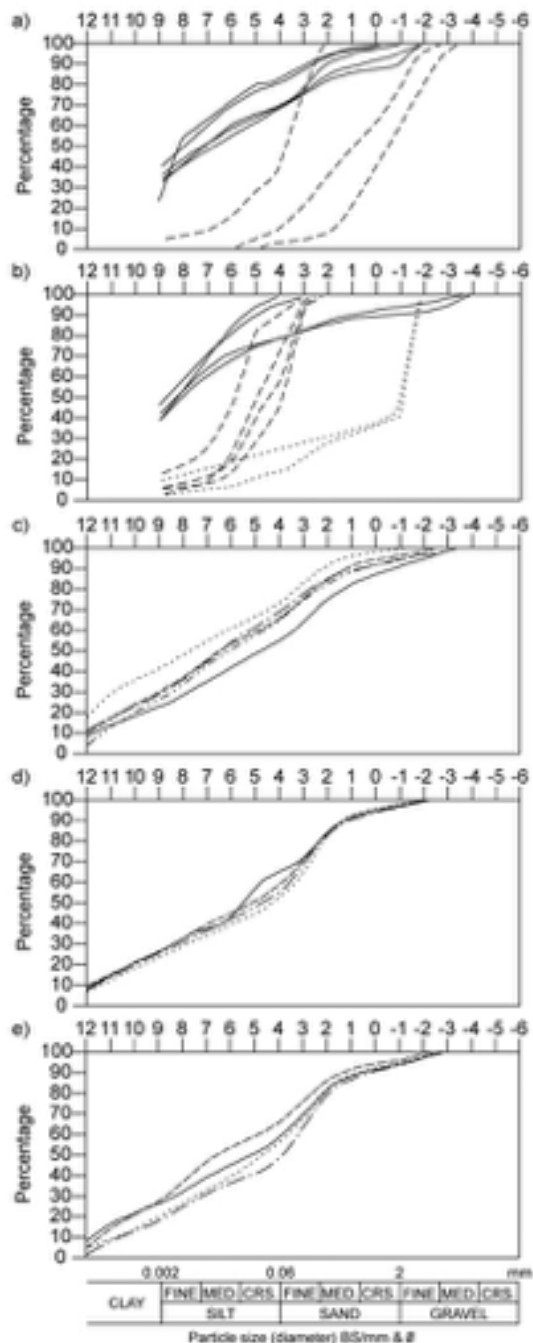


Figure 3.13 Particle size distributions (cumulative frequency curves) on the mm and ϕ (phi) scales showing the distinctive curves obtained from diamictons and sorted sediments a) and b) and the way in which the technique may distinguish between different diamictons c), d) and e). Note the more consistent frequency curves obtained from diamicton d) compared with those of c) and e). (a and b from McCarroll & Harris, 1992; c, d and e from Evans *et al.*, 1995).

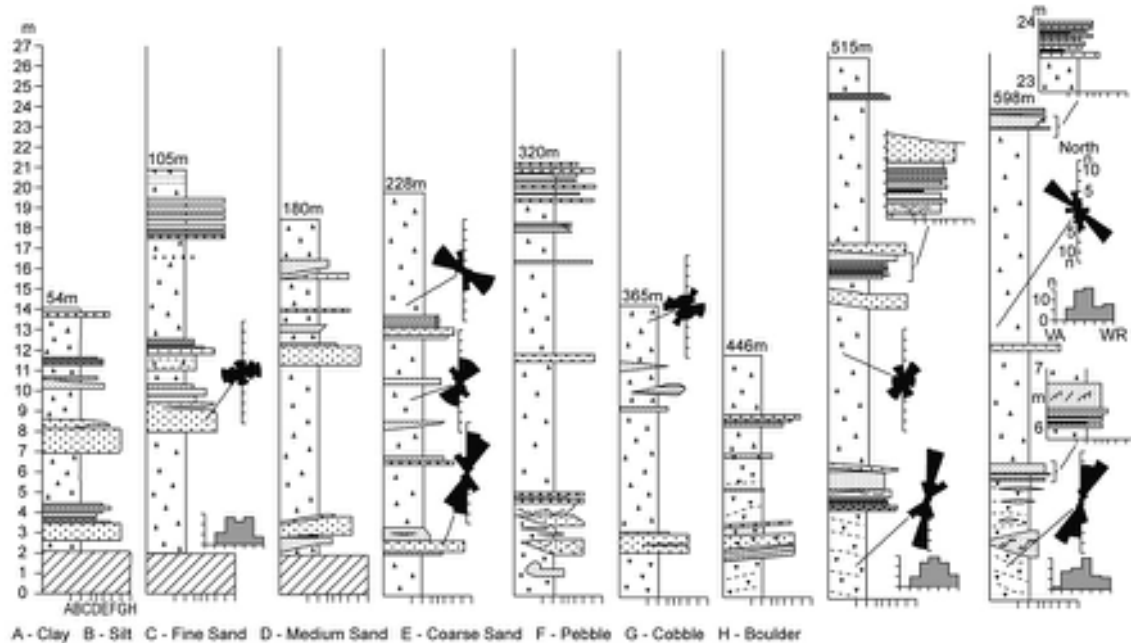


Figure 3.14 Schematic facies logs of glacigenic sediments in Wales, including rose diagrams of preferred orientations of long axes of clasts and clast roundness data (after McCarroll & Harris, 1992).

environment, while others have concluded that the coastal deposits around the Irish Sea were derived largely from wasting land-based glaciers (McCarroll *et al.*, 2001). There is no single set of sedimentary features that can conclusively resolve such differences of opinion; interpretation depends on an evaluation of all of the lithological (and geomorphological) evidence that is available, and the matching of this information with what are considered to be best-analogue facies sequences from contemporary glacial contexts. Much depends, therefore, upon having an adequate knowledge of the links between modern glacier, glaciomarine and glaciofluvial processes, and of the lithofacies variations they produce. Our understanding of Pleistocene glacigenic sequences is therefore an iterative and ongoing process, with constant refinement of the facies models upon which environmental reconstructions are based, and increasing recognition of the regional variation in glacigenic facies associations (Figure 3.15; Hambrey & Glasser, 2012).

3.3.6 Ice-directional indicators

It has already been shown how certain landforms, such as drumlins and *roches moutonnées*, can be used to infer the

direction of ice movement across a formerly glaciated area. However, some characteristics of glacial sediments can also yield valuable ice-directional information. The most widely used are indicator erratics, till fabrics and certain properties of the till matrix.

3.3.6.1 Erratics

The far-travelled particles found within, or on the surface of, a body of glacial sediment are known as **erratics**. The term is derived from the phrase *terrain erratique*, and was used initially by the French geologist Horace-Bénédict de Saussure in the late eighteenth century to describe areas where material of foreign origin overlay local bedrock. The shortened term is now generally applied to a particle of any size that is not indigenous to the area in which it is currently found. The most valuable types of erratic are those for which the sources are known, which are resistant to erosion, and which have distinctive appearances, unique mineral assemblages or unique fossil contents, thereby allowing unequivocal identification. These are usually termed **indicator erratics** and range in size from finely comminuted fragments to large blocks weighing several hundred tonnes. The famous Okotoks erratic ('The Big

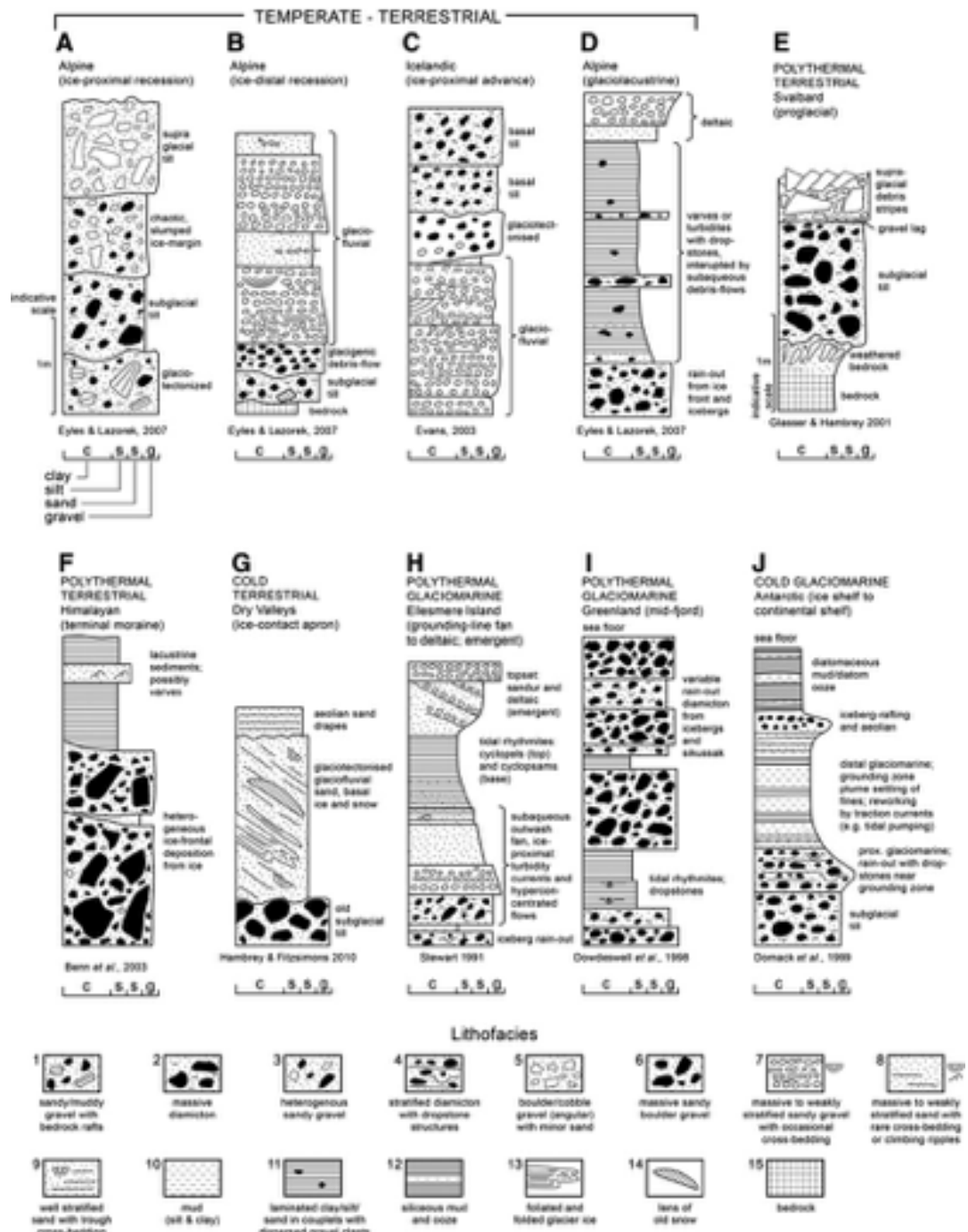


Figure 3.15 Idealized lithofacies associations for glacigenic sediment sequences that developed under different thermal regimes in terrestrial and marine settings. The depositional mechanisms inferred are also shown. The grain-size indicators (from left) are: c – clay; s – silt; s – sand; g – gravel (from Hambrey & Glasser, 2012, reprinted with permission from Elsevier).



Figure 3.16 The giant quartzite erratic ('The Big Rock') near Okotoks, southwest Alberta, Canada (photograph by Dave Evans, Durham University, UK).

'Rock': Figure 3.16) c.18 km southwest of Calgary in western Canada, for example, is the world's largest known glacial erratic, with a mass of c. 18,000 tonnes. It is part of the 'Foothills Erratics Train' that stretches more than 580 km from the Athabasca Valley in Jasper National Park along the eastern edge of the Rocky Mountain Foothills to the southern border of Montana, USA, and was carried into place during coalescence between Cordilleran glaciers and the Laurentide ice sheet during the Late Wisconsinan glaciation (Jackson *et al.*, 1997). At the other end of the scale, distinctive **indicator minerals** can also be used to infer till origin or *provenance* (e.g. Klassen, 2001; Roy *et al.*, 2007). Erratic distributions can provide information on both local and regional ice-flow directions (Figure 3.17), and they have also been used to reconstruct patterns of ice-sheet deglaciation, where changing flow pathways and migrations of ice divides can be inferred from erratic distributions (e.g. Ehrmann *et al.*, 2011). In this respect they are also an important data source for the development of ice-sheet models (section 2.3.4).

One problem with using erratics as ice-directional indicators, however, is that their presence in a glacial deposit may not always reflect primary derivation (i.e. an erratic could have been removed during a previous glacial episode and reincorporated into a younger till) and this can lead to erroneous interpretations of former patterns of ice movement. Hence, although erratics can frequently provide useful ice-directional information, they are perhaps best used in conjunction with other independent sources of evidence.

3.3.6.2 Till fabrics

The arrangement of particles in a till is termed the **till fabric**. It was observed at a very early stage in the development of

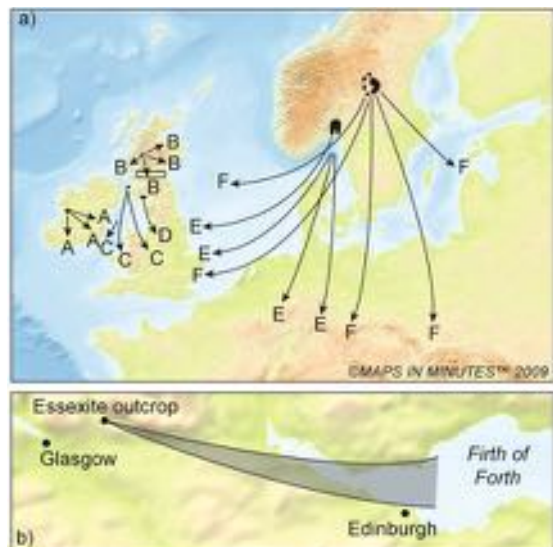


Figure 3.17 a) Distribution of some indicator erratics by ice in Britain and northwest Europe: A – Galway granite; B – Rannoch granite; C – Ailsa Craig riebeckite-eurite; D – Cribell granite; E – Oslo rhomb porphyry; F – Dala porphyries. b) The Lennoxtown boulder train in the Forth Valley lowlands of central Scotland (based on diagrams in Sissons, 1967 and West, 1977).

glacial geological studies that stones (clasts) within a till often displayed a preferred orientation, although it was somewhat later that a quantitative relationship was established between stone orientations in till and patterns of ice movement. Over the last few decades till fabric analysis, involving the measurement of orientation and dip of particles within a till matrix, has become one of the most widely used techniques for reconstructing former

ice-flow directions (e.g. Kjaer *et al.*, 2003). More recently, fabric data have been used to infer depositional processes and deformational mechanisms (Larsen & Piotrowski, 2003; Hart *et al.*, 2009). The technique rests on the assumption that, within the constantly deforming layer at the base of the ice, stones (clasts) will become orientated to adopt the line of minimal resistance to flow, that is, with their long axes parallel to the flow direction. In theory, therefore, subsequent deposition of the subglacial debris in the form of lodgement/deformation till should preserve a record of the former direction of ice movement, and this can be established by measuring the orientation of pebbles in lodgement/deformation till exposures using a compass. Measurement of the dip by means of a clinometer or a similar instrument may also provide useful ice-directional information, as a tendency has been observed for pebbles in a lodgement/deformation till to dip up-glacier.

Till fabric data are often presented in the form of stereonets or polar graphs. Where two-dimensional data only have been obtained, a rose diagram is constructed showing the number or proportion of pebbles in different azimuthal classes. However, because each measured stone is represented by two opposite azimuthal values (e.g. 30° and 210°), the rose diagram actually consists of two reflected halves or mirror images. The data can be shown by a line through the middle of each sector (Figure 3.18a), by the linking of such lines to form the typical rose diagram (Figure 3.18b) or by the shading of each azimuthal class to the extent of the line marking the outer limit of each class (Figure 3.18c). Where the dip of the pebbles has been recorded, orientation measurements are taken in the down-dip direction, and therefore each pebble is represented by a single dip and orientation value. In this case, the diagram will show a full 360° distribution (Figure 3.18d). Orientation and dip can be plotted together in the form of a scattergram with the radius divided into degrees showing the angle of dip, and the circumference divided into degrees showing the orientation of the pebble (Figure 3.18e). This is one of the most commonly used methods for depicting till fabric data, and in some cases the visual effect is enhanced by contouring the diagram as shown in Figure 3.18f.

While stereonets are useful in that they provide a good visual impression of fabric data, a quantitative basis for comparison between fabric data is often required. Perhaps the most widely used approach has been the eigen-vector method. **Eigenvalues** reduce large datasets to simple descriptive statistics. These reflect the strength and orientation of directional properties of a sediment, and thus allow the ready comparison of fabric data from several localities (Benn, 2004). This method has also been used as a basis for

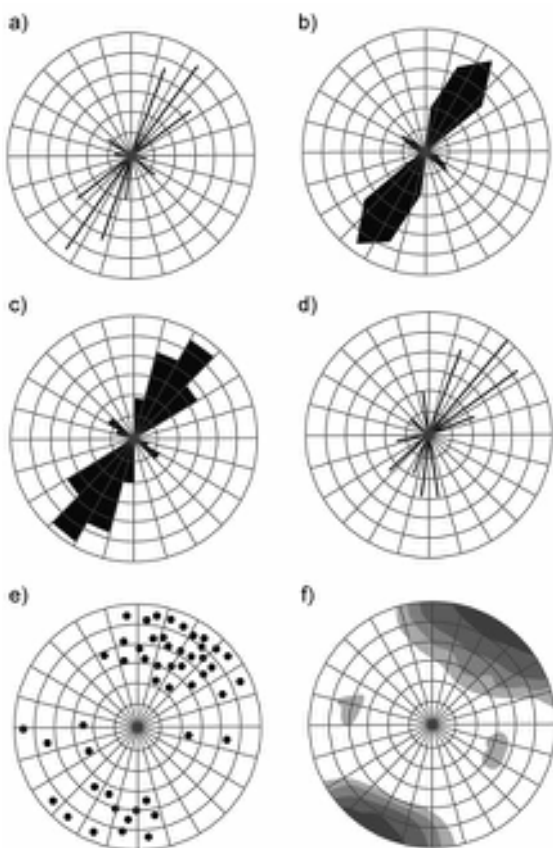


Figure 3.18 Different methods for representing till fabric data. For explanation see text.

differentiating between different types of sediment facies, for facies with contrasting depositional and deformational histories may have distinctive ranges of eigenvalues. If this is so, then it may be possible to employ the fabric characteristics (as reflected in eigenvalues) of sediments of known origin to assist in the interpretation of facies whose mode of genesis is not known (Benn, 1994; Hart, 1994). Not all authorities agree on the validity of this approach, however, and the use of fabric data in the discrimination of glaciogenic facies and in the genesis of tills continues to be debated (Benn & Ringrose, 2001; Carr & Rose, 2003).

In using fabric analysis as a basis for determining regional ice-flow direction, it is necessary to be certain of the genesis of the till under investigation. Mass flow tills, for example, which were generated under saturated conditions and flowed down a steep ice surface before settling, tend to show a very strong preferred orientation through-

out the sediment body. However, fabrics from such tills invariably indicate only very localized conditions of flowage with neighbouring till units often exhibiting markedly different flow directions. Other tills may show little preferred orientation where clast concentration was low and melting from within the ice was slow; in these cases, the englacial fabric may be retained (Johnson *et al.*, 1995), but as this is easily lost during the final melting phase, these too can be unreliable indicators of regional ice movement. The key, therefore, is to employ only tills that derive from the subglacial environment. However, fabrics in lodgement/deformation tills can also display considerable spatial variability, even within a single exposure with the lack of consistent pattern in relation to ice-flow direction perhaps reflecting stress field variability within the deforming glacier bed (Carr & Rose, 2003). Fabrics may also be affected by the morphology of the glacier bed, especially where basal ice is forced around prominent bedrock protuberances (Catto, 1990), and they may also show marked spatial variability where the tills were affected either by changes in the direction of regional ice movement during deposition (e.g. Hicock *et al.*, 1996), or by post-depositional modification of the sediment (e.g. Hambrey *et al.*, 2001). Till fabric analysis is, therefore, a technique that must be undertaken with care, and is perhaps best employed in association with other indicators of former ice movement.

3.3.6.3 Properties of the till matrix

Certain physical and chemical properties of the till matrix can be used to make inferences about regional ice movement, and also to differentiate between tills from different source areas. This approach rests on the assumption that tills will inherit certain textural and chemical characteristics from bedrock over which the glacier has travelled. In certain cases, where a particularly distinctive lithological type lies up-glacier, it may be possible to detect the influence of that rock outcrop on the till matrix. In a sense, therefore, certain properties of tills can be used in the same way as indicator erratics. A widely used technique has been the analysis of clay mineral ratios in the till matrix as, for example, in the establishment of ice-transport pathways for sediments lying beneath the McMurdo Ice Shelf in Antarctica, where it has been employed in conjunction with heavy mineral data (Georgetti *et al.*, 2009). Other methods that have been used for ‘fingerprinting’ till matrices are geochemical analysis of mineral composition (e.g. Kubala-Kukus *et al.*, 2013), mineral magnetic properties such as magnetic susceptibility (Ojala *et al.*, 2011a), major and trace element ratios and isotope analysis (Farmer *et al.*, 2006) and micropalaeontological content (Sjunneskog &

Scherer, 2005). In addition to providing insights into former patterns of ice movement, the analysis of indicator minerals in tills also has applications in economic geology, for ore bodies can be located using evidence of glacially transported debris (Lehtonen *et al.*, 2005; Sarala & Peuraniemi, 2007).

A recent development in studies of till matrices has been the analysis of cosmogenic nuclides. As we shall see in Chapter 5 (section 5.3.8), cosmogenic nuclides that are formed at the earth’s surface through interactions between incoming cosmic rays and certain terrestrial minerals can be used as a basis for dating. Here, however, variations in cosmogenic nuclide content of tills and exposed ground surfaces can be used to determine whether these surfaces were formerly covered by warm-based as opposed to cold-based ice. In Baffin Island, for example, the concentrations of two cosmogenic nuclides (^{26}Al and ^{10}Be) were higher in those areas where independent studies suggested cold-based ice predominated (Staiger *et al.*, 2006). This may reflect the fact that surfaces that were not subject to intense erosion (i.e. were covered by cold-based ice) have retained higher cosmogenic nuclide levels that were inherited from preglacial times. Greater effective erosion takes place under warm-based ice, which removes former regolith, exposing younger surfaces with a much lower cosmogenic nuclide content. This contrast is also reflected in the cosmogenic isotope content of tills associated with cold- or warm-based ice. A broadly similar finding emerged from the analysis of ^{10}Be content of regolith and tills in northern Sweden (Ebert *et al.*, 2012). Given the importance of distinguishing between cold-based and warm-based ice for understanding the behaviour of former ice masses, this new technique appears to offer a potentially useful independent method for reconstructing former glacier thermal regimes.

3.4 PERIGLACIAL SEDIMENTS

3.4.1 Introduction

In the ‘periglacial domain’ (section 2.4), freeze–thaw activity causes fracture of the country rock and the accumulation of coarse, angular debris. This material moves downslope through the combined processes of flowage (**gelification**) and creep induced by the growth and melt of interstitial ice and a landscape of low-angled slopes with smooth profiles results. The deposits are known by a variety of names, including ‘head’, ‘coombe rock’, ‘tjaele gravel’ and, where coarse stratification has developed, ‘stratified scree’ or ‘grèzes litées’ (e.g. Figure 2.28). Sediments that have been affected by periglacial action during the

Quaternary are widespread throughout the mid- and high-latitude regions of the world. Frequently, their presence reflects not only the breakdown of bedrock by cold-climate processes, but also the reworking and redistribution of pre-existing drift deposits. As described above (section 3.3.3.3), where such processes operate in proximity to glacier ice or in areas of recently deglaciated terrain where rates of sediment delivery are high, the term '**paraglacial**' is now used in preference to **periglacial** to describe the geomorphic processes that operate in such environments and the depositional sequences that are produced (Ballantyne, 2002a, 2002b).

Periglacial sediments can be recognized by a number of distinctive characteristics, including the occurrence of predominantly angular material within the sediment matrix as a result of frost-riveting, the vertical alignment of many stones reflecting the upward movement of particles with the expansion and melting of ice lenses, the presence of structures produced by ground cracking as well as flow of saturated sediment (see below) and, where the deposits have been moved by gelifluction, the preferred alignment of the larger particles downslope. Clast fabric analysis in particular may be used to distinguish between, for example, geliflucted and undisturbed glacial drift, for in periglacial deposits fabrics taken over a wide area should exhibit a consistent preferred orientation parallel with the local slope. Further details of the range of sediments and associated processes of the periglacial zone can be found in Ballantyne & Harris (1994), French (2007) and Martini *et al.*, (2011).

3.4.2 Structures associated with permafrost

Although the presence of frost-shattered bedrock and extensive spreads of gelifluction deposits is indicative of a former periglacial climatic regime within a particular area, it normally provides only the most generalized of information about former environmental conditions. However, where sediments show evidence of ground-ice activity, more precise palaeoclimatic inferences are possible. This section deals with two types of structure that result from the deep penetration of ground ice: **ice-wedge casts** and **involutions**.

Ice wedges are considered to be diagnostic structures of permafrost. When temperature falls rapidly, thermal contraction cracks open in the permafrost surface, and where these occur repeatedly at the same location, water seeps in and freezes, leading to the formation of a vertical wedge of ice. The incremental accumulation of ice in veins and fissures along the axes of the contraction cracks leads to the growth of wedges (Mackay & Burns, 2002).

They can be up to 3 m in width and 10 m in depth, but mature wedges are typically 1–1.5 m in width and 4 m in depth. They typically form in unconsolidated sediments, but on occasions have been recorded penetrating underlying bedrock (Owen *et al.*, 1998). If they develop some time after the accumulation of the sediments in which they form, they are referred to as **epigenetic ice wedges**. Occasionally, however, cracks form in sediments that are still accumulating, and the wedges extend upwards to keep pace with sediment aggradation; these are referred to as **syngenetic** (or **synsedimentary**) ice wedges and can grow to exceptional depths. Upon melting, the ice is replaced by material falling into the cracks from above and from the sides. In this way a cast or **pseudomorph** of the original form of the ice wedge is preserved (Figure 3.19a). Ice wedges typically form as part of a network of thermal contraction cracks which appear as interconnected polygons on the ground surface, although in sections they are often found as single features.

Active ice wedges in present-day cold regions can develop in a variety of sediments and soil, but they occur only in the zone of **continuous permafrost** (Ballantyne & Harris, 1994). They therefore provide unambiguous evidence of the former existence of perennially frozen ground. In the **discontinuous permafrost zone**, most ice wedges appear to be inactive. In arid and semi-arid periglacial regions and in some localities that are free-draining, frost fissures that develop from thermal contraction of the ground are frequently filled with wind-blown sediment and are termed **sand wedges** (Figure 3.19b). Occasionally,

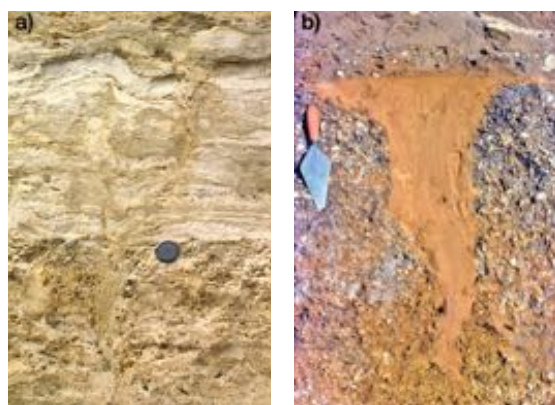


Figure 3.19 a) Ice-wedge cast or pseudomorph of Anglian age (MIS 12) penetrating sediments of the Cromerian complex, West Runton, Norfolk, Eastern England (photograph by Mike Walker). b) Anglian age sand wedge in profile, from Broomfield, Essex, UK (photograph by Peter Allen, Royal Holloway, University of London, UK).

though, they are filled with other materials, including soil, so that in eastern Europe the more general term of ‘**ground wedge**’ is used, while the term ‘**soil wedge**’ refers to those features that have a high soil content. Ancient/relict sand wedges of 2 m or more in depth probably indicate the former presence of permafrost (Murton *et al.*, 2000; Vandenberghe *et al.*, 2004), whereas narrow sand wedges (frost cracks) are more ambiguous as they form not only in the active layer above and within continuous permafrost, but also in seasonally frozen ground in non-permafrost areas.

Sand-wedge pseudomorphs can sometimes be distinguished from ice-wedge casts by the characteristics of the sediment infill, but a clear differentiation between the two is not always possible in the field, and the two forms may be found in close association in both present-day and former permafrost regions (Liu & Lai, 2013). Care also needs to be taken to distinguish ice-wedge casts from other deformational structures, such as water escape features which, at first sight, may often appear very similar. Characteristic features of wedges that can assist identification include: (1) depth/width ratios of between 3:1 and 6:1, which conform with the dimensions of modern wedges (Ballantyne & Harris, 1994); (2) slump structures and stratification within the cast-fill sediment, which is usually concave downwards ('sag' structures); (3) the presence of large joints and normal faults within the wedge structure and of associated micro-joint patterns in adjacent sediments, produced by freezing during the development of patterned ground; and (4) if the wedge cast has not been truncated by erosion, the top of the cast may merge with other evidence indicating the position of the former

permafrost table, such as a stone pavement or cryoturbated horizon.

In many areas where periglacial conditions prevailed, unconsolidated sediments in open sections frequently display contortions in bedding, the interpenetration of one layer by another, and pockets that resemble **load structures**.⁴ Such **cryostructures** are frequently termed **involution**, **cryoturbations** or **festoons** (Figure 3.20) and are considered to reflect differential pressures induced by freezing within the active layer above the permafrost table (French & Shur, 2010). They sometimes appear to be irregular in spacing and heterogeneous in form, but a close inspection often reveals a degree of order. Vandenberghe (1988) has recognized six different types of involution on the basis of their morphology (Figure 3.21): (1) isolated folds of small amplitude (i.e. depth of structure) but large wavelength; (2) regular, symmetrical and well-developed forms with amplitudes of 0.6–2 m; (3) smaller-scale versions of type 2; (4) solitary features of teardrop (4a) or diapiric (4b) form; (5) sediment injected upwards into polygonal cracks; and (6) irregular deformation structures.

Three main modes of formation have been proposed for involution structures. **Periglacial loading** involves the density inversion of sediments during the thaw of frozen ground. Melting may produce pockets or layers of mobile saturated sediment that become liquefied and injected into overlying deposits to be replaced by denser, less fluid material which sinks. This process probably accounts for most of the features classified as types 2, 3 and 4 in Figure 3.21. The second process involves the movement of material under **cryohydrostatic pressure**, as the ‘freezing front’ descends from the surface each autumn towards the upper



Figure 3.20

Involutions/cryoturbation structures, formed in Late Weichselian fluvial sediments during the Younger Dryas Stadial, exposed at the site of Bosscherheide, Netherlands (see Bohncke *et al.*, 1993) (photograph by Jef Vandenberghe, Free University, Amsterdam, Netherlands).

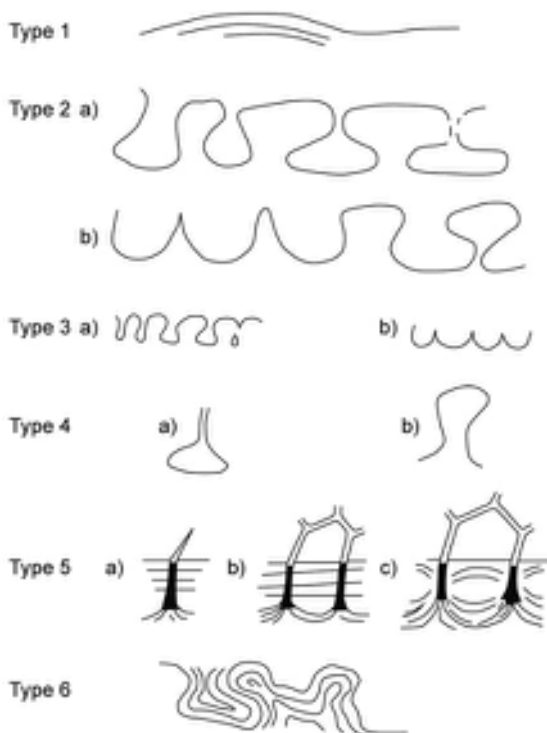


Figure 3.21 Classification of cryoturbation structures according to their form (symmetry, amplitude, wavelength and pattern of occurrence) (based on Vandenberghe, 1988, after Ballantyne & Harris, 1994). For further detail see text.

surface of the permafrost table at the base of the active layer. This leads to a build-up of high pore-water pressures in the material trapped within the unfrozen part of the active layer, and subsequent deformation of the liquefied sediments. The third mechanism is **differential frost heave**, which results from the differential rate of freezing in sediments of varying composition. Frost will penetrate coarser sediment more quickly than finer deposits, and the water in the latter has a lower freezing point. This results in differential pressures as the ground freezes, leading to mass displacement (heaving) of sediment (Ballantyne & Harris, 1994).

As is the case in the interpretation of ice-wedge casts, however, care has to be taken before attributing a periglacial origin to involutions, since very similar structures can also be produced under non-freezing conditions where, for example, high pore-water pressures build up and escape routes are created in overlying layers by tectonic effects, or where density variations lead to the injection of liquefied sediments into overlying sediment bodies. However, there

is often the close field relationship between cryoturbations and other undoubted periglacial phenomena, such as ice wedges, stone pavements and upturned stones, and thus where the depositional context is clearly periglacial, the involutions can be interpreted more confidently as frozen ground phenomena.

3.4.3 Palaeoclimatic significance of periglacial structures

As ice wedges and, in some cases, involutions are associated with permafrost, the former extent of permanently frozen ground can be deduced from the distribution of ice-wedge casts and involution structures. Thus, if the conditions under which permafrost is generated can be ascertained, then the fossil forms will enable climatic reconstructions to be made (Table 3.2). However, permafrost covers very large parts of the Northern Hemisphere, extending southwards into Alaska, Canada, Siberia and other parts of Asia (Figure 2.24). It occupies some 1.59 million km² (more than 15 per cent of the country) of China today (Ran *et al.*, 2012) and some 25 per cent of the southern circumpolar region (Bockheim, 1995). Clearly, with such an areal extent, there can be no single definition of what constitutes a ‘permafrost climate’. It is generally accepted, however, that permafrost will only occur where the mean annual air temperature (MAAT) drops below 0°C, although an upper MAAT limit for permafrost development of -2°C, especially for mountain regions, has also been suggested. The development of a thick permafrost layer requires centuries of sustained freezing. In North America, the present southern limit of continuous permafrost occurs between a MAAT of -6 and -8°C (Smith & Riesborough, 2002), while the southern limit of discontinuous permafrost in North America coincides with the -1°C isotherm. These relationships are not always consistent, however, for isolated but locally continuous areas of permafrost occur south of both of these isotherms. Altitudinal limits for permafrost have been identified in some mountain regions, such as Norway, where continuous permafrost occurs at MAATs that fall below -6°C and discontinuous permafrost below -1.5°C. In the Rocky Mountains of North America, discontinuous permafrost occurs where MAATs fall below -1°C.

More important in the context of palaeoclimatic reconstructions, however, are the specific climatic conditions required for the generation of ice-wedge casts and cryoturbations (Ballantyne & Harris, 1994). Where the ice wedges have developed in fine sediment, a MAAT of less than -4°C is probably required, and continuous permafrost is likely to be present (Table 3.2). If the feature is developed

Table 3.2 Range of air temperature thresholds for the formation of selected periglacial features estimated by different authorities in the field (after Matsuoka, 2011). MAAT – mean annual air temperature; MATCM – mean air temperature of the coldest month; a – value for fine (clay-silt) sediment; b – value for coarse (sand/gravel) sediment.

	Warm limits by MAAT (°C)			Warm limits by MATCM (°C)			
	Pewé, 1966	Washburn, 1980	Karte, 1983	Ballantyne and Harris, 1994	Huijzer and Isarin, 1997	Karte, 1983	Van Huissteden, <i>et al.</i> 2003
Earth hummocks			+3				
Small involutions, amplitude < 0.6 m					-1		
Large involutions, amplitude ≥ 0.6 m					-8 ^a , -4 ^b		
Sorted patterned ground, diameter < 1 m			+4				
Sorted patterned ground, diameter ≥ 1 m	0		-4	-2 to 0			
Rock glaciers	0		0 to +2	-2 to -1			
Organic palsas	0		-3 to 0				
Thermokarst depressions	-2 to 0		-1	-8 to -6			
Ice wedge polygons	-8 to -6	-5	-8 to -4	-6 ^a , -3 ^b	-8 ^a , -4 ^b	-20	-15
Soil wedge polygons			-4 to 0	-1 ^a , +1 ^b	-1	-8	
Open-system pingos	-2		-1	-5 to -4	-4		
Closed-system pingos	-6		-5		-6		

in sand and gravel, a MAAT of -8°C is implied, and almost certainly continuous permafrost (Matsuoka, 2011). Effectively, this means that mean annual air temperatures between -4 and -8°C produce continuous permafrost in loess regions, no permafrost in sandy-gravelly regions and discontinuous permafrost in regions with both coarse-grained and fine-grained soils (Renssen & Vandenberghe, 2003). Sand wedges are thought to develop under a similar climatic regime, although more severe conditions may be required, with a MAAT of as low as -12 to -20°C (Karte, 1983). However, sand wedges are known to form under warmer, and wetter, conditions where sand supply is abundant; indeed, small primary sand wedges may be associated with seasonally frozen ground where MAATs are very much higher (Murton *et al.*, 2000). Soil wedges can also occur in seasonally frozen ground, with a MAAT of $+1^{\circ}\text{C}$ (fine sediments) to -1°C (sand and gravel). Cryoturbation structures, on the other hand, reflect not only MAAT, but also the depth of the active layer, with large-scale structures (amplitude 0.6 m) indicating permafrost conditions and a MAAT of -4°C to -8°C (Huijzer & Isarin, 1997; French & Shur, 2010).

The distribution of ice and sand wedges and cryoturbations, in conjunction with other periglacial indicators (e.g. landforms), along with data from fossil Coleoptera (section 4.5.4.2), forms the basis for reconstructions of the periglacial environment of western Europe during the last cold stage (Huijzer & Vandenberghe, 1998). The evidence suggests that, in the period from *c.* $27\text{--}20\text{ k}^{14}\text{C yr BP}$ (prior to and during the Last Glacial Maximum: LGM), mean annual temperatures were below -8°C in the Netherlands, Belgium, England, Germany and Poland, and that the -4°C isotherm of mean annual air temperature was situated near the French–Belgian border (Figure 3.22a). The data therefore point to a transition from continuous permafrost across the former countries to discontinuous permafrost (northern France) during the maximum cold of the last cold stage. The southern boundary of permafrost lay across southern France. Mean annual temperatures remained below -8°C over much of the region immediately following the LGM (prior to *c.* 18 ka). During that interval, the southern boundary of the continuous permafrost zone was marginal to the decaying Weichselian ice sheet, and a zone of discontinuous permafrost extended from northern

France towards northern Germany. After 20 k¹⁴C yr BP, however, mean annual temperatures in Britain and Belgium rose by up to 10°C, and the permafrost zone shifted rapidly northwards (Figure 3.22b), so that by 17–15 k¹⁴C yr BP, only a narrow zone of permafrost existed near the retreating ice

sheets in Poland and northern Germany (Renssen & Vandenbergh, 2003). Precipitation reconstructions suggest an initial period of relatively high precipitation (around 30 ka), but an increasing trend to aridity thereafter (Huijzer & Vandenbergh, 1998).

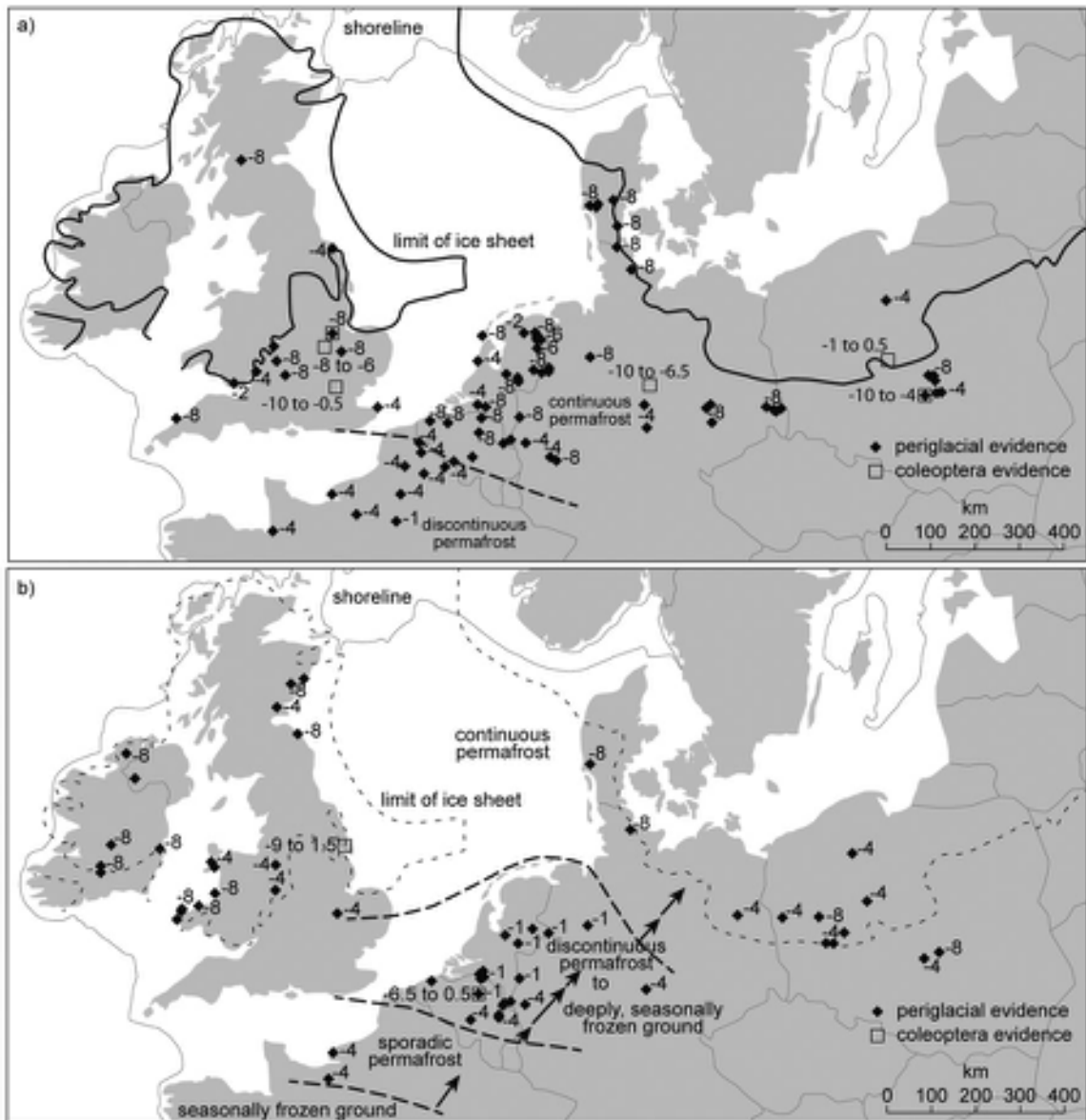


Figure 3.22 a) Mean annual temperature in northwest Europe during the 27–20 k¹⁴C yr BP interval based on a combination of periglacial and coleopteran evidence (after Huijzer & Vandenbergh, 1998). b) Mean annual temperature in northwest Europe during the 20–13 k¹⁴C yr BP interval based on a combination of periglacial and coleopteran evidence (after Huijzer & Vandenbergh, 1998).

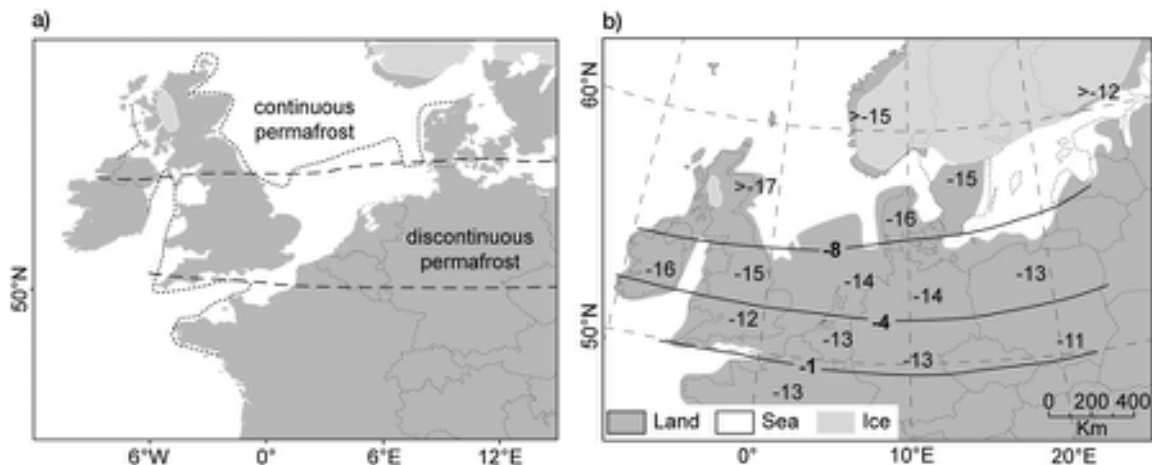


Figure 3.23 a) Permafrost limits in northwest Europe during the Younger Dryas based on periglacial evidence (after Renssen & Vandenbergh, 2003). b) Maximum mean annual isotherms in northwest Europe for the coldest part of the Younger Dryas Stadial based on periglacial evidence (after Isarin *et al.*, 1998).

During the Younger Dryas cold phase (*c.* 13–11.7 k¹⁴C yr BP), relict periglacial phenomena suggest that continuous permafrost existed north of 54°N in Fennoscandia, the northern parts of the British Isles, and Ireland during the coldest part of the phase (Figure 3.23a). Mean annual air temperatures at sea level near or below –8°C and mean temperatures of the coldest month well below –20°C (Figure 3.23b) characterized this zone. Discontinuous permafrost was present between 54°N and 50°N (*i.e.* in central and southern England and Ireland, the Netherlands, upland Belgium, northern Germany and Poland). In this zone, mean annual air temperatures were between –8 and –1°C, with mean temperatures of the coldest month above –20°C (Isarin *et al.*, 1997). These reconstructions suggest winter temperatures were depressed by as much as 20–30°C compared with today, with summer temperatures around 4–5°C below present values. The marked decrease in annual temperature range generated a Younger Dryas temperature regime in western Europe that may well be comparable to that of western Alaska today (Isarin & Renssen, 1999). A combination of the periglacial (and other proxy) evidence and atmospheric model simulation experiments suggests that during both the Younger Dryas and also early cold phases, the southern margin of permafrost in western Europe was controlled largely by the latitude of the winter sea-ice margin in the North Atlantic Ocean. Cold winds blowing off the ice pack (situated around 52°N during the Younger Dryas) would account for (1) the very low winter temperatures; (2) the low levels of precipitation; and (3) the resulting absence of a thick

snow cover and hence the relative abundance of ice wedges and related structures (Renssen *et al.*, 2002; Renssen & Vandenbergh, 2003).

Fossil periglacial phenomena, therefore, constitute a potentially valuable data source for the reconstruction of Quaternary environments. However, the use of this evidence is not without its difficulties (Murton *et al.*, 2000). Present-day Arctic areas are not necessarily good analogues for the periglacial regimes that prevailed in the mid-latitudes during former cold stages for, while the physics of the freeze–thaw process are essentially the same, mid-latitude environments would have experienced differences in insolation budgets, atmospheric circulation, vegetation cover and levels of ground instability (French, 2007). In particular, there would have been considerably more diurnal freeze–thaw cycles than in the present High Arctic where the seasonal periodicity of daylight and darkness favours longer, more severe cycles and deeper ground freezing. Certainly, mid-latitude areas did not experience the extremes of freezing that now characterize, for example, interior Siberia and Canada and, in view of the proximity of large glacier masses, probably had a climatic regime which differed in a number of respects from that of the present-day high latitudes, particularly in terms of precipitation, wind direction and wind intensity (French, 2007). Difficulties in palaeoclimatic reconstruction may also arise from the fact that geomorphological processes in periglacial regions are frequently determined as much by local site factors as by prevailing climatic conditions, giving rise to a complex variation in cryostatic facies (French & Shur,

2010). Hence, local variations in vegetation or snow cover, for example, can mean that mean annual ground temperature (MAGT) is more likely to be the determining factor in ice-wedge formation than MAAT (Smith & Riseborough, 2002). Indeed, modelling of ice-wedge networks suggests that the spacing, wedge width and fracture frequency in wedges may be more sensitive to infrequent climatic events and initial ground conditions, rather than prevailing climatic parameters such as MAAT (Plug & Twerner, 2008). Further interpretational problems may arise from the complex stages of wedge growth and degradation that have been observed in both relict Pleistocene wedges in mid-latitude sites (Kolstrup, 1993) and in High Arctic contexts (Murton *et al.*, 2000). Finally, the dating of periglacial structures is frequently problematic, and such features have only been dated either on the basis of their stratigraphy or on radiocarbon dating of sub-adjacent or supra-adjacent organic material. This difficulty has, to some extent, been overcome, at least in the dating of wedges, by measuring the luminescent properties of sand grains (section 5.3.6) in the sedimentary infill (Porter *et al.*, 2001; Kolstrup, 2004). These various limitations notwithstanding, the close agreement between palaeoclimatic inferences based on periglacial phenomena and those based upon other independent lines of evidence (see above) suggests that relict periglacial features can, when used judiciously, provide important insights into Quaternary climatic conditions, particularly during cold stages; however, they are perhaps best employed as a supplementary rather than as a primary data source.

3.5 PALAEOSOLS

3.5.1 Introduction

A ‘palaeosol’ is a soil that has developed on a land surface of the past, and which is preserved as a fossil soil usually (but not always) by burial beneath younger sediments (Retallack, 2001). Palaeosols frequently formed under environmental conditions that differ markedly from those currently prevailing at a site, and therefore by relating the fossil horizons to those of present-day soils, deductions can be made about environmental conditions that obtained at the time of their formation. In particular, inferences can often be made about two of the principal soil-forming factors, namely climate and vegetation. Additional palaeoenvironmental information may be derived from the fossil content of palaeosols, for acid soils frequently contain pollen and other microfossils, while molluscan remains may be found in calcareous soils. Palaeosols have also been used as a basis for the relative dating of landforms and sediments

(section 5.6.5) and, insofar as they form time-parallel marker horizons, they can be employed in the subdivision and correlation of Quaternary successions (section 6.2.3.4). In this respect, they have proved to be especially valuable as markers in loess sequences (section 3.6), where the interbedded palaeosols constitute key reference horizons for correlation at the local and regional scales (section 6.3.2.3).

3.5.2 The nature of palaeosols

Soils are formed by chemical, physical and biological processes operating in combination at the earth’s surface. Where the surface remains stable, near-surface layers will become progressively altered by soil-forming processes, in some instances resulting in well-differentiated horizons that are often diagnostic of particular bioclimatic zones (‘*zonal soils*’). Soils therefore evolve over time, and reflect the influences of prevailing environmental conditions. Where soils are buried beneath younger sediments, they may no longer be affected by soil-forming processes, and become relict features or palaeosols. **Buried palaeosols** may also be found in archaeological contexts where they may have been buried by either natural (e.g. alluvial or colluvial) processes, or as a consequence of anthropogenic activity. Frequently, palaeosols are often found beneath monuments, such as wall lines or field boundaries, sometimes in the form of a buried turf layer (Figure 3.24a).

The distinction between a soil and a palaeosol, however, is not always straightforward. Most soils are, in fact, **polygenetic** or **polycyclic**, for they can evolve over such long periods that environmental conditions may change significantly during the period of soil formation, and thus soils often contain **‘relict features’**, such as red colouration (Figure 3.24b) or cryoturbation structures (Figure 3.24c) inherited from a previous or subsequent climatic regime (Kemp *et al.*, 1993). In arid to semi-arid environments, for example, long-term changes in regional climate may lead to alternation between episodes of clay enrichment under more humid conditions and episodes of carbonate accumulation and surface salt deposition under arid conditions (Birkeland, 1999). Where relict features are particularly well developed in soils, therefore, these are referred to as **‘relict palaeosols’**.

When buried by sediment, a soil may be modified physically (e.g. by root penetration) or chemically (e.g. by solute percolation) through the action of subsequent soil-forming processes at the new ground surface. A **‘welded soil’** may develop if the younger soil profile is superimposed upon, or merges with, the older one, and is typical of a protracted period of pedogenesis (Olson & Nettleton, 1998). Welded soils are common in loess, alluvial and



Figure 3.24 Examples of palaeosols. a) A buried turf layer (dark horizon) beneath chalk upcast from a Neolithic ditch, Windmill Hill, Salisbury Plain, Southern England. b) Valley Farm Soil, Stebbing, Essex, eastern England, showing clay enrichment and 'rubification' under warm interglacial conditions (see text). c) Barham Arctic soil, Great Blakenham, Suffolk, eastern England showing cryoturbation structures and sand wedges that have been developed by ice that deposited the overlying till (photographs by Mike Walker).

colluvial sequences (Figure 3.26b). In these ‘pedocomplexes’, it often becomes difficult to distinguish the separate effects of the different phases of soil formation. A further problem arises in the case of **accretionary** or **cumulative soils**. These form where the deposition of colluvial, alluvial or aeolian sediment over a soil is so slow that soil formation can keep pace with aggradation at the surface (Hall & Anderson, 2000). The soil profile develops upwards and often generates very thick organic-rich horizons (A-horizons) as a result. It is possible, of course, that environmental conditions may change during the accretionary process, so that lower horizons contain relict features, and, where exceptional rates of accumulation are experienced, the lowest horizons may become isolated from soil-forming processes. Clearly, the distinction between active soil and palaeosol units may be difficult to make in these circumstances.

Distinguishing between relict, welded and accretionary soils is far from straightforward, and hence these types of pedocomplexes are more problematic for the student of

Quaternary environments than deeply buried soils. Equally difficult are **exhumed palaeosols**, which are those soils that were formerly deeply buried but have subsequently become exposed by erosion (e.g. Whiteman & Kemp, 1990). Exhumed palaeosols will be affected by contemporary pedogenic processes and they may therefore grade laterally into buried palaeosols and welded soils. Exhumed palaeosols have not been widely recognized, however, for in only a few areas, such as the loess landscape of the American Midwest, can they be shown to have emerged from beneath an eroding overburden and thus the exhumed nature of the palaeosol can be clearly demonstrated. In the absence of such stratigraphic evidence, it is often impossible to differentiate between relict and exhumed palaeosols, and thus the value of exhumed palaeosols in Quaternary research tends to be limited.

Buried soils may also be affected by **diagenesis**⁵ as a result of burial and other post-formational influences. These include disturbance by periglacial processes, compaction due to the weight of any overburden (especially

where glaciers advance over the sediments in which the palaeosols are developed: Figure 3.24c), or the effects of changing groundwater levels and conditions. All of these can lead to changes in the physical and chemical properties of soils, such as microfabric structures and iron oxide, carbonate and organic matter content (Kemp *et al.*, 1994). Where these changes have been particularly marked, it may be difficult to distinguish true palaeosols from '**pseudosoils**', which are distinctive, coloured horizons in sediment sequences, caused by the mobilization and subsequent accumulation of iron, manganese and other elements during diagenesis. True palaeosols can be distinguished, however, using criteria applied in the classification of modern soils, such as degree and nature of soil horizonation (see Krasilnikov & García-Calderón, 2006).

Where a palaeosol is exposed across a site or region, it may be possible to establish the extent to which the nature of the profile varies laterally as well as vertically, to form a **palaeocatena**. A soil catena (from the Latin word meaning 'chain'), or '**toposequence**', describes the gradational changes in soil profiles as a result of variations in surface gradient and the topographic position of the profile. In other words, it is a chain of related soil types (or facets) down a slope (e.g. Applegarth & Dahms, 2001). Relatively few examples of palaeocatenas have been published, but in a now classic study, Valentine and Dalrymple (1975) demonstrated their value in distinguishing true soil horizons from diagenetic or weathering phenomena, for the former should show lateral variations in development which bear a logical relationship to original topography (e.g. variations in clay content and mineral or salt concentrations) whereas the latter will not. Not surprisingly, therefore, greater attention is now being paid to the spatial variations in the nature and composition of modern soils in order to develop models of catenas that can assist in the identification and interpretation of palaeocatenas (Walkington, 2010).

3.5.3 Analysis of palaeosols

The recognition of buried palaeosols is not always easy, for a wide range of weathered materials will have been buried in Quaternary landscapes, which may or may not be soils. The most important property of a soil, and which distinguishes it from other sediments, is that it has developed distinctive, vertically differentiated layers or horizons in response to variations in physical, chemical and biological weathering, and the subsequent movement of weathering products up and down the profile (Krasilnikov & García-Calderón, 2006). The often abrupt nature of the horizon boundaries, the truncation of

underlying geological structures, and the areal or lateral continuity of soil are further characteristics that aid in the recognition of buried palaeosols.

The soil profile forms the upper part of the **weathering profile**, although some confusion has arisen, particularly in the American literature where the two terms have sometimes been used interchangeably. In certain cases, however, the weathering and soil profiles may be indistinguishable where, for example, erosion has removed the A and B horizons leaving only the weathered subsurface materials exposed in sections. In many palaeosols, the organic content of the A horizon is not retained after burial (it may be lost by decomposition or as a result of erosion), although the mineral part of the A horizon may still be present and may be recognized by a clay content that is markedly different from the underlying B horizon. Generally, however, it is the B horizon which is of greatest importance in the identification of buried palaeosols. Some important diagnostic features of the B horizon include colour, texture variations (e.g. clay-enriched or depleted horizons), weathered minerals, and enrichment (e.g. soils in semi-arid areas) or depletion (acid soils) in carbonate content. These properties can be used either singly or, more preferably, in combination, to demonstrate evidence of pedogenesis. A careful analysis of the properties of the B horizon may also establish the type of environmental conditions under which the soil evolved. Features that should be carefully recorded in the analysis of palaeosols, therefore, include colour changes (using Munsell colour charts), particle size distributions, clay mineral composition, organic matter content, evidence of soil macrostructures (e.g. peds, pans and nodules) and variations in calcium carbonate content (Kemp *et al.*, 2004).

Over the last two decades, increasing emphasis has been placed on **soil micromorphology** as both a descriptive and a diagnostic tool in palaeopedology (e.g. Stoops, 2003; Kühn *et al.*, 2006). Soil micromorphology is the term used to describe the distinctive arrangement of particles and voids making up a **soil fabric**, which can be established by an examination of soil thin sections under a microscope (Figure 3.25). It is now widely regarded as one of the most reliable methods for detecting evidence of pedogenesis, elucidating the pedosedimentary history of complex sedimentary sequences (such as loess–palaeosol sequences), and inferring changes in environmental conditions (Kemp *et al.*, 2003; Mroczek, 2013). Soil micromorphology has also been employed in archaeological research where it has been used to address a range of archaeological questions at both site and landscape scale (Davidson & Simpson, 2001; French, 2003). These include issues relating to site formation processes, agricultural practices, economic

activity and ritual practice. Soil micromorphological analysis can also reveal evidence of weathering alteration of minerals, packing or orientation of clay particles, concentration and arrangements of voids, presence and type of calcite crystal growths, animal excrements, clay coatings, rootlet pseudomorphs and a range of other features (Figure 3.25). Careful analysis of such evidence helps to decipher the history of soil formation and the changes in environmental conditions that may have occurred during pedogenesis.

A second technique that is being increasingly widely used in the investigation of palaeosols is **mineral magnetic analysis** (section 5.5.1). This involves the measurement of the magnetic properties of the mineral constituents of

soils in order to identify both the types and concentrations of minerals present (Walden *et al.*, 1999). The method offers a rapid way of analysing complex soil-stratigraphic sequences, for magnetic minerals produced or enriched through pedogenic processes generate diagnostic mineral magnetic signals. Further details can be found in section 3.6.

3.5.4 Palaeosols and Quaternary environments

The interpretation of Quaternary environments on the basis of palaeosol evidence rests, as in other fields of Quaternary investigation, on the uniformitarian principle of inferring past conditions from the observed relationships

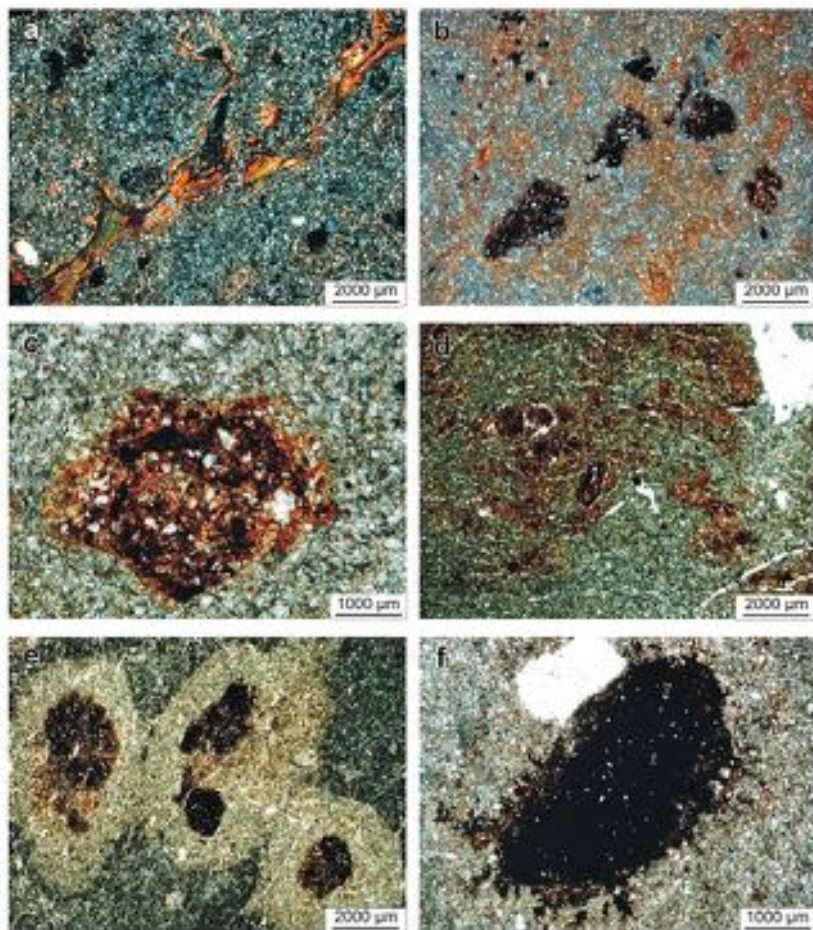


Figure 3.25 Photomicrographs of pedogenic structures in soil horizons within Weichselian loess deposits in southern Poland.
a) Clay particles infilling voids. b) Irregular Mn-Fe nodules (black) and disturbed clay infillings (orange). c) Irregular Fe nodule. d) Ferrous staining and lenticular pedogenic microstructures. e) MN-FE nodules with chemically depleted coatings. f) irregular large MN-FE nodule. (from Mrocze, 2013, reprinted with permission from Elsevier).

between present-day soils and environments. Although this approach seems to work reasonably well with most types of biological evidence (Chapter 4), it is, perhaps, less satisfactory in geomorphological and pedological contexts where the dangers of **equifinality** (different processes leading to the production of similar forms) are always present. Soils with very similar physical and chemical characteristics can develop through a variety of genetic pathways, and these may be impossible to differentiate in the fossil soil profile. Thus, although buried palaeosols may be similar in morphology and in other characteristics to soils forming at the present day, they may not necessarily be analogous in terms of palaeoenvironment and regional conditions. A further difficulty with the use of modern soils as analogues for Quaternary pedogenesis is that it is seldom possible to separate the influences of environmental variables (e.g. climatic regime) from those of other soil-forming factors (e.g. parent material). Moreover, some soils may not be in equilibrium with present-day environmental conditions. Although fossil soils have tended to be difficult to date, particularly by means of radiocarbon or uranium-series methods (section 5.3), new approaches using optical dating (Mauz & Felix-Henningsen, 2005; Ahr *et al.*, 2013), cosmogenic isotopes (Graham *et al.*, 2001) and mineral magnetism (Schellenberger *et al.*, 2003) have proved successful means of dating of palaeosols. In particular, a combination of dating methods, for example radiocarbon and luminescence (Clarke *et al.*, 2003) and mineral magnetism and luminescence (Dearing *et al.*, 2001), are now providing increasingly robust chronologies for many pedosedimentary sequences.

A number of inferences have been made about former environmental conditions on the basis of palaeosol evidence. For example, in southeast England, the widely developed Early and Middle Pleistocene palaeosol known as the *Valley Farm Soil* is clay enriched and distinctly reddish in colour ('**rubified**'), characteristics (Figure 3.24b) that are normally associated with a temperate or even Mediterranean environment. Hence it has been inferred that the soil formed under climatic conditions that were at least as warm as, or possibly warmer than, those prevailing in the region at the present time (Kemp, 1987). This contrasts with the *Barham Soil*, a Middle Pleistocene palaeosol which is frequently superimposed on the Valley Farm Soil unit, but which displays both macromorphological characteristics (incorporated aeolian sediments and ground-ice structures) and micromorphological features characteristic of severe arctic conditions (Rose *et al.*, 1985; Figure 3.24c). A key element in the palaeoenvironmental reconstruction based on these and other palaeosols is the soil microstratigraphy which shows, for

example, relatively stable phases with translocation of clay and calcium carbonate, a process that is characteristic of temperate soil climate, and intervening unstable phases with the physical disruption and mixing of soil material, typically as a consequence of cold-climate processes (Rose *et al.*, 2000).

In Europe, the textural B horizon of the last (Eemian) interglacial soil constitutes an important stratigraphic marker (Haesaerts & Mestdagh, 2000), and these interglacial palaeosols are especially well preserved in the loess sequences of central and eastern Europe. Comparisons between Eemian palaeosols and Holocene soils in Austria and the central Russian Plain showed that the former are better developed in terms of a range of soil-forming processes (weathering of primary minerals, clay transformation, etc.), reflecting not only a longer period of soil formation, but also a warmer and possibly moister climate during the Eemian (Sedov *et al.*, 2013). This accords with other proxy records for higher temperatures in many parts of Europe during the last interglacial (e.g. Coope, 2000). In central Asia, by contrast, data from a loess–palaeosol sequence in Tajikistan showed that the interglacial periods represented by the B horizons of the buried palaeosols of late, middle and early Pleistocene age were climatically similar to the Holocene (Bronger *et al.*, 1998). Warm intervals of different duration and intensity have also been inferred on the basis of palaeosols. In southern Spain, for example, strongly and weakly developed palaeosols have been correlated with interglacials and interstadials respectively (Günster *et al.*, 2001), while in the Basin of Persepolis in southern Iran, well-developed palaeosols have been correlated with major soil-forming episodes during MIS 5, while immature, weakly developed palaeosol horizons correspond with interstadials of MIS 3 (Kehl *et al.*, 2005). Younger palaeosols of Lateglacial age (typically late Allerød and Younger Dryas) are commonly found in aeolian sequences in western and north-central Europe. The Usselo soil, for example, has been found at sites in the Netherlands (see Figure 3.29), Germany and Poland, and widely dated to around 10,950 ^{14}C yr BP (Hoek, 1997). In Germany, the Finow Soil also began to form during the late Allerød (Kaiser *et al.*, 2009). These palaeosols have provided important palaeoecological data (e.g. both are rich in charcoal and reflect widespread burning), and they are also importantpedostratigraphical marker horizons across large areas of Europe.

Finally, palaeosols are often encountered in archaeological contexts, frequently marking former occupation horizons, for example in cave sequences (Mallol *et al.*, 2010). Careful analysis of pedogenetic features can establish whether a horizon was occupied several times, how much

disturbance has affected the archaeological layers, and what types of activity were conducted, for example micro-charcoal pieces preserved within soil horizons indicating the use of fire (Holliday, 2004). It can also reveal environmental factors that may have affected the archaeological record, such as changes in the position of the local water table or disturbance by animals (Tsatskin & Ronen, 1999).

Palaeosols, therefore, are of considerable value in Quaternary research. They constitute important stratigraphic markers, they provide a basis for correlation, they can be used as a means of relative dating and, above all, they can provide palaeoenvironmental information that is additional to, and often independent of, that derived from other sources such as fossil assemblages. Indeed, in some regions, they may provide the only source of palaeoenvironmental information for periods during which little or no sediment has accumulated. In some regions, buried soil sequences represent a substantial proportion of the Quaternary period (Hall & Anderson, 2000). While it is true that there is still much to be learned about modern soils that is crucial to the interpretation of palaeosols, it is equally the case that much can be learned by pedologists from the Quaternary archive of palaeosols, about the ways in which modern soils have evolved, and about the rates and effects of weathering and related pedogenic processes.

3.6 WIND-BLOWN SEDIMENTS

3.6.1 Introduction

Large areas of wind-blown sediment ([sand seas](#)) are currently forming in arid and hyper-arid regions of the world, while blankets of sandy material (grain size 64 µm to 2 mm) or [coversand](#) were deposited in many mid-latitude temperate regions during the last cold stage. Elsewhere, silt particles (2–64 µm) form the bulk of wind-blown sediment, material which is referred to as [loess](#). Spreads of loess are found throughout the world, and these often accumulate to great thicknesses. Analysis of these loess sequences has shown that not only are they frequently of considerable antiquity (some extend back into the Pliocene), but they also contain evidence of cyclical climatic change, with phases of aeolian sedimentation (reflecting cold stages) interspersed with episodes of soil formation during warm stages (section 3.5). Wind-blown sediments, both loess and coversands, are also valuable indicators of former wind directions. In addition, dust of terrestrial origin can be identified in marine and ice cores, and these archives enable both the former transport paths and the relative flux of air-transported dust to be reconstructed at a global scale.

3.6.2 Loess stratigraphy

Loess deposits cover about 10 per cent of the earth's land surface, blanketing hilltops, plateau surfaces and valley floors alike. Extensive spreads of loessic sediments occur on the 'Loess Plateau' of North China (see below), in central Asia and southern Siberia (Chlachula, 2003), in central Europe, where loess extends as a discontinuous belt from northern France to the Ukraine (Haase *et al.*, 2007), in the mid-continent United States (Bettis *et al.*, 2003), and in the Chaco-Pampean plains and adjacent mountain regions of southern South America (Zárate, 2003). The loess of North China frequently exceeds 100 m in thickness, and near the city of Lanzhou reaches 300 m (Derbyshire *et al.*, 1995). In central Asia, loess accumulations of about 90 m are common, but locally can exceed 200 m, whereas in Europe and North America, thicknesses of about 30 m are more usual. More restricted spreads of loess occur in many other parts of the world, including the Mediterranean region, the Middle East, India and Pakistan, the western USA, New Zealand and Alaska (Derbyshire, 2003).

Loess has a high carbonate content, sometimes exceeding 40 per cent by weight, and it frequently possesses a distinctive range of sedimentary properties, including heavy mineral and clay mineral suites, sediment magnetic variations and micromorphological features, all of which can be used to characterize and correlate loess sequences. The fine-grained and friable nature of loess deposits gives rise to unstable landscapes into which rivers are rapidly incised, and this creates numerous exposures for detailed study (Figure 3.26a). In section, the sediments usually display little visual evidence of stratification, although careful examination often reveals faint bedding. Microscopic and SEM examination of the particle fabric (micromorphology) can distinguish differences in texture that are important for palaeoenvironmental reconstruction (Kemp *et al.*, 2001; Josephs, 2010). These analyses have shown that there are two types of loess, one that is typical of areas such as China that have experienced arid conditions during glacial periods and humid conditions in interglacials, and a second type that has accumulated in areas with persistently high humidities, such as western Europe. The most distinctive features in loess sequences, however, are palaeosols, and these often show up in section as darker units in exposed profiles (Figure 3.26b). Differences in pedogenic history of these buried soil units revealed, for example, by grain size variations, micromorphological characteristics and the magnetic susceptibility record, provide a basis for correlation between individual loess–palaeosol sequences (Xiong *et al.*, 2001).



Figure 3.26 a) The early Quaternary 'Wucheng' sequence of loess units and soil horizons (darker bands) exposed at the Luochuan site on the Loess Plateau, China; prominent in the photograph are loess unit 15 (L15) and the Wucheng group of soil horizons (WS-1, comprising S15–S23) dating to between 1.2 and 1.6 Ma. b) The S1 (last interglacial) soil profile (dark red layer) exposed at the Lantian section, near Xi'an in the southern part of the Loess Plateau, where three separate soil horizons exposed in other areas converge to form a welded soil (section 3.5.2) due to unusually low rates of dust accumulation (photographs by Thomas Stevens, Royal Holloway, University of London, UK).

The largest area of loess deposits in the world is found on the Chinese Loess Plateau. This covers an area of around 440,000 km² between 33–40°N and 98–115°E (Figure 3.27). The sedimentary record contains a sequence of interbedded loess and palaeosol units which developed during successive cold (glacial) and warm (interglacial) episodes, with the earliest, the 'red clays', dated to c. 7 Ma (Ding *et al.*, 1999). The loess appears to have three principal sources: silt-sized material derived from adjacent deserts particularly to the north and west of the Loess Plateau, glacially derived material from the surrounding mountains, and recycled older loess that has been fluvially transported and deposited in river valleys within the Loess Plateau region (Kohfeld & Harrison, 2003). The loess–palaeosol sequence contains up to 37 soil units that have formed during the last 2.5 Ma (Figure 3.28). Some of these are very distinctive and widespread, such as the S₁ (last interglacial) and S₅ (MIS 13, 14, 15) palaeosols. However, a number have proved to be complex polygenetic units, consisting of several soil horizons separated by thin 'second order loess beds' with fainter 'second order pedogenic features' in some of the more distinctive soil units (Kemp *et al.*, 1995). These variations appear to reflect climatic change, the well-developed palaeosols probably indicating relatively long periods of pedogenesis during interglacial stages, while the less prominent soil units reflect much shorter episodes of soil formation during interstadial periods (section 3.5.4).

Numerous palaeosols, comparable in age with those of China, have also been discovered in central Asia. In

Tajikistan, for example, the loess–palaeosol record extends back to c. 1.77 Ma, and the climate cycles correspond closely with both the Chinese loess and deep-sea oxygen isotope records (Ding *et al.*, 2002a). In the middle and lower Danube basin of southeastern Europe, loess deposits extend to the base of the Pleistocene. The period from around 1 Ma onwards (MIS 27) was characterized by alternating loess deposition and pedogenesis during glacial and interglacial periods, respectively. Loess accumulation rates increased after ~700 ka reflecting a shift to a more steppic, and therefore relatively more arid, environment compared with the lower parts of the profiles (Fitzsimmons *et al.*, 2012). In South America, the beginning of loessic sedimentation dates back to the Late Miocene (c.10 Ma), although the Plio-Pleistocene record is mostly composed of loessic sediments modified by pedogenesis, which produced welded palaeosols (Zárate, 2003). The longest continuous loess–palaeosol sequence (La Carreras, northwest Argentina) contains thirty-one intercalated palaeosols and has a minimum age of 1.15 Ma for the onset of loess accumulation (Schellenberger *et al.*, 2003). In western Europe and North America, by contrast, the loess sequences are generally younger, and the deposits are usually thinner and span a much more limited age range. In southeast England, which lies at the western extremity of the central European belt of wind-blown sediments, loess-like deposits, locally termed 'brickearths', date largely from the last cold stage (MIS 2), but there are also localized patches of older (mainly MIS 6 and 12) loess, which are the dissected

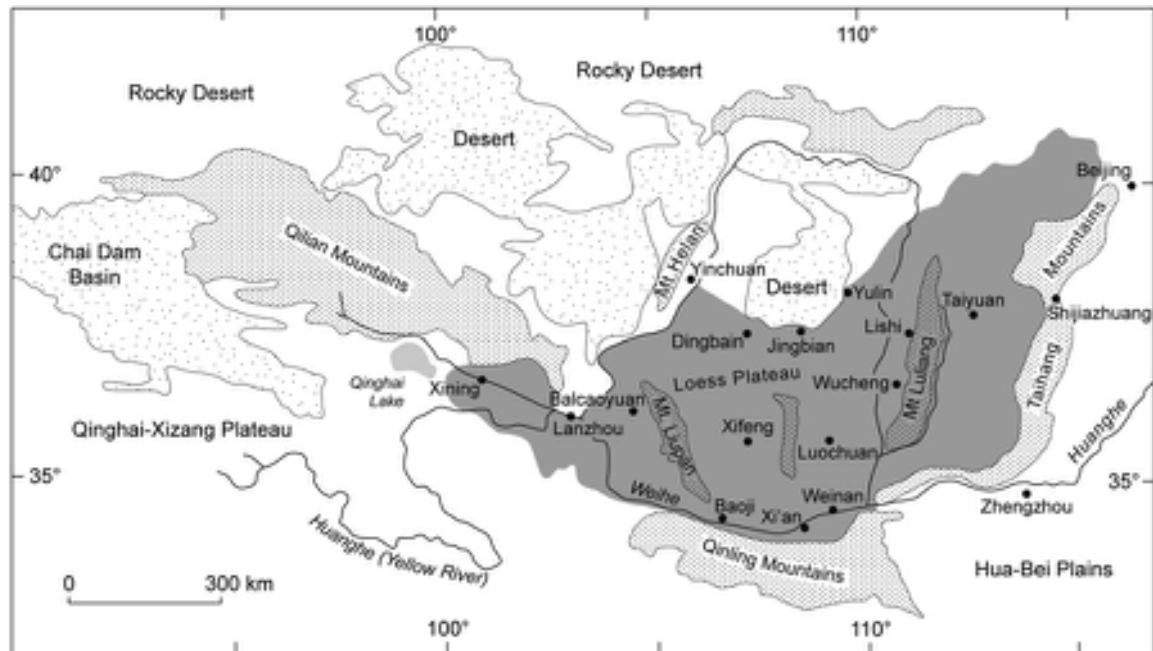


Figure 3.27 The Loess Plateau, major deserts and mountain regions of north-central China (from Ding *et al.*, 1994).

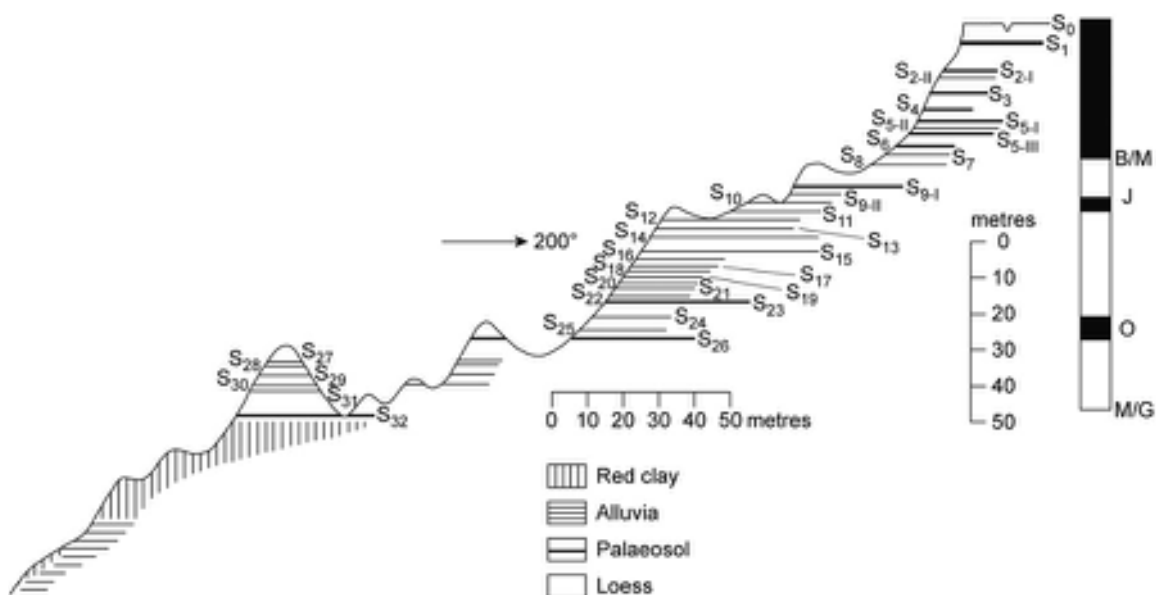


Figure 3.28 Loess-palaeosol succession at Baoji, in the southern Loess Plateau, north-central China (for location see Figure 3.27) showing thirty-two palaeosol units spanning the last 2 Ma. The palaeomagnetic timescale (see Figure 5.34) is shown on the right. B/M – Brunhes–Matuyama boundary c. 0.78 Ma; J – Jaramillo event, 1.07–0.99 Ma; O – Olduvai event; 1.956–1.79 Ma; M/G – Matuyama–Gauss boundary, c. 2.6 Ma (from Ding *et al.*, 1994).

remnants of originally more extensive deposits (Antoine *et al.*, 2003). In North America, complex successions of loess, sand units and at least four cycles of pedogenesis, dating approximately from the last 500–400 ka, have been reported from the central Great Plains (Feng *et al.*, 1994), but most loess sequences in the USA only span the period from the last interglacial (Bettis *et al.*, 2003), the most widespread being the Peoria Loess, dated to c. 25–14 ka, with the highest dust accumulation rates between 18 and 14 ka (Roberts *et al.*, 2003). In places, the loess is up to 48 m in thickness, making it probably the thickest Last Glacial Maximum loess accumulation in the world (Maat & Johnson, 1996).

3.6.3 Mid-latitude sand belts (coversands)

Coversands dating from the last cold stage are found in many parts of Europe and North America, their presence reflecting both availability of material and increased wind strength at that time. Much of the sediment was derived from the greatly expanded periglacial regions, where a combination of sparse vegetation and seasonally dry ground meant that large areas of unconsolidated and friable sediment were left exposed to wind action. Particularly vulnerable were the unvegetated surfaces of glaciogenic and outwash sediments, which were rapidly stripped of their finer components (Wright, 2001). Considerable quantities of sand were also removed from the continental shelves, which had been exposed by a eustatic fall in sea level of over 100 m, while unvegetated floodplains of large rivers provided a further source of material. A more vigorous atmospheric circulation around the ice sheets, coupled with strong katabatic winds blowing off the glaciers and ice sheets, resulted in the stripping of these surfaces and the deposition of the coversand and loess belts of the northern mid-latitude regions. In addition, aeolian sediments themselves are liable to severe erosion, and constitute a secondary source of mineralogic dust (Derbyshire *et al.*, 2000).

The coversands form a featureless surface, occasionally fashioned into undulating dunes, over large parts of the northern Great Plains of the USA and Canada (Forman *et al.*, 2008). In lowland Europe, they stretch from northern France, the Netherlands and Belgium, eastwards through Denmark, northern Germany and Poland into Russia. This mantle of yellow to grey sand is often several metres in thickness, and individual sand units are relatively homogeneous, with little or no stratification. The sediments are frequently deformed by folding and tension cracks, reflecting **niveo-aeolian deposition**, where both sand and snow



Figure 3.29 Coversands and interbedded Usselo soil of Lateglacial (late Allerød) age (section 3.5.4) exposed at a site in the Netherlands, with periglacial geomorphologist Kees Kasse of the Free University, Amsterdam (photograph by Mike Walker).

are driven by the wind to form interdigitating layers (Ballantyne & Harris, 1994). Subsequent melting of the snow destroys any bedding and leads to deformation and cracking of the sediment layers, collectively termed **denivation features**.

The European coversands typically comprise a number of distinctive sand units, which are interbedded with finer sand and loamy layers (Figure 3.29). In northwest Europe, these typically comprise an Older Coversand (mostly fluvially reworked aeolian sands) and dated to 25–22 ka, an Older Coversand II/Younger Coversand I (sandy to silty sand sheets) dated to 17–13 ka, and finally a Younger Coversand II (cross-bedded dune sands), with an age of 13–11.5 ka (Frechen *et al.*, 2001; Kasse *et al.*, 2007). This complex sequence suggests that, towards the end of the last cold stage, northwest Europe experienced abrupt but short-lived changes in climate from polar desert to relatively humid and more temperate conditions.

3.6.4 Low-latitude 'sand seas'

In addition to the extensive spreads of wind-blown sediment that form the present-day 'sand seas' of arid and hyper-arid low-latitude areas of the world, aeolian sands have been found beneath the present-day soils and vegetation of many savannah and forest regions, which indicates that these areas have experienced more arid conditions in the recent past. In South America, for example, some 25 per cent of the continent is covered with palaeo-aeolian features which reveal a complex history related to atmospheric circulation regime change during the Late Quaternary (Tripaldi & Forman, 2007). Similarly in northwest China, there are enormous spreads of aeolian material, much of which has been fashioned into dunes (section 2.7.2), and which provides evidence of the former development of extensive sand seas during the last cold stage (Wang *et al.*, 2004). The same is true of the great Sinai-Negev erg (sand sea) of Egypt and Israel which comprises aeolian material transported from the Nile delta region during the last cold stage (Muhs *et al.*, 2013). In Australia, the marine record for dust flux during the LGM is at least three times greater than that for the Holocene, driven by both weakened monsoon rains and drier westerly circulation (Hesse & McTainsh, 2003). Many present-day arid or hyper-arid regions contain evidence of earlier, wetter phases. Interbedded within, or buried beneath, the surficial sand seas and dunes can often be found palaeodrainage systems (Figure 2.59) that testify to the former existence of wetter conditions (e.g. Robinson *et al.*, 2000; Craddock *et al.*, 2010). In the Sahara, for example, satellite imagery reveals the presence of a dense palaeo-river network and this, combined with archaeological and fossil evidence, indicates a markedly more humid phase during the early Holocene (Drake *et al.*, 2010).

3.6.5 Wind-blown sediments and palaeoenvironmental reconstructions

Former wind directions can be reconstructed on the basis of grain-size or mineralogical variations of wind-blown sediments. For example, grain-size analysis of the Peoria Loess on the Great Plains of the USA shows that the deposit becomes progressively finer eastwards towards the Mississippi River (Mason, 2001). Maximum loess thickness also declines towards the east. The evidence suggests predominantly northwesterly loess-transporting winds across the Great Plains region during the last glacial period (Muhs & Bettis, 2000). In central and eastern Europe, spatial variations in loess grain-size distributions suggest a prevailing westerly wind during the Early and Middle

Pleniglacial periods (MIS 4 and 3), and a dominant northwesterly wind during the Late Pleniglacial (MIS 2: Bokhorst *et al.*, 2011). Proxy records from northwest Europe also indicate a predominantly westerly to northwesterly wind in winter during the Late Pleniglacial. Inferred easterly winds in more northern areas appear to reflect katabatic winds from the Scandinavian ice sheet. Modelling results suggest that the prevailing winds were stronger than the predominantly southwesterly winds over western Europe at the present day, caused by an eastward shift of the Icelandic Low pressure system, and an enhanced pressure gradient over northwest and central Europe during the last cold stage (Renssen *et al.*, 2007a).

In eastern Asia, a range of palaeoclimatic data has been obtained from the analysis of wind-blown sediments and related deposits. On the Chinese Loess Plateau, glacial-interglacial cycles are reflected in particle-size, geochemical and soil-micromorphological evidence from loess-palaeosol sequences, arid (glacial) phases being characterized by increased dust deposition and semi-arid episodes (interglacial/interstadials) by episodes of soil formation (Kemp & Derbyshire, 1998). The loess-palaeosol sequence has also provided a proxy record for the Asian monsoon which may have been initiated as long ago as the late Miocene (Porter, 2001). Different properties of the sediments have been used to reconstruct changes in monsoon intensity and circulation. For example, grain-size variations reflected in mineral magnetic signals demonstrate changes in both the strength and position of the Asian monsoon cell during the Late Quaternary. Horizons characterized by ultra-fine grains (high magnetic susceptibility) are typical of episodes of reduced aeolian deposition and pedogenesis, while periods of increased influx of wind-blown dust are indicated by lower magnetic susceptibility measurements. The latter represent periods when the winter monsoon (associated with dust transport from Siberia) was dominant, while evidence of pedogenic development reflects a reduction in the strength of northerly winds and an increase in intensity of the summer monsoon from the south (Liu & Ding, 1998). Hence the magnetic susceptibility record through a loess-palaeosol sequence can be used as a proxy index of the intensity of the summer monsoon (Figure 3.30). Changes in the strength of the Asian monsoon on the Chinese Loess Plateau have also been deduced from variations in the concentration of a range of chemical and isotopic indicators. For example, in the Huanxian profile in northern China, variations in $^{87}\text{Sr}/^{86}\text{Sr}$ and Zr/Rb ratios, and mean grain size, were interpreted as reflecting a weakening in the East Asian monsoon between 40 and 30 ka, but an increase in monsoon strength from 30–10 ka (Yang *et al.*, 2005). Finally, magnetic parameters have been

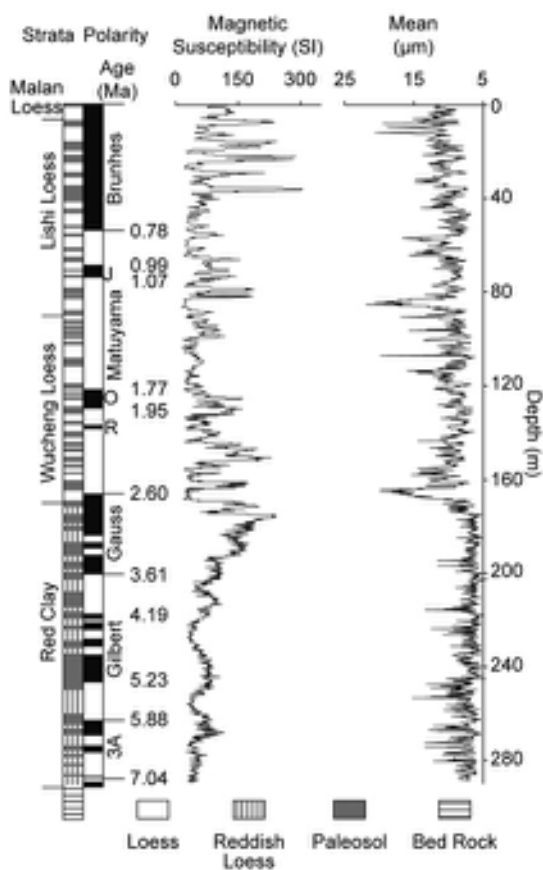


Figure 3.30 Magnetostratigraphy, lithology, magnetic susceptibility and grain-size variations of the Lingtai section ($35^{\circ}04'N$, $107^{\circ}39'E$) on the Chinese Loess Plateau (after An, 2000).

used, in association with other pedostratigraphic characteristics to obtain quantitative estimates of dust deposition on the Loess Plateau (Kohfeld & Harrison, 2003). From these, palaeoprecipitation estimates have been obtained which again enable the varying strength of the East Asian monsoon to be inferred (Liu & Ding, 1998). Variations in grain-size parameters also enable individual loess–palaeosol sequences to be correlated and resolved into a single ‘stacked’ climatic record which, in turn, can be correlated with the oxygen isotope record of the deep-ocean sequence (Ding *et al.*, 2002b).

Dust transport fluxes to the polar ice sheets can also be reconstructed using geochemical and isotopic tracers. For example, isotopic tracers in dust records from six different ice cores drilled on the east Antarctic Plateau suggest a

source in Patagonia and the Altiplano of Bolivia (Delmonte *et al.*, 2010). The Antarctic dust record extends back over 800 ka and shows a significant correlation with temperature, with a ~25-fold increase in dust concentration during glacial periods (Lambert *et al.*, 2008). Dust concentrations have also been measured in several ice cores from Greenland where again there is a strong relation with climate, the ice from the last glacial period containing dust concentrations 10–100 times higher than the Holocene; moreover, abrupt changes in climate tend to coincide with sudden changes in dust concentration (Steffensen *et al.*, 2008). Continental dust has been found in deep-marine cores using geochemical and magnetic methods and has been used, for example, to correlate marine and ice-core records (Pugh *et al.*, 2009). Increased aeolian flux to the oceans may also have climatic consequences, for increased concentrations of Fe-rich dust may be responsible for phytoplankton blooms in ocean waters, and these may draw down atmospheric CO₂. This scenario has been suggested for the Southern Oceans (Watson *et al.*, 2000), while enhanced dust flux from continental North America could have had significant effects on the productivity of the North Atlantic Ocean during the Last Glacial period (Bettis *et al.*, 2003).

Quaternary wind-blown sediments are therefore valuable data sources for palaeoenvironmental reconstruction. At the local and regional scales, they provide evidence of sediment source and transport, and hence of palaeo-wind directions. At the global scale, these data can be used to reconstruct former atmospheric pressure systems, and also to infer those times when atmospheric dust transport was greater than that of the present time. The loess–palaeosol sequences are important archives of palaeoenvironmental data, and constitute some of the longest and most detailed records of Quaternary climatic change. They also provide one of the principal sources of evidence for the correlation of terrestrial and marine sequences, a topic that is discussed in greater detail in section 6.3.3.

3.7 LAKE-LEVEL RECORDS FROM LOW-LATITUDE REGIONS

3.7.1 Introduction

The geomorphological evidence for environmental changes in low-latitude regions during the Quaternary was reviewed in section 2.7. However, much longer and more detailed lake-level histories can be reconstructed using sedimentological data. The records can be broadly divided into those from humid, low-latitude regions, and

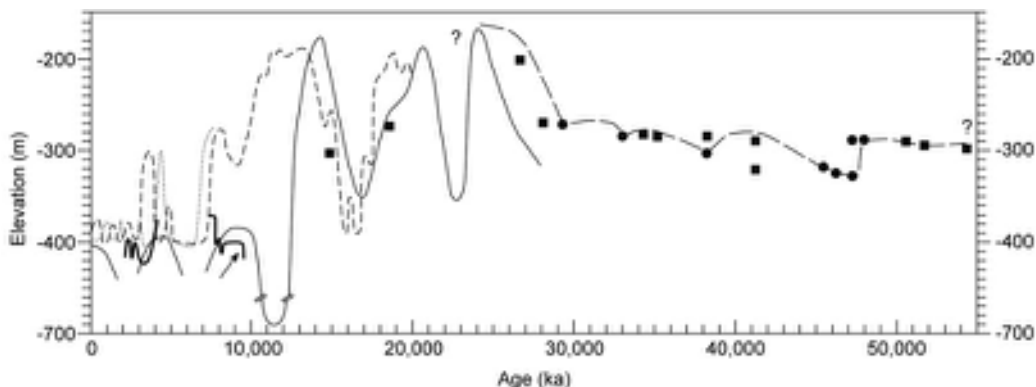


Figure 3.31 The water-level record for Lake Lisan over the course of the last 55 ka. The lake-level fluctuations reflect the hydrological conditions in the large watershed of the lake which, in turn, is influenced by the hydro-climatic conditions in the central Levant region. The highest lake levels occurred during MIS 2, while lower lake levels are recorded during MIS 3 and especially during the Holocene (MIS 1). The highest stand was reached at c. 26 ka during the coldest stage of the Last Glacial cycle. Note that lake-level heights are shown in metres below mean sea level (mbsl) (after Torfstein *et al.*, 2013).

those more typical of arid and semi-arid areas. In some low-latitude lakes, long sediment records are preserved, some of which span the whole of the Quaternary and extend back into the Pliocene (Torres *et al.*, 2013). Most attention has focused, however, on the ‘pluvial lake’ sequences (section 2.7.1) of the arid and semi-arid regions, for not only do these records provide some of the most dramatic evidence of Late Quaternary environmental change, but the data from these lakes are used in the construction of palaeoclimatic models at both the continental and global scales (Qin *et al.*, 1998; Kohfeld & Harrison, 2000).

3.7.2 Pluvial lake sediment sequences

Cores from saline lakes or from salt-encrusted pans of former playa lakes often reveal complex sequences of lake sediments (silts, marls, clays and organic muds), interbedded with units of alluvium, colluvium, aeolian sediments and occasional soil horizons. Unconformities are also common. In some places, for example in parts of Egypt and northern Kenya, the upper parts of the sequences are exposed and the intercalated lacustrine and terrestrial sediments can be examined in section (Brookes, 1993). Elsewhere in east Africa and further north in the Jordan Valley of Israel, sections through older lake sediments provide ‘snapshots’ of episodes of lake history (Hay & Kyser, 2001; Stein, 2001). The sedimentary sequences often reveal episodes of lake expansion (reflecting higher rainfall regimes) interrupted by periods of contraction during drier conditions (Figure 2.55), and some records extend back throughout the Quaternary. In the Searles Lake basin,

California, for example, the earliest sediments may be as old as Late Pliocene, with the most detailed part of the record (the last 150 ka) revealing a series of climatically related lake-level fluctuations that appear to be driven by orbital forcing (Smith, 2009). Further north in the Bonneville Basin of Utah, a long sequence of deep-lake cycles is also recorded, the oldest of which appears to correlate with MIS 16 (c. 650 ka) of the deep-ocean record (Oviatt *et al.*, 1999). In many cases, however, the borehole records and the majority of surface exposures span much shorter time intervals and hence a continuous sequence of lake-level change can usually only be constructed for the Holocene and last cold stage. In the Jordan Valley of Israel, for instance, the sedimentary record for ancient Lake Kinneret, the Last Glacial Dead Sea (Figure 3.31), extends back to around 70 ka (Torfstein *et al.*, 2013).

The sedimentary sequence in closed basin ([endoreic](#)) lakes is closely related to changes in water balance which, in turn, reflect changes in regional climatic regime. If the links between lithological variations and water balance can be quantified, it is possible to reconstruct the former climatic conditions under which the lake sediments accumulated. The hydrological budget of a lake is controlled by the balance between the inflows and outflows from the system as follows:

$$\frac{dV}{dt} = P + S_i + G_i - E - S_o - G_o$$

where dV is change in lake volume; dt , the time interval; P , precipitation on to the lake surface; S_i , surface inflow

from rivers and/or overland runoff; G_i , ground water inflow; E , evaporation from the lake surface; S_o , surface outflow; G_o , ground water outflow (Jones *et al.*, 2007b). Changes in lake area or volume could, therefore, reflect the influence of any of these variables. However, not all causes of lake-level changes are necessarily related to climate. For example, overspill from adjacent lakes, influx of glacial meltwaters during cold stages, changes in basin configuration due to tectonic activity, or the creation of dams by avalanche debris, talus cones or lava flows can all affect lake volume and lead to fluctuations in the lake-water level. Where sedimentary (and indeed geomorphological) evidence can be obtained from a number of lake basins within a particular region, and where these show a consistent trend in water balance changes for a given time period, a regional climatic signal may reasonably be inferred, and hence the lake sediment record can be used as a proxy for climate change.

As lakes change in volume, the sedimentary and geochemical environment also changes. In salt lakes, for example, salinity declines as water volumes increase, and hence clastic sediments of relatively low salinity tend to accumulate when lakes are expanded. By contrast, when lakes decrease in size, salinity levels rise, until primary carbonates are deposited first, followed by gypsum and then by halite. Algal limestone growths (**stromatolites**) may also develop at this stage. With seasonal drying of the

lake, secondary gypsum deposition occurs on the exposed sediment surface and clay pellets also form. Prolonged desiccation will result eventually in soil formation. A re-expansion of the lake will reverse these trends, the precise nature of the sedimentary sequence depending upon the rate and magnitude of the water-level changes. Other indicators of the fluctuating hydrologic balance of lakes include changes in magnetic properties, with reduced magnetic values being noted during episodes of high productivity during shallow water periods (Zic *et al.*, 2002), and in total inorganic carbon and $\delta^{18}\text{O}$, both of which decrease with increasing lake size (Benson *et al.*, 2003). The links between the hydrological balance and chemistry (e.g. stable isotope ratios) of a lake body can be quantified, using modified versions of the water balance equation presented above, and these are now widely used as palaeoclimatic proxies (Jones *et al.*, 2007b). The sedimentary and geochemical responses to lake-level fluctuations will vary considerably between individual lake basins, however, and each sedimentary sequence must therefore be interpreted in the context of local sediment chemistry, detrital input and hydrogeology. Detailed analysis of the geochemical variations in particular can enable water-level variations to be reconstructed which, in turn, may provide insights into former regional climatic controls, such as changes in the strength of monsoon circulation (Figure 3.32).

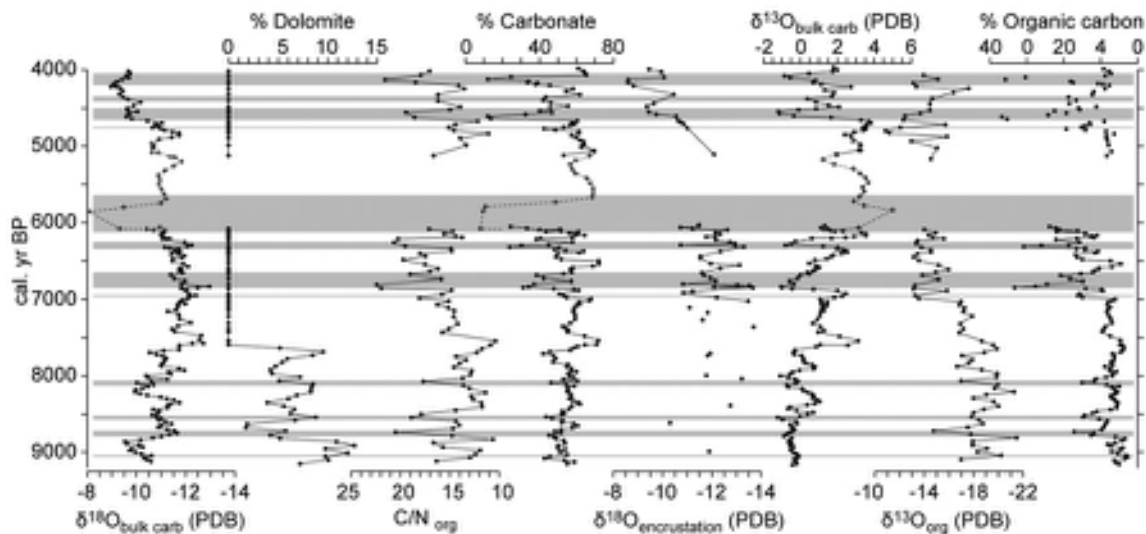


Figure 3.32 The geochemical record from a lake sequence in Tibet that developed between 9 and 4 ka. Lake geochemistry appears to have been particularly sensitive to water-level fluctuations driven by precipitation changes associated with variability in monsoon strength. The grey-shaded horizontal bars, for example, represent intervals of reduced carbonate content and the spread of the aquatic plant *Potamogeton*, reflecting lower water levels and a weakened monsoon (from Morrill *et al.*, 2006).

Quantifying the linkages between water balance and climate on the one hand, and between water chemistry and water budgets on the other, rests heavily on reference to modern analogues. Where present-day equilibrium conditions can be established for a lake basin, modelling techniques can be used to simulate the conditions that give rise to changes in either water budget or water chemistry. For Lake Malawi, for example, Kumambala & Ervine (2010) developed a water balance model based on a combination of lake outflow records and precipitation/evaporation estimates from climate stations along the lake shore, and combined this with climate change modelling using the IPCC emissions scenarios to assess the likely future behaviour of the lake. Further north in Ethiopia, Kebede *et al.* (2006) generated a hydrological model for Lake Tana based on similar series of parameters, which showed that in this case, the lake was less sensitive to recent rainfall variations than other large lakes in Tropical Africa. Using a different approach, Benson & Paillet (2002) developed a hydrologic-isotopic balance model for palaeolakes for application to palaeolake $\delta^{18}\text{O}$ records based on a combination of recent and historical datasets. Applications indicate that when lake volume increases, $\delta^{18}\text{O}$ decreases and vice versa. Hence the $\delta^{18}\text{O}$ record can be used to infer the direction of climate change, that is, whether climate is becoming drier or wetter (Benson *et al.*, 2002).

Other approaches to the study of the relationships between lake-level variations and climatic change include the use of biological indicators of lake salinity, particularly diatom and ostracod assemblages (sections 4.3 and 4.8), or the chemical analysis of sediments or fossils. The latter approaches include the analysis of the carbon, nitrogen and hydrogen isotopes of lake organic matter (Abbott *et al.*, 2000), the carbonate mineralogy of the sediments (Nelson *et al.*, 2005), and the oxygen isotope content of calcite, sediments, molluscs and ostracods (Benson *et al.*, 2003). Complementary information can be obtained from the study of fluvial sediments in low latitudes, since evidence of enhanced fluvial activity may reflect periods of higher precipitation, and might provide independent support for lake sediment evidence of 'pluvial' episodes (e.g. Blanchet *et al.*, 2013).

Prior to the 1980s, most chronologies of lake-level changes were based on radiocarbon dating of carbonate materials, such as algal limestones, calcite-cemented sands and mollusc remains. These are not ideal media for radiocarbon dating, however, for they are easily contaminated by older carbon residues (Licciardi, 2001). The problem is exacerbated by the mobility of CaCO_3 in arid and semi-arid environments, and by the fact that organic carbon that has been washed into lake sediments will often have spent a

considerable 'residence time' in soils around the catchment (section 5.3.2.5). Again, this will contribute to an 'ageing' effect in radiocarbon dates obtained from lake sediments. In addition, the effective age range of radiocarbon dating extends back only to c. 45 ka (section 5.3.2) and hence the technique is not applicable to the dating of long lake sediment sequences. Other techniques have therefore been employed to establish chronologies of lake-level change, including U-series dating of carbonates (Ma *et al.*, 2004) and stromatolites (Lisker *et al.*, 2009); amino-acid dating of molluscs and other organic materials (Kaufman, 2003a); magnetic stratigraphy and tephrochronology (Benson *et al.*, 2003); luminescence dating of lake sediments and interbedded aeolian or fluvial deposits (English *et al.*, 2001); and varve chronology (Prasad *et al.*, 2009). All of these methods are described in Chapter 5.

3.7.3 Lake-level changes and Quaternary palaeoclimates

Because of the potential value of lake-level changes in reconstructing Quaternary climates, a Global Lake Status Data Base of palaeo-lake records has been compiled (<http://www.ncdc.noaa.gov/paleo/lakelevel.html>), which classifies the records for particular time intervals on the basis of lake-level status (low, intermediate and high). When last updated (2011), the database contained modern lake-status data for 599 lakes, and estimates of the status of 413 lakes at 6 ka and of 103 lakes at 18 ka (Figure 3.33). The number of lakes in the record therefore decreases with age, and comparatively few lakes date from pre-Holocene times. There are also significant regional gaps, with very few records from South America, central and southwest Africa, or for large parts of Eurasia and the Far East. The classification into 'low', 'intermediate' and 'high' status is also rather generalized, while some of the lake sequences may not have been dated accurately. Despite these limitations, however, the database constitutes an important archive of palaeoclimatic information, and the palaeo-lake reconstructions also provide valuable benchmarks for evaluating numerical climate-model outputs (e.g. Qin *et al.*, 1998).

Street & Grove (1979) found that tropical lake records from Tropical Africa revealed evidence of widespread aridity at around the Last Glacial Maximum (LGM), but generally achieved their highest levels during the early Holocene, after which conditions became increasingly arid up to the present. They attributed this pattern to increased sea-surface evaporation following the global rise in eustatic sea level that resulted from the melting of the last ice sheets. In the southwest USA, the lake records showed a very

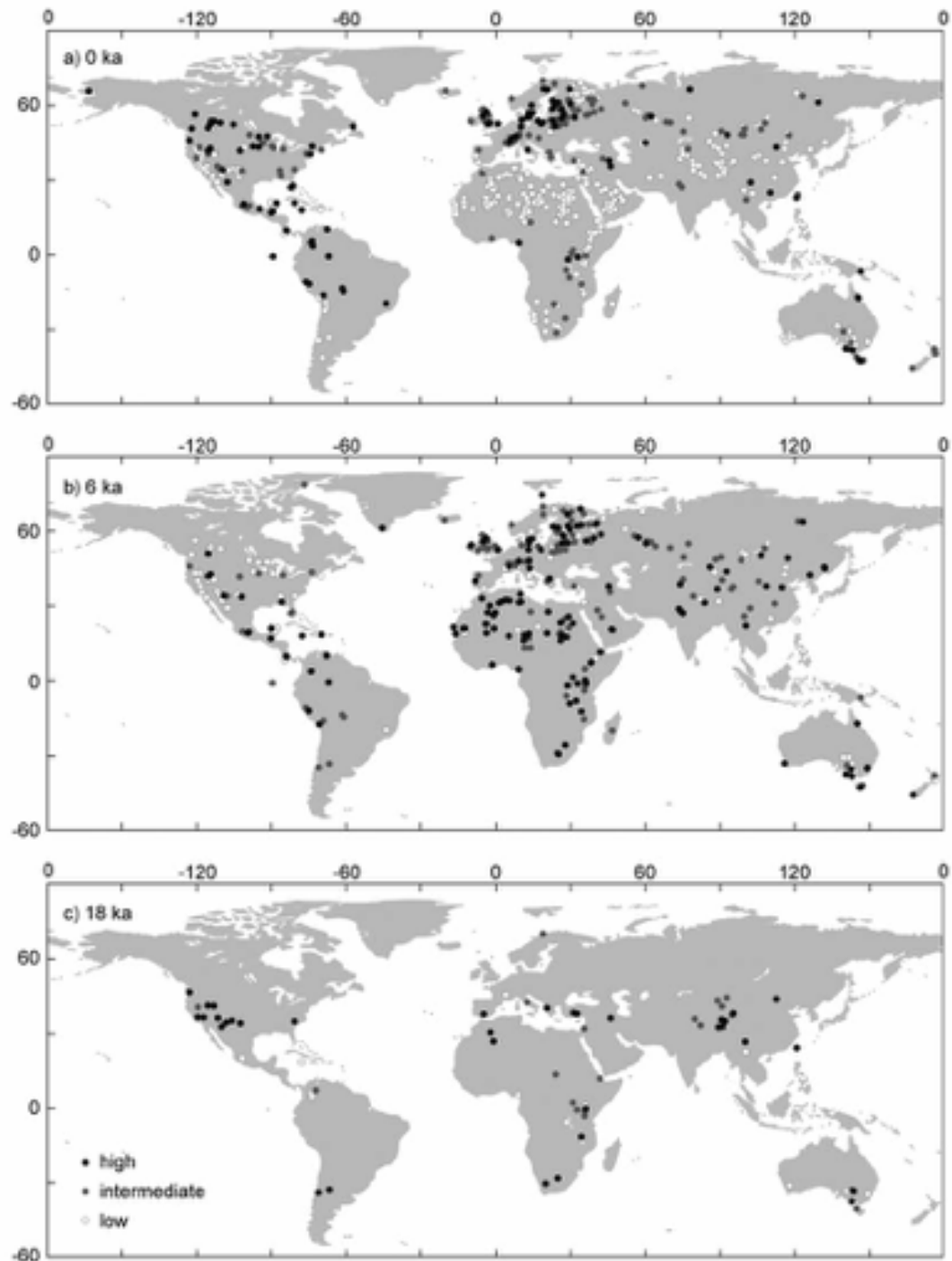


Figure 3.33 a) Locations of lakes for which lake-level data are lodged with the PMIP Global Lake Status Data Base (updated 2011). b) Lake status data for 6 ka. c) Lake status for 18 ka (source of data: <http://pmip2.lsce.ipsl.fr/synth/lakestatus.shtml>).

different pattern, with high levels from LGM times until the early Holocene, followed by arid conditions from c. 11–10 ka (Smith & Street-Perrott, 1983). The timing of lake-level variations in Australia appears to have been intermediate between those of Africa and the USA, with lake levels generally falling between c. 30 and 18 ka, rising steadily through the first half of the Holocene, and subsequently falling again after achieving maximum levels at c. 8 ka (Harrison & Dodson, 1993).

This general pattern of lake-level changes was broadly confirmed, and further developed, in a geostatistical analysis of the Global Lake Status Data Base by Vial & Gajewski (2001). They examined the data over the last 12 ka, and generated lake-status patterns (grids) at 3 ka intervals. The results suggest the following scenarios. By c. 12 ka, the northern ice sheets were in rapid retreat and most of North America and Europe was wet, perhaps due to the northward migration of the jet stream. At the same time, high lake levels in Africa probably reflected higher land–sea temperature contrasts and an enhanced African monsoon. By 9 ka, the Eurasian ice sheet had almost disappeared and the Laurentide ice sheet was significantly reduced in size. The northward migration of the jet stream was accompanied by the storm tracks that had previously delivered precipitation to the lakes in the American Southwest and this, in combination with higher levels of solar radiation (due to Milankovitch forcing) in the early Holocene, led

to an increase in aridity in this region. Higher lake levels in North Africa, Arabia and India reflected enhancement of the Afro-Asian monsoon circulation. In some parts of Africa, precipitation may have been around 15 per cent higher than at present (the ‘African Humid Period’, AHP; Bergner *et al.*, 2003). By 6 ka, a marked insolation anomaly over northern mid-latitudes led to further aridification of the American Southwest, and also of parts of Eurasia, while North Africa remained humid under a strong Afro-Asian monsoon (Figure 3.34). By 3 ka, declining seasonal insolation in the northern hemisphere was accompanied by an increase in precipitation in the American Southwest and a rise in lake levels, while a concomitant weakening of the Afro-Asian monsoon led to aridification in North Africa, Arabia and parts of Asia. Vial & Gajewski (2001) also compared the 6 ka lake-level status grids with simulations from four atmospheric circulation models (section 7.2.3) to underline their usefulness in validating broad-scale climate model outputs (e.g. Coe & Harrison, 2002). Conversely, because modelling methods can experiment with different climatic inputs, they can also inform the debate concerning the climatic parameters that lead to marked water balance differences, and hence to lake-level response (e.g. Li & Morrill, 2010).

Not all lakes are completely enclosed, however, or respond solely to climate changes in terms of the local evaporation–precipitation balance: a number of factors

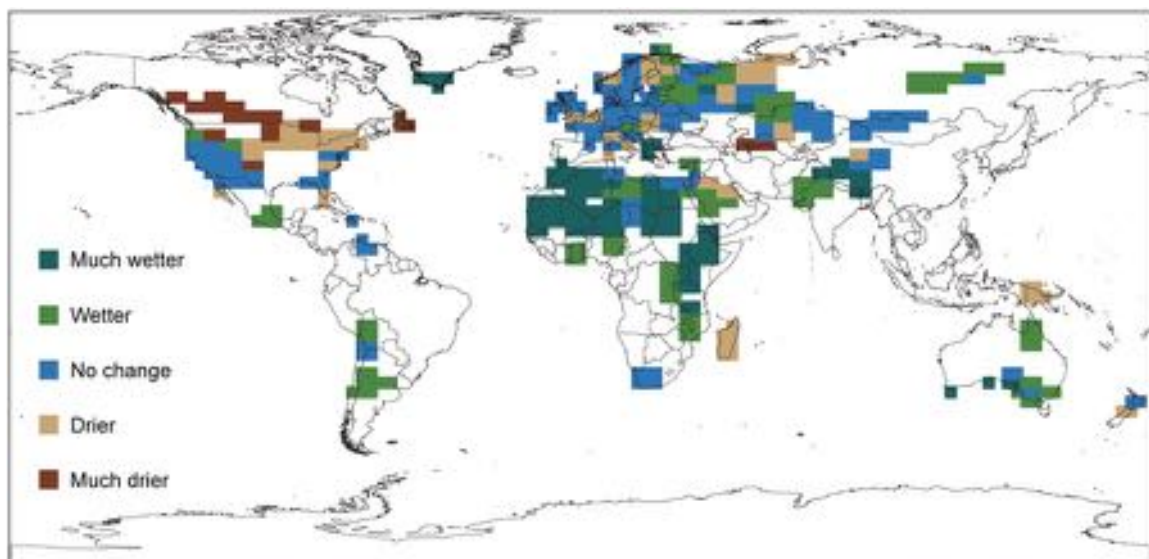


Figure 3.34 Lake-status data for 6 ka expressed as anomalies relative to long-term status. The site records are averaged for grid squares to enable comparisons with outputs from numerical modelling experiments (after Sawada *et al.*, 2004).

affect lake basins, such as tectonic or geomorphological processes that alter the dimensions of a drainage basin or the height of the overflow (section 2.7.1). In south-central Africa, for example, the Makgadikgadi Salt pans of northern Botswana are the desiccated remains of a former major inland lake system with well-preserved fossil shorelines, which have long been considered to be the result of Late Quaternary climate forcing, but which now seem more likely to reflect tectonically initiated changes in regional drainage pattern as the underlying control over lake evolution (Moore *et al.*, 2012). Furthermore, some lake basins may respond to climate changes more quickly than others, reflecting perhaps the size of the basin, drainage sources, or other factors. In certain cases, this may lead to a delay in, or an asynchronous lake response to climate forcing. In an analysis of lake status records from the north of the Tibetan Plateau, for example, Wünnemann (2007) found that while centennial- to millennial-scale changes in lake status during the last glacial stage were a direct response to synchronous feedbacks of variations in the Asian monsoon, since the onset of the Asian summer monsoon 13 ka ago, many desert lakes have responded asynchronously with temporal and spatial shifts of some 100 years between short-term climate-induced variations in moisture availability.

As with many other forms of proxy climate data, therefore, lake-level records are perhaps best used alongside independent lines of sedimentological and biological evidence. Hence, in Figure 3.34, for example, the inferred drier conditions in the north-central USA are consistent with independent pollen-based and numerical palaeoclimatic simulations which indicate a band of positive temperature anomalies across the continent at that time (Sawada *et al.*, 2004). In central Asia, lake-level records were one of a number of environmental proxies that provided the basis for a time-slice reconstruction of effective moisture changes across the monsoonal-affected areas over the past 13 ka (Figure 3.35). Although there is a considerable degree of complexity in the records, particularly during the Bølling-Allerød and Younger Dryas periods, there is a broader degree of consistency during the Holocene, with wetter conditions reflecting a strong summer monsoon and humid climate during the early and middle Holocene, but an increasingly drier climate indicating a weakened summer monsoon during the late Holocene (Herzschuh, 2006). In a similar multi-proxy study in arid central Asia (the region extending from the Caspian Sea eastwards across the northern Tibetan Plateau and into northeast China), a different spatial and temporal pattern emerged from the lake records, with a dry early Holocene (pre-8 ka), maximum moisture conditions during the mid-Holocene

(8–4 ka), and a decreasing moisture trend during the late Holocene. Across this region, the pattern of Holocene effective-moisture development appears to have been determined largely by westerly (as opposed to southerly monsoonal) airstreams, with a strong influence of North Atlantic sea-surface temperatures (Chen *et al.*, 2008).

Isotope variations in lake sediments (section 3.7.2) provide an additional index of past climatic variations that can be set alongside, or used in combination with, climatic inferences obtained from lake-level changes. For example, Zhang *et al.* (2011) compiled carbonate $\delta^{18}\text{O}$ records from eight lakes in the present-day Indian monsoon region, each spanning the Holocene. The records are remarkably consistent in the long-term trends they portray (Figure 3.36), indicating that climate changes during the Holocene were broadly synchronous across the monsoon region, with the wettest conditions during the early Holocene (11–7 ka) and progressive aridification since 7 ka. This confirms the general pattern of Holocene climate change inferred from other lake records (e.g. Figure 3.35). In the Mediterranean region, a comparison of $\delta^{18}\text{O}$ variations in biogenic and endogenic carbonates recovered from lake sediment sequences showed that conditions were arid around much of the Mediterranean at times of cooling in the North Atlantic, such as during Heinrich events (section 3.10.1) and the Younger Dryas. In addition, the records suggest that changes in local rainfall were more important than temperature in driving the isotopic signal in carbonate lake deposits in the eastern Mediterranean region, but not in the west, reflecting a strong west–east contrast across the region during the Holocene (Roberts *et al.*, 2008).

Much of the foregoing discussion has been on long-term (millennial-scale) climatic changes, but it now appears that lakes have also responded sensitively to shorter-term climatic oscillations over decadal and centennial timescales. Although these typically involve very small-scale shifts in the pattern of pressure cells, particularly around the inter-tropical convergence zone, they can lead to marked changes in regional precipitation patterns, and may perhaps be linked to short-term cycles of solar activity. For example, peaks in the ~11-year sunspot cycle (section 7.6.4.1) have been accompanied during the twentieth century by water-level maxima in Lake Victoria, reflecting positive rainfall anomalies ~1 year before solar maxima. Similar patterns occurred in at least five other East African lakes suggesting that these sunspot–rainfall relationships were broadly regional in scale (Stager *et al.*, 2007). Centennial-scale events in monsoonal climate have also been recognized in Asia (Wang *et al.*, 1999) and it is these, rather than Milankovitch-scale orbital forcing, that may be responsible

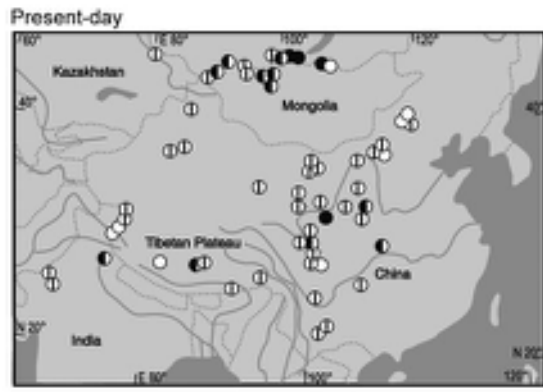
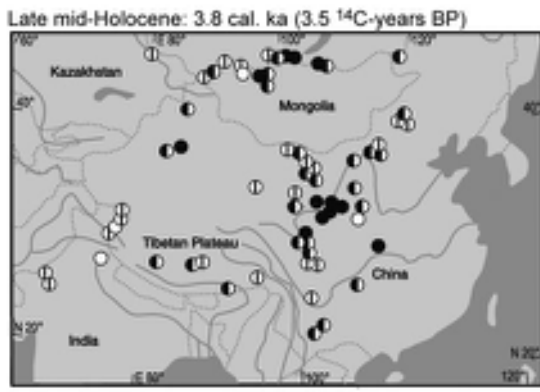
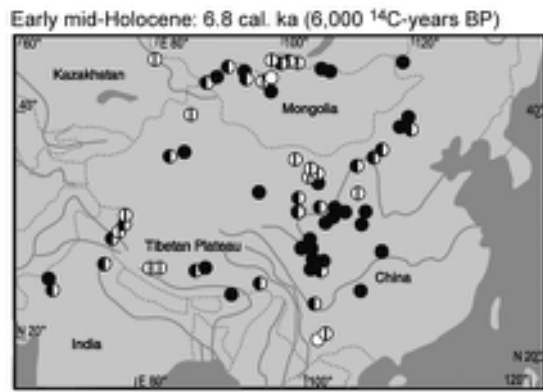
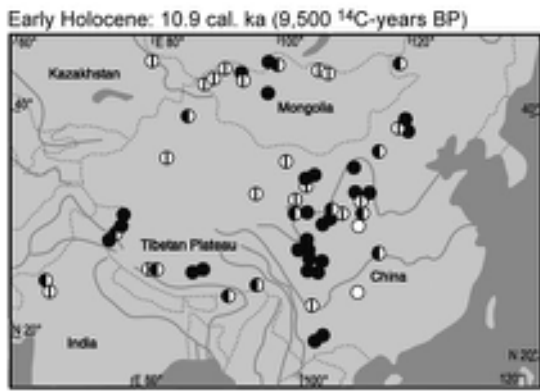
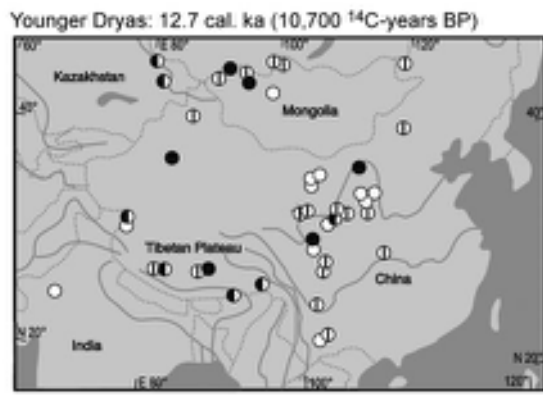
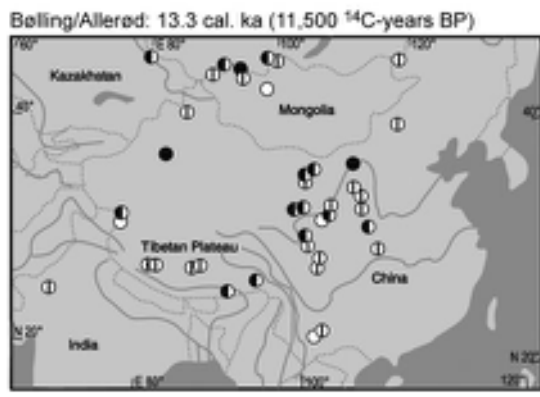


Figure 3.35 Spatial patterns of inferred effective moisture for six time-slices between the Bølling-Allerød period and the present time, based on lake-level variations and other palaeoclimatic records from Central Asia (after Herzschuh, 2006).

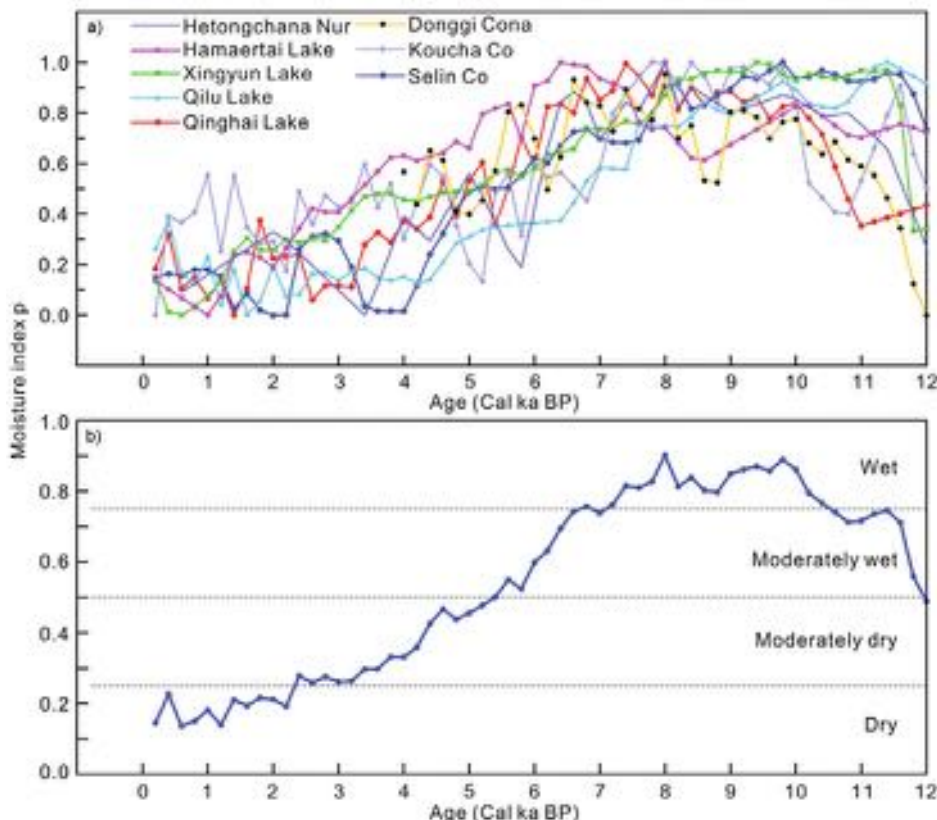


Figure 3.36 a) Carbonate $\delta^{18}\text{O}$ records from eight lake sediment sequences from the Indian monsoon region. Each isotope series has been normalized to reduce them to a common scale (shown in probability units: p). b) A regional moisture index based on the mean of the eight curves shown in a) (after Zhang *et al.*, 2011).

for a weakening of monsoonal circulation over central and northern Australia during the late Holocene, the subsequent trend to increasing aridity being reflected, *inter alia*, in palaeo-lake records (Wyrwoll & Miller, 2001; Hesse *et al.*, 2004).

Fluctuations in water level in closed-basin lakes, combined with isotopic studies and other proxy climate indicators, therefore, constitute a valuable means of investigating Late Quaternary climatic change. Most ‘pluvial’ lakes appear to respond rapidly to climate variations and are often more direct indicators of water balance than vegetation or soils. Moreover, many pluvial lake deposits are found in areas where biological and other indicators of former environmental conditions are scarce. Not only do they provide direct evidence of former precipitation regimes, but they also offer a basis for modelling climatic change and for reconstructing atmospheric circulation patterns in the low-latitude regions of the world.

3.8 CAVE SEDIMENTS AND CARBONATE DEPOSITS

3.8.1 Introduction

Caves form natural sediment traps in which the deposits are largely protected from the effects of subaerial weathering agencies and erosion (Gunn, 2003). In karstic regions especially, the sediments that have survived in caves frequently cover a much longer time interval than those on the neighbouring land surface. Three main types of material contribute to cave sediment sequences: clastic detritus, organic detritus and precipitated carbonates, the relative proportions of each depending upon rock type, size of fissure, groundwater regime, topographical or geological context and geographical location (section 4.11.5.1). Clastic detritus includes rock rubble, cave earth and water-lain sediments. Organic detritus may consist of skeletal parts of

animals that occupied the caves and those of their prey, while many caves acted as occupation sites for humans and so cave successions may contain a rich legacy of organic, artefactual and cultural material of anthropogenic origin. In limestone regions, reprecipitated carbonates, collectively known as **speleothem**, constitute a third important component of the sedimentary fill. Precipitation of carbonate from flowing or dripping water in caves can generate a variety of forms of **dripstone**, the best known of which are stalactites and stalagmites, or **flowstone**. In many caves, dripstone and flowstone production appears to have been periodic or even cyclic, resulting in inter-stratification of speleothem and detrital layers, and artefacts, bones and clastic material can often become wholly embedded (and very well preserved) within the precipitated carbonate (Figure 3.37; Ford, 2006).

In this section, the palaeoenvironmental potential of detrital and carbonate deposits in caves will be examined. Of particular importance is speleothem, since this material (1) provides the longest and most detailed palaeoenvironmental records from cave contexts (Fairchild & Baker, 2012); (2) contains stable isotopic signatures that form a basis for high-resolution palaeoclimatic reconstructions (Lauritzen & Lundberg, 1999); (3) can be dated by U-series dating (section 5.3.4) to provide a chronology both for the cave sedimentary sequences and for the derived

palaeoclimatic histories (Richards & Dorale, 2003); and (4) offers a basis for correlation between terrestrial, ice-core and ocean-core proxy climate records (Bar-Matthews *et al.*, 2003). Reference will also be made to other types of carbonate material that are found outside the cave environment (e.g. travertine and tufa), since the processes of formation, and the analytical techniques employed in their study, are often similar to those associated with speleothem (section 3.8.5).

3.8.2 Detrital sediment in caves

A major factor governing the processes of sedimentation in caves is the shape of the cave itself. A distinction is often made between **exogene** caves, which are shallow niches in the hillside, referred to by archaeologists and anthropologists as **rock shelters**, and **endogene** caves, which penetrate deep into the ground as chambers or passages (Figure 3.37). In the interior passages of endogene caves, relatively equable conditions prevail, for the air is protected from the temperature extremes that occur at the ground surface. Daily and seasonal changes in weather and climate therefore rarely penetrate, at least not directly, and therefore only the major and long-term climatic changes can affect the mode of sedimentation. Unless endogene passageways are near the ground surface, in which case exotic material

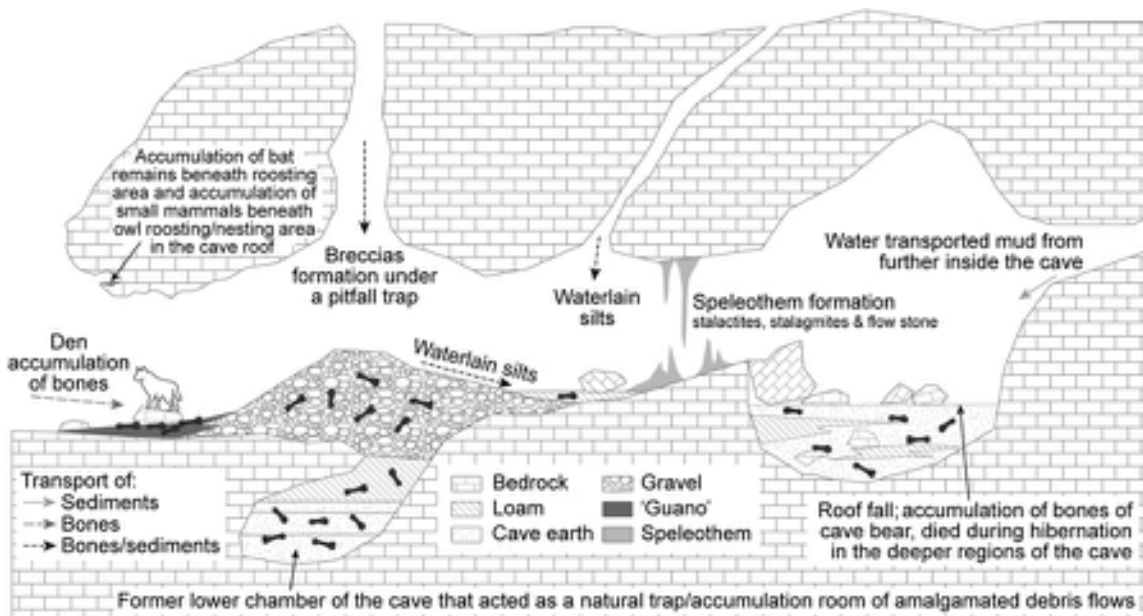


Figure 3.37 Generalized cross-section of a cave with various types of sedimentary infill and associated biological remains (modified from http://historyofgeology.fieldofscience.com/2010_10_01_archive.html).

may be introduced into the system through clefts in the cave roof, the majority of sediments are derived from the bedrock within which the fissures have formed, the principal exception being water-lain sediments from conduits connected to the surface.

In exogene caverns, and near the entrance to endogene caves, sedimentation is more directly influenced by prevailing weather conditions outside. Moreover, as the deposits are derived both from within the cave (autochthonous component) and from the surrounding area (allochthonous component), the stratigraphy in these situations is often complex. As a rule, exogene caves will tend to have a higher allochthonous component than endogene caves. The entrances of exogene caves in formerly glaciated terrain may contain till or other glaciogenic sediments, while coastal caves may contain beach gravels or (in the inner reaches) finer marine sediments. Wind-blown material is also commonly encountered in exogene cave sediments as well as colluvial and soliflucted sediment.

Autochthonous sediments consist principally of rock rubble and cave earth. Angular fragments of rock are common deposits in many caves and have been weathered from the roofs and walls to form **thermoclastic scree**. In the outer parts of caves, some rock fragments will have been derived from insulation weathering (expansion and contraction at the rock surface due to temperature changes), while in limestone areas, solutional weakening by percolating groundwaters will result in pieces of rock breaking off from the walls and roofs of a cave. **Cave earth** is composed of much finer materials (sand size and less) and may have a variety of origins. Near the cave entrance, it is often largely allochthonous, being composed of wind-blown or water-lain sand or silt, or even in washed colluvial sediment. In the deeper parts of limestone caves, however, cave earths are formed either from the acid-insoluble residues left by the solutional breakdown of the country rock, or from the secondary weathering of angular rock fragments that have accumulated on the cave floor. Cave earths are frequently red or brown in colour, due partly to the presence of oxides of iron and aluminium, but in some cases reflecting the influence of phosphate derived from fossilized faecal matter.

Until recently, relatively few detailed studies had been made of clastic sediments in caves, at least for the purposes of reconstructing Quaternary environments, since most interest has been focused on the fossil, archaeological or speleothem content of cave sequences. Indeed, many caves were excavated in the late nineteenth and early twentieth centuries primarily to recover archaeological remains, with scant regard for the stratigraphical context of this material. The situation has changed in recent decades, and

it is now widely recognized that cave sediment sequences constitute a potentially valuable archive of environmental and climatic change (Woodward & Goldberg, 2001; White, 2007), while important environmental and archaeological evidence can be obtained from both macro- and micromorphological analyses of sediments in caves (Mallol *et al.*, 2010). In a wider context, sedimentological analysis can provide a basis for correlating cave stratigraphies with the marine oxygen isotope record (Zhou *et al.*, 2001). However, cave sediment sequences are normally complex and characterized by numerous hiatuses in sedimentation. Furthermore, the facies variations found in cave sediments are often not as well understood as those associated with surface processes. The reconstruction of environmental conditions from clastic cave sediments is therefore not without its problems.

A wide range of organic materials can be found in cave sediments, incorporated within or interstratified with clastic material (e.g. Hearty *et al.*, 2004). The most obvious organic components are usually the skeletal remains of natural cave dwellers and their prey, and the analysis of such fossil assemblages can provide information on the nature and ecology of both predators and prey (Parmalee, 2005). Many caves contain rich snail assemblages, and in karstic regions, these may often be of considerable antiquity (Goodfriend & Mitterer, 1993). Pollen is often found in clastic cave sediments (Carrión *et al.*, 1999) and sometimes in speleothems (McGarry & Caseldine, 2004). Plant macroremains may also be preserved in cave sediment sequences (Hansen, 2001), such materials having been transported into caves either by natural processes, or by animals and people. These include the decayed parts of plants carried in for bedding, litter or food, plant macrofossils from animal excreta and carcasses, and charcoal deposits from former hearths. In addition, pollen and other microfossils (e.g. **phytoliths**⁶), derived from local vegetation may be carried in by animals and humans (Wallis, 2001). The fossil content (biostratigraphy) of caves is discussed in Chapter 4.

Many cave sequences are depositional palimpsests with successive cultural horizons superimposed (Auban *et al.*, 2001), and these may provide valuable insights into historic and prehistoric human activity, such as early agriculture (Peña-Chocarro *et al.*, 2005). Caves have also frequently been used in prehistory for stabling of animals, especially in upland areas that provided rich pasture in the summer months. Evidence of the use of caves for this purpose can be found in cave sediment layers that are rich in phosphates, coprolites (animal excreta), charcoal and concentrations of calcium oxalate crystals that are derived from coprolites (Canti, 1998). These and other cultural horizons can readily be identified by soil micromorphological and chemical

analysis of the cave sediment sequence, and provide evidence of, *inter alia*, transhumance in mountain regions during the Neolithic and Bronze Ages (Karali *et al.*, 2005). Human coprolites have also been recovered from cave sediments, sometimes in association with artefacts, and provide a basis both for DNA analysis and also for dating the cultural contexts (Jenkins *et al.*, 2012).

3.8.3 Speleothem

Speleothem is a secondary mineral deposit formed in caves in karst regions as **dripstones** or **flowstones**. Dripstones are deposits of calcium carbonate (although some may be composed of varying quantities of aragonite, gypsum or halite) formed by water dripping from the ceilings or walls of a cave, or from the overhanging edge of a rock shelter. The most common features that develop in this way are **stalactites** and **stalagmites**. Flowstones are deposits of calcium carbonate, gypsum or other mineral matter that have accumulated on the walls or floors of caves in places where water trickles or flows over the rock. Upon reaching the cave floor, water may percolate into the interstices of clastic sediments, cementing them into a coherent, often very hard porous rock known as **cave breccia**. In some cases, a complete cover of precipitated calcium carbonate blankets the floor of the cave, where it may become interbedded with the scree, breccias and cave earths (Figure 3.37). Such a flowstone cover has been referred to as a **stalagmite floor**. Other precipitated calcium carbonate deposits occasionally found in caves in karst regions include **travertine**, a light, compact and generally concretionary substance, extremely porous or cellular varieties of which are known as calcareous **tufa**, calcareous **sinter** or **spring deposit**. Compact banded varieties are sometimes referred to as '**cave marble**' or '**cave onyx**'. Many of these carbonate features are also common in subaerial environments in karstic regions, around streams and springs (section 3.8.5).

The precipitation of calcium carbonate is caused by degassing of CO₂. Water that drips or flows into the cave chamber has usually originated on the surface where it has acquired a high concentration of CO₂ from biogenic production in soils. Due to ventilation effects, the air in the cave chamber has a lower partial pressure of CO₂ than the incoming water and so automatic degassing of CO₂ from the water takes place, leading to supersaturation and then precipitation of carbonate. With a continuous supply of water over long periods, large speleothem structures can build up by successive **growth layers** of carbonate (Figure 3.38). It is this characteristic that makes speleothems so valuable for the reconstruction of Quaternary palaeo-environments, for they often preserve a continuous sedi-

mentary record capable of analysis at a very high resolution (Fairchild & Baker, 2012). In some sites the growth banding in speleothem may be annual in nature, while speleothem can also be dated using the U-series dating method (section 5.3.4) and, in some instances, by means of radiocarbon (Yadava & Ramesh, 2005). Once a chronology of speleothem growth has been established, palaeoenvironmental inferences can be made on the basis of (1) the rate and abundance of speleothem formation and (2) temporal variations in the isotope ratios contained within the carbonate structure. These aspects will now be discussed in more detail.

3.8.4 Speleothem growth and environmental reconstruction

Precise dating of speleothem has demonstrated that the development of carbonate growth bands in cave systems may be cyclic or intermittent. This largely reflects environmental controls on cave hydrology, and so an analysis of the growth frequency of speleothem within cave systems can be used to reconstruct a number of different aspects of former environmental conditions, as the following examples demonstrate.

3.8.4.1 Speleothem growth and climatic change

Carbonate precipitation is strongly influenced by prevailing climatic conditions. It is either strongly reduced or arrested during cold episodes and increases to a maximum during warm intervals. In permafrost environments, groundwater percolation is at a minimum, while CO₂ concentrations in these groundwaters are also reduced because of the restricted biogenic activity associated with skeletal periglacial soils. There may, however, be some limited or sporadic speleothem growth, depending upon local conditions. In Norway, for example, caves that were overlain by ice were flooded by meltwater, which resulted in **phreatic**⁷ conditions and the deposition of clastic sediments rather than speleothem carbonate (Lauritzen, 1993), whereas in Austria there are indications that speleothems were forming in some alpine caves when these were covered by glacier ice (Spötl & Magnini, 2007). During interglacial conditions, by contrast, higher precipitation levels result in greater water penetration, biological productivity increases, **vadose** (see note 7) conditions prevail in cave systems, and maximum speleothem formation occurs. In mid- and high-latitude regions, therefore, speleothem formation reflects the sequence of climatic conditions experienced during the course of a glacial-

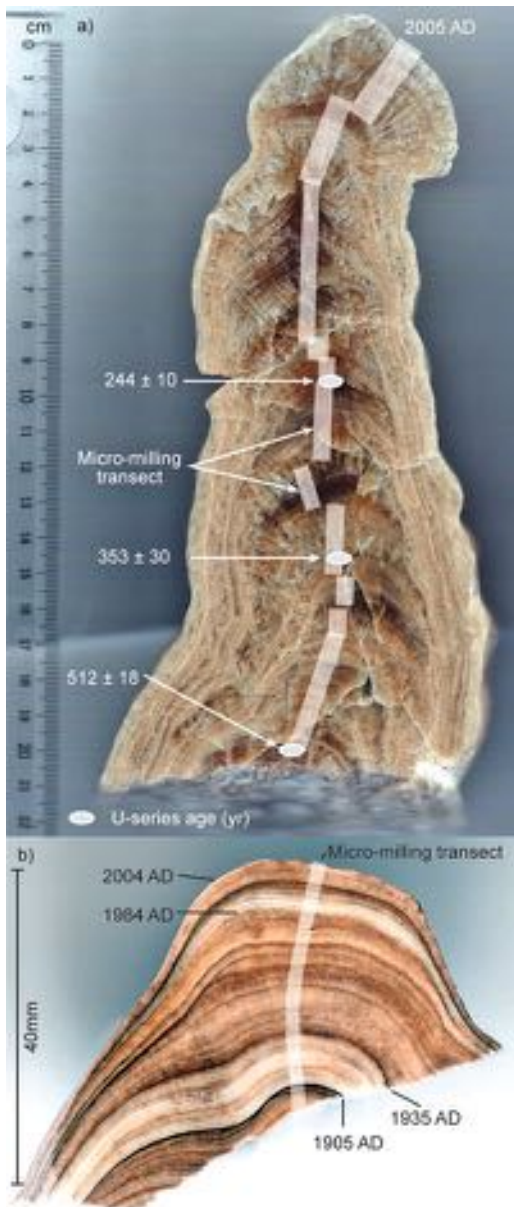


Figure 3.38 a) Cross-sectioned surface of a stalagmite from Akçakale Cave, northeast Turkey revealing annual growth layers spanning the last c. 500 years, the chronology confirmed by U-series dating. Small samples were extracted (micro-milled) at 0.1–1.0 mm sampling intervals along transects (light shading in the figure) where series of contiguous growth layers could be traced (Jex *et al.*, 2010). Stable isotope measurements obtained from these samples, cross-checked with modern instrumental records, provide a record of annual variations in local precipitation and have been successfully forward-modelled using GCM data for this region coupled with a karst hydrology model (Jex *et al.*, 2011). b) Cross-sectioned surface of a small stalagmite from Rukiessa Cave, southeast Ethiopia, spanning the last century. Seasonal layers are indicated by colour variations within the drip waters in the cave. Samples 1–3 mm in thickness were drilled along a continuous transect (light shading) that enabled seasonal climatic variations and land-use changes to be reconstructed (Baker *et al.*, 2007; Blyth *et al.*, 2007) (photographs by Andy Baker, Catherine Jex and Asfawossen Asrat, University of New South Wales, Sydney, Australia, reprinted with permission from Elsevier).

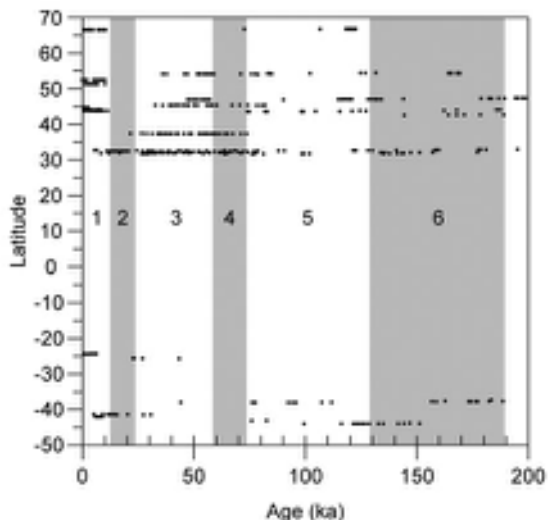


Figure 3.39 Compilation of c. 750 TIMS U-series speleothem dates plotted against the latitude of the relevant site. MIS stages are also shown. Note the virtual absence of dates from the mid- and high-latitude regions of the Northern Hemisphere during MIS 2 (after McDermott, 2004).

interglacial cycle. This pattern is clearly reflected in Figure 3.39, which shows a compilation of approximately 750 TIMS U-series dates (section 5.3.4.2) on speleothems that have been studied over the course of the last decade, plotted against the latitude of the relevant cave site. The absence of speleothem deposition in the mid- and high latitudes of the Northern Hemisphere during MIS 2 is striking. By contrast, speleothem deposition appears to have been essentially continuous throughout the glacial period at lower latitudes in the Northern Hemisphere (McDermott, 2004).

The correlation between interglacial intervals and periods of enhanced speleothem growth is evident at many sites around the world. In the Austrian Alps, for example, speleothems grew from around 127 ka, with peak interglacial conditions (high $\delta^{18}\text{O}$ values and growth rates)

between 127 and 124 ka. Speleothem growth terminated at c. 114 ka, which is in line with widespread ice rafting in the North Atlantic and the onset of full stadial conditions in MIS 5d (Meyer *et al.*, 2008). Further north at Rana, northern Norway, stalagmite deposition has been dated to between c. 123 and 73 ka, in other words spanning much of MIS 5. The most rapid growth phase ($\sim 46 \mu\text{m yr}^{-1}$) occurred between 123 and 119.5 ka, but had declined to $\sim 0.7 \mu\text{m yr}^{-1}$ by c. 107 ka. Between c.107 and 73 ka, growth is barely noticeable. The transition between rapid and slow growth rate between c. 119 and 107 ka reflects the termination of interglacial climate in the region (Linge *et al.*, 2001). In southern France, most of the major growth phases in stalagmite in the Grotte de Clamouse correspond with warmer intervals corresponding to MIS 5 and 7 (Plagnes *et al.*, 2002). Similar trends are apparent in evidence from the Southern Hemisphere. In Australia, for example, data from Tasmania indicate peak last interglacial conditions between c. 129 and 122 ka, which also coincides with a time of prolific coral growth in western Australia (Zhao *et al.*, 2001), while in New Zealand, U-series dating of almost 150 speleothems shows that calcite deposition has taken place somewhere in the country with little interruption for more than 500 ka, and that most growth also occurred during interglacial and interstadial episodes (Williams *et al.*, 2010).

Speleothem records may also reveal periods of more arid conditions. In caves in middle- to low-latitude regions, where variations in groundwater are strongly influenced by regional changes in precipitation regime, speleothem growth is often episodic. A change to drier climatic conditions will lead to a reduction in the amount of water percolating from the surface, while soil biogenic activity will also be reduced. In many caves in southern Australia, for example, speleothem deposition over the past 500 ka has been intermittent and concentrated during cooler and wetter stadials and interstadials of the past four glacial cycles (Aycliffe *et al.*, 1998; Desmarchelier *et al.*, 2000). For the Holocene, speleothem records indicate that, following an early phase of more effective precipitation, with peak moisture at 7–6 ka, an arid climate similar to present was established by 5 ka, reflecting the onset of an ENSO-like climate (section 7.6.4.2) across arid Australia (Quigley *et al.*, 2010).

3.8.4.2 Stable isotope ratios in cave speleothem

In deep caves, where there is no direct contact with the external atmosphere and there is little or no air circulation, the temperature remains more or less constant throughout the year and is similar to the mean annual air tempera-

ture in the vicinity of the site. Calcite deposition occurs by degassing from carbon-saturated dripwaters that enter the cave from the surface and the speleothem carbonate tends to form in **isotopic equilibrium**⁸ with the water from which it is precipitated. The isotopic composition of percolating water will be registered in the isotopic ratios locked into the carbonate crystal or in fluid inclusions trapped within it. By measuring the ratio of heavy (^{18}O) to light (^{16}O) oxygen isotopes (measured as a deviation, δ , from a standard: section 3.10.2) at regular intervals along the axis of speleothem growth bands, a record of isotope variations over time can be obtained. Such data have shown that the oxygen isotope ratios in cave speleothem often vary in a cyclic fashion (Figure 3.40) and that they contain a climatic signal (see below). Dating of these records by the uranium-series method allows direct correlation both with ice-core and marine oxygen isotope profiles, and also with other records of global climatic change (McDermott, 2004).

Not all speleothem is suitable for this type of research, however, for a number of conditions must be satisfied before the isotopic ratios can be regarded as providing reliable palaeoclimatic data. These include: (1) the carbonate precipitate must be in isotopic equilibrium throughout the period represented; (2) the oxygen isotope content of the water from which the carbonate was precipitated must be known; (3) no diagenetic alteration should have occurred; and (4) the deposit must be sufficiently free of detrital contamination for satisfactory dating of the sequence. Given the complexity of cave sediment sequences, it is not always easy to satisfy all four of these conditions. Perhaps the most difficult is (2), for isotope variations in cave carbonate can be the result of the combined influences of temperature, the **fractionation**⁹ which occurs when carbonate precipitates from dripwater (a decrease in cave temperature will lead to higher ^{18}O concentration in the carbonate precipitate), and changes in the isotopic ratios of dripwater before entry to the cave system. The extent of fractionation during carbonate precipitation can be estimated by analysing variations in other isotopes, such as carbon and hydrogen, since these are unaffected during crystal formation and they therefore enable the pre-fractionation ratios of oxygen isotopes in dripwater to be determined (Lauritzen, 1993).

As temperature is a major factor influencing temporal variations in $\delta^{18}\text{O}$ in cave speleothem, and numerous studies have been published in which quantitative estimates of past temperature have been derived from the oxygen isotope signal in speleothem calcite (e.g. Mangini *et al.*, 2005; Affek *et al.*, 2008). However, the temperature-dependence of $\delta^{18}\text{O}$ in rainfall is temporally and spatially variable, and is frequently site-dependent (Fricke & O'Neill, 1999).

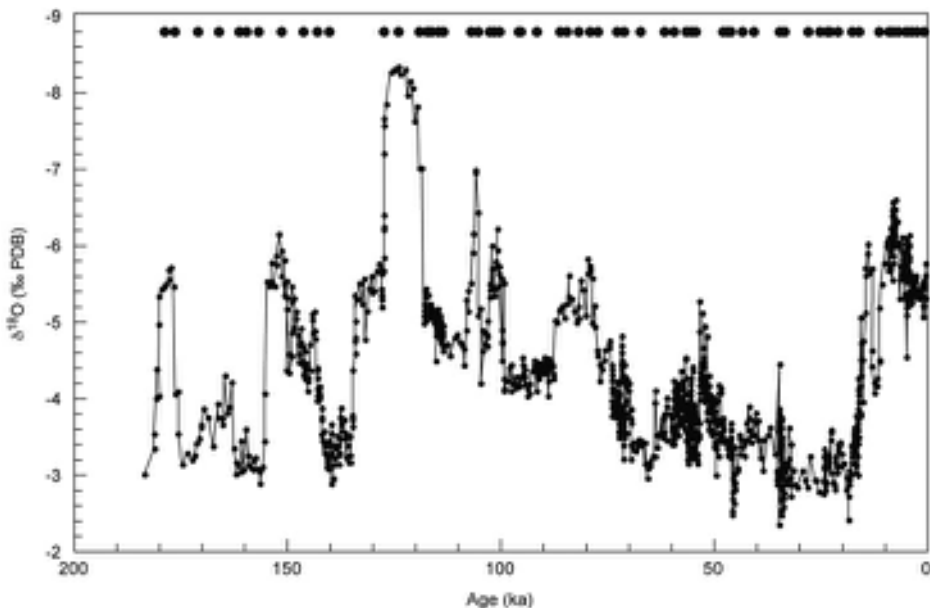


Figure 3.40 Composite $\delta^{18}\text{O}$ curve constructed from twenty-one overlapping speleothem records for the past 185 ka from Soreq Cave, Israel. The black circles at the top show the positions of samples dated by TIMS U-series (section 5.3.4.2) (after Ayalon *et al.*, 2002).

In addition, on centennial to millennial timescales, a range of factors other than temperature may lead to temporal variations in $\delta^{18}\text{O}$. These include changes in the $\delta^{18}\text{O}$ of the ocean surface due to fluctuations in continental ice volume (section 3.10); temporal variations in temperature difference between the sea-surface water vapour source area and the cave site of interest; long-term changes in moisture sources or storm tracks; changes in the proportion of precipitation that has been derived from non-oceanic sources, in other words obtained from rivers, lakes and other continental sources; and also the seasonally varying isotopic composition of precipitation (McDermott *et al.*, 1999; Fairchild & McMillan, 2007).

These and other interpretational difficulties have led, in more recent years, to a move away from quantitative temperature estimates to more qualitative climatic reconstructions, in which $\delta^{18}\text{O}$ shifts are interpreted in terms of warming and cooling trends (e.g. Onac *et al.*, 2002; Williams *et al.*, 2004a). Figure 3.41a shows a $\delta^{18}\text{O}$ record from a stalagmite in Höllloch Cave in the Bavarian Alps, Germany. The sequence spans the period from around 14 ka to the present and shows the climatic oscillation of the Lateglacial, with the marked cooling in the Younger Dryas cold interval (*c.* 13–11.5 ka) and the abrupt warming at the beginning of the Holocene (Wurth *et al.*, 2004). The marked oscillations in climate during the Holocene, including the

widely recognized 8.2 ka event (section 7.6.3.2), match very closely variations in the timberline in the eastern Austrian Alps (Figure 3.41b). In addition to reconstructing temperature trends, variations in oxygen isotope ratios can provide valuable chronological control on the timing of major shifts in $\delta^{18}\text{O}$ ratios in precipitation, which can then be interpreted in terms of changes in atmospheric circulation patterns, changes in the $\delta^{18}\text{O}$ of ocean vapour sources, or first order climate changes, such as the Dansgaard–Oeschger oscillations (section 3.11) of the last glacial cycle (McDermott, 2004). For example, a $\delta^{18}\text{O}$ record from Hulu Cave, China, shows a remarkable resemblance to the oxygen isotope record from the GISP2 Greenland ice core, suggesting that East Asian monsoon intensity changed in concert with Greenland temperatures between 75 and 11 ka (Figure 3.42). This record links North Atlantic climate with the meridional transport of heat and moisture from the warmest part of the ocean where the summer East Asian monsoon originates (Wang *et al.*, 2001).

In addition to $\delta^{18}\text{O}$ values, many recent studies have included the analysis of carbon isotope ratios ($\delta^{13}\text{C}$) in speleothem carbonate. The $\delta^{13}\text{C}$ record in the speleothem is a reflection of the nature of the overlying vegetation cover, albeit modified by fractionation and other processes and, in some instances, this can be interpreted as a palaeoclimatic record. In semi-arid and arid regions,

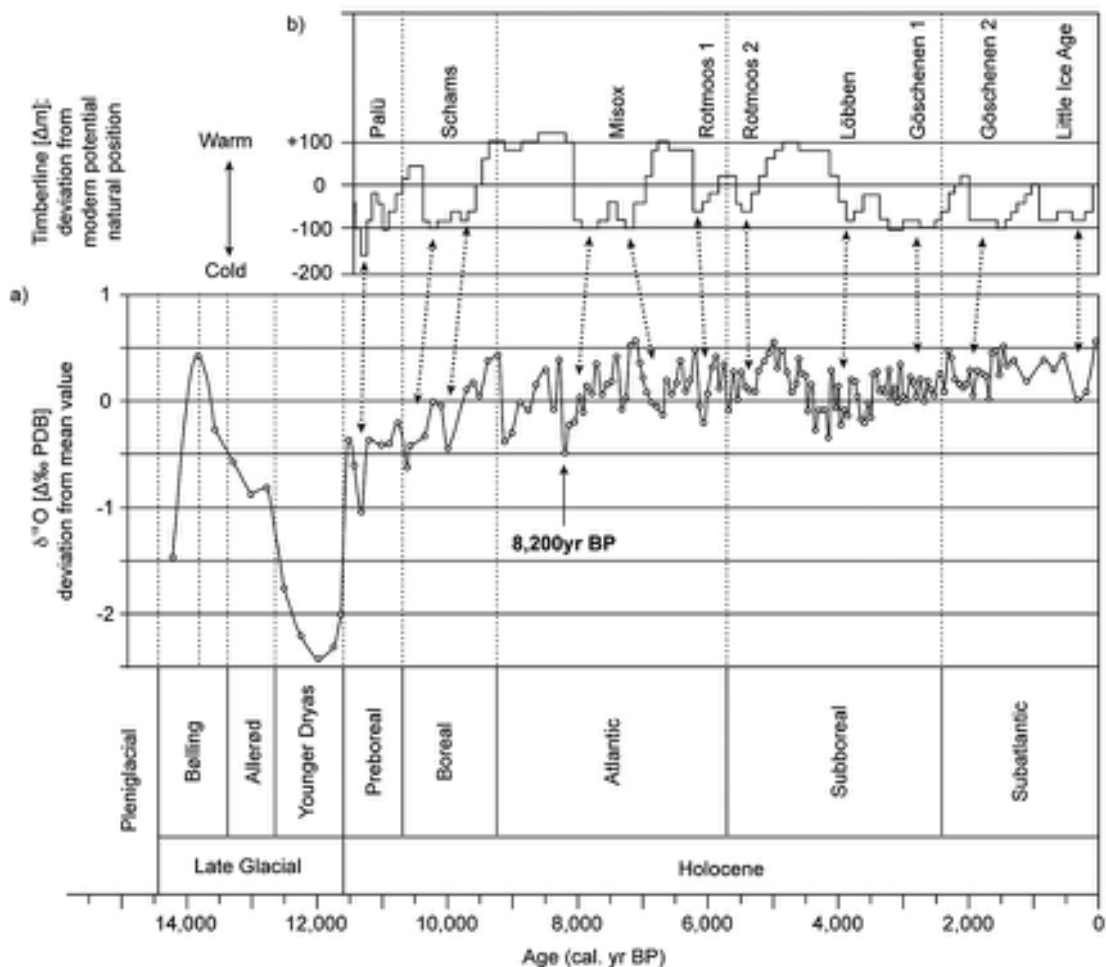


Figure 3.41 a) $\delta^{18}\text{O}$ measurements covering the period 14 ka to the present from Höllloch Cave, Bavarian Alps, Germany. Note the significant isotopic shift (to cooler conditions) between c. 13 and 11.5 ka (Younger Dryas) and the fluctuating nature of the Holocene climatic record. b) Timberline record from the Eastern Alps, Austria. Note the correlation between decline in timberline elevation (implying cooler climates) and the shifts to heavier values in the isotopic curve (after Wurth *et al.*, 2004).

significant shifts in $\delta^{13}\text{C}$ per mil values in speleothems may be reflective of climate-driven changes in vegetation (i.e. between C3 and C4 plant types), with 'lighter' $\delta^{13}\text{C}$ per mil values being associated with C3 plants and 'heavier' values with C4 vegetation (Bar-Matthews *et al.*, 1997). In eastern China, for example, Zhand *et al.* (2004) have interpreted $\delta^{13}\text{C}$ shifts in a 6,000-year Holocene stalagmite as a climatic proxy record, the lighter $\delta^{13}\text{C}$ values reflecting the dominance of C3 plants under relatively warm or rainy conditions, while heavier $\delta^{13}\text{C}$ values are associated with C4 plants that thrive under cooler, arid conditions. In temperate regions, however, the interpretation of the $\delta^{13}\text{C}$

record is often less straightforward, although a correlation has been suggested between $\delta^{13}\text{C}$ and changes in soil CO_2 production, with higher $\delta^{13}\text{C}$ values reflecting reduced soil CO_2 as, for example, during the Younger Dryas cold phase (Támas *et al.*, 2005). Another potentially fruitful area of research concerns hydrogen ratios (δD) in fluid inclusions that were trapped within the cave speleothem at the time of their formation. The $\delta^{18}\text{O}$ ratios of such inclusions may be ambiguous, because of the possibility of post-depositional changes between oxygen isotopes and the parent carbon material. Significantly, there is no post-depositional hydrogen isotope exchange. The correlation

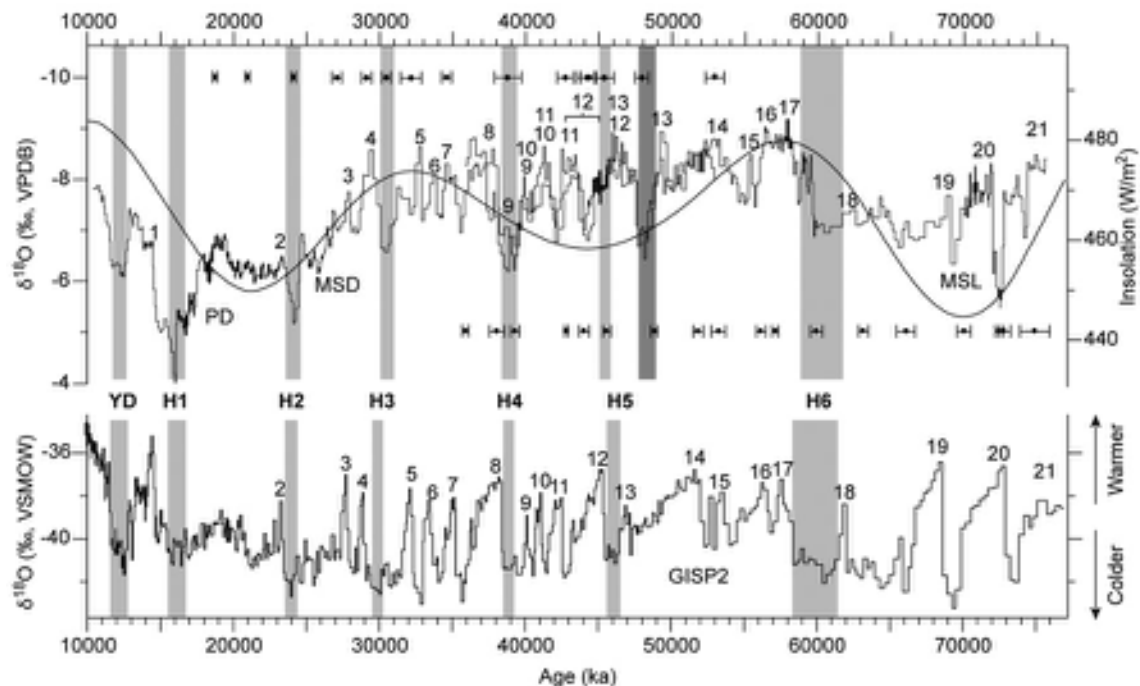


Figure 3.42 $\delta^{18}\text{O}$ record from Hulu Cave, China (upper) and the $\delta^{18}\text{O}$ trace from the GISP2 Greenland ice core. The Younger Dryas and Heinrich events (episodes of ice rafting reflecting cooler conditions in the North Atlantic: section 3.10) are shown by the vertical bars (after Wang *et al.*, 2001).

between D/H ratios and $\delta^{18}\text{O}$ is well known, and thus where δD and $\delta^{18}\text{O}$ are measured on the same fluid inclusions, D/H can be used as a proxy for $\delta^{18}\text{O}$. Because of the known temperature relationship between meteoric water (rainwater) and hydrogen isotopes, there is a basis for deriving a quantified temperature record from the $\delta^{18}\text{O}$ trace in the speleothem (Genty *et al.*, 2003). Using this approach on speleothems from three caves in Israel, McGarry *et al.* (2004) obtained a temperature range for the last interglacial (*c.* 130–120 ka) of 17–22°C and temperatures of the order of 10°C below modern values (18°C) for the Last Glacial Maximum. Further developments along these lines would not only enable unambiguous estimates to be derived from speleothem stable isotope records, but would also allow realistic estimates to be made of the uncertainties associated with reconstructed climatic parameters.

3.8.4.3 Trace elements in cave speleothem

In addition to stable isotopes, palaeoclimatic and palaeoenvironmental records can be derived from trace elements (e.g. Mg, Sr and Ba) contained within cave speleothem

(Fairchild, 2009). For example, at Soreq Cave, Israel, a marked decline in concentrations of strontium, barium and uranium, and in $^{87}\text{Sr}/^{86}\text{Sr}$ and $^{234}\text{U}/^{238}\text{U}$ ratios, that are recorded in cave speleothem, began around 17 ka and reached a minimum around 9 ka. This trend coincides with a climatic shift from a more arid to a wetter climatic regime. During the initial dry phase, the higher trace element concentrations are interpreted as reflecting an increase in the contribution of salts derived from exogenic sources (sea spray and aeolian dust) along with reduced weathering of local bedrock, while the subsequent lower concentrations are indicative of a reduction in exogenous material and enhanced weathering of the local dolomitic rocks (Ayalon *et al.*, 1999). In the Grotte de Clamouse, southern France, McMillan *et al.* (2005) showed that trace element Mg/Ca and Sr/Ca ratios in speleothem carbonate are enhanced during seasonally dry periods, and this led them to infer a multi-decadal period of aridity between *c.* 1.25 and 1.15 ka (AD 750–850). Interestingly, a comparable arid phase based on lake-level data (section 3.7) has been suggested for this time interval in Ethiopia, Niger and Mexico (Street-Perrott *et al.*, 2000).

3.8.4.4 Speleothem formation and sea-level variations

Submarine cave systems in coastal karst areas often contain speleothem structures, indicating that sea level must have been below the level of the caves at the time the speleothem formed. Dating the onset and cessation of speleothem growth throughout the cave systems has enabled the amplitude, rate and timing of global sea level to be reconstructed. In some instances, the age of low sea-level stands can be determined by radiocarbon dating organic inclusions in the speleothem (Smart, 2003), but in the majority of cases, long-term records of sea-level change are based on U-series dating of speleothem carbonate from the currently submerged caves. This approach has been used to develop a record of sea-level change during MIS 5a on the Adriatic coast of Croatia (Surić *et al.*, 2009), while a 215 ka history of sea-level oscillations in the Mediterranean region has been constructed from the dating of marine and continental layers in speleothems from the presently submerged Argentarola Cave in Italy (Antonioli *et al.*, 2004). These data are valuable in that they provide independent tests of the models of global ice volume based on oxygen isotope ratios from marine microfossils (section 3.10), since the changes in sea level inferred from the speleothem evidence should match the ice-volume changes deduced from the marine isotope records.

3.8.4.5 Speleothem formation and tectonic activity

Speleothem evidence also provides useful information on local and regional tectonic histories. In the Bahamian archipelago, for example, while speleothem growth is abundant in many submerged caves, it is less well developed in caves above sea level, being confined to a very narrow zone between *c.* +1 and +7 m. The restricted elevations of emerged caves, and the fact that speleothem older than 100 ka is absent within them, led Carew & Mylroie (1995) to conclude that the Bahamian banks have been tectonically stable throughout the Late Quaternary. By implication, therefore, it should be possible to derive a Late Quaternary eustatic sea-level curve from Bahamian shoreline evidence (section 2.5.2). On the east coast of Mallorca, caves partly filled with brackish water contain phreatic overgrowths on speleothems which mark sea-level positions during the Late Quaternary. The altitudinal positions of phreatic speleothems that formed during high sea-stands of MIS 5a, 5c and 5e are found at increasing elevations northwards and reflect significant southward tilting of

the island after MIS 5a. The overall differential displacement between the north and south of the east coast is ~1.5 m and, assuming that tilting has been continuous over the past 85 ka, this suggests an average rate of tilting of 0.02 mm yr⁻¹ (Fornós *et al.*, 2002).

3.8.4.6 Speleothem formation and rates of denudation

Dating of speleothem in mountain regions suggests that the oldest material is frequently found in the highest caves, while the onset of speleothem formation is progressively later in caves at lower altitudes. This may reflect long-term lowering of the water table through valley incision, which results in the higher caves being perched above the vadose zone so that carbonate precipitation will then cease (Atkinson & Rowe, 1992). As the water table falls, so new caves are formed or come within the vadose zone, and speleothem formation is initiated. Dating speleothems in different cave levels therefore enables rates of denudation to be inferred and may provide valuable insights into rates and processes of bedrock incision (Fei *et al.*, 2004). In northwest Scotland, for example, U-series dates on speleothems, in combination with geomorphological and other data from cave surveys, suggests that, over the course of the past 300 ka, the mean rate of valley deepening lies between 47 and 68 m per glacial–interglacial cycle. This indicates a glacial erosion rate of about 2 mm a⁻¹, a figure that is in agreement with modern process measurements (Hebdon *et al.*, 1997).

3.8.5 Other carbonate deposits

Other forms of carbonate accumulate in or around surface streams and springs in karstic regions. Some, such as **travertine** (carbonate coatings on bedrock), are produced in much the same manner as flowstone in caves (Pentecost, 2005). Groundwater saturated in CaCO₃ undergoes CO₂ degassing where it emerges into the open and carbonate is precipitated at the surface. In arid and semi-arid regions, the rate of production of CO₂-charged water depends upon local soil and microbial activity, and so the formation of travertine may reflect times of increased biological productivity associated, perhaps, with wetter climatic conditions. In some semi-arid regions, isolated patches of travertine may mark the levels at which higher, perched water tables developed during wetter periods. Dating of such features in the Grand Canyon, Arizona, for example, suggests that wetter episodes occurred at *c.* 338, 171, 71 and 15 ka, dates that correspond with those obtained for high lake-level stands in the region (Szabo, 1990). Travertine precipitation

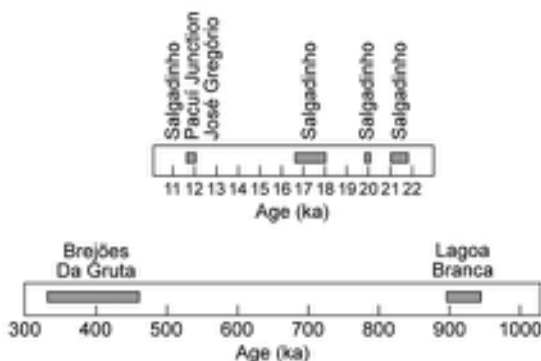


Figure 3.43 Growth phases of ^{230}Th -dated portions of travertine from sites in semi-arid northeastern Brazil extending over more than 600 ka. Note that the four phases of growth between 22 and 11 ka reflect periods of increased rainfall (after Auler *et al.*, 2004).

from hyper-alkaline springs in Northern Oman indicates wet conditions prior to 19 ka, a period of extreme aridity between 16.3 and 13 ka, a pluvial episode between 12.5 and 6.5 ka, and a late Holocene phase of hyper-aridity which continues to the present day (Clark & Fontes, 1990). Again, this is very similar to the climatic sequence obtained from lake-level records. In semi-arid northeastern Brazil, dating of travertines provides a record of pluvial activity extending back 900 ka (Figure 3.43), with the present dry conditions in the region being established at the onset of the present interglacial (Auler *et al.*, 2004).

Tufa is a calcareous crust that develops around lake margins, stream edges or springs. It can take a variety of



Figure 3.44 Tufa formations around the shore of Mono Lake, California. Many of these tufas occur on shorelines that are well above the level of the present-day lake and reflect highstands of formerly more extensive pluvial lakes (photograph by Mike Walker).

forms and can merge imperceptibly with other carbonate deposits, such as travertine, calcareous cements and stromatolites (see below). Tufas commonly mark the margins of high lake stands in arid and semi-arid regions (Figure 3.44), and the chronology of lake-level variations in such areas is frequently based upon the U-series dating of tufa deposits. Oxygen isotope ratios in freshwater tufa also appear to be a sensitive indicator of past climatic changes (Andrews & Brasier, 2005). Tufas are more difficult to date by U-series than most speleothems because of problems with detrital contamination (Garnett *et al.*, 2004).

A third category of carbonate growths is **stromatolites**, which are carbonate encrustations around algae, bacteria or other organisms. These can take a wide variety of forms, depending upon the range of organisms present, the chemical composition of the water and the nature of the climatic regime. Fossil stromatolites constitute the most ancient records of life on earth, with some remains dating to over 3.5 ba. In the contemporary littoral environment, they commonly accumulate to form reefs at the edges of lakes or in the intertidal zone where they are often found in association with travertines (Valero-Garcés *et al.*, 2001). As algal forms, they are reliant upon sunlight in the upper water layer, and they can therefore be used as proxies for water level changes in lakes; their aragonite mineralogy also means that they can be dated by U-series. As such, they constitute excellent proxies for reconstructing Late Quaternary lake-level sequences (Lisker *et al.*, 2009).

Finally, carbonate deposition is also an important pedogenic process, particularly in arid and semi-arid regions where **pedogenic carbonate** is deposited as nodules, root casings, pebble coatings and irregular concretions (Candy & Black, 2009). Precipitation is largely of inorganic carbonate, but biomineralization of carbonate in soils by soil fungi and other organisms also occurs. The analysis of pedogenic carbonate may provide evidence of climatic change, ground surface stability and substrate age, for the amount, type and depth of carbonate production in soils is climatically determined. In the western United States, pedogenic carbonate on alluvial gravels has been dated by U-series to provide a chronology for fluvial terrace sequences (Sharp *et al.*, 2003), while in western Europe, analysis of stable carbon and oxygen isotope ratios preserved in pedogenic needle fibre calcite (a particular form of pedogenic carbonate) at sites in France, Spain and the UK revealed a good correlation between mean monthly climatic parameters (including air temperature, frost-free days, humidity and precipitation), suggesting that stable isotope compositions preserved in carbonate in soil horizons may be a potential tool for palaeoenvironmental reconstructions (Millière *et al.*, 2011).

3.9 LAKE, MIRE AND BOG SEDIMENTS

3.9.1 Introduction

Preserved within sediments that have accumulated in lakes, mires and peat bogs is a diverse and often detailed record of environmental change. Given sufficient time, all lakes become infilled with sediment to form mires and bogs. Thus lake, mire and bog sediments are genetically related and frequently grade into one another. For this reason, the sediments are considered under a single heading. Lake, mire and bog deposits are important in a number of respects. First, the contained fossil flora and fauna provide evidence of both local and regional ecological changes. Second, the character of the sediments offers clues about former environmental conditions. This is particularly true in the case of lake sediments where variations in the physical and chemical properties reflect developments in the lake ecosystem, and also changes in the rates at which processes operated around the lake catchment. In both cases, the observed variations may be interpreted in terms of environmental change. Third, fossil lacustrine sediments and associated shoreline features often reveal a record of fluctuations in lake levels in response to climatic changes during the later part of the Quaternary. This topic is discussed in sections 2.7.1 and 3.7 in relation to lakes in arid and semi-arid regions, where prolonged episodes of drought frequently result in desiccation of the lakes. Here, however, we focus on lake sediments accumulating in the humid regions of the world, where drought is less of a hazard and sediment supply tends to be more continuous.

Lakes can have a variety of origins. In a classic contribution published more than thirty years ago, Håkansson and Jansson (1983) recognized eleven main types of lake (Table 3.3) of which three – tectonic, volcanic and ‘glacial’ – are of most interest to the Quaternary scientist, since it is within these that the most detailed sedimentary records have been found. **Tectonic lakes** form in areas of subsidence caused by folding or faulting, and include some of the largest lakes in the world, such as Lakes Baikal (Siberia), Titicaca (Bolivia), Tanganyika and Victoria (East Africa) and Biwa (Japan), and the Black, Dead and Caspian ‘Seas’. Some of these contain sediment sequences that span the whole of Quaternary time. **Volcanic lakes** (or **maars**) occur in calderas and craters, the length of the sediment record depending upon the time at which volcanic activity ceased. In Europe, a number of the maars in the French Massif Central, in central Italy and in Greece contain sediments that extend over several glacial–interglacial cycles (Reille *et al.*, 2000; Tzedakis *et al.*, 2003). ‘**Glacial lakes**’ are

the many hundreds of small lakes that typically form in glaciated regions. They include **kettle lakes** (which develop in hollows created by the melting of buried ice) and lakes dammed behind or between glacial landforms (e.g. terminal moraines or drumlins) as a result of the blocking of drainage outlets. In some respects the term is ambiguous, however, as it can also be used to refer to lakes that form on, or within, glacier ice (section 3.3) or to ice-marginal lakes where glaciers advance to block a drainage outlet. Other types of lake listed in Table 3.3 tend to be more ephemeral or to contain sediment records that span only short periods of time.

In the glaciated regions of Europe and North America, present-day lakes are no older than c. 15 ka, as they formed following the retreat of the last ice sheets, and hence the sediments in mires and bogs in these regions are usually

Table 3.3 Classification of lakes by mode of formation according to Håkansson & Jansson, 1983.

Type of lake	Mode of formation
Tectonic lakes	a. Epeirogenic movements (e.g. Caspian Sea); b. tilting, folding or warping (e.g. East African rift system)
Volcanic lakes	a. Maars, calderas and crater lakes (e.g. Crater Lake, Oregon); b. by damming of drainage by lava or volcanic debris (e.g. Lake Kivu, Sea of Galilee)
Landslide lakes	Rockslides, mudflows and screes
Glacial lakes	Large variety of lakes formed in glaciogenic sediments by ice-melting ('kettle' lakes) or through impeded drainage behind or between glaciogenic landforms (e.g. moraine, drumlins)
Solution lakes	Ground solution of limestone, other calcareous rocks, gypsum, rock salt
Fluvial lakes	Plunge pools, delta lakes, meander lakes (oxbows, levées)
Aeolian lakes	Deflation basins; lakes dammed by wind-blown sediment
Shoreline lakes	Damming by material transported by longshore drift; tombolas, spit-lakes
Organic lakes	Blocking by vegetation, beaver dams ('phytogenic' lakes); coral lakes
Anthropogenic lakes	Dams and excavation fills (e.g. Lake Mead, Arizona)
Meteorite lakes	Water accumulating in meteorite craters

considerably younger. In those areas that lay beyond the ice sheets, however, sediments continued to accumulate in lake basins throughout the last cold stage, and these sites often contain records extending back into the last interglacial and beyond. Coring of such open-water sites is technically difficult and relatively expensive, and it is only in the last two decades, with the development of sophisticated hydraulic coring equipment and the formation of international research teams to provide the necessary logistical and financial support, that long records have begun to be obtained from these deep lake basins (e.g. Brauer & Negendank, 2004; Nakagawa *et al.*, 2012).

The importance of these long lake sequences is that they provide a continuous record of changes in ecosystems, lake sediment processes and climate, sometimes over several glacial–interglacial cycles. Hence they offer a means of correlating terrestrial records with those obtained from deep-ocean sequences and from ice cores (section 6.3.3). In addition to these long lake records, fragmentary remains of lake and peat deposits dating to before the Last Glacial Maximum are also found in many localities. In higher latitudes these are often intercalated between tills and other terrestrial sediments (Figure 3.45) and usually reflect limnic accumulation during interglacials and interstadials or, in areas dominated by coarse-grained sediments that are free-draining, during intermittent periods of higher water tables when temporary lakes or mires developed. Although they are useful in stratigraphic subdivision, the palaeoenvironmental significance of these deposits usually lies more in the fossils they contain than in the nature of the sediments themselves. The faunal and floral remains



Figure 3.45 Middle Pleistocene (Cromerian Complex) organic deposits (the ‘Pakefield Rootlet bed’) exposed beneath till at Pakefield, Suffolk, UK (photograph by Mike Walker). The deposits contain a diverse range of plant and animal fossils, and date to around 700 ka. Flint artefacts recovered from the site represent some of the earliest evidence for human presence in northern Europe (Parfitt *et al.*, 2005).

that are commonly found in lake and bog sediments are discussed in Chapter 4.

In this section we are concerned with those *lithological* characteristics of lake, mire and bog deposits that can be used as a basis for palaeoenvironmental reconstruction. The emphasis is placed on sediments that have accumulated during the Late Quaternary (particularly during the Lateglacial and Holocene periods) in North America and northwest Europe, for these are often relatively accessible and can be sampled either in section or with hand-operated corers. As a consequence, they are frequently known in much greater detail than older deposits.

3.9.2 The nature of lake and bog sediments

Lake sediments are both allochthonous and autochthonous in origin, being derived partly from organic production within the lake ecosystem, and partly from the inwash of both organic and inorganic material from around the lake catchment (Cohen, 2003). If the lake is rich in mineral nutrients, organic productivity will be high and the conditions are described as **eutrophic**. The typical deposit will be a green-brown organic-rich sediment known as **nekton mud** or by the Swedish name **gyttja**. In deeper waters, this will be extremely fine in texture and will consist of comminuted and largely unrecognizable plant material, but will grade into **detritus gyttja** with recognizable plant macrofossils (fruits, seeds, leaves, etc.) in shallow waters. Where the lake substrate is calcareous, lime may be precipitated from the water by aquatic plants (e.g. by some of the pondweeds, such as *Potamogeton*, and algae such as *Chara*) and other organisms, and a fine cream-white clay-rich sediment (**marl**) will accumulate. In general, sediments deposited under eutrophic conditions are predominantly autochthonous. Where the lake is poor in nutrients and organic productivity is low (**oligotrophic**), allochthonous sediments will often predominate. If the inwashed materials are low in organic content, clastic sediments (sands, silts and clays) will dominate, the finer grades of sediment being encountered in deeper waters. Where organic productivity is low, but the inwashed materials are dominated by humic substances from, for example, peats around the lake catchment, the lake waters are typically brown in colour due to the dissolved humic acids. In some lakes, a dark-brown **gel-mud** composed largely of colloidal precipitates will accumulate. Such conditions are often described as **dystrophic** and the deposit is known by the Swedish term **dy**. Finally, where the lake waters support a rich diatom flora, the sediments are sometimes characterized by a white siliceous mud composed almost entirely

of diatom frustules (section 4.3), which is termed **diatomite**. These deposits may form under either eutrophic or oligotrophic conditions depending on the ecological affinities of the diatom species.

The nature of lake sediments is also partly related to lake size and the temperature and density variations experienced by lake waters. Lakes can be classified according to whether they are **chemically** or **thermally stratified**, a distinction that may be important for the interpretation of lake sediment sequences as well as their fossil content. The density structure of lake water is controlled by temperature, by solids in the water column and by dissolved compounds (Boehrer & Schultze, 2008). In freshwater, the temperature of maximum density is about 4°C at the surface and declines to about 3.4°C at a depth of 500 m due to increased pressure. In lakes where summer water temperatures exceed 4°C, the surface waters become less dense than bottom waters and a thermal stratification evolves. The warm surface waters (**epilimnion**) are separated from deeper, cooler water (**hypolimnion**) by a marked thermal gradient, termed the **thermocline**. Stratification may also occur in winter due to freezing at the surface. Most lakes in temperate regions therefore experience vertical mixing (breakdown of thermal stratification) twice a year (**diamictic** lakes), during what are called the spring and autumn '**overtur**s'. In high-altitude and high-latitude lakes, however, where warming does not exceed 4°C, mixing may occur only once per year (**monomictic** lakes). Similarly, lakes in low-latitude regions may not cool to below 4°C, and are also usually monomictic. Some lakes (**meromictic**) remain stable throughout the year, and do not overturn, usually because of a strong density gradient as a result of light freshwater overlying denser water at depth, the latter containing high concentrations of solids or dissolved salts. In very general terms, large (>10 km²) and deep (>10 m) lakes tend to be stratified, whereas shallow or small lakes tend to be unstratified.

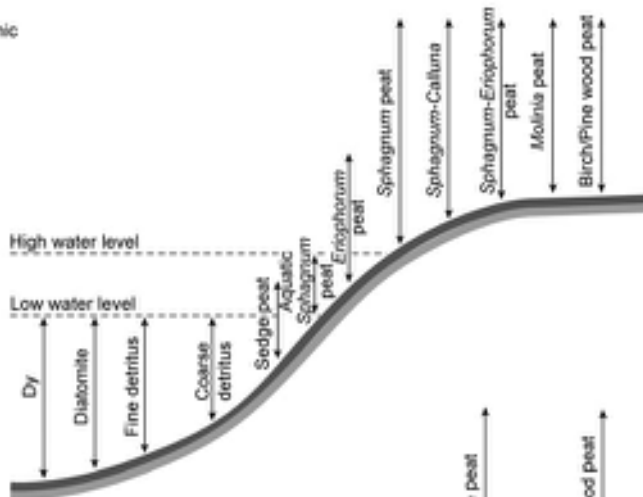
The importance of density/thermal stratification lies in its effects on oxygen levels in the water column, on the preservation of organic detritus and on the influences these have on lithological composition. The epilimnion is usually well oxygenated, while the hypolimnion is **anoxic** (anaerobic), and this leads to important differences in lake chemistry, lake biota and the types of sediment that accumulate. Organic remains, for example, are more likely to survive degradation under anoxic conditions. On the other hand, anoxic conditions may limit the variety and abundance of organisms inhabiting the lake, for they can lead to the production of hydrogen sulphide (H₂S) which, in high quantities, is toxic for most organisms. Exceptions include reducing bacteria that can thrive under

these conditions. Heavy metals are reactive with sulphides and form compounds that are typically black or blue-black in colour. These are usually very obvious in lake sediments, as they contrast markedly with the lighter-coloured oxidized clastic sediments or the brown colour of oxidized organic sediments. The former also often emit a pungent sulphurous odour and have a distinctive chemical composition. Changes in lake stratification and the former degree of oxygenation of lake waters can therefore be inferred from an analysis of sediment chemistry. In diamictic lakes which experience marked stratification, seasonal turnover may cause sudden and large-scale 'die-off' of aquatic organisms, such as algae (notably diatoms), and in some cases this can result in the formation of annual laminations (**organic varves**: Figure 5.23) in the sediments accumulating on the lake floor. A seasonal alternation between oxygenated and anoxic bottom waters may also lead to seasonal production of calcareous deposits, iron oxides or sulphur-rich sediments and hence **chemical varves**.

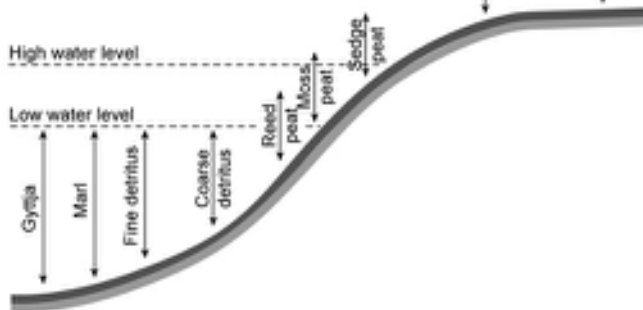
Over time, lakes silt up, plants encroach from the marginal zones, and areas of open water are progressively eliminated. The succession from open water to mire and bog is known as a **hydrosere** and the sediments gradually change in character from muds to peats. Three broad categories of peat can be identified and each is characteristic of a particular stage in the hydroseral succession. These are: (1) **limnic peats** which form beneath the regional water table and which are composed partly of transported plant debris and partly of decayed vegetation formerly growing *in situ*; (2) **telmatic peats** which form in the swamp zone between high and low water levels and which are largely autochthonous in origin; and (3) **terrestrial peats** which accumulate at, or above, the high water mark and which are entirely autochthonous in derivation. Each of these peat types will be composed of the remains of particular peat-forming plants, depending on the stage in the hydrosere and the trophic status of the lake water (Figure 3.46). The rate at which hydroseral succession progresses, and lakes become infilled, depends upon a number of factors, including the size of the lake, the size of the catchment, the rate of sediment supply and productivity within the lake. Many smaller lake basins in northwest Europe and North America have become completely infilled since the end of the last glacial stage, and are currently covered by peat deposits, whereas a number of larger lakes are still accumulating limnic sediments, except perhaps in shallow marginal areas where telmatic and terrestrial deposits have formed.

The terminology applied to peat-forming environments can be confusing. In Europe and Russia, all waterlogged areas where peat develops as a result of reduced vegetal

a) Oligotrophic

Terrestrial
(mires)Telmatic
(swamps)Limnic
(lakes)

b) Eutrophic

Terrestrial
(mires)Telmatic
(swamps)Limnic
(lakes)

decay under anaerobic (anoxic) conditions are usually termed mires. In North America, however, the term 'peatland' is more generally applied to such areas (Charman, 2004). Mires can be divided into those in which the high water table that induces peat formation is a consequence of groundwater conditions, either where drainage is impeded (**soligenous mires**) or where water accumulates in enclosed basins (**topogenous mires**), and those where the water table is maintained by high atmospheric moisture levels (**ombrogenous mires**). Topogenous mires are, of course, part of the hydroseral sequence and are usually referred to as **fens** if eutrophic and **valley bogs** if oligotrophic. Soligenous mires are almost always oligotrophic. Ombrogenous mires (usually termed bogs) can be subdivided into raised bogs and blanket bogs. Raised bogs develop mainly in lowland areas where the peat-forming plants, principally *Sphagnum* mosses, produce a domed surface above the level of the surrounding ground. Raised

Figure 3.46

Some sediment types deposited with increasing depth of water under oligotrophic a) and eutrophic b) conditions (after Birks & Birks, 1980).

bogs form the final stage of topogenous hydroseral successions (Figure 3.47) whereas blanket bogs are typical of upland areas and develop as a continuous cover over the landscape where rainfall is high.

3.9.3 Palaeoenvironmental evidence from lake sediments

Like caves, lakes form natural sediment traps, and analysis of the sedimentary record in lake basins enables inferences to be made about environmental changes around the lake catchment. These include changes in the composition of the vegetation cover, which may reflect both natural (climatically induced) or anthropogenic processes, and changes in the rates of operation of geomorphological processes on catchment slopes (solifluction, gelifluction, etc.). In addition, both the levels of lake waters and the pattern of sedimentation within the lake will be influenced

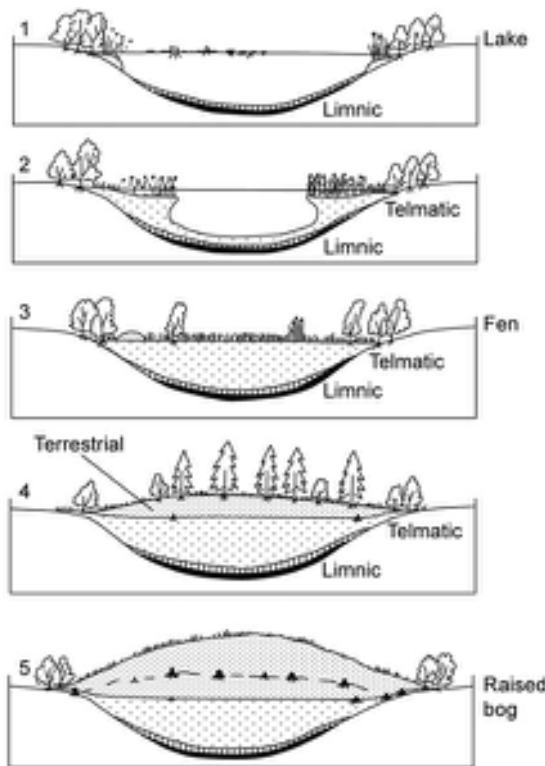


Figure 3.47 Schematic representation of gradual infill of a small lake with lake muds in deep water, fen peat in shallow water, and *Sphagnum* peat formed in a raised or domed bog (modified from Foss, 1987).

by changes in precipitation, while in calcareous lakes the isotopic record of the sediments will be determined, at least in part, by former temperature regimes. Hence it may be possible to make inferences about regional climatic change from the analysis of lake sediment records. These aspects of **palaeolimnology** (the study of ancient lake sediments) are considered in the following section.

3.9.3.1 Lake sediments and landscape changes

It has long been customary for those working on the pollen content of lake sediments to draw parallels between inferred vegetation changes and variations in sediment stratigraphy. In northwest Europe, for example, Lateglacial lake deposits typically consist of a threefold sequence of organic-rich lake muds (often gyttja or clay-gyttja) which overlie and are underlain by mineral sediments with a very low organic

content (see Figure 3.48). The whole sequence often rests upon glacial gravels or sands (deposited during the last cold stage) and commonly lies beneath Holocene peats and organic muds. Palaeobotanical evidence suggests that the two minerogenic horizons accumulated during periods of reduced vegetation cover, the former during the pioneer phase immediately following local deglaciation, while the latter represents the cold phase of the Loch Lomond or Younger Dryas Stadial when a periglacial regime prevailed. Minerogenic material was therefore transferred from the catchment to the lakes, especially during the Stadial phase, when surrounding slopes were affected by freeze-thaw activity, gelifluction and overland flow. The organic-rich sediments, however, contain a fossil record reflecting a vegetation of shrub or open woodland that developed under more stable conditions, as indicated, in turn, by a substantial reduction in the inwash of minerogenic material.

Other approaches to the investigation of lake deposits include analyses of the chemistry and magnetic properties of lake sediments. In Britain, pioneering research on Lateglacial sediments by John Mackereth, Winifred Pennington and colleagues (e.g. Pennington *et al.*, 1972) demonstrated how changes in the chemical composition of lake sediments could most readily be explained if the sediments were regarded as sequences of soils derived from the catchment. Increased soil erosion results in the transfer of large amounts of relatively unweathered material into lake basins, and the mineral fraction of the sediments that accumulates under such conditions is therefore characterized by higher proportions of metal elements, most notably sodium (Na), potassium (K) and magnesium (Mg) and, in certain cases, calcium (Ca), iron (Fe) and manganese (Mn), derived from exposed sediment or bedrock. During periods of reduced erosive activity and soil maturation under a vegetation cover, the mineral material transported into the lakes would be leached of its content of potassium, magnesium and sodium in particular, and during such 'stable' phases, the lake sediments record lower concentrations of those elements. Periods of reduced erosion also coincide with higher values for organic carbon, which result partly from increased aquatic productivity within the lake basins, and partly from the increase in organic matter washed in from the catchment. Where acid soils and peats develop in the catchment, this may result in high iodine/carbon ratios or a high Fe and Mn content in lake sediments.

Chemical data from lake sediments can therefore be used to augment pollen-stratigraphic and other palaeoenvironmental data in the reconstruction of lake catchment histories. Figure 3.49 shows chemical profiles from

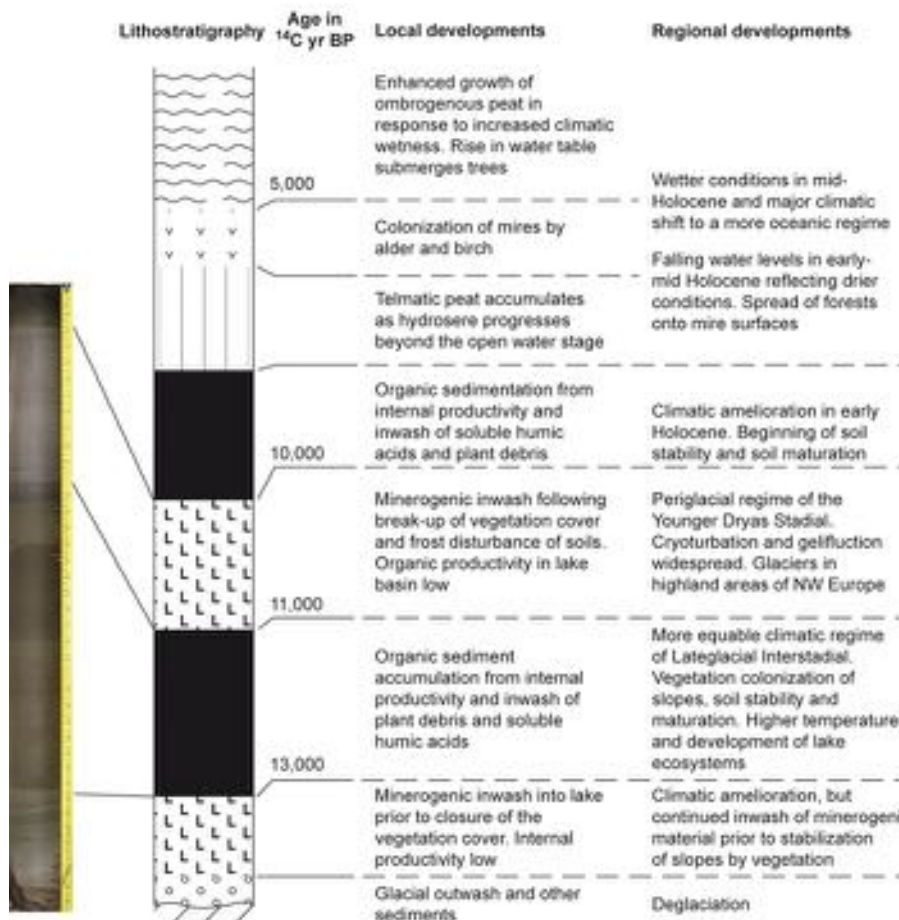


Figure 3.48 Lateglacial and early Holocene environmental changes inferred from lithostratigraphy of a typical northwest European lake and mire sequence.

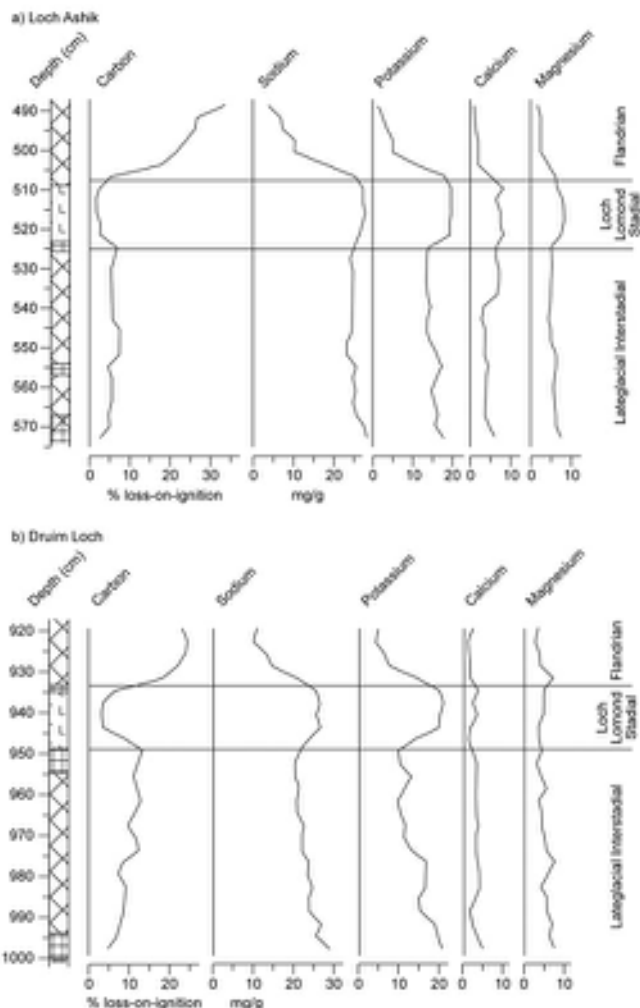
two lake sequences on the Isle of Skye, western Scotland, which date from the Lateglacial and early Holocene periods (c. 15–10 ka). The lowermost sediments accumulated in the basins following the wastage of the last ice sheet from Skye and contain relatively high quantities of Na, K, Ca and Mg, and a low organic carbon content. These data reflect the inwash into the lakes of unweathered, finely comminuted clastic material derived from freshly exposed glaciogenic sediments. Subsequently, an increase in carbon content reflects the gradual stabilization of slopes around the catchments and maturation of soils as the vegetation cover expanded in response to climatic amelioration. The reduction of mineral inwash is marked by the decline in base elements in the sediment profile. A return to cold conditions during the Loch Lomond (Younger Dryas)

Stadial (13–11.5 ka) led to the break-up of the interstadial vegetation cover, the destruction of soils by freeze-thaw and frost heave, and the renewed inwash of mineral material into the basins. These environmental changes are reflected in the reduced organic carbon content of the lake sediments and the significant increase in base element content. The abrupt climatic amelioration at the beginning of the Holocene is marked by a sharp upturn in the organic carbon curve and a marked decline in the curves for Na, K, Ca and Mg. In general terms, therefore, the chemical record from these lake sediments can be read as a proxy for regional climatic change (Walker & Lowe, 1990).

Anthropogenic effects on the landscape during the Flandrian can also be inferred from the chemical record of lake sediments. In his pioneering work, Mackereth

Figure 3.49

Variations in the abundance of selected chemical elements in Lateglacial and early Holocene sediments from two sites in the Isle of Skye, Inner Hebrides, Scotland: a) Loch Ashik; b) Druim Loch (from Walker & Lowe, 1990).



(1965) noted the increase in concentration of base elements in several lake cores in northern England following the decrease in woodland cover recorded in pollen records at c. 6 ka. This, he suggested, was a reflection of increased soil erosion around the lake catchments following forest clearance by Neolithic people. Accelerated soil erosion arising from human activity during the mid- and late Holocene is also reflected in the significantly increased sediment influx into lake basins in many parts of the world (Bell & Walker, 2005; Boardman & Poesen, 2006). Analysis of rates of sediment accumulation in fifty lakes in Britain and Ireland (Figure 3.50) has shown that accelerated sedimentation rates typically occur in those basins where there is pollen analytical evidence for human activity (Edwards & Whittington, 2001). For example, at Braeroddach Loch near

Aberdeen in northeast Scotland, the onset of pastoral activity after c. 5.39 ka, as indicated by the pollen record, resulted in a threefold increase in sediment accumulation, while during the period of modern agricultural practices (radiocarbon dated to 370 ± 250 years), about 25 per cent of the sediment deposited during the past 12 ka was accumulated (Figure 3.50b). Overall, lakes with no evidence for accelerated sedimentation, or where it occurs very late, are all found in the west or north of the British Isles (Figure 3.50a). Periods of increased sedimentation have been dated to 5.9, 4.9 and 3 ka (Figure 3.50c). Similar increased rates of erosion during the late Holocene have been noted at sites in Europe. A record from Dallun So in Denmark, for example, shows that the lake was relatively insensitive to catchment disturbance during the Neolithic and Early

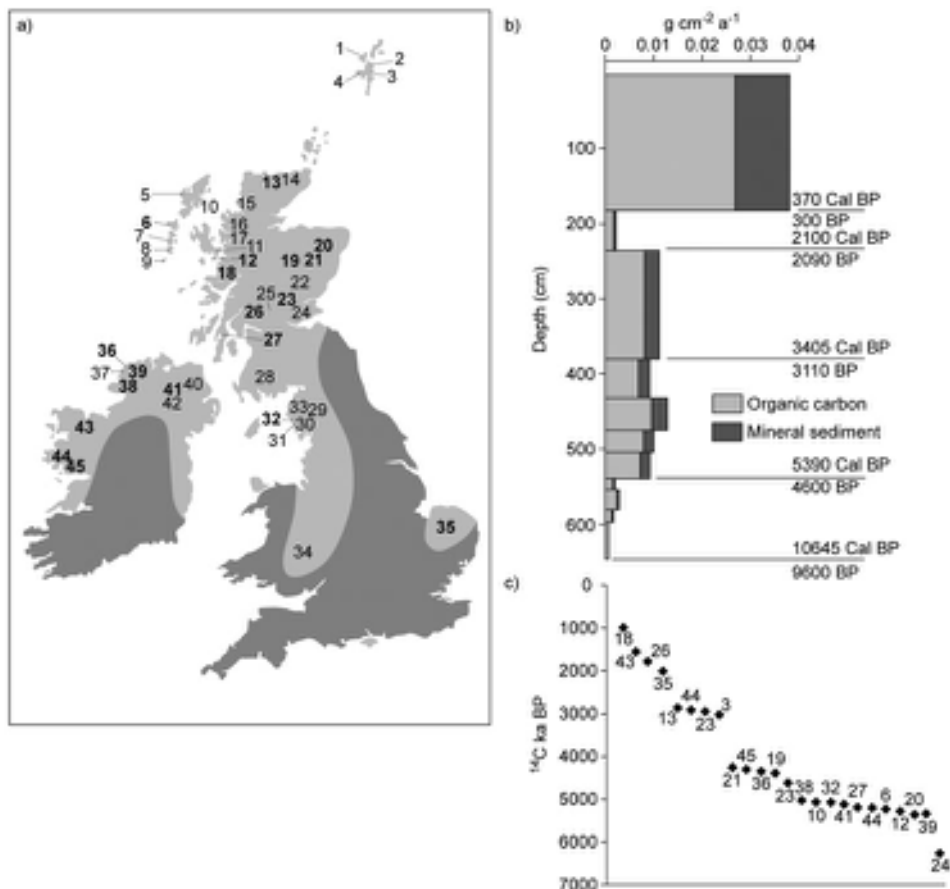


Figure 3.50 Lake sedimentation in the British Isles. a) Locations of studied lakes showing those with (bold) and those without accelerated late Holocene sediment accumulation. b) Record of sediment deposition at Braeroddach Loch, Scotland. c) Dates at which accelerated sedimentation occurs at sites in (a); note that the timescale is in ^{14}C yr BP in (c) and in both calibrated and ^{14}C yrs in (a) after Edwards & Whittington, 2001, b) after Edwards & Rowntree, 1980; from Bell & Walker, 2005).

Bronze Age periods (*c.* 5.9–3.0 ka), but there were dramatic impacts on the lake ecosystem by environmental changes and resultant erosion associated with a major phase of deforestation at the transition from the Late Bronze Age to the Pre-Roman Iron Age around 2.5 ka (Bradshaw *et al.*, 2005). Lakes in North America generally show few signs of increased sediment input resulting from human impact until after the European contact. At Crawford Lake, Ontario, Canada, however, there is evidence for increased nutrient input caused by Iroquoian horticultural activity from AD 1268–1486, and this elevated lake productivity caused bottom water anoxia and changed diatom community structure within the space of a few years. A second phase of cultural eutrophication starting in AD 1867 initiated by Canadian agricultural disturbance also

increased lake productivity but, interestingly, had comparatively less impact on diatom assemblages and carbon-storage pathways in the lake ecosystem than the initial Iroquois disturbance (Ekdahl *et al.*, 2004).

Changes in lake sediment chemistry are also associated with changes in the magnetic properties of the sediments, and these can often be diagnostic of the types of processes operating around the catchment. The quantity, size and mineralogy of ferrimagnetic particles in particular can be established using magnetic susceptibility measurements. In some lake sequences, magnetic parameters have been used to reconstruct vegetation patterns around the catchment and to relate these to patterns of climate change (e.g. Geiss *et al.*, 2003). In other lake contexts, magnetic data reflect increased erosion rates caused by human

disturbance, and offer insights into the type of land use practised in the catchments. For example, at Gormire Lake in northeast England, mineral magnetic properties combined with other proxy records (pollen analysis, organic biogeochemical analysis) formed the basis for the development of a catchment history which revealed major phases of deforestation and erosion during the Late Iron Age/ Romano-British and Medieval/post-Medieval periods. Before and between these periods, the lake catchment appears to have been mainly forest covered and erosion more limited and/or sporadic (Oldfield *et al.*, 2003).

3.9.3.2 Lake-level variations and climatic changes

Changes in water level in lake basins in temperate regions can be caused by a range of local factors, including the

silting up of the lake, blockage of outflowing streams by vegetation growth or by landslips, or the influence of human activity on lake catchments (see above). However, regionally synchronous changes in lake level can be assumed to be climatically driven, in other words they reflect changes in precipitation regime (Magny, 2007). A range of sedimentological characteristics can be employed to reconstruct histories of lake-level change (Figure 3.51). These include grain-size variations (coarser deposits correspond to near-shore areas); lithological properties (littoral sediments are often characterized by larger quantities of organic matter from near-shore vegetation, while fine lake marl is deposited in deeper water); sediment hiatuses, which mark either erosion or non-deposition during phases of lake lowering; and the macroscopic components of lake sediments (molluscan abundance increases in near-shore sediments; ostracods are more common in deeper

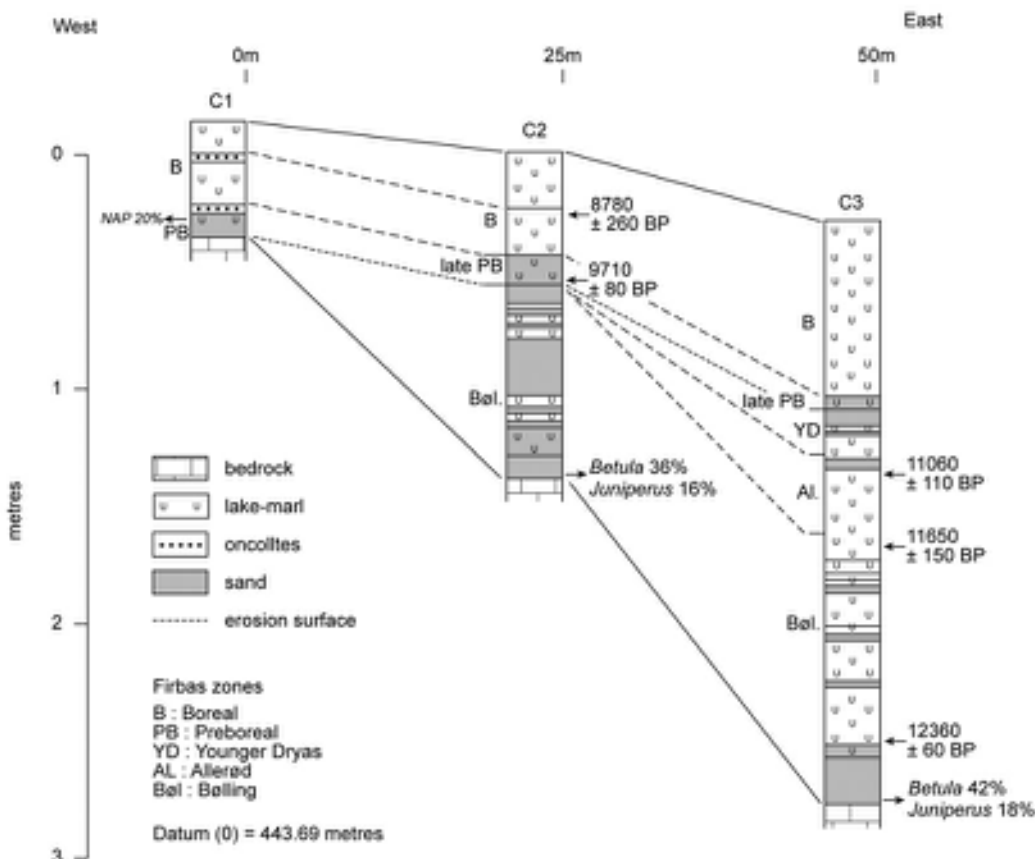


Figure 3.51 The lake sediment sequence at Sevrier-Les-Charretières, Lake Annecy, France. Deeper water phases are indicated by the marl units, and shallow water phases by sand layers and oncolites (carbonate concretions). Erosion surfaces in the marginal core mark episodes of very low lake level (after Magny, 2001, reprinted with permission from Elsevier).

water). Plant macroscopic remains also provide evidence of contrasting shallow and deeper water communities (Magny, 2001).

During the Lateglacial period in Europe, significant fluctuations in lake level have been recorded and have been linked to regional changes in climate. In the Netherlands, for example, higher water levels during the early and middle interstadial (Bølling–early Allerød: c. 14–13 ka), probably related to melting of permafrost under a warmer climatic regime, were followed by fluctuating lake levels in the later interstadial. During the Younger Dryas cold stage (12.9–11.7 ka), lake levels fell markedly as climate became drier (Bos *et al.*, 2006). In Switzerland, lake-level records for the Lateglacial and early Holocene show a close correlation with the climatic sequence reflected in the Greenland ice-core records (section 3.11). Lower lake levels are recorded during the warmer episodes of the Interstadial (GI-1e, GI-1c and GI-1a; Figure 1.7) during the middle period of the Stadial (GS-1), during the GS-1/Holocene transition, and immediately after the 11.2 ka event. Higher lake levels correspond with the colder phases of the Interstadial, that is, with GI-1d and 1b, early and late GS-1 and with the 11.2 ka event (Magny, 2001).

Even during the Holocene, however, regional climate changes appear to have been of sufficient amplitude to affect lake levels in temperate Europe. For example, a compilation of Holocene lake-level records obtained from twenty-six lake basins located in the French pre-Alps and Swiss Plateau show common tendencies, with evidence for as many as fifteen distinct lake-level highstands; these generally accord with episodes of increased climatic instability inferred from Greenland ice-core records and with North Atlantic ice-raftering events (Magny *et al.*, 2003). The data suggest that the Greenland ice sheet, the North Atlantic Ocean and north-central Europe were responding to common climatic forcing agencies over the course of the Holocene, with variations in solar activity (section 7.6.4.1) perhaps playing a major role (Magny, 2004). In similar vein, changes in level of a number of Swiss lakes during the last 3.5 ka correlate closely with fluctuations in extent of Swiss Alpine glaciers, suggesting regulation of both by winter cooling and summer moisture, a correspondence that has again been attributed to variations in solar activity (Holzhauser *et al.*, 2005).

Lake-level records also enable inferences to be made about changes in atmospheric circulation patterns. In northern Europe, for example, lakes during the early Holocene show conditions similar to or drier than present across southern Britain, southern Scandinavia and into the eastern Baltic, while wetter conditions obtained along the west coast and into central Europe. This pattern is

consistent with the development of an anticyclone over the decaying Scandinavian ice sheet with enhanced south-westerly flow along the west coast and easterlies south of the ice. After c. 9 ka, falling lake levels suggest drier conditions than at present over much of northern Europe, although wetter conditions are indicated by higher lake levels in the far north, along the west coast, in eastern Finland and in western Russia. Differences in lake status during the mid–late Holocene are consistent with strengthening of the blocking anticyclone over the Baltic Sea in summer, resulting in a more meridional circulation than that which obtains today (Yu & Harrison, 1995). Fluctuating lake status in central and southern Europe during the Holocene has been attributed to alternate southwards/northwards displacement of the Atlantic westerly jet stream. A southward movement of the jet could have led to enhanced cyclonicity, with the resulting increase in precipitation being reflected in higher lake levels (Harrison *et al.*, 1993; Magny *et al.*, 2003).

3.9.3.3 Lake sediments and palaeotemperatures

In calcareous lake sediments, a direct relationship has been found between stable isotope variations in lake sediments and palaeotemperatures, notably the relation between water temperature and $\delta^{18}\text{O}$ of lacustrine carbonates during equilibrium precipitation. For example, at Lake Torreberga in Sweden, the shift in $\delta^{18}\text{O}$ at the end of GS-1 was considered to represent an increase in mean annual air temperatures of c. 5.3°C (Hammarlund *et al.*, 1999), while in Hawes Water, northern England, a $\delta^{18}\text{O}$ record from carbonate sediments provided evidence for climatic warming at c. 12.5 ka, and four submillennial climatic events during the course of the Lateglacial Interstadial (GI-1) prior to the onset of the Loch Lomond/Younger Dryas Stadial (GS-1), that could be correlated with the climatic signal in the Greenland ice-core record (Jones *et al.*, 2002). Although interpretation of the $\delta^{18}\text{O}$ record in terms of temperature is not always straightforward (Leng & Marshall, 2004), and these data are perhaps best employed in conjunction with other palaeoclimatic and palaeoenvironmental indicators (e.g. Hammarlund *et al.*, 2002, 2003), stable isotope ratios in lake sediments do, nevertheless, offer a potentially valuable independent method of inferring palaeotemperature changes and trends.

In addition to palaeotemperature reconstructions, stable isotopes in lake sediments offer a basis for a number of other palaeoclimatic inferences. These include seasonal changes in precipitation and temperature, decadal and millennial variations in precipitation regime, and

linkages between lake sediment records and atmospheric circulation. Details of these and other aspects of climate-related isotopic records in lake sequences can be found in Leng (2004) and Leng *et al.* (2013).

3.9.4 Palaeoenvironmental evidence from mire and bog sediments

In topogenous mires and bogs that develop over former lake deposits, the different types of peat may also provide indications of former climatic conditions. The rate at which hydroseral succession has proceeded cannot usually be interpreted simply in terms of climatic change, as local site factors will often exert a degree of control over the direction and rate of the succession (Charman, 2004), but in certain circumstances, it may be possible to make inferences about variations in the height of former water tables and hence about former precipitation levels. Good examples would be where there is evidence for disturbance of the hydrosere (e.g. a transition from bog peat to reedswamp peat) reflecting a major change in local environmental conditions, such as a rise in silty water, possibly resulting from a change to a wetter climatic regime; or the occurrence of tree roots in a raised mire sequence, which may indicate invasion of the bog surface by trees during a drier climatic period.

3.9.4.1 Palaeoprecipitation records from ombrotrophic peats

Ombrotrophic peats can provide valuable palaeoclimatic information. A number of factors determine the rate and type of peat formed, including temperature (which affects metabolic and decomposition rates), local topography and groundwater pH. The most important control, however, is the height of the local water table. Above the water table, decomposition can take place relatively rapidly because of increased microbial activity under aerobic conditions. The height of the water table fluctuates throughout the year due to seasonal variations in regional drainage conditions but, when examined over a timescale of decades, it will tend to have a minimum level, below which little decomposition can take place. This lower permanently waterlogged zone is termed the **catotelm**. Above this, a shallow near-surface zone (the **acrotelm**) is regularly exposed for at least a brief period each year, and perhaps experiences prolonged dryness during the summer. The thickness of the acrotelm will be determined by a combination of water supply and summer drying, especially in ombrotrophic peats that are totally dependent upon precipitation for their water supply. Ombrotrophic peats therefore contain a record of past

climatic regimes and a range of palaeoclimatic data can be obtained from the careful analysis of peat stratigraphy. Peat chronologies are usually based on radiocarbon dating, although increasingly tephra horizons (section 5.5.2) are being used as a basis for correlation and dating (Langdon & Barber, 2004, 2005).

In the early years of the twentieth century, data from Scandinavian peat bogs enabled the Scandinavian botanists Blytt and Sernander to identify what they considered to be clearly defined climatic episodes (Pre-Boreal, Boreal, Atlantic, Sub-Atlantic, Sub-Boreal) in the plant macrofossil record of Holocene peat bog sequences in northern Europe. What became known as **the Blytt–Sernander climatic scheme** was subsequently related to regional pollen zones (section 4.2.4), and was enthusiastically adopted by palaeoecologists and particularly by archaeologists as the basis for climatic subdivision of the Holocene. For some time now, however, it has been apparent that the relationships between peat stratigraphy, pollen assemblage zones and climatic change are much more complicated than was envisaged in the 1920s and, as a consequence, the scheme has now been largely abandoned, although, curiously, the terminology still appears even in current literature (e.g. Roos-Barraclough *et al.*, 2004). Early work on peat stratigraphy also attempted to identify horizons in peat sequences where there had been rejuvenation of peat growth as reflected, for example, by a change from dark, well-humified peats to light-coloured, less humified *Sphagnum* peats (Figure 3.52a). These became known as **'recurrence surfaces'** and were believed to mark a change to wetter mire surface conditions brought about by an increase in precipitation. Perhaps the most famous (or infamous) of these was the **grenzhorizont** (boundary horizon) of northern Germany, first described by Weber more than 100 years ago, and radiocarbon-dated to c. 500 BC, the transition from the Bronze to the Iron Age on the archaeological timescale. As with the Blytt–Sernander scheme, however, questions have been raised about the validity of recurrence surfaces as regional palaeoprecipitation indicators. Radiocarbon dating has shown that not only do ages of inferred 'recurrence surfaces' from nearby sites differ by several hundred years, but that there may be considerable within-site variations in both age and stratigraphic position of individual 'recurrence surfaces' (Figure 3.52b). This partly reflects changing rates of peat growth on different parts of a mire surface, but it might also indicate mixing of carbon residues between peat horizons during oxidation and decomposition of the peat-forming materials. Where this has occurred, it can lead to major discrepancies between radiocarbon dates from the same stratigraphic horizon. A second problem relates to the



Figure 3.52 a) A peat profile at Bolton Fell Moss, northern England, showing a lower dark, well-humified peat overlain by a lighter-coloured, less well-humified peat. The boundary between the two peat units has often been described as a 'recurrence surface', reflecting a regional change from drier to wetter conditions (photograph by Mike Walker). b) A peat section from Store Vildmose, Denmark, showing both lateral and vertical alternations in darker and lighter peat layers. The boundaries between units characterized by different degrees of humification are marked by white pins in the peat face (photograph by Keith Barber, Southampton University, UK).

extent to which recurrence surfaces develop in response to regional climatic (i.e. precipitation) changes, or whether they may also form as a result of site-specific factors, such as local changes in mire hydrology, particularly where human activity has been a factor (Evans & Warburton, 2007).

More recent approaches to climatic reconstruction based on ombrotrophic peat sequences have focused on down-profile variations in indicators of surface wetness change, which provide a more realistic portrayal of trends in past climate than individual features of the peat stratigraphy (Charman, 2004). A widely used technique that has been applied to both blanket peats and raised mire peats is peat humification (Chambers *et al.*, 2011). This employs colorimetric methods, and the speed and relative ease of analysis means that high temporal resolution measurements are possible. Although most humification studies have been undertaken in Britain and Ireland, where proximity to the North Atlantic Ocean means that the peat bogs tend to be more sensitive to changes in effective precipitation (e.g. Blackford & Chambers, 1995; Charman *et al.*, 2009), mire surface wetness records have been generated from other parts of Europe (Roos-Barracough *et al.*, 2004; Andersson & Schoning, 2010), from New Zealand (McGlone & Wilmshurst, 1999) and from Alaska (Payne & Blackford, 2008). These records largely reflect changes in precipitation which, in western Europe, are due largely

to changes in the strength and location of the westerlies, linked to large-scale North Atlantic Ocean and atmospheric circulation (Charman *et al.*, 2009).

A second approach to the reconstruction of mire surface wetness records involves the use of plant macrofossils (Mauquoy *et al.*, 2010). This technique exploits the strong response of peatland plants, especially of bryophytes (notably *Sphagnum*) to changes in surface wetness. Some species (e.g. *Sphagnum* sect. *Cuspidata*) are associated with wetter conditions on the mire surface, whereas others such as *Sphagnum* sect. *Acutofolia* are characteristic of drier habitats. Hence, down-core changes in plant macrofossil assemblages will provide evidence of surface wetness changes and, by implication, of changes in effective precipitation (Barber *et al.*, 2000, 2003). Figure 3.53 shows a palaeoprecipitation record from Walton Moss, northern England, derived from plant macrofossil records. The sequence extends from the early Holocene to the present and shows significant wet shifts at 7.8 ka, 5.3 ka, 4.41–3.99 ka, 3.5 ka, 3.17–2.86 ka, 2.32–2.04 ka, 1.75 ka, 1.45 ka, 0.3 ka and 0.1 ka. Time-series analysis suggests that these climatic changes are not stochastic, but there are underlying periodicities of c. 600 and c. 100 years between wet-shifts (Hughes *et al.*, 2000).

A third technique that has been applied to ombrogenous peat sequences in order to derive a record of mire surface wetness is that of testate amoebae analysis. Testate amoebae

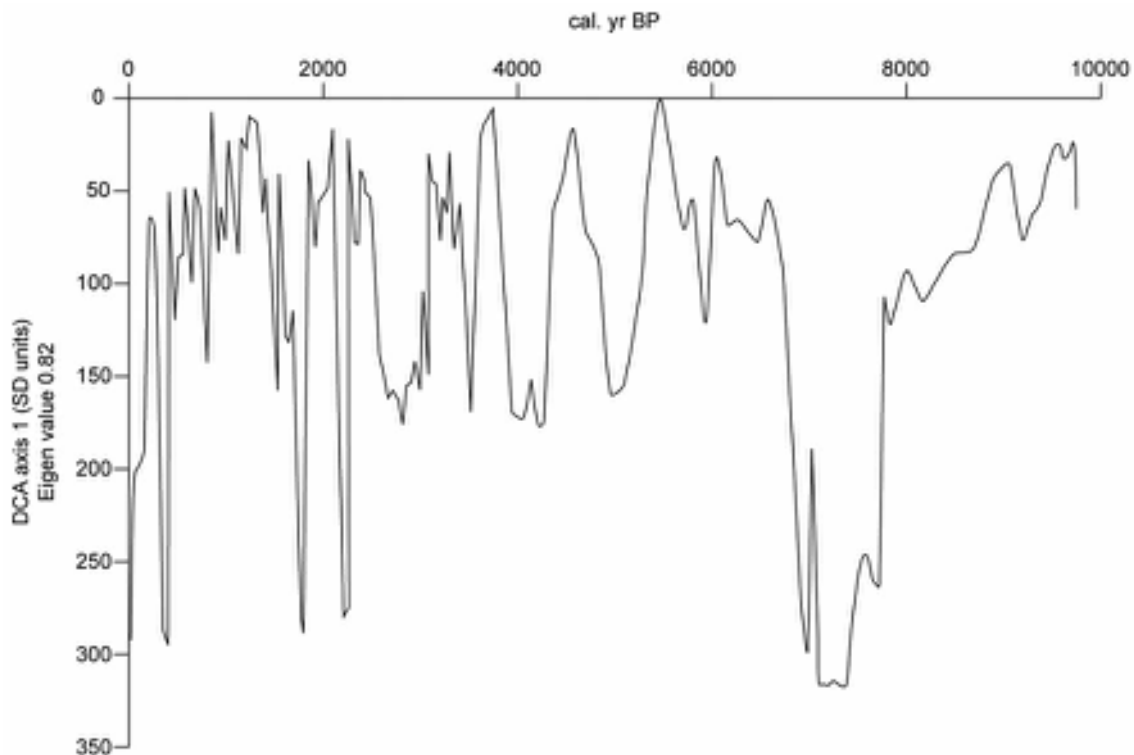


Figure 3.53 Reconstructed mire-surface wetness changes at Walton Moss, northern England. Increased wetness (and, by implication, higher levels of precipitation) is reflected in the higher values of detrended correspondence analysis (DCA) shown on the y axis. DCA is a standard multivariate statistical technique which is used here to analyse the variation in plant macrofossil components through the peat profile and to relate them to particular controlling factors (such as surface wetness) (after Hughes *et al.*, 2000, reprinted with permission of SAGE).

(rhizopods) are a group of the protozoa that are abundant in almost all peatland environments and certain species are reflective of surface wetness changes (Charman *et al.*, 2000). Again, therefore, down-core variation in fossil testate amoebae can be read as a record of surface wetness changes (Booth, 2002). Testate amoebae can also provide other insights into peatland environments, for example in characterizing hydroseral transitions from open water to fen, and from pioneer raised mire to ombrotrophic bog (Elliott *et al.*, 2012). Other proxies used to reconstruct variations in bog surface wetness include the ratios of abundances of *n*-alkanes (components of plant lipids) in selected plant macrofossils (Nichols *et al.*, 2006), and fungal spore records (see Chambers *et al.*, 2012, for an overview).

Increasingly, however, these various methods are being used in combination, for such a multi-proxy approach enables changes in each proxy reconstruction to be validated against another, thereby producing a more

reliable palaeoclimatic interpretation and strengthening the correlations with other climatic reconstructions (Mauquoy *et al.*, 2004; Langdon & Barber, 2005; Nichols *et al.*, 2006). A multi-proxy ombrogenous peat record for the past 7.5 ka from Temple Hill Moss, southeast Scotland is shown in Figure 3.54. The record not only contains a number of the wet-shifts identified at Walton Moss (Figure 3.53), but it also displays the same millennial-scale periodicity of 1,100 years suggesting that both sites are responding to a regional climatic forcing factor (Langdon *et al.*, 2003).

3.9.4.2 Stable isotope records from ombrotrophic peats

In ombrotrophic bogs, which are entirely rain-fed, the isotopic composition of rainwater (reflected in D/H and $^{18}\text{O}/^{16}\text{O}$ ratios) will be reflected in plant tissue and, in theory, isotopic variations through the peat sequence can

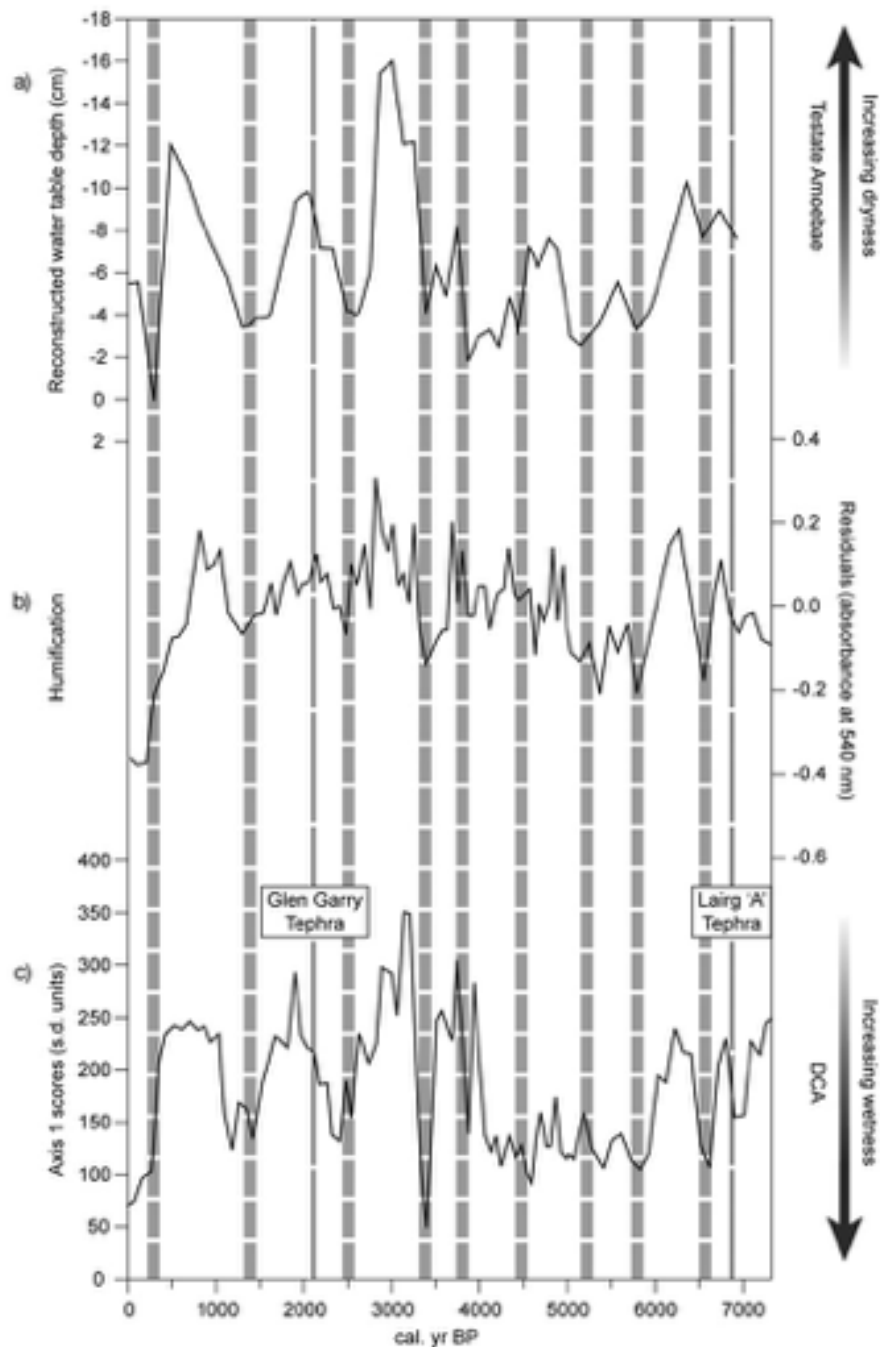


Figure 3.54 Proxy climate reconstructions from Temple Hill Moss, southeast Scotland. a) Variations in water table depth based on testate amoebae analysis. b) Peat humification record. c) Detrended correspondence (see Fig. 3.53) based on plant macrofossil data. The peaks in the curves represent drier intervals and the troughs wetter episodes. The vertical shaded bars highlight periods of wetter/coolier climate (after Langdon *et al.*, 2003).

be linked to past changes in temperature. If so, then the stable isotope record can be read in terms of past precipitation and temperature variations. In practice, however, the situation is much more complex, and there is considerable uncertainty about how isotopic ratios from peat should be derived and interpreted, principally because of strong inter-species variation between different plants in the ways in which water is moved to the growing tissues (Charman, 2004).

To a degree, some of these problems have been resolved by the recent development of more sophisticated analytical techniques (e.g. continuous flow isotope ratio mass spectrometry), which have enabled oxygen isotopic values to be measured on only a few mg of cellulose (Loader *et al.*, 2007). This means that genus-specific analysis can now be carried out, thereby avoiding complications arising from the different chemical signatures in different plants. Using the established relationships between modern temperature and the $\delta^{18}\text{O}$ precipitation signal, Daley *et al.* (2009, 2010) developed a Holocene climate record for Nova Scotia and northern England, although in the latter case the reconstructions show larger temperature anomalies than have been found in other archives. This may reflect a range of factors, including the influences of evaporation/peatland surface wetness, and changing $\delta^{18}\text{O}$ of the precipitation source. More promising appears to be the compound-specific analysis of hydrogen isotope ratios obtained from *Sphagnum* leaves; the reliability of this approach has been tested on modern peat surfaces and through comparisons with bog-surface wetness trends over the last 3 ka, obtained from other proxy indicators (Nichols *et al.*, 2010). The results suggest that the interpretation of stable isotope ratios in ombrotrophic peat is less problematic when restricted to selected compounds and plant species.

3.9.4.3 Human impact recorded in ombrotrophic peat

The effects of prehistoric and historic human activity are often preserved in the geochemical record of peat sequences. Arable farming, for example, may be reflected in an increase in the immobile elements silicon (Si) and titanium (Ti) as these are readily removed from bare ground by wind action and subsequently deposited on peat surfaces (Hölzer & Hölzer, 1998). The intensity and timing of farming activity can be corroborated by pollen-analytical and other evidence (Lomas-Clarke & Barber, 2006). The occurrence of these and other chemical elements (K, Ca, Rb, Sr, etc.) in peat profiles provide additional evidence of human impacts, such as an increase in atmospheric dust flux from exposed soils following anthropogenic

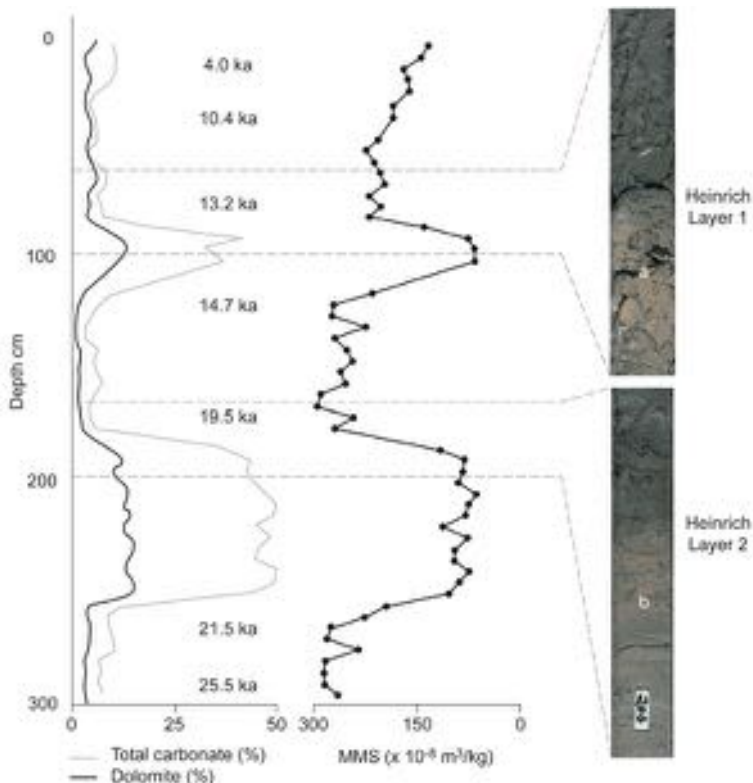
woodland clearance (Martínez-Cortizas *et al.*, 2005), while historic and prehistoric mining and metallurgy is reflected by the presence in peat sequences of heavy metals such as lead and mercury (Martínez-Cortizas *et al.*, 1997; Farmer *et al.*, 2009).

3.10 THE DEEP-SEA SEDIMENT RECORD

3.10.1 The nature and origin of ocean sediments

On the deep-ocean floors, sediments have been accumulating in a relatively undisturbed manner for thousands, or even millions, of years. They consist partly of terrigenous deposits, that is, detrital material derived from erosion of the land masses surrounding the ocean basins, and partly of biogenic sediments composed largely of accumulations of the calcareous and siliceous skeletal remains of micro-organisms that formerly lived in the ocean waters. Terrigenous detritus (ranging in size from fine sand to clay) arrives on the ocean floor by a number of different pathways, but the principal transporting agencies are turbidity currents, bottom currents, wind and ice. In the mid- and high latitudes, both coarse and fine terrigenous detritus appears to have been delivered to the ocean floors mainly during glacial periods, reflecting in particular the ice-rafting of glacially eroded debris (see below) and, to a lesser extent, the transport of aeolian sediments from the greatly expanded periglacial regions (section 3.4). Indeed, wind-blown sediment may have constituted a major proportion of the fine detrital input in low latitudes during glacial times. Sea-level lowering of over 100 m would also have resulted in the discharge of large quantities of terrestrial debris from the major rivers as they flowed across the continental shelves, and this material would subsequently have been spread down the continental slopes and across the abyssal plains in gravity-controlled sediment flow.

In many ocean sediment sequences, therefore, a broad correlation can be detected between the deposition of terrigenous material and former glacial episodes, and this is reflected most clearly in the large volumes of **ice-raftered debris (IRD)** that are found in deep-ocean sediments. In the North Atlantic, for example, IRD deposition appears to have been by far the most important mechanism for supplying terrigenous sediment to the ocean floor and it has been estimated that IRD may make up as much as 40 per cent of the total amount of sediment deposited in Quaternary cold stages (Robinson *et al.*, 1995). Cycles of IRD deposition in the North Atlantic during the course

**Figure 3.55**

Heinrich layers in deep-ocean sediments. The two core segments (right) were recovered from the northwestern Labrador Sea between Baffin Island and Greenland (lat. $61^{\circ}30'N$; long. $58^{\circ}26'W$). Sedimentological analyses (left) show that the Heinrich layers are characterized by significantly higher levels of carbonate and mass magnetic susceptibility (MSS), and in the cores they are reflected in a colour change from grey to brown ('a' and 'b' mark the end of Heinrich events 1 and 2, respectively). The two Heinrich layers shown here are radiocarbon-dated to 14.7–14.2 ka BP (c. 18.0–17.4 k cal. BP) and 21.5–19.5 ka BP (c. 25.6–23.3 k cal. BP), and are coeval with Heinrich events 1 and 2 in the eastern North Atlantic (sedimentological data from Andrews & Tedesco, 1992; photographs by John Andrews, University of Colorado, USA).

of the last cold stage are reflected in distinctive layers of glacially derived material in the ocean sediments around 45°N (Figure 3.55). These have been termed **Heinrich layers** and reflect episodic deposition of carbonate-rich IRD from icebergs drifting eastwards across the Atlantic from the margins of the Laurentide ice sheet (Heinrich, 1988; Hemming, 2004). The **Heinrich events** appear to have had a major effect on the global, or at least the Northern Hemisphere, climate system and their significance in the context of the history of the North Atlantic during the course of the last cold stage is discussed in section 7.4.

In the deeper oceans, the sediments tend to be finer grained and are often dominated by biogenic material consisting of the accumulations of the carbonaceous and siliceous remains of micro-organisms that formerly lived in the ocean waters. Such sediments are known as **marine oozes** (section 4.10) and are frequently characteristic of interglacial or warmer episodes. They contain recognizable fossil remains, and these provide a record of ocean circulation, ocean water temperature and, by implication, atmospheric temperatures throughout the Quaternary. The use of fossils in the reconstruction of changing patterns of oceanic circulation is considered in Chapter 4.

3.10.2 Oxygen isotope ratios and the ocean sediment record

3.10.2.1 General principles

An extremely important source of palaeoenvironmental information is the chemical and isotopic content of the marine organisms contained within ocean sediments. Variations in the ratios between, for example, aluminium, barium, calcium and cadmium, and between the isotopes of carbon, oxygen and uranium, reflect the combined influences of circulation, nutrient supply and water temperature, and therefore provide a basis for the reconstruction of oceanographical changes. Some of these lines of evidence are discussed in section 4.10. However, it is the application of oxygen isotope analysis to deep-ocean sediments that has had by far the greatest impact in Quaternary science. The method not only provides one of the principal indices of global environmental change during the Quaternary, but also serves as a basis for global stratigraphic subdivision and correlation (Chapter 6). Moreover, it was the marine oxygen isotope record that first convincingly demonstrated the influence of the

Milankovitch radiation cycles on the earth's climatic history (Imbrie & Imbrie, 1979). Oxygen isotope analysis has already been touched upon in the discussion of cave speleothems (section 3.8.4.2) and lake carbonates (section 3.7.3), but because deep-ocean oxygen isotope stratigraphy has such far-reaching implications for Quaternary science, the principles and applications of the method are discussed here in more detail. An overview and historical review of oxygen isotopes in marine Foraminifera is provided by Pearson (2012).

Oxygen can exist in three isotopic forms (^{16}O , ^{17}O and ^{18}O) but only two (^{16}O and ^{18}O) are of importance in oxygen isotope analysis of marine deposits. $^{18}\text{O}/^{16}\text{O}$ ratios in the natural environment vary between about 1:495 and 1:515, with an average of approximately 1:500. This means that only about 0.2 per cent of oxygen in natural circulation is ^{18}O . Ratios of oxygen isotopes are measured not in absolute terms but as relative deviations ($\delta^{18}\text{O}$ per mil) from a laboratory standard value. The standards normally employed are **PDB** (belemnite shell: see section 5.3.2) for the analysis of carbonates and **standard mean ocean water (SMOW)** for the analysis of water, ice and snow. The latter is used in the isotopic analysis of glacier ice cores (section 3.11). PDB is +0.2 per mil in relation to SMOW. The standard materials are monitored and distributed to laboratories by the International Atomic Energy Agency in Vienna.¹⁰ Mass spectrometric analyses are carried out on CO_2 gas prepared from the fossil material and on the standard reference material. Oxygen isotope ratios are then expressed as positive or negative values relative to the standard ($\delta = 0$), thus:

$$\delta^{18}\text{O} = 1000 \times \frac{{}^{18}\text{O}/{}^{16}\text{O}_{\text{sample}} - {}^{18}\text{O}/{}^{16}\text{O}_{\text{standard}}}{{}^{18}\text{O}/{}^{16}\text{O}_{\text{standard}}}$$

A $\delta^{18}\text{O}$ value of -3 per mil indicates that the sample is 0.3 per cent or 3.0 per mil deficient in ^{18}O relative to the standard. A $\delta^{18}\text{O}$ value of -10 per mil is even more deficient in ^{18}O and is therefore described as **isotopically lighter** than a value of -3 per mil. It is important to understand this because reference is commonly made in the literature to isotopically 'light' and isotopically 'heavy' segments of oxygen isotope records (see below).

The variation in the isotopic composition of ocean waters over time can be reconstructed from the $\delta^{18}\text{O}$ values of carbonate shells and skeletons preserved in deep-sea sediments. Many marine organisms secrete (or build) carbonate structures and oxygen is abstracted from seawaters for this purpose. Thus, the oxygen isotope ratios in fossil carbonates buried in sediments on the ocean floors should

reflect the ratios prevailing in the oceans at the time of their secretion. Analyses have been carried out on the remains of a range of marine micro-organisms, but by far the most widely used fossils are the tests of the planktonic (near-surface) and benthic (deep-water) Foraminifera (section 4.10). Data from a large number of ocean cores show that, over time, the isotopic balance of the world's oceans has changed. Several factors are involved in this process, but the two principal elements are the isotopic composition of the ocean waters at the time of secretion and water temperatures. The former largely reflects changes in land-ice volume, and it is important to appreciate why this is so before moving on to consider other influences on the marine isotope signal.

3.10.2.2 Glacial ice storage and the marine oxygen isotope record

Changes in $\delta^{18}\text{O}$ values in marine microfossils are a result of a natural **fractionation** of oxygen isotopes as water evaporates from the sea surface. During evaporation, the lighter H_2^{16}O molecule is drawn into the atmosphere in preference to the heavier H_2^{18}O molecule. This process is temperature dependent and so it is particularly marked at higher latitudes where colder air masses are increasingly less able to absorb the heavier isotope. Thus the moisture-bearing winds that nourish the polar glaciers contain relatively higher quantities of the lighter ^{16}O , and this, in turn, is reflected in the isotopic composition of glacier ice. During the cold phases of the Quaternary, with markedly expanded ice masses in both Northern and Southern Hemispheres, large quantities of H_2^{16}O were trapped in the ice sheets leaving the oceans relatively enriched in H_2^{18}O (i.e. isotopically more **positive**, or **heavier**). Conversely, the melting of the ice masses during interglacial periods liberated large volumes of water enriched in H_2^{16}O back into the oceans (Figure 3.56). The result, therefore, is a cyclical down-core oscillation in the marine oxygen isotope signal, reflecting alternating glacial (expanded land ice volume) and interglacial (reduced land ice volume) conditions (Figure 3.57). Analysis of $^{18}\text{O}/^{16}\text{O}$ ratios in Foraminifera has revealed that the overall glacial-interglacial variation in isotopic composition of ocean waters was relatively small, the $\delta^{18}\text{O}$ record from planktonic species suggesting that ocean waters at the Last Glacial Maximum (LGM) were typically about 1–1.5 per mil more positive than at the present day (Cortijo *et al.*, 2000). Isotopic data obtained from benthic species have much heavier $\delta^{18}\text{O}$ values than surface species, typically in the range +2.5 to +5.0 per mil (Shackleton *et al.*, 1990; Dwyer *et al.*, 1993), reflecting the higher $\delta^{18}\text{O}$ content of

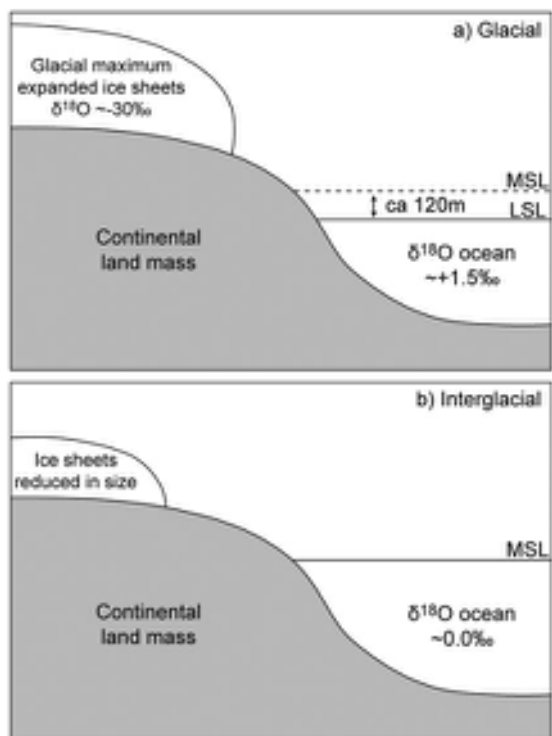


Figure 3.56 Variations in surface water oxygen isotope ratios during times of glacial maxima and interglacial high sea-level stands (minimal ice cover).

deep-ocean water. Overall, however, the glacial–interglacial oscillations reflected in isotope profiles from benthic species match very closely those obtained from planktonic species, which suggests that, in spite of the influence of other factors (see below), both isotopic signals contain a significant ice-storage component.

Oxygen isotope profiles from marine deposits can therefore be interpreted principally as a record of global palaeoglaciation. In Figure 3.57, the marine isotope signal has been drawn to show patterns of global ice accumulation and wastage over the course of the last 600 ka (the scale is the reverse of that normally depicted, with isotopically heavier values to the right). The isotopic trace is asymmetrical, reflecting a gradual increase in ice volume during the course of a cold stage, followed by a sudden decline indicating rapid ice wastage. These latter points on the isotope curve are referred to as **terminations** (I–VII in Figure 3.57). Small amplitude variations in isotope values between successive terminations suggest that the gradual build-up of land ice was interrupted by short-lived episodes of glacier retreat. The overall shape of the curve is

common to all marine isotope profiles, and hence the clearly defined terminations form marker horizons that can be used as a basis for inter-core correlation (section 6.2.3.5). The diagram also shows that, for much of the last 600 ka, global land ice cover was far greater and, by implication, the climate was cooler than at present. Hence, the current relatively equable climate is atypical when viewed in the context of the isotope records for the last 600 ka (section 7.3.3).

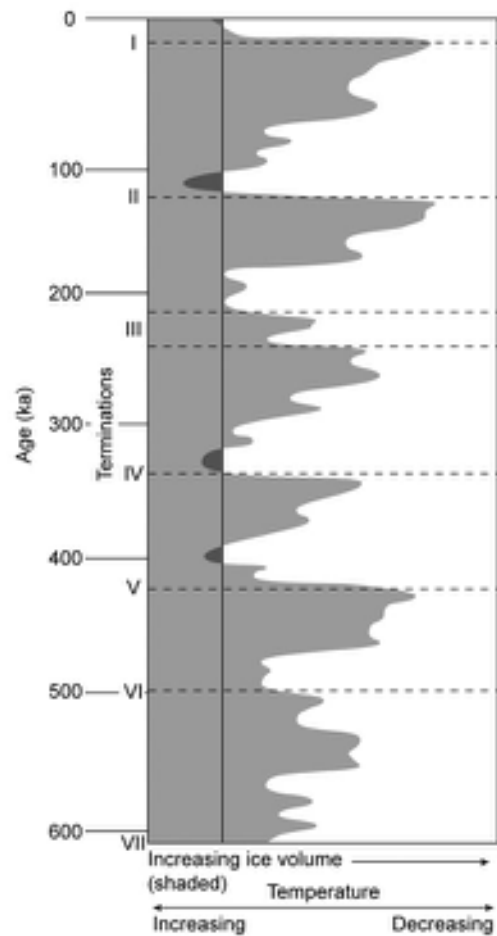


Figure 3.57 Schematic representation of oxygen isotope variations for the past 600 ka. Isotopically light values to the left, and isotopically heavier values to the right. The isotopic signal is interpreted as a proxy for extent of global palaeoglaciation. I–VII are termination events (section 6.2.3.5). The vertical line represents the isotope ratio that corresponds to the limited ice cover typical of the late Holocene. Only three short periods during the preceding 600 ka appear to have experienced comparable climatic conditions (after Broecker & Denton, 1990).

Oxygen isotope traces through cores of deep-ocean sediment reveal records of glacial-interglacial changes spanning, in many instances, the whole of the Quaternary. There is, moreover, a remarkable similarity between the isotopic profiles from different parts of the world's oceans, in terms of both the number and amplitude of oxygen isotopic cycles. This suggests that the oceans as a whole have been responding in a coherent fashion to a common forcing mechanism (the Milankovitch radiation cycles), and hence variations in the isotopic signals are broadly synchronous worldwide. The common peaks and troughs in the curves can therefore be designated as **isotopic stages**, and these form the basis for stratigraphic subdivision of the individual profiles and for correlation at the global scale. These aspects of oxygen isotope stratigraphy are considered further in sections 6.2.3.5 and 6.3.3.

3.10.2.3 Ice volumes, sea level and the marine oxygen isotope record

Given that there is a close relationship between the glacial storage of oxygen isotopes and the marine oxygen isotope record, it should, in theory, be possible not only to interpret the magnitude of the $\delta^{18}\text{O}$ shift between glacial and interglacial events in terms of fluctuating global ice volumes, but also to derive a quantitative estimate of global ice volume changes. Similarly, insofar as ice volumes are related to sea level, the marine $\delta^{18}\text{O}$ record could be employed as a proxy for global sea-level change. The planktonic $\delta^{18}\text{O}$ record is perhaps less suitable for these purposes because of temperature and other influences, hence ice volume and sea-level changes are usually inferred from benthic foraminiferal oxygen isotope signals.

Benthic Foraminifera inhabit the deep oceans of the world, which are generally more stable and uniform in terms of temperature and salinity than are ocean surface waters. As a consequence, it has generally been considered that temperature change in the deep oceans of the world has been minimal, and thus the deep-ocean isotopic signal is more readily interpreted as reflecting glacial storage variations, as opposed to the temperature-influenced fractionation effects of carbonate precipitation. However, it is now recognized that most benthic foraminiferal $\delta^{18}\text{O}$ curves, which typically range from 1.5–1.9 per mil, are also influenced to some degree by deep-sea temperature changes of as much as 4.5°C . This is equivalent to a $\delta^{18}\text{O}$ range in carbonate of *c.* 1.1 per mil, and clearly represents a significant proportion of the overall glacial-interglacial isotopic shift. In general, however, the likely temperature component is significantly less and, when other local effects are taken into account, benthic foraminiferal $\delta^{18}\text{O}$

suggests an LGM–Holocene change attributable to ice volume of 1.1–1.4 per mil (Mix *et al.*, 2001). This is roughly equivalent to an excess LGM ice volume (i.e. more ice than at present) of $48\text{--}59 \times 10^6 \text{ km}^3$ (modern ice volume being estimated at $32 \times 10^6 \text{ km}^3$). Other reconstructions of the ice volume component in the benthic isotopic record of the last glacial–present interglacial transition suggest a slightly lower isotopic shift. Shackleton (2000), for example, obtained an estimate of ~ 1.0 per mil based on a comparison of the benthic marine $\delta^{18}\text{O}$ record and the $\delta^{18}\text{O}$ signal from the Vostok (Antarctica) ice core (section 3.11), while Schrag *et al.* (1996) derived a value of 0.8–1.0 per mil from direct measurements of the isotopic composition of pore waters in deep-sea sediment cores. These estimates, if correct, would imply somewhat lower global ice volumes at the LGM.

In terms of sea-level changes, it has been suggested that a sea-level change of *c.* 10 m will be represented by a *c.* 0.1 per mil shift in the oxygen isotope signal (Shackleton and Opdyke, 1973). Based on the inferred ice-volume effect in the benthic $\delta^{18}\text{O}$ record noted above, this would imply a sea-level lowering at the LGM of -110 to -140 m, an estimate broadly confirmed by other $\delta^{18}\text{O}$ -based reconstructions (Waelbroeck *et al.*, 2002). This figure is also consistent with independent evidence for global sea-level change. For example, sea-level estimates from raised coral terraces in New Guinea point to a sea-level lowering of around 125–130 m at the LGM (Figure 3.58). A similar estimate (-125 ± 5 m) has been obtained by combining evidence from a range of low-latitude sites with data from ice modelling (Fleming *et al.*, 1998), while faunal and sedimentary records from the northwest Australian continental margin suggest sea level at the LGM at -135 to -130 m (Yokoyama *et al.*, 2000). A sea-level lowering of 125 ± 5 m corresponds to a volume of grounded ice in excess of the present volume (see above) of $46\text{--}49 \times 10^6 \text{ km}^3$,

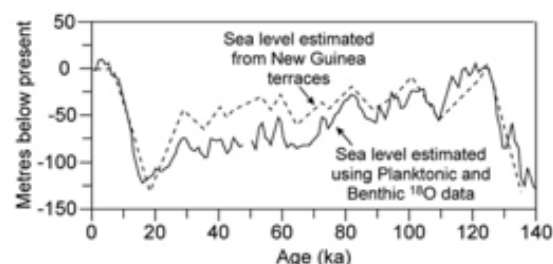


Figure 3.58 Comparison between estimates of sea-level variations for the last 140 ka based on marine isotopic variations and those derived from New Guinea coral reef records (based on Waelbroeck *et al.*, 2002).

while the lower sea-level value (-130 to -135 m) suggests an ice volume excess at the LGM of $52 \times 10^6 \text{ km}^3$.

Again, both these estimates are consistent with the figures for reconstructed ice volumes described above. Where the ice-volume component can be extracted from the benthic marine isotope record, therefore, this constitutes a useful proxy not only for global ice-volume variations, but also for glacio-eustatic sea-level change. For example, a long-term record of isotopically derived sea-level change, which links ice volume and sea level, suggests that the growth and decay of the Antarctic ice sheet from ~ 33.5 Ma caused variations of 50 – 60 m in sea level and that this amplitude of sea-level fluctuation also characterized the Early and Middle Quaternary, while from *c.* 780 ka onwards, a much larger range, of the order of ~ 100 m, is evident in the eustatic sea-level record (Miller *et al.*, 2011).

3.10.2.4 Sea-surface temperatures and the marine oxygen isotope record

In the early years of research on marine oxygen isotopes, the dominant influence on $\delta^{18}\text{O}$ was thought to be water temperature. This was because a second fractionation process, that which occurs when carbonate is precipitated slowly in seawater is, at least partly, temperature dependent. The pioneering work of the American scientist Harold Urey (published in 1947) suggested that former sea-water temperatures could be established by measuring the degree of isotopic fractionation that had occurred in marine carbonate fossils. Subsequently, Samuel Epstein and others developed an empirical equation for this relationship that gave a value of *c.* 0.23 per mil per 1°C . In order to use this equation to obtain palaeotemperatures, however, it was necessary to know the second component, namely the former isotopic composition of seawater (see above), and as this could not be established directly, it had to be estimated. Cesare Emiliani, who pioneered the stratigraphic application of oxygen isotope analysis in the 1950s, estimated that only about 0.4 per mil of the average 1.7 per mil $\delta^{18}\text{O}$ variation between glacial and interglacial stages reflected changes in the isotopic composition of seawater, and hence the more important factor was water temperature variation. Using Epstein *et al.*'s equation, he interpreted the fluctuations in isotopic content of planktonic Foraminifera in cores from the Caribbean and Equatorial Atlantic as reflecting palaeotemperature changes of 6°C between the last glacial and the postglacial periods.

In subsequent years, however, research has shown that the relationship between $\delta^{18}\text{O}$ values in planktonic Foraminifera is more complicated than was initially envisaged. This is reflected in the publication in recent years

of numerous empirically derived palaeotemperature relationships, which may produce results that differ by several degrees, even when applied to the same dataset. Planktonic foraminiferal data can be affected by a range of factors, including local changes in ambient temperature, fluctuations in the regional balance between evaporation and precipitation, and variations in salinity arising, for example, from river inflow or glacial meltwater discharge. Indeed, it has been suggested that as much as one third to one half of the total variability in planktonic $\delta^{18}\text{O}$ may reflect local environmental changes (Mix *et al.*, 2001). Studies of living planktonic Foraminifera indicate that the $\delta^{18}\text{O}$ signal is also affected by seasonal temperature variations and by the effects of vertical migration of foraminiferal species through the upper part of the water column. They also show that the $\delta^{18}\text{O}$ of living foraminiferal species is much lighter than that predicted by the equilibrium equations derived for calcite (Waelbroeck *et al.*, 2005).

These various limitations mean that the reconstruction of sea-surface temperatures using the $\delta^{18}\text{O}$ record in planktonic Foraminifera is far from straightforward and, where this approach is employed, it requires a careful analysis of the constraints that might influence the temperature reconstructions. This includes obtaining a realistic estimate of the likely ice-volume effect and, in northern oceans, of the effects of changing sea-surface salinity. An example of how this might be achieved is described by Meland *et al.* (2005) who reconstructed sea-surface salinity changes for the Nordic Seas at the LGM and then employed these data in the interpretation of the $\delta^{18}\text{O}$ record to construct a map of summer sea-surface temperature changes (see section 4.10.7 and Figure 4.46).

3.10.3 Limitations of oxygen isotope analysis

There are a number of limitations affecting the interpretation of oxygen isotope data. These include the following.

3.10.3.1 Stratigraphic resolution

Sedimentation rates vary markedly throughout the oceans. In deeper waters, where the terrigenous influx is often minimal and biogenic production is dominant, the rate of sediment accumulation is usually very low. Although long records, sometimes spanning the whole of the Quaternary, can occasionally be obtained from these deposits, an average sample for oxygen isotope analysis may span a time interval of several thousand years. Much higher temporal resolution can be obtained in sequences that

have accumulated more rapidly, such as those on or close to the continental shelves (Ebbesen & Hald, 2004) or from deep-water deposits dominated by IRD (Bond *et al.*, 2001b). However, these sedimentary records are often very much shorter, and are usually restricted to the last glacial-interglacial cycle.

3.10.3.2 Sediment mixing

Where mixing has occurred, as a result of bottom-dwelling burrowing organisms or through the action of turbidity currents, the clarity of the oxygen isotope record will tend to be blurred. Benthic organisms typically affect sediments to a depth of 20 cm as they feed and burrow, although in some cases the depth of bioturbation may be much deeper. Bioturbation is especially problematical where sedimentation rates are slow, and may lead to attenuation of millennial-scale events registered in the sediment record (Anderson, 2001). Reworking caused by the scouring of ocean bottom currents can also result in depositional hiatuses, while distortions of the sediment and contained microfossil record may occur during sampling.

3.10.3.3 Isotopic equilibrium between test carbonate and ocean water

Because of fractionation effects, some species of benthic Foraminifera do not secrete carbonate that is in isotopic equilibrium with the ocean water that they inhabit. Hence, when benthic tests are being measured, more importance is attached to species such as *Uvigerina senticosa* and *Globocassidulina subglobosa* that are known to deposit carbonate in isotopic equilibrium with deep-ocean waters. A number of planktonic species also calcify at different depths during their life cycle (e.g. some species of *Glororotalia*), and this can lead to differences in isotopic ratios between adults and juveniles of the same species. Some knowledge of the species dependence of such effects is therefore required and appropriate corrections can then be applied. Certain species are regarded as particularly good indicators of the original isotopic ratios of surface waters (e.g. *Globigerinoides sacculifer* and *Globigerina bulloides*), while others (e.g. *Glororotalia menardii* and *Neogloboquadrina pachyderma*) are selected because they are thought to provide reliable records of isotopic ratios in deeper waters.

3.10.3.4 Carbonate dissolution and diagenesis

After death, carbonate microfossils sink within the water column, and many will become dissolved or disaggregated

before reaching the ocean floor. Some foraminiferal species are more susceptible to dissolution than others, so that during settling there is a selective removal, usually of the species that lived closer to the surface. Between 3 and 5 km depth, CaCO_3 solution equals CaCO_3 supply, the level defined as the **carbonate compensation depth (CCD)**. Below that depth, only the most robust microfossils arrive on the seabed. Even where complete dissolution does not take place, the water depth plus depth of sediment burial may be sufficient to lead to diagenesis in the form of carbonate recrystallization (Carter *et al.*, 2000). Stratigraphic studies of foraminiferal assemblages are, therefore, usually restricted to sediments that have accumulated in waters that are shallower than the CCD, and where evidence of diagenesis is absent or negligible.

In spite of these potential limitations, however, oxygen isotope analysis of deep-sea sediments is a technique of great importance in Quaternary research. Indeed, in many respects it has revolutionized Quaternary science. Although perhaps not as secure an indicator of palaeotemperatures as was at one time believed, oxygen isotopes do, nevertheless, provide a unique record of glacial-interglacial cycles, of changing global ice volumes, and of glacio-isostatic oscillations of sea level. Moreover, the recognition of comparable isotope stages from different areas of the world's oceans provides a means of correlating environmental changes on a global scale (Chapter 6).

3.10.4 Carbon isotopes in marine sediments

The analysis of carbon isotopes in marine sediments can also provide valuable data on oceanographic changes during the Quaternary. As with oxygen, carbon has two naturally occurring stable isotopes (^{13}C and ^{12}C) that are fractionated during a range of natural processes (see section 5.3.2). $\delta^{13}\text{C}$ profiles in marine sediment sequences show cyclic variations, very similar to those in oxygen isotope traces, and it appears, therefore, that these also reflect important environmental changes. They can be used, *inter alia*, to reconstruct changes in ocean circulation patterns, marine productivity, air-sea gas exchange and biosphere carbon storage (Oliver *et al.*, 2009). Similar problems to those of oxygen isotope analysis are experienced in the analysis of carbon isotopes, including, for example, variations in carbon isotope content between microfossils caused by fractionation as a result of different vital effects, and regional variations due to localized circulation changes. Carbon isotope data in planktonic Foraminifera, however, provide information on former productivity changes in the upper layers of the oceans and on the flux of ^{12}C in surface

waters. This evidence also offers insights into factors affecting atmospheric variations in CO₂, for example during the last deglaciation (Tschumi *et al.*, 2010), and therefore forms a complementary source of information to the ice cores (section 3.11). Benthic Foraminifera record deep-water circulation changes in the oceans. Vertical circulation brings oxygenated waters into the deeper parts of the ocean, a process referred to as **ventilation** and, at times of reduced vertical mixing, oxygen levels fall, productivity is reduced and this will be reflected in the δ¹³C signatures obtained from the fossil records. For example, in the North Atlantic a close correspondence has been observed between IRD events and the δ¹³C record, with lighter δ¹³C values suggesting a ventilation minimum associated with IRD events (Boyle, 2000). In the Mediterranean, by contrast, fluctuations in δ¹³C values in benthic Foraminifera reflect a more vigorous thermohaline circulation during the cold stadials of Dansgaard–Oeschger oscillations of the last cold stage (Cacho *et al.*, 2000; Moreno *et al.*, 2005).

3.11 ICE-CORE STRATIGRAPHY

3.11.1 A brief history of deep-ice coring

Since the 1960s, groups such as CRREL (United States Army Cold Regions Research Engineering Laboratory), the Centre for Ice and Climate in Copenhagen, and the British Antarctic Survey have developed specialist coring equipment that can recover undisturbed cores from deep within the world's ice sheets. Analysis of deep cores from Greenland and Antarctica, and of shallower ones obtained from the smaller ice caps and glaciers, has revealed a record of annual increments of snow and ice accumulation extending back to the last interglacial and, in some cases, into deeper Quaternary time.

The first deep-ice core was recovered from Camp Century in northwest Greenland in 1966, and was followed by cores from Dye 3 (1981) and Renland (1988), also in Greenland (Figure 3.59a), and from Devon Island (1976) in northern Canada. Analyses of these cores not only yielded valuable stratigraphical and palaeoenvironmental information, but also led to technical improvements in drilling, core recovery and analytical techniques, as well as providing new insights into the behaviour of the great ice sheets. In the 1990s, two new deep cores were obtained from the summit of the Greenland Ice Sheet. The Greenland Ice-core Project (GRIP), coordinated through the European Science Foundation, reached bedrock at 3,029 m in 1992, while the North American Greenland Ice Sheet Project (GISP), which was drilled only 30 km or so away

from the GRIP site, reached bedrock at a depth of 3,053 m in 1993. In the last ten years, drilling has been completed on two new Greenland ice cores: NorthGRIP on the summit of the ice sheet to the north of the GRIP site where the ice is 3,085 m thick, and at NEEM in the far north of Greenland near the original Camp Century core where the ice is over 2,500 m in thickness (North Greenland Ice Core Project Members, 2004; NEEM Community Members, 2013). The oldest records from Greenland are from the last (Eemian) interglacial, with the NEEM core recording the onset of interglacial conditions around 130 ka.

In Antarctica, where rates of snow accumulation are lower than in Greenland, much longer ice-core records have been obtained. The earliest core was obtained from Byrd Station in the interior of West Antarctica (1968), and was followed by successful drilling at Dome C, the Concordia Research Station on the Antarctic Plateau (1979), and Vostok Station at the centre of the East Antarctic ice sheet (1985; Figure 3.59b). During the 1990s, deep ice cores were recovered from Taylor Dome on the East Antarctic ice sheet (1994) and Siple Dome in West Antarctica (1999), these sequences extending back to at least the last interglacial. Further work at the Vostok site resulted (in 1998) in the deepest ice core drilled to date (3,623 m), with a continuous record extending back over 400 ka. More recently, the European Project for Ice Coring in Antarctica (EPICA), has recovered a core (known as EDC) from Dome C near to Concordia Station with a logged depth of 3,260 m and spanning eight complete glacial–interglacial cycles; the basal ice has an age of around 800 ka, almost doubling the length of time covered by the Vostok record. Within the last ten years, further cores have been obtained from the Antarctic ice sheet. These include the Kohnen Station core (2005) in Dronning Maud Land (part of the EPICA programme and known as EDML), which provides a very high-resolution record of the last glacial–interglacial cycle and represents the first direct southern counterpart of the Greenland records; and the Talos Dome core (2007) obtained by the international TALDICE consortium from the edge of the East Antarctic plateau, which extends back over the last two glacial–interglacial cycles to around 250 ka (Barbante *et al.*, 2010; Buiron *et al.*, 2011).

In addition to these polar drilling programmes, ice cores have also been obtained from glaciers and ice caps in high-altitude regions in the mid-latitudes. These include cores from the Tibetan Plateau, from Africa (Mt Kilimanjaro), and from the Andes (Thompson, 2000; Thompson *et al.*, 2013). The records from these ice cores are much shorter than those from the polar ice sheets and typically contain only a Holocene or late last cold stage sequence.

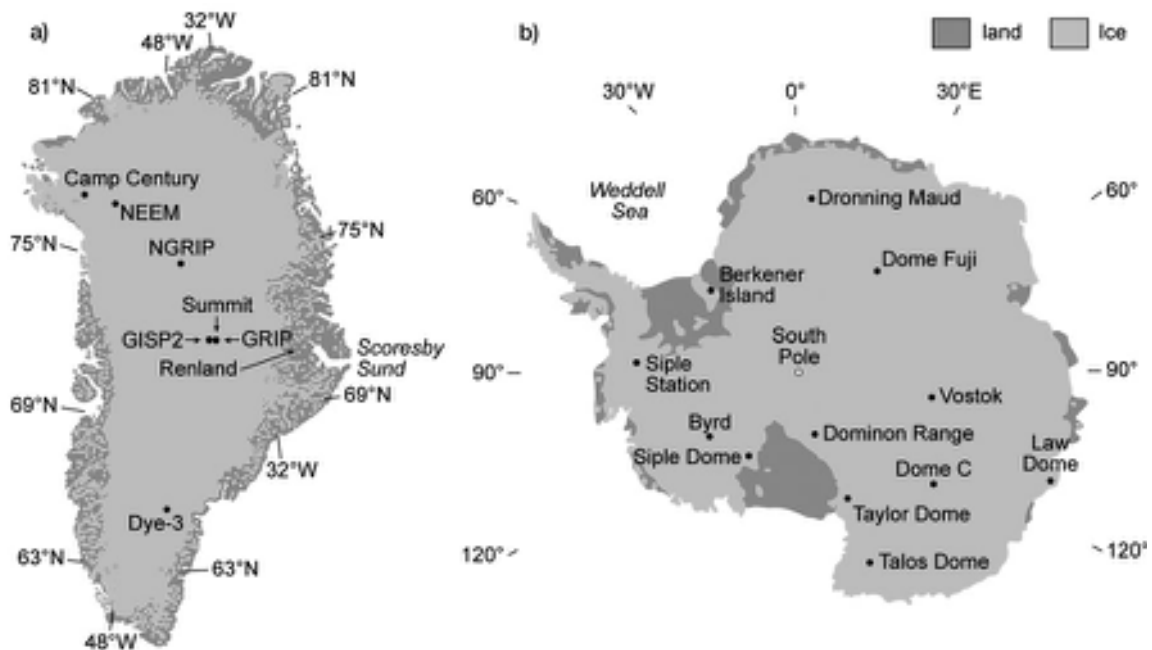


Figure 3.59 Location of some of the principal ice-core drilling stations in a) Greenland and b) Antarctica.

The data from these various investigations at both high and low latitudes have revolutionized our understanding of the patterns and rates of past global climatic change, and of the linkages between the ocean–atmosphere–terrestrial systems (Chapter 7).

3.11.2 Ice masses as palaeoenvironmental archives

Glacier ice accumulates in a sequence of annual layers, and analysis of cores from the high-latitude ice sheets has shown that these contain a wealth of palaeoclimatic evidence. The annual increments of ice reflect the balance between accumulation and ablation over the course of a year, and hence the variation in thickness of the annual layers may provide useful information on, for example, amount of winter snowfall, degree of melting (determined by summer temperature regimes), and so on. More detailed palaeoclimatic information can be obtained, however, from aerosol particles and other exotic material that has settled on the glacier and which subsequently becomes incorporated into the ice layers. These include dust particles from volcanic or desert sources, a variety of trace substances, and microbial or other biological materials (e.g. pollen grains and fungal spores), the relative abundance of these

various exotic materials reflecting the vigour of atmospheric circulation, wind direction and aerosol flux. Other sources of palaeoenvironmental data preserved in annual increments of ice sheets and glaciers include trace gases (e.g. carbon dioxide and methane) that become trapped in minute air bubbles within the ice crystals, and which provide evidence of both short- and long-term changes in atmospheric gas composition, and stable isotopes (particularly isotopes of oxygen), which not only act as a proxy for climate change but also offer a basis for correlation between marine and terrestrial records (section 6.3.3). Finally, natural and artificial radioactive isotopes contained within the ice layers provide an independent means of dating ice cores. Ice cores, therefore, contain a range of evidence that can be used to reconstruct past climatic conditions and are widely regarded as one of the most important archives of Late Quaternary palaeoenvironmental data (see below).

3.11.3 Analysis of ice cores

3.11.3.1 Annual ice increments

Near the surface of an ice sheet, the annual increments of ice comprise a darker and a lighter component. The winter layers are lighter in colour whereas those of the summer



Figure 3.60 Annual ice layers exposed in the Quelccaya ice cap, Peru (photograph by Lonnie G. Thompson, Ohio State University, USA).

melt season are darker (Figure 3.60), the lower rate of accumulation and partial melting in the summer leading to a higher concentration of impurities and hence a darker colour by comparison with the winter layers. In deeper ice, the annual layers are less obvious because they become thinner and distorted through pressure from the accumulating overburden, and as a result of flow deformation. They can be detected, however, using light transmission, X-ray methods or digital scanners (Figure 5.26), or on the basis of changes in physical or chemical properties of the annual ice increments (Figure 3.61). This ‘multi-parameter approach’ to ice layer counting is discussed further in section 5.4.3.

Once an incremental record has been established, each layer of ice can be assigned an age in **ice-accumulation years** (number of annual layers below present surface). For the youngest part of the record, these are equivalent to calendar years, but with increasing depth, the clarity of the seasonal increments diminishes, so that it becomes more difficult to distinguish between individual layers. The depth in the ice at which ice-accumulation years cease to provide reliable ages will vary, but in Greenland ice and in some Antarctic cores, ice-accumulation years have been established throughout the Holocene and into the last cold

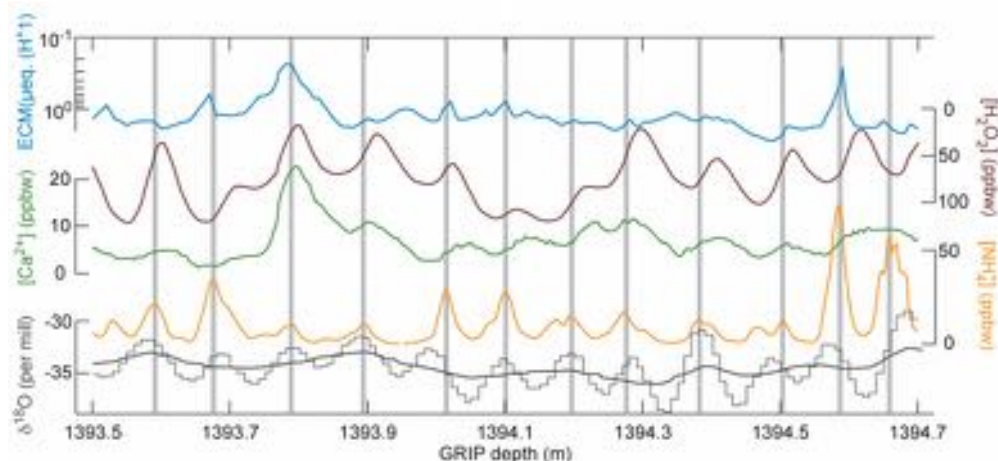


Figure 3.61 Seasonal variations in chemistry, dust content and stable oxygen isotope ratios in ice layers in a section of the NorthGRIP core. The annual layers (shown by the vertical grey bands) are identified as matching pairs of spring and summer indicators: spring is characterized by high dust content leading to peaks in Ca_2^+ and dips in the H_2O_2 curve, while summer is characterized by high NH_4^+ and corresponding minima in the ECM curve. Note that the ECM and H_2O_2 curves are plotted on reversed scales. The annual layer identifications are supported by high-resolution $\delta^{18}\text{O}$ data (after Rasmussen *et al.*, 2006; copyright 2006 by the American Geophysical Association).

stage. In general, however, dating of the older section of ice cores relies on other methods, and again these are considered in section 5.4.3.

3.11.3.2 Dust content

Wind-blown dust particles are an important stratigraphic component of ice cores. Studies of the variation of dust concentration with depth have shown that dust concentration in the ice varies seasonally, and hence the measurement of annual dust cycles along an ice core can help in the identification of annual layers of snow deposition. The concentration of dust particles, which typically have a grain size of 0.1–2 µm, can be measured using a Coulter (or Elzone) particle counter (section 3.2.3.1), but more rapidly and effectively by laser light scattering (LLS) along the length of the core (Ram *et al.*, 2012). Dust content can also be determined using **electrical conductivity measurements (ECM)** or measurements of the **dielectrical properties (DEP)** of ice. These methods involve the transmission of an electrical current through the ice, the strength being directly proportional to the balance of acids and bases present. The current increases with higher concentrations of strong acids, especially sulphuric and nitric acids, but a decrease occurs where the acids are neutralized by, for example, alkaline dust from aeolian sources (Taylor *et al.*, 1997). Dust records constitute valuable inputs to climatic models, and hence are important in palaeoclimatic reconstructions (sections 7.4 and 7.5).

3.11.3.3 Chemical content

Although the chemical content of ice can be determined using ECM and DEP analyses, most chemical analysis now involves **continuous flow analysis (CFA)** (Rasmussen *et al.*, 2005). This technique is carried out in specially constructed laboratories on the ice sheet and involves continuous melting of the inner parts of a newly drilled ice core. Air bubbles are removed from the meltwater and the sample stream is split into a number of analytical systems. Measurements are then made on a range of parameters, including the amount of insoluble dust and size distribution of the particles; the concentration of a range of chemical ions (NH_4^+ , Ca_2^+ , Na^+ , etc.); and the conductivity of the meltwater (which is closely related to the ion content). As the impurities come from different sources, they will reveal different information about the climate system. For example, Ca_2^+ (which is derived mainly from dust) has an annual cycle, and occurs in the highest concentrations in spring. Impurities in the ice also provide evidence of volcanic activity, and these too are detectable

in the CFA conductivity and sulphate profiles, as well as in ECM and DEP measurements (Svensson *et al.*, 2012).

3.11.3.4 Stable isotope records

The oxygen isotopic composition of ice is measured by mass spectrometry and is expressed as deviations ($\delta^{18}\text{O}$) per mil from a standard, which is SMOW (section 3.10; but see note 10). During evaporation from the ocean surface, atmospheric water becomes depleted in the heavier ^{18}O isotope by, on average, about 10 per mil; however, there is seasonal variability in this value, so that the range of $\delta^{18}\text{O}$ between summer and winter precipitation over the ice sheets is commonly about 15 per mil. Thus seasonal changes can be detected in ice cores by precise measurements of oxygen isotope variations. Although the amplitude of the $\delta^{18}\text{O}$ signal decreases with depth due to diffusion effects, significant variations are still detectable over at least the last 125 ka (Figure 7.15), and these predominantly reflect changes in regional and/or global climate (section 3.11.4). Hydrogen isotopes behave in much the same way as oxygen isotopes, the ratio of normal hydrogen to the heavier deuterium in atmospheric water (and hence in snow accumulation) being determined by saturation vapour pressure and molecular diffusivity in air. Hence in ice-core records, long-term variations in δD tend to match the trends in the $\delta^{18}\text{O}$ signal (Sime *et al.*, 2009).

3.11.3.5 Other trace substances

Seasonal variations in anions and, to a lesser extent, in some cations have been detected in many ice-core sequences, and the changing concentrations of, for example, Ca_2^+ , NH_4^+ and H_2O_2 , enable seasonal ice increments to be determined, and hence are important for the construction of ice-core chronologies (section 5.4.3). Trace gases, such as CO_2 and CH_4 , provide a record of changing atmospheric concentrations, reflecting both natural and anthropogenic influences; other trace substances, such as soot particles and heavy metal elements, are evidence of atmospheric pollution over both industrial and pre-industrial timescales (see section 3.11.4), while ash layers are evidence of past volcanic eruptions and form important time-stratigraphic markers in ice cores (Mortensen *et al.*, 2005).

3.11.4 Palaeoenvironmental significance of ice cores

Down-core variations in stable isotope content, and in the abundance of other trace elements in polar ice, provide a powerful tool for the reconstruction of the pattern and

amplitude of Late Quaternary climatic change. Moreover, because an independent chronology can be established for each ice core, a temporal framework is available for these continuous stratigraphic records. Where similar isotopic signals have been obtained from different cores within a single ice sheet, this provides compelling evidence for a regional/global climatic signal. Moreover, as the fractionation of isotopes is temperature dependent (section 3.10), the stable isotope variations provide a proxy record for air temperature change. Figure 3.62 shows continuous $\delta^{18}\text{O}$ profiles from five drill sites on the Greenland ice sheet. A distinctive feature of each of the records is the sequence of high-frequency oscillations during the course of the last 120 ka, with shifts in isotopic values of up to 8 per mil, reflecting amplitudes in air temperature change of between 5 and 16°C. These '**Dansgaard–Oeschger (DO events)**', as they have become known, were relatively

short-lived, each lasting for no more than 500–2,000 years, and appear to reflect the operation of a range of feedback mechanisms involving, *inter alia*, ice sheet fluctuations, oceanographic changes and atmospheric circulation variations (section 7.4).

In the Greenland NorthGRIP core where the DO cycles are particularly strongly registered (Figure 7.15), the isotopic value of the ice at the base of the core differs from the present by 3 per mil. If attributed solely to temperature, this would suggest that Eemian temperatures around 122 ka were at least 5°C warmer than the present day (North Greenland Project Members, 2004). This inference has recently been confirmed by data from the base of the most recently drilled core in Greenland, at NEEM (Figure 3.59a), which indicate that temperatures during the Eemian peaked at $8 \pm 4^\circ\text{C}$ (NEEM Community Members, 2013). In NGRIP, the subsequent slow decline in $\delta^{18}\text{O}$ values to

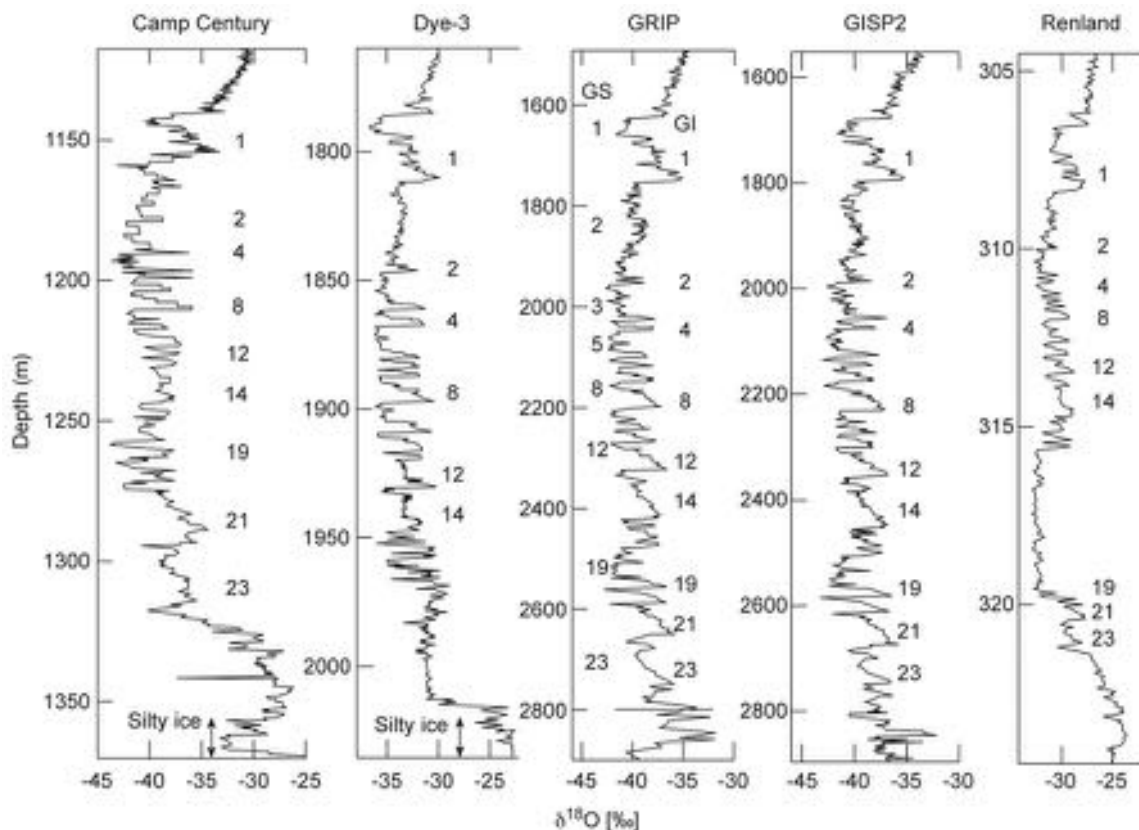


Figure 3.62 Continuous $\delta^{18}\text{O}$ profiles through five Greenland ice cores. Some of the warm Greenland Interstadials (GI) of the Dansgaard–Oeschger (DO) cycles are defined by reference to the GRIP $\delta^{18}\text{O}$ record and are numbered to the right of each profile; these were used to guide correlation between the isotope traces. Some of the cold Greenland Stadials (GS) are also numbered to the left of the GRIP record (after Johnsen *et al.*, 2001).

115 ka indicates that the last interglacial did not end with a rapid climatic change, but rather with a long and gradual decline in temperature. Within this overall trend, there is evidence for abrupt shifts in climate. Before full glacial conditions are reached, the record reveals an abrupt cooling, with the first $\delta^{18}\text{O}$ decrease at ~ 119 ka, followed by relatively stable depleted $\delta^{18}\text{O}$ (Greenland Stadial 26) and followed, in turn, by a sharp increase at ~ 115 ka, at the onset of the first interstadial of the DO cycles (Greenland Interstadial 25). What the record shows, therefore, is that the DO cycles, which constitute such a distinctive feature of the Greenland ice-core record during the course of the last cold stage, were registering in the isotopic signal at a time when the major ice caps were beginning to form. This is puzzling because one explanation for the DO events is that they were triggered, at least in part, by melting ice or other freshwater input to the North Atlantic (section 7.4).

An alternative method for obtaining past temperature variations from ice cores is to measure the temperature of layers in the ice directly by lowering specially designed **thermistors**¹¹ down the borehole, an approach termed **borehole thermometry**. As air diffuses through the surface layer of the ice sheet, the ice acquires a temperature attuned to contemporary climatic conditions. Because ice is a poor conductor, it retains this temperature after becoming buried beneath later layers. Each successive layer of ice therefore retains a ‘memory’ of the ambient climatic conditions at the time of formation (Johnsen *et al.*, 1995). This can be changed by other factors, such as geothermal heat flux, the local ice-flow pattern and the rate of ice accumulation, but these can be corrected for from a knowledge of modern surface temperature variations and the age-depth profile of the ice sheet (Dahl-Jensen *et al.*, 1998). Borehole thermometry generates palaeotemperature reconstructions that are broadly in line with those derived from isotopic measurements, and can clearly resolve distinct climatic events such as the Last Glacial Maximum (LGM), Holocene Climatic Optimum, Medieval Warm Period and Little Ice Age (section 7.6), although increasing statistical uncertainties down-core restrict the application of this method to the last *c.* 50 ka (Dahl-Jensen *et al.*, 1998). GCM simulation modelling (section 7.2) confirms that borehole palaeothermometry not only enables coherent temperature estimates to be inferred, but that these may constitute a correction for isotopic palaeotemperature reconstructions that may be biased by seasonality effects (Werner *et al.*, 2000). Borehole palaeothermometry can also provide other palaeoglaciological insights. For example, it has revealed unusually high rates of geothermal heat flux at the base of the West Antarctic ice sheet, which may explain the locations of some fast-flowing ice streams (Engelhardt,

2004), and also that the Antarctic Peninsula may have warmed faster than the globally averaged rate of warming over the last century (Barrett *et al.*, 2009).

Interpreting temperature records obtained from ice cores is not without its problems, however (Jouzel *et al.*, 1997). This is particularly the case in older records, where the deeper parts of the ice sheet may have flowed some considerable distance, and could therefore have originated in a different source region from the ice in the upper layers. If there is a significant isotopic gradient between the source area for the ice and the present drill site, this could be reflected in down-core isotopic variability that is independent of temperature. Corrections may have to be made for this effect, depending upon the regional isotopic variability of the ice. One advantage of the GRIP, GISP2 and NorthGRIP records, however, is that the drill sites were all close to the summit of the Greenland Ice Sheet (as also is NEEM) and hence, providing that the ice divide has not migrated significantly, flow within the ice sheet at these locations should have been minimal. A second problem concerns the relationship between stable isotope ratios and temperature. Evidence suggests a direct link between stable isotope ratios in precipitating snow and temperature of water vapour at the time of precipitation, assuming unchanged temperature and humidity in the moisture sources. Empirical evidence from the Greenland ice sheet shows a clearly defined relationship between $\delta^{18}\text{O}$ and mean annual surface air temperature, but it is uncertain whether this relationship obtained in the past. One way around this difficulty is to model the borehole temperature profile using parameters derived from instrumental records of recent temperatures, and the well-dated near-surface $\delta^{18}\text{O}$ profile. The modelled temperature profile can be fitted to the measured temperature profile and these data can then be employed to calibrate the deep-core $\delta^{18}\text{O}$ signal to temperature (Johnsen *et al.*, 2001). Using this approach, it has been estimated that Greenland temperatures were around 20°C colder than present during the LGM, and that the DO events were marked by extremely abrupt temperature shifts of around 15°C. We consider the Dansgaard–Oeschger cycles further in Chapter 7.

The Greenland ice-core records, therefore, provide a highly detailed record of climate change in the North Atlantic region extending back to the last interglacial. In Antarctica, however, ice cores spanning a much longer time period have been recovered, the oldest ice so far investigated being at the base of the EPICA core and dated to 960 ± 20 ka (EPICA Community Members, 2004). The climatic record therefore extends back over eight glacial–interglacial cycles. Figure 7.10 shows the inferred temperature profile (8D) from the EPICA core, plotted against carbon dioxide

178 LITHOLOGICAL EVIDENCE

(CO₂), methane (CH₄), dust flux and aerosols. The highest CO₂ and CH₄ mixing ratios are found during the interglacials and the lowest during the glacial maxima. The 100 ka periodicity reflected in these records provides striking confirmation of the Milankovitch hypothesis of long-term climate change described in section 1.7. However, the remarkable correlation between the CO₂ and CH₄ and the δD profiles in Figure 7.10 suggests that trace gases are also important as amplifiers of the initial orbital forcing (section 7.3). This record also reflects the dynamics of the oceanic and continental biospheric carbon reservoirs in relation to climatic changes.

The CH₄ signal in both Antarctic and Greenland ice-core records is of particular significance. Because the atmosphere is well mixed on timescales of a few years, variations in the concentrations of methane trapped in bubbles in the ice can be used as global time markers. By matching the methane records in Greenland and Antarctic cores, northern and southern records can be correlated. This is extremely important to climate scientists and modellers who are trying to understand the forcing mechanisms underlying millennial-scale climate change and, once again, it is a topic that we discuss further in Chapter 7 (section 7.3).

Over shorter timescales, the gas content in the upper layers of polar ice sheets constitutes an important record of recent human activity. This shows, in particular, an increasing anthropogenic influence over the last 200 years or so leading to present-day levels of atmospheric trace gas concentration (CO₂, CH₄, N₂O) that are unprecedented over the past 800 ka (Figure 7.10), or possibly over the past 20 Ma (Prentice *et al.*, 2001)! We consider these anthropogenic records in more detail in section 7.6 in the context of recent greenhouse warming. But the polar ice sheets may also provide evidence of earlier increases in atmospheric trace gases that predate the Industrial Revolution; for example, variations in CH₄ concentrations over the last two millennia have been linked to changes in population and land use during the decline of the Roman Empire, the Han dynasty in China and population expansion in Europe during the Medieval period (Sapart *et al.*, 2012). As well as changes in atmospheric trace gas, the ice sheets contain a record of recent pollution histories; these show soot, lead and other particulates all rising sharply during the industrial era (Weiss *et al.*, 1999; Osterberg *et al.*, 2008). Indeed, increased black carbon concentrations over the past 150 years have even been detected in an ice core from Mt Everest (Kaspari *et al.*, 2011). Trace substance records, such as for lead (Pb) and arsenic (As) in ice cores also provide a longer-term perspective on human industrial activity, including

contaminants from historic and prehistoric metallurgical industries (Krachler *et al.*, 2009).

In addition to the above, ice-core data have contributed to an understanding of many other aspects of environmental change. For example, the dust content of ice provides evidence of changes in atmospheric aerosol loadings and of the former extent of arid or poorly vegetated landscapes. Thus, data obtained from two ice cores in the north-central Andes of Peru suggest that during the last glacial stage the atmosphere may have contained 200 times as much dust as today, while a major phase of enhanced dust deposition around 4.5–4.2 ka marks an extensive drought event lasting for 300 years, and which may have impacted on both climate and culture throughout the world (Thompson, 2000; Walker *et al.*, 2012). Variations in sea-salt concentration in polar ice cores has been linked to changes in sea-ice formation (Rankin *et al.*, 2004), while ammonium and sulphate in the Antarctic ice have been used as an indicator of changes in biogenic productivity involving algae and bacteria in the Southern Ocean (Kaufmann *et al.*, 2010). Finally, acidity levels (**acidity profiles**) in ice cores, which can be established by ECM and CFA methods (see section 3.11.3), provide a record of changes in sulphuric acid content, reflecting variations in volcanic aerosols. Peaks in the acidity profiles constitute a proxy record of former volcanic eruptions, and constitute key marker horizons for the correlation of ice-core records (Parrenin *et al.*, 2012).

3.12 CONCLUSIONS

Almost all Quaternary sediments contain within their matrix important clues about their mode of deposition, and often about the climatic regime under which the sediments accumulated. This information can be extracted from the stratigraphic record by the application of various physical and chemical methods, such as those described at the beginning of this chapter, and by analogy with sedimentological processes that can be observed at the present day. Technological developments in field and laboratory methods, perhaps best exemplified by the extraction and analysis of cores from the world's ice sheets, have resulted in remarkable advances in our understanding of the operation of the global climate system over timescales ranging from decades to thousands of millennia. Equally impressive are the data that have been obtained from loess–palaeosol sequences, where the application of a range of analytical techniques has provided a high-resolution environmental record, in some cases spanning the whole of the Quaternary. It must be emphasized, however, that the sedimentary evidence can seldom be properly evaluated

in isolation. For example, in the analysis of glacigenic deposits, periglacial sediments or pluvial lake sequences, the stratigraphical record should, wherever possible, be integrated with the geomorphological evidence to produce a synthesis of landscape or climate change. The same applies equally to the fossil record, the third category of evidence used in the reconstruction of Quaternary environments, and which forms the subject matter of the following chapter.

NOTES

- 1 An electron microscope consists of a cathode-ray tube through which a beam of electrons is passed. The electrons are concentrated on, and pass through, the specimen to produce a magnified image on a photographic plate. After development, the electron photomicrograph shows the structure of the object in terms of its electron density.
- 2 The term 'diamicton' refers to non-sorted terrigenous sediments and rocks containing a wide range of particle sizes, regardless of genesis.
- 3 Deformation is the alteration of the primary (original) bedding or attitude of lithological units or their components through stress forces (e.g. compression, extension, or shear caused by traction) resulting in folding, faulting or alteration of internal structures and fabric (see also Chapter 2, note 13).
- 4 Load structures often form where coarse material (e.g. sand) is deposited over a hydroplastic or fluid mud layer. Under the weight of the sand, the mud layer becomes distorted and bent downwards. In some cases, the sand layer sinks and forms lobes; in others, the mud layer becomes pushed up to form tongues or 'flame' structures injected into the overlying material.
- 5 Diagenesis refers to the alteration of minerals and sediments by the influences of oxidation and reduction, hydrolysis, solution, biological changes (e.g. induced by anaerobic bacteria), compaction, cementation, recrystallization, and the alteration of the lattice structure of clays by expulsion of water and ion exchange.
- 6 Most plants secrete opaline silica bodies and these assume the shape of the cell in which they are deposited. These forms are known as phytoliths, and many are characteristic of the plants in which they are found. They may, therefore, provide important clues to components of past vegetation.
- 7 Water-filled passages in bedrock, which are below the ground-water table, are termed phreatic passages. Water flow is very slow and little, if any, downward erosion occurs. Immediately above the long-term water table, passages are only filled with water on a seasonal basis, or they may contain streams flowing down to the water table. This is termed the vadose zone, in which significant down-cutting can take place.
- 8 Biological or chemical compounds may contain isotopes of various elements that can be exchanged during reactions or that will be subject to fractionation (see note 9) until a stable ratio is attained, known as isotopic equilibrium.
- 9 Fractionation is the selective separation of chemical elements or isotopes during natural physical, chemical or biochemical processes, such as during evaporation, condensation, transpiration and metabolism.
- 10 In the 1990s, a problem arose because the supply of PDB (Pee Dee belemnite) standard material became exhausted and because SMOW (standard mean ocean water) does not have a unique definition; in other words, there is no globally accepted standard. This means that because laboratories do not use the same reference material to establish their isotopic ratio scales, they are reporting different values for the same material. In order to eliminate confusion, therefore, the Commission of Atomic Weights and Isotopic Abundances of the International Union of Pure and Applied Chemistry has recommended that the use of SMOW and PDB be discontinued, and that isotopic abundances of oxygen- (and also hydrogen- and carbon-) bearing materials should be reported relative to the reference water VSMOW (Vienna standard mean ocean water) and VPDB (Vienna Pee Dee belemnite). These are defined by adopting a $\delta^{18}\text{O}$ value of $-2.2\text{\textperthousand}$ and a $\delta^{13}\text{C}$ value of $+1.95\text{\textperthousand}$ for NBS (National Bureau of Standards) carbonate relative to VPDB. SLAP (standard light Antarctic precipitation) isotopic abundance scales should be normalized so that values for ^2H (or D, for deuterium) and $\delta^{18}\text{O}$ are $-427.5\text{\textperthousand}$ and $-55.5\text{\textperthousand}$, respectively, relative to SMOW (International Atomic Energy Agency, 2009).
- 11 A thermistor is a sensor that records temperature variations automatically through electrical resistance measurements which are temperature dependent.

This page intentionally left blank

Biological evidence

4.1 INTRODUCTION

Biological evidence, in the form of plant and animal remains, has always been a cornerstone in the reconstruction of Quaternary environments. The analysis of fossil evidence employs **uniformitarian principles**, namely that knowledge of the factors that influence the abundance and distribution of contemporary organisms enables inferences to be made about the dominant environmental controls on plant and animal populations in the past. Applying this approach to the interpretation of Quaternary fossil assemblages, therefore, the majority of which have living counterparts, it should be possible to reconstruct former environmental conditions with a reasonable degree of confidence. The use of modern ecological information in this way is an essential element of **palaeoecology**, the study of the interrelationships of organisms in the past, both with their physical environment and with other plants and animals (Battarbee, 2000; Birks & Birks, 1980, 2006). Variations in the type and diversity of plant and animal remains preserved within sedimentary sequences are also used to subdivide the geological record, a field of study known as **biostratigraphy**. This chapter is concerned almost entirely with the palaeoecological aspects of biological evidence; the principles and practices of biostratigraphy are considered more fully in Chapter 6.

4.1.1 The nature of the Quaternary fossil record

When sediments are disaggregated and closely examined, the organic components preserved within them can be surprisingly abundant and diverse. Even sediments that appear on first sight to be ‘barren’ may contain a rich array of tiny, but recognizable, plant and animal remains. These might include seeds, fruits, leaves, pieces of wood, charcoal, insect remains, molluscs, fish scales, teeth and so on.

Occasionally spectacular fossils, such as skeletons of large vertebrates (see Figure 4.49) and tree trunks or stumps (see Figure 5.21) are preserved. The range of biota that can be identified in Quaternary fossil material is extensive, and includes pollen, diatoms, plant macrofossils, insects, molluscs, ostracods, foraminifers and vertebrates, all of which are discussed in this chapter. Other organisms for which more limited palaeoecological data are available, including Cladocera, fungal spores and certain types of marine plankton, are considered more briefly.

Quaternary fossils fall broadly into three size categories. The largest, termed **macrofossils**, ranges from whole skeletons of large vertebrates to component parts (e.g. nuts or seeds) or fragments (e.g. pieces of leaf or wood) derived from plants or animals; these can be identified by eye or with low-power magnification (up to c. $\times 40$). **Microfossils** are those organic components that are generally less than 1 mm in size and hence require the use of more powerful microscopes for identification. They include the skeletal remains of tiny organisms (e.g. diatoms, Foraminifera, etc.) and any small components derived from larger organisms, such as pollen grains, stomatal cells, epidermal tissue, skeletal platelets or delicate scales. A third category comprises the **biomolecular products** of the degradation of organic tissue, such as DNA molecules, pigments, proteins and cellulose, which can account for a significant fraction of soil humus or of the fine organic muds that accumulate in some mires and lakes (Hofreiter, 2008). Sophisticated analytical methods are required to detect and identify these submicroscopic residues. Representatives of all three categories may be found together within the same organic unit, collectively providing an often detailed record of the biological communities from which they were derived, as well as insights into the nature of the sedimentary processes that operated during their burial.

4.1.2 The taphonomy of Quaternary fossil assemblages

The study of the processes that lead to the formation, deposition and burial of a fossil assemblage is referred to as **taphonomy**, and understanding the taphonomy of an assemblage is an essential prerequisite for palaeoenvironmental interpretation. Fossils are best preserved where deterioration resulting from the activities of micro-organisms and the operation of chemical agencies is minimal, and hence anaerobic environments are more likely to lead to survival rather than those where oxidation has occurred (Briggs, 2003). Some organisms may be found in the position of growth (***in situ*** fossils), such as tree stumps buried by the rapid accumulation of peat, volcanic ash or wind-blown sand. The majority of fossils, however, appear to have been transported from their growth or life position by, for example, wind (e.g. pollen and spores), water (a great range of fossils) and animals (e.g. prey of carnivorous taxa). These processes can introduce bias through the **selective transport** of fossils, or by **differential degradation** which selectively removes the less robust specimens. Following initial (primary) deposition, some fossils may subsequently become disturbed and remobilized by processes of erosion, bioturbation, solutional collapse or some other agency. As a result, they may be redeposited in a new locality and even in an entirely different sedimentary context as, for example, when rivers or tidal waves erode terrestrial peats, removing material which may then settle in a new repository, such as in a flood plain or estuarine basin. Fossils remobilized in this way are commonly referred to as **secondary, reworked or derived fossils**. Clearly, it is important to distinguish such secondary components from **primary fossils** in palaeoenvironmental reconstructions using this form of evidence.

4.1.3 The interpretation of Quaternary fossil assemblages

In addition to the taphonomical problems introduced above, other difficulties arise in the interpretation of the fossil record. First, fossil remains have to be identified to a sufficiently low taxonomic level for reasonably well-constrained inferences to be made about former environments. Whereas some types of fossil (e.g. beetles, diatoms) can be identified to species level and may show unambiguous ecological preferences, others, such as certain types of fossil pollen and spores, may only be identifiable to the genus or family level. This can pose problems where several different species within a genus, or genera within a family, have contrasting or very broad ecological affinities (see

section 4.2). Second, for valid inferences to be made using the uniformitarian approach, a number of assumptions about contemporary plant and animal populations must hold true. It must be assumed, for example, that the spatial distributions and population densities of present-day plant and animal taxa are fully known, that these reflect clear preferences for specific environmental conditions or niches, and that an equilibrium has been reached between a taxon's distribution and the dominant environmental factors that influence it. Third, similar assumptions have to be made when interpreting the fossil record in terms of what is known about the ecology and distribution of modern biota (the **modern analogue** approach). It is generally accepted, for example, that the taxa represented in fossil assemblages were themselves in equilibrium with the environmental conditions that prevailed at the time they lived, that plants and animals have coexisted in the past in communities that were similar to those than can be observed today (i.e. they closely match the modern analogues), and that the ecological affinities of plants and animals have not changed through time. The extent to which these assumptions hold true varies both with the type of fossil evidence (pollen grains, animal bones, shells, etc.) and with the nature of each fossil assemblage (how well preserved, how diverse, etc.). It is rare, however, for all of the above conditions to be satisfied. Indeed, given the frequency and rapidity of Quaternary climate change (Chapter 7), the question arises as to whether organisms ever achieve a state of complete equilibrium with their environment.

In this chapter, the different types of biological evidence that are routinely employed in the analysis of Quaternary environments are described and evaluated in the light of these qualifications. Although the different forms of evidence are discussed separately, organisms are of course integral components of **ecosystems**, and are dependent upon, as well as in competition with, other organisms for survival (Begon *et al.*, 2006). When attempting to reconstruct past environments, therefore, it is important to appreciate the complex interrelationships between different organisms, and hence the wider **palaeobiological context** of fossil assemblages. This is difficult to achieve in a **single proxy** study (i.e. one that focuses on only one fossil type). Increasingly, therefore, Quaternary scientists are collaborating in **multi-proxy** palaeobiological studies, where environmental reconstructions are based on the integration of evidence from a range of fossil types (e.g. Birks and Wright, 2000; Kucera *et al.*, 2005a). Moreover, while it is clear that palaeoecologists must have an understanding of the principles of modern ecology in order to draw reasonable inferences from fossil assemblages, knowledge of the Quaternary fossil record is equally vital for sound

interpretation of the origins and spatial distributions of the modern biota (MacDonald *et al.*, 2008). The present may indeed provide a key to the past, but the reverse is equally true: contemporary ecological theory is best served by a secure foundation in Quaternary palaeoecology (Willis *et al.*, 2007). Moreover, while the modern analogue approach is undoubtedly a valuable vehicle for making inferences about the past based on present-day climatic and environmental parameters, it may be that contemporary biota are attuned to increasingly unusual or atypical climatic circumstances, especially with respect to increasing levels of atmospheric CO₂ and the climatic consequences that follow from this (section 7.6.5.1). In addition, many species distributions have been markedly influenced by human activity, especially during the late Holocene (Jackson & Williams, 2004). We return to these matters towards the end of this chapter.

4.2 POLLEN ANALYSIS

4.2.1 Introduction

Of all the palaeobiological methods currently employed in the reconstruction of Quaternary environments, undoubtedly the most widely adopted and arguably the most versatile is pollen analysis (or, more correctly, pollen stratigraphy¹). The technique is also referred to as **palynology**. First developed in the 1920s, the method enables the history of late Quaternary vegetation change to be reconstructed at the local, regional, continental and, potentially, global scales (e.g. Williams *et al.*, 2004b; Gajewski, 2008). It can also be used as a basis for correlating Quaternary stratigraphic units (Magri, 2010), including continental-marine correlations (Roucoux *et al.*, 2005), for palaeoclimatic reconstructions (Seppä & Bennett, 2003), and for evaluating human impacts on late Quaternary vegetation and landscape (Mackay *et al.*, 2003). Pollen records are also increasingly being used in the formulation of conservation policies because of the important historical context that they provide (Froyd & Willis, 2008). An extensive literature on the principles and applications of pollen analysis is now available, and it is not possible to do full justice to the method within the space available here. The aim, therefore, is to provide a general introduction to pollen analysis as a palaeoenvironmental technique, and to outline the principal strengths and weaknesses of the method. More detailed accounts can be found in Birks & Birks (1980), Faegri & Iversen (1989) and Moore *et al.* (1991), while useful summaries are provided by Bennett & Willis (2001) and Chambers (2002).

4.2.2 The nature of pollen and spores

Pollen grains (Figure 4.1) are **reproductive propagules** formed in the anthers of the seed-producing plants (**angiosperms** or **gymnosperms**). They contain the **male gamete** of the plant and aim to reach the stigma of the female part of the flower where fertilization can take place. Spores, which are commonly included in pollen diagrams, represent the **sporophyte** stage of lower plants (**cryptogams**), such as ferns (*Pteridophyta*) and mosses (*Bryophyta*). The sporophyte is dispersed to suitable habitats where the second stage in plant generation, the **gametophyte**, can grow. Pollen grains and spores, particularly those that are spread by wind (see below), are frequently dispersed in very large numbers in order to maximize the opportunities for successful pollination or gametophyte growth, and many accumulate on the ground surface or in water bodies. Some will subsequently become incorporated and fossilized in sediments, and it is the extraction, identification and counting of these preserved fossil grains that form the basis of the technique of pollen analysis.

Most pollen grains and spores are extremely small, few exceeding 80–100 µm in diameter, with the majority falling in the size range 25–35 µm. A typical pollen grain consists of three elements. The central portion, the living part, which consists of one or two **generative cells** and one **vegetative cell**, is surrounded by a covering of cellulose known as the **intine**. None of these parts survives in the fossil form. The outer layer or **exine**, however, consists of a remarkably resistant, waxy coat of material called **sporopollenin**, a chemically complex substance consisting of biopolymers of carotenoids, phenolics and fatty acid derivatives. The prime function of this outer wall is to protect the inner, reproductive elements from desiccation and microbial attack. It achieves this so efficiently that pollen grains continue to be well preserved in sediments when almost all other organic constituents have been reduced to structureless and unrecognizable components. The exine is characterized by a variety of morphological and structural features which, along with the number and distribution of germinal apertures, and the overall size and shape of the grain, form the basis for pollen and spore identification (Figure 4.1).

Pollen grains and spores are disseminated by a variety of means. Spores are usually dispersed by wind, but pollen grains can also be spread by water, insects, birds and animals (including humans). Those plants that liberate wind-borne pollen are termed **anemophilous**, and generally produce far greater numbers of grains than **entomophilous** taxa, which rely on insects or other zoological vectors for

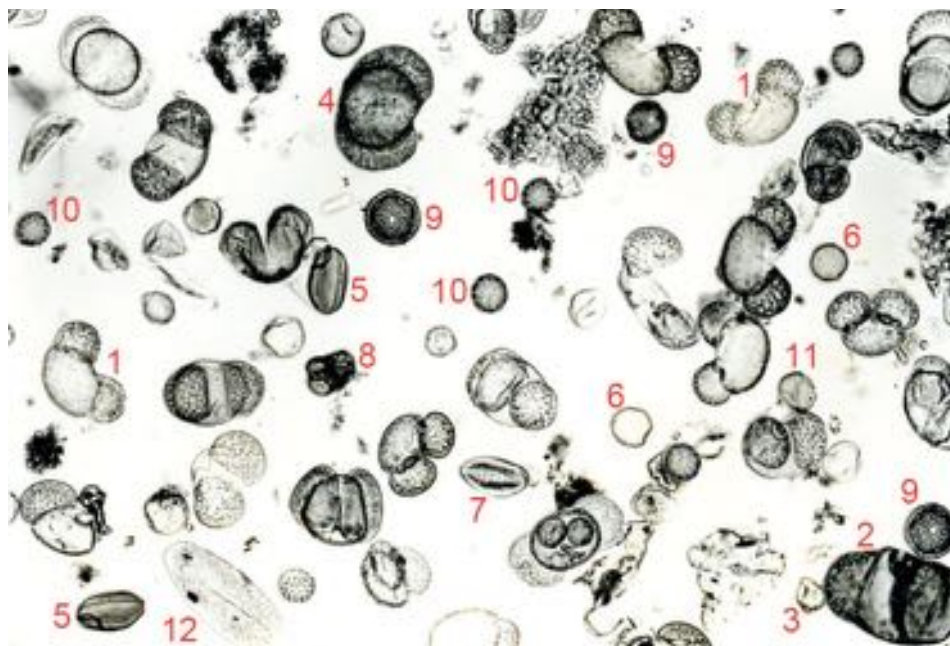


Figure 4.1 Subsample of a pollen assemblage typical of last cold stage deposits from the site of St Front, France. The arboreal component is dominated by *Pinus* (1), while *Picea* (2) and *Betula* (3) are also recorded in smaller numbers. Pollen of *Cedrus* (4) are atypical of this assemblage, and probably indicate long-distance transport. A wide variety of non-arboreal pollen is represented, including, for example, *Helianthemum* (5), *Plantago* (6), *Ephedra* (7), *Calluna* (8) and several genera within the families Caryophyllaceae (9), Chenopodiaceae (10), Poaceae/Gramineae (11) and Liliaceae (12). The long axis of the *Helianthemum* grain (5) is c. 45 µm (photo-montage courtesy of Maurice Reille and Valérie Andrieu-Ponel, Aix-Marseille University, France).

transfer. Wind dispersal is facilitated by the small size, smooth surface features and low specific gravity of the grains, while in the gymnosperms such as pine (*Pinus*) or spruce (*Picea*), air bladders or sacs have evolved enabling pollen of these taxa to stay airborne for very long periods and also to travel considerable distances. The entomophilous grains possess a hardy, armoured surface which often has prominent spines and a coat of sticky material that causes them to adhere to each other or to other surfaces, such as the bodies of insects or animals. Generally, these grains tend either to be large (>60 µm) or very small (<15 µm) and are usually less well represented in the fossil record than wind-dispersed types. Pollen production and dispersal is complex, and is considered in more detail in section 4.2.5.

4.2.3 Field and laboratory work

Pollen grains and spores are frequently well preserved in lake and pond sediments and in peats, and it is these deposits that have been most widely investigated in pollen

analytical work. They are also found in soils (Davidson *et al.*, 1999), cave earths (Navarro *et al.*, 2000), cave calcite deposits (McGarry & Caseldine, 2004), ocean floor sediments (Roucoux *et al.*, 2005), glacial ice cores (Liu *et al.*, 1998) and rodent middens in desert regions (Maldonado *et al.*, 2005). The degree of preservation of pollen and spores depends upon a range of factors, the most important of which are the chemical composition and grain size of the host material, the extent to which anaerobic conditions have persisted since deposition, and exine thickness and structure. Pollen grains tend to be poorly preserved in loosely compacted materials, such as certain types of peats or soils which allow aerobic or microbial attack, and they can also be damaged or destroyed by desiccation or by mechanical abrasion in, for example, coarse-grained sediments on river flood plains, in estuaries, or close to points of stream inflow into lakes.

Samples containing fossil pollen and spores can be extracted from sections exposed in river banks, cliffs, road cuttings or building excavations, or by digging pits. Alternatively, they can be obtained by coring (Last & Smol,

2001). Samples must be sealed air-tight and are best kept in a refrigerated store (at c. 2–3°C) to prevent dessication and/or microbial attack. This also protects them from contamination by pollen circulating in the atmosphere, especially during the pollen and spore production season. In the laboratory, following sediment dispersal, sieving and/or chemical flotation (density separation), samples are chemically treated in a variety of ways to remove as much of the sediment matrix as possible. Organic residues can be concentrated using oxidation, acetolysis and filtration methods, or by using thermochemical or ultrasonic techniques (Kim *et al.*, 2003). Minerogenic sediments can be removed by digestion in hydrofluoric acid or separated from an organic matrix by sieving through fine filters, by differential centrifugation or by flotation using a ‘heavy liquid’ such as sodium polytungstate. Carbonates and calcareous sediments can be treated with hydrochloric acid. The residues containing the pollen and spores may be stained with an organic dye such as safranin, which enhances the surface detail of some grains (although this stage is often omitted as some dyes limit the quality of photomicroscopy), and then mounted on glass slides in a suitable medium such as glycerine jelly or silicon oil. Counting is performed at magnifications of $\times 100$ to $\times 1,000$ depending on the resolution required for identification purposes. By traversing the slide in a systematic way, a count can be made of all of the identifiable pollen and spores until a predetermined number (the **pollen sum**) has been reached. This should be high enough to account for most of the variability in the spectrum. Pollen sums of 300–500 grains are usually employed, although there may still be significant statistical errors in counts of fewer than 1,000 (Weng *et al.*, 2006). Identifications, which can generally be made to family level, commonly to genus level but less frequently to species level, are based on distinctive exine characteristics using pollen keys, photographs and laboratory reference collections of modern pollen samples. Details of the laboratory procedures and examples of classification keys and photographs can be found in Moore *et al.* (1991), Reille (1995) and Colinvaux *et al.* (1999), and in pollen atlases (Hooghiemstra & van Geel, 1998). Because pollen counting can be time-consuming and subjective, attempts have been made to automate the process of pollen classification (Zhang *et al.*, 2004a), though these have yet to generate reliable procedures for routine use.

4.2.4 Pollen diagrams

Where samples have been taken from a stratified body of sediment, such as a lake or peat sequence, the pollen content of a single horizon will reveal a mixture of

pollen types; this is termed the **pollen assemblage** or **pollen spectrum**. Analysis of a series of horizons (or spectra) may reveal changes in pollen content which may, in turn, be interpreted as indicating vegetational changes in the area adjacent to the site. Pollen counts are displayed as pollen diagrams of which there are three principal types: those based on variations in the relative proportion of each taxon represented (**percentage** or **relative pollen diagrams**: Figure 4.2); those based on variations throughout the sequence in the actual concentrations of each pollen and spore type (**concentration pollen diagrams**: Figure 4.3); and those recording changes in the *rate* of accumulation of pollen and spores over specified stratigraphic intervals (**influx** or **pollen accumulation rate (PAR) diagrams**: Figure 4.4). The last mentioned are also sometimes referred to as ‘**absolute pollen diagrams**’.

In **percentage** (or **relative**) **pollen diagrams**, the proportion of each taxon represented in each spectrum is expressed as a percentage of the selected pollen sum (see section 4.2.3). Sometimes the data will be calculated as a percentage of the total pollen and spores counted, although this is not preferred by most analysts because not all plant types have an equal chance of being represented. In the case of a lake sediment sequence, for example, plants that were growing in or at the margins of the lake (e.g. pondweeds and water lilies) have more chance of being represented than those growing further away. Hence pollen derived from aquatic plants are usually excluded from the pollen sum. The same applies to spores, because they are formed in a different way and have a different function from pollen grains. In the majority of instances, therefore, the data are calculated on the basis of a ‘**total land pollen sum**’, that is, the total number of pollen derived from trees, shrubs and terrestrial herbaceous plants (Figure 4.2). Variations in the frequencies of aquatic and spore taxa are then expressed relative to the land pollen sum, and are also included on the diagram. In most instances, however, it is variations in the representation of the ‘land’ taxa that are the chief concern of the pollen analyst. Indeed, where researchers have been especially interested in forest history, they have often chosen to use an **arboreal pollen sum** as a basis of calculation. In this approach, all pollen and spore types are counted until a specified number of tree taxa have been identified, and each taxon is expressed as a percentage of the tree pollen sum. This style of presentation is still occasionally used in archaeological investigations and in studies of Holocene landscape change, where the focus is on the changing composition of forest communities (Booth *et al.*, 2004). Where sediments of the cold stages of the Quaternary are being investigated, much lower frequencies of tree pollen

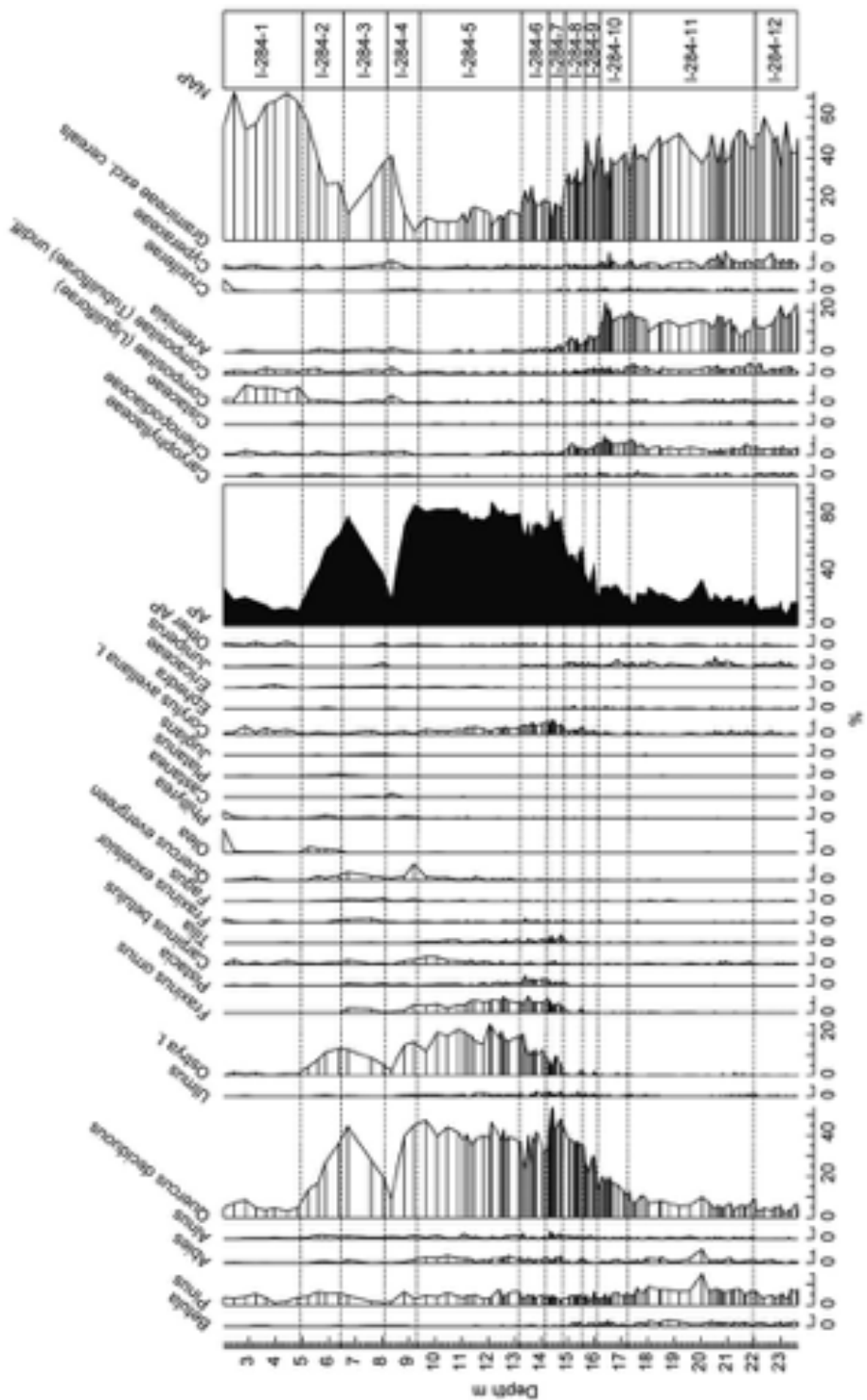


Figure 4.2 Relative pollen diagram showing variations in abundance of principal taxa in a lake sediment sequence (Core I-284) at Ioannina, northwest Greece. The data are based on a pollen sum of all terrestrial trees, shrubs and herbs. NAP – total non-arboreal pollen; AP – total arboreal pollen. The sequence spans approximately the last 20 ka (modified from Lawson *et al.*, 2004).

are usually recorded, and a 'land pollen sum' is considered more appropriate. In long sedimentary sequences spanning several glacial-interglacial cycles, simplified indices such as the ratio of arboreal to non-arboreal (AP/NAP) pollen may be employed to emphasize the changes in forest cover associated with successive warm and cold stages (Tzedakis *et al.*, 2004).

One problem arising from the representation of pollen data in percentage form is that the curves for individual taxa are, of necessity, *interdependent*. In other words, an increase in the influx of one type of pollen to

a site will automatically lead to a suppression of the percentages of other taxa represented in the pollen diagram. In the upper part of Figure 4.2, for example, where marked reductions in percentages of deciduous *Quercus* (oak) and *Ostrya* (Hop-hornbeam) coincide with an increase in Gramineae (grass) pollen, the question arises as to whether the rise in grass pollen percentages reflects a real ecological change, that is, an expansion of open grassland habitats at the expense of trees, or whether it represents a decline in tree pollen influx (e.g. from a reduction in flowering) and hence is a statistical artefact of that process.

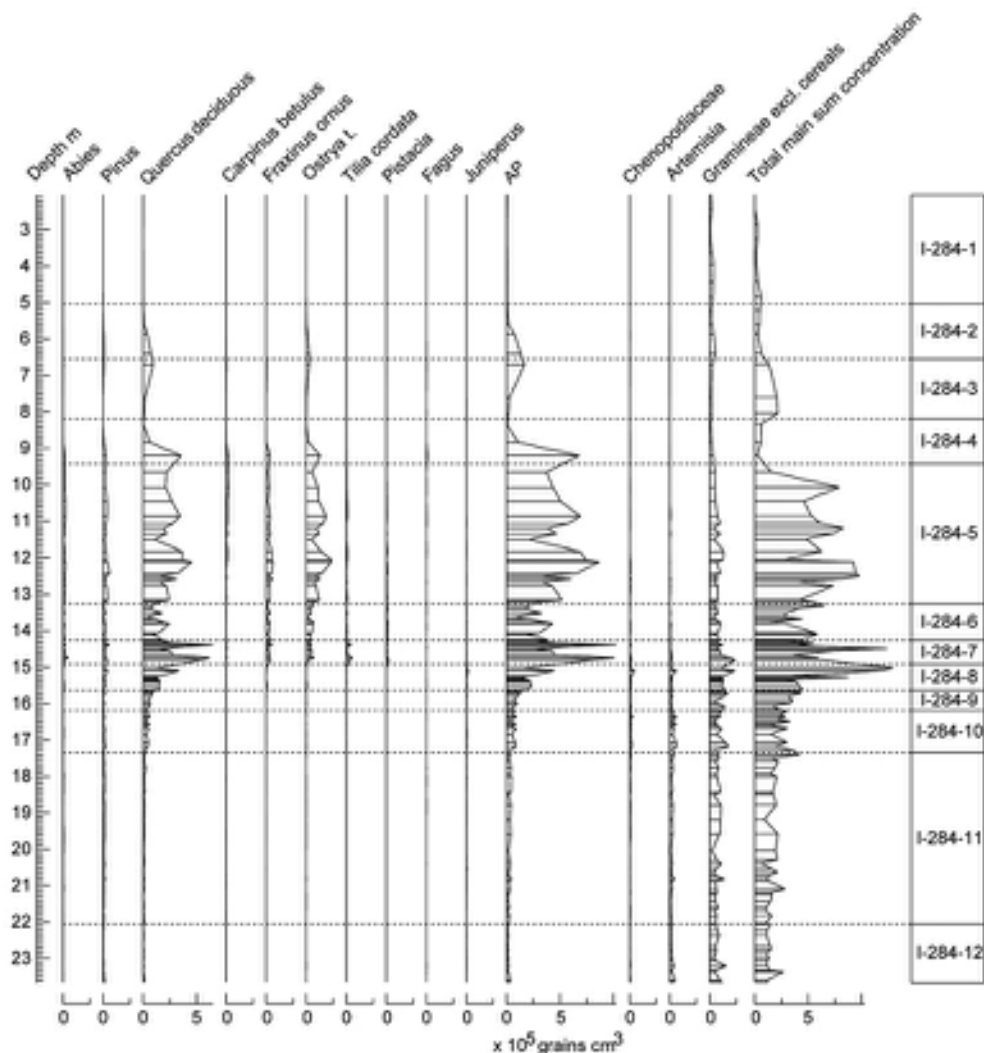


Figure 4.3 Pollen concentration diagram for some of the taxa represented in relative proportions in Figure 4.2 (from Lawson *et al.*, 2004).

One way of solving this problem is by the use of **pollen concentration** or **pollen influx diagrams** described above, as these are not based on percentage changes, but on changes in the total number of pollen grains per unit volume of sediment. A number of techniques are available for estimating pollen concentration, but the one most commonly employed involves the addition of a known quantity of **exotic pollen grains** (sometimes referred to as a '**spike**') to the fossil sample during laboratory preparation. In northwest Europe, tablets containing known amounts of *Eucalyptus* pollen are commonly used for this purpose, since the plant is exotic to the region and the pollen can therefore be easily distinguished from fossil grains. The spike is added to measured volumes of sediment and hence becomes mixed with the fossil pollen on the slides prepared from the residues. Since the quantity of exotic material added to the sample is known, then the observed ratio of exotic to fossil pollen enables the total number of fossil pollen per unit volume of sediment to be calculated, and thus changes in pollen concentrations

at different levels in a profile can be depicted diagrammatically (Figure 4.3).

Although this approach will overcome the difficulty of statistical interdependence of taxon curves, and is therefore potentially of considerable value in palaeoenvironmental reconstruction, it too has problems of application. Variations in rates of deposition within a body of sediment will affect pollen accumulation, and hence in a single profile, concentrations will vary between different types of sediment. In Figure 4.3, for example, pollen concentrations are generally low in the lower part of the diagram, increase markedly at c. 16 m, where a change in sediment type reflects the transition from the last cold stage to the Holocene interglacial, and decline abruptly at c. 9 m, where there is a further change to shallow-water type sedimentation. The extent to which the fluctuations in pollen concentrations reflect variations in pollen influx or in the rate of sediment supply is difficult to determine from these data alone. Supposing, for example, that both pollen and host sediment (clay, mud) are delivered to a lake basin

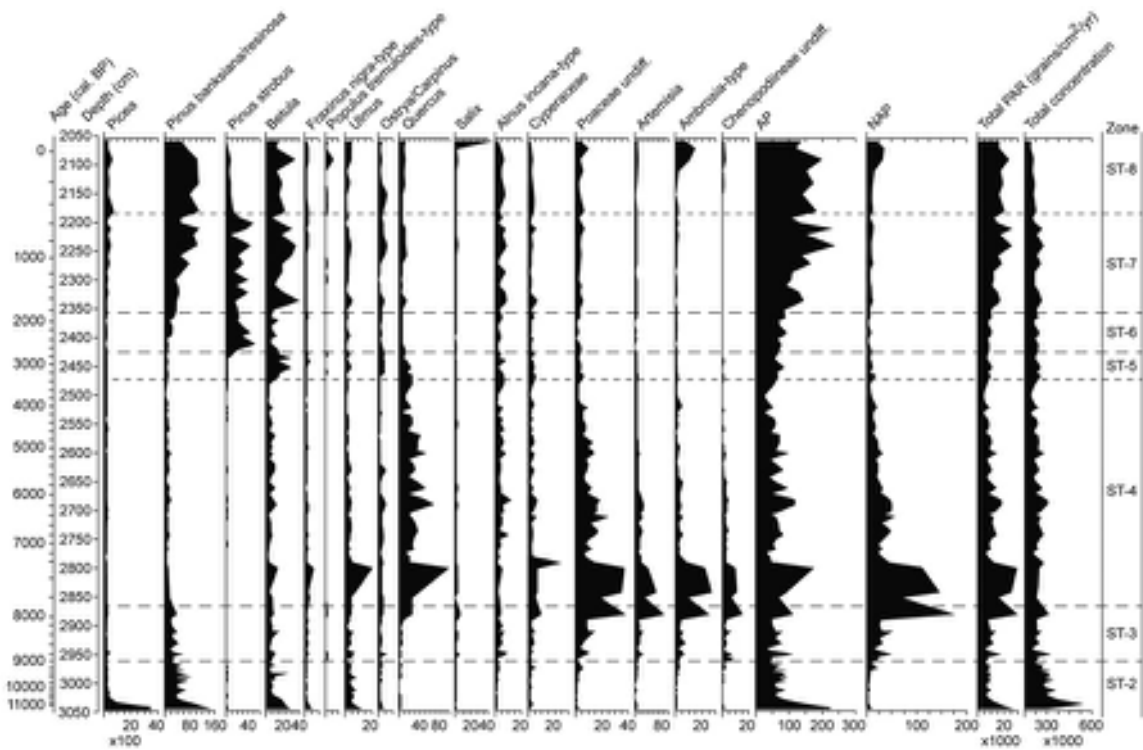


Figure 4.4 Pollen accumulation rate (PAR) data for a sequence spanning the last 11 ka at Steel Lake, central Minnesota, USA (from Wright *et al.*, 2004).

at constant rates, then the concentration of pollen will remain uniform. But pollen concentrations would increase if either the supply of pollen increased or the rate of sediment decreased, and vice versa.

In order to resolve this uncertainty, therefore, the rate of sediment accumulation must also be determined, so that 'absolute' changes in concentration per unit measure of time (pollen influx) can be established. This requires an independent chronology, which is usually provided by means of radiometric dating (Chapter 5). A series of age estimates from the profile enables the rate of sediment accumulation between dated horizons to be determined, and the **pollen concentration diagrams** can then be converted into **pollen influx diagrams**. These express the data in the form of number of pollen grains per square centimetre of surface of sediment per year or for some other unit of time. Again, however, care needs to be exercised when interpreting pollen influx data. In Figure 4.4, for example, the record appears to indicate an increase in the influx of arboreal taxa, notably *Pinus* (two species) and *Betula* (birch), after c. 3.4 ka. As is the case with many dated pollen records, however, the age scale has been derived from statistical curve-fitting through a series of radiocarbon dates, and is based on the assumption that the rate of sedimentation between the dated horizons was constant, something that can seldom be established unequivocally. Furthermore, in many palaeoecological studies, the constructed chronology is frequently based on a relatively low number of dates, all of which have statistical uncertainties (Chapter 5). In the case of calibrated radiocarbon dates, for example, the statistical errors are frequently centennial in scale (Telford *et al.*, 2004). Before interpreting pollen influx data, therefore, it is important to be aware of possible limitations in the age estimates and in the age-depth model upon which the influx calculations are based.

Pollen diagrams, whether percentage or 'absolute', are constructed in different ways, depending partly on tradition and partly on objective. Many diagrams show arboreal pollen on the left, and move through shrub, herb and aquatic taxa, with spores completing the record on the right-hand side. In other instances, the taxa may be arranged in alphabetical order or by plant families within the broad divisions of tree, shrub and herbaceous plants. In records from temperate regions, particularly from interglacial sequences, it is common to plot tree genera in the order in which they first appear, the advantage being that this may reflect the order of immigration of trees following their elimination from the landscape

during the preceding glacial episode (Figure 4.5). For many years, it was the convention in published pollen diagrams to show *all* pollen taxa counted, even where only single grains were recorded. More recently, however, it has become the practice to publish diagrams showing only the **principal pollen taxa**, as these fit more easily onto the printed page, and they focus attention on the key elements of the pollen record. The complete pollen counts may appear online as supplementary information, or are usually available on request from the author.

Diagrams are normally divided into a series of **pollen zones**, which are distinct stratigraphic intervals that are characterized by broadly similar pollen composition. Each zone is classified according to the dominant taxa, and highlights what are considered to be the key changes in vegetation cover reflected in the pollen record over the time interval represented. Until recently, pollen diagrams were traditionally zoned subjectively, but it is now more usual to employ multivariate statistical methods to avoid 'operator bias'. These include, for example, agglomerative ordination methods, such as principal components analysis, correspondence analysis and cluster analysis, which classify data according to degree of similarity as well as 'dissimilarity' (hierarchical partitioning techniques), and which enable a series of pollen spectra to be subdivided into discrete groups (Dale & Dale, 2002a). As Moore *et al.* (1991) have noted, however, all zonation systems are merely aids to interpretation and even an 'objective' system of zonation could be misleading if accepted without critical knowledge and appraisal of the ecological affinities of the taxa under consideration. Although some have questioned whether pollen zones need to be defined at all, there is a general consensus amongst palaeoecologists that in order to summarize, and ultimately to make sense of, the large body of complex multivariate data that is contained within a pollen diagram, some form of ordination scheme is essential (Bennett, 1996).

Most approaches to pollen zonation continue to follow principles first introduced by Cushing (1967), in that the pollen diagram is first divided into **local pollen assemblage zones**, usually on the basis of the principal terrestrial taxa. **Regional pollen assemblage zones** can then be established on the basis of observed common features between pollen diagrams obtained from neighbouring sites. These regional pollen zones therefore typify the suite of changes in vegetation that characterize given intervals, and examples include those for New England, USA (Shuman *et al.*, 2004), the Netherlands (Hoek, 1997) and North Island, New Zealand (Wilmshurst *et al.*, 2004).

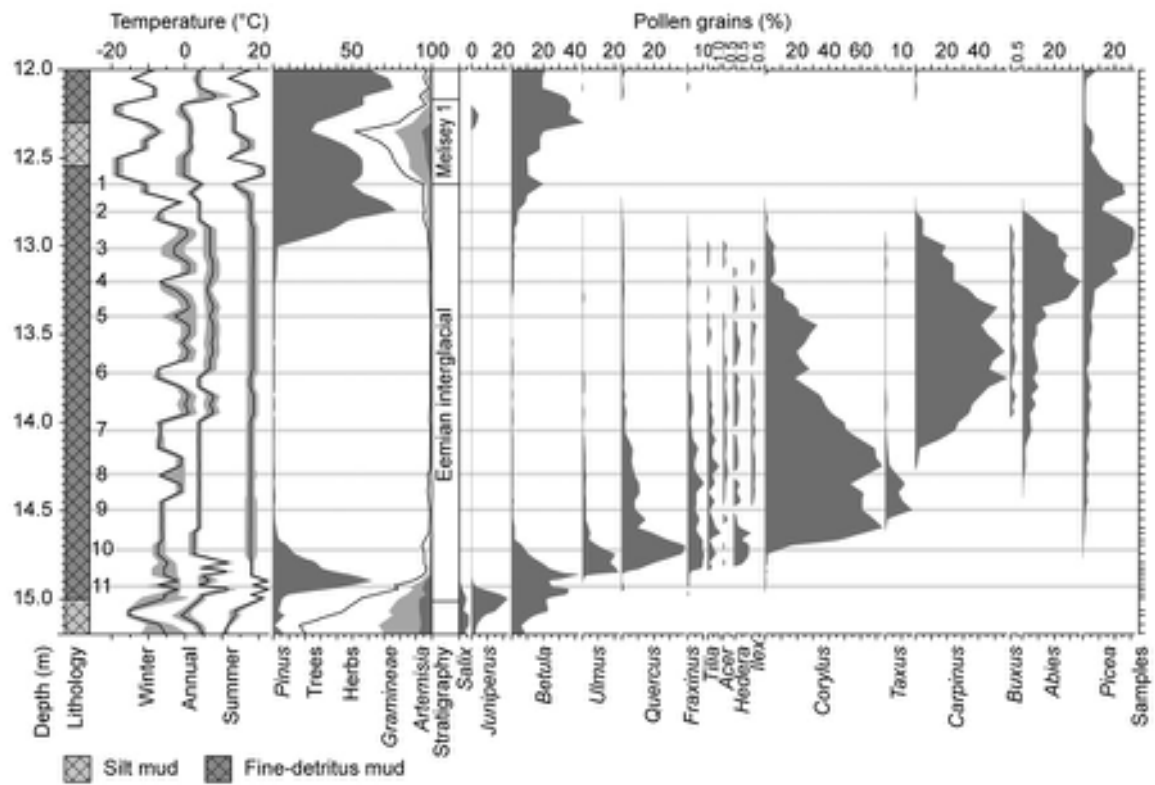


Figure 4.5 Arboreal pollen taxa recorded for last (Eemian) interglacial deposits at Jammtal, southwest Germany and palaeotemperature inferences based on the mutual present-day climate tolerances of the taxa. The grey horizontal bars, numbered to left, mark the positions of recurring short-lived cold events (from Müller *et al.*, 2005).

4.2.5 The interpretation of pollen diagrams

The interpretation of a pollen diagram is undoubtedly the most difficult part of pollen analysis, for it requires a knowledge of pollen production and dispersal, pollen source and deposition, pollen preservation and the relationship between fossil pollen and former plant communities. Only when these have been carefully evaluated can inferences be made about former vegetation cover and, by implication, about former climates and environments.

First, it is important to appreciate the fact that not all plants produce the same quantities of pollen. It has already been noted that entomophilous species usually produce much less pollen than anemophilous plants and will therefore be under-represented by comparison in modern surface samples and in the fossil record. Less well represented are the **autogamous** plants such as wheat (*Triticum*)

which are self-pollinating and which liberate very few pollen grains into the atmosphere, while in **cleistogamous** plants (e.g. *Viola*), the flowers never open and thus pollen is very rarely released. Within each of these plant types, however, there is considerable variation. Flowers of the lime (*Tilia cordata*) and ling (*Calluna vulgaris*), for example, are both insect-pollinated yet they usually liberate large quantities of pollen. On the other hand, beech (*Fagus sylvatica*) and oak (*Quercus petraea*) are both wind-pollinated, yet are often relatively low pollen producers. Table 4.1 gives some indication of the general variability in pollen production of some taxa that are commonly encountered in pollen diagrams from Europe. Although there are marked differences in the absolute quantities of pollen produced by these plants in different areas or vegetation associations, the rank order between them is often similar (Moore *et al.*, 1991). Indeed, some analysts have attempted to derive correction factors (or **R-values**) for tree and shrub taxa based on such rankings (e.g. Sugita,

Table 4.1 Estimates of the pollen production of various plant species. The index of relative pollen production in the final column is based upon estimates of the pollen production of an individual plant over a period of fifty years and is expressed relative to the estimated production of *Fagus* (beech) over the same period, which is used as a standard (from Erdtman, 1969).

Species	Number of pollen grains per anther	Number of pollen grains per flower	Number of pollen grains per catkin	Index of relative pollen production (cf. <i>Fagus</i> = 1.0)
<i>Trifolium pratense</i>	220			
<i>Acer platinoides</i>	1,000	8,000		
<i>Malus sylvestris</i>	1,400–6,250			
<i>Calluna vulgaris</i>	2,000 tetrads			
<i>Fraxinus excelsior</i>	12,500			
<i>Secale cereale</i>	19,000	57,000		
<i>Rumex acetosa</i>	30,000	180,000		
<i>Juniperus communis</i>		400,000		
<i>Pinus sylvestris</i>		160,000		15.8
<i>Picea abies</i>		600,000		13.4
<i>Betula pubescens</i>			6,000,000	
<i>Alnus glutinosa</i>			4,500,000	17.7
<i>Quercus robur</i>		1,250,000		
<i>Fagus sylvatica</i>				1.0
<i>Quercus petraea</i>				1.6
<i>Carpinus betulus</i>				7.7
<i>Betula pendula</i>				13.6
<i>Corylus avellana</i>				13.7
<i>Tilia cordata</i>				13.7

1994; Odgaard, 1999), based on the premise that taxa with high R-values are likely to be over-represented in the pollen record, while those with low values will be under-represented. Attempts to apply scaling or weighting ratios to correct for statistical biases caused by differential pollen production have proved problematic, however, as other factors (considered below) affect the mix of pollen delivered to sedimentary archives. Alternative approaches to calibrating fossil pollen spectra include modern analogue studies, which test for characteristic pollen suites associated with particular vegetation zones or niches (Whitmore *et al.*, 2005), and simulation models of pollen dispersal and deposition (Sugita, 2007).

Second, it is necessary to know something about the source of fossil pollen in a body of sediment. It is important to establish whether plants were growing on the bog surface or within the lake basin, around the margins of the site, in the immediate vicinity or some distance away. Moreover, it is necessary to know something of the

transport mechanisms by which the pollen are transferred from source to eventual point of deposition. Pioneering investigations by Tauber (1965) suggested that, in a forested region, airborne pollen arrives at a bog or lake surface by one of three pathways: either through the trunk space, through the forest canopy, or from raindrop impact. Factors such as wind speed through the trunk space and canopy, the density of woodland cover, thickness of foliage, time of pollination of the trees, and the size, shape and proximity of a bog or lake surface to pollen source, will all play a part in determining the composition of the pollen deposited. Since Tauber's innovative work, numerous studies have investigated the complexities of pollen dispersal and recruitment and their influence on pollen deposition in different sedimentary contexts (e.g. Nielsen & Odgaard, 2004). Contemporary pollen deposition can be monitored by analysing soil surface samples (Elenga *et al.*, 2000) or moss polsters collected from bog surfaces (Wilmshurst & McGlone, 2005b), or by the use of pollen

traps designed to capture pollen from the atmosphere, lake surface or sediment–water interface (Gosling *et al.*, 2003). These approaches provide valuable quantitative data on pollen compositional variation at the local, regional and continental scales (see section 4.2.6), and offer a basis for calibrations to correct for over- or under-representation of plant taxa in the pollen record (Sugita, 2007).

The mix of airborne pollen deposited at any one locality will also depend upon the surface area of a site in relation to surrounding vegetation. Pollen influx to a small lake basin surrounded by a dense tree cover will be dominated by pollen from the immediate vicinity, whereas a large open lake or bog surface will receive a higher proportion of airborne pollen derived from a larger regional catchment or from even further afield (Giesecke & Fontana, 2008). Analysis of sediment samples from the former site will, therefore, provide evidence of local vegetation composition, while data from the latter will be more likely to reflect the regional vegetation cover. According to Sugita (1994), the dominant source area reflected in pollen assemblages accumulating in small woodland hollows of 2 m radius lies within 50–100 m of the hollow, whereas the equivalent sources lie 300–400 m and 600–800 m from the edges of sites with radii of 50 and 250 m, respectively. Transport by inflowing streams is also an important process in pollen recruitment in lake sediments (Brown *et al.*, 2007a), and in some lakes in temperate regions, up to 90 per cent of the pollen accumulating on the lake bottom may be derived from inflowing streams and groundwater (e.g. Bonny, 1980). Data from Africa show that river-transported pollen is especially high around deltas (DeBusk, 1997), while in China, pollen transport by streams flowing from mountain areas into lowland lakes has generated pollen spectra that are markedly different from those obtained from plant communities in the lake hinterlands (Chen *et al.*, 2006). There will also be a local pollen input from aquatic plants growing in the lake or from mire plants growing on a bog surface or at the edges of a lake. Finally, there may also be a secondary component from pollen which has been deposited around the catchment and which has subsequently been remobilized and incorporated into lake sediments at a later date (see below).

Studies of contemporary pollen dispersal in relation to species composition of the vegetation around the sampling site suggest that most wind-borne pollen is deposited within a few kilometres of its source, and only a very small proportion of the pollen grains liberated into the atmosphere is likely to travel very far (e.g. Seppä & Bennett, 2003). In certain circumstances, however, and under particular synoptic conditions, some tree pollen grains may travel over considerable distances as reflected, for example, in the

presence of arboreal pollen in contemporary spectra from the Greenland tundra (Rousseau *et al.*, 2006) and the high alpine heathlands of Fennoscandia (Hicks *et al.*, 2001). Far-travelled arboreal pollen has even been found in high Arctic ice cores (Bourgeois *et al.*, 2000) and in small lakes in East Antarctica (Bera, 2004). These and other studies indicate that upper air currents often contain a ‘background’ component of long-distance pollen that can potentially contribute to local or regional pollen assemblages. This will tend to be insignificant (perhaps undetectable) where the local vegetation cover generates a high pollen influx, but in poorly vegetated polar or subpolar regions where local pollen influx is low, this far-travelled component may register more strongly and may be a feature of, for example, pollen assemblages in Quaternary cold stage deposits in mid- and high-latitude regions.

A third factor to be considered when pollen diagrams are being interpreted concerns the nature of pollen deposition. Differential settling velocities of pollen in lakes and ponds, coupled with the disturbance of sediment on the lake floor, either by currents or by burrowing organisms, can lead to complications in the fossil record. Equally misleading can be the occurrence of redeposited or secondary pollen that has been washed into the lake by stream flow, overland flow, solifluction or collapse of the basin edge sediments, and the subsequent redistribution of material across the lake floor (Campbell, 1999). These grains will clearly be of a different age from those arriving at the lake surface from the atmospheric pollen rain, and although they can often be distinguished from the primary pollen by signs of exine deterioration (see below), they are potential sources of confusion in the interpretation of the biostratigraphic record.

In general, there are fewer uncertainties where mire and bog sites are used in preference to lakes, although here too complications may still arise. Studies have shown that when pollen arrives on the surface of a bog, there may be a tendency for both lateral and vertical mixing to occur, with the larger grains remaining on the surface while smaller grains may migrate downwards into the peat (Clymo & Mackay, 1987). However, these movements are believed to be relatively insignificant when set against the timescales usually involved in peat accumulation. More problematical is the behaviour of pollen and spores in soils. A major difficulty with soil pollen analysis is that the processes of leaching and capillary action will have the effect of moving fossil grains up and down the profiles (Davidson *et al.*, 1999). Mixing by earthworms and other soil organisms further exacerbates the problem, although discrete pollen assemblages have been detected where earthworm populations have burrowed to progressively

shallower depths as soil profiles have developed (Miura, 1987). The analysis of pollen assemblages in cave sediment is also considered problematic, partly because of the possibility of downward migration of pollen in coarse-grained deposits (Bennett & Willis, 2001), and also because cave animals may disturb cave-floor deposits by trampling, or, in the case of bats, introducing pollen foraged from vegetation far removed from the cave (Hunt, 2005).

Fourth, many fossil pollen grains show signs of deterioration resulting from physical, chemical and biological attack on the exine. Experimental work has shown that pollen and spores vary in their susceptibility to such processes as oxidation and corrosion (Table 4.2). Some grains, for example spores of the clubmosses (*Lycopodium*) and certain ferns (*Polypodium*), show remarkable resistance to deterioration, while others, such as the more delicate grains of nettle (*Urtica*) and poplar (*Populus*), may be destroyed altogether. As a consequence, some pollen types tend to be under-represented in the fossil record while others may be over-represented. Damage to pollen may be chemical or physical in nature, the former caused by groundwater solutions, exposure to air (oxida-

tion) or bacterial attack, and the latter by mechanical abrasion, rupture or compaction during transportation, settling and burial. Four categories of deterioration in fossil pollen grains are commonly observed: **corrosion**, where the exine is pitted or etched; **broken**, where grains are ruptured or split, or where pieces have completely broken away; **crumpled**, where grains are folded, twisted or collapsed; and **degraded**, where the structural elements are fused together presenting a ‘solid’ or ‘fossilized’ (waxy) appearance to the grain. Fossil pollen grains frequently display more than one of these deterioration characteristics (Tweddle & Edwards, 2010).

The type of deterioration is largely a function of the nature of the depositional environment (Tweddle & Bunting, 2010). Corroded grains usually reflect oxidation in poorly compacted peats or soils subject to periodic drying, while degraded grains are frequently indicative of secondary deposition, the exine surfaces having undergone structural modification through reworking. As such, deteriorated pollen records may provide useful corroborative information on local environmental conditions, and may also reveal the occurrence of redeposited pollen (Wilmshurst and McGlone, 2005; Tweddle & Edwards, 2010). Pollen in soils and loess deposits are sometimes so poorly preserved that identification becomes difficult or even impossible (Tomescu, 2000), but even in undisturbed, waterlogged fen deposits some degree of pollen degradation may be encountered (Jones *et al.*, 2007a). Given that high levels of degradation might have led to the preferential removal of important plant types from the record, analysis of the amount and type of pollen degradation should perhaps be more widely employed in fossil pollen analysis.

Finally, there is the vexed question of how far it is possible to relate pollen assemblages to plant communities, and how far we are justified in making inferences about former climatic and environmental conditions on the basis of pollen analytical data. It is now generally accepted that many former plant communities, especially those dominated by herbaceous taxa, which were characteristic of large areas of the mid-latitude regions of the Northern Hemisphere during the cold phases of the Quaternary, have no analogues in the modern flora (West, 2000). Research in both western Europe and North America has shown that at times of climatic stress, each plant type responds individually, so that even though successive warm or cold stages were characterized by broadly similar climatic conditions, quite different plant associations developed (Williams *et al.*, 2004b). In some instances, it seems, plant communities may never have been in equilibrium with prevailing climatic conditions. Pollen records from the Colombian Andes, for example, indicate that low-latitude

Table 4.2 Corrosion and oxidation susceptibility of selected pollen and spores (from Havinga, 1964).

a) Sequence of increasing corrosion susceptibility of selected pollen and spores	
<i>Lycopodium</i>	LOW
Conifers	
<i>Tilia</i>	
<i>Corylus</i>	
<i>Alnus, Betula</i>	
<i>Quercus</i>	
<i>Fagus</i>	HIGH
b) Sequence of increasing oxidation susceptibility of selected pollen and spores	
<i>Lycopodium clavatum</i>	LOW
<i>Polypodium vulgare</i>	
<i>Pinus sylvestris</i>	
<i>Tilia</i> spp.	
<i>Alnus glutinosa, Corylus avellana</i>	
<i>Betula</i> sp.	
<i>Carpinus betulus</i>	
<i>Populus</i> spp.; <i>Quercus</i> spp.; <i>Ulmus</i> spp.	
<i>Fagus sylvatica, Fraxinus excelsior</i>	
<i>Acer pseudo-platanus</i>	
<i>Salix</i> spp.	HIGH

montane ecosystems were much more dynamic in the recent geological past than previously realized, and here it seems that the composition of the vegetation changed with such relative rapidity and frequency that stable plant communities rarely, if ever, existed (Hooghiemstra & van der Hammen, 2004).

These difficulties are further compounded by the limitations imposed on palaeoecological inferences by the taxonomic imprecision of pollen identification. Under normal microscopy, it is occasionally possible to identify pollen grains to the species level; distinctions can usually be made, for example, between species of plantain (*Plantago*), saxifrage (*Saxifraga*) or clubmoss (*Lycopodium*). More frequently, identifications are made only to the generic level, for example in identifying pollen of tree birch (*Betula*), willow (*Salix*) or mugwort (*Artemisia*), while in other cases it is often difficult to subdivide beyond the family level. Grass (Poaceae) and sedge (Cyperaceae), for example, are rarely taken to the generic or specific level. However, considerable progress has been made in recent years in the quality of instrumentation (e.g. SEM analysis and optics of higher resolution in standard microscopy) while detailed taxonomic studies have provided clearer diagnostic criteria for identifications to lower taxonomic levels (Reille, 1995; Punt *et al.*, 2009). Despite these technical and methodological advances, however, pollen diagrams remain a data bank at a variety of taxonomic levels, and this obviously imposes major constraints upon the reconstruction of former plant communities, particularly as some plant families and genera include species with markedly contrasting ecological affinities.

The reader may be forgiven for thinking that these difficulties in the interpretation of pollen data render the technique of dubious value to the analysis of Quaternary environments. That this is clearly not the case is demonstrated by the remarkable degree of consistency in the large number of pollen-based research publications that have appeared in the Quaternary literature in recent years. Some of the many important applications of pollen analysis are considered briefly in the following section.

4.2.6 Applications of pollen stratigraphy

In the ninety or so years since the technique was developed, fossil and modern pollen data have been published from a large number of sites around the world. While the density of records is highest in Europe and North America, numbers from other parts of the globe are increasing rapidly. This enormous body of data is difficult for individual researchers to store and to collate and so, in recent

years, a considerable international effort has been directed towards the development of [regional pollen databases](#). Under the aegis of approved nationally funded data centres (such as NOAA in the USA), or international collaborative initiatives (e.g. the European Pollen Database), pollen records are held in standardized formats in electronic archives for use by the global scientific community. The data can be remotely accessed and interrogated in a variety of ways. Individual site records can be downloaded, or pollen data can be synthesized to enable reconstructions of vegetation change to be made at a range of spatial scales (see below).

4.2.6.1 Local vegetation reconstructions

Tracing the course of local vegetation developments has been, and still remains, a central theme of pollen analysis. Pollen records from peat and lake cores enable inferences to be made about the history of a particular peat bog or lake ecosystem (Woolfenden, 2003), while in sites where pollen diagrams have been obtained from a number of different profiles ('three-dimensional pollen analysis'), changes in the local vegetation cover can be mapped through time (Bos *et al.*, 2006). In coastal regions, pollen analysis can help elucidate the history of sea-level change, as positive and negative sea-level tendencies (section 2.5.2.2) will be reflected in local pollen records by changes between saltmarsh and terrestrial or freshwater plant communities (Roe & van de Plassche, 2005). Understanding the nature of local vegetation changes is a prerequisite to establishing the scale and pattern of regional changes in vegetation, as well as the impact of humans on vegetation communities (section 4.2.6.4).

4.2.6.2 Regional vegetation reconstructions

For many years, pollen data have constituted one of the principal lines of evidence for reconstructing vegetational history at the regional and extra-regional scales. Not only does the technique enable large-scale vegetation patterns to be established, it allows the history of both individual species and entire vegetational assemblages to be traced through time (Webb *et al.*, 2003a). Regional biotic catastrophes may also be reflected in pollen records including, for example, the *Tsuga* (hemlock) decline at c. 4.9 ka in eastern North America (Bhairy and Filion, 1996) and the *Ulmus* (elm) decline at around 5.8 ka in western Europe (Parker *et al.*, 2002), both of which have been attributed to disease, although in the case of the elm decline, human activity may have been a contributory factor (Peglar & Birks, 1993).

4.2.6.3 Space-time reconstructions

Where a network of securely dated pollen records exists, maps can be compiled showing changes in vegetation pattern through time. These may be based on **isopollen maps** (sometimes referred to as ‘**isochrone maps**’), which provide ‘snapshots’ of regional vegetation cover for selected time periods (Birks, 1989). Pollen percentages of selected taxa are obtained from all sites within a region for a particular time interval; these are then plotted on maps which are contoured to reflect spatial variations in each taxon’s abundance. Data can be displayed for consecutive periods showing the changing distributions of selected taxa over time (Latalowa & Van der Knaap, 2006) and **palaeovegetation maps** can be generated to show the overall change in vegetation composition and distribution through time (Figure 4.6).

Isopollen and palaeovegetation maps for the Lateglacial and Holocene periods have been constructed for both Europe (Huntley, 1992) and North America (Williams, 2002). Such maps provide a basis for testing hypotheses relating, for example, to the responses of individual taxa or vegetation as a whole to global climatic changes or other environmental influences; to areas where temperate trees survived (**plant refugia**) during glacial stage conditions (Magri, 2010); and to patterns and rates of plant migration during climatic transitions (Klotz *et al.*, 2004). Isopollen maps also have applications in studies of faunal history, soil–vegetation relationships, human impacts on vegetation and the estimation of former **biomass** (Adams & Faure, 1998). The last-named is of particular importance in the development of global climate and earth system models, and particularly to the role that vegetation plays in carbon storage and the global carbon cycle (see Chapter 7). In comparisons between palaeovegetation reconstructions and general circulation models, however, the pollen data are usually simplified using the concept of **plant functional types (PFT)**² or **plant biomes**,³ in order to represent the dynamics of vegetation change over millennia at the continental or global scale (Williams *et al.*, 2004b; Edwards *et al.*, 2005).

4.2.6.4 Human impact on vegetation cover

Human impact has been the dominant factor affecting the vegetation cover of Europe since the beginning of the Neolithic period (around 7 ka in northwest Europe), and the effects of widespread woodland clearance, farming practices and the introduction of new plant species into regions have left clear imprints in pollen records, especially in sites closely associated with human activities. In southern

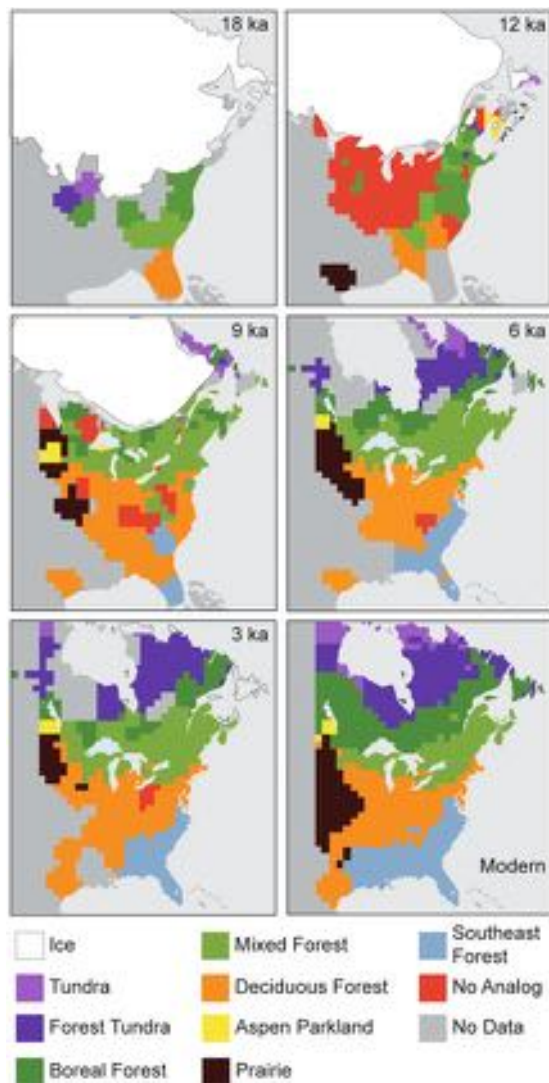


Figure 4.6 The changing vegetation cover of the eastern USA from 18 ka to present. These maps, lodged on the NOAA web site, are based on 11,700 fossil pollen samples and 1,744 modern pollen samples. Twenty-one pollen taxa were included in the analyses: *Alnus*, *Fraxinus*, *Populus*, *Tilia*, *Fagus*, *Betula*, *Ulmus*, *Abies*, *Celtis*, *Corylus*, *Tsuga*, *Carya*, *Ostrya/Carpinus*, *Quercus*, *Pinus*, *Prairie*, *Cyperaceae*, *Picea*, *Liquidambar*, *Platanus* and *Juglans* (based on original work by Overpeck & Webb, 1992, republished with permission of Geological Society of America; for additional information see the NOAA web site at <http://www.ncdc.noaa.gov/paleo/vegmap.html>).

Switzerland, for example, pollen records spanning the last 7 ka (Figure 4.7) show marked changes in woodland cover resulting from burning, with peaks of charcoal repeatedly associated with reductions in pollen of fir (*Abies*), ivy (*Hedera*), lime (*Tilia*), elm (*Ulmus*) and beech (*Fagus*), but with increases in hazel (*Corylus*), willow (*Salix*) and elderberry (*Sambucus*). In many northwest European pollen records, clearance of woodland to facilitate pastoral activities or cultivation is reflected not only by reduced frequencies of arboreal pollen, but also by increases in pollen of ruderal taxa that are characteristic of arable or pastoral land, or by the appearance of pollen grains of cereals. These pollen signals are commonly referred to as '**anthropogenic indicators**' (Behre, 1986), and an example of the way in which they register in pollen records is shown in Figure 4.8. This diagram, from the Aran Islands in western Ireland, demonstrates the degree to which people modified the vegetation cover during the mid-Holocene. Trees and shrubs begin to disappear from the record at the end of the Neolithic period, and are replaced by herbaceous plants associated with pastoral activity. A short-lived episode of woodland regeneration during the late Iron

Age is followed by a further reduction in tree/shrub pollen and by the appearance of cereal pollen, reflecting the establishment of a mixed farming economy from the Medieval period onwards (Molloy & O'Connell, 2004). Pollen diagrams with clear anthropogenic indicators can also provide insights into land management techniques (Berglund *et al.*, 2008), prehistoric and historic farming practices (Veski *et al.*, 2005b) and activities around ancient settlement sites, such as those of the initial colonization of the Faroe Islands and New Zealand (Wallin, 1996; Arge *et al.*, 2005). Pollen records can also reflect the environmental impacts of early mining operations, especially when combined with geochemical evidence from the same sequence (Breitenlechner *et al.*, 2010), and of military invasion and occupation (Manning *et al.*, 2007). Along with other indicators of human activity, such as increased sediment accumulation in lakes, the occurrence of charcoal into peat and lake sediments, and changes in soil characteristics, pollen-stratigraphic records provide important insights into the evolution of the '**cultural landscape**' in different regions of the world, particularly during the mid- and late-Holocene period (Hellman *et al.*, 2009).

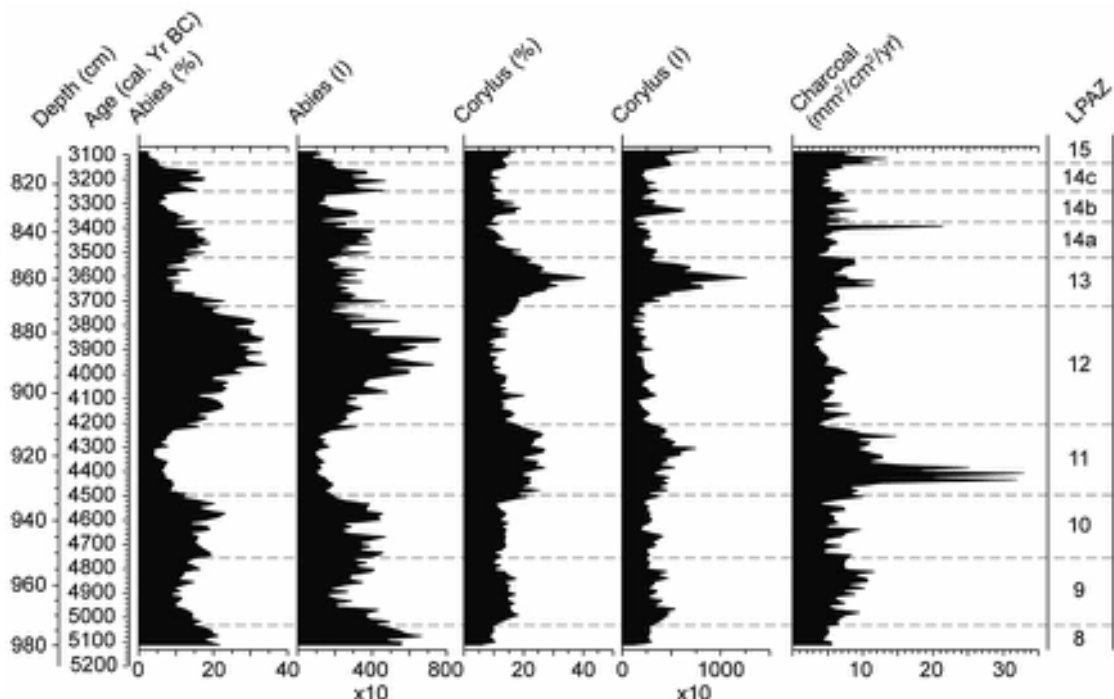


Figure 4.7 Pollen percentage (%) and influx (lI) diagram for *Abies* (fir) and *Corylus* (hazel), and charcoal influx record, from a site in south Switzerland spanning the period 5.1–3.1 cal. BC (from Tinner *et al.*, 1999).

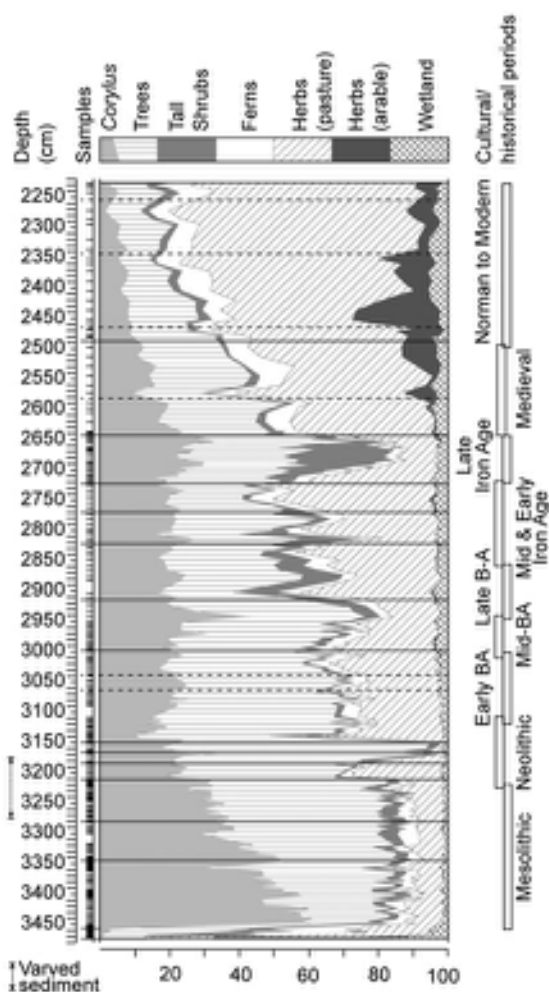


Figure 4.8 Holocene pollen diagram from the site of An Loch Mor, the Aran Islands, western Ireland. Apart from *Corylus*, which was a dominant shrub in the early Holocene, other taxa are grouped into plant types and their varying proportions are related to archaeological (cultural) and historical periods (from Molloy & O'Connell, 2004).

4.2.6.5 Pollen data and climatic reconstructions

Pollen data have long been used to reconstruct Quaternary climates. Indeed, some of the earliest systematic attempts to derive climatic parameters from fossil evidence employed pollen records (Faegri & Iversen, 1989). The initial approaches relied largely on **indicator species** in pollen diagrams, that is, individual plants with recognized

climatic affinities (Zagwijn, 1994). However, problems relating to the taphonomy of pollen assemblages (see section 4.1.2) and also the differential migrational response of plants, especially trees, to climatic change, can lead to erroneous palaeoclimatic inferences. More recent approaches to climatic reconstructions using pollen data have involved the development of **pollen response functions**, which measure, in a quantitative way, the dependence of a range of plant taxa or of broad-scale vegetation patterns on climate (Seppä & Bennett, 2003). Relationships are determined between spatial variations in modern vegetation and contemporary climatic parameters, usually mean annual or summer temperatures. These form the basis for a **pollen–climate training set** which enables the inter-dependence of these variables to be tested statistically. Selection of an optimal mathematical relationship provides a statistical **transfer function**⁴ that is used to infer past climatic conditions from analogous pollen assemblages (**calibration**). So long as the training set encompasses the full range of plants represented in the fossil record, then variations of climate through time can be inferred (Figure 4.9). However, the training set must accurately reflect the vegetation composition of the study area. Moreover, many of the plants commonly recorded in pollen spectra have wide climatic tolerances, and those with the narrow climatic preferences that are most valuable in palaeoclimatic reconstructions are frequently present in relatively low abundance. In addition, transfer functions assume equilibria between biota and the environment, and may produce aberrant results at times of climate–environment disequilibria (Birks & Seppä, 2004; Finsinger *et al.*, 2007). These limitations notwithstanding, however, pollen response functions are undoubtedly a powerful tool for climatic reconstruction, and are being increasingly widely used in integrated modelling of past climates at a range of spatial and temporal scales (Seppä *et al.*, 2004; St. Jacques *et al.*, 2008).

4.3 DIATOM ANALYSIS

4.3.1 Introduction

Although several members of the algal kingdom have been studied by Quaternary palaeoecologists, including the green algae, blue-green algae and chrysophytes (Armstrong & Brasier, 2005), it is **diatoms** that have attracted most attention, since their classification and ecological preferences are much better understood. Diatoms have been studied for over two centuries and the analysis of the diatom content of Quaternary sediments actually predates pollen analysis (Round *et al.*, 1990). By the end

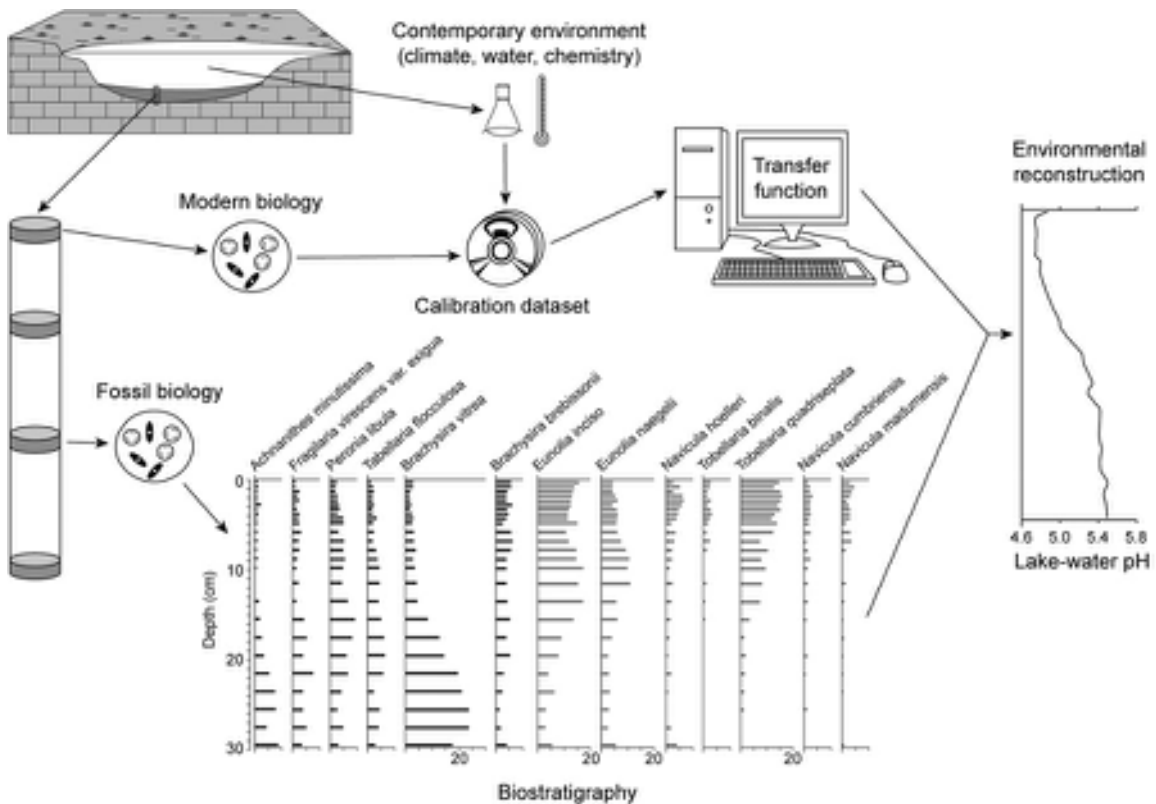


Figure 4.9 Schematic representation of the procedures employed to derive quantitative lake-water pH reconstructions from fossil diatom records (from Birks & Seppä, 2004, but based on an unpublished diagram by Steve Juggins, Newcastle University, UK). Although this schematic relates to diatoms, the procedure can be adapted to quantify the relationships between other biological proxies and environmental variables, for example pollen assemblages and climate.

of the nineteenth century, a considerable amount of work had been undertaken on diatom remains, and while most of these studies had little stratigraphic or palaeoecological value, they laid the foundations for later research on diatom taxonomy. Diatoms are ubiquitous, being found in virtually every body of water (Jones, 2007), while in the oceans, they generate most of the organic matter that supports marine life, accounting for something like one-fifth of all photosynthesis on earth (Armbrust, 2009). Quaternary diatom remains have proved extremely useful as indicators of local habitat changes, particularly in lake sediments, but also in both shallow and deep marine deposits. The analysis of diatom floras has provided new insights into a wide range of palaeoenvironmental issues, such as the reconstruction of lake-level changes, water chemistry variations, sea-level changes and the disturbance of lake ecosystems by human activities (Smol & Stoermer, 2010).

4.3.2 The nature and ecology of diatoms

Diatoms are microscopic, unicellular members of the Bacillariophyta of the algal kingdom (Figure 4.10). They secrete a siliceous shell or structure, known as a **frustule** which can range in length from 5 µm to c. 2 mm, depending on the species (Battarbee *et al.*, 2001). The frustule is often compared to a pill-box, as it consists of two overlapping valves or **thecae**, the larger one (**epitheca**) fitting over the smaller one (**hypotheca**) in a box fashion to enclose the living (protoplasmic) mass. The valves are linked together by connecting girdle bands (**copulae**). The wall of the frustule may be a single layer of silica or it may be more complex, consisting of a double silica wall separated by vertical silica slats. Frustules are commonly circular (**centric**) or elliptical to rod-like (**pennate**) in shape and are perforated by intricate patterns of tiny apertures (**punctae** or **areolae**).

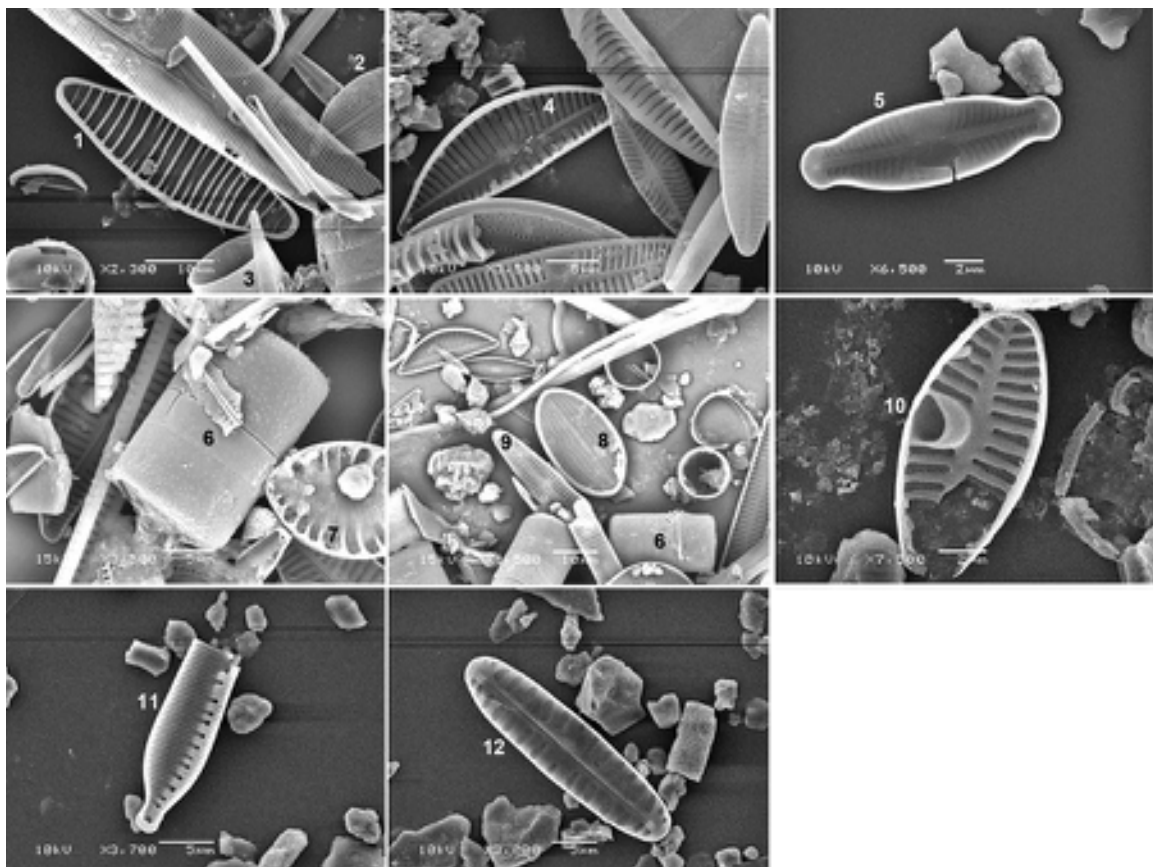


Figure 4.10 SEM images of common northwest European diatom frustules recovered from streams and soils in southeast England. 1 – *Diatoma* sp. (valve view). 2 – *Cocconeis placentula* (valve view). 3 – *Melosira varians* (girdle view). 4 – *Encyonema ventricosum* (valve view). 5 – Unknown naviculoid (valve view). 6 – *Melosira varians* (girdle view). 7 – *Surirella* sp. (valve view). 8 – *Cocconeis placentula* (valve view). 9 – *Achnanthes* sp. (valve view). 10 – *Planothidium frequentissimum* (valve view). 11 – *Hantzschia amphioxys* (fragment) (valve view). 12 – *Pinnularia borealis* (valve view) (images by Kirstie Scott, University College London, UK).

The arrangement of the perforations is one of the most important diagnostic characteristics of diatoms, although other structural details, as well as in tiny reticulations, canals and ribs, are important for classification below the generic level, so that careful scrutiny of the valves under a high-powered microscope is necessary for species identifications. The frustules are composed of amorphous hydrated silica, similar to opal, which enhances their preservation potential in different sedimentary environments.

Diatoms are found in a wide range of aqueous to subaqueous environments, including soils (Clarke, 2003), and make up about 80 per cent of the world's primary producers. They exist in bottom-dwelling (**benthic**), attached (**epiphytic** – attached to plants; **epilithic** – attached

to stones) and free-floating (**planktonic**) forms, and while all species require light and are therefore limited to the **photic zone** (usually less than 200 m water depth), they occupy a large number of ecological niches. In the sea, they are found in lagoons, shelf seas and deep oceans; they are common in the intertidal zone in estuaries and salt marshes; and they are often abundant in ponds, lakes and rivers. Certain species even live on wetted rocks, in the soil or attached to trees. The freshwater, soil or epiphytic niches are dominated by pennate diatoms, while the centric forms tend to be more common as free-floating plankton in ocean waters, especially in the subpolar and temperate latitudes. Marine benthic habitats, however, are characterized by pennate forms.

The distribution of diatom species is determined by a number of variables, including water acidity and salinity, oxygen availability, nutrient content and water temperature. Freshwater diatoms are controlled largely by salinity, pH and trophic status (Battarbee *et al.*, 2001), while sea-surface temperatures, oceanic frontal contrasts and nutrient up-welling influence the distribution of many marine taxa (Burckle, 1998). Changes in any of these parameters can have a major effect on the structure and composition of the diatom community. The autecology of modern diatoms has been extensively studied (Smol & Stoermer, 2010) and a range of quantitative methods has been developed to relate modern diatom assemblages to contemporary habitat and environmental conditions (see below).

4.3.3 Field and laboratory methods

Diatom valves, like pollen grains, are best preserved in fine-grained sediments since they can be easily damaged or destroyed in coarse-grained deposits. Samples for analysis can be obtained from vertical exposures in shallow water marine or estuarine deposits, though more frequently they are extracted from sediment cores obtained from lakes, shelf seas or the deep ocean floor (e.g. Koç, 2007; Barron & Bukry, 2007). Diatoms are not susceptible to oxidation or microbial degradation, but cores for diatom analysis are usually sealed air-tight to prevent drying out of the sediment, which can lead to fracturing of the valves.

Diatom frustules may be separated from the sediment matrix by a variety of laboratory procedures (Serieyssol *et al.*, 2011). Organic matter is removed by oxidation, the most common methods being by digestion in H₂O₂ or in a mixture of potassium dichromate and sulphuric acid, while carbonates and certain other salts can be dissolved by heating gently in dilute hydrochloric acid. Much more difficult is the removal of mineralogenic matter, since diatoms are soluble in some acids, and especially in hydrofluoric acid (HF) which is commonly used in the preparation of pollen samples. This means that diatom and pollen counts cannot be carried out on the same slides since the samples have to be prepared separately. Coarse mineral particles (> 500 µm) can be removed by sieving or by gentle swilling in a beaker, but finer particles require either some form of flotation using heavy liquids, or the less efficient differential centrifugation method. The residues are mounted on slides and counted under a microscope using phase-contrast illumination and magnification of up to ×1,000. Diatoms are often more abundant than pollen in sediment samples, and a count of 500 or 1,000 valves may form a statistically significant total (the ‘diatom sum’).

As with pollen grains, identifications are based upon type collections, keys and photographs in diatom manuals and catalogues (e.g. Round *et al.*, 1990). Nevertheless, diatoms are often difficult to classify and recent inter-comparison exercises have revealed discrepancies in taxonomic conventions between different countries, a problem that is being addressed by the development of international taxonomic quality control standards (e.g. Stoermer, 2001). Online guides to diatom identification are available, for example via the US Geological Survey at <http://westerndiatoms.colorado.edu/>, while attempts are being made to automate the process, such as the Automatic Diatom Identification And Classification (ADIAC) project (Bayer & Juggins, 2002).

Three principal methods have been developed for the determination of diatom concentrations in sediment samples. The **aliquot method** uses a measured volume of sample suspension which is pipetted on to a circular coverslip and the total number of frustules per unit volume is estimated. The **evaporation tray method** uses a measured volume of suspension which is added to a coverslip and from which the water is allowed to evaporate at room temperature. The diatoms are then counted and since the original volume is known, the concentration can be measured. The use of **microsphere markers** is the third method. These are tiny spherules made of glass or plastic which are added in known numbers to an aliquot of sample suspension, and concentrations of diatoms can be calculated from the ratio of diatoms to spherules. This third method is similar in principle to the estimation of pollen concentrations using exotic pollen markers, and sometimes yields better results (Wolfe, 1997). Measures of diatom concentration underpin estimates of diatom productivity, and are important for quantifying silica storage and flux in the global silica cycle (Bradtmiller *et al.*, 2006).

Diatom counts based on samples selected from a stratified sediment sequence are normally presented in the form of a percentage diagram using bar histograms (e.g. Figure 4.11). These can be subdivided in a similar way to pollen diagrams (see above), either subjectively on the basis of visual inspection of the data, or by statistical ordination techniques that test for structure and spatial variability within the data (Webster & Oliver, 2000). Other methods of data presentation that have been employed by diatom analysts include the tabular format, where counts are listed in percentages, and the **composite** or **ratio** diagram, whereby groups of diatoms with particular environmental affinities are added together to show the ratio variations between the different groups (e.g. Figure 4.12).

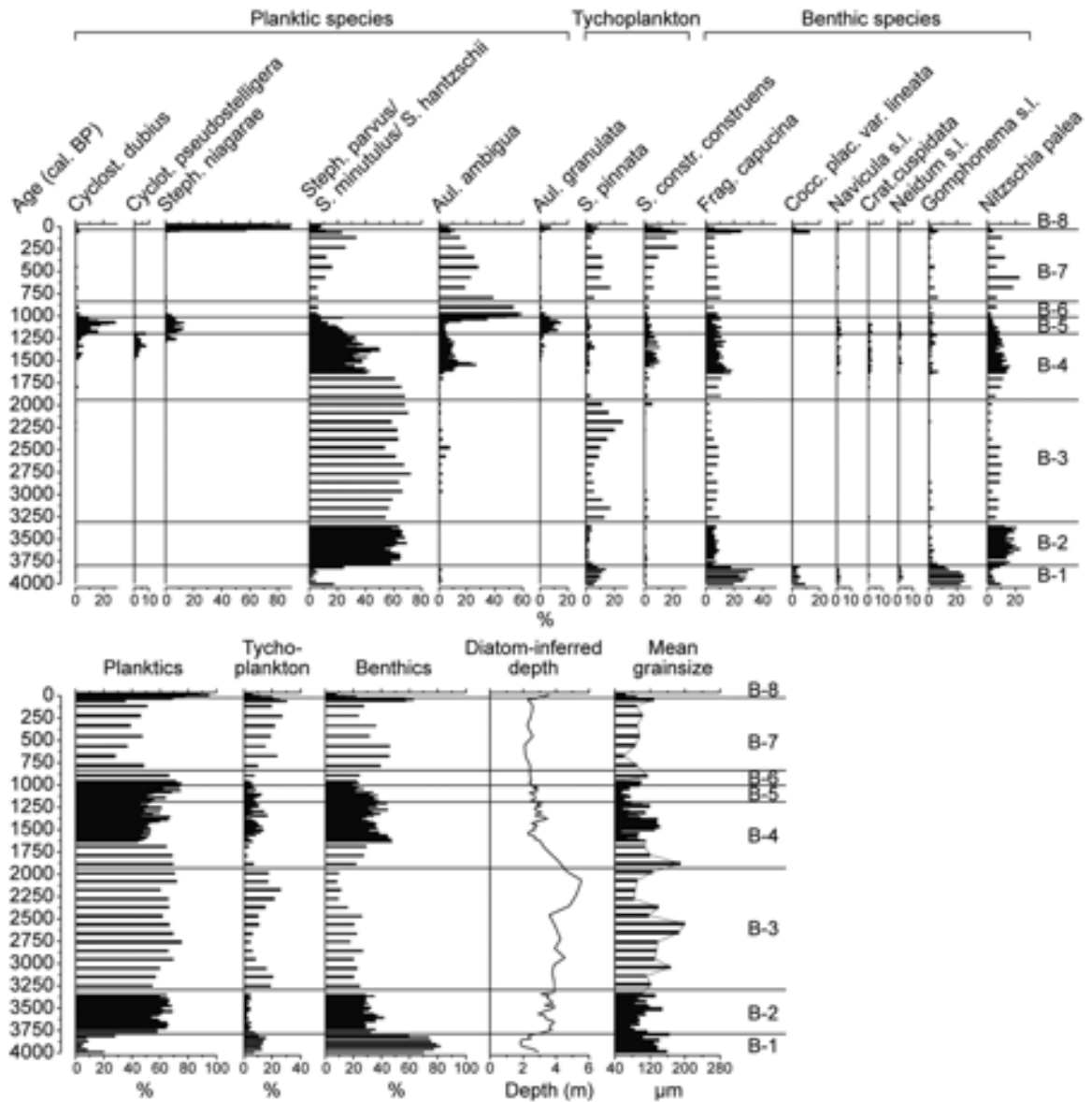


Figure 4.11 Late Holocene diatom stratigraphy from Beaver Lake in the Nebraska Sand Hills, USA. Variations in percentages of planktic, benthic and tychoplanktic species enable variations in lake-water depth to be inferred. Tychoplankton (or pseudo-plankton) are siliceous forms, particularly algae, that become enmeshed in vegetation mats near lake shores (from Schmieder *et al.*, 2011).

4.3.4 The interpretation of Quaternary diatom records

The difficulties that arise in the interpretation of diatom assemblages are, in many ways, similar to those discussed above for fossil pollen. Diatom valves are light and easily transported, and thus in estuarine sediments, for example, there is frequently an admixture of marine, brackish and freshwater forms, while lake muds may contain diatoms derived not only from the lake ecosystem itself, but also from inflowing streams and catchment soils. Freshwater diatoms often occur in marine sediments, having been blown in by the wind, while in the deep oceans, diatom remains have been found that have been transported many hundreds of kilometres from their source (Marshall & Chalmers, 1997). Selective destruction of diatoms is another potential error source, with complete or partial dissolution of the frustules under pressure at depth in the oceans, while in brackish and freshwater contexts, the less robust and weakly silicified forms will tend to dissolve where conditions are very alkaline. In these environments the diatom death assemblage will be biased in favour of the stronger and more heavily silicified forms. Grazing by herbivores may also affect the composition of fossil assemblages. Reworked diatom frustules can sometimes be detected where valves are broken or partially dissolved, or demonstrate signs of mechanical abrasion, although secondary diatoms within a body of sediment may not always be easily recognizable.

Moreover, diatom frustule size varies markedly between species. These various factors complicate the interpretation of diatom assemblages and the estimation of diatom productivity. Species-specific correction factors can be applied to the data in order to reduce some of the bias (Korholia, 2007), but an element of uncertainty will always remain.

Despite these problems, diatom analysis has proved to be a particularly valuable technique for environmental reconstructions, particularly in studies of eutrophication, acidification and salinity changes in lakes (Battarbee *et al.*, 2001; Smol & Stoermer, 2010). These and other applications of diatom analysis are discussed in the following section. In addition, diatoms in deep-ocean sediments constitute a valuable source of palaeoecological data, an aspect considered later in this chapter (section 4.10).

4.3.5 Applications of diatom analysis

4.3.5.1 Diatoms as salinity indicators

A major control on diatom distributions is salinity, and hence individual diatom species can be classified on the basis of their salinity preferences. The [halobian system](#) of classification, introduced by Robert in 1927 for application to marine and estuarine assemblages, and subsequently modified by Friedrich Hustedt in the 1950s, has four main groupings:

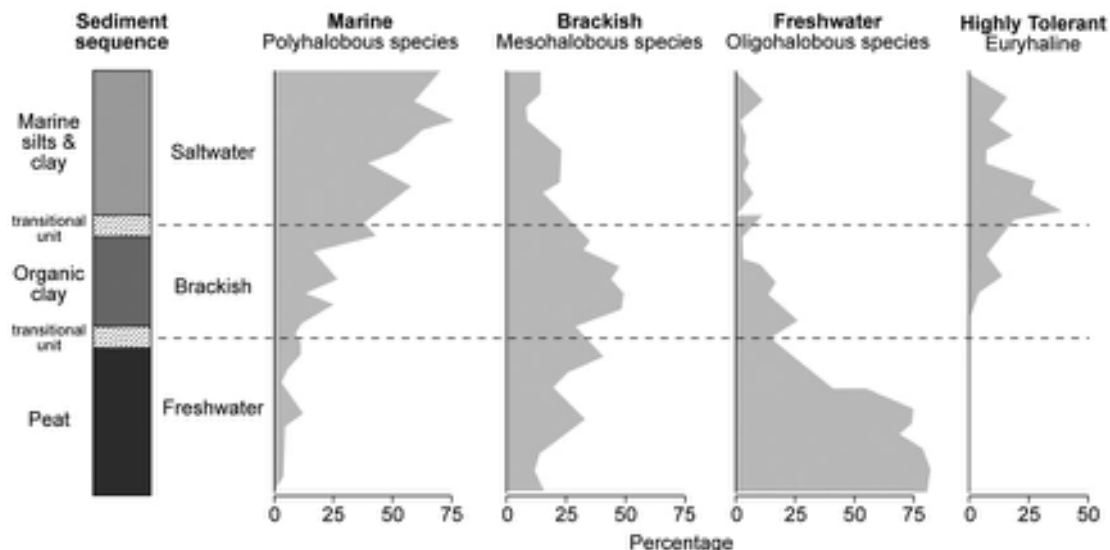


Figure 4.12 A marine incursion (positive sea-level tendency) as reflected in a diatom assemblage (from Carter, 1992).

- (a) **polyhalobous** diatoms: those that thrive in salt concentrations of >30 per cent;
- (b) **mesohalobous** diatoms: those that thrive in salt concentrations of 0.2–30 per cent;
- (c) **oligohalobous** diatoms: those that generally require salt concentrations of <0.2 per cent;
- (d) **halophobous** diatoms: those that cannot tolerate even slightly salty water.

Other terms commonly employed today are ‘**halophilous**’ for those diatoms that are particularly attracted to salt-rich waters and ‘**indifferent**’ or ‘**euryhaline**’, for those seemingly unaffected by variations in salt content, and hence not restricted to any of the above categories. The sensitivity of diatoms to salinity changes is exemplified in two particular areas of Quaternary research: sea-level change, and the environmental record preserved in closed-basin lakes.

Sea-level variations

Diatoms have long been employed as indicators of changing sea level, the earliest accounts being from Scandinavia in the 1920s, where evidence of marine or brackish water conditions in lakes now well above sea level formed an important line of evidence in the reconstruction of the extent of glacio-isostatic recovery following the wastage of the last ice sheet (Tuovinen *et al.*, 2008; section 2.5.4).

Subsequently, the analysis of diatom assemblages from coastal localities has become, as with pollen data (see above), a standard technique for identifying positive and negative sea-level tendencies (section 2.5.2.2; Figures 2.35 and 2.36) in littoral sediment sequences. Positive tendencies are characterized by the replacement of halophobous and oligohalobous diatoms first by mesohalobous and subsequently by polyhalobous forms (Figure 4.12), whereas the reverse is the case where negative sea-level tendencies have occurred (Figure 4.13). Hence changes in diatom assemblages can reflect precisely the highest point of marine influence, and can therefore provide important stratigraphic markers for the reconstruction of shoreline displacement curves and patterns of isostatic rebound. The evidence illustrated in Figure 4.13, for example, provides important indices of the timing and relative rate of sea-level fall in southeast Greenland as a result of land uplift following the retreat of the Greenland Ice Sheet (Long *et al.*, 2008). Similar investigations have provided valuable sea-level index points relating to the wastage of the last ice sheets in the British Isles (Selby & Smith, 2007), Scandinavia (Lohne *et al.*, 2007) and North America (Hutchinson *et al.*, 2004).

Closed-basin lakes

These lakes are frequently sensitive to changes in effective moisture, especially where this affects the salt content of the lake water (‘**salt lakes**’), and hence past variations in salinity can be used as a basis for reconstructing climatic change (Fritz, 2008). Fluctuations in lake volume and salt concentrations in lake waters will, in turn, be reflected in changing compositions in diatom assemblages, because of the wide range in salt tolerance between obligate freshwater and **hypersaline** species (Figure 4.14). The relationship between diatom assemblage variations and salinity concentrations in modern lakes can be measured and forms the basis for **diatom training sets** or **calibration sets**. These are now available for a number of regions throughout the world, and enable past variations in lake salinity to be quantified (Davies *et al.*, 2002a). For example, Laird *et al.* (2007) interpreted an abrupt increase in lake salinity in Oro Lake, western Canada at around 9.6 ka as marking the onset of a more arid climate that continued throughout much of the Holocene, albeit with several short episodes of reduced salinity that suggest shifts to wetter climatic conditions (Figure 4.14). Lake waters, however, are chemically complex and the ratios of the principal salts (chlorides, carbonates and sulphates) vary in response not only to hydrological changes, but also to a range of environmental variables that affect dilution and mineral supply (Fritz *et al.*, 2010a). Understanding the response of diatom communities to such changes is essential if valid inferences about palaeosalinity variations are to be made. Recent approaches to this problem have involved multivariate statistical analysis of modern diatom assemblages to gauge which chemical variables have the greatest influence on the structure and composition of diatom assemblages (Ryves *et al.*, 2003).

4.3.5.2 Diatoms and pH

The distribution and abundance of many diatom species also vary with water pH or with a wide range of environmental factors that co-vary with pH, such as alkalinity. Following pioneering work by Friedrich Hustedt in the 1930s, diatoms have traditionally been divided into the following groups according to their pH preferences:

- (a) **alkalibiotic**: occur in waters of pH values > 7;
- (b) **alkaliphilous**: occur at pH values of about 7, but with widest distribution at pH > 7;
- (c) **circum-neutral**: occur equally above and below a pH of 7;
- (d) **acidophilous**: occur at pH values of about 7, but with widest distribution at pH < 7;

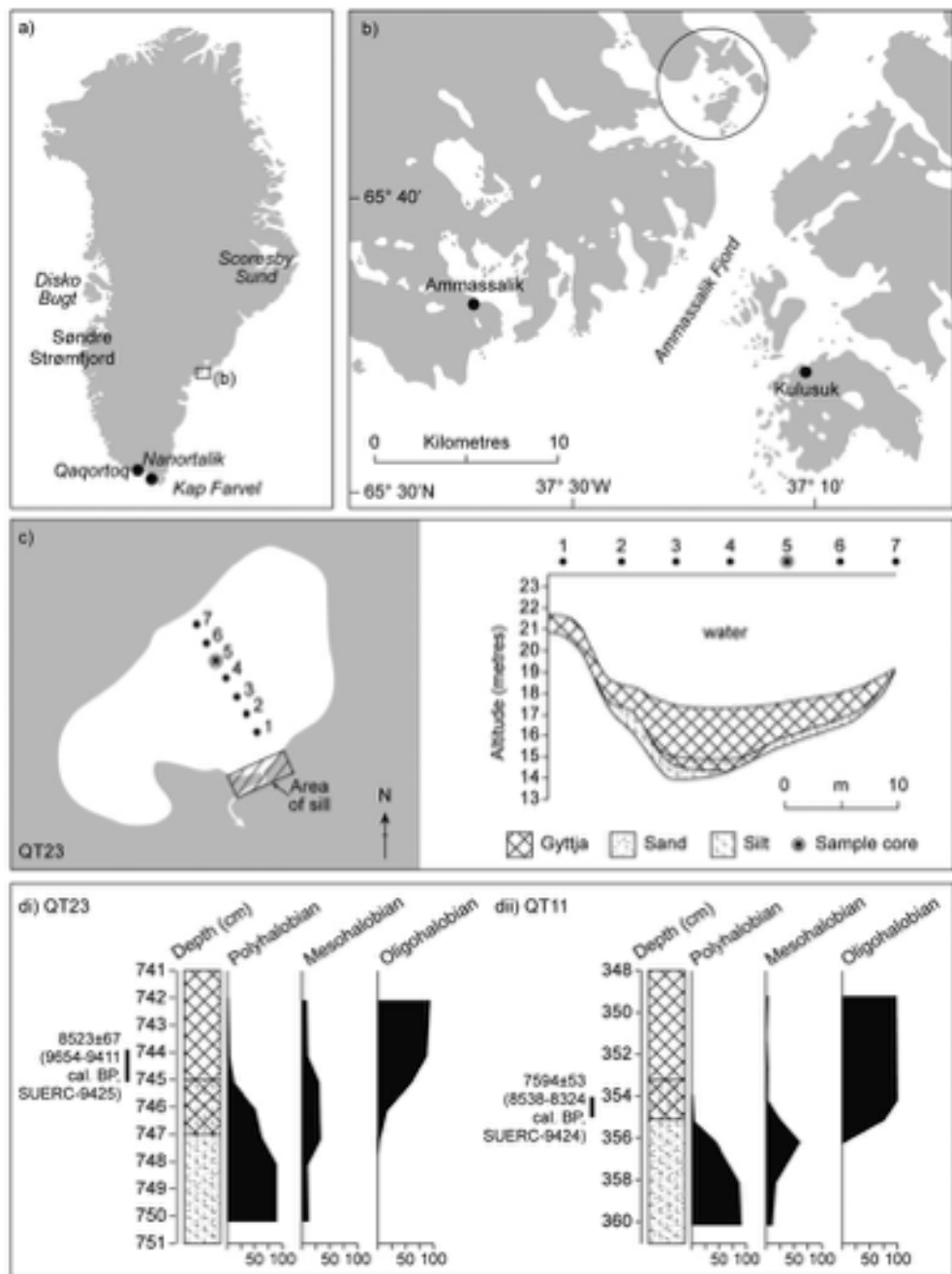


Figure 4.13 Isolation basin studies in southeast Greenland. Transects of sediment cores were obtained from six small basins on islands in Ammassalik Fjord (circle in b). c) shows an example of the sediment infill recorded from a transect of boreholes for one of the basins, and d) the changes in diatom content in two of the basins. The change from polyhalobous to oligohalobous assemblages marks the time when the basin became isolated from the sea due to land uplift after wastage of the Greenland Ice Sheet, the timing of basin isolation being dependant on the height of each basin's sill (from Long *et al.*, 2008). For further explanation see text.

- (e) **acidobiotic**: occur at pH values of less than 7, with optimum distribution at pH of 5.5 or under.

Fossil diatom assemblages that can be classified in this way provide a basis for inferring changes in lake water pH in the past (Battarbee *et al.*, 2010). The links between modern diatom assemblage variations and pH are tested and quantified using transfer functions based on a range of multivariate statistical methods (Holden *et al.*, 2008) and these provide a basis for inferring past variations in pH from fossil diatom records (Simpson *et al.*, 2005). This approach has enabled palaeolimnologists to demonstrate the acidification of many lakes during the late Holocene (Figure 4.15), partly as a consequence of increased levels of acid deposition caused by atmospheric pollution (Stoddard *et al.*, 1999), but possibly linked also to climate change (Wolfe, 2002).

4.3.5.3 Diatoms and trophic status

Diatom communities are also very sensitive to changes in nutrients and are therefore good indicators of trophic status (section 3.9.2). Many lakes have experienced a trophic stability through most of the Holocene. However,

for some lowland lakes, deforestation and the spread of farming in the mid- to late Holocene has led to marked changes in nutrient balance (Hall & Smol, 2010), whilst the recent increase in sewage effluents, phosphorus-rich detergents and intensive agricultural methods has resulted in a rapid nutrient enrichment of many lakes throughout the world (Battarbee & Bennion, 2011), as well as impacting on coastal waters (Clarke *et al.*, 2006a). Such **cultural eutrophication** is marked in diatom records from lake sediments (Ekdahl *et al.*, 2004), particularly in lakes that were naturally oligotrophic, by increases in overall diatom productivity, in the relative abundance of planktonic taxa, or in diatom-inferred phosphorus concentrations.

4.3.5.4 Diatoms and the archaeological record

Diatom assemblages are increasingly widely used as indicators of past human activity (Juggins & Cameron, 2010). Archaeological applications include the identification of prehistoric agricultural practices (Horrocks *et al.*, 2002), the detection and mapping of traces of ancient dwellings (Bathurst *et al.*, 2010), and the provenancing

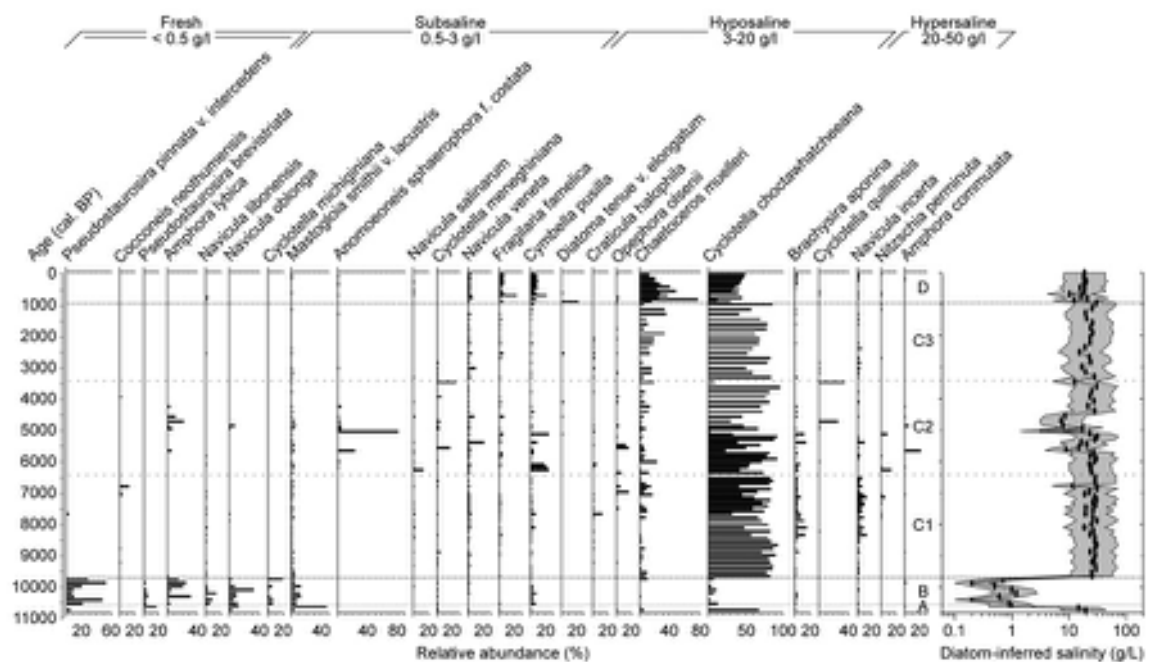


Figure 4.14 Diatom-inferred palaeosalinity through a sediment sequence in Oro Lake, Saskatchewan, Canada, based on variations in abundance of dominant diatom species (from Laird *et al.*, 2007).

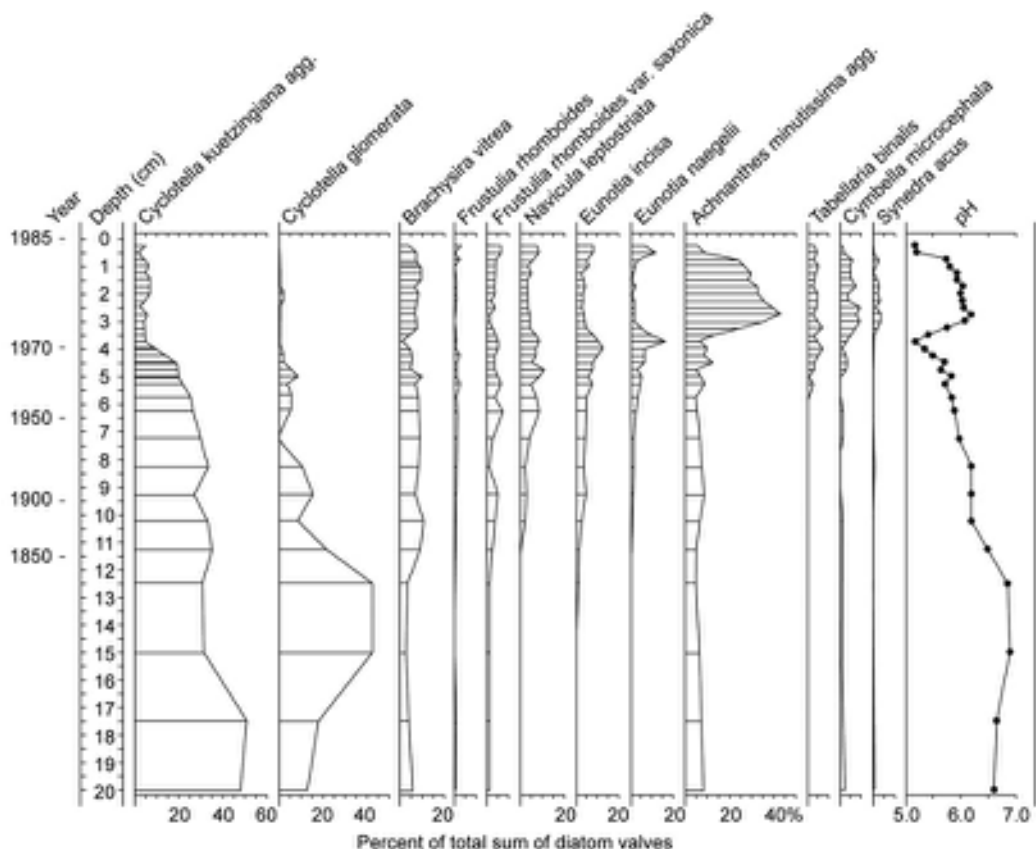


Figure 4.15 Diatom-inferred pH history of Lysevatten Lake, southwestern Sweden, suggesting increased acidification since the 1960s. Note how the alkaliphilous diatom species on the left are progressively replaced by diatoms which are associated with more acid conditions (centre and right). The curve for inferred pH change is shown on the right (from Renberg *et al.*, 2009).

of manufactured materials such as pottery and bricks (Kligmann & Calderari, 2012). Diatom stratigraphy is also frequently employed in multi-proxy investigations of archaeological sites, especially those associated with waterfronts (e.g. Veski *et al.*, 2005a) or lake dwellings, such as crannogs (O'Brien *et al.*, 2005). As outlined above, diatoms also reveal the impacts of humans on local ecosystems and water bodies, from the introduction of agriculture in the early to mid-Holocene (Bradshaw *et al.*, 2005) through to the toxic effects of metal pollution in the industrial era (Cattaneo *et al.*, 2004).

4.3.5.5 Other environmental applications

Because diatoms respond sensitively to a range of variables, they are proving to be useful indicators for evaluating

long-term changes in a number of other environmental contexts. They can provide evidence of variations in, *inter alia*, lake-water depth (Wolin & Stone, 2010), the extent and duration of ice cover over lakes (Thompson *et al.*, 2005) and sea surfaces (Gersonde & Zielinski, 2000), wind trajectories and strength (Romero *et al.*, 2003) and rates of ocean upwelling (Anderson *et al.*, 2009). They have also been used to detect prehistoric tsunami activity (Dawson & Smith, 2000) and to reconstruct high-resolution climate histories (Fritz, 2008). Finally, while most of this section has focused on diatom evidence from the late Quaternary, diatom analysis has also been applied to earlier Quaternary records, for example, in the investigations of long lake sediment sequences such as that in Lake Baikal in central Asia (Mackay, 2007), and diatom-rich oozes on the deep ocean floor (Romero & Schmieder, 2006).

4.4 PLANT MACROFOSSIL ANALYSIS

4.4.1 Introduction

The study of fossil plant remains is one of the earliest branches of Quaternary research, the Quaternary floras of the British Isles being investigated from as long ago as the 1840s. Similar studies were being undertaken in Denmark and Germany and the results of these nineteenth-century investigations were synthesized in Clement Reid's remarkable volume *The Origin of the British Flora* published in 1899 (Birks, 2008). This book contained the first clear statement of Quaternary vegetation changes in western Europe, and appeared almost twenty years before the development of pollen analysis as a palaeoenvironmental technique. The analysis of plant macrofossils can provide valuable complementary information to microfossil data, but it can also provide an independent approach to the reconstruction of environmental conditions.

4.4.2 The nature of plant macrofossils

Plant macrofossils range in size from minute fragments of plant tissue or tiny seeds, to pieces of wood, and even to whole trees that can be measured in cubic metres (Birks, 2001, 2007). They include recognizable remains of both

vascular plants (plants with specialized tissues for transporting water), such as fruits, seeds, stamens, buds, scales, rhizomes, roots and bark, and non-vascular plants, mainly the leaves of bryophytes (mosses) and liverworts, but also oospores of algae, the latter being especially abundant in calcareous lakes (Figure 4.16). Carbonized plant macrofossils, usually in the form of wood or seeds, are also commonly encountered, especially in archaeological contexts (van der Veen, 2007).

Plant macrofossils are found in a variety of depositional environments, but most commonly in lacustrine and fluvial sediments, especially fine alluvium, and in acid peats. Occasionally, rich assemblages of plant remains are recovered from soils or sediments on archaeological sites where the fossil remains may include those of cultivated plants, weeds associated with cultivation, and uncultivated species collected for food (e.g. Kubiak-Martens, 1999). Fossil dung or animal middens may also preserve plant remains in good condition, and in some regions these have provided valuable records of vegetational and environmental change (van Geel *et al.*, 2008). However, it is in acid peat deposits that the remains are often best preserved, as the fossils have been protected from oxidation, and may even be found in growth position.

The preservation of fossil plant material is very variable. Wood may survive in recognizable condition for many thousands of years, either in waterlogged sites or in very dry

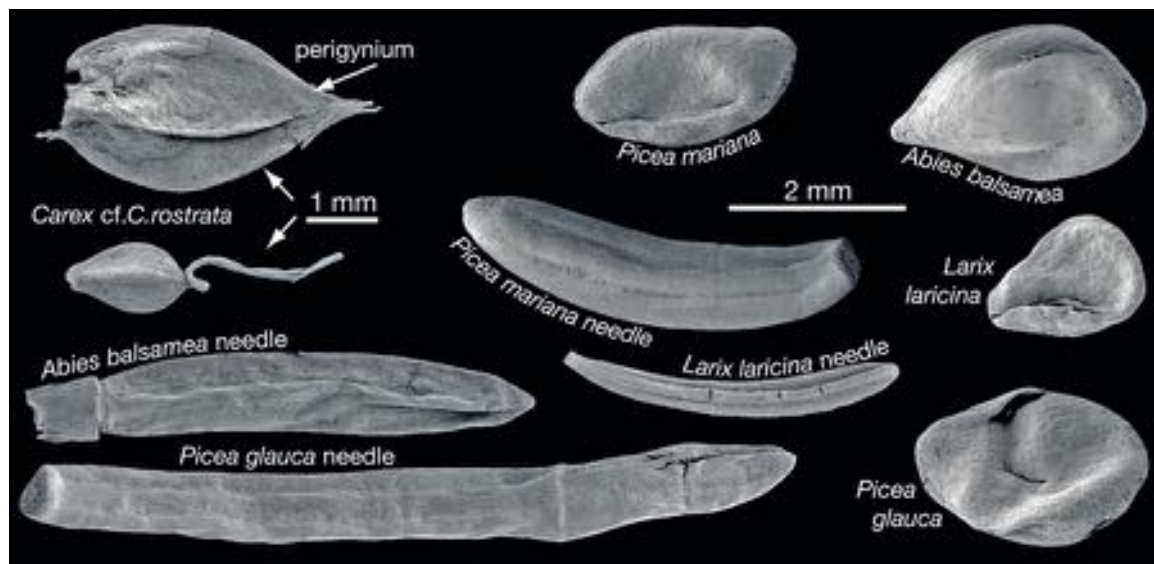


Figure 4.16 Scanning electron photomicrographs of terrestrial macrofossils from a 12 ka peat layer in North Dakota, USA (from Fisher *et al.*, 2008, reprinted by permission of SAGE; image provided by Timothy Fisher, University of Toledo, USA and Catherine Yansa, Michigan State University, USA).

soils in arid environments, but in other situations decomposition can be extremely rapid. Seeds and fruits will survive in most deposits, their resistance to decay reflecting adaptation to periods of dormancy. Some of the very small seeds, however, such as those produced by orchids and by certain members of the heather family (Ericaceae), are rarely preserved. The leaves of deciduous trees, with their delicate structure, are particularly vulnerable to mechanical breakdown and decomposition and hence are usually preserved as very small fragments. Perfect specimens can survive, however, especially in annually laminated fine-grained sediments (Staff *et al.*, 2011) or in deposits in sinkholes with water deep enough to be anoxic (Steadman *et al.*, 2007). Needles from coniferous trees are often abundant as macrofossils, occurring in a variety of depositional situations (Tobolski & Ammann, 2000), while leaves of dwarf shrubs from tundra environments such as willow (*Salix*), dwarf birch (*Betula nana*) and bilberry (*Vaccinium*) have also been found in a good state of preservation in lake sediments (Rundgren & Björck, 2003). Of the lower plants, mosses preserve very well in the macrofossil form, but lichen and liverwort remains are seldom found, though impressions of the latter occur in tufa and travertine deposits (Ali *et al.*, 2003). In the majority of cases, therefore, Quaternary macrofossil analysis is concerned primarily with the study of wood, seeds, fruits and mosses, augmented by information provided by a limited number of easily identifiable plant remains such as conifer needles and certain leaves.

4.4.3 Field and laboratory work

The larger plant macrofossils can be collected in the field from exposed sections or from sediment cores, but in most cases extraction takes place in the laboratory. There is a variety of techniques for the removal of the fossil remains from the sediment matrix, but the majority involve disaggregation of the material with either dilute hydrochloric acid or sodium/potassium hydroxide, followed by sieving (Birks, 2007; Mauquoy *et al.*, 2010). Use of stronger chemicals, such as nitric acid or hydrogen peroxide tends to be avoided as these can degrade delicate plant tissues. Finer lake sediments and ombrotrophic peat can usually be broken down simply with the aid of a jet of water and washing through sieves (90–250 µm in mesh size), in order to capture tiny seeds (Beaudoin, 2007). During disaggregation, some fruits, seeds or leaves will rise to the surface of the liquid and these can be picked off with a fine paintbrush, while macrofossils can be removed in a similar fashion from the mesh of the sieves. Some fossils, such as fruit stones, can be kept dry, but others need to be stored in alcohol,

glycerine or other preserving fluids. The more delicate structures such as translucent leaves and seeds are best kept mounted on microscope slides. Wood, except in the case of some very obvious species (e.g. birch), must be either macerated or prepared in thin section for identification. Most plant macrofossil remains can be examined on a white plate under binocular scanners or low-powered stereo-microscopes. On occasions, however, high-powered microscopy is required, and in recent years, the electron microscope (Figure 4.16) has been employed for the differentiation of closely similar taxa (Carlquist, 2001). As with pollen analysis, identifications are based on a reference collection of seeds, fruits, leaves, wood and so on from the present flora, on atlases of macroscopic plant remains and, in certain cases, on keys of particular plant families (e.g. Hather, 2000; Velichkevich & Zastawniak, 2008).

4.4.4 Data presentation

The results of plant macrofossil analysis can be presented in a number of different ways. At many sites, particularly where archaeological investigations are being carried out or where a single stratum is being investigated, a simple species list is compiled of all taxa discovered. Where several levels are being examined, the presence or absence of particular plant remains may be indicated by simple dot symbols (Figure 4.17) or the results may be shown in tabular format. Alternatively, the data may be expressed as estimates of abundance using such descriptive terms as rare, occasional or frequent, and thus an impression can be gained of changes in frequency of taxa through time.

More commonly, however, plant macrofossil data are presented in quantitative form, where the plant remains from different levels in a profile are expressed as a percentage of the total number of macrofossils identified from each sample, and these are plotted on a vertical time sequence. A major problem with this type of diagram, however, is that certain macrofossil types (such as seeds of aquatic plants in limnic sediments or stems and leaves of sedge or moss in peat) will be over-represented and thus the curves for other taxa will be suppressed. Equally, it may be difficult to arrive at a satisfactory macrofossil sum, particularly when a range of different types of plant macrofossil material is present. An alternative strategy, therefore, is to construct a concentration diagram showing the occurrence of total numbers of plant macrofossils per unit volume of sediment at different levels in the profile, and this may be converted to a macrofossil influx diagram showing accumulation per year if a secure dating framework can be established (Figure 4.18). As with pollen concentration diagrams, however, fluctuations in

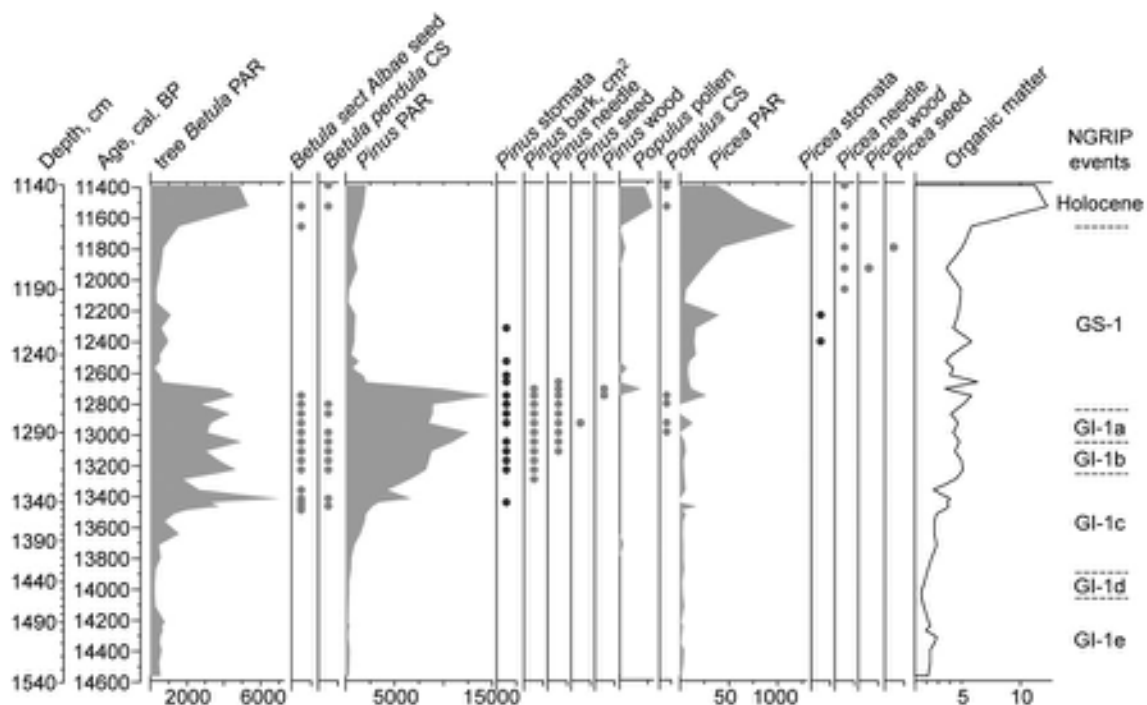


Figure 4.17 Arboreal plant macrofossils (shown as dots) in a Lateglacial sediment sequence in Latvia, plotted against the pollen record of the same taxa (from Veski *et al.*, 2012).

sedimentation rates and an insufficiently sensitive timescale can pose interpretative problems and, as yet, comparatively few influx diagrams have been constructed for plant macrofossil data. Another approach to data analysis is to use a square grid graticule for the quantitative estimation of macrofossil remains examined under a low-power microscope, and the resulting data can be analysed statistically using, for example, weighted averages, and then presented in tabular form (e.g. Mauquoy *et al.*, 2010).

4.4.5 The interpretation of plant macrofossil data

The majority of plant macrofossils found in a body of sediment are derived locally (autochthonous) and provide data on the composition of former plant communities growing in and around the site of deposition. Important information can often be gained, therefore, on local hydroseral developments and also on changes in the trophic status of lake waters and associated fens. Interpretation of the record is aided by the fact that, unlike pollen grains, a very large number of plant macrofossil remains can be

identified to the species level, and therefore many of the problems arising from taxonomic imprecision which often prove so frustrating in pollen analysis are not encountered to the same degree in the study of plant macrofossils. Moreover, there are some plants, such as the rushes (*Juncaceae*) and poplar (*Populus*), whose pollen seldom survive in the fossil form, and which are only occasionally represented in the pollen record. The former presence of these types in a vegetation community may, however, be revealed by their macrofossil remains. The same applies equally to those plants that are low pollen producers.

Unfortunately, however, the occurrence of plant macrofossils tends to be sporadic. Many deposits, while rich in fossil pollen, are entirely devoid of recognizable plant remains (and vice versa). Other sediments may contain plant macrofossils, but a large quantity of material is often needed in order to produce relatively few fragments of fossil vegetative matter. Moreover, although identification is frequently possible to the species level, the abundance of diagnostic detail in different fossil remains is very variable, and while there are seeds and fruits that are relatively easy to recognize, the identification of small fragments of achene

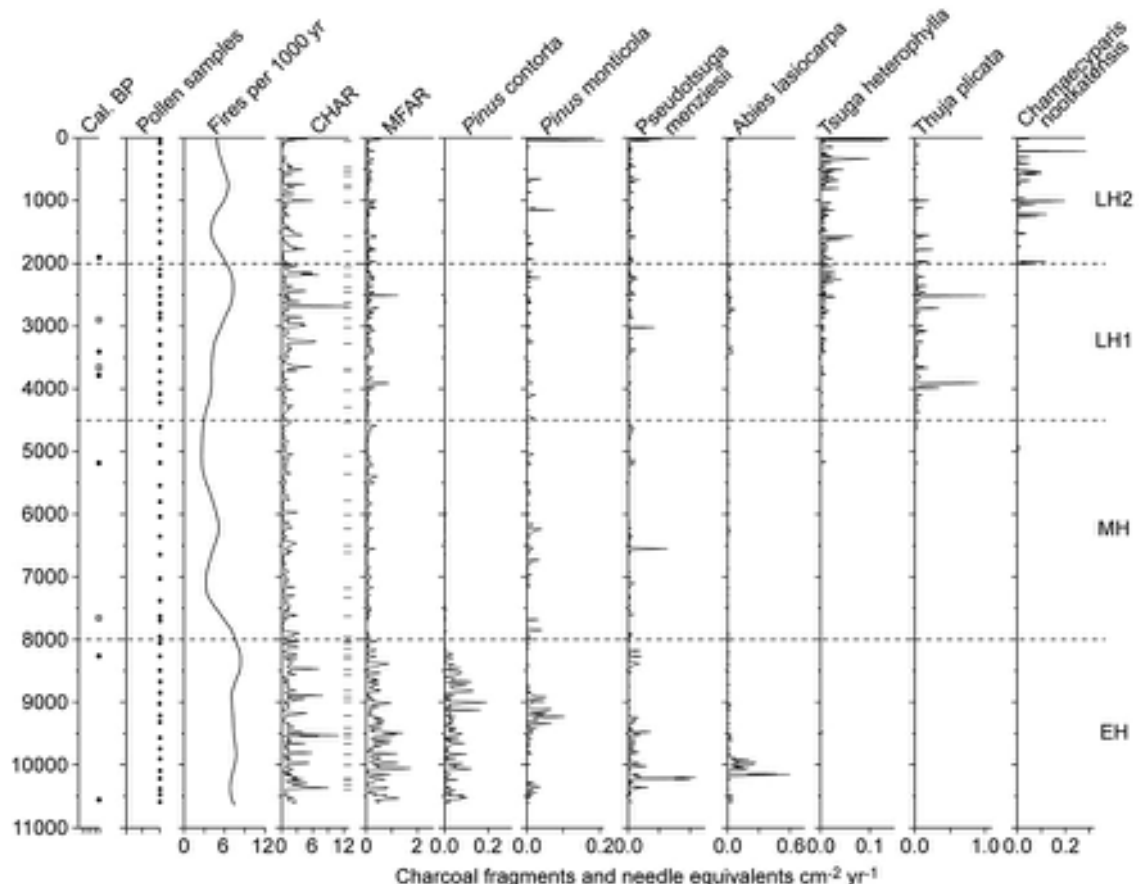


Figure 4.18 Influx of charcoal fragments (CHAR), total plant macrofossils (MFAR) and macrofossils of selected plant taxa in a lake sediment sequence in the North Cascade Range, Washington State, USA (from Prichard *et al.*, 2009).

or epidermis, for example, may require a great deal of work. For these reasons, plant macrofossils may be worth studying only if they are abundant, well preserved and easily extracted from the sediments in which they occur, or where they make up most, if not all, of the sediment body, such as ombrotrophic peats. In some cases, however, it may be worth examining the macrofossil content of a site where relatively few remains are preserved, either because it might help to solve a particular ecological problem, encountered in pollen analysis, or because the macrofossil remains are required for radiocarbon dating (section 5.3.2).

As with pollen analysis, a proper understanding of the origins of a plant macrofossil assemblage is required before palaeoecological inferences can be attempted. In fen or bog sites, macroremains tend to be almost entirely of local origin (Figure 4.19), apart from a few with very good wind

dispersal such as fruits of birch (*Betula*) or seeds of sycamore (*Acer*). Hence, these records will usually be dominated by the remains of the peat-forming plants such as *Sphagnum* mosses and the cotton sedge (*Eriophorum vaginatum*), accompanied by species such as the bog myrtle (*Myrica gale*) and common heather (*Calluna vulgaris*) which are often found growing on bog surfaces (Hughes *et al.*, 2000). In lake sediments, however, plant macrofossil assemblages are more diverse, for although locally derived fossils (particularly those of aquatic plants) will tend to predominate, exotic elements from outside the lacustrine ecosystem may also be present and will have been brought into the lake by wind, stream or animal transportation (Figure 4.19). The proportion of autochthonous to allochthonous fossil material will therefore be determined by a range of taphonomic factors affecting the production and

dispersal of seeds, fruits, leaves, etc., the mode of transportation to and within the lake, and sedimentary processes operating during and after deposition.

Vegetational productivity varies considerably between species, and even between individuals of the same species, depending upon reproductive strategies (in the case of fruits and seeds) and vegetational response to environmental conditions. Woodland shrubs and herbs tend to produce relatively few seeds, while certain trees and annual weeds, especially those found growing on muddy surfaces around lakes with fluctuating water levels, may have a higher rate of seed production. Other factors will also come into play. Many seeds and fruits will not find their way into the fossil record because they are taken for food by birds and animals, while others may be subject to attack by fungal parasites. Different plants have different strategies for combating predation, which affects the seed survival ratio (Nathan & Casagrandi, 2004), and hence some taxa have a much higher probability of being represented in death assemblages than others. The potential dispersal range of seeds also varies widely between taxa due primarily, but not exclusively, to seed size: small-seeded species usually produce more seeds per plant that persist longer in seed stores than is the case with larger-seeded species (Dieffenbacher-Krall, 2007). Dispersal efficiency depends upon the mode of transportation. The most effective agent for transporting seeds to lake surfaces is wind, especially where propagules or other plant parts such as leaves are launched from the canopies of tall trees. Transport by streams and surface runoff is also important, especially during periods of high rainfall (Hölzel & Otte, 2004). Seeds that are not waterlogged remain afloat and tend to be carried into shallow water by wind and wave action; indeed, studies of the seed content of surface sediments in modern lakes show low numbers in the deeper areas and a much greater concentrations close to the shores (Zhao *et al.*, 2006). Seeds of some species, however, become rapidly waterlogged and sink, and are then moved along the lake bed by currents and turbulence until they settle in the coarser marginal sediments or are trapped near the lake shore by submerged plants.

Although the foregoing discussion has been concerned largely with lake sites, many of the points apply equally to plant macroremains found in riverine sediments. In fluvial deposits, however, a further complicating factor is the occurrence of plant macrofossils from different time periods that have been incorporated into a single assemblage. Hence reworked or secondary macrofossils are frequently encountered in river terrace sequences. Mixed assemblages of plant macrofossil material are also occasionally encountered in lake sediments where, for example,

there have been marked fluctuations in lake-water level and intermittent erosion of the shoreline. Unlike secondary pollen, however, it is not always easy to detect reworked plant macrofossil material by signs of physical or chemical deterioration, and often a meticulous evaluation of the assemblage is necessary in order to isolate such exotic components.

There are, finally, a range of broader environmental factors that may affect the formation of plant macrofossil assemblages. These include lake bathymetry and catchment

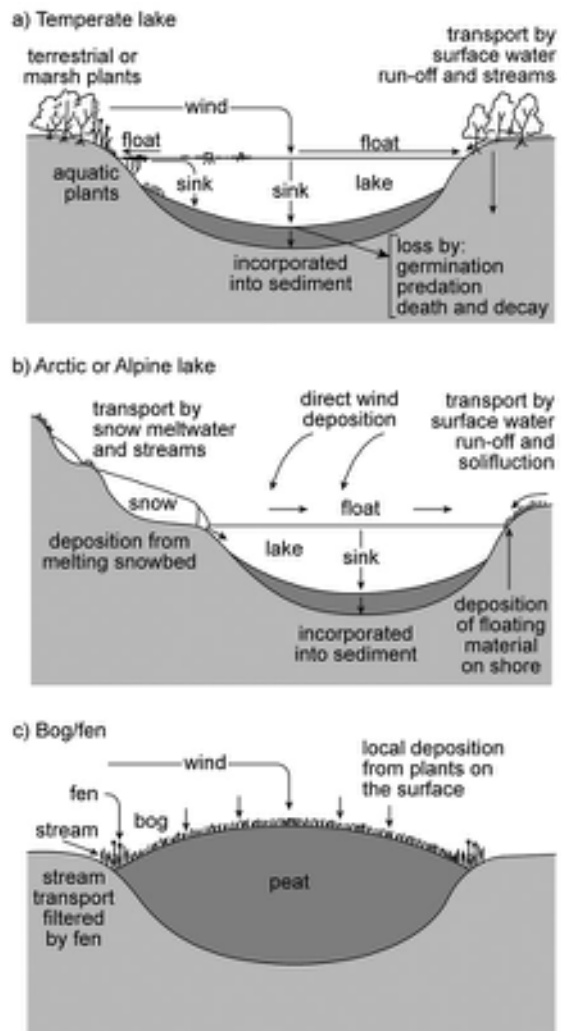


Figure 4.19 Recruitment pathways and processes by which plant macrofossil remains are delivered to lakes in a) a temperate environment, b) an arctic or alpine environment, and c) to a bog or fen site.

size, the type and density of vegetation surrounding a site (dispersal through a woodland stand, for example, is less efficient than wind transport over open ground), and both annual and longer-term climatic variations that can modulate seed production. In addition, there are geographically determined influences, such as the role of melting ice and snow in the transportation of plant debris in arctic landscapes (West, 2000), the activities of animals in the creation of plant macrofossil assemblages in arid and semi-arid terrains (McCarthy & Head, 2001), and the ecological dynamics in areas of frequent burning, either by natural forest fires or initiated by humans, where charred macrofossils predominate in the palaeobotanical record (section 4.4.6.3).

Understanding the complex web of taphonomic processes leading to the development of plant macrofossil assemblages has been aided in recent years by the use of modern analogue studies. Some of these are based on observation of contemporary ecological processes, which inform interpretations of palaeoecological records. For example, Stearta *et al.* (2009) studied the present-day decay rates of the leaves of five Australian tree species (*Acacia*, *Atherosperma*, *Eucalyptus*, *Lomatia* and *Nothofagus*) in order to establish which species might be over- or under-represented in the fossil record. Cellot *et al.* (1998) examined the drift of aquatic macrophyte propagules along the River Rhône during flood conditions, and were able to demonstrate the importance of floods in propagule dispersal, while Dilcher *et al.* (2009) compared the characteristics of leaf litter on the floor of a Florida swamp woodland with those of leaves in the adjacent woodland canopy, from which the litter was derived.

Other modern analogue studies have focused on the relationships between the mix of plant remains that initially accumulate on land surfaces, and those that survive decay and predation to become preserved in sedimentary sequences, in order to determine how well observed death assemblages reflect the local or regional vegetation cover from which they were derived. For example, Goman (2001) studied the seed and vegetal remains dispersed across modern tidal marshes in San Francisco Bay to develop a calibration dataset of seed assemblages for the last 4,000 years, while Kalis *et al.* (2006) linked fossil plant assemblages recovered from a fen in the Vosges Mountains, France, with typical phyto-sociological communities currently occupying the region, and Davidson *et al.* (2005) compared documentary evidence of changes in the composition of submerged vegetation in a small lake with plant macrofossil assemblages in the lake sediments that accumulated over the same period. Modern analogue studies such as these are an important means by which

palaeoenvironmental reconstructions can be refined. They also aid the Quaternary palaeoecologist in a number of other ways, for example by indicating the degree of bias associated with assemblage types, the sedimentary niches (e.g. type of lake) where bias is best constrained, and the optimal locations within a site for the collection of plant macrofossil samples (Dieffenbacher-Krall, 2007). One problem, however, is that some associations of plant species appear to have no modern analogues. Jackson & Williams (2004) attribute these non-analogue vegetation types to unique climatic regimes and possibly to lower atmospheric CO₂ levels in the past, while in Europe they may also reflect the long-term impacts of humans (van der Knaap *et al.*, 2011). Future research may clarify the nature and origins of these non-analogue vegetation types and their implications for contemporary plant ecology, evolutionary biology and palaeoecology (Jackson & Williams, 2004).

These various difficulties notwithstanding, plant macrofossil analysis remains a valuable tool in palaeoecology. While pollen analysis is perhaps the more widely used technique in vegetational reconstructions, plant macrofossil analysis is an important adjunct to palynological studies and, when used in conjunction, the two methods offer a more secure basis for palaeoecological inference than either technique used in isolation.

4.4.6 Palaeoenvironmental applications of plant macrofossil studies

4.4.6.1 Palaeoclimatic reconstructions

Climatic inferences can be drawn from plant macrofossil remains in a number of different ways. First, the *indicator species* and *transfer function* approaches used to derive pollen-climate relationships (section 4.2.6.5) can also be applied to plant macrofossil assemblages. The former was used by Isarin & Bohncke (1999) to infer mean July temperatures of 12–13°C (c. 5°C below those of the present) in western Europe during the Younger Dryas cold period, while the latter, when applied to deposits of Eemian age from a site in Germany by Kühl *et al.* (2002), indicated that summer temperatures were similar to those at the present day. The *mutual climatic range* method, developed for deriving quantitative climatic estimates from fossil beetle assemblages (section 4.5.4.2), can also be applied to fossil plant remains (Sinka & Atkinson, 1999). The precision with which former climatic conditions can be reconstructed using these methods depends, however, on the number of taxa in a fossil assemblage for which modern climatic parameters can be quantified, and on the range of climatic

conditions that each indicator species can tolerate (Pross *et al.*, 2000).

A different approach to palaeoclimate reconstruction involves the analysis of stomata (guard cells) found on the surface (epidermis) of plants, as both *stomatal density* (number of stomata per unit area of leaf) and *stomatal index* (percentage of epidermal cells that are stomata) vary inversely with atmospheric CO₂ concentration (Beerling & Royer, 2002; Hetherington & Woodward, 2003). Measurement of these indices on fossil leaves enables past variations in atmospheric CO₂ concentration to be inferred, and these data complement those derived from other methods, such as the analysis of gas bubbles in polar ice cores (section 3.11.3). The results not only contribute to global models of environmental change (Chapter 7), but provide additional insights into the possible role of atmospheric CO₂ variations as a driver of climatic changes during the Late Quaternary (McLwain *et al.*, 2002).

A third line of evidence for past climate change comes from the analysis of plant remains in bog peat. The stratigraphy of ombrotrophic bogs has long been

considered to be linked to variations in local hydrological conditions (bog surface wetness) which are, in turn, influenced by regional climatic conditions (section 3.9.4.1). The composition and state of preservation of plant macrofossils in ombrotrophic peats provide a basis for measuring these relationships (Chambers *et al.*, 2012) and are reflected, for example, in changes in the proportions of different species of the bog moss *Sphagnum*, since each species has a different tolerance to bog-surface wetness, or in the relative importance of macrofossils of plants requiring drier bog conditions, such as *Erica* (e.g. Langdon *et al.*, 2003). These changes can be quantified using weighted averaging methods, and the results often show a correlation with independent temperature reconstructions (Barber & Langdon, 2007). Moreover, a number of peat macrofossil studies reveal cyclic variations in bog-surface wetness during the Holocene (Figure 4.20), which may reflect solar variations (e.g. Mauquoy *et al.*, 2004; section 7.6.4.1).

Finally, plant remains concentrated and preserved through the actions of animals can provide valuable climatic

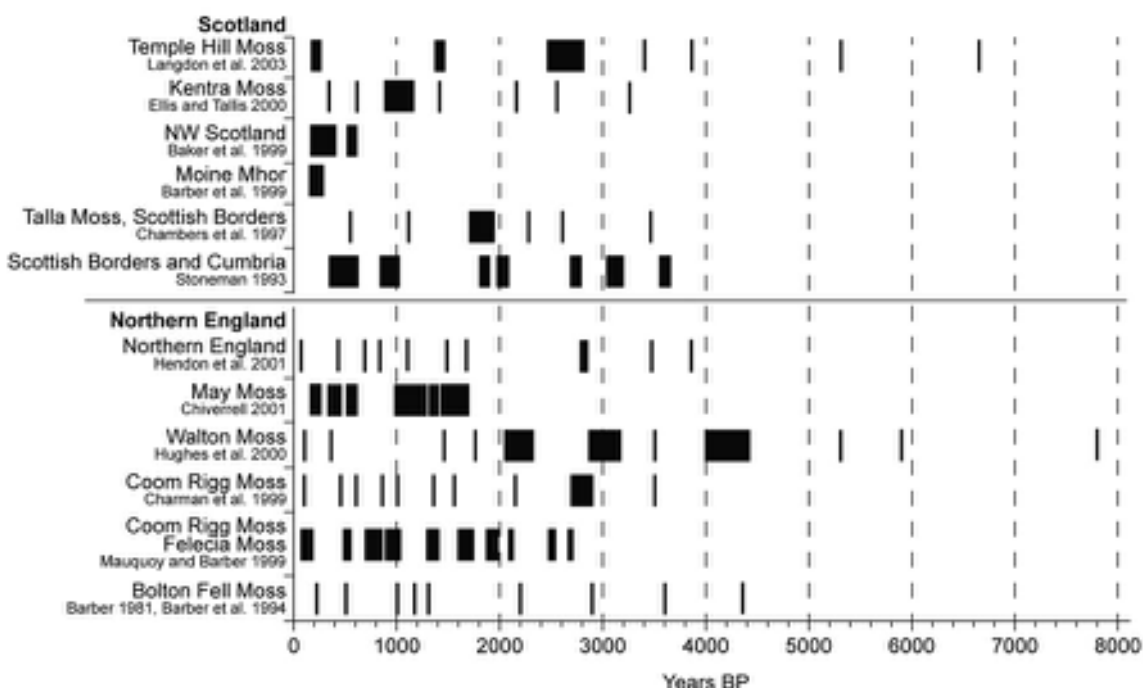


Figure 4.20 Episodes of climatic deterioration in northern Britain during the past 7.5 ka based on plant macrofossil evidence for increased bog-surface wetness. Thin bars represent wet shifts and thicker bars wet phases (from Langdon *et al.*, 2003). See also Figures 3.53 and 3.54.

information in places where there are few alternative lines of evidence. For example, remains of the aquatic plants *Najas flexilis* and *Typha latifolia* found among a rich array of other plant macrofossils in a beaver dam in central Alaska indicate that temperatures were significantly warmer during the early Holocene than today (Robinson *et al.*, 2007), while in the desert regions of the USA, plant macrofossil remains preserved in packrat middens (nests) provide a record of changes in vegetation and climate, notably precipitation, in some instances extending back over 40 ka (Jackson *et al.*, 2005).

4.4.6.2 Forest history

A long-standing debate in Quaternary palaeoecology concerns the altitudinal and latitudinal positions of former treelines. During full glacial conditions, temperate trees are believed to have receded to ‘refugia’ in lower-latitude warmer areas, but the location and nature of many of these refugia remain to be established. Determining forest limits during warmer episodes has also proved problematic. The main difficulty has been the reliance on pollen-stratigraphic evidence for detecting past treelines, because the proportion of trees can be over-estimated in pollen assemblages obtained from areas with few or no trees (Eide *et al.*, 2006), but also under-estimated in pollen records obtained from wooded areas (Opgenoorth *et al.*, 2010). Macrofossil tree remains, on the other hand, are unequivocal evidence for tree presence, and are providing important new insights into former forest refugia. It has long been assumed, for example, that the key refugia in Europe during the Last Glacial Maximum lay in areas such as the Balkans, Italy and Iberia, but plant macrofossil data now suggest that coniferous and some deciduous trees were growing much further north and east than previously envisaged (Willis & van Andel, 2004). Macrofossil evidence also shows that both black spruce (*Picea mariana*) and white spruce (*P. glauca*) were able to regenerate in an unglaciated enclave of Yukon Territory, Canada, after the onset of harsh glacial conditions between 26 and 24 ka when most of the territory was arctic tundra (Zazula *et al.*, 2006). Similarly, in the Himalayas, near the highest known treelines in the world, macrofossil evidence indicates that trees survived in small refugia throughout the last cold stage. These small protected enclaves of persistent tree growth through harsh glacial conditions are referred to as **cryptic refugia** or **glacial microrefugia** (Opgenoorth *et al.*, 2010), and woody macrofossil evidence from these localities is providing new insights into the history of trees and how they responded to the major climatic changes of the Late Quaternary.

4.4.6.3 Charcoal and fire history

Some regions, such as the western mountains of North and South America, experience regular wildfires as part of a natural ecological cycle, and records of historical fire activity are reflected in fossil charcoal records. Analysis of the charcoal content of lake sediments in the North Cascade Mountains in Washington State, USA, for example, suggests significant changes in fire frequency throughout the last 10.5 ka, with climate probably the key driver (Prichard *et al.*, 2009). Charcoal studies from the Argentinian Andes also implicate climate as the principal forcing factor in fire frequency, with increases in fire incidence coinciding with increased ENSO strength (section 7.6.4.2) and greater climatic variability (Whitlock *et al.*, 2006). The relationship between fire and climate may not always be straightforward, however, because changes in forest composition also modulate fire dynamics by altering the mix of species susceptible or resistant to fire (Prichard *et al.*, 2009). In addition, local factors may over-ride regional climatic controls, while the intensity of fire damage also varies at the local and regional scales (Gavin *et al.*, 2007). A further complication in the interpretation of charcoal records is that charcoal fragments can be transported over considerable distances, due to the powerful convection currents generated by intense forest fires (Pisaric, 2002). Hence, although charcoal stratigraphy in lake sediments provides a basis for reconstructing fire histories, care is required in the interpretation of the data.

In many areas of the world, fire histories reflect human activity as opposed to climate. Throughout North America, for example, there is abundant ethnohistorical and charcoal evidence for burning, with fire being used as part of hunting practices to drive animals, to improve pasture and human mobility, and to increase species diversity of food plants (Boyd, 1999). Anthropogenic burning inferred from charcoal records has also been described, *inter alia*, from the British Isles (Barton *et al.*, 1995), Madagascar (Burney *et al.*, 2004) and Australia (Wroe & Field, 2006). The principal difficulty with attributing fire to human agency, of course, is that in many areas, with long, seasonally dry climates, such as the American Midwest, it is difficult to distinguish between natural and anthropogenic burning from the charcoal record alone (Bell & Walker, 2005). This is exemplified by evidence from Australia where fire incidence after the arrival of humans from c. 60 ka onwards has been interpreted on the one hand as indicating burning as part of a hunting strategy which led to the eventual extinction of the Australian megafauna (Miller *et al.*, 2005), while on the other it has been suggested that the fire regime in Australia has been predominantly

forced by climate, with a strong similarity in temporal variation to the Dansgaard–Oeschger cycles of the last cold stage (Mooney *et al.*, 2011; section 3.11.4).

4.4.6.4 Archaeological records

Humans have altered natural vegetation in a variety of ways, through woodland clearance for pastoral and agricultural activities, exploitation of aquatic resources, land irrigation and reclamation, domestication of grain and crop species, and transfer of selected plants to new territories as ‘exotic’ newcomers; evidence for all of these changes can be discerned in the plant macrofossil record (Jacomet, 2007). Plant macrofossil data augment inferences drawn from pollen records about anthropogenic activity, and the two are collectively referred to as **archaeobotanical evidence**. Macrofossils may provide important dietary information; for example, remains of wild fruits found in sediments from Neolithic and Bronze Age dwellings at Lake Neuchatel, Switzerland, reveal that the occupants consumed *Prunus spinosa* (sloe), *Cornus sanguinea* (dogwood), *Malus sylvestris* (apple), *Rubus* species (raspberry/dewberry/blackberry), *Fragaria vesca* (wild strawberry), *Rosa* sp. (hip), *Quercus* sp. (acorn), *Corylus avellana* (hazelnut) and *Fagus sylvatica* (beechnut) (Karg & Märkle, 2002). Plant macrofossil remains also provide evidence of the earliest farming activity, with charred cereal grains indicating cultivation in the Euphrates Valley, Syria around 13 ka (Hillman *et al.*, 2001), while in the New World, peanut, squash and cotton appear to have been grown as early as 10 ka in the Peruvian Andes (Dillehay *et al.*, 2007). Other archaeobotanical evidence reveals the nature of plants used in the dyeing of fabrics (Hall, 1996), the development of plant-based fabric industries, such as flax and hemp (Viklund, 2011), and the types of plants adopted for sacrificial ceremonies (Megaloudi, 2005). In addition, evidence of routine domestic practices such as the preparation of animal fodder, and the plant types and parts preferred for bedding, tempering agents, insulation and roofing, may also be preserved in the archaeobotanical record.

4.5 FOSSIL INSECT REMAINS

4.5.1 Introduction

Fossil insects are often abundant in a wide range of Quaternary deposits. Typically these include sediments that accumulated in ponds or near lake margins, in backwaters of rivers, in peats or indeed in any depositional environment conducive to the preservation of plant debris.

Many different orders of fossil insects have been observed in Quaternary deposits, including bugs (Hemiptera–Homoptera), two-winged flies (Diptera), caddis flies (Trichoptera), stink bugs (Pentatomidae), seed bugs (Lygaeidae), leaf hoppers (Cicadidae), bees, ichneumons (Hymenoptera), dragonflies (Odonata), non-biting midges (Chironomidae), water striders (Gerridae), shore bugs (Saldidae), water boatmen (Corixidae), backswimmers (Notonectidae) and beetles (Coleoptera) (Elias, 2010), while members of the ant family (Formicidae) have also been investigated. Although not technically insects, the mites (Arachnida), especially oribatid mites, have been considered together with insect assemblages, and are particularly important components of the soil fauna of arctic and alpine ecosystems (Elias, 1994).

It is the beetles, however, that are the best-known of this array of fossils (Figure 4.21). This is because in a body of sediment they are often visible to the naked eye and commonly display brilliant and often iridescent colouring of blues and greens. As a consequence, their presence in Quaternary sediments has long been a source of fascination to laymen, naturalists and entomologists alike. More recently, however, and largely through the pioneering work of Russell Coope (see section 4.5.4), fossil Coleoptera have proved to be a powerful tool for the investigation of Quaternary environments, and particularly of past climatic conditions. Although fossils of the other insect groups have occasionally proved useful in palaeoecological studies, such as caddis flies and oribatid mites (Greenwood *et al.*, 2003; Hodgson & Convey, 2005), they tend to be less well preserved due to their delicate structures, some of the groups are difficult to identify beyond generic level, and their present-day distributions are less well known than those of the Coleoptera. As a consequence, the remainder of this section is devoted mainly to Coleoptera, although Chironomidae are also considered as they too have proved to be useful palaeoclimatic indicators.

4.5.2 Coleoptera

Coleopteran remains are usually the most diverse group of insect fossils in Quaternary deposits and often they are the most abundant. The chitinous exoskeletons of which they are composed are highly robust and contain sufficient structural detail to permit a large number of beetle fossils to be identified to species level (Figure 4.22). They have been collected and studied by entomologists in many parts of the world and there is now a considerable body of knowledge in the form of atlases and monographs that summarize their distribution and ecological associations. The order Coleoptera is one of the

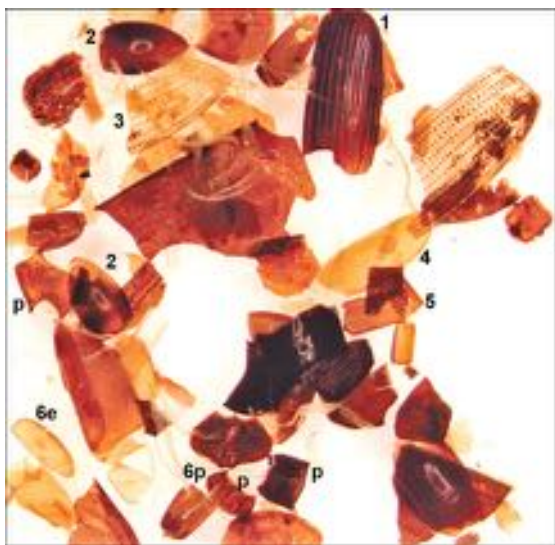


Figure 4.21 Subfossil coleopteran sclerites (see Figure 4.22) recovered by flotation from peat deposits overlying a Bronze Age occupation site near Ballyarnet Lake, Co. Derry, Northern Ireland. Elytra (wing-cases) dominate in this view with an occasional pronotum (p). 1. *Pterostichus nigrita* – a predatory ground beetle (10–15 mm) widespread in marshes and water margins. 2. *Cercyon atomarius* – a small (1.5–4.5 mm) dung beetle. 3. *Helophorus* spp. – a water scavenger genus, with most species occupying emergent vegetation in standing or slow-moving water. 4. *Trechus rubens* – a small (5–6.5 mm) subterranean ground beetle, under stones and leaf piles on riverbanks and lake shores. 5. *Anobium punctatum* – a beetle that bores into and feeds upon wood (3–4.5 mm). 6. *Hydraena brittani* elytrum (6e) and pronotum (6p) – a water beetle common in shallow lake margins (photograph by Nicki Whitehouse, Plymouth University, UK).

largest in the animal kingdom, accounting for 25 per cent of all known species of organisms. They form the most important insect order, with more than 300,000 known species, 30,000 of which occur in North America while within Britain alone there are over 3,800 named species. They occupy a very wide range of habitats, having colonized almost every terrestrial and freshwater niche, some even being found within the intertidal zone. Many of these species are **stenotopic**, which means that they show a marked preference for particular environments (e.g. those adapted to narrow temperature ranges or specific habitats or substrates), and it is this characteristic above all others that makes the Coleoptera such valuable palaeoecological indicators.

4.5.3 Laboratory methods

In the laboratory, insect fragments can be removed by hand from the sediment matrix where, for example, they occur on bedding planes in clays or felted peats. More frequently, however, flotation techniques are employed (Elias, 2007a). The most commonly used method involves disaggregation of the sediment in water or in a sodium carbonate solution, followed by sieving (300 µm), and the residues remaining on the sieves are then mixed with kerosene (paraffin), which adheres to insect sclerites but not to plant detritus. When water is subsequently added, the insect remains float to the surface, along with some plant macrofossils. The floating fraction is decanted, washed gently in detergent and dehydrated in 95 per cent ethanol before being sorted under a low-power microscope. The insect fossils range in size from less than 1 mm to several centimetres, and close examination may be necessary at this stage in order to ensure that very small specimens are not overlooked and that the subsequent collection is not heavily biased in favour of the more conspicuous species.

The fossil remains are then glued onto cards or stored in dilute (*c.* 20 per cent) alcohol and examined under a microscope. Electron microscopy may be necessary where examination of very fine structural detail is required for identification of some species. Since the entire insect fossil is rarely recovered from the sediment body (commonly identification is made on an elytron [wing cover] or thorax, or even a small fragment of an elytron), keys to identification are of limited value and identifications require careful comparisons with modern specimens. A comprehensive comparative collection of modern beetles is therefore essential for palaeoecological research. Some parts of the fossils possess few diagnostic features, but in many cases the heads, thoraces, elytra and genitalia (particularly in the male specimens) display a wealth of characters, which enable specific determinations to be made (Figure 4.22).

Data from fossil insect analysis are usually presented in the form of a species abundance list showing numbers of individuals occurring within a particular sample. The results tend to be presented in tabular form because of the size of the overall dataset, although subsets of particular interest, such as stenothermic species, may be displayed graphically (Figure 4.23). Occasionally, further information is provided in species lists on the specific parts of insects that have been recovered, for example heads and elytra. The numbers listed are the minimum numbers of individuals that are represented by the recorded skeletal parts. Thus a collection of three elytra, one head and two thoraces of the species *Olophrum fuscum* (Grav.) obtained from one stratigraphic horizon would indicate a minimum number of two individuals of that species.

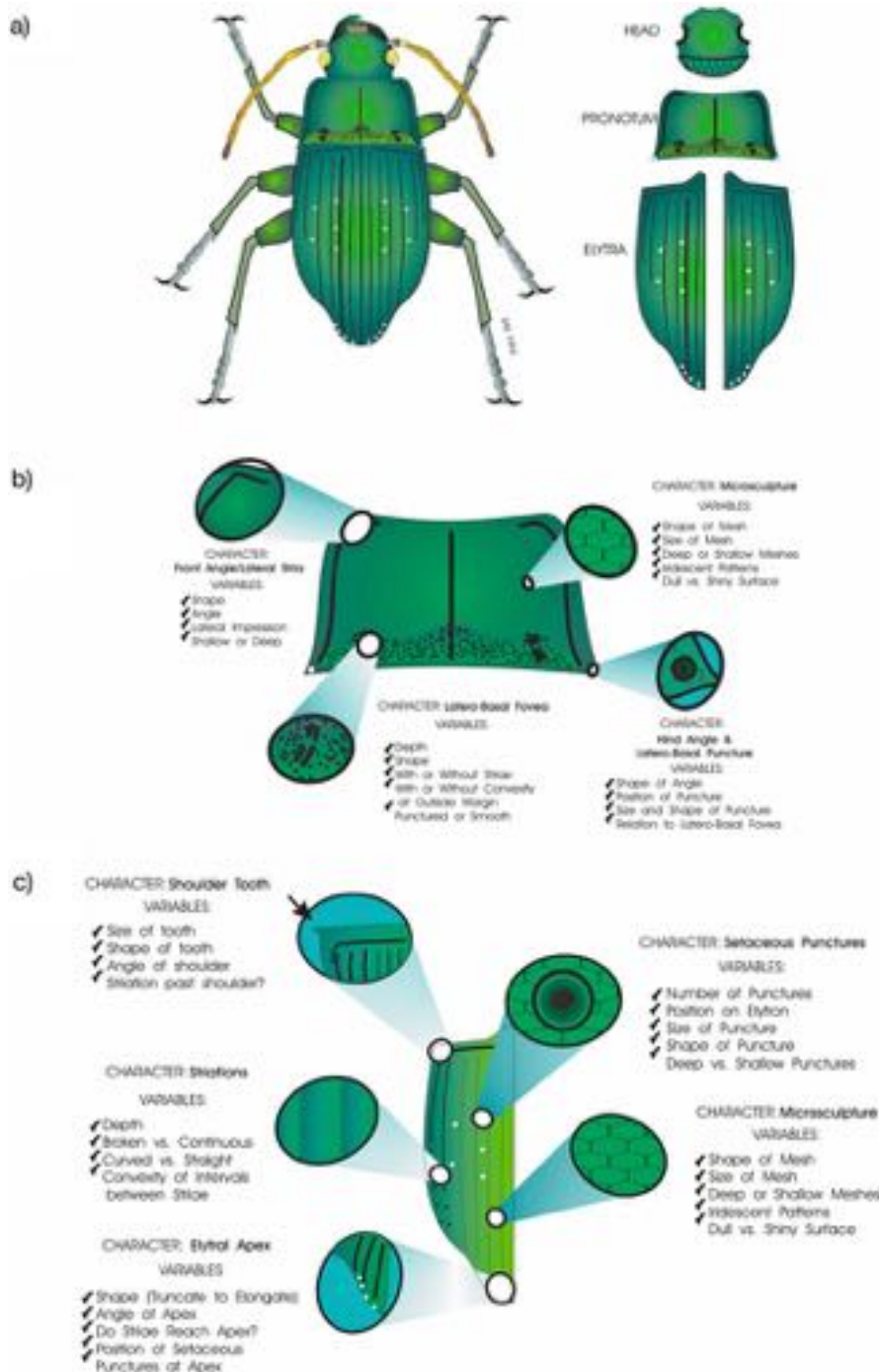


Figure 4.22 Generalized drawings of coleopteran sclerites frequently preserved as Quaternary fossils, showing a range of diagnostic features used in fossil identification: a) dorsal surface, b) pronotum and c) elytron of a ground beetle (Carabidae) (from Elias, 1994).

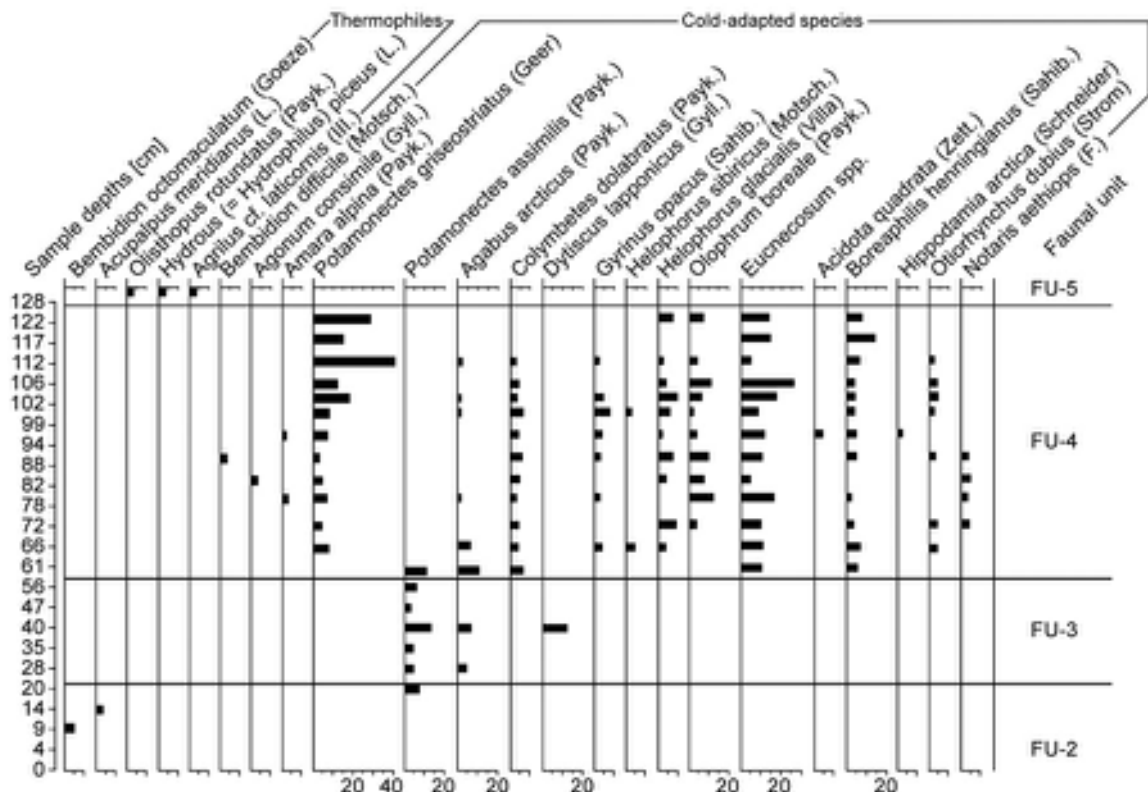


Figure 4.23 A coleopteran record from the Lateglacial (c. 14.7–11.5 ka) site of Llanilid, south Wales, UK. The warmest part of the sequence (early Interstadial) is represented by faunal unit FU-2, cooler conditions are recorded in FU-3 (later Interstadial) and marked by the arrival of cold-adapted species, while the cold Younger Dryas/Loch Lomond Stadial is characterized by an increased number of cold-adapted species. Note how these disappear in the early Holocene (FU-5) to be replaced by thermophiles (from Walker *et al.*, 2003).

A useful aid for the study of palaeoentomology, entomology and ecology is the Bugs-CEP web site: <http://www.ncdc.noaa.gov/paleo/insect.html> or <http://www.bugscep.com>. This provides a comprehensive set of search and reporting functions, including pictorial images of species, information on their habitat and distributions, guidelines for data collection and storage, and tools for climatic and environmental reconstruction (Buckland & Buckland, 2006).

4.5.4 Coleopteran analysis and Quaternary environments

Coleoptera exhibit a number of characteristics which make them one of the most valuable components of the terrestrial biota for the reconstruction of Quaternary environments. Not only are they relatively abundant in a wide range

of deposits, but they appear to combine both evolutionary and physiological stability with acute sensitivity to climatic change (Elias, 2010). In addition, they frequently display a marked preference for very restricted environmental niches or conditions.

Our present understanding of the ways in which fossil beetles can be used to reconstruct Quaternary environments stems, in large measure, from the work of Russell Coope (Ashworth *et al.*, 1997). He noted, in particular, that the skeletal elements of the fossil insects showed a remarkably close similarity in shape and fine anatomical detail to the corresponding parts of living species, and that this remained the case irrespective of the age and context of the Quaternary assemblages (Coope, 1967). Subsequent research has confirmed his view that the vast majority of beetle species have remained morphologically identical, possibly since Miocene times; moreover,

there is only one confirmed record of species extinction during the Pleistocene (Elias, 2010; Marra & Leschen, 2011). This apparent long-term **evolutionary stasis** (anatomical stability) initially seemed counter-intuitive, for it was assumed that the cyclical climatic changes that characterize the Quaternary would have resulted in a high species turnover. Coope's research suggested quite the opposite: repeated environmental disruption appears to have engendered stasis, at least as far as beetles were concerned (Coope, 2004).

Coope's second key observation related to the mechanism by which stasis in beetle populations was maintained, for he noted that the ecological preferences of most coleopteran species also appear to have remained unchanged during the Quaternary. The available evidence suggested that, in the great majority of cases, species of beetles are found in similar associations in both fossil and living assemblages. In Britain, for example, the warm-adapted insect assemblages of one interglacial period are essentially similar to those of others, even though the interglacials may differ in age by hundreds of thousands of years (Coope, 2010). The beetle assemblages of various cold stages, in particular, have a large number of species in common. Moreover, independent palaeobotanical and geological evidence indicates that most fossil beetle species were associated with environments that are similar to those that they occupy today. It does seem, therefore, that in the majority of cases, physiological stability of coleopteran species was accompanied by morphological and ecological constancy throughout the greater part of the last two million years, and exceptions to this rule are comparatively rare (Coope, 1977). The key point is that beetles, being highly mobile, did not need to evolve to cope with marked climatic or ecosystem change: they simply moved to maintain their association with migrating climatic and vegetational zones, thereby remaining within their ecological comfort zones and avoiding pressures to adapt.

Although the evidence for morphological stasis appears strong, however, recent developments in molecular research are beginning to reveal that more speciation of beetles may have taken place during the Quaternary than has been recognized hitherto. For example, on the Iberian Peninsula, eighteen to nineteen new species appear to have emerged during the Quaternary (Ribera & Vogler, 2004), while in North America, tiger beetles have continued to diversify over the course of the last 5 Ma, and at an increasing rate during the Quaternary (Barraclough & Vogler, 2002). However, most studies suggest that beetle speciation during the Quaternary was confined to low-latitude areas not directly affected by glaciation, or to mountain micro-refugia, where beetle faunas became

isolated for long periods (Previsic *et al.*, 2009; Marra & Leschen, 2011). In such areas, therefore, the habitat preferences of some beetle species might possibly have changed over the course of the Quaternary. It is also worth noting that the current global databank of Quaternary fossil beetle records is biased towards northern temperate and Palearctic regions and to records from the last 15 ka. The database may therefore reflect a greater emphasis on species that were forced to migrate over long distances as a consequence of repeated expansion and demise of the great ice sheets. In other areas, by contrast, past changes in the geographical and temporal ranges of beetle species appear to have been much more conservative (Abellán *et al.*, 2011).

4.5.4.1 Habitat preferences

Any assemblage of fossil insect remains will contain species from a variety of local habitats. Botanical factors, soil type, microclimatic environment, hydrological conditions and chemical variations will all restrict the distribution of insects at the local scale (Elias, 1994, 2010). To a palaeoecologist who is interested in the environmental history of a particular site, therefore, it is important that the range of habitats represented by the fossil assemblage is identified and, as far as is possible, quantified. Some beetle species are substrate dependent, such as *Bembidion obscurum*, which lives on dry, sandy soils; *Dyschirius globosus*, which requires moderately humid soils with clay, sand or peat and a sparse vegetation cover; and *Bembidion schueppeli*, which is restricted to river banks. A large number of beetles are associated with aquatic habitats. Thus actively flowing water is indicated by *Esolus*, *Limnius volckmari* and *Ochthebius pedicularius* while *Potamoneutes depressus (elegans)* and *Halyplus obliquus* live in clear ponds with sandy or silty bottoms. Other beetles indicate the presence of particular plants or other animals upon which they depend for food. Most of the staphylinid beetles, for example, are predators, living on small arthropods and worms in leaf litter. A profusion of dung beetles in an assemblage would indicate the local presence of mammals; indeed, some beetle species are selectively associated with the dung or decaying carcasses of particular animals, for example mammoths (Allen *et al.*, 2009). A number of phytophagous Coleoptera feed only on reeds, such as several species of the *Donacia* genus which live on *Carex*, *Scirpus*, *Sparganium* and tall marsh grasses. *Hydnobius punctatus* feeds on fungal hyphae, *Hypera postica* is dependent upon various leguminous plants, such as *Medicago*, *Melilotus* and *Trifolium*, and *Simplocaria semi-striata* feeds exclusively on moss.

Beetle assemblages can therefore provide valuable information on a diverse range of contemporaneous habitats or co-dependent biota, and may provide environmental insights that are difficult to obtain from other lines of evidence. For example, large numbers of the genus *Bledius* were found among the earliest colonizers of the surface of the lower cover sands (deposited during the last cold stage) in the Netherlands in deposits containing remains of the blue-green alga *Gleotrichia* (Van Geel *et al.*, 1989), an important nitrogen fixer. The algae may have provided an important food source for these beetles at a time when few other organisms had succeeded in colonizing the area. Large numbers of *Bledius* recovered from early Lateglacial sands in a site in eastern England may therefore indicate that nitrogen-fixing algae played an important role in the colonization process at that site also (Walker *et al.*, 1993). Some beetle species are obligate dwellers in tree bark or leaf litter, and fossil remains of such

beetles have been used to augment palynological evidence for the presence of trees and to establish the changing composition of woodland over time (Figure 4.24; section 4.5.4.3). Fossil insect assemblages preserved in packrat middens in the deserts of the southwest USA contain a mixture of temperate and desert species not found together in any part of North America today (Elias, 2007b). This may indicate a late Pleistocene climatic regime for which there is no modern analogue.

In addition to these macro-scale environmental reconstructions, mosaics of former micro-habitats may also be inferred from fossil beetle assemblages. For example, Olsson & Lemdahl (2009) used fossil beetle records from southern Sweden to amplify the history of woodland changes during the Holocene, with different species groups providing evidence of variation in woodland density and diversity, of the amount of deadwood on the ground, of the impacts of grazing and fire, and of the eventual

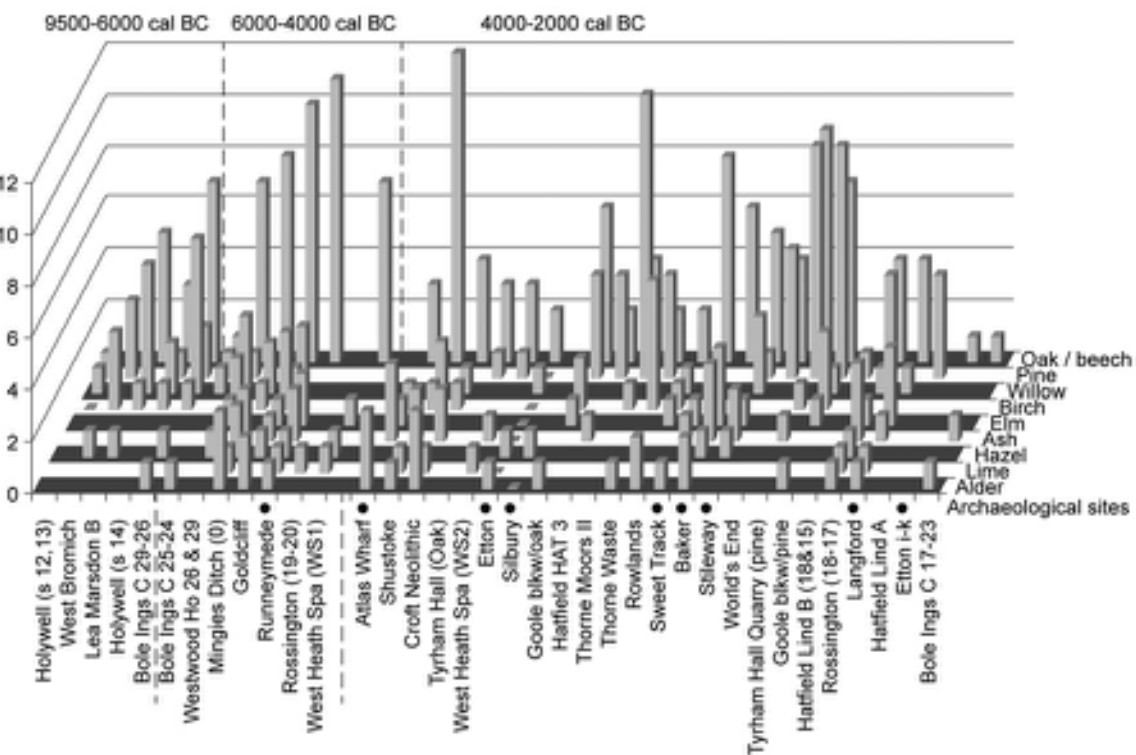


Figure 4.24 Number of obligate beetle species (key indicates tree affinities) recorded in Holocene sediment sequences from southern and central England. The site names are listed along the base; archaeological sites are indicated by closed circles; the remainder are considered 'palaeoecological' (not disturbed by archaeological activities). For further explanation see text (from Whitehouse & Smith, 2010).

replacement of woodland by heathland at c. 2.8 ka. Similarly, Davis *et al.* (2007) were able to decipher small-scale variations in the topography and channel patterning of lowland river flood plains from the characteristic fossil beetle assemblages that occupy different flood-plain micro-habitats, while Kuzmina *et al.* (2011) used evidence of micro-habitat preferences of modern beetles in present-day arctic tundra regions to reconstruct climatic gradients for the former periglacial zone of the exposed continental shelf around the Bering Sea during the last cold stage. These various examples show how a knowledge of the autecology of beetles can provide valuable additional insights into Quaternary palaeoenvironments at a range of spatial and temporal scales.

4.5.4.2 Palaeoclimatic inferences based on coleopteran assemblages

One of the most important factors that has governed the distribution of most insect species during the Quaternary has been climate, particularly thermal conditions (Coope, 1990, 2004). Distribution maps of modern beetles show that the geographical range of many species corresponds with well-defined climatic zones (Figure 4.25) and especially with summer temperature thresholds. Those insect species whose distributions are narrowly restricted are termed **stenotherms**, while those that can tolerate a broader range of climatic conditions are termed **euerytherms**. The former are much more important in palaeoclimatic research,

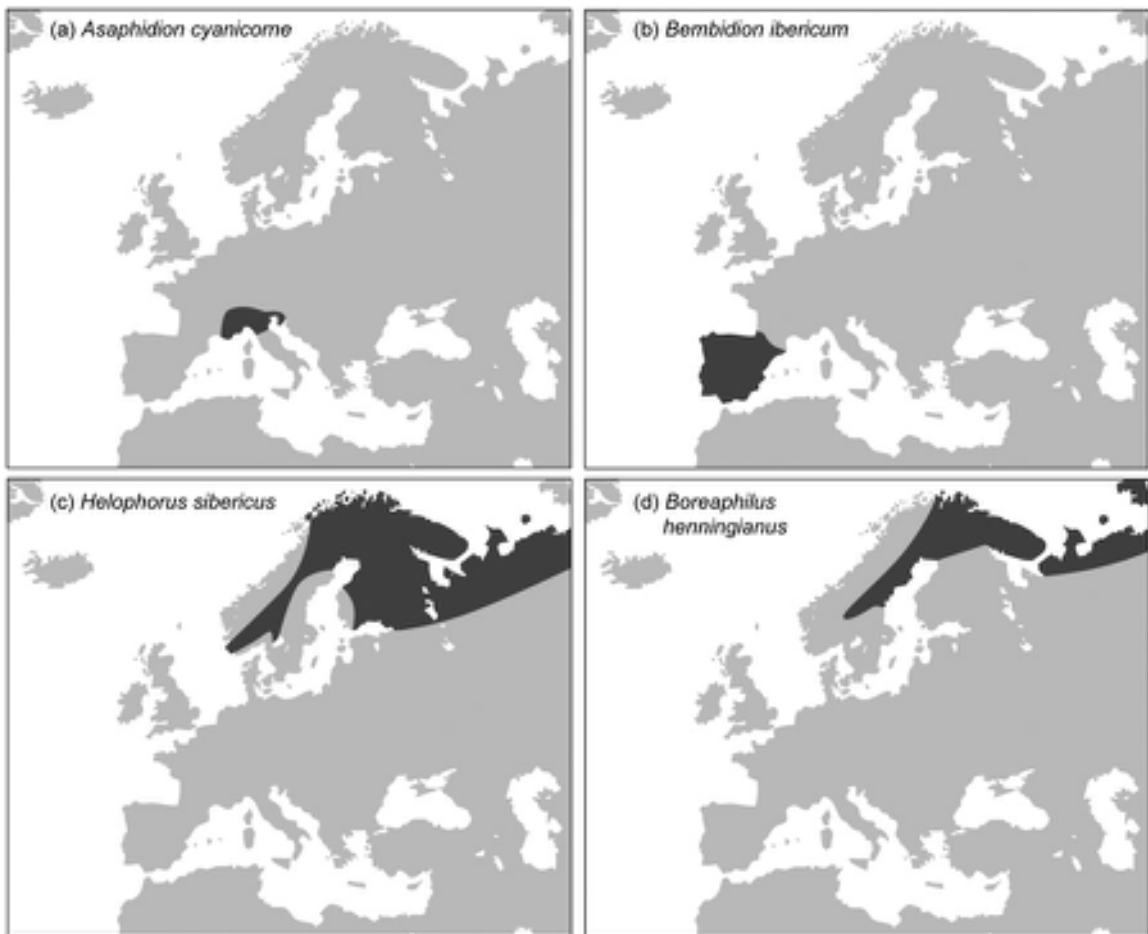


Figure 4.25 Present-day European distributions of four coleopteran species found in Lateglacial deposits (c. 14.7–11.5 ka) at the site of Glanllynau, north Wales (from Coope & Brophy, 1972).

since they enable more precise inferences to be made about former temperature regimes. The acute sensitivity of beetles to temperature variations is reflected in the growing body of evidence that reveals how beetles have adjusted their modern geographical ranges in response to global climate change within the last century or so (e.g. Parmesan, 1999; Hill *et al.*, 2011).

As with most other lines of fossil evidence, however, there are problems in utilizing fossil beetles as climatic proxies. It can never be established for certain that an insect species has colonized the entire climatic range to which it is suited, nor that past distributions were entirely in equilibrium with the prevailing climatic conditions. On the other hand, Coope (1977) has argued that the enormous scale of the changes in geographical distribution of species in response to climatic shifts during the Quaternary, and the rapidity of many of these changes in species range, indicate that Coleoptera must have been able to colonize new available habitats extremely quickly. In the majority of cases where the range limit of a coleopteran species coincides with a climatic boundary, this relationship has, therefore, long been used to derive quantitative palaeotemperature estimates. For the British Isles, Coope (1987) classified fossil coleopteran species ranges into eight categories:

- (a) southern European species;
- (b) southern species whose normal ranges just fail to reach Britain;
- (c) southern species whose normal ranges are south of central Britain;
- (d) widespread species whose normal ranges are north of central Britain;
- (e) boreal and montane species whose normal ranges extend down into the upper part of the coniferous forest belt;
- (f) boreal and montane species whose normal ranges are above the tree line;
- (g) eastern Asiatic species, some of which also range into North America;
- (h) cosmopolitan species with very wide geographical ranges.

Hence, an interglacial assemblage might therefore be dominated by fossils from categories (a), (b) and (c) with representatives of group (h), while cold-stage faunas are more likely to have a high representation of categories (d), (e) and (f) with some elements of (h). The problem, however, is how to make a quantitative estimate of prevailing macroclimate from such data.

Early attempts to derive macroclimatic reconstructions from fossil assemblages employed the **range overlap**

method, in which the modern distributions of species (indicator species) represented in a fossil assemblage are plotted, and the zone of overlap of the ranges is identified (e.g. Coope, 1959). Modern climatic statistics obtained from meteorological stations that lie within the zone of overlap, such as mean annual temperature or the annual temperature range, can then be used to provide a quantitative estimate of the regional macroclimate that prevailed at the time the fossil taxa coexisted. In practice the method works best when a large number of stenothermic species are represented in an assemblage, and this often enabled relatively precise palaeoclimatic estimates to be inferred. The main difficulty with this approach, however, is that a species might not occupy its full potential geographical range. Furthermore, some taxa may temporarily coexist during a transitional phase of adaptation to new climatic conditions, and the resulting mix of fossils may therefore be largely an ephemeral one, with no modern analogue (a **non-analogue assemblage**). This problem may be particularly acute in the interpretation of fossil insect assemblages derived from sediments that accumulated during an episode of abrupt climatic change, since insects appear to have responded much more rapidly than other biota to changing climatic conditions. One of the challenges of Quaternary palaeoecology, therefore, is to distinguish such temporary associations from those representing more stable climatic episodes, and, while meeting this challenge, to note that non-analogue faunas do not necessarily imply non-analogue environments.

In an attempt to avoid the errors that may arise from the use of the indicator species approach, the **mutual climatic range (MCR)** method was developed to obtain more representative palaeotemperature estimates from beetle records (Atkinson *et al.*, 1987). This is an extension of the range overlap method, but it employs the ranges of *all* of the taxa included. Modern distribution maps are first obtained for as many as possible of the species in the fossil assemblage, and the climatic range of each beetle type is then established using contemporary meteorological data. The two most important variables governing beetle distributions appear to be the temperature of the warmest month (T_{MAX}) and the temperature range between the warmest and coldest months (T_{RANGE}), the latter providing an index of seasonality. By knowing the distribution in terms of T_{MAX} and T_{RANGE} , the geographical range of each species may be plotted in 'climate-space', and for each species a 'climatic envelope' is thus produced (Figure 4.26). For any fossil assemblage, therefore, the **mutual climatic range** can be determined from a computer-generated plot of the climatic parameters relating to each beetle in the assemblage. From these plots, the values of T_{MAX} , T_{RANGE}

and T_{MIN} (temperature of the coldest month) can be obtained, and these constitute the 'best estimates' of the mutual climatic conditions within which the particular mix of fossils formerly coexisted. The method is most successful (i.e. produces the narrowest range estimates) where an assemblage contains a large number of species, and where a number of these are obvious stenotherms. The method can be tested by deriving MCR values for modern beetle assemblages and measuring their statistical relationship with modern climate data (Figure 4.27). The results usually show a stronger linear relationship for summer than for winter temperatures, mainly because many beetle species can survive a wide range of winter temperatures (Elias, 1997). The advantages of the MCR method over the indicator species approach are that it avoids subjective interpretations and possible bias, as well as over-generalization from the use of geographical overlays. Moreover, geographical range limits are often too broad, and cannot take into account such factors as altitude, oceanicity, microclimatic variations and so on. The MCR approach ignores geographical location, and focuses entirely on climatic parameters governing species distributions. Hence a complex geographical distribution may be reduced to a narrow climatic range, reflecting the fact that the often diverse geographical locations in which a species occurs may, in fact, have common characteristics when plotted in climate-space. Also, and most importantly, it does not really matter if the species does not occupy its

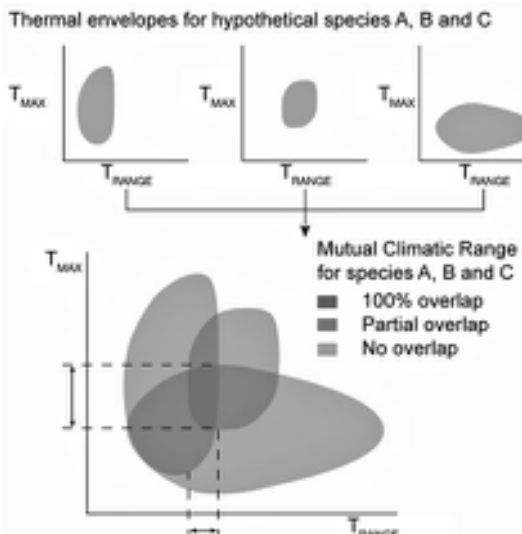


Figure 4.26 Schematic representation of the mutual climatic range (MCR) method of quantitative temperature reconstructions (courtesy of Adrian Walkling).

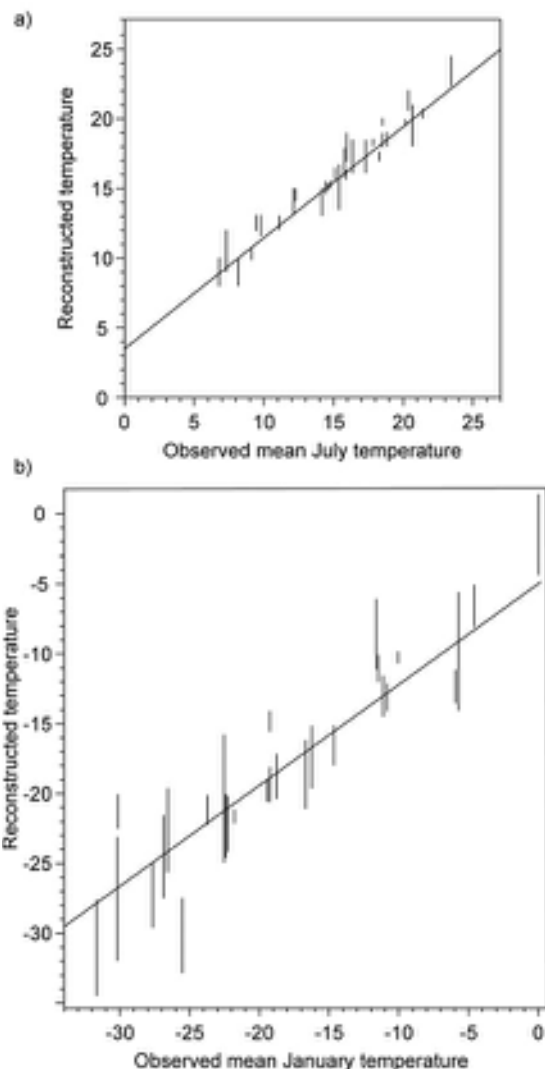


Figure 4.27 Test of the MCR method on assemblages of species found living today at thirty-five localities in North America. The reconstructed mean July temperatures (T_{MAX}) are shown on the vertical axis of graph a); the reconstructed mean January temperatures (T_{MIN}) on the vertical axis of graph b). Vertical bars represent the mutual climatic range of the beetles found living at the localities studied. The horizontal axes of the two graphs show the observed T_{MAX} and T_{MIN} values for the thirty-five sites. The slopes and positions of the gradient lines are linear regressions of predicted against observed values for the test sites (from Elias, 1997).

full (potential) geographical range, so long as it reaches potential climatic boundaries in a sufficient number of places.

Climatic reconstructions based on beetle MCR data from the British Isles (Figure 4.28 main curve) bear a striking resemblance to those derived from Greenland ice-core records (section 3.11.4), most notably in respect of the abrupt increases (by around 7°C) in mean July temperatures at around 14.7 and 11.5 ka where the rate of warming may have been as rapid as 1°C per decade (Atkinson *et al.*, 1987), and the episode of markedly lower temperatures between c. 12.9 and 11.5 ka, in the Younger Dryas period or Greenland Stadial 1 (GS-1: section 1.6). So close is the match between the British and Greenland records, that it seems likely that both areas were climatically phase-locked at times during the Lateglacial period (Walker *et al.*, 2012). This does not appear to have been the case for other parts of Europe, however, for MCR reconstructions from Poland, Sweden, Norway and France (Figure 4.28) show significant differences in regional temperature trends (Ponel *et al.*, 2005). These largely reflect the delayed melting of the Scandinavian ice sheet compared with its British counterpart, with the former maintaining cooler climatic conditions around its periphery for longer. This is clearly indicated by the beetle MCR data which reveal marked thermal gradients between Britain and Scandinavia throughout the Lateglacial period (Coope *et al.*, 1998). In contrast to Europe, fossil beetle MCR data from many parts of North America indicate a relatively smooth transition from glacial to interglacial climates from around 17 ka onwards, and few sites record a climatic reversal

coincident with the Younger Dryas interval, again reflecting the prevailing influence on climate of the last ice sheets (Elias, 2007a). The two exceptions are the Maritime Region of Canada, where beetle MCR temperature evidence from a number of Lateglacial sites shows a significant decline in temperature (c. 5°C) around 13.0–12.5 k BP, coincident with the onset of the Younger Dryas in Europe (Miller & Elias, 2000), and arctic Alaska, where again beetle data appear to indicate a Younger Dryas equivalent cooling (Elias, 2000).

The MCR method is not without its problems, however. One drawback is the incomplete knowledge of the present geographical ranges of many species, especially in Asia. As a result, the palaeoclimatic significance of records of the many cold-adapted Asian species that migrated to Europe and Alaska during cold intervals is difficult to quantify precisely (Zinovjev, 2006; Alfimov and Berman, 2009). A different constraint affects the use of the MCR method in geographically isolated regions, such as Australia: although conditions appear to have been much colder in the past than is experienced in any part of Australia today, these lower temperatures are not reflected in the fossil beetle record, because no inward migration of cold-adapted species was possible (Poroch, 2010). Other problems with the MCR method include the possibility that some modern species are prevented from attaining their full climatic range because of physical barriers to migration, while the range of climate states that exists today may not include the extreme conditions or variants that some species could potentially tolerate (Poroch, 2010). Finally, the MCR method has been challenged on statistical grounds, mainly because beetle data are unlikely to have normal (Gaussian) distributions in climate-space, but are dispersed in more complex ways throughout their ranges (Bray *et al.*, 2006). These and other difficulties notwithstanding, there is no doubt that the MCR method has proved to be a valuable tool in palaeoclimatology, and remains one of the key techniques for quantifying the magnitude and rate of past temperature change.

A recent development in the use of fossil beetles as palaeoclimatic indicators involves the analysis of the hydrogen isotope chemistry of the chitin in fossil beetle carapaces (Gröcke *et al.*, 2006). Data from modern beetles suggest that this varies predictably with changes in mean precipitation and annual temperature. The methodology is still at an early stage, however, and requires further experimentation to establish the degree to which H-isotope varies both within and between beetle specimens in a systematic and predictable way, and the extent to which these variations correlate with climatic parameters (Gröcke *et al.*, 2011).

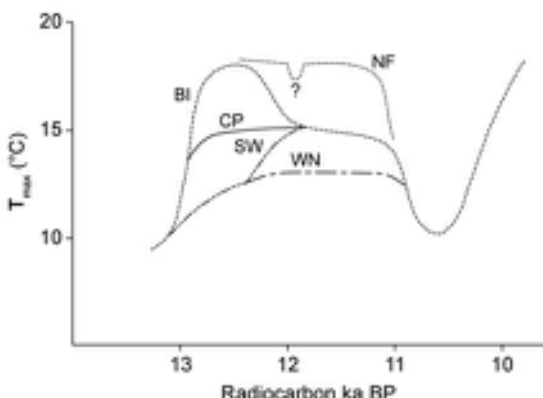


Figure 4.28 Generalized climatic curves of estimated T_{MAX} variations during the Lateglacial–early Holocene for the British Isles (BI), central Poland (CP), southern Sweden (SW), western Norway (WN) and northern France (NF) (from Coope & Lemdahl, 1995).

4.5.4.3 Insect fossils and archaeology

Coleopteran assemblages, in common with a number of other proxy biological indicators, clearly record the effects of human impact on the landscape of Europe during the mid-Holocene (Elias, 2010). Obligate woodland beetle species not only record natural changes in woodland composition throughout the Holocene (Figure 4.24) but also reveal the degree to which woodland in large parts of Europe was reduced in density or cleared completely to meet increasing agricultural or pastoral demands (Whitehouse & Smith, 2010). This in turn led to the elimination of a number of beetles dependent on natural woodland cover and their replacement by species associated with farming practices and human settlements (Whitehouse, 2006). The latter include pests of grain production (Smith & Kenward, 2011), dung and parasitic beetles associated with domesticated or working animals (Buckland *et al.*, 2009), and beetles that are associated with human occupation, and are found in house floors, waste pits, roofing structures and fills, tanneries, cess or refuse pits, stables and textile stores (Kenward & Carrott, 2006; Kenward *et al.*, 2012). Human activity is also reflected in the occurrence of **synanthropic** species (those closely associated ecologically with humans), especially parasitic species or predators on human corpses (Panagiotakopulu *et al.*, 2012), while other bio-indicator species are indicative of more specialized human practices, such as ancient mining and metal-working (Mighall *et al.*, 2002).

A number of factors serve to complicate the study of **archaeoentomology**, however. Fossil beetle assemblages from sites of human occupation often consist of a mix of fossils derived from several different habitats, or are dominated by species that are not restricted to very specific niches (Kenward & Carrott, 2006). Also, while most assemblages from occupation sites contain a large proportion of insect remains that originated from near the point of deposition, they often also contain an element of '**background**' fauna composed of insects that have flown to the site, or that have been derived from the regurgitated pellets or faeces of birds and other animals. Because of the complexities of insect death assemblages in archaeological contexts, therefore, large samples (over fifty species) should be analysed, in order that the full species diversity is adequately represented and that the background component can be isolated. A further difficulty arises, however, where people have created a range of wholly artificial environments, for ecological changes may have occurred in certain insect species as they adapt to these new biotopes (Anderson, 2000). Many natural and artificial environments, while being very different in terms of

macro-environment, may contain microclimatic niches that are very similar, and in some cases identical. Moreover, it would be expected that, in those insects that are markedly synanthropic, such as the grain weevil (*Sitophilus granarius*), slight physiological changes may have occurred to adapt to these artificial habitats. Although in most cases the general archaeological interpretation will not be affected, care clearly needs to be exercised in the palaeo-ecological inferences that are drawn from entomological records from archaeological sites based upon the known ecological affinities of modern insect species.

Recent technological developments may help to resolve some of these problems, and may also shed new light on past human activities. An important advance has been in the extraction of DNA preserved in fossil beetle material as, for example, from exoskeletal fragments of *Sitophilus granarius* discovered in deposits of Roman and Medieval age (King *et al.*, 2009b). Although DNA in beetle remains is susceptible to contamination and requires relatively large specimens for analysis (Reiss, 2006), this approach may provide important new insights into the ways in which beetles have developed adaptational traits in response to human influences. A second potentially important development for archaeology is the analysis of isotopic fractionation within subfossil beetle chitin, as this enables inferences to be made about past farming practices, such as transhumance, or changes in the types of herds or crops managed by humans during different archaeological periods (King, 2012).

4.5.5 Chironomidae

Chironomidae are non-biting midges, a family of the Diptera (true flies), and their species abundance and composition are related to such factors as pH, salinity, water depth, temperature, oxygen concentration and trophic status (e.g. Porinchu & MacDonald, 2003). This makes them potentially valuable for Quaternary palaeoenvironmental reconstruction, although it is their use as palaeotemperature indicators that has attracted the greatest interest (Brooks, 2006).

Chironomidae produce larvae in the bottom of almost all freshwater habitats, and these eventually develop into mature forms that consist of a robust, strongly sclerotized head capsule made of chitin (Figure 4.29) and a body that resembles a maggot. The final, adult stage is mosquito-like but lacks a proboscis and a biting habit. It is the head capsules of the larval stage that are often abundant and well preserved in freshwater sediments. Most genera possess head capsules with diagnostic forms, structures or surface markings that enable them to be identified, using both type

material and keys (e.g. Brooks *et al.*, 2007b). Chironomid head capsules can be separated from most sediment matrices by procedures that include deflocculation in KOH (or, for calcareous deposits, HCl), the use of a sonic bath, and removal of fine sediment by sieving (Lang *et al.*, 2003). Kerosene flotation, used to extract beetle remains, also works well with chironomid head capsules (Rolland & Larocque, 2007). After concentrating the head capsules,

they can be picked individually using forceps under low-power magnification and mounted on slides in a suitable medium, commonly Euparal or Hydromatrix (Brooks *et al.*, 2007b).

A number of studies have demonstrated a close relationship between summer air and lake surface water temperatures and the distribution of chironomid species in arctic, subarctic, temperate and tropical zones of both

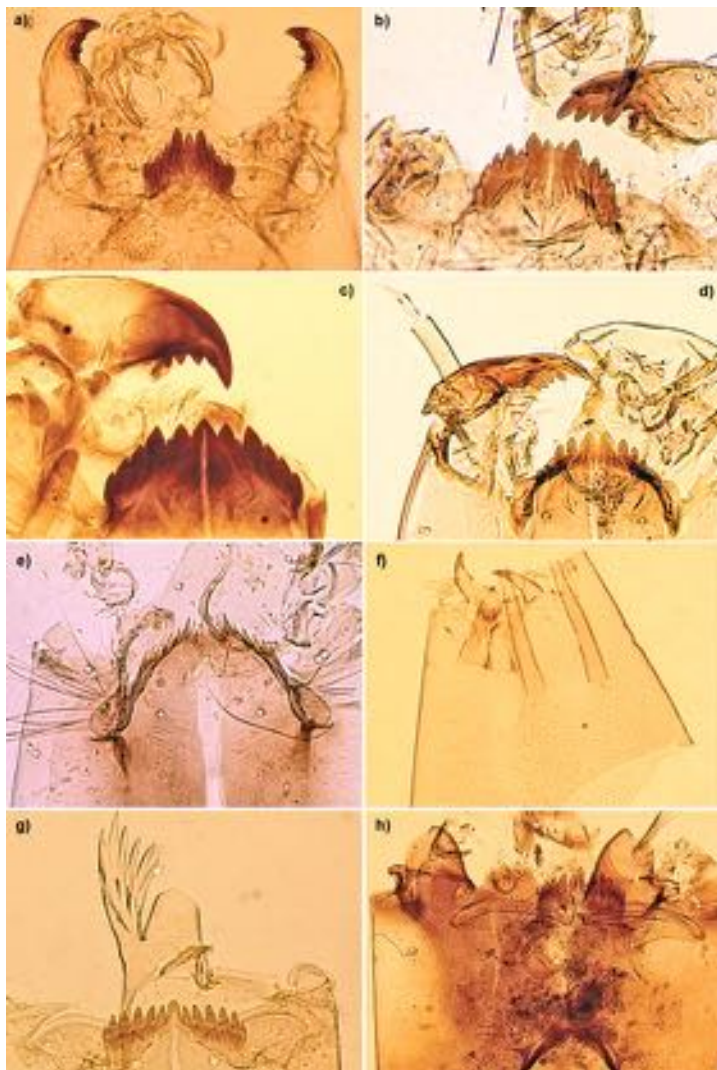


Figure 4.29 Head capsules of common chironomid taxa recovered from late Quaternary lake sediment sequences from northwest Europe: a) *Glyptotendipes severini*-type (tribe Chironomini); b) *Phaenopsectra flavipes*-type (tribe Chironomini); c) *Cricotopus obnixus*-type (Orthocladiinae); d) *Heterotriassocladus grimshawi*-type (Orthocladiinae); e) *Prodiamesa olivacea*-type (Prodiamesinae); f) *Guttipelopia* (Tanytarsinidae); g) *Stempellina* (Tanytarsini); h) *Micropsectra radialis*-type (Tanytarsini) (images provided by Steve Brooks, Natural History Museum, London).

hemispheres (Eggermont & Heiri, 2012). Calibration datasets have been generated that measure the strength of the relationship between *predicted* (i.e. chironomid-inferred, mainly using weighted-average regression methods) and *measured* summer surface water temperatures. Research was initially concentrated in Europe (e.g. Heiri *et al.*, 2011) and North America (e.g. Porinchu *et al.*, 2009), but has subsequently been extended to Africa, Australia, New Zealand and South America (Verschuren & Eggermont, 2006; Vandergoes *et al.*, 2008). Some studies have also shown a close relationship between chironomid-

inferred and instrumental temperature measurements, which suggests that chironomids could provide useful proxy climate data over the course of recent centuries (Larocque & Hall, 2003).

Interest in the palaeoclimatic potential of chironomid stratigraphy has grown considerably over the past ten to fifteen years, principally because this approach offers two important advantages over other methods of Quaternary palaeotemperature reconstruction. First, many hundreds of head capsules can be obtained from as little as 1 cm³ of sediment. This should enable a higher-resolution record

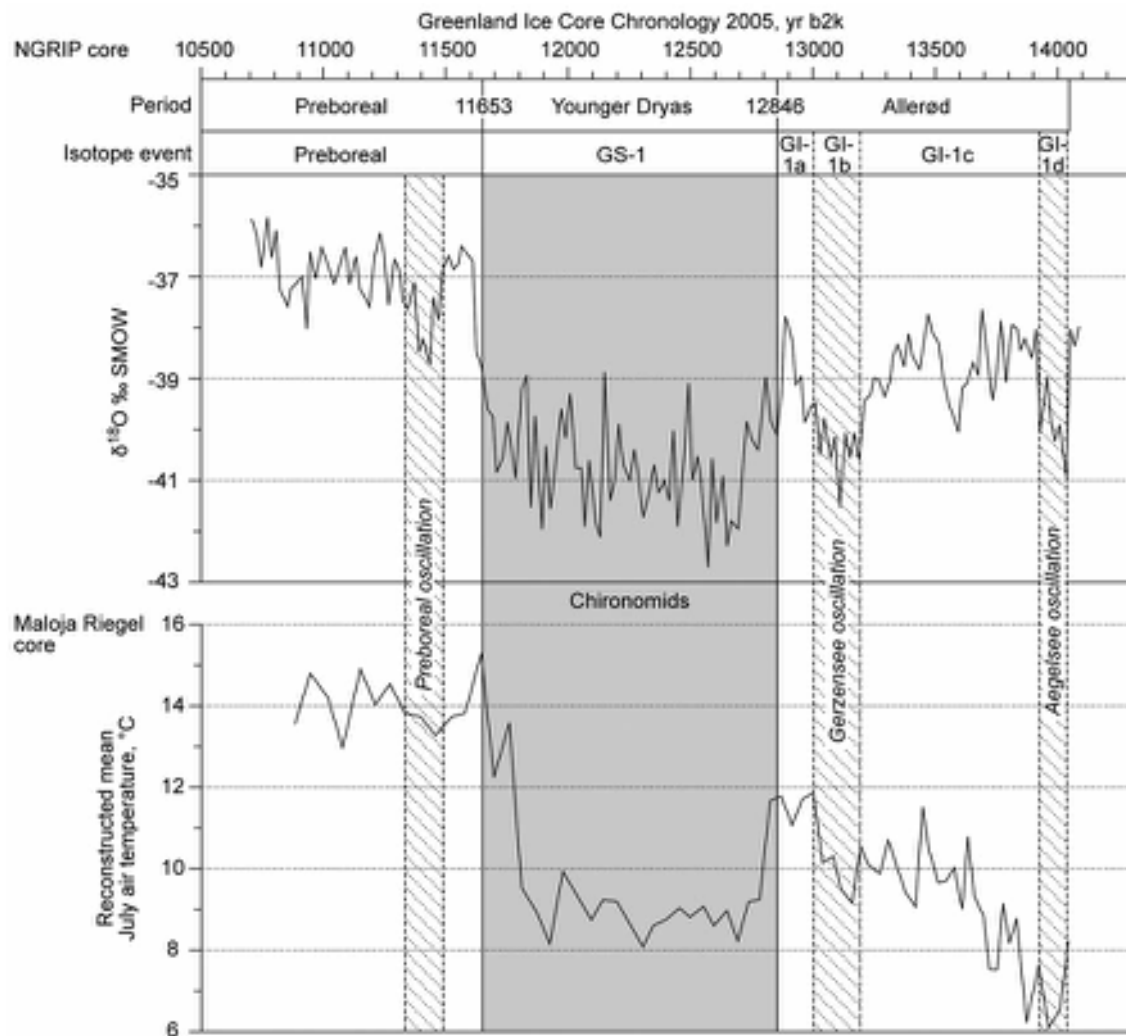


Figure 4.30 Chironomid-inferred temperature variations for the Lateglacial sequence from a former lake near the Majola Pass in the Swiss Alps, compared with the NGRIP oxygen isotope record and climatic event sequence (from Ilyashuk *et al.*, 2009).

than is possible using other proxies, such as fossil Coleoptera, where far larger samples of sediment are required. This is particularly well illustrated in chironomid-inferred temperature reconstructions for the Lateglacial period, which enable detailed comparisons to be made with Greenland ice-core records (Figure 4.30). Second, the method enables summer water-surface temperatures of small lakes to be inferred, providing valuable microclimatic information which can be compared with independently derived ambient air or ground temperature estimates. In some Lateglacial records, for example, the chironomid data suggest a steady increase in temperatures over intervals for which pollen and other proxies suggest the opposite. This is thought to reflect different forcing factors within the overall climatic environment, with the midges responding exclusively to summer season conditions, while land plants were more sensitive to changes in seasonality or to variations in annual precipitation (Lotter *et al.*, 2012). Chironomids therefore have much to offer in palaeoclimatic reconstructions, a potential that may be further enhanced by the discovery that $\delta^{18}\text{O}$ abundance in head capsules may also be temperature-dependant (e.g. Wooller *et al.*, 2004).

While the palaeoclimatic applications of chironomid analysis have attracted most attention, the technique is proving to be useful in other areas of Quaternary research. In archaeological investigations, for example, chironomid assemblages have enabled changes in lake levels resulting from the construction of dwellings or drainage channels

to be inferred (Ruiz *et al.*, 2006). Elsewhere, they have provided evidence of changes in lake productivity or degree of eutrophication (Brodersen & Quinlan, 2006), of flow regime within fluvial palaeochannels (Howard *et al.*, 2010), and of palaeosalinity variations and hence changes in sea level (Heinrichs & Walker, 2006).

4.6 NON-MARINE MOLLUSCA

4.6.1 Introduction

Mollusc shells are some of the most common fossil remains in terrestrial Quaternary sediments (Figure 4.31) and consequently they have a long history of investigation. As in other branches of palaeontology, much of the early work in the eighteenth and nineteenth centuries was concerned with taxonomy and, by comparison, little consideration was given to the palaeoecology of molluscan assemblages. In the late nineteenth and twentieth centuries, however, workers in Britain such as Alfred Kennard, Bernard Woodward and Frederick Harmer began to utilize molluscs as palaeoclimatic indicators, and also as a means of dating geological events (Keen, 2001). The increasing use of pollen analysis as a palaeoenvironmental technique led to a gradual decline in interest in molluscan studies in the period before and after the Second World War, and the modern phase of molluscan investigations did not begin until the 1950s with the first quantitative analyses of shell-bearing deposits (Miller & Tevesz, 2001). This approach,

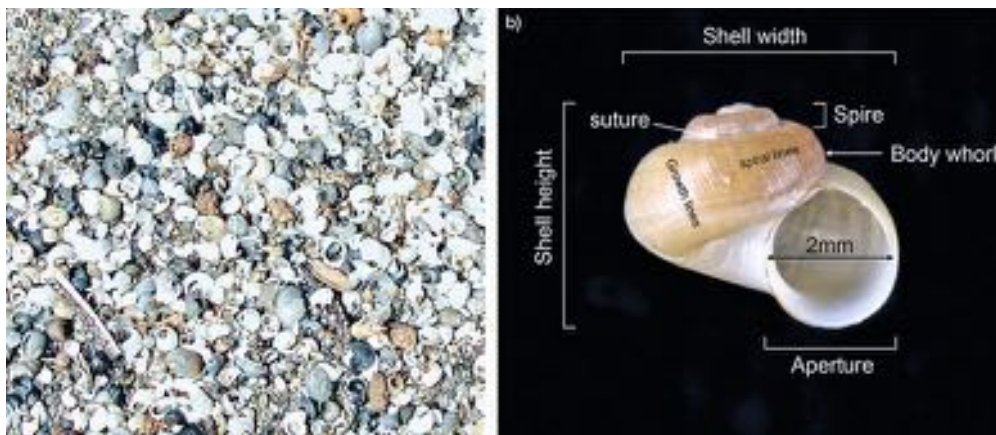


Figure 4.31 a) Fossil shells of freshwater molluscs (principally gastropods) exposed on an abandoned beach of Pluvial Lake Lahontan (section 2.7.1) on the eastern side of Pyramid Lake, Nevada, USA (photograph by Allan Ashworth, North Dakota State University, USA). b) *Valvata piscinalis*, a small gastropod (up to 5 mm height and width) that inhabits streams, rivers and lakes, preferring running water and tolerant of low calcium levels. Such small specimens can be readily identified, when magnified, by examination of morphological and ornamental details, some of which are illustrated (photograph by Jenni Sherriff, Royal Holloway, University of London, UK).

developed initially for the investigation of non-marine Mollusca, has since been applied to the study of marine shells (section 4.7) and, over the last thirty years or so, has produced a considerable body of data on local environmental and climatic changes during the Quaternary. More recently, however, attention has also turned to other palaeoenvironmental aspects of molluscan studies, such as shell morphology and colour-banding on the shells of certain species, stable isotopic composition of shell organic matter and shell carbonate, and processes of amino-acid diagenesis (Ellis *et al.*, 1996; Rousseau, 2001).

Mollusca possess a number of advantages over other terrestrial and freshwater fossil groups that have been used in the reconstruction of Quaternary environments. First, specimens can nearly always be identified to species level and therefore more secure palaeoenvironmental conclusions can be drawn. Second, fossil shells are often present in oxidized sediments, such as slope-washes, loess or tufa, in which other fossil remains, such as pollen or Coleoptera, are either absent or poorly preserved. Third, many specimens are large enough to be identified in the field (Cameron, 2003; Sturm *et al.*, 2006) and hence a good idea of the general palaeoecological context of each mollusc can generally be gained. This may help to determine where samples should be taken for other fossil groups. Fourth, much is known about their present-day ecology and geographical distributions (Dillon, 2000; Barker, 2001) and, since molluscs are frequently sensitive to changes in the physical or chemical environment (Horsák, 2005), they provide useful insights into past changes in both the local and regional environment.

4.6.2 The nature and distribution of molluscs

Molluscs are invertebrates in which the soft parts of the body are generally enclosed within a hard shell or exoskeleton composed of calcium carbonate bound by proteins. They have a wide range of morphological characteristics, many of which are shared between marine and continental species. The two principal classes as far as the Quaternary palaeoecologist is concerned, however, are the **Gastropoda** (snails) or **univalves**, which usually possess a single spiral or conical shell (although in the case of the slugs the shell is reduced to an internal remnant), and the **Bivalvia** (mussels and clams), in which the animal possesses two hinged valves. Other classes include the **Polyplacophora** (commonly known as chitons, sea cradles or ‘coat-of-mail’ shells), **Scaphopoda** (tusk-shells) and the Cephalopoda. The last-named are the most highly organized of the Mollusca and range from *Nautilus*, which has a

large calcareous, external, coiled shell, through the squids, which have only a thin horny vestige of a shell embedded in the mantle, to the octopuses which have no shell. Some gastropods breathe by gills (**prosobranchs**) and are mainly aquatic, while others such as snails and slugs breathe by a rudimentary lung (**pulmonates**) and, although they can live in water, are primarily terrestrial in habitat. The crystalline form of calcium carbonate in the shells of most molluscs is pure aragonite, although the internal shells of certain slugs are composed of calcite. In both cases, the shells are subject to little change in either their crystalline or their chemical composition following the death of the organism, frequently retaining residues of the organic compounds bound within the carbonate matrix, and are therefore sometimes referred to as **subfossil** rather than fossil.

Land and freshwater Mollusca are extremely useful palaeoecological tools because of their wide distribution and preservation in a variety of deposits. They show a marked preference for habitats that contain sufficient lime for building their shells, although they are found not only in chalk and limestone regions, but also in calcareous drifts, in colluvial deposits, in cave earths, in loess, on coastal dunes and beaches, and in estuarine muds. Molluscs do occur in non-calcareous environments, for some species are strongly calcifuge and are found only in non-calcareous regions (e.g. *Zonitoides excavatus*, which lives in acid litter of birch or alder). In such cases, however, the number of species is more restricted, shells are often thinner and less well preserved, and weathering and leaching in acid environments are more likely to lead to shell dissolution. In general, the richer the base status of the locality, whether it be land or freshwater, the richer the fauna, and molluscan remains would be expected to be discovered in a wide range of river, marsh, lake, woodland and open-land sediments (Miller & Tevesz, 2001; Sturm *et al.*, 2006). Terrestrial molluscs are also found in a variety of archaeological deposits including soils, ditch, pit and well sediments, ploughwash and other colluvial deposits, and occupation horizons and building debris (Allen *et al.*, 2009).

4.6.3 Field and laboratory work

Although molluscan remains can be collected from open sections in the field by hand, they are best extracted under laboratory conditions because hand-picking of individual shells will bias the resulting samples towards the larger species (Kidwell, 2002). Bulk samples from sections or from cores are air dried and immersed in water, a small quantity of a dispersive agent such as H_2O_2 or NaOH being added if there is organic material present. The froth, which includes the snails, is then decanted through a 0.5 mm

sieve. The process is repeated several times until no more snails are present in the froth and the residual slurry is then poured into a second 0.5 mm sieve. Both sieves are dried and the residues passed through another set of sieves (1 mm, 710 µm, 2,411 µm) for ease of sorting. Molluscan remains can be either removed by hand or with the aid of a moistened brush under a low-powered binocular microscope or scanner. Identifications are always based on type collections of modern shell material aided by the numerous molluscan reference works that are now available (e.g. Kerney, 1999; Perez *et al.*, 2008). In many respects, identification of molluscan remains is not as difficult as in other branches of palaeontology. This is particularly true of land and freshwater molluscs, for which not only is there an extensive taxonomic literature but also, in Britain at least, the total number of species (both living and extinct) in late Quaternary assemblages does not

exceed 200 (cf. the 3,800 or more species of Coleoptera). Nevertheless, identifications can be complicated by the fact that many mollusc species vary markedly in morphology and in markings from juvenile to adult stage, while both colouring and fine sculpture can be affected by local site condition. Some fossils may also be damaged by mechanical abrasion, some can have their surface markings masked by carbonate overgrowths, while others, particularly the fragile specimens, may be highly comminuted. In certain cases, specialized techniques allow even small fragments to be identified. For example, the marine genera *Mytilus*, *Modiolus* and *Pinna* have shells which possess a characteristic crystal structure that can be recognized with a high-powered microscope. Similarly, differences in shell microsculpture are often diagnostic of land Mollusca, so that specific determination of fragmentary remains can be made using a light microscope,

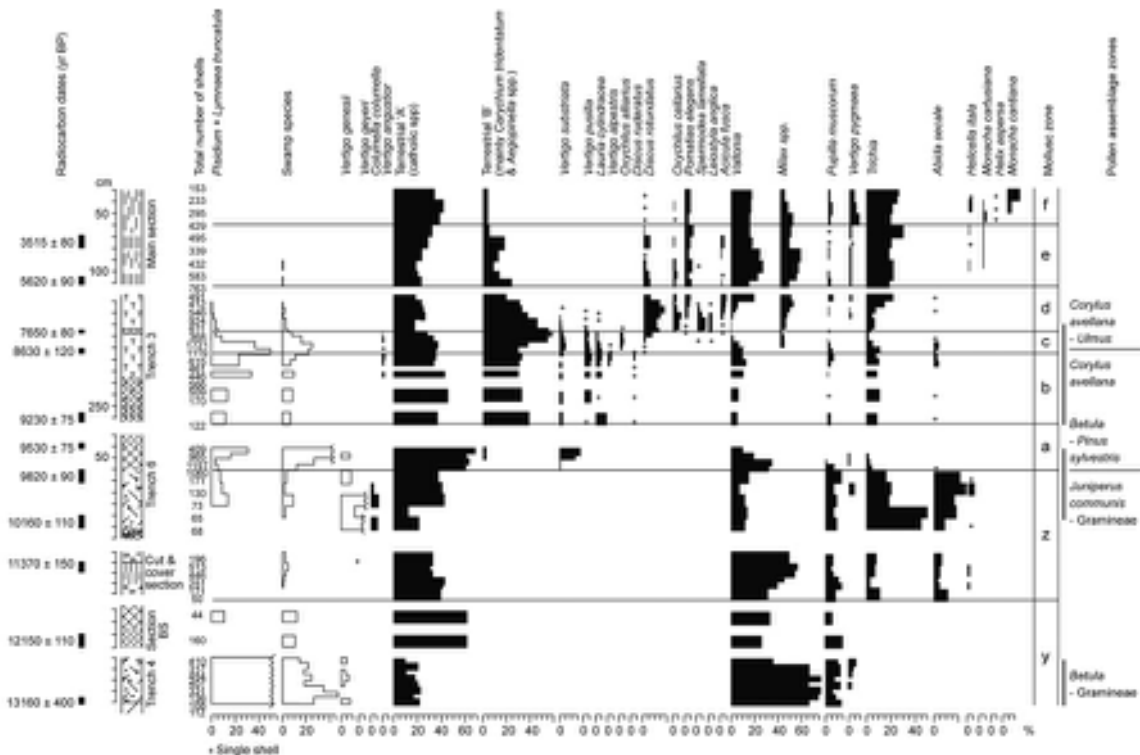


Figure 4.32 Variations in relative abundance of molluscan species from the Lateglacial to mid-Holocene sequence at Holywell Coombe, southern England. Several taxa have been combined to produce Terrestrial Group A ('catholic' species, of wide environmental tolerance, mainly open ground), and Terrestrial Group B (more narrow in environmental tolerance, mainly deciduous woodland). Note how Group B taxa expand in molluscan zone b, which coincides with woodland expansion (*Corylus avellana*) as reflected in the pollen record (right) (from Preece & Bridgland, 1999).

augmented by the use of scanning electron photomicrographs (Karney *et al.*, 2011).

The results of molluscan analyses can be presented in a variety of ways. Early studies tended to employ species lists, perhaps using symbols to depict the frequency of occurrence (+ = presence; * = common; 0 = abundant, etc.). Nowadays the data are more usually depicted graphically, either in histogram form for single samples or, where a sequence of sediments is being investigated, on a diagram which has the vertical axis for depth in the sequence and the horizontal axis for the number of species plotted. The results can be presented in terms of relative abundance (Figure 4.32) or absolute numbers (Figure 4.33), in both cases the histogram bars showing the depth below ground datum or a timescale, and being drawn proportional to the thickness of the sampled horizons. Once constructed, the diagram can be divided into **molluscan assemblage zones** (Figure 4.32) which allow further palaeoecological or biostratigraphical inferences to be made. These zones will initially be of local significance only, but may be extended (as in pollen analysis) to form a zonation scheme that has regional applicability, implying an orderly immigration sequence of molluscan species within the region (Meyrick & Preece, 2001; Meyrick & Karrow, 2007).

4.6.4 Taphonomy of non-marine molluscan assemblages

The interpretation of molluscan assemblages can be complicated by a number of taphonomic problems that should be taken into account before palaeoenvironmental reconstructions are attempted. Species bias in fossil snail assemblages has long been recognized, for example by marked differences between the characteristic assemblages found in modern river flood plains compared with those associated with older, abandoned flood plains (river terraces); these differences are likely to reflect the combined effects of selective transportation, burial and preservation (Briggs *et al.*, 1990). Species with fragile shells are generally under-represented in subfossil assemblages, for example in shell middens, primarily due to the action of predatory animals such as birds (Carter, 1990). Although abundant and well-preserved molluscan remains are often found in caves where an equable microclimate (temperature and humidity) is maintained and greater protection from erosion and weathering is afforded, the taphonomy of cave molluscan assemblages is still not well understood. The assemblages are frequently diverse, with material being derived from the litter and vegetation that accumulate

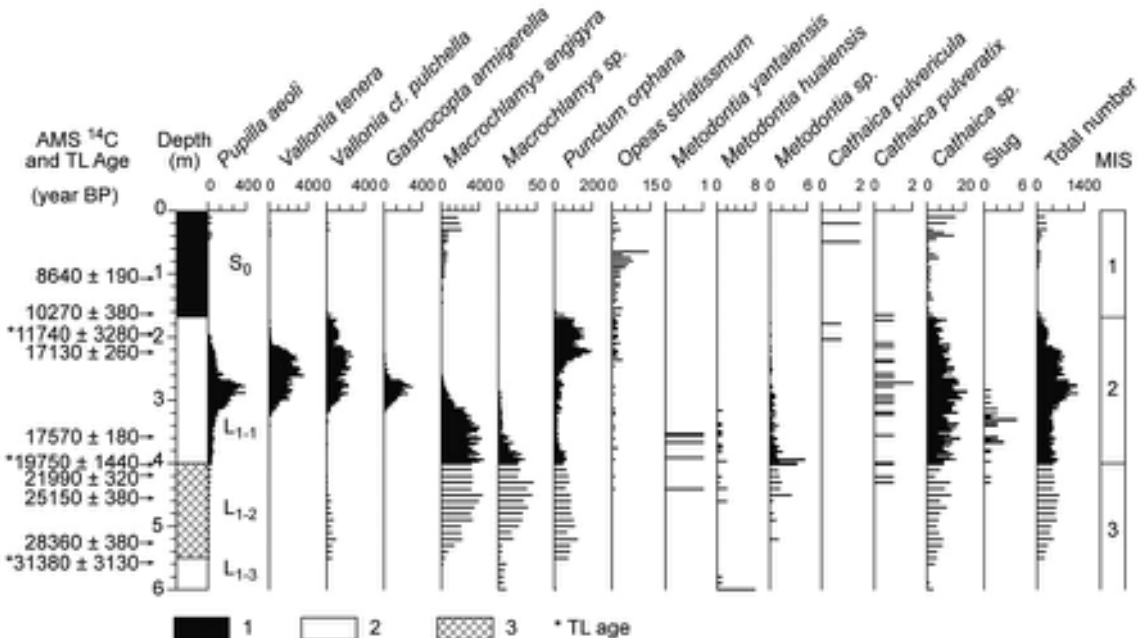


Figure 4.33 Variations in absolute abundance (number of individuals per 15 kg of sediment) of terrestrial molluscan species through a Late Quaternary loess and palaeosol succession at Weinan, China. Note that species abundance and diversity are dependent on weathering intensity (pedogenic alteration). 1: Holocene soil; 2: Loess; 3: Weakly-weathered soil (from Wu *et al.*, 2002).

close to the cave mouth, from the action of scavenger animals that inhabited the cave, from washing in of specimens either from surface soils through fissures, or from rock faces, and from the dropping of shells into cave fissures by birds (Hunt, 1993).

These various taphonomic problems have led, in recent years, to the increasing application of quantitative taphonomic studies that test the degree of compatibility, or ‘**fidelity**’, between life, death and fossil molluscan assemblages. Results have shown a relatively close correspondence between life and death assemblages in a range of sedimentary environments, for example in calcareous soils (Yanes *et al.*, 2011) and in stream and lake deposits (Cummins, 1994; Tietze & De Francesco, 2012), although in estuarine sediments, death assemblages may contain large amounts of reworked material (De Francesco & Hassan, 2008). Much greater differences are to be found, however, between life and death assemblages on the one hand, and ancient (subfossil) assemblages on the other. The principal reasons for this appear to be post-burial taphonomic processes, including weathering, fragmentation of shell material, chemical decomposition and carbonate secretions,

while the transfer and subsequent spread of ‘alien’ species by humans when colonizing new areas is a problem that particularly affects the interpretation of Holocene records (Erthal *et al.*, 2011).

4.6.5 Interpretation of non-marine molluscan assemblages: habitat groups and indices of species diversity

Terrestrial Mollusca can be classified in a number of ways that allow inferences to be made about former local habitats and environmental change. One approach is to divide modern species into groups according to their common habitat preferences. The most widely recognized subdivisions include a ‘**catholic**’ group (species tolerant of a wide range of habitats), an **aquatic** group (species associated with standing or running water, such as ditches, pools and streams), **marsh or ‘swamp’** species, **open ground** species (intolerant of shade), and **shade-tolerant** species, i.e. those normally associated with woodland. The last group can be further subdivided according to their preferences for light, medium or heavy shade. Figures 4.32 and 4.34

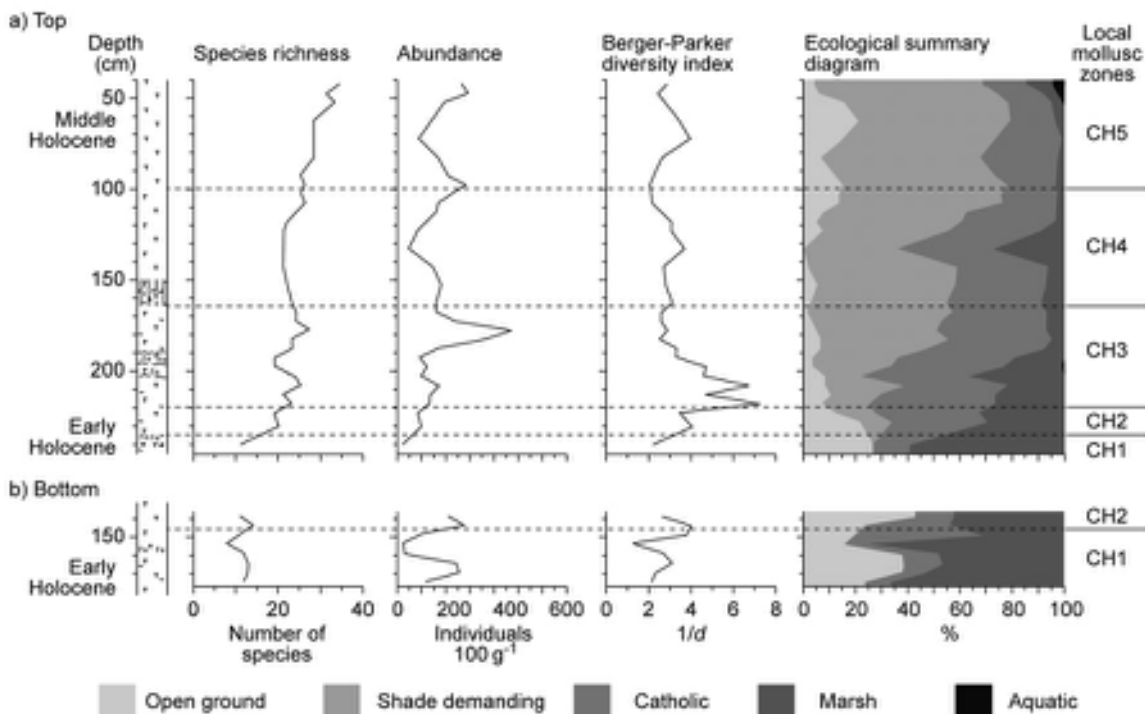


Figure 4.34 Variations in species richness, abundance, diversity and habitat types in Holocene tufa sequences at Courteenhall, near Northampton, UK (from Meyrick & Preece, 2001). For explanation see text.

(right-hand column) show how this type of classification enables temporal trends in the dominant groups in a molluscan record to be identified, and corresponding local and regional environmental changes to be inferred. The habitat data summarized in Figure 4.34, for example, show a decline in open-ground taxa in biozones CH1 to CH3 during the early Holocene, and a gradual increase in shade-tolerant species through CH3 to CH5, culminating in the mid-Holocene with a predominance of species tolerant of heavy woodland cover (Meyrick & Preece, 2001).

Non-marine molluscan populations have also been classified into groups on the basis of the overall diversity of the fossil assemblage, and various indices are used to reflect this diversity. Some of these are shown in Figure 4.34. They include **species richness** (a count of the number of different species represented in a sample) and **abundance** (the number of **individuals** recovered from a unit weight or volume of sample: in Figure 4.34, the number per 100 g of sample). **Species diversity** is also an important indicator, for it shows the relative abundance of each species represented in the assemblage. Two such indices that are commonly used are the **Berger–Parker index (BPI)** and the **Shannon diversity index (SDI)**. The former is a measure of species dominance (d), and reflects the proportional abundance of the most common species in the assemblage; the inverse of this measure ($1/d$) gives an indication of relative diversity. Hence an increase in $1/d$ indicates an increase in diversity and reduction in dominance by a few species. In Figure 4.34, for example, species richness generally increased throughout the Holocene, the greatest abundance and diversity of species occurring in zone CH3, during the transition from open ground to woodland. The **SDI** also measures the degree to which faunal assemblages are dominated by a small number of species, and shows the degree of evenness or equitability of species in an assemblage on a scale of 0 (dominated by one species) to 1 (even representation of several species). The SDI has been widely used in modern ecological studies to reveal how molluscan species richness and diversity vary systematically with environmental variables, for example with altitude (Aubry *et al.*, 2005) or regional rainfall patterns (Tattersfield *et al.*, 2001). Application of this index to molluscan assemblages in loess sequences has revealed how their diversity co-varies with changes in rates of loess accumulation, presumably because an increase in dust flux reduces the range of mollusc species able to survive (Rousseau, 2001; Rossignol *et al.*, 2004). In a sediment record from the coastal plain of Tuscany, Italy, the SDI was used to discriminate between fully marine, lagoonal and alluvial faunal assemblages (molluscs and Foraminifera), and

thereby to reconstruct the history of local sea-level change between MIS 4 and MIS 2 (Carboni *et al.*, 2010).

4.6.6 Applications of Quaternary non-marine molluscan records

4.6.6.1 Biostratigraphic correlation

It has long been recognized that molluscan assemblages offer a basis for relative dating and correlation, because the species composition of the assemblages changes over time, while certain species are confined to discrete intervals, and hence constitute *range fossils* (see section 6.2.3.2). The development of regional molluscan ‘biozonation’ schemes, for example, has proved particularly useful for correlating loess units and sequences, such as the Peoria Loess in North America, within which molluscan remains are particularly abundant and well preserved (Rousseau, 2001). In the British Isles, some interglacial deposits of different age can be discriminated by virtue of diagnostic molluscan assemblages (Keen, 2001; Preece, 2001). In part, this reflects climatic influences, for certain thermophilous taxa, such as the gastropod *Belgrandia marginata* (Michaud) and the freshwater mussel *Unio crassus* (Philipsson), could only survive in Britain during periods slightly warmer than the present interglacial (Candy *et al.*, 2010). A second important control was the periodic isolation of the British Isles as a result of sea-level rise: the mix of molluscan species able to migrate from the continent during transitions between cold glacial and warm stages depended on the time it took for rising sea levels to flood the English Channel and form an effective barrier to migration (Meijer & Preece, 1995). Insofar as some interglacials can be recognized by different combinations of non-marine molluscan species, this therefore provides a basis for correlation (Bridgland *et al.*, 2004; Schreve & Candy, 2010). Interglacial deposits on the European continent, however, tend to show less marked differences in molluscan species because there were fewer effective barriers to migration, although there is one notable exception. A distinctive assemblage found in the Somme and Seine Valleys of northern France, and that dates to the Middle Pleistocene, is characterized by the presence of shells of a small extinct land snail of the genus *Retinella* (*Lyrodiscus*) and by the remains of several species found well beyond their modern ranges. This marker bio-assemblage, locally termed the ‘*Lyrodiscus* biome’, is thought to correlate with the Hoxnian Interglacial molluscan assemblages of the British Isles, and provides a unique basis for linking British and western European sequences (Limondin-Lozouet & Antoine, 2006).

4.6.6.2 Palaeoclimatic reconstructions

Many palaeoclimatic reconstructions from molluscan records have been based on the indicator species approach. Candy *et al.* (2010) employed this methodology to identify interglacial episodes in Britain that were warmer than present, while Wu *et al.* (2002) also used variations in the abundance of selected molluscan indicator species (both warm- and cold-adapted) to reconstruct the climatic history of part of the Loess Plateau, China, during the MIS 12 to MIS 10 interval. In southern Siberia, Horsák *et al.* (2010) identified eight 'index species' for extreme cold (*Columella columella*, *Pupilla alpicola*, *P. loessica*, *Vallonia tenuilabris*, *Vertigo genesisii*, *V. parcedentata* and *V. pseudosubstriata*), and concluded that these indicator molluscs would indicate 'full glacial' conditions in other parts of Eurasia during the Pleistocene.

Other palaeoclimatic reconstructions have been based on the statistical analysis of the range of species recorded in molluscan assemblages. For example, a transfer function derived from a modern calibration or training dataset suggests that contemporary non-marine molluscan assemblages reflect two main climatic influences, a temperature gradient and a moisture gradient, and that these can be determined from characteristic groupings of species (Rousseau *et al.*, 1993). Using this approach, temperature and moisture variations in Burgundy, eastern France, during the Holocene have been reconstructed from fossil molluscan assemblages, the data showing a two-step warming at the beginning of the Holocene, which is similar to that inferred from oceanic evidence (Rousseau *et al.*, 1994). The mutual climatic range method (section 4.5.4.2) has also been applied to fossil molluscan records, although the resulting temperature estimates often tend to have relatively large uncertainties (Moine *et al.*, 2002). This may be due, in part, to the fact that climate is only one of a number of variables that affects molluscan distribution, and that the climatic influence may be difficult to isolate from other factors, such as vegetation cover or soil chemistry, which may be more important especially at the local scale (Horsák, 2011). A further problem is that modern molluscan distributions may not provide reliable analogues for fossil assemblages because of the degradation of their natural habitats over recent millennia by human activity, most notably through woodland clearance, drainage alteration and farming practices (Kiss *et al.*, 2004, and see below).

In recent years, stable isotope ratios in molluscan shells have increasingly been used to infer past environmental and climatic conditions. Studies of modern shells have shown that carbon isotope ratios are largely determined

by diet (as opposed to climate) and in some areas reflect variations in the proportions of C3, C4 and CAM plants in the local vegetation. Oxygen isotope ratios, on the other hand, appear to be governed by climate, and hence offer a basis for palaeoclimatic reconstruction. For example, regional variations in the $\delta^{18}\text{O}/\delta^{16}\text{O}$ ratio of modern land snails closely accords with regional isotopic trends in meteoric water (Kehrwald *et al.*, 2010), and hence variations in $\delta^{18}\text{O}$ in fossil shells provide insights into long-term changes in precipitation source and/or amount. Oxygen isotope data from mollusc shells has been used to reconstruct, *inter alia*, shifts in the northern margin of the African summer monsoon in Sudan during the Holocene (Abell & Hoelzmann, 2000), an episode of increased humidity and cooler temperatures in New Mexico, USA, at the end of the last cold stage (Balakrishnan *et al.*, 2005), and the history of drought phases in central Mexico between 40 and 8 ka (Stevens *et al.*, 2012). In some instances it has proved possible to obtain palaeoclimatic data from single mollusc shells. For example, high-resolution measurement of $\delta^{18}\text{O}$ variations along the growth axis of a land snail shell from Ethiopia revealed a cyclic periodicity that may reflect seasonal changes in rainfall, temperature and evaporation (Leng *et al.*, 1998). If these inferences are correct, it shows that palaeoclimatic records at annual or even seasonal resolution can be generated from freshwater molluscs, as has also proved to be the case with marine mollusc shells (see Figure 4.37).

4.6.6.3 Archaeological relevance

Both land and freshwater snails have also proved valuable in archaeological investigations, allowing inferences to be made about the environmental contexts of former occupation sites (Preece *et al.*, 2006), about human-induced vegetation changes (see Figures 4.32 and 4.34) and about agricultural activities and associated erosional effects (Davies, 2008). In this respect, non-marine Mollusca have proved to be particularly useful in chalkland areas where the archaeological evidence is often abundant, but where there is little scope for pollen analysis due to the general absence of peats or limnic sediments (Davies & Griffiths, 2005). Mollusc shells are also important indicators of foraging practices, ornamental craftwork and trading operations: although most usually associated with marine species (see section 4.7.4), land snails have also featured in these prehistoric activities (Stiner, 1999). Over the course of the late Quaternary, and especially during the late Holocene, the impacts of humans on non-marine molluscan populations has been considerable. These include 'alien' introductions, either deliberate or accidental, of species

not endemic in areas to which humans have migrated, and which have often led to ecological destabilization and the favouring of synanthropic species, a process that has extended to even the remotest of islands (Ó Foighil *et al.*, 2011). In addition, progressive alteration and loss of natural habitats has led to a general reduction in species diversity, with many now in danger of extinction (Lydeard *et al.*, 2004; Cuttelod *et al.*, 2011).

4.7 MARINE MOLLUSCA

4.7.1 Introduction

The shells of marine Mollusca have been found in a range of deposits in coastal areas. They often occur in beach gravels, sands and estuarine clays now lying some distance above or below sea level, having been isostatically raised following uplift of areas formerly glaciated or submerged by rising sea levels, and dating of these marine fossils provides a chronology of sea-level change and deglaciation (Dyke *et al.*, 1996; Pedoja *et al.*, 2011; section 2.5). Molluscan assemblages have been recovered from boreholes both onshore and from the seabed, while shell remains, often highly fragmented, are found at localities inland, having been stripped from a former seabed and transported to their present position by glacier ice (England *et al.*, 2000). Although perhaps less widely used in Quaternary studies than their freshwater counterparts, marine Mollusca are nonetheless an important additional source of palaeoenvironmental information. Indeed, the Pleistocene epoch was originally defined on the basis of the composition of marine molluscan faunas.

Marine molluscs occupy a great range of ecological niches from pools and rock outcrops in the intertidal zone to the deeper waters off the edge of the continental shelf, although they are seldom found at depths greater than 1 km. The mode of life of marine molluscs varies considerably, but many taxa are **infaunal**, burrowing with a muscular foot into soft sediments (e.g. *Turritella*, *Mya*, *Macoma*, *Arctica*, *Nucula*) or boring into bedrock (*Hiatella*, *Zirfaea*). Others are **epifaunal**, attaching themselves by threads to surfaces or other organisms (*Mytilus*, *Modiolus*) or by cementing one valve to the surface (*Ostrea edulis*). Only a few bivalves are free-swimming (e.g. *Chlamys*) while some species (mainly pectinids, or scallops) are unattached and are recumbent on the sea bed (Saxena, 2005). The gastropods, scaphopods and bivalves are principally benthic and sedentary in life and, upon death of the individual, often become fossilized *in situ* to form autochthonous death assemblages. Marine Mollusca are often well preserved in Quaternary sediments (Figure 4.35),

although those from the intertidal zone may be fragmented by wave action.

4.7.2 Analysis of marine molluscan assemblages

Approaches to the analysis of marine molluscan assemblages are essentially the same as those employed in the study of terrestrial and freshwater forms. Marine molluscs are affected by a number of environmental factors, such as substrate, food supply, temperature, salinity, oxygen level, nutrient availability, 'depth' (which affects, in combination,

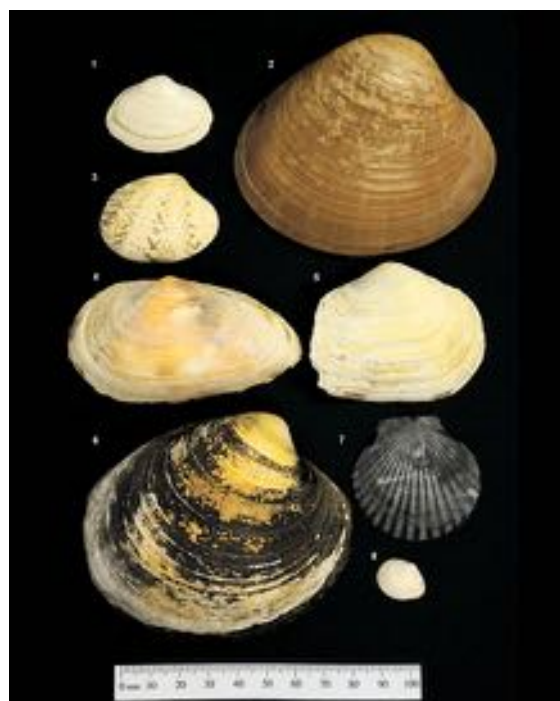


Figure 4.35 Examples of some common marine bivalves of the North Atlantic and their water depth preferences. 1. *Spisula elliptica* – open water, on various substrates, to 100 m depth. 2. *Callista chione* – continental shelf to 200 m depth. 3. *Tapes decussatus* – lower shore and shallow sublittoral. 4. *Mya arenaria* – inter-tidal mudflats. 5. *Mya truncata* – widely distributed on sandy substrates to 70 m depth. 6. *Arctica islandica* – widespread on muddy sand substrates from very shallow tidal to (exceptionally) 200 m depth; noted for its longevity. 7. *Aequipecten opercularis* – typically found on hard surfaces in depths of 20–45 m in shallow subtidal areas, but can extend to 180 m depth. 8. *Macoma balthica* – open sea in inter-tidal zone, and to 100 m depth in the brackish Baltic Sea (photographs by David Roberts and James Scourse, School of Ocean Sciences, Bangor University, UK).

food supply, habitat, shelter, light, temperature and degree of turbulence), competition, predation and life strategy. The main controls over their distribution and abundance, however, are current flux and water temperature (Hiscock *et al.*, 2004). As a result, marine fauna can be grouped into distinct **zoogeographical provinces**, the boundaries of which are determined by marked temperature gradients that are, in turn, influenced by major ocean currents and gyres (Spalding *et al.*, 2007). The latter not only regulate water temperature, but also affect nutrient supply as well as the dispersal of larval stages. Within the Northeast Atlantic and adjacent seas, for example, modern and fossil molluscan assemblages can be categorized on the basis of their thermal and ecological affinities as Lusitanian (warm, southern species),⁵ Boreal (temperate), Subarctic or Arctic on the basis of a strong south–north temperature gradient and the impacts of dominant surface water currents (Figure 4.36). These groupings provide the basis for palaeoenvironmental reconstruction, although there are no universally accepted definitions of the provinces in which they occur, or of the geographical locations of the province boundaries. Furthermore, the taphonomy of fossil marine molluscan assemblages is generally not well known, although relationships between life, death and fossil assemblages are increasingly being investigated by marine biologists (Walker & Goldstein, 1999; Powell *et al.*, 2011).

4.7.3 Marine Mollusca and palaeoclimatic inferences

There are four main approaches to deriving palaeoclimatic information (changes in sea-surface or water-column temperature) from marine molluscan assemblages. The first is based upon evidence of past migrations of the principal zoogeographical provinces referred to above (Figure 4.36), and has been characteristic of attempts to use molluscs as palaeoclimatic indicators, particularly in the North Atlantic (e.g. Peacock, 1993). Other oceanic regions that show clearly defined province migrations during the late Quaternary include the Pacific Shelf adjacent to North America (Roy *et al.*, 1995), and the Southern Atlantic off the coast of Argentina (Aguirre *et al.*, 2011).

The second approach employs indicator species. Mangerud (1977), for example, used the variation in occurrence through a sequence of marine deposits at Ågtnes, Norway, of three species (*Modiolus modiolus*, *Littorina littorea* and *Mytilus edulis*) whose present-day distribution and ecology are well known, to plot the palaeo-positions of the **North Atlantic Polar Front**⁶ off the west coast of Norway during the Lateglacial period. A similar approach was adopted by Ingólfsson *et al.* (1997) to reconstruct water mass variations close to Iceland during the Lateglacial period, in which *Macoma calcarea* and *Chlamys islandica* were identified as key indicators of boreal–arctic

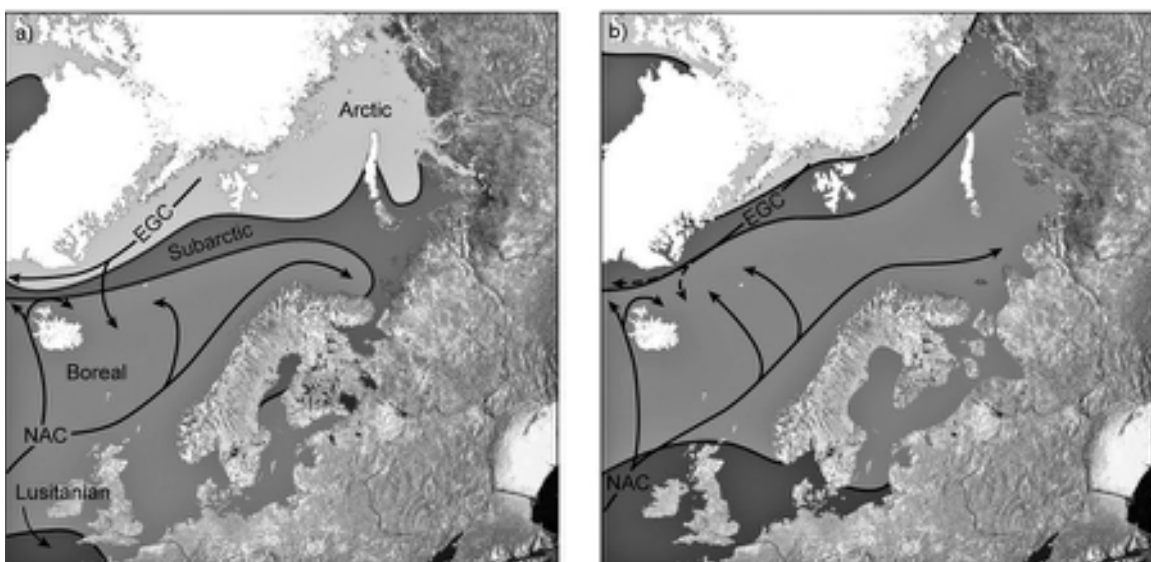


Figure 4.36 Distribution of marine zoogeographical provinces in the Northeast Atlantic: a) present time; b) during the Eemian (Last) Interglacial. NAC – North Atlantic Current; EGC – East Greenland Current (based on Funder *et al.*, 2002 – province boundaries; and Knudsen *et al.*, 2001 – surface current flows).

conditions and *Portlandia arctica* and *Buccinum groenlandicum* as arctic indicators. In a similar study, five 'guide fossils' (*Mytilus edulis*, *Modiolus modiolus*, *Arctica islandica*, *Littorina littorea* and *Zirphaea crispata*) were selected by Salvigsen *et al.* (1992) to infer variations in the temperature of the sea close to Svalbard during the Holocene. Molluscan indicator species were also employed in a multi-disciplinary reconstruction which suggested that summer temperatures were 4–5°C above present over Arctic regions during the last interglacial (CAPE-Last Interglacial Project Members, 2006). In addition, the projected northward migration of marine Mollusca in the North Atlantic as a consequence of current and expected ocean warming has involved the use of key indicator species (Lima *et al.*, 2007).

The third approach involves the analysis of elemental or isotope ratio variations within marine molluscan shells which are considered to reflect, *inter alia*, changes in sea-water temperature. The most frequently employed indices are Mg/Ca, $^{18}\text{O}/^{16}\text{O}$, $^{13}\text{C}/^{12}\text{C}$ and Sr ratios. Examples of the types of palaeoclimatic inference that have been based on this approach include the effects of a freshwater outburst from Glacial Lake Agassiz into the Champlain Sea (eastern Ontario) at the start of the Younger Dryas episode (Brand & McCarthy, 2005), and variations in sea-surface temperature (SST) values and also in ENSO strength (section 7.6.4.2) in the Pacific Ocean adjacent to Peru during the Holocene (Carré *et al.*, 2005).

A final approach involves the detailed analysis of the structure and/or isotopic composition of shells of certain marine molluscan species that secrete growth layers on an annual or seasonal basis (Wanamaker *et al.*, 2011). As is described in section 5.4.5.2, annual growth layers of specimens of long-lived species, such as *Arctica islandica*,

can be matched to develop a growth chronology (**sclerochronology**) that may span several centuries (Figure 4.37). The isotopic profile obtained from such shells provides an annually resolved palaeoclimatic record over the same interval (Scourse *et al.*, 2006). Using this approach, Schöne & Feibig (2009) compared seasonal and inter-annual temperature patterns in the North Sea for Allerød Interstadial and Medieval and modern times, while Butler *et al.* (2013) were able to develop a c. 1,350-year proxy marine climate record for the North Icelandic shelf using growth increments in *Arctica islandica*.

4.7.4 Other applications of fossil marine molluscan records

Marine molluscs also contribute to other areas of Quaternary research. For example, they provide a basis for biostratigraphic correlation, as exemplified by the work of Garilli (2011) who employed selected range fossils and a distinctive group of thermophilous molluscan taxa (the 'Senegalese fauna') to differentiate glacial from interglacial assemblages in long Quaternary sequences from the Mediterranean region. Marine molluscan assemblages also provide palaeosalinity data, which underpin long-term sea-level histories for a number of tectonically active basins including, for example, the Wanganui Basin, New Zealand (Hughes & Kennedy, 2009), the eastern Mediterranean (Lécuyer *et al.*, 2012) and the Black Sea, the last-named being a basin with a particularly complex history of marine incursion since the Last Glacial Maximum (Major *et al.*, 2006). Fossil marine molluscs also have archaeological importance, as they have been a key part of hominin diet since the Lower Palaeolithic, and shell middens provide evidence of the importance of marine shellfish in prehistoric foraging and other subsistence strategies (Colonese *et al.*, 2011). Many sites of former human occupation are now submerged beneath the sea, but can be identified through characteristic midden assemblages, and are therefore key elements in the reconstructions of long-term migration and habitation patterns (Bailey & Flemming, 2008). The analysis of seasonal climatic variations reflected in annually layered shells (section 4.7.3) can also have archaeological significance, for example, in the provision of an environmental context for the demise of the Norse colonies in Iceland and Greenland (Patterson *et al.*, 2010). Finally, marine molluscan assemblages are proving particularly valuable in the development of conservation strategies, notably in the identification of reserves for the protection of marine biota (Gladstone, 2002) and for the modelling of biotic responses to future global climate change (Belanger *et al.*, 2012).

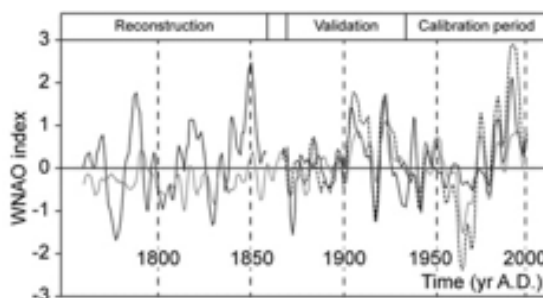


Figure 4.37 Variations in the dynamics of the winter North Atlantic Oscillation (dotted curve: section 7.6.4.3) and of annual growth increments of the bivalve *Arctica islandica* obtained from the central North Sea and the Norwegian Shelf: all values shown as deviations from long-term means (from Schöne *et al.*, 2003).

4.8 OSTRACOD ANALYSIS

Ostracoda ('mussel shrimps') are small, laterally compressed, bivalved crustaceans whose time range extends over 450 million years from the Ordovician to the present (Rodriguez-Lazaro & Ruiz-Muñoz, 2012). During that period they have expanded from exclusively marine habitats to colonize most aquatic environments, encompassing a wide range of salinity and temperature conditions, including ephemeral lakes and ponds. An estimated 20,000 species exist today, though many have never been formally described. Some have restricted ecological preferences and are therefore useful palaeoenvironmental indicators. Their fossil record is well documented, the first fossil ostracod having been described as long ago as 1746. Most stratigraphical research has been devoted to investigation of marine ostracods, where the majority of species are to be found, although there is an expanding databank on the stratigraphical occurrence and ecological preferences of brackish and freshwater species (Forester *et al.*, 2005; Martens *et al.*, 2008). Recently, the analysis of isotopic ratios and trace element contents of ostracod carapaces has provided an additional basis for inferring past environments, and especially for differentiating salinity conditions (Holmes & Chivas, 2002; Horne *et al.*, 2012).

4.8.1 The nature and distribution of ostracods

The majority of ostracods are generally between 0.2 and 2.0 mm in adult length, but exceptionally up to 30 mm. They consist of an outer shell or **carapace**, which contains the soft body parts of the living organism. The carapace is usually ovate, kidney-shaped or bean-shaped (Figure 4.38) and consists of two chitinous or calcitic bivalve-like valves that hinge above the dorsal region of the body. The biological classification of recent ostracods rests very largely on the characteristics of the soft parts, but as these features are very rarely preserved in the fossil form, the taxonomic classification of extinct species has to be based on the nature of the carapace, which fossilizes relatively easily.

The majority of marine ostracods are bottom-dwelling forms, and only a small number occupy the planktonic realm. Moreover, pelagic species usually possess weakly calcified shells and are therefore relatively rare in fossil assemblages. The distribution patterns of living ostracod communities are governed by a wide range of factors (Mesquita-Joanes *et al.*, 2012), including physical parameters such as water temperature, salinity and nature of the substrate, and biological factors such as food chains,

parasitism and natural associations. However, it is often difficult to cite any one controlling factor as being universally dominant, for while many feel that, in the case of marine ostracods in particular, water temperature is the most important, others would argue that salinity is more fundamental, while in the freshwater situation the nature of the substrate may be the overriding influence (Holmes, 2002; Lord *et al.*, 2012). Nevertheless, where autecological studies have been able to establish, with some degree of confidence, the principal parameters that govern ostracod distributions, those species may be of value in palaeoenvironmental reconstruction (Holmes & Chivas, 2002).

4.8.2 Collection and identification

Fossil ostracods are often collected, along with Foraminifera and molluscs, from lacustrine and marine sediments. The deposits are usually disaggregated in water (although occasionally hydrogen peroxide may be required), sieved and then dried. The ostracod carapaces and valves can be picked out by hand, using a very fine brush. The use of a low-powered binocular scanner of $\times 40$ or $\times 60$ magnification allows the majority of determinable remains to be collected. Individual ostracods are then mounted on a slide and examined under a high-powered microscope. The carapaces possess a considerable range of morphological features that aid identification, including extensive ornamentation of frills and spines, and internal details such as muscle scars, pore canals and duplicature.⁷ A distinction is made between the valve (hard parts) and the body with its appendages (soft parts). Many zoologists distinguish several ostracod species on the basis of the number of bristles on their appendages, whereas palaeontologists are forced to use other (less satisfactory) criteria. Ostracods are usually studied under reflected light, but transmitted light may be necessary to see the internal features. Identifications are based on modern type collections, stereoscan photographs and descriptions in micropalaeontological manuals, and the data are expressed either as species lists or in diagrammatic form showing the change in frequency of occurrence through time. Further details on collection, preparation, taxonomy and study can be found in Holmes & Chivas (2002), Cohen *et al.* (2007) and Namiotko *et al.* (2011). In the case of specimens selected for elemental or isotopic chemical analysis (section 4.8.3), more stringent preparation procedures are required in order to remove minute organic or clay particles that may have adhered to carapace surfaces. These include soaking in ethanol or methanol, or heating in H_2O_2 , oxygen plasma or a vacuum, although of these, multiple methanol ultrasonic cleaning tends to yield optimal results (Jin *et al.*, 2006).

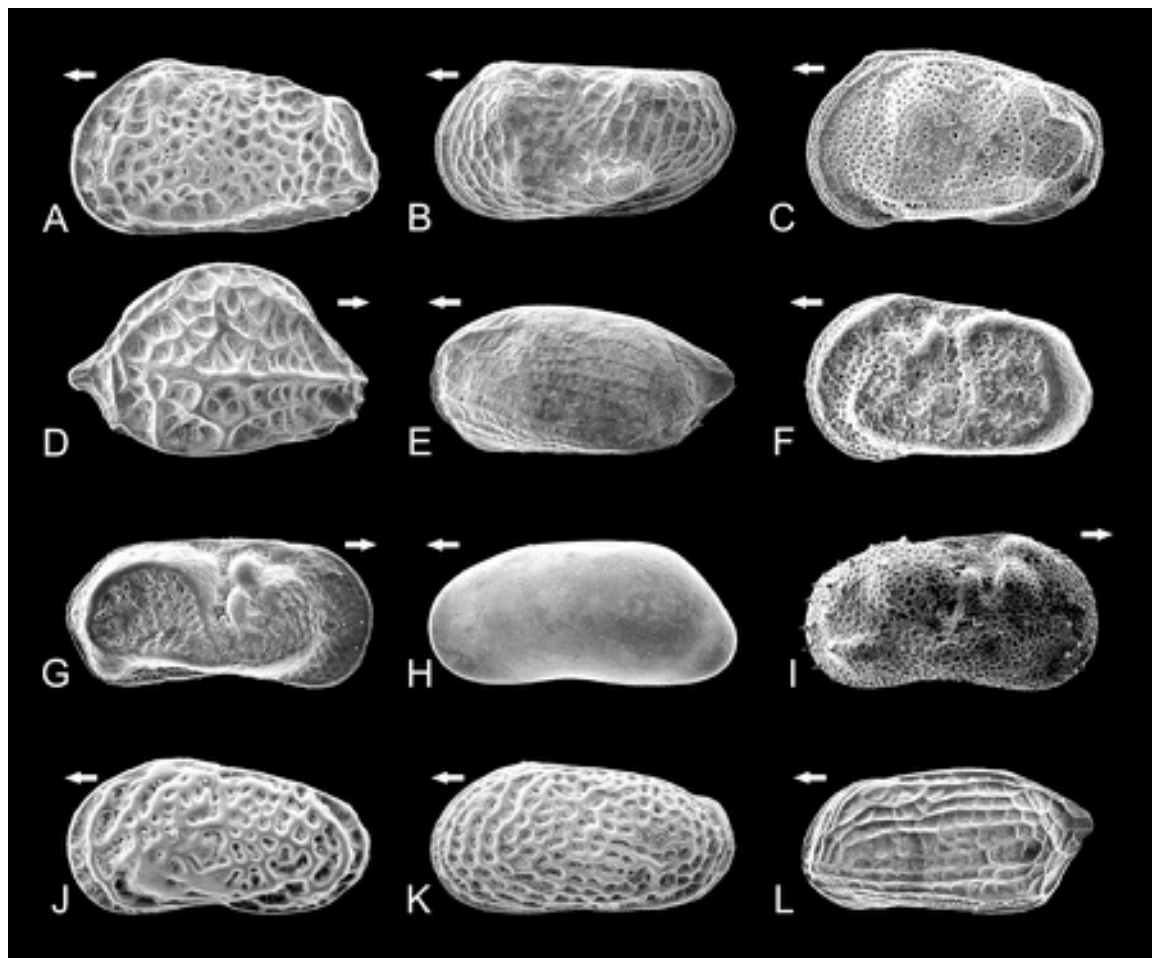


Figure 4.38 Climatically significant ostracods from the Pleistocene of the British Isles. A–H are cold-adapted taxa (A–E marine; F–H freshwater) and I–L are warm-adapted (I, freshwater; J–L brackish/marine). A. *Baffinicythere howei*, flv (female left valve) 910 µm. B. *Roundstonia globulifera*, mlv (male) 450 µm. C. *Cluthia cluthae*, flv 360 µm. D. *Hemicytherura clathrata*, frv (right valve) 490 µm. E. *Semicytherura affinis*, mlv 520 µm. F. *Leucocythere batesi*, flv 700 µm. G. *Limnocythere falcata*, frv 660 µm. H. *Amplocypris tonnensis*, flv 1,870 µm. I. *Ilyocypris salebrosa*, frv 800 µm. J. *Callistocythere curryi*, flv 470 µm. K. *Leptocythere cribrosa*, flv 520 µm. L. *Semicytherura arcachonensis*, flv 560 µm. The measurements are valve lengths and arrows point in anterior direction (SEM images provided by David Horne, Queen Mary University of London, UK).

4.8.3 Ostracoda in Quaternary studies

Certain rapidly evolving ostracod lineages are useful markers in marine biostratigraphic sequences, especially where Foraminifera are absent (Griffiths, 2001). However, as they lack planktonic larvae, many shallow- and warm-water species cannot cross physical barriers and are therefore restricted to particular geographical areas. Moreover, some of the problems already considered in the interpretation of terrestrial fossil assemblages are also found

in ostracod analysis. At the generic level, the poor state of taxonomy often inhibits the comparison of fossil and recent forms. Also there is evidence to suggest that several ostracod species that are now benthic in character developed from shallow-water ancestors. Fortunately, it appears that migration in the opposite sense, in other words from deep and cold to shallow and warm water, seems unlikely to have occurred. Further, there are indications that the dominant elements in certain benthic fossil assemblages may be due less to environmental factors than to selective

preservation of the more thick-shelled species. Where these difficulties can be overcome, however, marine ostracods can be extremely useful for reconstructing a range of palaeoenvironmental conditions, including salinity, temperature, hydrodynamic balance, substrate characteristics, sea-level variations, oxygenation levels and nutrient availability (Frenzel & Boomer, 2005). The most frequently inferred parameters, however, are palaeotemperature, palaeosalinity and (by association) palaeobathymetry, which co-vary between ocean masses and currents. They are also the principal controlling factors in the distribution and abundance of non-marine ostracods in freshwater and saline lakes (Mesquita *et al.*, 2005).

Some palaeoclimatic reconstructions obtained from ostracod assemblages have used the indicator species approach. For example, two modern Lusitanian (Mediterranean) ostracod species, *Aurila arborescens* and *Callistocythere badia*, which are found in the seas adjacent to northern Denmark only during the mid-Holocene, suggest that sea-surface temperatures during the coldest month at that time were more than 5–6°C above present values (Vork & Thomsen, 1996). Similarly, Bennike *et al.* (2010) concluded that the optimum warmth of the seas around west Greenland during the Holocene was achieved between 7 and 6.5 ka, as the thermophilous (non-Arctic) ostracod species *Ilyocypris bradyi* is confined to records dating from that period. On a longer timescale, glacial and interglacial episodes in a 130 ka sediment sequence in south-central Illinois could be identified using the ostracod species *Limnocythere friabilis* as a cold indicator and *Candonia caudata* and *Heterocypris punctata* as warm indicators (Curry & Baker, 2000). Although this approach has been less extensively used with non-marine ostracods, because fewer species appear to be controlled exclusively by temperature, some recent research suggests that a number of non-marine ostracod species do show common distributional patterns with respect to modern climatic variables, and where this is the case their **mutual temperature range** can be calculated enabling an estimation to be made of former temperatures (Horne *et al.*, 2012). This approach constitutes a variant of the MCR technique developed for the analysis of fossil beetle assemblages (section 4.5.4.2).

Some ostracod species, such as *Cyprideis torosa*, appear to be particularly sensitive to salinity variations and have therefore been used as salinity indicator species (Pint *et al.*, 2012). Other ostracods are able to survive in the inter-tidal zone, where salinity, light, degree of oxygenation and other properties vary markedly over a diurnal cycle, and these constitute useful indicator taxa for the reconstruction of past variations in sea level (Yasuhara *et al.*, 2003).

In general, however, the abundance and distribution of most present-day ostracod species (both marine and non-marine) co-vary with *both* temperature and salinity, and it is not always clear which of these is the dominant controlling variable. As a consequence, multivariate statistical methods and modern training sets tend to be used to determine the association between the species composition of modern ostracod communities and selected environmental factors, the resulting transfer function informing interpretations of the fossil assemblage data (Viehberg & Mesquita-Joanes, 2012). This approach has been used, for instance, to reconstruct variations in lake level and salinity in regions susceptible to seasonal or longer-term evaporation cycles (Kemp *et al.*, 2012a). Multivariate statistical methods are also increasingly being employed in studies of sea-level variations based on ostracod assemblages. For example, Reeves *et al.* (2007) used cluster analysis to identify characteristic faunal assemblages associated with marine, marginal marine, tidal, estuarine and non-marine sediment facies in the Gulf of Carpentaria, and then employed the results to develop a sea-level history for the shallow shelf that formed a land bridge between Australia and New Guinea at times of low sea level. A similar approach, based on the taxonomic composition of ostracod assemblages, was adopted by Boomer *et al.* (2010) to reconstruct the complex history of the Black Sea, which over the course of the late Quaternary has been periodically joined to, and isolated from, the Mediterranean Sea.

An alternative and increasingly important palaeoenvironmental approach is the analysis of variations in the chemical composition of fossil ostracod carapaces. Recent studies have shown that the ratios of chemical elements (e.g. Mg, Sr, Ba, measured proportionately to the abundance of Ca) and of isotopes of oxygen, carbon and strontium in modern ostracod carapaces vary predictably with environmental gradients (Holmes & Chivas, 2002; Horne *et al.*, 2012). The chemical composition of ostracod carapaces has been used to reconstruct the history and pattern of lake-level variations during the Late Quaternary in North America (Bright *et al.*, 2006), to determine the strength of the East Asian monsoon system (Zhai *et al.*, 2011), to identify sources of water delivered to lake systems in southern Spain (Anadón & Gabàs, 2009), and to establish rates of dissolved load influx and weathering in the catchment of Lake Constance in central Europe (Kober *et al.*, 2007).

Fossil ostracod assemblages have also been employed in other areas of Quaternary research, for example in the study of high-energy tsunami deposits (Ruiz *et al.*, 2010), and in the reconstruction of pollution histories in both marine and freshwater environments (Yasuhara *et al.*,

2003). They can also provide useful archaeological information on the nature of sites occupied or exploited by humans (Holmes *et al.*, 2010; Lord *et al.*, 2011). Finally, they are an important component of current micro-palaeontological work that is providing new insights into deep-sea biodiversity and ecosystems, and the degree to which these vary over glacial–interglacial cycles (e.g. Yasuhara *et al.*, 2012).

4.9 FORAMINIFERAL ANALYSIS

Foraminifera are **protists** (or **prokaryotes** – single-celled organisms⁸) that possess a hard calcareous shell often distinctively coiled to resemble that of a gastropod or cephalopod. They were first described and illustrated in the sixteenth century, but were not studied systematically until the latter part of the nineteenth century following the remarkable voyage of HMS *Challenger* which began in 1872. The discovery during that expedition of living Foraminifera in deep-sea waters, and of fossil remains in sediments that were dredged from the sea floor, revolutionized marine micropalaeontology. Since then, Foraminifera have become staple tools in Quaternary stratigraphy, palaeoceanography and palaeoclimatic reconstruction.

4.9.1 The nature and distribution of Foraminifera

Foraminifera consist of a soft body (protoplasm) enclosed within a shell or **test** secreted by the organism, which is variously composed of organic matter, minerals (calcite or aragonite) or **agglutinated** (foreign particles held together

by various cements) components. The tests may be single chambered, but more frequently consist of a number of chambers separated by **septae**. Connections between the chambers, through which cytoplasmic material can move, are formed by small holes in the septae known as **foramina**, from which the group derives its name. In many common species, the chambers are added in a spiral pattern, producing a coiled shell, while others develop far more complicated structures (Figure 4.39). They are classified on the basis of a number of characteristics, such as the **rhizopodia** (cytoplasmic extensions used in locomotion and feeding), degree and form of coiling, number of chambers, number and pattern of apertures, and surface ornamentation. Not all of these, however, are preserved in fossil forms.

Foraminifera range in size from less than 0.40 mm (the planktonic forms) to some of the benthic species which may measure up to 10 cm in width (so-called larger Foraminifera). They are tolerant of a range of salinity and temperature, being found in saltmarshes, shallow brackish water in estuaries, on the continental shelf and in the waters of the deep oceans of the world. Most Foraminifera are marine and benthic, although a few genera are pelagic, while a very small number of species (**thecamoebids**) are adapted to freshwater environments. The marine planktonic and benthic forms have proved to be particularly useful in global correlation and climatic reconstruction and these will be considered in the next section of this chapter. The present discussion will be concerned principally with foraminiferal remains in shelf seas and inshore waters. Further details on the nature, distribution and ecology of Foraminifera can be found in Haslett (2002), Sen Gupta (2002) and Murray (2006).

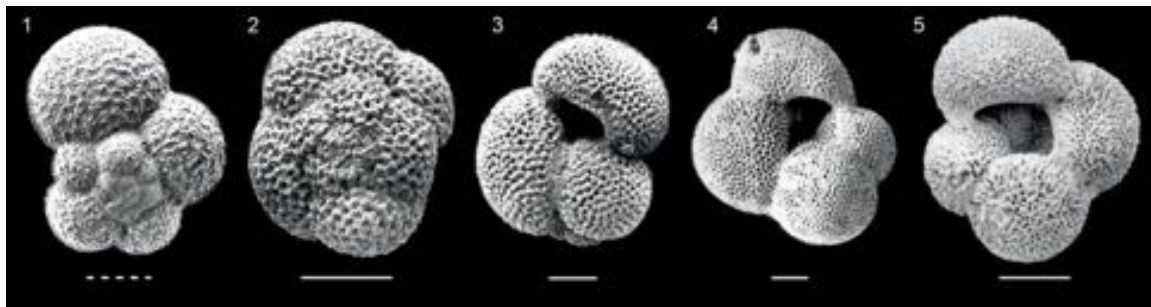


Figure 4.39 Examples of planktonic foraminiferal species widely employed in Quaternary palaeoceanographical studies. The use of sinistral (1) and dextral (2) forms of *Neogloboquadrina pachyderma* as palaeoclimatic proxies in high-latitude surface waters is referred to in section 4.10.7. *Globigerinoides ruber* (3) and *G. sacculifer* (4) are abundant today in subtropical waters (Figure 4.43) and hence employed as proxy indicators of warm SSTs. *Globigerina bulloides* (5) can tolerate a wide range of temperatures but is most abundant in cool upwelling ocean waters. (SEM images provided by Alessandra Asioli, CNR Institute of Geoscience and Geo-resources, Padua, Italy.)

4.9.2 Collection and identification

Foraminifera can be extracted from sediments obtained from surface samples or from cores. The matrix is usually disaggregated using either water or Calgon solution, but boiling in a dilute solution of hydrogen peroxide may prove necessary for strongly cemented sediment matrices. The samples are then washed through sieves and the residues dried; the retained Foraminifera can be picked out by hand with the aid of a binocular microscope. Where large numbers of sand grains are present (e.g. in some shelf sediments), the foraminiferal remains can be concentrated using a heavy liquid such as ethylene bromide/absolute alcohol solutions, the tests being ‘floated’ from the sand using detergent (Lehmann & Röttger, 1997). Removal of surface contaminants, which is essential where elemental or isotope ratio measurements (e.g. Mg/Ca) are to be obtained from foraminiferal tests, is usually achieved by dilute acid leaching, although care needs to be exercised in the application of this procedure as it may lead to partial dissolution of sample carbonate, which can affect the isotopic ratios (Barker *et al.*, 2003).

The smaller Foraminifera are examined under a high-powered microscope using reflected light. Occasionally staining (e.g. with malachite green or a similar food dye) is required to bring out the surface structures more clearly. Larger Foraminifera are often studied in thin section where wall and growth plan may be better seen under transmitted light. As with ostracods, identifications are based on type collections, descriptions and stereoscan photographs in foraminiferal manuals, which can be explored through online resources, such as the *World Modern Foraminifera Database* (<http://www.marinespecies.org/foraminifera/>), the *Marine Species Identification Portal* (<http://species-identification.org>) or *eForams* (<http://www.eforams.org/>). The data can be presented simply as species lists or, more commonly, as ‘range charts’ expressed in percentage form or as abundance per unit volume of sediment (e.g. Lloyd *et al.*, 2012). Further information on the collection and study of Foraminifera can be found in Green (2001) and Schönfeld (2012).

4.9.3 Foraminifera in Quaternary inshore and shelf sediments

Foraminiferal remains in sediments of most inshore waters and the shelf seas are dominated by benthic forms, in contrast with the deep-sea sediments in which planktonic Foraminifera are more abundant. These bottom-water assemblages are influenced by a number of factors, which include light, oxygenation, organic and nutrient flux within

the water column, and (to a lesser degree) water temperature. But because these conditions can change quickly in shallow marine environments, most benthic forams possess wide environmental tolerances (Van der Zwaan *et al.*, 1999), and are therefore less valuable as palaeoenvironmental indicators than planktonic species (see section 4.10). Palaeoenvironmental inferences are also constrained by taphonomic factors such as reworking and redeposition, the resulting mixed assemblages being indicated by wear, poor preservation and unusual population structure. Further problems arise from the pyritization or permineralization of some tests, which makes them heavier leading to segregation during transport (Berkeley *et al.*, 2007), and differential dissolution, which particularly affects calcareous tests (Murray & Alve, 1999), although agglutinated forams are more susceptible to dissolution than either calcareous or siliceous forms.

These problems notwithstanding, benthic foraminiferal studies have provided valuable data on inland and shelf-sea sequences, some examples of which are summarized below.

4.9.3.1 Sea-level change

A number of studies have shown a strong statistical relationship between the altitudinal distribution of modern benthic foraminiferal species and tide level, while calibrations between benthic foram assemblages and tide-gauge records indicate that some species track changes in tidal reach (Edwards, 2007). Transfer functions that quantify these relationships have provided a basis for the reconstruction of Holocene changes in sea level on, for example, the Great Barrier Reef complex, Australia (Horton *et al.*, 2007), mangrove swamps on various Pacific shores (Woodroffe *et al.*, 2005), saltmarshes in North America (Kemp *et al.*, 2009) and inter-tidal mudflats and inter-dune slacks in the British Isles (Edwards & Horton, 2006). There is a limit to the precision with which mean tidal altitude can be inferred using this approach, however, due partly to taxonomic issues, but also to the fact that most inter-tidal species seem able to tolerate a range of salinity and other conditions, so that small-scale changes in sea level may be difficult to detect (Edwards, 2007; Woodroffe, 2009). Where significant changes in sea level are sustained over longer periods, however, the corresponding changes in benthic foraminiferal assemblages are more evident. In the Western Mediterranean, for example, benthic foram records from shallow-water shelf sequences reflect a rise in sea level over the last 12 ka that matches reconstructions based on independent lines of evidence (Figure 4.40).

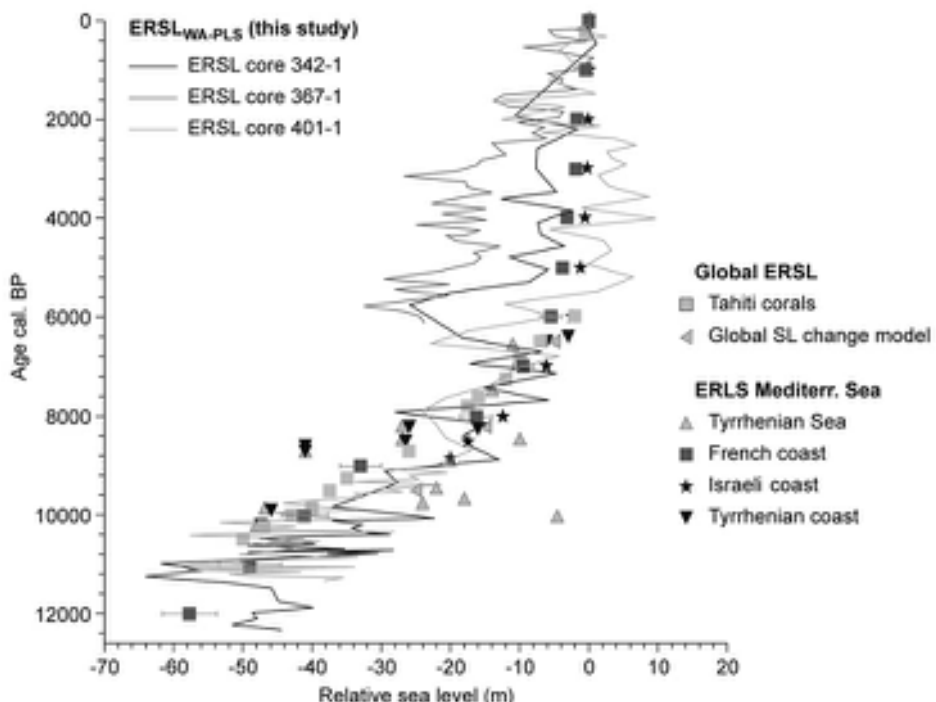


Figure 4.40 Relative sea-level (ERSL) curves for the last 12 ka for the Western Mediterranean based on benthic Foraminifera-based transfer functions. Data from three shelves (core 342-1: Alboran Platform; core 367-1: Oran Bight; and core 401-1: Mallorcan Shelf) show broadly similar trends to independent reconstructions of sea-level change over the same period (from Milker *et al.*, 2011).

4.9.3.2 Shallow marine water mass and temperature variations

Most palaeotemperature reconstructions based on foraminiferal evidence are derived from planktonic or deep marine benthic species, and particularly on the chemical composition of their tests (see section 4.10). Nevertheless, shallow-water benthic species can also provide important palaeoclimatic insights, because shelf and estuarine assemblages are sensitive to changes in water mass, the positions of dominant surface currents, or migrations of important sea-surface boundaries such as the North Atlantic Polar Front, and indicator species can be used to reconstruct these past changes in marine conditions. For example, Perner *et al.* (2011) identified the benthic foram species *Cassidulina reniforme* as an indicator of an Atlantic water mass, and *Elphidium excavatum f. clavata*, *Cuneata arctica* and *Spiroplectammina biformis* as indicators of an Arctic water mass, in their reconstruction of centennial-scale climate variations off West Greenland over the past 3.6 ka. They attributed changes in water mass to variations in the

influences of the West Greenland and East Greenland Currents during the Roman Warm Period, the Medieval Climate Anomaly and the Little Ice Age. Eberwein & Mackensen (2008) also employed benthic foraminiferal indicator species as one of a number of tools to reconstruct changes in palaeoproductivity and water mass in an upwelling region of the Atlantic off the coast of northwest Africa. In the eastern Pacific, benthic foraminiferal assemblages from the Santa Barbara Basin, California, show distinctive faunal ‘switches’ during the Late Quaternary, which Cannariato *et al.* (1999) attributed to the influence of Dansgaard–Oeschger climatic oscillations (section 3.11.4). Other studies of shallow benthic foraminiferal assemblages have employed a transfer function approach, for example in the reconstruction of water mass temperature and salinity variations over the North Icelandic Shelf during the Holocene (Knudsen *et al.*, 2012). Finally, modern benthic foraminiferal assemblages have been used to establish the rate and magnitude of the warming of shallow seas in response to the recent increase in global temperatures (Saher *et al.*, 2012).

4.9.3.3 Other palaeoenvironmental applications

Apart from the palaeoclimatic and sea-level applications described above, the wider palaeoenvironmental potential of shallow marine benthic Foraminifera has been relatively under-exploited until quite recently (Schönfeld, 2012). For example, some modern benthic species have been found to be diagnostic of glacimarine margins; hence equivalent fossil assemblages can be used to locate the positions of former ice margins and grounding lines, and these have contributed to the mapping of retreat stages of the Laurentide Ice Sheet (Jennings *et al.*, 1996), the Antarctic ice sheet (Pudsey *et al.*, 2006) and fjord glaciers in Spitsbergen (Korsun & Hald, 1998). Other assemblages appear to be indicative of seasonal or permanent sea ice, and provide evidence of sea-ice cover in the past (Scott *et al.*, 2008). Many benthic species are now known to be sensitive to changes in water chemistry, and are proving to be valuable monitors of past and current pollution levels and water quality (Bouchet *et al.*, 2012), while others provide evidence of submarine methane seepage (Panieri *et al.*, 2012). Shallow marine benthic forams also have important archaeological applications, for example for provenancing of pottery (Santacreu & Vicens, 2012), discriminating between natural and cultural shell deposits (Rosendahl *et al.*, 2007) and deciphering the detailed coastal context of ancient settlements now isolated from the sea (Bernaconi *et al.*, 2010).

Shallow water benthonic Foraminifera, therefore, can be used as indicators of both local and regional environmental conditions although, as with ostracod assemblages described earlier, they are best employed in conjunction with other fossil remains, particularly molluscs, ostracods, diatoms and pollen. But it is the planktonic and deeper-water benthic Foraminifera that have made the most significant contributions to Quaternary environmental reconstruction, as explained in the following section.

4.10 MICROPALAEONTOLOGY OF DEEP-SEA SEDIMENTS

4.10.1 Introduction

It has already been shown (section 3.10) how the ratios of oxygen isotopes in marine microfossils can provide a record of the expansion and contraction of ice sheets during the Quaternary, and the applications of this technique in Quaternary stratigraphy will be considered further in Chapter 6. However, the marine microfaunal

and microfloral assemblages themselves can also provide valuable palaeoenvironmental data, since they commonly retain a record, at least in part, of former ocean-water temperatures that will, in turn, be a reflection of former climatic conditions. From an analysis of the biostratigraphy of the deep-sea sediments, therefore, it is possible to make reasoned inferences about climatic regimes that prevailed over large areas of the world's oceans at different times during the Quaternary period. In addition, marine microfossil records have been used to reconstruct changes in oceanic circulation (palaeceanography) and in nutrient supply (palaeoproductivity), as well as in the dissolved oxygen content of ocean waters and bathymetry.

Some of the marine organisms found in the deposits of the deep-ocean floors that are employed in palaeoclimatic research have been discussed above in relation to fresh- or brackish-water situations, or to relatively shallow shelf seas. These include foraminifers, diatoms and ostracods. Of the remaining organisms, the most valuable in terms of their application to palaeoclimatic research have proved to be Radiolaria, coccolithophores and dinoflagellates (Armstrong & Brasier, 2005; Hillaire-Marcel & De Vernal, 2007).

4.10.2 Radiolaria

Radiolaria are marine, amoebic protozoans that secrete elaborate skeletons composed largely of amorphous (opaline) silica, which is extracted from seawater in the same way that Foraminifera extract calcium carbonate, a group with which they have close affinities in terms of ecological and environmental requirements (Haslett, 2004). The skeleton, which consists of a complex network of elements, is contained within the living protoplasm and thus the hard parts forming the fossil do not dissolve in seawater until the creature dies. The single-celled radiolarians are commonly circular in shape and average between 100 and 2,000 µm in diameter, though their skeletal tests vary markedly in form, measuring c. 30–300 µm in length (Figure 4.41a). There are about 400–500 relatively common species and these are found in all ocean waters from the tropics to the subpolar seas, in surface waters down to depths of over 4 km. Most of the taxa have specific, sometimes narrow, bathymetric preferences, though some can occur in a very wide range of water depths (**erybathyal**) (Baumgartner *et al.*, 2006).

The composition of modern radiolarian communities appears to be influenced by water depth, water masses, hydrographic boundaries (e.g. surface frontal systems) and

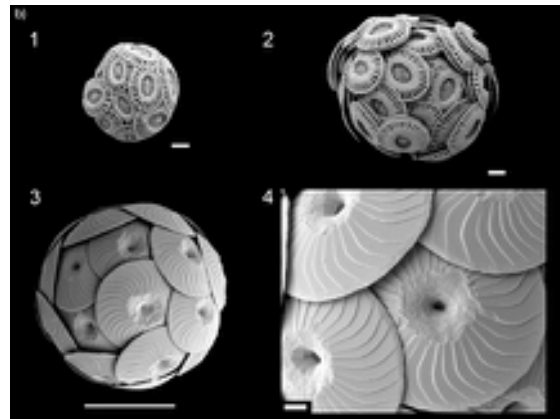
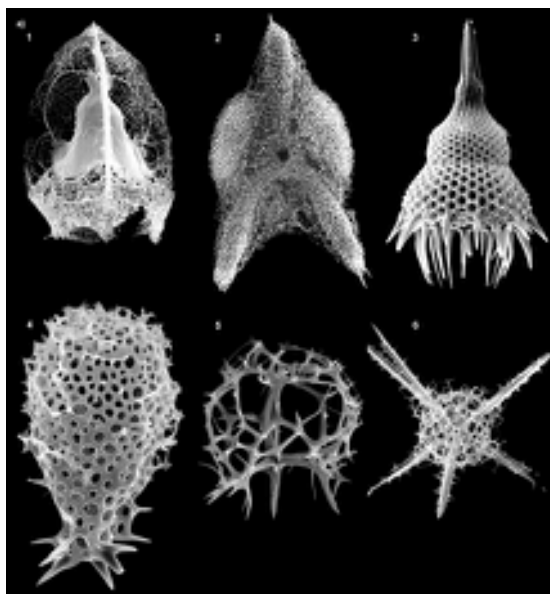


Figure 4.41 a) Examples of siliceous skeletons (tests) of the radiolarian groups Spumellaria (S) and Nassellaria (N), important biomarkers commonly preserved in Late Quaternary deep marine sediment; their tests range in size from c. 30–300 µm. 1. *Callimitra carolotae* (N). 2. *Euchitonia elegans* (N). 3. *Lamprocyclas maritalis* (S). 4. *Mitrocalpis araneafera* (N). 5. *Nephrosypyris knutheieri* (N). 6. *Rhizoplegma boreale* (S), recently renamed *Cleveiplegma* (from Dumitrica, 2013; SEM images provided by Kjell Rasmus Bjørklund, Natural History Museum, University of Oslo, Norway). b) SEM scans of coccolithophore specimens from the central Adriatic Sea. 1. CoccospHERE of *Emiliania huxleyi* TYPE A comprising an outer (single) layer of calcitic platelets (coccoliths) which enclose the living organism. This form of the species is typical of nutrient-rich environments and is characterized by rapid growth during bloom conditions (scale bar: 1 µm). 2. *Emiliania huxleyi* TYPE A with multiple layers of coccoliths, a larger form that is typical of nutrient-poor environments and which grows more slowly (scale bar 1 µm). 3. Complete coccospHERE of *Calcidiscus leptoporus* (ssp. *quadriperforatus*), an important carbon storage species that thrives in tropical and temperate latitudes (scale bar: 10 µm). 4. Close-up of 3 showing coccolith detail (scale bar: 1 µm) (images provided by Luka Supraha, Uppsala University, Sweden).

nutrient availability (Abelmann & Gowing, 1997), and hence past variations in these parameters can be inferred from fossil assemblages. Examples include the reconstruction of variations in the strength of the East Asian monsoon over the last glacial cycle (Ikehara & Itaki, 2007), and of the upwelling currents in the Atlantic close to northwest Africa over the past 40 ka (Haslett & Smart, 2006). Radiolarian stratigraphy has also been used to estimate past variations in SSTs, for example in the East China Sea during the past 10.5 ka (Chang *et al.*, 2008a), to reconstruct stratification and current patterns in the southwest Pacific over the past 600 ka (Lüer *et al.*, 2008), and to assess oceanographic responses to orbital glacial–interglacial cycles (Itaki *et al.*, 2007). In addition, Quaternary radiolarian records often contain distinct biostratigraphic marker horizons (e.g. range boundaries of certain taxa), and these provide a basis for correlation between palaeoceanographical records (Haslett, 2004).

4.10.3 Coccolithophores

Coccolithophores are the most common members of a group of unicellular autotrophic marine algae known as **calcareous nanoplankton**. They are generally spherical or oval in shape, and are mostly less than 100 µm in diameter (Figure 4.41b). The living organism is covered by a layer of organic scales upon which small calcite platelets, commonly ranging in size from 1–25 µm and called **coccoliths**, are secreted (Flores & Sierro, 2007). These may envelop the cell completely to form a hollow sphere (**coccospHERE**) which eventually disintegrates and falls to the ocean bed. The individual button-shaped coccoliths are usually all that remain of the former living creature. Like other marine flora, coccolithophores are autotrophic, possessing chloroplasts that are used to photosynthesize food. They possess whip-like threads (**flagella**) to generate motion, and a few are known to ingest bacteria and small algae. They are therefore difficult to classify, possessing

characteristics of both plants and animals. Although a few species are adapted to either fresh or brackish water, the majority of present-day coccolithophores are marine, but are much less common at salinities greater than 37 per mil or less than 32 per mil. Being photosynthetic, they are mostly confined to the photic zone, predominantly within the upper 80 m of the water column, and are rarely encountered below 200 m depth (Baumann *et al.*, 2005).

Coccolithophores are found in very large numbers in present-day ocean surface waters where they rival diatoms as the most abundant phytoplankton (Flores *et al.*, 2012). Their abundance and species distributions are governed by a combination of light, salinity and temperature, but it was their temperature requirements that initially attracted ocean scientists, the down-core variations of key coccolith indicator species forming the basis of some of the early research on Quaternary palaeoceanography (McIntyre & Ruddiman, 1972; McIntyre *et al.*, 1972). This approach continues to be used today, providing evidence, for example, of shifts in the position of the Inter-Tropical Convergence Zone (ITCZ) during the late Quaternary (Mertens *et al.*, 2009), the effects of Dansgaard–Oeschger cycles (section 3.11.4) and Heinrich Events (section 3.10.1) in the Atlantic and Mediterranean basins over the past 50 ka (Colmenero-Hidalgo *et al.*, 2004), and precession orbital forcing effects on the Arabian Sea over the last 200 ka (Rogalla & Andrleit, 2005). Recent research has also focused on the link between climate change and coccolith productivity, particularly over glacial–interglacial cycles, with marked increases in coccolith abundance apparent during glacial periods and peak abundances reached during Terminations (section 6.2.3.5) (Flores *et al.*, 2012). Coccolith productivity also appears to have fluctuated in concert with the precession orbital cycle (e.g. Ivanova *et al.*, 2012). Over shorter timescales, however, the factors affecting coccolith productivity are more complex, and appear to reflect the positions and strengths of dominant marine currents (Giraudeau *et al.*, 2010). It now seems that the body size and morphology of some coccoliths, such as *Emiliania huxleyi* (Figure 4.41b), may be controlled by temperature, for an increase in size appears to correspond with successive colder episodes; if so, this would be a useful additional palaeoclimatic indicator (Flores *et al.*, 2010).

4.10.4 Dinoflagellates (dinocysts)

Dinoflagellates are microscopic, usually unicellular, protists measuring up to 2 mm in diameter, though the majority are considerably smaller. They are members of the algae (division Dinoflagellata), and are free-swimming, being

propelled by the spiralling motion of two flagella. The cell wall of many dinoflagellates is protected by armoured plates, called **theca**, the distinctive structure and arrangement of which provides a basis for classification (Figure 4.42a). Their life cycles are complex and frequently involve a non-motile stage during which a cyst, composed of sporopollenin, is formed; it is this resistant **dinocyst** that is commonly preserved in fossil form (Figure 4.42b). Dinoflagellates are one of the most abundant types of marine plankton, occasionally generating ‘algal blooms’ that colour the sea surface red or brown (so-called ‘red tides’), caused by the pigments that their living cells contain. Further details can be found in Haq & Boersma (1998) and Dale & Dale (2002b).

Comparatively little was known about the potential of dinoflagellates for Quaternary stratigraphy and palaeoenvironmental reconstruction until the early 1990s (Harland, 1988). Over the last twenty years, however, dinoflagellate records have been obtained from many of the world’s oceans and a range of palaeoenvironmental parameters have been inferred, including sea-surface temperatures (Esper & Zonneveld, 2007), palaeosalinity (Mudie *et al.*, 2001), ocean palaeoproductivity (Höll *et al.*, 1999), ocean stratification (Marret & Scourse, 2002) and the limits of sea-ice extent (Harland *et al.*, 1999). Past variations in the strength and location of major oceanographic currents have also been reconstructed, for example periodic incursions of Atlantic waters into the Eurasian Arctic (Matthiessen *et al.*, 2001) and latitudinal migrations of the Antarctic Circumpolar Current (Verleye & Louwey, 2010). A number of statistical methods have been employed in these studies, again including transfer functions. The latter approach, however, tends to generate SST estimates that are higher than those derived from other proxies, such as forams, diatoms and radiolarians, and this has been attributed either to selective degradation of the more delicate dinocyst types (Esper & Zonneveld, 2007) or to inherent statistical bias (Telford, 2006). Nevertheless, dinoflagellate records not only add to the Quaternary scientist’s proxy toolkit, but also have applications in non-marine contexts. For example, seasonal dinoflagellate blooms in large freshwater lakes have formed annually laminated sediment, allowing past environmental changes to be reconstructed at a high temporal resolution (Chu *et al.*, 2008).

4.10.5 Marine microfossils in ocean sediments

Planktonic Foraminifera are the major contributors to deep-sea sediments and, along with coccoliths, account

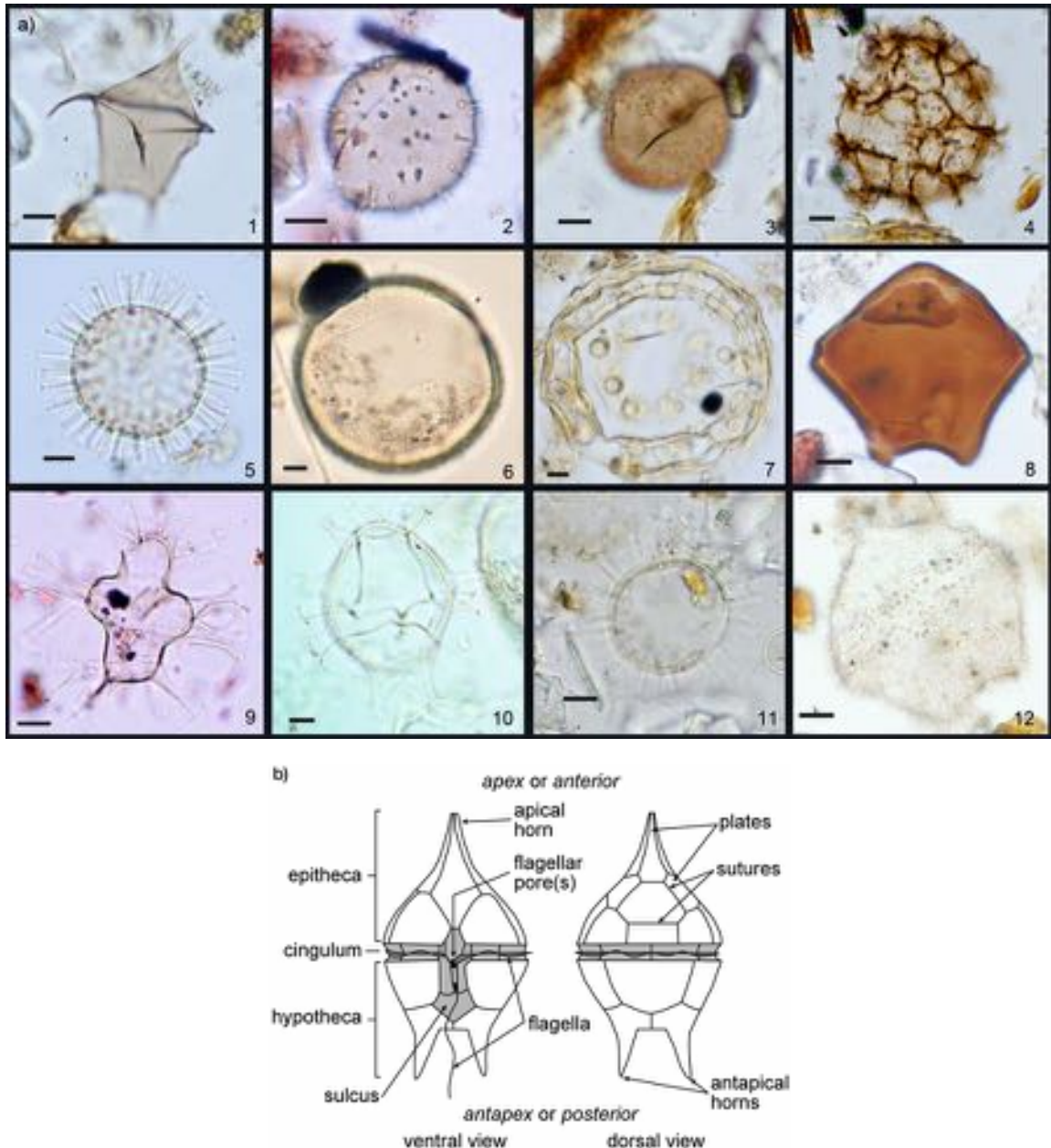


Figure 4.42 a) Examples of common Quaternary dinocysts. 1. *Proteroperidinium stellatum* (Black Sea Holocene sediments). 2. *Echinidinium transparantum* (Black Sea Holocene sediments). 3. *Peridinium ponticum* (Black Sea Holocene sediments). 4. Cyst of *Polykrikos schwartzii* (Black Sea Holocene sediments). 5. *Operculodinium centrocarpum* (North Icelandic Shelf Recent sediments). 6. *Bitectatodinium tepikiense* (Celtic Sea Recent sediments). 7. *Tuberculodinium vancampoae* (Gulf of Guinea Recent sediments). 8. *Quinquecuspis concreta* (Celtic Sea Recent sediments). 9. *Spiniferites cruciformis* (Black Sea Holocene sediments). 10. *Spiniferites ramosus* (Celtic Sea Recent sediments). 11. *Lingulodinium machaerophorum* (Black Sea Holocene sediments). 12. *Trinovantedinium applanatum* (Celtic Sea Recent sediments). Scale bar represents 10 µm (images provided by Fabienne Marret, University of Liverpool, UK). b) Structural features of some dinoflagellate cysts (dinocysts) at motile stage.

for more than 80 per cent of modern carbonate deposition in seas and oceans (Hüneke & Mulder, 2011). Most of the tests now being deposited are from planktonic species of *Globigerina* and it has been estimated that about 30 per cent of the present ocean floor (over 60 million km²) is covered by the grey mud known as *Globigerina ooze*. These oozes, forming at depths up to 5 km in ocean waters between 50°N and 50°S, are fed by a continuous rain-out from the water column of mixed organic detritus, termed ‘marine snow’. Coccolith oozes form principally in the tropical and subtropical regions, where the remains may average up to 30 per cent by weight of the sediments. In arctic regions, by comparison, the values may be as low as 1 per cent. By contrast with Foraminifera, however, coccolith remains settle much more slowly, and are therefore more susceptible to carbonate dissolution. Although some coccoliths may settle out more rapidly if they are contained within the faecal pellets of planktonic grazers, it has been estimated that less than 25 per cent of all coccolith species are actually preserved in the fossils of ocean sediments, though precise census studies of coccolithophore production and survival are rare (Robert, 2009). Below 3–5 km, the calcium carbonate compensation depth, nearly all CaCO₃ enters into solution, and thus only the most resistant calcareous fossils will be found. The sediments there will be dominated by siliceous remains, predominantly of Radiolaria.

Radiolaria accumulate in abundance in equatorial sediments where productivity is high in the water column above. However, as the productivity of calcareous organisms is also high, the radiolarian remains are often masked by foraminiferal and coccolith fragments. Only in areas such as the tropical northern Pacific and Indian Ocean, where large areas of the sea floor lie below the carbonate compensation depth, are radiolarian oozes encountered. Diatomaceous oozes are also found in the abyssal depths of the Pacific and Indian Oceans and in parts of the Atlantic (Sverdrup & Kudela, 2011). Some of these oozes are laminated and appear to have formed along oceanic temperature ‘fronts’ where upwelling leads to large concentrations of diatoms near the surface, and periodic die-off promotes sudden accumulation (diatom mats) on the sea floor (Shimada *et al.*, 2008). Siliceous oozes are most common in the high-latitude areas of the north Pacific and around Antarctica, locally containing a high abundance of siliceous dinoflagellate cysts (e.g. Marret & Zonneveld, 2003). In these regions, calcareous fossils are rare and both radiolarian and diatom remains are abundant. As with carbonates, however, silica is soluble in seawater, dissolution being especially rapid in the upper levels of the water column. Only those radiolarian species with a solid opaline skeleton reach the sea floor and, overall, it has been

estimated that perhaps as few as 10 per cent of all Radiolaria find their way into the fossil record. Similar low values have been suggested for diatoms. Both Radiolaria and diatoms are prone to exhumation and reburial in younger sediments and this poses further problems of interpretation for the marine biostratigrapher.

4.10.6 Laboratory separation of marine microfossils

Faunal and floral remains are extracted from deep-ocean cores in the laboratory by disaggregation of the sediment using a water jet to flush sediment through a series of sieves of varying mesh size. This procedure alone may be sufficient to recover most specimens from soft, unconsolidated sediment, but for more resistant materials, immersion in dilute hydrogen peroxide (Foraminifera, Radiolaria), nitric acid or hydrochloric acid (Radiolaria), or, in the case of coccoliths, sodium hexametaphosphate (Calgon), may be required. The larger fossils can be hand-picked from the meshes of sieves, while for the smaller remains, particularly coccoliths and dinoflagellate cysts, it is necessary to concentrate the microfossils into a liquid which can then be mounted on a microscope slide (‘smear slides’). Diatoms and some other small siliceous microfossils (less than 100 µm) require a more lengthy laboratory preparation procedure involving several chemical immersion steps and centrifugation. High-powered microscopy (up to ×1,600) may be necessary for ultra-detailed study using transmitted, reflected and polarized light and, as in other micropalaeontological work, increasing use is being made of the electron microscope. Identifications may be made difficult by the solution of diagnostic parts, by the mechanical wear of the skeletal remains, and by the tendency, especially in the case of carbonate fossils, for calcite overgrowth and recrystallization to obscure the morphology of the surface features. Further detail on extraction procedures can be found in De Vernal *et al.* (2010) and on identification in Armstrong & Brasier (2005).

4.10.7 Marine palaeoclimatology

The distributions of Foraminifera, Radiolaria, coccolithophores, dinoflagellates and marine diatoms are partly determined by nutrient requirements. The planktonic forms are all found in abundance in zones of upwelling, for example, or pronounced vertical mixing, where mineral nutrients are readily available. For this reason, large numbers of these micro-organisms are frequently encountered just seaward of the continental slope. In most cases, however, the fundamental determinant is water

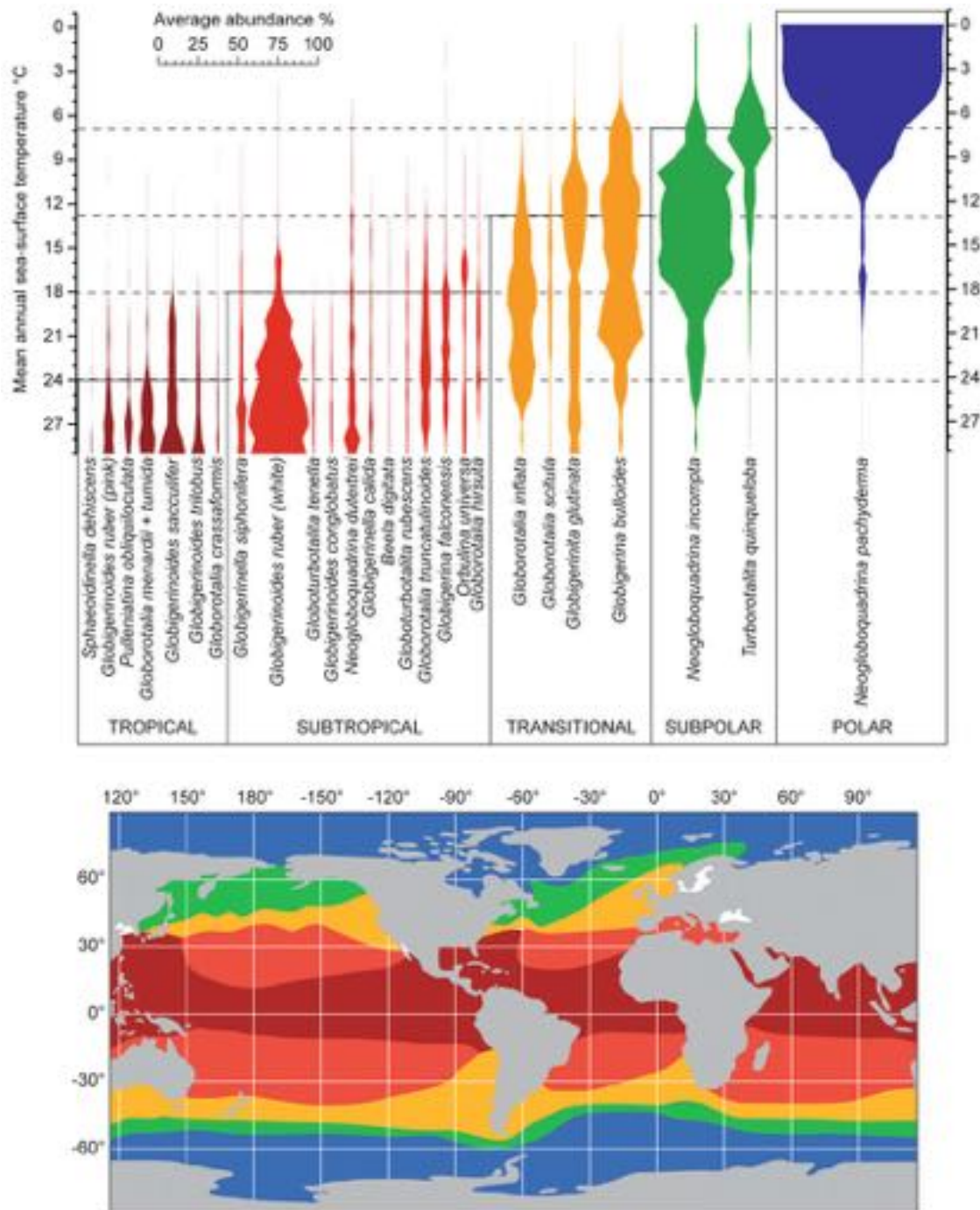


Figure 4.43 Planktonic foraminiferal provinces in the modern ocean showing the close relationship between sea-surface temperature gradients and species abundances. The species abundance plots (top) are averaged at 1°C intervals (from Kucera, 2007, reprinted with permission from Elsevier).

temperature, and detailed ecological studies have shown that many species are associated with water masses that possess distinctive thermal characteristics. From the present distribution of marine plankton, and allowing for current circulation and Coriolis effects, it is possible to recognize distinct equatorial, tropical, subarctic and arctic provinces (Figure 4.43). Hence, the analysis of marine microfossil assemblages can provide a unique source of information on ocean palaeotemperatures and, by implication, on former climatic conditions.

The initial approach to Quaternary temperature investigations using data from deep-ocean cores was based simply on the presence or absence of certain key species in fossil assemblages. Early work demonstrated that the abundance of the planktonic foraminiferal species *Globorotalia menardii* could be used to infer climatic change, an idea developed by David Ericson and his colleagues (e.g. Ericson & Wollin, 1968) to construct a series of palaeotemperature curves based on the abundance of *G. menardii* in sediments from the floors of the Caribbean and subtropical Atlantic. High percentages of *G. menardii* were interpreted as indicating warmer, possibly interglacial periods, while reduced frequencies reflected cold, glacial periods. In a series of influential papers during the 1970s, McIntyre *et al.* (1972), McIntyre & Ruddiman (1972) and Kellogg (1976) used selected planktonic faunal indicators, particularly the markedly polar foraminifer *Neogloboquadrina pachyderma*, along with the absence of coccolith remains at certain levels in cores from the North Atlantic, to record the migration of the North Atlantic Polar Front since the last interglacial. This important indicator

is a left-coiling species, whereas right-coiling species, e.g. *N. incompta*, favour warmer waters (Figure 4.44). Both the abundance of *N. pachyderma* and the ratio of left- to right-coiling *Neogloboquadrina* species are still widely employed in palaeoceanography as key palaeotemperature indicators (see Kucera, 2007).

Although this work provided valuable insights into Quaternary climatic changes, the foraminiferal assemblage evidence was not always easy to interpret. It has already been shown that only a small proportion of the planktonic ocean fauna and flora actually reaches the sea floor to enter the fossil record due largely to dissolution, a process that favours the preservation of cold-adapted species, since they tend to have more robust skeletal parts. The death assemblage in a body of ocean sediment, therefore, rarely reflects accurately the former living assemblage in the water column above. Indicator species associated with these biased death assemblages are therefore not always a reliable index of palaeotemperature change. Moreover, although temperatures are generally believed to be the major determinant in the distribution of planktonic fauna and flora, other factors need to be considered such as salinity variations, seasonal temperature fluctuations and food supply, and the prime factor may not be the same for all species in a given assemblage.

In an attempt to overcome this problem, Imbrie and Kipp (1971) developed a transfer function approach to derive palaeotemperature estimates from microfossil data which led to one of the important milestones in palaeoceanography and palaeoclimatology: the establishment of the CLIMAP research programme (see especially Cline & Hays, 1976). This generated a considerable body of data on the Quaternary history of the world's oceans and atmosphere, and laid the foundations for high-resolution palaeoceanographic reconstructions that form such an important component of contemporary Quaternary research (see Chapter 7). Within the North Atlantic, for example, where most of the late Quaternary palaeoceanographic investigations were initially concentrated, Ruddiman & McIntyre (1976) and Kellogg (1976) were able to reconstruct time-space variations in surface-water mass boundaries for the last 225 ka based on the occurrence of distinctive foraminiferal and coccolith assemblages in the deep-ocean cores (Figure 4.45). These water masses appear to have migrated across more than 20° of latitude (some 2,000 km) at rates of up to 200 m per year. From these data it would appear that glacial surface water temperatures in the area were up to 12.5°C lower in winter and 13.0°C lower in summer than at present, and within the last 600 ka alone, at least eleven separate prolonged southward movements of polar water occurred.

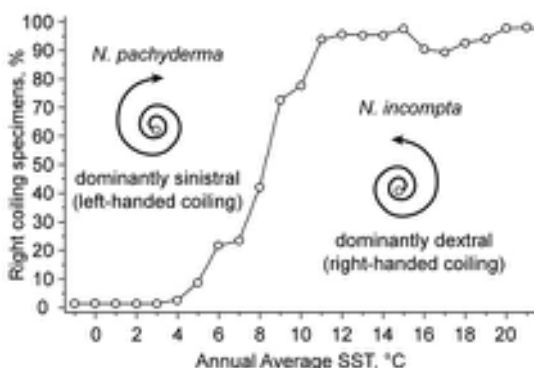


Figure 4.44 Changes in coiling direction of tests of the high-latitude species *Neogloboquadrina*. The proportion of right-coiling specimens increases markedly in surface waters with mean temperature of between 6 and 10°C, reflecting the replacement of *N. pachyderma*, which produces mainly sinistral tests, by the dextral-coiling *N. incompta* (modified from Kucera, 2007).

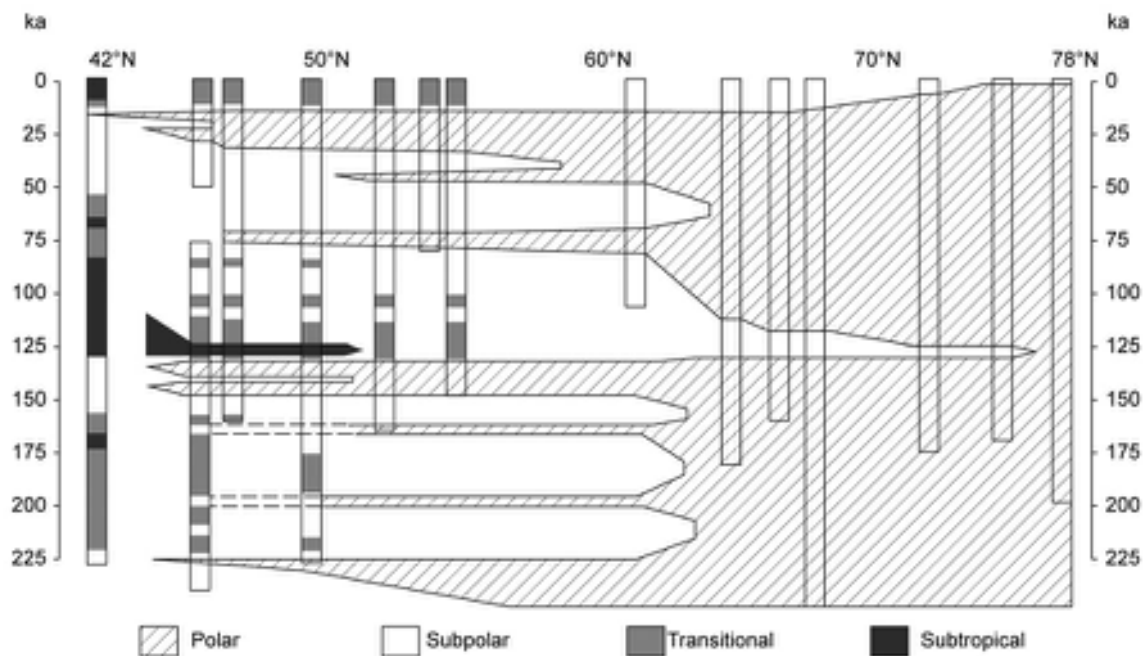


Figure 4.45 Changes in ecological water masses in the Norwegian Sea and the northern North Atlantic over the past 225 ka; the reconstruction is based on analysis of foraminiferal assemblages in a transect of marine sediment cores obtained from the sea bed (after McIntyre & Ruddiman, 1972).

The CLIMAP Project (1981) produced maps showing inferred sea-surface temperatures (SSTs) for the world's oceans at the Last Glacial Maximum (LGM, c. 18 k ^{14}C yr BP) compared with the present. Not only did these provide the first quantified model of the state of the oceans during full glacial conditions, but they also highlighted those parts of the oceans that experienced the largest temperature differences between the LGM and the present day, with the major change in the North Atlantic perhaps being the most distinctive feature. Such reconstructions provide essential **boundary conditions**⁹ for the development of global circulation models (GCMs) which aim to simulate past climatic changes at a global scale (section 7.2). For example, models of the global climate at 18 k ^{14}C yr BP developed by the COHMAP group employed the CLIMAP global SST reconstructions as boundary conditions for the ocean surface (COHMAP Members, 1988).

CLIMAP and COHMAP were landmark collaborative programmes that provided new insights into the way the global ocean-climate system operates. Since then, however, a marked increase in the number of published fossil marine records, a more detailed knowledge of the distribution and ecology of marine organisms, and refinements to

transfer function models have provided a basis for more sophisticated palaeoceanographical and palaeoclimatic reconstructions (Kucera, 2007). A significant methodological advance has been the development of SIMMAX, a modern analogue technique that uses similarity indices. CLIMAP employed a limited number of indicator species and hence could not accommodate the diversity of fossil assemblages commonly encountered in Quaternary oceanographical records. As a result, too many fossil samples deviated appreciably from any known modern assemblage ('non-analogue samples'), and hence could not be calibrated satisfactorily. SIMMAX is based on a more comprehensive species list with closer palaeoecological constraints (Pflaumann *et al.*, 1996). It is periodically updated and now underpins most palaeoclimatic reconstructions based on marine microfossil assemblages (e.g. Meland *et al.*, 2005; Kandiano *et al.*, 2012). SIMMAX results are often significantly different from those generated by CLIMAP: for example, the latter suggests that the Nordic Seas were permanently frozen during the LGM (Figure 4.46a), whereas seasonal ice-free conditions extending much further north are implied by SIMMAX data (Figure 4.46b). A further difference is the location of the strongest

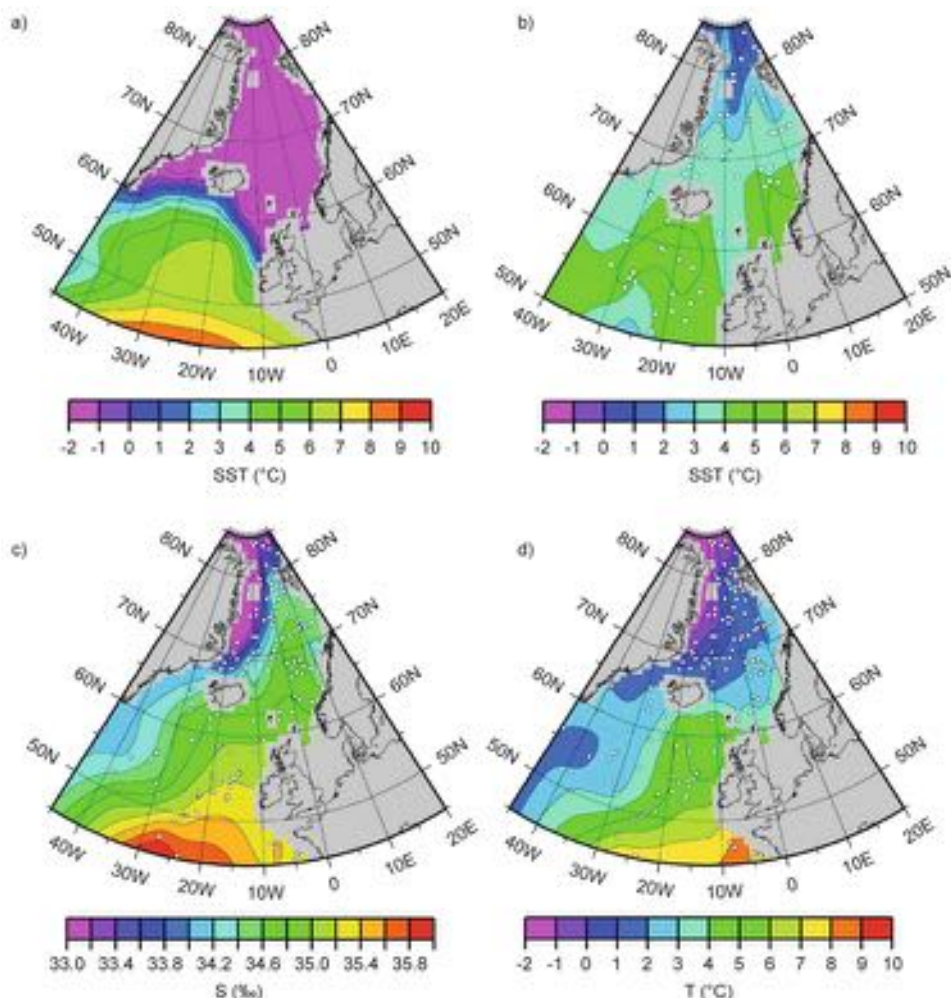


Figure 4.46 Reconstructions of surface conditions in the Northeast Atlantic during the Last Glacial Maximum (LGM) based on marine microfossil records. a) Summer SSTs based on CLIMAP (1981). b) Summer SSTs based on SIMMAX. c) and d) More detailed reconstructions for LGM salinities and SSTs based on a larger number of palaeo-data sites and calibrated using SIMMAX (from Meland *et al.*, 2005).

salinity and temperature gradients, which SIMMAX data place to the north, not south, of Iceland (Figure 4.46, b–d). Equally detailed palaeoceanographic reconstructions using SIMMAX have been generated for other marine sectors, such as the Mediterranean Sea (e.g. Hayes *et al.*, 2005), the Pacific Ocean (Chen *et al.*, 2005), and the Indian Ocean and Australian margin (Barrows & Juggins, 2005).

Marine palaeotemperature estimates have also been obtained from the chemical composition of planktonic foram tests (Katz *et al.*, 2010), the most widely used being Mg/Ca palaeothermometry (Barker *et al.*, 2005). The

Mg/Ca ratio in planktonic foram tests appears to be closely related to temperature at the time of carbonate secretion, an association confirmed by studies of living organisms recovered from sediment traps and by laboratory culture experiments (Anand *et al.*, 2003; Lea *et al.*, 1999), while many species show remarkably similar temperature responses (Figure 4.47). In addition, some species are restricted to narrow temperature ranges that accord with their habitat requirements, and this enables temperature differences and gradients through the water column to be reconstructed. Finally, the measurement of Mg/Ca ratios is a

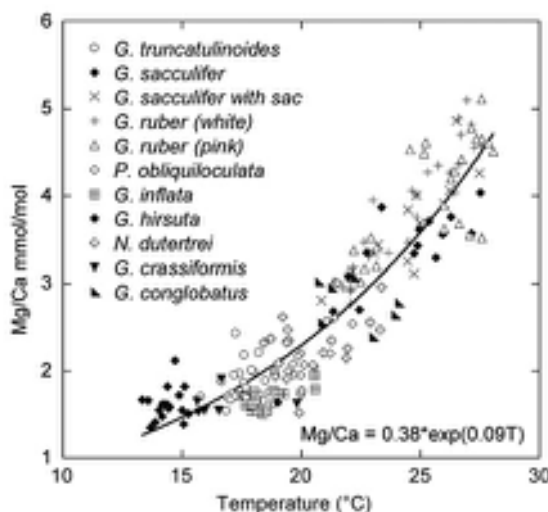


Figure 4.47 Mg/Ca calibration results for several species of planktonic Foraminifera. Temperatures shown are the isotopically derived calcification temperatures; the equation defines the correspondence between temperature and calcification ($r = 0.93$) (based on Anand *et al.*, 2003).

relatively rapid process and requires only small samples, enabling temperature estimates to be generated at a high temporal resolution (James & Austin, 2008).

Another approach to marine palaeoclimatology involves the measurement of long-chain carbon compounds (C_{37-39} ketones, or ‘alkenones’) preserved in microfossil remains, one of a number of trace organic derivatives (**biomarkers**) now employed in Quaternary palaeoenvironmental research (see section 4.12.6). The compound most commonly measured, the alkenone unsaturated U_{37}^k index, is biosynthesized by certain algae, including coccolithophores (Rosell-Melé & McClymont, 2007). This process is temperature-sensitive, and hence down-core variations in U_{37}^k abundance enable temperature fluctuations to be quantified. The method has generated highly resolved palaeotemperature records for the last glacial cycle that correlate closely with Greenland ice-core records (Figure 4.48); moreover, it appears to have application throughout the entire Quaternary period (Cacho *et al.*, 1999; McClymont & Rosell-Melé, 2005).

A range of palaeoclimate proxies is therefore now available to the Quaternary palaeoceanographer and, as is the case with other aspects of Quaternary research, multi-proxy datasets are being compared in order to test the degree of compatibility between different indices, and hence to generate more secure palaeoceanographical reconstructions. A good example is the MARGO

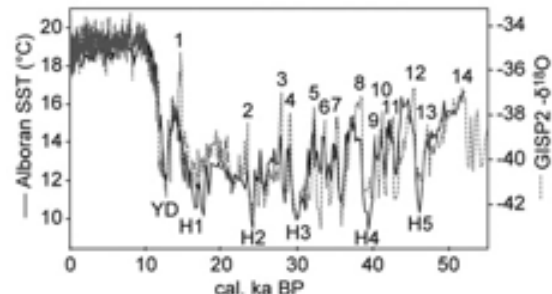


Figure 4.48 Rapid changes in SST in the Alboran Sea (Mediterranean Sea) over the past 50 ka, inferred from variations in U_{37}^k abundance, and correlation with Greenland ice-core events; note that marked declines in temperature in the Alboran Sea coincide with Heinrich Events and the Younger Dryas cold stage (from Cacho *et al.*, 1999).

initiative (Multiproxy Approach for the Reconstruction of the Glacial Ocean), which has synthesized and quality-tested all the available proxy palaeotemperature records in order to reconstruct the global ocean surface temperature pattern during the LGM (Kucera *et al.*, 2005b; MARGO Project Members, 2009). MARGO has provided a snapshot of ocean circulation at the time of maximum ice extent, and it has computed ocean surface temperature gradients that differ markedly from those in other climate model simulations. Similarly, the EPILOG project (Environment Processes of the Ice Age: Land, Ocean, Glaciers) has integrated surface temperature data for the LGM in the Southern Ocean, a sector that appears to have played a major role in past global climate change (Gersonde *et al.*, 2005). Collaborative programmes such as these represent the cutting edge in current palaeoceanographical research, providing important new insights into the ocean’s role in global climate behaviour (Chapter 7).

4.10.8 Marine palaeoproductivity and palaeocirculation

Just as the gyres, thermal stratification, major currents and climate fronts (water mass boundaries) of the contemporary oceans are determined by the prevailing circulation pattern, so too are the distribution of nutrients and the rate of exchange between the ocean and the atmosphere on the one hand, and between shallow and deep ocean water on the other. Changes in any of these parameters will be reflected in chemical changes in the water column and in ocean sediments. In addition to oxygen isotope signals (section 3.10), marine microfossils contain a record of former trace element variations in ocean water. This is a

powerful new tool in palaeoceanography, enabling past variations in circulation and productivity to be reconstructed, and related to changes in atmospheric gas content (Sigman & Boyle, 2000). A number of **chemical tracers** (often chemical ratios) are now widely employed (Elderfield, 2006). Some provide evidence of water mass and productivity changes, including Mg/Ca, Cd/Ca, Ba/Ca, Mn/Ca and Zn/Ca ratios, while others, such as ^{14}C content and $^{231}\text{Pa}/^{230}\text{Th}$ ratios, provide information on the pattern and rates of circulation (Lynch-Stieglitz *et al.*, 2007). Some tracers, such as isotopes of neodymium (Nd), are useful for detecting the mixing of water masses or significant influx of freshwater into the marine realm (Scrivner *et al.*, 2004). An important indicator of past variations in nutrient supply is phosphorus (P), a vital nutrient for all living organisms. Past variations in P concentration cannot, however, be measured directly, but are inferred from Cd/Ca ratios. Cd is preferentially taken up by planktonic forams during skeletal building, and because Cd/Ca ratios in foram tests are proportional to the amount of P in the ocean, they can be used as a proxy for nutrient (P) levels (Elderfield & Rickaby, 2000). Other marine water mass properties that can be inferred from chemical tracers in palaeoplankton include alkalinity, pH, degree of oxygenation and nutrient uptake (Henderson, 2002). Chemical tracers can be measured in deep-water benthic species and hence provide information on ocean circulation at depth, allowing inferences to be made about intermediate and deep-ocean properties and behaviour (Flower *et al.*, 2000; Rickaby and Elderfield, 2005). By analysing chemical tracer information for particular time-periods therefore, ocean density stratification and overall circulation can be inferred (Rogerson *et al.*, 2011), information that is key to understanding the role of oceans in the global climate system (Rahmstorf, 2002).

4.11 VERTEBRATE REMAINS

4.11.1 Introduction

Fossil animal bones and teeth, particularly those of large vertebrates, have long been an attraction for amateur collectors and, as a result, museums are full of the skeletal parts of Pleistocene mammals. Many of these remains were removed from exposures in cliffs and in river valleys towards the end of the last century by well-meaning Victorian enthusiasts who, unfortunately, often paid scant regard to the stratigraphic context within which they lay, or indeed to the less spectacular but equally important collecting of smaller animal remains which together formed the total assemblage of the stratum (Schreve, 2007). Thus,

although the fossil remains indicate that extinct animals such as the mammoth (*Mammuthus primigenius*), woolly rhinoceros (*Coelodonta antiquitatis*) and straight-tusked elephant (*Palaeoloxodon antiquus*) were to be found in many areas of the Northern Hemisphere during the Quaternary (Stuart, 2005), and also that creatures such as the hippopotamus (*Hippopotamus amphibius*) and musk-ox (*Ovibus moschatus*) formerly occupied ranges that are very different from those of their present-day counterparts, albeit at different times, until comparatively recently much less was known about the smaller vertebrates and their Quaternary distributions. In the last few decades, however, considerable progress has been made in understanding the spatial and temporal variations in both large and small animal populations during the Quaternary, and their relationships to environmental changes.

A range of vertebrate remains is found in Quaternary sediments. Occasionally hair, muscle and horn-sheaths are preserved, and, in exceptional locations such as the permafrost of arctic Siberia, tar pits and peat bogs, mummified carcasses have been found (Spencer *et al.*, 2003b; Fisher *et al.*, 2012). Other evidence of the former presence of animals includes nests and middens of rats, burrows, hyena dens, coprolites (droppings: section 3.8), bird pellets, diagnostic teeth marks by predators on other bones, ‘trace fossils’ (prints and tracks) and skincasts. Overall, however, it is teeth and bones (and, occasionally, antlers) that make up the majority of fossil vertebrate remains (Figure 4.49), and these form the principal focus of the following discussion.

4.11.2 The structure of teeth and bones

Teeth are structurally complex but in most mammals consist of three distinct substances of differing hardness: the hard brittle outer casing (**enamel**), the softer **dentine** of which the greater part of the tooth is composed, and **cement** which covers the dentine of the roots and occasionally the valleys and folds of the main tooth body. In the fossil, the enamel provides the most durable element except where burning has affected the original dental material, in which case the dentine of the tooth roots may prove to be the most resistant. Teeth are of considerable importance in palaeoenvironmental work for not only do they provide data on the age (years of life) of the animal, but they also give an indication of dietary preferences (i.e. herbivore or carnivore), while isotopic analysis can provide additional information on diet, habitat and climatic conditions (Kohn & McKay, 2012). In more recent sediments, teeth tend to be outnumbered by remains of bone, but in older Quaternary deposits, teeth are occasion-



Figure 4.49 a) Nigel Larkin cleaning the fossil right femur (length 145 cm) of a mammoth of Middle Pleistocene age discovered at the site of West Runton, Norfolk, UK (photograph by Nigel Larkin, Norfolk Museums & Archaeology Service, Norfolk, UK; from Larkin, 2010, reprinted with permission from Elsevier). b) Occlusal surface (top) and roots of the first lower molar of the ancestral water vole (*Mimomys savini*) recovered from sediments of early Middle Pleistocene age at Pakefield, Suffolk, UK. Variations in dentition enable fossil vole teeth to be assigned to species and the relative age of temperate stages to be inferred (section 5.5.4). Scale bar represents 1.0 mm (photograph by Harry Taylor & Simon Parfitt, Natural History Museum, London, UK; from Maul & Parfitt, 2010, reprinted with permission from Elsevier). c) Reconstruction of woolly mammoth (*Mammuthus primigenius*) based on soft tissue, skin, hair, parts of the intestines and delineation of toes recovered from one of the best preserved mammoth carcasses ever discovered, in Yakutia, arctic Siberia (reconstruction and photograph by Remie Bakker of Mammal Works & Dick Mol of the Natural History Museum, Rotterdam, Netherlands; from van Geel *et al.*, 2008, reprinted with permission of Elsevier; Lister & Bahn, 2009).

ally more strongly represented than elements of the postcranial skeleton (Dayan *et al.*, 2002).

Fresh animal bone consists of both organic material and inorganic material in the approximate ratio by weight of 30:70. The organic fraction is contained within the shafts of long bones (e.g. femurs, tibias and vertebrae) and comprises cell tissue (fats, etc.) and a fibrous protein called **collagen**. The collagen is very resistant to decay and may survive for thousands of years following the death of the animal, while the remaining organic matter undergoes autolysis¹⁰ after death and is rapidly decomposed. Surrounding the collagen fibre is bone mineral material, the principal component of which is a phosphate of calcium, **hydroxyapatite** ($\text{Ca}_{10}\text{OH}(\text{PO}_4)_6$). The structure and composition of animal bones are of considerable interest to the palaeoenvironmentalist as they affect the way in which fossilization takes place, and the chemical structure of bones in particular provides a means of dating the fossil material (see section 5.6.2).

4.11.3 Fossilization of bone material

Quaternary vertebrate remains have been recovered from a wide range of deposits. These include cave and fissure sediments, lacustrine and marine deposits, fluvial sediments (especially river terraces), peat bogs, soils and a variety of situations associated with human activities such as middens, cesspits and burial chambers. At some sites, whole skeletons have been found, but more frequently the fossil assemblages consist of disarticulated skeletons and a mixture of bones of varying sizes and in differing states of preservation. Animal bones are perhaps more vulnerable to physical and chemical changes than any other biological remains encountered in Quaternary deposits. They are highly susceptible to ‘weathering’ by a variety of processes, if exposed to oxidation, temperature extremes or chemical exchange with ground solutions. In some instances, the extent of weathering has been used to estimate duration of exposure of bone assemblages, but this is no longer considered to be a reliable approach, because bones degenerate differentially, even within the same site and sedimentary layer (Nielsen-Marsh & Hedges, 2000), and more sophisticated methodologies are needed to establish the diagenetic history of bones and teeth (Szostek, 2009).

As soon as a bone becomes incorporated into a body of sediment, it begins to undergo chemical changes that vary in nature and degree with the chemistry of the surrounding matrix. In most deposits where air is freely circulating, the mineral parts of bone will tend to be more resistant to decay, while the organic substances will break down rapidly into simple compounds such as ammonia, carbon dioxide

and water. Mineral salts in solution in the surrounding sediment, particularly calcium and iron, will be deposited in the vacant pore spaces and the bone may eventually become completely **permineralized**, and more resistant to further decay (Turner-Walker, 2008). This is one reason why mammalian remains tend to be well preserved in cave deposits in limestone regions. However, Quaternary fossil bones are often mechanically weak, because loss of structural collagen happens quickly, while the hardening process of mineralization is usually much slower; particular care is needed, therefore, during excavation and sample transfer, especially with large bones (Larkin, 2010; Figure 4.49a). In acid soils and peats, which are depleted in bases, both the organic and mineral fractions decompose quickly and the bone will disappear completely, leaving no trace of its former existence. Thus while prehistoric burials on chalklands in areas such as southern England have often yielded well-preserved bones, those in adjacent regions where porous, sandy soils are found contain few bone remains.

In waterlogged contexts, a completely different set of reactions occurs. In deep lakes in limestone regions where bases are abundant, bones are not only well preserved but are often extremely hard. In some cases, even the organic elements have been converted into a stable wax-like substance, composed of fatty acids, known as **adipocere** (Ubelaker & Zarenko, 2011). At the other extreme, in peat bogs or in oligotrophic lakes, the anaerobic nature of the depositional environment often results in the organic portions of the bones being preserved, while attack by humic acids leads to complete destruction of the mineral fraction. Skeletal remains will, therefore, be found in a soft or pulpy state in advanced stages of decalcification (Adams *et al.*, 2007).

Finally, there are the effects of burial on bone that are purely physical. The seasonal drying of clay soils, for example, will result in the fissuring and eventual destruction of even the strongest bones. Bones may be similarly shattered by frost-heaving and by the action of ground ice. Soil creep, solifluction and mechanical abrasion in river gravels will have similar damaging effects and will result in the progressive fragmentation of bone remains.

4.11.4 Field and laboratory techniques

Before any excavation of bone assemblages can take place, legal and ethical requirements must be considered, not only in the interests of conservation, but also because of the possibility that human remains form part of the assemblage. It should not be assumed that all the bones are ancient, while some sites have particular religious or cultural

importance and may be protected by legislation (Marquez-Grant & Fibiger, 2011). Appropriate permissions must be obtained in advance, and excavation protocols strictly followed.

Because bones can be found in such a variety of conditions, particular care must be exercised in the excavation of bone-bearing deposits. Mapping and surveying augmented by field description, sketches and photographs should precede the removal of bone fragments from the sediment matrix. In some cases, it may be possible to remove the larger bones by hand. These can be left to dry out and then cleaned with a brush or by gentle agitation in water. Large bones that are cohesive can be protected by encasing in plaster of Paris and hessian, prior to removal (Larkin, 2010). Many bone remains, however, even if heavily mineralized, are quite brittle and it may be necessary to treat these with a penetrative epoxy resin hardener before removal from the matrix can be attempted; this process is best preceded by anatomical examination of subsamples of the bones to establish the degree of decay (Jans *et al.*, 2002). If the bones are wet, resins or emulsions of lower viscosity may be needed in order for the strengthening material to penetrate deeply into the bone fibres (Smith, 2003). Bones that are so treated, however, cannot be used for subsequent chemical analysis or for radiocarbon dating. The presence of very small bones or teeth of **micro-vertebrates** (e.g. rodents) can usually only be detected by sieving the matrix following the removal of the larger faunal remains by hand, but all sample material needs to be examined for small bone fragments to reduce sampling bias (Stahl, 1996). The smaller specimens (< 2 mm in size) are identified under a binocular microscope (Maul & Parfitt, 2010).

Identification of bone remains is usually carried out in the laboratory and often proceeds in two stages. As most identifications are based upon fragmentary evidence, the first step is to identify the bone of which the fragment is a part. This is usually achieved by comparing the fragment with fresh skeletal material from a range of animals of different sizes. The second, and more difficult, stage is to track down the animal from which the unknown bone was derived. Here a reference collection of type material is essential, although the development of a type collection for the Quaternary vertebrates involves many more difficulties (and considerably more expense) than are encountered in the construction of a reference collection for Quaternary pollen grains or coleopteran remains. The Mammalia, for example, include a proportion of taxa that are now extinct, while evolution and speciation during the Quaternary pose additional complications. Moreover, few museums possess a reference collection that is suitable for identifi-

cation purposes. In spite of these difficulties, however, positive identifications of Quaternary vertebrate remains are steadily increasing and it is now proving possible to construct fairly detailed faunal lists for the major stages of the Quaternary (Kurtén, 2009; Currant & Jacobi, 2011). In addition, the palaeobiogeography and evolutionary trends in many groups of animals can now be reconstructed in detail, and are frequently accompanied (and enhanced) by DNA analysis (section 4.11.6.4).

4.11.5 The taphonomy of fossil vertebrate assemblages

The first stage in the interpretation of fossil bones and teeth is to establish how a particular grouping of vertebrate remains came to be associated together. The various factors that can influence the reconstruction of the living community that is represented in the fossil assemblage are reviewed by O'Connor (2005). Three different depositional environments will serve to demonstrate the complexities of fossil vertebrate assemblages.

4.11.5.1 Cave and fissure deposits

Some of the richest vertebrate assemblages in the world are those found in cave sediments, particularly in limestone regions, yet the ecological history of cave faunas is frequently very difficult to interpret because of the multiple origins of the fossil material (Jass & George, 2010). Some bones, for example, may have been washed into the caves or fissures by streamflow and are therefore allochthonous to the site (Figure 3.37). Caves were often occupied during the Quaternary by carnivores including cave bear (*Ursus*), wolf (*Canis lupus*), red fox (*Vulpes vulpes*), sabre-toothed cats (e.g. *Smilodon*) and spotted hyena (*Crocuta crocuta*), and hence many cave assemblages will be biased towards the prey of these animals. Small vertebrate remains could, for example, have been derived almost entirely from birds of prey, especially from pellets dropped by owls nesting in the cave roof, and could include either woodland or open-country rodents depending on the species involved (Marín-Arroyo *et al.*, 2009). Many of the large vertebrate bones will have been dragged into the cave by predators so that the resulting assemblage will give some indication of the original large vertebrate fauna of the vicinity. However, the cave assemblages will inevitably be biased towards the predators themselves as many would have eventually died in the caves and thus contributed their bones to the assemblage. This is particularly the case where caves acted as natural pitfall traps with animals having fallen in through holes in the cave roof (Kos, 2003), or where the

configuration of a cave opening allows animals to enter the cave but from which they were unable to escape. In both instances, the resulting bone assemblages will be partly biased towards scavenging animals, such as the hyena, which would have been attracted to the cave by dead and dying animals. Early humans may also have been attracted to such easy prey, and it is frequently difficult to distinguish their activities from those of other scavengers (Kuhn *et al.*, 2010). The difficulties of interpretation of vertebrate assemblages in cave sites are further exacerbated by the often complex stratigraphy of cave sediments (Figure 3.37; section 3.8).

4.11.5.2 Lacustrine sediments

Lake sediments often contain whole or partial skeletons of mammals, amphibians and fish. Remains of large mammals such as elk (*Alces alces*), reindeer (*Rangifer tarandus*) and mammoths (e.g. *Mammuthus primigenius*) found in lake deposits probably represent animals that died either by drowning after breaking through thin ice, or after having become trapped in the soft mud on the lake floors in their efforts to drink, wallow or feed (Lister, 2009). Often the adjacent sediments will have been disturbed by the struggles of the animal to become free. Many human occupation sites, such as the early Mesolithic hunting settlement at Star Carr in Yorkshire, were by lakes and rivers and therefore a proportion of the remains of animals that were hunted also found their way into the lake (Milner *et al.*, 2011). Fish and amphibians clearly reflect the former presence of these animals in the lake waters, but again humans may have been responsible for the concentration of faunal remains in the littoral sediments.

4.11.5.3 Fluvial sediments

The origins of vertebrate remains in river sediments can be almost as diverse as those found in cave deposits, and the assemblages may include the bones of a wide variety of species, particularly if deposited by rivers with large catchments (Rogers *et al.*, 2007). Large vertebrate remains become incorporated in riverine deposits in similar ways to those outlined above for lacustrine contexts, though allochthonous material is common because corpses can float downstream. From an analysis of the assemblage, it may be possible to gain some impression of relative population densities, of the lifespan of particular taxa, and of the distance of their habitats from the site of deposition (Faith *et al.*, 2009). Fish and amphibian remains will be locally derived and will tend to be over-represented in the assemblage. The small animal remains

are, however, more difficult to interpret. Some may be the remains of waterside creatures such as voles and rats, while others may have been delivered to stream banks or the water directly by carnivore droppings or by predator birds (Louchart *et al.*, 2009). Bird remains, however, are seldom preserved in lacustrine or fluvial deposits due to the extreme fragility and buoyancy of their bones; as a consequence the Quaternary history of the avian fauna is still poorly understood.

A further difficulty in the interpretation of animal remains from fluvial deposits is that the assemblages are frequently biased as a result of hydraulic sorting. Fluvial transportation, particularly during floods, leads to selective fragmentation or removal of bones according to size and state of fragility, a process that tends to be more common in open channels where stream power is high and bed material coarser ([channel-lag assemblages](#)) than in overbank or meander beds ([channel-fill assemblages](#)) (Behrensmeyer, 1988), and careful analysis of both the bones and their host sediment is needed in order to gauge the possible effects of hydraulic sorting (Price & Webb, 2006). An additional complication is that vertebrate remains of different ages may be incorporated into the sediments as the river banks are eroded. Because similar (but not necessarily identical) animal populations existed during successive warm and cold stages of the Quaternary, the likelihood of erroneous ecological interpretations from mixed bone assemblages is very real, and care needs to be taken to establish the degree to which the mix of skeletal remains is contemporaneous (Lewis *et al.*, 2006). Sometimes it may be possible to recognize bones of different ages on the basis of varying degrees of physical deterioration. Alternatively, relative ages of bones may be established by chemical means, for example by the use of amino-acid ratios (section 5.6.1) or of the fluorine, uranium or nitrogen content of bones (section 5.6.2), although in some cases direct dating using the U-series method may be possible (section 5.3.4).

4.11.6 Quaternary vertebrate records

The record of Quaternary vertebrates in both space and time is extremely patchy, for fossil bone assemblages, particularly those of large mammals, tend to accumulate episodically. In river terrace deposits, for example, they are often found in channel fills that were quickly abandoned because rivers change course (Bridgland & Schreve, 2009), while in caves, intermittent occupancy by predators or humans, flooding of cave passages and collapse of roofs and walls means that cave bone assemblages are commonly discontinuous. In addition, vertebrate species have

experienced marked and recurrent shifts in territorial range in response to Quaternary environmental and climatic changes, and many have been characterized by a degree of biogeographical, and in some cases evolutionary, change. In this section we consider these different aspects of the Quaternary vertebrate record, but we begin with vertebrate biostratigraphy, as this provides the foundation on which the other studies depend.

4.11.6.1 Vertebrate biostratigraphy

Analyses of Quaternary vertebrate assemblages have enabled Quaternary **stratigraphic ranges** (appearance and extinction dates) to be established for many vertebrate species in Europe (Kurtén, 2009; Currant & Jacobi, 2011), North America (Webb *et al.*, 2003b), Africa (Werdelin & Lewis, 2005) and South America (Prevosti *et al.*, 2009). The stratigraphic ranges of individual vertebrates and of vertebrate assemblages have proved to be of particular value in distinguishing between interglacial deposits of different ages in fluvial records (Schreve, 2007). In the lower Thames Valley, for example, diagnostic vertebrate assemblages in terrace sequences enabled a detailed biostratigraphy for the interglacials of the Middle Pleistocene to be established (Figure 5.44), and this could be used to correlate these fluvial records with those from central Germany (Bridgland *et al.*, 2004). Although the majority of such studies have tended to focus on large mammals, first appearance and extinction evidence has also been obtained for a number of small mammal species, from which distinctive faunal assemblages or ‘provinces’ (also termed ‘guilds’) have been identified, and which are diagnostic of particular Quaternary intervals. For example, Cuénca-Bescós *et al.* (2010) have shown that the stratigraphic record of the last 1.5 Ma in Spain is characterized by seven distinct provinces defined by changes in the fossil assemblages of small mammals, while Markova (2005) subdivided the stratigraphic record of the last 1 Ma in Russia using fossil rodent remains. In other cases, a combination of small and large vertebrate data have been used as biostratigraphic indicators as, for example, in the differentiation between MIS 9 and MIS 11 interglacial stages in fluvial deposits from Essex, eastern England (Roe *et al.*, 2009). In addition to being diagnostic fossils of particular time intervals, some vertebrates have been employed as biomarkers in stratigraphic sequences, most notably the evolutionary transition from *Arvicola* to *Mimonyx* in the vole lineage, which forms an important marker horizon within Cromerian (Middle Pleistocene) deposits in western Europe, and which is discussed further in section 5.5.4.

4.11.6.2 Vertebrate biogeography

Correlation of vertebrate stratigraphic records also enables the **geographical ranges** of individual species to be reconstructed, and the ways in which these have changed in response to climatic and other environmental influences. These range shifts were especially marked in the high latitudes with the successive advances and retreats of the great continental ice sheets, and the corresponding latitudinal shifts in the permafrost zone. Although much remains to be learnt about the consequent changes in faunal population dynamics (Lyons, 2005), it is clear that many large mammals, particularly carnivores, had more extensive distributions in the past than they do today (Hofreiter & Stewart, 2009). The cave lion (*Panthera spelaea*), for example, was widespread in northern Eurasia and the Yukon–Alaska region during the late Pleistocene, but became extinct at the end of the last cold stage, allowing the modern lion (*Panthera leo*) to expand into some of its former territory during the Holocene (Stuart & Lister, 2011). The European spotted hyena (*Crocuta crocuta*) was common throughout Europe (Figure 4.50) until the end of the last cold stage, when it contracted in range and is now confined to Africa (Varela *et al.*, 2010). It appears that larger-bodied vertebrates were able to expand their ranges more readily and over greater distances than smaller-bodied species, perhaps because the former had better dispersal abilities and were less inhibited by physical barriers (Lyons *et al.*, 2010).

The Quaternary fossil vertebrate record shows how many mammals adapted to changing habitats during the Quaternary, some to exploit new niches that arose as global climate cooled, while others became more flexible in their

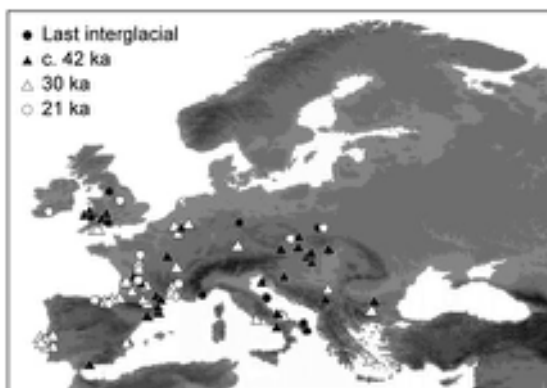


Figure 4.50 Age estimates of Pleistocene records of the spotted hyena (now confined to Africa) in Europe (from Varela *et al.*, 2010).

requirements and were able to exploit a range of different habitats (Lister, 2004). Also apparent from the fossil record is the gradual decline, from the early Pleistocene onwards, in the importance of solitary carnivore hunters. By the middle Pleistocene, these had become increasingly outnumbered by larger, more social predators such as *Panthera leo*, *Crocuta crocuta* and *Canis lupus*, perhaps reflecting the expansion of grasslands that supported large herbivores (Croitor & Brigal, 2010).

One feature of the Quaternary vertebrate record is evidence for changes in animal morphology, particularly in isolated populations. It has long been known that when animals become isolated for long periods of time they can change size: some small mammals grow progressively larger (**gigantism**) while others become smaller (**dwarfism**). The Quaternary fossil vertebrate record contains many instances of such changes, including the skeletal remains of ‘pygmy’ hippopotami and elephants (Figure 4.51) as well as giant rodents (Millien *et al.*, 2006). In the case of predator–prey dynamics, it has been suggested that there is a reduction in the size of large predators if the size or number of prey declines, whereas small animals become larger when isolated from their natural predators (Raia & Meiri, 2006). Of particular interest are islands, where a marked change in body mass, reduced species diversity and accelerated evolution in animal communities is such a recurrent phenomenon that it has come to be known as ‘**the island rule**’ (van der Geer *et al.*, 2010). Indeed, this rule may also apply to hominids, for on the island of Flores, Indonesia, the skeletal remains of a dwarfed hominid species (*Homo floresiensis*) have been found in association with bones of other animals showing signs of either dwarfism or gigantism, and are believed to be the result of isolation sometime between 90 and 17 ka (Van den Bergh *et al.*, 2009). In these and other instances, evolutionary change

appears to have occurred spontaneously when species competition and population dynamics have been altered. But there are examples where the island rule has not applied consistently, as in the vertebrate record from Santa Rosa Island, California, where a pygmy mammoth, *Mammuthus exilis*, seems to have coexisted with the much larger *M. columbi* (Figure 4.51) between c. 200 and 11 ka (Agenbroad, 2012). Much clearly remains to be learned about morphological changes in both current and historical isolated animal populations, and the Quaternary vertebrate record is an important source of evidence in these lines of enquiry into faunal biogeography.

4.11.6.3 Vertebrate fossils and Quaternary environments

It has long been assumed that there is a close link between Quaternary vertebrates and prevailing climatic regime (Blois & Hadly, 2009). In low-latitude regions, vertebrate records tend not to reflect major thermal changes between glacial and interglacial episodes, but rather longer-term trends related mainly to precipitation. In central Queensland, Australia, for example, contrasting mammalian assemblages indicate that tropical rainforests were present throughout the early and middle Pleistocene (until c. 280 ka), after which there was a switch to the arid regime that characterizes the region today (Hocknull *et al.*, 2007). In the Turkana Basin, east Africa, vertebrate records indicate that a savannah regime persisted in that region for almost the whole of the Quaternary, whereas rainforest and deciduous woodland had characterized the earlier Pliocene period (Fernández & Vrba, 2006). In the Pampas region of South America, the modern wet subtropical fauna was established as recently as 1.5–1 ka, prior to which conditions were drier, especially during the Last Glacial Maximum when the area was largely a cold desert (Tonni *et al.*, 1999).

In higher latitudes, however, vertebrate faunal assemblages are more reflective of contrasting thermal conditions of interglacial and glacial episodes (Lister, 2004), although the relationships between faunal assemblages and prevailing climate have not been quantified to the same degree as for other biological proxies discussed earlier in this chapter. Traditionally, the indicator species approach has been used to derive palaeoclimatic information from fossil vertebrate records. During the last interglacial, for example, hippopotamus (*Hippopotamus amphibius*), the pond tortoise (*Emys orbicularis*) and the lesser white-toothed shrew (*Crocidura cf. suaveolens*) were all found in southern Britain. The hippopotamus is now confined to tropical Africa, the pond tortoise is now found only in the

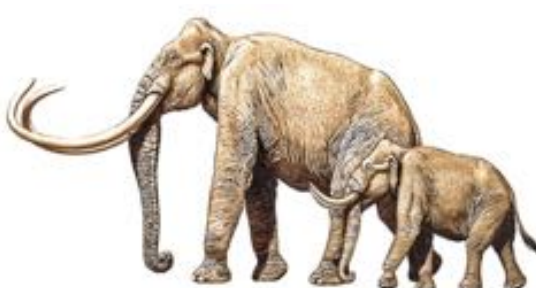


Figure 4.51 Reconstructions, based on skeletal remains, of the large (*Mammuthus columbi*) and pygmy (*M. exilis*) mammoth species that co-inhabited Santa Rosa Island, California between c. 200 and 11 ka (from Agenbroad, 2012, reprinted with permission of Elsevier).

Mediterranean and in southeast Europe with its northern breeding range apparently limited by the 18°C July isotherm, while the lesser white-toothed shrew is also essentially southern European in its distribution. These data are, therefore, strongly suggestive of warmer summers and milder winters in the British Isles during the Last (Ipswichian) Interglacial by comparison with the present day, a hypothesis supported by both palynological and coleopteran evidence (Stuart, 1979).

More recent studies have attempted to derive quantified climatic envelopes for groups of vertebrate species with common thermal preferences. For example, Fernández (2006) applied modern bioclimatic limits for rodent species to fossil rodent assemblages in order to reconstruct temperature variations in continental Europe over the last interglacial–glacial cycle. Polly & Eronen (2011) used an approach similar to the MCR method described above (section 4.5.4.2) to construct **ecological niche models** for groups of vertebrate animals typical of cold (*Alopex lagopus*, *Lemmus lemmus*, *Ovibos moschatus* and *Rangifer tarandus*), warm (*Crocuta crocuta*, *Panthera leo* and *Hippopotamus amphibius*) and temperate climates (*Arvicola terrestris*, *Cervus elaphus* and *Sus scrofa*). Application of these models to British fossil vertebrate records generated maximum probability temperatures that accorded with independent estimates based on other proxies, and particularly on beetle MCR data. However, a straightforward relationship between animal distribution and climatic parameters cannot always be assumed for, as pointed out by Frederick Zeuner in 1959, the primary adaptation of many vertebrates during the Quaternary may well have been to vegetation and only secondarily to climate. In the fifty years since Zeuner made that observation, a number of other problems have emerged. For example, from an analysis of the fossil mammal record of the United States, Graham *et al.* (1996) concluded that climatic change could not by itself explain the changing distributions of mammals during the late Quaternary, and that other factors, such as habitat change, species interactions and stochastic events must also have been involved. A further difficulty is that it now seems that many fossil vertebrate assemblages have no modern analogues, which clearly creates a problem in using modern bioclimatic data to infer past climatic conditions (Hofreiter & Stewart, 2009). This problem has been thrown sharply into focus by recent work on animal refugia during the Quaternary. The traditional view has been that in Eurasia and North America, temperate-adapted vertebrates were confined to shared southern refugia during glacial periods and cold-adapted fauna to northern refugia during interglacials. The vertebrate fossil record shows, however, that species responded individually to rapid environmental

change, some in scattered cryptic refugia. As we saw earlier (section 4.4.6.2), these are refugia that are situated at different latitudes or longitudes than would normally be expected, and often resemble climatic islands in which conditions differ, often favourably, from the surrounding areas. The manner by which animal communities were subsequently reassembled depended on complex population interactions and perhaps an element of serendipity (Stewart *et al.*, 2010). As a result of this continuous mixing and renewal of faunal associations during successive glacial–interglacial cycles, non-analogue species combinations may have been the rule rather than exception, the degree of divergence between ancient and modern faunal groups seemingly increasing with the age of the assemblage (Stewart, 2009).

A further constraint on the use of modern bioclimatic data as a basis for inferring past environmental conditions is the degree to which humans have affected animal populations and distributions during the late Quaternary, either through hunting or domestication, the latter being accompanied by accelerated genetic modification (Bar-Oz & Nadel, 2013). Humans have been implicated in the **mass extinction** of large mammals between c. 50 and 7 ka, when more than 178 of the world's largest mammals disappeared. In North America, for example, some thirty-five genera (more than seventy species) became extinct between 13 and 11 ka (Faith & Surovell, 2009). Many small mammals also disappeared at around the same time (Blois *et al.*, 2010), but it is the fate of the larger animals that has attracted most attention. The peopling of the Americas appears to have occurred shortly before this extinction event (Davidson, 2013), but the demise of the mammals also coincided with the climatic warming at the Pleistocene–Holocene transition, and the debate continues as to which of these factors was primarily responsible for the disappearance of large numbers of the megafauna from the American landscape (Haynes, 2009). In northern Eurasia, megafaunal extinctions seem to have begun earlier, at around 50 ka, close to the time of the arrival of anatomically modern humans, who brought superior hunting tools and skills, but again this was also a time of rapid environmental change, with the major climate shifts associated with the Dansgaard–Oeschger cycles (section 3.11.4). As in North America, there appears to have been a further wave of extinctions around the time of rapid warming at the onset of the Lateglacial at c. 14.7 ka (Stuart & Lister, 2012). In the Australia–New Guinea region, about sixty megafaunal species disappeared during the Middle to Late Pleistocene, which some have linked to the arrival of humans, perhaps from c. 60 ka onwards, although here too a climatic influence cannot be excluded (Field *et al.*, 2008). That said, however, it is clear

from the fossil record that extinctions on this scale did not occur earlier in the Quaternary at similar times of marked climate change and, moreover, that the selective disappearance of large mammals is unusual, both of which would tend to favour human agency and lend support to the '[overkill hypothesis](#)' which attributes the mass extinctions to the indiscriminate slaughter of animal herds (Koch & Barnosky, 2006). The consensus view, however, is that a combination of these two factors may have been responsible, with abrupt climatic changes reducing and scattering the large mammal populations, before the development of human hunting technology tipped the balance towards extinction (Haynes, 2013). Other theories of the cause of extinctions involving, for example, transmission of pathogens and spread of disease by humans or animals (e.g. dogs) travelling with them (Fiedel, 2005), or the environmental effects (e.g. wildfires) of a cometary impact (Firestone *et al.*, 2007), have proved more controversial and have not gained widespread support (Boslough *et al.*, 2012).

4.11.6.4 Vertebrate fossils and faunal evolution

The frequent climatic and environmental changes that characterized the Quaternary appear to have resulted in accelerated rates of morphological adaptation, and to a degree of evolution, certainly when compared with preceding geological periods. This is reflected in calculations of '[turnover rate](#)' (the sum of first and last appearances of species during a geological interval, divided by the total number of species recorded for that interval), and estimates for the Quaternary are very much higher than for comparable time spans during the Neogene. Remarkably, nearly all the mammal species present in Europe at the start of the Quaternary have now disappeared, while none of the present-day mammal species were present at around 2.5 Ma (Lister, 2004). DNA analysis has certainly shown that genetic diversity changed more often, and in unpredictable ways, during the Quaternary, much more so than had been anticipated from previous studies of bone assemblages (Hofreiter & Stewart, 2009).

In considering adaptation of animals to environment, a distinction needs to be made between short-term changes in animal traits (e.g. body shape, skin colour and markings), which is termed [phenotypic plasticity](#) (a phenotype is the sum of all the traits that make up the physical appearance of an individual organism), and [genetic modification](#), which is a much longer process that results in irreversible changes that lead to speciation. Data from Quaternary mammals provide evidence of the rate and manner in which these processes take place. For example, there has

been an assumption, seemingly initially confirmed by DNA analysis (Lindqvist *et al.*, 2010), that the polar bear (*Ursus maritimus*) is a relatively recent evolution from the brown bear (*U. arctos*), though more recent DNA results suggest that the polar bear is a much older and distinct bear lineage that evolved during the Middle Pleistocene (c. 600 ka: Hailer *et al.*, 2012), or maybe even earlier (Miller *et al.*, 2013).

DNA analysis is also proving to be important in vertebrate [phylogeography](#), i.e. the study of how the modern distributions of different animals evolved, which has provided new insights into animal history and behaviour, including the identification and locations of key animal refugia and colonization routes (Hewitt, 2011). In North America, for example, DNA analysis of fossils of the woodland caribou (*Rangifer tarandus caribou*) indicates that this animal withdrew during the last glacial stage to three geographically discrete refugia: in the Rocky Mountains, east of the Mississippi and the Appalachian Mountains (Klütsch *et al.*, 2012). The present phylogeography of this animal comprises three genetic lineages that reveal a pattern of expansion from these refugia after the wastage of the Late Wisconsinan ice sheet. Miller *et al.*'s (2013) study of polar bears (see above), suggests that these probably came into contact and interbred with brown bears during interglacial stages at times when their territories overlapped; hence, although polar bears are now exclusively Arctic animals, they must have been sufficiently adaptable throughout the Quaternary to cope with a long series of climatic fluctuations. In Europe, DNA analyses of fossil remains of the collared lemming (*Dicrostonyx torquatus*) indicate that this animal was driven to extinction on numerous occasions as a result of climatic fluctuations and, since this small mammal is an important prey species, this must have impacted on the wider steppe–tundra animal community (Brace *et al.*, 2012). This process of episodic extinction and regeneration led to a significant loss of genetic diversity in collared lemmings, a trend that is also noted in a number of other vertebrate species during the late Quaternary (Hofreiter & Barnes, 2010; Barnosky *et al.*, 2011).

These various studies attest to the dynamic nature of phenotypic and phylogenetic interchange during the Quaternary, and it seems clear that Quaternary climate oscillations had a marked effect on the gene pools and phenotypic adaptability of vertebrate animals (Stewart, 2009). As noted in Chapter 1, Milankovitch-driven climatic oscillations became more pronounced after the mid-Pleistocene Revolution, in turn forcing the biota to respond. This may have militated against specialization in species, leading instead to the development of animal guilds that

were more adaptable, had larger territorial ranges and were able to disperse quickly. This evolutionary trend, a product of serial environmental upheaval, has been termed ‘orbitally forced species range dynamics’ (Dynesius & Jansson, 2000). Over shorter timescales, the question arises as to how animals coped with the rapid climatic and environmental changes that occurred during, for example, the last glacial stage and where temperature fluctuations of several degrees Celsius occurred in a matter of decades (section 3.1.4). The possible phylogenetic effects that may have resulted from these changes are only now beginning to attract the attention of geneticists and evolutionary biologists (e.g. Hof *et al.*, 2011).

4.12 OTHER FOSSIL GROUPS

4.12.1 Chrysophytes

Chrysophytes are a group of planktonic ('golden') algae that produce resting cysts (**stomatocysts** or **statospores**) during their life cycle, while a subset are also covered by siliceous scales ('scaled chrysophytes'). As siliceous organisms, chrysophyte cysts and scales are commonly found in association with diatoms, and are frequently analysed together. Chrysophyte remains are deposited in great abundance and preserve well in sediments, while the majority can be identified to species level. Since most are sensitive to a range of environmental variables, including pH, lake chemistry, nutrient status and metal concentration, they have been widely employed in palaeolimnology (Zeeb & Smol, 2001), but they can also be useful palaeoclimatic indicators. In Alpine lakes, for example, variations in stomatocyst assemblages have been found to co-vary with the time of spring thaw (Kamenik & Schmidt, 2005), while in lakes in southwest Greenland, they show a strong relationship with longitudinal temperature gradients (Pla & Anderson, 2005). They also appear to be influenced by seasonal changes in lake temperature (Pla-Rabes & Catalan, 2011), and constitute one of the few biological proxies that provide a basis for reconstructing former winter temperatures (De Jong & Kamenik, 2011). In addition they are proving to be a key proxy for monitoring the response of lake systems to recent global warming (e.g. Moos *et al.*, 2009).

4.12.2 Cladocera

Cladocera are small invertebrate crustaceans, commonly called 'water fleas', the chitinous exoskeletons of which are often abundant in lake sediments. Although they are an important component of freshwater ecosystems, they have

been less well studied than other lake biota (Eggermont & Martens, 2011). They mainly occupy the littoral zones of lakes and ponds, though a number of species are planktonic and occur in open water, but skeletal fragments of both forms accumulate in the deeper parts of lakes. They have been most widely used as indicators of past changes in lake level, because cladoceran assemblages and the ratio of planktonic to littoral cladoceran species vary with water depth (Nevalainen *et al.*, 2011). Their potential as palaeoclimatic indicators is less clear, however. For example, Kattel *et al.* (2008) developed a Cladocera-based temperature transfer function for small lakes in Scotland, but found that inferring a relationship between cladoceran assemblages and climate was complicated by other environmental factors. A similar problem was encountered in Canadian Arctic lakes, where the response of Cladocera to recent global warming appears more muted compared with that of diatoms (Sweetman *et al.*, 2008). These and other studies seem to suggest that the climatic signal in fossil cladoceran assemblages may be masked by the influence of additional ecological variables, including trophic state, water depth and habitat availability (Eggermont & Martens, 2011).

4.12.3 Coral polyps

Coral reefs are formed by a number of interlocking elements, including autochthonous and allochthonous remains of animals and plants, clastic sediment and chemical alteration processes (Montaggioni & Braithwaite, 2009). The main 'builders', however, are **coral polyp** colonies that are normally long-lived, spanning hundreds to thousands of years. Together with the other elements mentioned above, they produce massive calcareous structures close to mean sea level. Growth rates of about 10–30 mm yr⁻¹ are common. Gradual changes in sea level have enabled reefs to build vertically, maintaining their shallow-water habitat over time, and thus provide important records of sea-level variations (section 2.5). As the reef grows, the growth rates and chemical composition of coral are affected by the physical and chemical condition of the surrounding seawater as well as by biological factors, and a record of variations in these influences is therefore contained within the coral structure. The most important parameters governing rate of reef growth appear to be water temperature and water depth. Since these vary seasonally, many species of coral produce seasonal growth bands with clear density differences that are visible by X-radiography or fluorescence techniques (Lough & Cooper, 2011). The rapid growth and annual banding of coral provide a basis for palaeoenvironmental

reconstruction at high temporal resolution, potentially as detailed as records based upon tree rings (section 5.4.1). Moreover, a number of chemical indices can be used in conjunction with ‘coral stratigraphy’ as a basis for palaeoenvironmental reconstructions. The most widely employed are stable isotopic composition (mainly oxygen and carbon) and trace element composition, such as barium/calcium (Ba/Ca) and strontium/calcium (Sr/Ca) ratios. While a number of environmental variables can affect these ratios, the principal controlling factor appears to be variations in SST, which can be measured on seasonal to millennial timescales (Corrège, 2006). A global compilation of coral $\delta^{18}\text{O}$ records shows temporal trends dominated by El Niño Southern Oscillation (ENSO) variability (section 7.6.4.2), in terms of both long-term freshening of the oceans and decadal- to seasonal-scale SST fluctuations (Grottoli & Eakin, 2007). Coral stratigraphic records also provide the long-term historical context for assessing the scale of ecological problems affecting modern reefs, such as coral ‘bleaching’ (Baker *et al.*, 2008a).

4.12.4 Fungal remains

Fungal remains, especially hyphae and fruiting structures (which resemble spores), are very common in Quaternary deposits, and are often encountered during routine pollen analysis. They are especially common in lake sediments and peats. The fossil components are difficult to classify, even to genus level, although systematic recording and classification of the most common types found in late Quaternary deposits have led to the identification of key ‘marker’ fossils (e.g. Van Geel & Aptroot, 2006). Fungal remains appear to offer considerable potential for Quaternary palaeoenvironmental reconstruction. For example, the identification in a sediment profile of saprophytic fungi known to invade peats and organic lake sediments during phases of desiccation could provide evidence of previous drier episodes (Yeloff *et al.*, 2007). Episodes of catchment erosion may be reflected in lake sediment records by high numbers of spores of fungi associated with disturbed ground (Kramer *et al.*, 2010). Phases of natural or human-induced burning can be inferred from the presence of **pyrophilous fungi**, species that appear after plant communities have been destroyed by fire (Riera *et al.*, 2006). Parasitic fungi associated with crop plants, for example those that cause rust disease, have been used to reconstruct past farming practices of indigenous peoples and European settlers in Canada (McAndrews & Turton, 2010). The most widely employed, however, have been **coprophilous** (dung-loving) fungi, some of which are indicative of the dung of pastoral animals. These have

been used in studies of past agricultural activity, as in Norse Greenland during the early Middle Ages (Gauthier *et al.*, 2010), and in the Pyrenees Mountains where fluctuations in grazing pressure over the last two millennia were inferred from coprophilous fungal assemblages (Cugny *et al.*, 2010). Others are associated with the dung of wild animals. For example, ascospores of three types of coprophilous fungi, *Sordaria*, *Sporormiella* and *Podospora*, are often found together in Quaternary records, where they are indicative of the dung of large herbivores, such as mammoth (Van Geel *et al.*, 2007). Their importance in palaeoenvironmental reconstruction is reflected in the work of Gill *et al.* (2009), who found a marked decline in influx of *Sporormiella* spores in sites in North America around 14.8–11.3 ka, and which provides further evidence of the late Pleistocene megafaunal collapse (section 4.11.6.3). Finally, the unique insight that fungal spores can provide into Quaternary palaeoecology is demonstrated by the contents of the lower intestine of a preserved mammoth carcass from Siberia, which contained fruit-bodies of coprophilous fungi that require at least one week of exposure to air for germination, suggesting that the last meal of this particular mammoth must have included some dung (Van Geel *et al.*, 2008)!

4.12.5 Testate amoebae

As we saw in Chapter 3 (section 3.9.4.1), **testate amoebae** are a large and diverse group of Protozoa, classified together with Foraminifera in the taxonomic superclass Rhizopoda. Unlike forams, however, the amoebae are found predominantly in lakes and ponds, rivers, mire deposits and wet soils, though a few inhabit estuaries. Some amoebae have thin shells, or tests, that they build through secretion or the agglutination of organic or mineral particles to protect the cytoplasm (section 4.9), and it is the shells of these **testate amoebae** (occasionally referred to as ‘testaceans’ or ‘thecamoebians’, or imprecisely as ‘Rhizopods’) that are preserved in sediments (Charman *et al.*, 2000). They are morphologically distinctive, permitting identification to species level.

Testate amoebae have proved to be valuable palaeoecological indicators in a range of palaeoenvironmental contexts (Charman, 2001). They are particularly sensitive to variations in water table depth, a relationship that has again been quantified using transfer functions. Applying these to data from ombrotrophic peat bogs, for example, shows that the western Great Lakes region in North America experienced severe drought between 1,000 and 700 years ago (Booth *et al.*, 2006). Testate amoebae have also been employed in the interpretation of archaeological

records. In bog sequences adjacent to archaeological sites in County Tipperary, Ireland, for example, records of testate amoebae indicate episodes of low water table level that accord with independent archaeological evidence for increased anthropogenic activity (Gearey & Caseldine, 2006). Other applications include the reconstruction of sea-level variations (Charman *et al.*, 2010) and of palaeolimnological properties of Arctic lakes, such as pH, oxygen levels and degree of eutrophication (Patterson & Kumar, 2002).

4.12.6 Biomarkers (ancient biomolecules)

The decay of organic tissue leads ultimately to chemical breakdown and the release of organic molecules, some of which have chemical structures that are species-specific and are frequently preserved in sedimentary deposits. Because they provide useful palaeoecological and palaeoenvironmental information, they can be considered as **chemical fossils**, though they are more commonly referred to as chemical **biomarkers** (Eglinton & Calvin, 1967). An example is vestigial DNA, which is ubiquitous in the environment. In addition to its role in phylogeographical and evolutionary studies (section 4.11.6.4), DNA analysis is important in taxonomy, for it enables taxa to be identified to subspecies level, and can thus be a more powerful and reliable classificatory mechanism than one based on the morphological characteristics of organisms alone (Hofreiter *et al.*, 2012). In some deposits lacking visible fossil material, a diverse range of DNA molecules may have been preserved, reflecting the mix of plants and animals that once inhabited the vicinity of the site, including some that are rarely preserved as fossils (Willerslev *et al.*, 2007). Further details can be found in Willerslev & Cooper (2005) and Hofreiter *et al.* (2012).

A number of other organic molecular proxies have applications in Quaternary palaeoenvironmental research, particularly in palaeoceanography (Rosell-Melé & McClymont, 2007). The majority are derived from long-chain alkenones and lipids, such as the alkenone-based U_{37}^k index that co-varies with sea-surface temperature (section 4.10.7). Another marine palaeotemperature biomarker that is widely employed is the lipid-based **TEX_{86} index** (TetraEther indeX), a group of tetraether compounds consisting of eighty-six carbon atoms, the composition of which co-varies with mean annual temperature of surface ocean water (Kim *et al.*, 2008). A further recently discovered biomarker that indicates the presence of sea ice is the **IP₂₅ index** (Ice Proxy with 25 carbon atoms), a lipid-based compound derived from diatoms during the Spring (Belt & Müller, 2013). Detection of this compound in marine

sediment sequences allows the former extent of sea-ice cover to be reconstructed (Stein & Fahl, 2013).

Palaeoenvironmental biomarkers have also been found in terrestrial and freshwater sediments. A peat sequence in China, for example, showed that lipids derived from subaerial plants could be distinguished from those of waterlogged plants, the ratio between the two providing an index of effective precipitation over the past 16 ka (Zhou *et al.*, 2010). Romero-Viana *et al.* (2012) have applied a similar approach in order to reconstruct past rainfall anomalies from lake sediment records, using a measure termed the **DiTe index** which is derived from the ratio of two molecular compounds. Analysis of the concentration of lipids derived from *Archaea* (single-celled microbes that are abundant in soils and peat) provides a basis for estimating past changes in methane production and cycling (Pancost *et al.*, 2011). Some biomarkers also have archaeological applications, for example organic molecules derived from human and animal faeces, which can indicate the onset of human settlement (D'Anjou *et al.*, 2012).

4.13 MULTI-PROXY PALAEO-ECOLOGICAL STUDIES

For many years, Quaternary palaeoecological research projects generally involved the analysis of only one or two lines of biological evidence. This is a reflection both of the time-consuming nature of palaeoecological research, and of the particular specialisms of most palaeoecologists. Increasingly, however, research in Quaternary science has followed a multi-proxy, as opposed to a single-proxy, approach, principally because more sophisticated environmental reconstructions are possible when several different proxies provide converging and mutually supporting data. A much wider range of biological evidence is now being investigated, and a great deal more is known about the ecological affinities of modern biota and, in particular, about their environmental controls. In an increasing number of cases, therefore, it is now possible to model environmental change using these different lines of evidence, but the models are, of course, much more powerful when they combine evidence from more than one climatic or environmental proxy. As a consequence, Quaternary research is now characterized by teams of scientists, each perhaps with a different expertise, cooperating in collaborative research programmes which are not only multidisciplinary but frequently interdisciplinary in nature. Perhaps the first modern example of such collaboration was the CLIMAP project in which marine micro-palaeontologists, marine geochemists and atmospheric

scientists came together to develop models of ocean–atmosphere–biosphere–cryosphere interactions for the Last Glacial Maximum (section 4.10). Multi-proxy investigations such as CLIMAP are essential if the multi-faceted nature of the Quaternary record is to be properly interpreted and reasonable inferences drawn about patterns, processes and causes of environmental change. The validity of the inferences that we make depends, however, on establishing the past distribution of biota (the palaeobiogeography of the period under investigation) as accurately as possible, and also on improving still further our understanding of the palaeoecology of former organisms whose remains make up the fossil record. Just as the interpretation of modern distributions of individual species requires a knowledge of their mutual associations, so must be the case for palaeoecosystems. This, however, is a two-way process: studying the past is just as important to contemporary ecology as modern ecology is to understanding past conditions, a point that we have been stressing throughout this chapter.

4.14 CONCLUSIONS

Palaeobiological evidence, in the form of fossil fauna and flora, is probably the most effective and direct means we have at our disposal for reconstructing past environmental conditions. The analysis of all forms of biological evidence, however, is time-consuming, often costly and requires a very high level of expertise. These factors must be weighed against the type of information required, the level of sophistication in the data that are being sought and the importance of the research topic to which they are being applied. No single technique can provide all of the evidence that we need in order to understand fully the nature of Quaternary environmental changes. Each data source outlined in this chapter offers a slightly different perspective, and the point has been made repeatedly that the most fruitful lines of enquiry are frequently those in which several techniques are employed in conjunction, or where biological evidence is supported by geomorphological, sedimentological or geochemical data. In these circumstances, the tools are available to enable Quaternary scientists to attempt reconstructions not only of environments that existed at specific times in the past, but also of the history of environmental changes and of specific responses of the biota over time. Before these steps can be taken, however, two further aspects of Quaternary research need to be examined, namely the establishment of a timescale for environmental change and the means whereby Quaternary sequences at widely separated localities can

be correlated in both the spatial and temporal dimensions. These form the subject matter of the following two chapters.

NOTES

- 1 Used literally, the term ‘pollen analysis’ refers to the description and classification of pollen grains, whereas environmental reconstruction is based upon interpretation of pollen assemblages and their stratigraphical variations. However, the term is so widely used that it is retained here, though strictly the term ‘pollen stratigraphy’ is perhaps more appropriate.
- 2 **Plant function types (PFTs)** is a system employed in vegetational modelling by climatologists and ecologists to classify plants according to their physical, phylogenetic (evolutionary relationships) and phenological (life cycle) characteristics.
- 3 **Plant biomes** are communities of plants occupying a major geographical area and usually related to climate that are characterized by similarity of vegetation structure rather than by similarity of species composition.
- 4 **Transfer functions** are essentially variants on multiple linear regression models. In palaeoecological studies, they have been employed to establish quantitative relationships between biological data and environmental variables. If it is assumed that an assemblage of organisms is related to the environment by some complex function (the transfer function), and if these relationships can be determined for modern situations, then multivariate numerical analysis should allow that function to be applied to the fossil assemblages, thereby enabling former environmental parameters to be reconstructed quantitatively (Birks & Birks, 1980).
- 5 **Lusitanian**, a term used to denote warm-adapted fauna and flora in or adjacent to the Northeast Atlantic, is named after the province (Lusitania) established in Portugal by the Romans.
- 6 The North Atlantic Polar Front is a prominent hydrographic/oceanographic boundary, also termed the Subarctic Convergence, which separates warm water of high salinity flowing northwards from cold low-salinity water flowing from the Arctic. Weather patterns are usually ‘trained’ along the southern flank of this boundary, which is informally termed the atmospheric ‘Polar Front’ in the literature.
- 7 The term ‘duplicature’ in ostracod anatomy refers to calcified inner lamellae that extend along the free margin of the two valves that encase the soft parts of the animal.
- 8 Prokaryotes differ from all other organisms principally because the DNA within their cell is loosely organized and not bounded by a membrane into a nucleus. They lack chromosomes.
- 9 **Boundary conditions** are the assumed or measured surface conditions used to constrain global climate models, and include such factors as sea-surface temperatures, albedo values, incoming solar radiation and atmospheric transparency. For further explanation see section 7.2.
- 10 **Autolysis** is the self-‘ingestion’ of organic matter caused by organic chemical reactions triggered by the enzymes of which it is partly composed.

Dating methods

5.1 INTRODUCTION

There are three broad categories of Quaternary dating methods. First, there are **techniques that provide age estimates**, in other words techniques that enable the age of fossils, sediments or rocks to be established directly in years. These include **radiometric methods**, which are based on the radioactive decay of certain unstable chemical elements or related phenomena (such as damage to crystal lattices caused by radiation), and **incremental methods**, which involve measurements of regular accumulations of sediment or biological materials through time. Second, there are **techniques that establish age-equivalence** based on contemporaneous horizons in separate and often quite different sedimentary sequences. Certain distinctive stratigraphic marker horizons are regionally and, in some cases, globally synchronous, and where these can be traced laterally between sediment profiles, they represent common time-planes in the stratigraphic records. If the age of the markers can be established in one locality by the application of any of the age-estimate methods (above), then equivalent horizons within other sequences can be indirectly dated by correlation. Third, there are **relative age methods**, techniques that establish the **relative order of age** of fossils or stratigraphic units. The relative antiquity of geological materials is most obvious where superposition¹ can be established but, under certain circumstances, the relative age of Quaternary landforms and sedimentary units can be determined from the degree of degradation or alteration resulting from the operation of chemical processes through time. Further details of these various approaches can be found in Walker (2005).

5.2 PRECISION AND ACCURACY IN QUATERNARY DATING

Many of the dating techniques currently employed in Quaternary research can be applied only to restricted spans of Quaternary time (Figure 5.1), and each method has its own distinctive set of problems which lead to uncertainties in interpretation. In evaluating any age determination, particularly those obtained by radiometric means, it is important to make a distinction between **precision** and **accuracy**. The former refers to the **statistical uncertainty** that is attached to any physical or chemical measurement, while the latter relates to the degree of correspondence between true age and that obtained by the dating process (Figure 5.2). In other words, it refers to the extent of **bias** in an age determination. In considering accuracy and precision, it is useful to think of the analogy of a watch. A *precise* watch that tells the time to the nearest second may actually be inaccurate by 10 minutes; conversely, an *imprecise* watch with no second hand may still be *accurate* and tell exactly the correct time. Both accuracy and precision determine the **reliability** of dates, but establishing whether or not a date can be regarded as reliable also requires a knowledge of other factors such as contexts of deposition, taphonomy of fossil material and post-depositional diagenetic processes. For example, precise measurements can be obtained from fossils containing contaminants, but if the contaminants are not recognized as such and corrected for, then the inferred age will be inaccurate and therefore invalid.

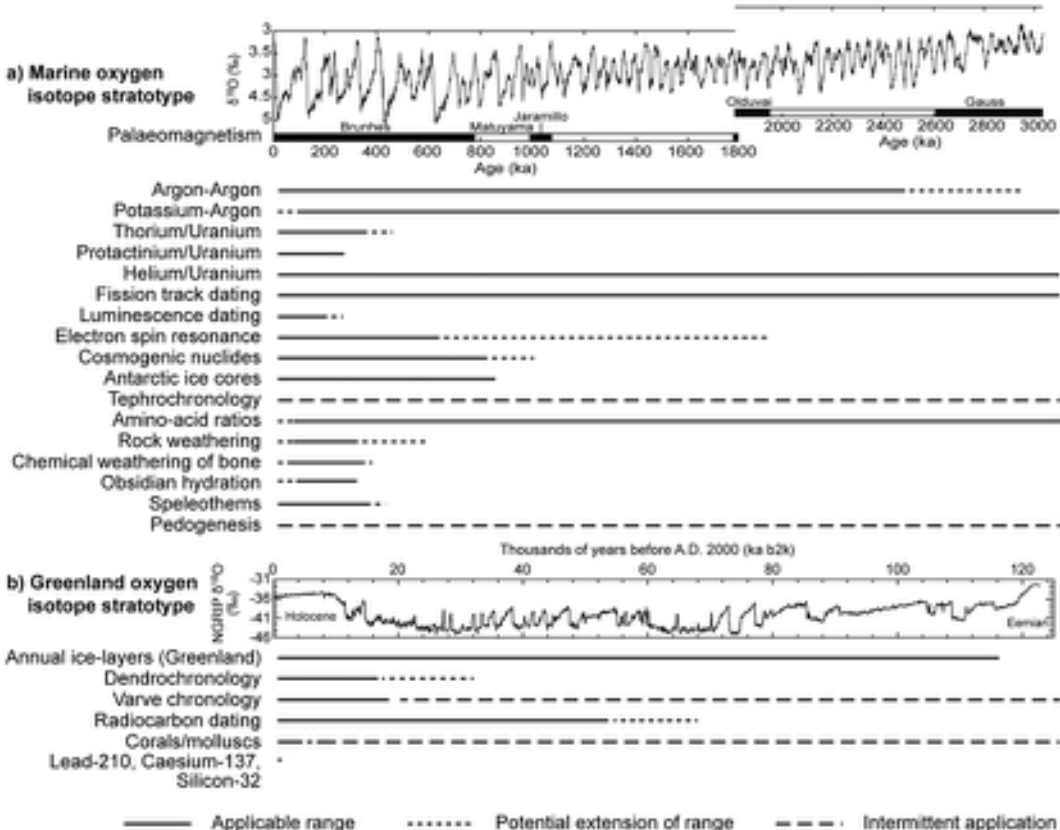


Figure 5.1 The ranges of various dating methods discussed in the text, divided into a) those that apply to the longer Quaternary timescale and b) those generally restricted to the Holocene and last glacial cycle. Broken lines with short dashes indicate where extensions to dating ranges may be possible with further methodological improvements; broken lines with larger dashes indicate time ranges in which a method can presently only be applied intermittently.

5.3 RADIOMETRIC DATING TECHNIQUES

Radiometric dating methods are based on the radioactive properties of certain unstable isotopes which undergo spontaneous changes in atomic organization in order to achieve a more stable atomic form. A number of radioactive elements, such as uranium, occur naturally and are commonly found in rocks, sediments and fossils. **Radioactive decay** (atomic transformation) is **time-dependent**, and if the rate of decay is known, the age of the host rocks or fossils can be established. Rates of radioactive transformations vary markedly: some elements decay in days or even seconds, whereas others transform gradually over millions of years. A range of radiometric dating

methods has now been developed, some of which are capable of dating the oldest rocks on earth (Macdougall, 2008), but in this section only those techniques that are directly applicable to the Quaternary timescale are discussed.

5.3.1 The nucleus and radioactivity

The nucleus of an atom contains positively charged particles called **protons** and particles with no electrical charge known as **neutrons**. These are densely packed in the nucleus so that although the nucleus occupies only about 10^{-14} of the volume of an atom, it contains nearly all of the mass. The other major type of particle contributing to the structure of an atom is the **electron**. These are tiny particles of negative charge and negligible mass that spin

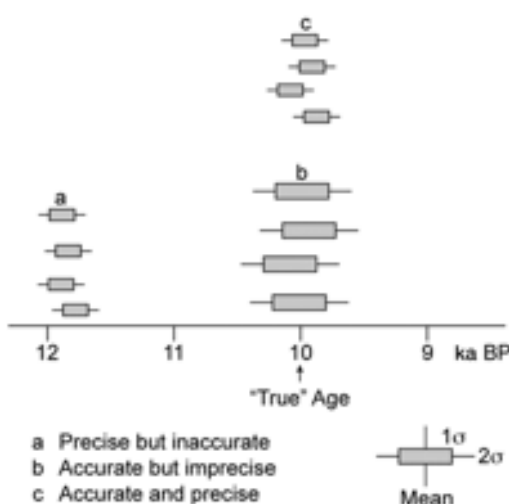


Figure 5.2 Accuracy and precision with respect to age estimates derived for a sample with a true age of 10 ka BP.

around the nucleus, and they vary in number for different chemical elements. At one time, it was believed that electrons orbited the nucleus in shells (or orbitals), and that in each of these orbits they had a certain energy level. It now appears, however, that this is too simplified a view, for modern physics has shown that it is not possible to determine both the location *and* velocity of subatomic particles. Electrons are now considered to exist in *volumes of space* around the nucleus, even though their precise location cannot be established. These volumes are known as **atomic orbitals**, and the build-up of electrons within these orbitals enables scientists to account for many of the properties of elements, and forms the basis of modern chemistry.

As atoms gain or lose electrons, they acquire a net electrical charge, in which case they are referred to as **ions**. The charge can be positive or negative; a positively charged ion is known as a **cation** and a negatively charged ion as an **anion**. The degree of electrical charge is determined by the number of protons minus the number of electrons and is termed the valence. For example, a chemical element with six protons and six electrons has a net electrical charge of zero. If it loses two electrons, it develops a positive charge (valence = 2^+) and becomes a cation; conversely, if it gains two electrons it now has a negative charge (valence = 2^-) and becomes an anion. The process whereby electrons are removed (usually) or added (occasionally) to atoms is known as **ionization**, and is an important element in radiation (see below).

Chemical elements are classified according to **atomic number (Z)**, which is the number of protons contained in the nucleus. Hydrogen has an atomic number of 1, oxygen 8 and uranium 92. The **atomic mass number (A)** of an element is the number of protons plus neutrons; that of hydrogen is 1 and of oxygen is 16. It is convention to give the numerical value of A as a superscript and Z as a subscript on the left-hand side of the symbol for a chemical element, for example, $^{238}_{92}\text{U}$ (uranium-238). The atomic mass number of elements can vary, since the number of neutrons in the nucleus is not always constant. As we saw in Chapter 1, elements with the same number of protons, but a different number of neutrons (e.g. ^{16}O and ^{18}O ; ^{12}C and ^{14}C) are known as **isotopes**. They have the same chemical properties, since the number of electrons remains constant for each element, but isotopes differ in mass. Each isotope of an element is called a **nuclide**. The particles that constitute the nucleus are bound together in a way that is not fully understood, but if a nucleus contains too many or too few neutrons, it becomes unstable and the repulsive forces between the similarly charged particles overcome the binding forces keeping them together. This results in spontaneous emission of particles or energy, which is the basis of radioactivity. Isotopes involved in such radioactive processes are known as **radioactive nuclides**.

Three types of energy emission occur during radioactive decay. **Alpha (α) particles** consist of two protons plus two neutrons and are the positively charged nuclei of helium atoms. They collide with surrounding atoms and acquire electrons to form helium gas. Nuclides that emit alpha particles lose mass and positive charge. By this process, the atomic number changes, and thus one chemical element can be formed by the ‘decomposition’ of others. **Beta (β) particles** are negatively charged electrons, and their emission does not alter mass, but changes atomic number. **Gamma rays (γ)** are powerful forms of radiation that occur during radioactive decay. They are not important in the calculation of decay constants but do contribute to the build-up of thermoluminescence properties in minerals (section 5.3.6). Moreover, the cosmic rays that constantly bombard the earth’s upper atmosphere (section 5.3.2) consist largely of gamma rays.

The atom that undergoes atomic transformation is termed the **parent nuclide** (or ‘mother nuclide’) and the product is the **daughter nuclide**. This single-stage transformation is known as **simple decay**. Many radioactive transformations, such as uranium-series (section 5.3.4), involve more complex pathways where the transformation of the nuclide with the highest atomic number to a stable nuclide involves the production of a number of intermediate unstable nuclides. This is known as **chain decay**.

(see Figure 5.14). Intermediate nuclides involved in such chains are both the product of previous transformations and the parents in subsequent radioactive decay, and such nuclides are termed **supported**. **Unsupported decay** involves the transformation of a parent nuclide that is not, in itself, the product of decay, or is separated from earlier nuclides in the chain as a result of physical, biogenic or sedimentary processes (section 5.3.4.1).

Radioactive decay processes are governed by atomic constants. The number of transformations per unit time is proportional to the number of atoms present, and for each decay scheme there is a **decay constant (λ)** which represents the probability that an atom will decay in a given period of time. The transformation of an individual atom occurs spontaneously and unpredictably, but where a large number of atoms of a particular nuclide are considered, there is a predictable time rate at which overall disintegration proceeds. The law of radioactive decay is given by:

$$\frac{-\delta N}{\delta t} = \lambda N$$

where N is the number of atoms, t is a time constant and λ is the decay constant for that nuclide. For all nuclides, the decay is exponential (see Figure 5.3), and is best considered in terms of the **half-life ($t_{0.5}$)**. This is the period of time required to reduce a given quantity of a parent nuclide to one half. For example, if 1 g of a parent nuclide is left to decay, after $t_{0.5}$ only 0.5 g of that parent will remain. It will then take the same period of time to reduce that 0.5 g to 0.25 g, and to reduce the 0.25 g to 0.125 g, and so on. The relation between the half-life and the decay constant is given as:

$$\text{Half-life } (t_{0.5}) = \frac{\log_e 2}{\lambda} = \frac{0.693}{\lambda}$$

The application of the principle of radioactivity to geological dating requires that certain fundamental conditions be met. If an event (such as the cooling of a magma, the formation of salt precipitates, the death of an animal and the burial of its bones, etc.) is associated with the incorporation of a radioactive nuclide, then assuming that (a) none of the daughter nuclides are present in the initial stages, and that (b) no parent or daughter nuclides are added to or lost from the materials to be dated (i.e. the radioactive process has proceeded within a **closed system**), then an estimate of the age of that event can be obtained, providing that the ratio between parent and daughter nuclides can be established, and that the decay rate is known. All estimates of time derived by radioactive decay are termed **radiometric clocks**; some methods are based on

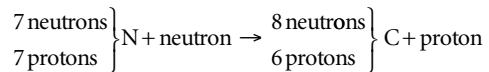
measurements of the progressive disappearance of nuclides during disintegration, while others ('accumulation clocks') measure the increasing quantity of a particular nuclide through time. The principal radiometric methods employed by Quaternary scientists are discussed in the following sections.

5.3.2 Radiocarbon dating

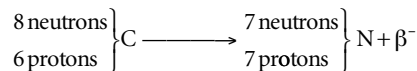
5.3.2.1 General principles

This was one of the earliest radiometric methods to be developed and, despite the fact that it is only applicable to a small proportion of Quaternary time (Figure 5.1), radiocarbon dating has perhaps been the most widely used of all the radiometric techniques. A useful overview can be found in Bowman (1990), while the journal *Radiocarbon*, along with its website (<http://www.radiocarbon.org>) and associated links, is a valuable source of information on recent developments in, and applications of, the method.

The basic principles were formulated during the late 1940s by the American scientist Willard Libby who synthesized evidence from radiochemistry and nuclear physics to determine the effects of high-energy cosmic radiation (the cosmic-ray flux) on the atmosphere (Libby, 1955). Free neutrons resulting from nuclear reactions in the upper atmosphere collide with other atoms and molecules, and one effect is the displacement of protons from nitrogen atoms to produce carbon atoms:



The carbon nucleus produced by this reaction, ^{14}C , is a radioactive isotope of carbon which eventually decays to form the stable element ^{14}N :



Decay is by beta (β) transformation, i.e. the emission of β^- particles.

^{14}C atoms are rapidly oxidized to carbon dioxide and, along with other molecules of carbon dioxide ($^{12}\text{CO}_2$), become mixed throughout the atmosphere and absorbed by the oceans and by living organisms. Thus ^{14}C , which is continually being produced in the upper atmosphere, becomes stored in various **global reservoirs**, the atmosphere, the biosphere and the hydrosphere. All living matter absorbs carbon dioxide during tissue building in a ratio that is *broadly* in equilibrium with atmospheric

carbon dioxide. As long as the organism is alive, carbon used to build new tissues will be in isotopic equilibrium with (i.e. will exist in similar isotopic ratios to) those in the contemporaneous atmosphere. Upon death, ^{14}C within the organic tissues will continue to decay, but no replacement takes place. Hence, if the rate of decay of ^{14}C is known, date of death can be calculated from the measured residual ^{14}C activity.

The activity of ^{14}C in the atmosphere is approximately 15 dpm/g (15 disintegrations per minute per gram), and this activity is halved every 5,700 years or so (Figure 5.3). The half-life of ^{14}C was originally calculated at $5,568 \pm 30$ years, but this was subsequently more accurately determined as $5,730 \pm 40$ years. However, because a large number of ^{14}C dates were published prior to the measurement of the new half-life, it has been convention to base radiocarbon dates on the former half-life value, and $5,570 \pm 30$ years remains the internationally agreed fixed constant for all radiocarbon measurements. This avoids confusion as dates calculated using the same half-life, irrespective of value, are directly comparable. Similarly, all radiocarbon age estimates are expressed in years before present (BP), the reference year being AD 1950.

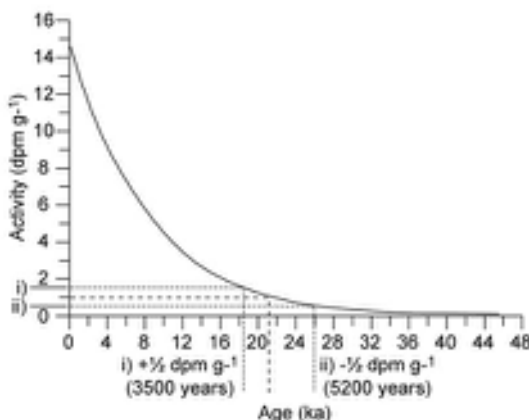


Figure 5.3 Decay curve for radiocarbon. See sections 5.3.2.1 and 5.3.2.2 for further explanation.

5.3.2.2 Measurement of ^{14}C activity

In order to detect ^{14}C activity in organic materials, extremely sensitive equipment is required. This is because the natural occurrence of ^{14}C is so small that for every one million atoms of ^{12}C in a living organism, there is only one atom of ^{14}C . Moreover, ^{14}C is a low-energy β particle emitter. Two approaches are used to measure the

residual ^{14}C activity in a sample: (1) **radiometric dating** or '**beta decay**', which involves the detection and counting of β emissions from ^{14}C atoms over a period of time in order to determine the rate of emissions and hence the activity of the sample; and (2) **accelerator mass spectrometry**, which uses particle accelerators as mass spectrometers to determine the isotope ratio of ^{14}C relative to that of the stable isotopes of carbon (^{13}C and ^{12}C), and age is then determined by comparing this ratio with that of a standard of known ^{14}C content. The development and refinement of these very different approaches to ^{14}C measurement are reviewed by Povinec *et al.* (2009).

Radiometric dating

Two methods are employed in radiometric radiocarbon laboratories to detect emissions of beta particles: **gas proportional counting** and **liquid scintillation counting**. In the former, a suitable gas (usually carbon dioxide, ethylene or methane) is prepared from the carbon in the sample and collected in a chamber, down the centre of which runs a charged wire. This detects, and counts, pulses of current that flow through the gas when it is ionized by radioactive decay. The current is *proportional* to the energy of the β particle (electron), and hence it is possible to discriminate between decays from different radioactive elements in a proportional counter. In liquid scintillation counting, samples are first combusted to CO_2 , reacted with molten lithium metal to give lithium carbide, mixed with water to release acetylene and finally polymerized to benzene. A 'scintillator' is then added, usually a phosphoric substance that emits pulses of light (photons) in response to radioactive disintegrations, and these can be counted by photo-electrical means.

From the decay curve (Figure 5.3), it can be seen that material approximately of 10 ka age will have an activity of only 4 dpm/g, and older samples correspondingly lower values. The limit of practical counting using conventional methods is eight half-lives (about c.45 ka), for beyond that age the curve becomes so flat and insensitive that it is difficult to separate samples of different activities with any statistical certainty. However, greater ages have been measured by the technique of **isotopic enrichment** where the amount of ^{14}C present in a sample is enhanced so that the frequency of decay can be more accurately determined by gas or liquid scintillation counters. This method, which takes advantage of isotopic fractionation (Chapter 3, note 9) uses either thermal diffusion or photo-dissociation by means of a laser beam. With the former, finite ages in excess of 60 ka have been obtained (Grootes, 1978; Woillard & Mook, 1982). However, the technique has not been widely applied, for it requires relatively large samples of material

and long counting times and, by comparison with standard dating procedures, it is time-consuming and hence more costly. Another approach to extending the radiocarbon timescale is to use large-volume, high-precision counters in which very old samples (up to ten half-lives) can be measured, and finite ages in the range 50–60 ka have been obtained in this way (Behre & van der Plicht, 1992). Again, however, substantial quantities of sample material and extended counting times are needed.

In the calculation of radiocarbon dates obtained by conventional methods, laboratories compare sample activities with a **modern reference standard**. The internationally accepted reference standard for all ^{14}C dating is the modern activity level of NBS oxalic acid held by the American Bureau of Standards. Because of the relative scarcity of this material, however, some laboratories now use a secondary standard, such as Australian National University (ANU) sucrose, or a paper cellulose sample provided by the International Atomic Energy Authority (IAEA). The reason why such standards are necessary is that there have been variations in ^{14}C production rates through time, and modern levels are artificially high (see below). Comparability between laboratories and between samples of different ages therefore requires reference to a standard. The time in years (R) since the death of an organism can be calculated from the following equation:

$$R = \frac{1}{\lambda} \log_e \left(\frac{A_0}{A} \right)$$

where λ is the decay constant of ^{14}C , A_0 is the ^{14}C activity of the modern reference standard, and A is the measured ^{14}C activity of the sample of unknown age. In arriving at a measure of R , account has to be taken of a number of factors that affect the determination of the activity of a sample. These include sample volume or gas pressure, dilution ratio (especially for small samples), atmospheric pressure (which affects background radiation during measurement), and loss of sample during counting (which results in samples having to be reweighed at the end of counting and a correction applied). Because these cannot always be accurately determined, however, some uncertainty is always associated with the calculated age of a sample. One source of uncertainty that can be quantified is the probable effects of the randomness of radioactive decay on the counting statistics. As a consequence, radiocarbon dates along with other radiometric age determinations are always reported as mean determinations with a plus or minus value of one standard deviation (1σ) about the mean. A radiocarbon date of $2,000 \pm 100$ years should be interpreted as indicating that there is a 68 per cent

probability that the true age of the sample lies between 1,900 and 2,100 years BP, or, for a 95 per cent probability (2σ), the age is within the range 1,800–2,200 years BP. Even with two standard deviations on the ‘date’, there is still a one in twenty chance that the true age lies outside the range 1,800–2,200 years BP.

It is important to remember, however, that age is not the quantity that is being measured, but *activity of the sample* which, on the basis of a number of assumptions, is interpreted as indicating ‘age’. The plus-or-minus refers to the uncertainty associated with determining activity, and this is why on older dates the plus value of the standard deviation is often quoted as being larger than the minus value. This can be seen in Figure 5.3 by considering an activity of $1 \text{ dpm/g} \pm 0.5 \text{ dpm/g}$ which, translated into ‘age’, gives a significantly higher plus than minus value. Because of the asymptotic decay curve, technically there is always a difference between the plus and minus value, but this is regarded as insignificant for younger material.

Accelerator mass spectrometry (AMS dating)

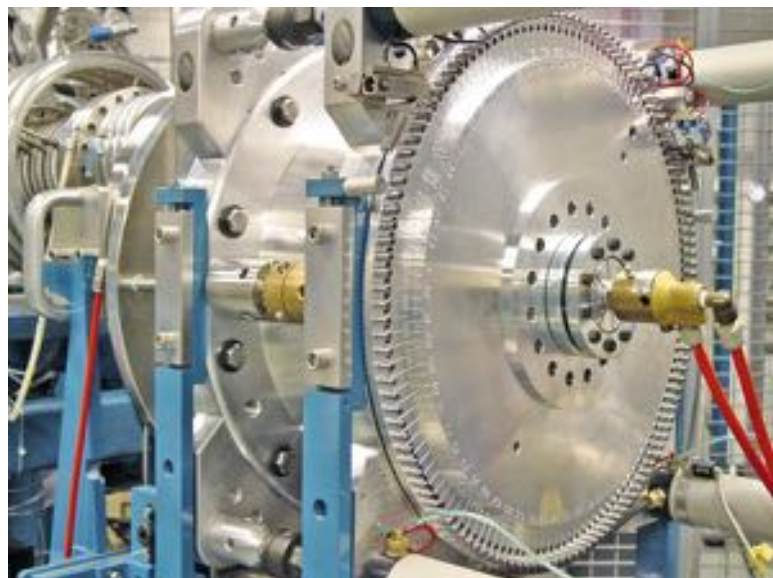
Mass spectrometers are widely used in physics to detect atoms of specific elements based on differences in atomic weights (section 3.10). Charged particles moving in a magnetic field will be deflected from a straight path by a factor that is in proportion to atomic weight; the lighter the particle, the greater will be the amount of deflection. Normal mass spectrometers cannot discriminate, however, between ^{14}C and other elements of similar weight (e.g. ^{14}N), but if the particles are subjected to large voltage differences so that they travel at very high speeds, even the very small number of ^{14}C atoms in a sample can be detected. This is the principle of **accelerator mass spectrometry**. The most commonly used system is a **tandem accelerator** (Figure 5.4), so called because there are two stages of acceleration (see below). Samples are converted to graphite (although a number of laboratories use a CO_2 source) and mounted on a metal disc (Figure 5.5). Caesium ions are then fired at this ‘target’ and the negatively ionized carbon atoms (C^-) produced are accelerated towards the positive terminal through the two focusing devices and injection magnet (Figure 5.6). Nitrogen does not form negative ions, and hence almost all of the ^{14}N , which tends to mask the ^{14}C signal in a conventional mass spectrometer, is eliminated before it can reach the detector. During passage through the ‘stripper’, four electrons are lost from the C^- ions and they emerge with a triple positive charge (C^{3+}). Other molecules are also lost at this stage. Repulsion from the positive terminal leads to a second acceleration of the carbon ions through focusing magnets where deflection occurs according to mass, and the concentration of ^{14}C and

Figure 5.4

The 5 MV National Electrostatics Corporation Accelerator Mass Spectrometer (AMS) at the Scottish Universities Environmental Research Centre, East Kilbride, UK. The accelerator itself is on the left of the photograph, while the target wheel or ion source (Figure 5.5) is in the screened area to the right (photograph by Sheng Xu, Scottish Universities Environmental Research Centre, East Kilbride, UK).

**Figure 5.5**

The exposed sample target wheel (ion source) of the AMS in Figure 5.4. The wheel holds 134 graphite samples, but not all of these will be of fossil material as standards of known age are interspersed at regular intervals (photograph by Sheng Xu, Scottish Universities Environmental Research Centre, East Kilbride, UK).



of the stable carbon isotopes ^{13}C and ^{12}C can therefore be measured.

In order to obtain an age for the sample material, the $^{14}\text{C}/^{12}\text{C}$ ratio measured for the sample is compared with those for the targets in the same set which are made up from a material of known ^{14}C activity (usually oxalic acid – see above). This gives a sample/modern ratio from which, after corrections, a radiocarbon age can be calculated. It is

important to stress, however, that it is not the absolute number of ^{14}C atoms that is being measured: the abundance of ^{14}C atoms is so small that it would be extremely difficult to measure total amounts. Rather, it is the ratio between ^{14}C and the stable isotopes that form the basis for determining age, and thus this approach is often referred to as **isotope ratio mass spectrometry**. The plus-or-minus value that accompanies all AMS dates reflects, as in conventional

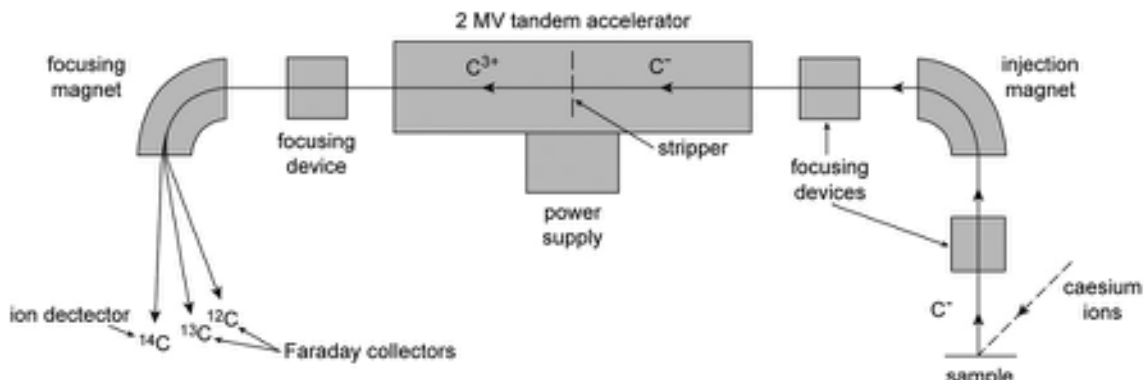


Figure 5.6 Schematic diagram of the components of a tandem accelerator. For further explanation see text (after Bowman, 1990).

dating, statistical uncertainties associated with the precise measurement of the ^{14}C decay curve, difficulties in quantifying the natural background ^{14}C , as well as random and systematic errors that inevitably occur during the measurement process. These can arise, for example, from contamination by modern carbon of samples, targets or the ion beam itself.

Evaluation of counting techniques

There are two principal advantages of AMS dating over gas proportional or liquid scintillation counting. First, very small samples of material can be dated, with most AMS laboratories routinely counting samples containing 1 mg of organic carbon or less. This compares with a typical sample size of 5–10 g of organic carbon required by most radiometric dating laboratories. The second advantage of AMS is one of time. The actual determination can take only a matter of hours whereas typical liquid scintillation or gas proportional counters may be occupied for days. Hence an AMS laboratory could perform more than 1,000 analyses per year, far more than most decay counters can measure to a comparable precision. It was initially envisaged that AMS would enable the radiocarbon timescale to be significantly extended, and while it still has not equalled the isotope-enriched beta counting dates in excess of 70 ka (see above), it is possible that the dating of large samples, possibly back to 80 ka, might become feasible in due course (Hedges, 2001). Indeed, recent developments involving more stringent pretreatments (e.g. the ‘ABOX pretreatment’, and filtered gelatin preparations) and innovations in target preparation for AMS dating (‘stepped combustion’) to remove contaminants have resulted in finite ages for charcoal samples in the range 50–60 ka BP (Bird *et al.*, 2003; Higham *et al.*, 2004).

The potential of AMS is therefore clearly considerable, and its versatility is shown by a range of applications which include the dating of small plant macrofossils (Hillman *et al.*, 2001), fossil pollen grains (Vandergroes and Prior, 2003), charcoal fragments (Meyrick, 2003), fossil insect remains (Walker *et al.*, 2001) and microfauna from marine cores (Flower *et al.*, 2009), as well as more unusual materials such as fragments of cloth from the Shroud of Turin (Damon *et al.*, 1989), pieces of old parchment (Donahue *et al.*, 2002), carbon residues (from smelting) in iron artefacts (Hüls *et al.*, 2004) and in calcium oxalate skins covering ancient rock engravings (Smith *et al.*, 2009), organic-rich coatings (from food) on ancient pottery (Stott *et al.*, 2001) and lime mortar from old buildings (Heine-meyer *et al.*, 2010).

AMS dating does have certain disadvantages, however. The capital cost of establishing an AMS facility is an order of magnitude greater than that involved in developing a conventional radiocarbon laboratory, and running costs are also commensurately higher. Hence AMS dates are still more costly than radiometric radiocarbon age determinations. Initially, analytical precision was also a problem, with AMS laboratories unable to match the levels of precision obtained by radiometric dating where the error estimate is typically around 1 per cent; in other words, ± 50 years at 5.5 ka and 120 years at 12.0 ka. However, over the last decade or so, counting statistics have rapidly improved, and many AMS facilities are now more or less comparable with conventional radiometric laboratories in terms of analytical precision. Neither of these can compare with the high-precision radiometric laboratories (such as Belfast, Groningen, Heidelberg, Pretoria and Seattle) which can produce dates with a standard deviation of less than 20 years, and sometimes as low as ± 12 years,

although in order to achieve these levels of precision, large amounts of sample material (up to 20 g carbon) and markedly longer counting times are required.

5.3.2.3 Quality assurance in radiocarbon dating

Because different practices have been adopted in different laboratories, the international radiocarbon community has agreed to participate in regular inter-laboratory comparison programmes designed to ensure reliability of, and consistency between, results from radiocarbon laboratories. The most recent of these, VIRI (the fifth international radiocarbon intercomparison) which was completed in 2008, involved the preparation and distribution of typical sample materials (peat, bone, shell, etc.) to more than sixty laboratories worldwide. In this exercise, many more AMS than radiometric laboratories participated but, on average, the results showed little evidence of differences between laboratory types (Scott *et al.*, 2010a, 2010b). These intercomparison programmes are an essential part of the quality assurance process in radiocarbon dating, for they demonstrate to the user community that laboratories worldwide are delivering results that are reliable and in accordance with good practice.

5.3.2.4 Sources of error in radiocarbon dating

Temporal variations in ^{14}C production

A fundamental assumption in radiocarbon dating is that atmospheric ^{14}C concentrations (expressed as the decay-corrected deviation from the standard pre-industrial atmospheric ^{14}C concentration, and indicated by $\Delta^{14}\text{C}$) have not varied significantly over time. We now know, however, that this is not the case. Over forty years ago, scientists working on tree-ring chronologies found a clear discrepancy between ages of wood obtained by dendrochronological dating (section 5.4.1) and those based on radiocarbon, with the dendrochronological dates being older than the radiocarbon ages (Renfrew, 1973). These data showed, for example, that wood with a radiocarbon age of c. 5.0 ka BP corresponds approximately to 5.8 ka BP on the dendrochronological timescale. In addition, comparisons between dendrochronological and radiocarbon dating series indicated that atmospheric ^{14}C activity has fluctuated markedly throughout the Holocene, apparently in a quasi-periodic manner (Sonnett & Finney, 1990). The record of long-term ^{14}C variations shows pronounced ‘plateaux’ of constant radiocarbon age, for example at 10.4, 10.0 and 9.6 ka BP,

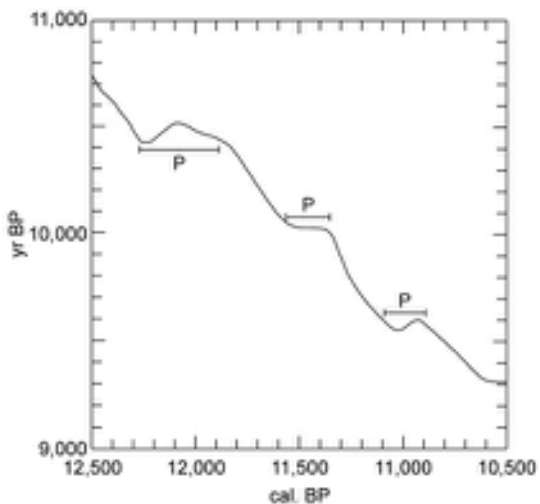


Figure 5.7 Radiocarbon years (y axis) versus calendar ages for the period 9.0–11.0 ka BP (10.5–12.5 cal. BP). Note the marked ‘radiocarbon plateaux’ at c. 10.4, 10.0 and 9.6 ka BP. Radiocarbon dates that fall on these plateaux will have calendar age ranges of up to several hundred years (after Goslar *et al.*, 2000).

each plateau is considered to reflect an episode of reduced $\Delta^{14}\text{C}$ (Figure 5.7). On a longer timescale, comparisons between AMS determinations of ^{14}C and uranium isotopes on carbonate materials such as coral and cave speleothem (section 5.3.4) indicate that radiocarbon dates underestimate true age by as much as 3.5 ka at 20 ka BP, with even greater discrepancies beyond 25 ka BP (Hughen *et al.*, 2004a).

The divergence between radiocarbon age determinations and those obtained by other dating methods means that it is necessary to make a clear distinction between ‘radiocarbon years’ and ‘calendar years’ when discussing Late Quaternary chronologies. The two timescales can be reconciled, however, by comparing radiocarbon dates with those obtained from the same samples of material using independent dating methods. In this way it is possible to **calibrate the radiocarbon timescale** against calendar years (see section 5.3.2.6).

The causes of the long-term atmospheric variations in $\Delta^{14}\text{C}$ remain to be established, but several factors seem to be involved. Of particular significance are variations in the strength of the earth’s geomagnetic field and changes in the intensity of solar activity (Stuiver *et al.*, 1991). A reduction in magnetic field intensity could result in a weakening of the earth’s geomagnetic shield and the resultant increase in the number of cosmic rays entering the atmosphere would lead to an increase in ^{14}C production.

Similarly, a reduction in the strength of the solar wind (the stream of charged particles emitted by the sun) would also enable more cosmic rays to enter the atmosphere, which again would result in an increase in ^{14}C production (van Geel *et al.*, 2003). A further factor may have been changes in the carbon distribution in the ocean–atmosphere system, especially in the oceans, which constitute one of the major global carbon reservoirs (Beck *et al.*, 2001). During the last glaciation, for example, lower atmospheric CO_2 levels were accompanied by increased atmospheric radiocarbon concentrations, reflecting greater storage of CO_2 in deep ocean basins. The end of the last cold stage was marked by a rapid increase in atmospheric CO_2 as this old, ^{14}C -depleted CO_2 was released back into the atmosphere (Rose *et al.*, 2010). One consequence of this process is the plateaux in radiocarbon ages at the onset of the Holocene described above. Over longer timescales, palaeomagnetic records suggest a close relationship between changes in the earth's geomagnetic field and ^{14}C production, with fewer radiocarbon nuclides being produced during periods of high magnetic field intensity and more during low geomagnetic field intensity phases (Muscheler *et al.*, 2005). Data from sediment cores in the Iceland Sea, for example, show that over the time interval from 27–54 ka, three intervals of highly increased atmospheric $\Delta^{14}\text{C}$ have been recorded (*c.* 34 ka cal. BP; *c.* 38 ka cal. BP; *c.* 41 ka cal. BP) and these are coincident with low values of magnetic field intensity (Voelker *et al.*, 2000). The palaeoenvironmental significance of long-term changes in ^{14}C is considered further in section 5.3.2.6.

In addition to natural variations, atmospheric ^{14}C content has recently been affected by human activity. Over the past 200 years, ^{14}C levels have been progressively diluted as a result of the combustion of fossil fuels, which has liberated large quantities of ‘inert’ ^{12}C into the atmosphere (Solomon *et al.*, 2007). In the last forty-five years or so, however, this **industrial effect** has to some extent been offset by greatly increased production of ^{14}C resulting from the detonation of thermonuclear devices. The combined effects of industrial activity and atomic explosions mean that modern organic samples are unsuitable as reference samples for radiocarbon activity. A value of 0.95 times the measured activity of the NBS standard is regarded as equivalent to the natural ^{14}C activity of AD 1890 wood (pre-industrial effect), and this is corrected to AD 1950 which is, as noted above, the reference year for all ages quoted in radiocarbon years BP.

Isotopic fractionation

Of the three naturally occurring isotopes of carbon about 98.9 per cent is ^{12}C , 1.1 per cent is ^{13}C and only 1 part in

10^{10} is ^{14}C . In nature, however, a fractionation of this ratio commonly occurs. Photosynthesis, for example, results in an enrichment of ^{12}C relative to the other isotopes in most plant tissues, whereas ocean waters preferentially absorb ^{14}C . These effects are small, but can significantly affect radiocarbon dates where measurement to less than ± 1 per cent error is required. In addition, fractionation can also occur in the laboratory during the conversion of sample carbon to the gas or liquid form. Most radiocarbon laboratories today make corrections for the probable effect of fractionation based on thermodynamic laws which show that the heavier isotope ^{14}C is twice as enriched as ^{13}C . The latter can be measured in a small subsample of the material to be dated. Originally, the $^{13}\text{C}/^{12}\text{C}$ ratio was compared with a standard from carbonate of a marine fossil from the Pee Dee Formation in South Carolina, USA (PDB belemnite), but this material has now been exhausted and has been replaced by a new limestone standard using marble, and referred to as Vienna PDB or VPDB (Chapter 3, note 10). Values are published as deviations from this standard:

$$\delta^{13}\text{C}_{\text{‰}} = \frac{{}^{13}\text{C}^{12}\text{C}_{\text{sample}} - {}^{13}\text{C}^{12}\text{C}_{\text{standard}}}{{}^{13}\text{C}^{12}\text{C}_{\text{standard}}}$$

Most terrestrial samples have a negative $\delta^{13}\text{C}$ value compared with the PDB standard. Different photosynthetic pathways exist in plants so that very different levels of fractionation occur (Table 5.1). However, it is practice to ‘normalize’ ^{14}C activities during calculations of radiocarbon age, by treating each sample as if an average enrichment had taken place. The normal value is taken to be -25 per mil, which is the mean isotopic composition of wood. If the $\delta^{13}\text{C}$ value of a sample is found to be -25 per mil, then no adjustment is made. With a value of -30 per mil, however, a 5 per mil depletion in the $^{13}\text{C}/^{12}\text{C}$ ratio is implied, which in turn indicates a probable 10 per mil depletion in the $^{14}\text{C}/^{12}\text{C}$ ratio. Thus, the measured ^{14}C activity would be increased by 10 per mil, which is equivalent to about 83 years.

Circulation of marine carbon

Because ^{14}C is transferred from the atmosphere to the oceans only across the ocean surface, and because the mixing rate of surface and deep waters is very slow, ^{14}C in deep ocean waters decays without replenishment. Seawaters therefore have an **apparent age** (known as the **reservoir age**). The ageing effect in ocean surface waters ranges from *c.* 30 years or less in parts of the northern Indian Ocean (Dutta *et al.*, 2001), to around 400 years in the North Atlantic (Bard *et al.*, 1991) and over 700 years in parts of the northwestern Pacific (Kuzmin *et al.*, 2001).

Table 5.1 Approximate $\delta^{13}\text{C}$ values for various materials. The ranges on these data are typically ± 2 or 3 per mil, but substantially more variability is possible. With each per mil deviation from -25 per mil representing *c.* 16 years, these data clearly illustrate the need for fractionation corrections to be applied to measured ^{14}C age results (from Bowman, 1990).

Material	$\delta^{13}\text{C}$ value (‰)
Wood, peat and many C3 plants	-26
Bone collagen*	-19
Freshwater plants (very variable)	-16
Arid zone plants (C4 plants)	-13
Marine plants	-15
Atmospheric CO_2	-8
Marine carbonates	-0

* For direct or indirect C3 consumers.

In the deep oceans, however, longer **residence time** means that seawater may have an apparent age in excess of 2,000 years. Hence, radiocarbon dates on Foraminifera from deep-ocean cores have to be corrected for the age of seawater, with different correction factors being applied to planktonic and benthic species. Similarly, corrections have to be made to dates on marine molluscan fossils and also to other samples with a marine component, such as human bone from coastal regions. At present, the global average marine reservoir age of surface waters, $R(t)$, determined from measurements on modern marine organisms, is *c.* 400 radiocarbon years, but regional values deviate from this as a function of climate and ocean circulation systems (Ascough *et al.*, 2005). These local deviations from $R(t)$ are expressed as δR values and have been collated in an online global database (<http://www.calib.org>; see also <http://radiocarbon.1deo.columbia.edu/research/resage.htm>). In general, polar waters tend to exhibit greater reservoir ages ($\delta R = +400$ to $+800$ radiocarbon years) than equatorial waters ($\delta R = c. 0$ ^{14}C years), but there is considerable local and/or regional spatial variation in the data. For example, empirical values for modern Mediterranean surface waters vary between 280 and 665 radiocarbon years, and are, exceptionally, in excess of 1,000 radiocarbon years (Reimer & Reimer, 2001). It is difficult, therefore, on present evidence, to specify a δR that would be representative of the Mediterranean region as a whole, and this appears to be the case for other marine sectors as well. An online marine reservoir correction database is now available and can be accessed at the website <http://www.calib.qub.ac.uk/marine>.

A further problem is that the apparent age ($R(t) + \delta R$) of present-day marine molluscs in a region may not represent an appropriate correction factor for earlier periods of the Quaternary. This is partly because of spatial and temporal changes in patterns of ocean water movement, but may also reflect oceanographical responses to variations in atmospheric ^{14}C . Data from the high-latitude North Atlantic, for example, indicate that during Greenland Stadial 1 (GS-1)/Younger Dryas, the marine reservoir age increased to 590 (± 130) radiocarbon years (Cao *et al.*, 2007), while even greater values (1,000 ± 250 radiocarbon years) have been suggested for the same time interval for the Norwegian Sea (Björck *et al.*, 2003). These age estimates are significantly higher than those obtained from modern marine molluscs from the North Atlantic region. Even during the late Holocene (post 4.5 ka), there is evidence from the Icelandic Sea that marine reservoir ages varied from tens to hundreds of radiocarbon years as a result of changes in water mass distribution (Eiriksson *et al.*, 2004). Collectively, these data suggest that finding the appropriate correction factor for marine radiocarbon dates may be more problematical than has hitherto been envisaged.

Contamination

Contamination can occur in organic sediments because younger or older carbon has been added to the sample material. The former can arise from root penetration through a profile, infiltration by younger humic acids through older peat or soil horizons, and the downward movement of younger sediments through bioturbation. The possible effects of contamination by younger carbon are shown in Table 5.2a. Because of the high activity of modern carbon in comparison to fossil material, relatively small amounts of contaminant can result in major errors in radiocarbon dates.

Contamination by older carbon can also take a number of forms. Inwash of older inorganic carbon residues (graphite, coal, chalk, etc.) into lake basins leads to a dilution of the local $^{14}\text{C}/^{12}\text{C}$ ratio and hence an ageing factor (**mineral carbon error**) will affect radiocarbon dates from such sediments. In formerly glaciated regions, such older carbon may have been brought into the area by the passage of glacier ice (Walker *et al.*, 2001). In late Holocene sediments, inwash of soils or sediments can arise as a consequence of anthropogenically induced erosion around lake catchments (e.g. Oldfield *et al.*, 2003). Sub-aquatic photosynthesis, water uptake in carbonate-rich groundwaters, and carbonate secretion by freshwater or offshore organisms may also be affected by diluted ^{14}C levels. In these instances, the resulting age error is termed **hard-water error**, and may add up to 1,200 years to the apparent age

Table 5.2 The effect of contamination on true age of samples selected for radiocarbon dating, a) by modern carbon, b) by inert carbon (after Harkness, 1975).

a) Measured age as a result of weight % contamination of sample by modern carbon

True age (years)	1% contamination	5% contamination	10% contamination
600	540	160	Modern
1,000	910	545	160
5,000	4,870	4,230	3,630
10,000	9,730	8,710	7,620
Infinitely old	36,600	24,000	18,400

b) Effect of contamination by inert carbon on true ^{14}C age

Contamination (%)	Years older than true age
5	400
10	850
20	1,800
30	2,650
40	4,100

of limnic material. One way around this problem is to date inwashed terrestrial materials (such as leaves and fruits) as these are unlikely to have been influenced by hard-water contamination if the plants have been growing above the level of the carbonate-rich water table.

Contamination of lake sediments may also arise from the inwashing of older organic carbon detritus, and this redeposited or allochthonous carbon will also produce an ageing effect in dated samples. The extent to which contamination by older carbon can affect radiocarbon dates is shown in Table 5.2b. In general, samples that are initially rich in organic carbon will only be significantly affected where the amount of contaminant is high. Many organic sediments such as lake gyttjas, however, typically consist of only 4–5 per cent (and sometimes as low as 1 per cent) organic carbon, and therefore relatively small amounts of inert carbon incorporated into the sediments can introduce significant errors into radiocarbon dates.

A further problem in the dating of limnic sediments arises because the $^{14}\text{C}/^{12}\text{C}$ ratio in lake waters may be lower than that in the atmosphere (the **reservoir effect**). This is partly a consequence of the fact that the exchange rate at the lake surface is relatively slow and hence lake waters may have a somewhat lower activity than the atmosphere, but it may also reflect seepage into lakes of groundwater containing dissolved carbonates. Some lakes in central and eastern Europe show variations in reservoir age of almost 1,000 years (Geyh *et al.*, 1998), while in two lakes on the

Tibetan Plateau, reservoir ages of 2,010 and 3,260 radiocarbon years have been measured in samples of bulk organic matter (Wu *et al.*, 2010).

Problems of contamination are often encountered where shells are used for dating, since carbon exchange takes place more readily in carbonate structures. Contamination may be by older or younger carbon, depending on the dissolved contaminants introduced, and can result from the gradual accumulation of particulates or solutional carbon in the interstices of the carbonate matrix, or from the recrystallization of the carbonate matrix and an **exchange** of sample carbonate with contaminant carbon. Exchange usually affects the outer part of a shell more than the inner layers, and it has therefore become practice to remove the external portion prior to dating. Procedures vary between laboratories, but up to 25 per cent of the outer part is typically leached and discarded. The remainder is then treated to produce an ‘outer’ and an ‘inner’ fraction which are dated separately, the inner date being preferred where a noticeable difference between the two ages occurs. The development of AMS dating has resolved some of the difficulties that have arisen with the dating of shell, however, for age determinations can now be made on very small samples of inner shell material. Moreover, radiocarbon dates on Mollusca can now be obtained from hitherto unpromising contexts, such as marine boreholes, where only small amounts of shell carbonate are available.

In the case of bone material, carbon exchange after death is always likely to have occurred, and hence although in theory both elements of bone (calcium hydroxyapatite and collagen) can be dated, it is usually only the proteinaceous fraction which is used for ^{14}C measurements, although careful sample selection and biochemical purification is needed in order to obtain reliable dates (van der Plicht *et al.*, 2004; Higham *et al.*, 2006). With the development of AMS dating, however, it has proved possible to obtain age determinations on individual amino acids (section 5.6.1) within the collagen to check for consistency in dates and hence for the presence of contaminants (McCullagh *et al.*, 2010).

Biogeochemistry of lake sediments

AMS dating has enabled radiocarbon ages to be obtained on different biogeochemical components of lake sediments (humic acid fractions, lipids, chlorite treatment residues, HF/HCl treatment residues, etc.). Where this type of dating has been carried out, significant age differences have been found within a single sediment sample and between samples from contemporaneous horizons (Lowe *et al.*, 1988). Moreover, marked discrepancies have also been recorded in ^{14}C activity between macrofossil cellulose and the sediments from which the plant macrofossils have been obtained, with macrofossils typically providing younger radiocarbon ages than the sediments within which they were contained (Turney *et al.*, 2000; Walker *et al.*, 2003). Clearly, more needs to be learned about the biogeochemistry of lake sediments, if reliable age estimates are to be obtained from these media by means of radiocarbon dating.

5.3.2.5 Radiocarbon dating of soils

One of the most difficult materials to date by radiocarbon is soil. All soils contain both organic and inorganic carbon, but soils are dynamic systems and receive organic matter over long time periods. Any radiocarbon date on a soil will therefore be heavily influenced by the **mean residence time** of the various organic fractions in the soil. The continual addition of organic matter throughout its development means that the measured radiocarbon age of a soil is normally younger than its true age (Pessenda *et al.*, 2001). When a soil is buried, addition of organic matter ceases and a radiocarbon age will reflect both the mean residence time and the time that has elapsed since burial. The date at which pedogenesis commenced, which is of primary interest to the stratigrapher, will be almost impossible to establish. Further complications are caused by the constant recycling that takes place within the soil profile, notably by humic acid filtration and root penetra-

tion. However, buried soils are important components of the Quaternary stratigraphic record (section 3.5) and a considerable amount of effort has been directed towards obtaining coherent radiocarbon dates from such contexts (Scharpenseel & Becker-Heidemann, 1992). Meaningful dates have been obtained from soil profiles by dating and comparing different organic components, such as soil organic matter, the humin (acid-insoluble) fraction and charcoal (Pessenda *et al.*, 2001), by modelling the measured ^{14}C content of soil organic matter (Wang *et al.*, 1996), or by verifying radiocarbon dates from soils against results obtained from other dating methods (Dalsgaard & Odgaard, 2001).

5.3.2.6 Calibration of the radiocarbon timescale

Bases for calibration

Long-term variations in atmospheric $\Delta^{14}\text{C}$ which were first detected over forty years ago through comparisons between radiocarbon and tree-ring chronologies have resulted in an increasing divergence back in time between radiocarbon and calendrical ages (section 5.3.2.4). Over the course of the past thirty years, and particularly following the advent of AMS and the radiocarbon dating of small samples of material, the international radiocarbon community has devoted a considerable amount of effort to the development of calibration programmes that enable radiocarbon years to be converted to 'actual' or 'calendar' years (Kromer, 2009). A major focus has been dendrochronological records, as these enable a direct comparison to be made between the ages of wood as determined by counting annual tree rings (section 5.4.1) and radiocarbon dates obtained from individual wood increments. High-precision radiocarbon measurements on bristlecone pine from the western United States, on Irish oak and, for the earliest part of the sequence, on German oak, have generated a continuous dendrochronological calibration curve extending back over 10,000 years (Stuiver *et al.*, 1998). By linking this European oak-based record to tree-ring series from subfossil pines, the tree-ring calibration record has been extended to 12,594 cal. (calibrated) years BP (Hua *et al.*, 2009). Beyond the limit of continuous dendrochronological series, calibrations have been based on matched uranium-series (U-series: section 5.3.4) and radiocarbon dates on fossil corals (Fairbanks *et al.*, 2005), radiocarbon-dated organic material from laminated (i.e. annually accumulating) marine sediments, and synchronized palaeoclimatic signatures in ice cores and U-series dated cave speleothems (Hughen *et al.*, 2006; Weninger & Jöris, 2008). A number of radiocarbon calibration models have been

generated for the period 0–50 ka (Figure 5.8), and some of these are considered below.

IntCal: Probably the most widely employed calibration model has been developed by an international Working Group ([IntCal](#)) of specialists in radiocarbon dating and in other areas of Quaternary geochronology. Their remit is to produce the most coherent calibration model, and to make this available to the wider user community. The latest iteration at the time of writing is [IntCal13](#) which is based on radiocarbon-dated tree-ring samples back to 13.9 ka BP, and then extended to 50 ka BP using ^{14}C and independently dated samples from both terrestrial and marine contexts (Reimer *et al.*, 2013). These include ^{14}C -dated plant macrofossils from the varved sequence in Lake Suigetsu, Japan (section 5.4.2.7), ^{14}C measurements from U-series-dated speleothem samples from the Bahamas and China, paired ^{14}C and U-series dates from pristine corals and planktonic foraminifera from a number of localities in the Atlantic and Pacific Oceans, and a ^{14}C -dated

foraminiferal record from the Cariaco Basin in Venezuela, where parts of the sediment sequence are also laminated (section 5.4.2.7). The radiometric ages provide the tie-points for matching (or tuning) the different records (e.g. Figure 5.9). The temporal trends in the calibration datasets were statistically analysed and averaged using a ‘random walk’ procedure (Buck & Blackwell, 2004). This generates and tests various iterations within the data, and selects the most coherent results that are then statistically smoothed. The calibration curve confirms a progressive divergence between radiocarbon and calendar time (Figure 5.8), but also shows fluctuations (‘[radiocarbon wiggles](#)’) which reflect both long-term variations in atmospheric ^{14}C production and statistical noise in the radiocarbon dataset.

Calibration procedures and effects: Calibrating radiocarbon to calendar time, which takes account of the statistical errors in both the original radiocarbon measurement and in the relevant part of the calibration curve, can be achieved by the use of online programs such as CALIB

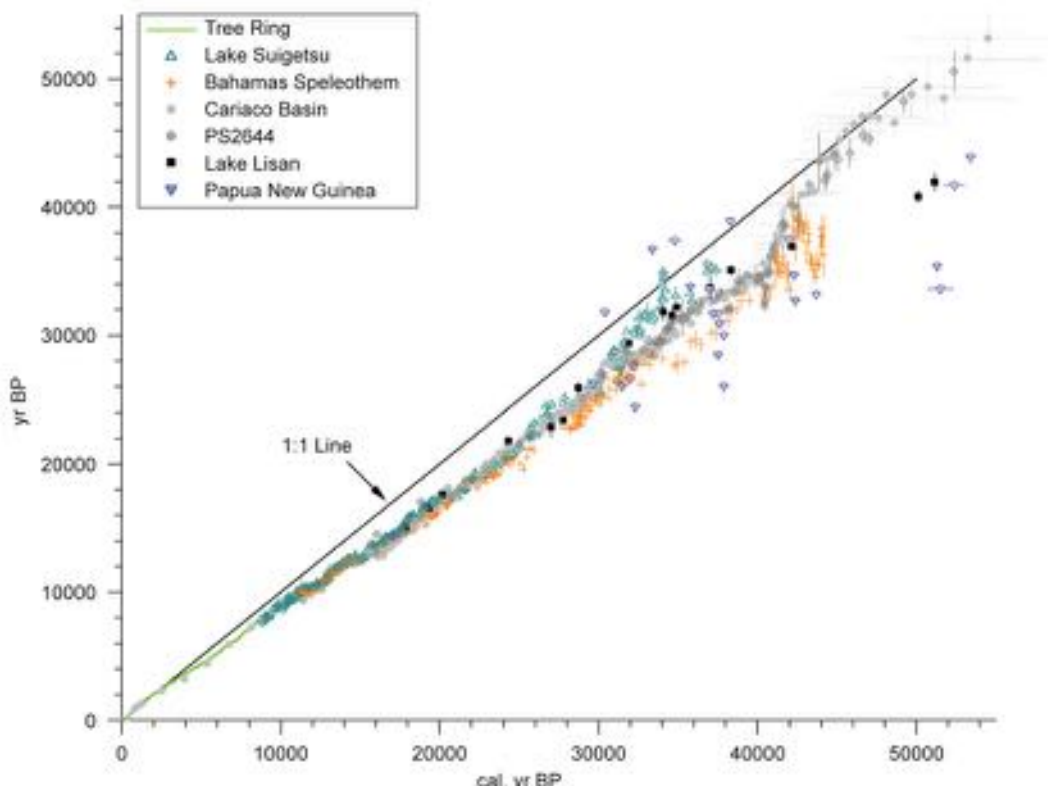


Figure 5.8 Radiocarbon calibration dating series for the period 0–50 ka; some of the IntCal datasets are shown by the light green (dendro) and grey (Cariaco) records (after Fairbanks *et al.*, 2005).

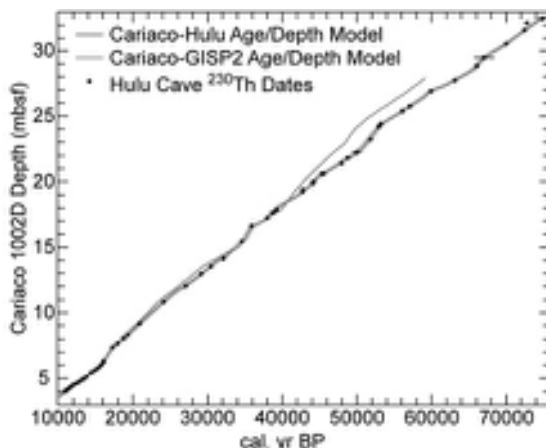


Figure 5.9 Age–depth plot of Cariaco Basin sediments after being tuned (matched) to the Hulu Cave record (Wang *et al.*, 2001). The close convergence between the two datasets suggests that both are reflecting past variations in $\Delta^{14}\text{C}$ (after Hughen *et al.*, 2006).

7.0 (IntCal: <http://calib.qub.ac.uk/calib/>; Stuiver *et al.*, 2013) and OxCal (Oxford Radiocarbon Accelerator Unit: <http://c14.arch.ox.ac.uk/>). It is important to distinguish between calibration datasets (the raw data), such as IntCal13, and the programs developed to interrogate the datasets (i.e. to perform the calibration calculations) such as CALIB and OxCal, as they are often confused. Once the user has selected the calibration model and conversion software of preference, the radiocarbon data can be input and the output generated fairly quickly, although interpretation of the results is frequently far from straightforward. In Figure 5.10, for example, radiocarbon date RD1 intersects a steep part of the calibration curve, and a calibration with a small error range is obtained; indeed, in this instance, calibration leads to an apparent reduction in age uncertainty. The opposite is the case with radiocarbon date RD2, where the age estimate intersects a part of the calibration curve that is flatter and also uneven. Here, calibration leads to an increased uncertainty in age. Furthermore, due to the vagaries of the calibration curve, the *chronological order* of samples measured in radiocarbon time can, in some instances, be reversed after calibration (see Bowman, 1990). An additional difficulty is that whereas radiocarbon dates have Gaussian (normally distributed) errors, the calibrated equivalents are statistically more complex and may be multi-modal, which makes interpretation of age even more complicated (Figure 5.11). Site chronologies should no longer be expressed in radiocarbon time, therefore, since radiocarbon time is not

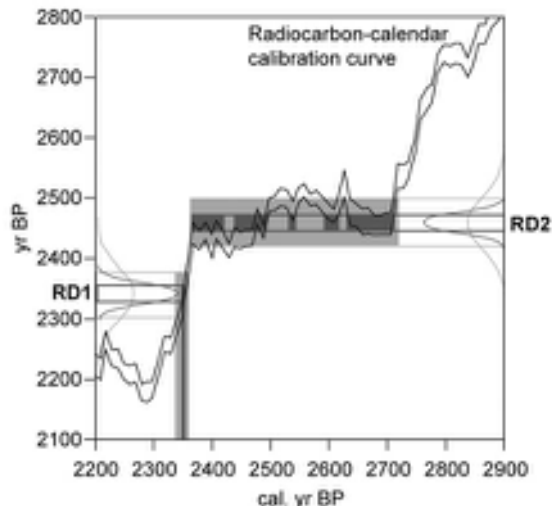


Figure 5.10 The influence of the shape of the radiocarbon curve on calibration. Radiocarbon date RD1 intercepts a steep part of the curve, while RD2 intercepts a flatter part of the curve. The consequence for calibrating radiocarbon dates are discussed in the text.

linear; calibration is *essential* if the true order and temporal precision of a series of radiocarbon dates is to be determined.

Other calibration models: In addition to IntCal, a number of other curves for calibration are now available. These include the Fairbanks (2005) calibration model (<http://radiocarbon.ldeo.columbia.edu/research/radiocarbon.htm>), which is based on high-precision paired U-series and radiocarbon dates on pristine coral samples, and the CalPal (Cologne Radiocarbon Calibration and Palaeoclimate Research Package) calibration which synchronizes the palaeoclimatic signature of several radiocarbon dating series with the uranium-series dated Hulu cave speleothem sequence and the Greenland ice-core record (Weninger & Jöris, 2008; <http://www.calpal.de/>). The differences (sometimes marked) between the various datasets partly reflect the limited analytical precision with which samples of low residual ^{14}C activity can be measured, but they also arise from both systematic and stochastic errors that affect each dataset. For example, marine records may be affected by reservoir errors that are not yet sufficiently constrained (section 5.3.2.4); varved records may be inaccurate because of missing or indistinct annual layers (section 5.4.2.6); speleothems often contain old carbon residues from soil (dead carbon fraction: DCF) which results in aberrantly older radiocarbon dates; other carbonate materials, such

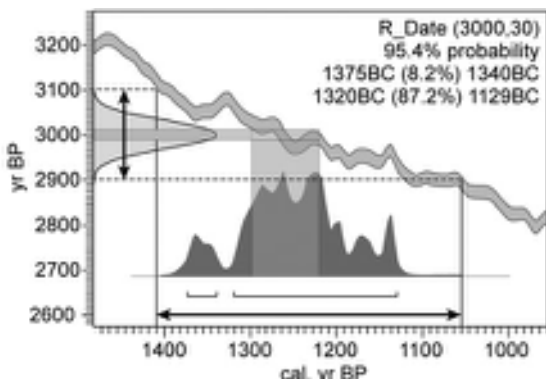


Figure 5.11 The conversion of a Gaussian radiocarbon error range (1σ : at left-hand edge) to a non-Gaussian, multi-modal error distribution in calibrated time (lower curve), using IntCal04. The 1σ error range of c. 200 radiocarbon years is spread over nearly 300 cal. years but there is no single dominant mode. The probability distribution of the radiocarbon error is proportionally distributed according to the pattern of intercept with the calibration curve. Hence, those parts of the Gaussian curve close to the mean value (transparent shading) are allocated a commensurately higher probability intercept value than those nearer to the tails of the radiocarbon error range (figure obtained from the University of Oxford Radiocarbon Web-Info site at <http://www.c14.arch.ox.ac.uk>).

as aragonite and mollusc shells, are generally unreliable media for radiocarbon dating due to fractionation and other chemical effects; while freshwater lake sediments may include in-washed secondary organic materials. Each dataset, therefore, has limitations and, while the IntCal calibration is perhaps the most widely used, there is, as yet, no consensus on which calibration curve is the most reliable.

Age modelling based on calibrated radiocarbon data

So far we have addressed the calibration of individual radiocarbon dates and the resulting output; a more complicated task, however, is the calibration of a whole series of radiocarbon dates from a single section and the construction of calibrated age-depth models. Two main approaches have evolved, both of which attempt to find the optimal match of a series of radiocarbon dates to a calibration model where the stratigraphic order of the dated samples is known: visual matching to the radiocarbon calibration curve, and statistical matching. The first, termed **radiocarbon wiggle-matching**, takes advantage of the short-term fluctuations in the radiocarbon calibration curve, and which should also be evident in a dated sequence, providing there are sufficient data-points. Where high-

precision radiocarbon-dated tree-ring series are available, for example, the curve derived by plotting dendro-age against radiocarbon age should show undulations that correspond to those in the calibration curve; in other words, the ‘wiggles’ should match (Figure 5.12). This approach has also been applied to the dating of peat sequences, although here only the radiocarbon age of individual horizons is known, and the independent (i.e. non-radiocarbon-based) timescale has to be derived using assumptions about the rate of peat accumulation (Blaauw *et al.*, 2003, 2004). The wiggle-matching approach is best used over a short section of the calibration curve where, in some cases, it may prove possible to match the dated section to within a few years on the calendar timescale (Hogg *et al.*, 2003).

A more sophisticated way of achieving optimal matches between a radiocarbon dataset and a calibration curve involves the use of statistical methods, particularly **Bayesian-based statistical modelling**. Bayesian probability differs from classical statistics in that prior knowledge and assumptions are expressed explicitly in the calculation of probability, allowing such prior information to be incorporated into the radiocarbon calibration process. This approach can be most usefully applied in the generation of age-depth models for sedimentary sequences, especially where there is a degree of scatter in the original radiocarbon dates and inversions in age-depth relationships (Walker *et al.*, 2003; Blockley *et al.*, 2004). In such cases, it is difficult to judge the coherency of the dataset and the degree to which individual values represent statistical ‘outliers’ merely by visualizing the plotted data, particularly because the probability densities of the calibrated dates are not normally distributed (Figure 5.11). Bayesian-based age-modelling approaches have therefore been developed to deal with this problem and are now widely employed in Quaternary stratigraphic and archaeological studies (e.g. Wohlfarth *et al.*, 2006; Dee *et al.*, 2013); the relevant software is available online through the OxCal web site (see above). The models use a Bayesian form of Markov Chain Monte Carlo analysis and a prior rule that age must increase with sediment depth (Bronk Ramsey, 2008). The method tests sequentially through all possible combinations for the highest probability match between the new site chronology and the radiocarbon calibration model. The probability distributions of individual radiocarbon age measurements are treated independently in the analysis, so that the outcome is not based on knowledge of the other radiocarbon dates in the set, or on a pre-judgement of the order in which the dates should plot; the data only need to satisfy the prior rule. The appeal of this approach is that it provides an objective test that is independent of stratigraphic

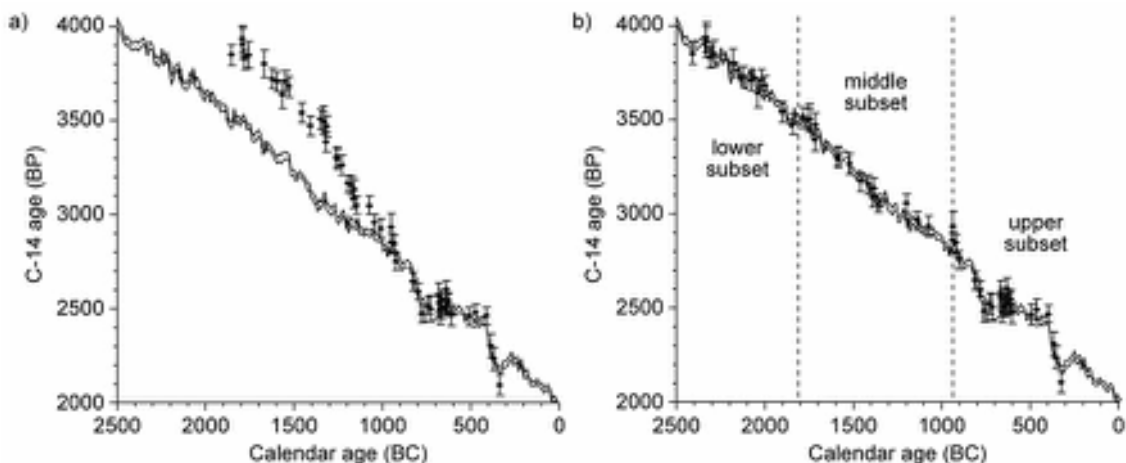


Figure 5.12 Wiggle-match dating of a peat sequence in the Netherlands. a) The individual radiocarbon ages (shown with error bars) have been wiggle-matched to the radiocarbon calibration curve based on the assumption of a constant rate of accumulation for the peat, with the younger part of the series showing the closest pattern match. b) The most probable calendar-year conversions for all dated horizons in the peat profile are shown, if the constant growth rate assumption is relaxed (after Blaauw *et al.*, 2004).

assumptions, it employs the full radiocarbon inventory available for each sequence (no data are excluded until analysis is complete) and it makes any data selection explicit (Blockley *et al.*, 2007a).

Extending and refining radiocarbon calibration models

The most secure bases for radiocarbon calibration are radiocarbon-dated tree-ring chronologies that extend back continuously from the present day. Further refinement of radiocarbon calibration would therefore be best achieved by extending the dendrochronological calibration beyond the current limit of 12,556 cal. BP (Reimer *et al.*, 2013). A 1,500-year extension to the present record may be provided by the radiocarbon wiggle-matched Huon Pine chronology from Tasmania and the Stuttgart-Hohenheim chronologies from Europe (section 5.4.1.3), as this has enabled a continuous record of atmospheric ^{14}C variations to be established back to 14 ka cal. BP (Hua *et al.*, 2009). In addition, linking of currently ‘floating’ tree-ring chronologies (i.e. tree-ring series that are currently not anchored to a calendrical timescale) to the present continuous central European tree-ring record could extend the radiocarbon calibration back to 14.2 ka cal. BP (section 5.4.1.3). Although older dendrochronological records have been obtained from a number of sites around the world, the best prospects for deriving an even longer dendrochronology-based radiocarbon calibration appear to be

from the fossil kauri (*Agathis australis*) trees preserved in peats in North Island, New Zealand (section 5.4.1.3), as these have been growing since at least MIS 5 (D’Costa *et al.*, 2009), and radiocarbon dates back to 60 ka have been obtained from wood samples (Hogg *et al.*, 2006). An alternative approach to the provision of an extended radiocarbon calibration is to use annually laminated (varved) sediments in long lake sequences (section 5.4.2.7). The most promising site in this regard is currently Lake Suigetsu, Japan (Nakagawa *et al.*, 2012), where a continuous varved sequence extends back over at least the last 70 ka, and from which a comprehensive radiocarbon inventory has been obtained that spans the whole of the radiocarbon time range (Bronk Ramsey *et al.*, 2012).

Palaeoenvironmental applications

As noted above (section 5.3.2.4), $\Delta^{14}\text{C}$ in the atmosphere is modulated, *inter alia*, by geomagnetic and solar influences, and hence the long-term deviations in $\Delta^{14}\text{C}$ that are reflected in the radiocarbon calibration curve provide a record of variations in the earth’s magnetic field and in solar activity over the past 50 ka (Laj *et al.*, 2002; Muscheler *et al.*, 2005). The level of detail that can be obtained from the ^{14}C data is remarkable, as exemplified by Miyahara *et al.*’s (2007) study of the modulation of the eleven-year sunspot cycle between AD 1413 and 1745. Such precise reconstructions of past geophysical behaviour enable temporal fluctuations in the global carbon

cycle to be quantified, and this has applications in global carbon modelling (Naegler & Levin, 2006), and in the evaluation of other influences on global climate change, such as fluctuations in ocean circulation and ventilation (Muscheler *et al.*, 2004).

5.3.3 Argon-isotope dating

5.3.3.1 Potassium–argon dating

Two approaches are employed in argon isotope dating. **Potassium–argon dating** is a technique that allows the age of volcanic rocks to be established using the radioactive isotope of potassium, ^{40}K . This is a radioactive nuclide that undergoes branching decay, leading to one of two daughter nuclides depending on the type of transformation (Figure 5.13). Most ^{40}K decays by β^- emission to produce ^{40}Ca , each particle emitted from the nucleus resulting in the conversion of a neutron to a proton. The atomic number is therefore increased by one, resulting in an element of different chemical properties, but with a virtually unchanged atomic mass. Electron capture (from the surrounding atomic orbitals) by the nucleus is the alternative

radioactive process. This converts a proton into a neutron (Figure 5.13) to reduce the atomic number by one and yield argon, a gas. Only one of these branches, the $^{40}\text{K}/^{40}\text{Ar}$ pathway, is useful for dating, for ^{40}Ca is so ubiquitous in nature that it is not possible to separate ^{40}Ca atoms produced by the decay of ^{40}K from those already present in rocks at the time of formation.

$^{40}\text{K}/^{40}\text{Ar}$ transformation is an accumulation radiometric clock. Once a volcanic rock has cooled, ^{40}Ar from the decay of ^{40}K becomes trapped within the lattice, and its abundance increases with time. Hence measurement of the amount of ^{40}Ar enables an estimate to be made of the time that has elapsed since the formation of the rock. It has to be assumed, however, that no original ^{40}Ar is present and that the system remains closed to both ^{40}Ar and ^{40}K after crystallization; hence dates will only be valid for host rocks from which argon gas cannot escape. Fortunately, many mineral lattices retain argon, and it is only if rocks become melted, recrystallized or heated to a critical temperature that substantial loss of argon will occur. In the case of a volcanic rock that has been reheated or metamorphosed, therefore, the method will determine the age at which the final phase of modification ceased and not the age of initial formation. It also has to be assumed that no non-radiogenic ^{40}Ar is present (i.e. argon from the atmosphere). In practice, some atmospheric ^{40}Ar will be included in rocks and minerals, but this can be corrected for by comparing the $^{36}\text{Ar}/^{40}\text{Ar}$ ratio in the host rock with the known atmospheric ratio for the two gases. Potassium concentrations are measured by means of atomic absorption spectrophotometry or flame photometry, while the abundance ratios of the three argon isotopes (^{36}Ar , ^{38}Ar and ^{40}Ar) are determined by gas isotope mass spectrometry (Lanphere, 2000).

Radiometric dating by the $^{40}\text{K}/^{40}\text{Ar}$ method is largely restricted to volcanic and metamorphic rocks, since sedimentary rocks do not retain argon. Yet not all volcanic and metamorphic rocks are suitable, for sufficient potassium must be present to make dating possible. The nature of the mineral lattice is also an important factor, for not all minerals retain argon over long time periods, particularly when under stress. Orthoclase and microcline, for example, do not retain argon well. Biotite, on the other hand, is one of the most suitable minerals, for not only does it retain argon, but it is also rich in potassium. The long half-life of ^{40}K (1,250 million years) means that it can be used to date some of the oldest rocks on earth. In the Quaternary, however, the $^{40}\text{K}/^{40}\text{Ar}$ method is only appropriate for dating volcanic rocks that are older than c. 100 ka. Although dates younger than this have been obtained, the large standard errors (typically ± 100 per cent) mean that these have little

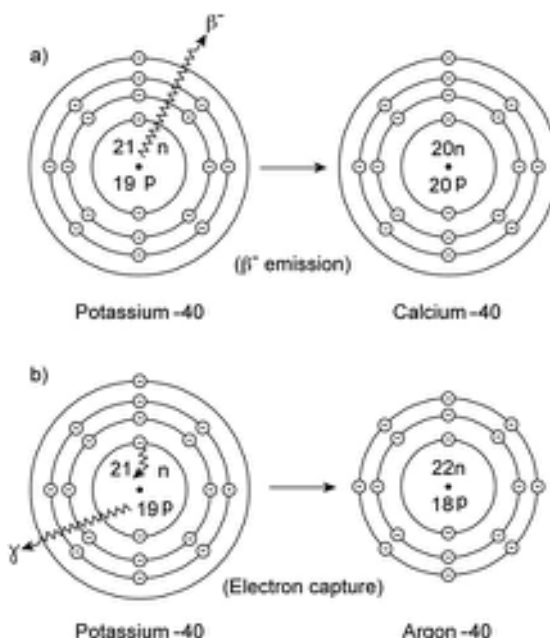


Figure 5.13 Branching decay of ^{40}K . a) Conversion of atoms of ^{40}K to ^{40}Ca through the emission of a β^- particle from the nucleus. b) Conversion of ^{40}K to ^{40}Ar through electron capture by the nucleus from one of the atomic orbitals. The latter are shown in schematic form.

practical value. However, recent methodological developments have enabled meaningful ages to be obtained from volcanic rocks as young as 30 ka (Chernyshev *et al.*, 2006), suggesting that the method may now have a much wider application in Late Quaternary geochronology.

5.3.3.2 Argon–argon (Ar/Ar) dating

One difficulty with $^{40}\text{K}/^{40}\text{Ar}$ dating is that measurements have to be made on separate aliquots (equal proportions of a sample) and this can lead to erroneous results where the sample material is heterogeneous (e.g. in basalts). The development of **argon–argon dating** circumvented this problem, for here measurements are made on a single sample of material. In this method, the ^{40}Ar content is measured directly, but the ^{40}K concentration is determined indirectly by using the known proportions between the potassium and argon isotopes. Sample grains are placed in a nuclear reactor and irradiated. This converts a portion of the stable ^{39}K isotopes to another form of argon, ^{39}Ar . The ^{39}Ar abundance is proportional to that of ^{39}K which is, in turn, proportional to ^{40}K . Hence a single mass spectrometric analysis can be employed to determine the $^{40}\text{Ar}/^{40}\text{K}$ ratio (McDougall & Harrison, 1999). The advantage of this approach is that dating can be carried out using very small samples, typically less than 10 g of material (e.g. tephra). Indeed, recent refinements to the technique enable single mineral crystals of the order of 1 mg or less to be targeted. This method, which employs a high-powered laser to drive off the argon for measurement using a super-sensitive mass spectrometer, is known as **single laser crystal fusion (SLCF) $^{40}\text{Ar}/^{39}\text{Ar}$ dating**, and has led to a significant improvement in both accuracy and precision of argon–argon age estimates (Wintle, 1996). Although this technique has been most widely employed in the dating of older volcanic materials, such as the 2.1 Ma old Huckleberry Ridge Tuff in Yellowstone, northwest USA (Ellis *et al.*, 2012), it has been used to date more recent volcanic events, such as the Laacher See eruption of 12.9 ka in the Eifel region of Germany (Van den Bogaard, 1995) and the Toba eruption in Indonesia around 73 ka (Mark *et al.*, 2013). Over shorter timescales, the dating of the eruption of Vesuvius in AD 79 (Renne *et al.*, 1997) demonstrates that the $^{40}\text{Ar}/^{39}\text{Ar}$ method can provide a practical geochronometer into the late Holocene.

5.3.3.3 Problems and limitations of argon-isotope dating

Two fundamental assumptions underlie argon-isotope dating. The first is that the system remains closed follow-

ing a volcanic event; in other words, there has been no loss of argon following crystallization. This could occur if the mineral sample has been weathered or if a further episode of heating has occurred; in both cases, an underestimate of age will result. Careful petrographic examination may reveal evidence of weathering, while the presence of secondary minerals (e.g. xenocrysts) may indicate that recrystallization has occurred. If older mineral material has become incorporated into rocks, a relatively common phenomenon in volcanic materials, this may lead to an over-estimate of age (Richards & Smart, 1991). Over-estimate of age can also be caused by the presence of excess argon in the sample; in other words, previously accumulated gas that has failed to escape while the rock was molten.

A second key assumption is that all the ^{40}Ar in the sample has been derived from the decay of ^{40}K . The problem here is that ^{40}Ar is also a constituent of the atmosphere and hence a proportion of this atmospheric ^{40}Ar (as opposed to radiogenic ^{40}Ar) will be present in minerals. This can be corrected for, however, by using another argon isotope, ^{36}Ar , which accompanies atmospheric ^{40}Ar , and which will only be present in the sample as a result of atmospheric contamination (Kelley, 2002a). Measurement of ^{36}Ar in the sample will therefore enable a correction to be made for the presence of atmospheric ^{40}Ar , using the known ratio of $^{40}\text{Ar}/^{36}\text{Ar}$ in the contemporary environment. A further difficulty occurs in argon–argon dating, however, because ^{36}Ar is produced from calcium when the sample is exposed in a nuclear reactor. In this case, correction for the presence of atmospheric argon involves the measurement of the non-naturally occurring argon isotope, ^{37}Ar , which is also produced from calcium (Aitken, 1990). A good overview of the principles and problems of both Ar–Ar and K–Ar dating can be found in Kelley (2002b).

5.3.3.4 Some applications of argon-isotope dating

The principal contributions of argon-isotope dating in Quaternary research include the dating of early hominid sites in Africa (McDougall *et al.*, 2005) and the provision of an outline timeframe for early hominid migration from Africa to eastern Europe and the Far East (Garcia *et al.*, 2010; Sémaah *et al.*, 2000). The method has also been used in the development of glacial chronologies by dating tephras interbedded with glacial deposits, for example in the Yukon (Westgate *et al.*, 2001) and Patagonia (Singer *et al.*, 2004), and it provides a chronology for the palaeomagnetic timescale (section 5.5.1).

5.3.4 Uranium-series (U-series) dating

5.3.4.1 General principles

^{238}U , ^{235}U and ^{232}Th all decay to stable lead isotopes through complex decay series of intermediate nuclides with widely differing half-lives (Figure 5.14). The helium (He) gas formed by a particle emission may become trapped within host rocks, or may slowly diffuse out, ultimately to be liberated into the atmosphere. In theory, the age of a rock or mineral can be obtained from the amount of stable lead produced, or from the amount of He liberated, but these measures are usually restricted to the dating of much older rocks (but see below). Within the more limited timescale of the Quaternary, only those intermediate nuclides with relatively short half-lives can usually be employed. However, nuclides with half-lives of only a few years or less are impractical for dating and even the intermediate nuclides with half-lives of hundreds or thousands of years cannot be used for dating of materials where radioactive disintegration has proceeded in an undisturbed system. This is because in most rocks, an equilibrium state has been achieved in which nuclides formed by decay are disintegrating at rates similar to their rate of production by the parent nuclide. If the decay chain remains unbroken, parent and daughter isotopes remain in radioactive equilibrium. However, if the decay chain is broken, then the system will be in disequilibrium until equilibrium is restored through subsequent radioactive decay. Disequilibrium between the longer-lived isotopes

can occur in natural systems for a variety of reasons. These include the loss of radon (Ra) by gaseous diffusion through a porous rock matrix, and the separation of different chemical elements during weathering, transport and deposition in the hydrosphere. Where the U-decay is interrupted, and some decay products selectively removed, the **uranium-series disequilibrium dating method** can be applied. Overviews can be found in Smart (1991a) and Latham (2001), while more in-depth accounts are provided by Ivanovich & Harmon (1995), Bourdon *et al.* (2003) and van Calsteren & Thomas (2006).

Disequilibrium methods are based on the following geochemical principles. Uranium (U) and weathering products containing U are highly soluble, whereas other products of the uranium decay chain, such as thorium (^{230}Th) and protactinium (^{231}Pa) are readily absorbed or precipitated. Thus ^{230}Th and ^{231}Pa are co-precipitated with other salts to accumulate on the floors of lakes and on the seabed, while U remains in solution. A selective separation (fractionation) of these decay products therefore occurs. Accumulating sediments will contain quantities of ^{230}Th and ^{231}Pa but will be deficient in U, whilst organisms that secrete carbonate direct from ocean waters (such as molluscs and corals) will build a carbonate shell or skeleton that contains U but very little ^{230}Th or ^{231}Pa . The same principles apply to carbonate precipitates such as speleothems and travertines, where fractionation results in the separation of uranium from decay products, and the age of precipitation can be measured from the renewed accumulation of radioactive decay products in

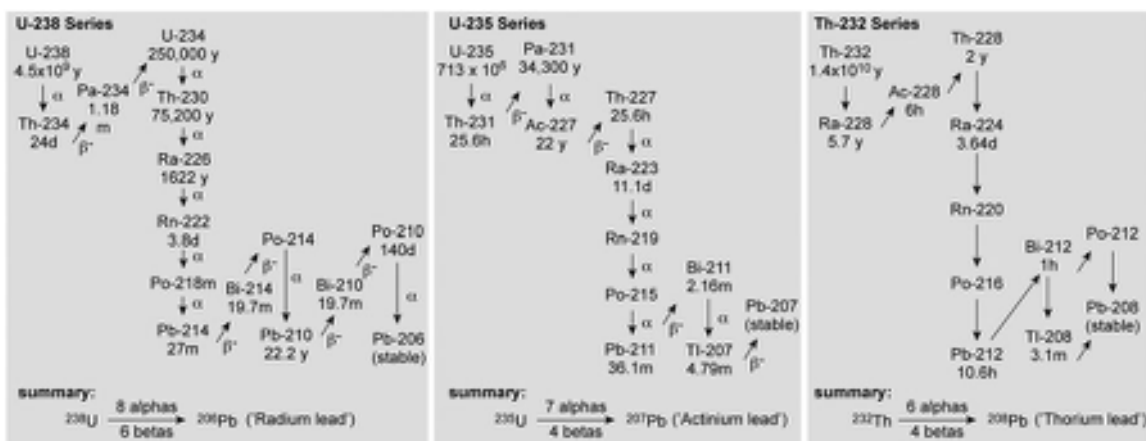


Figure 5.14 Chain decay pathways and half-lives of intermediate nuclides during the decay of ^{238}U , ^{235}U and ^{232}Th to stable lead. The elements are arranged vertically according to atomic number. Loss of an α particle results in a decrease in atomic number, whereas emission of a β^- particle leads to an increase. Some of the very short-lived nuclides within the decay chain have been omitted; d – days; h – hours; m – minutes.

the speleothem calcite. Age of lake or ocean floor sediments can be estimated by measuring the rate of decay of ^{230}Th or ^{231}Pa down a sediment profile, while the age of carbonate fossils, speleothems, teeth and bone can be derived from measurement of the accumulation of decay products of U within the carbonate matrix. The former has been referred to as the **daughter excess (DE)** type of U disequilibrium series dating method, that is, the daughter nuclides are initially present in excess of concentration at secular equilibrium before decaying over time, while the latter is termed the **daughter deficient (DD)** group of methods, in which the daughter nuclide is initially absent but increases with time until equilibrium is achieved. DE methods have been most widely used in the dating of ocean sediments using the decay of ^{230}Th or ^{231}Pa , while the DD methods are principally based on measurement of $^{230}\text{Th}/^{234}\text{U}$ ratios in a variety of materials including tufa, speleothem, shell, bone and phosphates, all of which are initially deficient in thorium.

5.3.4.2 Measurement, problems and age range

Conventional measurement of U-series ages is by means of alpha spectrometry following chemical extraction of thorium and uranium from the sample material. Since the late 1980s, however, **thermal ionization mass spectrometry (TIMS)** has been employed to determine U-isotope ratios. This approach enables individual atoms to be counted directly as opposed to the monitoring of alpha particles emitted during radioactive decay. It is therefore more rapid and, as count rates are not restricted by the half-life of the isotope, there is the potential for extending the age range of the technique. In addition, the method offers a greater level of analytical precision enabling, for example, meaningful ages to be obtained from Lateglacial and Holocene materials (Camoin *et al.*, 2012). Over the past decade, further advances have been made in thermal ionization techniques, and the advent of alternative mass spectrometric methods, especially **multi-collector inductively coupled-plasma mass spectrometry (MC-ICPMS)** (Goldstein & Stirling, 2003) and **laser-ablation ICPMS** (Eggins *et al.*, 2005), have continued to improve the quality of U-series studies.

A number of assumptions underlie the U-series disequilibrium method. It must be assumed that the decay coefficients have been accurately determined and that the activity ratio of daughter to parent nuclide can be measured to a high level of precision. These two requirements can largely be met. A third assumption, namely that there has been no loss or gain of nuclides since deposition, is more

difficult to satisfy, and a number of materials show evidence of departure from **closed system** behaviour (Table 5.3). Dating of such material necessitates the use of correction factors which, in turn, requires a detailed knowledge of the geochemistry that gives rise to the isotope disequilibrium (see below). Open-system behaviour may be reflected in reversals in isotopic ages in stratigraphic sequence or the samples themselves may show evidence of open-system activity. For example, petrographic study of calcite may indicate recrystallization and similar evidence may be detected in bone (Scholz *et al.*, 2004). A fourth assumption is that the sample has not been contaminated at the time of formation by detrital materials that already contain daughter nuclides. Hence in the measurement of the $^{234}\text{U}/^{230}\text{Th}$ ratio in speleothem calcite, for example, it is assumed that the ^{230}Th content was zero at the time of crystal formation, for any residual ^{230}Th in the sample would result in an age that was too old. Again, empirical evidence has shown that this assumption does not always hold, and that dated materials may contain varying amounts of detrital ^{230}Th . The presence of detrital ^{230}Th can be detected by measuring the amounts of ^{232}Th in a sample. This long-lived isotope occurs in water as a trace impurity and, where present, is indicative that contamination has occurred. The $^{232}\text{Th}/^{230}\text{Th}$ ratio may then be used as a basis for the correction of detrital contamination. One way to identify the effects of detrital contamination and to correct for them is by the isochron technique (Dorale *et al.*, 2007). This involves measuring the activity ratios of different minerals, or of whole rock fragments, obtained from the dated sample. If straight line plots are obtained, this indicates that the different mineral phases were formed simultaneously, and the best estimate of age is that ratio at which the isochron lines intersect. A large scatter in the dataset indicates that detrital contamination is a major problem.

The age range of the uranium-series disequilibrium method varies with the nuclides employed. The practical dating range using alpha-particle spectrometric methods is around five half-lives, and hence $^{230}\text{Th}/^{234}\text{U}$ has been employed to date samples in the range 5–350 ka, while $^{231}\text{Pa}/^{235}\text{U}$ and $^{231}\text{Pa}/^{230}\text{Th}$ have upper limits of around 200 ka and 250 ka, respectively. Recent developments in mass spectrometric counting (TIMS, ICPMS), however, have reduced the lower limits of the $^{230}\text{Th}/^{234}\text{U}$ method to less than 100 years, while increasing the upper age limit to c. 500 ka. Materials in the range 100 ka to 10 Ma may, in theory, be dated using $^4\text{He}/\text{U}$ ratios, while the $^{234}\text{U}/^{238}\text{U}$ method has a potential age range of up to 1.5 Ma. Although the very long half-life of ^{238}U (4.5×10^9 yr) means that U-Pb (lead) methods had previously been largely applied

Table 5.3 Reliability of uranium-series dates for terrestrial materials due to deviations from closed system behaviour and contamination by ^{230}Th and ^{234}U from detritus (after Smart, 1991a).

Reliability	Material	Closed system?	Contaminated?
Reliable	Unaltered coral	Closed	Clean
	Clean speleothem		Clean
	Volcanic rocks		–
	Dirty speleothem		Contaminated
Possibly reliable	Ferruginous concretns	Possibly closed	Contaminated
	Tufa		Contaminated
	Mollusc shells		Contaminated
	Phosphates		Contaminated
Generally unreliable	Altered coral*	Open	Clean
	Bone		?
	Evaporites		Contaminated
	Caliche		Contaminated
	Stromatolites		Contaminated
	Peat and wood		?

* Diagenetically altered.

only to the dating of old rocks, under certain favourable circumstances (e.g. radiogenic speleothems with very low common Pb) and using recently developed MC-ICPMS analytical methodologies, it has proved possible to generate excellent age resolution on much older materials (Woodhead *et al.*, 2006). Examples include the dating of an Early Pleistocene Italian cave stalagmite (Bajo *et al.*, 2012), and flowstones of around 1 Ma in caves from South Africa (Pickering *et al.*, 2013). Further refinements in this area could eventually lead to a combination of U-Th and U-Pb methods covering the whole of the Quaternary time range and beyond (Latham, 2001).

5.3.4.3 Some applications of U-series dating

Speleothems

$^{230}\text{Th}/^{234}\text{U}$ dating has been widely applied to the dating of cave calcite precipitates – stalagmites, stalactites, flowstones, etc., the palaeoclimatic significance of which has already been considered (section 3.8). ^{234}U is precipitated from karst waters during the formation of speleothem carbonate, and almost all of the ^{230}Th subsequently found appears to be authigenic, that is, it has originated from decay of ^{234}U that forms part of the speleothem chemistry. Because not all speleothems can be layer-counted, age-depth models have been produced using U-series determinations spread along the length of the speleothem (Scholz *et al.*, 2012), and in some instances, Bayesian

analysis has been used, as in radiocarbon, in the development of speleothem chronologies (Millard, 2006). The dating of cave speleothem and associated material forms the chronological basis for a range of environmental applications (Richards & Dorale, 2003); these include climatic reconstructions (Fleitmann *et al.*, 2004), cave archaeology (Pike & Pettitt, 2003), the depositional history within caves (Hearty *et al.*, 2004), sea-level change (Surić *et al.*, 2009), and in an unusual application, the dating of cave art (Pike *et al.*, 2012). Further applications and details of recent developments in speleothem dating can be found in Drysdale *et al.* (2012).

Corals

Corals are generally regarded as one of the best media for U-series dating for, after death, coral skeletons act as closed systems until the coral is dissolved or changes to calcite. Moreover, they contain sufficient uranium (typically 2–3 ppm) for the application of both the $^{230}\text{Th}/^{234}\text{U}$ and $^{231}\text{Pa}/^{235}\text{U}$ methods. Since these are independent decay chains, they can provide an internal check on calculated ages. U-series dating of raised coral reef complexes has been widely employed in studies of Late Quaternary environmental change, with high stands of sea level during the recent interglacials commonly recorded in raised reef complexes (Thompson *et al.*, 2011) although corals of Middle Pleistocene age have also been dated using this method (Stirling & Andersen, 2009). In addition, the

technique has been used to determine the duration of interglacial periods as reflected in periods of high sea level (Edwards *et al.*, 2003). As noted above (section 5.3.2.6), U-series dating of fossil corals provides a basis for calibrating the radiocarbon timescale (Fairbanks *et al.*, 2005), and can also be used to calibrate orbitally tuned timescales based on the marine oxygen isotope record (Thompson & Goldstein, 2006; section 5.5.3).

Carbonate deposits

These include such diverse materials as travertines, calcrites, lake marls, stromatolites, phosphates and evaporites. Travertines and calcareous tufa can be difficult materials to date because of their complex growth mechanisms and contamination by detrital and organic particles (Garnett *et al.*, 2004), but reliable U-series age determinations can be obtained providing they are based on primary calcite (e.g. micrite and spar), and iron (Fe) and aluminium (Al) levels are low (Mallick & Frank, 2002). Dating of pedogenic calcareous nodules in alluvial terrace sequences is possible, but only if multiple ages are generated from a single site and are shown to be stratigraphically consistent (Candy *et al.*, 2005). U-series dating of lake sediments usually requires significant corrections to account for detrital inputs of Th and U, but the technique has enabled coherent long chronologies and sediment accumulation histories to be established (Torfstein *et al.*, 2009).

Molluscs

Thus far, U-series dating of fossil molluscs has been relatively unsuccessful, due partly to the fact that they contain initially only very small amounts of uranium (e.g. one-fiftieth of that contained in corals), and also to the fact that they do not function as geochemically closed systems, for diagenetic uptake of uranium is common following death of the organism (McLaren & Rowe, 1996). Hence, uranium-series dates on molluscs have tended to be regarded as unreliable. On the other hand, coherent age estimates on molluscs have been obtained in some instances (Jedouï *et al.*, 2003), and particularly from contexts where these can be compared with the results from other dating methods, such as radiocarbon (Magnani *et al.*, 2007). As many shorelines are not characterized by coral (a more suitable dating medium), but often contain shells, attempts are likely to continue to find a means of obtaining reliable U-series dates from fossil molluscs.

Bone

Following the death of an animal, U from groundwater enters and is trapped within the bone apatite. In theory,

therefore, the reappearance of Th and Pa in bone apatite can be determined using either the $^{230}\text{Th}/^{234}\text{U}$ or $^{231}\text{Pa}/^{235}\text{U}$ ratios, but discrepancies between $^{230}\text{Th}/^{234}\text{U}$ and $^{231}\text{Pa}/^{235}\text{U}$ dates on the same sample, and between ^{14}C dates and U-series dates on bone, suggests that problems of leaching (resulting in U depletion) and open-system behaviour (resulting in U enrichment) remain. However, because both human and animal bone is such an important and relatively common fossil material (Pike & Pettitt, 2003), considerable efforts have been made to resolve the problem of open-system behaviour in buried bone (Pike *et al.*, 2002; Grün *et al.*, 2010). These have largely involved the development of uptake models to try to describe how and when the U was absorbed into bone (e.g. Sambridge *et al.*, 2012), but these may need to be calibrated using other dating techniques, such as electron spin resonance (section 5.3.7). Further progress is still required before reliable U-series dates can be obtained from bones and teeth.

Peat and other applications

Peat, along with other organic material, takes up U from groundwaters and can become relatively enriched in the element. Since peat has a high adsorption capacity, any percolating groundwater will transfer its U content to the upper peat surface layer, thus protecting the older layers from further acquisition of U. As with bone, the incorporation of U-bearing inorganic detrital material into the peat deposits has proved to be a problem. However, some encouraging results have been obtained on peat (Walker *et al.*, 1992; Vaughan *et al.*, 2004), and refinement of the method offers the prospect of dating interglacial peats and other organic deposits that currently lie beyond the range of radiocarbon (Frechen *et al.*, 2007).

U-series has also been employed in the dating of young volcanic rocks (Miallier *et al.*, 2004) and of wood samples from fluvial sediments (Allard *et al.*, 2012).

5.3.5 Fission track dating

5.3.5.1 General principles

This method, which dates uranium-bearing crystals, is based on the **spontaneous fission** of ^{238}U : that is, the nucleus (of atomic number 92) divides to form elements of medium atomic number from about 30–65 (e.g. barium 56). An important consequence of spontaneous fission is that the energy released leads to high-speed collisions between fission fragments and neighbouring atoms. In rocks containing uranium, fission fragments cause **damage trails** or **tracks** in the wake of their movement through the host crystal lattice. The ‘damage’ induced is a result of

ionization of the atoms that come into contact with fission fragments. The positive charge acquired by adjacent atoms leads to mutual repulsion and therefore disorder in the crystal lattice. The tracks can be retained for millions of years and their number is a function of both U content and time. Fission track (FT) dating is mostly applicable to volcanic extrusive rocks such as basalts, tephras and tuffs, where the fission track clock is zeroed by the heating event, although it has also been applied to volcanic glasses such as obsidian and pumice. Zircon is the most widely used mineral because of its naturally high U content and also its widespread occurrence in volcanic rocks. Details of fission track dating can be found in Wagner & van den Haute (1992) and van den Haute & Corte (1998).

A variant of FT dating is **alpha-recoil track (ART) dating**. This method is also based on the analysis of damage trails etched in crystals by natural radioactivity, but ARTs are formed by recoil of the nucleus that emits alpha particles during the decay of U and Th, as well as from other daughter nuclei. Although relatively new and not yet as widely applied as FT dating, tests of the concentrations of ARTs in dark mica from the Quaternary volcanics of the Eifel region, Germany, suggest that this technique may have considerable potential for dating Quaternary events (Gögen & Wagner, 2000).

5.3.5.2 Measurement and problems

The age of a mineral or glass can be obtained by counting 'spontaneous' ^{238}U fission tracks under a microscope after the surface has been polished and treated with a chemical etchant to enlarge the fission tracks. In order to use these data to infer age, it is necessary to know the original U content of the sample and while this cannot be determined by direct measurement, it can be inferred indirectly by measuring the amount of ^{235}U . After the 'spontaneous' fission tracks have been counted, therefore, the sample is irradiated in a nuclear reactor with thermal neutrons to induce fission in atoms of the less abundant U isotope ^{235}U ; this produces a new set of fission tracks which can also be etched and counted. The 'induced' fission track count provides a measure of ^{235}U abundance, from which the concentration of ^{238}U in the sample can be obtained from the known $^{235}\text{U}/^{238}\text{U}$ ratio in volcanic rocks (Hurford, 1991).

The method, however, is not without its problems. Fission tracks can 'heal' or be erased (a process known as **fading** or **annealing**) through the heating of the host materials or through spontaneous diffusion of ions. The result is that the tracks become narrower and shorter over time until they eventually disappear completely. Partial

fading is reflected in a reduced number of fission tracks and, if not detected, will lead to an under-estimate of age. Not all materials show the same tendency to anneal, however; in some minerals, such as zircon and titanite, fission tracks are relatively stable and fading is less of a problem. Apatite, by contrast, is much less stable, while in glasses stability decreases with decreasing silica content. A number of experimentally established correction procedures can be applied to counter this problem. These involve the step-wise heating of paired samples containing spontaneous and induced tracks until the ratio of the spontaneous track density in the natural sample to the induced track density in the irradiated sample reaches a plateau level, this plateau value providing a corrected age for the sample (**plateau correction procedure**). A variant on this method is the **isothermal plateau fission track technique (ITPFT)** in which paired samples are subjected to a single heat treatment until a pre-determined temperature is achieved and sustained for a specified period (Westgate, 1989). Since the density of fission tracks depends on U content and age, the method cannot be applied where the density of tracks is too low (typically in samples of less than 100 ka) or, at the other extreme, so high that counting becomes impossible. Ironically, rocks with a rich U content are not suitable because of the very high density of tracks, and in these instances the selection of minerals with a low U content, such as sphene, may form a more suitable counting medium.

5.3.5.3 Some applications of fission track dating

Materials that have been dated by this method range from glass manufactured in the nineteenth century to some of the oldest rocks on earth (Wagner, 1998). In the context of the Quaternary, the most significant contribution of the technique has been in the dating of tephras and tuffs in the age range 50 ka (the upper limit of radiocarbon) to 500 ka. Where these have been found interbedded with glacial deposits, fission track dating can provide a timescale for glacial events, as has been the case, for instance, in western Argentina (Espizua *et al.*, 2002), the west-central United States (Colgan, 1999) and Alaska (Westgate *et al.*, 2001). Widespread tephras form key marker horizons (section 5.5.2) and fission track dating may enable ages to be assigned to these. Examples include the Rockland Tephra (c. 400 ka), a widespread pyroclastic layer and hence a key stratigraphic marker horizon in western North America (Meyer *et al.*, 1991), and the much older but equally significant Bishop Tuff (c. 700 ka) also from the western United States (Izett & Naeser, 1976). Other

applications include the dating of the Early Pleistocene hominid colonization of southeast Asia (O'Sullivan *et al.*, 2001), of Middle Pleistocene (800–900 ka) stone tool assemblages on the island of Flores in Indonesia (Morwood *et al.*, 1998) and of Middle Pleistocene glacial–interglacial sequences in Italy (Marcolini *et al.*, 2003). The technique has also provided chronologies for uplift and erosion in the Himalayas (Burbank *et al.*, 2003) and for the Pleistocene drainage history of the European Alps (Bernet *et al.*, 2004). In addition, the method has also been used in the tracing of trade routes in the Andes based on fission track dates obtained from obsidian artefacts (Dorighel *et al.*, 1998).

5.3.6 Luminescence dating

5.3.6.1 General principles

Any material that contains U, Th or potassium (K) (all sediments and volcanic rocks contain all three), or lies in close proximity to other materials containing these radioactive substances, is subject to continuous bombardment by α , β and γ particles. This leads to ionization in the host materials and the ‘trapping’ of metastable electrons within minerals. These electrons can be freed by heating, and under controlled conditions, a characteristic emission of light occurs which is proportional to the number of electrons trapped within the crystal lattice of mineral grains, principally quartz and feldspar. This is termed **thermoluminescence** and is the basis of **thermoluminescence (TL) dating**. The electrons can also be released from traps by shining a beam of light onto the sample, and again the luminescent signal is a reflection of the number of electrons trapped within the crystal lattice. This is **optically stimulated luminescence** and hence the technique is referred to as **optically stimulated luminescence (OSL) dating**, although this is now often abbreviated to **optical dating** (Aitken, 1998).

All electron traps can be emptied by exposure to heat, but only some are sensitive to light. The luminescent clock is reset by heating, for example by firing of pottery or, in the case of sediments, by exposure to heat from a campfire or forest fire, or by exposure to sunlight. This process is often referred to as **bleaching**. In both cases, the majority of the electron traps are effectively emptied but then progressively fill following burial of the pottery or sediment. The ‘natural luminescence signal’ therefore provides an indication of the time that has elapsed since firing, in pottery, or, in the case of sediment, since burial and removal from sunlight. In volcanic rocks, the zeroing of the electron clock will be a direct consequence of both heat and mineral formation. Further details on

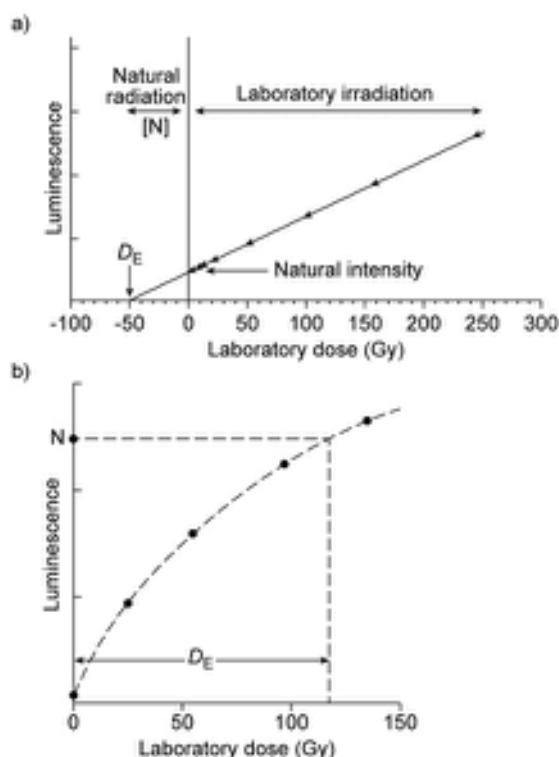


Figure 5.15 Methods of measuring palaeodose (D_E) after the natural TL intensity of a sample (N) has been established. a) In the **additive method**, different aliquots of the sample are irradiated in the laboratory at increasing intensities of irradiation and the corresponding TL properties measured. b) In the **regenerative method**, aliquots of the sample are initially bleached to low radiative intensities and then progressively irradiated by known amounts, with corresponding TL values noted. Method b can be applied using multiple or single aliquots (**single aliquot regeneration**, or **SAR**) of a sample. Each approach establishes the mathematical correspondence between D_E , N and TL. Radiation intensity is measured in units of gray (Gy) (based on Grün, 2001 and Aitken, 1998).

luminescence dating can be found in Aitken (1998), Lian & Huntley (2001), Duller (2004) and Wintle (2008). Case studies are described in two recent symposium volumes on luminescence and ESR dating (Grün, 2010; Grün & Preusser, 2012).

5.3.6.2 Measurement and problems

TL measurements are carried out on a sample of mineral material, usually a separated quartz or feldspar fraction. This is heated to temperatures in excess of 500°C and as

light (photons) is emitted from the luminescence centres, these photons are converted to electric pulses using a sensitive light detector. The light emission (TL intensity) is then plotted against heating temperature to produce a **glow curve**, in which the peaks are reflective of the thermal lifetimes of the various electron trap populations within the sample. The most important are the traps with long thermal lifetimes ('deep traps') because the electrons within them will remain there over relatively long periods of time. Once a 'natural signal' has been obtained, this is compared with the 'artificial signals' obtained from a portion of the sample to which known doses of radiation have been administered from a calibrated laboratory radioisotope source (Figure 5.15). This enables the **equivalent dose (D_E)** to be determined, which is a measure of the amount of radiation that would be needed to generate a TL signal equal to that which the sample has acquired subsequent to the most recent firing (zeroing) event or exposure to sunlight. The D_E is sometimes referred to as the **palaeodose** or **palaeodose equivalent**.

Many of the principles of TL dating underlie OSL dating, but the major difference is that the trapped electrons are released by light rather than by heat. In the earlier studies, a beam of green light from an argon ion laser was employed, but other light sources have subsequently been used, including filtered halogen lamps and high-powered light-emitting diodes (LEDs). A further development has been the employment of **infrared stimulated luminescence (IRSL)**, although this approach can only be applied to feldspar grains as electron traps in quartz are insensitive to infra-red stimulation. For quartz grains, high-powered blue-green LEDs are now routinely used.

In order to arrive at an estimate of age using either TL or OSL, the environmental **dose rate** (or **annual dose rate**) has to be determined. This is a measure of the radiation dose per unit of time absorbed by particular minerals since the zeroing of the luminescence clock either by firing or by exposure to sunlight. The dose rate is calculated from an analysis of the radioactive elements in both the sample and its surroundings, the so-called internal dose rate and external dose rate. However, the determination of the total radiation dose that the sample has received since burial is not straightforward for, in addition to radiation from the surrounding sediments, the sample will also have been affected by cosmic rays from deep space, and these need to be corrected for. In addition, water and organic matter, where present in a body of sediment, absorb radiation at a different rate from mineral sediment, and this has to be accounted for in dose rate calculations. Overall, this can usually be measured with a precision of around 5 per cent (Grün, 2001).

Once the dose rate has been established, then TL/OSL age can be calculated from the following:

$$\text{TL/OSL age (yr)} = \frac{\text{Equivalent dose}}{\text{Annual dose}}$$

Possible sources of error in luminescence dating include systematic errors in the calibration of laboratory radiation sources, light contamination during field sampling, and the accurate determination of the dose rate discussed above. A number of potential difficulties surround the zeroing of the luminescence clock because, particularly in TL dating, there may be a residual TL component which, if not corrected for, will result in an aberrant age. Reworking of sediments, intermittent exposure to sunlight, and grain-to-grain variability in the extent of bleaching are all problems encountered in the dating of sediments. Inadequate bleaching and reworking of older sediments may be particularly problematical in the dating of glacial sediments (Lukas *et al.*, 2007). Dating errors can also arise as a result of the leakage of electrons from thermally stable electron traps, a problem that affects both TL and OSL dating of feldspars (but not quartz) and which is usually referred to as **anomalous fading** (Huntley & Lamothe, 2001). This results from disequilibrium in the uranium decay chain and variations in past water content of sediments, the latter in particular being very difficult to assess.

5.3.6.3 Developments in luminescence dating

The increasing use of OSL in the dating of sediments has stimulated a number of methodological developments. An important advance was the **single aliquot regeneration method (SAR)** which uses repeated measurements on a single sample rather than multiple aliquots from the same sample, as is the case in TL, to determine D_E (Wintle & Murray, 2000). This enables much smaller samples of material to be dated, and it also avoids the problems of differing luminescence sensitivity resulting from grain-to-grain variations within a sample (section 5.3.6.2). A second important development has been the ability to obtain OSL measurements from single grains of quartz or feldspar. Again, this makes it possible to determine whether all of the grains in a sample of sediment possess the same apparent age (Duller, 2004). More recently, studies have been undertaken into a new signal from quartz, termed the **thermally transferred optically stimulated luminescence (TT-OSL)**. This appears to have the potential to date sediments over much longer periods than OSL, but further comparisons with independent chronological methods are needed (Duller & Wintle, 2012). These and other technolo-

logical advances are reviewed in Wintle (2008, 2010). Although OSL is a relatively recent development, it has effectively replaced TL in the dating of sediments, partly because of the technical innovations described above, but also because residual signals are usually much smaller for OSL than for TL dating, which enables younger sample materials to be dated (Lian & Huntley, 2012).

5.3.6.4 Age ranges and applications of luminescence dating

The lower age range of luminescence dating reflects the sensitivity of the sample and the efficiency of the zeroing mechanism, while at the upper end of the dating range, **saturation** (the point at which the electron traps become completely filled) and the long-term stability of the TL/OSL signal are the principal constraints. At the younger end of the dating range, TL ages of around 100 years have been obtained from fired pottery, while OSL dates obtained on quartz grains from dune sands in Denmark that accumulated during the last few centuries are entirely consistent with independent dates from historical sources (Clemmensen & Murray, 2006). At present, the upper practical limit for quartz appears to be around 150–200 ka, although luminescent ages of around 450 ka have been obtained on quartz from fluvial sediments in the Thames Valley which were consistent with an independently assigned age (MIS 12) for the deposits (Pawley *et al.*, 2010). Optical dates on feldspar may have a similar upper age limit to quartz. Here, problems of anomalous fading are a major limitation, but recent studies using infra-red IRSL and the application of carefully selected correction factors suggest that this range might, in due course, be extended (Kars *et al.*, 2008). With the TT-OSL method, there is the potential for dating sediments back to one million years (Duller & Wintle, 2012). This has been recently confirmed by the dating of quartz from cave sediments in South Africa, where TT-OSL dates of around 1 Ma were supported by independent age estimates based on U-series and palaeomagnetic evidence (Pickering *et al.*, 2013).

The range of luminescence dating applications is considerable, and the technique is now used almost as widely as radiocarbon in the dating of Late Quaternary events. It has been applied to the dating of a variety of archaeological contexts, including stratified cave sequences with interbedded artefacts (Barton *et al.*, 2009), burnt flints from Palaeolithic contexts (Richter, 2007), ancient hearths (Sun *et al.*, 2012), historic iron smelters (Godfrey-Smith & Casey, 2003), pottery (Zink *et al.*, 2012) and calcite overgrowths on ancient rockwall cave paintings (Watanabe *et al.*, 2003a). Other applications include the

dating of beach sands (Roberts & Plater, 2007), glacial deposits (Puthusserry *et al.*, 2008), lake deposits (Wilkins *et al.*, 2012), colluvial deposits (Fuchs *et al.*, 2004) and fluvial sediments (Popov *et al.*, 2012). The technique has proved to be especially valuable in the dating of sediment sequences and landforms in desert regions, where there is frequently no alternative chronometric method (Singhvi & Porat, 2008; Singhvi *et al.*, 2010).

5.3.7 Electron spin resonance (ESR) dating

5.3.7.1 General principles and measurement

Electron spin resonance (ESR) dating was initially used in Quaternary research to determine the age of speleothem calcite, but it has since been employed to date a variety of materials, most notably tooth enamel, but also coral, molluscs, quartz-bearing rocks and sediments, and burnt flint. The basic principles of the technique are similar to those of optical dating in that it involves the direct measurement of radiation-induced paramagnetic electrons trapped in crystal defects in a body of rock or other material (indeed, the technique is sometimes referred to as **electron paramagnetic resonance**). These ‘free’ electrons are generated by α , β and γ radiation from natural radioelements (e.g. U, Th and K) and have accumulated in the crystal lattices of minerals over time. Exposure to high-frequency electromagnetic radiation in a strong magnetic field ‘excites’ the electrons and their resonance can be detected as the magnetic field is changed. This is because when the trapped electrons (or ‘spins’) are in resonance, electromagnetic power is absorbed in proportion to the number of electrons present; the greater the number of electrons, the greater the absorption. Hence the latter is a reflection of age and, as in luminescence dating, is known as the **palaeodose** or **equivalent dose**. Again, this is a measure of the amount of radiation that would be needed to generate an ESR signal equal to that which the sample has acquired subsequent to the most recent zeroing event.

In order to obtain an age for the sample, an estimate has also to be made of the **dose rate** (or **annual dose**), which is a measure of radiation dose per unit of time since the zeroing of the electron clock. This includes both internal and external radiation, plus cosmic ray radiation. The age of a sample can then be obtained by dividing the value for equivalent dose by the dose rate. It is important to note, however, that in ESR dating, the electron traps are not emptied, as in the case of luminescence dating, and this means that replicate measurements can be made on a single sample of material. Overviews of ESR dating can be

found in Rink (1997), Blackwell (2001a) and Schellmann *et al.* (2008).

5.3.7.2 Sources of error in ESR dating

Almost all of the error sources discussed above in relation to luminescence dating apply equally to ESR dating. These include the non-zeroing of the electron clock, leakage from electron traps and problems relating to sample context, such as reworking of materials or the effects of ground-water movement. The last-named poses particular difficulties in estimating the annual dose, for while ideally both the dated sample and surrounding deposit should form a geochemically closed system with regard to the relevant isotopes, in practice erosion or deposition of relatively radioisotope-rich sediments surrounding the sample can often result in major changes in the radiation flux over time (Smart, 1991b). A further complication is that many materials conventionally dated by ESR show post-depositional uranium uptake, the extent of which cannot normally be established, and recourse has to be made to models to attempt to simulate the process (Grün, 2001). As a consequence, although ESR dates may be *accurate* (in other words, they provide a reasonable approximation of the true age of the sample: section 5.2), they tend to be of low analytical precision. Precision will also be affected by the strength of the ESR signal: a weak signal, for example, could result in a precision of no better than ± 100 per cent. Overall, therefore, ESR dating is a technique that seldom generates ages with errors of < 10 per cent (Rink, 1997).

5.3.7.3 Some applications of ESR dating

ESR dating has a greater time range than many of the techniques discussed in this book, extending from a few thousand years to about 2 Ma in the case of tooth enamel. Most of the applications on other materials lie in the time range between 20 and 700 ka. Examples include the dating of glacial sediments in western China up to 710 ka of age (Zhou *et al.*, 2002); of teeth from a site of Hoxnian interglacial age (MIS 11) in eastern England (Grün & Schwarcz, 2000); of the first human settlements of the Loire Basin, western France, around 1.1 Ma (Voinchet *et al.*, 2010); of molluscs associated with Palaeolithic artefacts in Egypt of MIS 2 and MIS 4 age (Blackwell *et al.*, 2012); and of quartz phenocrysts from the Mt Toba super-eruption where the ESR ages (mean value of 81 ± 17 ka) accord with the previously derived argon isotope ages of 74 ± 4 ka (Wild *et al.*, 1999). Dating of corals from the Netherlands Antilles has shown not only that the method is appropriate for the dating of older Pleistocene corals, but

that coherent ESR ages can be obtained from younger coral material that was formed only a few hundred years or even a few decades ago (Radtke *et al.*, 2003). Further applications of the ESR method can be found in Grün (2010) and Grün & Preusser (2012).

5.3.8 Cosmogenic radionuclide (CRN) dating

5.3.8.1 General principles

Cosmogenic nuclides form when high-energy cosmic rays entering the earth's atmosphere collide with nuclei, triggering a cascade of high-energy neutrons that impact on the earth's surface. The collisions between these neutrons and target nuclei within certain minerals cause these nuclei to fragment (a process known as **spallation**) resulting in the creation of new radioactive nuclides. These accumulate in the surface layers of rocks and boulders and their abundance is directly related to the time that the surfaces have been exposed to cosmic ray activity. By measuring the concentration of cosmogenic nuclides in rock surface samples, therefore, an estimate can be obtained on the time of exposure of that rock surface. This is the basis of **cosmogenic radionuclide (CRN) dating**, also known as **terrestrial in situ cosmogenic nuclide (TCN) dating**. Details of the method and its applications can be found in Gosse & Phillips (2001), Ivy-Ochs & Kober (2008), Dunai (2010) and Balco (2011).

In addition to **surface exposure dating**, however, CRN dating can be used to estimate weathering and erosion rates and therefore to develop timescales for long-term landscape evolution, and also to determine ages for buried depositional sequences. The first approach involves modelling measured surface concentrations of cosmogenic nuclides in an eroding rock outcrop, and has been used to establish site-specific denudation rates in different geomorphological contexts (Cockburn & Summerfield, 2004). Cosmogenic burial dating uses a pair of nuclides (usually ^{10}Be and ^{26}Al) that are produced in a rock or mineral, but with different decay constants. On an exposed surface, the concentrations of the two nuclides conform to the production ratio. Once buried, however, nuclide production ceases and the inventories of both nuclides decline due to radioactive decay. As they decay at different rates, the ratio between the two nuclides gradually diverges from the surface production ratio. Hence by measuring this ratio in a body of sediment, the time when these nuclides were first shielded from the effects of cosmic rays (i.e. buried beneath a surface overburden) can be determined (Dehnert & Schlüchter, 2008).

5.3.8.2 Measurement and problems

For surface exposure dating, samples 1–2 cm in thickness are chiselled off exposed rock surfaces or off boulders lying on the rock surfaces or on deposits such as moraines. Sampling sites should be horizontal or near-horizontal surfaces where there are no obvious signs of weathering or erosion in order to ensure that the layers of sampled rock contain representative nuclide concentrations.

A number of cosmogenic nuclides are now commonly used as a basis for dating (Table 5.4). Beryllium-10 (^{10}Be), carbon-14 (^{14}C), aluminium-26 (^{26}Al) and chlorine-36 (^{36}Cl) are radioactive and are measured using AMS, while the ‘noble gases’ helium-3 (^3He) and neon-21 (^{21}Ne) are stable and can be measured by mass spectrometry. The different half-lives of the various nuclides mean that they are appropriate to different time ranges. For the dating of surfaces less than 5 ka in age, ^3He and ^{36}Cl are most generally employed, although technical advances in extraction and measurement suggest that *in situ* produced ^{14}C may become more widely used in the future (Naysmith *et al.*, 2004). For longer time periods, ^{10}Be , ^{21}Ne , ^{26}Al and ^{36}Cl are more applicable. Cosmogenic ^3He and ^{21}Ne are

usually determined on a particular mineral such as olivine or garnet; ^{14}C , ^{10}Be and ^{26}Al are measured on pure quartz; whereas ^{36}Cl analyses are generally undertaken on whole rock samples.

There are two principal sources of error in CRN dating, the first relating to factors affecting the CRN signal in the dated rock surface, and the second to the determination of CRN production rates. In terms of the first, it is assumed that there has been no erosion or weathering of the surface since the time exposure. On bedrock surfaces, this can be checked by replicate measurements, but it is a problem in other contexts, for example in the dating of boulders on moraines where erosion and exhumation of fresh boulders can cause an under-estimate of age (Putkonen & Swanson, 2003). Under-estimates of age may also result if the surface has been shielded from cosmic rays by snow cover or by soil and/or sediment (Benson *et al.*, 2004). It must also be assumed that the surfaces have acted as closed systems since exposure and that there has been no loss of nuclides or contamination by others. Similarly, it has to be assumed that there is no inherited signal from earlier exposure events; in other words, the ‘exposure accumulation clock’ has been effectively zeroed. This may

Table 5.4 Summary of characteristics and scope of nuclides used in surface exposure (CRN) dating (from Ivy-Ochs & Kober, 2008). Production rates (atoms per grams per year) are from Gosse & Phillips (2001).

Nuclide	Half-life	Other isotopes	Target elements	Production rate	Advantages	Disadvantages
^{10}Be	1.51 Ma	^9Be	O, Si	5	Quartz resistant; ubiquitous	Low production rate; ^{10}Be interference in AMS; generally restricted to quartz
^{26}Al	716 ka	^{27}Al	Si	31	High production rate; quartz resistant ubiquitous	Restricted to quartz (low Al); accurate measure of ^{27}Al required
^{36}Cl	301 ka	^{35}Cl ^{37}Cl	Ca, K, ^{35}Cl	10, granite 20, limestone	Low detection limit; low AMS background; any rock type; silicates and carbonates	Complex production; ^{36}S interference in AMS; accurate measure of total Cl required
^{14}C	5.73 ka	^{12}C ^{13}C	O	16	Useful for short time-scales; quartz resistant; ubiquitous	Short half-life; atmospheric ^{14}C contamination
^3He	Stable	^4He	Many	120	High production rate; useful for long time-scales; pyroxene; olivine	Diffuses out of quartz or volcanic groundmass; corrections required; pre-exposure possible
^{21}Ne	Stable	^{20}Ne ^{22}Ne	Mg, Si	20	Useful for long time-scales (> 50 ka); quartz, olivine, pyroxene	High air background possible; corrections required; pre-exposure possible

be a particular problem in the dating of glacial and fluvial sediments and careful field sampling is needed to resolve the difficulty.

Obtaining a reliable estimate of CRN production rates is also problematic as these are known to vary with altitude, latitude, depth below ground surface and degree of shielding from cosmic rays (Stone, 2000; Gosse & Phillips, 2001). Changes in past cosmic ray flux also have to be taken into account (Florinski *et al.*, 2004). In order to address these issues, CRN production rate calibration datasets have been developed, including the globally averaged dataset of Balco *et al.* (2008) which can be accessed online (<http://hess.ess.washington.edu>). This enables scientists to calculate exposure ages and erosion rates and to compare previously published exposure ages or erosion rate measurements on a common basis. However, because of the marked geographical variations in CRN production, regional calibration sets are now being generated for different areas of the world, for example for western Norway (Goehring *et al.*, 2012), Greenland (Briner *et al.*, 2012) and the Baffin Bay region of Arctic Canada (Young *et al.*, 2013). A further complication is that some cosmogenic isotopes may occur naturally in rocks. For instance, ^{36}Cl may be produced in rocks as part of the decay series of uranium and thorium isotopes, while cosmogenic nuclides can occur in rocks not as a result of spallation reactions, but by direct adsorption from the atmosphere. In both instances, those nuclides have to be identified and their presence corrected for.

All of the above mean that there are, at present, considerable uncertainties in CRN ages, which are typically in the range 10–20 per cent. When these are added to the analytical errors arising from laboratory measurement (7 per cent or less for AMS; ± 3 per cent for mass spectrometry), this means that CRN dating is the least precise of all the radiometric methods considered so far. However, in view of the ubiquity of rock surfaces (e.g. by comparison with ancient organic deposits), the potential of the technique is clearly considerable and hence sustained efforts are being made to improve both the accuracy and precision of CRN dating. A major initiative is the CRONUS (Cosmic-Ray Produced Nuclide Systematics)-Earth Project, an international consortium of scientists from Europe and North America, whose goals are not only to develop and refine the calibrations for CRN production rates referred to above, but also to evaluate the sources of uncertainty in CRN production with a view to reducing current levels of uncertainty in measurements to around 5 per cent. If this could be achieved, it would bring CRN dating more into line with other radiometric techniques currently employed in Quaternary dating.

5.3.8.3 Some applications of CRN dating

CRN dating has evolved rapidly over the past two decades, and the applications of the technique have been extremely varied (Dunai, 2010). Some of the earliest uses were in glacial geology to determine surface exposure ages of moraines and glaciated surfaces (Figure 5.16), and this approach has since been extensively applied in the development of glacial and deglacial chronologies (Kelly *et al.*, 2004; Balco *et al.*, 2013), and in developing constraints on the lateral and vertical dimensions of ice sheets (Ballantyne *et al.*, 2008; Fabel *et al.*, 2012). Other applications include the dating of landslide and rock avalanche deposits (Ivy-Ochs *et al.*, 2009), of alluvial fans (Machette *et al.*, 2008), of pluvial lake shorelines (Kurth *et al.*, 2010), of granite tor forms (Gunnell *et al.*, 2013) and of river terrace sequences (Rixhon *et al.*, 2011). The cosmogenic burial approach has been less widely used than surface exposure dating, but has been successfully applied in a number of depositional contexts including cave (Anthony & Granger, 2007) and fluvial sequences (Dehnert *et al.*, 2011).

Cosmogenic radionuclides are also found in glacier ice. These are not produced at the earth's surface but by spallation processes in the atmosphere (as in the case of ^{14}C), and they become incorporated into glacier ice via precipitation. They can be used in the dating of older ice (greater than 100 ka); for instance, a ^{36}Cl age of c. 760 ka was obtained from near the base of the Guilya ice cap on the Qinghai-Tibetan Plateau (Thompson *et al.*, 1997), but they are more widely used in the correlation of ice-core records. An example is the clearly defined peak in ^{10}Be concentration at c. 41 ka which has been used to link Greenland and Antarctic ice cores (Raisbeck *et al.*, 2007). Because cosmogenic radionuclide production in the atmosphere is influenced by changes in the earth's geomagnetic field, past variations in the geomagnetic field can also be reconstructed from the record of cosmogenic radionuclides preserved in glacier ice (Wagner *et al.*, 2000). In addition, since cosmogenic radionuclide production is also modulated by solar activity (the 'solar wind'), fluctuations in solar activity can be inferred from the record of cosmogenic radionuclides, such as ^{10}Be in polar ice (Vonmoos *et al.*, 2006).

5.3.9 Short-lived radioactive isotopes

Radioisotopes with much shorter half-lives that have been used in dating Late Quaternary events include lead-210 (^{210}Pb : half-life 22.26 yr) and caesium-137 (^{137}Cs : half-life 30 yr). These have, in the main, been applied to the dating of lake sediments that have accumulated over the past two



Figure 5.16 a) Glacial moraine near Leh in the Indus Valley, Ladakh, northern India. b) ^{10}Be ages on the boulders from the moraine surface indicate formation during the Leh glacial stage (Owen *et al.*, 2006) which dates to 317 ± 57 ka, that is, in MIS 9/10 (Dortch *et al.*, 2013; photographs by Mike Walker).

or three centuries, although other depositional contexts have also been dated. A third radioisotope, silicon-32 (^{32}Si), has a longer half-life (178 ± 10 yr) and is applicable over a timescale of 30–1,000 years. Dating of recent sediments using these various isotopes is reviewed by Appleby (2008).

5.3.9.1 Lead-210

Lead-210 dating uses the radiogenic isotope ^{210}Pb , which forms in the atmosphere from terrestrial radon-226 (^{226}Ra). The ‘unsupported’ ^{210}Pb is subsequently removed from the atmosphere by precipitation to accumulate in lacustrine and marine sediments, and in soils, peats and glacier ice, where it subsequently decays to stable ^{206}Pb . Measurement of the remaining ‘unsupported’ ^{210}Pb as a function of depth in a body of sediment provides an estimate of the time that has elapsed since the lead was deposited (up to a maximum of *c.* 150 years, i.e. 5–7 half-lives), and hence enables the rate of sediment accumulation to be established. The main problem encountered with this method is that most sediments contain small amounts of ^{210}Pb derived from the decay of ^{226}Ra , and this ‘supported’ ^{210}Pb must be determined and subtracted from the ‘unsupported’ ^{210}Pb produced in the atmosphere (Appleby & Oldfield, 1992). Other difficulties arise from the fact that the fluxes of ^{210}Pb and its carriers are site-specific and may vary through time, while bioturbation and reworking of sediments provide further constraints on the technique. Particular problems are encountered in the dating of peat sequences as a result of erosion and sediment loss in the upper parts of the profile and the downwash of ^{210}Pb in the lower levels (Oldfield *et al.*, 1995).

^{210}Pb has been widely used in the dating of recent lake sediments, and especially in studies of human impacts on lake catchments and ecosystems (Oldfield *et al.*, 2003). It has also been used to date recent peat accumulations (Hendon & Charman, 2004), salt-marsh sediments (Kemp *et al.*, 2012b) and marine deposits (Zillén *et al.*, 2012), while ^{210}Pb dates have also been obtained from ice cores (Eichler *et al.*, 2011).

5.3.9.2 Caesium-137

^{137}Cs is an artificially generated radioactive nuclide that has only been produced in significant quantities as a result of thermonuclear weapons testing which began in 1945. The first pronounced atmospheric increase in the Northern Hemisphere was detected in 1954 and a clear maximum in 1963, after which atmospheric concentrations declined significantly with successive nuclear test-ban treaties. The 1963 maximum, however, shows up clearly in many recent lacustrine sequences, and forms a distinctive time-stratigraphic marker horizon. In Europe, the ^{137}Cs peak due to the Chernobyl fallout (1986) is more strongly marked than the weapons peak, but the latter is global whereas the Chernobyl signal is regional. Applications of ^{137}Cs include the dating of pollution histories of lake sediments (Rember *et al.*, 1993) and the determination of rates of erosion on archaeological sites (Davidson *et al.*, 1998). ^{137}Cs has also been used as an independent check on ^{210}Pb chronologies (Abril, 2003).

In addition to ^{137}Cs , other artificially generated isotopes, including plutonium-239 (^{239}Pu : half-life 2.4×10^4 yr), plutonium-240 (^{240}Pu : half-life 6.5×10^3 yr) and

americium-241 (^{241}Am : half-life 432.7 yr), also show 1963 maxima and can be used in the dating of recent peat and lake sediment sequences (Böllhofer *et al.*, 2004).

5.3.9.3 Silicon-32

Cosmic-ray produced ^{32}Si is removed from the atmosphere by precipitation and accumulates in lake and marine sediments, and also in snow. It can therefore be used in the dating not only of sediment sequences, but also of glacier ice. The principal difficulty in ^{32}Si dating relates to the detection of ^{32}Si because of its very low natural specific activity compared with stable Si. Hence, in the dating of sediments, stringent radiochemical purification procedures are required. AMS can be used for samples of rain, snow and ice, but for limnic and marine sediments where biogenic silica (diatoms and radiolaria) forms the dating medium, the $^{32}\text{Si}/\text{Si}$ ratio is below the detection limit for AMS, and hence beta radiation radiometry has to be employed (Morgenstern *et al.*, 2000).

Applications of ^{32}Si include the dating of glacier ice (Morgenstern *et al.*, 2000) and the dating of recent lacustrine and marine sequences (Nijampurkar *et al.*, 1998; Suckow *et al.*, 2001). The applicable timescale of ^{32}Si dating (30–1,000 years) means that it bridges the time gap between the present and the younger end of the ^{14}C range (Fifield & Morgenstern, 2009), and it could therefore be especially valuable for archaeologists in the dating of historical events over the course of the last millennium (Morgenstern *et al.*, 2001).

5.4 INCREMENTAL DATING METHODS

Incremental dating methods are those based on regular additions of material to organic tissue or to sedimentary sequences. Those which have been most widely used are **dendrochronology** (tree-ring dating) and **varve chronology**, which is based on annual accumulations of sediments in lakes or in the sea. **Annual layers in glacier ice** also form a basis for dating. Measurements of variations in lichen size (**lichenometry**) can be used to determine the age of exposure of rock surfaces, while annual increments of calcite can also be detected in **speleothems**. Annual banding in **corals** and **molluscs** enable short-term chronologies (**sclerochronologies**) to be established in marine environments.

5.4.1 Dendrochronology

5.4.1.1 General principles

In most softwood (coniferous) trees, new water- and food-conducting cells (tracheids) are added to the outer perimeter of the trunk each growth season following an inactive period in winter. The new cells that begin to grow in the spring tend to be larger and more thin-walled than those produced in late summer, as a result of heavier demands on water supply early in the growth season. Later in the year, the cells become gradually smaller and develop thicker walls. There is normally, therefore, a distinct 'line' between successive annual increments of wood growth (Figure 5.17), and counting of these lines (**tree rings**) allows the age of the tree to be established. In hardwood (deciduous) trees, growth trends are more variable, however. They can be divided into **ring-porous** types where the spring vessels are normally distinctly larger than those of the summer wood (e.g. oak, ash, elm) and **diffuse-porous** types in which the pores are more uniform in size (e.g. beech, birch, alder, lime). The result is a considerable difference in the nature of tree rings between species, and as some do not display clearly defined annual bands, not all trees are suitable for dendrochronology. The most widely used are oak (*Quercus*) and pine (*Pinus*), although tree-ring chronologies have also been obtained from *Sequoia* and Douglas fir (*Pseudotsuga*). The principles and applications of dendrochronology are described by Baillie (1995), Schweingruber (1996), Fritts (2001) and Speer (2010), while the journal *Dendrochronologia* provides a regular update on recent developments in the technique.

5.4.1.2 Measurement and problems

Subfossil or dead trees may be obtained from a range of contexts: they may be buried in peats, in riverine deposits or on archaeological sites, or they may form part of a standing or former building. In all of these cases, the wood can be cut to enable a complete cross-section to be examined, allowing comparisons of ring width to be made in several radial directions. Living trees can be sampled with a metal increment corer which extracts small-diameter cylinders of wood from the tree trunk. In the laboratory, samples are dried, polished and mounted prior to examination, or else cut with a sharp blade while still damp. Counting and measuring can be carried out by visual inspection of the rings under normal magnification, or on a moving stage under a binocular microscope. Other approaches employ electronic measuring equipment linked to both micro- and main-frame computers, or

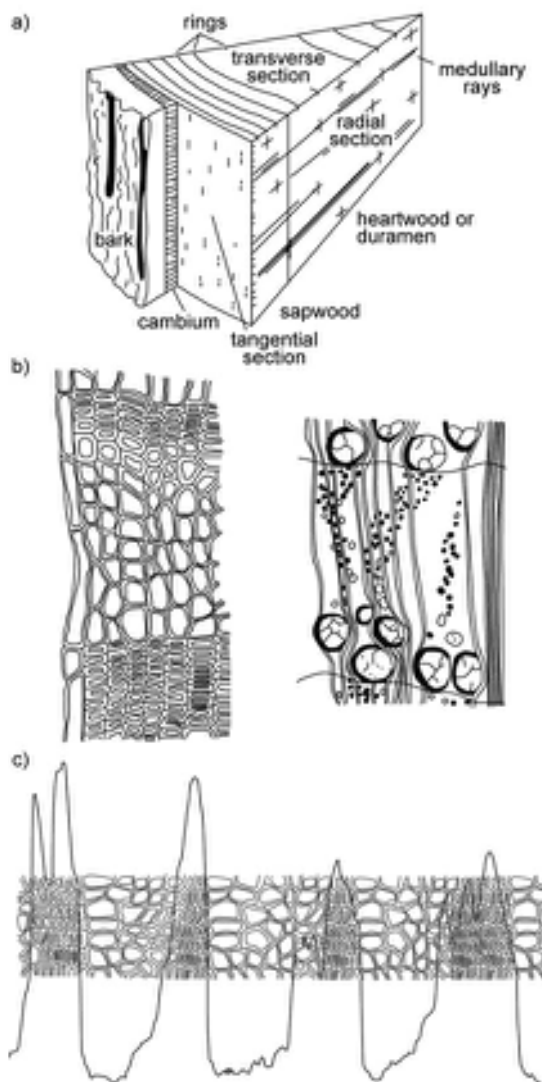


Figure 5.17 a) Cross-cut of a tree trunk showing seasonally differentiated growth rings, reflecting variations in wood cell density. b) X-ray negatives of wood surfaces can be magnified and analysed using a high-resolution microdensitometer: the optical density of the X-ray negatives is inversely proportional to wood density, as illustrated schematically in c).

X-ray densitometry which detects annual variations in wood density by degree of penetration of X-ray beams.

Tree-ring width is seldom uniform, for tree growth is influenced by a range of environmental factors, variations within which will produce different physiological

responses in the trees. The most important determining factor for many trees is climate. Under conditions of stress, growth is retarded, and a narrow tree-ring will result; conversely, under more favourable conditions, growth rates are increased, and wider annual rings are produced. As a consequence, climatic variations over very short and precisely dated timescales can often be inferred, a field of study known as **dendroclimatology**. In temperate areas, such as northwest Europe, there is usually sufficient moisture available all year round, and hence the primary limiting factor to tree growth is temperature (accumulated summer degrees). In semi-arid regions, such as parts of the southwest USA, moisture availability is more important. Climatic changes over time are reflected in a ring-width pattern within which distinctive rings (representing particularly good or bad growth years), or characteristic groups of rings, form **markers** and these, in turn, form a basis for cross-matching or **cross-dating** between wood of overlapping ages. Tree-ring records can therefore be extended back in time and a **master chronology** developed (Figure 5.18). Where wood samples are recovered from peat bogs, for example, or from old buildings, counting of the tree-ring sequences enables a **floating chronology** to be established. This can be matched to the master chronology by cross-dating and thus wood of hitherto unknown date can be assigned a precise calendar age.

Trees tend to grow more vigorously in youth than in old age, and as a result there is usually a reduction in ring-width with age. This may cause difficulties in cross-dating for the climatically induced ring-width variations can be masked by ring-width variations due to age. A further problem is that the width of tree rings tends to vary with the height of the trunk, and there is no way of knowing precisely where on the trunk a piece of subfossil wood originated. Each tree-ring series is therefore **standardized**, by transforming the measured ring-width values to **ring-width indices**, for example by fitting a regression line to the measured ring-width values to provide an indication of the general decline in tree-ring width with age (see Figure 5.19). Further difficulties arise from the lack of variations in ring width, from intermittent absence of rings, or from the presence of false rings. Where trees are growing in situations where there is little or no climatic variation or where minimal climatic stress is exerted on the trees, ring widths may show little variation through time. A tree-ring series of this type is termed a **complacent series**, and is of little value in dendrochronology as the distinctive markers that form a basis for cross-dating are absent. Dendrochronologists therefore prefer to select trees from stressed situations, where some climatic factor has been critical to growth.

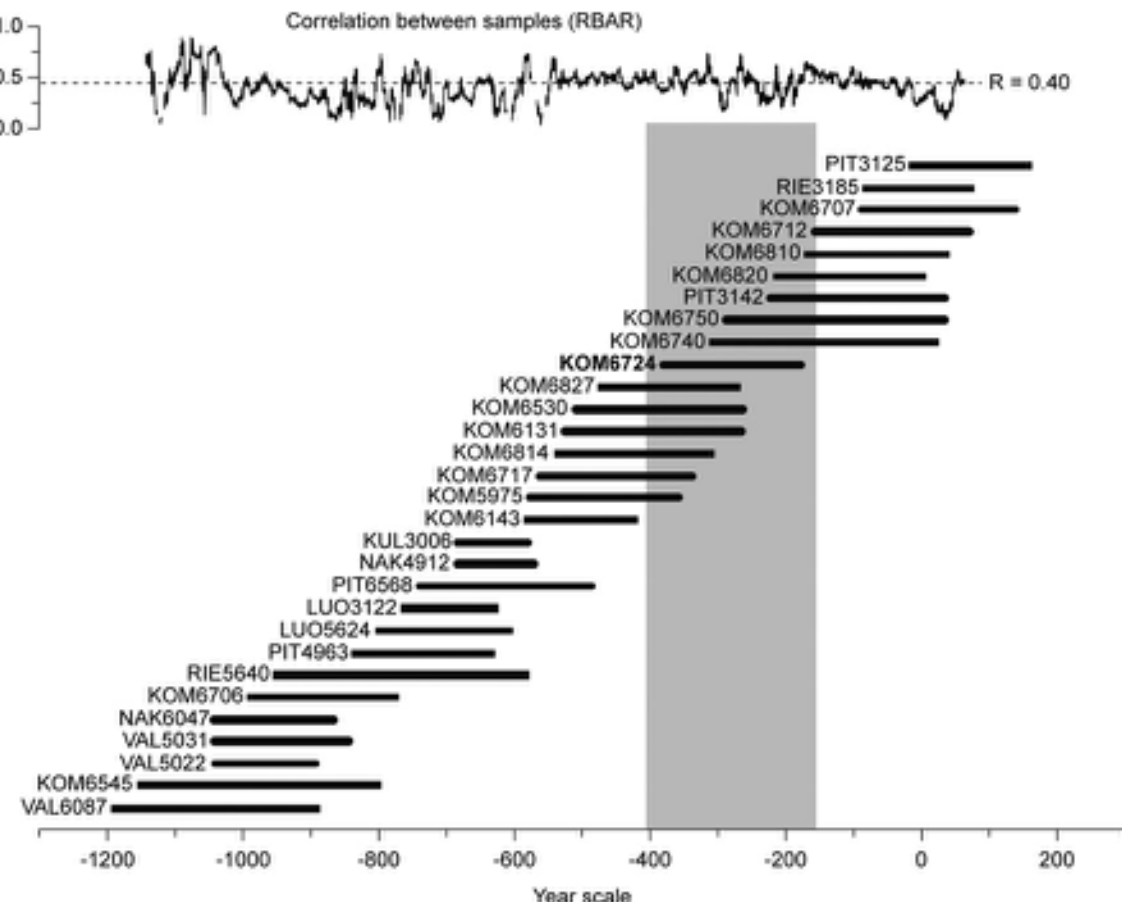


Figure 5.18 Age profile of cross-matched tree-ring series from Finnish Lapland for the period AD 1200–160 BC, showing part of the record with many overlapping tree-ring series (after Eronen *et al.*, 2002). The complete record of which this forms a part, and which extends over the past 7,519 years, is shown in Figure 5.22.

Wood production will be reduced at times of stress, and this is shown by a **sensitive series** of rings. However, if the stress is too extreme, there is always the possibility that during certain years a tree may fail to manufacture new cells, or may only produce new material on restricted parts of the trunk. The result is **missing** or **partial rings**. On the other hand, where the spring growth period is interrupted or curtailed by late frosts, it is possible for more than one growth band to develop in a particular year (**false rings** or **intra-annual growth bands**). These may not be easy to identify in individual tree-ring series, and can only be corrected for by replication of a number of records through systematic cross-dating.

5.4.1.3 Dendrochronological records

Dendrochronological records are now available from many parts of the world (Briffa, 2000), and form the basis for dating environmental change, as well as providing a chronology for climatic and environmental reconstructions derived from dendroclimatological data (section 5.4.1.4). They are also key to the calibration of the radiocarbon timescale (section 5.3.2.6). Moreover, as tree-ring sequences contain a record of long-term atmospheric ^{14}C variations, they offer insights into the forcing mechanisms (solar variability, ocean circulation variations, geomagnetic changes, etc.) that influence atmospheric ^{14}C variability over both long and short timescales (Hua *et al.*, 2009).

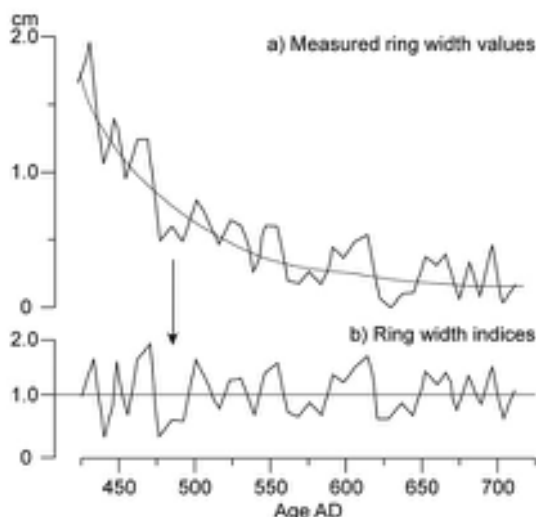


Figure 5.19 Standardization of ring-width measurements to generate ring-width indices. a) A linear regression line has been fitted to the measured ring widths and this provides an indication of the overall decrease in ring width with age. The value for each year is then divided by the value for that year obtained from the regression curve. b) The derived ring-width indices (after Baillie, 1982).

North America

In the arid mountain environments of the southwest United States are the oldest living trees in the world. The bristlecone pine (*Pinus longaeva*, formerly *Pinus aristata*) thrives on dry and rocky sites up to 4,000 m and in the White Mountains of California, in the rain shadow of the Sierra Nevada, large numbers of twisted and stunted bristlecone pines are found (Figure 5.20), with the famous ‘Methuselah Tree’ being more than 4,700 years old. These trees are growing under particularly stressed conditions, and the limited growth period (perhaps only one or two months each year) produces very narrow rings and a ring width that is highly sensitive to climatic change (Johnson, 1999). By cross-dating between living and dead wood and then between subfossil samples, a continuous master chronology has been developed which extends back to 8681 years BP (Ferguson & Graybill, 1983). This has since been extended to 6828 BC (8778 BP) and may eventually link with an older 3,000-year floating chronology (Harlan & Robertson, 2006). Other relatively long tree-ring chronologies have been established in North America on species of *Sequoia*, Douglas fir (*Pseudotsuga*), and pine, the longest of which, based on foxtail pine (*Pinus balfouriana*), presently extends back over 3,000 years. In due course, even



Figure 5.20 Ancient bristlecone pines growing in the White Mountains of California (photograph by Mike Walker).

longer chronologies may be developed, as floating chronologies from subfossil remains of *Quercus* from the central USA have been radiocarbon dated up to 13.8 ka cal. BP (Stambaugh & Guyette, 2009), while in New York State, floating chronologies from *Picea* have been radiocarbon dated back to c. 14.5 ka cal. BP (Griggs & Kromer, 2008).

Western Europe

In western Europe, there are no trees with an age range comparable to the bristlecone pine, and hence long chronologies have only been established by the laborious cross-dating of large numbers of subfossil wood samples whose ring patterns often span no more than 100–200 years. The most commonly used species are the oaks (*Quercus robur* and *Quercus petraea*) and the Scots pine (*Pinus sylvestris*), obtained from fen and raised bog peats, or from river gravels. In the British Isles, the longest chronologies so far developed have been on oak, with a record from Ireland extending back 7,429 years (Brown & Baillie, 1992). In central Europe, a continuous oak chronology has been constructed from the remains of oak found in the riverine deposits of southern and eastern Germany (Figure 5.21), the oldest oak in the German Hohenheim master chronology being dated at 10,429 years (Friedrich *et al.*, 2004). By linking the sequence based on oak to a chronology based on pine, the European dendro-record has now been extended back to 12,594 years; in other words, beyond the onset of the Holocene and into the Younger Dryas period (Hua *et al.*, 2009). For the Lateglacial, two floating chronologies (the Hohenheim series: 1,116 rings; the Swiss Dättnau series: 1,606 rings) have been synchronized into a combined chronology, the youngest section of which extends forward into the Younger Dryas (Kromer, 2009; Kaiser *et al.*, 2012). If these floating records can, in due



Figure 5.21 a) Fossil oak trunks excavated from gravel beds of the River Danube valley, with dendrochronologist Michael Friedrich of the University of Hohenheim, Germany. b) A section through one of the trunks of subfossil oak, with the late Bernd Becker, one of the pioneers of European dendrochronology (photographs by Bernd Kromer, University of Heidelberg, Germany).

course, be linked to the Hohenheim master chronology, this will extend the continuous European dendro-curve back beyond 14,000 years. For earlier periods, there are floating pine and larch chronologies from northern Italy, the oldest of which dates to around 17,500 years (Kromer, 2009). Long tree-ring records based on pine have also been constructed for northern Scandinavia, with a 7,400-year chronology from Swedish Lapland (Grudd *et al.*, 2002) and a 7,500-year chronology from Finnish Lapland (Figure 5.22). In both North America and Europe, there are shorter chronologies spanning the last 1.0–1.5 ka (Watson & Luckman, 2001; Gunnarson & Linderholm, 2002). Floating chronologies have been used, *inter alia*, to date prehistoric trackways (Hillam *et al.*, 1990), ancient boat timbers (Nayling & McGrail, 2004) and prehistoric tombs (Panyushkina *et al.*, 2007).

Australia and New Zealand

Although long continuous tree-ring chronologies comparable with those from North America and Europe have yet to be developed from the Southern Hemisphere, some trees offer the potential for the construction of long dendrochronological records. These include the Huon Pine (*Lagarostrobus franklinii*) from Tasmania from which a 4,136-year annual tree-ring chronology has been reconstructed, and the Silver Pine (*Lagarostrobus colensoi*) from the South Island of New Zealand which has yielded a cross-matched chronology extending back to 323 BC (Cook *et al.*, 2006). Of particular significance in terms of its dendrochronological potential, however, is the Kauri (*Agathis australis*), a conifer which grows on the North Island of New Zealand. This long-lived tree (over 500 years) has produced a continuous chronology that extends

back 3,722 years (Boswijk *et al.*, 2006). More importantly, perhaps, the remains of subfossil Kauri have been found buried in peats that pre-date the Last Glacial Maximum, and a preliminary group of chronologies has been developed that combine to produce a floating chronology spanning 10,719 years of MIS 3 (Palmer *et al.*, 2006). This tree, therefore, not only has potential for the construction of long and continuous Holocene dendrochronological series but it may, as discussed above (section 5.3.2.6), also offer a basis for a dendrochronological calibration of the radiocarbon timescale well beyond that provided by the Northern Hemisphere tree-ring series.

5.4.1.4 Dendroclimatology

Dendroclimatology is the science of reconstructing past climatic conditions and histories from tree rings. The importance of dendroclimatological records is that palaeoclimatic information can be precisely dated, and inferences can even be made about seasonal variations (Linderholm *et al.*, 2010). Further, as a proxy record of climate, it enables the record to be extended beyond those based on instrumental measurements (Hughes *et al.*, 2011).

Palaeoclimatic reconstructions based on tree rings rest on assumed or demonstrable relationships between ring width, or some other ring characteristic, and climatic parameters. These relationships are often complicated by lag effects between climatic inputs and tree response, for trees have the ability to store food reserves and water that may then be used in adverse years. Once the linkages between climatic and tree-growth parameters have been established, however, inferences can be made about past climate for the timespan of the dendrochronological record.

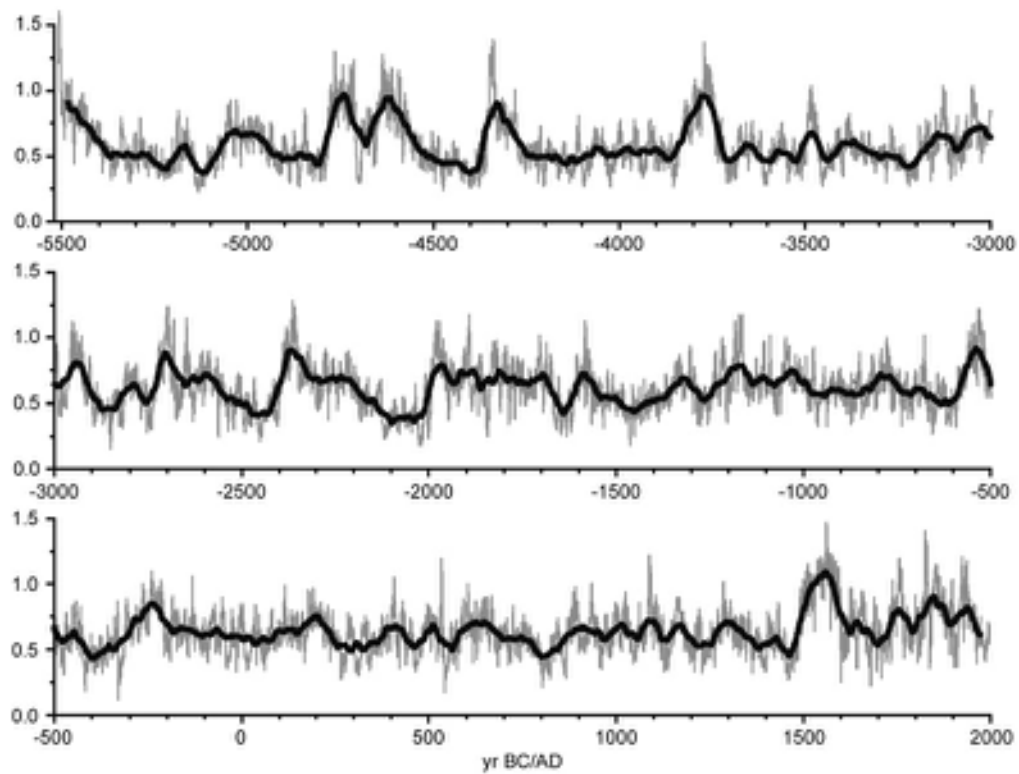


Figure 5.22 Part of a continuous 7,519-year pine tree-ring chronology from Finnish Lapland. The average ring width remains remarkably constant at about 0.6 mm yr^{-1} throughout the whole length of the chronology. The thin line indicates annual ring-width variability (in mm) and the bold line the 50-year running mean (after Eronen *et al.*, 2002).

Dendroclimatology has become an integral tool in the study of environmental change, particularly over the course of the last millennium, allowing inferences to be made about temporal variations in summer temperature (Helama *et al.*, 2002), precipitation regimes (Watson and Luckman, 2001), summer drought patterns (Zhang *et al.*, 2004b), extreme arid events (Stahle *et al.*, 2007), linkages between streamflow and climate (Cleaveland, 2000), and relationships between climatic change and late Holocene volcanism (Gervais & MacDonald, 2001). Moreover, because tree-ring sequences provide very high-resolution records of climate change, they constitute one of the key sources of information for the reconstruction of short-term climatic events, such as the Pacific Decadal Oscillation (PDO) or the North Atlantic Oscillation (NAO: section 7.6.4.3).

An alternative approach to dendroclimatology involves variations in wood density and, in some instances, this may provide clearer palaeoclimatic information than simple ring-width measurements. As wood densities respond primarily to conditions during restricted growth periods,

particularly during the summer, they offer the prospect for finer resolution of climatic relationships than ring widths which integrate the effects of conditions over several seasons. Studies from North America (Wilson & Luckman, 2003), Europe (Büntgen *et al.*, 2006) and China (Wang *et al.*, 2010) have shown that late-wood width and maximum density appear to be closely related to climate, while dendrochronological records from Tasmania suggest a link between maximum density and regional streamflow at the end of the growing season (Allen *et al.*, 2012). Although much still remains to be learned about the precise nature of the climatic signal in wood density variations, density measurements are becoming increasingly widely employed alongside conventional ring-width values in dendroclimatic research (Briffa, 2000; Mannes *et al.*, 2007).

A further climatic index derived from tree-ring data is based on stable isotope ratios of carbon, hydrogen and oxygen in wood cellulose, a field of research known as **isotope dendroclimatology**. The carbon isotope composition in cellulose of trees is determined by the ratio between

the CO₂ concentrations in the cell fluid and that in the atmosphere. Warmer and drier conditions generally lead to more restricted CO₂ availability and to an enrichment in the heavier isotope of carbon, ¹³C, relative to ¹²C. The D/H and ¹⁸O/¹⁶O ratios in tree rings are largely determined by the isotopic signature of the source water available for tree growth. If this is mainly meteoric water (rainwater), then the isotopic ratios in the tree rings reflect the isotopic effects in the regional precipitation, and in mid- and high-latitude regions, these are closely related to surface air temperatures. Hence δ¹³C, δD and δ¹⁸O values in tree-ring series can be employed as proxy climatic indicators (Tang *et al.*, 2000). Examples include the reconstruction of precipitation patterns over the last millennium in the Canadian Rockies (Watson & Luckman, 2001), the detection of a mid-Holocene warm and dry phase in northwestern Russia (Boettger *et al.*, 2003), and the development of a record of temperature and sunshine for northern Sweden over the past 100 years (Loader *et al.*, 2013). The majority of these studies have been carried out on coniferous trees growing in remote high-latitude/high-altitude areas, but recent results from west Wales, where a 160-year palaeoclimate signal has been obtained from sessile oak (*Quercus petraea*) and which correlates closely with the central England temperature record, suggest that it may be possible to derive robust palaeoclimate records from trees in more temperate regions, and particularly from the well-replicated oak chronologies of western and central Europe described above (Young *et al.*, 2012).

Despite these encouraging results, there are a number of problems in isotope dendroclimatology that remain to be resolved, particularly in relation to the nature of the fractionation and equilibrium processes that determine isotopic ratios in tree rings. For example, it appears that the stable carbon isotope signal in tree-ring cellulose from northern pines reflects a combination of stomatal conductance (controlled by air humidity and soil moisture status) and photosynthetic rate, the latter controlled primarily by sunshine and air temperature. As the balance of these controls varies spatially, and perhaps also locally, during the Holocene, without some independent estimate of either stomatal conductance or photosynthetic rate, the δ¹³C value alone cannot provide a clear and consistent climatic signal. One solution is to adopt a multi-proxy approach in which stable isotope data are analysed alongside other potential climatic proxies (ring width, wood density, etc.). By combining the proxies, the strength of climate correlations is increased and the range of extractable climatic parameters extended. This type of study provides a powerful new means of extracting climatic information from long tree-ring chronologies (McCarroll *et al.*, 2003),

but needs to be combined with experimental studies of isotopic pathways and exchanges during cellulose synthesis in living trees (Barbour, 2007).

5.4.2 Varve chronology

5.4.2.1 The nature of varved sediments

Rhythmic sediment layers in lacustrine deposits are common in the geological record and are generally referred to as **rhythmites**. Where these reflect an annual cycle of accumulation, they are termed **varves**, from the Swedish *varv* for lap, turn or revolution. They usually consist of couplets of alternating sediment colour, grain size or fabric, resulting from seasonal differences in depositional processes. **Clastic varves** are minerogenic and reflect variations in rate or type of sediment influx, the best known being **glacigenic varves** which accumulate in lakes close to a glacier margin. Organic varves form as a result of seasonal changes in the deposition of organic materials, for example alternations between microfossil-rich summer accumulation formed during plankton ‘blooms’, and lower-productivity winter layers (Figure 5.23). **Chemical varves** develop where the seasonal contrasts in the water column (e.g. in oxygen content or temperature) lead to the precipitation of different chemical compounds. Some varves may be the product of all three of these seasonal influences. Where varved sequences can be dated by independent means (e.g. by radiocarbon), then the events and intervals that they represent can be estimated in calendar time, potentially at an annual resolution. Even if their calendar age is unknown, they nevertheless provide a ‘floating chronology’ (section 5.4.1.2) for the interval of time over which the varved sequence has accumulated.

5.4.2.2 Clastic varves

Large quantities of sediment are deposited in proglacial lakes and shallow seas from rapid ice melt during the spring and early summer. The coarser particles settle quickly, but the silts and clays remain in suspension throughout the summer season as the water column is agitated by surface winds and currents. During winter, however, when the lake is frozen, the smaller particles settle out to form a fine silt- or clay-dominated layer that contrasts with the coarser summer layer, thereby forming glacigenic varves (Figure 5.23). Clastic varves can also form in non-glacial lakes that receive a mixed-grade sediment supply and freeze over in winter.

The potential of glacigenic varves as a basis for dating was first recognized by the Swedish geologist Gerard De

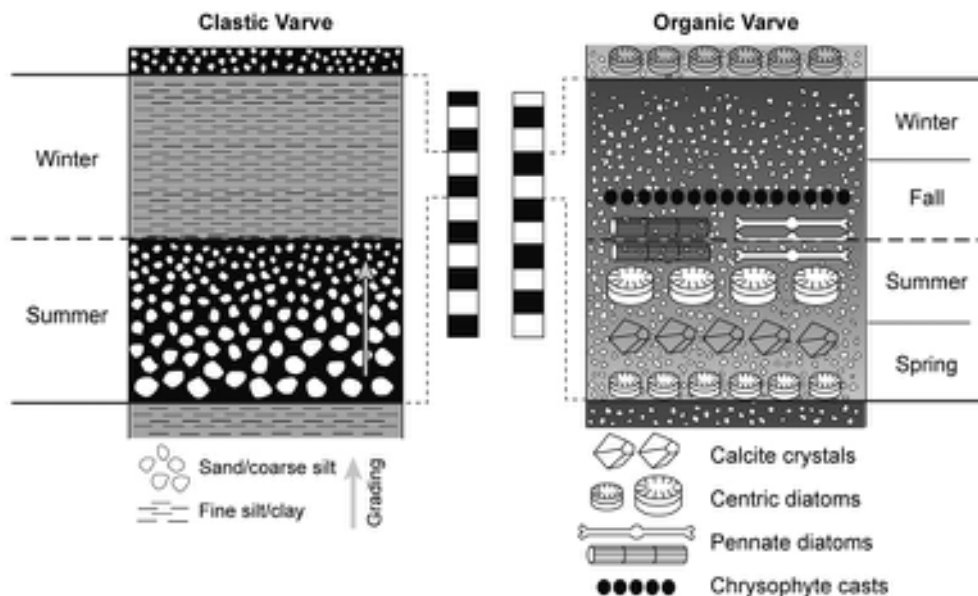


Figure 5.23 Simplified model of clastic and organic varve formation, showing variations in sedimentological and biological characteristics of annual layers (after Sturm & Lotter, 1995).

Geer who, as early as 1884, was investigating the exposed varve sequences in the Stockholm area (Petterson, 1996). He discovered that as the last ice sheet wasted northwards across southern Sweden, it left behind a complex of moraines and proglacial lakes. In many places, overlaps of varve ‘histories’ had developed, the uppermost varves in one lake sequence being of the same age as those in the lower part of a neighbouring series. In a now classic publication, De Geer (1912) first presented measurements of individual varves and curves of relative thickness for each site investigated. Comparisons between sites enabled correlations to be established using similar principles to those now employed in the matching of ring-width series in dendrochronology. By methodically extending his master chronology northwards and southwards across Sweden, De Geer compiled a long varve sequence which was believed to extend back continuously to the beginnings of deglaciation. This seminal work laid the foundations for all subsequent work on ice recession in the Baltic region (section 5.4.2.7).

Finely graded laminated sequences have also been found in other ice-marginal locations, and especially in shallow marine settings (Ó Cofaigh & Dowdeswell, 2001). However, it is now apparent that the pulsed supply of sediment that is responsible for the formation of the laminations may not always be a seasonal phenomenon, and hence

the clastic couplets may not necessarily represent annual incremental accumulations. In order to establish whether such sequences are true varves, reference may need to be made to independent age estimates from the same sedimentary sequence, or the use of stratigraphic markers of known age (e.g. Lekens *et al.*, 2005). Another approach is to employ some of the techniques described below (section 5.4.2.6) to compare the fine internal detail of clastic varve series with modern analogues (Hambley & Lamoureux, 2006).

5.4.2.3 Organic (biogenic) varves

Many lakes do not contain laminated sediments because of reworking of deposits by currents or by bottom-dwelling organisms (**holomictic lakes**). In deeper waters, however, there are fewer bottom-dwelling fauna, and vertical circulation (caused by thermal lake stratification and its seasonal breakdown: see section 3.9.2) does not extend to the bottom of the water column. In these **meromictic lakes**, fine laminations (organic/biogenic varves) may form. Laminae that develop during the summer typically exhibit higher organic content, reflecting increased biological productivity within the lake and reduced allochthonous influx from the catchment, while the reverse is the case in laminae formed during the winter. Fossil assemblages (pollen,

diatoms, etc.) may be preserved in the summer layers (Baier *et al.*, 2004; Nakagawa *et al.*, 2005) and, in some cases, increments laid down in spring, summer and autumn can be identified on the basis of these assemblages (St. Jacques *et al.*, 2009). However, in many lake systems, organic varves are thin and comprise only decomposed organic detritus, in which case seasonal layers can only be established by molecular and isotopic analytical methods (Fuhrmann *et al.*, 2004).

Similar processes lead to the formation of organic varves in the marine realm. Most common are diatom-rich varves that develop where biological productivity is high, notably where upwelling occurs (Pike & Stickley, 2007). In some marine basins, such as the Gulf of California, productivity is so high that diatom frustules form ‘mats’ on the seabed (Kemp, 2003). However, as in lakes, the number of fossils reaching the sea floor is likely to be low. In the Cariaco Basin off Venezuela, for example, estimates suggest that only 1–2 per cent of the organic carbon generated in the water column accumulates on the seabed, with perhaps less than half of that subsequently preserved in the sediment record (Thunell *et al.*, 2000). Diatom-rich varved sediments are found throughout the world’s oceans, and even in areas adjacent to the Antarctic ice sheet, where diatom oozes develop in response to seasonal changes in nutrient availability and ocean stratification caused by seasonal fluctuations of the sea-ice margin (Stickley *et al.*, 2005).

5.4.2.4 Chemical varves

Water bodies vary in the degree to which dissolved chemicals precipitate out to form crystalline compounds (carbonates, oxides, hydroxides) which may combine with other particulate matter raining out of the water column to the lake or sea floor. The chemical processes may be seasonally affected, for example through summer–winter temperature contrast or degree of oxygenation, resulting in **chemical varves** that can be recognized on the basis of colour or texture. In temperate lakes, sediments deposited in summer are frequently much darker than winter accumulations, caused by the enrichment in iron sulphide (FeS) or Fe reduction in deoxygenated water (Hongve, 2003). Water enriched in dissolved calcium carbonate may precipitate carbonatic compounds in the warmest months, through either inorganic or biologically enhanced processes, to form **carbonate varves** (Wittkop *et al.*, 2009). In semi-arid and arid regions, **evaporitic varves** may form in high-salinity lakes where water levels are reduced during summer droughts (Zolitschka, 2007).

5.4.2.5 Complex varves

Some varve series have complex origins, reflecting the various physical, chemical and biological factors that affect productivity and deposition in lacustrine and marine systems. The varves that form around the Antarctic ice margin (section 5.4.2.3), for example, are characterized not only by contrasts in diatom content, but by seasonal grain-size (clastic) alternations. Moreover, some varve sequences that have developed over long time intervals contain different types of varve, reflecting changes in local and regional environmental conditions. In Lac d’Annecy, France, for example, the varves that developed after the end of the last glacial stage are clastic, indicating low initial lake productivity, but these gradually change into chemical varves as the lake waters warmed and biological activity increased (Brauer & Casanova, 2001). Similarly, in the long lacustrine record of Lake Lisan, Jordan, that spans MIS 4 to MIS 2, there are marked variations between aragonite-dominated and clastic-dominated varved sequences that reflect cyclical changes in lake water depth (Schramm *et al.*, 2000).

5.4.2.6 Sources of error in varve counting

Problems are encountered in varve counting that are similar in many respects to those in dendrochronology. Local site factors can lead to incorrect estimates of age, and also cause difficulties in the correlation (cross-dating) between individual varve sequences. For example, adverse weather conditions in particular years can result in a reduced input of sediment into a proglacial lake, or to reduced biomass or chemical precipitation in summer, so that an individual varve fails to develop, or is too thin to be recognized. Seasonal increments of sediment may also be absent because of the intermittent erosion of bottom layers. Alternatively, more than one set of laminae (**sub-laminations**) can develop within an annual increment of sediment reflecting, for example, episodic sedimentation from intermittent local wind-driven currents, or two or more periods of snowmelt during the course of a year (Lamoureux *et al.*, 2001). Further complications can arise as a result of subaqueous slumping and/or the action of turbidity currents (Hambley & Lamoureux, 2006), and as a result of flocculation of sediment which can affect the formation of glaciolacustrine varves (Hodder, 2009). Chronological errors may also arise through inconsistencies in varve counting, either by a single operator or between operators, although where attempts have been made to quantify error estimates, these may amount to no more than 1–3 per cent (Ojala *et al.*, 2011b).

Overcoming these difficulties requires careful assessment of each of the potential error sources. For example, structural disturbance of sedimentary sequences may be identified by a survey of sediment architecture using 3-D seismic reflectors that can provide high-resolution images of internal sedimentary structures (Vardy *et al.*, 2010). Ultra-thin varves and fine-scale sub-laminations can be detected using a range of imaging methods, including X-ray radiography (Ojala & Alenius, 2005) and thin-section micromorphology (Palmer *et al.*, 2010). Variations in chemical composition can be established by, for example, ITRAX (high-resolution continuous microfluorescence-X) or CAT-scan (computerized axial tomographic) analyses (Guyard *et al.*, 2007). Also, the use of replicated records from different parts of a basin, and the employment of different operators in the varve counting of each core sequence provide a basis for identifying and quantifying errors in the resulting chronology (Ojala & Tiljander, 2003). Finally, correlation between varve sequences is increasingly being based on other parameters, including the palaeomagnetic properties of the sediments and pollen-stratigraphic records, coupled with calibrated radiocarbon dates on plant macrofossils from the varved sequences (Lundqvist & Wohlfarth, 2001; Nakagawa *et al.*, 2005).

5.4.2.7 Applications of varve chronologies

Patterns of regional deglaciation

The development of a regional varve chronology spanning a long period of deglaciation has, hitherto, been an approach largely confined to Scandinavia. In the British Isles and throughout most of western Europe, relatively few varved sequences have been recorded and analysed; consequently, there has been little interest in the use of varves as a basis for dating ice recession, although in Britain, glaciolacustrine varves have recently been used as a climate proxy and to correlate climatically inferred events with those in polar ice cores (Palmer *et al.*, 2012). In North America too, there are relatively few studies that have involved varved sediments as deglacial chronometers. However, the early work of Ernst Antevs who, between the 1930s and 1950s, developed preliminary varve chronologies for Lake Agassiz and for the Great Lakes region has been revisited in recent years, and his original New England Varve Chronology (NEVC) has been consolidated and recalibrated to produce a continuous (5,659-year) varve sequence spanning the retreat of the Laurentide ice sheet (18.2–12.5 ka BP), and which again has been linked to the Greenland ice-core records (Ridge *et al.*, 2012).

In Scandinavia, however, following on from the pioneering studies of Gerard De Geer in Sweden (see

section 5.4.2.2) and Matti Sauramo in Finland, glaciolacustrine varves have continued to attract considerable interest as a means of dating the wastage of the last ice sheet. The starting point for De Geer's timescale was a key marker varve in a section in the Indalsälven Valley of north-central Sweden, which he considered to reflect the sudden input of large quantities of meltwater following the bipartition of the residual Scandinavian ice mass. By reference to this varve year 'zero', which was taken to mark the change from glacial to postglacial conditions, older varves were given negative numbers and younger varves positive numbers. Subsequently, De Geer's master chronology has been repeatedly revised as more data have become available, while the connection of the upper part of the varve sequence to the present (AD 1978) has enabled a calendrical age of 9,238 years to be assigned to the 'zero year'. The Swedish Timescale (STS) now extends back for 13,300 varve years and is based on more than 1,000 inter-connected varve-thickness records. The youngest varves in the sequence are still being deposited today in the estuary of the Ångerman River in northeastern Sweden. However, independent evidence, including AMS dating of plant macrofossils extracted from the varved clays, indicates that several hundred years are missing from the varve chronology (Wohlfarth & Possnert, 2000). This means that, at present, the STS is effectively a 'floating varve chronology'. Considerable efforts are now being made to identify and quantify the extent of the time gaps resulting from the missing varves, for example by wiggle-matching, calibration and/or synchronization of the AMS ^{14}C -dated intervals (Wohlfarth & Possnert, 2000); by correlating the STS with independently dated records such as the Greenland ice cores (Andrén *et al.*, 1999); and by linking individual varve sequences using, *inter alia*, pollen stratigraphy, palaeomagnetic secular variations (section 5.5.1.2) and lead-pollution chronologies (Stanton *et al.*, 2010). These difficulties notwithstanding, the STS remains a valuable chronological tool, particularly at the regional scale, and has enabled the deglacial history in parts of southern Sweden to be reconstructed in considerable detail. It also provides an overall temporal framework for the deglaciation of the Baltic region as a whole (Figure 5.24).

Duration of Quaternary time intervals

Varve chronology offers a basis for estimating the duration of Quaternary time intervals. For example, analysis of the annually laminated sequence in Lago Grande di Monticchio, Italy, indicates that the last (Eemian) interglacial spanned an interval of 17.7 ± 0.20 ka (Brauer *et al.*, 2007). Varved sequences have been used to date the



Figure 5.24 The pattern and rate of ice retreat across Scandinavia based on a combination of clay-varve chronology and radiocarbon dating. The dates from northern Sweden and along the southwest Baltic coast are based on clay-varve chronology and should be corrected by +365 years (Cato, 1985). Other dates are based on radiocarbon (after Lundqvist, 1986, with permission from Elsevier). While subsequent radiocarbon dating may have revised the ages of some of the retreat stages, the overall pattern of ice wastage remains essentially unchanged.

duration of earlier European interglacial periods (Bittman & Müller, 1996), as well as more recent, shorter time periods, such as the Younger Dryas Stadial (Litt *et al.*, 2001). Non-climatic periods can also be dated by varve chronology. At Diss Mere in southeast England, the *Ulmus* (elm) decline, a feature common to most western European mid-Holocene pollen records and dated to c. 5.8 ka cal. bp, is preserved in a series of annually laminated sediments. The record shows that *Ulmus* pollen values fell by 73 per cent over a six-year interval, such a rapid decline being

consistent with the hypothesis that this was a result of a pathogenic attack (Peglar, 1993). Varve records have also been employed to determine the duration of former ice-dammed lakes, and different phases of their development (Palmer *et al.*, 2010).

Dating Late Quaternary events

Where annually laminated sediment sequences, which are effectively floating chronologies (section 5.4.2.1), can be linked to calendar time by, for example, calibrated

radiocarbon dates, the varve sequence can provide the basis for a high-resolution timescale of climatic and environmental changes. For example, a 14,000-year composite carbon isotope record from Lake Holzmaar in the Eifel region of western Germany, which shows evidence of significant ecosystem reorganizations at around 14.2, 9.6, 5.5 and 2.7 ka, each reflecting major changes in climatic regime, has been dated by varve chronology, the mean time resolution for the isotope sequence being 14 years (Lücke *et al.*, 2003). Varve chronology has also been used to provide a similar high-resolution timescale for a palynological record from a lake in the Hartz Mountains of Germany, which shows land-use changes from Bronze Age to Roman times (Zolitschka *et al.*, 2003). In the marine Cariaco Basin, a seasonally resolved titanium influx record from the varved sequence shows that the collapse of the Mayan civilization in the Terminal Classic Period occurred during an extended regional dry episode, punctuated by more intense multi-year droughts centred at approximately AD 810, 860 and 910 (Haug *et al.*, 2003).

Climatic cycles and patterns

Statistical analysis of varved sequences suggests that a history of cyclical climatic activity and patterns may be imprinted in varve records. Holocene varves in the Santa Barbara basin, California, for example, show evidence of a c. 1,000-year cycle, similar to that recorded in the Greenland ice cores, suggesting a teleconnection (similar response to a common stimulus) between the Pacific and Polar realms (Nederbragt & Thurow, 2005). Some varved sequences appear to reflect the influence of more than one climatic rhythm, such as Turkish lake deposits which appear to have responded to variations in both the Indian monsoon and the North Atlantic winter climate regime (Jones *et al.*, 2006). Other varve records contain evidence of decadal-scale climate cycles, such as the North Atlantic Oscillation (NOA) (Hubeny *et al.*, 2006; section 7.6.4.3) and the El Niño Southern Oscillation (ENSO) (Boës & Fagel, 2008; section 7.6.4.2). In addition, solar and lunar periodicities may be recorded in some varved sequences (Berger & von Rad, 2002).

Atmospheric dust and pollutants

Dust in the atmosphere can be an important factor affecting climate, and varved sediments are key records for quantifying past variations in atmospheric dust flux (Maher *et al.*, 2010). In northeast China, Schettler *et al.* (2006) analysed the annual concentrations of atmospheric dust in a varve record for the past 220 years and related these to seasonal variations in the East Asian monsoon regime, while in Minnesota, USA, a varved sediment sequence

provided evidence for a higher dust flux in the mid-Holocene compared with the Little Ice Age and more recent 'dust bowl events' (Dean, 1997). Dust and other pollutants in varved sediments also provide records of human activity. In China, Chu *et al.* (2009) found evidence for intensive dust storms during the historic period (AD 1050–1330, 1590–1690 and over the past 200 years) which they linked to expanding populations and associated farming activity, while Renberg *et al.* (2002) detected increases in lead pollutants in a Swedish varve record, with markedly higher levels in Roman and Medieval (AD 1000, 1200 and 1530) times, and especially in the period post World War II. An increase in metal pollutants over the past 150 years has also been observed in varved sequences in Arctic lakes (Sun *et al.*, 2006a).

Palaeoseismicity

Deformed laminated deposits caused by seismic events (**seismites**) provide evidence of past earthquake and associated activity. In the Dead Sea graben, there is a record in varved sediments of major earthquakes occurring in 31 BC, and AD 749, 1033, 1212, 1837 and 1927 (Migowski *et al.*, 2004). Seismic events are also reflected in the Swedish varve record, with evidence for increased tectonic activity in the Stockholm area just after the onset of ice-sheet wastage (Tröften, 2000).

Calibration of the radiocarbon timescale

The IntCal13 calibration described in section 5.3.2.6 incorporates marine-varve data from the Cariaco Basin, Venezuela, where lighter layers, rich in the remains of diatoms, are formed during the winter–spring upwelling season, and these alternate with darker laminae formed largely of terrestrial material inwashed into the basin during the late summer–autumn rainy season. The varve chronology, which spans the time period 15–10 ka, is floating but it can be anchored to the calendrical timescale by cross-correlating radiocarbon dates obtained on planktonic Foraminifera with the ^{14}C record in the pine tree-ring chronology (Hughen *et al.*, 2004b). A more extended timescale for the Cariaco varve sequence, spanning the interval 55–15 ka, has been cross-matched with the annual-layer counted chronology of the GISP2 ice core (Hughen *et al.*, 2004b).

The longest continuous varve record in a terrestrial site is that from Lake Suigetsu, Japan (Figure 5.25) which extends back over 70 ka (Nakagawa *et al.*, 2012). The varves consist of lighter-coloured, diatom-rich, spring–summer units alternating with darker, diatom-poor, autumn–winter horizons. Radiocarbon dating of organic materials from the laminated sediment sequence provides

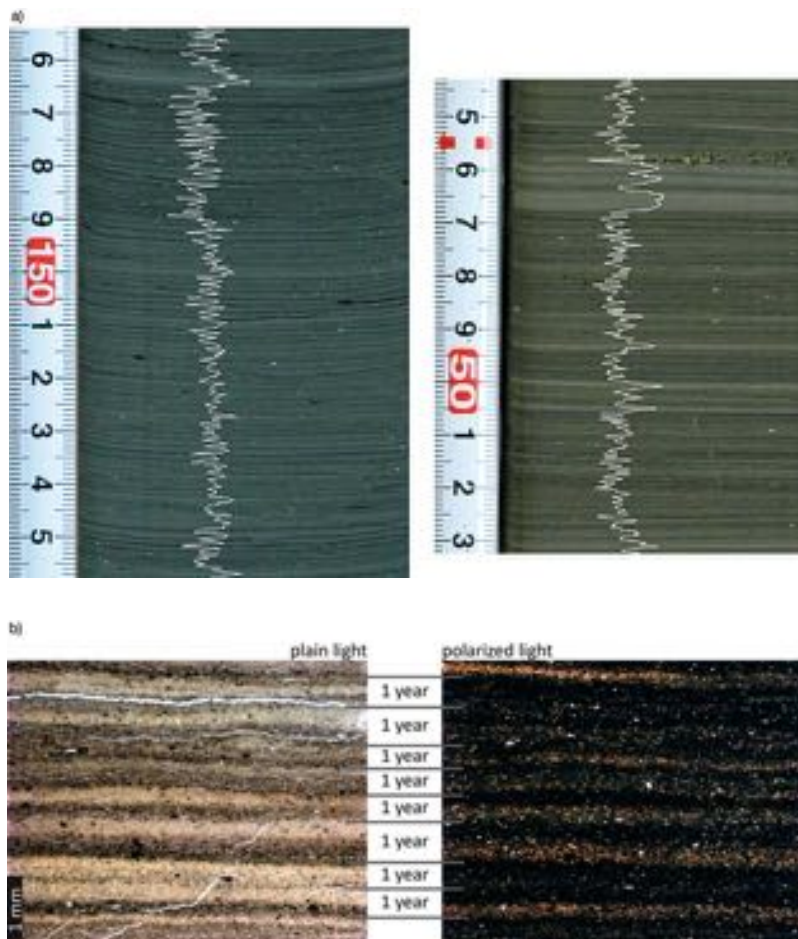


Figure 5.25 a) Part of a varved sequence from Lake Suigetsu, Japan. The white curves reflect measured grey-scale variations which are proportional to sediment colour (lighter to the right). In the left-hand image, the ages of the varves range from $49,951 \pm 168$ vyr (varve years) (top) to $50,088 \pm 171$ vyr (base), and in the right-hand image from $51,497 \pm 201$ vyr to $51,627 \pm 204$ vyr. b) Photomicrographs of part of the Suigetsu varve sequence in plain light (left) and polarized light (right). The varves are composed primarily of amorphous biogenic material and diatoms (the latter appear black in polarized light), along with chemical precipitates, principally siderite (yellowish in polarized light) and recycled iron (Fe). While biogenic material makes up most of the sediment generated in a year, there is a marked seasonal component in the varve record, with distinct diatom-rich layers forming in spring and siderite layers in the late autumn. The latter are the most frequent seasonal layers in the Lake Suigetsu core, and varve counting relies mainly on these horizons. This part of the sequence dates to c. 26.8 k vyr (photographs and micrographs by Takeshi Nakagawa, Ritsumeikan University, Kyoto, Japan).

a comprehensive calibration based on terrestrial samples for the period 52.8–11.2 ka and constitutes a unique source of information on the connection between global atmospheric and marine radiocarbon levels (Bronk Ramsey *et al.*, 2012). This remarkable record may, in due course, enable even further improvements to be made in radiocarbon calibration (section 5.3.2.6).

5.4.3 Annual layers in glacier ice

5.4.3.1 General principles

Annual additions of snow can be observed as clearly defined layers in the upper parts of many glacier masses and these provide a high-resolution chronology for environmental

change (section 3.11). Annual layering has been observed both in polar ice sheets (Taylor *et al.*, 2004; Rasmussen *et al.*, 2006) and in smaller ice masses, such as those found on the summits of high mountains in the tropics (Vimeux *et al.*, 2009). In addition to changes in the visual properties of the ice, seasonal layering can also be detected by measurements of such physical and/or chemical parameters as stable isotope ratios ($\delta^{18}\text{O}$, δD), electrical conductivity of the ice, dust content, microparticle content and chemical element composition. More recent approaches using digital scanners, powerful computers and large storage media (Svensson *et al.*, 2005) have enabled the visual stratigraphy of ice cores to be determined with extraordinary clarity

(Figure 5.26). Identification and subsequent counting of annual layers in ice cores can be based on a single parameter that is known to exhibit annual cycles, but where parallel data series with sufficient resolution are available from the same segment of an ice core, then it is preferable to use all of the data in the development of a chronology. This **multi-parameter approach** is now routinely employed in the construction of ice-core timescales (Meese *et al.*, 1997; Rasmussen *et al.*, 2006).

In deeper ice, however, the annual layers are more closely spaced and they become increasingly deformed and diffuse, hence annual variations are more difficult to distinguish. Older ice, therefore, cannot be dated by

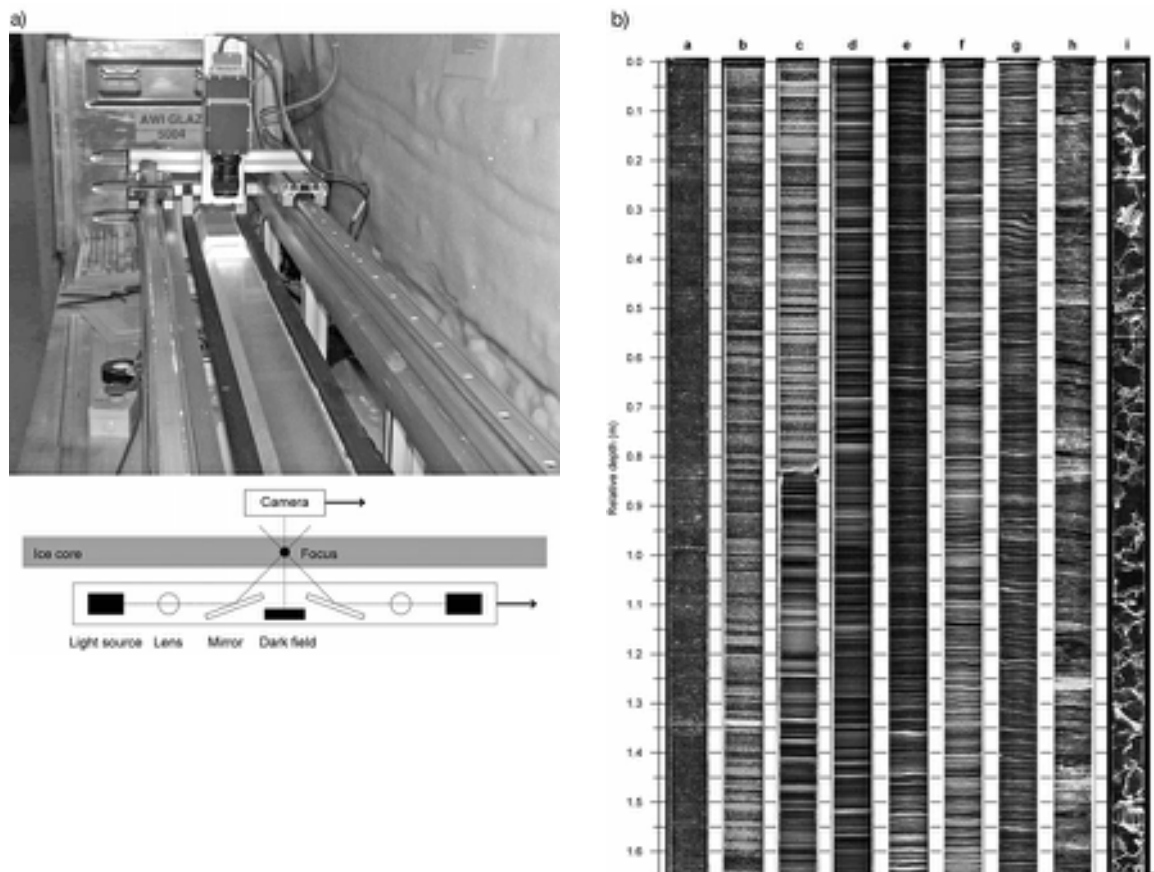


Figure 5.26 Line-scan images from the NorthGRIP ice core. a) A camera moves along the upper side of an ice-core section while an indirect light source is moving below the ice. The light enters the ice at an angle of 45° so that the camera detects only light that is scattered in the ice. Transparent ice thus appears black in the record, whereas the cloudy bands appear white. b) The images show alternating darker and lighter layers, the latter containing relatively high amounts of impurities, in particular micrometre-sized dust particles from dry areas in eastern Asia. The visual stratigraphy is essentially a seasonal signal. However, other impurities also show on the line-scan images; for example, the bright layer at 1.33 m in core b is the Vedde Ash (after Svensson *et al.*, 2005; images by Anders Svensson, Niels Bohr Institute, University of Copenhagen, Denmark).

straightforward incremental means, and recourse has to be made to other techniques. For example, age estimates can be derived from theoretical ice-flow models based on a knowledge of ice dynamics. This method is often combined with the use of marker horizons, such as tephra and sulphate from volcanic eruptions, cosmogenic nuclides (e.g. ^{10}Be , ^{14}C) and geomagnetic events (section 5.5.1.2) to provide ‘pinning points’ for the ice-core chronology (Parrenin *et al.*, 2007). Alternatively, the isotopically defined events in the ice cores can be correlated with independently dated events (based on radiocarbon or U-series dating) in marine cores or in speleothem records, and the ice-core timescale can then be ‘calibrated’ using these age measurements (Shackleton *et al.*, 2004). Other methods include the **tuning** (matching) of proxy climate records obtained from ice cores, such as atmospheric trace gases (e.g. methane) to variations in the earth’s orbital parameters (section 1.7) which have an independent chronology based on astronomical calculations (Ruddiman & Raymo, 2003). A difficulty with this approach, however, is that there will be an age difference between the trapped gas and the surrounding ice matrix. This is because the gas itself is trapped several tens of metres below the ice-sheet surface where it is surrounded by ice that was deposited as surface snow, possibly hundreds or even thousands of years earlier, and firm densification models are required in order to evaluate this ice age–gas age difference (Loulerge *et al.*, 2007). More recently, an integrated method for dating of ice cores has been developed which combines the modelling and empirical approaches and develops a ‘best compromise’ between model-based dating scenarios and chronological information from data (direct measurements; age markers, etc.). This probabilistic technique employs a Bayesian framework (section 5.3.2.6) in order to estimate confidence intervals for the new dating scenario (Lemieux-Dudon *et al.*, 2010).

5.4.3.2 Errors in ice-core chronologies

Errors in ice-core chronologies arise from two sources: imperfections in the nature of the record and human (or technical) errors that occur during sampling, recording and interpreting the ice-core sequence. The former includes loss of material from the ice surface through wind scour which will leave gaps in the ice-core stratigraphy, and deformation within the ice which causes folding and possible loss of stratigraphic continuity (Alley *et al.*, 1997). It also includes the ice age–gas age difference described above. Technical or human errors include incomplete core recovery, which means that interpolations of age may have to be made to bridge the missing parts of the sequence, as well

as inconsistencies in the counting of annual (or, in some cases, subannual) horizons. While replicate counts by at least two different operators are the norm, some degree of error will be inevitable. All ice-core chronologies therefore contain an element of uncertainty. For example, in the younger part of the Greenland NGRIP ice core (14.8–7.9 ka BP), the **maximum counting error (MCE)** (broadly equivalent to a 2σ error in a Gaussian distribution) ranges from 2 per cent in the Holocene to 3 per cent in the Late-glacial. The base of the Holocene at 11,700 has an MCE of 99 years, and the onset of the Lateglacial at 14,692 an MCE of 190 years (Rasmussen *et al.*, 2006). In the deeper part of the core where the chronology extends to *c.* 60 ka, the MCE varies between 4 per cent in the warm interstadial periods to 7 per cent in the cold stadials, although the overall MCE is *c.* 5 per cent or 950 years (Andersen *et al.*, 2006; Svensson *et al.*, 2008).

In Antarctica, while annual layer counting has been possible at some sites (Taylor *et al.*, 2004), in general low rates of snow accumulation mean that layer counting is not feasible, especially in deeper ice, and age–depth profiles have largely been based on ice-flow modelling constrained by marker horizons and by orbital tuning of trace gas records. The longest continuous chronology dated in this way is the EDC3 timescale from the EPICA Dome C site in East Antarctica (EPICA Community Members, 2004; Wolff *et al.*, 2010). The 2σ error on the timescale is estimated to be of the order of 100 years at 6–2 ka, increasing to 400 years at 14 ka, 1.5 ka at 40 ka, 3 ka at 100 ka and 6 ka at 130 ka, after which it remains stable to the base of the record (Parrenin *et al.*, 2007).

5.4.3.3 Ice-core chronologies

In the Greenland ice sheet, where snow accumulation was relatively rapid, chronologies span the last glacial–interglacial cycle. They include the GRIP (Greenland Ice Core Project) core, which is ice-layer counted back to 14.5 ka (Johnsen *et al.*, 2001), and GISP2 (Greenland Ice-Sheet Project 2), where multiparameter continuous counting has been possible down to a depth of 2,800 m and where the ice is dated at *c.* 110 ka (Meese *et al.*, 1997). These chronologies agree within 750 years back to *c.* 40 ka, but diverge by up to several thousand years beyond that time. The most highly resolved chronology from Greenland is the **Greenland Ice Core Chronology (GICC05)** extending back to 60 ka (Figure 5.27; Table 5.5). GICC05 is a composite stratigraphic timescale and is based on multiparameter counting using $\delta^{18}\text{O}$ and δD variations, electrical conductivity measurements (ECM) and continuous flow analysis (CFA) of water-soluble ions in three separate

Greenland ice cores: Dye-3, GRIP and NGRIP (Rasmussen *et al.*, 2006). Ages are expressed in years before AD 2000, which is abbreviated to b2k; hence the Holocene boundary in the core referred to above is dated at 11,700 b2k, i.e. before AD 2000. As radiocarbon ages are measured in years before 1950, this means that ice-core ages on the GICC05 timescale are 50 years older than radiocarbon ages. The 7.9–0 ka section of GICC05 is based on annual layer counting in the Dye-3, GRIP and NGRIP ice cores, the 14.8–7.9 interval on ECM and CFA in the GRIP and NGRIP cores, while the chronology for the 60–14.8 ka section is based on the counting of annual layers identified by visual stratigraphy and in ECM and CFA data in the NGRIP core only (Svensson *et al.*, 2008).

The NorthGRIP ice-core record extends to bedrock at 3,085 m depth below the ice surface and dates to *c.* 123 ka BP, the later part of the last (Eemian) interglacial (North Greenland Ice Core Project Members, 2004). Dating by layer counting may, in due course, be possible to a depth of 2,700 m (*c.* 90 ka BP), but below this the annual layers are extremely thin, indistinct and deformed (Svensson *et al.*, 2005). The age of the lower parts of the ice-core record, therefore, will still have to be estimated using ice-flow models based on observed physical relationships between

ice thickness, heat flow, ice melt and integral ice-flow dynamics (Johnsen *et al.*, 2001; Dahl-Jensen *et al.*, 2003). As we saw in section 3.11.1, the oldest ice so far investigated in Greenland is in the 2,540 m long NEEM core from the northern part of the ice sheet which contains the onset of the Eemian interglacial (NEEM Community Members, 2013). By linking the CH₄ and δ¹⁸O profiles from the bottom section of the core with other records from Greenland (NGRIP) and Antarctica (EPICA), the Eemian sequence in the NEEM ice core can be placed on the EDML timescale (see below).

A number of chronologies have been generated from Antarctic drilling programmes, including the Vostok Station and Dome Fuji records, dated by ice-flow modelling to *c.* 420 and 340 ka respectively (Petit *et al.*, 1999; Watanabe *et al.*, 2003b). The oldest record obtained so far is the EPICA core, which has reached ice estimated to date to 960 ± 20 ka (EPICA Community Members, 2004). The EDC3 timescale from that core is based on snow accumulation rates and a mechanical ice-flow model, and by reference to a set of age markers along the core. These include volcanic events and independently dated cosmogenic records; geomagnetic events; and dated CH₄ profiles in other ice-core records (e.g. GICC05). Construction of the timescale

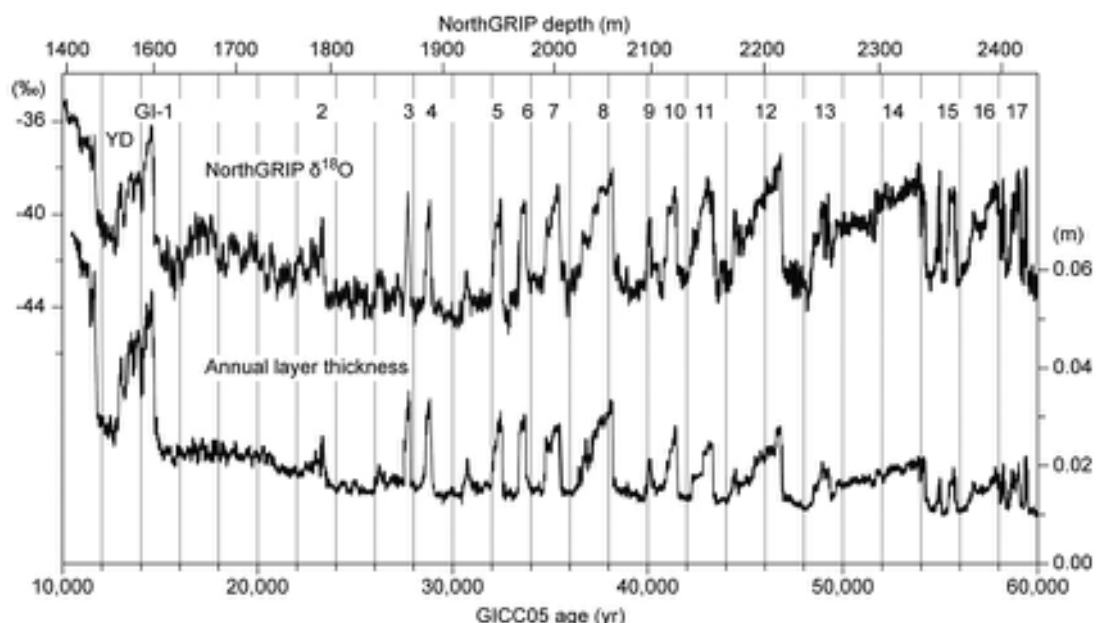


Figure 5.27 The NorthGRIP (NGRIP) oxygen isotope record and variations in annual ice-layer thickness plotted against the GICC05 timescale. GI indicates Greenland Interstadials; GI-1 – Bølling-Allerød Interstadial; YD – Younger Dryas Stadial (after Svensson *et al.*, 2008).

314 DATING METHODS

Table 5.5 GICC05 chronology of climatic events represented in the NGRIP and GRIP ice-core records for the period c. 47 to c. 8.1 b2k (years before AD 2000). GS – Greenland Stadial; GI – Greenland Interstadial (from Blockley *et al.*, 2012).

Event	Depth in NGRIP core (m)	GICC05 age (years b2k)	Maximum counting error (2σ) in years	Uncertainty of definition (years)	Depth in GRIP core (m)
End of 8.2 ka BP event	1,219.47	8,140	45	+50/-10	1,325.11
Volcanic peak, 8.2 ka BP event	1,228.67	8,236	47	1	1,334.04
Start of 8.2 ka BP event	1,234.78	8,300	49	+10/-40	1,340.5
End of 9.3 ka BP event	1,322.88	9,240	68	+30/-10	1,432.43
Start of 9.3 ka BP event	1,331.65	9,350	70	+10/-20	1,442.10
Start of Holocene	1,492.45	11,703	99	4	1,624.27
Start of GS-1	1,526.52	12,896	138	4	1,662.41
Start of GI-1a	1,534.5	13,099	143	30	1,671.7
Start of GI-1b	1,542.1	13,311	149	+30/-10	1,680.5
Start of GI-1c	1,570.5	13,954	165	+30/-10	1,713.7
Start of GI-1d	1,574.8	14,075	169	10	1,718.5
Start of GI-1e	1,604.64	14,692	186	4	1,753.39
Start of GS-2a	Feature not consistent between records; no date recommended				
Start of GS-2b	1,745.31	20,900	482	100	1,899.7
Start of GS-2c	1,783.62	22,900	573	40	1,940.28
Start of GI-2	1,793.19	23,340	596	60	1,950.46
Start of GS-3	1,861.69	27,540	822	20	2,018.09
Start of GI-3	1,869.12	27,780	832	20	2,025.39
Start of GS-4	1,882.62	28,600	887	20	2,037.7
Start of GI-4	1,891.57	28,900	898	20	2,046.05
Start of GS-5	1,938.95	32,000	1,103	60	2,087.33
Start of GI-5	1,951.66	32,500	1,132	20	2,098.82
Start of GS-6	1,964.3	33,360	1,191	20	2,109.73
Start of GI-6	1,974.56	33,740	1,212	20	2,118.58
Start of GS-7	1,990.28	34,740	1,286	20	2,131.77
Start of GI-7	2,009.45	35,480	1,321	20	2,148.69
Start of GS-8	2,026.66	36,580	1,397	40	2,162.56
Start of GI-8	2,070.03	38,220	1,449	20	2,200.32
Start of GS-9	2,094.64	39,900	1,569	20	2,219.69
Start of GI-9	2,099.62	40,160	1,580	20	2,223.6
Start of GS-10	2,109.71	40,800	1,615	20	2,231.55
Start of GI-10	2,124.03	41,460	1,633	20	2,243.27
Start of GS-11	2,134.99	42,240	1,682	20	2,251.94
Start of GI-11	2,157.49	43,340	1,736	20	2,270.77
Start of GS-12	2,170.0	44,280	1,780	60	2,280.48
Start of GI-12	2,222.3	46,860	1,912	20	2,324.22

also involves tuning of atmospheric trace gas records in the EPICA core to orbital parameters (Parrenin *et al.*, 2007). More recently, a multi-site, multi-proxy timescale, the Antarctic Ice Core Chronology 2012 (AICC2012), has been developed for four Antarctic ice cores: Vostok, EPICA Dome C (EDC), EPICA Dronning Maud Land (EDML) and Talos Dome (TALDICE). The section from 120–0 ka includes data from the Greenland NGRIP GICC05 timescale and has been constructed using the Bayesian tool DATICE (Lemieux-Dudon *et al.*, 2010) that combines both glaciological inputs and a wide range of relative and absolute gas and ice-stratigraphic markers (Veres *et al.*, 2012). The record from 800–120 ka also employs DATICE, and is based on a combination of modelling (snow accumulations rates, snow densification into ice, and ice flow), and observational data (absolute ages of key reference horizons, stratigraphic links between the different cores, and orbitally derived ages). The new chronology shows only small differences, well within the uncertainty range, when compared with the previous Antarctic ice-core reference age scale, EDC3, described above (Bazin *et al.*, 2012).

5.4.4 Lichenometry

5.4.4.1 General principles

Lichens are complex organisms consisting of algae and fungi living together symbiotically. The algae provide carbohydrates via photosynthesis, while the fungi provide the protective environment in which the algal cells can function. Although lichens had been used as a basis for dating by Knut Faegri in the 1930s, the technique was

pioneered and developed by Roland Beschel a decade or so later, and rests on the principle that there is a direct relationship between lichen size and age. Where a surface has been recently exposed to lichen colonization, providing (a) that the growth patterns of the lichens are known and (b) that no major time lapse has occurred between surface exposure and lichen colonization, an estimate of the age of the substrate can be made. In studies of glacial retreat, for example, lichen size (usually maximum diameter of the largest lichen) is first established for morainic surfaces of known age (dated by radiometric methods or by historical evidence such as old photographs) and a **lichen growth curve** can then be constructed based on these ‘fixed points’ (Figure 5.28). Surfaces of unknown age can then be dated by relating lichen diameters on those surfaces to the growth-rate curve and deriving a calendar age. In this way, a detailed deglacial chronology can be established for an area. The biological basis of lichenometry is discussed by Loso & Doak (2006) who confirm its reliability as a dating method.

Some lichen species (e.g. *Rhizocarpon geographicum*) will continue to grow for several thousand years and therefore, in theory, lichenometry is a technique that may be applicable to most of the Holocene. In practice, however, the dating limit is around 4,500 years in extremely cold and dry continental regions, such as west Greenland, whereas in the majority of cases the age range for lichenometry as a dating technique is 500 years or less (Matthews, 1992).

5.4.4.2 Sources of error in lichenometric dating

Not all lichens are suitable for lichenometrical purposes, for only those that show a gradual and progressive rate of growth can be employed. Moreover, lichen growth is affected by local environmental conditions that vary with both latitude and altitude, for example air temperature, day length and snow cover. A lichen growth curve must therefore be constructed for specific lichens and will only be applicable to particular geographical areas (Figure 5.28). Moreover, recent climate change will probably result in changed lichen growth curves over time (Hansen, 2010). However, in remote regions, such as the mountains of Norway or Greenland, no documentary or other evidence may be available for establishing fixed points on a lichen growth curve (Winkler *et al.*, 2003). Further, it is assumed that in the study of glacier recession, for example, there is no significant delay in lichen colonization of exposed surfaces following ice retreat. This, however, can never be proved and must always remain a source of uncertainty. Conversely, lichens are found on actively forming medial

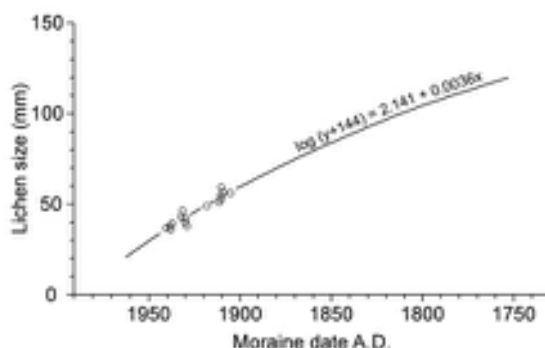


Figure 5.28 Lichenometric growth curves for *Rhizocarpon* spp. from West Greenland, West Spitsbergen and Baffin Island. The ages of unknown surfaces (moraines, etc.) can be obtained by measuring average lichen size on those surfaces (y axis) and reading off the appropriate age on the x axis (after Forman *et al.*, 2007).

moraines and therefore in some areas lichen growth must have preceded ice wastage. Finally, problems have been encountered in sampling and measurement of lichens in the field and very thorough preliminary investigations are required to establish reproducibility of results within any one region. These and other constraints on lichenometric dating are reviewed by Hansen (2008).

5.4.4.3 Some applications of lichenometry

Lichenometry has been most widely employed in the dating of Late Holocene moraines, particularly those of the Little Ice Age period, for example in Scandinavia (Matthews, 2005), Alaska (Wiles *et al.*, 2010), the North American Cordillera (O’Neal & Schoenenberger, 2003) and New Zealand (Winkler, 2004). However, lichenometry has a range of other applications. These include the provision of a timescale for plant colonization of newly exposed

substrates in proglacial areas (Matthews, 1992); and the dating of talus accumulations (McCarroll *et al.*, 1998), glacier outburst floods (Winchester & Harrison, 2000), fluvial deposits (Gob *et al.*, 2003), debris-flow activity (Innes, 2006), and historic and late prehistoric earthquakes (Bull, 2003). The technique has also been used to date structures built of lichen-covered rock, and may have other applications in archaeology (Benedict, 2009).

5.4.5 Other materials dated by annual increments

5.4.5.1 Speleothems

As we saw above (section 5.3.4.3), speleothems, which often contain valuable palaeoclimatic evidence, can be dated by U-series. However, in certain circumstances, it may be possible to identify individual growth bands in the

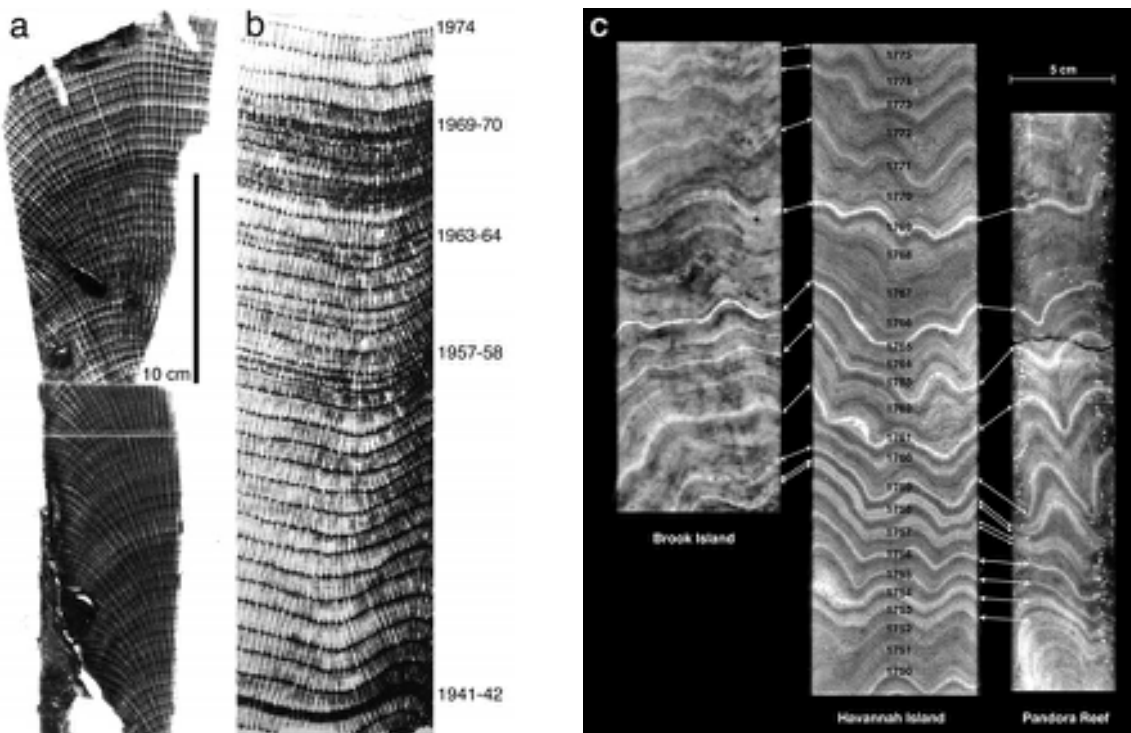


Figure 5.29 Radiographs of core-slabs cut from a) Pleistocene and b) modern coral reefs (*Montastraea*) in Florida Bay, Gulf of Mexico, showing seasonal growth layers (from Gischler *et al.*, 2009; images supplied by Eberhard Gischler, University of Frankfurt, Germany). c) Cross-matching of growth layers of *Porites* coral from three locations on the central Great Barrier Reef, Australia, using images enhanced by UV luminescent illumination, an approach that enabled a 373-year chronology of ENSO variations to be reconstructed (from Hendy *et al.*, 2003, reprinted with permission of SAGE; image supplied by Erica Hendy, Bristol University, UK).

speleothem (Figure 3.38) that represent annual accumulations of calcite, and counting these laminations forms the basis for a timescale (Baker *et al.*, 2008b). The floating chronology that results can be anchored to calendar years either by counting back from the present day or by using other dating techniques (U-series; ^{210}Pb) to calibrate the sequence (Paulsen *et al.*, 2003). Speleothem laminae can be identified visually using UV and visible light, or they can be detected by fluorescence (or luminescence), the signal reflecting seasonal variations in concentrations of organic matter derived from the overlying soil by percolating groundwaters (McGarry & Baker, 2000). Annual banding in speleothems has been used to provide a timescale for recent precipitation records (Fleitmann *et al.*, 2004), to calibrate climatic reconstructions over the course of the last millennium (McMillan *et al.*, 2005) and to provide an independent chronology for Dansgaard–Oeschger events (Spötl & Mangini, 2002).

5.4.5.2 Sclerochronology

Many organisms in the aquatic realm display clear annual growth bands reflecting seasonal controls over the

physical and chemical processes of skeletal construction. The construction of a timescale based on these growth increments is referred to as **sclerochronology**, and the most widely employed media thus far have been corals and molluscs (Gröcke & Gilliken, 2008; Oschmann, 2009).

Coral

Corals grow rapidly through successive increments of aragonite that can accumulate at up to several centimetres per year. Some species contain clear evidence of annual banding (Figure 5.29) which can be detected by X-radiography or UV luminescence (Hendy *et al.*, 2003). The annual bands are characterized by variations in chemical properties, such as stable isotope and trace-element ratios, which reflect seasonal variations in environmental conditions (Grottoli & Eakin, 2007), and from which past sea-surface and salinity changes can be reconstructed with an annual, monthly or even weekly temporal resolution (Figure 5.30). Although coral growth bands can be cross-matched in the same manner as tree-ring sequences, there are, as yet, few records extending back more than c. 400 years. Typical errors associated with coral-chronology are of the order of 1–2 years per century.

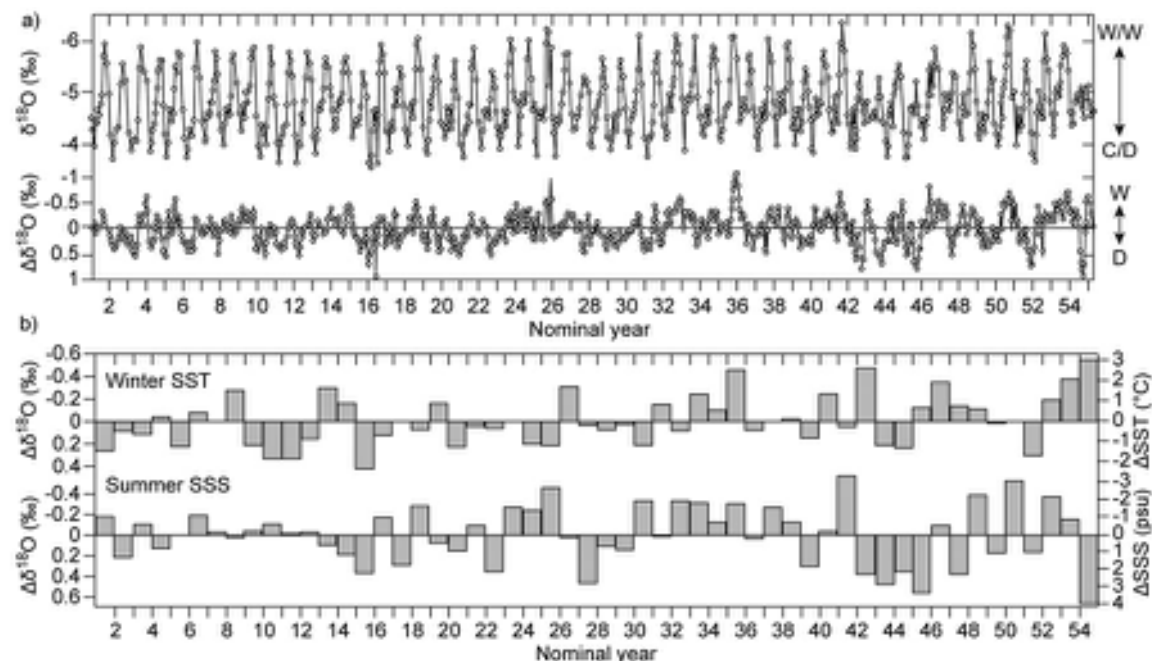


Figure 5.30 A 54-year annual coral stable isotope record from the mid-Holocene. a) The $\delta^{18}\text{O}$ record (above) and deviations in $\delta^{18}\text{O}$ ($\Delta\delta^{18}\text{O}$) after removal of the sea-surface temperature component W/W – warm/wet; C/D – cold/dry. b) Annual variability in winter (December–February) sea-surface temperatures and in summer sea-surface salinity (SSS) (after Sun *et al.*, 2005).

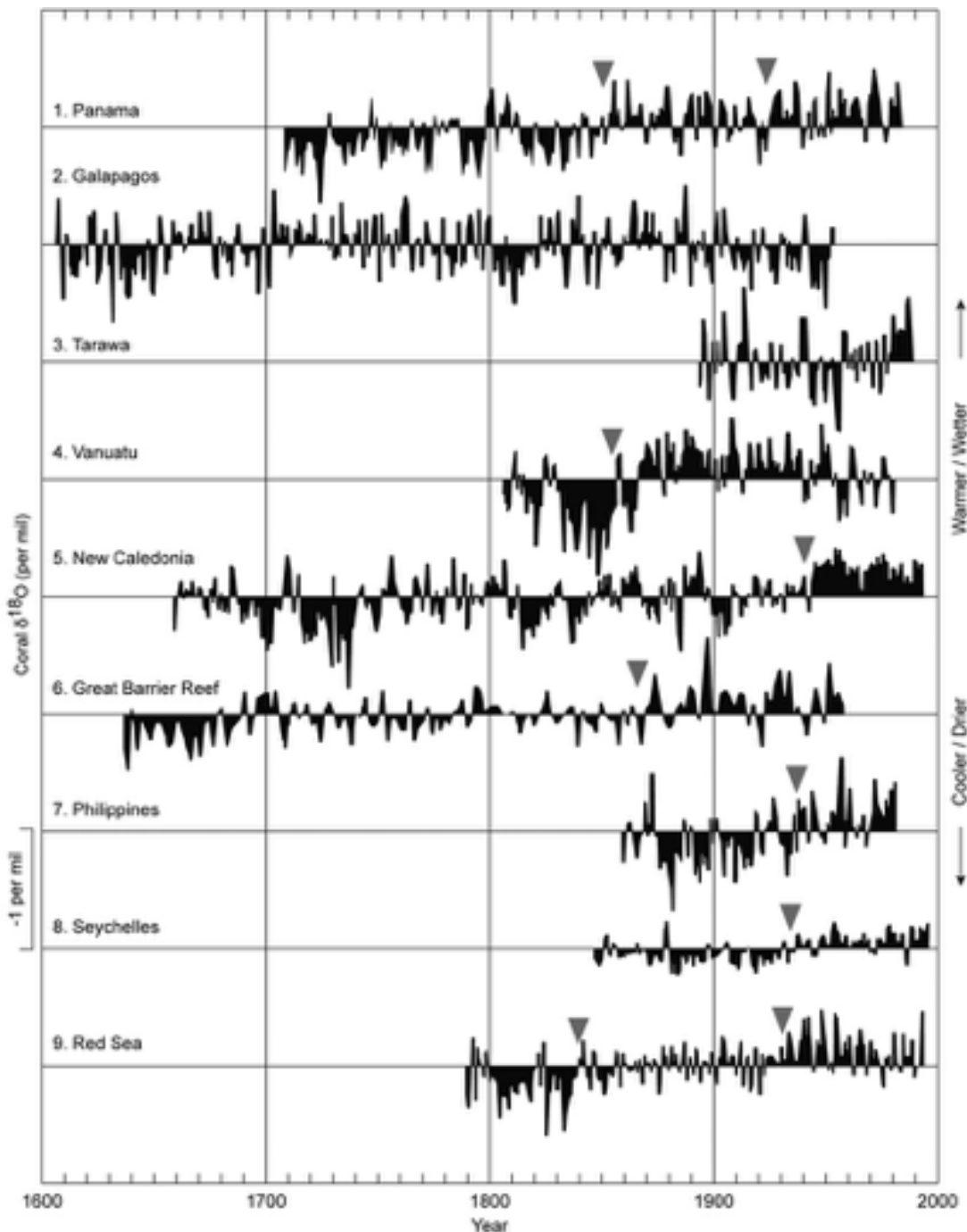


Figure 5.31 Annual coral $\delta^{18}\text{O}$ records from various sites in the Pacific and Indian Oceans. Horizontal lines represent the mean $\delta^{18}\text{O}$ value for each site. Black triangles mark approximate times of abrupt shifts in $\delta^{18}\text{O}$, heralding warmer/wetter conditions related to ENSO variations (after Gagan *et al.*, 2000).

As global sea levels have fluctuated, so too has the tidal range within which corals live, and hence fossil corals of varying ages occur at different altitudes, while many are submerged below present sea level. Coral records have been used to reconstruct past sea-surface temperature changes (McCullough & Esat, 2000), ENSO events (Figure 5.31; section 7.6.4.2), variations in coastal run-off (Hendy *et al.*, 2003) and Holocene precipitation changes (Deng *et al.*, 2009). In addition, samples of fossil corals have been used to develop floating chronologies for older (interglacial) reef sequences (Tudhope *et al.*, 2001).

Molluscs

Like corals, some marine molluscs also develop annual growth bands in their shells. These range from semi-diurnal to annual and reflect the influence of a range of environmental factors, including water temperature, salinity and, in particular, nutrient and food availability (Goodwin *et al.*, 2001). Variations in growth banding may provide valuable palaeoenvironmental data, as well as the basis for a timescale for geochemical proxies such as $\delta^{18}\text{O}$ and $\delta^{13}\text{C}$ from which variations in, for example, bottom-water temperature can be inferred (Weidman *et al.*, 1994). The shells of some freshwater molluscan species may also contain evidence of former climatic/environmental conditions, such as changes in air temperature (Schöne *et al.*, 2004). Composite sclerochronologies have also been developed, in which living molluscs are linked to subfossil species using distinct 'marker' bands or sequences of bands, following the principles of cross-dating employed in dendrochronology (section 5.4.1.2). Many of these chronologies are relatively short (< 100 years) because of the limited lifespan of most Mollusca (Schöne, 2003), but some are longer-lived and hence longer chronologies may be possible. One example is *Arctica islandica*, a relatively long-lived (over 100 years) species from the North Atlantic, from which a continuous chronology back to AD 1843 has been obtained for northwest Scotland (Stott *et al.*, 2010). An even older *Arctica* record has been obtained from the North Sea where a cross-matched floating chronology spanning the period from c. AD 1000–1400 has been constructed, and which includes a 267-year continuous series from the longest-living *Arctic islandica* specimen yet recorded from the area (Scourse *et al.*, 2006). Further development of these sclerochronological records could have major implications, not only for palaeoceanographical reconstructions, but also for our understanding of spatial and temporal variations in the marine radiocarbon reservoir (section 5.3.2.4). In addition, sclerochronology of shell middens provides an opportunity for the examination of climate and environmental change in relation to human activity (Andrus, 2011).

5.5 AGE-EQUIVALENT STRATIGRAPHIC MARKERS

In many Quaternary deposits, distinctive marker horizons are found that are broadly synchronous and form time planes across different sedimentary sequences. The horizons themselves cannot be used in the first instance to date Quaternary successions, for other methods are required to establish their age. However, once dated by radiometric or incremental methods at one locality, they allow age estimates to be extended to other sequences where the marker horizon is present. As such, they form an indirect means of dating. Moreover, in view of their often widespread distribution, they also form a basis for stratigraphic subdivision and time-stratigraphic correlation (Chapter 6).

Four methods of dating using age-equivalent stratigraphic markers are considered here: **palaeomagnetism**, which is based on the changes in the earth's magnetic field preserved in rocks and sediments; **tephrochronology**, the use of volcanic ash layers as a means of dating; **oxygen isotope chronostratigraphy**, which employs globally synchronous changes in the oxygen isotope signal in deep-ocean sediments; and **biostratigraphy**, in which dating is based on palaeoecological or evolutionary events recorded in stratigraphic sequences. Other marker horizons that are more widely employed in stratigraphic subdivision and correlation than in dating, such as palaeosols and shorelines, are discussed further in section 6.3.2.

5.5.1 Palaeomagnetism

5.5.1.1 Geomagnetic field and remanent magnetism

The earth's geomagnetic field is **dipolar** in that it possesses two poles that we refer to as north and south. Over time, the magnetic field changes in both field strength and direction. There are two components to these changes: major **dipole changes** where the dynamo currents that generate the main dipole field become reversed so that effectively the magnetic north pole becomes the magnetic south pole and vice versa (**polarity changes**), and **secular variations**, which operate largely through a process known as 'dipole wobble' whereby the axis of the dipole field (magnetic north) precesses around the earth's axis of rotation (true north). The major polarity changes are measurable over timescales of thousands or millions of years, whereas, secular variations occur over centuries or less during which field direction changes at a rate of 1° every

few decades, while field strength changes by several per cent per century (Sternberg, 2001).

A record of both of these magnetic changes can be found in rocks and sediments containing magnetic minerals, for these are magnetized during formation and hence individual crystals or particles will reveal a **natural remanent magnetism (NRM)** which is a reflection of the geomagnetic field at the time of rock or sediment formation (McElhinney & McFadden, 2000). Volcanic rocks will acquire a remanence through heating, and this is referred to as **thermoremanent magnetization (TRM)**. Archaeological materials that have been reheated, such as pottery and hearths, will also contain a TRM signal, and again this will reveal the direction of the earth's magnetic field at the time of firing. Sedimentary rocks and unconsolidated sediments accumulating on the sea floor or in lakes also contain evidence of former geomagnetic fields, for a record is preserved in the alignment of ferromagnetic sedimentary particles as they settle in water or in water-saturated sediments. This is referred to as **detrital remanent magnetism (DRM)**. In some sediments, however, NRM can also be acquired by chemical action, where the crystallization of ferromagnetic oxides results in a **chemical remanent magnetism (CRM)**. This process may occur later than, and under a different magnetic field from, that of DRM in the same sediment unit. In this way, a **secondary magnetization** is introduced into both volcanic and sedimentary rocks, which serves to complicate the study of palaeomagnetic variations. Thompson and Oldfield (1986) provide further details of the magnetic properties of minerals, rocks and sediments, while various aspects of environmental magnetism are discussed in Walden *et al.* (1999), Evans & Heller (2003) and Maher (2007).

There are three components in the earth's magnetic field. **Declination** is the angle between magnetic north and geographic (true) north, while **inclination** refers to the angle of dip of the magnetic field. Hence, a freely suspended needle at the surface of the earth will align with the prevailing magnetic field (declination), and the amount of dip exhibited by the needle relative to the horizontal is a measure of the inclination. The inclination value varies from 0° at the magnetic equator to 90° at the magnetic poles. The third component, **intensity**, refers to the strength of the geomagnetic field. At the present day, the field strength at the geomagnetic poles is twice that at the geomagnetic equator. The strength of the field can be estimated in the following way. Suppose a magnetic needle is fixed to a horizontal axle, so that the axle passes through the centre of gravity of the needle and is orientated along magnetic east–west. If the needle (aligned north–south) is allowed to swing freely, it would eventually stabilize at the

angle of magnetic dip. Magnetic intensity can be measured by the amount of torque required to prevent the needle returning to the angle of magnetic dip after it has been rotated through 90°.

5.5.1.2 Magnetostратиграфија

The study of variations in magnetic properties through a sequence of rocks or sediments is termed **magnetostратиграфија**. Geomagnetic field variation can be detected in rocks or sediments that contain even small amounts of magnetic minerals, and the identification of major polarity changes in volcanic rocks, in ice cores, and in deep-sea sediment records, or variations in inclination or declination (secular changes) in different depositional sequences, provides a basis for relative dating and correlation (Roberts *et al.*, 2013). In addition, however, **mineral magnetic 'potential'**, that is, the concentration and magnetic susceptibility of magnetic minerals, also varies within sediments, and under certain circumstances this too can provide a basis for correlation.

Secular variations

Secular variations, which are due to both dipole and non-dipole field activity, are variable in both space and time, and are reflected in changes in declination, inclination and field intensity. Past variations in these three parameters are referred to as **palaeosecular variations (PSV)**. Direct measurements of values of field declination, inclination and intensity have been collected over the past 400 years² for cities such as London, Rome and Boston (Figure 5.32). These suggest complex radial variations in field activity around the globe and may hold the key to understanding the causes of major excursions and reversals (Jackson *et al.*, 2000). In London, for example, declination has varied from 11°E in AD 1570 to 24°W in AD 1820. Since then, declination has decreased to the present values of 5°W, and it continues to decrease at a rate of 9 minutes each year (Thompson & Oldfield, 1986). Magnetic inclination has varied from a maximum of over 74° in AD 1700 and is now near to 66°. Figure 5.32 shows that secular magnetic variations in London and Rome have been similar whereas in Boston, some 5,000 km from Europe, the pattern has been very different. These curves, based on observational evidence, can be extended into the historic period and beyond by using **archaeomagnetic measurements** from features dated by documentary sources, pottery typology, dendrochronology or other methods (Batt, 1997). Within the historic period, data from a number of sites in western Europe and the eastern Mediterranean suggest that the region experienced 'archaeomagnetic jerks' (significant

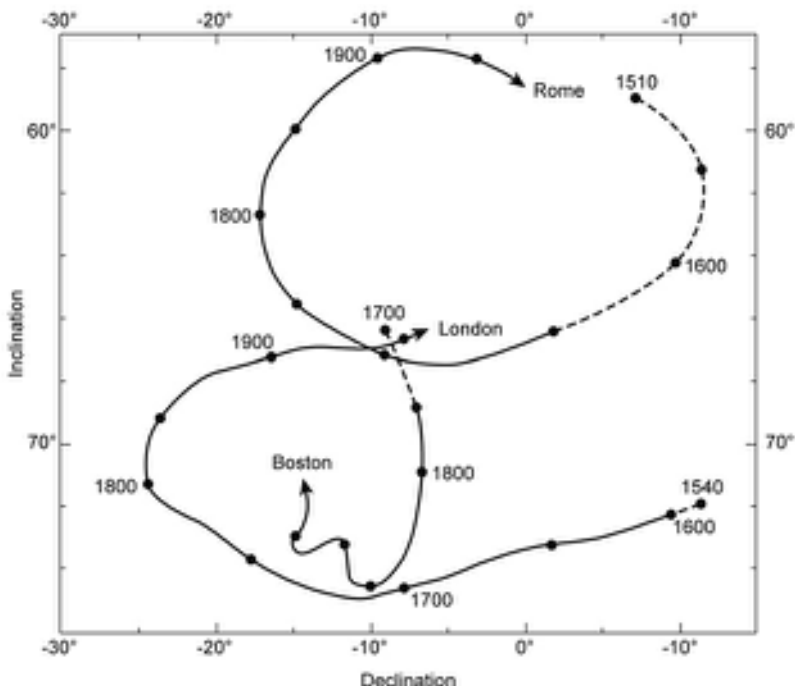


Figure 5.32 Secular changes in magnetic declination and inclination as observed in London, Rome and Boston. The solid curves begin at the time of the first declination measurements at each locality. The earlier inclination changes (dashed lines) are based on archaeomagnetic data (after Thompson & Oldfield, 1986).

short-term departures in geomagnetic field direction and intensity) on at least two occasions, most notably at c. AD 200 and 1400 (Gallet *et al.*, 2003).

Long-term records of secular geomagnetic variations can also be obtained from lake sediment sequences, and these can be used as regional chronostratigraphic tools (Barletta *et al.*, 2008). High-resolution magnetostratigraphic sequences, which can be dated by independent methods such as radiocarbon and varve chronology (Snowball & Sandgren, 2002), constitute type profiles against which other secular magnetic records can be matched (Figure 5.33). These **master curves**, some of which extend back into the early Holocene, may be applicable to sediments found up to 2,000 km from the type site. Core matching can be achieved using the distinctive inflections or **turning points** in the magnetic profiles. Secular geomagnetic variations recorded in lake sediments have been employed in the correction of errors in Holocene varve sequences in west central Sweden (Stanton *et al.*, 2010) while, on a longer timescale, a 50 ka palaeomagnetic record of secular variation has been obtained from a lake sequence in southern Argentina. This compares with other magnetic

profiles from the mid- and high latitudes of the Southern Hemisphere, and reveals consistent millennial-scale variability (Lis  -Pronovost *et al.*, 2013). The derivation of an accurate record of long-term secular variations is not always straightforward, however, partly because of the difficulties in obtaining an accurate independent timescale for lake sediment profiles, and partly because secular variation patterns rarely have amplitudes of more than 20° (compared with 180° for polarity changes) and hence the palaeomagnetic signal may not always be easily distinguishable from background ‘noise’ (Snowball *et al.*, 2007).

Field reversals and the palaeomagnetic timescale

From time to time, the geomagnetic field reverses so that the geomagnetic poles change relative positions through 180°. These **polarity reversals** can be detected in the geological record and are of fundamental importance in palaeomagnetic studies. The present-day magnetic field is regarded as possessing **normal polarity**, and the opposite is referred to as **reversed polarity**. Periods of long-term fixed polarity (10^5 – 10^7 years) are known as **polarity epochs**.

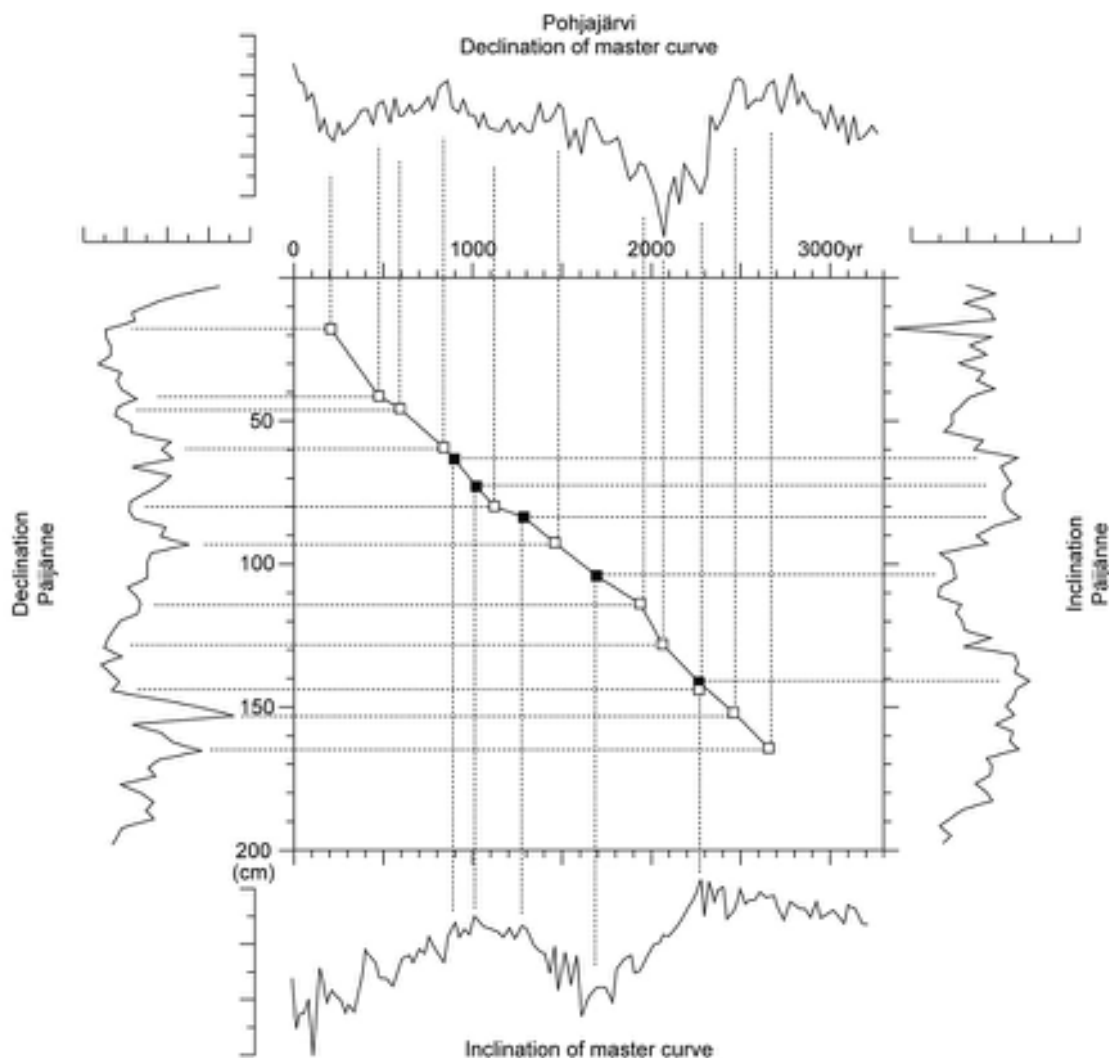


Figure 5.33 Palaeomagnetic dating of sediments from Lake Päijänne, Finland, based on a correlation of the declination (left) and inclination (right) record with the dated PSV master curves from Lake Pohjajärvi. Open boxes indicate matching declination features and solid boxes show matching inclination features (after Saarinen, 1999).

These are interrupted by a large number of polarity reversals of shorter duration (10^4 – 10^5 years), which are termed **polarity events**, and also by **polarity excursions**, in which the geomagnetic pole changes direction through 45° or more for a short period only (100–1 ka). Polarity epochs and polarity events are experienced globally and can be used as a basis for worldwide correlations.

Where polarity epochs and events are found in volcanic rocks, they can be dated by the argon isotope dating method (section 5.3.3), thereby enabling a palaeomagnetic

timescale to be established for the Quaternary and parts of the pre-Quaternary sequence (Figure 5.34). Three polarity epoch boundaries are shown on Figure 5.34: the Brunhes–Matuyama, which is K–Ar dated at c. 0.73 Ma, the Matuyama–Gauss at c. 2.47 Ma and the Gauss–Gilbert at c. 3.41 Ma. Important polarity events include the Jaramillo ‘normal’ event, which has a K–Ar age of between 0.90 and 0.97 Ma, and the Olduvai ‘normal’ event between 1.67 and 1.87 Ma. Argon isotope dating is, however, not sufficiently precise to date some of the relatively short-lived polarity

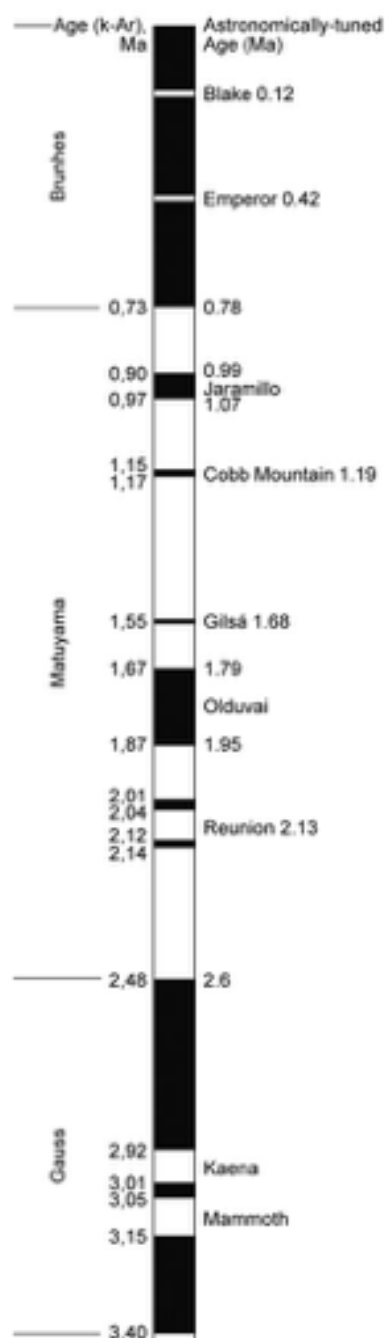


Figure 5.34 The palaeomagnetic timescale of the last 3.5 Ma. Shaded areas indicate periods of normal polarity; unshaded areas show episodes of reversed polarity. K-Ar ages are shown on the left; astronomically tuned ages are on the right (after Cande & Kent, 1995; Funnell, 1995).

events, and their positions on the palaeomagnetic timescale have therefore been established by extrapolation based on the ages of epoch boundaries. As a consequence, the dating of polarity events tends to be less secure.

An alternative approach to dating the palaeomagnetic timescale involves the use of the ocean sediment record. As sediments accumulate on the deep-ocean floors, individual particles adopt the direction of the earth's magnetic field, and hence a continuous record of geomagnetic changes is preserved within the sediment sequence. Astronomical tuning of the oxygen isotope signal obtained from the microfossil record within these sediments (sections 5.5.3 and 6.3.3) provides the basis for a timescale for the geomagnetic changes that is independent of that based on argon isotope dating of volcanic rocks (Bassinot *et al.*, 1994). Ages of the polarity epochs and principal polarity events that have been obtained using this method are shown on the right of Figure 5.34. In general, the dates tend to be older than those based on K-Ar. Hence, the Brunhes–Matuyama boundary is dated at c. 0.78 Ma and the Matuyama–Gauss boundary at c. 2.6 ka BP, while the ages of the Jaramillo and Olduvai events are 0.99–1.07 Ma and 1.79–1.95 Ma BP, respectively. The resolution and length of the polarity timescale in the ocean sediment record is, however, dependent on rates of sedimentation. For example, in parts of the oceans experiencing comparatively slow sedimentation rates (e.g. 0.1–1.2 m per 1,000 years), a core may contain a complete record of Pleistocene polarity changes. Conversely, in some areas of the oceans, such as the North Atlantic, where sedimentation rates are rapid (e.g. 0.25–0.5 m per 1,000 years), coring may fail to reach the first major geomagnetic boundary, the Brunhes–Matuyama transition.

The causes of these geomagnetic changes are not fully understood, but some have pointed to a possible link between magnetic variations and astronomical cycles. For example, Yamazaki & Oda (2002) have detected a 100 ka periodicity in a 2.25 Ma palaeomagnetic inclination and intensity record from the equatorial Pacific (Figure 5.35), and have suggested that the earth's magnetic field may be modulated by orbital eccentricity. A relationship has also been proposed between geomagnetic polarity reversals/excursions and glacial–interglacial cycles, with the suggestion that the growth of polar ice sheets may affect the differential rotation between the earth's field and core, and that increased ice volumes are accompanied by a weakened geomagnetic field (Westaway, 2009). Other possible causes of geomagnetic reversals are discussed by Gubbins (2008).

The use of palaeomagnetic stratigraphy as a means of correlating between individual deep-sea cores, and also

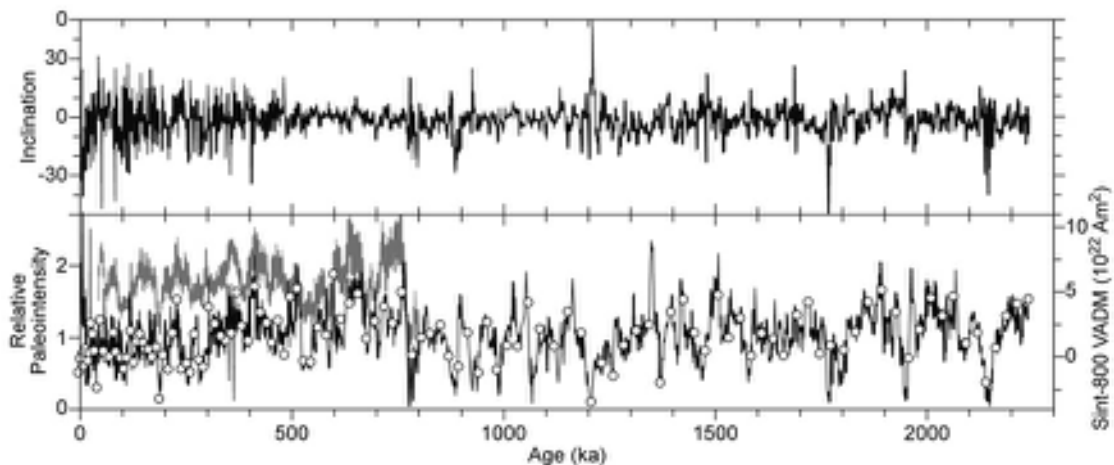


Figure 5.35 Variations in the earth's magnetic inclination and field strength (palaeointensity) during the last 2.5 Ma (from Yamazaki & Oda, 2002).

between the marine and terrestrial records, is discussed further in Chapter 6.

Magnetic susceptibility, isothermal remanent magnetism and coercivity

A number of magnetic characteristics of sediments do not depend on variations in the earth's magnetic field, but rather reflect the nature and origins of magnetic minerals in the sediments (Walden *et al.*, 1999). While these properties cannot in themselves be used as a basis for a chronology, they offer a potential basis for correlation. This is because changes in mineral magnetic potential are often a reflection of environmental change, and as these will be broadly synchronous, the magnetic signal in sediments may offer a means of correlation between depositional contexts and across a range of timescales.

Mineral magnetic susceptibility (MS): This measures the degree to which a material can be magnetized, that is, its 'magnetizability'. Variations in natural magnetic assemblages, which will be reflected in susceptibility measurements, have been used to make inferences about a number of environmental processes (e.g. as an indicator of sediment flux and erosion in lake catchments). Applications include the correlation of Holocene lake sediment cores (Evans & Slaymaker, 2004), the relative age correlation of alluvial fans (Harvey *et al.*, 2003) and the correlation of magnetic susceptibility variations in cave sediments with the MIS record to date Neanderthal skeletal remains (Ellwood *et al.*, 2004). On a longer timescale, magnetic susceptibility measurements have been obtained from loess–palaeosol sequences from China extending back over

3.5 Ma (Sun *et al.*, 2006b). The magnetic susceptibility signal, which is usually higher in soils than in loessic sediments, reflects the production or concentration of magnetic minerals with pedogenesis, and therefore forms a basis for correlation between widely separated profiles (Figure 5.36).

Isothermal remanent magnetization (IRM): This is the magnetic moment activated in and retained by a sample placed in a magnetic field at room temperature. With a gradual increase in the strength of the field, IRM will increase non-linearly until **saturation isothermal remanent magnetization (SIRM)** is reached. This is the level at which a further increase in the magnetic field will not result in any increase in IRM in the sample. SIRM measurements have been used in a range of environmental studies, for example in reconstructions of fire and pollution histories (Gedye *et al.*, 2000; Rosen & Dumayne-Peaty, 2001), and again these properties have been employed in the correlation of Holocene lake sediment records (Snowball & Thompson, 1992).

Coercivity of IRM: This is the reversed field strength required to reduce the remanent magnetism to zero after saturation. Low coercivity values appear to be characteristic of large-grained magnetite, while high coercivities tend to be associated with fine-grained haematite. In practice, coercivity curves may differentiate between assemblages of soil and sediment types, and offer a further means whereby correlation between sediment sequences, and between components of those sequences, can be effected (Andrews *et al.*, 2003).

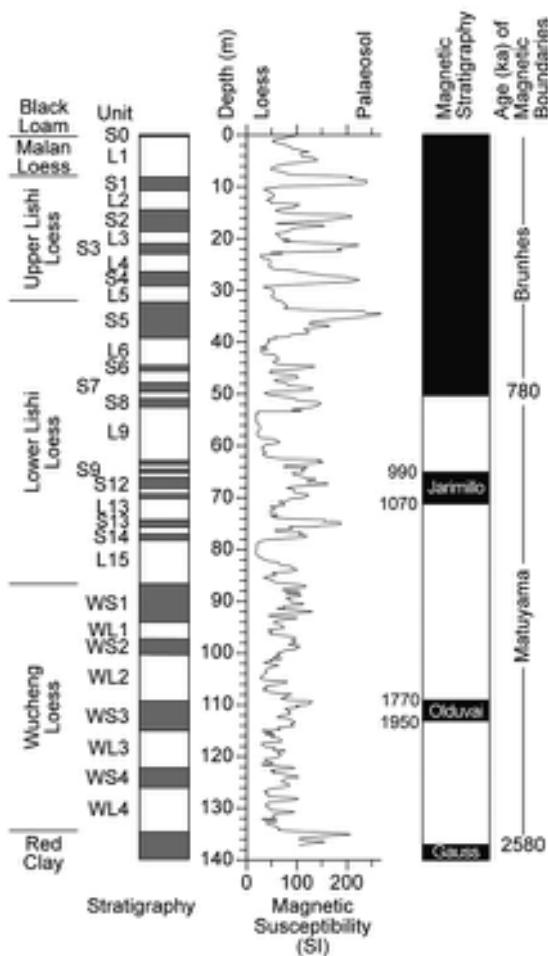


Figure 5.36 Magnetic susceptibility variations through a complete Quaternary loess sequence at Luochuan on the Loess Plateau, Central China. The sequence is divided into pedogenetically altered loess (S – soil, or palaeosol) and unaltered loess (L) units. The strong magnetic signals in the soil units reflect higher concentrations of iron oxides (after Balsam *et al.*, 2004).

5.5.2 Tephrochronology

5.5.2.1 General principles

Following a volcanic eruption, ash or **tephra** is often spread rapidly over a relatively wide area and forms a thin cover over peat surfaces, lake-floor sediments, estuarine sediments, river terraces, etc. Thin ash layers have also been found in deep-sea sediments. As the deposition of the tephra layers is effectively instantaneous in geological time,

these horizons constitute distinctive isochronous marker horizons that provide a basis for inter-site correlation. Many tephra layers contain a unique geochemical fingerprint relating to the source of eruption, and it is often possible to date the tephra layers using radiometric or other techniques (see below). Tephras therefore provide a basis for dating (**tephrochronology**) and also for correlation (**tephrostratigraphy**). Good overviews can be found in Alloway *et al.* (2007a) and Lowe (2011).

In areas close to a volcanic eruption, tephras may be visible as distinctive light-coloured horizons in stratigraphic sections and in cores of peats or lake sediments. Such ash-fall deposits are usually referred to as **proximal tephras**, in contrast to **distal tephras** that can be deposited hundreds or even thousands of kilometres downwind of the point of eruption (Figure 5.37a). For example, the Y5 tephra from the Campanian Ignimbrite eruption near Naples (c. 39 ka) reached southwest Russia, more than 2,500 km away (Figure 5.37c; Pyle *et al.*, 2006), and it is likely that non-visible distal ash layers (microscopic glass shards known as **microtephras** or **cryptotephras**) travelled even further afield. Meticulous laboratory procedures involving, for example, density and magnetic separation, are required to extract these from minerogenic lacustrine and marine sediments where the volcanic glass shards are often present in very low concentrations (Turney & Lowe, 2001). The tephras can be identified on the basis of their physical characteristics (colour, grain-size distribution, lithic content, refractive indices, etc.), but for distal tephras in particular, the chemical composition of the glass shards has proved to be a more effective basis for identifying and distinguishing between particular tephras. This **geochemical fingerprinting** not only enables a distinctive signature to be obtained for each tephra, but it also provides a basis for linking tephras directly to centres of eruption. The geochemical composition is usually determined by electron probe micro-analysis (EPMA), and usually about ten major elements (expressed as oxides) are selected for analysis (Davies *et al.*, 2002b). More sophisticated geochemical techniques involving, for example, mass spectrometric analysis of rare earth or trace elements and isotopic composition are now being employed to distinguish tephras, particularly where low numbers of shards have been recovered (Pearce *et al.*, 2004). Considerable efforts are also being made to standardize the analytical protocols used in different laboratories, the reporting procedures and the ways in which tephrochronological data are presented.

The age of a tephra can be established by radiocarbon dating of associated organic material such as plant macrofossils (Plunkett *et al.*, 2004) or, in older deposits, by argon isotope dating (Mark *et al.*, 2013), fission track

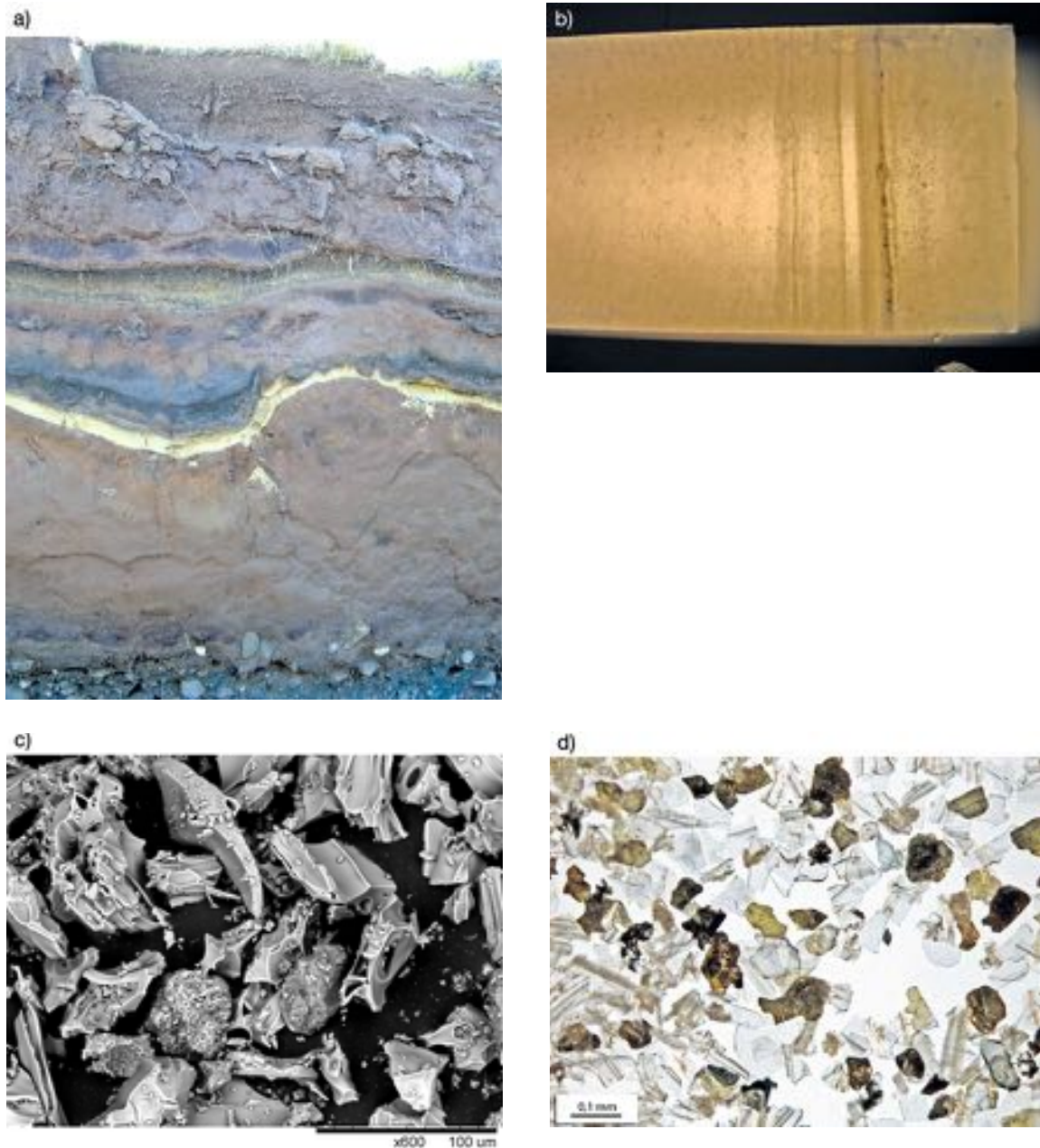


Figure 5.37 a) Yellow and black tephra layers exposed in a soil–peat complex in Iceland (photograph by Christopher Bronk Ramsey, Oxford University, UK). b) The North Atlantic Ash Zone 2 tephra layer (dark grey band) preserved at 2,359 m depth in the NGRIP ice core, and with an age of 55.4 ka BP (photograph by Inger Seierstad, Niels Bohr Institute, University of Copenhagen, Denmark). c) Fluted distal shards of the Campanian Ignimbrite from Campania, Italy, with an age of c. 39 ka (SEM by Suzanne MacLachlan, National Oceanography Centre, Southampton, UK). d) Platy distal shards of the Vedde Ash from Katla Volcano, Iceland. In the Greenland GICC05 ice-core chronology, this tephra is dated to 12,171 with a maximum counting error (MCE) of 114 years (photograph by Jan Mangerud, Bergen University, Norway).

dating (Marcolini *et al.*, 2003), or ESR and luminescence dating (Toyoda *et al.*, 2006) of some of the primary mineral constituents. Where tephras are found in ice cores (Figure 5.37b), the date of the ash fall can be obtained by annual layer counting (Davies *et al.*, 2008), and calendar ages for tephras can also be obtained from varved sediment sequences (Blockley *et al.*, 2007b). Other means whereby tephra can be dated include stratigraphical position in relation to other tephra layers, palaeomagnetic correlations and relationships to oxygen isotope stage boundaries in deep-ocean sediments (Wastegård & Rasmussen, 2001).

5.5.2.2 Sources of error in tephrochronology

Two major difficulties constrain the effectiveness of tephra as a chronological and correlative tool: the first relates to the distribution of tephra and its incorporation into sedimentary sequences, while the second involves ongoing analytical problems. In terms of distribution, it is clear that tephrochronology can, at best, only form a basis for regionally applicable schemes of dating and correlation, for individual ash layers are restricted spatially by factors such as the magnitude and type of volcanic eruption, the strength of the prevailing wind, and the direction of the prevailing wind at the time of eruption. Many volcanic plumes appear to have been relatively narrow, and hence the spatial distribution of tephra fall-out will be restricted. Post-depositional processes will also influence tephra presence in the sedimentary record. Tephras falling over the high-latitude oceans may be prevented from reaching the seabed by surface ice cover; moreover, these tephras may subsequently be transported by ice-rafting and deposited only when the ice melts. In this case, older tephras would be incorporated into younger stratigraphic horizons (Bond *et al.*, 2001a). In peatland areas, a combination of protracted snow cover, wind scour and redeposition by meltwater on the bog surface may result in only a fragmentary tephra record being preserved in peat sequences (Bergman *et al.*, 2004).

In terms of analytical problems, correct geochemical sourcing to a particular eruptive event may not always be possible because of a lack of data on volcanic histories and diagnostic chemistries of eruptive events. Moreover, some tephras (especially basaltic layers), once deposited in sediments, may have a poor chemical stability. This could result in major alterations to the tephra geochemistry and pose problems for the correct geochemical typing and provenancing of the tephra (Pollard *et al.*, 2003). Further difficulties arise because successive tephras from the same volcanic source can have very similar chemical signatures, while individual tephras can be generated by magmas of

heterogeneous chemical composition, further complicating geochemical classification (Shane *et al.*, 2008). Finally, not all geochemical data have been obtained using the same analytical procedures and protocols, leading to inconsistency and a lack of comparability in the published data (Pollard *et al.*, 2006).

5.5.2.3 Applications of tephrochronology

Tephrochronology is now widely and routinely employed to correlate and date Quaternary sequences. A large number of tephras have been discovered since the mid-1990s, and with the associated technical advances, particularly in the detection and geochemical fingerprinting of non-visible distal tephras (section 5.5.2.1), the global tephra database has expanded enormously (Froese *et al.*, 2008). The result is that regional tephrostratigraphic frameworks have been developed for many parts of the world, particularly for the Late Quaternary (Haflidason *et al.*, 2000; Shane, 2005; Lane *et al.*, 2010). In each of the regional schemes, there are normally distinctive marker tephras that form the thickest and most widely distributed of the layers, and that can be detected even in the most distal locations. These have usually resulted from cataclysmic, caldera-forming events ('super-eruptions': Mason *et al.*, 2004). Examples include the Lava Creek B tephra from the Yellowstone Caldera that was spread across much of the western USA at c. 640 ka (Alloway *et al.*, 2007a) and the Y5 tephra from Campania (see below). The largest known eruption of the last two million years, the Toba Caldera in Sumatra (c. 74 ka), deposited tephra over India, Malaysia, much of the Indian Ocean, and the Arabian and South China Seas (Williams *et al.*, 2009). Tephras from eruptions of lower magnitude, such as Glacier Peak and Mt St Helens (c. 7.5 ka) in the northwest USA, tend to have more limited geographical distributions (Figure 5.38). Some volcanoes have been active over long periods during the Quaternary, leaving multiple tephra layers that can help address a number of chronological issues.

The rate of dissemination of tephra in the atmosphere and the potential extent of its distribution was graphically illustrated by the eruption of Eyjafjallajökull in southeastern Iceland in April 2010. Following the onset of the eruption, satellite imagery showed the rapid transportation of ash by westerly winds over western Europe, eventually expanding to large swathes of the North Atlantic Ocean and the eastern seaboard of Canada. This event caused unprecedented disruption to air traffic over Europe, a region generally considered to be free from hazards associated with volcanic eruptions, and it constitutes a remarkable modern analogue for Late Quaternary Icelandic

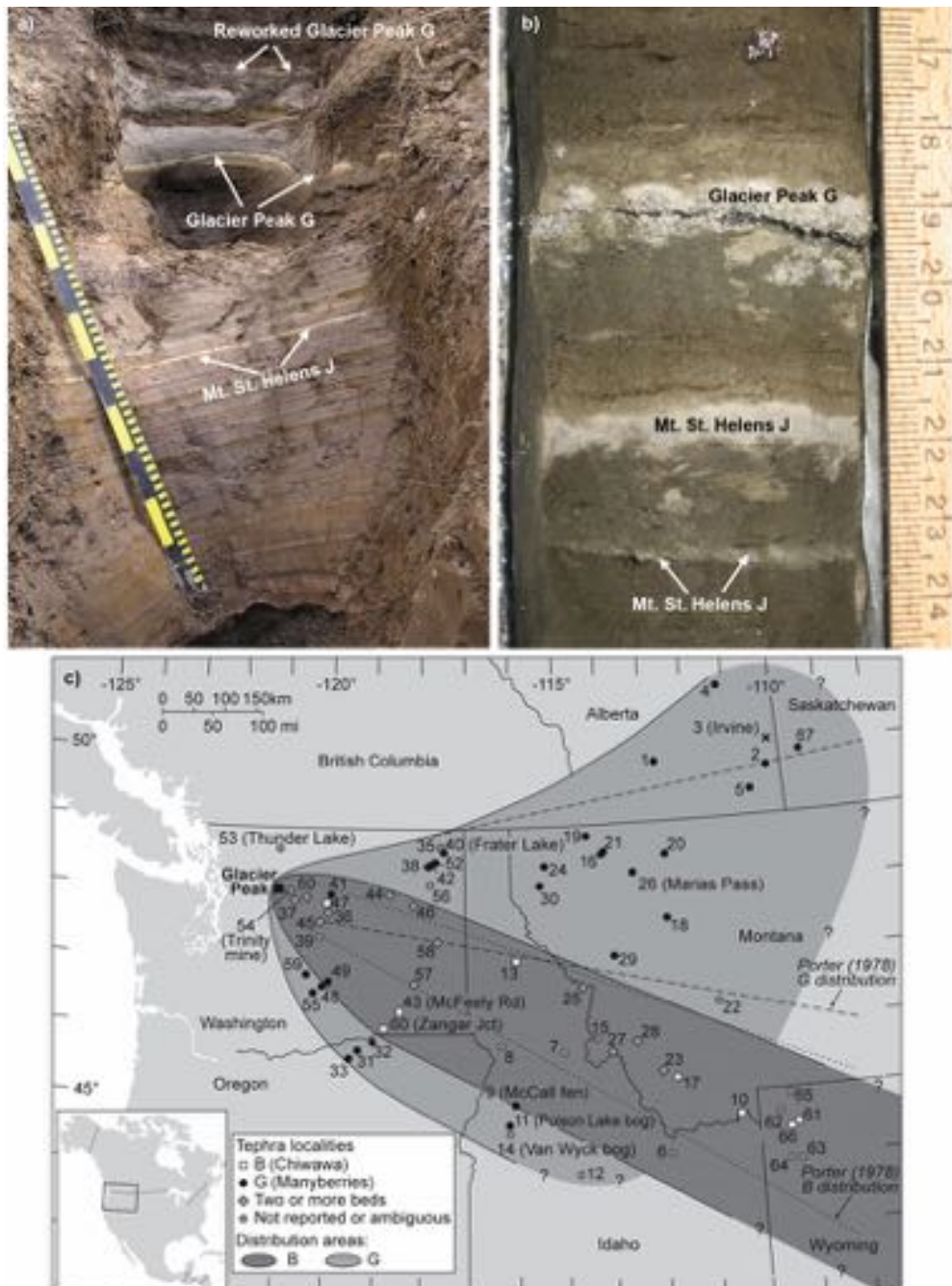


Figure 5.38 Tephra layers exposed in sections at two sites in Montana, northwest USA: a) Maris Pass and b) Frater Lake. The tephras are from the Glacier Peak G and Mt St Helens J volcanic eruptions, the former dating to c. 11,600 ^{14}C yr BP and the latter to a few decades earlier (from Kuehn *et al.*, 2009, reprinted with permission of Elsevier; photographs by Steve Kuehn, Concord University, West Virginia, USA). c) Mapped distributions ('footprints') of the Glacier Peak G and B eruptions, the ages of which are too close to discriminate between.

eruptions and their potential effects throughout the North Atlantic region and adjacent land areas (Davies *et al.*, 2010). As in other parts of the world, some Icelandic volcanoes have been active over long periods of the Quaternary, leaving multiple tephra layers that can be used as a basis for dating and correlation. Some examples are considered in the following section.

Land–marine–ice correlations

Tephra isochrons constitute one of the most important bases for correlating terrestrial records. For example, the Y5 tephra mentioned above is one of several clear tephra isochrons that link central Mediterranean and eastern European stratigraphical records (Figure 5.39), while the Icelandic Vedde Ash (Figures 5.26 and 5.37d) provides a basis for correlation of Lateglacial sequences across large areas of northwest Europe (Blockley *et al.*, 2007c; section 7.5.5). Tephra layers can also be used to link terrestrial and marine sequences, for example New Zealand to the western

Pacific (Newnham *et al.*, 2003), Japan to the Pacific (Machida, 1999) and Latin American to the Caribbean (Jordan *et al.*, 2006). Ash layers in polar ice sheets enable correlations to be established between ice-core records and those from both the marine and terrestrial realms (Davies *et al.*, 2008). Examples from Antarctica, and parts of the Southern Ocean and adjacent lands, are described by Narcisi *et al.* (2005, 2010), and from Greenland and the North Atlantic region by Hafslidason *et al.* (2000) and Wastegård & Rasmussen (2005). Also in the North Atlantic province, tephra isochrones underpin an event stratigraphy (section 6.3.2.6) for the Last Termination which links ice-core, marine and terrestrial records (Lowe *et al.*, 2008b).

Marine reservoir errors

Radiocarbon marine reservoir errors (section 5.3.2.4) can be estimated for times in the past by comparing radiocarbon dates on marine fossils with those from contemporaneous terrestrial materials (preferably plant

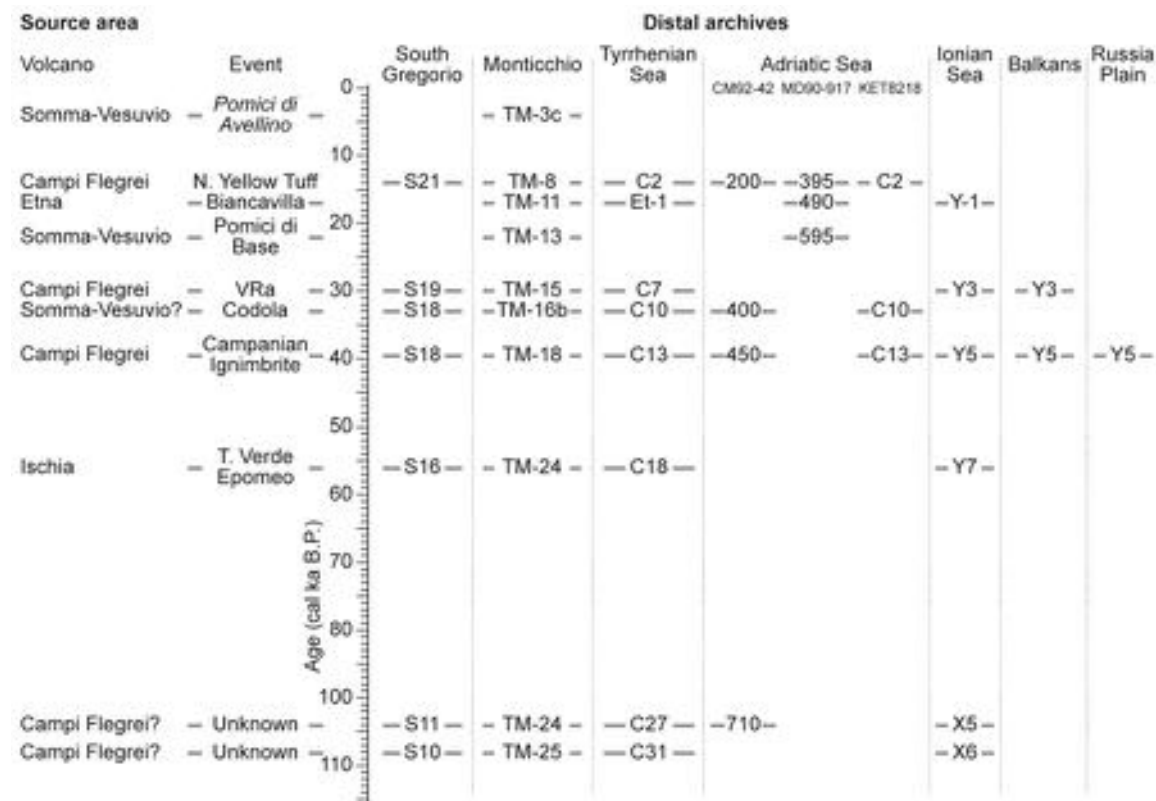


Figure 5.39 Widespread tephra marker horizons in marine and terrestrial sequences in the central Mediterranean and eastern Europe (after Sulpizio *et al.*, 2008).

macrofossils), and one way of establishing contemporaneity is by tephrochronology. For example, by using tephra horizons as time-stratigraphic markers, Eiríksson *et al.* (2004) found that the magnitude of the marine reservoir error in the Iceland Sea varied by several hundred years over the last 4,500 years, probably as a result of periodic incursions of Arctic water masses. A similar approach using tephra isochrones has been employed to determine the extent of marine reservoir offsets in the Mediterranean and Black Seas (Kwiecien *et al.*, 2008).

Volcanic histories

Eruption histories for individual volcanic centres are often incomplete because of destruction of older beds by younger explosions, and the limited registration of minor volcanic eruptions (Bacon & Lanphere, 2006). Furthermore, older volcanic materials may be buried by younger deposits and hence are inaccessible. Distal records of tephra deposition can therefore provide evidence of volcanic activity that is missing from the proximal sequences (Wulf *et al.*, 2004). Well-dated eruption histories are particularly important for establishing the recurrence patterns of volcanic activity (Marra *et al.*, 2009). These form the basis for the development of hazard prediction models (Turner *et al.*, 2008), and for evaluating the effects of, for example, glacial unloading (Jellinek *et al.*, 2004) and sea-level change (D'Argenio *et al.*, 2004) on long-term volcanic behaviour.

Volcanism and climate

Possible links between volcanic activity and climate remain controversial, with some arguing that there is little evidence for significant climatic impacts from recent eruptions (Shindell *et al.*, 2003), while others point to coincidences between volcanic activity and recurrent climatic phenomena such as ENSO (Adams *et al.*, 2003; section 7.6.4.2). Over longer timescales, Bay *et al.* (2004) have noted a possible causal connection between increased volcanic activity (as reflected in ash layers in polar ice) and millennial-scale climate change, while Prueher & Rea (1998) have suggested that a tenfold increase in the number and thicknesses of volcanic ash layers across the North Pacific implicates volcanic activity in the rapid onset of global cooling at 2.67 Ma. There is also the possibility that climatic change could, by contrast, have affected volcanic activity, perhaps through increased stress on the lithosphere by ice sheet loading and unloading, by associated fluctuations in global sea level, and perhaps also by changes in the earth's axial spin rate, all modulated by Milankovitch harmonics (Rampino *et al.*, 1979). Tephrostratigraphical records are important in the examination of these issues, as they not only provide a basis for quantifying past volcanic

activity, but they form time-stratigraphic frameworks within which different environmental processes can be compared and evaluated.

Volcanism and human evolution

Volcanism has also been implicated as an influence in human evolution. For example, in the East African Rift Valley, volcanic activity may have been part of a range of tectonic processes that affected behaviour or even speciation within early human groups (King & Bailey, 2006). Similarly, it has been suggested that volcanic winters initiated by major volcanic eruptions, such as Toba, may have caused 'population bottlenecks', that is, marked reductions in human population levels which catalysed genetic drift and local adaptations in behaviour (Ambrose, 1998), although this proposal has proved to be contentious (Petruglia *et al.*, 2007). In Europe, the Campanian Ignimbrite tephra fallout at c. 39 ka may have fostered the expansion of *Homo sapiens* at the expense of Neanderthals who were less adaptable to cope with the disaster (Fedele *et al.*, 2002), although in this case also other evidence suggests that the volcanic effects on human populations may have been less far-reaching (Lowe *et al.*, 2012). In all of these instances, however, tephrochronology provides a basis for evaluating the competing hypotheses by providing a secure chronological framework within which to examine the different lines of evidence.

5.5.3 Oxygen isotope chronology

It has already been seen (section 3.10.2) that the oxygen isotope trace in deep-ocean sediments represents a proxy record of long-term climatic change. Moreover, as the isotopic signal is geographically consistent and can be replicated in cores taken from different areas of the world's oceans, inflections in the isotopic profiles are essentially time-parallel events, and constitute age-equivalent marker horizons. As we explained in Chapter 1, these form the basis for a globally applicable scheme of **oxygen isotope stages** (section 1.6) and, moreover, it is possible to derive ages for the major isotopically defined horizons using the technique of **orbital tuning**; in other words, using the astronomical forcing frequencies of the 23 ka (precession), 41 ka (obliquity) and 100 ka (eccentricity) Milankovitch variables to time the cycles reflected in the marine oxygen isotope records. This approach was pioneered by Imbrie *et al.* (1984) in their production of a standard template for oxygen isotope records known as the **SPECMAP timescale**. A high-resolution chronology was based on the amalgamation of several isotopic records ('stacked' records), and the composite curve which spans

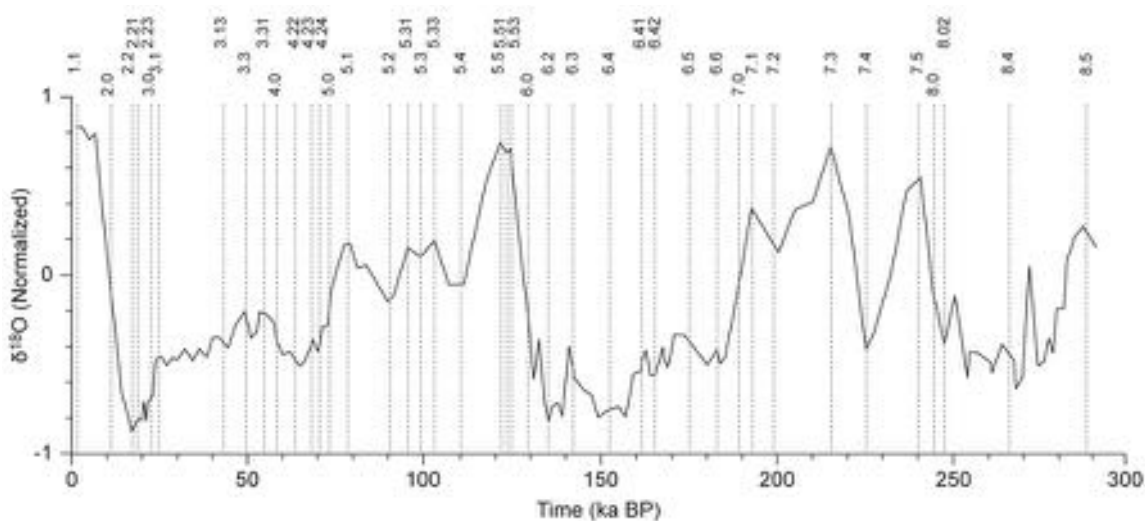


Figure 5.40 Orbitally tuned chronostratigraphy for a composite ('stacked') deep-ocean isotopic record spanning the last 300 ka. The numbered vertical lines indicate distinctive features in the record. In the hierarchical numbering scheme, each number before the decimal point refers to the marine isotope stage (1, 2, 3, 4, 5 . . .) while the number following the decimal refers to substages within each of the major isotopic stages (see section 6.2.3.5) (after Martinson *et al.*, 1987).

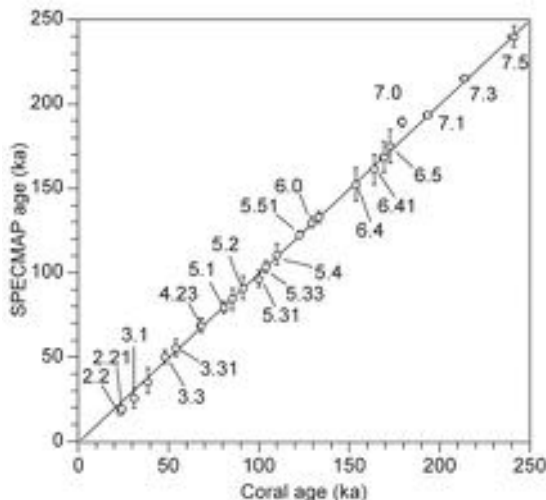


Figure 5.41 Comparison of orbitally tuned age estimates based on SPECMAP and independently dated U-series coral ages. The numbered data points correspond to the SPECMAP marine isotopic events as defined by Martinson *et al.* (1987): 5.51 – Last Interglacial; 7 – Penultimate Interglacial (after Thompson & Goldstein, 2006).

the last 300 ka was then smoothed, filtered and tuned to the known cycles of the astronomical variables (Figure 5.40). This now classic orbitally tuned chronology has since been confirmed by independent dating of fossil corals using U-series (Figure 5.41). Since then, a number of tuned stacked records have been constructed (e.g. Martinson *et al.* 1987; Karner *et al.*, 2002), the longest and most comprehensive of which is the LR04 stack of Lisiecki & Raymo (2005). This consists of fifty-seven globally distributed benthic $\delta^{18}\text{O}$ records, and forms a continuous orbitally tuned sequence extending back into the early Pliocene (Figures 1.5 and 5.1). The stacked record shows a significant coherency with insolation as reflected in the obliquity band throughout the entire 5.3 Ma record, and in the precession band throughout more than half of that time interval. As such, it constitutes the most detailed oxygen isotope chronostratigraphy developed to date, and forms a 'type sequence' against which all palaeoceanographic measurements can be compared.

5.5.4 Biostratigraphy and molecular clocks

As noted in Chapter 4, within a restricted geographical area, vegetational changes will have been broadly synchronous, and hence the boundaries between **regional pollen assemblage zones** will be effectively time-parallel. In

essence, therefore, these form marker horizons in lake or peat profiles and can be used as a basis for correlation and dating. They have been of particular value in the dating of Holocene sequences. In Britain, for example, regional pollen assemblage zones have been established largely on the basis of the establishment and expansion of key indicator taxa, notably particular woodland trees. Radio-carbon dating enables the events to be set within a time-stratigraphic framework, and includes the arrival of *Corylus avellana*, dated to 10.5–10.0 ka, and the expansion of *Alnus* around 8.0 ka. A key marker horizon is the *Ulmus* decline, an event that is considered to be broadly synchronous and has been widely dated in both Britain and in western Europe to c. 5.8 ka (Parker *et al.*, 2002). Such data form the basis for isopollen maps (Chapter 4) showing the patterns of expansion of arboreal taxa and threshold ages for the arrival of certain tree species in particular localities (van der Knaap *et al.*, 2005). Planktonic assemblage zones can provide similar biochronological frameworks for the marine realm (Capotondi *et al.*, 1999), while sapropels (Chapter 1, note 6) may also form isochronous marker horizons that offer a basis for correlation of some marine deposits (Meyers, 2006).

Although not common, evolutionary changes do occur within the Quaternary (section 4.11.6.3) but one that is of particular significance for dating the Middle Pleistocene in Europe involves the lineage of the large water vole, *Arvicola terrestris cantiana*. This species, with unrooted molars, is thought to have evolved from an earlier species of vole, *Mimomys savini* (with rooted molars) during the ‘Cromerian’, that part of the Middle Pleistocene record which may contain at least five temperate episodes (Preece & Parfitt, 2012). The *Mimomys*–*Arvicola* boundary, which occurs after the Brunhes–Matuyama geomagnetic boundary (~MIS 19) but earlier than the Elsterian–Anglian glaciation (MIS 12), forms an important marker horizon within Cromerian deposits at sites in western Europe (van Koenigswald & van Kolfschoten, 1996). It has proved extremely valuable in dating and correlating sites for a time period for which few other dating methods are available (e.g. Stuart & Lister, 2001; Preece *et al.*, 2009).

Recent developments in the recovery and sequencing of mitochondrial DNA from fossil remains, however, indicate that evolutionary changes may be a more common feature of the Quaternary fossil record than hitherto considered. Evidence from a number of different fossil residues, including reptiles (Douglas *et al.*, 2006), mammals (Lister, 2004) and birds (Lambert *et al.*, 2002), suggests that faunal turnover and speciation may have been both common and significantly increased during the Quaternary (Barnes *et al.*, 2007). If evolutionary turnover can be shown

to occur at predictable rates, then **molecular clock analysis**, which is based on the timings of genetic mutations, may enable dates to be assigned to events or to stratigraphic sequences (Bromham & Penny, 2003; Kumar, 2005). This approach has already been applied to the dating of river drainage and other geological processes (Craw *et al.*, 2007, 2008).

5.6 RELATIVE CHRONOLOGY BASED ON PROCESSES OF CHEMICAL ALTERATION

Fossils, sediments and rocks are affected by a number of chemical reactions that are partly time-dependent. Upon the death of an organism, tissues are broken down by a variety of chemical processes to produce compounds of a more simple chemical structure; the surfaces of fossils or minerals may be altered by the effects of hydration or the accumulation of precipitates of certain chemicals in groundwaters, while weathering and pedogenic processes will gradually effect changes on rock and sediment surfaces. In all of these cases, the degree of alteration brought about by different chemical reactions increases with time, and this therefore offers a basis for relative dating. Some of the more widely used techniques are considered in the following section.

5.6.1 Amino-acid geochronology

Living bone consists of approximately 23 per cent collagen (protein-bearing) fibrils bound within a phosphatic–calcitic matrix. Proteins can survive in bones and shells for extremely long periods,³ but undergo a number of molecular changes. Protein residues were discovered in fossil bones and shells in the 1950s, and since then the study of protein transformation in the geological record has developed rapidly. Some of the chemical changes in proteins that occur after the death of organisms are time-dependent, and thus the characteristics of certain protein residues from the Quaternary record can provide the basis for a relative chronology. Useful overviews of amino-acid geochemistry and its applications in geochronology can be found in Goodfriend *et al.* (2000), Wehmiller & Miller (2000), Blackwell (2001b) and Penkman (2010).

5.6.1.1 Chemistry of proteins

Proteins are large and complex molecules and are basic ingredients of all living organisms. They are composed of **amino acids**, which have the generalized chemical formula

shown in Figure 5.42a. The 'R' linkage differs for each amino acid, ranging from a simple hydrogen atom in glycine, to a methyl group (CH_3) in alanine, and to highly complex chemical structures in other amino acids. Around eighty amino acids occur in nature, of which about twenty are commonly found in proteins. Proteins form through the combination of several amino acids into **peptide chains**, each amino acid linked to the next by a **peptide bond** following the loss of a water molecule (Figure 5.42b and c). The patterns formed in this way are specific to each protein type, and the various amino-acid arrangements create thousands of different proteins, including enzymes and antibodies. Some of the larger proteins may contain up to 3,000 amino-acid residues. A list of the more common amino acids includes alanine, glycine, isoleucine, leucine and aspartic acid.

With the exception of glycine, all amino acids

commonly found in proteins can exist in two molecular forms (**isomeric forms**). The chemical and biochemical properties of the two forms of amino acid are similar, but they rotate plane-polarized light in opposite directions. Effectively, they constitute two non-superimposable mirror images (Figure 5.42d), rather like left and right hands, and these optical isomers are referred to as **L-amino acids** and **D-amino acids** (after the Latin *laeva* – left-handed, and *dextra* – right-handed). The carbon atom at the centre of the isomers (the **chiral carbon atom**) forms the point of asymmetry and allows the development of the two optical isomers. The biological significance of this distinction between the L- and D-configuration in amino acids is that only L-isomers occur in living (active) proteins. D-isomers can occur in a free state as components of non-protein structures, and in fossil organic materials as a result of the break-down of proteins (see below).

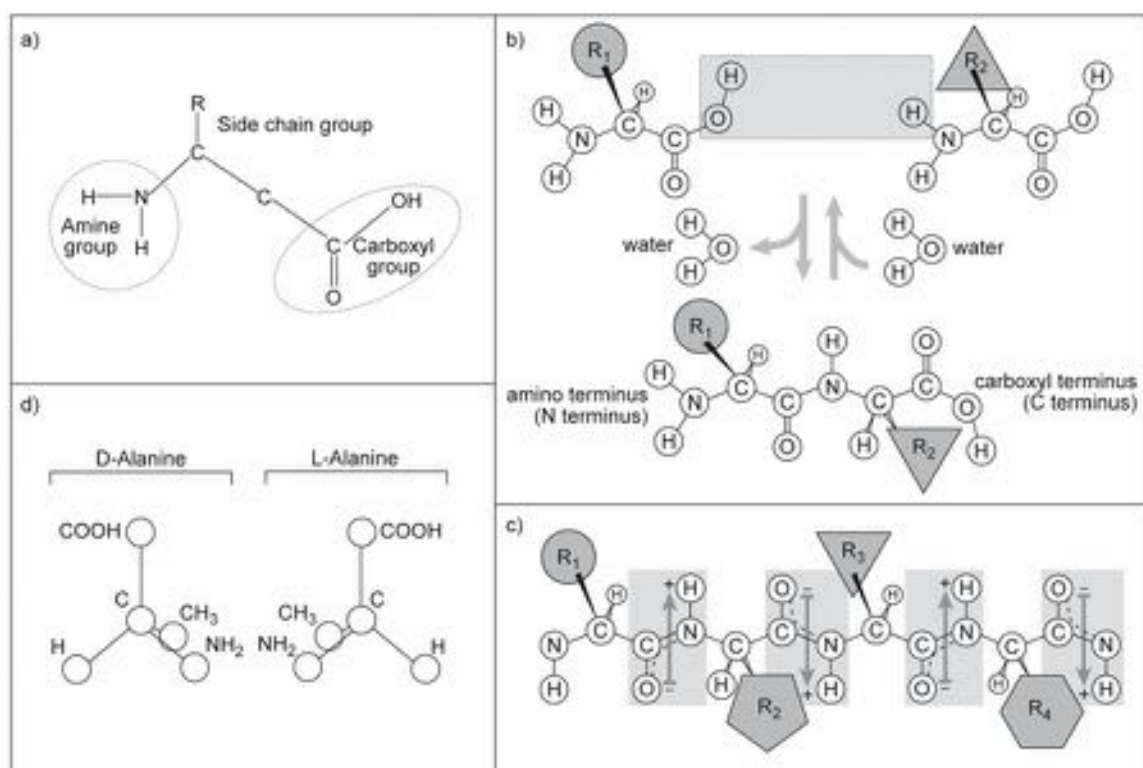


Figure 5.42 Chemistry of amino acids. a) Generalized formula for amino acids. b) Schematic representation of chemical combination of amino acids through loss of water molecule to form a peptide bond. c) Combination of carboxyl and amino groups between amino bonds to form peptide chains. d) Isomers (mirror-image molecular arrangements) of alanine (from Petsko & Ringe, 2004).

5.6.1.2 Amino-acid diagenesis

Chemical alteration in proteinaceous residues following the death of an organism results in the disruption of peptide chains to release free amino acids. Where proteins are exposed to the atmosphere or to biological processes, very rapid degradation will take place, but if they are protected by skeletal hard parts so that a 'closed' system prevails, then much slower chemical alterations occur. Some reaction times are in the range of 50 ka to a few million years, whereas other amino-acid reactions operate over a timescale of only a few thousand years.

Several indices have been employed to measure the amount and rate of degradation of amino acids in fossil samples, including the ratio between bound- to free-amino acids, with respect to either the total amino compounds in the sample, or for selected amino acids. From the point of view of Quaternary geochronology, however, the most important diagenetic change that takes place in subfossil material is the inversion (or intraconversion) of L- to D-configured molecules in the constituent amino-acid residues, a reaction that proceeds until an equilibrium state has been achieved. In the case of amino acids that form stereoisomers, this conversion is called **racemization**. However, some common amino acids (e.g. aspartic acid) are **diastereomers**: their D- and L-molecules are not mirror images of each other. In this instance, the conversion process is known as **epimerization**. D/L ratios start at zero at the time of death of an organism and increase to an equilibrium ratio, which for the process of epimerization in some molluscan species is a value of 1.30 ± 0.05 . Fossil ratios are measured proportional to position on the degradation continuum from 0–1.30 (e.g. a ratio of 0.65 indicates that the sample is half of the way along the conversion continuum, which is reported as a value of 0.5). Amino-acid ratios (AARs) are normally measured by means of ion-exchange chromatography or gas–liquid chromatography coupled to mass spectrometers, and kinetic models are employed to determine the trend of protein diagenesis.

Although in theory amino-acid determinations can be made on any protein-bearing materials, such as hair, teeth, Foraminifera, shells, bones and tusks, in practice suitable samples are restricted to those with 'tight' skeletal carbonate matrices (Penkman *et al.*, 2008). The most widely used media have been marine molluscan shells which form an essentially closed system that is affected by a minimum of external factors. Other materials have been used with some degree of success, however, including freshwater molluscs, land snails and ostracods (Ellis *et al.*, 1996; Kaufman, 2003a), ostrich eggshells (see below),

and organic residues in cave speleothems that were originally derived from surface soils (Blyth *et al.*, 2008). AARs have also been obtained from organic materials incorporated into carbonate rocks in coastal areas, often referred to as 'whole-rock aminostratigraphy' (Hearty & Kaufman, 2000; Hearty, 2003). More problematic media include wood, where difficulties arise from such non-carbonaceous materials not being buffered against changes in environmental pH (Sykes, 1991), and bone, where open-system behaviour results in post-burial loss of proteins through leaching or contamination by younger amino acids from the surrounding sediment matrix (Collins *et al.*, 2000; Fernández *et al.*, 2009).

5.6.1.3 Aminostratigraphy and age control

Amino-acid racemization (or epimerization) does not progress at the same rate in all species, nor in fossils of the same species recovered from different sites (see below). By themselves, therefore, AARs cannot provide numerical age estimates. The rate of the degradation process needs to be calibrated for individual sites and species, and for different types of host material, using independent dating methods such as radiocarbon, U-series or luminescence measurements (Owen *et al.*, 2007; Kosnik *et al.*, 2008). Calibrated AAR age models (**AAR chronology**) show that D/L conversion values can be traced back over considerable periods, for well-preserved amino acids have been recovered from ostracods (Ortiz *et al.*, 2004) and marine molluscs in deposits older than 1 Ma (Table 5.6). Aminostratigraphy appears to be potentially applicable to the entire timespan of the Quaternary (and beyond?), for it has been employed to date, *inter alia*, some of the earliest Pleistocene marine formations in the British Isles (Bowen, 1991), Plio-Pleistocene raised marine sediments in New Zealand (Bowen *et al.*, 1998) and Pliocene glacial sediments in Antarctica (Colhoun *et al.*, 2009).

5.6.1.4 Problems with amino-acid geochronology

The relationship between D/L ratio and time is complicated by a number of factors. All reactions are temperature-dependent, with epimerization proceeding more rapidly at higher ambient temperatures. Hence, meaningful comparisons of amino-acid ratios can only be made between sites that have experienced a similar climatic, and particularly thermal, history. Amino-acid composition, relative abundances of amino acids, and rates of various amino-acid reactions are all genus- and, in some cases, species-dependent, and hence precise identifications of shell

Table 5.6 Age calculations based on D/L ratios of five amino acids measured in fossil terrestrial ostracods recovered from alluvial and travertine sequences in central and southern Spain. All error ranges are 1σ (from Ortiz *et al.*, 2004).

Level in sequence above datum (m)	D-alloisoleucine/ L-isoleucine	D/L leucine	D/L aspartic acid	D/L phenylalanine	D/L glutamic acid	Age (ka)
206.5	0.997 ± 0.021	0.710 ± 0.030	0.780 ± 0.066	0.805 ± 0.007	0.703 ± 0.083	1,012 ± 169
223.8	1.045 ± 0.035	0.735 ± 0.007	0.820 ± 0.014	0.780 ± 0.000	0.725 ± 0.092	1,008 ± 125
228.1	0.819 ± 0.000	0.828 ± 0.000	0.711 ± 0.000	0.678 ± 0.000	0.594 ± 0.000	863 ± 173
253.0	0.725 ± 0.046	0.570 ± 0.061	0.700 ± 0.013	0.502 ± 0.035	0.534 ± 0.042	743 ± 88
269.3	0.736 ± 0.055	0.544 ± 0.055	0.683 ± 0.040	0.519 ± 0.094	0.579 ± 0.100	736 ± 115
281.2	0.877 ± 0.046	0.603 ± 0.031	0.687 ± 0.004	0.603 ± 0.029	0.599 ± 0.007	737 ± 68
303.4	0.675 ± 0.021	0.490 ± 0.014	0.605 ± 0.021	0.435 ± 0.007	0.445 ± 0.007	517 ± 56
314.0	0.520 ± 0.071	0.373 ± 0.051	0.534 ± 0.006	0.436 ± 0.099	0.376 ± 0.037	407 ± 58
323.3	0.529 ± 0.106	0.397 ± 0.098	0.522 ± 0.016	0.429 ± 0.085	0.397 ± 0.031	409 ± 95
327.1	0.492 ± 0.011	0.397 ± 0.031	0.492 ± 0.004	0.430 ± 0.040	0.342 ± 0.015	389 ± 62
329.8	0.395 ± 0.037	0.336 ± 0.001	0.481 ± 0.054	0.320 ± 0.000	0.40 ± 0.000	339 ± 68
352.5	0.332 ± 0.001	0.279 ± 0.081	0.441 ± 0.019	0.346 ± 0.051	0.325 ± 0.005	279 ± 77

samples, for example, are necessary before analyses are undertaken (Miller & Clarke, 2007). A further difficulty is that proteins in different structural layers of a shell may often differ in terms of their amino-acid composition and rate of epimerization (Penkman *et al.*, 2008). In theory, therefore, comparable portions of different shells should be used for analysis, but this principle is difficult to apply where samples are taken from fragmented molluscan assemblages. Degradation of proteins due to microbiological activity and varying degrees of oxygenation, particularly during the early stages of diagenesis, may also result in significant differences in amino-acid ratios in molluscs from sites of the same age and with the same thermal histories (Takano *et al.*, 2005). Furthermore, some AAR diogeneses may be characterized by non-linear and reversible reactions (Clarke & Murray-Wallace, 2006). Finally, AARs are naturally variable, and it will frequently be the case that a range of values will need to be obtained in order to generate an index that adequately reflects the AAR signature of any one stratigraphic context. In other words, relative age estimates must be sufficiently large to capture this natural variability (McCarroll, 2002). These difficulties are not insurmountable, however, and a number have been resolved by some recent developments in AAR analysis, which are discussed in the following section.

5.6.1.5 Recent developments in amino-acid geochronology

Since the mid-1990s, there have been a number of methodological advances in amino-acid geochronology. These involve improvements in sample pretreatment and new analytical methods (Sykes *et al.*, 1995; Kaufman & Manley, 1998), including the technique of sample bleaching to remove the leachable, open-system matrix of shell protein. This leaves a component, known as the **intra-crystalline fraction**, that exhibits closed system behaviour, and within which protein degradation is dependent on only two variables, time and temperature (Penkman *et al.*, 2008). In this fraction, it has proved possible to isolate five amino acid D/L pairs (aspartic acid, glutamic acid, serine, alanine and valine). As these racemize at different rates, this provides a cross-check on the geochemical integrity of the sample (see also Table 5.6), and also enables different aspects of diagenesis to be monitored within a closed system. Moreover, as the overall extent of inter-crystalline protein decomposition is being measured, the method offers a significantly improved temporal resolution over earlier analyses based on the racemization of a single amino acid (Penkman *et al.*, 2007). A further development has been the use of the calcitic component of shell as opposed

to aragonite. As the former is more stable, inter-crystalline proteins should be better preserved in this biomineral, and hence are likely to provide better temporal resolution than those in aragonitic shells. This has been confirmed by recent analyses of calcitic opercula⁴ from the freshwater mollusc *Bithynia* from sites in southeastern England and the Netherlands, the results of which have formed the basis for a coherent aminostratigraphic framework for the whole of the Quaternary. In addition, samples from the Eocene demonstrate the persistence of closed system protein within the calcitic opercula extending back over 30 Ma (Penkman *et al.*, 2013).

5.6.1.6 Some applications of amino-acid geochronology

Correlation and dating of Quaternary sequences

One of the most widely used applications of this technique has been in the correlation and dating of stratigraphic sequences containing molluscs. This involves the development of **aminozones**, each of which is characterized by a distinctive range of D/L ratios. Stratigraphic units can be correlated on the basis of comparable D/L values, providing they were obtained from the same species and molecular compounds. This approach is applicable only to regions that are likely to have experienced the same thermal histories during the Quaternary, however. Order of superposition of the stratigraphic units provides an independent test of the integrity of the aminozones, which is important in view of potential constraints on aminostratigraphy outlined above, and the sequence can be calibrated to real time using radiometric or other methods. For example, Ortiz *et al.* (2004) used palaeomagnetic dating to test the AAR chronology for central and southern Spain shown in Table 5.6. Amino-acid geochronology has been employed to date eustatic changes and interglacial marine sequences in, for example, the Bahamas, western Australia, the eastern United States and South Africa (Hearty & Kaufman, 2000; Parham *et al.*, 2007; Carr *et al.*, 2010). Coastal aeolianite sequences, in some cases extending back over 500 ka (Figure 5.43), have been dated by this method, but it has also been applied to the dating and correlation of much younger deposits (Hearty *et al.*, 2004).

The extension of the amino-acid technique to non-marine Mollusca has provided a basis for the dating and correlation of terrestrial deposits, such as loess–palaeosol sequences (Oches & McCoy, 2001) and fluvial terrace sequences (Westaway, 2009). In the lower Thames Valley of southeast England, for example, D/L ratios from opercula of the freshwater gastropod *Bithynia* provided a chronological context for the terrace sequence extending back to

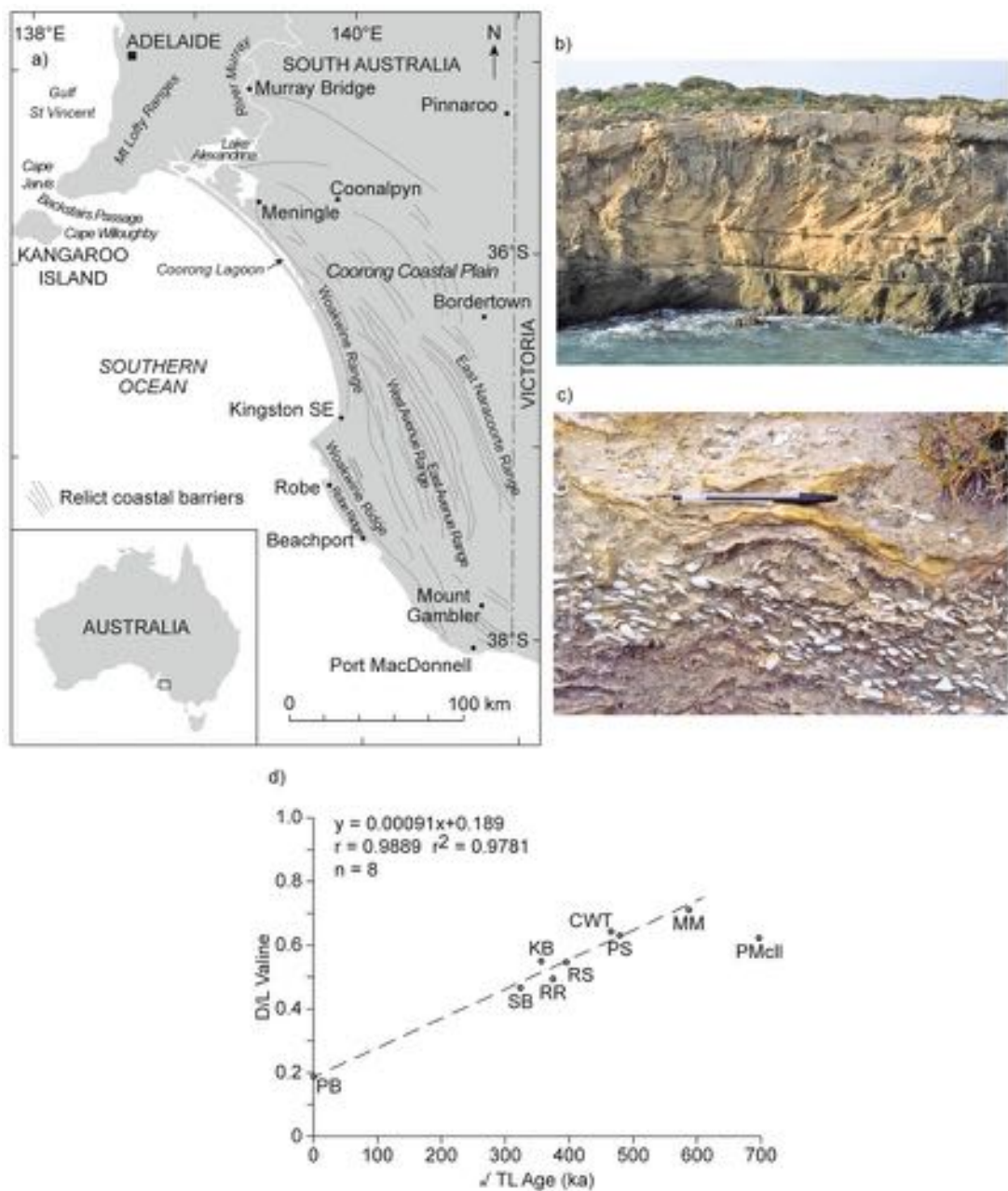


Figure 5.43 Amino-acid geochronology of coastal barrier sediments (aeolianites) in the region of the Murray River mouth, South Australia. a) Location of the aeolianite ridges. b) Cliff section in one of the barrier ridges showing cross-bedded aeolianite deposits (dune limestone or calcarenite) of MIS 5a and 5c age overlain (at surface) by Holocene coastal dunes. c) Backbarrier shell-rich lagoonal facies of the last interglacial age, dominated by the cockle *Donax deltoides*, exposed on Hindmarsh Island, Murray River mouth. d) Extent of valine racemization (total hydrolysable amino acids) in 'whole-rock' sediment samples plotted against the square root of TL age. Letters indicate names of beach and spit sections from which the samples were obtained (after Murray-Wallace *et al.*, 2010, reprinted with permission of Elsevier; photographs by Colin Murray-Wallace, University of Wollongong, Australia).

MIS stage 11 (Figure 5.44a), while data from a number of sites in southern and eastern England enabled a temporal framework based on aminostratigraphy to be reconstructed for faunal (Figure 5.44b) and archaeological (Figure 5.44c) records that extends back into the Middle Pleistocene, that is, beyond MIS 12 (Penkman *et al.*, 2013). Elsewhere in Europe, terrace sequences of the River Danube in eastern Europe (Oches & McCoy, 1995) and the River Dnieper in the Ukraine (Oches *et al.*, 2000) have also been differentiated on the basis of aminostratigraphy. Similarly, in the Somme Valley of northern France, the chronology of a well-developed staircase of fluvial terraces is based on a combination of aminostratigraphy, radiometric and palaeomagnetic dating, enabling the sequence to be correlated with the marine oxygen isotope record (Bridgland *et al.*, 2004).

Dating of ratite eggshell in archaeological contexts

Unlike bone or mollusc shell, ratite eggshell (ostrich, emu and the extinct ratite, *Genyornis*) has a compact structure which protects the protein within it from changes in soil chemistry. Indeed, experimental work has shown that ostrich eggshell more closely approximates a closed system for amino acids than any other biomineral yet evaluated (Miller *et al.*, 1992), and that in tropical and subtropical regions, isoleucine epimerization in egg shell should allow dating back to 200 ka (Brooks *et al.*, 1990).

AARs on ostrich shell, calibrated to a timescale using radiocarbon, have been used to develop an aminostratigraphic context for human occupation at the key site of Border Cave in South Africa (Miller *et al.*, 1999a). The reconstructed chronology showed that anatomically modern human remains were present in levels more than 100 ka old, thereby lending support to an African origin for *Homo sapiens*. Other examples of the use of AARs in eggshell include an analysis of the likely role of humans in the extinction of *Genyornis newtoni* (a flightless, ostrich-sized bird) in Australia, around 50 ka (Miller *et al.*, 1999b), possible human-induced ecosystem collapse and megafaunal extinction, also in Australia (Miller *et al.*, 2005), and Late Holocene faunal extinctions in Madagascar (Clarke *et al.*, 2006b).

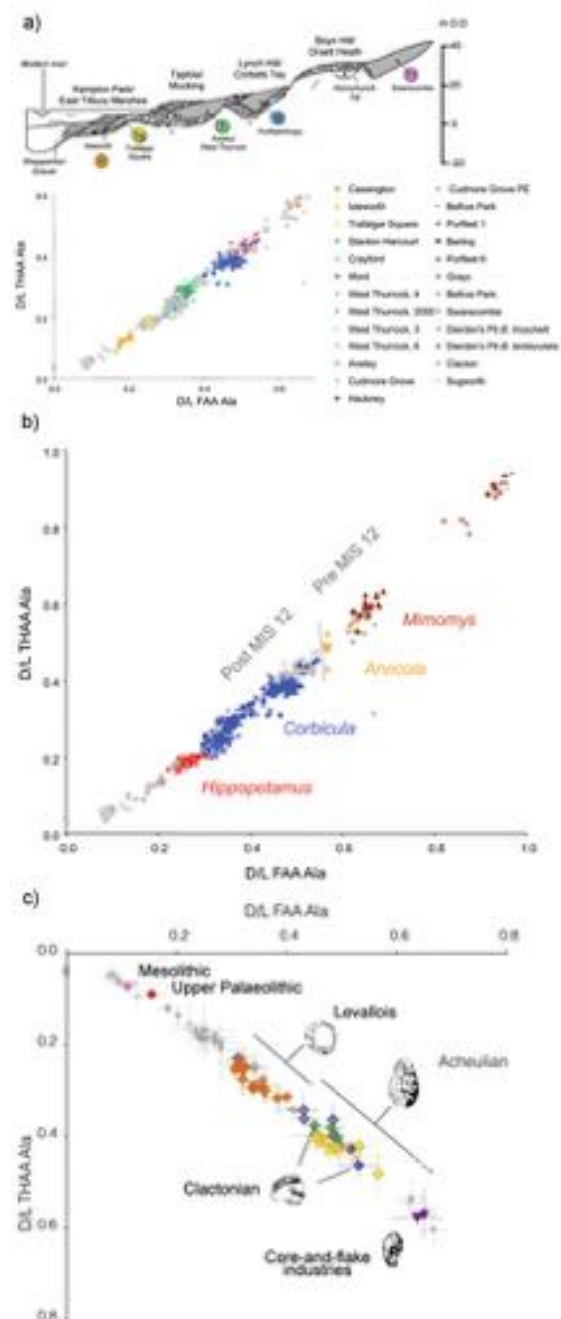


Figure 5.44 An aminostratigraphic framework for the Thames terraces of southeast England (section 2.6.3): a) the terrace deposits; b) the faunal record; c) the archaeological record. The numbers in a) refer to MIS stages; in b) and c) THAA refers to the total hydrolysable amino-acid fraction of the sample; FAA refers to the free amino acids analysed; Ala is the amino acid alanine (after Penkman *et al.*, 2013).

Dating of molluscs in archaeological contexts

One of the most widespread indicators of human exploitation of marine resources and occupation of coastal environments are shell middens. Dating of these deposits using conventional techniques such as radiocarbon can be problematic, however, as the shell middens accumulated relatively rapidly, and there is often a mixing and inversion of materials (Stein & Deo, 2003). Middens have been successfully dated by AAR, however (Bateman *et al.*, 2008), and recent work involving the isolation and extraction of amino acids from the inter-crystalline fraction of shell offers the potential for even more secure dating of middens (Demarchi *et al.*, 2011). Not only is establishing a reliable chronology for these molluscan accumulations important for understanding human activity in the coastal zone, but it may also be significant in studies of human evolution and dispersal.

Palaeothermometry

Since racemization rates are temperature-dependent, where the age of a fossil protein can be established, amino-acid ratios can be used to infer the ambient temperature conditions that affected the proteins since the onset of diagenesis (McCoy, 1987). On this basis, Miller *et al.* (1997) found that AARs from emu eggshells indicated low-latitude cooling in the southern hemisphere during the last glacial stage, while Oches *et al.* (1996) inferred depressed north-south temperature gradients in the Mississippi Valley during the past 25 ka on the basis of AARs from fossil gastropod species, the southern part of the valley having cooled by up to 13°C at the Last Glacial Maximum. Using AARs from fossil ostracods, Kaufman (2003b) suggested that temperatures in the Bonneville Basin, Utah were about 10°C cooler during the last glacial stage by comparison with the late Holocene, and concluded that reduced evaporation rather than increased precipitation could have accounted for an expanded ancient Lake Bonneville (section 2.7.1). While these temperature estimates broadly concur with those from independent lines of evidence, other studies suggest that local environmental and preservation factors can cause problems for the application of amino-acid palaeothermometry (Reichert *et al.*, 2011), and the technique, at present, remains largely experimental.

Screening of fossils for sample integrity

Because amino-acid racemization studies are relatively inexpensive, they provide a cost-effective basis for screening fossils prior to other analyses, such as radiometric dating (Kosnik & Kaufman, 2008) or the extraction of DNA (Collins *et al.*, 2009). Unusual variations in amino-acid diagenetic behaviour may reveal atypical site conditions, or the contamination of the assemblage (O'Donnell

et al., 2006). Screening is particularly important for establishing the integrity of archaeological sequences and their contained fossils (Ellis *et al.*, 1996).

5.6.2 Fluorine, uranium and nitrogen content of fossil bones

Hydroxyapatite, the principal mineral constituent of bones and teeth (section 4.11), absorbs fluorine from groundwater progressively over time. The rate at which the fluorine content increases varies from locality to locality, but bones that have been buried for the same length of time in a particular deposit will have approximately the same fluorine content. As the fluorine fixed in the bone is not readily removed, a specimen that is washed out of an older deposit will show a much higher fluorine content than bones that are contemporaneous with the bed, while bones from a younger stratum will have accumulated substantially less fluorine. Hence the technique is useful in the relative dating of bones in a deposit, and it also enables intrusive (i.e. younger or older) material in a fossil assemblage to be identified (Demetsopolous *et al.*, 1983). The fluorine to phosphate ratio is established by X-ray diffraction techniques, or by the use of an ion-selective electrode (Schurr & Gregory, 2002). The latter approach has been employed in the dating of mammal bones in a range of archaeological contexts (e.g. Johnsson, 1997; McFarlane & Blake, 2005).

The analysis of uranium incorporated into fossil bones from groundwater has been employed in a similar way to the fluorine method, the former having the advantage that the counting of uranium emissions does not involve the destruction of the bone material, but it has the disadvantage that bone material does not always conform to the assumptions of a closed system (Millard & Hedges, 1996). The relative ages of fossil bones in assemblages can also be established by analysing the nitrogen content of fossil bone, for as proteinaceous materials disappear from bone collagen, so too will nitrogen. Hence decreasing nitrogen content will reflect increasing age.

A further means of dating using fluorine content of bone involves the establishment of **fluorine profiles** through sections of bone using a nuclear microprobe. In older bones, the profile is relatively flat, whereas in younger samples, the concentration of fluorine falls off steeply with increasing distance into the bone. The shape of the profile is therefore age-dependent and offers the basis for dating. The technique can be used to establish relative age in mixed bone assemblages, providing useful data on the taphonomy of animal bone assemblages (Johnsson, 1997; Tankersley *et al.*, 1998). It may also be a useful screening

process in the selection of samples for radiocarbon dating, and may provide approximate ages for very recent materials, that is, over the timespan of the last few hundred years. However, uranium profiling suffers from the same problems of non-uniform alteration and low levels of accuracy and reliability as other chemical methods considered in this section; moreover, the distribution of fluorine in archaeological samples appears to be strongly influenced by local environmental factors (Gaschen *et al.*, 2008). Indeed, it has been suggested that fluorine (or fluoride⁵) dating can only be considered a valid dating method where the chronological validity of its results are confirmed by independent chronometric data (Lyman *et al.*, 2012).

5.6.3 Obsidian hydration dating (OHD)

5.6.3.1 General principles

Freshly exposed surfaces of obsidian (a form of volcanic glass) absorb water from their surroundings to form a hydration layer known as **perlite**. This external rind should not, however, be confused with the patina that develops on many materials as a result of chemical weathering (section 5.6.4). One factor governing the thickness of the perlite layer is time, and hence by measuring the thickness of this layer, it may prove possible to estimate the relative age of exposure or the breaking of the obsidian surface, working on the assumption that the thicker the perlite layer, the older the exposed surface. This is the basic principle of **obsidian hydration dating (OHD)**. In addition to time, however, the thickness of the hydration layer depends on the rate at which hydration proceeds and this, in turn, reflects a range of factors including the chemical composition of the obsidian, and the temperature and humidity of the hydrating environment (Beck & Jones, 1994). The thin hydration layer (sometimes less than 1.0 µm) can be seen in section under a microscope when illuminated by polarizing light, but computer-assisted imaging technology is now also used (Ambrose, 1994). More recently, **secondary ion mass spectrometry (SIMS)** has been employed to measure the concentration of hydrogen as a function of depth in obsidian samples, a technique known as **obsidian diffusion dating** (Liritzis, 2006). OHD dates have been reported in the age range from 200–100 ka.

5.6.3.2 Problems with obsidian hydration dating

Numerous difficulties are encountered in the use of OHD. Some of these relate to analytical constraints, but more

serious are problems relating to the determination of the hydration rate which, as noted above, is influenced by a number of different factors. Calibration of obsidian hydration rates to an absolute timescale is even more problematical. These and other limitations have led some to question the validity of the method (Ridings, 1996; Anovitz *et al.*, 1999). Others, however, have come to the defence of OHD, pointing out that although the temporal resolution of the method may not be as good as was once anticipated, as a relative dating technique it can, nevertheless, provide quite rapid answers to site-specific problems (Hull, 2001; Rogers, 2007).

5.6.3.3 Some applications of obsidian hydration dating

Applications of OHD dating include the dating of volcanic activity (Friedman & Obradovich, 1981), glacial events (Pierce *et al.*, 1976), and fluvial terrace sequences (Adams *et al.*, 1992). The technique has been most widely used, however, in the dating of archaeological contexts, and particularly of artefacts (Ambrose, 1994; Tripcevich *et al.*, 2012). It now appears that hydration rims may also develop on quartz and, if so, this could provide a basis for the dating of a much wider range of artefacts (Ericson *et al.*, 2004). Indeed, the greatest value of the technique may be in the establishment of relative order of antiquity of artefacts, for on many archaeological sites, this may be the only dating method available (Hull, 2001). As with other techniques, greater awareness of the constraints has led to refinements of OHD and more coherent age estimates. For example, in a study of more than thirty sites in the southern Nazca region, Peru, estimated OHD ages were within 15 per cent of independently obtained radiocarbon ages (Eerkens *et al.*, 2008).

5.6.4 Weathering characteristics of rock surfaces

5.6.4.1 General principles

A range of rock-weathering parameters has been employed to assign ages to rock surfaces (Mills, 2005). Degree of weathering of stones or boulders, which is a reflection of time, is indicated by a range of characteristics including the relative decomposition or exfoliation of boulders, lack of soluble materials (e.g. limestones) on older surfaces, the crumbly nature of sandstone or volcanic clasts on older drifts, and the relative concentration of more durable materials (e.g. quartz, chert, siliceous rocks) at the surface.

The extent of weathering may also be established by recording the sound produced by boulders being struck with a hammer. Fresh boulders produce a sharp ring and a strong hammer rebound whereas weathered stones emit a dull sound and a weaker recoil. More quantitative estimates may be obtained from a **Schmidt hammer** where rock-hardness is measured by the distance of rebound of the controlled impact of a calibrated spring-loaded mass, and which has been widely employed in geomorphological research (Goudie, 2006). Indeed, the Schmidt hammer may also offer a basis for calibrated-age dating, particularly in Holocene contexts (Figure 5.45a; Shakesby *et al.*, 2006). The thickness and chemical composition of the **weathering rind**, the outer layers of boulders or stones which have been oxidized and discoloured by iron-bearing minerals, can also be used to establish relative order of antiquity of rock surfaces (Figure 5.45a). One approach is **cation-ratio dating**, which is based on the relative stability of chemical constituents of **rock varnish**, the coating of clay minerals, manganese, iron oxides, etc., that form on rock surfaces in arid areas (Gordon & Dorn, 2005). Certain bases, notably potassium (K) and calcium (Ca), are easily mobilized whereas others, such as titanium (Ti), are more stable. Hence the K + Ca/Ti ratio in rock varnish decreases with time and provides an indication of age. Magnification of rock varnish rinds shows that they are composed of microscopically thin layers, or **micro-laminations**, the number and structure of which also provide an index of relative age, a technique termed **varnish micro-lamination (VML) dating** (Liu & Broecker, 2008). Rock varnish also contains minute quantities of organic material, and where sufficient can be obtained for AMS radiocarbon dating, the relative chronologies obtained from cation-ratio dating can be calibrated to a radiometric timescale (Liu, 2003). Where well-jointed rock crops out at the surface, variations in depth of jointing can also be employed to determine relative order of age, the deeper and more expanded joints indicating a longer exposure to weathering agencies, for example under periglacial conditions (Ballantyne *et al.*, 1998).

5.6.4.2 Problems in using surface weathering features as indicators of relative age

Although degree of weathering on rock surfaces and boulders is a function of age, it may also be affected by other factors such as local climate, altitude, aspect and bedrock type. Thus variations in local lithology may influence Schmidt hammer readings, as also might wind polishing and case hardening of weathering rind surfaces in high

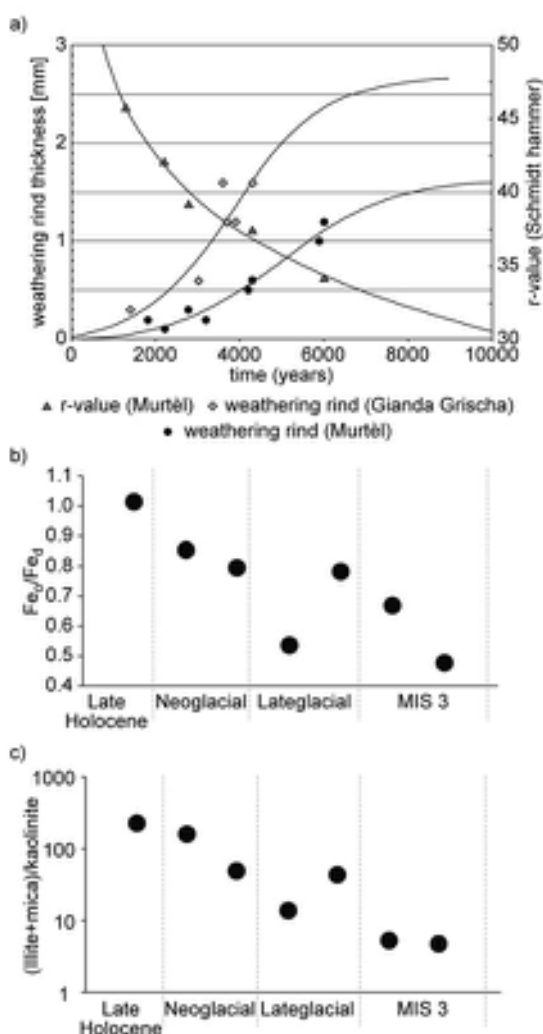


Figure 5.45 Weathering and soil-forming indices used to establish relative age of landform surfaces. a) Weathering rind thickness measurements and Schmidt hammer rebound values (*r*-values) for boulders on the Murtel rock glacier surface in Switzerland (from Haeberli *et al.*, 2003). Weathering rind thickness measurements from the neighbouring Glanda Grischa rock glacier reveal that weathering rates vary as a result of factors such as rock type and micro-climatic conditions. b) Iron oxide and c) clay mineral ratios in top soils on moraines of different age in Nepal (from Zech *et al.*, 2003). Active non-crystalline iron oxides (Fe_O) dominate in young soils but are progressively reduced to the crystalline state (Fe_2O_3) over time.

arctic regions (Viles *et al.*, 2011). In glaciated regions, the incorporation of older rocks and boulders into younger glacial landforms can also result in anomalous Schmidt hammer data (Evans *et al.*, 1999). Cation-ratio dating has proved to be particularly problematical, with questions being raised about the precise nature of the processes that lead to cation-ratio variations, and also about the long-term stability of ultra-thin varnishes on rock surfaces (Bierman & Gillespie, 1994). The validity of radiocarbon dates on organic residues from rock varnish has also been queried (Beck *et al.*, 1998; Watchman, 2000). However, the recent application of varnish microlamination dating to rock surfaces in the arid southwest USA has generated results that not only correlate with the SPECMAP oxygen isotope record (section 5.5.3), but accord well with independently derived CRN ages, suggesting that VML dating can provide a reliable basis for determining relative age (Liu & Broecker, 2008).

5.6.4.3 Some applications of surface weathering dating

Variations in rock weathering characteristics have been widely employed in the establishment of Late Quaternary glacial chronologies, where moraines and other glacial features have been placed in relative order of age on the basis of, *inter alia*, degree of weathering of contained rocks and boulders (Shakesby *et al.*, 2004). Rock surface weathering contrasts have also been used to delimit the upper level of glacial erosion on mountain summits (the trim line: section 2.3.1), from which the former vertical extent of ice sheets can be reconstructed (Ballantyne *et al.*, 2008), while in arid regions, rock varnish laminations (see above) have enabled ages to be assigned to a range of landforms and deposits, including alluvial fans, colluvial boulder deposits, lava flows and rock pavements (Liu, 2003; Liu & Broecker, 2008). Surface exposure dating has also been used in archaeological contexts, in relation to the physical and/or chemical weathering of rock surfaces. Initially, this approach appeared to generate equivocal results (see e.g. Watchman, 2000), but more recent investigations have shown a close correspondence between surface exposure and radiometrically determined age estimates from archaeological artefacts (e.g. Zerboni, 2008). Finally, an increasingly important role for surface exposure dating is in the selection of surface samples for cosmogenic radionuclide dating (Gordon & Dorn, 2005).

5.6.5 Pedogenesis

5.6.5.1 General principles

Key pedological (soil) properties can be used to estimate ages of Quaternary deposits from various deposition environments, estimate long-term stability and instability of landscapes, and make inferences about past climatic changes (Birkeland *et al.*, 2003). This approach rests on the concept of a **soil chronosequence**, that is, a series of related soils developed when all factors of soil formation except time (climate, organisms, parent material and topography) are held more or less constant (Huggett, 1998). Hence contrasts between soil profiles, such as grain size variations, physical and chemical properties, micromorphology and depth of soil development, along with other parameters, such as magnetic susceptibility or clay fraction mineralogy, can be interpreted as a function of time and so provide a basis for relative dating (Birkeland, 1999). Although qualitative assessments of soil development have proved useful in the establishment of local glacial chronologies, a more quantitative methodology has been adopted in recent years. Examples include **soil development indices**, which reduce soil property data from a profile to a single value that reflects the degree of pedogenic development. Inter-site comparisons enable temporal and regional trends in soil development to be identified and profiles can be ranked in terms of relative order of age (Goodman *et al.*, 2001). Soil development indices can then be employed in **soil chronofunctions** in which changes in soil properties are modelled as functions of time (Dahms *et al.*, 2012). These provide a quantitative framework for the construction of timescales of soil development (Figure 5.45b).

5.6.5.2 Problems in using pedogenesis as a basis for dating

The major difficulty in using degree of pedogenesis as a basis for chronology lies in the requirement that all soil-forming factors, apart from time, must be held constant, for numerous studies have shown that factors such as topography and vegetation cover are frequently as important as time in controlling soil genesis (Almond *et al.*, 2007; Douglass & Mickelson, 2007). Rates of pedogenesis also appear to be influenced by regional climatic parameters (Birkeland, 1999) and this imposes further constraints on models of soil evolution where time is considered to be the major independent variable. An additional problem, which particularly affects older (pre-Holocene) glacial substrates, is that episodic erosion and redeposition can result in soils that may be an order of magnitude younger than underlying

sediments (Rodbell, 1990). As with weathering characteristics of rock surfaces, therefore, pedogenic development tends to be used in an auxiliary, as opposed to a primary, role in the establishment of relative chronologies (Mark *et al.*, 2004). Indeed, with the advent of surface exposure dating, U-series dating of soil carbonates and OSL dating, pedogenic differentiation as a dating approach is now less widely used than before.

5.6.5.3 Some applications of relative dating based on degree of pedogenesis

Pedogenic contrasts as a basis for relative chronologies have perhaps been most widely employed in North America. In many formerly glaciated areas of the western Cordillera, for example, systematic changes in morphology and soil development reflect increasing age of parent material. These include the sequence and thickness of genetic horizons; increase in clay content of the B-horizon; depth of oxidation of the B- and C-horizons; and clay mineral alteration (Figure 5.45b). A clear trend is often apparent in pedogenesis with older soils showing evidence of, for example, deeper profiles, thicker horizons and increased clay accumulation. Using this type of evidence, it has been possible to assign relative ages to, and to establish correlations between, moraines in, for example, the Rocky Mountains, USA (Dahms, 2002), the Peruvian Andes (Goodman *et al.*, 2001) and the Himalayas (Zech *et al.*, 2003). An alternative approach involves the use of **soil catena chronosequences**, that is, the evolution of soils at different positions on slopes of moraines of different ages, in order to provide a more secure basis for pedologically derived timescales of glacier activity (e.g. Mahaney *et al.*, 2009). Soil development indices and pedo-chronosequences have also been used to determine the relative ages of marine terraces (Scarciglia *et al.*, 2006), sand dunes (Botha & Porat, 2007) and river terrace sequences (Tsai *et al.*, 2007), while pedogenic and weathering parameters have been employed in combination with other techniques (radiocarbon, ^{10}Be , dendrochronology) to reconstruct glacial histories and other aspects of landscape evolution during the Late Pleistocene and early Holocene (Zech *et al.*, 2003; Favilli *et al.*, 2009).

5.7 STRATIGRAPHIC AND TEMPORAL RESOLUTION

Although techniques that establish age equivalence on the basis of stratigraphic markers, and methods that determinate the relative order of antiquity of rocks or

fossils, are being increasingly used in Quaternary research, the most important methods for establishing the age of Quaternary events are likely to remain the radiometric and incremental techniques. Because they allow events to be dated in years, their application has often been referred to as ‘absolute dating’. However, this term has not been used here as it implies a level of exactitude that is rarely attainable. Nor have we used ‘geochronometric’, which has frequently been employed to describe dating techniques from all of the categories described above, including methods which, at best, only provide relative age relationships at a very broad scale. Again, a degree of precision is implied by the use of this term that is often not reflected in the results produced. But irrespective of the techniques employed, the key question that needs to be addressed in formulating a sampling strategy for dating Quaternary events is: how can the highest level of **geochronological resolution** be achieved on samples from a single stratigraphic sequence? This involves assessment of both **stratigraphic** and temporal **resolution**.

In Figure 5.46a, cores (or monoliths) have been obtained from bodies of Quaternary sediment, each 1 m in length. The left-hand core is subsampled in 10 cm blocks, while the core on the right is subsampled in 2 cm increments. Hence, the right-hand core is sampled at a much higher **stratigraphic resolution**. The former may have been sampled for coleopteran analysis (which requires greater quantities of material), while the latter may have been sampled for pollen or diatom analysis, for which much smaller samples are needed. The level of sampling resolution is therefore dictated by the nature of the analytical programme. But the temporal dimension also needs to be considered (Figure 5.46b). The left-hand core may have accumulated over an interval of 1.0 ka while the right-hand spans 10 ka. Assuming a constant rate of sedimentation in both cases, each increment from the left-hand core would have taken 100 years to accumulate, and those on the right 200 years. Hence, the sequence on the left would have been sampled at a **higher temporal resolution**, albeit with a **lower stratigraphic resolution**. If we are seeking to date these two sequences (Figure 5.46c), and a specific volume of sediment (or abundance of fossil material) is required to satisfy the analytical constraints of the particular dating method (e.g. radiocarbon or OSL), then the **geochronological potential** of that method (in theory, at least) can be determined. For example, a 5 cm or 20 cm thick sample of material from the left-hand core could potentially provide age estimates at a temporal resolution of 50 years and 200 years, respectively. In the right-hand core, by contrast, a sample of no more

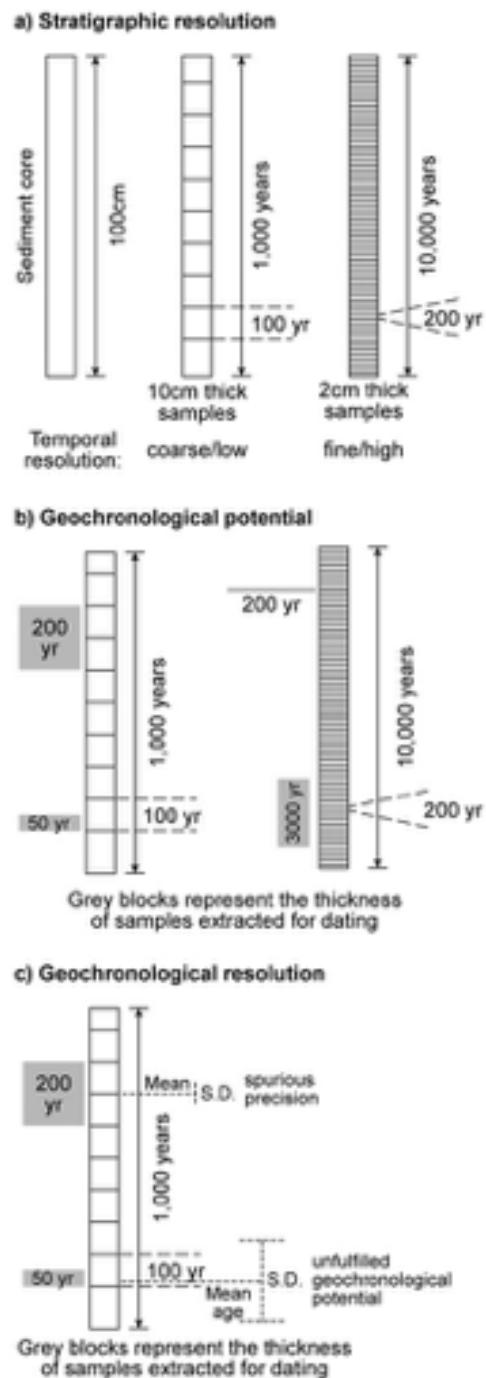


Figure 5.46 Stratigraphic and temporal resolution in Quaternary sediment sequences. S.D. – standard deviation (2σ). For explanation see text.

than 2 cm in thickness would be required to provide a geochronological resolution of 200 years. The value for a 20 cm sample would be 2,000 years. From a research design perspective, therefore, if the aim is to achieve decadal resolution or better, then only the sequence on the left can provide this, but only if a small sample size is used. Finally, as has been shown throughout this chapter, all dating methods have uncertainties, and so the full theoretical geochronological potential of a sedimentary sequence will rarely be achieved. Thus, in Figure 5.46c, the error range for a 5 cm thick sediment sample may be much greater than for the 20 cm thick sample, perhaps because there is less material (organic carbon for radiocarbon dating; quartz grains for OSL dating) for analysis. Hence there will have to be a trade-off between sample size and analytical precision. This is **geochronological resolution** (as opposed to potential). But even if it proved possible to reduce the analytical error, this might generate spurious results, depending on how long the sediment has taken to accumulate. This is illustrated in Figure 5.46c where a standard deviation of ± 30 years for Date 1 implies an unrealistic level of temporal precision on a sediment sample that took 200 years to accumulate, whereas better age resolution is possible for Date 2 if analytical precision can be improved.

Clearly, the situation depicted in Figure 5.46 is an oversimplification of reality, as most sedimentary sequences are complicated by non-linear (irregular) sedimentation rates, depositional hiatuses, and perhaps recycled or deformed components. Moreover, when confronted by a stratigraphic sequence, it is very difficult to make an initial assessment of the geochronological potential of that sequence. However, given the increasing imperative in Quaternary science to conduct analyses at the highest possible levels of temporal resolution, it is essential that consideration be given to these matters in the formulation of sampling and dating strategies, and that preliminary investigations involving, for example, the use of range-finder dates, should be an essential first step in the establishment of a chronology for Quaternary sedimentary records.

5.8 CONCLUSIONS

In addition to ensuring that sites are sampled at the highest levels of geochronological resolution, the major challenge now in Quaternary dating would appear to be how to achieve a greater degree of reliability in age estimates based on methods that, in some cases, have somewhat uncertain foundations. Progress in this respect depends not only

on achieving higher levels of both accuracy and precision in individual dating techniques, but also on replication of results from a given method, and on the implementation of integrated dating strategies, involving the application of more than one technique to the dating of a fossil assemblage, body of material, stratigraphic horizon or event. Although the approaches reviewed in this chapter have gone a considerable way towards providing a coherent dating framework, particularly for the Late Quaternary, it is important that new techniques continue to be developed. One area that appears to offer considerable potential in this regard is biomolecular dating (section 5.5.4), in particular **molecular clock analysis** based on timings of genetic mutations, and which could eventually provide a complete chronology for human evolution. Not only do techniques such as this offer new bases for determining Quaternary time, but they provide further scope for the calibration of existing methods. Bearing these points in mind, we now turn to the wider question of stratigraphic subdivision and correlation of the Quaternary record.

NOTES

- 1 The **principle of superposition** states that, in the absence of evidence for disturbance or reworking, the overlying sediments in a sequence are younger than those lying beneath them. This applies both to lithological units, such as tills, solifluction deposits, etc., and to biostratigraphic units, such as pollen or molluscan assemblage zones. In this way, pollen analysis, for example, can be employed as a relative dating technique.
- 2 The secular magnetic database analysed by Jackson *et al.* (2000) contains more than 83,000 individual measurements of declination for more than 64,000 locations, all collected prior to AD 1800.
- 3 For example, protein residues have been found in Ordovician and Devonian shells, and collagen-like proteins have been recovered from Cretaceous dinosaur bones.
- 4 The **operculum** (pl. **opercula**) in a mollusc shell is the small lid that is attached to the upper surface of the foot and serves as a 'trapdoor' to close the aperture of the shell when the soft parts of the animal are retracted.
- 5 Some analyses use **fluoride**, which is the negative ion of the element **fluorine**, as a basis for dating of fossil bone.

This page intentionally left blank

Approaches to Quaternary stratigraphy and correlation

6.1 INTRODUCTION

In previous chapters, the various methods employed in palaeoenvironmental reconstruction have been examined and the techniques used in the dating of Quaternary events have been discussed. Of particular interest to the Quaternary scientist, however, is the way in which environments have changed through time, and how such information can be gained from the stratigraphic record. There are two aspects to the interpretation of that record, namely the ordering of the evidence at any one locality into a time sequence (*temporal dimension*) and the relationship of the evidence at one locality to that at another (*spatial dimension*). The temporal dimension involves principles of **stratigraphy**, while the spatial dimension involves principles of **correlation**. A proper understanding of the procedures involved in these two aspects of geological investigation is fundamental to a correct interpretation of Quaternary palaeoenvironmental records.

If stratigraphic sequences were complete at all places on the earth's surface, and if every important horizon could be dated accurately, then elements of the record could be arranged into stratigraphic order based on increments of time. In this way a **time-stratigraphic** framework for the history of environmental change could be established, and correlation between even the most widely separated localities would present few problems. In practice, however, this is not achievable. The terrestrial record is frequently incomplete, and dating control inadequate, due either to the absence of suitable dating materials or to limitations of the techniques employed (Chapter 5). Only on the ocean

floor, and in certain exceptional terrestrial situations, such as deep lakes or regions with thick loess deposits, are long continuous stratigraphic records preserved, although even in those contexts the dating of events may be difficult. For the most part, therefore, the Quaternary stratigrapher is confronted by a highly fragmented and partial sedimentary record that can be dated securely only in certain circumstances and over limited time ranges. As a consequence, very careful analysis of the stratigraphic relationship between sediment sequences is required before records can be ordered at one locality and correctly related to those at another.

In this chapter, the principles of, and the procedures involved in, Quaternary stratigraphy and correlation are examined, and the means through which time-stratigraphic correlation can be achieved are explored. Although deep-sea sediment records are considered, this discussion will relate primarily to the terrestrial record, for it is terrestrial evidence that provides the greatest obstacles to the application of conventional stratigraphic and correlation procedures.

6.2 STRATIGRAPHIC SUBDIVISION

6.2.1 Principles of Quaternary stratigraphy

Stratigraphy is the study of the chronological order of rocks and sediments, and also of the sequence of events reflected within them (Rawson *et al.*, 2002). The fundamental building blocks are units of geological strata that

can be identified on the basis of visible attributes, such as colour, grain-size variations or structural elements (bedding, deformation features, etc.). These units comprise the basic elements of **lithostratigraphy**, which involves the ranking or ordering of local rock or sediment sequences according to observable variations in lithology. Increasingly, however, a range of instruments and sensors are being employed in the analysis and classification of geological units, including the various remote sensing methods described in section 2.2.2, as well as geophysical data-logging procedures such as digital imaging or X-ray core scanning (Rothwell, 2006). These enable the properties of rock or sediment units to be examined in much more sophisticated ways than is achievable by the human eye. A wide range of physical and chemical properties, reflecting changes in the constituent materials within rocks or sediments, can be analysed. Examples include **magnetostratigraphy** (variations in strength or direction of magnetic signals), **seismic stratigraphy** (variations in strength of penetration or reflectance of directed signal beams) and **chemical stratigraphy** (variations in abundance of chemical compounds or of their isotopic ratios). Some methods have particular applications in Quaternary research, such as **oxygen isotope stratigraphy** (a form of chemical stratigraphy) that provides the foundation for subdividing the Quaternary timescale (section 3.10.2), and **electrical conductivity measurements** (a geophysical logging method) developed specifically for the analysis of ice-core sequences. Where clearly defined ‘events’ are recorded in the stratigraphic record, such as magnetic reversals, volcanic eruptions (indicated by tephra layers) or inflections in isotopic profiles marking abrupt climatic changes, these can form the basis for an **event stratigraphy** (Alloway *et al.*, 2007b). As the event horizons are essentially time-parallel (**isochronous**), they offer a means of correlation at a range of spatial scales (section 6.3.2.6).

Modern stratigraphical investigations normally involve a range of approaches, and geological sequences are usually subdivided after integration of all the available evidence. In most situations, however, it is still the visible features that are of primary importance in the formal subdivision of the stratigraphic record: the parameters derived from instrumentation, such as geophysical or chemical data, provide supplementary information only. In some important cases, however, visible lithological variations may be absent or imperceptible, while important stratigraphic changes, which may be crucial in subsequent palaeoenvironmental reconstructions, can be detected only by instrumental techniques. The isotopic and trace-gas signals in deep-ocean sediments and ice cores (sections 3.10 and

3.11) are important examples of such instrumentally derived stratigraphic records.

There are a number of other important ways in which stratigraphic units can be subdivided and ordered, however. **Biostratigraphy** involves the classification of sediment units according to observable variations in fossil content, and enables a sediment sequence to be divided into **biostratigraphic units** or **biozones**, each characterized by a distinctive fossil assemblage. In Quaternary stratigraphy, landforms can be classified according to their relative order of age (**morphostratigraphy**), with each landform or landform suite constituting a distinct **morphostratigraphic unit**. **Climatostratigraphy** is concerned with the division of a stratigraphic sequence into **geological-climatic units** on the basis of inferred changes in climate, while **chronostratigraphy** involves the classification of stratigraphic units according to age, the interval of time during which a geological unit has developed being referred to as a **geochronological unit** (section 6.2.3.7). Climatostratigraphy and chronostratigraphy are essentially *inferential* methods of stratigraphic subdivision, whereas both lithostratigraphy and biostratigraphy are more direct, being based on empirical properties of the sediment record.

Codes of practice have been produced to aid the geologist in the task of stratigraphic subdivision and classification (e.g. Salvador, 1994; Rawson *et al.*, 2002; North American Commission on Stratigraphic Nomenclature, 2005). These aim to provide a clear and unambiguous terminological framework, as well as guiding principles on stratigraphic procedures. All of these codes, however, have been developed for use in pre-Quaternary geology, and have limitations when applied to Quaternary stratigraphy. This is because Quaternary sediment sequences can be examined in far greater detail and at a much higher level of temporal resolution than their pre-Quaternary counterparts. The result is that the Quaternary scientist often has to deal with sedimentary sequences of unusual geological complexity, and this gives rise to problems of classification, interpretation and correlation that are not encountered in earlier parts of the geological record. For example, boundaries between lithological units are placed at positions of lithological change (section 6.2.3.1), but in many Quaternary sequences these cut across the limits of fossil ranges (reflected in biozones) and the boundaries of other types of stratigraphic unit (Figure 6.1). Moreover, they frequently cut across time-horizons (**time-transgression**), and this poses particular problems in the correlation of stratigraphic sequences at the scale of resolution required in Quaternary research.

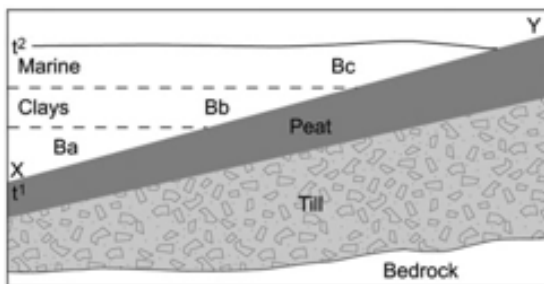


Figure 6.1 Time-transgression in lithostratigraphic and biostratigraphic boundaries. A till unit is overlain by a peat layer which has, in turn, been buried by marine sediments. The marine deposits accumulated during a gradual marine transgression (t^1-t^2) and therefore the lithostratigraphic boundary between peat and the overlying marine sediments (X–Y) will be time-transgressive. During the deposition of the marine sediments, changes in fossil content have occurred, represented by biozones Ba, Bb and Bc. The lithostratigraphic boundary X–Y therefore cuts across the biozone boundaries.

6.2.2 Stratotypes

According to conventional geological procedures, a locality where a particular stratigraphic unit is clearly and fully recorded, or where its lower boundary is securely defined, is termed a **type site** or **stratotype**. This can then be used as a reference standard against which other sequences, where the equivalent unit or its boundaries are only partially or poorly represented, can be compared. The type section should be accessible and durable, so that it may be available for further study, and perhaps reassessment where necessary. In a review of the role of stratotypes, Walsh (2005) defines three types: **exemplary stratotypes**, which provide concrete examples of important, widely recognized stratigraphic units; **boundary stratotypes**, which show the clearest exemplification of the nature of the boundaries between internationally recognized stratigraphic units; and **nominal stratotypes**, which are internationally agreed reference sites to which the formal name of the stratotype applies. Walsh draws an analogy between these procedures for classifying rock or sediment sequences, and the code of practice used in the naming of new biological species and for establishing their hierarchical importance.

Ideally, all stratigraphic units should be defined by reference to a stratotype. However, this is often difficult in Quaternary stratigraphy because of the highly fragmented nature of the terrestrial stratigraphic record, the considerable spatial variation in type and thickness of Quaternary sediments, the limited lateral continuity of many Quaternary deposits, the spatial and temporal

contrasts in Quaternary environments as reflected in the biostratigraphic record and, above all, the markedly time-transgressive nature of terrestrial stratigraphic boundaries (Figure 6.1). In many situations, therefore, a stratotype will have little more than local application and, as a consequence, the concept of the stratotype has been less widely adopted by Quaternary workers than by geologists dealing with older segments of the stratigraphic record. However, in the interests of clarity and precision, a strong case can be made for the more widespread adoption of Quaternary stratotypes than has been the practice in the past. Certainly, if effective communication between scientists is to be achieved with respect to the subdivision of the Quaternary stratigraphic record, the establishment of **regional stratotypes** where the lithostratigraphic and biostratigraphic units constitute clear reference standards is an integral component of that process (McMillan, 2005). An example is the isotopic record in the GRIP Greenland ice core that has been proposed as a stratotype for the Late Quaternary in the North Atlantic region (Walker *et al.*, 1999). At a larger scale, **global stratotypes** are required by the international geological community for defining major geological boundaries and, as explained in section 1.3, these are referred to as **Global Boundary Stratotype Sections and Points (GSSPs)**. Hence, as we saw in Chapter 1, the GSSP for the base of the Quaternary system/period and Pleistocene series/epoch is located at Monte San Nicola in Sicily (Figure 1.3) while the GSSP for the base of the Holocene series/epoch is in the NGRIP Greenland ice core (Walker *et al.*, 2009). The Subcommission on Quaternary Stratigraphy (Chapter 1, note 3) is now working towards the definition of global stratotypes for the Lower–Middle and Middle–Upper Pleistocene boundaries (Head *et al.*, 2008b; Litt *et al.*, 2008).

6.2.3 Elements of Quaternary stratigraphy

6.2.3.1 Lithostratigraphy

In theory, lithostratigraphic units should be recognized and defined on the basis of sediment properties alone, such as colour, particle shape and size, and grain-size variations. In practice, however, Quaternary scientists have also tended to classify sedimentary units on the basis of inferred mode of origin (till, aeolian sand, glaciofluvial gravel, etc.). The problem with such genetically based classifications is that if the mode of origin is incorrectly inferred, then the subsequent stratigraphic reconstruction may be undermined. Hence many Quaternary geologists now prefer the use of sedimentological terms that are free from such genetic connotations. One such term is

diamicton, which simply refers to any sedimentary unit with a heterogeneous mix of particle sizes from clay through to boulders. The mode of genesis of a diamicton is inferred at a later stage in the analysis on the basis of such diagnostic criteria as fabric data, clast size and shape, and micro-morphological properties (section 3.3.5). When confronted by a complex stratigraphic sequence (Figure 6.2), the approach should be first to identify **beds**, which are individual sediment units or bodies that are considered to have originated during the same or similar depositional event. Careful examination of a sand unit, for example, may reveal a series of large- or small-scale cross-bedded layers, each reflecting changes in the environment of deposition. Similarly, alternations between sand and gravel beds, layers of silt- or clay-dominated beds, and diamicton units (which frequently form individual beds), may indicate important variations in mode of deposition. In some instances, even

finer subdivisions of the stratigraphy may be possible where, for instance, very thin layers of perhaps 1 cm or less (**laminae**) occur throughout a bed, each reflecting a very short-lived sedimentary episode. Once such individual units have been identified, the second stage is to establish mode of genesis; in other words, *description* and *classification* should always precede *interpretation* of the stratigraphic record.

Where several beds can be shown to be related and have accumulated through similar depositional processes, they comprise larger lithostratigraphic units known as **members**. Hence the stratified sediments in Figure 6.2 are grouped together to form a member that can be differentiated lithologically from the overlying and underlying unstratified diamicton (till) members. Members that accumulated sequentially during a major depositional event (e.g. a glacial episode or a marine transgression) form lithostratigraphic

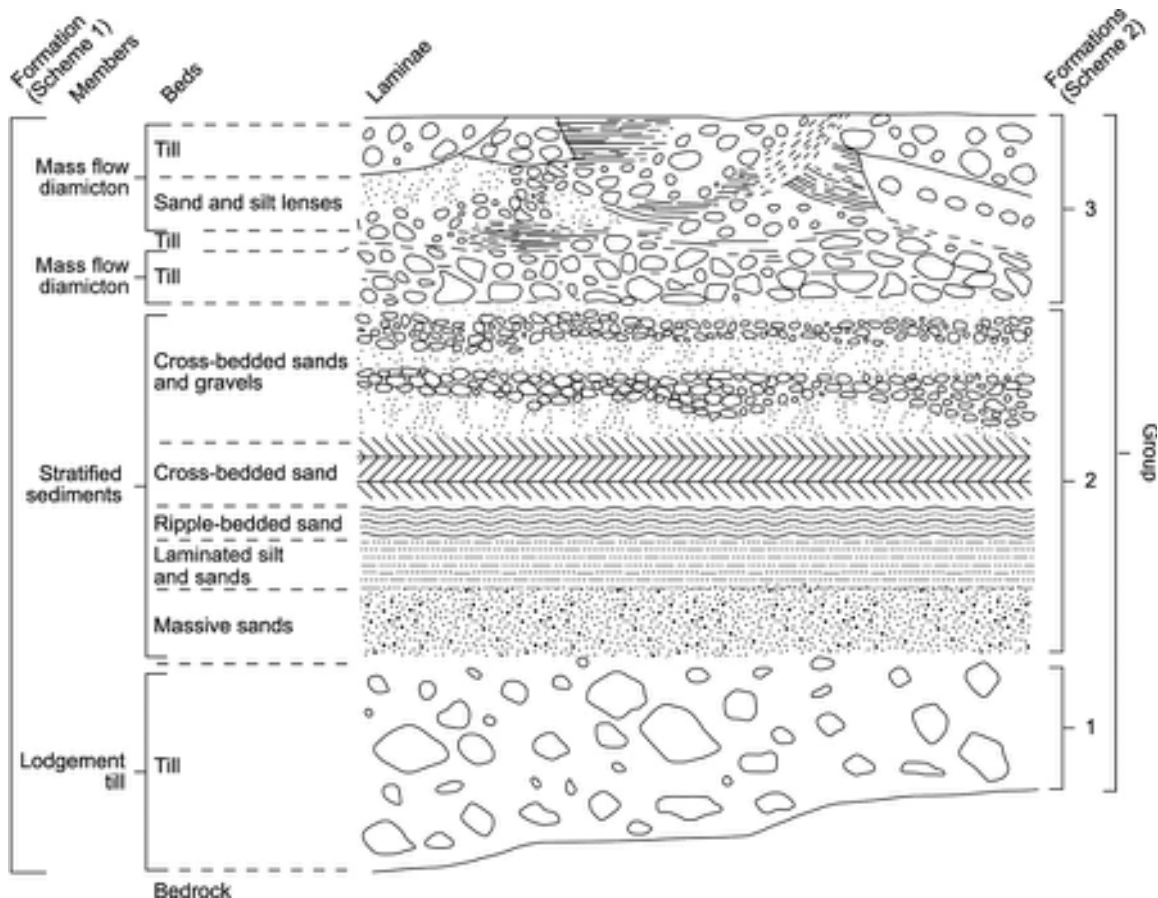


Figure 6.2 Lithostratigraphic subdivision of a glacigenic sequence.

units of higher rank, termed **formations**. Two or more contiguous formations that possess common lithological properties (particle size characteristics, clast lithologies, etc.) may be aggregated into **groups**. Distinctive lithostratigraphic units that appear regularly in sediment records, and provide a basis for correlation between sequences (such as tephra layers), are referred to as **markers**. Units of formation or group rank, displaying common properties or associations of members and beds, may also constitute markers. In such cases, these higher-ranking lithostratigraphic units are given formal status and may be accorded proper names. In southeast England, for example, extensive spreads of glaciofluvial gravels dating from the Anglian Glacial Stage have been termed the '*Barham Formation*'. A more extensive suite of river sediments that formed over 1.2 Ma prior to the Anglian Glaciation, the '*Kesgrave Sands and Gravels*' (Figure 2.51c), accumulated over many warm and cold stages. This lithostratigraphic unit, which contains two major formations (Colchester and Sudbury) and which can be traced over large areas of the River Thames basin and East Anglia, is referred to as the '*Kesgrave Group*' (Rose *et al.*, 1999). Further examples of the ways in which these stratigraphic procedures have been applied in Quaternary research can be found in Bowen (1999), Rose *et al.* (2001) and Lee *et al.* (2004).

An alternative approach to stratigraphic subdivision stems from detailed studies that have been undertaken on contemporary depositional environments. These have shown that different sedimentary contexts (estuarine, glacial, fluvial, aeolian, etc.) give rise to distinctive associations of sedimentary units or **facies** (section 3.3.3.2). Key diagnostic properties (colour, grain-size variations,

geometry, bedding, external contacts, etc.) can be established for each facies, and these data can then be used to define **lithofacies** in rock or sediment sequences, that is, ancient equivalents of modern facies types. Facies may be subdivided into **subfacies** or grouped together into **facies associations**, while at the regional scale they can be considered three-dimensionally in terms of **facies architecture**. In Quaternary stratigraphy, facies analysis has been most widely employed in the study of glacigenic (including glaciofluvial) deposits (Benn & Evans, 2010), although this approach has also been employed in the examination of other sequences, including fluvial and deltaic sediments (Amorosi *et al.*, 2003), and lacustrine records (van Leeuwen *et al.*, 2000). As in conventional lithostratigraphic procedure, however, it is important to begin with a descriptive facies analysis, using the sort of criteria shown in Table 6.1. Non-genetic terms such as 'diamict' should be applied, and a shorthand notation (Gm for massive gravels, Sh for horizontally laminated sands, etc.) should be used to describe each lithofacies. Again, interpretation of the sediment record in terms of mode of genesis then constitutes the second stage of the analysis.

In some depositional contexts, recurrent or cyclic processes lead to the repetitive formation of similar sedimentary 'packages' (discrete stacks of sediment units), each separated by distinct unconformities or hiatuses. The order of superposition and overall architecture of these accretionary 'prisms' can be established by lateral tracing of their bounding unconformities (**sequence stratigraphy**), an approach that is now widely applied in geology (Miall, 2000). This has, perhaps, been most widely employed in the

Table 6.1 Principal descriptive criteria used in defining lithofacies in glacigenic sequences (after Hambrey, 1994).

Lithology	Bedding characteristics	Bedding geometry	Sedimentary structures	Boundary relations
Diamict(on/ite)	Massive	Sheet	Grading: normal, reverse, coarse-tail	Sharp
Gravel	Weakly stratified	Discontinuous	Cross-bedding: tabular, trough	Gradational
Sand(stone)	Well stratified	Lensoid	Dropstones	Disconformable
Mud(stone)	Laminated	Draped	Clast supported	Unconformable
	Rhythmic lamination	Prograding	Matrix supported	
	Wispy stratification		Clast concentration: layers, pockets	
	Inclined stratification		Ripples	
			Scours	
			Load structures	
			Mottling (poss. bioturbation)	

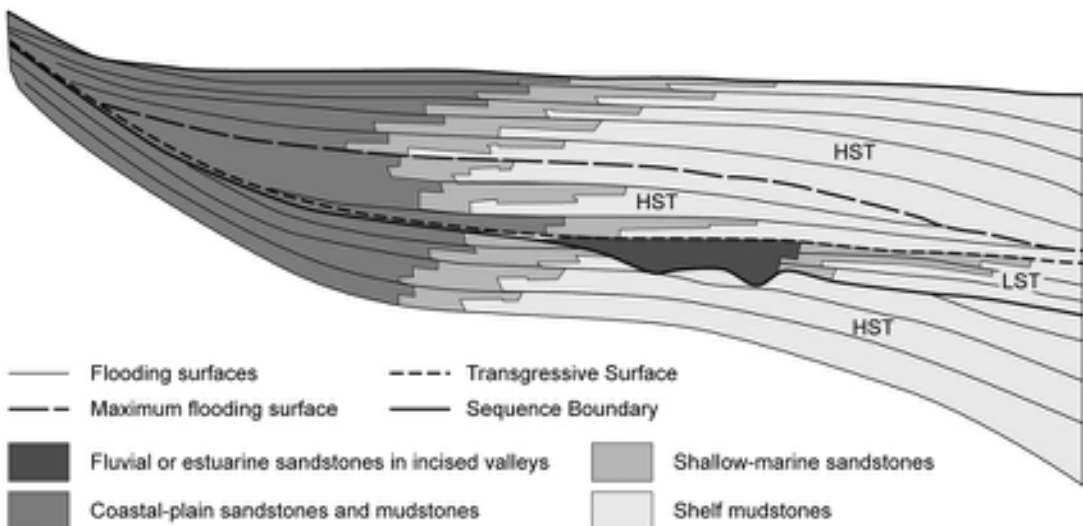


Figure 6.3 Sequence of sedimentary units deposited near continental margins during cycles of sea-level fall and rise. HST, Highstand stage; LST, Lowstand Stage. Other terms are explained in the text.

analysis of marine deposits that have accumulated close to continental margins. Repeated rises and falls in sea level lead to landward and seaward migration of the zones in which shallow- and deep-water sediments accumulate. Each cycle has two characteristic stages: a **lowstand** and **highstand** (Figure 6.3) and two transitional phases: **transgressive** and **falling**. During a fall in sea level, marine sediments may become exposed and hence subject to erosion, but a subsequent transgressive phase will lead to the burial of the remaining deposits by a new accretionary layer, the base of which is marked by an obvious unconformity. Although sequence stratigraphy was initially developed for the analysis of pre-Quaternary rock formations, particularly in the search for petroleum reserves, it has also been used in the mapping and interpretation of unconsolidated Quaternary marine facies (Ridente & Trincardi, 2002; Browne & Naish, 2003).

Lithologically similar accretionary sediment stacks can also be generated by other depositional processes that operate in a cyclic manner, for example in fluvial, glacial or aeolian systems. Some stratigraphic codes now include the wider generic term '**allostratigraphy**' to refer to the classification and sequencing of the depositional stacks (**alloformations**) that these systems generate (North American Commission on Stratigraphic Nomenclature, 2005; Hughes, 2010). The difference between lithostratigraphy and allostratigraphy is that the former often ignores significant breaks in the sediment sequence (e.g. unconformities or flooding surfaces), whereas allostratigraphy, as in

sequence stratigraphy, uses discontinuities and surfaces to subdivide the sedimentary record. Hence an **allostratigraphic unit** is a body of sediment or rock that is defined and identified solely on the basis of its bounding discontinuities. As such, allostratigraphic units differentiate between individual bodies of superposed deposits, for example between a sequence of lithologically similar alluvial and lacustrine deposits separated by a palaeosol, or between onlapping lobes of geliflucted material from different cold-climate episodes (Rawson *et al.*, 2002). Whether this form of stratigraphic classification represents a significant advance over more traditional methods of classifying Quaternary deposits, however, is still being debated (Räsenen *et al.*, 2009; Johnson *et al.*, 2009).

Irrespective of the approach adopted, the level of lithostratigraphic subdivision of a Quaternary depositional sequence depends on the local complexity of the record, and on what are frequently subjective decisions on the nature or rank of a particular stratigraphic unit. However, interpretation is often complicated by the fact that apparently similar sediments and sedimentary sequences can result from different geological processes. Fluvial, glaciofluvial and aeolian sediments, for example, can appear lithologically similar despite the fact that they have accumulated in markedly different depositional environments. This problem, referred to as **equifinality**, can also arise in the interpretation of Quaternary soils and landforms (Kemp, 1998; Evans, 2009). In addition, many Quaternary sedimentary sequences (such as fluvial deposits) show considerable

lateral and vertical variation, and these local facies changes frequently pose problems of interpretation and classification when using traditional lithostratigraphic criteria (Clague, 2000; Winsemann *et al.*, 2007). Deformation of sediments is a further complicating factor, particularly in the analysis of glaciogenic deposits (Lee & Phillips, 2008). Even where the origin of the sediments can be unequivocally established, the subdivision of very complex sequences into lithostratigraphic units is not always straightforward. In Figure 6.2, for example, the beds of stratified sediments can be grouped together to form a member that can be differentiated lithologically from the unstratified diamictons above and below. Analysis shows the sediments to have been derived from episodes of glacial and glacio-fluvial activity during a single glacial event, and hence the whole sequence can be classified as a formation (scheme 1: left). Alternatively, the upper and lower diamictons and the intervening stratified unit might be regarded as representing discrete depositional events, and under this interpretation, each could be classified as units of formation rank (scheme 2: right). Consistency of interpretation between individual workers may, therefore, be difficult to achieve. Nevertheless, insofar as it emphasizes the need for careful analysis and interpretation, this is still the best approach to the subdivision of the Quaternary rock-stratigraphic record.

6.2.3.2 Biostratigraphy

Biostratigraphic classification organizes rock strata into units based on the variety and abundance of fossils. Biostratigraphic units are usually termed **biozones**, and the following types are commonly employed in stratigraphic classification (Figure 6.4):

- Total range biozone:** a group of strata containing the full stratigraphic and geographical range of a particular fossil or group of fossils.
- Acme biozone:** a group of strata based on the acme or maximum development of a particular taxon.
- Partial range biozone:** the stratigraphic interval described by that part of the range of a particular taxon that lies above that of a second taxon and below that of a third. Hence in Figure 6.4, PRB-b is that part of the range of taxon b which lies above the range of taxon a and below that of taxon c.
- Concurrent range biozone:** defined on the basis of the overlapping ranges of several taxa.
- Consecutive range biozone:** where speciation changes can be clearly established (**phylogenetic lineage**), biozones can be defined on the basis of the consecutive ranges of fossils in an evolving lineage.

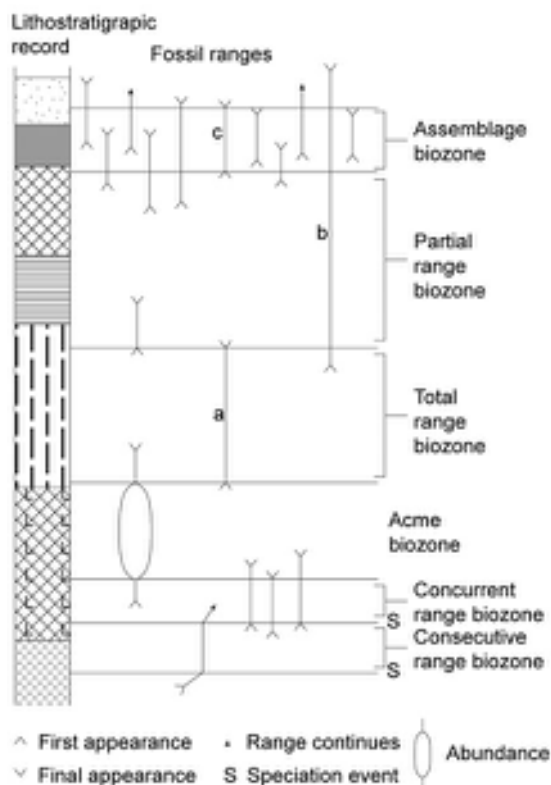


Figure 6.4 Various types of biozone used in the subdivision and correlation of strata. The **consecutive** and **concurrent** ranges are defined on the basis of the appearance and disappearance of taxa, normally in the context of evolutionary lineages. Others are defined in the text.

6. **Assemblage biozone:** biozones that are defined on the basis of a characteristic mix and relative abundance of fossil types.

In pre-Quaternary geology, the biostratigraphic record is subdivided largely on the basis of evolutionary changes in organisms, and thus acme biozones and range biozones reflect those episodes of geological time where a species appeared, thrived for a while, and then died away. Acme and range biozones constitute valuable stratigraphic markers, and often form the basis for correlation. Although there is some evidence of evolutionary development in lineages of rodents (van Koenigswald & van Kolfschoten, 1996) and beetles (Elias, 1994), and perhaps also in ostracods (Griffiths, 2001) and fish (Craw *et al.*, 2007), evolutionary changes are generally less common over much of the Quaternary biological record, and thus acme

and range biozones are not as widely used as in pre-Quaternary geology. Quaternary biostratigraphy is, therefore, based almost entirely on **assemblage biozones**, and these largely reflect the ecological response of organisms to environmental change rather than evolutionary developments in flora and fauna. The biostratigraphic approach to Quaternary subdivision has perhaps been most widely applied in the British Isles and western Europe where a range of biological indicators has been used to characterize warm- and cold-stage sequences and to differentiate between them (Schreve & Thomas, 2001). Unlike evolutionary trends, however, ecological changes are both reversible and repeatable. Hence Quaternary assemblage biozones of different ages may contain essentially the same mix of fossils (Thomas, 2001), in which case they are potentially flawed as stratigraphic tools. This situation differs from that in pre-Quaternary strata where evolutionary changes over much longer time periods have resulted in assemblage biozones that can be unique.

Because of the time-transgressive nature of climatic and environmental change, the boundaries of biozones (pollen assemblage zones, molluscan assemblage zones, diatom assemblage zones, etc.) cut across time horizons and frequently transgress the boundaries of other stratigraphic units. In parts of the deep oceans, however, where sedimentation rates are comparatively slow, assemblage biozone boundaries may *appear* to be time-parallel. In reality, however, all assemblage biozone boundaries examined at the resolution required in Quaternary science are time-transgressive, since it takes time for organisms to migrate and to adapt to changes in environmental conditions. Whether the degree of time-transgression can be ascertained depends on the nature of the changes and, as in all biostratigraphical investigations, on the temporal resolution of the stratigraphic record. Difficulties may also be encountered in the establishment of Quaternary

biozones as a result of the reworking and selective destruction of fossils, and because of problems of identification and ecological interpretation of fossil assemblages (see Chapter 4).

6.2.3.3 Morphostratigraphy

Morphostratigraphy is rarely discussed in stratigraphic codes, yet is an essential stratigraphic method in Quaternary science. A **mohostratigraphic unit** has been defined as 'a body of rock that is identified primarily from the surface form it displays' (Willman and Frye, 1970, p. 43), and was intended to be used by geological surveyors unable to unravel the complexities of glacial stratigraphy on the basis of lithology alone. A range of geomorphological features can be recognized that possess distinctive forms and which are diagnostic of specific geological processes. These include glacial and glaciofluvial landforms, aeolian landforms and coastal features, such as beaches. A morphostratigraphic unit may therefore be defined as that part of the lithostratigraphic record represented by a particular geomorphological feature. Often a series of landforms reflects a temporal succession of phases of formation, such as river-terrace sequences, a series of raised shorelines or a suite of glacial landforms (Schellman & Radtke, 2004; Lukas, 2006). As a distinct category of stratigraphy, morphostratigraphic units are integral components of the Quaternary stratigraphic record.

The role of morphostratigraphy and its relation to the lithostratigraphic record is shown schematically in Figure 6.5. Here the landforms have been identified as glacial features (moraines) on the basis of morphology and geomorphic context. Between the moraine ridges are lake basins (B1, B2) that contain limnic sediments and peats. In order to provide a full account of the stratigraphy of this area, the morphological evidence must be integrated

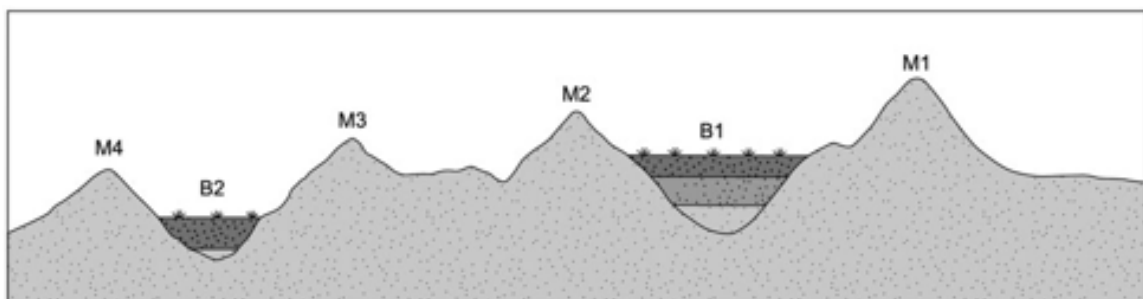


Figure 6.5 Schematic diagram showing a series of moraine ridges (M1 oldest to M4 youngest) between which sediments have accumulated in lake basins (B1 and B2) following deglaciation. For further explanation see text.

with the lithostratigraphic and biostratigraphic record. One interpretation is that the moraines formed sequentially during a period of glacier retreat, with M1 being the oldest and M4 the youngest. If this was so, the base of the lake sediments in B1 would post-date M1, but pre-date the formation of M2. Similarly, the base of the limnic deposits in B2 would post-date both M2 and M3, and the basal sediments in B1. The complete stratigraphic record would therefore consist of morphostratigraphic unit (m.u.) M1 > (= older than) B1 base > m.u. M2 > m.u. M3 > B2 base > m.u. M4. Alternatively, all of the ridges might have formed in a very short period of time and hence the accumulation of the basal lake sediments in both B1 and B2 post-dates the entire morphostratigraphic sequence. Only the application of other methods (e.g. biostratigraphic analysis, radiometric dating) can resolve such an issue.

6.2.3.4 Soil stratigraphy

Palaeosols (section 3.5) occur in many Quaternary sediment sequences. Well-developed palaeosols that evolved during a specific soil-forming interval and which possess sufficiently distinctive characteristics to enable them to be traced over a wide area can be considered as **soil-stratigraphic units**. A soil-stratigraphic unit was initially defined by the American Commission on Stratigraphic Nomenclature (1961, p. 654) as ‘a soil with physical features and stratigraphic relations that permit its consistent recognition and mapping as a stratigraphic unit’. A better term than ‘physical’ might be ‘pedological’, since soils are now identified and categorized on the basis of a range of properties, including chemical, magnetic and micro-morphological characteristics. The North American Commission on Stratigraphic Nomenclature (1983) subsequently introduced the term **pedostratigraphic unit** to describe ‘a buried, three-dimensional body of rock that consists of one or more differentiated pedologic horizons’ (p. 864), and has recommended that the term ‘**geosol**’ replace the term ‘soil’ in stratigraphic usage. Here, however, we retain the terms ‘palaeosol’ and ‘soil-stratigraphic unit’ to refer, respectively, to fossil soils and to the stratigraphic units that they represent, since these terms are still the most widely employed in the Quaternary literature.

Soil-forming processes will begin to operate in most areas immediately after surfaces become exposed to the atmosphere. The subsequent degree of pedogenesis will depend, however, on a range of site and climatic factors, as well as on regional history, which includes length of exposure of the land surface. In many regions, the typical soil features of horizonation may not be present, while in other situations, distinct and clearly demarcated horizons

will develop. Many soils are polygenetic, such as the Valley Farm Soil (Figure 3.24b) of East Anglia and south-east England (Kemp *et al.*, 1993). This particular soil is rubified (displays a characteristic reddening) and mottled with a high translocated clay content. It is a complex soil-stratigraphic unit with evidence for several episodes of soil development spanning a number of warm and cold intervals over a period (at its fullest development) of more than one million years. In the North American Midwest, the Sangamon Geosol, which can be differentiated from the modern soil by virtue of a greater mineral alteration, a thicker solum, a redder colour under oxidized conditions and deeper carbonate leaching, is also polygenetic and appears to have formed over a period of around 100 ka between MIS 5 and 3, during which time the climate shifted from cold to warm to cold again (Hall & Anderson, 2000; Grimley *et al.*, 2003). The stratigraphic importance of such soil-stratigraphic units is that they provide clear evidence for a major hiatus in the lithostratigraphic record. In addition, because the soils are very distinctive, they constitute key stratigraphic markers, and may be used as a basis for correlation between individual sequences (see below).

Where sedimentation is episodic, pedogenesis will occur during intervening periods of landscape stability and hence, over time, sequences of soils may form (Kemp, 2001). This is most clearly demonstrated in the loess regions of the world, where numerous soil-stratigraphic units are found interbedded with suites of aeolian sediment, for example in South America (Kemp *et al.*, 2006), North America (Jacobs & Mason, 2007) and parts of eastern Europe (Marković *et al.*, 2007). The best known and most widely studied, however, are the long loess–palaeosol sequences that have developed on the Loess Plateau in China (section 3.6.2). In the 160 m Baoji loess section in the southern part of the Plateau, for example, up to thirty-seven separate palaeosols have been identified, the lowermost of which has been dated to around 2.5 Ma (Rutter & Ding, 1993). The palaeosols have formed through a combination of carbonate eluviation and illuviation, clay translocation, pseudogleization and rubification. Most display Bt horizons that have developed in forest and/or steppe-forest environments. This sequence, like those elsewhere in China, reflects a long history of loess deposition with intermittent episodes of stability during which vegetation became established and soils formed.

6.2.3.5 Oxygen isotope stratigraphy

It has already been shown that, in the deep oceans of the world, long sequences of relatively undisturbed sediments

are preserved that may extend back to the beginning of the Quaternary and, indeed, into the Tertiary. The microfauna and microflora within these sediments contain a record of changing oxygen isotope ratios that not only provides evidence for former glacial and interglacial oscillations (section 3.10), but which also forms a basis for stratigraphic subdivision and long-distance correlation. It must be appreciated, however, that marine oxygen isotope profiles are not appropriate for *high-resolution* stratigraphic subdivision, as the slow mixing of the deep oceans means that asynchronous changes are impossible to detect, and thus at the centennial scale, the underlying concept of the oxygen isotope stratigraphic scheme becomes meaningless (Shackleton, 2006). In other, better resolved sequences, however, such as ice cores, speleothems and tree-ring series, oxygen isotope profiles can provide a basis for subdivision at the centennial and, in some instances, at the decadal scale.

As noted in sections 1.6 and 3.10.2, oxygen isotope profiles from deep-ocean cores can be divided into marine isotope stages (MIS), and these stages and substages are fundamental units in Quaternary stratigraphy. Recall that those parts of the marine isotope curve interpreted as representing warm stages (lighter $\delta^{18}\text{O}$ values) are assigned odd numbers, and the cold stages (heavier $\delta^{18}\text{O}$ values) even numbers. MIS 1 represents the Holocene period, and higher numbers indicate successively older cold and warm stages. The allocation of stage numbers is therefore a ‘count from the top’ division of a sinusoidal curve, the underlying assumptions being (1) that inflections in the curve reflect changes in global ice volume and deep-ocean temperature (Shackleton, 2000); and (2) that no major interruption in sedimentation has occurred. Twenty MISs can be recognized in the ocean sediment record of the last 800 ka or so (Figure 6.6a), which implies that ten interglacials (or near interglacials) and ten glacial episodes have occurred during that time interval. The record of isotopic stages formally designated in Quaternary deep-ocean cores extends back to MIS 103 at *c.* 2.6 Ma (Figures 1.5 and 1.6). These stages can be dated by reference to the palaeomagnetic timescale (Figure 5.34) with the Brunhes–Matuyama boundary located in MIS 19, the reversal marking the onset of the Olduvai chron at the base of MIS 63, and the Gauss–Matuyama boundary in MIS 104. This MIS subdivision has now been continued back to 5.3 Ma (Lisiecki & Raymo, 2005), but in the Pliocene record, the isotopic stage prefixes are designated by the geomagnetic subchron in which they are found. Hence in the early Gauss polarity epoch, the warm stages are numbered G-1 to G-21, while in the earlier part of the Gauss, through the Kaena and Mammoth polarity events,

the isotopic stages are designated by the prefixes K-, KM-, M- and MG-, respectively. The deep-sea isotopic signal is geographically consistent, and can be replicated in cores from different oceanic areas, thus emphasizing the fact that the oxygen isotope signal provides a proxy climatic record of global significance (see section 6.3.2.7).

In the main, the isotopic stage numbers equate with conventional glacial and interglacial episodes inferred from the terrestrial Quaternary stratigraphic record, although MIS 3 is anomalous, for while it is recognized as a ‘warm’ stage, it is regarded only as a period of interstadial status. It should also be noted that the later ‘interglacial’ stages have been subdivided into separate warmer and colder episodes. MIS 5, for example, contains five substages, with 5a, 5c and 5e interpreted as warmer phases while 5b and 5d reflect colder intervals. The last (Eemian, Ipswichian, Sangamonian) interglacial (as defined on land) is represented in the isotope record by substage 5e. An alternative approach to substage notation is to employ a decimal system in which negative (warm) and positive (cold) excursions are given odd and even numbers, respectively (Figure 6.6b). In this scheme, first applied in the SPECMAP timescale (section 5.5.3), the warmer substages in MIS 5 that were previously referred to as 5a, 5c and 5e, are designated 5.1, 5.3 and 5.5 (last interglacial); the colder substages (5b and 5d) are numbered 5.2 and 5.4. The three warmer intervals of MIS 7 are designated 7.1, 7.3 and 7.5, with the intervening colder phases denoted as 7.2 and 7.4. In the case of MIS 7, however, there is some uncertainty over which of the warmer intervals represents the penultimate interglacial (*sensu stricto*), for the warmest climate signal registers in MIS 7.5 in Antarctic ice cores (Masson-Delmotte *et al.*, 2010), in MIS 7.3 in pollen and benthic foraminiferal data (Desprat *et al.*, 2006) and in MIS 7.1 in some cave speleothem stable isotope records (Spötl *et al.*, 2008). The boundaries between the major isotopic stages are indicated by integers: hence the boundary between MIS 5 and MIS 6 is designated as 6.0, while that between MIS 7 and MIS 8 is 8.0. A similar numerical notation has subsequently been applied to older parts of the marine oxygen isotope record. The rationale underlying this approach is that the exact stratigraphic level of a peak or trough in the isotope curve can be defined unambiguously in one curve and correlated with the same level in another.

As noted above (section 3.10.3) a distinctive feature of most deep-ocean oxygen isotope profiles is the ‘saw-tooth’ appearance of the curves (Figures 1.5 and 6.6), with the most rapid isotopic changes occurring at the end of glacial episodes. These seemingly rapid changes from inferred glacial to interglacial conditions have been referred to as

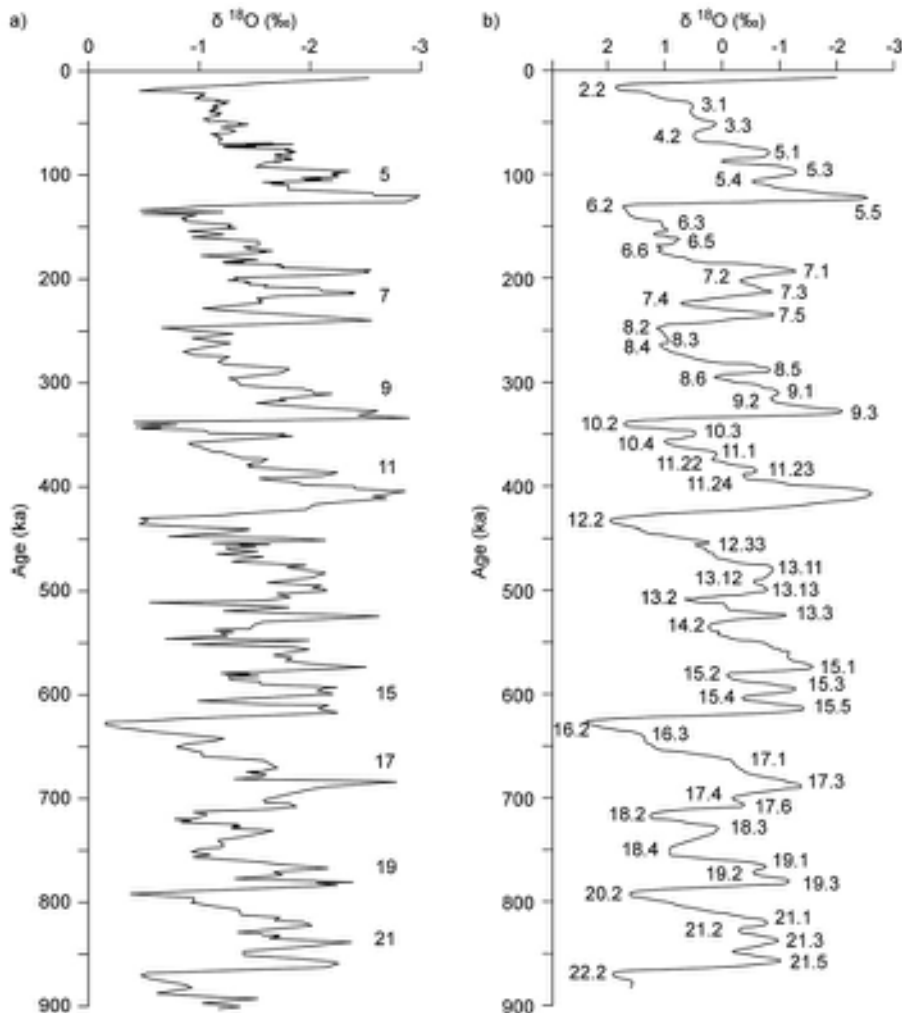


Figure 6.6 a) Oxygen isotope stratigraphy in a 53 m core (core MD900963) obtained from a water depth of 2,446 m in the Indian Ocean to the east of the Maldives Platform. The record spans c. 900 ka and extends back to MIS 22; prominent interglacial stages are numbered. b) A stacked record of Core MD900963 and ODP core 677 from the eastern equatorial Pacific, which has been tuned to a model of changes in global ice volume. The isotopic stages are designated using the decimal MIS notation, as explained in the text (based on Bassinot *et al.*, 1994).

terminations and constitute major **events** (section 6.3.2.7) in the isotope stratigraphy (Cheng *et al.*, 2009). As with the isotopic stages, the terminations have been numbered from the top down. Hence Termination I refers to the sudden relative decrease in ^{18}O content of the world's oceans at the end of the last glacial stage (MIS 2). However, as MIS 3 is not considered to be a warm interval of full interglacial rank, Termination II marks the transition from MIS 6 to MIS 5, and not from MIS 3 to MIS 2. The most recent termination

has been subdivided into Termination Ia (dated mid-point 15 ka BP) and Termination Ib (dated mid-point 10.5 ka BP), and these constitute key marker horizons in the oceanic isotopic record at the end of the last cold stage. These terminations are also evident in proxy records from terrestrial contexts (Figure 6.7), and therefore provide a basis for land–ocean correlations (see below). We return to the importance of terminations in the Quaternary record in Chapter 7.

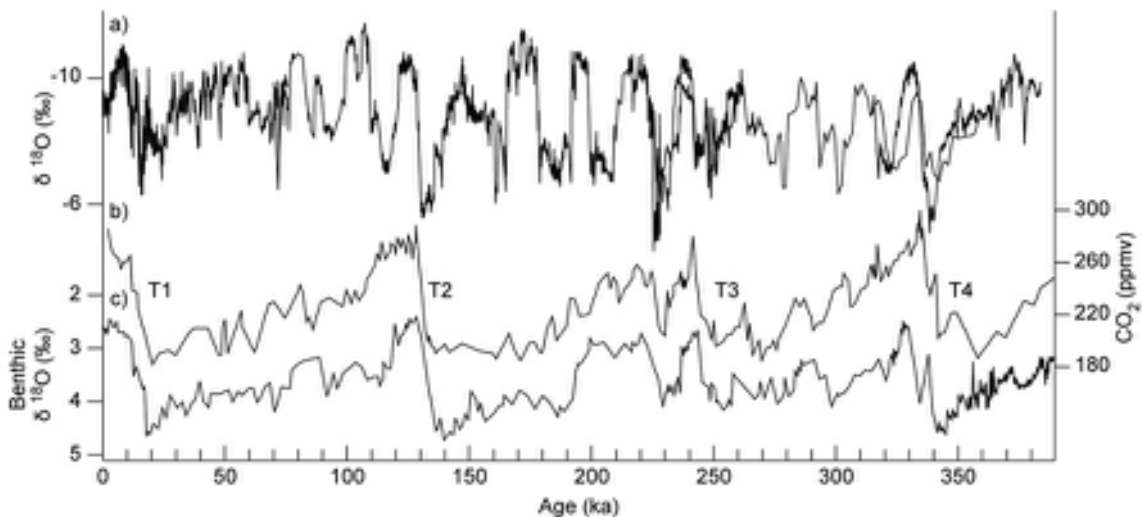


Figure 6.7 The last four terminations in different proxy records. a) Composite $\delta^{18}\text{O}$ profile from speleothem carbonate from four caves (Hulu, Dongge, Linzhu, Sanbao) in China. b) Vostok CO_2 record from Antarctica. c) Benthic $\delta^{18}\text{O}$ values from marine core ODP 980 from the North Atlantic (after Cheng *et al.*, 2009).

6.2.3.6 Climatostratigraphy

A universally employed basis for the subdivision of the Quaternary is climatic change, for the characteristics of the stratigraphic record that are distinctive, and therefore used in the identification of stratigraphic units, frequently reflect processes driven by former climatic conditions. This was recognized half a century ago by the American Commission on Stratigraphic Nomenclature (1961, 1970) who proposed a stratigraphical subdivision termed a **geologic-climatic unit**, which was ‘an inferred widespread climatic episode defined from a subdivision of Quaternary rocks’ (1970, p. 31). In areas affected by Quaternary glaciation, *glacials* and *interglacials* constitute the principal geologic-climatic units, while *stadials* and *interstadials* form units of lesser rank. In areas not affected by glacier ice, it was anticipated that other geologic-climatic units, such as *pluvials* and *interpluvials*, would form units of equivalent status.

Geologic-climatic units are undoubtedly useful concepts and, insofar as the Quaternary sequence in mid- and high latitudes is usually subdivided into *glacials* and *interglacials* (section 1.6), they form the basis for stratigraphic subdivision at the regional and continental scales. However, because climatic change is time-transgressive, the boundaries of geologic-climatic units are diachronous. Strictly speaking, therefore, it is not appropriate to use geologic-climatic terms (*glacial*, *interglacial*, etc.) and chronostratigraphic terms (*stage*, *substage*) interchange-

ably, although in practice this is often done. In a formerly glaciated region, for example, the stratigraphic record of the presence of ice may comprise only sediments that were deposited during deglaciation (Figure 6.8). Hence the time interval reflected in the stratigraphic record by a suite of glaciogenic sediments (which comprise the geologic-climatic unit) represents only a small part of the glacial or cold stage. At other sites, a more protracted period of glacial sedimentation may be preserved, but again this may only have occurred during a limited part of the glacial stage. Hence the duration of the latter will have to be inferred from other lines of evidence, such as the biostratigraphic record in lake sediment sequences. Here, the suite of minerogenic sediments containing that record (the geologic-climatic unit) may span the entire cold stage. Reconciling diachronous climatic signals, which may have contrasting expressions in different geologic units, is therefore a major difficulty in climatostratigraphy.

The fundamental problem, of course, is that it is not climate that is directly recorded in the stratigraphic record, but *manifestations* of climate, namely the results of climatic influences on, for example, biota, soils, sediments and glaciers. Climatic reconstructions are, therefore, two steps removed from the observable data, and at each stage in the analysis, interpretation is required. If, for example, pollen assemblage zones are being used as the basis for geologic-climatic units, the first step is to infer vegetational communities and patterns of vegetational change from

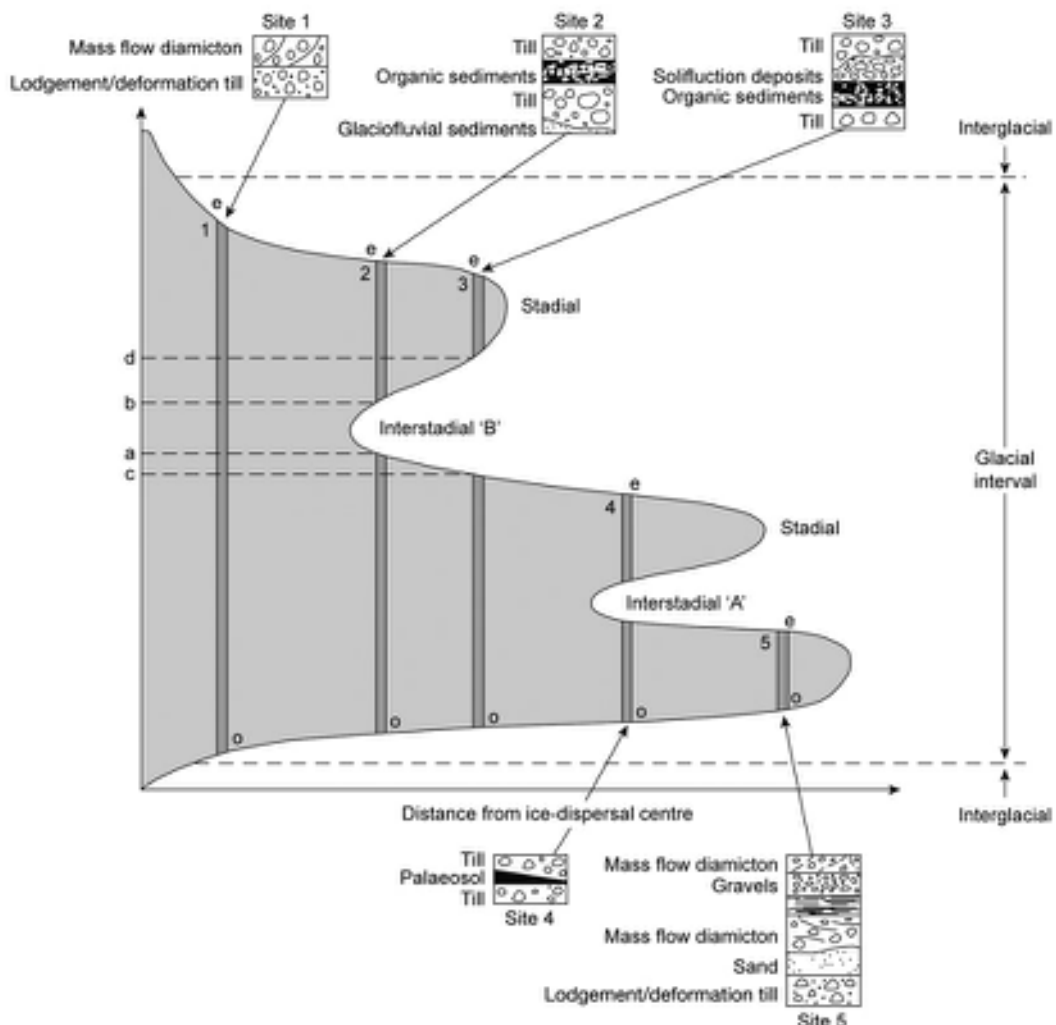


Figure 6.8 A time–distance diagram showing the onset (o) and end (e) of glaciation at sites at increasing distance from the ice-dispersal centre. Time is shown schematically on the y axis and distance on the x axis. Possible glaciogenic sequences and relative sediment thickness at each site are also indicated. For further explanation see text.

the pollen record, and the second is to use these reconstructions to infer climatic changes. Inferences are therefore being made which are themselves based on inferences; errors can enter into both stages of the analysis, but those resulting from the first will be compounded in the second. These complications will arise irrespective of the form of lithostratigraphic or biostratigraphic evidence that is being employed.

The American Stratigraphic Commissions (1961, 1970) originally intended the boundaries of geologic-climatic units to follow the boundaries of the rock or biostrati-

graphic unit that formed the basis for their definition. This may be relatively straightforward when dealing with pre-Quaternary successions where, because of the long time intervals and low temporal resolutions involved, climatic change appears in the geological record to have been virtually instantaneous. In the Quaternary, however, where temporal resolution of stratigraphic sequences is usually so much greater, geological boundaries based on evidence of climatic change are much more difficult to locate, and correlation based on these boundaries is more problematical. Consider, for example, Figure 6.9 which

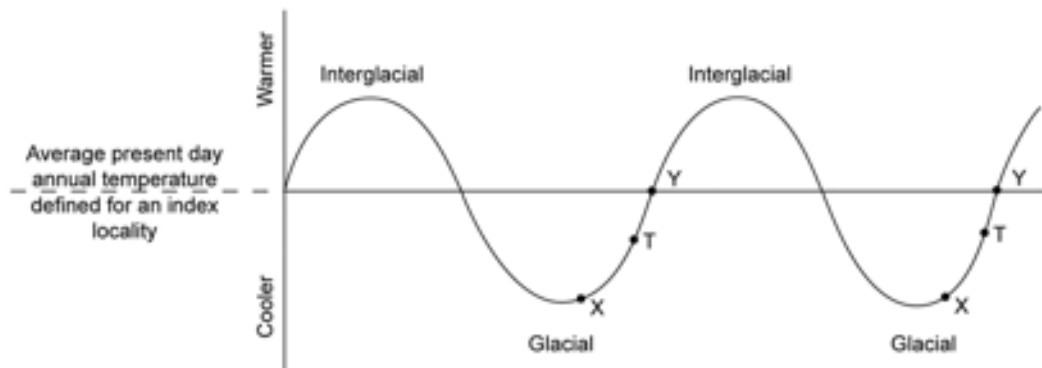


Figure 6.9 Different ways of defining the onset of an interglacial. The curve is schematic and represents temperature oscillations between interglacial and glacial cycles. The three possible points of onset for an interglacial are explained in the text.

shows temperature change through a glacial–interglacial cycle and represents, in a schematic way, one of the climatic cycles reflected in the oxygen isotope signal (Figure 6.6). Where on the curve does the geologic-climatic unit of the interglacial begin? It could be argued that the boundary should be placed at that point on the curve where temperature increases following a thermal minimum (point X). Alternatively, the boundary could be located where a temperature similar to that of today is achieved (point Y). A third view would be to place the boundary at a point where a particular temperature threshold is crossed (point T) as indicated, for example, by the first occurrence of a certain indicator species in the fossil record. The problem, of course, is that we are attempting to fix a point boundary on what is a continuum of climatic change. Any of the above could be used as a basis for defining the onset of an interglacial but, because of the diachronous nature of climatic change, it is unlikely that an interglacial established in one region will be a temporally equivalent geologic-climatic unit to that in another. Similar problems are encountered in determining the end of an interglacial. Moreover, the extent to which climatic episodes will be represented in the stratigraphic record will depend both on the amplitude and duration of climatic shifts, and also on the sensitivity of the proxy evidence upon which climatic inferences are based.

Further complications arise when different types of evidence are being employed in environmental reconstruction. In Figure 6.10, a transgressive sequence of marine sediments has been divided on the basis of different lithostratigraphic and biostratigraphic criteria. Each particular line of evidence may define a different geologic-climatic unit, however. On the basis of the molluscan records, for example, the boundary between warm and cold

climatic conditions may be placed between assemblage zones 1 and 2; the pollen data might indicate a climatic change between pollen zones 4 and 5, while the boundary between cold and temperate Coleoptera may occur between assemblage zones a and b. These contrasts reflect different response rates of biota to climatic change and also, insofar as the taxa are derived from both marine and terrestrial environments, time delay between atmospheric and oceanic temperature changes. Within a single sequence, therefore, the boundary of a geologic-climatic unit could be placed at any one of several levels. Once again, the problems that this can pose for inter-regional comparisons and correlations are clear.

The designation of geologic-climatic units is therefore frequently intuitive, often arbitrary, and much less precise than other forms of stratigraphic subdivision. Indeed, this was recognized in a subsequent code of practice produced by the North American Commission on Stratigraphic Nomenclature (1983), where the concept of geological climatic units was abandoned because ‘inferences regarding climate are subjective and too tenuous a basis for the definition of formal geologic units’ (p. 849). That stance is unhelpful to the Quaternary researcher, however, since repeated climatic change is undoubtedly the dominant characteristic of the Quaternary, and it is difficult to envisage a stratigraphic scheme that does not explicitly acknowledge this fact. For example, in the marine oxygen isotope record discussed in the preceding section, the isotopic signal mainly reflects fluctuations in global ice volume (section 3.10.2) and these, in turn, are driven principally by changes in climate. In essence, therefore, the subdivision of the marine record into distinct isotope stages is a climatostratigraphic scheme. Hence, despite the problems surrounding definition and application, geologic-

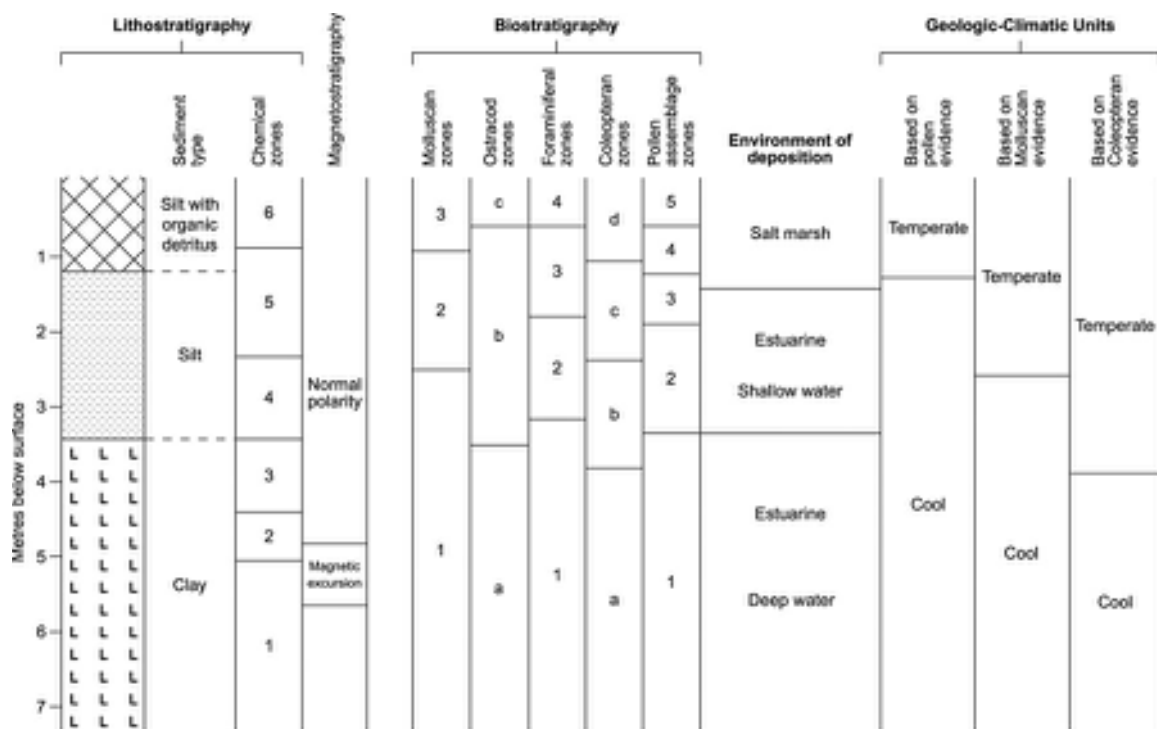


Figure 6.10 Stratigraphic subdivision of a Quaternary sedimentary sequence based on different criteria and the geologic-climatic units that can be inferred.

climatic units seem destined to remain an integral and necessary tool in Quaternary stratigraphy.

6.2.3.7 Chronostratigraphy

Chronostratigraphy is the classification of the stratigraphic record in terms of time. Once stratigraphic units have been established on the basis of visible, instrumental, biological or inferred climatic characteristics, and a relative chronology determined by superposition and correlation, it is important (wherever possible) to relate the sequence of events preserved in the rock-stratigraphic record to time. The purpose of chronostratigraphy is to divide sequences of strata into **chronostratigraphic units** that correspond to intervals of geological time. Such units are bounded by isochronous surfaces or **chronohorizons**. Chronostratigraphic units can be defined on the basis of geological age, where this can be established, or in terms of time intervals between isochronous horizons. In other words, where chronostratigraphic comparisons are being effected between sites, reference can be made to the time period encompassed by two designated stratigraphic

horizons, even where the age of each horizon is unknown and many of the rocks are missing. For example, reference can be made to the time interval between two biozones or two lithological boundaries. If these boundaries prove to be time-parallel, they can be employed as chronostratigraphic boundaries, and the biozone or lithofacies or, indeed, any other stratigraphic unit, can be considered as a chronostratigraphic unit. Chronostratigraphy, like clinostratigraphy, is inferential, since it is not based in the first instance on the characteristics of the sediment record (Salvador, 1994).

The division of the stratigraphic record on the basis of time is termed **geochronology**. As explained in section 1.3, chronostratigraphic units represent a time period between boundaries and, where the actual ages of such boundaries are known, the interval of time itself is referred to as a **geochronological unit**. It is worth re-emphasizing the distinction between a *chronostratigraphic unit* and a *geochronological unit* since the two are frequently confused (Table 6.2). The term ‘*chronostratigraphic unit*’ refers to the rock sequence laid down during a particular time interval. Hence the term ‘Quaternary system’ is used to

Table 6.2 Conventional hierarchy of chronostratigraphic and geochronological units (after Hedberg, 1976).

Chronostratigraphic	Geochronological	Examples
Eonothem	Eon	Phanerozoic
Erathem	Era	Cenozoic
System	Period	Quaternary
Series	Epoch	Pleistocene
Stage	Age	Devensian
Chronozone	Chron	Younger Dryas

describe the rocks and sediments that have accumulated over a time range that is called the Quaternary. The geochronological equivalent (**geochronological unit**), that is, the time interval itself, is referred to as the ‘Quaternary period’. The same applies to the Holocene ‘series’ (chronostratigraphy) and Holocene ‘epoch’ (geochronology). It has been suggested, however, that this distinction in stratigraphic terminology between time-rock units (chronostratigraphy) and geologic time units (geochronology) should now be abandoned, and that the term ‘chronostratigraphy’ should, henceforth, be the term used to define intervals of geologic time within rock strata. As a consequence, ‘geochronology’ would revert to its original meaning of numerical age dating (Zalasiewicz *et al.*, 2004). Under this scheme, the terms ‘eonothem’, ‘erathem’, ‘system’, ‘series’ and ‘stage’ (Table 6.2) would become redundant in favour of ‘eon’, ‘era’, ‘period’, ‘epoch’ and ‘age’. Whether this proposal, which represents a fundamental change to the traditional time-stratigraphic subdivision of the geological record, will prove to be acceptable to the wider community remains to be seen.

The foregoing notwithstanding, the current basic working units in Quaternary stratigraphy are **stages**. Conventional stages in pre-Quaternary time typically range from 3–10 million years, but in the Quaternary, stages are measured in tens of thousands of years. Stages can be divided into smaller units or substages as, for example, in the marine oxygen isotope record (section 6.3.2.7). The basic chronostratigraphic unit is the **chronozone**, the timespan of which is usually defined in terms of the timespan of a previously designated stratigraphic unit such as a formation, or a member, or a biozone. Chronozones have been most widely employed in Quaternary research where biozones have been dated by radiometric methods, for example radiocarbon-dated pollen assemblage zones (section 4.2.4).

The division of Quaternary strata into chronostratigraphic units is seldom straightforward, however, and here again problems arise that are not encountered in the earlier geological record. In the main, these result from the

comparatively short timespan of the Quaternary, and from the fact that the relatively fine divisions of the Quaternary stratigraphic sequence are of equal importance to the much coarser subdivisions of the earlier geological record. Only a relatively small number of geochronological methods cover the whole of Quaternary time (Chapter 5), while dating aberrations are likely to pose particular problems in Quaternary research because of the more limited time range involved. Moreover, if the statistical uncertainty associated with the dates (i.e. the quoted \pm value) is as great as or greater than the stratigraphic intervals that are under examination, then clearly these age determinations are insufficiently precise either to define the boundaries of such units, or to distinguish subdivisions within those units. A further difficulty arises over the recognition of isochronous horizons in the stratigraphic record. As we have already explained, in pre-Quaternary strata, lithostratigraphic and biostratigraphic boundaries, although inherently time-transgressive, appear to be synchronous when set against the vast span of geological time. As such, they are frequently used as time-stratigraphic markers. In the Quaternary stratigraphic record, by contrast, most boundaries are manifestly time-transgressive, particularly biozones whose boundaries reflect biological response to climatic change which is spatially and temporally diachronous (Walker, 1995). Nevertheless, some Quaternary stratigraphic units or boundaries do provide a basis for time-stratigraphic correlation, and it is to these that we now turn our attention.

6.3 TIME-STRATIGRAPHIC CORRELATION

6.3.1 Principles of Quaternary correlation

The stratigraphic methods outlined above all provide a basis for **correlation**; in other words, the relationship of stratigraphic sequences or events at one locality to those at another. Throughout most of the geological column, lithostratigraphic and biostratigraphic boundaries are, at the level of resolution applied, effectively time-parallel, and

are therefore regarded as being almost of equivalent status to chronostratigraphic units in time-stratigraphic subdivision and subsequent correlation. This assumption cannot be made in the correlation of Quaternary successions, however, except perhaps at the local scale. Not only are stratigraphic boundaries time-transgressive (see above), but the repetitive nature of Quaternary climatic change means that at any given locality, similar depositional sequences may be preserved that are of markedly different age. In view of the fragmented and highly diverse nature of the Quaternary stratigraphic record, effecting meaningful correlations between often widely separated sites is therefore seldom straightforward.

Some of the difficulties that can arise in the correlation of Quaternary sequences are exemplified by Figure 6.8 which shows, in a diagrammatic way, the extent of glaciation over time, the shaded area representing the time period during which ice covered the ground at increasing distance from an ice-dispersal centre. Site 1 was affected by glacier ice for almost the whole of the 'glacial' time interval; sites 2 and 3 were occupied by ice for a shorter period, while site 4, and especially site 5, were ice-covered for only a small proportion of the glacial episode. Sites 2, 3 and 4 also experienced interstadial conditions between successive glacial advances. At each site, the environmental history is recorded in sequences of glaciogenic sediments, interbedded at sites 2, 3 and 4, with organic deposits (peat or soil).

At site 1, which for much of the glacial interval lay some distance up-glacier, erosion probably dominated and the only record of glacier activity is a thin layer of lodgement till deposited during glacier wastage. By contrast, a complex sequence of glaciogenic sediments accumulated at site 5 near the ice margin. There are two points to note here: first, the thickest and most complex sequence of sediments is preserved at the site that was covered by glacier ice for the shortest length of time; and second, although the glacier reached site 1 before site 5, on a time-stratigraphic basis, the deposits that are actually *preserved* at site 1 may, in fact, be *younger* than those at site 5. At sites 2, 3 and 4, two till units occur, but from the stratigraphic evidence alone, it is far from clear which till unit is the correlative of the glaciogenic sequence recorded at site 5. Moreover, because sites 2, 3 and 4 have experienced two periods of glaciation separated by an interstadial interval, almost identical stratigraphic sequences (till–organic sediments–till) have developed. In the absence of other evidence, correlation might therefore be unwittingly effected between these sequences. Yet, as the diagram shows, the sequence of deposits at site 4 relates to an earlier period of time and to a stadial–interstadial oscillation which is different from that at sites 2 and 3. Where units of similar composition and

mode of origin, but of very different ages, are incorrectly correlated, such errors of correspondence are referred to as **homotaxial errors**.

This type of error can also arise in biostratigraphy. It is entirely possible, indeed likely, that a very similar environment existed during both interstadials A and B, and this would be reflected in the fossil evidence preserved in the organic horizons at sites 2, 3 and 4. Again, the inference of a single interstadial based on the pollen evidence from the three sites would be homotaxially incorrect. Finally, the diagram illustrates the time-transgressive nature not only of the lithostratigraphic and biostratigraphic units, but also of the geologic-climatic units. At site 2, the geologic-climatic unit (interstadial) inferred from the fossil content of the organic deposit spans the time interval a–b, while at site 3, the same interstadial covers the time interval c–d.

These complications arise partly because the deposits of varying ages are not arranged vertically in order of superposition, and partly because lateral correlation often has to be made between numerous short-lived depositional records. The above example relates to a single glacial interval, yet when it is recalled that at least twenty glacial–interglacial cycles affected the mid- and high-latitude regions of the world during the last 800 ka alone, the scale of the problem begins to emerge. Moreover, it is not only in formerly glaciated areas that difficulties are encountered. Repeated climatic changes had a profound effect on those regions that lay beyond the margins of the ice sheets, and there too the complicated erosional and depositional history of the Quaternary presents the stratigrapher with major problems of correlation. Clearly, therefore, at the regional and continental scales, lithostratigraphy, biostratigraphy and climatostratigraphy are not sufficiently sensitive tools with which to effect meaningful time-stratigraphic correlations. A geochronological basis is required, although as yet no single radiometric dating method has been developed that is applicable to the whole of the Quaternary period at the required level of temporal resolution. There are, however, a number of ways in which sequences may be correlated on a time-stratigraphic basis, and some of these are examined in the following section.

6.3.2 Bases for time-stratigraphic correlation

6.3.2.1 Palaeomagnetic correlation

Magnetostratigraphy utilizes stratigraphical variations in the magnetic properties of rocks as a basis for geological correlation. The palaeomagnetic record can be divided into **magnetozones** (units of rock with a specific magnetic

signature), the boundaries of which reflect abrupt changes in the earth's magnetic field (see section 5.5.1), and are therefore clearly defined. Because these changes are experienced globally, geomagnetic reversals and prominent excursions provide a basis for correlating Quaternary events at the global scale. Palaeomagnetic stratigraphy has also been employed to correlate marine, terrestrial and, in some cases, ice-core records (see below). On the other hand, the method is restricted to certain rock types (e.g. volcanic rocks) and specific depositional environments (such as lake sites or aeolian contexts), while the timing of some palaeomagnetic events remains to be established and the temporal precision, particularly of older geomagnetic boundaries, is relatively low. At the regional scale, **secular magnetic variations** (section 5.5.1.2) can be used as a basis for correlation between lake sequences, the distinctive inflections or turning points in the magnetic field measurements providing a basis for correlation between different sedimentary records (Snowball *et al.*, 2007). Thus far, however, this aspect of palaeomagnetic correlation has been applied routinely only to Holocene lake deposits.

6.3.2.2 Correlation using tephra layers

Tephra layers (section 5.5.2) constitute marker horizons in the stratigraphic record that are essentially isochronous, and hence have the potential to serve as the basis for time-stratigraphic correlation between sediments formed on land, in lakes and on the seabed, and between these sequences and polar ice. Although correlation on the basis of tephra deposits is not as universally applicable as that based on palaeomagnetism (e.g. the Brunhes–Matuyama boundary), because individual ash beds have relatively limited geographical ranges, **tephrochronology** (the dating and correlation of deposits based on distinctive tephra horizons) is proving to be an increasingly powerful correlative tool at the regional or sub-hemispherical scales. Examples of the use of tephrochronology in different depositional contexts are discussed in section 5.5.2.3.

6.3.2.3 Correlation using palaeosols

Palaeosols (section 3.5) have been perhaps most widely employed as a correlative tool in North America where it has traditionally been assumed that pedogenesis during interglacials and certain interstadials alternated with periods of negligible profile development or arctic soil formation in the intervening cold phases. Hence well-developed buried soils (such as the Sangamon Soil of the American Midwest) have been considered to constitute stratigraphic

marker horizons and have been used for both local and long-distance time-stratigraphic correlation. Subsequently, however, a more cautious approach has been adopted to the use of buried palaeosols in stratigraphy and correlation, for it is now recognized that degree of soil development as a direct function of time can only be assumed where other soil-forming factors (parent material, climate, slope and biological factors) can be shown to have been constant (section 5.6.5.2). Moreover, insofar as most soils are polygenetic, any buried profile may be the product of more than one phase of pedogenesis. Indeed, the Sangamon Soil of North America, hitherto widely considered to be of last interglacial age, appears to have formed over a period of up to 50 ka (MIS 5–3) during which time the climate shifted from cold to warm and back to cold again (Hall & Anderson, 2000).

Despite these limitations, however, palaeosols have been used successfully in the development of both local histories and wider correlative schemes. In northern France and the American Midwest, fossil soils of Late Pleistocene age constitute key correlative elements in the stratigraphic record (Antoine *et al.*, 2003; Rutter *et al.*, 2006). A particularly useful example in the latter region is the Farmdale Geosol of Illinois, which is radiocarbon dated to 28–25 ka and which forms an important stratigraphic marker for correlating Late Wisconsinan events at both local and regional scales (Jacobs *et al.*, 2009). In areas of the world where palaeosols are found in loess sequences, such as those on the Chinese loess plateau, soil-stratigraphic units provide a basis for correlation between different loess profiles (Bronger, 2003) and also, in a much wider context, between loess–palaeosol sequences, global ice volume cycles and the marine oxygen isotope record (Dearing *et al.*, 2001)

6.3.2.4 Shoreline correlation

Marine shorelines and deposits may also, in certain contexts, provide a basis for time-stratigraphic correlation. If world sea levels are stable for long enough to allow the development of shoreline features, then these essentially isochronous reference surfaces potentially offer a basis for inter-regional correlation. Isochronous shorelines can often be traced around a coastline, even in regions affected by glacial isostasy or tectonic uplift (Fjeldskaar *et al.*, 2000). If the shoreline cuts certain sedimentary units, but is overlain by others, then the shoreline can be used as a time-stratigraphic reference plane for separating deposits of different age. Sedimentary units formed as a result of catastrophic marine events, such as tsunamis, also constitute

marker horizons for correlating between marine and terrestrial sequences (Smith *et al.*, 2004). At the broader scale, evidence of former sea levels (raised beaches and corals, submerged corals, submerged clifflines, etc.) may provide a basis both for inter-regional correlation, and also for linking terrestrial and deep-sea records (Hearty & Kaufman, 2000). However, problems can arise from complexities in the coastal records induced by variations in amounts and rates of local tectonic activity (Marquardt *et al.*, 2004), and perhaps also from the phenomenon of geoidal eustasy (section 2.5).

In addition to marine shorelines and deposits, lake shorelines can also provide timelines for correlating between, and establishing the order of superposition of, local geological features (Orme & Orme, 2008). Moreover, as some lake shorelines reflect climatically driven fluctuations in lake-water level (section 3.7.3), they provide a basis for correlating climatic events in terrestrial and marine records (Benson *et al.*, 1998).

6.3.2.5 Correlation on the basis of radiometric dating

These methods, which were considered in section 5.3, are an extremely important independent means of long-distance correlation, for they form time-planes across the stratigraphic record against which the time-transgressive litho-, bio- and morphostratigraphic boundaries can be measured. There is, however, a substantial body of opinion in support of the view that the subdivision of the Quaternary should rest primarily on the stratigraphic record, with radiometric dates being merely a means whereby that record can be underpinned. Certainly, any date applies only to the locality and to the horizon from which it was obtained, and it can only be related to other sequences on the basis of the observed stratigraphic record at the different localities. As has already been shown, no radiometric date is free from analytical errors and, in some cases, the error (\pm) associated with the age determination may be so great that the date cannot be used effectively in time-stratigraphic correlation. Equally, all dated samples are prone to errors of contamination, some of which may go undetected. Each date should not only be carefully checked against other age determinations, therefore, but must be thoroughly evaluated in the light of its stratigraphic context before it is used as an aid in correlation. Overall, radiometric dating is perhaps best regarded as a means of corroborating and validating other stratigraphic and correlative procedures, rather than as the primary basis for time-stratigraphic correlation.

6.3.2.6 Event stratigraphy and correlation

Events may be broadly defined as comparatively rare and geologically short-lived occurrences that have left some trace in the rock records. The stratigraphic signatures of these sudden events are effectively isochronous markers, and hence constitute a tool for correlating geological sequences. This is the basis of what has been termed **event stratigraphy** or **event chronostratigraphy** (Gale, 2009). The products of some events (tephra from volcanic eruptions; tsunami deposits in marine sequences) have already been discussed, but others might include the geological manifestations of storms, floods, earthquakes, mass movement and turbidity flows, although clearly not all of these will be sufficiently widespread to constitute a basis for inter-regional correlation. Other event products, however, such as the layers of carbonate-rich debris in North Atlantic Ocean sediments formed during major ice-raftering events ('Heinrich events'; section 3.10.1) of the last cold stage, offer a means both for inter-core correlation, and also for linking oceanic and terrestrial sequences (Hemming, 2004). Other characteristics of the geological record that reflect widespread and large-magnitude events may also offer a basis for broader time-stratigraphic correlation. These include palaeomagnetic changes preserved in Quaternary sediments (see sections 6.3.2.1 and 5.5.1), and a range of geochemical indices, including stable isotopes of oxygen, carbon, sulphur and strontium, that form stratigraphic markers. For example, an event stratigraphy has been proposed for the Last Termination in the North Atlantic region based on the oxygen isotope signal in Greenland ice cores (Björck *et al.*, 1998; Lowe *et al.*, 2008b; section 6.3.3), while a pollen-based event stratigraphy for the same time interval has been developed for the Lake Suigetsu sequence in Japan (Nakagawa *et al.*, 2005). An unusual type of event stratigraphy has involved the use of the 'plateaux' in atmospheric ^{14}C activity during the Lateglacial and early Holocene (section 5.3.2.6) as a basis for time-stratigraphic correlation, working on the assumption that the individual plateaux reflect essentially isochronous and universal marker horizons (Hajdas *et al.*, 2003). Certain biological events may also be used for correlation purposes. For instance, the sudden decline in *Ulmus* in Holocene pollen records from western Europe, which has been radiocarbon dated to around 5.8 ka cal. BP and which appears to reflect a rapid and widespread biotic catastrophe (Parker *et al.*, 2002), could be employed in time-stratigraphic correlation. In earlier Quaternary sequences, mammalian extinction or evolutionary events might also offer a basis, not only for relative dating (section 5.5.4), but also for regional and inter-regional correlation.

6.3.2.7 Correlation using the marine oxygen isotope record

Although the low sedimentation rate and slow mixing times in the deep oceans means that oxygen isotope profiles from ocean cores cannot be used in the correlation of recent marine sequences, or as a basis for high-resolution correlation below the centennial scale (Shackleton, 2006), on millennial and longer timescales, the isotopic stage boundaries, and especially the Terminations, are essentially synchronous. They therefore constitute key marker horizons within the ocean sediment sequences and offer the potential for the development of a correlative chronology that is globally applicable over most of the Quaternary time range (Hilgen *et al.*, 2006). Moreover, the stage boundaries can be dated by orbital tuning (section 1.4), and hence the marine oxygen isotope record, and particularly the LR04 ‘stacked record’ (Figure 1.5), constitute the type sequence for the Quaternary against which other isotopic profiles can be compared.

Deep-ocean records undoubtedly hold a number of advantages over terrestrial sequences from the point of view of stratigraphic subdivision and correlation. First, the sediments from which the isotopic data have been obtained appear to be relatively undisturbed. Second, a common technique (oxygen isotope analysis) can be used to compare profiles from widely scattered localities on the deep-ocean floors. Third, the Terminations can be used as universal reference points in inter-core correlation. Fourth, although the isotopic changes are a consequence of climatic changes, and are therefore time-transgressive, this to a very large extent is masked by the slow rate of sediment accumulation. As a consequence, the major isotopic stage boundaries and Terminations can be interpreted as *essentially* time-parallel horizons. Fifth, orbital tuning enables a timeframe to be established for the isotope curves, with key levels in the cores being dated on the basis of periodicities obtained from astronomical calculations. Moreover, marker horizons such as the Brunhes–Matuyama boundary can also be dated by the independent method of palaeomagnetic stratigraphy (Hilgen *et al.*, 2006).

Interpretation of the isotopic evidence is not always straightforward, however. Continuity of sedimentation can never be proved, and it is questionable whether, in practice, gaps in the sedimentary record can ever be reliably detected. Problems also arise over poor stratigraphic resolution, over bioturbation and reworking of sediments, and over the recognition and precise definition of stage boundaries in some isotopic profiles. Moreover, although the records can be dated by orbital tuning and by reference to the palaeomagnetic timescale, correlation between

individual isotopic profiles is based largely on a ‘count from the top’ principle, and hence the possibilities of homotaxial error are always present. In addition, the quantification of orbital cyclicity, which is fundamental to precise orbital tuning, may be compromised by ‘signal noise’ in the marine isotope records, resulting from time distortion (non-linear sedimentation rates), diagenesis, different sampling protocols and analytical errors (Meyers *et al.*, 2008). A further potential source of uncertainty arises from the differentiation between interglacials and interstadials. It has already been shown that MIS 3 is regarded as being of interstadial rather than interglacial status. The possibility cannot, therefore, be excluded that some previous interglacials and interstadials have been confused, particularly in the earlier part of the Quaternary record. If this has occurred, then it clearly has implications for the status attached to isotope stages, and could lead to problems in correlating between continental records and the marine oxygen isotope sequence (section 6.3.3.1). By the same token, the complexities of MIS 5 and 7 (section 6.2.3.5) are surely not unique to the upper parts of the isotopic sequence. Consistency of interpretation between different isotopic profiles may not, therefore, be easy to achieve, particularly in those cores where stratigraphic resolution is low.

Although the above difficulties have yet to be satisfactorily resolved, there is no doubt that the isotopic trace in the ocean sediments constitutes a remarkable record of Quaternary climatic change, and it is now widely accepted that this, and not the terrestrial sequence, provides the basic framework for a global scheme of Quaternary correlation. Because the isotopic stages are a reflection of climatic change, they are essentially geologic-climatic units and, as such, should have correlatives in the terrestrial record. How these two can be linked is considered in the final section.

6.3.3 Correlation between continental, marine and ice-core records

If correlations are to be established with oceanic sequences, terrestrial records should possess certain characteristic features: (1) evidence of climatic change that is clear and unequivocal so that the climatic signal can be compared directly with that in marine oxygen isotope profiles, or other elements of the deep-ocean sequence; (2) a history of sediment accumulation that has been continuous, or more or less continuous; and (3) an independent chronology based on radiometric, incremental, or age-equivalent dating, and which therefore enables a time-stratigraphic correlative framework to be established. In practice, it is perhaps the third of these that poses the greatest problem

for land–sea correlations, partly because of the technical limitations of the methods (Chapter 5), partly because of the restricted time ranges of some techniques, and partly because many stratigraphic records lack either suitable material for dating, or clearly defined time-stratigraphic marker horizons (palaeomagnetic boundaries, tephra layers, etc.). As a consequence, correlating terrestrial successions to the deep-ocean sequence is frequently based on **record** or **event alignment** (sometimes referred to informally as ‘wiggle-matching’ in the literature), whereby inflections in curves of proxy climate data form a basis for aligning events in one record with their assumed closest equivalents in another. Once such matches have been established, it may be possible to **tune** one record against the other. This involves changing the chronology of a record, either by matching it against a better-dated one, or by matching it with a known **cyclicity** based on an established cause-and-effect relationship, as in the tuning of the marine isotope signal and isotopic/trace gas records in polar ice cores to the astronomical (or orbital) timescale (sections 5.4.3 and 5.5.3).

Although alignment and tuning of palaeoenvironmental records are now routinely employed in the correlation of Quaternary sequences, these approaches are also not without problems. The assumption in sequence alignment is that the climate signal that is reflected in proxy records in different terrestrial and oceanic archives is broadly time-parallel. But as we have already seen, climate change at decadal, centennial and, sometimes, at millennial timescales may be diachronous. Moreover, some elements of the biosphere, such as insects, respond more rapidly to climate change than, for example, plants, and hence there will often be a degree of time-transgression in climate signals from different proxy records. In highly resolved stratigraphic sequences, therefore, alignment of, and tuning the climate signal between, different land and ocean archives may not be a straightforward procedure. In the deep oceans, by contrast, slow rates of sedimentation on the deep-ocean floor tend to mask any spatial variation in the marine oxygen isotope signal, and hence the major inflections in the isotopic trace, especially the Terminations, constitute essentially time-parallel markers for correlating between the different isotopic records (section 6.3.2.7). On the other hand, the relatively low stratigraphic resolution of this record by comparison with some terrestrial sequences, such as polar ice, means that aligning and tuning the terrestrial record to the marine isotope signal may fail to reveal possible leads and lags in the earth–ocean–atmosphere system. In other words, the tuning process may tend to ‘blur’ or smooth out what may be a complex climate signal. As noted above, however, these and other

difficulties may be resolved if independent chronological data are available to underpin the records. These enable time-stratigraphic equivalence to be established, in which case it may prove possible to **synchronize** the different records, which is the optimum situation in land–ocean correlation (section 6.3.3.3).

Ideally, terrestrial sequences that are being used for correlation should span the whole Quaternary time range, as does the marine oxygen isotope signal, and thus comparisons can be made on **Milankovitch** (or **orbital**) **timescales**. In reality, however, it is only in a few depositional contexts, such as tectonic basins and deep lakes, where there are continuous sedimentary sequences that extend back to the beginning of the Quaternary and beyond. But there are a number of terrestrial sites where continuous depositional records are preserved that span several glacial–interglacial cycles, and these also enable land–marine correlations to be effected at the Milankovitch scale. In addition, there are other contexts where the sedimentary successions are shorter and more fragmented, but these may be better resolved, both stratigraphically and temporally. As such, they allow more precise correlations to be established between components of terrestrial and marine sequences, often on **sub-Milankovitch timescales** (section 1.5). Some examples of the types of record that can provide a basis for terrestrial and marine time-stratigraphic correlation on long-, medium- and short-term timescales are considered in the next two sections.

6.3.3.1 Long-term correlation on Milankovitch timescales

In recent years, technological advances in subsurface exploration and in coring have revealed long sedimentary sequences in some continental localities which, in certain exceptional cases, span much or all of the Quaternary and beyond. Proxy climate records reveal long-term climatic cycles that appear to have resonated at Milankovitch periodicities, and hence offer a potential basis for correlation with marine oxygen isotope records throughout the entire Quaternary time range. Some of the longest sequences are preserved in the great **tectonic basins** of the world, such as that beneath the high plains of Bogotá in the Eastern Cordillera of Colombia, the pollen record from which extends continuously back into the Pliocene (Torres *et al.*, 2013), and the Wanganui Basin of New Zealand, where great thicknesses of Plio-Pleistocene shallow-water marine deposits can be linked to the marine oxygen isotope record using a combination of biostratigraphy, magnetostratigraphy and fission track dating of interbedded rhyolitic tephra layers (Pillans *et al.*, 2005). In the Northern

Hemisphere, the Central Graben of the southern Netherlands contains fluvial and marine sediments extending back to the Reuverian Stage of the upper Pliocene, and the quantified temperature record derived from pollen evidence shows clear parallels with the marine oxygen isotope record (Figure 6.11).

In some of the world's larger lakes, such as Lake Titicaca in Bolivia/Peru (Fritz *et al.*, 2007) and Bear Lake, Utah/Idaho (Colman *et al.*, 2006), sediment accumulations may span several glacial–interglacial cycles, but few lakes contain a record that extends continuously through the full Quaternary timespan. Exceptions include Lake Biwa in

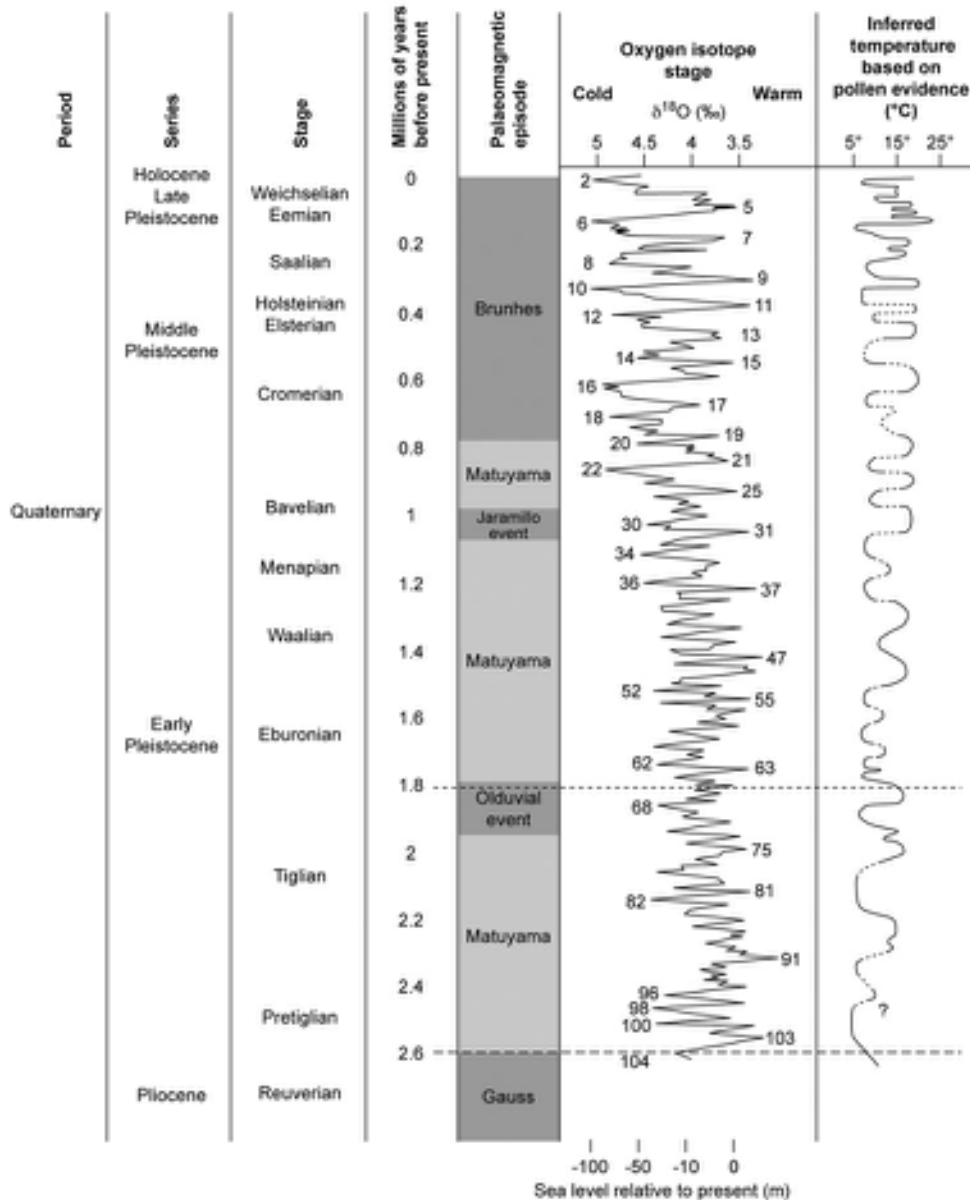


Figure 6.11 The Quaternary sequence in the Netherlands matched against the marine oxygen isotope record. Pollen-based temperature reconstructions are shown on the right (after de Mulder *et al.*, 2003).

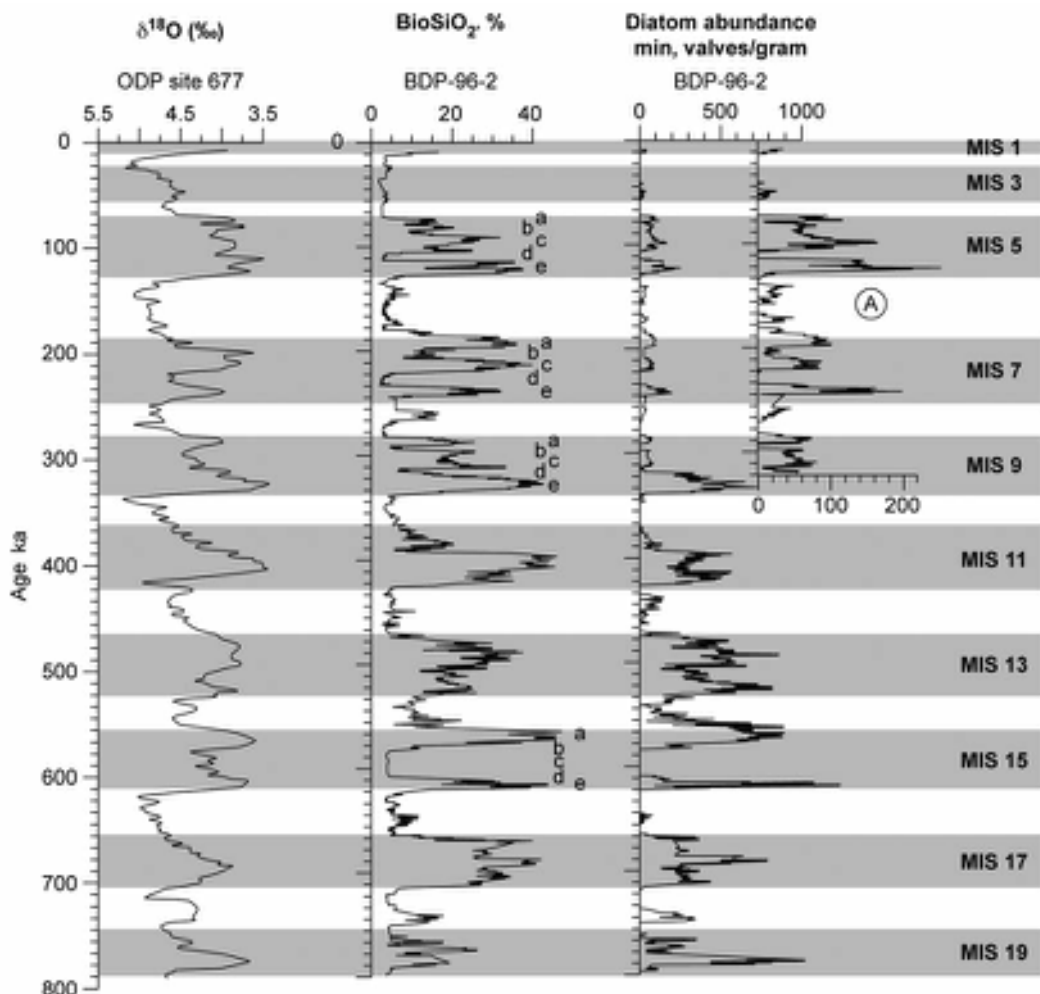


Figure 6.12 Comparison of biogenic silica and diatom records from Lake Baikal with the marine oxygen isotope signal from ODP site 677. Diatoms were relatively less abundant in the upper part of the record, but the amplified curve (inset A) shows that the cyclical pattern of diatom abundance continues to parallel the BioSiO_2 profile throughout the MIS 9c-1 interval (after Khurshovich *et al.*, 2001).

Japan (Miyoshi *et al.*, 1999) and Lake Baikal in Siberia. The latter is the deepest lake in the world and, in parts of its basin, sediments exceed 5 km in thickness and may be between 20 and 40 Ma in age (Williams *et al.*, 2001). Close correlations have been established between biogenic silica and diatom data from Lake Baikal and the marine oxygen isotope sequence (Figure 6.12), a comparison that now extends beyond 1.8 Ma (Prokopenko *et al.*, 2006) and which may have the potential to reach as far back as 12 Ma

(Kashiwaya *et al.*, 2001). In East Africa, records extending back to the late Pliocene have been obtained from the Rift Valley (Trauth *et al.*, 2005), although the sedimentary regimes in these lakes reflect a complex interplay of climatic and tectonic factors (Bergner *et al.*, 2009).

There are other terrestrial sedimentary successions that span much or all of the Quaternary, most notably the thick loess deposits of the continental interiors (section 3.6.5) in which aeolian and soil units provide a remarkable

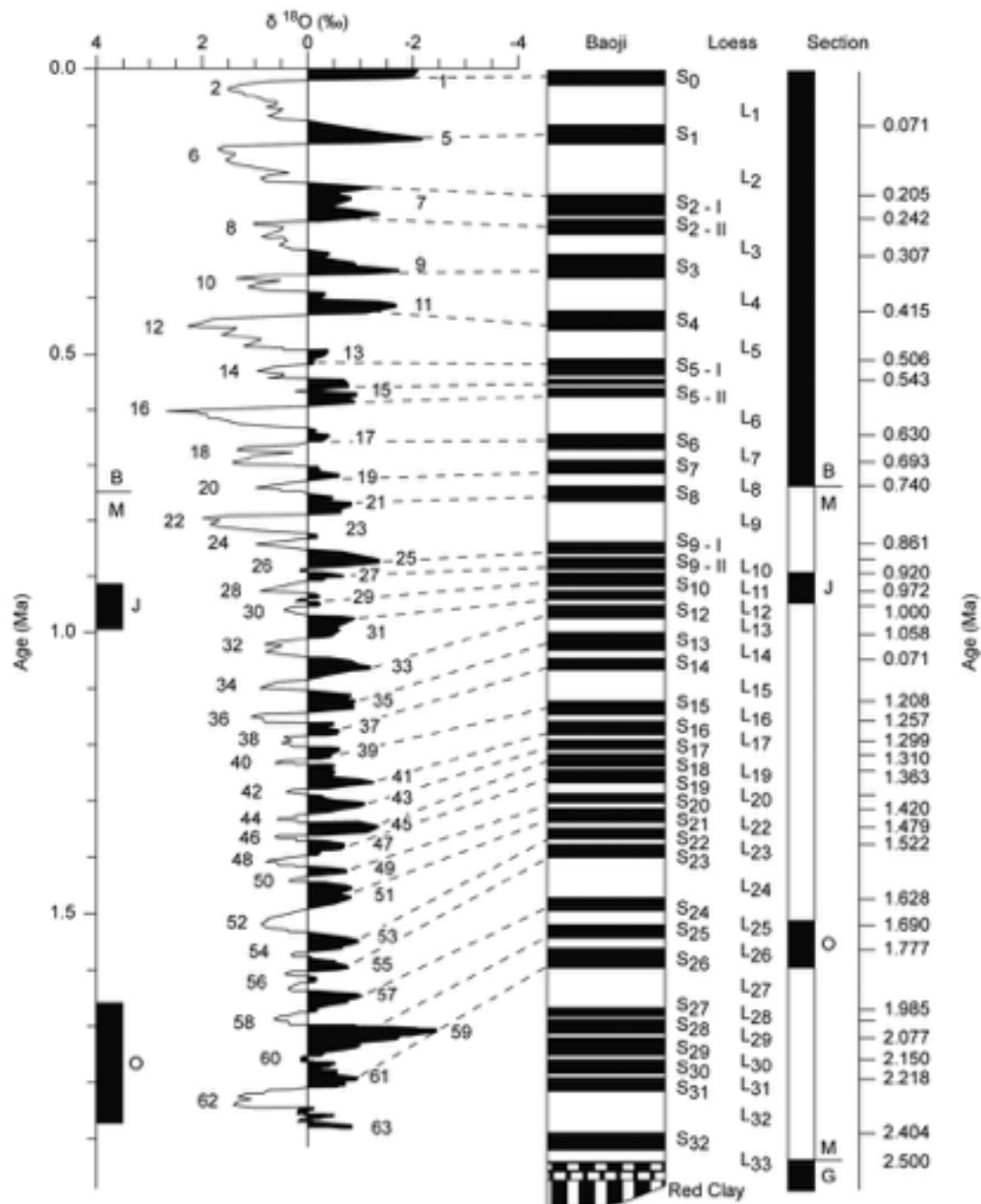


Figure 6.13 The sequence of loess-palaeosol units preserved at the Baoji site on the Loess Plateau, China, plotted against the marine oxygen isotope record. B/M – Brunhes-Matuyama boundary; J – Jaramillo Event; O – Olduvai Event; M/G – Matuyama-Gauss boundary. Note the isotopic record extends back to c. 1.8 Ma (MIS 63), whereas the loess-palaeosol record goes back to 2.5 Ma (the beginning of the Quaternary/Pleistocene) (after Rutter *et al.*, 1996).

record of glacial–interglacial cycles. The potential of these loess–palaeosol sequences for linking terrestrial and marine records was first recognized by George Kukla who compared the aeolian records from Moravia in eastern Europe with the oxygen isotope timescale, a correlation that was eventually extended back into the early Quaternary (Kukla, 1977). Other loess–palaeosol sequences from eastern Europe and central Asia have subsequently been correlated with the deep-ocean oxygen isotope signal (Brögger, 2003). However, it is the loess–palaeosol records on the Loess Plateau region of central China (section 3.6.2) that offer the greatest potential for terrestrial–marine correlations (Ding *et al.*, 2002b; Sun *et al.*, 2006b). Loess began to accumulate more than 2.6 Ma ago, and these sediments and their interbedded soils are another depositional record that can form a basis for time-stratigraphic correlation throughout the entire Quaternary period (Figure 6.13).

Long polar ice-core records also provide a means of land–ocean correlation on Milankovitch timescales as the $\delta^{18}\text{O}$ values in the two archives are inter-related, the isotopic signal in the ice cores being the reverse of that in the marine record (section 3.11). In one of the earliest attempts to utilize this relationship as a basis for correlation, Dansgaard *et al.* (1982) were able to identify the equivalents of MIS 1–5e in the Camp Century ice core from northern Greenland, the isotopically ‘warmest’ $\delta^{18}\text{O}$ values being recorded in levels equating to MI substages 5e. With the recovery of much longer cores from Antarctica, however, the ice–marine isotopic correlation has been extended back to MIS 20.2 (*c.* 800 ka BP), in the EPICA core from the Dome C drill site (Jouzel *et al.*, 2007).

Another proxy climate record that can be used to link terrestrial and marine sequences is the oxygen isotope signal in cave speleothems (section 3.8.4.2). In some cave sites, particularly those located in low latitudes where speleothem growth is more likely to have been continuous over relatively long periods of time (McDermott, 2004), a close relationship has been observed between episodes of more rapid speleothem growth and warmer (and wetter) periods, as inferred from other proxy climatic data. Records from the Hoti Cave in northern Oman, for example, show enhanced phases of speleothem growth at 132–125 ka, 200–180 ka and 325–300 ka, in other words during MI stages 5e, 7 and 9, reflecting episodes of increased monsoon rainfall (Burns *et al.*, 2001). U-series dated stalagmite records from the Hulu and Sanbao Caves in China show evidence of 23 ka (precessional) cycles over the last 224 ka which are linked to changes in the East Asian monsoon, and which can be correlated with MI stages back to MIS 7.3 (Wang *et al.*, 2008).

6.3.3.2 Correlation on sub-Milankovitch timescales

As we saw in Chapter 3 (section 3.11.4), the last glacial cycle in the Greenland ice-core record was characterized by a series of twenty-five abrupt warming events, the Greenland Interstadials (GI) or Dansgaard–Oeschger (DO) events, and these have been shown to be consistent in number and amplitude in different Greenland ice cores (North Greenland Ice Core Project Members, 2004). Equivalent features have been detected in marine and other terrestrial archives (e.g. lakes and speleothem deposits) that span the last glacial period (see below). This sequence of short-lived but distinctive climatic events was not unique to Greenland, therefore, but appears to reflect widespread, perhaps global, climatic perturbations (Schulz, 2002). The same may be equally true of the Heinrich events (H), six prominent cooling episodes that occur in records of the mid- and later part of the last glacial cycle (section 3.10.1). Their signatures have been detected in both marine and terrestrial archives and in widely separated localities, prompting the suggestion that these too represent short-term, globally significant, climatic ‘pulses’ (Voelker, 2002). In combination, these two sets of marker events, GI1–GI25 in the ice cores and H1–H6 in ocean sediments, provide the basis for high-resolution correlations of marine, continental and ice-core sequences.

The signatures of the Heinrich events, which are marked in North Atlantic marine sediments by distinctive layers

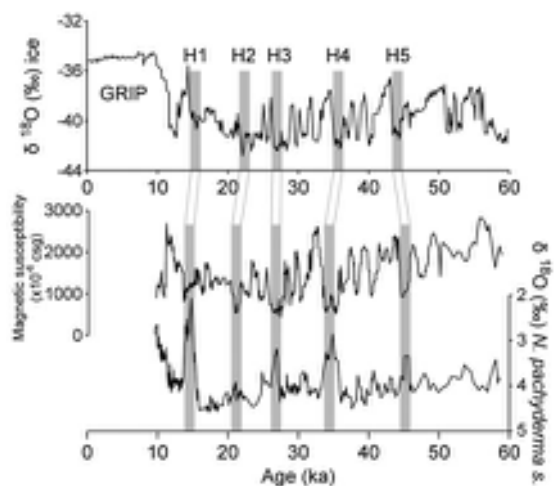


Figure 6.14 Matching of marine sediments in core ENAM93-21 from the northeast Atlantic Ocean with the GRIP $\delta^{18}\text{O}$ ice-core record using Heinrich events (H1–H5) as tie-points (after Cortijo *et al.*, 2000).

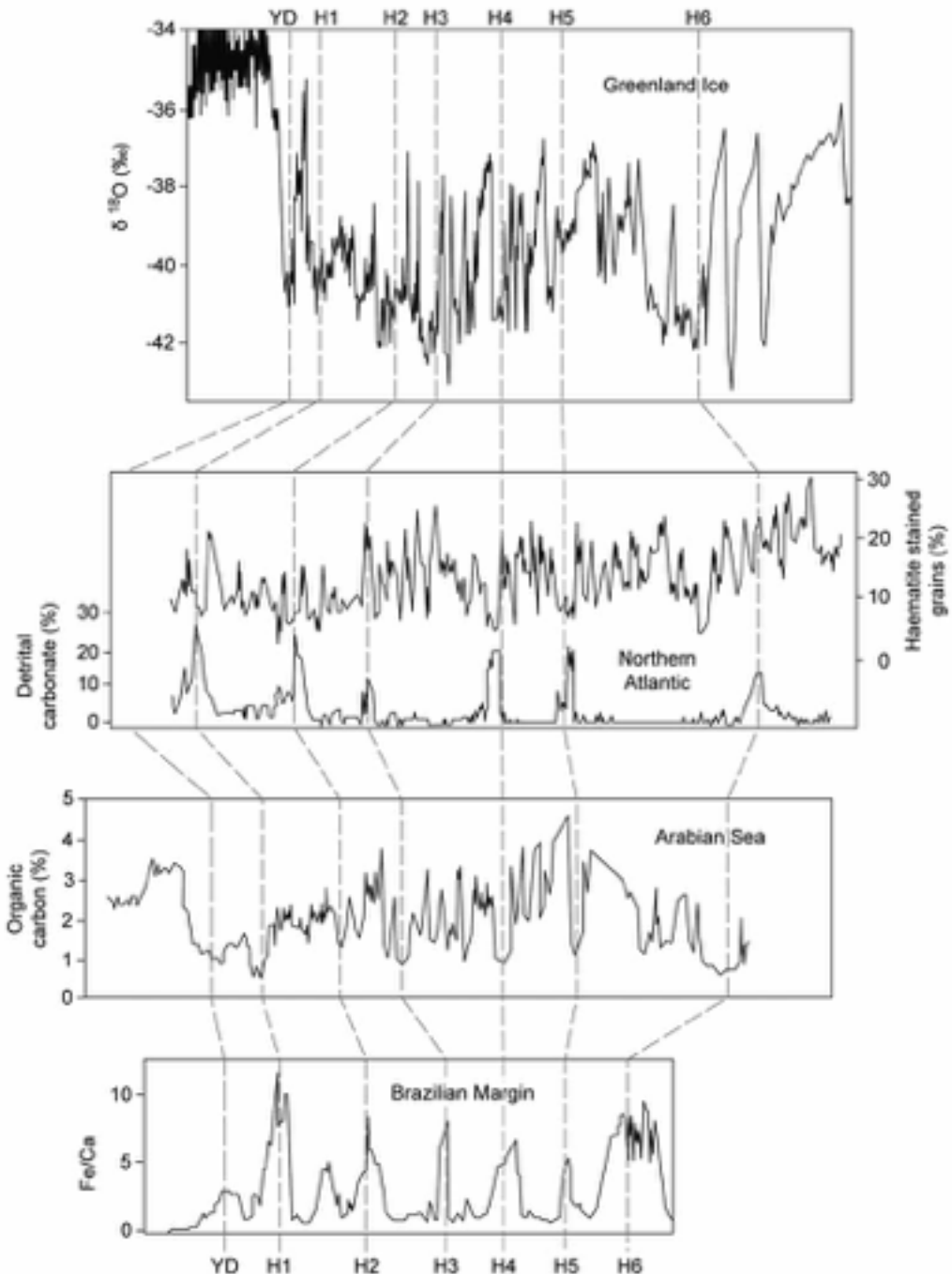


Figure 6.15 Tentative correlations between records from the Greenland ice sheet, northern North Atlantic, Arabian Sea and Brazilian Atlantic margin, using a variety of proxies to define Heinrich events (H1–H6), and the intervening DO events. YD – Younger Dryas cold event (after Broecker & Hemming, 2001).

of ice-rafter debris (IRD; section 3.10.1), register clearly in the oxygen isotope record in the Greenland ice cores (Figure 6.14), and this not only enables correlations to be established between the marine and ice sheet archives, but also allows calendar ages to be ‘imported’ into the marine record from the annually counted 60 ka Greenland ice-core chronology (Svensson *et al.*, 2008). This is important because dating of the Heinrich IRD layers by radiocarbon has proved problematical, due largely to uncertainties over the marine reservoir effect (section 5.3.2.4). Although the IRD record of Heinrich events is confined to the mid- and high latitudes of the North Atlantic, changes have been observed in other marine proxies that may parallel the Heinrich events. These include short-lived increases in algal productivity in the sub-Antarctic Ocean, implying major reorganizations of ocean circulation (Sachs & Anderson, 2005), variations in Fe/Ca ratios in cores from near the Brazilian margin of the South Atlantic which reflect enhanced sediment supply (increased run-off), and reductions in the organic carbon content of sediments in the Arabian Sea, indicating colder water temperatures (Broecker & Hemming, 2001). If these are indeed the correlatives of the North Atlantic Heinrich events, then the HE marker horizons can be used to link marine sequences in different ocean basins (Figure 6.15).

Further linkages between marine and terrestrial events in the North Atlantic province have been established using evidence from ocean cores from the Iberian margin of southwest Europe. These have yielded both marine micro-fossil data (from which sea-surface temperatures have been reconstructed) and pollen evidence, the latter enabling direct comparisons to be made with pollen-based climate reconstructions from terrestrial sites. The proxy records suggest a close link between millennial-scale oscillations in the North Atlantic and vegetation responses on the adjacent western European landmass (Sánchez Goñi *et al.*, 2008). This land–ocean correlation has now been extended back through the last two glacial periods (de Abreu *et al.*, 2003).

Attempts have also been made to compare marine and Greenland ice-core records on the basis of equivalent Interstadial (IS) or DO events. For example, in a sequence of sediments from the Cariaco Basin, located in the tropical Atlantic off the Venezuelan coast, the colour reflectance record (which indicates changes in marine productivity) has been tuned to the sequence of interstadials and stadials in the GISP2 ice core, using prominent IS events as tie-points (Figure 6.16). A similar correlation has been suggested between the oxygen isotope profile from speleothem in Hulu Cave, China, which has also been tuned to the GISP2

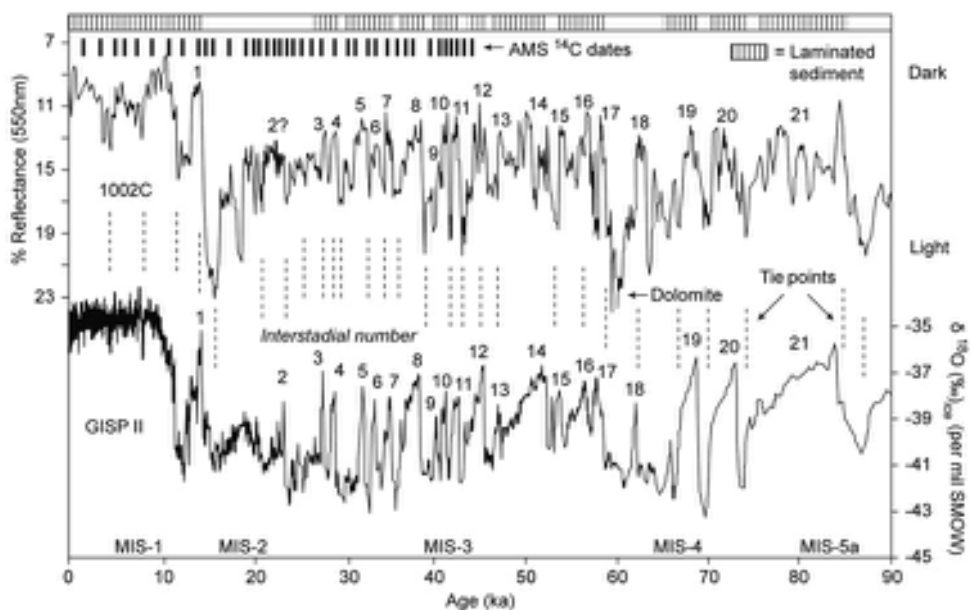


Figure 6.16 Comparison between colour reflectance of Cariaco Basin sediments and the GISP2 $\delta^{18}\text{O}$ record over the last glacial cycle. The interstadial (IS) events correspond with darker layers in the sediment sequence which reflect higher levels of organic productivity. The Cariaco record has been tuned to the GISP2 isotopic signal on the basis of matching (equivalent) interstadial events, with the key tie-points shown by dashed lines (after Peterson *et al.*, 2000).

ice-core sequence, while some of the most prominent shifts in the isotopic signal are considered to reflect the North Atlantic Heinrich events (Figure 6.17). There the tuning is based on eighteen distinctive marker events and the similarity between the two isotopic records suggests a link between the East Asian monsoon and North Atlantic atmospheric circulatory systems (Wang *et al.*, 2001). Other speleothem sequences that provide the potential for this degree of close matching to the ice-core records include those from cave sites in Europe (Genty *et al.*, 2003), the American Midwest (Serefiddin *et al.*, 2004) and Israel (Frumkin *et al.*, 1999).

Correlations have also been made between the central European loess–palaeosol record and Heinrich Events (Shi *et al.*, 2003), while in the Malan Loess of central China, high-frequency fluctuations in dust influx include peaks that appear to correlate with events in the North Atlantic (Porter, 2001). In addition, loess sequences have been correlated with the Greenland ice-core record. In the American Midwest, for example, a series of palaeosols (reflecting warmer episodes) have been correlated with the IS events in Greenland ice cores (Wang *et al.*, 2003), while a link has also been suggested between features of the Chinese loess–palaeosol sequences and Greenland IS events (Huang *et al.*, 2000).

6.3.3.3 Synchronizing records of past environmental change

In the foregoing examples, correlation between the different land and ocean archives is based on alignment and, in some cases on tuning, of curves from proxy climate records. Where correlations can be underpinned by independent dating, however, it may be possible to synchronize records of past environmental change. This is important for not only does it enable more secure comparisons to be effected between marine and terrestrial records, it also provides a means whereby leads and lags between different components of the earth–atmosphere system can be detected.

The principles and some potential problems of aligning and synchronizing stratigraphic records are illustrated in Figure 6.18. Here, there are two sediment cores, one of which is from a lake sequence (core 1), while core 2 contains a marine record. Six common marker horizons or tie-points (M1–M6) are shown; these might be Heinrich events in the marine core and their inferred terrestrial equivalents in the terrestrial lake sequence. The markers provide the basis for aligning the proxy climate records from the two cores (Figure 6.18a). However, in order to establish a precise time-stratigraphic correlation (synchronization) and to show that the alignment is valid, additional

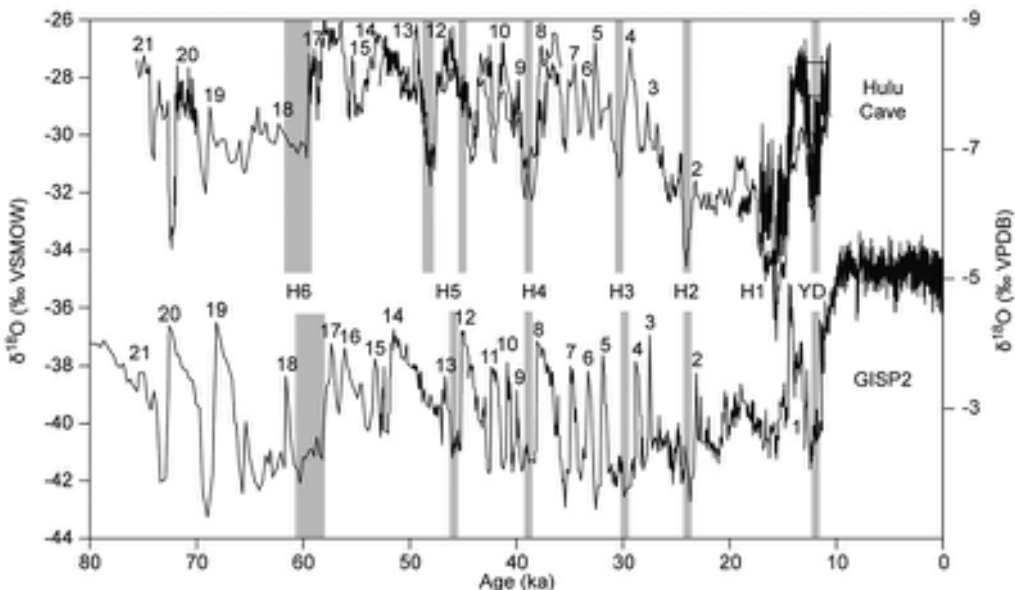


Figure 6.17 Correlation between the $\delta^{18}\text{O}$ record from Hulu Cave, China, and the $\delta^{18}\text{O}$ profile from the GISP2 Greenland ice core. The numbers above the isotopic traces denote Greenland Interstadial (DO) intervals. The vertical bars mark the positions of Heinrich events 1–6 in the two sequences; YD – Younger Dryas (after Wang *et al.*, 2001 and Genty *et al.*, 2003).

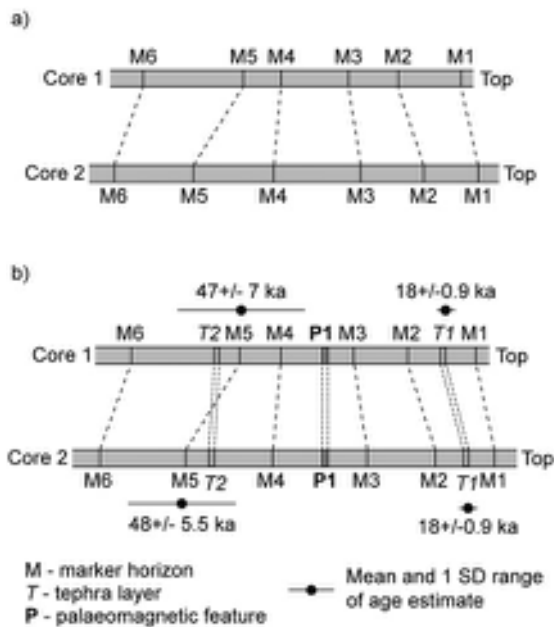


Figure 6.18 Schematic diagram showing the principles and limitations of tuning palaeoenvironmental records from two cores. For explanation see text.

chronological data are needed. In Figure 6.18b, as well as the six tie-points, there are two tephra horizons (T1 and T2), a palaeomagnetic boundary (P1) and three radiometric dates. T1 has been provenanced and securely dated in another lake profile, and hence that age can be ‘imported’ into both cores. By contrast, T2 has not been radiometrically dated elsewhere, and the only available age estimates for this tephra are those that have been obtained from cores 1 and 2. The stratigraphical relationships between T1 and P1 and the marker horizons M1–M4 are consistent in the two cores, and the imported radiometric date with a small standard error provides a precise age for T1. The alignment of M1 with M4 is therefore underpinned by superposition, by two time-stratigraphic markers and by radiometric dating; hence the two records are effectively synchronized. This is not the case with the alignment at M5 where the tephra T2 occurs above M5 in core 1 and below M5 in core 2. Several explanations are possible for this: (1) M5 has been incorrectly identified or positioned within either core 1 or 2 (or both); (2) M5 is diachronous between the two records; or (3) different tephras, of different age, with virtually identical chemical signatures occur in the two cores. Note that the radiometric dates for T2 both have large standard errors, and as the age range brackets M5 in both cores, they do not help in resolving the issue.

In this instance, therefore, the records cannot be synchronized and, indeed, there may be doubts over the reliability of the proposed alignment.

One of the most effective approaches to the synchronization of records from different depositional archives is the use of event stratigraphy (section 6.3.2.5), such as that proposed for the North Atlantic region by the International Working Group known as INTIMATE (INTegration of Ice-core, MARine and TERrestrial records). INTIMATE initially outlined a North Atlantic Event Stratigraphy for the Last Termination (15–8 ka) based on the annually dated isotopic signal in the GRIP Greenland ice core (Björck *et al.*, 1998), but with the subsequent construction of the high-resolution GICC05 timescale from the NorthGRIP ice core (Rasmussen *et al.*, 2006), NGRIP has now been adopted as the regional stratotype and the Event Stratigraphy extended back initially to 30 ka (Lowe *et al.*, 2008b), and subsequently to 48 ka (Blockley *et al.*, 2012). The INTIMATE group has recommended a series of protocols for synchronizing Last Termination records from the North Atlantic region, including the use of quantified proxy climate data from both marine and terrestrial contexts, secure ^{14}C dating frameworks based on high-resolution sampling and age modelling, and tephrochronology, and with inter-archive correlations established on the basis of a high-quality ^{14}C chronology and tephrochronology. This approach provides a secure time-stratigraphic framework for inter-regional comparisons as, for instance, in the synchronization of varved lake sediment records from sites in north-central Europe which is based on a combination of pollen stratigraphy and tephrochronology (Figure 6.19). As noted above, this approach is also important in palaeoenvironmental reconstruction as it may reveal temporal variations in terrestrial and marine responses to changes in the climate system. An example is provided by the detailed pollen record and associated high-resolution ^{14}C age model from Crystal Lake, Illinois, which shows that although vegetational changes in the American Midwest were broadly coeval with millennial-scale trends in the NGRIP ice-core record over the period 17–11 ka, major shifts in vegetation lag the NGRIP record by 300–400 years (Gonzalez & Grimm, 2009). This probably reflects the proximity of the Laurentide ice sheet, which could have affected regional climate through its influence on atmospheric frontal boundaries and the position of the jet stream.

In the Southern Hemisphere, the New Zealand INTIMATE Group has also developed a climate event stratigraphy for the past 30 ka (Alloway *et al.*, 2007b). This is based on a series of well-dated, high-resolution onshore and offshore proxy records from a variety of latitudes and elevations. These include long peat and lacustrine sediment

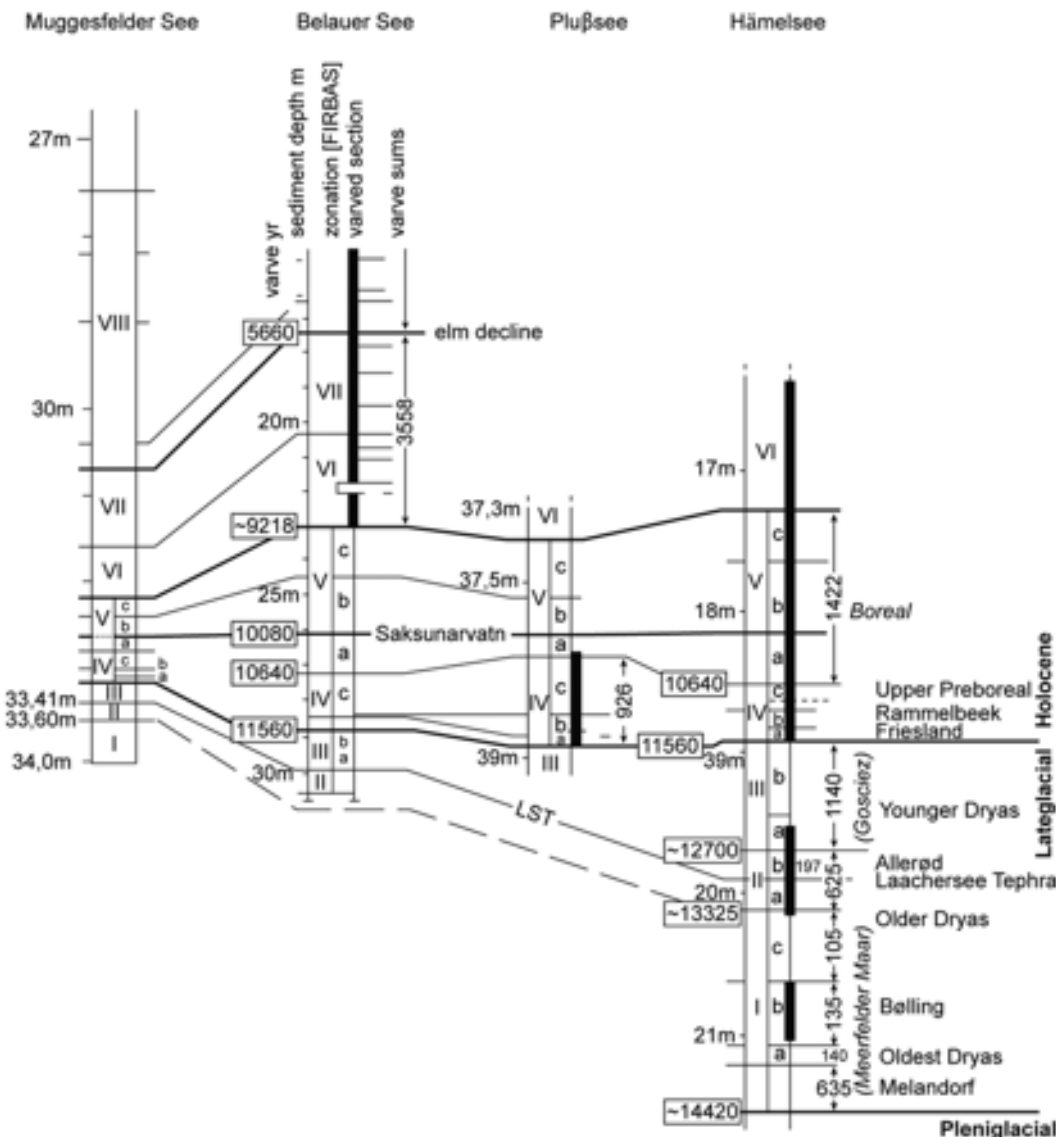


Figure 6.19 Synchronization of four Lateglacial and early mid-Holocene lake records from northern Germany, using a combination of pollen analyses (key pollen zone boundaries such as the 'Elm Decline'), tephra isochrones (Saksunarvatn Ash and Laacher See Tephra) and varve chronology (after Litt *et al.*, 2001).

accumulations, speleothem and marine-core records, and more fragmented glacial, fluvial and aeolian sequences. The records are linked by a combination of high-precision radiometric dating (radiocarbon, U-series, OSL) and (with the exception of the speleothem) by well-dated tephra marker beds (twenty-two in all) provide the

principal means of synchronizing the different stratigraphic sequences (Lowe *et al.*, 2008a). Further south in Antarctica, older tephras, dating from MIS 5 and 6, have been detected in both ice and marine cores, and while the dating and provenancing of these tephras is currently uncertain, they may in due course provide a basis for synchronizing Antarctic and marine records (Hillebrand *et al.*, 2008).

Volcanic events marked by acidity or sulphate peaks, or by the presence of tephra particles, have also been used to synchronize different ice-core records. In Greenland, for example, volcanic reference horizons were used to link the Holocene sections of the Dye-3, GRIP and NGRIP cores for the construction of the GICC05 timescale (Vinther *et al.*, 2006), and also to synchronize proxy records from those ice cores spanning the later part of the last cold stage (Rasmussen *et al.*, 2008). At the global scale, Greenland and Antarctic ice-core records have been synchronized using isotopic and trace gas data (Blunier *et al.*, 2007). Millennial-scale variations in water isotope ratios ($\delta^{18}\text{O}$) are evident in both NGRIP (Greenland) and EPICA (Antarctica) ice cores, and these can be coupled to the globally applicable methane (CH_4) profiles to align Greenland and Antarctic records, for example in the period of MIS 5 between 123 and 80 ka (Capron *et al.*, 2010a). Other approaches to linking Greenland and Antarctic ice cores involve the use of cosmogenic ^{10}Be at the Laschamp palaeomagnetic excursion around 41 ka (Raisbeck *et al.*, 2007), and bipolar volcanic markers, such as the acidity spikes in the cores that reflect the major Toba eruption around 74 ka (Svensson *et al.*, 2012), evidence that is discussed in more detail in Chapter 7.

On longer timescales, the sapropels of the Mediterranean region offer a remarkable basis for correlating terrestrial and marine sequences, and for synchronizing these different records. As explained in Chapter 1 (note 6), sapropels are layers rich in organic material which accumulate under anoxic conditions in ocean basins. In the Mediterranean, sapropels have formed episodically from Pliocene times onwards (Emeis *et al.*, 2000), and are found in both marine cores and in uplifted marine sequences, particularly around the coastlines of Italy and Sicily, where they occur in repetitive cycles of organic and inorganic sediment accumulations (Figure 1.3). The sapropels are believed to reflect near-synchronous oceanographical changes across the Mediterranean region, and have been related to increased run-off or river discharge, and associated increases in nutrient input during periods of higher precipitation (Cane *et al.*, 2002). These wetter episodes coincide closely with minima in the Milankovitch precessional index (*c.* 21 ka), which allows the **MPRS (Mediterranean precession-related sapropels)** sequence to be tuned to the astronomical timescale (Lourens, 2004). The sapropel layers can be correlated with microfaunal and microfloral biozones, and with the marine $\delta^{18}\text{O}$ signal, while further tie-points are provided by radiometric dating of younger parts of the sequence, and magnetostratigraphy on earlier parts of the record (Figure 6.20). These unique stratigraphic sequences therefore provide a basis for ocean-

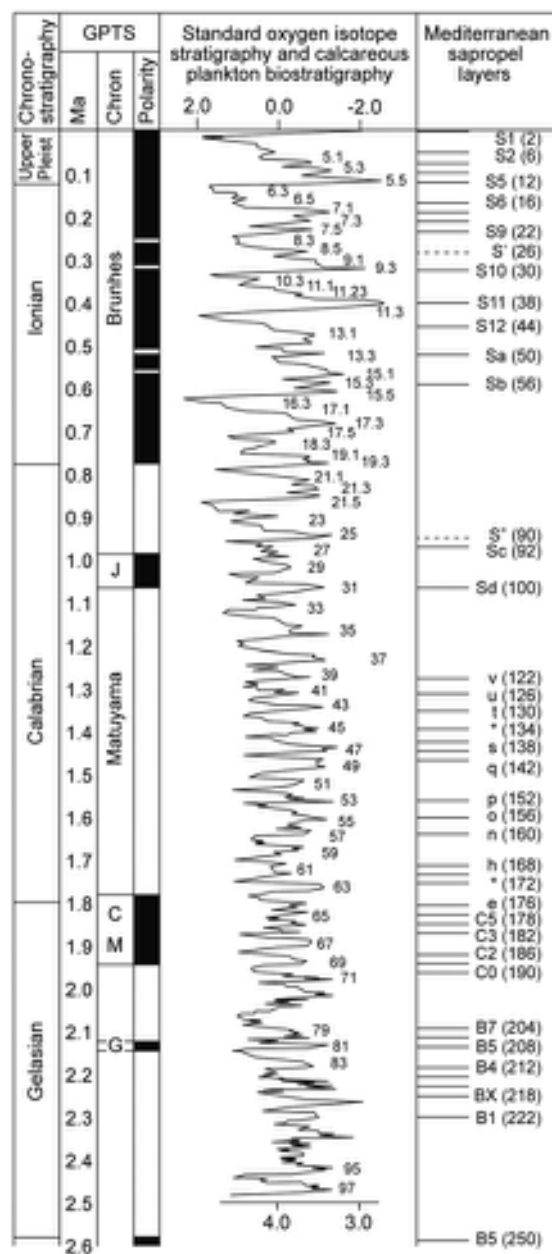


Figure 6.20 Stratigraphic framework for Quaternary marine sequences in the Mediterranean, showing regionally isochronous sapropel units, foraminiferal biozones and magneto-zones, linked to the astronomical timescale. The three principal magnetic excursions of the Matuyama chron are indicated: J – Jaramillo; CM – Cob Mountain; G – Gilse (after Massari *et al.*, 2004).

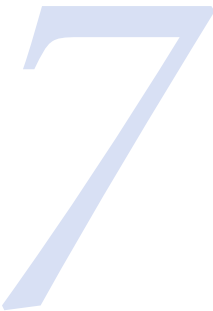
ocean, and land–ocean correlation and synchronization within the Mediterranean region throughout the entire Quaternary period and beyond.

6.4 CONCLUSIONS

There is now a broad consensus that subdivision of the Quaternary stratigraphic record should follow as closely as possible conventional geological procedures, although the higher levels of resolution and analytical precision that are required in the classification of the most recent part of the geological record mean that a strict adherence to these principles may pose particular problems for the Quaternary stratigrapher. Nevertheless, it is generally acknowledged that, wherever possible, lithostratigraphy should comprise the basic building blocks of the Quaternary terrestrial stratigraphic sequence, augmented by empirical evidence from bio- and morphostratigraphy along with inferential

data from chrono- and clinostratigraphy. Ultimately, geologic-climatic units will be established, and these form the basis for correlation at the regional and continental scales. Geologic-climatic units are also the basis for correlating marine and terrestrial sequences, while the essential reference standard for global correlation at Milankovitch frequencies is the oxygen isotope stratigraphy of the deep-ocean sediments. At sub-Milankovitch frequencies, well-defined events in marine, terrestrial and ice-core records provide a basis for correlation, with the event stratigraphic approach offering perhaps the best prospects for establishing time-stratigraphic correlation between these different archives. Secure correlations are an essential prerequisite for reconstructing spatial and temporal patterns of climate change, and for understanding the forcing factors that drive those changes, and it is to these aspects of the Quaternary record that we turn our attention in the final chapter.

Global environmental change during the Quaternary



7.1 INTRODUCTION

Thus far, we have considered the different types of evidence that can be used to reconstruct Quaternary environments, the means by which a timescale for environmental change can be established, and the stratigraphic procedures that enable sedimentary records to be interpreted and meaningful correlations to be effected between often widely scattered localities. In this final chapter, we will show how results obtained using these different methods and approaches can be synthesized to produce an overview of global environmental change and, in particular, to reveal the **forcing factors** behind these changes. Data compilation and syntheses at regional, continental or, indeed, global scales are important aspects of contemporary Quaternary science for, in addition to providing snapshots of past environmental conditions, they offer a means of cross-checking evidence from different proxy sources, they focus attention on the linkages between processes and components of the global environmental system (e.g. between the glacial, oceanic and terrestrial realms) and they may provide new insights into the causes of environmental changes. All of these aspects were exemplified by the revolutionary CLIMAP and COHMAP projects of the 1970s and 1980s (section 4.10.7), and they underpin more recent research initiatives, some of which are considered in this chapter.

In the second edition of this book (published in 1997), we examined these various interlocking themes by focusing on the interval from *c.* 130–10 ka, the last interglacial–glacial cycle of the Quaternary record, and we centred our discussions on the North Atlantic. We chose this region and this time period partly because the evidence obtained from the Greenland ice-core records in the early 1990s had

provided the first high-resolution records of climatic changes during the last glacial cycle (section 3.11.1), and partly because North Atlantic Ocean circulation was considered by many to be the principal driver behind these changes. Since 1997, however, data from other regions of the world have begun to reveal the true scale and complexity of Quaternary environmental changes, not only during the past 130 ka, but also over earlier glacial–interglacial cycles. The evidence shows that while the North Atlantic does indeed play an important role in the world's ocean circulation regime and has a profound effect on Northern Hemisphere climate, it is but one component of a highly complex pan-global ocean–climate system. To understand that system and its role in Quaternary climatic and environmental change, it is now clear that a global perspective is necessary, and it is such an overview that this final chapter aims to provide. We freely acknowledge, however, that this is a daunting task and is worthy of a book in its own right. Hence, we will not be able to cover all aspects of the subject; nor will we have the space to go into the level of detail that the topic really demands. As a consequence, we have opted to focus the discussion on what we consider to be some of the key questions about the nature, causes and consequences of global environmental change, and to show how these issues are central to many areas of contemporary Quaternary research.

A recurrent theme throughout this book has been the fundamental imprint on the Quaternary environmental record of climate change, operating at Milankovitch, sub-Milankovitch and much shorter (decadal) timescales. It should not be assumed, however, that climate is always the prime instigator of change, with other environmental processes (soil development or erosion, glacier expansion or contraction, changes in atmospheric gas content, etc.)

being mere responders. The climate system is itself reactive to precursor and contemporaneous environmental conditions: one of the main challenges confronting Quaternary scientists, therefore, is that of the ‘chicken-and-egg’ problem, of identifying within continuous and sometimes cyclic proxy environmental records those factors that are causally connected, and those that are initiators of change. To meet that challenge, it is important to define the precise order and timing of key signals in the proxy data, as these may point to **leads** and **lags** between environmental variables, distinguishing forcing factors from responders. The degree to which leads and lags can be clearly resolved, however, in part depends on the temporal resolution at which the stratigraphical record can be examined. It also depends on the quality of the proxy data available, and on the nature of the environmental processes inferred as these operate over a range of timescales. We illustrate the problems of defining leads and lags, and of establishing causal relationships between proxy indicators, by considering the evidence at four temporal scales: the Milankovitch timescale (section 7.3), the sub-Milankovitch (centennial to millennial) timescale (section 7.4), the sub-centennial timescale, for which we focus on evidence from the Last Termination (section 7.5), and finally at a decadal to annual resolution, with a particular emphasis on the Holocene (section 7.6).

7.2 ENVIRONMENTAL SIMULATION MODELS (ESMs)

7.2.1 Introduction

While the geological record can reveal the precise order of events or environmental changes this, by itself of course, does not demonstrate causality. In the experimental sciences, causality can be established by controlled manipulation of selected properties or processes and measurement of their effects, an approach that is not possible with geological evidence. Instead, causality in geology is inferred from observations of repeated associations of, or sequential changes in, proxy variables that are common to a number of stratigraphical records. A causal link is difficult to prove, however, from such observations alone, since it may arise by chance or may reflect the operation of other factors or processes not yet detected. An alternative approach is the simulation of natural environmental processes by numerical modelling. The construction of environmental simulation models (ESMs) enables inputs to be varied in a controlled manner and ‘what-if?’ experiments to be conducted by exaggerating or suppressing selected components, or by omitting or replacing variables.

The sensitivity of a model to changes in particular parameters can then be tested, and their relative importance deduced. Because ESMs are now so widely employed in Quaternary research, we preface our discussion of timescales of change with a consideration of the bases and capabilities of ESMs, and of their importance in the study of land–ice–ocean–atmosphere interactions over the course of the Quaternary record.

7.2.2 Box models

The simplest ESMs are box models that reduce complex components of the global environmental system (e.g. the global ocean, atmosphere or polar ice) to artificial ‘reservoirs’, within which conditions are homogenized; the reservoirs are connected by ‘pipes’ that control mass transfer between the reservoirs (see McGuffie & Henderson-Sellars, 2005). The principal properties of each reservoir (e.g. volume, density, salinity and temperature changes) can be varied in order to see the effect that each change imposes on the operation of the model. These models are not meant to represent the complexity of the real environmental system; rather, they are deliberately simplified to allow the operator to study the feedback links between selected components of the system (Claussen *et al.*, 2002). Figure 7.1, for example, shows a schematic of the elements of a box model that represents (proportionately) the global atmosphere, polar ice, sea ice and ocean. When the model was run, the output generated a 100 ka climatic cycle that is self-sustaining (i.e. it works without any external forcing), and the key driver was found to be the extent of sea-ice cover in the polar oceans, which regulates the growth and decay of polar ice sheets (Gildor & Tziperman, 2001; Gildor *et al.*, 2002). The degree to which this reflects reality can be explored through a combination of further modelling runs calibrated against empirical data. Other simple box model experiments have been used to explore ideas about the operation and impacts of the North Atlantic limb of the global thermohaline circulation (Rahmstorf, 1996). They were also used for some of the earliest ‘**freshwater hosing experiments**’, which simulate the injection of glacial meltwaters into the ocean in order to assess their climatic significance (Kageyama *et al.*, 2010). Over longer timescales, box models have been used, *inter alia*, to simulate bottom water salinity changes in the Southern Ocean, the outputs suggesting that these processes could have played a key role in modulating the rhythm of climate change during the Quaternary, and particularly the change from the 41 ka to 100 ka cycle around 900–800 ka (sections 1.7 and 7.3; Paillard & Parrenin, 2004).

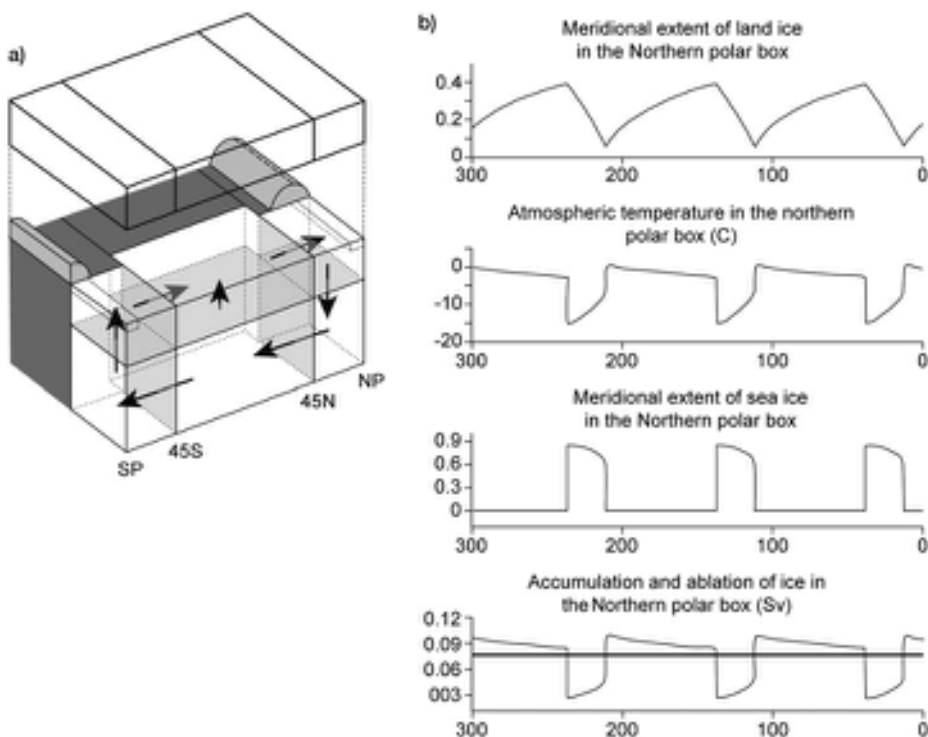


Figure 7.1 a) Schematic representation of a coupled box model showing atmospheric boxes (upper slab), thermohaline circulation (black arrows), parabolic land ice sheets (grey semi-cylinders), and a partial sea-ice cover (grey slabs) in the polar ocean boxes. All of these components are allowed to vary in model equations. Ocean biogeochemistry and atmospheric CO₂ interact with physical climate components. NP – North Pole; SP – South Pole; 45°N and 45°S indicated (from Gildor & Tziperman, 2001). b) Box model results simulating the 100 ka Milankovitch climatic cycle. The horizontal axis is model run-time in simulated ka (from Gildor *et al.*, 2002). For further explanation see text.

The advantage of box models is that they are computationally simple, and hence results can be obtained quickly. They are useful, therefore, for testing the efficacy of selected global environmental feedback loops, with the results feeding into the design of more complex models, often leading to considerable saving of time and resources. The principal disadvantage of box models, however, is that they tend to underestimate the complexity of global systems and their processes. In nature, the oceans and atmosphere are dynamic systems with complicated zonal and non-linear flow mechanisms, which in the reservoirs and slabs of box models are reduced to uniform mass properties. Box models also tend to isolate elements of the global environmental system from other feedback mechanisms that could modulate their operation. As a consequence, therefore, box models may simplify natural processes to the extent that they can deliver misleading outputs (Marotzke, 2000; Wunsch, 2010), and thus

attention is increasingly being directed towards more sophisticated models, which we now move on to consider.

7.2.3 General circulation models (GCMs)

Some of the most advanced environmental models yet developed are those that simulate the global climate system, and have been generated primarily as a response to the demand for improved weather forecasting and climate prediction capabilities (Randall *et al.*, 2007). They are widely referred to as **general circulation models (GCMs)** but technically, perhaps, should be called climatic general circulation models, to distinguish them from those that incorporate simulations of other environmental processes (sections 7.2.4 and 7.2.5). GCMs are designed to simulate the complex three-dimensional structure and dynamic flows of the earth's atmosphere and oceans. The input data fall into two categories. The first are **boundary conditions**,

which are the prescribed surface values for such physical parameters as sea-surface temperatures (SSTs), surface albedo, radiation receipt, atmospheric transparency, sea-ice cover and topography. For simulations of modern climate, the input values are based on direct measurements of current physical parameters, while boundary conditions that prevailed during earlier periods are based on estimates derived from proxy (geological) data. **Dynamic conditions (fluxes or flows)** can then be added by parameterization of surface and ocean processes. For the atmosphere, these might include heat and moisture exchange gradients between surfaces, moisture convection, Coriolis and shear constants, atmospheric pressure equilibria, and cloud formation and effects; and for the oceans, salinity flux, surface and subsurface currents, upwelling and overturning, eddy interference and density mixing (Randall *et al.*, 2007).

GCMs vary in their construction in three main ways. First, the earth's surface is represented by a geometrical Cartesian grid, the size of the grid cells depending upon the type and amount of information to be computed, and the capabilities of the computer employed (Figure 7.2). The grid in early GCMs varied between $4^\circ \times 5^\circ$ and $11.5^\circ \times 11.25^\circ$, but recent advances in computer capabilities and computational algorithms have allowed cell sizes of $1^\circ \times 1^\circ$ or less to be employed. Second, the atmosphere and oceans can be represented as a series of layers (or slabs), enabling both horizontal and vertical flows to be calculated (Figure 7.2). Third, the number of properties measured for each grid cell and the type of algorithms used for dynamic flow calculations also vary between GCMs, and these inevitably affect model performance.

The most sophisticated GCMs operating at the present time have been developed at specialist research centres sponsored by national organizations with research budgets large enough to meet the heavy technical and resource demands. Examples are those developed by NASA-GISS (Goddard Institute of Space Studies) and NOAA (National Oceanographic and Atmospheric Administration) in the USA, the Hadley Centre for Climate Prediction and Research of the Meteorological Office in the UK, the Meteorological Research Institute in Japan, the Bjerknes Centre for Climate Research in Norway and the Max Planck Institute for Meteorology in Germany. The models have been developed independently, although there is regular collaboration and cross-checking between research teams, and sharing of technical developments (e.g. Covey *et al.*, 2003; Jacob *et al.*, 2007). Over time, a degree of specialization has developed, with different teams focusing on improving the performance of specific components of the climate system, such as the UK Hadley Centre's project to

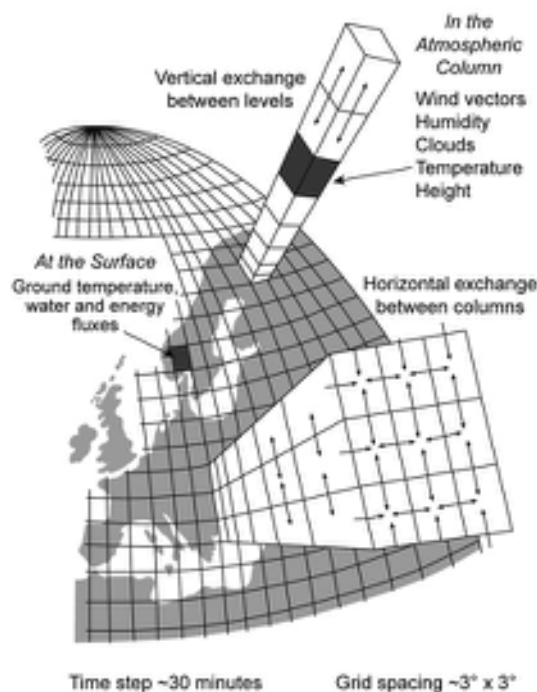


Figure 7.2 Cartesian grid arrangement for a GCM using a six-layered atmosphere and a grid cell size of $13^\circ \times 13^\circ$ (latitude and longitude). Physical parameters (wind vectors, humidity, clouds, etc.) are assigned to each grid block, and horizontal and vertical flows between adjacent blocks also have to be parameterized for each interface (i.e. for six interfaces for each cube within the stack).

develop a 'Fast Ocean' GCM, with improved representation of ocean gyres (Jones, 2003).

The performance of individual GCMs can be tested by comparing the extent to which they simulate modern weather patterns and conditions (Phillips *et al.*, 2004), or longer-term climate trends for which instrumentally measured data are available (Randall *et al.*, 2007). The latter approach is shown in Figure 7.3, where the model simulations tend to track the long-term instrumental temperature record, and the majority also pick out four short-term climatic downturns that immediately followed significant volcanic eruptions. The scatter in the model outputs (the 'noise' in the data) reflects differences of design between each GCM, for example Cartesian grid cell size, number of atmospheric and oceanic layers involved, and the computational algorithms employed. Inevitably, all models are characterized by a degree of uncertainty, since even the most powerful of computers

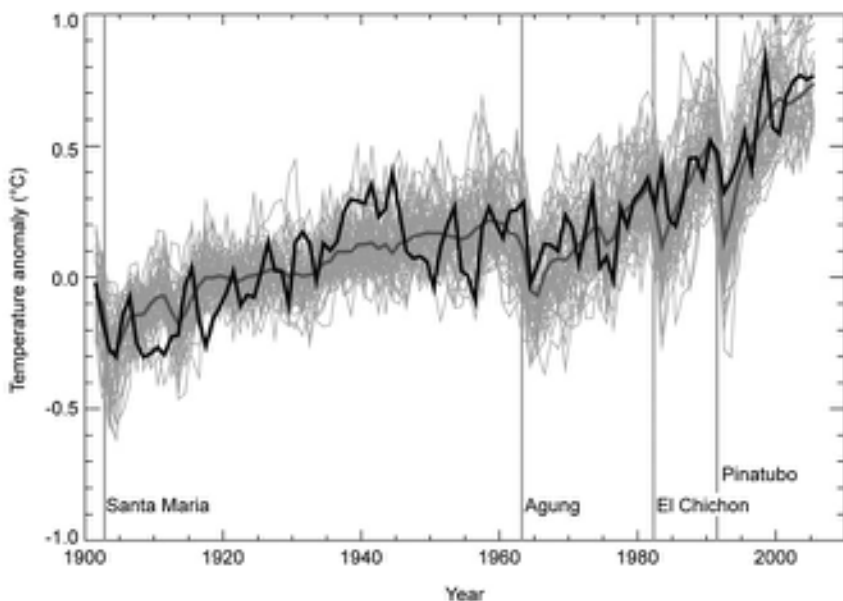


Figure 7.3 Comparison of fifty-eight individual GCM simulations of global temperature change since AD 1950 (thin light-grey curves, with mean trend shown in thicker, dark-grey line) compared with instrumentally measured temperature variations over the same period (black curve). The data are shown as deviations (anomalies) from the 1901–1950 mean value. Vertical grey lines indicate the timing of four major volcanic eruptions that occurred during the period (from Randall *et al.*, 2007). For further explanation see text.

cannot adequately represent the true scale and complexity of the global climate system.

Climate GCMs have generally been tuned to simulate modern climatic conditions especially, as noted above, in climatology and weather forecasting. Of particular interest to the Quaternary scientist, however, are environmental simulations for times in the past when the earth's surface boundary conditions were markedly different, and the information that such experiments can provide about the factors driving long-term climate change. In order to address these issues fully, however, additional environmental parameters need to be considered, as is explained in the following section.

7.2.4 Earth system models of intermediate complexity (EMICs)

Attempts to model the global climate system under different boundary conditions have tended to focus on the last 18 ka, the period for which the appropriate proxy data are most abundant (e.g. COHMAP Members, 1988). Atmospheric temperatures over land areas can be reconstructed using palaeoecological evidence (botanical records, coleopteran records, etc.); SSTs from marine micropalaeontological

data; glacier ice and sea-ice cover from glacial geomorphological and palaeoceanographic data; and atmospheric aerosol content from ice-core records. Orbitally induced solar radiation receipt can be calculated from radiation tables. Figure 7.4 shows, in a schematic way, how these boundary conditions may have varied at a global scale over the last 18 k ^{14}C yr (Kutzbach & Webb, 1993). The figure also illustrates the ways in which the earth's surface can be depicted in contrasting states or 'modes': (1) a 'glacial mode' at c. 18 k ^{14}C yrs BP (the Last Glacial Maximum: LGM), when the earth's orbital configuration was similar to that of today, but ice cover was much greater, sea level lower, and SSTs well below those of the present; (2) a period of enhanced seasonality around 11–10 k ^{14}C yrs BP; (3) a period when ice cover was significantly reduced and sea levels were close to those of the present day, but when seasonal differences remained high (at c. 6 k ^{14}C yrs BP); and (4) the present-day situation. The figure emphasizes how the climate system is constantly adapting to transient boundary conditions, which are very difficult to simulate: indeed, it has taken several decades to develop GCMs to the point where they can successfully model the modern climatic situation, and it is likely to take another step-change in computer power, as well as greatly increased operator

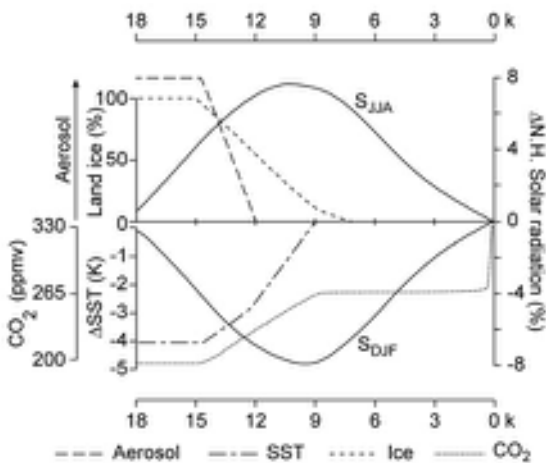


Figure 7.4 Boundary conditions for the COHMAP simulation for the last 18 k ^{14}C yrs BP. External forcing is shown for Northern Hemisphere solar radiation in June–August (S_{JJA}) and December–February (S_{DJF}) as the percentage difference from present-day radiation receipts. Internal boundary conditions include land ice as a percentage of 18 kyr ice volume; global mean SSTs are expressed as a difference from present-day SSTs. The excess glacial-age atmospheric aerosol content is shown on an arbitrary scale, while atmospheric CO_2 concentration is shown in parts per million by volume (ppmv). The horizontal scale shows the time interval of seven sets of ‘time-slice’ simulation experiments conducted by COHMAP (after Kutzbach & Webb, 1993).

time, before GCMs will be capable of simulating moving boundary conditions at the global scale (see section 7.2.4).

In order to circumvent this problem, a time-slice approach has often been adopted, whereby the prevailing (static) global climate state is simulated for specified time periods or intervals, effectively the approach that was adopted by COHMAP (Figure 7.5). Such models employed fixed SSTs, which is clearly unrealistic since the real oceans and atmosphere interact in a dynamic and mutually responsive way. They also adopted a relatively coarse grid size without any topographic detail, did not build in changes in global sea level, vegetation cover or ocean circulation, and the amount and quality of palaeodata available was far less than is the case today. Nevertheless, these models represented a significant breakthrough in Quaternary science, for they brought sharply into focus the scale and complexity of the changes in boundary conditions that typically occur during the course of a glacial–interglacial cycle and which would, in turn, have modulated the various feedbacks within the global environmental system. Examples of important linkages that the

COHMAP project highlighted include (1) the close correspondence between enhanced summer insolation and the strength of the monsoon cells in the Northern Hemisphere (Kutzbach & Guetter, 1986); (2) the deflection (or splitting) of the northern jet stream by the build-up of the Laurentide ice sheet (Figure 7.5), leading to marked changes in regional moisture distribution throughout the Northern Hemisphere (Kutzbach *et al.*, 1993); (3) the downstream modification of climate in Europe caused by sea-surface temperature changes in the North Atlantic (Rind *et al.*, 1986); and (4) the delay (by some 2–2.5 kyr) of the Northern Hemisphere interglacial thermal maximum following the summer insolation peak at c. 10 k ^{14}C yrs BP (Figure 7.4) as a consequence of the delayed melting of the great northern ice sheets (Webb *et al.*, 1993).

Although the situation has changed considerably since the COHMAP experiments, particularly as more comprehensive palaeo datasets have become available and models of much higher spatial resolution have been developed, two major problems remain. First, it is still not possible to generate circulation models for times in the past that are as sophisticated as the GCMs employed to simulate the modern climate, since quantified values for past boundary conditions (inferred from proxy data) have varying degrees of uncertainty (as discussed in Chapters 2–4), and there are still many areas of the world from which the requisite high-resolution data are simply not available. Second, the climate system is affected by other global circulation processes, not routinely incorporated into climate GCMs, for example the regulation of atmospheric gas content by the biogeochemical cycle. The amount of CO_2 and CH_4 present in the atmosphere at any one time reflects a balance between, on the one hand, release of these gases through a variety of processes and routeways (from terrestrial vegetation, disturbed peatlands, wildfires, permafrost melting, etc.) and, on the other, the amount that is absorbed into (and effectively trapped in) various reservoirs, for example the ocean ([carbon sinks](#)). A further influence is the amount and distribution of glacial and sea ice at any specific time, as this affects albedo. Other surface features that influence global climate include the extent and type of terrestrial biomes, ocean biomass, distribution and thickness of permafrost, ocean circulation and sea level. In addition, the climate system may experience a degree of inertia, with delayed response to effects inherited from these long-term processes.

The need to capture more of these processes and influences has led to the development of a new set of advanced models, which are referred to as [earth system models](#) (Figure 7.6). These attempt to identify and simulate as many as possible of both the short- and long-term

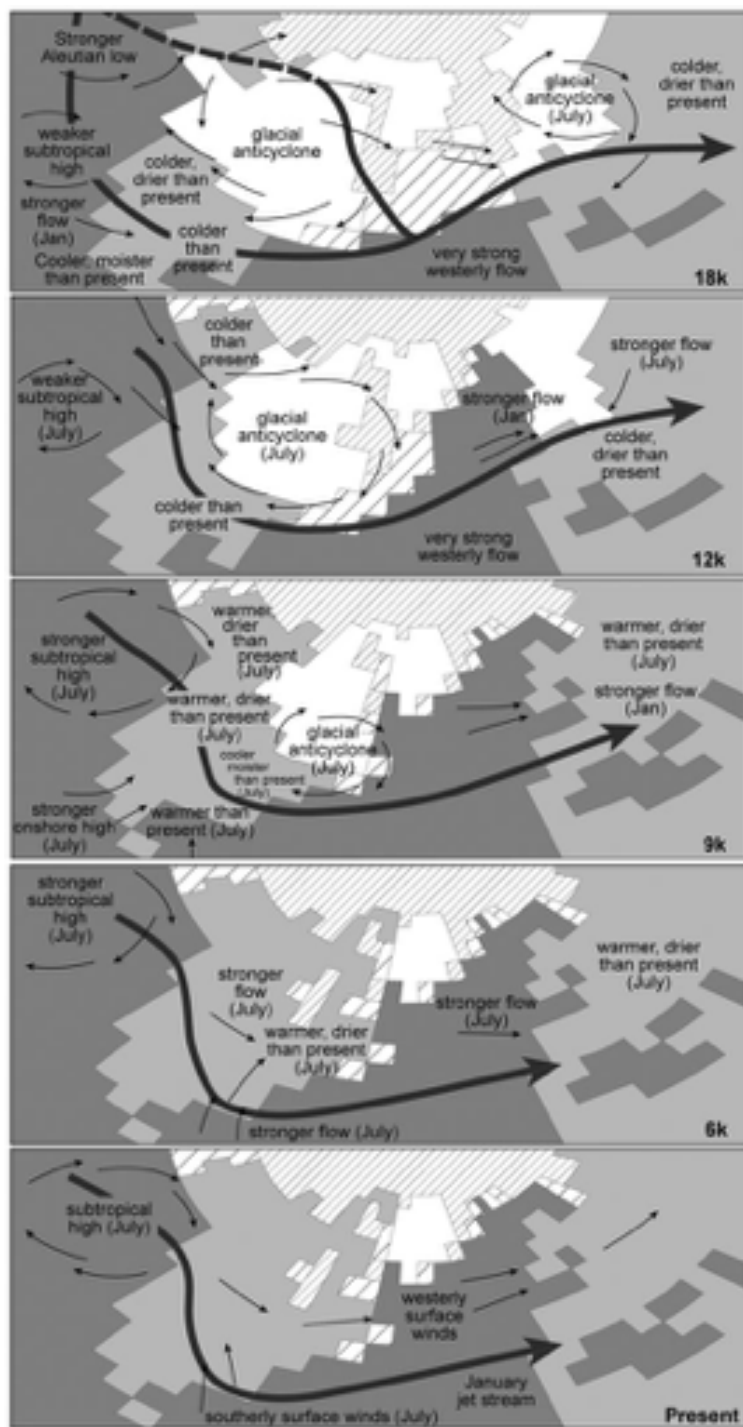


Figure 7.5 Palaeoclimatic model simulations for the last 18 k ^{14}C yrs BP (after Kutzbach *et al.*, 1993).

processes acting on the atmosphere and oceans (Flato, 2011). However, because it is still not feasible to build into the models *all* of the environmental parameters that exert an influence on the atmosphere, ‘**sub-models**’ have been constructed, which include a degree of simplification in terms of the inputs required for the simulation of long-term environmental feedback processes (Prinn, 2011). These ‘reduced’ models, intermediate in terms of computer power and complexity between conceptual box models on the one hand and top-of-the-range climate GCMs on the other, are termed **earth system models of intermediate complexity (EMICs)**. Since the computations performed are simpler than in GCMs, EMICs are able to generate results reasonably quickly, while several of these lower-order models can be coupled to each other or to GCMs in order to test the ways in which different subsystems integrate and feed in to the climate system. Figure 7.6 shows a schematic of the type of integrated earth system model array being developed by the Massachusetts Institute of Technology

in the USA (Prinn *et al.*, 2011). A second example is the GENIE initiative (Grid ENabled Integrated Earth system), developed in the UK for experiments designed to identify the ‘**tipping points**’ that affect Atlantic thermohaline circulation; in other words, those critical conditions that can tip the system into instability (Lenton *et al.*, 2009). Because EMICs can simulate changes over long time-scales, including the 100 ka cycles (Weber, 2010), they are becoming increasingly important in the study of Quaternary environmental change, as is illustrated in later sections.

7.2.5 Transient simulations

A further difficulty with full-scale GCMs is that they are most often used to simulate the climate at equilibrium, and the results therefore provide ‘snap-shots’ of the climate state at particular points in time. In order to examine change in the system, new boundary conditions and feedback fluxes

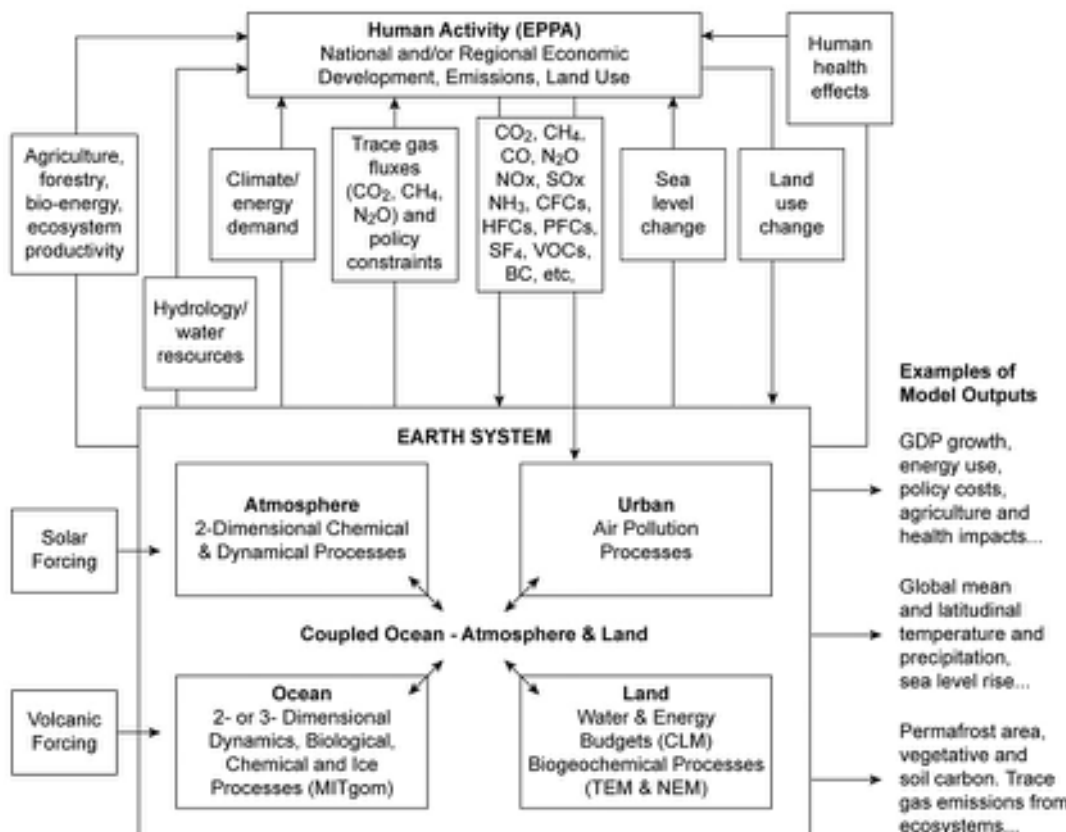


Figure 7.6 Feedback framework for the Integrated Global System Model of MIT (Massachusetts Institute of Technology, USA; <http://mit.edu/globalchange>).

must be prescribed, and the model set to run until it achieves equilibrium with the new controls. In other words, the model effectively ‘jumps’ from one climate state to the next, unlike the real climate system which is continually responding to a range of forcing factors and feedback loops, some of which change gradually, while others may cross thresholds that trigger more sudden adjustments (tipping points). Of particular interest to Quaternary scientists are the transitions between climate states, for example those that characterize the last glacial cycle (DO cycles), and the factors that initiate a change from one climatic episode to another. Current GCMs are not able to simulate these non-equilibrated (transient) climatic shifts, due to excessive computational demand (Timm & Timmermann, 2007). But by improving the design and performance of EMICs, which have fewer climatic components but include computations for geological variables such as ice-sheet variations, ocean circulation or volcanic forcing, **transient models** can be constructed which are capable of responding to continuously adjusting variables and which can deliver *transient accelerated palaeosimulations* (Lunt *et al.*, 2006). These require specialized sub-models representing different components of the environmental system, which are coupled together in order to test their interactions. One example is the EC–Bilt–CLIO model (<http://csdms.colorado.edu/wiki/Model:ECBILT-CLIO>), which consists of three coupled sub-models simulating the global atmosphere, ocean dynamism and sea-ice variations (Renssen *et al.*, 2007b). This transient model features in a range of model experiments designed to test the operation and regional impacts of thermohaline circulation (Timmermann *et al.*, 2005). EC–Bilt–CLIO can also be coupled with other sub-models, for example those that simulate changing vegetation cover, to include additional feedbacks in palaeoenvironmental experiments (Renssen *et al.*, 2005). Further examples of the EMIC arrays used in transient models and an assessment of their simulation performance and limitations can be found in Petoukhov *et al.* (2005).

7.2.6 Palaeodata-model comparisons

Palaeoenvironmental proxy data (commonly shortened to ‘palaeodata’) make important contributions to the development of ESMs in two main ways: first, in providing estimates of the boundary conditions that prevailed in former times, and second, in evaluating the results of ESM experiments that are designed to ‘predict’ (or ‘retrodict’) past climate states. The former application was discussed above, while the latter works in the following way. If a number of site records provide continuous palaeodata

spanning a specific time interval, for example from the LGM to the present, boundary conditions for selected times can be inferred and fed into the ESM. If the changes in boundary conditions for the early stages only are fed into the model, then it can be set to run with these prescribed boundary conditions, and allowed to continue to simulate how the climate might evolve at a later stage. The model outputs can then be compared with independent empirical data for the later period in order to determine how well they match. Because the ‘predicted’ (forecast) outcome in this instance is for some time in the past, this procedure is often referred to as **‘post-diction’** (or **‘hind-casting’**). This is extremely important in Quaternary research, for it is the only way in which ESMs (including GCMs) can be tested for their ability to predict climate states not experienced within the period of instrumental records, which at most extend over the past 150–200 years. However, the data have to satisfy a number of criteria if they are going to deliver reliable information that can be used for this purpose (Kohfeld & Harrison, 2000). First, they should be continuous or near-continuous over the period concerned, although small gaps can be filled by data interpolation techniques. Second, they should be reliably dated, to ensure that the boundary conditions prescribed for specific times are derived from contemporaneous evidence. Third, they should be spatially extensive, to discriminate local anomalies from more general changes. Fourth, the former environmental conditions should preferably be quantified and in a form that can be directly compared with model output data (e.g. seasonal or annual mean temperatures, precipitation or moisture change, etc.). Fifth, realistic statistical uncertainties should be integral to the data (Kohfeld & Harrison, 2000).

Insights into Late Quaternary climates from palaeodata-model comparisons, therefore, require a close dialogue between climate modellers on the one hand, and Quaternary scientists who collect and interpret proxy data on the other. The models are, of course, only as secure as the data upon which they are based, and against which they are ultimately to be tested. The *onus* therefore falls squarely on the Quaternary community to provide the necessary high-quality, high-resolution proxy records to enable climatic modelling to begin to provide answers to questions, not only about the pattern of past climatic changes, but also about their causes. To meet these objectives, global palaeo-datasets are now usually assembled through collaborative (community) research initiatives that are subject to strict **quality control** measures, with the resulting archives being held in publicly accessible data-centres. These include, for example, **DIRTMAP** (Dust Indicators and Records from Terrestrial and Marine Palaeoenviron-

ments), an integrated record of variations in quantified rates of aeolian dust accumulation (Bullard, 2010), the **Global Lake Status Data-base**, which collates information on past variations in lake level (Qin *et al.*, 1998; section 3.7.3), and **BIOME-6000**, a global synthesis of palaeo-vegetation records based mainly on pollen data which are classified into a series of different biome types, an initiative established primarily to test ESM simulations (Wu *et al.*, 2007). Global databases are also being assembled for marine records, for example the multiproxy MARGO database referred to in section 4.10.7. There are also major interdisciplinary initiatives that foster closer collaboration between scientists who collect palaeodata and modellers interested in performing ‘hindcasting’ experiments, such as **PMIP** (the Paleoclimate Model Intercomparison Project), which focuses on experimental design and capabilities (Weber *et al.*, 2007).

7.2.7 Limitations of ESMs

Although numerical modelling has provided important new insights into the workings of the global environmental system, even the most sophisticated of models continue to have limitations. Some of the remaining areas of concern are the following:

1. Models invariably (and inevitably) oversimplify environmental complexity for, as we have seen, they cannot represent every component and synergistic interaction that occurs in nature. New discoveries continue to show how small-scale processes, such as feedback mechanisms involving cloud formation, for example, can have far bigger impacts on climate (and also model output) than might have been anticipated (McGuffie & Henderson-Sellars, 2005).
2. Because numerical models can only handle a finite number of calculations, all the global processes and interactions represented in the models must be scaled down in order to be manageable, and this inevitably leads to a difficulty in scaling-up when it comes to interpreting the output. This is the reverse-logic problem of knowing whether or not the scaled-down, almost artificial, microcosm created in the model truly reflects the operation of the system at the global scale.
3. Interactions between global subsystems (the atmosphere, hydrosphere, cryosphere, biosphere, geosphere) are invariably non-linear. Hence, while it may be possible to predict responses within a simplified subsystem when only a few variables are involved,

the greater the number of variables, the greater the complexity in terms of links between different subsystems. This almost inevitably means that the outcomes are less predictable (Schellnhuber, 1999).

4. Only very small changes in one or more parameters can have significant effects on model output. Running the same model twice using exactly the same parameters and boundary conditions can generate quite different outputs (Sivakumar, 2004), which may help explain why GCMs often tend to produce different predictions of future climatic scenarios.

Despite these limitations, however, if an element of chaotic behaviour is involved in all natural processes, then, paradoxically perhaps, the only viable way forward in the search for an understanding of the global climate system, and predicting its behaviour, is through numerical modelling. If this challenge is to be met, future generations of numerical models must become even more sophisticated. They will have to incorporate a much wider range of variables and linkages to reflect more realistically the complexity of the global environmental system.

7.2.8 The importance of ESMs in Quaternary research

Despite their limitations, ESMs of all categories are playing an increasingly important role in Quaternary science. They provide a means of synthesizing a wide range of environmental information at the global scale, of quantifying the major processes influencing global climate, and of conceptualizing the cause-and-effect pathways involved in climate change, and their environmental impacts. ESMs have also focused attention on the important time lags that appear to have occurred between climate-forcing signals on the one hand, and the response of climatic circulation and other environmental processes on the other, examples of which are discussed in later sections. Palaeodata-modelling collaborations are critical for testing and improving ESMs, and hence for reducing uncertainties in their results, which is one of the key issues highlighted by the **IPCC** (Intergovernmental Panel on Climate Change) in its latest reports (Schmidt, 2010). The threat of accelerating anthropogenically induced climate change, with its environmental, economic, political and societal ramifications, and the need for appropriate remedies and policies, places an increasing responsibility on environmental scientists to provide a realistic context within which future climatic scenarios can be assessed. Quaternary science has a key role to play in this regard, for the Quaternary stratigraphic

record provides the all-important data archive against which climate models can be tested and evaluated. With this in mind, we now turn our attention to the record of the past, and begin with environmental change over longer timescales.

7.3 CLIMATIC CHANGE OVER MILANKOVITCH TIMESCALES

7.3.1 Introduction

Although there is a general consensus that the precessional (*c.* 21 ka), obliquity (*c.* 41 ka) and eccentricity (*c.* 100 ka) Milankovitch cycles are key elements in explanations of long-term climate change (section 1.7), it is now clear that these alone cannot account for all aspects of the Quaternary climate record. Indeed, despite the fact that the astronomical theory has been a central tenet of Quaternary research ever since the publication of the seminal paper by Hays *et al.* (1976), it is a curious fact that there is still no universally accepted account of the individual and combined effects of the Milankovitch variables on global climate (Elkibbi & Rial, 2001). Moreover, while a Milankovitch signal is clearly evident in many proxy records, in some the astronomical rhythms are more subdued, while in others there are clear off-sets between astronomically predicted and empirically based climatic cycles. One reason for this may be because the former are approximations of complex planetary harmonics: the *c.* 21 ka cycle, for example, is an average of two separate but interlocked cycles, while the *c.* 100 ka cycle is a derivative of at least five separate cycles of varying power, ranging in frequency between 95 and 107 ka, and each reflecting varying orbital interference between Mars, Mercury, Venus, Earth and Jupiter (Berger *et al.*, 2005). And there are other orbital factors that might influence global insolation, for example changes in the Earth's orbital plane (the imaginary surface marked out by the Earth's orbital path) which is known to vary in terms of its inclination over a quasi-100 ka cycle (Muller & MacDonald, 1997). Off-sets between empirically derived and astronomically driven climatic cycles may also reflect chronological and stratigraphical uncertainties associated with geological age models (Ao *et al.*, 2011), or the fact that climatic responses may lag changes in insolation because of delays in environmental feedbacks, for example mass balance changes of large continental ice sheets (see Ruddiman, 2006) which influence the $\delta^{18}\text{O}$ signal in the oceans through variations in ice mass volume (section 3.10.2). Furthermore, the detail in empirical records may be blurred by the application

of data-smoothing and tuning of the results to the Milankovitch timescale, a procedure frequently adopted in the analysis of isotopic profiles from deep-sea sediments, but which may conceal differences in detail between records by assuming, rather than testing for, contemporaneity between inferred climatic events (Blaauw, 2012; Berger 2013a, 2013b; section 6.3.3.3).

Accounting for the amplitude and frequency of the climate signal in Quaternary stratigraphic sequences in terms of the Milankovitch rhythms is also often difficult. For example, while there may be strong empirical evidence pointing to the influence of precession and obliquity in proxy climate records, the influence of the 100 ka cycle is more difficult to explain, because calculations have shown that variations in insolation forcing resulting from eccentricity changes are, by themselves, too small (of the order of 0.1 per cent) to be the direct cause of glacial–interglacial changes over the past 900 ka (Imbrie *et al.*, 1993). This '100 kyr problem' of Milankovitch theory is further compounded by the fact that the longer 413 ka eccentricity cycle, which appears to be the largest component of eccentricity forcing, does not register clearly in the marine oxygen isotope records (Rial & Anacleto, 2000). The pacing of recent glacial–interglacial cycles is also problematic, for although the climatic mode (as reflected in marine isotope records) of the last 800–900 ka is around 100 ka, the duration of consecutive glacial periods actually varies from *c.* 80–120 ka. The interval between the last two interglacials is 120 ka, while around 400 ka, the interval was *c.* 80 ka, with three successive interglacials occurring in less than 200 ka (Raymo, 1997). These and other apparent inconsistencies between observation and theory have prompted questions about whether we can indeed match the geological record to the astronomical variables (Meyers *et al.*, 2008) and, moreover, whether the earth's climate system does actually respond in a linear fashion to the Milankovitch influences, or that the nature of the response is non-linear or stochastic (Wunsch, 2004; Huybers & Wunsch, 2005). While this is still perhaps a minority view, it does highlight the fact that an understanding of long-term climate change requires additional explanatory mechanisms.

In this section we look again at the Astronomical Theory in the light of some of these difficulties and we focus on two particular aspects of the Quaternary record: the switch from 41 ka to 100 ka cycles at the Middle Pleistocene Transition (MPT), and the factors driving glacial–interglacial cycles during the last 800 ka. The latter, in particular, have importance for evaluating developments during the present interglacial (Holocene), including the

extent to which humans may have exerted an influence over natural environmental processes, and to which we return later in the chapter (section 7.6).

7.3.2 The Mid-Pleistocene Transition (MPT)

As we noted in Chapter 1, the terms ‘Middle Pleistocene Transition’ (MPT) or ‘Mid-Pleistocene Revolution’ refer to a shift in spectral frequency in oxygen isotope records, between the ‘41 kyr world’ that characterizes the early to Mid-Pleistocene and the ‘100 kyr world’ of the late Pleistocene (Raymo & Nisancioglu, 2003). For the sake of convenience, this change in spectral dominance is often described as having occurred around 900–800 ka but, in practice, there is considerable variability between different proxy records in the timing of the onset of the MPT (e.g. Head *et al.*, 2008b; Elderfield *et al.*, 2012). Moreover, the transition is often gradual, spanning several hundred thousand years. In the marine isotope record from the

Pacific shown in Figure 7.7, for example, the isotopic signal, reconstructed sea-level history, and inferred sea-surface temperature records (SSTs) are clearly dominated by the 41 ka cycle before c. 1.25 Ma, but this is followed by a period up to c. 700 ka where the pattern is much less clear (Siddall *et al.*, 2010a). Thereafter, the 100 ka cycle becomes dominant, and this accords with the majority of other records which show that by c. 650 ka, the start of what has been termed the **Milankovitch chron** (Berger *et al.*, 1994), global climate was locked into the 100 ka rhythm of change (Figure 7.8a). It is important to remember, however, that what we are seeing in Figure 7.8a are variations in the strength of the global climatic *response* to astronomical forcing factors, and this record appears to show that the global climate system became much *more responsive* to the 100 ka insolation cycle after the MPT. But herein lies one of the problems referred to above, namely that despite this increased sensitivity of global climate to the Milankovitch rhythms post the MPT, astronomical calculations suggest that eccentricity variations are insufficient *in themselves*

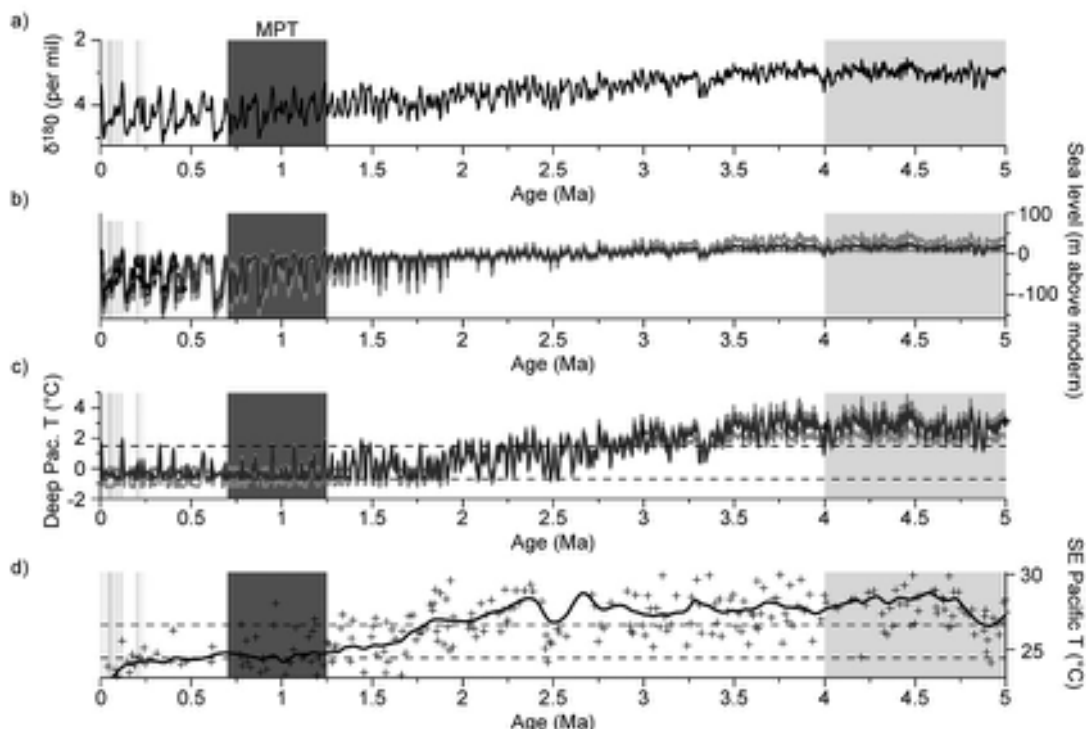


Figure 7.7 Deep Pacific records of environmental change during the past 5 Ma. a) Composite oxygen isotope record based on benthic Foraminifera. b) Variations in global sea level interpolated from the isotopic data. c) Temperature residuals of the isotopic data that cannot be explained by the sea-level component. d) Surface ocean temperature variations based on Mg/Ca analysis of marine microfossils. The crosses are the primary data, the curve is a moving average trend-line, and the two dashed lines represent an arbitrary 2°C interval used as a guide to long-term trends in SST. For further detail see Siddall *et al.* (2010a).

to account for the large-amplitude oscillations that characterize the late Pleistocene mode of climatic behaviour; in other words, the repeated shifts between glacial and interglacial conditions (Paillard, 2001). Furthermore, when considered over the timescale of the last 1 Ma or so, the strength of the correlation between marine records (reflecting climate response) and insolation data (possible forcing) indicates a considerable (and surprising) variability in sensitivity of the climate system to changes in the Milankovitch variables (Figure 7.8b). Particularly curious is an interval of unusually weak correlation between the proxy records and insolation data, which Berger (2013b) has described as a ‘deaf zone’ (a period when the global climate system seems to have been relatively inert to astronomical forcing), and which is interposed between

periods of more agitated or excited behaviour. The latter appear to be exaggerated responses to the low-amplitude eccentricity signal, as for example during the last 400 ka, a period informally termed the *Emiliani chron* (Figure 7.8b). Since these marked shifts from muted to excited behaviour of the climate system cannot be explained by Milankovitch forcing alone, they must reflect the influence of additional factors. Efforts to establish what these factors might be and how they might have influenced global climate rhythms prior to and post the MPT have involved three main approaches: the analysis of terrestrial, oceanic and atmospheric records; investigations of what is termed ‘phase interference’ between the astronomical cycles; and the use of numerical models. Each of these will be considered in turn.

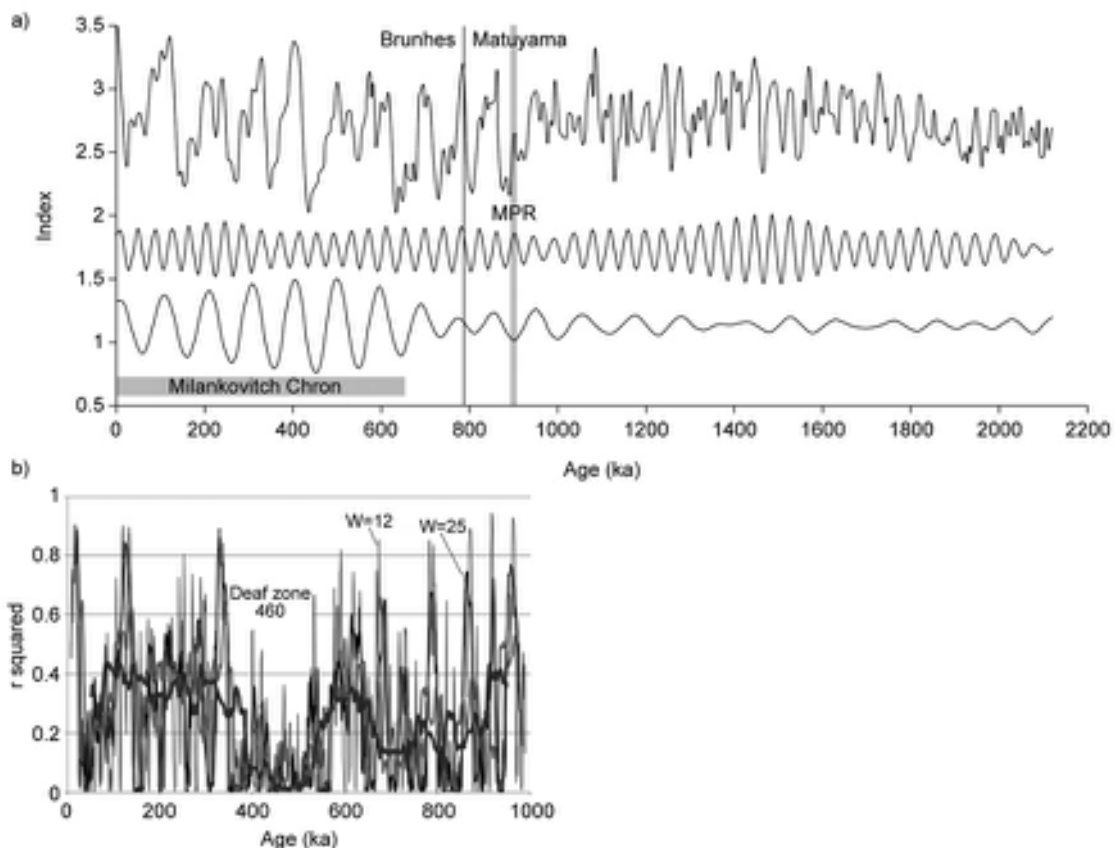


Figure 7.8 a) Marine oxygen isotope record for the last 2.1 Ma (ODP Site 806) and the spectral signal of the 41 ka and 100 ka cycles from this record. b) A measure of the strength of correlation between the stacked oxygen isotope record and Milankovitch forcing over the past 1 Ma. The method employs ‘sliding windows’ (W) of 50 ka (darkest grey and thickest line), 25 ka (mid-grey; $W = 25$) and 12 ka (lightest grey; $W = 12$) intervals in the correlations. The data reveal a period (centred on 460 ka) of particularly low correlation coefficients (r^2 -values) suggesting a time of low sensitivity of the earth system to insolation, which Berger (2013b) refers to as a ‘deaf zone’ (from Berger, 2013b). For further explanation see text.

A number of potential amplification agents have been proposed from an analysis of geological records. Considerable attention has focused on variations in atmospheric CO₂ and other greenhouse gases, as ice-core data in particular have shown a close relationship between the Milankovitch variables, atmospheric CO₂ and inferred temperature changes (see Figure 7.13). Physical processes within the atmosphere have also been suggested as forcing factors for the MPT, such as intensification of the Walker circulation cells leading to increased moisture transport to high latitudes, thereby accelerating the growth of the northern continental ice sheets (McClymont & Rosell-Melé, 2005). In addition, there are indications of a significant increase in Antarctic ice volume at around 900 ka which some have seen as a potential trigger for the MPT (Elderfield *et al.*, 2012), while others have invoked variations in atmospheric dust flux, which alters surface albedo (especially over ice sheets) and insolation receipt (Bar-Or *et al.*, 2008; Martinez-Garcia *et al.*, 2011). A widely held view is that the change in climatic periodicity around the MPT and the concomitant intensification of Northern Hemisphere glaciation could be due to tectonic activity, with progressive land uplift (e.g. in the Himalayas) leading to the transgression of critical altitudinal thresholds and accompanying changes in atmospheric circulation regime (Raymo *et al.*, 1992). Other explanations for the shift in climatic phasing prior to and post the MPT, however, involve a complex interplay of Milankovitch forcing (principally on precessional and obliquity timescales), and feedback mechanisms involving ocean circulation changes, ice-sheet build-up and atmospheric gases. For example, Raymo (1997) has suggested that prior to 900 ka, ice sheets melted during each precession- or obliquity-induced warm stage, but around 900 ka, Northern Hemisphere temperatures had cooled to a critical threshold which allowed ice to persist through weaker insolation maxima and hence to grow to a larger size over each successive cycle. Because high-amplitude precession maxima only occur in every fourth cycle (100 ka), due to eccentricity modulation, ice sheets would tend to grow and melt with a periodicity of 100 ka. Such effects would have been increasingly amplified by CO₂ feedback (Ruddiman, 2003a). Denton (2000) has pointed to the effects of the ocean in such feedback loops. He envisages ice sheets growing steadily over the course of a 100 ka cycle, extracting waters from the world's oceans and leading to major reorganization of deep-water circulation from an 'interglacial' to 'glacial' mode. The Milankovitch variables will eventually trigger ice-sheet collapse which then shifts circulation back into an interglacial mode and the cycle begins again. He also invokes a possible tectonic component in the development of the 100

ka climate rhythm, pointing to the uplift of the submarine Greenland–Scotland ridge which occurred between 900 and 650 ka BP, and which may have led to marked changes in North Atlantic deep-water circulation.

As noted above, a characteristic of the Mid-Pleistocene Transition (MPT) is that post the MPT, global ice volume was greater and ice sheets appear to have been substantially thicker than in pre-transition times. Clark and Pollard (1998) attributed this change in ice thickness (and volume) to the gradual removal by ice-sheet erosion of a thick regolith. Prior to the MPT, this 'low-friction' regolith led to the development of extensive, but relatively thin ice sheets that responded linearly to the 41 ka obliquity cycle. As this mantle of debris was removed by successive glaciations, large areas of Precambrian Shield crystalline bedrock were exposed, and this 'high-friction' substrate induced thicker ice sheets with a fundamentally different response to orbital forcing after the MPT. In addition, regolith erosion and exposure of crystalline bedrock could have caused an increase in silicate weathering rates (section 1.7), and carbon-cycle modelling suggests that the drawdown in atmospheric CO₂ that would have accompanied this process could have led to a decrease of around 7–12 ppm in atmospheric CO₂ (Clark *et al.*, 2006). If this was indeed the case, then the global cooling resulting from this secular decrease in atmospheric CO₂ may have been an important feedback in causing the MPT (Mudelsee & Schultz, 1997; Raymo, 1997). In a radically different interpretation, it has been suggested that the apparent shift in pacing from c. 40 to c. 100 ka cycles that characterized the MPT can be seen not as a response to changes in atmospheric CO₂, continental regolith exposure or other external control, but rather as a reflection of glacial variability spontaneously switching between long and short period modes; in other words, it is another aspect of the chaotic or non-linear response to orbital forcing referred to above (Huybers, 2009).

There is, therefore, a range of factors within the earth's terrestrial, oceanic and climate systems that could, through a complex network of linkages and feedback mechanisms, have affected the astronomical pacing of global climate and instigated the MPT, and the subsequent shift to the 100 ka mode (McClymont *et al.*, 2013). It is, however, difficult to establish which, if any, of these individual factors could have been *driving* climate change, as opposed to being secondary effects, an issue we return to in later sections of this chapter.

The second approach to resolving the conundrum of the MPT focuses on the analysis of the amplitude, frequency and phasing (concordancy) of the different Milankovitch rhythms, and their integrated effects, the principles and

language used in these analyses being borrowed from the study of electromagnetic wave-forms. The process of modifying a wave's amplitude while keeping frequency constant is termed **amplitude modulation**, while the opposite (constant amplitude but variable frequency) is referred to as **frequency modulation**. In theory, natural earth surface processes could modulate insolation waves in both ways. On the other hand, the wave-forms themselves could self-regulate through a process termed **phase-locking**: two waveforms can be locked into harmonious frequencies, but shifted in phase, by the operation of a feedback loop. The combined effect of this could either amplify or dampen the output signal, and could do so in either a linear or non-linear fashion, the latter having less predictable outcomes.

As we have seen, time-series data from the Quaternary record, whether they be isotopic signals from ice cores or ocean cores, long trace-gas records, or palaeotemperature reconstructions, are characterized by wave amplitude and frequency variations, and are amenable to a number of mathematical or statistical methods for analysing the strength of, and resonance between, interacting wave forms. Perhaps the most widely applied has been spectral analysis (see Chapter 1, note 7), but other techniques have also been employed. For example, Huybers (2007) applied a probability statistic (Rayleigh's R)¹ in an analysis of the relationship between the timing of deglacial events and orbital variations. He focused on thirty-six deglaciation signals identified in the records for the past 2 Ma and found that thirty-three of them occurred when the *obliquity* signal was anomalously large: during the early Pleistocene, they align closely with the obliquity signal, and hence have a 40 ka rhythm, while in the late Pleistocene, deglaciation occurred every 80 or 120 ka, giving an average frequency of 100 ka. Maslin & Ridgwell (2005) have linked the 100 ka glacial–interglacial mode of behaviour to resonance between the *precession* and *eccentricity* cycles, with eccentricity *pacing* the changes, but the climate response being enhanced by concordant phasing with the obliquity cycle. Other studies have suggested that strengthening of a **semi-precession signal** (periods of about 11.5 ka) during the late Pleistocene was responsible for the development of 100 ka cycles (Rutherford & D'Hoydt, 2000). Possible support for this contention comes from Chinese loess records, which reveal evidence of well-defined semi-precessional cycles during the most recent interglacial–glacial cycle, and which are attributed to periodic strengthening and weakening of the East Asia summer monsoon (Sun & Huang, 2006). More recently, however, spectral analysis by Rial *et al.* (2013) of climatic variations over the past 4 Ma suggests that the 400 ka eccentricity cycle has been more important

than previously realized, with the global climate system having apparently synchronized to this frequency around 1.2 Ma, after which an increasing alignment between the 41 ka, 100 ka and 400 ka cycles culminated in enhanced amplitude of the 100 ka cycle.

The third approach uses numerical modelling to test observations or ideas obtained from empirical evidence or from statistical analyses of long Quaternary records. Reference has already been made (section 7.2.1) to the use of simple box models to evaluate the hypothesis that growth of sea ice initiated and regulated the late Pleistocene 100 ka oscillations (Tziperman & Gildor, 2003). A more comprehensive ice-sheet–ocean temperature model was developed by Bintanja & van de Wal (2008) to quantify changes in global surface air temperature, ice volume and sea level from marine benthic $\delta^{18}\text{O}_2$ measurements spanning the last 3 Ma. The results suggest that the evolution of the 100 ka cycles coincided with a change in the relative importance of the North American and European ice sheets, with the latter apparently dominating before the MPT, but the former exerting an increasingly greater influence during the Milankovitch chron (i.e. post-650 ka BP; Figure 7.9). This was probably a result of the merging of the Cordilleran and Laurentide ice sheets, enabling the combined ice mass to survive insolation maxima during each successive glacial cycle. Ultimately, this compound ice sheet grew to the extent that it became unstable, initiating rapid terminations (Bintanja & van de Wal, 2008).

Ganopolski & Calov (2011) used an earth system model of intermediate complexity to demonstrate that both strong 100 ka periodicity in the ice-volume variations and the timing of glacial terminations during the past 800 ka can be successfully simulated as a direct, strongly non-linear response of the climate-cryosphere system to orbital forcing, providing that the atmospheric CO₂ concentration stays below its typical interglacial value. Their modelling results suggest that the existence of long glacial cycles during the late Pleistocene is primarily attributed to the North American ice sheet, and requires the presence of a large continental area with exposed rocks, and that temporal variability in CO₂ concentration plays an important role in the amplification of the 100 ka cycles. These modelling results accord with empirical evidence referred to above for increased ice volume during the later Pleistocene, and with amplification of the astronomical signal by atmospheric CO₂ variations. They also reinforce the view that non-linear amplification of astronomical forcing may be necessary for the generation of the 100 ka cycle that has dominated climatic behaviour during the Milankovitch chron (see for example Ditlevsen, 2009).

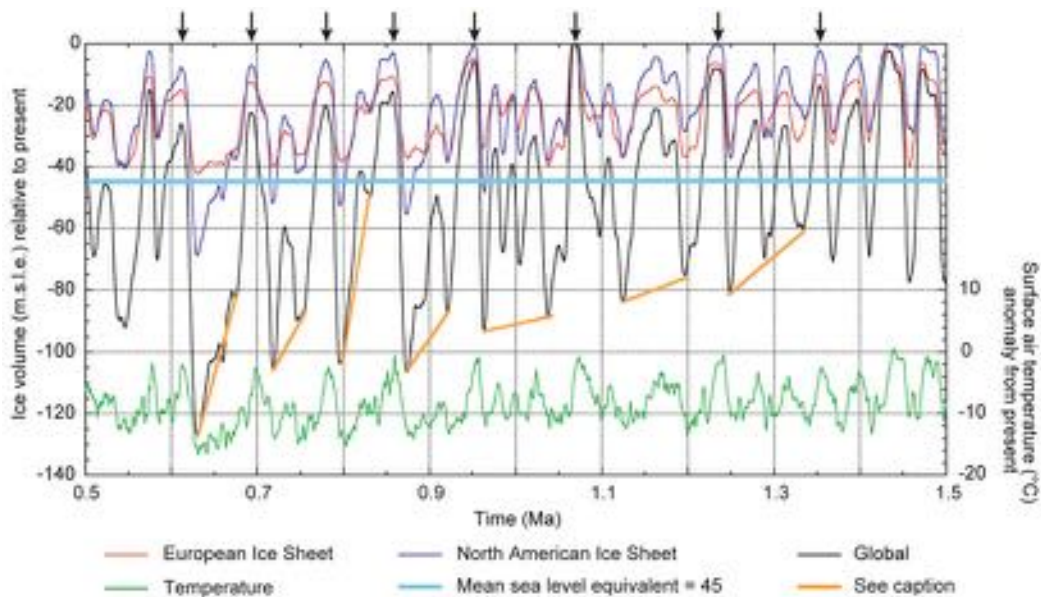


Figure 7.9 Modelled time-series of ice volume (top three curves) and Northern Hemisphere subarctic surface air temperatures (green) from 1.5–0.5 Ma, encompassing the Mid-Pleistocene Transition. The model simulates changes in global sea level (black curve) and contributions to global sea-level variations made by the European (red) and North American (blue) ice sheets, all shown relative to long-term mean sea level (msl: pale blue horizontal line). The vertical black arrows indicate positions of msl maxima (interglacials), approximately every 100 ka. The model results suggest an increasing influence of the North American ice sheet on global sea levels, with progressively lower global sea level minima (orange bars), over the course of the last 1 Ma (from Bintanja & van de Wal, 2008).

While these different approaches to the problem have undoubtedly thrown new light on the nature and causes of the MPT, there are many questions about this enigmatic section of the Quaternary record that remain unresolved. These are exemplified by a recent analysis of global sea-surface temperature variations over the past 2 Ma (McClintock *et al.*, 2013). This shows that although a common cooling trend is manifest in all records between 1.2 Ma and 800 ka, and that the majority are characterized by significant cooling steps at 1.2 Ma and 900 ka, some oceanic records appear to show earlier responses. Moreover, for some regions, the coldest glacial stages occur after 900 ka, whereas in other regions, predominantly in the Southern Hemisphere, the glacial stages post-900 ka were *warmer* than those in the mid- and early Pleistocene. In addition, the shift towards dominant 100 ka cyclicity occurs gradually in some records, emerging as early as 1.2 Ma, while in others it is not evident until after 800 ka. We return to these and related matters in section 7.3.3, after first examining the nature and form of the 100 ka oscillations reflected in the fossil record of the past 800 ka.

7.3.3 The glacial-interglacial cycles of the last 800 ka

The high-resolution palaeoenvironmental records for the last 800 ka obtained from recent deep-ice drilling of the Antarctic ice sheet (section 3.11) have provided important templates for climatic variability over the last eight glacial–interglacial cycles. These records have revolutionized the study not only of long-term climatic change, but also of potential forcing factors that drive those fluctuations, because they contain information on atmospheric conditions (notably greenhouse gas [GHG] content and dust flux); on global temperature, principally through the proxy of deuterium (δD); on ice-volume changes; and on a range of other environmental variables. Importantly, these are co-registered in the same ice core (Figure 7.10), and hence precise temporal relationships between each of them can be determined. Moreover, records are available from ice from a number of different drilling sites (e.g. Vostok, Dome C, Dome F and Dronning Maud Land), which enables local influences to be identified and quantified. The remarkable degree of overall compatibility

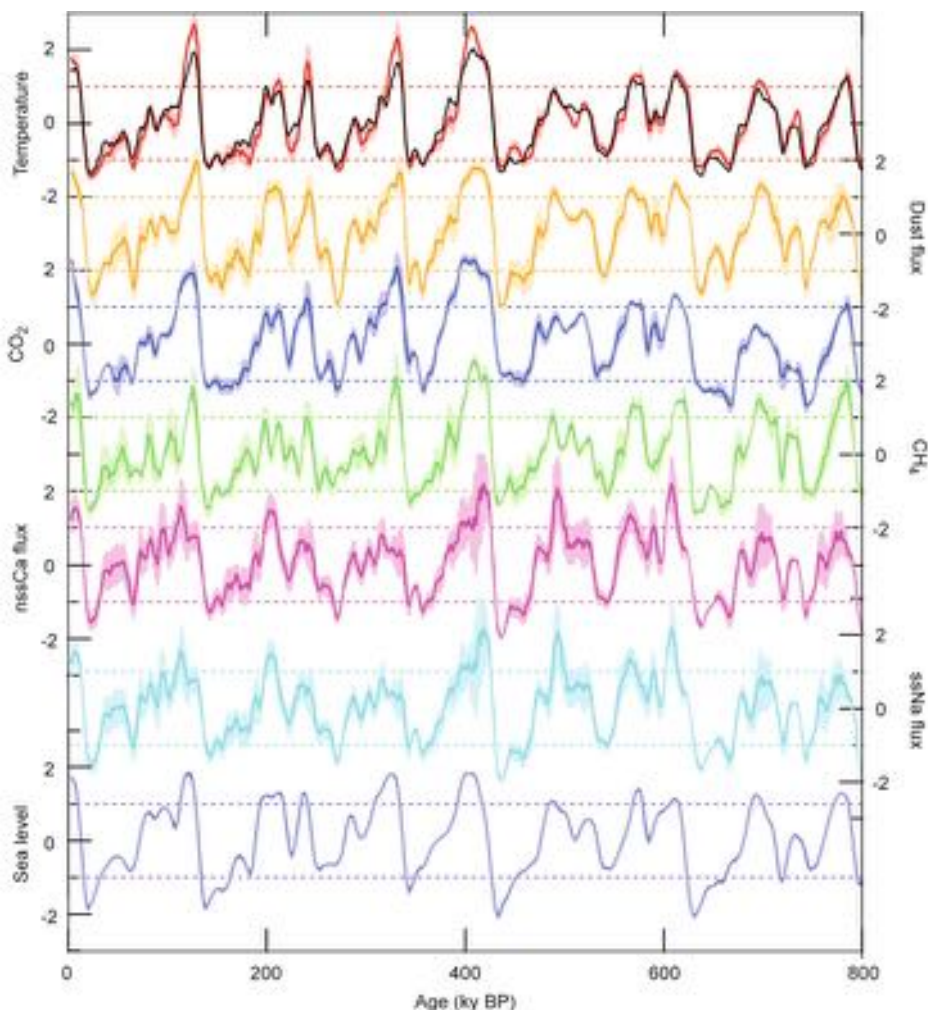


Figure 7.10 Records of deuterium (δD), dust flux and aerosols (CO_2 , CH_4 , Ca and Na flux) over the last 800 ka obtained from the EPICA Dome C (EDC) ice core, East Antarctica, compared with sea-level changes inferred from the LR04 marine isotope record (Figure 1.5). The data are shown as variations in standard deviation units from the long-term means; the thick lines indicate forcing on orbital timescales, while the shaded areas reflect non-orbital influences – a combination of data uncertainty and feedback variability (after Masson-Delmotte *et al.*, 2010).

between different Antarctic ice-core records is illustrated in Figure 7.11.

Antarctic ice-core data have provided new insights into glacial–interglacial climate dynamics, particularly in regard to radiative and climate feedback forcing mechanisms, and also in the estimations of time lags between forcing factors and climatic response. **Radiative forcing** is any change in the intensity of the solar radiation signal transmitted through the atmosphere to the earth’s surface. Changes in greenhouse gas content, cloud properties,

impurities (e.g. dust), and in other variables, can alter the atmosphere’s radiative balance and, if sustained, can lead to a new climatic regime. As we saw in Chapter 3, variations in atmospheric gas content can be determined from ice-core records, and their radiative forcing impacts can then be estimated from laboratory measurements of the radiative effects of individual gases (e.g. CO_2 , CH_4 , measured in Watts per square metre: W m^{-2}), or from records of the impacts of recent changes in atmospheric greenhouse gas content on modern temperatures (see for example the

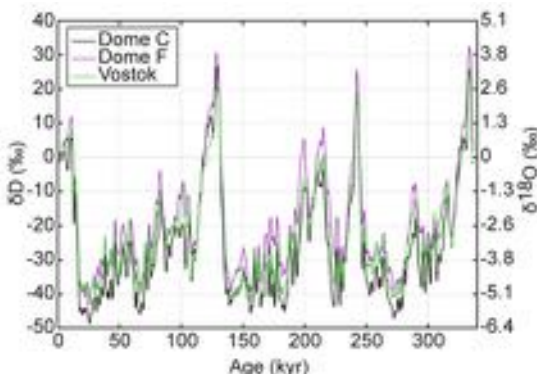


Figure 7.11 Isotope time-series data for the past c. 360 ka from three East Antarctic ice-core records: EPICA Dome C (EDC; δD), Dome F (Fuji; $\delta^{18}\text{O}$) and Vostok (δD). Although the data have been converted to a common timescale (an EDC age model), nevertheless the degree of similarity between all three suggests synchronous changes within the East Antarctic ice sheet (from Sime *et al.*, 2009).

NOAA Annual Greenhouse Gas Index [AGGI]: <http://www.esrl.noaa.gov/gmd/aggi/>). In Figure 7.12, a radiative forcing component has been estimated for the 800 ka long EPICA Dome C (EDC) ice core (7.12a), and subtracted from the original temperature record obtained from the δD signal (7.12b). The residual values are plotted against the orbital element of the temperature record (Figure 7.12c), which reveals the component of the EDC temperature record that cannot be explained by radiative or orbital forcing. This represents the amount of unexplained orbital forcing which must therefore be caused by feedback processes.

To be able to quantify and compare potential atmospheric forcing factors with such a high temporal resolution over a period of eight glacial–interglacial cycles represents a major advance in the search for causes of Quaternary climate change and, in particular, of possible linkages between long-term climatic patterns and forcing factors. In Figure 7.12, for example, it is apparent that the EDC temperature record for the last 800 ka has a strong obliquity component (Figure 7.12d), and that climate sensitivity (as reflected by the amplitude of variations in Figure 7.12b and c) was significantly higher during the last 450 ka (the Emiliani chron) than in the period 800–450 ka. In addition, it appears that the pattern of climatic variability differed significantly between individual glacial and interglacial stages: MIS 11 and 5.5 appear to have been the warmest interglacials, MIS 16, 12 and 2 had the strongest glacial maxima, while glacials MIS 13 and MIS 17 were notably weaker in intensity. Moreover, the high residual values (Figure 7.12c) indicate that although climate feedback

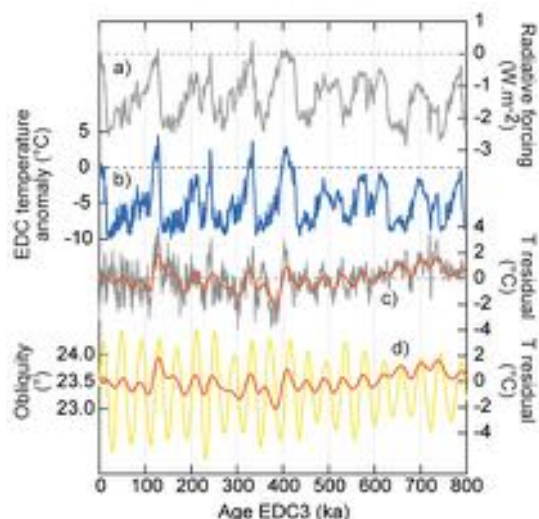


Figure 7.12 Radiative forcing, temperature profile and the obliquity signal in the EPICA Dome C (EDC) ice core over the past 800 ka. a) The estimated radiative forcing component of the EDC record. b) The EDC temperature profile reconstructed from δD . c) The residual temperature component that cannot be explained by either radiative forcing or obliquity (thin grey line); the thick orange line is the long-term orbital trend. d) The orbital component of the EDC record superimposed on the obliquity cycle (from Masson-Delmotte *et al.*, 2010).

mechanisms were clearly important, their effects appear to have consistently lagged the obliquity signal by c. 5 ka. Finally, the EDC record reveals evidence for a gradual long-term cooling trend between 700 and 400 ka (Figure 7.12c). These and other Antarctic ice-core data provide a further confirmation that the Milankovitch rhythms are mediated by other factors. This is further underlined by the contrast between the symmetrical wave-form of astronomical forcing (Figure 7.13a) compared with the strongly asymmetrical form of the proxy records of glacial–interglacial climatic oscillations reflected in the ice-core data (Figure 7.13b). This asymmetry in climate signal first appears at around 2.5 Ma and becomes increasingly accentuated in the late Pleistocene (Lisiecki & Raymo, 2007), particularly during the Emiliani chron (i.e. post-400 ka). As explained earlier (section 3.10.2.2), the end of each cold or glacial stage in the isotopic records (**terminations**) is often abrupt, but the cooling trends that precede each termination are more gradual (Figure 7.14), a pattern that again cannot be explained by astronomical forcing alone, but which must reflect feedback processes within the global climate system once a critical threshold has been trans-

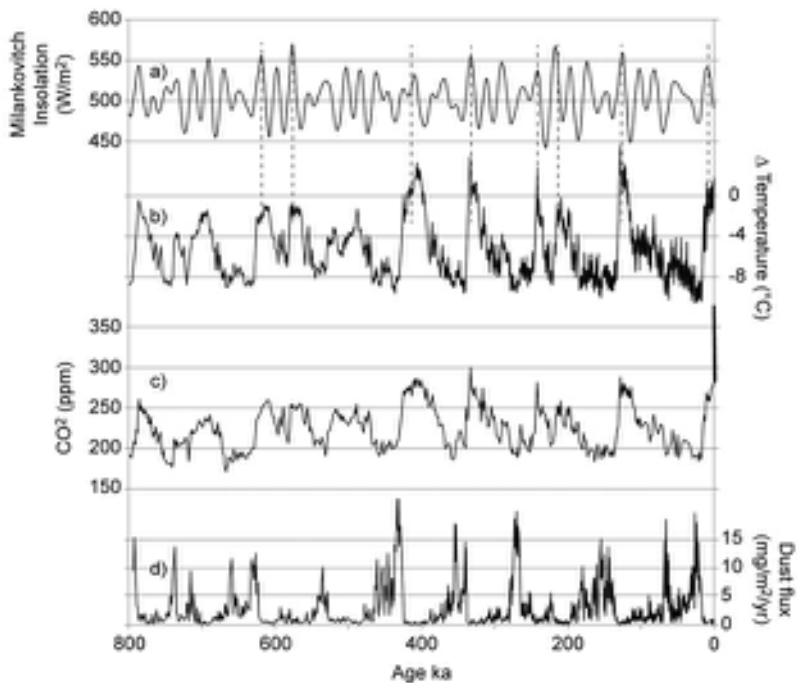


Figure 7.13 Milankovitch insolation record for the past 800 ka a), compared with temperature b), CO₂ c) and dust profiles d) from the EPICA Dome C (EDC) ice core, Antarctica. The dashed vertical lines show correspondence between peak interglacial temperatures (curve b) and insolation power (curve a) (data from <http://www.climatedata.info>).

gressed. Possible feedbacks that could trigger terminations include changes in snow-ice albedo, which feeds the growth of ice in the early stages until the ice sheets become too large to sustain the process (Stott *et al.*, 2007); the release of CO₂ stored in the deep ocean during cold stages but released as the ocean warms, the process being subsequently accelerated by a positive feedback greenhouse effect (Skinner *et al.*, 2010); or changes in ocean circulation in the Southern Ocean which initiates positive feedbacks through altered albedo or CO₂ release in both hemispheres and which, in turn, leads to what has been referred to as ‘runaway global warming’ (Wolff *et al.*, 2009).

Data from Antarctic ice-core records are also beginning to challenge some long-held views concerning the dominant role that the Northern Hemisphere has played in global climate change. Following Milankovitch’s initial proposal, it has tended to be assumed that climatic patterns in the Southern Hemisphere were largely controlled by Northern Hemisphere insolation, a view that is still current in some quarters today (e.g. Kawamura *et al.*, 2007), although one that has become increasingly contentious (Laepple *et al.*, 2011). For example, statistical analysis of midsummer

insolation in both hemispheres over the past 2 Ma indicates that at each termination insolation increased in both hemispheres in concert, but with the Southern Hemisphere having a slight lead (Schulz & Zeebe, 2006). This has been supported by records from Antarctica which suggest that warmings or terminations are led from the Southern Hemisphere, although specific conditions (ice-volume changes, ocean circulation, etc.) in the Northern Hemisphere are needed in order for the climate state to complete its shift from glacial to full interglacial conditions (Wolff *et al.*, 2009). Hence, although it is clear that the Northern Hemisphere generated the greatest volume increase in glacial ice during successive glacial stages, it now seems that processes operating in the Southern Hemisphere played the key role in terminating the glacial stages, a subject that we return to in section 7.4, where we consider climatic oscillations operating over shorter timescales.

7.3.4 Overview

From the foregoing accounts, it might be thought that feedback effects within the global terrestrial–oceanic–

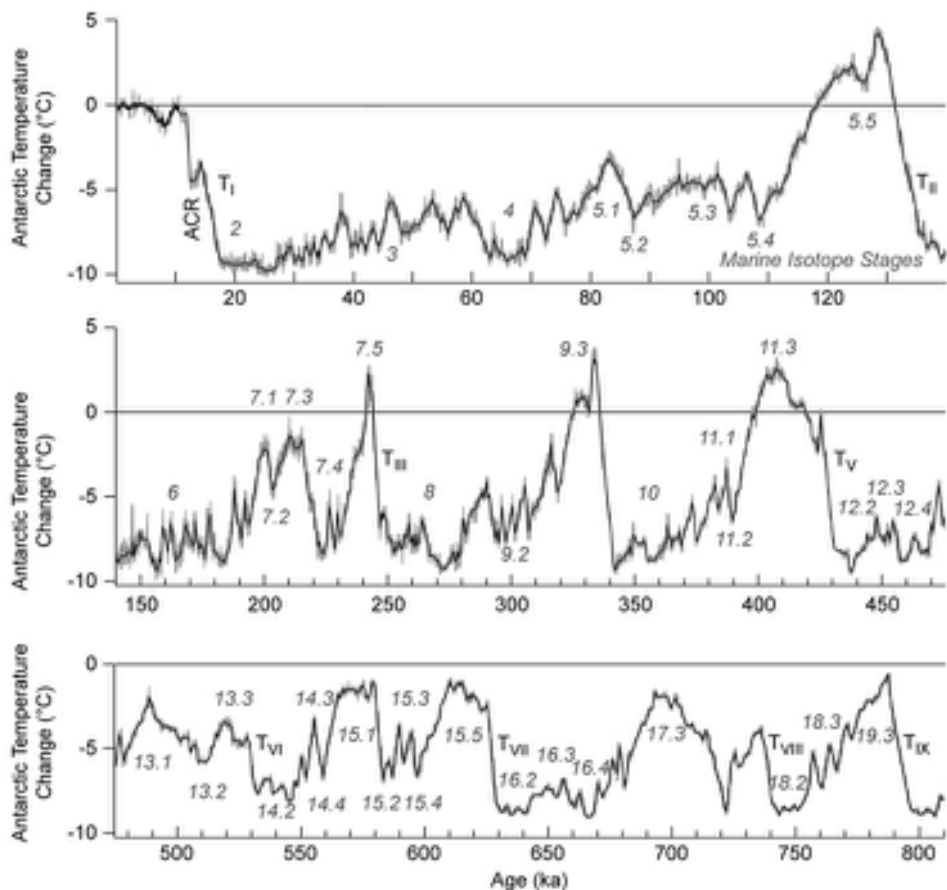


Figure 7.14 Temperature anomaly record (deviation from late Holocene mean, the zero line in the figure) for the last 800 ka derived from the EPICA Dome C (EDC) ice-core deuterium record. The record matches closely the LR04 benthic marine record (Figure 1.5) so that marine isotope stages and substages (numbered) back to MIS 19.3 can be readily identified. Also shown are the nine terminations (T_1 - T_9) that are prominent features in the record (from Jouzel *et al.*, 2007).

climatic system have assumed such prominence in interpretations of the Quaternary climate record that the Milankovitch hypothesis as an explanatory vehicle for long-term climate change no longer has currency. This is most certainly not the case. Modulation of the astronomical cycles fails to obscure the characteristic astronomical climatic rhythms, which persist as indelible hallmarks in marine and ice-core records, and which therefore remain as fundamental components in the formulation of any comprehensive theory of Quaternary climate change (Roe, 2006; Meyers *et al.*, 2008; Berger & Loutre, 2010). But while the Milankovitch theory remains a key element in the explanation of glacial-interglacial cycles, it must now be acknowledged that it provides only a partial explanation of the pattern and magnitude of long-term climate change.

Modulation of the underlying astronomical signal by other factors is evident throughout the Quaternary record, and is implicated not only in the long-term cooling trend reflected in the marine oxygen isotope profiles (Figure 1.5), but also in shifts in climatic phasing in both marine and ice-core time-series data (such as the MPT), as well as in the amplitude and frequency of the climatic signal in different proxy records. The increase in prominence of the 100 ka glacial-interglacial cycles and their abrupt terminations are further signs of signal amplification, operating over shorter timescales. But uncertainties continue to obscure the precise physical processes and linkages involved in the modulation process: for example, the MPT appears to have occurred without any significant change in insolation forcing; the prominence of the 100 ka cycle

during the Milankovitch chron remains enigmatic; and additional (non-Milankovitch) spectral peaks have been detected in some Quaternary records which cannot yet be explained (Huybers, 2007). A key challenge for Quaternary science in the future, therefore, is to try to understand not only what the key modulation/amplification processes are, but how they operate, how they are interlinked and, above all, how they complement insolation variations.

These problems and difficulties notwithstanding, there can be little doubt that our knowledge of climate evolution at the Milankovitch timescale has advanced considerably in recent years. We are now able to match the high-resolution ice-core isotopic variations with those of the marine isotope record for the past 800 ka or so (Figure 7.14), which clearly suggests a close coupling between ice-sheet growth and decay and ocean temperature changes over that time period. This further confirms a linkage that has long been considered, namely the reciprocal relationship between ice sheet, ocean temperature and, by implication, air temperature variations. Some general trends are discernible throughout this period, for example the greater amplitude of the climatic cycles (differences between thermal maxima and minima) post-400 ka compared with earlier in the record, but what is also apparent is that over the past 800 ka, no two glacial or interglacial episodes show precisely the same climatic pattern. This is very curious given that the same underlying climatic rhythms (astronomical variables) and modulating factors were operating throughout that period. Lang & Wolff (2011) attribute this variability to preconditioning of the environment, in that the climatic evolution of an individual isotopic stage is determined by three principal influences: insolation variations, natural feedbacks (modulation), and baseline conditions inherited from the preceding stage. As in a game of cards, although the rules remain the same, each hand unfolds differently, according to the cards that are dealt at the start.

Finally, it is worth noting one particularly enigmatic feature of the record of the last 800 ka, and that is the very limited time that temperatures have been as warm as those of the present. In Figure 7.14, where the black line across the diagram equates with the mid- to late Holocene thermal maximum, it is clear that in only four earlier interglacials did temperatures exceed this value: MIS 7 and MIS 9 for a short period only, while in MIS 5 and MIS 11 the thermal maxima were sustained for longer. Indeed, from the data in Figure 7.14, it would appear that the total amount of time during which temperatures were as warm as or warmer than the present day appears to represent, at most, only 10 per cent of the last 800 ka. In other words, present-day conditions are highly unusual, when viewed in

the long-term context. Global climates were generally colder, sea levels lower (at times much lower) and a great deal more glacier ice existed than is the case today. If this was so, then perhaps the maxim ‘the present is the key to the past’, which underpins much of our work in Quaternary science (section 1.5), might therefore require some qualification!

7.4. ENVIRONMENTAL CHANGE OVER SUB-ORBITAL (MILLENNIAL) TIMESCALES

7.4.1 Introduction

As we saw in Chapter 3, the most highly resolved and continuous records spanning the last glacial cycle are to be found in the Greenland ice cores. Of these, perhaps the most important in terms of the last cold stage and the Last Termination (section 7.5) is the core from NorthGRIP (NGRIP), as this has been dated by multiparameter annual layer counting (section 5.4.3.3) and therefore constitutes a stratotype against which other records can be compared (Svensson *et al.*, 2008; Blockley *et al.*, 2012; section 7.5). The most distinctive feature of the NGRIP record is the sequence of twenty-five short-lived stadial–interstadial oscillations, the so-called **Dansgaard–Oeschger (DO) events** (section 3.11.4). The onset of each event was abrupt, with peak warmth achieved in some cases in less than fifty years (Steffensen *et al.*, 2008), while the amplitude of warming ranged between 5 and 16°C (Figure 7.15). This sequence of DO events reflects repeated instability in the climate–ocean system of the North Atlantic region over millennial timescales, and is unusual in the Quaternary record in terms of the amplitude and frequency and, above all, in the resolution of the climatic oscillations.

Although the DO events are most clearly reflected in the Greenland ice cores, climatic instability during the last cold stage was not only a feature of the Greenland record, for it is evident in proxy data from a range of terrestrial contexts and is apparent in a number of profiles from the deep ocean (section 6.3.3.2; Figures 6.14–6.16). Evidence for climatic instability is also found in Antarctic ice-core records. The question arises, therefore, as to whether these various archives are related and reflect contemporaneous climatic events, or whether there are spatial and temporal variations in the respective climate signals.

The linkage of climatic anomalies over great distances (i.e. at the global scale) is referred to as **teleconnection**. These linkages are a result of energy transport and wave propagation in the atmosphere and ocean, enabling the

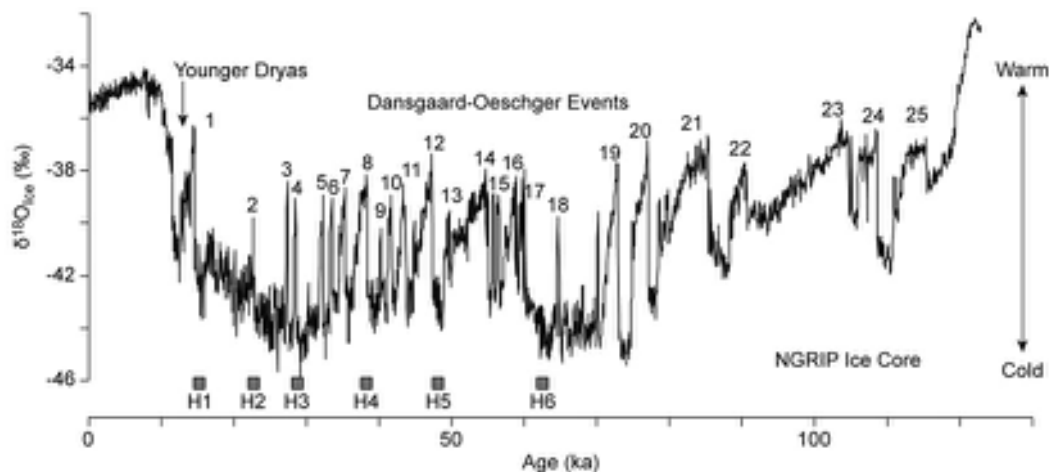


Figure 7.15 The $\delta^{18}\text{O}$ record from the NorthGRIP ice core over the last 125 ka. Short-lived warming (Dansgaard–Oeschger) events are numbered from most recent (1) to oldest (25). H1–H6 are the six Heinrich events, explained in the text (from Clement & Peterson, 2008).

atmosphere to act as a ‘bridge’ between different parts of the ocean, and the ocean to act as a ‘tunnel’ linking different atmospheric regions (Liu & Alexander, 2007). In this section we examine the degree to which the marked climatic, oceanographic and cryospheric changes that characterize the last cold stage do indeed reflect teleconnected events. We first consider the role of ocean–ice interactions in the North Atlantic region, long regarded as having had a dominant influence on climate during the last cold stage, then assess the evidence for oceanic effects at the global scale, and finally evaluate other factors that may have generated rapid and repeated climatic fluctuations over millennial to centennial timescales.

7.4.2 Ice–ocean–climate interplay in the North Atlantic

Prior to the publication of the Greenland ice-core records, interpretations of the climatic history of the last cold stage were based largely on marine oxygen isotope records. While these have proved invaluable in Quaternary science (section 3.10), many were obtained from areas of the seabed where sediment accumulation was slow. As a result, the temporal resolution of the last glacial cycle was relatively low and, while the major isotopic stages could usually be discerned, finer structures of the ocean–climate record were often obscured. In the 1990s, however, Gerard Bond and his colleagues showed, for the first time, that high-resolution ocean–climate records could be obtained from deep-ocean sediments by sampling areas of the North

Atlantic where sediment accumulation rates were exceptionally high (Bond *et al.*, 1993). Sea-surface temperature variations reconstructed from these cores, based on the abundance of the left-coiling cold-water foram species *N. pachyderma* (section 4.10.7; Figure 4.44), closely mirror the Greenland isotope records in the number and relative duration of inferred DO events; in the abrupt onset and asymmetric form of each DO event, particularly noticeable for events of longer duration; and in the tendency for interstadials to be grouped into longer-term cooling cycles, in which successive DO events have progressively lower thermal maxima (Figure 7.16). These longer-term composite cycles have subsequently been termed **Bond cycles** (Rasmussen & Thomsen, 2004). Initially, it was believed that they approximated a quasi-regular ~1,500-year periodicity (Bond *et al.*, 1997). However, subsequent high-resolution dating on both the ice-core records and on marine sequences, and the application of new age models to one of the key profiles investigated by Bond *et al.*, suggest that the 1,500-year cycle may, in fact, be an admixture of ~1,000- and ~2,000-year cycles. Overall, the 1,500-year number, which has been widely cited in the literature, now appears to be an artefact of averaging and seems to have little statistical justification (Obrochta *et al.*, 2012). This is not to say that the Bond cycles do not exist (for we return to these below), but that there remains a question over their periodicity.

Ocean-core records obtained by Bond and others show that both surface and deeper circulation in the North Atlantic varied markedly in strength and direction during

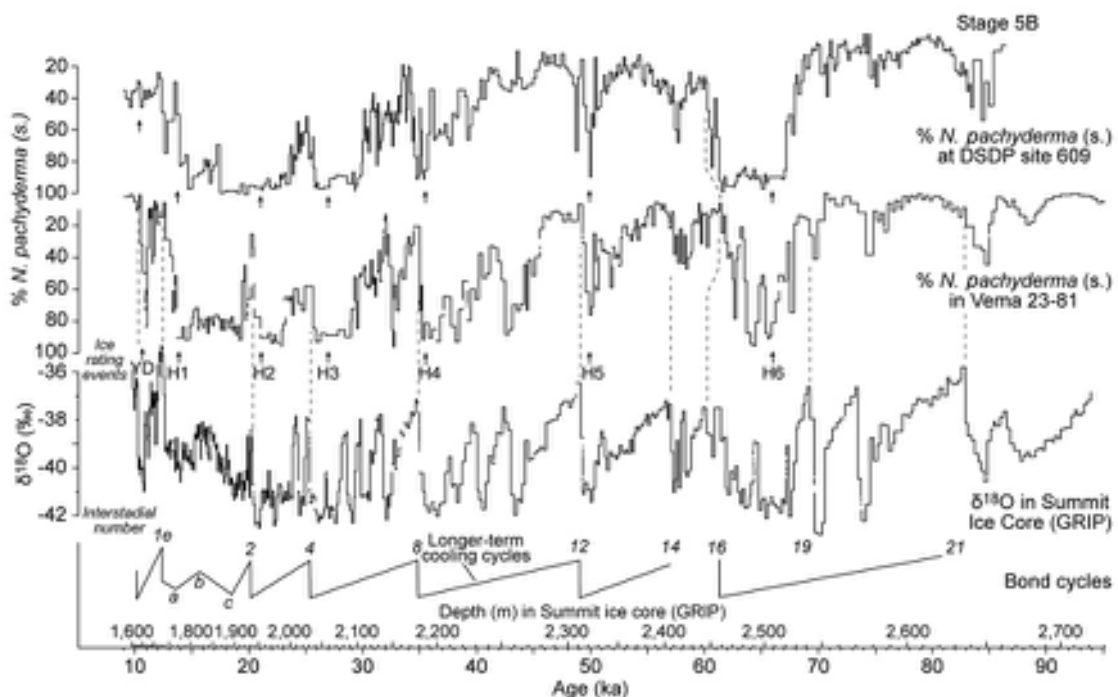


Figure 7.16 Correlation between variations in abundance of *N. pachyderma*, a cold-tolerant foraminiferal species, from North Atlantic deep marine sites DSDP-609 and V23-81, and the $\delta^{18}\text{O}$ record from the GRIP Summit ice core. Also shown are the long-term Bond cycles, defined by grouping the Dansgaard–Oeschger cycles and Heinrich events (H1–H6) (after Bond *et al.*, 1993).

the last cold stage (Rahmstorf, 2002). The principal circulation system that operates at the global scale is known as the ‘ocean’ or ‘global conveyor’ (Figure 7.17) and is driven by variations in water temperature and density (**thermohaline circulation: THC**). A number of processes contribute to the global THC flow pattern, but a key driver is surface wind. The trade winds, which blow constantly from east to west, lead to evaporation of surface waters in the tropical Atlantic and the net export of moisture into the Pacific where it is precipitated. As a result, the surface Atlantic is saltier and hence more dense than the Pacific. Density variations also arise from the cooling of waters in subpolar regions, aided by expulsion of brine as sea ice forms, and are particularly evident in the North Atlantic and circum-Antarctic (Clark *et al.*, 2002). The result is a sinking of surface waters and the formation of deep-water currents that link to surface flows by upwelling, for example in the eastern Pacific close to Chile and Peru (Humboldt Current) and the west coast of the USA (California Current), and in the eastern Atlantic close to the coasts of the Cape of Good Hope (Benguela Current) and northwest Africa (Canary Current). A schematic for the THC is shown

in Figure 7.17 (see Summerhayes & Thorpe, 2002, or visit the NASA web site [or YouTube] for animated films of the system in operation).

The surface flow of the North Atlantic is dominated by the Gulf Stream, warm salty water that is driven north-eastwards by prevailing winds, keeping northwest Europe significantly warmer than equivalent latitudes on the western Atlantic seaboard. As this salty water cools, its density increases and in the vicinity of south Greenland and the Norwegian Sea it sinks (Figure 7.18) to feed a **North Atlantic Deep Water (NADW)** current that flows southwards to compensate for the north-flowing Gulf Stream; in combination, these currents comprise the **Atlantic Meridional Overturning Circulation (AMOC)**. Cold water sinking from the margins of Antarctica forms an **Atlantic Bottom Water (ABW)** current that is denser than NADW, and which feeds an overturning cell in the Southern Ocean that is generally weaker than the AMOC. Although other factors serve to complicate this picture, such as episodic deep-water flow (Praetorius *et al.*, 2008), eddy and wind-field influences (Lozier, 2010), and the outflow into the Atlantic of more saline Mediterranean waters

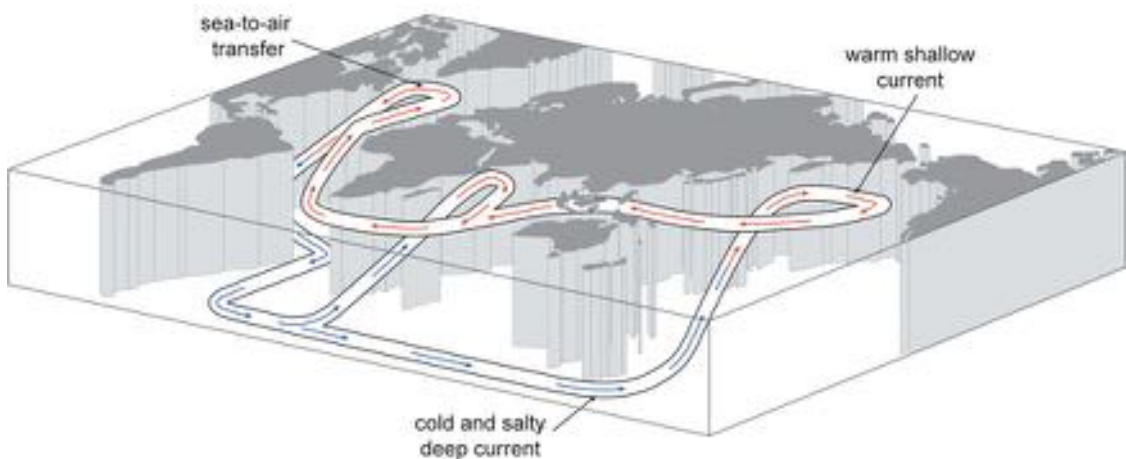


Figure 7.17 Schematic model of the main currents of the global 'ocean conveyor': surface (warm) currents are red, bottom (cold) currents are blue; upwelling of deep water and sinking of surface waters through density variations complete the circuit (modified from National Earth Science Teachers Association web site, http://www.windows2universe.org/earth/Water/deep_ocean.html). For further explanation see text.

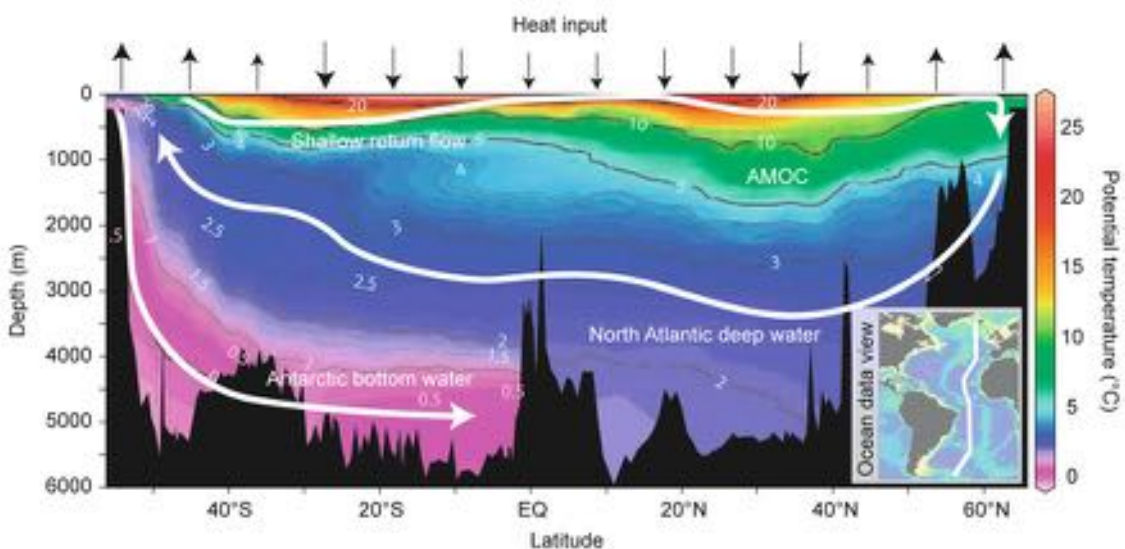


Figure 7.18 Cross-section of the Atlantic Ocean basin showing thermal stratification, principal flows and surface heat exchange. The black arrows represent, schematically, net gain to, or heat loss from, the ocean surface. Heat penetrates into the ocean surface layer and is subducted into the upper ocean along surfaces of equal density. The isolines and colour coding show pressure-adjusted (potential) temperature variations. A combination of winds, sinking processes and ocean circulation leads to heat transport (white arrows) and Atlantic Meridional Overturning Circulation (AMOC) (from Hegerl & Bindoff, 2005, reprinted with permission of the AAAS; based on Schlitzer, 2003).

(Rogerson *et al.*, 2012), this general model of the AMOC remains a useful vehicle for explaining North Atlantic Ocean circulation.

It now appears that there were three dominant circulation modes in the North Atlantic during the last cold stage (Rahmstorf, 2002; Clark *et al.*, 2002). During warmer intervals, the AMOC dominated, as it does at the present time (Figure 7.19a); during colder ('glacial') episodes, the AMOC still operated, but through reduced density and buoyancy, was confined to shallower depths with a more sluggish flow (7.19b); and during Heinrich events (episodes of iceberg and freshwater injection following ice-sheet collapse: see below), water derived from the Antarctic filled the North Atlantic basin, except perhaps for the top 1,000 m (Figure 7.19c) when flow was almost switched off (Clark *et al.*, 2002).

In the late 1980s–early 1990s, Wally Broecker and colleagues suggested that the abrupt climate changes of the last cold stage evident in Greenland records could be explained by salinity-driven variations in the strength of the AMOC (Broecker & Denton, 1989; Broecker *et al.*, 1990). This '[salt oscillator hypothesis](#)' envisaged two competing influences that drove the surface ocean to switch between climate states. The first is when too much freshwater is injected into the Atlantic near sites of deep-water formation, which reduces surface-water density to the point where sinking can no longer take place, thereby slowing or shutting down the AMOC. The effect would be to reduce the amount of heat being transferred northwards from the tropics because the Gulf Stream would be less effective, thereby enabling northern ice sheets to grow. However, evaporation would still be taking place in more southerly and temperate latitudes, so salt would accumulate there during times of low AMOC strength, and would do so until the surface water was sufficiently dense to sink, starting up the AMOC once again (the second competing influence). The sudden onsets of DO events could therefore be explained by the latter process reaching a threshold, or 'tipping point', and initiating a positive feedback process through which northward heat transport would, for example, check or reverse the build-up of sea ice or ice sheets.

The salt oscillator hypothesis is now an accepted paradigm in Quaternary palaeoclimatology and palaeoceanography (Alley, 2007). It is supported by a substantial body of data from ocean-core records that enable changes in strength of North Atlantic circulation during the last glacial stage to be reconstructed in considerable detail (Gherardi *et al.*, 2009; dos Santos *et al.*, 2010; Thornalley *et al.*, 2010). These allow variations in temperature, density and flow speed associated with the AMOC to be inferred.

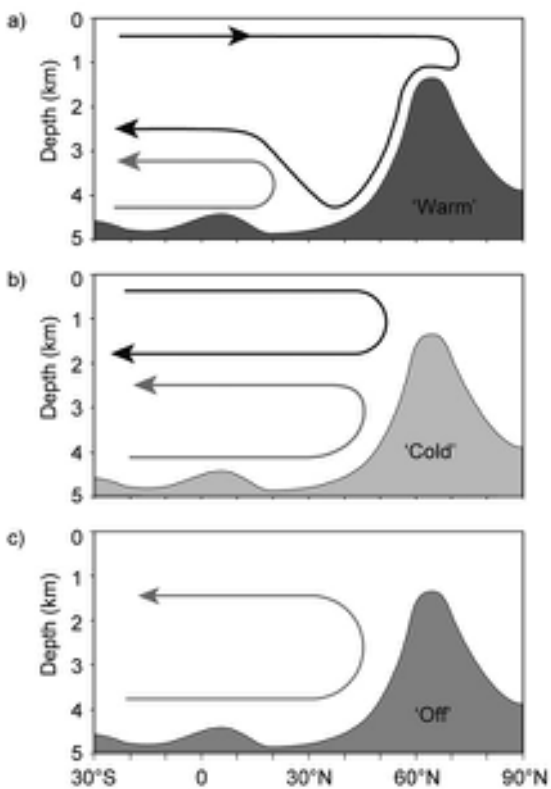


Figure 7.19 Schematic model of three dominant types of Atlantic circulation that recurred throughout the last cold stage. The black line indicates North Atlantic overturning; the grey line, Antarctic Bottom Water; the infill at the base of each block represents bottom topography, with the rise in the north representing the shallow sill between Scotland and Norway near which deep-water formation occurs. Circulation is represented for a) a warm interval, b) a cold interval, and c) a Heinrich event (based on Rahmstorf, 2002). For further explanation see text.

The records also show that episodic injections of freshwater occurred throughout the last cold stage, either from ice sheet collapse (see below) or release from ice-dammed lakes, which led to temporary shutdowns of the AMOC (Clark *et al.*, 2001). Indeed, simulations of the AMOC in coupled numerical models indicate that the Atlantic Ocean is sensitive to relatively small changes in freshwater supply (Otto-Bliesner & Brady, 2010). Contemporary monitoring of modern flow rates and physical properties in the Atlantic show that the AMOC varies markedly on time-scales of weeks to months, also suggesting a high degree of sensitivity to minor variations in water density and pressure (Rayner *et al.*, 2011). These may be contributory factors to

present-day short-term variations observed in Atlantic circulation, such as the North Atlantic Oscillation (section 7.6.4.3).

While changes in AMOC strength may have been contributory factors in DO cycles, the sequence and pacing of the cycles is more difficult to explain. External factors, such as orbital or solar forcing (section 7.6.4.1) seem unlikely to have driven the changes, and although the ~1,000- and ~2,000-year periodicity that now seems to have been associated with the Bond cycles (see above) matches evidence for changes in solar irradiance at around these frequencies, the amplitude of the cycles in terms of inferred temperature change seems unlikely to be accounted for by solar forcing alone. The answer, therefore, seems to lie in some sort of reorganization and associated feedbacks within the ocean–cryosphere–climate systems. Precisely how this might operate, however, remains unclear, but ice-sheet activity appears to be an important part of the process, for the similarity between the oceanic and cryospheric records suggests that ocean and ice-sheet behaviour were strongly coupled.

This linkage is underlined by the record in North Atlantic cores of the six Heinrich events (H1–H6). As explained in Chapter 3, these are reflected in layers of ice-raftered debris (IRD) that mark episodic deposition of carbonate-rich glacially derived sediments from icebergs drifting mainly eastwards across the Atlantic from the margins of the Laurentide ice sheet (section 3.10.1). The IRD layers tend to coincide with the final cold phase of a Bond cycle, immediately preceding an abrupt increase in temperature (Hulbe *et al.*, 2004). Periodic collapse of the ice margins is indicated by repeated IRD layers after which the ice was able to stabilize and build again, a process MacAyeal (1992) has termed ‘binge-purge’. This process appears to reflect a complex interplay between ice-sheet volume, subglacial processes and sea level. As the ice sheets reached a critical size a ‘tipping point’ was reached, caused, for example, by increased basal melting and lubrication beneath thicker ice margins, and/or by advance of the ice fronts beyond the grounding line near the edges of Laurentide continental shelves, enabling seawater to penetrate beneath the ice margin (Hemming, 2004; Marcott *et al.*, 2011). This combination of factors could have been sufficient to destabilize ice margins, leading to collapse and release of meltwater and icebergs into the northern oceans. Moreover, as the ice sheets expanded, their margins encroached closer to the places where deep-water formation occurs, and hence where meltwaters could more directly affect AMOC strength, again contributing to ice-sheet destabilization.

Although the early work on ice-rafting in the North Atlantic suggested that the IRD layers were derived from

the Laurentide ice sheet (e.g. Alley & McAyeal, 1994), subsequent studies have revealed a more complex history of IRD deposition in the North Atlantic during the last cold stage, reflecting non-synchronous behaviour between the Laurentide, Greenland, British and Fennoscandian ice sheets (Dowdeswell *et al.*, 1999; Scourse *et al.*, 2009). This is an important discovery because it means that ice-sheet instability and collapse, which may have been a factor in the termination of the Bond cycles (see above), was not necessarily a circum-North Atlantic phenomenon reflecting a common forcing factor (or factors); in other words, the ice-rafting events are ice-sheet specific, and are driven by internal as opposed to external processes. However, it is possible that collapse of one ice sheet could have led to the break-up of others, for as one ice sheet failed and surged, the rise in sea level could have destabilized ice masses elsewhere. For example, it has been suggested that during Heinrich events 1, 2, 4 and 5, European ice break-up appears to have preceded the onset of ice-sheet melting by ~1,500 years (Maslin *et al.*, 2001).

A key element in ice-sheet collapse was not simply the release of icebergs, but the injection of large quantities of freshwater into the northern oceans. As we saw above, the North Atlantic is highly sensitive to freshwater input, and even relatively minor quantities of freshwater could cause profound changes in ocean circulation (Rahmstorf *et al.*, 2005). One possible scenario that follows from this is that as each DO event was associated with ice-sheet melting and freshwater release into the Nordic Seas, this could have been sufficient to reduce the strength of NADW, weaken the Northern Hemisphere circulation and thus conserve heat in the southern oceans. The resultant warming around Antarctica would trigger accelerated ice-sheet melting and contraction of sea-ice extent in the Southern Hemisphere, a reduction in strength of the Antarctic Bottom Water current, and eventually the re-establishment of NADW formation, initiating the next DO cycle. Ice-sheet build-up over a number of DO cycles would, in due course, lead to ice-sheet destabilization and a Heinrich event. This would bring an end to the final DO event within a Bond cycle and the resetting of the DO ‘clock’ (Maslin *et al.*, 2001).

While the above account may explain some aspects of the North Atlantic record during the last cold stage, other issues remain to be resolved. For example, the scenario does not offer an explanation for the amplitude, pacing and frequency of the DO events in the ice cores. In the first part of the DO sequence in Figure 7.15 (c. 110–65 ka), only eight events occurred, and these tend to have higher temperature maxima and minima and, on average, longer durations than later ones. Double this number of DO events occur post-65 ka, each of which was shorter. It is also notable that

Heinrich events are confined only to the middle and later part of the record, and there is no evidence of major IRD events pre-65 ka. The period from DO event 17 onwards therefore appears to have been more climatically unstable as reflected in increasing DO cycle frequency, which may reflect more frequent ‘binge–purge’ episodes around the much larger northern ice sheets that developed during that period. But if the absence of Heinrich events from the pre-65 ka record is indicative of more restricted ice-sheet growth, then ice-sheet collapse may not have been a primary mechanism for driving these earlier DO cycles. Finally, there is the question of the pacing of the DO cycles. Although some have argued that the abrupt climatic events reflected in the ice cores are paced by a regular cycle with a periodicity of ~1,500 years (e.g. Rahmstorf, 2003; Braun *et al.*, 2005), others have suggested that the recurrence times of the DO events are indistinguishable from a random occurrence (Ditlevsen *et al.*, 2007). Much clearly still remains to be learned about the nature and origin of the climatic changes that occurred around the North Atlantic during the last cold stage. Indeed, despite the fact that the Dansgaard–Oeschger events were first identified in the ice-core records as long ago as 1993, there is still no coherent

explanation of what initiates and sustains DO behaviour (Clement & Peterson, 2008).

7.4.3 A bipolar teleconnection

Ice-core records from Antarctica show a pattern of climatic variability remarkably similar to, at least in terms of rhythm, those recorded in the Greenland ice cores (Figure 7.20). A major difficulty in comparing the records, however, is that Antarctic ice cores are seldom annually resolved because the layers are thinner than those encountered in Greenland and diffuse more rapidly with depth. An exception is the upper part of the core from Dronning Maud Land (EDML) in which annual layers can be identified (Fischer *et al.*, 2004), although how far back in time these can be traced has not yet been determined. In the absence of annual chronologies, therefore, synchronization of Antarctic records with the NGRIP record relies on other methods.

As explained in Chapter 6, Greenland and Antarctic ice-core records have been linked using atmospheric trace gases, particularly methane (CH_4). Changes in the methane content of the atmosphere are quickly equilibrated globally,

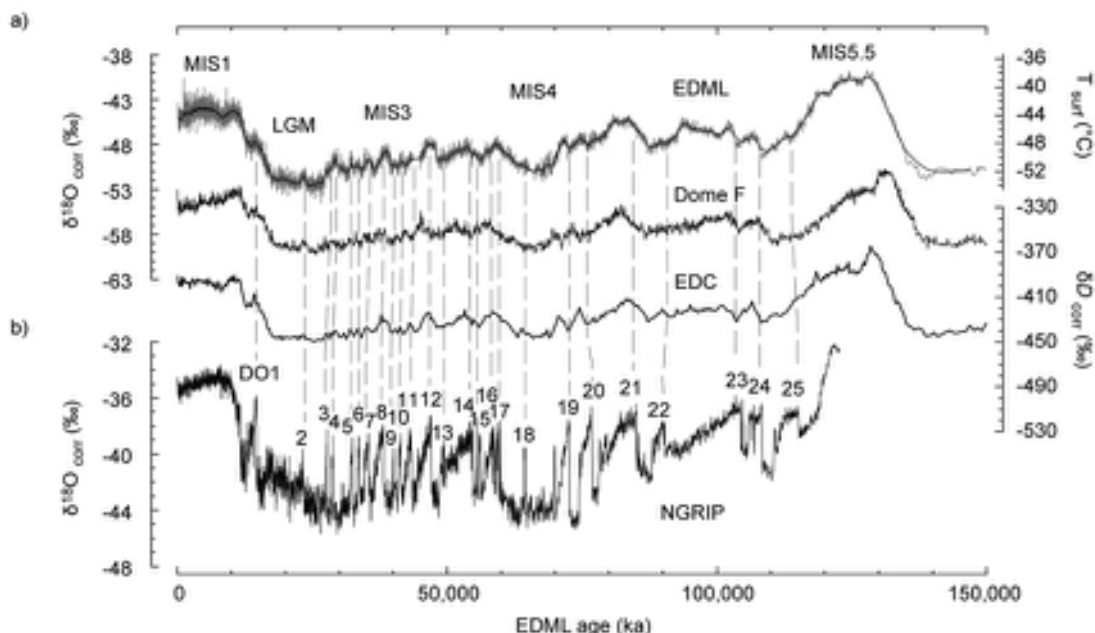


Figure 7.20 Stable isotopic records spanning the last glacial cycle from Dronning Maud Land (EDML), Dome F and EPICA Dome C (EDC), Antarctica, aligned with the NGRIP isotopic record from Greenland. All four records are plotted on a common timescale (explained in text). MIS – marine oxygen isotope stages; LGM – Last Glacial Maximum; DO – Dansgaard–Oeschger events, 1–25 (from EPICA Community Members, 2006).

and hence variations in atmospheric methane concentration should register contemporaneously in both polar ice sheets and should serve as a basis for correlating Greenland and Antarctic records (Barker *et al.*, 2009). Although this approach may be compromised to some extent by ice age–gas age differences in ice cores (section 5.4.3.3), comparison of the records shows that there is a close correlation between the methane profiles in Antarctica and Greenland over the period between *c.* 10 and 52 ka (Figure 7.21 lower). The matched record is currently confined to this period because the age uncertainties for older layers are much larger (EPICA Community Members, 2006). In addition to the methane signal, ice-core profiles can be linked using atmospherically generated cosmogenic nuclides (^{10}Be); geomagnetic events, such as the Laschamp excursion at *c.* 41 ka (Raisbeck *et al.*, 2007); and volcanic eruptions, such as Mt Toba at *c.* 74 ka (Williams, 2012; section 6.3.3.3).

For the part of the record shown in Figure 7.21, linking the Greenland and Antarctic ice cores using methane fluctuations and marker horizons also provides a basis for comparing the stable isotope records (Figure 7.21 upper). But this produces a surprising result: the Antarctic and Greenland isotopic variations are in *anti-phase* with each other (Figure 7.21), suggesting that cooling episodes in Greenland coincide with warming in Antarctica and vice versa. It is worth noting in passing that a quite different (and erroneous) conclusion might have been drawn had the polar ice cores been linked (or tuned) using stable isotope variations alone (section 6.3.3).

Consistent anti-phase behaviour between the two polar ice sheets over several millennia indicates that they are coupled to a driving mechanism that transfers energy alternately between the two hemispheres, which has been termed the '**bipolar seesaw**' (Broecker, 1998; Stocker, 1998). Central to this process are changes affecting AMOC

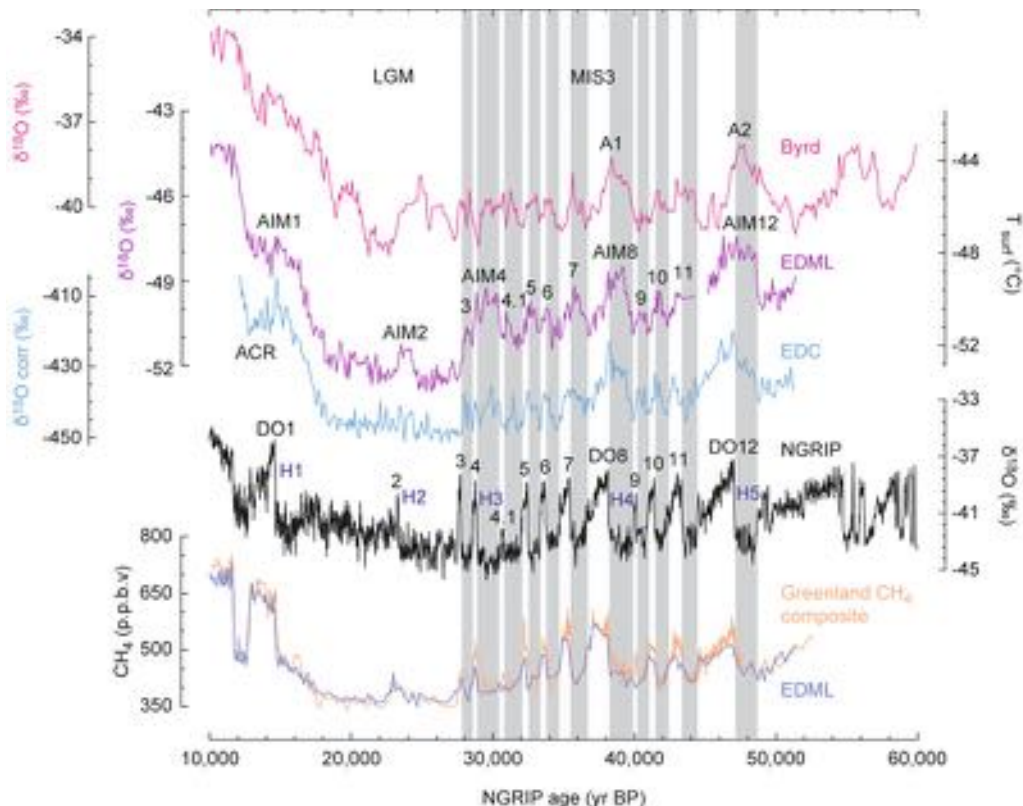


Figure 7.21 Synchronization of isotopic records from Antarctic and NGRIP ice cores between 10 and 52 ka using common variations in methane (CH_4 ; lower curve). All records have been converted to the Greenland GICC05 timescale. H1–H5 – Heinrich layers; DO – Dansgaard–Oeschger events; A and AIM – Antarctic Isotope Maximum Events (distinct warming events); ACR – Antarctic Cold Reversal (after EPICA Community Members, 2006). For further explanation see text.

behaviour: as explained earlier, when the AMOC is closed down by injections of cold water into the northern North Atlantic, heat can no longer be carried northwards by the Gulf Stream, and is consequently stored in the southern oceans. Hence cooling in the North Atlantic coincides with a warming trend in the south. Sustained heating of the south would, however, increase evaporation rates and hence sea-surface salinity, which ultimately leads to re-establishment of the AMOC, thereby transferring stored heat northwards and allowing the southerly latitudes to cool. Once initiated, this process of alternating surface heat and mass transfer between the hemispheres, which Seidov & Maslin (2001) refer to as ‘heat piracy’, becomes a self-perpetuating system, although how it is initiated is still not yet fully understood (Severinghaus, 2009; Rial, 2012).

The bipolar seesaw hypothesis has gained wide support because it provides an elegant explanation of the anti-phase relationship reflected in the aligned polar ice-core records, and it is a concept that accords with reconstructions of Atlantic circulation reorganization during the last cold stage (Hoogakker *et al.*, 2007; Barker *et al.*, 2009). Moreover, simple box models (Stocker & Johnsen, 2003) and some GCM experiments (Manabe & Stouffer, 1997) reproduce this oscillatory bipolar climatic behaviour when set to run from a fixed set of input variables, suggesting that it is an integral component of the ocean system during a glacial stage (Rial, 2012). It could also operate in warmer periods, however, for twentieth-century Arctic and Antarctic temperatures have been shown to vary in an anti-phase seesaw pattern, with warming in the Arctic being accompanied by cooling in the Antarctic and vice versa (Chylek *et al.*, 2010).

While the concept of the bipolar seesaw has gained widespread acceptance in recent years, there are several aspects of the polar ice-core records that are not adequately explained by this mechanism. For instance, there appear to have been significant time lags in temperature shifts between the two poles, though it is uncertain as to which pole leads in the process. Some have concluded that temperature shifts in Greenland preceded the corresponding opposite trends in Antarctica by around 400–800 years (Schmittner *et al.*, 2003), while others have suggested that temperature changes in the Antarctic preceded those in Greenland by as much as 1,000–2,000 years (Hinnov *et al.*, 2002). Brook *et al.* (2005) support the view that Antarctica led the changes, but found that the lead time was not constant. Moreover, Capron *et al.* (2010b) have noted that when the northern ice sheets were extensive, Antarctica did not always stay warm during entire Greenland stadials. These observations do not fit well with the seesaw

hypothesis, for if the AMOC was the sole or dominant driver, then the opposing polar climate shifts should be broadly synchronous (Seidov *et al.*, 2001). It may be, therefore, that while the essence of the theory is correct, as with the Milankovitch theory discussed above, other factors serve to influence or modulate climatic response. This is seemingly confirmed by numerical simulation experiments which reveal the sensitivity of AMOC behaviour to a range of additional environmental factors. These include the much larger ocean volume in the Southern Hemisphere compared with the north, the former taking much longer to warm up and cool down; variable rates, durations and loci of the injection of cold water into the North Atlantic; similar variations in the timing and volume of freshwater release into the Southern Ocean from the Antarctic ice sheet; and atmospheric processes and feedbacks that amplify the effects of ocean circulation changes (Dokken & Nisancioglu, 2004; Knutti *et al.*, 2004; Barreiro *et al.*, 2008; Swingedouw *et al.*, 2009). In combination, these may suppress or delay the transfer of energy and mass via the bipolar teleconnection, in particular slowing the rate of response of the Southern Ocean to abrupt climate shifts in the north (Severinghaus, 2009).

7.4.4 Global teleconnections: linking mechanisms

There is now increasing evidence that the millennial-scale climate oscillations reflected in the polar ice-core records affected not just the Atlantic region, but all parts of the globe (Voelker, 2002; Fritz *et al.*, 2010b). The question, therefore, is precisely how the global climate system responded to the abrupt climatic shifts of the last cold stage reflected in the North Atlantic DO cycles and, in particular, whether other regions responded synchronously to these changes, or whether there were significant leads and lags between them. First, however, it is necessary to examine some of the processes that are involved in the propagation of North Atlantic-driven climatic fluctuations to other regions of the globe, and how these may relate to the operation of the bipolar seesaw. These include CO₂ storage in the oceans, displacements of the **Inter-Tropical Convergence Zone (ITCZ)**, atmospheric dust supply and fluctuations in sea level.

It has long been recognized that the oceans have a capacity to store CO₂ and that the amount stored is dependent on water temperature. High-resolution ice-core and palaeoceanographic records now enable the rate of exchange of CO₂ between different carbon reservoirs to be quantified, in turn informing the design of GCM experiments used to test the climatic significance of CO₂

variations (Meissner *et al.*, 2007). Changes in the CO₂ content of **Antarctic Bottom Water (ABW)**, the largest single ocean store of CO₂, appear to have played an important role in modulating the bipolar seesaw during the last cold stage, particularly during MIS 3 (Martin *et al.*, 2005). A number of factors regulate the CO₂ content of the Southern Ocean (the source of ABW), including SST and salinity, marine biomass, deep-ocean temperature and circulation, storage of CO₂ in the ocean, sea-ice extent and fertilization of the ocean surface by Fe (derived from dust influx). These various components account for about 80 per cent of the calculated millennial-scale fluctuations in CO₂ exchange during the last cold stage, which implies that some important sources and processes are not yet accounted for (Fischer *et al.*, 2010b). It is also clear that no single factor can explain all of the observed patterns of CO₂ exchange during the last cold stage, which suggests that different factors assumed greater importance at different times.

An example of the kinds of impact that millennial-scale climate changes could have had on global ocean circulation systems and, in turn, on CO₂ exchange between the oceans and the atmosphere is provided by Bereiter *et al.* (2012). They noted an important difference in CO₂ and Greenland temperature in MIS 5a-d on the one hand, and in MIS 3 on the other: during the former, peak CO₂ values lag the onset of Greenland DO events by around 250 ± 190 years, whilst in MIS 3 this lag increases to around 850 ± 90 years, and peak CO₂ values are also higher (Figure 7.22). It appears that during MIS 5a-d, the North Atlantic was not much cooler than during interglacial times (MIS 5e), with a circulation similar to that of the present (note that NADW extends to the ocean floor). After the onset of a DO event, therefore, the AMOC remained strong enough to prevent the northward spread of ABW. During the colder MIS 3 period, however, the starting conditions were very different as ABW occupied the whole of the Atlantic deep (Figure

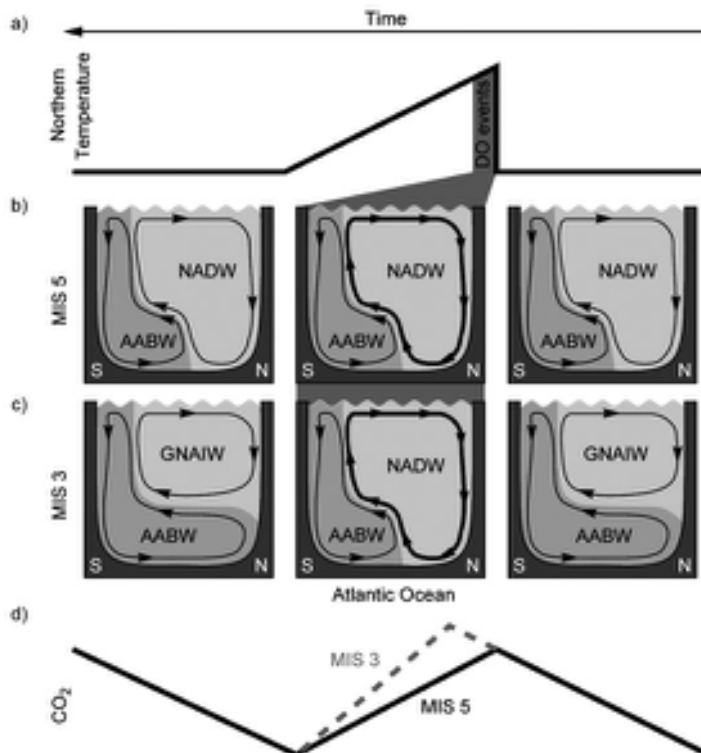


Figure 7.22 Schematic representation of Atlantic water mass changes during DO cycles. a) Simplified, schematic asymmetric temperature oscillation. b) Time slices of water mass distribution and circulation before, during and after a DO event during MIS 5. c) As for b), but representing the sequence of changes during MIS 3. d) Idealized changes in atmospheric CO₂ concentration leading into, and following on from, a DO event during MIS 5 (in black) and during MIS 3 (black plus grey dashed line). NADW – North Atlantic Deep Water; ABW – Atlantic Bottom Water; GNAIW – Glacial North Atlantic Intermediate Water (from Bereiter *et al.*, 2012). For further explanation see text.

7.22). This would have restricted the North Atlantic overturning to a shallower circuit, termed **Glacial North Atlantic Intermediate Water (GNAIW)**. As a consequence, the surface area of ocean where deep water could exchange directly with the atmosphere would have been reduced, so that the CO₂ storage capacity of the ABW was increased. At the start of a DO event, when NADW circulation was reinstated, this enhanced deep-water store of CO₂ could then be released (Figure 7.22). The effect would have been not only to return much greater quantities of CO₂ to the atmosphere compared with MIS 5, but also to prolong that release by 500–1,000 years. Since CO₂ is a greenhouse gas that mixes and diffuses rapidly in the atmosphere, this should have had an immediate and significant feedback effect on climate at a global scale.

Whether the above example adequately explains all aspects of CO₂ storage and release from the ocean reservoir during the last cold stage is open to question, but it does serve to highlight the various linkages and feedback mechanisms involved in ocean circulation, CO₂ storage and release, and the possible climatic effects. It also highlights the important role of the oceans in regulating the carbon cycle (Doney *et al.*, 2009). For example, it appears that increased CO₂ storage may have led to acidification of the deep ocean while the shallower layers became more alkaline; the latter process would increase the rate of uptake of atmospheric CO₂ by the surface ocean layer and its transfer to the deep, thereby enhancing the capacity of the deep ocean to act as a reservoir for storing (and subsequently releasing) CO₂ during millennial-scale climatic fluctuations (Sigman *et al.*, 2010).

The second mechanism that is key to understanding global climate shifts over millennial timescales is the displacement of the ITCZ. Proxy records from marine and terrestrial sites located within, or close to, the Tropics suggest that the mean position of the ITCZ shifted southwards during Greenland DO and Heinrich events, which reduced the strength of the East Asian and Indian monsoons (Fritz *et al.*, 2010b; Weldeab, 2012). In a speleothem isotopic time-series from northern Australia, for example, higher summer monsoon rainfall coincides with Heinrich stadials and also with the Younger Dryas, while decreased rainfall characterizes the DO interstadials (Denniston *et al.*, 2013). This precipitation response is anti-phased with sites from around the Indo-Pacific warm pool and with Chinese records of the East Asian summer monsoon. It also finds parallels with anti-phase behaviour between the Northern and Southern Hemispheres inferred from other records, for example opposing trends in palaeomonsoon strength inferred from isotopic signals in speleothems from sites in China and Brazil (Wang *et al.*,

2006). These provide further confirmation that a southward migration of the ITCZ coincided with periods of high northern-latitude cooling and, moreover, that North Atlantic forcing was a primary driver of millennial-scale monsoonal variability during the last cold stage (Denniston *et al.*, 2013).

That these shifts are closely associated with the operation of the bipolar seesaw tends to be generally assumed, because they approximate the temporal sequence of millennial-scale climate variations evident in polar ice-core and other high-latitude records. However, the extent to which low-latitude records align with high-latitude datasets appears to vary. In some cases, these appear to match the Greenland signals quite closely, for example climatic oscillations reflected in a sediment record from Lake Malawi (Brown *et al.*, 2007b), and wet phases seemingly related to intensification of the South American summer monsoon recorded in sediments in Lake Titicaca (Fritz *et al.*, 2010b). The implication is that in these examples, excursions of the ITCZ were being driven by climatic variability in Greenland. By contrast, other archives seem to bear the imprint of Antarctic signals, such as climatic variations revealed in South African speleothems (Holmgren *et al.*, 2003), and in marine sediment records from the subtropical Indian and Southern Atlantic Oceans (De Deckker *et al.*, 2012). In yet other cases from the low latitudes, however, the imprints of both polar signals have been detected. For instance, planktonic and benthic microfossil records from MIS 3 from the western tropical Pacific indicate that while variations in sea-surface temperatures and salinities show close affinities with the Greenland rhythm, changes in deep-water conditions more closely resemble the Southern Ocean–Antarctic sequence (Saikku *et al.*, 2009).

The position of the ITCZ is also a barometer of changes in position and strength of the monsoon belts. During the last cold stage, there appear to have been significant latitudinal displacements of the monsoon cells which, in turn, brought about major regional changes in seasonal and annual precipitation. Such changes, which reflect repeated shifts in the ITCZ, are evident, *inter alia*, in the marked fluctuations in low-latitude lake levels throughout the tropical zone (section 3.7). The recurrent changes in precipitation, which are often accompanied by changes in meridional temperature gradients, are indicative of major reorganizations of atmospheric circulation at the global scale. This may have been driven by (or at least related to) the bipolar seesaw. One possible consequence of the climatic reorganization that follows a shift in the ITCZ is the replacement of the zonal (latitudinal) pattern of monsoon belts that dominates at the present time by a more meridionally dominated circulation (Fritz *et al.*, 2010b).

If so, this would weaken the northern monsoon cells, preventing, for example, moisture from the Indian and Pacific Oceans reaching the Himalayas and Tibet (Aizen & Aizen, 1996), and leading to greater aridification in those regions (Herzschuh, 2006). This, in turn, would lead to an expansion in mid-latitude continental deserts, thereby increasing the potential source of global dust.

We have already seen that the dust content in polar ice cores varies inversely with ambient temperature over Milankovitch timescales (section 7.3.3), and that atmospheric dust transport increases during colder periods. This relationship also appears to hold true on millennial timescales. Over Greenland, for example, there was a significant increase in dust flux during the stadial events of the last 80 ka (Figure 7.23), while the same association between dust and cold intervals is also a feature of Antarctic ice-core records from the last cold stage (Fischer *et al.*, 2007). The most remarkable feature of Figure 7.23, however, is the abruptness of the changes in the dust record: it appears as though the dust flux to the polar ice sheets could be switched on and off quite suddenly. This might reflect

sudden shifts in the trajectory of dust-bearing winds over the polar regions, caused by adjustments in global atmospheric circulation, but is more likely to be the result of variation in the quantities of mineral dust removed from the source regions and advected into the upper atmosphere. In addition to the mid-latitude inland deserts referred to above, which increased in area and dust transport capacity during colder episodes (Maher *et al.*, 2010; Muhs, 2013), additional sources of aeolian material include outwash deposits near glacier and ice sheet margins (Sugden *et al.*, 2009) and continental shelves that became exposed during times of lower global sea level (Gaiero, 2007). A further factor leading to enhancement of atmospheric dust flux could have been higher wind variability during cold intervals, that is, an increase in frequency and intensity of storms due to steepening of meridional temperature gradients (McGee *et al.*, 2010). Overall, it seems that global cooling is invariably associated with an increase in aeolian activity, with the higher atmospheric dust loading leading to important albedo feedback effects (Arimoto, 2001). The abrupt changes in atmospheric dust content indicated in

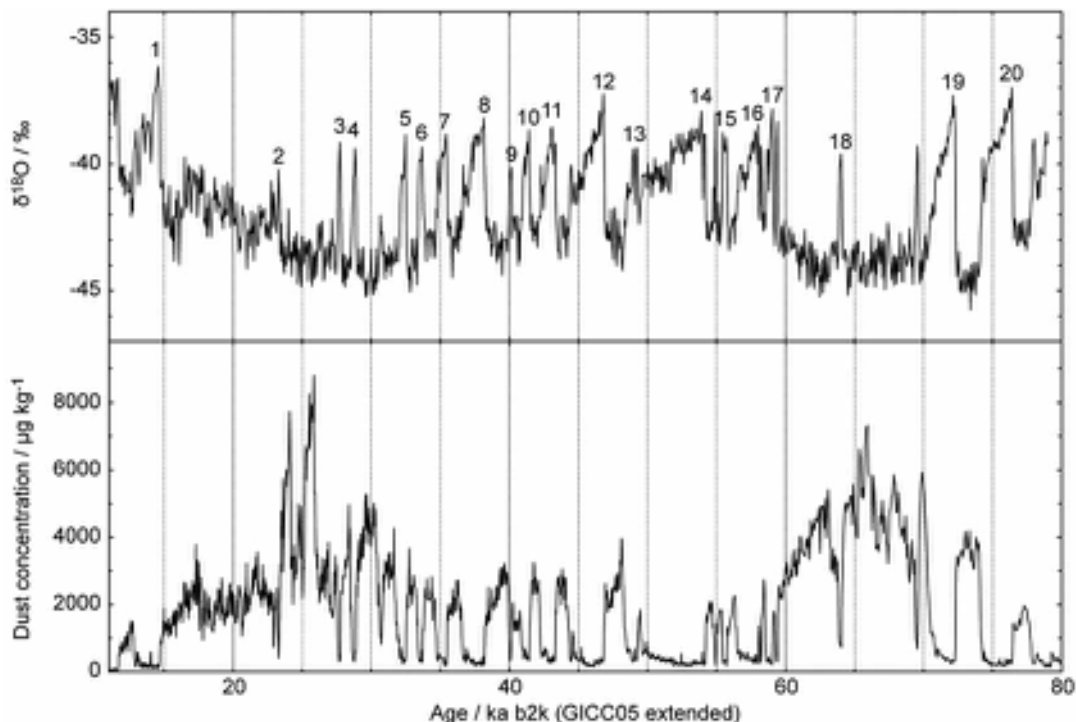


Figure 7.23 Variations in concentration of terrestrial dust (lower panel) over the last 80 ka shown against $\delta^{18}\text{O}$ variations, a proxy for temperature fluctuations (upper panel), in the NGRIP ice core; Greenland DO events are numbered in the upper panel (from Wolff *et al.*, 2010).

Figure 7.23 suggest that dust emission and flux are closely coupled to other environmental factors, a point we return to below.

The final factor to consider is sea-level change (section 2.5). The trend of falling sea level between MIS 5 and MIS 2 (Figure 2.33), which reflects the effects of expanding ice sheets, was interrupted by a number of short-lived rises in sea level, some of which are linked to the climatic variability reflected in the polar ice-sheet records. For example, four distinct fluctuations in sea level of around 20–30 m amplitude during MIS 3 have been linked to millennial-scale warming phases that have been recorded in Antarctic records (Siddall *et al.*, 2008; see below), while short-lived rises in sea level in the China Sea appear to coincide with North Atlantic Heinrich events (Huang & Tian, 2012). Whether these fluctuations in sea level instigated, or resulted from, ice-sheet mass balance changes is not yet clear, and may in any case be difficult to determine, as they are interdependent processes.

Sea-level events in the two hemispheres may be further complicated by the operation of the bipolar seesaw. As we saw above, under this hypothesis, colder conditions in Greenland were accompanied by warming in Antarctica, and vice versa. That this was indeed the case is demonstrated by a core sequence (GeoTü-KL11) from the Red Sea, where the terrestrial dust record matches that in the GISP-2 Greenland ice core (Figure 7.24), while variations in sea level based on independent proxies match more closely the Antarctic Byrd Station isotope profile (Rohling *et al.*, 2008). Since the different proxies were co-registered in the same core sequence and their separate signal affiliations are consistent throughout the core sequence, it seems reasonable to conclude that a regional terrestrial process (dust influx) was responding to the north polar climatic signal, while a global index (eustatic sea-level change) was forced by a south polar signature. A number of implications follow from this. First, the Antarctic ice mass appears to have had the largest influence on millennial-scale sea-level variations, and could have instigated changes that affected the north polar region, such as sea-level rise that may have been a factor in triggering Heinrich events (Flückiger *et al.*, 2006). Second, the Red Sea record underlines the importance of being able to discriminate between, and to quantify, the separate contributions that the south and north polar ice masses made to millennial-scale sea-level variations, but a satisfactory means of achieving this has yet to be developed (Rohling *et al.*, 2004). Third, care needs to be exercised when tuning sea-level records to climate curves in order to establish phase relationships between them, for the outcome will depend upon which polar record is selected. For example, Sierro *et al.* (2009)

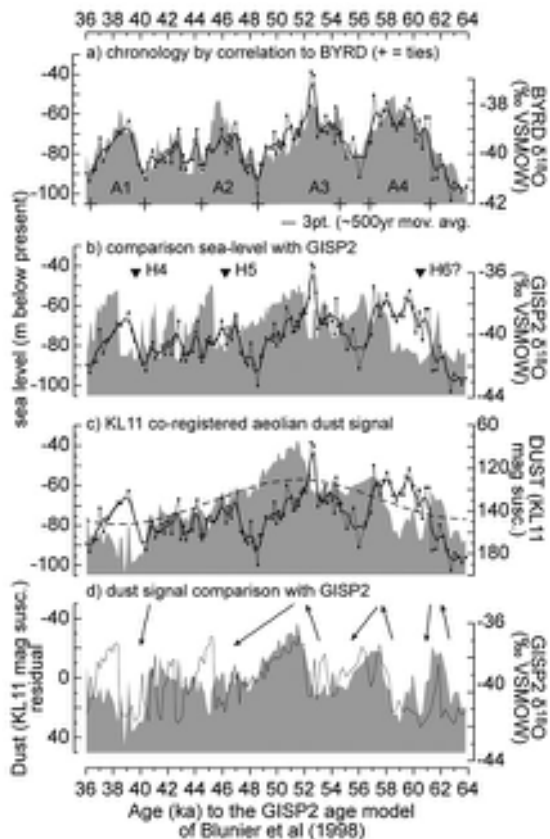


Figure 7.24 Terrestrial dust flux and sea-level reconstruction for the period 36–64 ka BP based on analysis of proxy records obtained from core GeoTü-KL11 in the Red Sea. a) Sea-level fluctuations (KL11; thin line) compared with the corresponding part of the Byrd Station (Antarctic) isotope record (grey shade). A1–A4 are Antarctic warm periods (AIMS). b) KL11 sea-level fluctuations compared with the GISP2 isotopic record (grey shade); H4, H5, H6 are Heinrich events. c) KL11 sea-level fluctuations compared with the KL11 magnetic susceptibility data (grey shade), a proxy for dust influx. d) KL11 dust influx record (thin line) compared with the GISP2 isotope record (grey shade). Arrows indicate places of particularly strong agreement (from Rohling *et al.*, 2008).

tuned a sediment record of sea-level change from the Mediterranean continental shelf to the Greenland ice-core record, from which they inferred that a series of marine flooding events in the Mediterranean was generated by rapid melting of Northern Hemisphere ice sheets. Had the sea-level record been tuned to the Antarctic ice cores, a somewhat different conclusion might have been reached!

7.4.5 Overview

Although we have focused our discussion on the last cold stage, it is now apparent that millennial-scale perturbations appear to be a persistent feature of earlier glacial stages also (Poli *et al.*, 2000; Loulerge *et al.*, 2008; Margari *et al.*, 2010), which suggests that processes such as the salt oscillator and the bipolar seesaw are integral components of the earth–atmosphere system. While some tentative explanations have been advanced to account for the series of climatic changes that took place during the last cold stage, it is clear that we are still some way from formulating a theory that explains all aspects of the climate record for this time period. A particular difficulty relates to the establishment of the precise order of events, and hence the determination of leads and lags in the system. There are a number of reasons for this. First, there are problems of chronology, for with the exception of annually resolved ice-core records and some (relatively rare) varved sequences, the age uncertainties on radiometric dates are often large (Chapter 5). In the absence of close dating control, the tendency has often been to tune individual records to selected master sequences but, as we have seen, this has its problems, because different models (Greenland, Antarctic, Hulu Cave, etc.) are employed in the tuning process, some records contain the imprint of more than one climatic rhythm, while in others there may be compound signals with ‘overprints’ from different regional or global contexts. In relation to the last point, for example, if it is indeed the case that Antarctic warmings are implicated in DO and possibly also Heinrich events, then North Atlantic and Greenland records reflect a compound signal showing the influence of both north (ice-sheet fluctuations, ocean circulation changes, climate change) and south (ocean circulation change, sea-level change) polar regions. But if we are to understand fully the sequence of changes reflected in these signals and establish the leads and lags (and causes and effects), then we need to improve the precision and accuracy of dating and correlation methods, so that records can be compared more objectively.

A second difficulty concerns the relatively limited number of high-resolution records that extend through the last cold stage. Although the number is steadily increasing, as yet they are barely sufficient to develop the databases that are required to underpin global-scale modelling and simulation programmes (Kageyama *et al.*, 2010). Furthermore, much of the published work on millennial-scale oscillations during the last cold stage has focused on individual components of the system, such as AMOC behaviour, the influence of sea-ice cover, or ice-sheet fluctuations. Maybe because of this, some interpretations

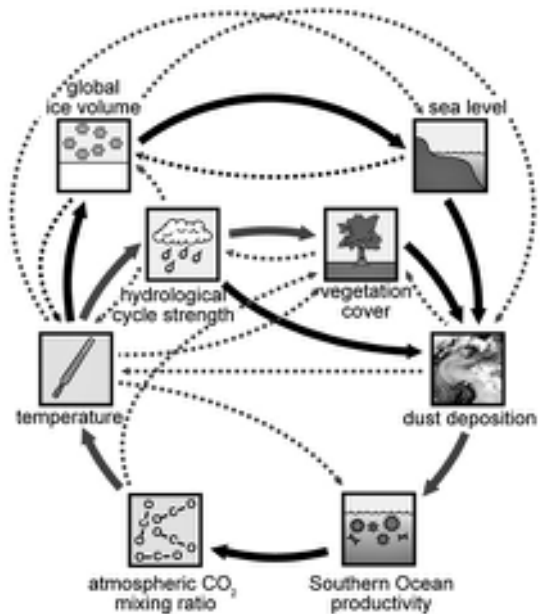


Figure 7.25 Schematic representation of the role of dust in the earth feedback system. The components link in three possible ways: by positive response, where an increase in one component results in a corresponding increase in another (grey arrows); by negative response, where an increase in one component leads to a decrease in others (black arrows); and neutral or no influence. If the sum of the connections between components is positive, this gives rise to a positive feedback, where an initial perturbation is amplified, and vice versa for negative feedback, which dampens the initial change. Solid arrows in the diagram are primary interactions or links, and dashed lines are additional linkages (from Ridgwell, 2002).

of the causes of millennial-scale climatic perturbations can seem contradictory, for example the contrasting views over which pole takes the lead in driving the bipolar seesaw, or the nature and sequence of processes that are involved in the generation of Heinrich events. A major aim for Quaternary science over the coming years, therefore, is to develop more comprehensive databases of high-resolution palaeo-records as a basis for meaningful simulations of millennial-scale climate fluctuations operating at the global scale.

A third problem arises from the interdependency of the processes and agencies that contribute to millennial-scale climate variation. This point is exemplified in Figure 7.25 which shows how an increase in the earth’s dust flux, once initiated, can induce a number of negative responses, some, for instance, relating to albedo effects and leading to an overall negative feedback in the climate system. This is

an example of the close coupling that often exists between key environmental variables. But something has to initiate the change in dust flux in the first instance, perhaps vegetation change, and that in turn must be responding to some other causal factor. Whichever variable we choose, this will always be the case: all of the variables are mutually interacting in some way, and hence it is difficult to isolate one as the genuine instigator of change. It could be argued that astronomical forcing, which is external to the earth system, initiates change at Milankovitch timescales, but, as we have seen, millennial-scale climate fluctuations during the last cold stage appear to have been induced by internal regulatory mechanisms, such as the bipolar seesaw, and hence could reflect some form of what has been termed **stochastic resonance**² (Claussen *et al.*, 2003). Once the resonance is set, then it is difficult to single out any one point in the sequence as being of particular causal significance, since all components in the process are responding to precursor conditions and events. The challenge, therefore, is to establish how the cycle starts in the first place, the key feedbacks that keep the cycle going, and how quickly global teleconnections operate, that is, how rapidly the changes in climatic conditions are transmitted through the global system. To answer these questions, strategic collaboration between the palaeodata and climate modelling communities will be required, and the former will need to supply time-series of palaeoenvironmental data based on improved age models. This may seem a tall order, but may not be beyond the bounds of feasibility!

7.5 THE LAST TERMINATION

7.5.1 Introduction

At several points in this book, we have made reference to **terminations**, the abrupt shifts in the marine oxygen isotope signal that mark the change in the global climate system from glacial to interglacial mode (sections 3.10.2 and 6.2.3.5). Although the terminations are generally considered to reflect a combination of astronomical forcing and associated climate feedback processes (Schulz & Zeebe, 2006; Cheng *et al.*, 2009), the relatively low resolution of the records means that the precise sequence of events and the interplay between the different components of the earth–atmosphere system during the course of each termination is not well understood. The situation is very different for the Last Termination (Termination 1), the transition from the last cold stage (MIS 2) to the present interglacial (MIS 1: the Holocene). The various stratigraphical records that span this time interval are

undoubtedly the best resolved of any that cover one of these major global climate shifts, and hence provide unique insights into the sequence, spatial pattern and timing of events that occurred during Quaternary terminations. In this section, we examine some of the evidence for Termination 1, and consider the implications for our understanding of how these major climatic transitions occurred at the regional, hemispherical and global scales.

7.5.2 Definition of the Last Termination

The term ‘Last Termination’ has not so far been formally defined, but is widely used to refer to the interval between the Last Glacial Maximum (LGM: also not formally defined, but generally acknowledged to have occurred around 21 ka: Mix *et al.*, 2001) and 11.7 ka, the onset of the Holocene (Walker *et al.*, 2009). This time interval includes the period widely referred to as the **Lateglacial** (or **Late Glacial**), and which, from a Northern Hemisphere perspective at least, has been considered to encapsulate the Last Termination. Indeed, the Lateglacial, the onset of which is marked in many Northern Hemisphere proxy records by an abrupt rise in temperature at ~14.7 ka (e.g. Walker *et al.*, 2003; Steffensen *et al.*, 2008), has frequently been referred to as the **Last Glacial–Interglacial Transition** (e.g. Björck *et al.*, 1998).

As we saw in Chapter 1 (section 1.6), the Lateglacial was initially subdivided on the basis of inferred climatic events in northwest Europe. An initial amelioration (the **Bølling Interstadial**) was followed, in turn, by the short-lived **Older Dryas (OD)** cold oscillation, a further mild climatic period, the **Allerød Interstadial** (interrupted by the short-lived **Inter-Allerød Cold Phase: IACP**) and the much colder **Younger Dryas (YD) Stadial**; this last episode spanned the time interval from 12.9–11.7 ka, and was terminated by the abrupt warming at the start of the Holocene (Figure 7.26). This terminology formed the basis for a climato-stratigraphic subdivision of terrestrial records not only from northern Europe but, somewhat paradoxically, from many other regions for which the subdivision was never initially intended (see below). It was, moreover, never related to a type site or stratotype (section 6.2.2). As explained previously (sections 1.6 and 6.3.3.3), however, the Bølling–Allerød–Younger Dryas terminology has, to a large degree, been superseded by an event stratigraphy based on the oxygen isotope signal in the Greenland cores, with the NGRIP record now constituting a stratotype sequence for the Last Termination in the North Atlantic region (Lowe *et al.*, 2008b). The parallel set of isotopically defined terms that is now increasingly being employed for events during the Last Termination,

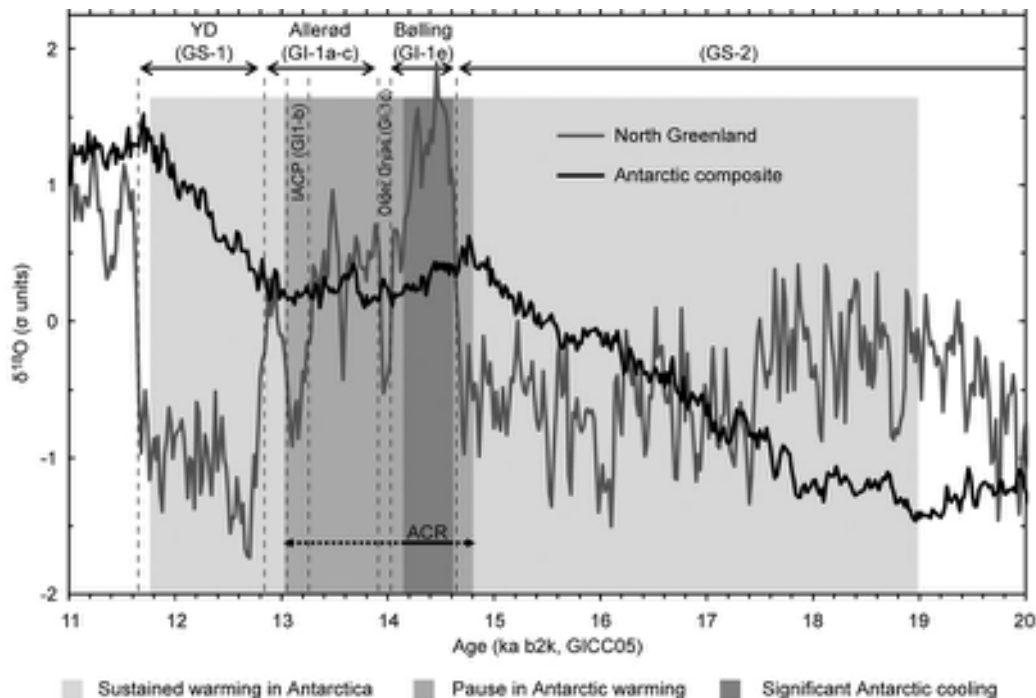


Figure 7.26 Isotopic records from Antarctica (black line: a composite of four Antarctic ice-core records) and Greenland (NGRIP, grey line) for the Last Termination, defined here as the interval between 20 and 11.7 ka. Vertical light-grey shading denotes an episode of sustained warming in Antarctica, the vertical medium-grey band a pause in Antarctic warming, and the dark-grey band a significant Antarctic cooling (the Antarctic Cold Reversal: ACR). The NGRIP record shows the marked warming in Greenland at c. 14.7 ka that defines the start of the Lateglacial period. b2k – years before AD 2000 (from Pedro *et al.*, 2011). For further explanation see text.

based on Greenland stadial (cold: GS) and interstadial (warm: GI) units, is shown in Figure 7.27. In this scheme, **GS-2a** denotes the cold period between the LGM and the onset of Lateglacial warming (sometimes also referred to as the *Oldest Dryas* period), while the succeeding warmer period encompassing the Bølling and Allerød interstadials equates with **GI-1** in the NGRIP sequence. **GI-1** is subdivided into five subunits on the basis of inferred climatic variability: **GI-1e** broadly corresponds with the Bølling, **GI-1d** with the OD and **GI-1c** to **GI-1a** with the Allerød, the IACP seemingly marked by a short-lived cooler episode (GI-1b). **GS-1** corresponds with the YD Stadial. Strictly speaking, however, these terms are not synonymous, nor time-parallel, and should not be assumed to be so, as explained in section 7.5.5.

Although the NGRIP ice core constitutes a viable regional (and indeed hemispherical) stratotype for the Last Termination in the North Atlantic region, it is evident from Figure 7.26 that it cannot represent the sequence of events in both the north and south polar regions. This is because

the two hemispheres experienced very different climatic histories during the Last Termination. Whereas conditions remained cold in the north until the abrupt rise in temperatures at c. 14.7 ka, warming in Antarctica began perhaps as early as c. 19 ka, and was more gradual. Other differences between northern and southern records include a significant period of cooling in Antarctica, the **Atlantic Cold Reversal (ACR)**, which coincided with the warmest phase of the Lateglacial period in the north; the absence of a reciprocal change in Antarctica when the IACP (GI-1b) affected Greenland; and gradual warming in Antarctica during the North Atlantic YD (GS-1) cold event. In this context, therefore, the YD/GS-1 cold episode, which had such a profound effect on the environment of large areas of North America and Eurasia, can be seen as a uniquely Northern Hemisphere event. Moreover, while from a north polar perspective, the marked rise in temperatures at 14.7 ka constitutes the first unequivocal sign that the last glacial period had ended, this major event is signalled much earlier in the south, and accords with the marine isotope evidence

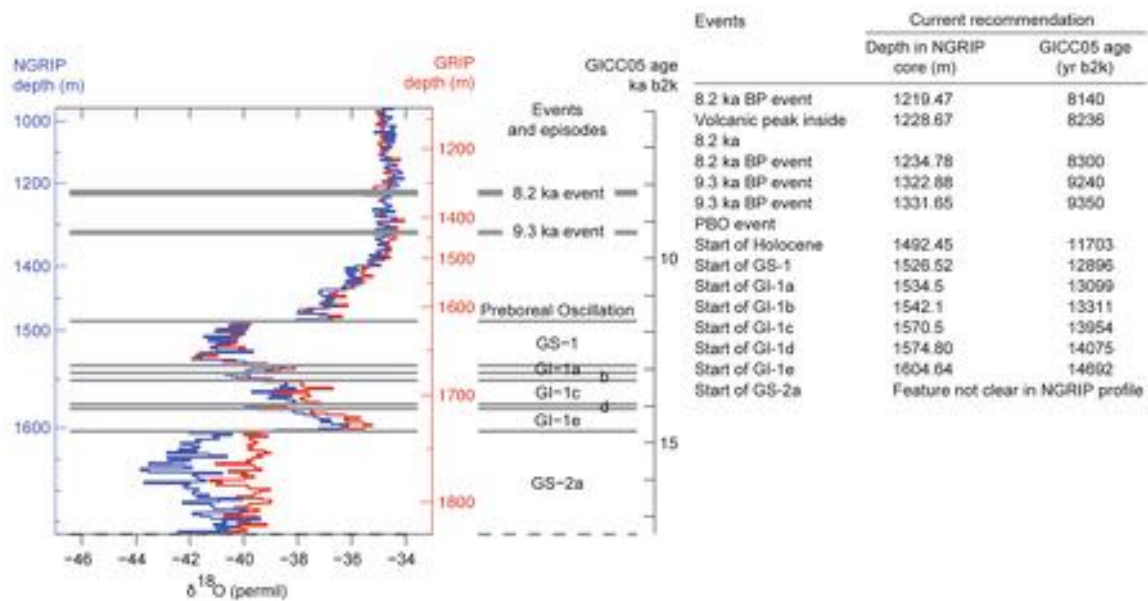


Figure 7.27 Stratotype scheme for the Lateglacial–early Holocene in the North Atlantic region. The figure on the left shows the NGRIP (blue) and GRIP (red) isotope records and corresponding isotopic events and sub-events: GI – Greenland Interstadial; GS – Greenland stadial. The table on the right defines the boundaries between each isotopic event in years before 2000 (b2k) (from Lowe *et al.*, 2008b).

that points to a significant decline in global ice cover from c. 20 ka onwards. On a global scale, therefore, the Last Termination did indeed begin as early as 19 or 20 ka, and markedly predated the beginning of the Northern Hemisphere Lateglacial.

7.5.3 Onset of the Last Termination

In section 6.2.3.5 we noted that a distinctive feature of the deep-ocean marine isotope profiles is the ‘saw-tooth’ appearance of the curves reflecting the fact that while glacial inceptions are usually progressive over tens of thousands of years, the transitions from full glacial to full interglacial conditions (the terminations) occur within maybe 10 ka or less. Why, after a long period of sustained cold climate, glaciations should end so abruptly remains a puzzle, because the orbitally forced increase in solar insolation (Figure 7.28) cannot alone account for such a sudden and pronounced climatic shift (Denton *et al.*, 2010). One possibility is that the trigger may lie in the Southern Hemisphere, because of the early manifestation of an increase in temperatures shortly after the LGM (Stott *et al.*, 2007). For example, comparisons between Antarctic ice-core records, Pacific Ocean marine records

and Southern Hemisphere insolation changes suggest that temperatures in the southern Pacific (both deep-water and sea-surface temperatures: SSTs) started to warm around 1 ka *before* warming of tropical Pacific SSTs and the rise in atmospheric CO₂ content as reflected in the ice cores (Figure 7.28). This would appear to rule out increased atmospheric CO₂ or tropical climate circulation as the forcing agents that initiated the onset of the last termination (Peeters *et al.*, 2004; Timmermann *et al.*, 2009). One plausible scenario is that increased solar radiation over Antarctica initiated a retreat of sea ice which, in turn, led to increased ventilation of the Southern Ocean, and therefore higher atmospheric CO₂ levels, which enhanced the warming trend (Stott *et al.*, 2007).

Others have suggested, however, that the onset of the Last Termination was triggered by processes operating in the north. Denton *et al.* (2010), for example, note that as the northern ice sheets reached their maximum extent during the closing stages of the last glacial period, the Greenland stadial events became more prolonged (see Figure 7.15). This in turn would have led to longer periods of warming of more southerly latitudes (because of the effects of the bipolar seesaw: section 7.4.3). Warming was further induced by an associated increase in ventilation in

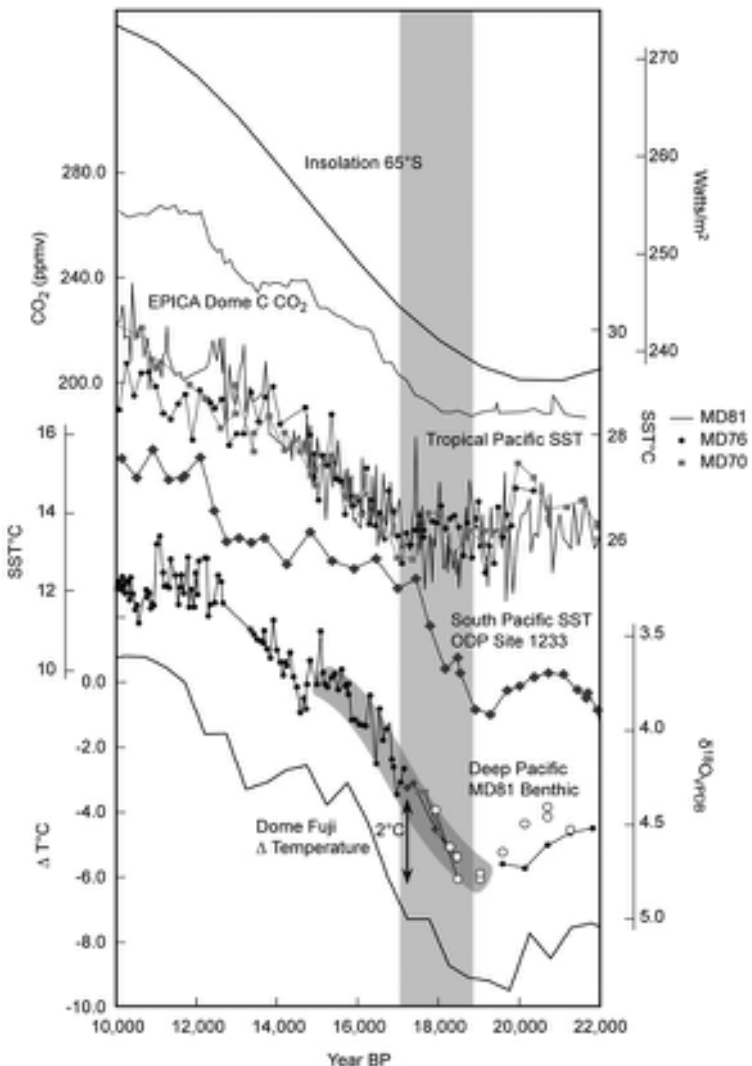


Figure 7.28 Temperature variations in the Pacific Ocean at the surface (SST) and at depth (benthic) during the Last Termination inferred from foraminiferal assemblages, shown against ice-core CO₂ data (EPICA Dome C), ice-core temperature reconstructions (Dome Fuji) and summer insolation in the Southern Hemisphere (upper curve). The vertical grey shading highlights the difference in timing between the onset of deep-water warming (close to 19 ka) and Tropical Pacific SST warming. The grey shading on the MD81 benthic curve represents a 200-year uncertainty on the ages obtained from benthic foraminiferal samples (from Stott *et al.*, 2007). For further explanation see text.

the southern oceans and in the release of CO₂ to the atmosphere. These combined effects led eventually to the transgression of a critical threshold, when stored warmth in the south grew to a level sufficient to prevent a return to stadial conditions in the north, save for some short-lived reversals such as the IACP and YD (see above). Cheng *et al.* (2009) arrived at a broadly similar conclusion, based

in this case on the analysis of variations in strength of the northern monsoon. In their scenario, periods of northern ice-sheets collapse and associated sea-level rise coincide with times of low monsoon strength and an increase in atmospheric CO₂. The relative strength of the northern monsoons appears to have been a critical factor in the prolongation of stadials in the North Atlantic region, again

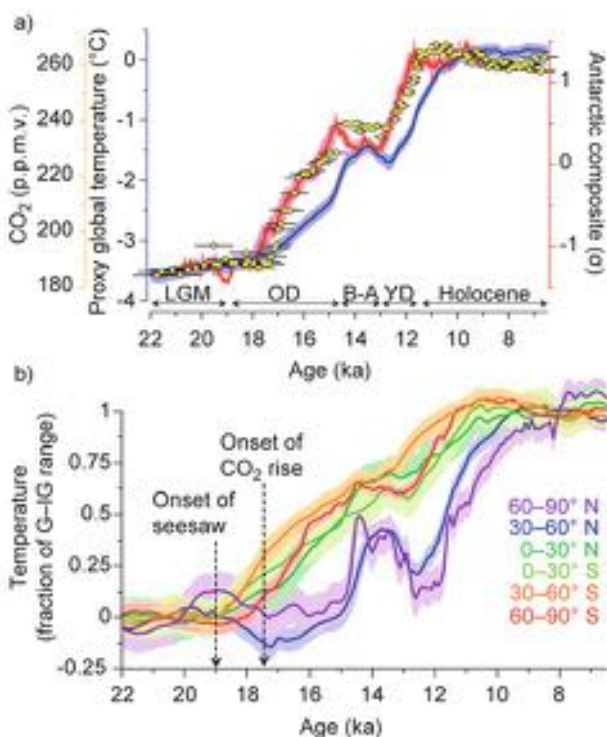


Figure 7.29 a) Global temperature stack for the Last Termination based on eighty globally distributed records (blue curve), compared with temperature (red curve) and atmospheric CO₂ concentration (yellow dots) records from Antarctic ice-cores. All data are shown with 1σ error ranges. LGM – Last Glacial Maximum; OD – Oldest Dryas; B–A – Bølling–Allerød interval; YD – Younger Dryas. b) Mean temperature variations (with 1σ error ranges) for stacks of proxy records arranged in 30° latitude bands. The mean values have been normalized to fractions or percentages of the total glacial–interglacial (G–IG) temperature range (from Shakun *et al.*, 2012, reprinted with permission from Macmillan Publishers Ltd: *Nature* (Shakun, J.D., Clark, P.U., Feng, H. *et al.*) copyright 2012). For further explanation see text.

allowing longer periods of CO₂ release from the southern oceans, and resulting in an amplification of the solar signal and the demise of the last great ice sheets.

A compilation of global temperature records for the Last Termination (Figure 7.29) suggests that air temperature over Antarctica had started to rise by at least 18 ka, before atmospheric CO₂ concentrations rose, but then increased in concert with CO₂ after c. 17 ka (Figure 7.29a). The composite for mean *global* temperature, however, clearly lags these developments during the period 18 to c. 11 ka, except during the Bølling–Allerød (B–A) interval. All three curves converge near the start of the Holocene. When the data are resolved into latitudinal belts, however, it can be seen that the global composite temperature curve shown in Figure 7.29a is biased by the data obtained from sites located between 30°N and 90°N (Fig. 7.29b). These partitioned data show that the first net increase in temperature, albeit small, is recorded in the high-latitude

Northern Hemisphere records at around 19 ka, preceding the more marked warming in the Southern Hemisphere, again implicating events in the Northern Hemisphere as a possible trigger for the Last Termination (He *et al.*, 2013).

A possible sequence of events during the Last Termination is shown in Figure 7.30. An increase in boreal summer insolation beginning c. 22 ka (1 in Figure 7.30) caused the northern ice sheets to melt, reducing surface reflectivity, allowing Greenland to warm (2). Meltwater released from the wasting ice sheets and glaciers caused a shutdown in the Atlantic Meridional Overturning Circulation (AMOC), and a cooling in the North Atlantic. Southwards heat transfer led to a warming of Antarctica and the Southern Oceans (3) and subsequently the release of CO₂ into the atmosphere (4). A consequent increase in global-scale warming accelerated northern ice-sheet melting, keeping the north cool, the south warm and further CO₂ release (a positive feedback loop). Ultimately, this led to the

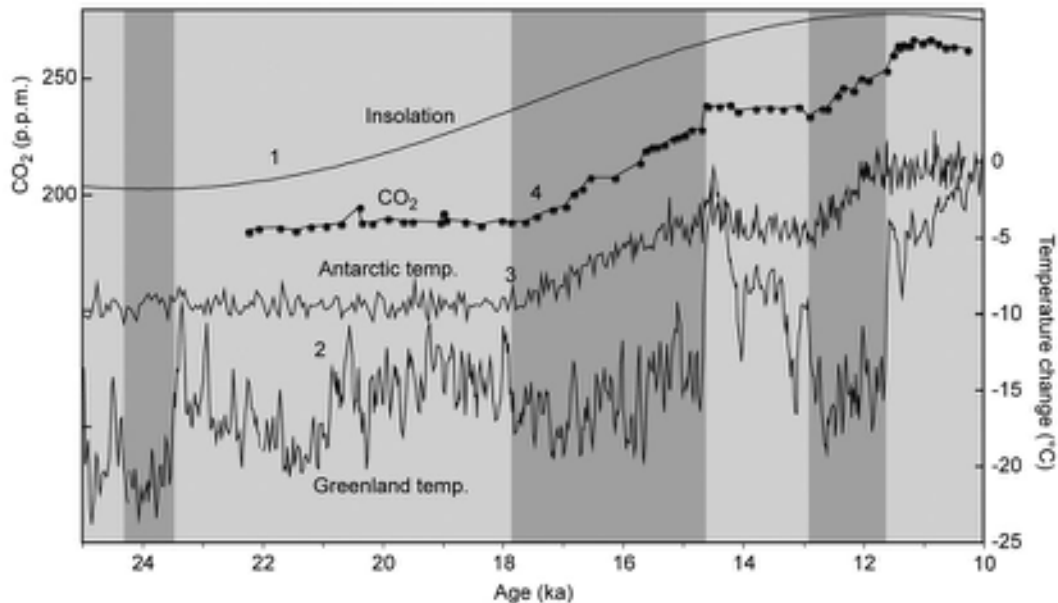


Figure 7.30 Hypothesized chain of events during the Last Termination; the sequence (1–4) is explained in the text (from Severinghaus, 2009).

termination of the last glacial stage (Severinghaus, 2009). This scenario, based initially on empirical evidence, has been supported by transient simulation modelling which suggests that the last deglaciation was initiated by rising insolation during spring and summer in the mid- and high northern latitudes. AMOC changes associated with this orbitally induced retreat of Northern Hemisphere ice sheets led to early Southern Hemisphere deglacial warming, with the ensuing rise in atmospheric CO₂ providing the critical feedback for global deglaciation (He *et al.*, 2013).

7.5.4 Global teleconnections during the Last Termination

In previous sections, we examined the evidence for teleconnections between the polar regions, monsoon cells, the Inter-Tropical Convergence Zone (ITCZ) and other elements of the global circulation system over the last glacial cycle. Here we consider further evidence for the close coupling of these regional elements of global climate during the Last Termination.

As we saw in section 7.4, a distinctive feature of the ocean-atmosphere system over the course of the last glacial cycle was the operation of the bipolar seesaw, and this also appears to constitute a working hypothesis for the pattern of environmental changes in the two hemispheres during

the course of the Last Termination. In the Southern Hemisphere, for example, records that are closely in-phase with the Antarctic climate rhythms include glacier oscillations in the Southern Alps, New Zealand and Patagonia, including a marked readvance during the ACR (Putnam *et al.*, 2010; Garcia *et al.*, 2012); sea-surface temperature (SST) variations along the Chilean coastal margin (Lamy *et al.*, 2004), the tropical Indian Ocean (Naidu & Govil, 2010), the Arabian Sea (Huguet *et al.*, 2006) and around South Australia (Calvo *et al.*, 2007); air temperature records from South Africa (Holmgren *et al.*, 2003); and palaeohydrological trends in the Dry Valley lakes of Antarctica (Hall *et al.*, 2010). Throughout most of the Northern Hemisphere, by contrast, palaeoenvironmental records tend to align closely with the Greenland ice-core climate signal. Examples include variations in strength of the Indian, Asian and African monsoons (Chang *et al.*, 2008b); lake-level variations in North America (Benson *et al.*, 1998); SST variations and circulation in the central Mediterranean Sea (Cacho *et al.*, 1999) and tropical Atlantic (Lea *et al.*, 2003); air temperature variations in Japan (Kossler *et al.*, 2011); and glacial and aridity cycles in the Spanish Pyrenees (González-Sempériz *et al.*, 2006).

Some low- and mid-latitude regions, however, appear to have been affected by both Northern and Southern hemisphere factors. For example, warming of the Cali-

fornian margin of the North Pacific appears to have predated the start of the GI-1e warming in Greenland by c. 2 ka, but post-dates the start of warming in Antarctica, perhaps reflecting both northern and southern circulation influences in this region (Hill *et al.*, 2006). Similarly, large-scale retreat of mid-latitude LGM glaciers in both hemispheres seems to have commenced at broadly the same time, but the timing of retreat is consistent with the onset of temperature and CO₂ increases in Antarctic ice cores, suggesting a Southern Hemisphere driver for deglaciation in some Northern Hemisphere regions (Schaefer *et al.*, 2006). There is also evidence suggesting the operation of an Atlantic–Pacific seesaw teleconnection during the Last Termination, with deep-water formation in the northern Pacific when the AMOC was closed down in the North Atlantic (Okazaki *et al.*, 2010). More puzzling are some records from the Southern Ocean that appear to accord more closely with the Greenland climatic record, for example a cooling phase in the Great Australian Bight and the South Atlantic that was contemporaneous with the GS-1 event (Kim *et al.*, 2002; Andres *et al.*, 2003). Clearly, therefore, some events during the Last Termination cannot be accounted for by the bipolar seesaw alone (Seidov *et al.*, 2005). Indeed, despite the numerous proxy records now available from the Last Termination, it is not clear how climate changes initiated at the poles are propagated throughout the global climate system. There is, nevertheless, a considerable body of evidence to support the view that the bipolar seesaw remained a key element of the ocean–atmosphere system during the Last Termination (e.g. Stenni *et al.*, 2011), and we return to this matter below.

7.5.5 Synchronizing records of Lateglacial age

7.5.5.1 Introduction

Thus far, we have been considering the Last Termination in its broadest sense; in other words, the whole time period from the end of the LGM to the onset of the Holocene. We now turn our attention to the Lateglacial, that 3 ka interval of the Last Termination when, in the Northern Hemisphere at least, profound and often extremely rapid changes occurred in the climate–environment system.

The study of the Lateglacial period has a long history, and it is undoubtedly one of the most intensively investigated episodes in the entire Quaternary record. This is because the geomorphological, lithostratigraphical and biostratigraphical evidence from the Lateglacial can be examined at a much higher temporal resolution, and

potentially dated more precisely, than is the case for earlier Quaternary phases (Walker, 2001). Realizing the chronological potential of these records, however, has proved to be a major challenge, for the ice cores and their accompanying timescales set new standards in terms of stratigraphic resolution and chronological precision that other archives have not always been able to match. In this section, we consider the development of new time-stratigraphic frameworks for the Lateglacial that are increasingly enabling us not only to distinguish spatial and temporal patterns of environmental change during this key interval of the Quaternary record but, equally importantly, to begin to quantify leads and lags in climate change and accompanying environmental response.

7.5.5.2 Lateglacial stratigraphy and chronology

The subdivision of the Lateglacial outlined above (section 7.5.2) was based originally on pollen-based biozones (section 6.2.3.2) identified in southern Scandinavia (the ‘Norden model’: Mangerud *et al.*, 1974). The pollen zone boundaries were dated by radiocarbon, and hence assumed the status of chrono-zones (section 6.3.7). This has since proved problematical, however, partly because of errors that can affect radiocarbon dates (section 5.3.2.4), but also because biozone boundaries (which reflect response of vegetation to climate/environment thresholds) are time-transgressive, whereas chronozone boundaries, by definition, are time-parallel (Walker, 1995). Indeed, this was one of the principal reasons why the INTIMATE Working Group (section 6.3.3.3) advocated replacement of the Norden Model by the Greenland event stratigraphy (Björck *et al.*, 1998). Yet the terms Bølling, Older Dryas, Allerød and Younger Dryas (section 7.5.2; Figure 7.26) were widely adopted, and are still applied today, often in parts of the world distant from Scandinavia, to stratigraphic units that are considered to approximate, in time or climatic characteristics, those in the Norden Model (Peteet, 1995). The use of the term ‘Younger Dryas’ (YD) to define climato-stratigraphic units in sites remote from northwest Europe, especially those in the high-latitude Southern Hemisphere, appears particularly incongruous, given that that part of the globe was warming at the time of the YD cold period in the north!

As we saw in Chapter 5, the Greenland ice-core record is underpinned by the high-resolution GICC05 timescale, an annually resolved record based on multiparameter layer counting, with a maximum counting error (MCE) in the Lateglacial of ~3 per cent (section 5.4.3.3). Thus at the GS-1–Holocene boundary, the MCE is of the order of

99 years, while at the onset of the Lateglacial (onset of GI-1e), it is 190 years (Rasmussen *et al.*, 2006). It is worth recalling that the MCE is broadly equivalent to a 2σ error in a Gaussian probability distribution, and hence the MCE in the GICC05 chronology equates approximately to a 68 per cent probability value (1σ) on a conventional radiocarbon date. At the GS-1–Holocene boundary, therefore, the MCE of 99 years corresponds broadly to a *c.* 50-year error on a radiocarbon date. However, many dates from the Lateglacial have standard errors that are in excess of the MCE in GICC05, and hence, until comparatively recently, there were considerable chronological uncertainties in age models for the Lateglacial sequence, sometimes millennial in scale (Lowe *et al.*, 2007). This meant that the degree of correspondence between Lateglacial terrestrial and marine sequences, and between these archives and the Greenland ice cores, could not be rigorously tested, and correlations therefore tended to be assumed rather than convincingly demonstrated. This was especially the case where sequences were either poorly dated or where radiocarbon dates were lacking. In these instances, alignment of climatically derived signals from fossil records with the oxygen-isotope record from the Greenland ice cores became standard procedure (section 6.3.3.2). But this brought with it additional problems, particularly in terrestrial sites (lakes and bogs) where sedimentation was slow and hence stratigraphic resolution was poor, for contemporaneity of events could never be conclusively demonstrated.

In recent years, therefore, there has been a concerted attempt to refine dating procedures and to establish stratigraphic protocols in order to provide a more secure basis for correlating between, and synchronizing, Lateglacial records. We examine some of these initiatives in the following sections.

7.5.5.3 Lateglacial age models and correlation procedures

A number of parallel developments have helped to refine Lateglacial age models and the synchronization of ice-core, marine and continental records. The first of these is the gradual fine-tuning of the IntCal radiocarbon calibration model (section 5.3.2.6), which has significantly reduced the uncertainties of calibrated ages within the Lateglacial time frame. For example, although the latest iteration, IntCal13, employs a tree-ring dataset that extends back to 14.2 ka BP, the dendrochronologically based calibration model has been terminated at 13.9 ka because of sparse measurements in the early part of the record (Reimer *et al.*, 2013). However, if these problems can be resolved, and currently floating chronologies can be linked

to the continuous dendrochronological record, calibration may in due course be extended back to the early Lateglacial (GI-1e: Kaiser *et al.*, 2012). Other developments involve the use of more reliable dating media, for example through the careful targeting of fossil types or chemical fractions most likely to yield coherent results (Blockley *et al.*, 2007a; Howarth *et al.*, 2013), and by refining the procedures employed for sample pretreatment and ^{14}C activity measurement so that samples with low ^{14}C content yield more accurate age estimates (Watanabe *et al.*, 2009).

A second important advance has been refinements in tephrochronology, especially the employment of cryptotephra layers (section 5.5.2.1) to identify distal volcanic ash horizons and to use these to correlate Lateglacial records and to synchronize climatic events (Figure 7.31). Some distal tephras detected in marine cores are also found in continental records, and so terrestrially based age estimates can be imported into marine sequences, circumventing the problems caused by marine reservoir effects on ^{14}C dates (section 5.3.2.5) and thereby ensuring more secure marine–land correlations (Thornalley *et al.*, 2011). Of particular value are those tephra layers that are co-registered in the polar ice cores and in continental or marine records, for they provide well-dated tie-points. For example, the widely dispersed Vedde Ash, which originates in Iceland (Katla volcano), is found in the Greenland ice-core sequences (Figure 5.26), where it is dated on the GICC05 timescale to 12,171 years with an MCE of 114 years (*c.* 57 years at 1σ), placing it within the YD/GS-1 Stadial (Lane *et al.*, 2012). It occurs in marine sediments in the North Atlantic, and can be traced throughout much of Europe, from the British Isles in the west to the Ural Mountains in the east, and from Norway to as far south as Slovenia and North Italy (Lane *et al.*, 2011). It therefore constitutes a key time-stratigraphic marker horizon for the Lateglacial across a large area of the Northeast Atlantic region.

A third key innovation has been the analysis of increasing numbers of varved sediment records and the construction of varve chronologies (section 5.4.2). Since these are based on annual-layer counting, they perhaps come closest to ice-core records in terms of the potential they offer for discriminating environmental changes with a high temporal resolution (e.g. Litt *et al.*, 2001; Brauer *et al.*, 2008). Some Lateglacial varved records also contain distal tephra layers (Blockley *et al.*, 2007b), which have proved particularly valuable for refining the timing of regional events, and showing how they align with the polar ice-core records.

The fourth important development has been the emergence of statistical tools that aid the evaluation of complex chronological data and form the basis for the

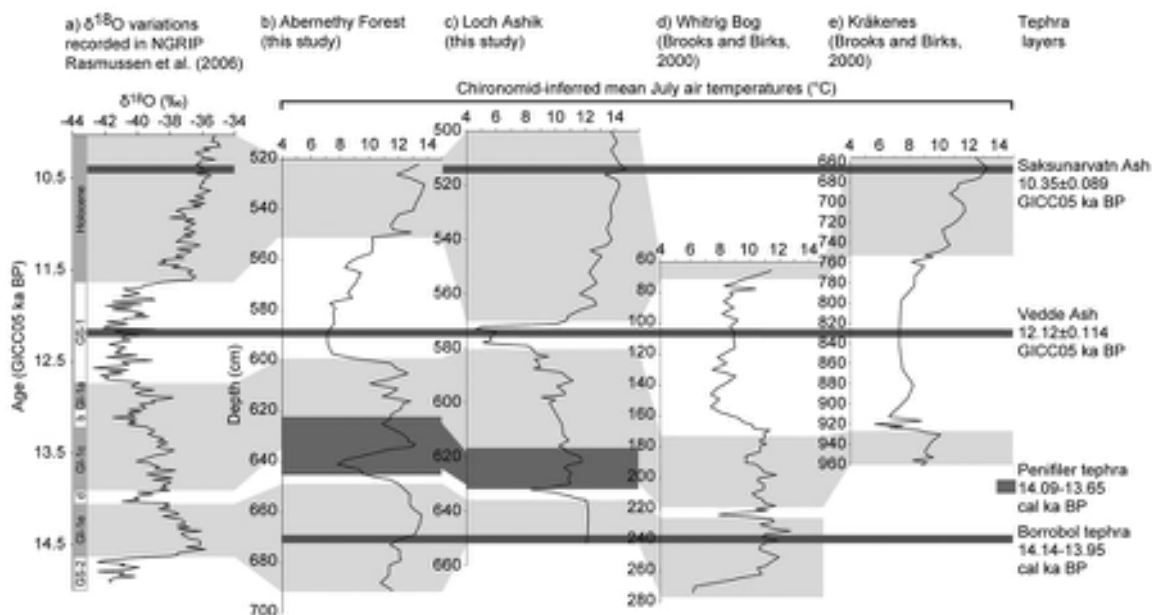


Figure 7.31 Quantified palaeotemperature records for the Lateglacial and early Holocene from three sites in Scotland and one (Kräkenes) in Norway aligned using four tephra isochrons. The temperature reconstructions are based on the analysis of fossil chironomid assemblages. Two of the isochrons, the Saksunarvatn Ash and Vedde Ash, occur in the Greenland ice cores (left) and are therefore dated by ice-core chronology. The ages of the Borrobol and Penitifer tephra are based on calibrated radiocarbon-based ages. The grey shading indicates relatively warmer phases (Bølling, Allerød, early Holocene). The timescales for b)–e) are in ka cal. BP (from Brooks *et al.*, 2012). For further explanation see text.

construction of age models (section 5.3.2.6). These take into account all information concerning the stratigraphic order of dated samples and additional evidence relating to the stratigraphic sequence and its context, and combine this information using Bayesian probability procedures (Blockley *et al.*, 2007a; Bronk Ramsey, 2008). The models can be adjusted using different assumptions (e.g. about changes in sedimentation rate, possible hiatuses in the sequence) until an optimized age–depth profile has been achieved. This approach is particularly useful where more than one chronological method, for example radiocarbon dating and tephrochronology, is being employed.

Finally, there has been the formulation of protocols for the stratigraphic subdivision and correlation of Lateglacial sequences. As we explained in Chapter 6, the INTIMATE Group has proposed that the NGRIP ice-core record should be the stratotype for the Lateglacial period for the North Atlantic region (section 6.3.3.3), and that the ages of the event boundaries should be dated using the GICC05 timescale (Figure 7.27; Lowe *et al.*, 2008b; Blockley *et al.*, 2012). While the NGRIP isotopic signal constitutes the regional stratigraphic template, the INTIMATE proposal

is that individual site records should be subdivided on the basis of local or regional criteria, and should be assigned *local* stratigraphic terms, with ages and durations determined by independent dating, prior to correlation with the ice-core records. It must be recognized, however, that the NGRIP stratotype is applicable only to the North Atlantic province, and will not provide a suitable template for regions that have experienced a quite different sequence of climatic events during the Last Termination. Finally, a common misconception is that INTIMATE has simply replaced one set of general stratigraphic terms (Bølling, Allerød etc.) with another (GI-1e, GS-1, etc.). This is *not* the case, as that defeats the purpose of stratigraphy and correlation, which is to *test* how each sequence has evolved, and how the inferred climate signal correlates with that in other stratigraphic records.

7.5.5.4 Rapid environmental change during the Lateglacial

There are strong indications in the ice-core records that the bipolar seesaw was influential in determining the pattern

of climate changes during the course of the Lateglacial (Stenni *et al.*, 2011) although, as we saw above, there remains some uncertainty over how, and how rapidly, the climate signals were transmitted from high- to low-latitude regions. Here we examine some recent evidence of the processes involved, and of their response times. The focus will be on the Northern Hemisphere and on three key events or episodes: (1) the marked warming at the start of GI-1e (Bølling); (2) the cooling trend between GI-1d and GI-1a; and (3) the YD Stadial (GS-1; Figure 7.26).

Prior to the GI-1e event, the North Atlantic region experienced markedly colder conditions with the shutdown of the AMOC and widespread formation of sea ice leading to more severe winter conditions, not only in the North Atlantic region but also in Asia (Denton *et al.*, 2005). This period of extreme cold was followed by the re-establishment of the AMOC and rapid warming at the onset of the Lateglacial (GI-1e). Precisely what caused the shutdown and subsequent re-establishment of the AMOC remains unclear, but it could reflect retreat of sea ice in the Southern Ocean leading to export of heat northwards (Bianchi & Gersonde, 2004), or rapid melting of the Antarctic ice sheet leading to sudden sea-level rise which destabilized the ice margins in the north (Deschamps *et al.*, 2012). Alternatively, it may have been triggered by events in the Northern Hemisphere, most probably the release into the northern oceans of large quantities of meltwater from the wasting ice sheets. As we saw above, the first signs of warming in the northern high latitudes occurred *c.* 22 ka, and this may have been the trigger for ice-sheet wastage. Oceanographic records from the North Atlantic certainly show that the onset of meltwater release from the collapsing ice sheets began *c.* 19 ka, and was followed by the deposition of ice-raftered debris (Heinrich event 1) between *c.* 17.5 ka and 16.5–15 ka. This appears to have been accompanied by a ‘pooling’ of freshwater in the Nordic Seas which was subsequently purged into the North Atlantic, thereby preconditioning the Nordic Seas for convective deep-water formation (Stanford *et al.*, 2011). This, in turn, allowed an abrupt restart of the AMOC and North Atlantic Deep Water (NADW) formation at the GI-1e warming (14.7 ka). Greenland ice-core records suggest that the major reorganization in North Atlantic hemispherical circulation that accompanied this warming occurred within one to three years and resulted in a centennial-scale rise in temperatures of up to 10°C (Figure 7.27; Steffensen *et al.*, 2008). In the Southern Hemisphere, by contrast, Antarctic ice-core records show a gradual warming throughout this period, while the North Pacific experienced three short warmings, each lasting between 500 and 1,500 years (Sarnthein *et al.*, 2006). Moreover, the high-resolution

record from Lake Suigetsu in Japan (section 5.4.2.7) suggests that the onset of the warming at the beginning of the Lateglacial occurred 300–500 years earlier than in Greenland (Figure 7.32; Nakagawa *et al.*, 2005), suggesting that other areas of the Northern Hemisphere were experiencing climate shifts that differed significantly in character and timing from those in the North Atlantic.

Peak thermal conditions in Greenland during GI-1e lasted for perhaps only 100 years or so, before temperatures started to decline. A long-term cooling trend between *c.* 14.5 and 12.9 ka was interrupted by several short-lived, and colder excursions. Two of these are defined in the Greenland stratotype sequence (Figure 7.27) – events GI-1d (onset 14.075 ka; MCE 169 years; duration 121 years) and GI-1b (onset 13.111 ka; MCE 149 years; duration 203 years) – while a third, of much shorter duration (< 100 years), is sandwiched between them. In each of these cases, both the cooling and subsequent warming associated with each of these events appears, from the Greenland isotope signal at least, to have occurred relatively rapidly. Many palaeoclimatic records from lake sediment sequences around the North Atlantic region tend to show a similar pattern of climate variation during the Bølling–Allerød interval (GI-1), although the number of clearly identified cold intervals varies between sites. Frequently only one of these events can be detected, usually the Older Dryas (GI-1d) in European sites, but the Inter-Allerød Cold Phase (GI-1b) is evident in some North American records (Yu & Wright, 2001). In a number of high-resolution records from Europe, however, up to four such cold episodes have been recognized (Brauer *et al.*, 1999; van Raden *et al.*, 2013). There may be a number of explanations for this. Slow rates of sediment accumulation in many lake basins could have compressed the stratigraphic record and made these short-lived climatic phases difficult to detect, a problem that may have been further compounded by inadequate sampling resolution. In other cases, the climatic signals might not have registered in proxy data, either because of the low amplitude of the climatic fluctuations, or because the changes in temperature and/or precipitation regime were insufficient to overcome critical geomorphic and ecological thresholds to produce, for example, changes in lake sedimentation or in regional plant communities. As a consequence, and perhaps surprisingly as many hundreds of Lateglacial sites have now been investigated in Europe and North America, a complete climatic picture for the Lateglacial Interstadial around the North Atlantic region has yet to be established.

Antarctic records (Figure 7.26), by contrast, do not show any matching reciprocal signals for these short-lived cooler events, while the Lake Suigetsu record (Figure 7.32) reveals

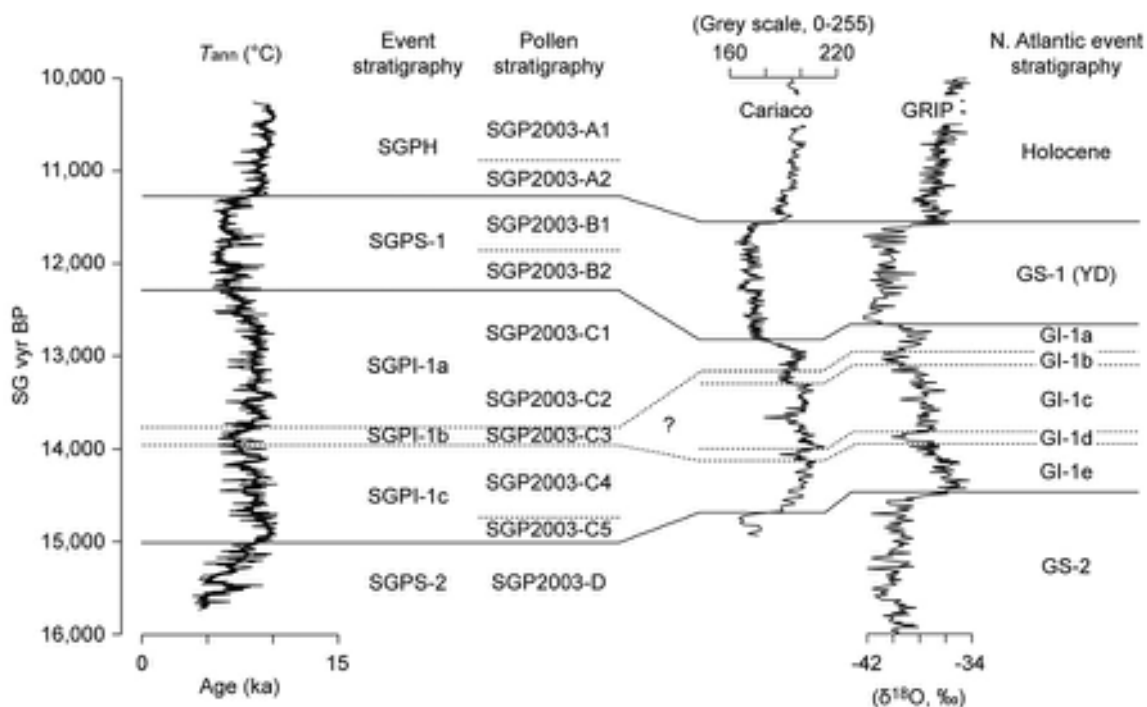


Figure 7.32 Lateglacial temperature record from Lake Suigetsu Japan, derived from a pollen-based transfer function. The timescale is based on varve chronology and high-precision radiocarbon dating (section 5.4.2.7; Figure 5.25). The black (thick) curve on the left is a running mean through individual temperature uncertainty ranges. The record is plotted against the Cariaco Basin (Venezuela) grey-scale record (also dated by a combination of radiocarbon and varve chronology), the Greenland (GRIP) ice-core record, and the North Atlantic event stratigraphy scheme dated using independent chronologies (from Nakagawa *et al.*, 2005).

only one similar event, the age of which lies between those of GI-1d and GI-1b. The pattern of climate variability during GI-1 described above appears, therefore, to be confined largely to the North Atlantic region, and is probably attributable to episodic phases of meltwater influx released during the continuing demise of the northern ice sheets (Clark *et al.*, 2001).

The final climatic episode of the Lateglacial is the clearly defined Younger Dryas (YD) Stadial, dated in the Greenland stratotype sequence to between 12.9 and 11.7 ka (GICC05: MCE of 138 and 99 years, respectively; Figure 7.27). This is one of the best-known and most intensively studied intervals in the entire Quaternary record, partly because it constitutes a clearly defined time-stratigraphic unit in both lithological and pollen-stratigraphic sequences (e.g. Figure 3.48), and partly because it constitutes the most recent and accessible example in the recent geological record of a high-resolution millennial- (or even centennial-) scale stadial event and, as such, is readily amenable to climate modelling (Broecker *et al.*, 2010). The

YD is occasionally referred to as ‘Heinrich event 0’ (H-0), because a detrital sediment layer has been identified in North Atlantic marine sediments from the YD interval (Andrews *et al.*, 1995). This term has not been widely adopted, however, as the detrital layers appear to be much more limited in terms of their spatial extent, unlike the widespread IRD deposits that characterize H1–H6 (Hemming, 2004).

In the Greenland ice-core records, the YD is the ‘end member’ of the progressive cooling trend that characterizes the GI-1 interval (Figure 7.26). While its onset is marked by a marked shift in isotopic values (reflecting a fall in temperature), this is no steeper or greater in magnitude than the two preceding thermal declines (GI-1e to GI-1d and GI-1c to GI-1b). The records therefore suggest that the YD is the product of a longer, incremental cooling trend, though many consider it to be a unique event. The most widely accepted explanation for the onset of YD cooling again involves the injection of meltwater into the North Atlantic, this time on a sufficient scale and for a sufficiently

long period to lead to a significant decrease in the rate of NADW formation and a weakening (or complete disruption) of the AMOC, with the resulting spread of sea ice and a hemispherical drop in atmospheric temperature. This hypothesis has gained a great deal of support, because there is clear evidence of extensive ice-dammed lakes trapped by the retreating ice margin and of episodic catastrophic drainage from these lakes (Leverington *et al.*, 2002), while marine cores show clear evidence of lower salinity and bottom-water flow rates during the YD interval (Roberts *et al.*, 2010). In addition, 'hosing' simulation experiments have confirmed that meltwater influx on a sufficiently large scale would seriously disrupt AMOC behaviour (Tarasov & Peltier, 2004). The routing of meltwater into the North Atlantic appears to have been via the St Lawrence Seaway and the Champlain Valley of the northeast USA (Barber *et al.*, 1999; Rayburn *et al.*, 2011), although there may well have been a more northerly flux of meltwater and icebergs from the Arctic Ocean via the Fram Strait and into the Greenland–Iceland–Norwegian Seas (Tarasov & Peltier, 2004). Re-diversion of North American meltwater drainage and a reduction in iceberg meltwater influx into the North Atlantic led to a density increase in surface waters and reactivation of the AMOC. The associated heat release generated a hemispherical-scale warming and brought an end to the YD (Alley, 2000).

An alternative, and more recent, hypothesis attributes the onset of the YD to the impact of an extraterrestrial object (bolide) at c.12.9 ka that exploded above North America and partially destabilized the Laurentide ice sheet. This, it has been argued, caused, *inter alia*, continental-scale wildfires, extinction of many megafaunal species, the disappearance of the Clovis (palaeo-Indian) culture and, perhaps most significantly, the onset of YD cooling (e.g. Firestone *et al.*, 2007; Bunch *et al.*, 2012). The impact hypothesis has proved to be highly controversial, however, because of questions over the stratigraphical evidence, consistency in analytical results, and the nature of the physical mechanisms proposed (e.g. Pinter *et al.*, 2011). It is also the case that the Younger Dryas is not a unique event in the recent geological record, and hence does not require a particular (and in this instance, catastrophist) explanation to account for its onset and character. Rather, as we have seen, it is the latest of a series of millennial- or centennial-scale climatic perturbations that occurred during the last cold stage and shares a number of common characteristics (and therefore, by implication, causal mechanisms) with its predecessors (Broecker *et al.*, 2010).

Recent studies of the YD based on high-resolution analysis of European lake deposits not only provide further support for the North Atlantic, and particularly the AMOC

as a driver of YD climate changes, but they also reveal the remarkable temporal resolution that is now possible in the reconstruction of Lateglacial climatic events. Two lake records serve to illustrate this point (Figure 7.33). In Meerfelder Maar in the Eifel district, Germany, the sediments are varved throughout the entire YD interval, and the series has been tied to an absolute timescale by the well-dated Laacher See Tephra (LST), and by a calibrated radiocarbon chronology based on sixty-nine AMS radiocarbon dates (Brauer *et al.*, 2008). Evidence from sub-annual microfacies and geochemical variations within the varve layers indicates that the lake experienced a significant increase in stormy conditions at the onset of the YD. This is attributed to a reduction in strength of the AMOC, which enabled North Atlantic sea ice to expand, driving the oceanic Polar Front southwards (Figure 7.33), blocking off ocean heat, and diverting strong westerly winds across central Europe. The registration of this marked climatic shift in the Meerfelder Maar sequence is precisely dated at 12,679 varve years. As such, it post-dates the onset of the YD in Greenland by over 200 years, reflecting the length of time it took for the sea ice to build up and the Polar Front to migrate southwards to the latitude of the Eifel region of Germany.

A similar high-precision Lateglacial record is available from Kråkenes Lake in western Norway. There the age model is based on ninety-six calibrated radiocarbon dates,

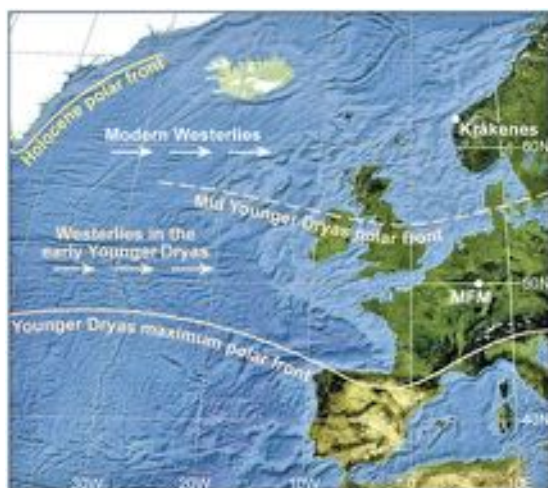


Figure 7.33 Location of the Kråkenes and Meerfelder Maar (MFM) sites that contain high-resolution records of the GS-1 (Younger Dryas Stadial) interval (see Figures 7.34 and 7.35 and text) and inferred positions of the Polar Front (from Lane *et al.*, 2013).

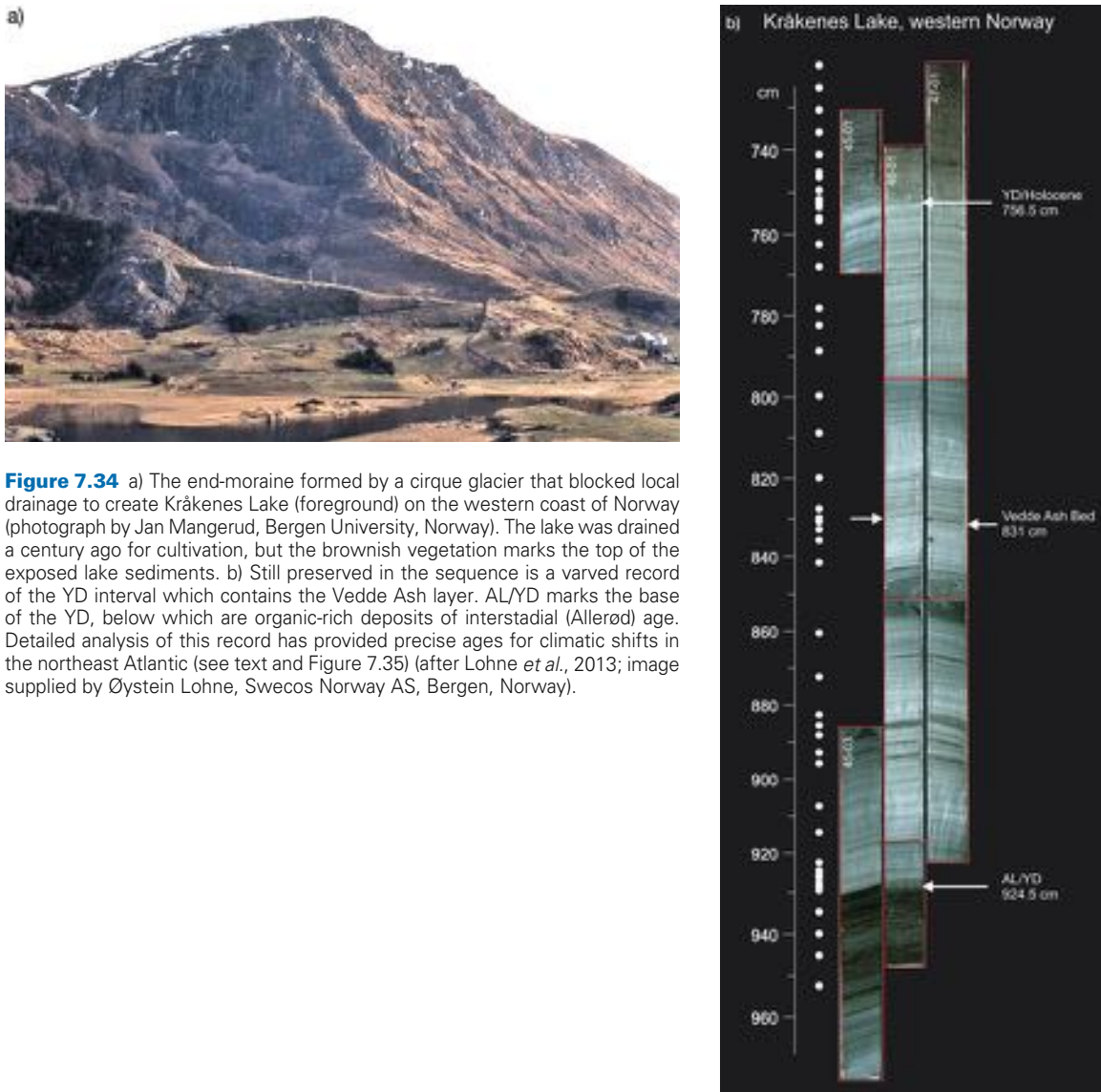


Figure 7.34 a) The end-moraine formed by a cirque glacier that blocked local drainage to create Kråkenes Lake (foreground) on the western coast of Norway (photograph by Jan Mangerud, Bergen University, Norway). The lake was drained a century ago for cultivation, but the brownish vegetation marks the top of the exposed lake sediments. b) Still preserved in the sequence is a varved record of the YD interval which contains the Vedde Ash layer. AL/YD marks the base of the YD, below which are organic-rich deposits of interstadial (Allerød) age. Detailed analysis of this record has provided precise ages for climatic shifts in the northeast Atlantic (see text and Figure 7.35) (after Lohne *et al.*, 2013; image supplied by Øystein Lohne, Swecos Norway AS, Bergen, Norway).

and tied to the NGRIP stratotype by the Vedde Ash, which is present in both the Kråkenes Lake and in Greenland ice-core sequences (Bakke *et al.*, 2009). The lake is located close to a cirque that was occupied by a glacier during the YD and which delivered sediment directly into the Kråkenes basin (Figure 7.34). A significant increase in Ti content (followed by greater variability in the record) and also in sediment heterogeneity (as reflected in the XRF data) occurs around 12.5 ka cal. BP (Figure 7.35), these trends reflecting a more erratic sedimentation pattern due to

increased glacier melting. Evidence from marine cores off western Norway indicates that periodic incursions of warm salty water began at around the same time. The evidence suggests that the Nordic seas were permanently frozen during the early YD but, as the Polar Front retreated northwards, sea ice started to break up with largely ice-free conditions being achieved around 12.15 ka BP (Bakke *et al.*, 2009). This is around 400 years before the end of the YD as recorded in the Greenland ice cores (Walker *et al.*, 2009).

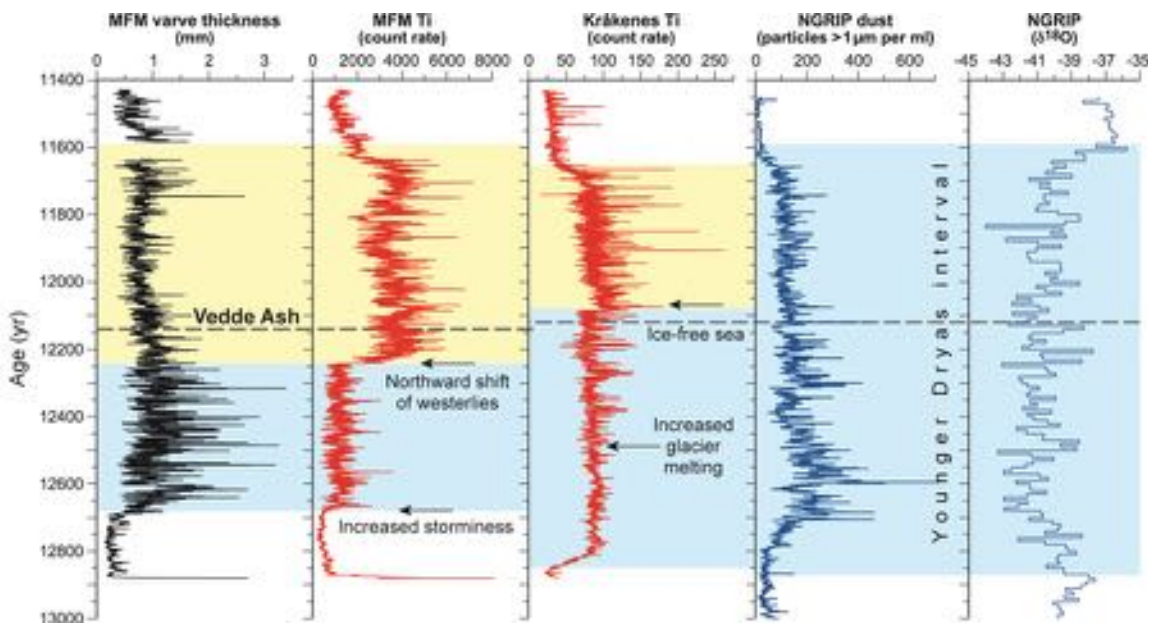


Figure 7.35 Comparison of the timing of the mid-YD transitions reflected in the Kråkenes Ti, and Meerfelder Maar (MFM) Ti and varve thickness records. The age models for the two sites agree within twenty years at the level of the co-registered Vedde Ash (dashed line). The position of the Vedde Ash in the NGRIP ice core is shown on the right. The main mid-YD transition in the lake records is marked by the colour change from blue to yellow (from Lane *et al.*, 2013). For further explanation see text.

The Kråkenes record is one of a number from both terrestrial and marine contexts that point to a marked change in atmospheric and oceanic circulation regimes not just at the onset and end of the YD, but as a transitional episode in the mid-YD (e.g. Isarin *et al.*, 1998; Elmore & Wright, 2011). It has been suggested that this was a broadly synchronous event across the North Atlantic realm (e.g. Bakke *et al.*, 2009), a hypothesis that can now be tested by comparing the records from the Kråkenes and Meerfelder Maar sites. The key stratigraphic marker linking the two records is the Vedde Ash which is dated at $12,140 \pm 40$ years on the Meerfelder Maar varve chronology. In that lake sequence, an abrupt climatic amelioration, marked by a northward shift of westerly wind systems (reflected in the XRF Ti record: Figure 7.35), occurs at 12,240 varve years, which is precisely 100 years *before* the deposition of the Vedde Ash. In Kråkenes Lake, a similar shift in the Ti signal occurs *c.* 20 years *after* the deposition of the Vedde Ash, in other words *c.* 120 years after the reduction in storminess recorded in the Meerfelder Maar sequence. This temporal offset between the two records must reflect the time taken for the Polar Front to move northwards from the latitude of central Europe to that of southwestern Norway. Moreover, it clearly demonstrates that the mid-YD climatic

transition was not a single synchronous event, but rather was a time-transgressive northward shift of polar air masses whose average rate of retreat was around 10 km per yr (Lane *et al.*, 2013).

These examples show the extraordinary level of temporal precision that can now be achieved when Lateglacial records are dated and correlated using the approaches outlined in section 7.5.5.2. Given suitable sites and the appropriate evidence (varved sequences, media for high-resolution and high-precision radiocarbon dating, tephra isochrones), it now becomes possible to compare and to correlate records that are greater than 10 ka in age, at a centennial or, in some instances as we have seen, at a decadal scale. It is by using such high-precision and high-resolution archives that we will, in due course, be able to distinguish, with a degree of confidence, those records that are synchronous from those that are not. In this way, we will be able to begin to resolve one of the longest-standing problems in Quaternary palaeoclimate research, namely whether there is indeed a temporal order in events, and which of those events constitute the leads and which the lags; in other words, we will be much better equipped to tackle the ‘chicken-and-egg’ conundrum to which we have referred in earlier sections of this chapter.

7.6 CLIMATE AND THE HOLOCENE

7.6.1 Introduction

The Holocene is the most recent period within the geological record and covers the time interval from 11.7 ka until the present day. The term *Holocene*, which means ‘entirely recent’ (or ‘wholly modern’), refers to the warm episode that began with the end of the last glacial period (the Younger Dryas). In many ways, the Holocene is no different in terms of climatic trends from previous interglacial periods of the Quaternary record, but what distinguishes the Holocene from these earlier warm stages is the evolution of the human environment. Indeed, it is this anthropogenic signature that is the hallmark of the Holocene and that not only sets it apart from previous interglacials, but that justifies its status as a time-stratigraphic unit of series/epoch rank in the geological timescale (section 1.3). Here we examine some of the key climatic events that have occurred during the course of the present interglacial, the evidence for cyclical climate changes during the later Holocene and their possible causes, and the anthropogenic effects on Holocene climate. But we begin by considering the major trends that are evident in the Holocene climate record.

7.6.2 Holocene climate trends

When viewed in the long-term perspective of the Quaternary, the Holocene appears as a relatively stable climatic episode. The Greenland oxygen isotope records, for example, show relatively few significant fluctuations during the course of the Holocene, and certainly nothing to compare with the regular, pronounced and often abrupt climatic swings of the last cold stage and the Last Termination. Global temperature reconstructions suggest a warming of around 0.6°C from the early Holocene to a temperature plateau extending from 9.5–5.5 ka (Figure 7.36), a period often referred to as the ‘**Holocene Thermal Maximum**’ (or the ‘Hypsithermal’, ‘Altithermal’, or ‘Climatic Optimum’), this warm interval being followed by a long-term 0.7°C cooling from 5.5 ka to c. 100 years ago. This general pattern appears to have been globally variable, however, with the extra-tropical Northern Hemisphere (north of 30°N) showing a cooling of c. 0.7°C from 7.0 ka onwards. In the low latitudes (30°N–30°S), by contrast, there appears to have been a lesser warming of 0.4°C from 11.0–5.0 ka, with temperatures levelling off thereafter. In the Southern Hemisphere (south of 30°S), however, where the thermal maximum occurred near the beginning of the Holocene, cooling (of around 0.4°C) is recorded from

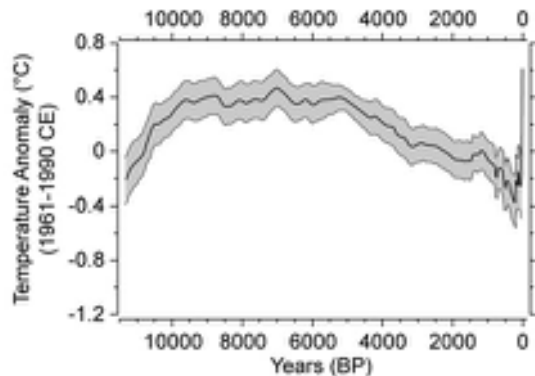


Figure 7.36 Temperature anomalies for the Holocene derived from the mean of seventy-three globally distributed temperature records (dark line) with its 1σ uncertainty (grey band) (after Marcott *et al.*, 2013).

11.0–7 ka followed by relatively constant temperatures over subsequent millennia (Marcott *et al.*, 2013). Early Holocene warmth in the Southern Hemisphere at a time when Northern Hemisphere climate was still to recover fully from glacial conditions may reflect the persistence of the bipolar seesaw (section 7.4) into the Holocene epoch.

This broad tripartite pattern of Holocene climate change, which is reflected in proxy climate records from both marine and terrestrial realms, can be largely attributed to orbital forcing. For example, in the high northern latitudes, the Milankovitch variables for 65°N predict maximum insolation values around 11–10 ka, due to a combination of summer perihelion and enhanced obliquity, with a subsequent decline by a factor of 10 per cent since that time interval (Ritchie *et al.*, 1983). However, it is now apparent that, when examined at a finer scale of resolution, Holocene climate records were more temporally and spatially variable than the above generalized patterns might suggest. Indeed, there appear to have been significant changes in climate often over very short timescales. For example, Mayewski *et al.* (2004) have identified six distinct periods of rapid climate change over the course of the last 11.5 ka (9.0–8.0 ka, 6.0–5.0 ka, 4.3–3.8 ka, 3.5–2.5 ka, 1.2–1.0 ka and 600–150 years ago), each characterized by polar cooling, tropical aridity and major atmospheric circulation changes. More recently, Wanner *et al.* (2011) also recognized six distinct episodes during the Holocene when periods of more stable and warmer climate were interrupted by clearly defined cold relapses (c. 8.2 ka, 6.3 ka, 4.7 ka, 2.7 ka, 1.55 ka and 550 years ago). We consider some of these climatic events in the following sections.

7.6.3 Holocene climatic events

7.6.3.1 The Pleistocene–Holocene transition

The transition from the last cold stage (Younger Dryas) to the Holocene, defined in stratigraphic records by the Pleistocene–Holocene boundary (Walker *et al.*, 2009), is manifest in a range of proxy records. These include, for example, the replacement of cold-climate elements by more thermophilous taxa in pollen profiles; the (often abrupt) lithostratigraphic change from minerogenic to organic sediment in limnic sequences; rapid isotopic shifts (reflecting changing temperature values) in isotopic records from lake sediment and from speleothems; and the change from cold- to warm-dominated microfaunal and microfloral assemblages in marine sediment cores. All of these indicate a marked reorganization in the global climate system, and there are indications that the transition from a glacial to an interglacial mode was very rapid. However, the most impressive manifestation of the nature and speed of climate change at the onset of the Holocene is to be found

in the high-resolution records from the Greenland ice sheet, as these indicate that the major climatic shift at the beginning of the Holocene occurred within a century or less.

Figure 7.37 shows that part of the Greenland NGRIP ice core that spans the Pleistocene–Holocene boundary, while Figure 7.38 presents a multiparameter dataset from the same section of core. The stratigraphic record of impurities and chemicals within the ice is at subannual resolution, and provides a unique insight into the onset and evolution of the rapid climatic shift that occurred at the end of the Pleistocene (Steffensen *et al.*, 2008). The $\delta^{18}\text{O}$ profile, which is a proxy for past air temperature at the coring site, records a warming during the Pleistocene–Holocene transition of the order of 10°C over 60 years. It was accompanied by a decline (by a factor of 5–7) in dust concentration and in calcium, both reflecting a marked change in atmospheric circulation regime, notably a reduction in dust flux from the low-latitude Asian deserts. But the speed of the climatic transition is most clearly evident in the curve for deuterium excess (d-excess). This

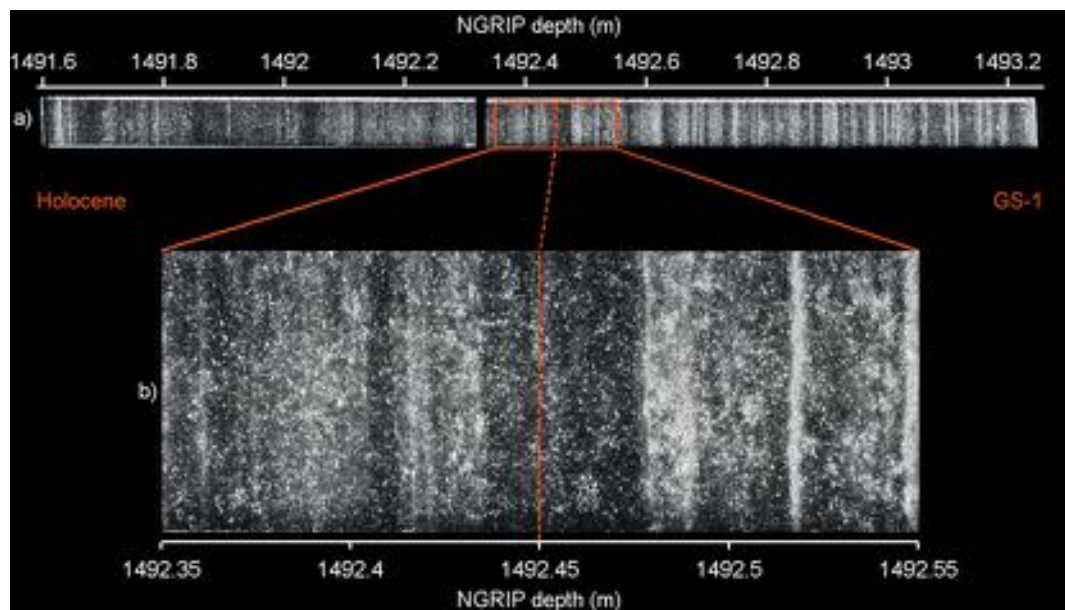


Figure 7.37 a) Visual stratigraphy of the NGRIP ice core across the Pleistocene–Holocene boundary obtained using digital line scanning (section 5.4.3.1). As explained in Figure 5.26, this process produces a ‘reversed’ image, so that clear ice shows up black, whereas the cloudy bands, which contain relatively large quantities of impurities, in particular micrometre-sized dust particles from dry areas in eastern Asia, appear white. This is essentially a seasonal signal that is reflected in annual banding in the ice. Note that the dust concentrations are much higher in the Pleistocene (GS-1) section of the core than in the Holocene, reflecting a markedly increased dust flux during colder periods. b) The precise location of the Pleistocene–Holocene boundary at 1,492.45 m is shown in the enlarged lower image (after Walker *et al.*, 2009; image provided by Sune Rasmussen, Niels Bohr Institute, University of Copenhagen, Denmark).

value, which is derived from the relationship between deuterium and oxygen, is an important isotopic tracer of precipitation and, in the Greenland ice-core records, is indicative of changes in the moisture source areas of the precipitation that falls on the ice sheet. It can also be considered as a proxy for sea-surface temperatures in those moisture source areas. The NGRIP d-excess record shows a 2–3 per mil decrease at the onset of the Holocene, corresponding to an ocean-surface temperature decline of 2–4°C in the regions from which the precipitation was being advected; in other words, it reflects a change in the source of Greenland precipitation from the warmer mid-Atlantic during glacial times to colder high latitudes in the early Holocene (Masson-Delmotte *et al.*, 2005). The NGRIP record shows that this change in d-excess occurred over a timescale of no more than 1–3 years! It is accompanied by

a 40 per cent increase in ice-layer thickness (Figure 7.38), reflecting an abrupt increase in precipitation, the two proxies marking a sudden and major reorganization of Northern Hemisphere atmospheric circulation, which is believed to be related to the rapid northward movement of the oceanic Polar Front at the end of the Younger Dryas Stadial/Greenland Stadial 1. This extraordinary record from the Greenland ice sheet shows that an abrupt shift between two radically different climatic states can occur within a matter of a few years.

7.6.3.2 The 8.2 ka event

During the course of the early Holocene, three climatic cooling events are evident in the Greenland ice cores at c. 11.5 ka, 9.3 ka and 8.2 ka (Rasmussen *et al.*, 2007). These

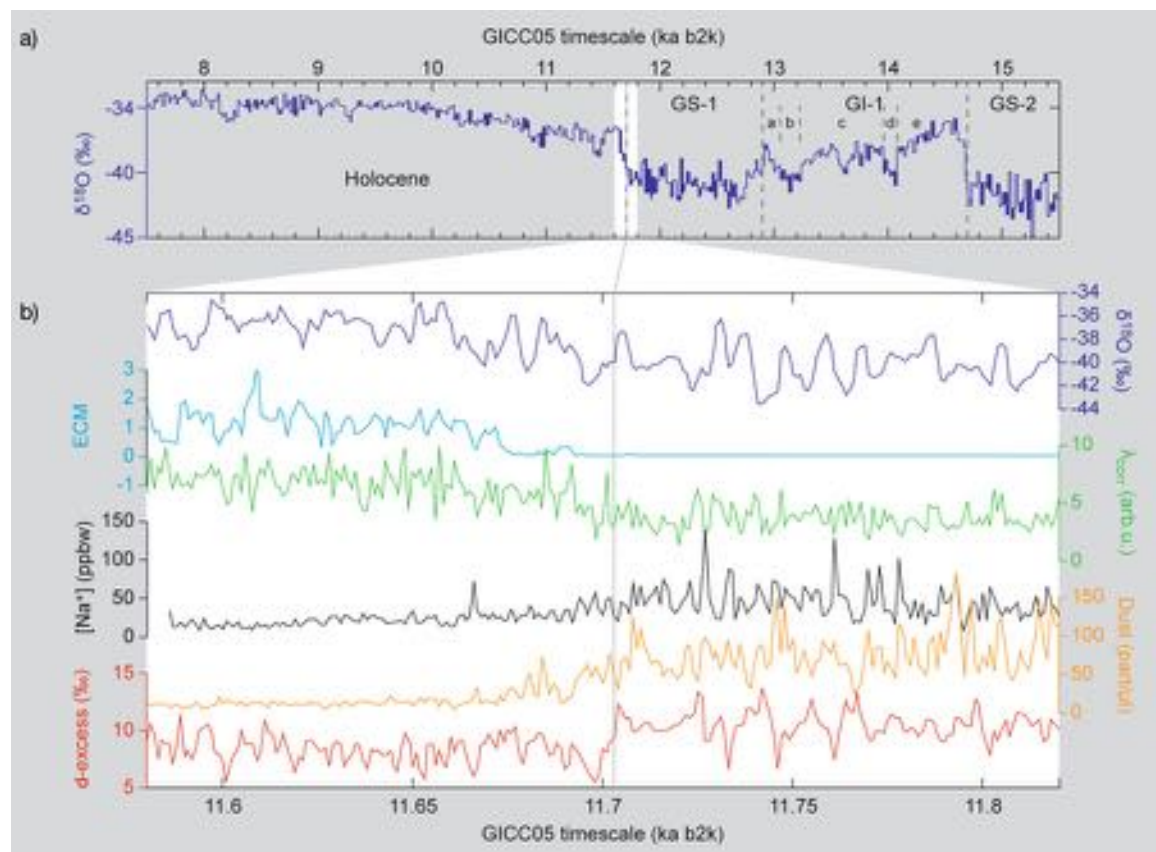


Figure 7.38 a) The $\delta^{18}\text{O}$ record through the last glacial-interglacial transition, showing the position of the Pleistocene–Holocene boundary in the NGRIP core. b) High-resolution multiparameter record across the Pleistocene–Holocene boundary: $\delta^{18}\text{O}$, electrical conductivity (ECM), annual layer thicknesses corrected for flow-induced thinning (λ_{corr}) in arbitrary units, Na concentration, dust content, and deuterium excess (after Walker *et al.*, 2009. Copyright © 2008 John Wiley and Sons, Ltd).

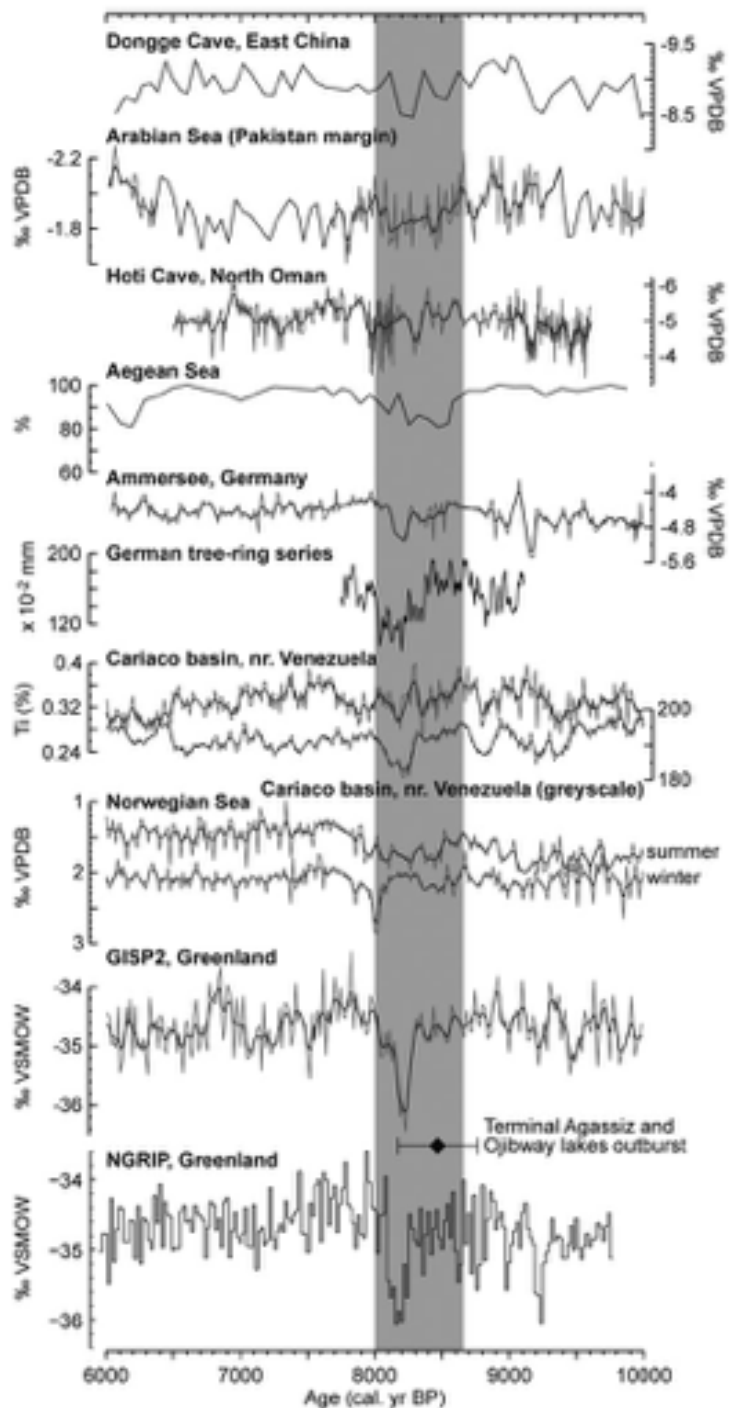


Figure 7.39 Proxy records for the 8.2 ka event. The vertical grey bar marks the approximate duration of the climatic anomaly associated with the 8.2 ka event (after Walker *et al.*, 2012. Copyright © 2012 John Wiley and Sons, Ltd).

lasted for no more than c. 150 years, and each is marked by a pronounced $\delta^{18}\text{O}$ anomaly (abrupt shift to low isotopic values) in the ice-core records (Figure 7.39 lower two panels). The most significant of these cooling episodes in terms of a global climate signal is that which occurred around 8.2 ka.

This event is also registered in the ice cores in a decline in ice-layer thickness and deuterium excess, in a conspicuous minimum in atmospheric methane (a ‘global event’), and in a subsequent increase in atmospheric CO_2 , and the duration is estimated to be 160 ± 10 years. It is generally considered that the event reflects curtailment of North Atlantic Deep Water (NADW) formation and its associated northward heat transport, due to catastrophic meltwater release from glacial lakes Agassiz and Ojibway into the North Atlantic during the later stages of the wastage of the Laurentide ice sheet (Kleiven *et al.*, 2008). It is possible that the earlier Holocene oscillations resulted from a similar process, as climate modelling experiments have shown that freshwater fluxes into the North Atlantic can also trigger centennial-scale cooling events with temperature anomalies resembling proxy evidence for the cooling event at 8.2 ka (Renssen *et al.*, 2007b). The 8.2 ka event has been detected in a range of proxy records (Figure 7.39), particularly from round the North Atlantic region, but also in Africa, Eastern Asia, South America and perhaps New Zealand (Walker *et al.*, 2012). In the South Atlantic, there are indications that the event may be associated with an increase in sea-surface temperatures, and coupled climate model simulations appear to show a warm response at around 8.2 ka in the Southern Oceans (Wiersma *et al.*, 2011), again perhaps reflecting the continued operation of the bipolar seesaw referred to above. Overall, therefore, although the trigger mechanism for the 8.2 ka event lies in the North Atlantic, it is unusual in late Quaternary records in being a climatic event that is near global in nature (Rohling & Pälike, 2005).

7.6.3.3 The 4.2 ka event

Throughout the middle and low-latitude regions of the world, there is widespread evidence for a pronounced, but relatively short-lived (200–300 years), aridification event which occurred around 4.2 ka. This is again reflected in a range of proxy climate records (Figure 7.40), including fluvial archives, lake sediment sequences and cave stalagmite profiles from North America, through the Middle East to China; and from Africa, parts of South America to Antarctica where there is also evidence from ice-core records of drier conditions (Mayewski *et al.*, 2004).

In higher latitudes, by contrast, there are indications of colder conditions that appear to be coeval with the lower-latitude aridification event. In the Southern Hemisphere, these include deuterium-derived temperature reconstructions from Antarctica (Masson-Delmotte *et al.*, 2004) and ocean-core records off South Australia (Moros *et al.*, 2009), while in the mid- and high latitudes of the Northern Hemisphere, a climatic shift to cooler and wetter conditions is reflected, for example, in European peat sequences (Barber *et al.*, 2003), in glacier readvances in northwest Canada (Menounos *et al.*, 2008) and in ice-core records from the Yukon (Fisher *et al.*, 2008).

The forcing mechanisms behind the global reorganization of climate that is marked by the 4.2 ka event are less obvious than is the case with the climatic shift at 8.2 ka. There is, for example, no evidence for massive meltwater releases into mid- and high-latitude oceans; nor is there evidence for major increases in atmospheric trace gases or volcanic aerosols which might have served to trigger the event. Similarly, there is nothing in the Holocene solar irradiance record to suggest that solar activity might have played a part (Figure 7.41). Mayewski *et al.* (2004) have suggested that the southward migration of the Inter-Tropical Convergence Zone (ITCZ) might account for enhanced low-latitude aridity, and would be consistent with the increase in strength of the westerlies over the North Atlantic, and increased precipitation and the consequent glacier advances in western North America. The onset of aridification also coincides with a 1–2°C cooling of North Atlantic surface waters (Bond *et al.*, 1997), while in the Pacific, tropical deep waters may also have cooled sufficiently to allow the switch-on of the modern El Niño Southern Oscillation (ENSO) regime. The climatic significance of ENSO and associated La Niña climatic regimes is discussed further in section 7.6.4.2.

The global impacts of the 8.2 and 4.2 ka events and their registration in a range of stratigraphic and proxy climate records has led to the suggestion that these might constitute time-stratigraphic marker horizons for a subdivision of the Holocene (Walker *et al.*, 2012). Hitherto, there has been no formal subdivision of the Holocene epoch (the only epoch in the geological record so far not to be so divided), and it has been proposed that the Holocene be formally subdivided into three sub-epochs: the Early Holocene (11.7–8.2 ka); the Middle Holocene (8.2–4.2 ka); and the Late Holocene (4.2 ka to the present). This is currently (2014) under consideration by the Subcommission on Quaternary Stratigraphy and the International Commission on Stratigraphy (section 1.3) and, if approved, will be forwarded to the International Commission on Stratigraphy for formal ratification.

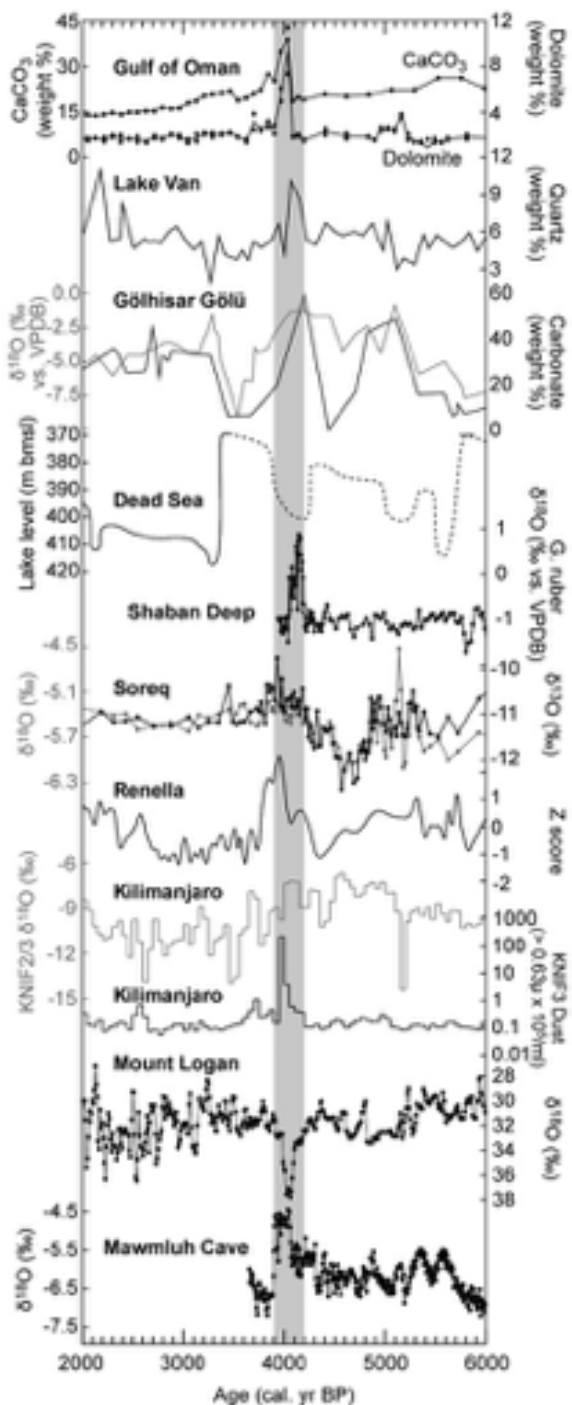


Figure 7.40 Proxy records for the 4.2 ka event. The vertical grey bar marks the likely onset and termination of the event (after Walker *et al.*, 2012. Copyright © 2012 John Wiley and Sons, Ltd).

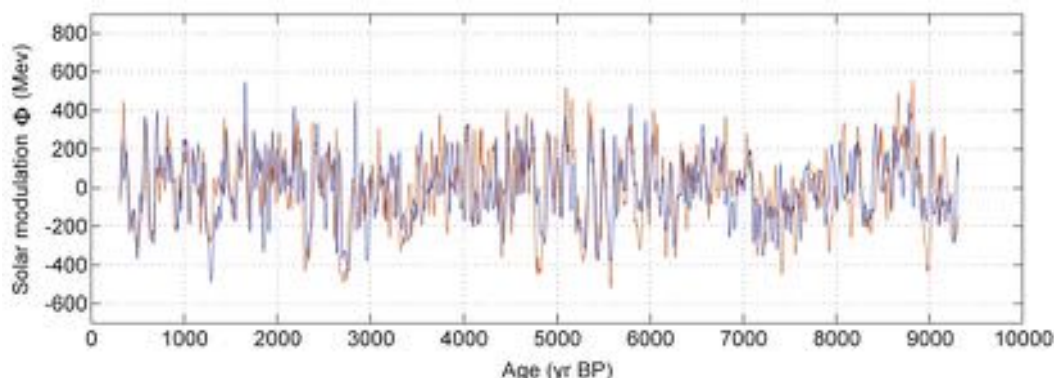


Figure 7.41 Solar activity throughout the Holocene. The solar modulation parameter (Φ) is based on ^{14}C data from IntCal04 (orange curve) and ^{10}Be from the GRIP ice cores (blue) (after Knudsen *et al.*, 2009). Note the significant decline in solar irradiance at around 2.8 ka; note also that there is no similar decline at c. 4.2 ka suggesting that solar forcing was unlikely to be implicated in this event.

7.6.3.4 The 2.8 ka event

An abrupt climatic deterioration marked by the onset of cooler and wetter conditions and beginning at around 2.8 ka cal. BP has been widely recorded in both proxy climate and archaeological records from Europe (e.g. van Geel *et al.*, 1996; Speranza *et al.*, 2002). For example, wet-shifts at about that time have been found in peatland sites in Britain (Charman *et al.*, 2006) and Ireland (Swindles *et al.*, 2007), while a similar change to wetter conditions has also been reported from Germany (Barber *et al.*, 2004) and Siberia (van Geel *et al.*, 2004), and in the Southern Hemisphere from the Andean region of South America (Chambers *et al.*, 2007). In addition, cooler ocean surface waters and an increase in ice-rafting at around 2.8–2.7 ka is evident in marine cores from the North Atlantic (Bond *et al.*, 1997). Over the broader time interval of 3.5–2.5 ka, there is evidence for a weakening of westerly winds over North America, cooling over the northeast Mediterranean related to winter-time continental/polar air outbreaks, advances of alpine glaciers and a decline in the treeline limit in Scandinavia (Mayewski *et al.*, 2004).

The principal factor driving this climatic change is widely considered to be a reduction in solar activity (Bond *et al.*, 2001b). Long-term variations in solar activity can be determined from the record of cosmogenic radionuclides (^{14}C and ^{10}Be) preserved in tree rings and ice cores (Knudsen *et al.*, 2009; Steinhilber *et al.*, 2012). We have already seen (sections 5.3 and 5.6) that both of these radionuclides are produced in the atmosphere from incoming cosmic rays, but the cosmic ray flux reaching the earth is modulated by both the solar magnetic field and the

earth's geomagnetic field. At times of increased solar activity when the solar magnetic field is strengthened, fewer cosmic rays reach the earth's atmosphere, and thus the production of radionuclides such as ^{14}C and ^{10}Be is reduced; the reverse obtains at times of lower solar intensity. Holocene records show a significant increase in radionuclide concentrations at c. 2.8 ka, and hence a decline in solar intensity (Figure 7.41). This, coupled with the fact that evidence for the 2.8 ka event is found in both hemispheres and is broadly synchronous, provides strong supporting evidence for the hypothesis that a worldwide climatic shift at 2.8 ka is driven principally by solar forcing.

7.6.3.5 The Little Ice Age

Of all the climatic events in the Holocene, none has attracted more attention than the Little Ice Age (LIA), the short-lived cold interval from approximately the sixteenth to the nineteenth centuries. One of the reasons for this is that although the Little Ice Age was not a true 'ice age' in the conventional sense, it was nevertheless a colder episode that, particularly in northern Europe, had considerable effects on late- and post-Medieval societies. In alpine areas, glaciers readvanced, in some cases destroying farms; crop failure and resultant famine were widespread, while expanded sea ice disrupted coastal communications and fisheries (Grove, 1988; Fagan, 2000). When viewed at the global scale, however, the Little Ice Age appears to have been a relatively modest cooling of the Northern Hemisphere with an overall temperature decline of less than 1°C relative to late twentieth-century levels. On the other hand, these generalized values conceal considerable regional and temporal differences (Crowley & Lowery, 2000).

For example, in Europe, the coldest periods appear to have occurred in the eighteenth century, with temperatures in some regions 2°C below twentieth-century levels, while in North America, the coldest decades were experienced during the nineteenth century and were close to 1.5°C colder (Mann *et al.*, 1998).

Whether the Little Ice Age was largely a Northern Hemisphere, and indeed a North Atlantic phenomenon, has been much debated (and indeed the global relevance of the term ‘Little Ice Age’ itself has been questioned: Jones & Mann, 2004), principally because of the spatial bias towards Northern Hemisphere proxy and meteorological records (Jones *et al.*, 2009). However, there is now an emerging body of evidence from the Southern Hemisphere to suggest a climate cooling broadly coterminous with the LIA in the Northern Hemisphere. There are, for example, indications of glacier advances in New Zealand during the eighteenth century (Winkler, 2000); stalagmite data from South Africa point to a cold period between AD 1500 and 1800 (Holmgren *et al.*, 2001); borehole records from Australia suggest that the seventeenth century was the coldest in Australia over the last 500 years (Pollack *et al.*, 2006); while stable isotope data from a coastal ice core from Antarctica indicate that the area experienced 1.6–1.4°C cooler average temperatures prior to AD 1850 compared with the last 150 years (Rhodes *et al.*, 2012). Nonetheless, the question still remains as to whether these events are indeed synchronous with periods of anomalous cold further north and whether they reflect a globally significant climate signal.

The LIA occurred against a backdrop of long-term Northern Hemisphere temperature decline driven by orbital forcing. In the Arctic, for example, it has been estimated that the rate of cooling has been of the order of 0.02°C per century (Kaufman *et al.*, 2009). But this alone would be insufficient to generate the levels of cooling evident in Europe and North America during the LIA. A possible causal factor might have been a reduction in North Atlantic Deep Water Formation and the disruption of thermohaline circulation, although so far the oceanographic evidence in support of this hypothesis is equivocal (Broecker, 2000). More likely explanations appear to lie in climatic forcing from solar or volcanic activity (Grove, 1988). It has long been known that two significant episodes of reduced sunspot activity (reflecting a reduction in solar output) occurred during the LIA: the Maunder Minimum between 1645 and 1715, and the Dalton Minimum from 1790–1830, and these are well represented in the radionuclide records of ^{14}C and ^{10}Be from tree rings and ice cores (Steinhilber *et al.*, 2012). The reduction in solar irradiance during the LIA is apparent in Figure 7.41.

The second hypothesis, involving volcanic forcing has also been long espoused. During an eruption, large quantities of ash and sulphur are ejected into the atmosphere, the former blocking the sun’s rays beneath the spreading ash cloud, while the latter interacts with atmospheric constituents to create sulphuric acid particles that are disseminated globally and which also screen out incoming solar radiation (Oppenheimer, 2011). Recent work in Arctic Canada and Iceland, using a combination of empirical evidence and climate simulation modelling, has shown that the onset of the LIA can be linked to an unusual 50-year-long episode with four large sulphur-rich explosive eruptions around the end of the thirteenth century, the subsequent cold being maintained by sea ice–ocean feedbacks long after the volcanic aerosols were removed (Miller *et al.*, 2012). Under this scenario, the climatic patterns of the LIA can be explained without recourse to changes in solar irradiance.

7.6.4 Holocene climatic cycles

A distinctive feature of many Holocene records from both marine and terrestrial realms is the apparently rhythmical or cyclic nature of climatic fluctuations over the course of the past 11.7 ka or so. Unlike the longer-term climatic cycles that characterize the Pleistocene record, however, these are not driven by orbital influences; rather, they appear to reflect external forcing principally through variations in solar irradiance, or to be the consequence of internal reorganization and feedback within the ocean–atmosphere system. Some of these cyclical climate changes are discussed in this section.

7.6.4.1 Late Holocene solar cycles

We have already seen that a proxy record of past solar variability can be obtained from cosmogenic nuclides in tree rings and ice cores (Figure 7.41), and indeed that some events in the Late Holocene palaeoclimate record, such as the 2.8 ka event and the Little Ice Age, have been linked to changes in solar irradiance. It is also apparent from these proxy records, and also from observational and instrumental measurements, that there is a cyclical pattern in solar variability. These periodicities include the 11-year Schwabe sunspot cycle, the 22-year Hale cycle, the 88-year Geisberg cycle, the ~200-year Suess cycle, and the ~1,000-year and ~2,200-year (Hallstattzeit) cycles (Chambers & Blackford, 2001).

Until relatively recently, an influence of solar variability on climate, whether through cycles or trends, was usually dismissed because climate simulations with simple energy

balance models indicated that the responses to the decadal solar cycles would be too small to be detected in observations and hence in proxy records. However, more recent modelling studies have found indications of positive feedbacks in the ocean–atmosphere system that may amplify the response to solar irradiance variations, and now solar cycles and trends are widely recognized as important components of natural climatic variability on decadal to centennial timescales (Lean, 2009). For example, although the variation in solar irradiance that is associated with a Schwabe cycle is only of the order of $\sim 1 \text{ W m}^{-2}$ between solar maximum and minimum, winter and spring temperatures in the Northern Hemisphere nevertheless show a response even to this small-scale variability (Engels & van Geel, 2012).

Over the course of the Holocene, perhaps the most pervasive cycles have been those at $\sim 1,000$ and maybe also $\sim 2,000$ years. Of these, the $\sim 1,000$ -year cycle has been the most widely detected, registering in such diverse archives as lake sediments in Alaska (Hu *et al.*, 2003), varved sediments in the Santa Barbara Basin off California (Nederbragt & Thurow, 2005), foraminiferal records and sea-surface reconstructions off the east coast of North America (Cléroux *et al.*, 2012) and loess–palaeosol sequences in southern Siberia (Kravchinsky *et al.*, 2013). The extent to which these solar cycles have influenced Holocene climatic variability remains uncertain, but they may have served to amplify or modulate climate changes arising from other forcing mechanisms such as variations in deep-water flow, sea-surface temperature changes, sea ice formation and the effects of the ENSO regime (see below).

7.6.4.2 El Niño–Southern Oscillation (ENSO)

The term ‘El Niño’ was first used by Peruvian fishermen to refer to the annual warming of coastal waters that often occurs around Christmas time, but scientists now reserve the term for an anomalous periodic warming, reflected in an increase in sea-surface temperatures (SSTs) of the eastern equatorial Pacific. The ‘**Southern Oscillation**’ is a seesawing of atmospheric mass, and hence of sea-level pressure (SLP) between the eastern and western Pacific. Records over the past 100 years or so show a striking similarity between the SST and SLP indices, one oceanic and the other atmospheric, despite the fact that they are widely separated in space: El Niño accompanies high surface pressure in the western Pacific, while the cold phase (known as **La Niña**) coincides with low surface pressure in the western Pacific. Oscillations occur approximately every 4 years (2–7 years normally defines the ENSO band); some

periods, such as the late nineteenth and early twentieth centuries, are marked by high-amplitude oscillations, but others (such as the 1930s) are more quiet (Cane, 2004).

The causes of the oscillation are not fully understood, but appear to be associated with a reduction in upwelling of colder waters off the South American coast as a result of the weakening of the trade winds (part of the atmospheric Walker circulation). There is a surface-water heat transfer from the western to the eastern Pacific. As the Pacific Ocean is a major heat reservoir that drives global wind patterns, the changes in temperature that result from this redistribution of surface water exert an influence on weather patterns at the global scale. For example, rainfall shifts from the western Pacific towards the Americas, while Australia, Indonesia and India experience droughts.

The ENSO cycle is apparent in proxy climate records (such as tropical corals) extending back to the last interglacial (Tudhope *et al.*, 2001). During the present interglacial, it appears that the ENSO cycle was markedly weaker during the early and middle Holocene, but proxy records indicate that a major climatic transition in the Pacific region, characterized by an increasing ENSO influence, is evident from *c.* 5–3 ka onwards (e.g. Gomez *et al.*, 2004). An enhanced ENSO regime between 4 and 2 ka is also evident along the Pacific coastline of North America (Barron & Anderson, 2010). This increase in ENSO variability during the later Holocene may be an oceanic response to changing insolation (Loubere *et al.*, 2013). Over the past 1.0 ka, data from corals show both decadal and longer variations in the strength of the ENSO cycle, possibly due to a combination of volcanic and solar forcing, and amplified by internal feedbacks within the ocean–atmosphere system (Cane, 2004). Atmospheric general circulation modelling suggests that with rising temperatures from global warming (section 7.6.5.1), ENSO-induced drought and floods are likely to be more intense in future El Niño years (Power *et al.*, 2013).

7.6.4.3 Late Holocene Atlantic and Pacific Oscillations

The North Atlantic Oscillation (NAO)

This is one of the principal modes of climatic variability in the North Atlantic region, and affects surface air temperatures, winds, storminess and precipitation (Hurrell & Deser, 2009). It is driven by variations in atmospheric pressure at sea level between the Icelandic low and the Azores anticyclone. During a positive NAO phase, strengthening of the high-pressure cell over the subtropical Atlantic and a weakening of the Icelandic low accentuates the pressure gradient between the two cells, and this results

in warmer and wetter conditions over northwest Europe and the eastern USA, whereas Greenland, northern Canada and the Mediterranean tend to be cooler and drier. In negative NAO phases, when the gradient between the Azores high and the Icelandic low is reduced, this situation is reversed. The oscillation is driven entirely by changes within the atmosphere and there is no discernible periodicity; indeed, it displays considerable inter-decadal and inter-annual variability (Thompson *et al.*, 2003). The NAO has been detected in both instrumental and proxy records. For example, the exceptionally cold winter of 2009–10 in Britain and western Europe coincided with an extremely negative phase of the NAO, while the observed shifts during the 1990s towards a pattern of anomalously wet summers in northern Europe and concomitant hot and dry summers in southern Europe have been related to warming of the North Atlantic following a positive phase of the NAO (Robson *et al.*, 2012). In southern Norway, rapid glacier advances during the early eighteenth century have been attributed to increased precipitation in milder and wetter winters during a positive NAO mode (Nesje & Dahl, 2003). On the east coast of the USA, marine Foraminifera interbedded in littoral marsh sediments reflect coastal inundation resulting from hurricanes, and have been linked to changes in the position of the Bermuda (or Azores) high-pressure cell, which influences the direction of storm paths for North Atlantic hurricanes (Scott *et al.*, 2003).

The Atlantic Multidecadal Oscillation (AMO)

This was first identified in 1994 and is marked by variations in North Atlantic sea-surface temperature. These have been linked to small changes in the North Atlantic branch of the thermohaline circulation. The AMO appears to have a quasi-cycle of around 50–90 years, with past recorded peaks around AD 1880 and 1950, and the next likely peak between 2000 and 2040 (Enfield & Cid-Serrano, 2010). The AMO has been linked to variations in air temperature and rainfall throughout the Atlantic region. Warmer waters in the North Atlantic have been associated, for example, with increased rainfall in southern Florida, the African Sahel and India, and with increased Atlantic hurricane activity (Zhang & Delworth, 2006). The AMO has also been linked with drought conditions in the American Midwest and over large areas of West Africa (Shanahan *et al.*, 2009).

The Pacific Decadal Oscillation (PDO)

Periodic spatial changes in sea-surface temperatures have been detected in the Pacific Ocean north of 20°C; a cooling in the west Pacific is accompanied by a warming in the east ('warm' or 'positive' phase), while during a 'cool' or

'negative' phase, the opposite pattern occurs. This Pacific Decadal Oscillation operates over a timescale of 20–30 years, and has been linked to ENSO, marked sea-surface temperature changes in subsequent winters and atmospheric forcing (Newman *et al.*, 2003). During positive phases, warmer conditions are experienced in the Pacific Northwest and Alaska, whereas lower temperatures are recorded in Mexico and the southeastern USA (Mantua & Hare, 2002). Droughts over the northern and southwestern USA have been associated with a positive AMO, especially when linked to a negative PDO (McCabe *et al.*, 2004). In India, increased summer rainfall and decreased temperatures have been associated with the negative phase of the PDO (Krishnan & Sugi, 2003). Tree-ring records from western North America provide a history of the PDO, for example a combined tree-ring record from California and Alberta reveals PDO changes over the course of the last millennium (MacDonald & Case, 2005).

7.6.5 People and climate

Thus far in this chapter, we have considered climate change on a range of temporal and spatial scales, and have examined the various forcing factors and feedback mechanisms that have fashioned global climate over the course of the middle and later part of the Quaternary. To date, however, we have said relatively little about people, and have focused our attention largely on the impacts of climate change on the natural environment. We have tended also to consider the larger-scale changes in climate as reflected, for example, in the high-amplitude temperature fluctuations that occurred during the DO cycles. But it is evident that these temperature (and precipitation) changes must, equally, have impacted on plants and animals and, especially, on humans, where even comparatively small variations in climatic regime may have had a profound impact on human societies. This is particularly so as globally averaged temperatures (with which we have largely been dealing) tend to mask the spatial variations of climate shifts, so that some regions would have experienced more pronounced climatic effects than others. The extent to which climate, and especially the DO cycles and Heinrich events, impacted on the lives of Neanderthals and early modern humans in the Old World during the last cold stage has been much debated (e.g. Gilligan, 2007; Jiménez-Espejo *et al.*, 2007) as, of course, have the climatic and other factors (such as ice-sheet extent) that determined the timing of the arrivals of humans in the Americas (e.g. Davidson, 2013; Rabassa & Ponce, 2013).

The most recent of these pronounced climatic shifts, the transition from the last cold stage to the Holocene,

coincides with the beginnings of agriculture, one of the most important innovations in human history, and the transition from the hunter-gatherer economies of the last cold stage to the sedentary cultivation-based societies of the Holocene. And with that cultural change began the first significant impacts of humans on the natural environment, with widespread forest clearance, the development of urban societies and industrialization. One consequence of this, of course, was to reverse the former scenario in which climate was a limiting (in some cases, perhaps, even a forcing) factor in human activity and behaviour, to one where humans themselves are exerting an increasing influence on the global climatic environment, and it is this human dimension in recent climate and environmental change that we address in the final sections of this chapter.

7.6.5.1 The greenhouse effect

During the later years of the nineteenth century, pioneering experimental work by John Tyndall had shown that gases, such as carbon dioxide, can effectively absorb infrared radiation. Later, the Swedish scientist, Svante Arrhenius, used these results to estimate the sensitivity of global temperatures to increases in carbon dioxide. This was the first articulation of what we now refer to as the 'greenhouse effect', although in the early 1900s, the theory that an increase in atmospheric carbon dioxide could change climate was not widely accepted. In a seminal paper published in 1938, however, an amateur scientist, Guy

Callendar, showed that the planet had warmed by about 0.3°C over the previous 50 years and suggested that carbon dioxide (CO_2) could be partly to blame (Hawkins & Jones, 2013). Remarkably, Callendar's global land temperature estimates agree well with more recent analyses (Figure 7.42) which show a sustained rise in the earth's temperature over the course of the last 100 years or so. Although some still remain sceptical about the nature and extent of the greenhouse effect (for both scientific and political reasons!), a combination of empirical data from instrumental and proxy sources, coupled with the results of increasingly sophisticated climate modelling, have provided a powerful confirmation of the hypothesis that the recent rise in global temperatures can be attributed, in very large measure, to the effects of human activity. Indeed, the most recent report by the Intergovernmental Panel on Climate Change (IPCC) published in September 2013 states that scientists are now 95 per cent certain that humans are the dominant cause of global warming since the 1950s.

The principal contributors to atmospheric greenhouse warming are the trace gases CO_2 (carbon dioxide), CH_4 (methane) and N_2O (nitrous oxide), along with CFCs (chlorofluorocarbons). The most valuable archives of changes in these greenhouse gases are the polar ice sheets from which records of both long-term (section 3.11) and more recent (post-industrial) atmospheric concentrations have been obtained (Figure 7.43). These show that for CO_2 , the mean concentration of late Holocene pre-industrial levels was around 280 ppmv (parts per million

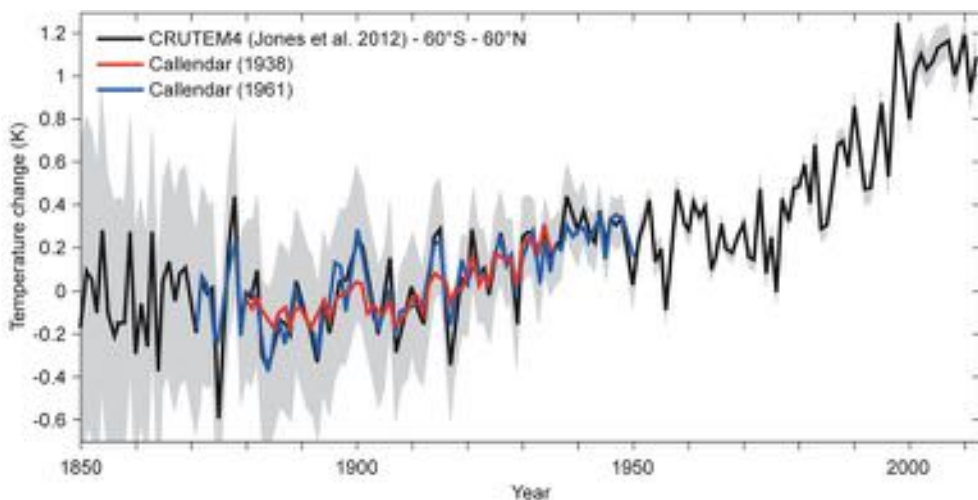


Figure 7.42 Comparing historical reconstructions of near-global land temperatures ('CRUTEM4': Jones *et al.*, 2012) with Callendar (1938) and Callendar (1961), using a reference period of 1880–1935. The CRUTEM4 estimates are for 60°S–60°N (to accord with Callendar's series), with grey shading representing the 95 per cent uncertainty.

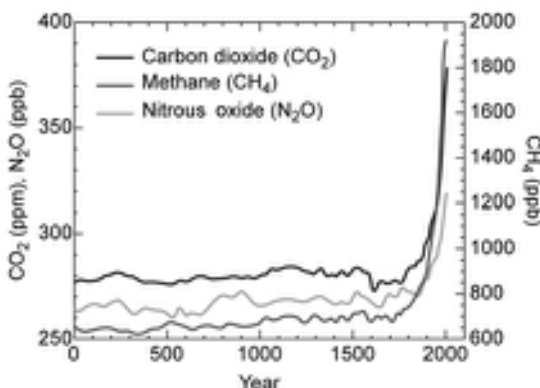


Figure 7.43 Atmospheric concentrations of greenhouse gases over the past 2 ka. The increase since c. AD 1750 is largely attributable to human activities in the industrial era (from Intergovernmental Panel on Climate Change, 2007).

by volume). Following the Industrial Revolution in Europe and North America in the eighteenth century, the records show a progressive rise to values of around 315–320 ppmv by the 1950s, and to around 380 ppmv by the year 2000. In May 2013, continuous monitoring of atmospheric CO₂ at the Maua Loa research facility in Hawaii revealed that the gas had reached an average daily level of 400 ppmv, higher than at any time in the past 3 Ma. Since c. AD 1750, atmospheric concentrations of CH₄ have risen from a pre-industrial level of around 700 ppbv (parts per billion by volume) to a value in excess of 1,950 ppbv by 2000, and N₂O has increased from around 275 ppbv to more than 310 ppbv. The consequences of these increases on global temperatures have been dramatic. For example, in the NOAA National Climatic Data Center annual list (<http://www.ncdc.noaa.gov>), each of the twelve years from 2001–12 features as one of the warmest in a record that began in 1880. There were only two years in the pre-AD 2000 list where broadly comparable global temperatures were achieved. Indeed, we have to go back to 1911 to find the coolest year in the NOAA record. These data are compelling, and it seems very difficult to deny the likelihood that human influence on the global climatic environment is now all-pervasive.

7.6.5.2 Early human impact?

Much of the literature on global warming focuses on the post-industrial period, with the ‘tipping point’ in the anthropogenic impact scenario occurring around AD 1750, when the byproducts of the industrial revolution began to

add measurably to the natural greenhouse gas levels already in the atmosphere. But this interpretation of the atmospheric trace-gas record was challenged by Bill Ruddiman, who argued that anthropogenic influences on Holocene climate predated by several millennia the eighteenth-century increase in greenhouse gases (Ruddiman, 2005a, 2005b). He first proposed that the natural decrease in atmospheric CH₄ that accompanied the decline in orbitally driven solar insolation since the early Holocene was reversed around 5 ka, principally as a consequence of the spread of rice farming throughout southeast Asia (Ruddiman & Thomson, 2001). The irrigated rice paddies with their rich biomass would have been a natural source of methane, and the release of these gases to the atmosphere was, Ruddiman suggested, largely responsible for the progressive upward trend in methane concentration that is evident in the ice-core records from the mid-Holocene onward (Figure 7.44a). He further proposed that humans also reversed the natural decrease in atmospheric CO₂ values around 8 ka by beginning the process of forest clearance (Ruddiman, 2003b), again the resultant release

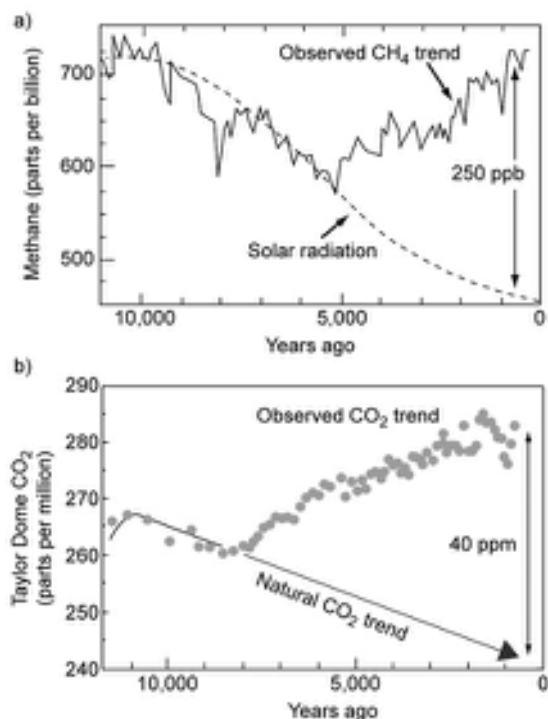


Figure 7.44 Concentration of CH₄ a) and CO₂ b) over the last 11 ka, showing departures (increases) from the natural trace-gas trends (after Ruddiman, 2005a).

of CO₂ to the atmosphere being marked in the CO₂ record in polar ice-core records (Figure 7.44b). If these arguments are correct, then human influence on the atmosphere, in terms of increased trace-gas concentration, does indeed long precede the industrial era (Ruddiman, 2013).

7.6.5.3 Delayed glaciation?

A second element in the Ruddiman scenario concerns the extent to which trace-gas emission as a consequence of human activity during the course of the Holocene could have caused an anthropogenic warming sufficient to counter the orbitally driven natural cooling trend, and to prevent the onset of the next glaciation. For the pre-industrial period, Ruddiman estimated that global climate would have warmed by around 0.8°C. This is around 15 per cent of the global cooling at the Last Glacial Maximum, and when amplified polewards, this would have led to a temperature decrease of ~2°C which, modelling results suggest, would be more than sufficient to generate permanent snow and ice cover over parts of northeastern Canada (Ruddiman *et al.*, 2005); in other words, to initiate the next glaciation. Ruddiman also noted that in all of the last interglacial stages (MIS 1, 5, 7, 9 and 11), summer insolation reached late deglacial/early glacial peaks and then fell for the next 11.0 ka or so. Through each of those intervals, CO₂ and CH₄ concentrations also declined in every case but one: the Holocene, where the trend is reversed (Figure 7.13). Indeed, modelling evidence and analogies with earlier interglacials suggest that had CO₂ levels been lower (below 240 ppmv, the baseline in Figure 7.44b), the end of the current interglacial would occur within the next 1,500 years (Tzedakis *et al.*, 2012). The implication, therefore, is that human-induced increases in atmospheric trace gases have delayed the onset of the next glaciation.

Both of these ideas, namely that early and mid-Holocene increases in atmospheric trace gases have resulted from prehistoric human activity, and that these have been sufficient to prevent the onset of glaciation, have proved controversial, some critics questioning whether there were sufficient people in prehistory capable of clearing and burning sufficient forest in order to create the observed CO₂ anomaly in the ice-core records, while others have argued that the later Holocene increase in CO₂ could be accounted for by delayed ocean carbonate compensation and atmospheric CO₂ release, in part associated with coral reef formation (Joos *et al.*, 2004; Elsig *et al.*, 2009). However, preliminary reconstructions of possible rates of early and mid-Holocene forest clearance, based partly on analogies with contemporary cultures that still employ shifting

cultivation methods, yield CO₂ emission estimates that are in line with pre-industrial trajectories (Ruddiman & Ellis, 2009), while natural explanations for the CO₂ increase still confront the problem that, when compared with the previous four interglacial episodes, the late Holocene CO₂ increase is anomalous (Ruddiman *et al.*, 2011).

7.6.6 The Anthropocene

The term ‘Anthropocene’ (meaning *anthrōpos* ‘human being’ and *kainos* ‘new’) has become increasingly widely used since it was proposed by Crutzen & Stoermer (2000) to denote the present time interval during which the earth’s climate and many geologically significant processes (ranging from erosion and sediment transport to sea-level rise) have been, and continue to be, affected and altered by human activities. These anthropogenic effects, which have become especially marked since the Industrial Revolution in northern Europe, have resulted in marked changes not only to global climate (see above), but also to the earth’s surface, and almost every aspect of the contemporary global environment is now modified, or at least influenced, by human activity (Steffen *et al.*, 2011).

Although the term ‘Anthropocene’ was initially invoked in an *informal* sense to describe this period of expanding human influence on the global environment (Crutzen, 2002), there is a body of opinion within the geological community that this accelerated human impact may be reflected in recent stratigraphic sequences, where it can be distinguished from natural ‘background’ conditions (Zalasiewicz *et al.*, 2008). As a consequence, the term is increasingly being applied to the geological record, where it is viewed by some as being equivalent to those used as series-status divisions of the Cenozoic Erathem, notably ‘Pleistocene’ and ‘Holocene’. Indeed, a Working Group of the Subcommission on Quaternary Stratigraphy is currently looking into the matter to determine whether the stratigraphic signature of the Anthropocene is now sufficiently clearly defined to warrant its formal definition as a new period of geological time that is additional to, and separate from, the Holocene (Zalasiewicz *et al.*, 2011). The Group aims to conclude its deliberations by 2016.

There are, however, a number of problems relating to formal definition of the Anthropocene in this way. Where to place the onset of the Anthropocene, for example, has proved to be a contentious issue. Many have advocated the increase in trace-gas concentrations at around AD 1750 in the ice-core records as providing the key marker horizon for the first significant impact of humans on the climatic environment (Gibbard & Walker, 2013). But it is now clear that human influence on global climate may

considerably predate this event (see above). Alternative suggestions include the ‘Great Acceleration’ of the second half of the twentieth century when many human activities reached their take-off points in terms of their environmental impacts (Steffen *et al.*, 2011), and the short-lived atmospheric radiogenic nuclide peak around AD 1963 resulting from nuclear bomb testing of the mid-twentieth century (Zalasiewicz *et al.*, 2011). Again, however, these simply mark one of the many stages in human technological development; they do not coincide with the onset of environmental changes resulting from human activity and hence, it has been suggested, have little value in defining the initiation of human impact (Gale & Hoare, 2012). A further difficulty is that the impact of human activity is time-transgressive, the effects of industrialization, for example, occurring at different times in different parts of the world. Hence it is difficult to isolate a single boundary within the geological record that marks the global ‘tipping point’ where natural processes have been overtaken by human-induced environmental changes (Gibbard & Walker, 2013; Ruddiman, 2013).

There is no doubt that the term ‘Anthropocene’ has caught the imagination, and it is being widely used in both the popular and scientific literature. The problem, however, is over the status of the term in the geological record, and whether a formal designation of the Anthropocene as a time-stratigraphic unit that is equivalent to a series or epoch division within the geological timescale would prove to be acceptable to the wider geological community. If not, then the term might simply become another name for the Late Holocene, with a usage similar, perhaps, to ‘Dark Ages’ or ‘Middle Ages’. In a geological sense, therefore, its status would remain unchanged, and it would continue to be employed *informally* to denote the recent period of accelerated human influence on the global environment.

7.7 CONCLUDING REMARKS

In this chapter we have reviewed the evidence for the pattern and tempo of climate change during the Quaternary, and considered some of the more important factors that appear to have influenced global climates over this time period. In this final section of the book, we highlight some of the key themes that have emerged from recent investigations into Quaternary environmental change, and briefly consider their relevance to current concerns over potential future climate and environmental change.

Perhaps the most striking discovery to emerge from recent palaeoclimatic research is the apparent rapidity with which the global climate system is able to shift from one dominant mode to another. It is now widely accepted that

the earth can switch from a ‘glacial’ to an ‘interglacial’ state within a matter of hundreds, as opposed to thousands, of years, a timescale that was considered almost inconceivable prior to the recent findings in the polar ice cores. Indeed, there is clear evidence that wholesale atmospheric reorganizations, involving temperature changes of more than 10°C, can occur within centuries (in some cases decades) during ‘glacial’ stages, and perhaps did so on more than twenty-five separate occasions during the last glacial stage.

Until recently, major climate shifts appeared to be more or less synchronous events in proxy records from ocean basin, polar ice and terrestrial contexts, but improvements in dating precision, coupled with the analysis of more highly resolved stratigraphical archives, are increasingly revealing that this is not the case, but there are clear leads and lags in the climate system. This work has also highlighted the importance of coupled variables, such as atmospheric gas and dust content, sea ice and ice-sheet extent, sea-level change, and ocean circulation, and their respective roles in influencing global climate. Although the inter-relationships are complex, simulation modelling is beginning to tease out key cause-and-effect linkages that drive the global climate system. Moreover, while it still remains the case that Milankovitch-induced variations in insolation are the principal forcing factors underlying glacial–interglacial cycles, it is equally clear that internal feedback mechanisms modulate the astronomical cycles, and may promote irregular, non-symmetric climatic behaviour. The bipolar seesaw is but one example of a number of important mechanisms that we need to understand if we are to explain (often abrupt) climate change at the global scale. A future research agenda will need to examine the ways in which other components of global climate, such as the ITCZ, monsoon cells and ENSO, interconnect with the bipolar rhythm of climate change.

We know that the global climate system is in a constant state of flux, with a variability that is hard to predict (Figure 7.45), and this is one of the reasons why models that attempt to postdict or predict the climate system have large uncertainties. The new polar ice-core records have revealed that while long-term cycles are clearly evident, no two glacials or interglacials, or even DO events for that matter, were exactly the same, in terms of either duration or climate signal. Indeed, there is no precise analogue for the current interglacial or for any of its substages. This is partly because each climatic stage contains the imprint of a series of superimposed climatic rhythms (Figure 7.45). The phasing between these climate frequencies and their integrated product is constantly changing. In addition, each individual climatic event starts from a different combination of initial boundary conditions, for the earth’s

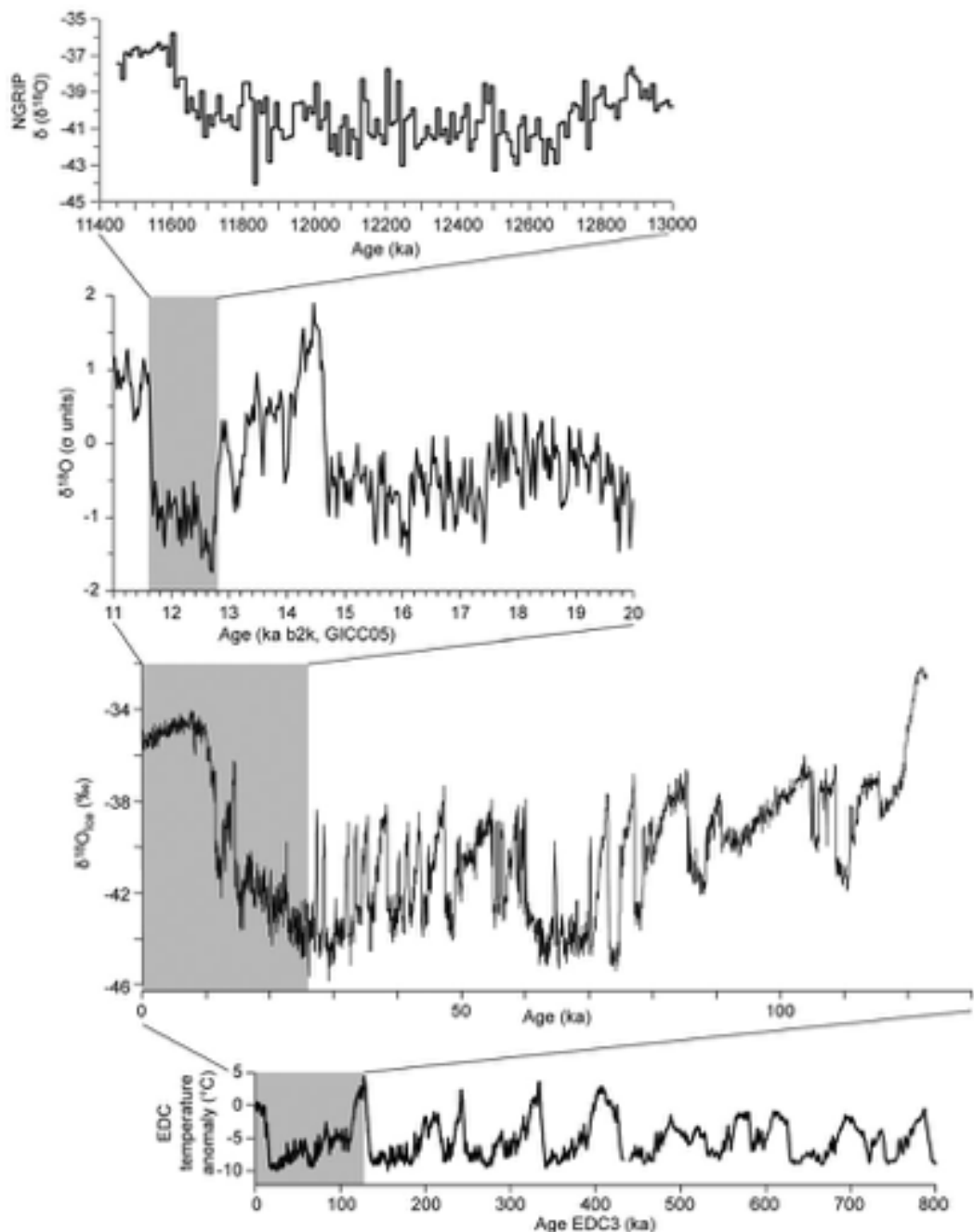


Figure 7.45 Schematic diagram showing superimposition of global climatic variations at different frequencies, from glacial-interglacial (bottom) to centennial scale (top).

surface is also in a constant state of flux. Modelling these changes, and deriving predictions from them, represents one of the biggest challenges facing the science community, and it is one that will require improved stratigraphical records, more precise geochronological methods, more robust and reliable proxy data, integrated global databases, and collaborations with the numerical modelling community. As we hope this book has shown, these tools and their associated approaches have been dramatically refined since 1990, and the foundations have been laid for the multidisciplinary cooperation that is increasingly needed if we are to understand fully the workings, both spatially and historically, of the global climate–environmental system.

A final point concerns the possible link between climate change and humans, which we considered in section 7.6. The Quaternary record shows that we live in unusual times, with global atmospheric levels of CO_2 and CH_4 higher than at any time during the last 800 ka. While some concerns that have been raised about this matter could well prove to be exaggerated, they most certainly cannot be ignored, as they might prove prescient! For example, one prediction suggests that the earth's surface will be heated beyond what humans can tolerate by AD 2300 (Sherwood & Huber, 2010). Other assessments suggest that atmospheric greenhouse gas concentrations are approaching levels last seen during the Pliocene, when the world was much warmer and sea levels significantly higher than today (Raymo *et al.*, 2011).

The impact that humans have had on earth surface processes and biota over what is a very small interval of geological time cannot be overestimated (Figure 7.46). While it is difficult to gauge human population numbers in prehistoric times, these are generally considered to be no more than 2 million at around 50 ka. By the start of the Holocene, population may have increased to 5 million, and by the start of the Christian (or Common) Era was around 300 million, the steep rise over the course of the Holocene reflecting the combined benefits of farming, settlement and metal tool production. Figures are more certain for recent historical times: global population has grown from 0.5 billion in AD 1650 to today's total of nearly 7 billion (Population Reference Bureau, 2011). At a number of points in this book, we have touched upon the various impacts that this inexorable rise in global human population may have had, especially with respect to the extinction, forced migration and range restriction of plant and animal species, over-exploitation of resources (especially water), forest destruction, soil degradation and so on. It is scarcely surprising, therefore, that this level of environmental impact, combined with the polluting effects of the industrial revolution, and successive regional industrializations, has contributed to the current abnormal levels of greenhouse gases in our atmosphere (see Sapart *et al.*, 2012). Humans are arguably a product of climate change, stimulated into learning to cope with its constant upheavals and associated stresses (Figure 7.46), but they may also

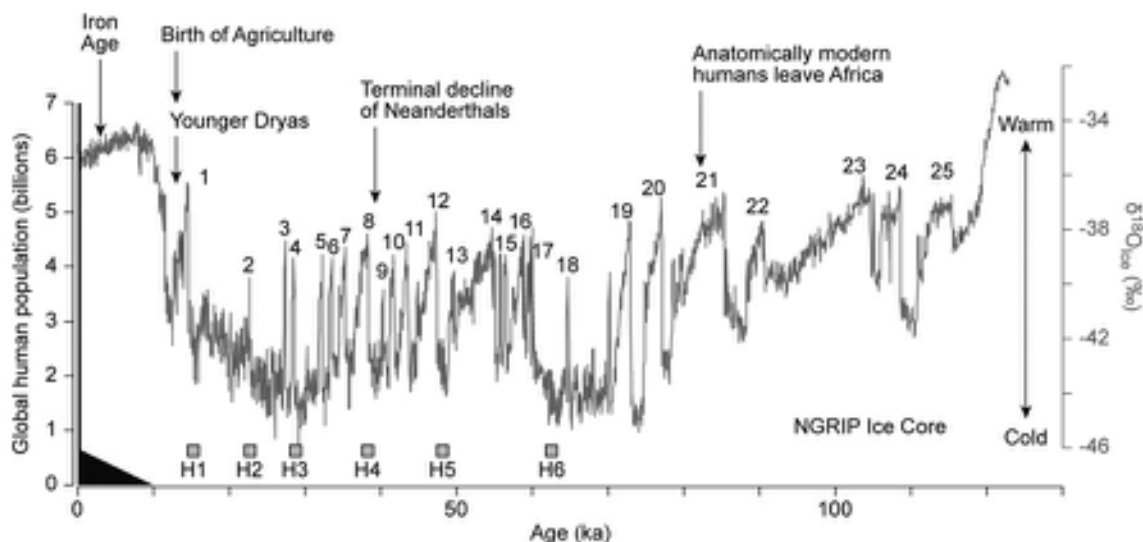


Figure 7.46 Significant developments in human history plotted against the NGRIP climate record for the last glacial–interglacial cycle. The total global human population (Population Reference Bureau, 2011, <http://www.prb.org>) is shown on the left of the diagram.

be the architects of future distress, if some of the predictions about future climate change and its consequences are proved correct. It is here that Quaternary science can play a leading role, for it not only informs the debate in terms of the land–air–ocean–cryosphere processes, but it also provides the all-important historical dimension, best exemplified by the contribution of the Intergovernmental Panel for Climate Change (IPCC), on international policy making. One of the basic dictums of Quaternary science, as we noted in Chapter 1, is that the ‘present is the key to the past’. But the past is also the key to the future, and it is by providing that key that Quaternary science can perhaps make its greatest contribution to the evaluation of future risks to humankind.

NOTES

- 1 The **Rayleigh test** is a statistical procedure for determining whether a circular distribution is random or non-random; in other words, whether the azimuths of a distribution are clumped in a particular direction.
- 2 **Stochastic resonance** is a term used by physicists to describe a situation where a signal that is normally too weak to be detected by a sensor can be boosted by adding white noise (a random signal) that contains equal power across a range of frequencies. The frequencies within the white noise that correspond to those in the original signal’s frequencies will resonate with each other, thereby amplifying the signal and making it easier to detect.

This page intentionally left blank

References

- Abbott, M.B., Wolfe, B.B., Aravena, R., *et al.* 2000. Holocene hydrological reconstructions from stable isotopes and paleolimnology, Cordillera Real, Bolivia. *Quaternary Science Reviews* 19, 1801–1820.
- Abell, P.I., Hoelzmann, P. 2000. Holocene palaeoclimates in northwestern Sudan: stable isotope studies on molluscs. *Global and Planetary Change* 26, 1–12.
- Abellán, P., Benetti, C.J., Angus, R.B., *et al.* 2011. A review of Quaternary range shifts in European aquatic Coleoptera. *Global Ecology and Biogeography* 20, 87–100.
- Abelmann, A., Gowing, M.M. 1997. Spatial distribution pattern of living polycystine radiolarian taxa – baseline study for paleoenvironmental reconstructions in the Southern Ocean (Atlantic sector). *Marine Micropaleontology* 30, 3–28.
- Abrial, J.M. 2003. Constraints on the use of ^{137}Cs as a time-marker to support CRS and SIT chronologies. *Environmental Pollution* 129, 31–37.
- Adams, J.B., Mann, M.E., Ammann, C.M. 2003. Proxy evidence for an El Niño-like response to volcanic forcing. *Nature* 426, 274–278.
- Adams, J.M., Faure, H. 1998. A new estimate of changing carbon storage on land since the last glacial maximum, based on global land ecosystem reconstruction. *Global and Planetary Change* 16–17, 3–24.
- Adams, J.W., Herries, A.I.R., Kuykendall, K.L., *et al.* 2007. Taphonomy of a South African cave: geological and hydrological influences on the GD 1 fossil assemblage at Gondolin, a Plio–Pleistocene paleocave system in the Northwest Province, South Africa. *Quaternary Science Reviews* 26, 2526–2543.
- Adams, K.D. 2010. Lake levels and sedimentary environments during deposition of the Trego Hot Springs and Wono tephras in the Lake Lahontan basin, Nevada, USA. *Quaternary Research* 73, 118–129.
- Adams, K.D., Locke, W.W., Rossi, R. 1992. Obsidian-hydration dating of fluvially reworked sediments in the West Yellowstone region, Montana. *Quaternary Research* 38, 180–195.
- Affek, H.P., Bar-Matthews, M., Ayalon, A., *et al.* 2008. Glacial/interglacial temperature variations in Soreq Cave speleothems as recorded by ‘clumped isotope’ thermometry. *Geochimica et Cosmochimica Acta* 72, 5351–5360.
- Agenbroad, L.D. 2012. Giants and pygmies: mammoths of Santa Rosa Island, California. *Quaternary International* 255, 2–8.
- Aguire, E., Pasini, G. 1985. The Pliocene–Pleistocene boundary. *Episodes* 8, 116–120.
- Aguirre, M.L., Donato, M., Richiano, S., *et al.* 2011. Pleistocene and Holocene interglacial molluscan assemblages from Patagonian and Bonaerensian littoral (Argentina, SW Atlantic): palaeobiodiversity and palaeobiogeography. *Palaeogeography, Palaeoclimatology, Palaeoecology* 308, 277–292.
- Ahr, S.W., Nordi, L.C., Forman, S.L. 2013. Soil genesis, optical dating, and geoarchaeological evaluation of two upland Alfisol pedons within the Tertiary Gulf Coastal Plain. *Geoderma* 192, 211–226.
- Aitken, M.J. 1990. *Science-based Dating in Archaeology*. Longman, London.
- Aitken, M.J. 1998. *An Introduction to Optical Dating*. Oxford University Press, Oxford.
- Aizen, V.B., Aizen, E.M. 1996. Glaciers and snow cover in Central Asia as indicators of climate change in the Earth–Ocean–Atmosphere system. In *Regional Hydrological Response to Climate Change* (edited by J.J.A. Jones). Kluwer Academic Publishers, Dordrecht, 269–286.
- Alfimov, A.V., Berman, D.I. 2009. Possible errors of the Mutual Climatic Range (MCR) method in reconstructing the Pleistocene climate of Beringia. *Entomological Review* 89, 487–499.
- Alho, P., Russell, A.J., Carrivick, J.L., *et al.* 2005. Reconstruction of the largest Holocene jökulhlaup within Jökulsáá Fjöllum, NE Iceland. *Quaternary Science Reviews* 24, 2319–2334.
- Ali, A.A., Carcaillet, C., Guendon, J.-L., *et al.* 2003. The Early Holocene treeline in the southern French Alps: new evidence from travertine formations. *Global Ecology and Biogeography* 12, 411–419.
- Al-Juaidi, F., Millington, A.C., McLaren, S.J. 2003. Merged remotely sensed data for geomorphological investigations in deserts: examples from central Saudi Arabia. *The Geographical Journal* 169, 117–130.
- Allard, G., Roy, M., Richard, P.J.H., *et al.* 2012. Constraining the age of the last interglacial–glacial transition in the Hudson Bay lowlands (Canada) using U–Th dating of buried wood. *Quaternary Geochronology* 7, 37–47.

446 REFERENCES

- Allen, J.R.M., Scourse, J.D., Hall, A.R., *et al.* 2009. Palaeoenvironmental context of the Late-glacial woolly mammoth (*Mammuthus primigenius*) discoveries at Condover, Shropshire, UK. *Geological Journal* 44, 414–446.
- Allen, K., Drew, D.M., Downes, G.M. 2012. Ring width, climate and wood density relationships in two long-lived Tasmanian tree species. *Dendrochronologia* 30, 167–177.
- Alley, R.B. 2000. Ice-core evidence of abrupt climate changes. *Proceedings of the National Academy of Sciences of the United States of America* 97, 1331–1334.
- Alley, R.B. 2007. Wally was right: predictive ability of the North Atlantic ‘conveyor belt’ hypothesis for abrupt climate change. *Annual Review of Earth and Planetary Sciences* 35, 241–272.
- Alley, R.B., MacAyeal, D.R. 1994. Ice rafted debris associated with binge/purge oscillations of the Laurentide Ice Sheet. *Paleoceanography* 9, 503–511.
- Alley, R.B., Gow, A.J., Meese, D.A., *et al.* 1997. Grain-scale processes, folding, and stratigraphic disturbances in the GISP2 ice core. *Journal of Geophysical Research* 102, 26819–26830.
- Alley, R.B., Clark, P.U., Huybrechts, P., *et al.* 2005. Ice-sheet and sea-level changes. *Science* 310, 456–460.
- Alloway, B.V., Larsen, G., Lowe, D.J., *et al.* 2007a. Tephrochronology. In *Encyclopedia of Quaternary Science* (edited by S.A. Elias). Elsevier, Amsterdam, 2869–2898.
- Alloway, B.V., Lowe, D.J., Barrell, D.J.A., *et al.* 2007b. Towards a climate event stratigraphy for New Zealand over the past 30 000 years (NZ-INTIMATE project). *Journal of Quaternary Science* 22, 9–35.
- Almond, P., Roering, J., Hales, T.C. 2007. Using soil residence time to delineate spatial and temporal patterns of transient landscape response. *Journal of Geophysical Research* 112, F03S17, doi: 10.1029/2006JF000568.
- Alonso-Zarza, A.M., Wright, V.P. 2010. Calcretes. *Developments in Sedimentology* 61, 225–267.
- Ambrose, S.H. 1998. Late Pleistocene human population bottlenecks, volcanic winter, and differentiation of modern humans. *Journal of Human Evolution* 34, 623–651.
- Ambrose, W.R. 1994. Obsidian hydration dating of a Pleistocene age site from the Manus Islands, Papua New Guinea. *Quaternary Science Reviews* 13, 137–142.
- American Commission on Stratigraphic Nomenclature. 1961. Code of Stratigraphic Nomenclature. *American Association of Petroleum Geologists Bulletin* 45, 645–665.
- American Commission on Stratigraphic Nomenclature. 1970. Code of Stratigraphic Nomenclature, 2nd edn. *American Association of Petroleum Geologists Bulletin* 60, 1–45.
- Amorosi, A., Centineo, M.C., Colalongo, M.L., *et al.* 2003. Facies architecture and latest Pleistocene–Holocene depositional history of the Po Delta (Comaccio area), Italy. *Journal of Geology* 111, 39–56.
- An, Z. 2000. The history and variability of the East Asian paleomonsoon climate. *Quaternary Science Reviews* 19, 171–187.
- Anadón, P., Gabàs, M. 2009. Paleoenvironmental evolution of the Early Pleistocene lacustrine sequence at Barranco León archeological site (Orce, Baza Basin, Southern Spain) from stable isotopes and Sr and Mg chemistry of ostracod shells. *Journal of Paleolimnology* 42, 261–279.
- Anand, P., Elderfield, H., Conte, M.H. 2003. Calibration of Mg/Ca thermometry in planktonic foraminifera from a sediment trap time series. *Paleoceanography* 18, doi: 10.1029/2002PA000846.
- Andersen, B.G., Mangerud, J., Sørensen, R., *et al.* 1995. Younger Dryas ice-marginal deposits in Norway. *Quaternary International* 28, 147–169.
- Andersen, K.K., Svensson, A., Rasmussen, S.O., *et al.* 2006. The Greenland Ice Core Chronology 2005, 15–42 ka. Part 1: constructing the time scale. *Quaternary Science Reviews* 25, 3246–3257.
- Anderson, D. 2001. Attenuation of millennial-scale events by bioturbation in marine sediments. *Paleoceanography* 16, doi: 10.1029/2000PA000530.
- Anderson, J. 2000. What is the origin of the carabid beetle fauna of dry, anthropogenic habitats in western Europe? *Journal of Biogeography* 27, 795–806.
- Anderson, R.F., Ali, S., Bradtmiller, L.I., *et al.* 2009. Wind-driven upwelling in the Southern Ocean and the deglacial rise in atmospheric CO₂. *Science* 323, 1443–1448.
- Andersson, S., Schoning, K. 2010. Surface wetness and mire development during the late Holocene in central Sweden. *Boreas* 39, 749–760.
- André, M.-F. 2009. *From Climatic to Global Change Geomorphology: Contemporary Shifts in Periglacial Geomorphology*. Geological Society of London, Special Publication 320. Blackwell Scientific Publications, Oxford, 5–28.
- Andrén, T., Björck, J., Johnsen, S. 1999. Correlation of Swedish glacial varves with the Greenland (GRIP) oxygen isotope record. *Journal of Quaternary Science* 14, 361–371.
- Andres, M.S., Bernasconi, S.M., McKenzie, J.A., *et al.* 2003. Southern Ocean deglacial record supports global Younger Dryas. *Earth and Planetary Science Letters* 216, 515–524.
- Andrews, J.E., Brasier, A.T. 2005. Seasonal records of climatic change in annually laminated tufas: short review and future prospects. *Journal of Quaternary Science* 20, 411–421.
- Andrews, J.T. 1970. A geomorphological study of Postglacial uplift with particular reference to Arctic Canada. *Institute of British Geographers, Special Publication* 2.
- Andrews, J.T., Tedesco, K. 1992. Detrital carbonate-rich sediments, northwestern Labrador Sea: implications for ice-sheet dynamics and iceberg rafting (Heinrich) events in the North Atlantic. *Geology* 20, 1087–1090.
- Andrews, J.T., Principato, S.M. 2002. *Grain-size Characteristics and Provenance of Ice-proximal Glacial Marine Sediments*. Geological Society of London, Special Publication 203. Blackwell Scientific Publications, Oxford, 305–324.
- Andrews, J.T., Dyke, A.S. 2007. Late Quaternary in North America. In *Encyclopedia of Quaternary Science* (edited by S.A. Elias). Elsevier, Amsterdam, 1095–1101.
- Andrews, J.T., Jennings, A.E., Kirby, K.M., *et al.* 1995. A Heinrich-like event, H-0 (DC-0): source(s) for detrital carbonate in the North Atlantic during the Younger Dryas chronozone. *Paleoceanography* 10, 943–952.
- Andrews, J.T., Hardadottir, J., Stoner, J.S., *et al.* 2003. Decadal to millennial-scale periodicities in North Iceland shelf sediments

- over the last 12 000 cal yr: long-term North Atlantic oceanographic variability and solar forcing. *Earth and Planetary Science Letters* 210, 453–465.
- Andrus, C.F.T. 2011. Shell midden sclerochronology. *Quaternary Science Reviews* 30, 2892–2905.
- Anisimov, O.A., Nelson, F.E. 1996. Permafrost distribution in the Northern Hemisphere under scenarios of climatic change. *Global and Planetary Change* 14, 59–72.
- Anovitz, L.M., Elam, J.M., Riciputi, L.R., et al. 1999. The failure of obsidian hydration dating: sources, implications and new directions. *Journal of Archaeological Science* 26, 735–752.
- Anthony, D.M., Granger, D.E. 2007. A new chronology of Appalachian erosional surfaces determined by cosmogenic nuclides in cave sediments. *Earth Surface Processes and Landforms* 32, 874–887.
- Antoine, P., Lautridou, J.-P., Laurent, M. 2000. Long-term fluvial archives in NW France: response of the Seine and Somme rivers to tectonic movements, climatic variations and sea-level changes. *Geomorphology* 33, 183–207.
- Antoine, P., Catt, J., Lautridou, J.-P., et al. 2003. The loess and coversands of northern France and southern England. *Journal of Quaternary Science* 18, 309–318.
- Antonioli, F., Bard, E., Potter, E.-K., et al. 2004. 215-ka history of sea-level oscillations from marine and continental layers in Argentarola Cave speleothems (Italy). *Global and Planetary Change* 43, 57–78.
- Ao, H., Dekkers, M.J., Qin, L., et al. 2011. An updated astronomical timescale for the Plio–Pleistocene deposits from South China Sea and new insights into Asian monsoon evolution. *Quaternary Science Reviews* 30, 1560–1575.
- Appleby, P.G. 2008. Three decades of dating recent sediments by fallout nuclides. *The Holocene* 18, 83–93.
- Appleby, P.G., Oldfield, F. 1992. Applications of lead-210 to sedimentation studies. In *Uranium Series Disequilibrium, Applications to Earth, Marine and Environmental Sciences* (edited by M. Ivanovich, R.S. Harmon). Clarendon Press, Oxford, 731–779.
- Applegarth, M.T., Dahms, D.E. 2001. Soil catenas of calcareous tills, Whiskey Basin, Wyoming, USA. *Catena* 42, 17–38.
- Aref, M.A.M. 2003. Classification and depositional environments of Quaternary pedogenetic gypsum crusts (gypcrete) from east of the Fayum, Depression (Egypt). *Sedimentary Geology* 155, 87–108.
- Arge, S.L., Sveinbjarnardóttir, G., Edwards, K.J., et al. 2005. Viking and Medieval settlement in the Faroes: people, place and environment. *Human Ecology* 33, 597–620.
- Arimoto, R. 2001. Eolian dust and climate: relationships to sources, tropospheric chemistry, transport and deposition. *Earth-Science Reviews* 54, 29–42.
- Armbrust, E.V. 2009. The life of diatoms in the world's oceans. *Nature* 459, 185–192.
- Armstrong, H., Brasier, M. 2005. *Microfossils*. Blackwell Publishing, Oxford and Malden, MA.
- Arnold, N., Sharp, M. 2002. Flow variability in the Scandinavian ice sheet: modelling the coupling between ice sheet flow and hydrology. *Quaternary Science Reviews* 21, 485–502.
- Ascough, P., Cook, G., Dugmore, A. 2005. Methodological approaches to determining the marine radiocarbon reservoir effect. *Progress in Physical Geography* 29, 532–547.
- Ashworth, P.C., Buckland, P.C., Sadler, J.P. (eds). 1997. *Studies in Quaternary Entomology: An Inordinate Fondness for Insects*. Quaternary Proceedings 5, John Wiley, Chichester and New York.
- Atkinson, T.C., Rowe, P.J. 1992. Applications of dating to denudation chronology and landscape evolution. In *Uranium-Series Disequilibrium: Applications to Earth, Marine and Environmental Science*, 2nd edn (edited by M. Ivanovich, R.S. Harmon). Clarendon, Oxford, 669–702.
- Atkinson, T.C., Briffa, K.R., Coope, G.R. 1987. Seasonal temperatures in Britain during the last 22,000 years, reconstructed using beetle remains. *Nature* 325, 587–592.
- Auban, J.B., Barton, C.M., Rapol, M.P. 2001. A taphonomic perspective on Neolithic beginnings: theory, interpretation and empirical data in the western Mediterranean. *Journal of Archaeological Science* 28, 597–612.
- Aubry, S., Magnin, F., Bonnet, V., et al. 2005. Multi-scale altitudinal patterns in species richness of land snail communities in south-eastern France. *Journal of Biogeography* 32, 985–998.
- Auler, A.S., Wang, X., Edwards, R.L., et al. 2004. Quaternary ecological and geomorphic changes associated with rainfall events in presently semi-arid northeastern Brazil. *Journal of Quaternary Science* 19, 693–701.
- Ayalon, A., Bar-Matthews, M., Kaufman, A. 1999. Petrography, strontium, barium and uranium isotope ratios in speleothems as paleoclimate proxies: Soreq Cave, Israel. *The Holocene* 9, 715–722.
- Ayalon, A., Bar-Matthews, M., Kaufman, A. 2002. Climatic conditions during marine oxygen isotope stage 6 in the eastern Mediterranean region from the isotopic composition of speleothems of Soreq Cave, Israel. *Geology* 30, 303–306.
- Aycliffe, L.K., Marianelli, P.C., Moriarty, K.C., et al. 1998. 500 ka precipitation record from southeastern Australia: evidence for interglacial relative aridity. *Geology* 26, 147–150.
- Bacon, C.R., Lanphere, M.A. 2006. Eruptive history and geochronology of Mount Mazama and the Crater Lake region, Oregon. *Geological Society of America Bulletin* 118, 1331–1359.
- Badding, M.E., Briner, J.P., Kaufman, D.S. 2013. ^{10}Be ages of late Pleistocene deglaciation and Neoglaciation in the north-central Brooks Range, Arctic Alaska. *Journal of Quaternary Science* 28, 95–102.
- Baier, J., Lücke, A., Negendank, J.F.W., et al. 2004. Diatom and geochemical evidence of mid- to late-Holocene climatic changes as Lake Holzmaar, West-Eifel (Germany). *Quaternary International* 113, 81–96.
- Bailey, G.N., Flemming, N.C. 2008. Archaeology of the continental shelf: marine resources, submerged landscapes and underwater archaeology. *Quaternary Science Reviews* 27, 2153–2165.
- Baillie, M.G.L. 1982. *Tree Ring Dating and Archaeology*. Croom Helm, London.
- Baillie, M.G.L. 1995. *A Slice Through Time*. Batsford, London.

- Baily, B., Collier, P., Farres, P., et al. 2002. Comparative assessment of analytical and digital photogrammetric methods in the construction of DEMs of geomorphological forms. *Earth Surface Processes and Landforms* 28, 307–320.
- Bajo, P., Drysdale, R., Woodhead, J., et al. 2012. High-resolution U-Pb dating of an Early Pleistocene stalagmite from Corkhia Cave (central Italy). *Quaternary Geochronology* 14, 5–17.
- Baker, A., Caseldine, C.J., Gilmour, M.A., et al. 1999. Stalagmite luminescence and peat humification records of palaeo-moisture for the last 2500 years. *Earth and Planetary Science Letters* 165, 157–162.
- Baker, A., Asrat, A., Fairchild, I.J., et al. 2007. Analysis of the climate signal contained within $\delta^{18}\text{O}$ and growth rate parameters in two Ethiopian stalagmites. *Geochimica et Cosmochimica Acta* 71, 2975–2988.
- Baker, A.C., Glynn, P.W., Riegl, B. 2008a. Climate change and coral reef bleaching: An ecological assessment of long-term impacts, recovery trends and future outlook. *Estuarine, Coastal and Shelf Science* 80, 435–471.
- Baker, A., Smith, C.J., Jex, C., et al. 2008b. Annually laminated speleothems: a review. *International Journal of Speleology* 37, 193–206.
- Bakke, J., Dahl, S.O., Nesje, A. 2005. Lateglacial and early Holocene palaeoclimatic reconstruction based on glacier fluctuations and equilibrium-line altitudes at northern Folgefonna, Hardanger, western Norway. *Journal of Quaternary Science* 20, 179–198.
- Bakke, J., Lie, Ø., Dahl, S.O., et al. 2008. Strength and spatial patterns of the Holocene wintertime westerlies in the NE Atlantic region. *Global and Planetary Change* 60, 28–41.
- Bakke, J., Lie, Ø., Heegaard, E., et al. 2009. Rapid oceanic and atmospheric changes during the Younger Dryas cold period. *Nature Geoscience* 2, 202–205.
- Balakrishnan, M., Yapp, C.J., Meltzer, D.J., et al. 2005. Paleo-environment of the Folsom archaeological site, New Mexico, USA, approximately 10,500 ^{14}C yr B.P. as inferred from the stable isotope composition of fossil land snail shells. *Quaternary Research* 63, 31–44.
- Balascio, N.L., Kaufman, D.S., Briner, J.P., Manley, W.F. 2005. Equilibrium-line altitudes during the Last Glacial Maximum across the Brooks Range, Alaska. *Journal of Quaternary Science* 20, 821–838.
- Balco, G. 2011. Contributions and unrealised potential contributions of cosmogenic-nuclide exposure dating to glacier chronology. *Quaternary Science Reviews* 30, 3–27.
- Balco, G., Stone, J.O., Lifton, N., et al. 2008. A complete and easily accessible means of calculating surface exposure ages or erosion rates from ^{10}Be and ^{26}Al measurements. *Quaternary Geochronology* 3, 174–195.
- Balco, G., Schaefer, J.M., LARISSA Group. 2013. Exposure-age record of Holocene ice sheet and ice shelf change in the north-east Antarctic peninsula. *Quaternary Science Reviews* 59, 101–111.
- Ballantyne, C.K., 1989. The Loch Lomond Advance on the Isle of Skye, Scotland: glacier reconstruction and palaeoclimatic implications. *Journal of Quaternary Science* 4, 95–108.
- Ballantyne, C.K. 2002a. Paraglacial geomorphology. *Quaternary Science Reviews* 21, 1935–2017.
- Ballantyne, C.K. 2002b. The Loch Lomond Readvance on the Isle of Mull, Scotland: glacier reconstruction and palaeoclimatic implications. *Journal of Quaternary Science* 17, 759–771.
- Ballantyne, C.K. 2007a. Loch Lomond Stadial glaciers in North Harris, Outer Hebrides, north-west Scotland: glacier reconstruction and palaeoclimatic implications. *Quaternary Science Reviews* 26, 3134–3149.
- Ballantyne, C.K. 2007b. The Loch Lomond Readvance on north Arran, Scotland: glacier reconstructions and palaeoclimatic implications. *Journal of Quaternary Science* 22, 343–359.
- Ballantyne, C.K. 2010. Extent and deglacial chronology of the last British-Irish Ice Sheet: implications of exposure dating using cosmogenic isotopes, *Journal of Quaternary Science* 25, 515–534.
- Ballantyne, C.K., Kirkbride, M.P. 1986. The characteristics and significance of some Lateglacial protalus ramparts in upland Britain. *Earth Surface Processes and Landforms* 11, 659–671.
- Ballantyne, C.K., Benn, D.I. 1994. Glaciological constraints on protalus rampart development. *Permafrost and Periglacial Processes* 5, 145–153.
- Ballantyne, C.K., Harris, C. 1994. *The Periglaciation of Great Britain*. Cambridge University Press, Cambridge.
- Ballantyne, C.K., McCarroll, D., Nesje A., et al. 1998. The last ice sheet in north-west Scotland: reconstruction and implications. *Quaternary Science Reviews* 17, 1149–1184.
- Ballantyne, C.K., Stone, J.O., McCarroll, D. 2008. Dimensions and chronology of the last ice sheet in Western Ireland. *Quaternary Science Reviews* 27, 185–200.
- Ballantyne, C.K., Schnabel, C., Xu, S. 2009. Readvance of the last British-Irish Ice Sheet during Greenland Interstadial 1 (GI-1): the Wester Ross Readvance, NW Scotland. *Quaternary Science Reviews* 28, 783–789.
- Balsam, W., Ji, J., Chen, J. 2004. Climatic interpretation of the Luochan and Lingtai loess sections, China, based on changing iron oxide mineralogy and magnetic susceptibility. *Earth and Planetary Science Letters* 223, 335–348.
- Bamber, J.L., Rivera, A. 2007. A review of remote sensing methods for glacier mass balance determination. *Global and Planetary Change* 59, 138–148.
- Bamber, J.L., Alley, R.B., Joughin, I. 2007. Rapid response of modern day ice sheets to external forcing. *Earth and Planetary Science Letters* 257, 1–13.
- Bannister, A., Raymond, S., Baker, R. 1998. *Surveying*, 7th edn. Prentice Hall, Harlow.
- Barbante C., Fischer., Masson-Delmotte, V., et al. 2010. Climate of the last million years: new insights from EPICA and other records. *Quaternary Science Reviews* 29, 1–7.
- Barber, D.C., Dyke, A., Hillaire-Marcel, C., et al. 1999. Forcing of the cold event of 8,200 years ago by catastrophic drainage of Laurentide lakes. *Nature* 400, 344–348.
- Barber, K.E. 1981. *Peat Stratigraphy and Climatic Change: A Palaeoecological Test of the Theory of Cyclic Peat Bog Regeneration*. Balkema, Rotterdam.
- Barber, K.E., Langdon, P.G. 2007. What drives the peat-based palaeoclimate record? A critical test using multi-proxy climate records from northern Britain. *Quaternary Science Reviews* 26, 3318–3327.

- Barber, K.E., Chambers, F.M., Maddy, D., *et al.* 1994. A sensitive high resolution record of Late Holocene climatic change from a raised bog in Northern England. *The Holocene* 4, 198–205.
- Barber, K.E., Maddy, D., Rose, N., *et al.* 2000. Replicated proxy-climate signals over the last 2000 years from two distant UK peat bogs: new evidence for regional palaeoclimatic teleconnections. *Quaternary Science Reviews* 19, 481–487.
- Barber, K.E., Chambers, F.M., Maddy, D. 2003. Holocene palaeoclimates from peat stratigraphy: macrofossil proxy climate records from three oceanic raised bogs in England and Ireland. *Quaternary Science Reviews* 22, 521–539.
- Barber, K.E., Chambers, F.M., Maddy, D. 2004. Late Holocene climatic history of northern Germany and Denmark: peat macrofossil investigations at Dosenmoor, Schleswig-Holstein, and Svanemose, Jutland. *Boreas* 33, 132–144.
- Barbour, M.M. 2007. Stable oxygen isotope composition of plant tissue: a review. *Functional Plant Biology* 34, 83–94.
- Barclay, D.J., Wiles, G.C., Calkin, P.E. 2009. Holocene glacier fluctuations in Alaska. *Quaternary Science Reviews* 28, 2034–2948.
- Bard, E., Arnold, M., Duplessy, J.-C. 1991. Reconciling the sea level record of the last deglaciation with ^{18}O spectra from deep sea cores. In *Radiocarbon Dating: Recent Applications and Future Potential* (edited by J.J. Lowe). *Quaternary Proceedings* 1, Quaternary Research Association, Cambridge, 67–73.
- Bard, E., Hamelin, B., Delanghe-Sabatier, D. 2010. Deglacial meltwater pulse 1B and Younger Dryas sea levels revisited with boreholes at Tahiti. *Science* 327, 1235–1237.
- Barker, G.M. (ed.). 2001. *The Biology of Terrestrial Molluscs*. CABI Publishing, Wallingford.
- Barker, S., Greaves, M., Elderfield, H. 2003. A study of cleaning procedures used for foraminiferal Mg/Ca paleothermometry. *Geochemistry, Geophysics, Geosystems* 4, doi: 10.1029/2003GC000559.
- Barker, S., Cacho, I., Benway, H., *et al.* 2005. Planktonic foraminiferal Mg/Ca as a proxy for past oceanic temperatures: a methodological overview and data compilation for the Last Glacial Maximum. *Quaternary Science Reviews* 24, 821–834.
- Barker, S., Diz, P., Vautravers, M.J., *et al.* 2009. Interhemispheric Atlantic seesaw response during the last deglaciation. *Nature* 457, 1007–1102.
- Barletta, F., St-Onge, G., Channell, J.E.T., *et al.* 2008. High-resolution palaeomagnetic secular variation and relative palaeointensity records from the eastern Canadian Arctic: implications for Holocene stratigraphy and geomagnetic field behaviour. *Canadian Journal of Earth Sciences* 45, 1265–1281.
- Bar-Matthews, M., Ayalon, A., Kaufman, A. 1997. Late Quaternary paleoclimate in the eastern Mediterranean region from stable isotope analysis of speleothems at Soreq Cave, Israel. *Quaternary Research* 47, 155–168.
- Bar-Matthews, M., Ayalon, A., Gilmour, M., *et al.* 2003. Sea-land oxygen isotope relationships from planktonic foraminifera and speleothems in the Eastern Mediterranean region and their implication for palaeorainfall during interglacial intervals. *Geochimica et Cosmochimica Acta* 67, 3181–3199.
- Barnes, I., Barnett, R., Shapiro, B. 2007. Ancient DNA. In *Encyclopedia of Quaternary Science* (edited by S.A. Elias). Elsevier, Amsterdam, 3249–3253.
- Barnosky, A.D., Matzke, N., Tomiya, S., *et al.* 2011. Has the Earth's sixth mass extinction already arrived? *Nature* 471, 51–57.
- Bar-Or, R., Erlick, C., Gildor, H. 2008. The role of dust in glacial–interglacial cycles. *Quaternary Science Reviews* 27, 201–208.
- Bar-Oz, G., Nadel, D., 2013. Worldwide large-scale trapping and hunting of ungulates in past societies. *Quaternary International* 297, 1–7.
- Barracough, T.G., Vogler, A.P. 2002. Recent diversification rates in North America tiger beetles estimated from a dated mtDNA phylogenetic tree. *Molecular Biology and Evolution* 19, 1706–1716.
- Barreiro, M., Fedorov, A., Pacanowski, R., *et al.* 2008. Abrupt climate changes: how freshening of the northern Atlantic affects the thermohaline and wind-driven oceanic circulations. *Annual Review of Earth and Planetary Sciences* 36, 33–58.
- Barreto, A.M.F., Bezerra, F.H.R., Suguió, K., *et al.* 2002. Late Pleistocene marine terrace deposits in northeastern Brazil: sea-level change and tectonic implications. *Palaeogeography, Palaeoclimatology, Palaeoecology* 179, 57–69.
- Barrett, B.E., Nicholls, K.W., Murray, T., *et al.* 2009. Rapid recent warming on Rutford Ice Stream, West Antarctica, from borehole thermometry. *Geophysical Research Letters* 36, doi: 10.1029/2008GL036369.
- Barron, J.A., Bukry, D. 2007. Development of the California Current during the past 12,000 yr based on diatoms and silicoflagellates. *Palaeogeography, Palaeoclimatology, Palaeoecology* 248, 313–338.
- Barron, J.A., Anderson, L. 2010. Enhanced Late Holocene ENSO/PDO expression along the margins of the eastern North Pacific. *Quaternary International* 235, 3–12.
- Barrows, T.T., Juggins, S. 2005. Sea-surface temperatures around the Australian margin and Indian Ocean during the Last Glacial Maximum. *Quaternary Science Reviews* 24, 1017–1047.
- Bartoli, G., Sarnthein, M., Weinelt, M., *et al.* 2005. Final closure of Panama and the onset of northern hemisphere glaciation. *Earth and Planetary Science Letters* 237, 33–44.
- Barton, R.N.E., Berridge, P.J., Walker, M.J.C., *et al.* 1995. Persistent places in the Mesolithic landscape: an example from the Black Mountain Uplands of south Wales. *Proceedings of the Prehistoric Society* 61, 81–116.
- Barton, R.N.E., Bouzouggar, A., Colclutt, S.N., *et al.* 2009. OSL dating of the Aterian levels at Dar es-Soltan 1 (Rabat, Morocco) and implications for the dispersal of modern *Homo sapiens*. *Quaternary Science Reviews* 28, 1914–1931.
- Bassiotis, F.C., Labeyrie, L., Vincent, E., *et al.* 1994. The astronomical theory of climate and the age of the Brunhes–Matuyama magnetic reversal. *Earth and Planetary Science Letters* 126, 91–108.
- Bateman, M.D., Carr, A.S., Murray-Wallace, C.V., *et al.* 2008. A dating intercomparison study of Late Stone Age midden deposits, South Africa. *Geoarchaeology* 23, 715–741.
- Bathurst, R.R., Zori, D., Byock, J. 2010. Diatoms as bio-indicators of site use: locating turf structures from the Viking Age. *Journal of Archaeological Science* 37, 2920–2928.

450 REFERENCES

- Batt, C.M. 1997. The British archaeomagnetic calibration curve: an objective treatment. *Archaeometry* 39, 153–168.
- Battarbee, R.W. 2000. Palaeolimnological approaches to climate change, with special regard to the biological record. *Quaternary Science Reviews* 19, 107–124.
- Battarbee, R.W., Bennion, H. 2011. Palaeolimnology and its developing role in assessing the history and extent of human impact on lake ecosystems. *Journal of Paleolimnology* 45, 399–404.
- Battarbee, R.W., Jones, V.J., Flower, B.P., et al. 2001. Diatoms. In *Tracking Environmental Change Using Lake Sediments. Volume 3: Terrestrial, Algal and Siliceous Indicators* (edited by J.P. Smol, H.J.B. Birks, E.F. Stoermer). Kluwer, Dordrecht, 155–201.
- Battarbee, R.W., Charles, D.F., Bigler, C., et al. 2010. Diatoms as indicators of surface-water acidity. In *The Diatoms: Applications for the Environmental and Earth Sciences*, 2nd edn (edited by J.P. Smol, E.F. Stoermer). Cambridge University Press, Cambridge, 98–121.
- Baumann, K.-H., Andrleit, H., Bockel, B., et al. 2005. The significance of extant coccolithophores as indicators of ocean water masses, surface water temperature, and palaeoproductivity: a review. *Paläontologische Zeitschrift* 79, 93–112.
- Baumgartner, P.O., Aitchison, J.C., De Wever, P., et al. (eds). 2006. *Radiolaria: Siliceous Plankton Through Time. Eclogae Geologicae Helvetiae Supplement 1*, S63–S66, Birkhäuser, Basel.
- Bay, R.C., Bramall, N., Price, P.B. 2004. Bipolar correlation of volcanism with millennial climate change. *Proceedings of the National Academy of Sciences of the United States of America* 101, 6341–6345.
- Bayer, M.M., Juggins, S. 2002. ADIAC imaging techniques and databases. In *Automated Diatom Identification* (edited by H. du Buf, M.M. Bayer). World Scientific Press, Singapore, 55–73.
- Bazin, L., Landais, A., Lemieux-Dudon, B., et al. 2012. An optimised multi-proxy, multi-site Antarctic ice and gas orbital chronology (AICC2012): 120–180 ka. *Climate of the Past Discussions* 8, 5963–6009.
- Beaudoin, A.B. 2007. On the laboratory procedure for processing unconsolidated sediment samples to concentrate subfossil seed and other plant macro-remains. *Journal of Paleolimnology* 37, 301–308.
- Beck, C., Jones, G.T. 1994. Dating surface assemblages using obsidian hydration. In *Dating in Exposed and Surface Contexts* (edited by C. Beck). University of New Mexico Press, Albuquerque, 47–75.
- Beck, J.W., Donahue, D.J., Jull, A.J.T., et al. 1998. Ambiguities in direct dating of rock surfaces using radiocarbon measurements. *Science* 280, 2132–2135.
- Beck, J.W., Richards, D.A., Edwards, R.L., et al. 2001. Extremely large variations in atmospheric ^{14}C concentrations during the last glacial period. *Science* 292, 2453–2458.
- Beerling, D.J., Royer, D.L. 2002. Reading a CO_2 signal from fossil stomata. *New Phytologist* 153, 387–397.
- Begon, M., Townsend, C.R., Harper, J.L. 2006. *Ecology: From Individuals to Ecosystems*, 4th edn. Blackwell Publishing, Malden, MA and Oxford.
- Behre, K.-E. (ed.). 1986. *Anthropogenic Indicators in Pollen Diagrams*. Balkema, Rotterdam.
- Behre, K.-E., van der Plicht, J. 1992. Towards an absolute chronology for the last glacial period in Europe: radiocarbon dates from Oerel, northern Germany. *Vegetation History and Archaeobotany* 1, 111–117.
- Behrensmeyer, A.K. 1988. Vertebrate preservation in fluvial channels. *Palaeogeography, Palaeoclimatology, Palaeoecology* 63, 183–199.
- Belanger, C.L., Jablonski, D., Roy, K., et al. 2012. Global environmental predictors of benthic marine biogeographic structure. *Proceedings of the National Academy of Sciences of the United States of America* 109, 14046–14051.
- Bell, M., Walker, M.J.C. 2005. *Late Quaternary Environmental Change: Physical and Human Perspectives*. Pearson: Prentice Hall, London.
- Belt, S.T., Müller, J. 2013. The Arctic sea ice biomarker IP25: a review of current understanding, recommendations for future research and applications in palaeo sea ice reconstructions. *Quaternary Science Reviews* doi: 10.1016/j.quascirev.2012.12.001.
- Benedict, J.B. 2009. A review of lichenometric dating and its applications to archaeology. *American Antiquity* 74, 143–172.
- Benn, D.I. 1994. Fluted moraine and till genesis beneath a temperate glacier: Slettmarkbreen, Jotunheimen, Norway. *Sedimentology* 41, 279–292.
- Benn, D.I. 1997. Glacier fluctuations in western Scotland. *Quaternary International* 38–39, 137–147.
- Benn, D.I. 2004. Macrofabric. In *A Practical Guide to the Study of Glacial Sediments* (edited by D.J.A. Evans, D.I. Benn). Arnold, London, 93–114.
- Benn, D.I., Lemkuhl, F. 2000. Mass balance and equilibrium-line altitudes of glaciers in high-mountain environments. *Quaternary International* 65/66, 15–29.
- Benn, D.I., Ringrose, S. 2001. Random variation of fabric eigenvalues: implications for the use of a-axis fabric data to differentiate till facies. *Earth Surface Processes and Landforms* 26, 295–306.
- Benn, D.I., Ballantyne, C.K. 2005. Palaeoclimatic reconstruction from Loch Lomond Readvance glaciers in the West Drumochter Hills, Scotland. *Journal of Quaternary Science* 20, 577–592.
- Benn, D.I., Lukas, S. 2006. Younger Dryas glacial landsystems in north west Scotland: an assessment of modern analogues and palaeoclimatic implications. *Quaternary Science Reviews* 25, 2390–2408.
- Benn, D.I., Evans, D.J.A. 2010. *Glaciers and Glaciation*, 2nd edn. Hodder-Arnold, London.
- Benn, D.I., Hulton, N.R.J. 2010. An Excel TM spreadsheet program for reconstructing the surface profile of former mountain glaciers and icecaps. *Computers and Geosciences* 36, 605–610.
- Benn, D.I., Kirkbride, M.P., Owen, L.A., et al. 2003. Glaciated valley landsystems. In *Glacial Landsystems* (edited by D.J.A. Evans). Arnold, London, 372–406.
- Benn, D.I., Owen, L.A., Osmaston, H.A., et al. 2005. Reconstruction of equilibrium-line altitudes for tropical and sub-tropical glaciers. *Quaternary International* 138–139, 8–21.
- Bennett, K.D. 1996. Determination of the number of zones in a biostratigraphical sequence. *New Phytologist* 132, 155–170.

- Bennett, K., Willis, K.J. 2001. Pollen. In *Tracking Environmental Change Using Lake Sediments. Volume 3: Terrestrial, Algal and Siliceous Indicators* (edited by J.P. Smol, H.J.B. Birks, E.F. Stoermer). Kluwer Academic Publishers (Springer), Dordrecht and Boston, 5–30.
- Bennett, M.R., Glasser, N.F. 2009. *Glacial Geology: Ice Sheets and Landforms*, 2nd edn. Wiley-Blackwell, Chichester and Oxford.
- Bennike, O., Anderson, N.J., McGowan, S. 2010. Holocene palaeo-ecology of southwest Greenland inferred from macrofossils in sediments of an oligosaline lake. *Journal of Paleolimnology* 43, 787–798.
- Benson, L., Paillet, F.L. 2002. HIBAL: a hydrologic-isotopic-balance model for application to paleolake systems. *Quaternary Science Reviews* 21, 1521–1539.
- Benson, L.V., Lund, S.P., Burdett, J.W., et al. 1998. Correlation of late-Pleistocene lake-level oscillations in Mono Lake, California, with North Atlantic climate events. *Quaternary Research* 49, 1–10.
- Benson, L., Kashgarian, M., Rye, R., et al. 2002. Holocene multi-decadal and multicentennial droughts affecting northern California and Nevada. *Quaternary Science Reviews* 21, 659–682.
- Benson, L., Lund, S., Negrini, R., et al. 2003. Response of North American Great Basin Lakes to Dansgaard–Oeschger oscillations. *Quaternary Science Reviews* 22, 2239–2251.
- Benson, L., Madole, R., Phillips, W., et al. 2004. The probable importance of snow and sediment shielding on cosmogenic ages of north-central Colorado Pinedale and pre-Pinedale moraines. *Quaternary Science Reviews* 23, 193–206.
- Bera, S.K. 2004. Late Holocene palaeo-winds and climatic changes in Eastern Antarctica as indicated by long-distance transported pollen-spores and local microbiota in polar lake core sediments. *Current Science* 86, 1485–1488.
- Bereiter, B., Lüthi, D., Seagrist, M., et al. 2012. Mode change of millennial CO₂ variability during the last glacial cycle associated with a bipolar marine carbon seesaw. *Proceedings of the National Academy of Sciences of the United States of America* 109, 9755–9760.
- Berger, A., Loutre, M.F. 2010. Modeling the 100-kyr glacial–interglacial cycles. *Global and Planetary Change* 72, 275–281.
- Berger, A., Mélice, J.J., Loutre, M.F. 2005. On the origin of the 100-kyr cycles in the astronomical forcing. *Paleoceanography* 20, PA4019, doi: 10.1029/2005PA001173
- Berger, W.H. 2013a. Milankovitch tuning of deep-sea records: Implications for maximum rates of change of sea level. *Global and Planetary Change* 101, 131–143.
- Berger, W.H. 2013b. On the Milankovitch sensitivity of the Quaternary deep-sea record. *Climate of the Past Discussions* 9, 1237–1257.
- Berger, W.H., von Rad, U. 2002. Decadal to millennial cyclicity in varves and turbidites from the Arabian Sea: hypothesis of tidal origin. *Global and Planetary Change* 34, 313–325.
- Berger, W.H., Yasuda, M.K., Bickert, T., et al. 1994. Quaternary time scale for the Ontong Java Plateau: Milankovitch template for Ocean Drilling Program Site 806. *Geology* 22, 463–467.
- Berglund, B.E., Gaillard, M.-J., Björkman, L., et al. 2008. Long-term changes in floristic diversity in southern Sweden: palynological richness, vegetation dynamics and land-use. *Vegetation History and Archaeobotany* 17, 573–583.
- Bergman, J., Wastegård, S., Hammarlund, D., et al. 2004. Holocene tephra horizons at Klocka Bog, west-central Sweden: aspects of reproducibility in subarctic peat deposits. *Journal of Quaternary Science* 19, 241–249.
- Bergner, A.G.N., Trauth, M.H., Bookhagen, B. 2003. Paleo-precipitation estimates for the Lake Naivasha basin (Kenya) during the last 175 k.y. using a lake-balance model. *Global and Planetary Change* 36, 117–136.
- Bergner, A.G.N., Strecker, M.R., Trauth, M.H., et al. 2009. Tectonic and climate control on evolution of rift lakes in the Central Kenya Rift, East Africa. *Quaternary Science Reviews* 28, 2804–2816.
- Berkeley, A., Perry, C.T., Smithers, S.G., et al. 2007. A review of the ecological and taphonomic controls on foraminiferal assemblage development in intertidal environments. *Earth-Science Reviews* 83, 205–230.
- Bernasconi, M.P., Stanley, J.-D., Caruso, C. 2010. Sybaris–Thuri–Copia deltaic settings in Calabria, Italy: molluscs, associated biogenic components and ecobiostatigraphy applied to archaeology. *Journal of Coastal Research* 26, 377–390.
- Bernet, M., Brandon, M.T., Garver, J.I., et al. 2004. Downstream changes of Alpine zircon fission-track ages in the Rhône and Rhine Rivers. *Journal of Sedimentary Research* 74, 82–94.
- Berthier, E., Schiefer, E., Clarke, G.K.C., et al. 2010. Contribution of Alaskan glaciers to sea-level rise derived from satellite imagery. *Nature Geoscience* 3, 92–95.
- Bettis III, E.A., Muhs, D.R., Roberts, H.M., et al. 2003. Last Glacial loess in the coterminous USA. *Quaternary Science Reviews* 22, 1907–1946.
- Birhy, N., Filion, L. 1996. Mid-Holocene hemlock decline in eastern North America linked with phytophagous insect activity. *Quaternary Research* 45, 312–320.
- Bianchi, C., Gersonde, R. 2004. Climate evolution at the last deglaciation: the role of the Southern Ocean. *Earth and Planetary Science Letters* 228, 407–424.
- Bierman, P.R., Gillespie, R.A. 1994. Evidence suggesting that methods of rock-varnish cation-ratio dating are neither comparable nor consistently reliable. *Quaternary Research* 41, 82–90.
- Bintanja, R., van de Wal, R.S.W. 2008. North American ice-sheet dynamics and the onset of the 100,000-year glacial cycles. *Nature* 454, 869–872.
- Bintanja, R., van de Wal, R.S.W., Oerlemans, J. 2005. Modelled atmospheric temperatures and global sea levels over the past million years. *Nature* 437, 125–128.
- Bird, M.I., Fifield, L.K., Santos, G.M., et al. 2003. Radiocarbon dating from 40 to 60 ka BP at Border Cave, South Africa. *Quaternary Science Reviews* 22, 943–947.
- Bird, M.I., Taylor, D., Hunt, C. 2005. Palaeoenvironments of insular Southeast Asia during the Last Glacial Period: a savanna corridor in Sundaland? *Quaternary Science Reviews* 24, 2228–2242.
- Birkeland, P.W. 1999. *Soils and Geomorphology*. Oxford University Press, Oxford.

- Birkeland, P.W., Shroba, R.R., Burns, S.F., et al. 2003. Integrating soils and geomorphology in mountains – an example from the Front Range of Colorado. *Geomorphology* 55, 329–344.
- Birks, H.H. 2001. Plant macrofossils. In *Tracking Environmental Change Using Lake Sediments. Volume 3: Terrestrial, Algal and Silicic Indicators* (edited by J.P. Smol, H.J.B. Birks, E.F. Stoermer). Kluwer Academic Publishers, Dordrecht, 49–74.
- Birks, H.H. 2007. Plant macroossil introduction. In *Encyclopedia of Quaternary Science* (edited by S.A. Elias). Elsevier, Amsterdam, 2266–2287.
- Birks, H.H. 2008. The Late-Quaternary history of arctic and alpine plants. *Plant Ecology & Diversity* 1, 135–146.
- Birks, H.H. and Wright, H.E. (eds). 2000. The reconstruction of the late-glacial and early-Holocene aquatic ecosystems at Kråkenes Lake, Norway. *Journal of Paleolimnology* 23, 1–114.
- Birks, H.H., Birks, H.J.B. 2006. Multi-proxy studies in palaeolimnology. *Vegetation History and Archaeobotany* 15, 235–251.
- Birks, H.J.B. 1989. Holocene isochrone maps and patterns of tree-spreading in the British Isles. *Journal of Biogeography* 16, 503–540.
- Birks, H.J.B., Birks, H.H. 1980. *Quaternary Palaeoecology*. Edward Arnold, London.
- Birks, H.J.B., Seppä, H. 2004. Pollen-based reconstructions of late-Quaternary climate in Europe – progress, problems, and pitfalls. *Acta Palaeobotanica* 44, 317–334.
- Bitinas, A. 2012. New insights into the last deglaciation of the south-eastern flank of the Scandinavian Ice Sheet. *Quaternary Science Reviews* 44, 69–80.
- Bitinas, A., Karmazienė, D., Jusienė, A. 2004. Glaciolacustrine kame terraces as an indicator of deglaciation in Lithuania during the Last Deglaciation. *Sedimentary Geology* 165, 285–294.
- Bittman, F., Müller, H. 1996. The Kärlich Interglacial site and its correlation with the Bilshausen sequence. In *The Early–Middle Pleistocene in Europe* (edited by C. Turner). Balkema, Rotterdam, 187–193.
- Björck, S. 1995. A review of the history of the Baltic Sea, 13.0–8.0 ka BP. *Quaternary International* 27, 19–40.
- Björck, S., Walker, M.J.C., Cwynar, L.C., et al. 1998. An event stratigraphy for the Last Termination in the North Atlantic region based on the Greenland ice-core record. *Journal of Quaternary Science* 13, 283–292.
- Björck, S., Koç, N., Skog, G. 2003. Consistently large marine reservoir ages in the Norwegian Sea during the last deglaciation. *Quaternary Science Reviews* 22, 429–435.
- Blaauw, M., 2012. Out of tune: the dangers of aligning proxy archives. *Quaternary Science Reviews* 36, 38–49.
- Blaauw, M., Heuveldink, G.B.M., Mauquoy, D., et al. 2003. A numerical approach to C-14 wiggle-match dating of organic deposits: best fits and confidence intervals. *Quaternary Science Reviews* 22, 1485–1500.
- Blaauw, M., Van Geel, B., Mauquoy, D., et al. 2004. Radiocarbon wiggle-match dating of peat deposits: advantages and limitations. *Journal of Quaternary Science* 19, 177–181.
- Blackford, J., Chambers, F.M. 1995. Proxy climate record for the last 1000 years from Irish blanket peat and a possible link to solar variability. *Earth and Planetary Science Letters* 133, 145–150.
- Blackwell, B.A.B. 2001a Electron spin resonance (ESR) dating in lacustrine environments. In *Tracking Environmental Change using Lake Sediments. Volume 1: Basin Analysis, Coring and Chronological Techniques*, 2nd edn (edited by W.M. Last, J.P. Smol). Kluwer, Dordrecht, 283–369.
- Blackwell, B.A.B. 2001b. Amino acid racemisation (AAR) dating and analysis in lacustrine environments. In *Tracking Environmental Change Using Lake Sediments. Volume 1: Basin Analysis, Coring and Chronological Techniques*, 2nd edn (edited by W.M. Last, J.P. Smol). Kluwer, Dordrecht, 391–450.
- Blackwell, B.A.B., Skinner, A.R., Mashriqi, F., et al. 2012. Challenges in constraining pluvial events and human activity: examples of ESR dating molluscs from the Western Desert, Egypt. *Quaternary Geochronology* 10, 430–435.
- Blanchet, CL., Tjallingii, R., Frank, M., et al. 2013. High- and low-latitude forcing of the Nile River regime during the Holocene inferred from laminated sediments of the Nile deep-sea fan. *Earth and Planetary Science Letters* 364, 980–110.
- Blockley, S.P.E., Lowe, J.I., Walker, M.J.C., et al. 2004. Bayesian analysis of radiocarbon chronologies: examples from the European Late-glacial. *Journal of Quaternary Science* 19, 159–175.
- Blockley, S.P.E., Blaauw, M., Bronk Ramsey, C., et al. 2007a. Building and testing age models for radiocarbon dates in Lateglacial and Early Holocene sediments. *Quaternary Science Reviews* 26, 1915–1926.
- Blockley, S.P.E., Bronk Ramsey, C., Pyle, D.M. 2007b. Improved age modelling and high-precision age estimates of late Quaternary tephras, for accurate palaeoclimate reconstruction. *Journal of Volcanology and Geothermal Research* 177, 251–262.
- Blockley, S.P.E., Lane, C.S., Lotter, A.F., et al. 2007c. Evidence for the presence of the Vedde Ash in central Europe. *Quaternary Science Reviews* 26, 3030–3036.
- Blockley, S.P.E., Lane, C.S., Hardiman, M., et al. 2012. Synchronisation of palaeoenvironmental records over the last 60,000 years, and an extended INTIMATE event stratigraphy. *Journal of Quaternary Science* 36, 2–10.
- Blois, J.L., Hadly, E.A. 2009. Mammalian response to Cenozoic climatic change. *Annual Review of Earth and Planetary Sciences* 37, 181–208.
- Blois, J.L., McGuire, J.L., Hadly, E.A. 2010. Small mammal diversity loss in response to late-Pleistocene climatic change. *Nature* 465, 771–774.
- Blott, S.J. and Pye, K., 2008. Particle shape: a review and new methods of characterization and classification. *Sedimentology* 55, 31–63.
- Blott, S.J., Croft, D.J., Pye, K., et al. 2004. *Particle Size Analysis by Laser Diffraction*. Geological Society of London, Special Publication 232. Blackwell Scientific Publications, Oxford, 63–73.
- Blum, M.D., Törnqvist, T.E. 2000. Fluvial responses to climate and sea-level change: a review and look forward. *Sedimentology* 47 (Suppl. 1), 2–48.
- Blunier, T.J., Chappellaz, J., Schwander, J., et al. 1998. Asynchrony of Antarctic and Greenland climate change during the last glacial period. *Nature* 394, 739–743.
- Blunier, T., Spahni, R., Barnola, J.-M., et al. 2007. Synchronisation of ice core records via atmospheric gases. *Climate of the Past* 3, 325–330.

- Blyth, A.J., Asrat, A., Baker, A., et al. 2007. A new approach to detecting vegetation and land-use change using high-resolution lipid biomarker records in stalagmites. *Quaternary Research* 68, 314–324.
- Blyth, A.J., Baker, A., Collins, M.J., et al. 2008. Molecular organic matter in speleothems and its potential as an environmental proxy. *Quaternary Science Reviews* 27, 905–921.
- Boardman, J., Poesen, J. (eds). 2006. *Soil Erosion in Europe*. Wiley, Chichester and New York.
- Bockheim, J.G. 1995. Permafrost distribution in the Southern Circumpolar Region and its relation to the environment: a review and recommendation for further research. *Permafrost and Periglacial Processes* 6, 27–45.
- Boehrer, B., Schultze, M. 2008. The stratification of lakes. *Review of Geophysics* 46, doi: 10.1029/2006RG000210.
- Boenigk, W., Frechen, M. 2006. The Pliocene and Quaternary fluvial archives of the Rhine system. *Quaternary Science Reviews* 25, 550–574.
- Boës, X., Fagel, N. 2008. Relationship between southern Chilean varved lake sediments, precipitation and ENSO for the last 600 years. *Journal of Paleolimnology* 39, 237–252.
- Boettger, T., Hiller, A., Kremenski, K. 2003. Mid-Holocene warming in the northwest Kola Peninsula, Russia: northern pine-limit movement and stable isotope evidence. *The Holocene* 13, 403–410.
- Bohacs, K.M., Carroll, A.R., Neal, J.E. 2003. Lessons from large lake systems – thresholds, nonlinearity, and strange attractors. *Geological Society of America, Special Paper* 370, 75–90.
- Bohncke, S., Vandenberghe, J. and Huijzer, A.S. 1993. Periglacial environments during the Weichselian Late Glacial in the Maas valley, the Netherlands. *Geologie en Mijnbouw (Netherlands Journal of Geosciences)* 72, 193–210.
- Bokhorst, M.P., Vandenberghe, J., Sümegei, P., et al. 2011. Atmospheric circulation patterns in central and eastern Europe during the Weichselian Pleniglacial inferred from loess grain-size records. *Quaternary International* 234, 62–74.
- Boles, J.R., Clark, J.F., Leifer, I., et al. 2001. Temporal variation in natural methane seep rate due to tides, Coal Oil Point area, California. *Journal of Geophysical Research* 106, 27,077–27,086.
- Böllhofer, A., Mangini, A., Lenhard, A., et al. 2004. High-resolution ^{210}Pb dating of Lake Constance sediments: stable lead in Lake Constance. *Environmental Geology* 24, 267–274.
- Bond, G., Broecker, W., Johnsen, S., et al. 1993. Correlations between climatic records from North Atlantic sediments and Greenland ice. *Nature* 365, 143–147.
- Bond, G., Showers, W., Cheseby, M., et al. 1997. A pervasive millennial-scale cycle in North Atlantic Holocene and glacial climates. *Science* 278, 1257–1266.
- Bond, G.C., Mandeville, C., Hoffman, S. 2001a. Were rhyolitic glasses in the Vedde Ash and in the North Atlantic's Ash Zone 1 produced by the same volcanic eruption? *Quaternary Science Reviews* 20, 1189–1199.
- Bond, G., Kromer, B., Beer J., et al. 2001b. Persistent solar influence on North Atlantic climate during the Holocene. *Science* 294, 2130–2136.
- Bondevik, S., Mangerud, J. 2002. A calendar age estimate of a very late Younger Dryas ice sheet maximum in western Norway. *Quaternary Science Reviews* 21, 1661–1676.
- Bonny, A.P. 1980. Seasonal and annual variations over 5 years in contemporary airborne pollen trapped at a Cumbrian lake. *Journal of Ecology* 68, 421–441.
- Boomer, I., Wünnemann, B., Mackay, A.W., et al. 2009. Advances in understanding the late Holocene history of the Aral Sea region. *Quaternary International* 194, 79–90.
- Boomer, I., Guichard, F., Lericolais, G. 2010. Late Pleistocene to Recent ostracod assemblages from the western Black Sea. *Journal of Micropalaeontology* 29, 119–133.
- Booth, R.K. 2002. Testate amoebae as paleoindicators of surface-moisture changes on Michigan peatlands: modern ecology and hydrological calibration. *Journal of Paleolimnology* 28, 329–348.
- Booth, R.K., Jackson, S.T., Gray, C.E.D. 2004. Paleoecology and high-resolution paleohydrology of a kettle peatland in upper Michigan. *Quaternary Research* 61, 1–13.
- Booth, R.K., Notaro, M., Jackson, S.T., et al. 2006. Widespread drought episodes in the western Great Lakes region during the past 2000 years: geographic extent and potential mechanisms. *Earth and Planetary Science Letters* 242, 415–427.
- Bos, J.A.A., Bohncke, S.J.P., Jannsen, C.R. 2006. Lake-level fluctuations and small-scale vegetation patterns during the Late Glacial in the Netherlands. *Journal of Paleolimnology* 35, 211–238.
- Böse, M. 2005. The Last Glaciation and geomorphology. In *The Physical Geography of Western Europe* (edited by E.A. Koster). Oxford University Press, Oxford, 61–74.
- Boslough, M., Nicoll, K., Holliday, V., et al. 2012. Arguments and evidence against a Younger Dryas impact event. *Geophysical Monographs Series* 198, 13–26.
- Boswijk, G., Folwer, A., Lorrey, A., et al. 2006. Extension of the New Zealand kauri (*Agathis australis*) chronology to 1724 BC. *The Holocene* 16, 1–12.
- Botha, G., Porat, N. 2007. Soil chronosequence development in dunes on the southeast African coastal plain, Maputaland, South Africa. *Quaternary International* 162/163, 111–132.
- Bouchet, V.M.P., Alve, E., Rygg, B., et al. 2012. Benthic foraminifera provide a promising tool for ecological quality assessment of marine waters. *Ecological Indicators* 23, 66–75.
- Boulton, G.S. 1980. Classification of till. *Quaternary Newsletter* 31, 1–12.
- Boulton, G.S., Eyles, N. 1979. Sedimentation by valley glaciers: a model and genetic classification. In *Moraines and Varves* (edited by C. Schlüchter). Balkema, Rotterdam, 11–23.
- Boulton, G., Hagdorn, M. 2006. Glaciology of the British Isles Ice Sheet during the last glacial cycle: form, flow, streams and lobes. *Quaternary Science Reviews* 25, 3359–3390.
- Boulton, G.S., Dobbie, K.E., Zatsepin, S. 2001. Sediment deformation beneath glaciers and its coupling to the subglacial hydraulic system. *Quaternary International* 86, 3–28.
- Bourdon, B., Henderson, G.M., Lundstrom, C.C., et al. (eds). 2003. *Uranium Series Geochemistry. Reviews in Mineralogy and Geochemistry* 52, 1–656.

- Bourgeois, J.C., Koerner, R.M., Gajewski, K., et al. 2000. A Holocene ice-core pollen record from Ellesmere Island, Nunavut, Canada. *Quaternary Research* 54, 275–283.
- Bowen, D.Q. 1981. The 'South Wales End Moraine': fifty years after. In *The Quaternary in Britain* (edited by J. Neale, J. Flenley). Pergamon Press, Oxford, 60–67.
- Bowen, D.Q. 1991. Time and space in the glacial sediment systems of the British Isles. In *Glacial Deposits in Great Britain and Ireland* (edited by J. Ehlers, P.L. Gibbard, J. Rose). Balkema, Rotterdam, 3–11.
- Bowen, D.Q. 1999. On the correlation and classification of Quaternary deposits and land-sea correlations. In *A Revised Correlation of Quaternary Deposits in the British Isles* (edited by D.Q. Bowen). Geological Society of London, Special Report 23. Geological Society, Bath, 1–9.
- Bowen, D.Q., Gibbard, P.L. 2007. The Quaternary is here to stay. *Journal of Quaternary Science* 22, 3–8.
- Bowen, D.Q., Pillans, B., Sykes, G.A., et al. 1998. Amino acid geochronology of Pleistocene marine sediments in the Wanganui Basin: a New Zealand framework for correlation and dating. *Journal of the Geological Society of London* 155, 439–446.
- Bowen, D.Q., Phillips, F.M., McCabe, A.M., et al. 2002. New data for the Last Glacial Maximum in Great Britain and Ireland. *Quaternary Science Reviews* 21, 89–101.
- Bowman, S. 1990. *Radiocarbon Dating*. British Museum, London.
- Boyd, R. (ed.). 1999. *Indians, Fire and the Land*. Oregon State University Press, Corvallis, OR.
- Boyle, E.A. 2000. Is ocean thermohaline circulation linked to abrupt stadial/interstadial transitions? *Quaternary Science Reviews* 19, 255–272.
- Brace, S., Palkopoulou, E., Dalén, L., et al. 2012. Serial population extinctions in a small mammal indicate Late Pleistocene ecosystem instability. *Proceedings of the National Academy of Sciences of the United States of America* 109, 20532–20536.
- Bradley, R.S. 1999. *Paleoeclimatology. Reconstructing Climates of the Quaternary*, 2nd edn. Academic Press, London.
- Bradshaw, E.G., Rasmussen, P., Nielsen, H., et al. 2005. Mid- to late-Holocene land-use change and lake development at Dallund Sø, Denmark: trends in lake primary production as reflected by algal and macrophyte remains. *The Holocene* 15, 1130–1142.
- Bradtmiller, L.I., Anderson, R.F., Fleisher, M.Q., et al. 2006. Diatom productivity in the equatorial Pacific Ocean from the last glacial period to the present: a test of the silicic acid leakage hypothesis. *Paleoceanography* 21, PA4201, doi: 10.1029/2006PA001282.
- Bradwell, T., Stoker, M.S., Larter, R. 2007. Geomorphological signature and flow dynamics of The Minch palaeo-ice stream, NW Scotland. *Journal of Quaternary Science* 22, 609–622.
- Bradwell, T., Stoker, M.S., Golledge, N.R., et al. 2008a. The northern sector of the last British Ice Sheet: maximum extent and demise. *Earth-Science Reviews* 88, 207–226.
- Bradwell, T., Fabel, D., Stoker, M., et al. 2008b. Ice caps existed throughout the Lateglacial Interstadial in northern Scotland. *Journal of Quaternary Science*, 23, 410–407.
- Bradwell, T., Stoker, M.S., Krabbendam, M. 2008c. Megagrooves and streamlined bedrock in NW Scotland: the role of ice streams in landscape evolution. *Geomorphology* 97, 135–156.
- Brand, U., McCarthy, F.M.G. 2005. The Allerød–Younger Dryas–Holocene sequence in the west-central Champlain Sea, eastern Ontario: a record of glacial, oceanographic, and climatic changes. *Quaternary Science Reviews* 24, 1463–1478.
- Brauer, A., Casanova, J. 2001. Chronology and depositional processes of the laminated sediment record from Lac d'Annecy, French Alps. *Journal of Paleolimnology* 25, 163–177.
- Brauer, A., Negendank, J.F.W. (eds). 2004. High resolution lake sediment records in climate and environment variability studies: European lake drilling program. *Quaternary Proceedings* 122, 1–133.
- Brauer, A., Endres, C., Gunter, C., et al. 1999. High resolution and sediment and vegetation responses to Younger Dryas climate change in varved lake sediments from Meerfelder Maar, Germany. *Quaternary Science Reviews* 18, 321–329.
- Brauer, A., Allen, J.R.M., Mingram, J., et al. 2007. Evidence for last interglacial chronology and environmental change from Southern Europe. *Proceedings of the National Academy of Sciences of the United States of America* 104, 450–455.
- Brauer, A., Haug, G.H., Dulski, P., et al. 2008. An abrupt wind shift in western Europe at the onset of the Younger Dryas cold period. *Nature Geoscience* 1, 520–523.
- Braun, H., Christl, M., Rahmstorf, S., et al. 2005. Possible solar origin of the 1470-year glacial climate cycle demonstrated in a coupled model. *Nature* 438, 208–211.
- Bray, P.J., Blockley, S.P.E., Coope, G.R., et al. 2006. Refining mutual climatic range (MCR) quantitative estimates of palaeotemperature using ubiquity analysis. *Quaternary Science Reviews* 25, 1865–1876.
- Brazier, V., Kirkbride, M., Owens, I. 1998. The relationship between climate and rock glacier distribution in the Ben Ohau Range, New Zealand. *Geografiska Annaler* 80, 193–207.
- Breemer, C.W., Clark, P.U., Haggerty, R. 2002. Modeling the subglacial hydrology of the late Pleistocene Lake Michigan Lobe, Laurentide Ice Sheet. *Geological Society of America Bulletin* 114, 665–674.
- Breitenlechner, E., Hilber, M., Lutz, J., et al. 2010. The impact of mining activities on the environment reflected by pollen, charcoal and geochemical analyses. *Journal of Archaeological Science* 37, 1458–1467.
- Bridgland, D.R. (ed.). 1994. *Quaternary of the Thames*. Chapman and Hall, London.
- Bridgland, D.R. 2000. River terrace systems in northwest Europe: an archive of environmental change, uplift and early human occupation. *Quaternary Science Reviews* 19, 1293–1303.
- Bridgland, D.R. 2006. The Middle and Upper Pleistocene sequence in the Lower Thames: a record of Milankovitch climate fluctuation and early human occupation of southern Britain. *Proceedings of the Geologists' Association* 117, 281–305.
- Bridgland, D.R. 2010. The record from British Quaternary river systems within the context of global fluvial archives. *Journal of Quaternary Science* 25, 433–446.
- Bridgland, D.R., Westaway, R. 2008a. Climatically controlled river terrace staircases: a worldwide Quaternary phenomenon. *Geomorphology* 98, 285–315.

- Bridgland, D.R., Westaway, R. 2008b. Preservation patterns of Late Cenozoic fluvial deposits and their implications: results from IGCP 449. *Quaternary International* 189, 5–38.
- Bridgland, D.R., Schreve, D.C. 2009. Implications of new Quaternary uplift models for correlation between the Middle and Upper Thames terrace sequences, UK. *Global and Planetary Change* 68, 346–356.
- Bridgland, D.R., Schreve, D.C., Keen, D.H., et al. 2004. Biostratigraphical correlation between the late Quaternary sequence of the Thames and key fluvial localities in central Germany. *Proceedings of the Geologists' Association* 115, 125–140.
- Bridgland, D.R., Harding, P., Allen, P., et al. 2013. An enhanced record of MIS 9 environments, geochronology and geoarchaeology: data from the construction of the High Speed 1 (London–Channel Tunnel) rail-link and other recent investigations at Purfleet, Essex, UK. *Proceedings of the Geologists' Association* 124, 417–476.
- Briffa, K.R. 2000. Annual climatic variability in the Holocene: interpreting the message of ancient trees. *Quaternary Science Reviews* 19, 87–105.
- Briggs, D.E.G. 2003. The role of decay and mineralization in the preservation of soft-bodied fossils. *Annual Review of Earth and Planetary Science* 31, 275–301.
- Briggs, D.J., Gilbertson, D.D., Harris, A.L. 1990. Molluscan taphonomy in a braided river environment and its implications for studies of Quaternary cold-stage river deposits. *Journal of Biogeography* 17, 623–637.
- Bright, J., Kaufman, D.S., Forester, R.M., et al. 2006. A continuous 250,000 yr record of oxygen and carbon isotopes in ostracode and bulk-sediment carbonate from Bear Lake, Utah–Idaho. *Quaternary Science Reviews* 25, 2258–2270.
- Briner, J.P. 2007. Supporting evidence from the New York drumlin field that elongate subglacial bedforms indicate fast ice flow. *Boreas* 36, 143–147.
- Briner, J.P., Young, N.E., Goehring, B., et al. 2012. Constraining Holocene ^{10}Be production rates in Greenland. *Journal of Quaternary Science* 27, 2–6.
- Brocklehurst, S.H. 2010. Tectonics and geomorphology. *Progress in Physical Geography* 34, 357–383.
- Brodersen, K.P., Quinlan, R. 2006. Midges as palaeoindicators of lake productivity, eutrophication and hypolimnetic oxygen. *Quaternary Science Reviews* 25, 1995–2012.
- Brodzikowski, K., Van Loon, A.J. 1987. A systematic classification of glacial and periglacial environments, facies and deposits. *Earth-Science Reviews* 24, 297–381.
- Broecker, W.S. 1998. Paleocean circulation during the last deglaciation: a bipolar seesaw? *Paleoceanography* 13, 119–121.
- Broecker, W.S. 2000. Was a change in thermohaline circulation responsible for the Little Ice Age? *Proceedings of the National Academy of Sciences of the United States of America* 97, 1339–1342.
- Broecker W.S., Denton, G.H. 1989. The role of ocean-atmosphere reorganizations in glacial cycles. *Geochimica et Cosmochimica Acta* 53, 2465–2501.
- Broecker, W.S., Denton, G.H. 1990. What drives glacial cycles? *Scientific American* 262, 42–50.
- Broecker, W.S., Hemming, S. 2001. Climate swings come into focus. *Science* 294, 2308–2309.
- Broecker, W.S., Bond, G., Klas, M.A. 1990. A salt oscillator in the glacial Atlantic? 1. The concept. *Paleoceanography* 5, 469–77.
- Broecker, W.S., Denton, G.H., Edwards, R.L., et al. 2010. Putting the Younger Dryas cold event into context. *Quaternary Science Reviews* 29, 1078–1081.
- Bromham, L., Penny, D. 2003. The modern molecular clock. *Nature Reviews Genetics* 4, 216–224.
- Bronger, A. 2003. Correlation of loess–paleosol sequences in East and Central Asia with SE Central Europe: towards a continental Quaternary pedostratigraphy and paleoclimatic history. *Quaternary International* 106/107, 11–32.
- Bronger, A., Winter, R., Sedov, S. 1998. Weathering and clay mineral formation of two Holocene soils and of buried paleosols in Tajikistan: towards a Quaternary climatic record in Central Asia. *Catena* 34, 19–36.
- Bronk Ramsey, C. 2008. Depositional models for chronological records. *Quaternary Science Reviews* 27, 42–60.
- Bronk Ramsey, C., Staff, R.A., Bryant, C.L., et al. 2012. A complete terrestrial radiocarbon record for 11.2 to 52.8 kyr BP. *Science* 338, 370–374.
- Brook, E.J., White, J.W.C., Schilla, A.S.M., et al. 2005. Timing of millennial-scale climate change at Siple Dome, West Antarctica, during the last glacial period. *Quaternary Science Reviews* 24, 1333–1343.
- Brook, M.S., Williams, J. 2012. A relict pronival (protalus) rampart in the Tararua Range, North Island, New Zealand. *Permafrost and Periglacial Processes* 24, 67–74.
- Brookes, L.A. 1993. Geomorphology and Quaternary geology of the Dakhla Oasis region, Egypt. *Quaternary Science Reviews* 9, 273–280.
- Brookes, L.A. 2003. Geomorphic indicators of Holocene winds in Egypt's Western Desert. *Geomorphology* 56, 155–166.
- Brookhaven, B., Fleitmann, D., Nishiizumi, K., et al. 2006. Holocene monsoonal dynamics and fluvial terrace formation in the northwest Himalaya, India. *Geology* 34, 60–1604.
- Brooks, A.J., Bradley, S.L., Edwards, R.J., et al. 2007a. Postglacial relative sea-level observations from Ireland and their role in glacial rebound modelling. *Journal of Quaternary Science* 23, 175–192.
- Brooks, A.S., Hare, P.E., Kokis, J.E., et al. 1990. Dating Pleistocene archaeological sites by protein diagenesis in ostrich eggshell. *Science* 248, 60–64.
- Brooks, S.J. 2006. Fossil midges (Diptera: Chironomidae) as palaeoclimatic indicators for the Eurasian region. *Quaternary Science Reviews* 25, 1894–1910.
- Brooks, S.J., Birks, H.J.B. 2000. Chironomid-inferred Late-glacial air temperatures at Whitrig Bog, southeast Scotland. *Journal of Quaternary Science* 15, 759–764.
- Brooks, S.J., Langdon, P.G., Heiri, O. 2007b. *The Identification and Use of Palearctic Chironomidae Larvae in Palaeoecology*. Technical Guide 10. Quaternary Research Association, London.
- Brooks, S.J., Matthews, I.P., Birks, H.H., et al. 2012. High resolution Lateglacial and early-Holocene summer air temperature

- records from Scotland inferred from chironomid assemblages. *Quaternary Science Reviews* 41, 67–82.
- Brown, A.G., Carpenter, R.G., Walling, D.E. 2007a. Monitoring fluvial pollen transport, its relationship to catchment vegetation and implications for palaeoenvironmental studies. *Review of Palaeobotany and Palynology* 147, 60–76.
- Brown, D.M., Baillie, M.G.L. 1992. Construction and dating of a 5000-year English bog oak tree-ring chronology. *Lundqua Report* 34, 72–75.
- Brown, E.T., Johnson, T.C., Scholz, C.A., et al. 2007b. Abrupt change in tropical African climate linked to the bipolar seesaw over the past 55,000 years. *Geophysical Research Letters* 34, doi: 10.1029/2007GL031240.
- Browne, G.H., Naish, T.R. 2003. Facies development and sequence architecture of a late Quaternary fluvial–marine transition, Canterbury Plains and shelf, New Zealand: implications for forced regressive deposits. *Sedimentary Geology* 158, 57–86.
- Brugal, J.-P., Croitor, R. 2007. Evolution, ecology and biochronology of herbivore associations in Europe during the last 3 million years. *Quaternaire* 18, 129–151.
- Buck, C.E., Blackwell, P.G. 2004. Formal statistical models for estimating radiocarbon calibration curves. *Radiocarbon* 46, 1093–1102.
- Buckland, P.C., Edwards, K.J., Panagiotakopulu, E., et al. 2009. Palaeoecological and historical evidence for manuring and irrigation at Garðar (Igaliku), Norse Eastern Settlement, Greenland. *The Holocene* 19, 105–116.
- Buckland, P.I., Buckland, P.C. 2006. Bugs coleopteran ecology package, v7.63, <http://www.bugscep.com>.
- Buiron, D., Chapellaz, J., Stenni, B., et al. 2011. TALDICE-1 age scale of the Talos Dome deep ice core, East Antarctica. *Climate of the Past* 7, 1–16.
- Bull, W.B. 2003. Lichenometry dating of coseismic changes to a New Zealand landslide complex. *Annals of Geophysics* 46, 1155–1167.
- Bullard, J. 2010. Bridging the gap between field data and global models: current strategies in aeolian research. *Earth Surface Processes and Landforms* 35, 496–499.
- Bunch, T.E., Hermes, R.E., Moore, A.M.T., et al. 2012. Very high-temperature impact melt products as evidence for cosmic airbursts and impacts 12,900 years ago. *Proceedings of the National Academy of Sciences of the United States of America* 109, doi: 10.1073/pnas.1204453109.
- Büntgen, U., Frank, D.C., Nievergelt, D., et al. 2006. Summer temperature variations in the European Alps, AD 755–2004. *Journal of Climate* 19, 5606–5623.
- Burbank, D.W., Blythe, A.E., Putkonen, J., et al. 2003. Decoupling of erosion and precipitation in the Himalayas. *Nature* 426, 652–655.
- Burckle, L. 1998. Marine diatoms. In *Introduction to Marine Micropaleontology* (edited by B.U. Haq, A. Boersma). Elsevier, Amsterdam, 245–266.
- Burney, D.A., Burney, L.P., Godfrey, L.R., et al. 2004. A chronology for late prehistoric Madagascar. *Journal of Human Evolution* 47, 25–63.
- Burns, S.J., Fleitmann, D., Matter, A., et al. 2001. Speleothem evidence from Oman for continental pluvial events during interglacial periods. *Geology* 29, 623–626.
- Burrough, S.L., Thomas, D.S.G., Baillie, R.M. 2009. Mega-Lake in the Kalahari: A Late Pleistocene record of the Palaeolake Makgadikgadi system. *Quaternary Science Reviews* 28, 1392–1411.
- Busschers, F.S., Kasse, C., van Balen, R.T., et al. 2007. Late Pleistocene evolution of the Rhine–Meuse system in the southern North Sea basin: imprints of climate change, sea-level oscillation and glacio-isostacy. *Quaternary Science Reviews* 26, 3216–3248.
- Butler, P.G., Wanamaker, A.D., Scourse, J.D., et al. 2013. Variability of marine climate on the North Icelandic Shelf in a 1357-year proxy archive based on growth increments in the bivalve *Arctica islandica*. *Palaeogeography, Palaeoclimatology, Palaeoecology* 373, 141–151.
- Cacho, I., Grimalt, J.O., Pelerejo, C., et al. 1999. Dansgaard–Oeschger and Heinrich event imprints in Alboran Sea paleotemperatures. *Paleoceanography* 14, 698–705.
- Cacho, I., Grimalt, J.O., Sierro, F.J., et al. 2000. Evidence for enhanced Mediterranean thermohaline circulation during rapid climatic coolings. *Earth and Planetary Science Letters* 183, 417–420.
- Callendar, G. 1938. The artificial production of carbon dioxide and its influence on temperature. *Quarterly Journal of the Royal Meteorological Society* 64, 223–240.
- Callendar, G. 1961. Temperature fluctuations and trends over the earth. *Quarterly Journal of the Royal Meteorological Society* 87, 1–12.
- Calvo, E., Pelejero, C., De Deckker, P., et al. 2007. Antarctic deglacial pattern in a 30 kyr record of sea surface temperature offshore South Australia. *Geophysical Research Letters* 34, doi: 10.1029/2007GL029937.
- Cameron, R. 2003. *Land Snails in the British Isles*. FSC Publications, Preston Montford.
- Campbell, I.D. 1999. Quaternary pollen taphonomy: examples of differential redeposition and differential preservation. *Palaeogeography, Palaeoclimatology, Palaeoecology* 149, 245–256.
- Camoin, G.F., Ebren, Ph., Eisenhauer, A., et al. 2001. A 300,000-yr coral reef record of sea level changes, Mururoa atoll (Tuamotu archipelago, French Polynesia). *Palaeogeography, Palaeoclimatology, Palaeoecology* 175, 325–341.
- Camoin, G.F., Montaggioni, L.F., Braithwaite, C.J.R. 2004. Late glacial to post glacial sea levels in the Western Indian Ocean. *Marine Geology* 206, 119–146.
- Camoin, G.F., Seard, C., Deschamps, P. et al. 2012. Reef response to sea-level and environmental changes during the last deglaciation: Integrated Ocean Drilling Program Expedition 310, Tahiti Sea Level. *Geology* 40, 643–646.
- Cande, S.C., Kent, D.V. 1995. Revised calibration of the geomagnetic polarity timescale for the Late Cretaceous and Cenozoic. *Journal of Geophysical Research* 100, 6093–6095.
- Candy, I., Black, S. 2009. The timing of Quaternary calcrete development in semi-arid southeast Spain: the role of climate on calcrete genesis. *Sedimentary Geology* 218, 6–15.
- Candy, I., Black, S., Sellwood, B.W. 2005. U-series isochron dating of immature and mature calcrites as a basis for constructing Quaternary landform chronologies for the Sorbas basin, southeast Spain. *Quaternary Research* 64, 100–111.

- Candy, I., Coope, G.R., Lee, J.R., et al. 2010. Pronounced warmth during early Middle Pleistocene interglacials: investigating the Mid-Brunhes Event in the British terrestrial sequence. *Earth-Science Reviews* 103, 183–196.
- Cane, M.A. 2004. The evolution of El Niño, past and future. *Earth and Planetary Science Letters* 164, 1–10.
- Cane, A., Molnar, P. 2001. Closing of the Indonesian seaway as a precursor to East African aridification around 3–4 million years ago. *Nature* 411, 157–162.
- Cane, T., Rohling, E.J., Kemp, A.E.S., et al. 2002. High-resolution stratigraphic framework for Mediterranean sapropel S5: defining temporal relationships between records of Eemian climate variability. *Palaeogeography, Palaeoclimatology, Palaeoecology* 87–101.
- Cannariato, K.G., Kennett, J.P., Behl, R.J. 1999. Biotic response to late Quaternary rapid climate switches in Santa Barbara Basin: ecological and evolutionary implications. *Geology* 27, 63–66.
- Canti, M.G. 1998. The micromorphological identification of faecal spherulites from archaeological and modern materials. *Journal of Archaeological Science* 25, 435–444.
- Cao, L., Fairbanks, R.G., Mortlock, R.A., et al. 2007. Radiocarbon reservoir age of high latitude North Atlantic surface water during the last deglacial. *Quaternary Science Reviews* 26, 732–742.
- CAPE-Last Interglacial Project Members. 2006. Last Interglacial Arctic warmth confirms polar amplification of climate change. *Quaternary Science Reviews* 25, 1383–1400.
- Capotondi, L., Borsetti, A.M., Morigli, C. 1999. Foraminiferal ecozones, a high resolution proxy for the late Quaternary biochronology of the central Mediterranean Sea. *Marine Geology* 153, 253–274.
- Capron, E., Landais, A., Lemieux-Dudon, B., et al. 2010a. Synchronising EDML and NorthGRIP ice cores using $\delta^{18}\text{O}$ of atmospheric oxygen ($\delta^{18}\text{O}_{\text{atm}}$) and CH_4 measurements over MIS5 (80–123 kyr). *Quaternary Science Reviews* 29, 222–234.
- Capron, E., Landais, A., Chappellaz, J., et al. 2010b. Millennial and sub-millennial scale climatic variations recorded in polar ice cores over the last glacial period. *Climate of the Past* 6, 345–365.
- Carbone, M.G., Bergamin, L., Di Bella, L. 2010. Palaeoenvironmental reconstruction of late Quaternary foraminifera and molluscs from the ENEA borehole (Versilian plain, Tuscany, Italy). *Quaternary Research* 74, 265–276.
- Carew, J.L., Mylroie, J.E. 1995. Quaternary tectonic stability of the Bahamian Archipelago: evidence from fossil coral reefs and flank margin caves. *Quaternary Science Reviews* 14, 145–154.
- Carlquist, S.J. 2001. *Comparative Wood Anatomy: Systematic, Ecological and Evolutionary Aspects of Dicotyledon Wood*. Springer, Berlin.
- Carr, S.J. 2004. The North Sea basin. In *Developments in Quaternary Science. Volume 2: Quaternary Glaciations: Extent and Chronology* (edited by J. Ehlers, P.L. Gibbard). Elsevier, Amsterdam, 261–270.
- Carr, S.J., Rose, J. 2003. Till fabric patterns and significance: particle response to subglacial stress. *Quaternary Science Reviews* 22, 1415–1426.
- Carr, S.J., Coleman, C. 2007. An improved technique for the reconstruction of former glacier mass-balance and dynamics. *Geomorphology* 92, 76–90.
- Carr, S.J., Holmes, R., van der Meer, J.J.M., Rose, J. 2006. The Last Glacial Maximum in the North Sea Basin: micromorphological evidence of extensive glaciation. *Journal of Quaternary Science* 21, 131–153.
- Carr, A.S., Bateman, M.D., Roberts, D.L., et al. 2010. The last interglacial sea-level high stand on the southern Cape coastline of South Africa. *Quaternary Research* 73, 351–363.
- Carré, M., Bentaleb, I., Fontugne, M., et al. 2005. Strong El Niño events during the early Holocene: stable isotope evidence from Peruvian sea shells. *The Holocene* 15, 42–47.
- Carrión, J.S., Mumuera, M., Navarro, C., et al. 1999. The palaeo-ecological potential of pollen records in caves: the case of Mediterranean Spain. *Quaternary Science Reviews* 18, 1061–1073.
- Carter, L., Neil, H.L., McCave, I.N. 2000. Glacial to interglacial changes in non-carbonate and carbonate accumulation in the SW Pacific Ocean, New Zealand. *Palaeogeography, Palaeoclimatology, Palaeoecology* 162, 333–356.
- Carter, R.W.G. 1992. Sea-level changes: past, present and future. In *The Applications of Quaternary Research* (edited by J.M. Gray). Quaternary Proceedings 2, Quaternary Research Association, Cambridge, 111–130.
- Carter, S.P. 1990. The stratification and taphonomy of shells in calcareous soils: implications for land snails analysis in archaeology. *Journal of Archaeological Science* 17, 495–507.
- Casana, J. 2008. Mediterranean valleys revisited: linking soil erosion, land use and climate variability in the Northern Levant. *Geomorphology* 101, 429–442.
- Catani, F., Farina, P., Moretti, S., et al. 2004. On the application of SAR interferometry to geomorphological studies: estimation of landform attributes and mass movements. *Geomorphology* 66, 119–131.
- Cato, I. 1985. The definitive correction of the Swedish geochronological time scale with the present, and the new date of the zero year in Döviken, northern Sweden. *Boreas* 14, 117–122.
- Cattaneo, A., Couillard, Y., Wunsam, S., et al. 2004. Diatom taxonomic and morphological changes as indicators of metal pollution and recovery on Lac Dufault (Québec, Canada). *Journal of Paleolimnology* 32, 163–175.
- Catto, N.R. 1990. Clast fabric of diamictites associated with some roches moutonnées. *Boreas* 19, 289–296.
- Catto, N.R. 1998. Comparative study of striations and basal till clast fabrics, Malpeque-Bedique region Prince Edward Island, Canada. *Boreas* 27, 259–274.
- Cellot, B., Mouillet, F., Henry, C.P. 1998. Flood drift and propagule bank of aquatic macrophytes in a riverine wetland. *Journal of Vegetation Science* 9, 631–640.
- Chambers, D.P. 2006. Observing seasonal steric sea level variations with GRACE and satellite altimetry. *Journal of Geophysical Research* 111, doi: 10.1029/2005JC002914.
- Chambers, F.M. 2002. The environmental applications of pollen analysis. In *Quaternary Environmental Micropalaeontology* (edited by S.K. Haslett). Arnold, Oxford and New York, 241–258.
- Chambers, F.M., Blackford, J.J. 2001. Mid- and Late-Holocene climatic change: a test of periodicity and solar forcing in proxy-climate data from blanket peat bogs. *Journal of Quaternary Science* 16, 329–338.

- Chambers, F.M., Barber, K.E., Maddy, D., Brew, J., 1997. A 5500-year proxy-climate and vegetation record from blanket mire at Talla Moss, Borders, Scotland. *The Holocene* 7, 391–399.
- Chambers, F.M., Mauquoy, D., Brain, S.A., et al. 2007. Globally synchronous climate change 2800 years ago: proxy data from peat in South America. *Earth and Planetary Science Letters* 253, 439–444.
- Chambers, F.M., Beilman, D.W., Yu, Z. 2011. Methods for determining peat humification and for quantifying peat bulk density, organic matter and carbon content for palaeostudies of climate and peatland carbon dynamics. *Mires and Peat* 7(art. 7), 1–10.
- Chambers, F.M., Booth, R.K., De Vleeschouwer, F., et al. 2012. Development and refinement of proxy-climate indicators from peats. *Quaternary International* 268, 21–33.
- Chang, F., Li, T., Zhuang, L., Yan, J. 2008a. A Holocene paleotemperature record based on radiolaria from the northern Okinawa Trough (East China Sea). *Quaternary International* 183, 115–122.
- Chang, P., Zhang, R., Hazeleger, W., et al. 2008b. Oceanic link between abrupt changes in the North Atlantic Ocean and the African monsoon. *Nature Geoscience* 1, 444–448.
- Chappell, J. 2002. Sea level changes forced ice breakouts in the Last Glacial cycle: new results from coral terraces. *Quaternary Science Reviews* 21, 1229–1240.
- Charman, D.J. 2001. Biostratigraphic and palaeoenvironmental applications of testate amoebae. *Quaternary Science Reviews* 20, 1753–1764.
- Charman, D. 2004. *Peatlands and Environmental Change*. John Wiley, Chichester and New York.
- Charman, D.J., Hendon, D., Packman, S. 1999. Multiproxy surface wetness records from replicate cores on an ombrotrophic mire: implications for Holocene palaeoclimate records. *Journal of Quaternary Science* 14, 451–463.
- Charman, D.J., Hendon, D., Woodland, W.A. 2000. *The Identification of Testate Amoebae (Protozoa: Rhizopoda) in Peats*. Technical Guide 9. Quaternary Research Association, London.
- Charman, D.J., Bludell, A., Chiverrell, R.C., et al. 2006. Compilation of non-annually resolved Holocene proxy climate records: stacked Holocene peatland palaeo-water table reconstructions from northern Britain. *Quaternary Science Reviews* 25, 336–350.
- Charman, D., Barber, K.E., Blaauw, M., et al. 2009. Climate drivers for peatland palaeoclimate records. *Quaternary Science Reviews* 28, 1811–1819.
- Charman, D.J., Gehrels, W.R., Manning, C., et al. 2010. Reconstruction of recent sea-level change using testate amoebae. *Quaternary Research* 73, 208–219.
- Cheetham, P. 2005. Forensic geophysical survey. In *Forensic Archaeology: Advances in Theory and Practice* (edited by J. Hunter, M. Cox). Routledge, Abingdon and New York.
- Chen, F., Cheng, B., Zhao, Y., et al. 2006. Holocene environmental change inferred from a high-resolution pollen record, Lake Zhuyeze, arid China. *The Holocene* 16, 675–684.
- Chen, F., Yu, Z., Yang, M., et al. 2008. Holocene moisture evolution in arid central Asia and its out-of-phase relationship with Asian monsoon history. *Quaternary Science Reviews* 27, 351–364.
- Chen, M.-T., Huang, C.-C., Pflaumann, U., et al. 2005. Estimating glacial western Pacific sea-surface temperature: methodological overview and data compilation of surface sediment planktic foraminifer faunas. *Quaternary Science Reviews* 24, 1049–1062.
- Cheng, H., Ewards, R.L., Broecker, W.S., et al. 2009. Ice age terminations. *Science* 326, 248–252.
- Chepalyga, A.L. 2007. The late-glacial Great Flood in the Ponto-Caspian Basin. In *The Black Sea Flood Question* (edited by V. Yanko-Hombach, A.S. Gilbert, N. Panin, et al.). Springer, Dordrecht, 119–148.
- Chernyshev, I.V., Lebedev, V.A., Arakelyants, M.M. 2006. K-Ar dating of Quaternary volcanics: methodology and interpretation of results. *Petrology* 14, 1556–2085.
- Chiverrell, R.C., 2001. A proxy record of late Holocene climate change from May Moss, northeast England. *Journal of Quaternary Science* 16, 9–29.
- Chiverrell, R.C., Thomas, G.S.P. 2010. Extent and timing of the Last Glacial Maximum (LGM) in Britain and Ireland: a review. *Journal of Quaternary Science* 25, 535–549.
- Chiverrell, R.C., Thrasler, I.M., Thomas, G.S.P., et al. 2013. Bayesian modelling the retreat of the Irish Sea ice stream. *Journal of Quaternary Science* 28, 200–209.
- Chlachula, J. 2003. The Siberian loess record and its significance for reconstruction of Pleistocene climate change in north-central Asia. *Quaternary Science Reviews* 22, 1879–1906.
- Christiansen, H.H. 2005. Thermal regime of ice-wedge cracking in Adventdalen, Svalbard. *Permafrost and Periglacial Processes* 16, 87–98.
- Chu, G., Sun, Q., Rioual, P., et al. 2008. Dinocyst microlaminations and freshwater ‘red tides’ recorded in Lake Xiaolongwan, northeastern China. *Journal of Paleolimnology* 39, 319–333.
- Chu, G., Sun, Q., Zhaoyan, G., et al. 2009. Dust records from varved lacustrine sediments of two neighbouring lakes in northeastern China over the last 1400 years. *Quaternary International* 194, 108–118.
- Church, J.A., White, N.J., Aarup, T., et al. 2008. Understanding global sea levels: past, present and future. *Sustainability Science* 3, 9–22.
- Church, M., Ryder, J.M. 1972. Paraglacial sedimentation, a consideration of fluvial processes conditioned by glaciation. *Geological Society of America Bulletin* 83, 3059–3072.
- Chylek, P., Folland, C.K., Lesins, G., et al. 2010. Twentieth century bipolar seesaw of the Arctic and Antarctic surface air temperatures. *Geophysical Research Letters* 37, L08703, doi: 10.1029/2010GL042793.
- Ciliberto, E., Spoto, G. 2000. *Modern Analytical Methods in Art and Archaeology*. John Wiley, Chichester and New York.
- Claessens, L., Veldkamp, A., ten Broeke, E.M., et al. 2009. A Quaternary uplift record for the Auckland region, North Island, New Zealand, based on marine and fluvial terraces. *Global and Planetary Change* 68, 383–394.
- Clague, J. 2000. Recognizing order in chaotic sequences of Quaternary sediments in the Canadian Cordillera. *Quaternary International* 68–71, 29–38.
- Clague, J.J., James, T.S. 2002. History and isostatic effects of the last ice sheet in southern British Columbia. *Quaternary Science Reviews* 21, 71–87.

- Clague, J.J., Menounos, B., Osborn G., *et al.* 2009. Nomenclature and resolution in Holocene glacial chronologies. *Quaternary Science Reviews* 28, 2231–2238.
- Clark, C.D. 1997. Reconstructing the evolutionary dynamics of former ice sheets using multi-temporal evidence, remote sensing and GIS. *Quaternary Science Reviews* 16, 1067–1092.
- Clark, C.D., Evans, D.J.A., Khatwa, A., *et al.* 2004. Map and GIS database of glacial landforms and features related to the last British Ice Sheet. *Boreas* 33, 359–375.
- Clark, C.D., Hughes, A.L.C., Greenwood, S.L., *et al.* 2009b. Size and shape characteristics of drumlins, derived from a large sample, and associated scaling laws. *Quaternary Science Reviews* 28, 677–692.
- Clark, C.D., Hughes, A.L.C., Greenwood, S.L., *et al.* 2012. Pattern and timing of retreat of the last British–Irish Ice Sheet. *Quaternary Science Reviews* 44, 112–146.
- Clark, I.D., Fontes, J.-C. 1990. Palaeoclimatic reconstruction in Northern Oman based on carbonates from hypersaline groundwaters. *Quaternary Research* 33, 320–336.
- Clark, J., McCabe, A.M., Schnabel, C., *et al.* 2009a. Cosmogenic ^{10}Be chronology of the last deglaciation of western Ireland, and implications for sensitivity of the Irish Ice Sheet to climate change. *Geological Society of America Bulletin* 121, 3–16.
- Clark, P.U. 1994. Unstable behaviour of the Laurentide Ice Sheet over deforming sediment and its implications for climate change. *Quaternary Research* 41, 19–25.
- Clark, P.U., Pollard, D. 1998. Origin of the middle Pleistocene transition by ice sheet erosion of regolith. *Paleoceanography* 13, 1–9.
- Clark, P.U., Marshall, S.J., Clarke, G.K.C., *et al.* 2001. Freshwater forcing of abrupt climate change during the last glaciation. *Science* 293, 283–287.
- Clark, P.U., Pisias, N.G., Stocker, T.F., *et al.* 2002. The role of the thermohaline circulation in abrupt climate change. *Nature* 415, 863–869.
- Clark, P.U., Brook, E.J., Raisbeck, G.M., *et al.* 2003. Cosmogenic ^{10}Be ages of the Saglek Moraines, Torngat Mountains, Labrador. *Geology* 31, 617–620.
- Clark, P.U., Archer, D., Pollard, D., *et al.* 2006. The middle Pleistocene transition: characteristics, mechanisms, and implications for long-term changes in atmospheric pCO_2 . *Quaternary Science Reviews* 25, 3150–3184.
- Clarke, A.L., Weckström, K., Conley, D.J., *et al.* 2006a. Long-term trends in eutrophication and nutrients in the coastal zone. *Limnology and Oceanography* 51, 385–397.
- Clarke, J. 2003. The occurrence and significance of biogenic opal in the regolith. *Earth-Science Reviews* 60, 175–194.
- Clarke, M.J., Vogel, J.C., Botha, G.A., *et al.* 2003. Late Quaternary hillslope evolution recorded in eastern South African colluvial badlands. *Palaeogeography, Palaeoecology, Palaeoclimatology* 197, 199–212.
- Clarke, S.J., Murray-Wallace, C.V. 2006. Mathematical expressions used in amino acid racemisation geochronology – a review. *Quaternary Geochronology* 1, 261–278.
- Clarke, S.J., Miller, G.F., Fogel, M.L., *et al.* 2006b. The amino acid and stable isotope biogeochemistry of elephant bird (*Aepyornis*) eggshells from southern Madagascar. *Quaternary Science Reviews* 25, 2343–2356.
- Claussen, M. 2009. Late Quaternary vegetation–climate feedbacks. *Climate of the Past Discussions* 5, 635–670.
- Claussen, M., Mysak, L.A., Weaver, A.J., *et al.* 2002. Earth system models of intermediate complexity: closing the gap in the spectrum of climate system models. *Climate Dynamics* 18, 579–585.
- Claussen, M., Ganopolski, A., Brovkin, V., *et al.* 2003. Simulated global-scale response of the climate system to Dansgaard/Oeschger and Heinrich Events. *Climate Dynamics* 21, 361–370.
- Cleaveland, M.K. 2000. A 963-year reconstruction of summer (JJA) streamflow in the White River, Arkansas, USA, from tree-rings. *The Holocene* 10, 33–41.
- Clement, A.C., Peterson, L.C. 2008. Mechanisms of abrupt climate change of the last glacial period. *Review of Geophysics* 46, doi: 10.1029/2006RG000204.
- Clemmensen, L.B., Murray, A. 2006. The termination of the last major phase of aeolian sand movement, coastal dunefields, Denmark. *Earth Surface Processes and Landforms* 31, 795–808.
- Cléroux, C.M., Debret, M., Cortijo, E., *et al.* 2012. High-resolution sea surface temperature reconstructions off Cape Hatteras over the last 10 ka. *Paleoceanography* 27, doi: 10.1029/2011 PA002184.
- CLIMAP Project Members. 1976. The surface of ice-age earth. *Science* 191, 1131–1137.
- CLIMAP Project Members. 1981. *Seasonal reconstructions of the earth's surface at the last glacial maximum*. Geological Society of America Map and Chart Series, MC-36.
- Cline, R.M., Hays, J.D. 1976. *Investigation of Late Quaternary Paleoceanography and Paleoclimatology*. Geological Society of America Memoirs, 145.
- Clymo, R.S. and Mackay, D. 1987. Upwash and downwash of pollen and spores in the unsaturated surface layer of *Sphagnum*-dominated peat. *New Phytologist* 105, 175–183.
- Cockburn, H.A.P., Summerfield, M.A. 2004. Geomorphological applications of cosmogenic isotope analysis. *Progress in Physical Geography* 28, 1–42.
- Coe, M.T., Harrison, S.P. 2002. The water balance of northern Africa during the mid-Holocene: an evaluation of the 6 ka BP PMIP simulations. *Climate Dynamics* 19, 155–166.
- Cohen, A.C., Peterson, D.E., Maddocks, R.F. 2007. Ostracoda. In *The Light & Smith Manual: Intertidal Invertebrates from Central California to Oregon*, 4th edn (edited by J.T. Carlton). University of California Press, Berkeley and Los Angeles, 417–446.
- Cohen, A.S. 2003. *Paleolimnology: The History and Evolution of Lake Systems*. Oxford University Press, Oxford and New York.
- Cohen, K.M., Gibbard, P.L. 2011. *Global Chronostratigraphical Correlation Table for the Last 2.7 million years. V. 2011*. Sub-commission on Quaternary Stratigraphy, Cambridge, <http://www.qpg.geog.cam.ac.uk/>.
- Cohen, T.J., Nanson, G.C., Jansen, J.D., *et al.* 2011. Continental aridification and the vanishing of Australia's megalakes. *Geology* 39, 167–170.
- COHMAP Members. 1988. Climatic changes of the last 18,000 years: observations and model simulations. *Science* 241, 1043–1052.

- Colgan, P.M. 1999. Early Middle Pleistocene glacial sediments (780000–620000 BP) near Kansas City, northeastern Kansas and northwestern Missouri, USA. *Boreas* 28, 477–489.
- Colhoun, E.A., Kiernan, K.W., McConnell, A., et al. 2009. Late Pliocene age of glacial deposits at Heidemann Valley, East Antarctica: evidence for the last major glaciation in the Vestfold Hills. *Antarctic Science* 2009, doi: 10.1017/S0954.
- Colinvaux, P., de Oliveira, P.E., Moreno Patino, J.E. 1999. *Amazon Pollen Manual and Atlas*. Harwood Academic Publishers, Amsterdam.
- Collins, M.J., Gernaey, A.M., Nielsen-March, C.M., et al. 2000. Slow rates of degradation of osteocalcin: green light for fossil bone protein? *Geology* 28, 1139–1142.
- Collins, M.J., Penkman, K.E.H., Rohland, N., et al. 2009. Is amino acid racemization a useful tool for screening for ancient DNA? *Proceedings of the Royal Society B* 276, 2971–2977.
- Colman, S.M., Kaufman, D.S., Bright, J., et al. 2006. Age model for a continuous, ca 250-ka Quaternary lacustrine record from Bear Lake, Utah–Idaho. *Quaternary Science Reviews* 25, 2271–2282.
- Colmenero-Hidalgo, E., Flores, J.-A., Sierra, F.J., et al. 2004. Ocean surface water response to short-term climate changes revealed by coccolithophores from the Gulf of Cadiz (NE Atlantic) and Alboran Sea (W Mediterranean). *Palaeogeography, Palaeoclimatology, Palaeoecology* 205, 317–336.
- Colonese A.C., Mannino, M.A., Bar-Yosef, D.E., et al. 2011. Marine mollusc exploitation in Mediterranean prehistory: an overview. *Quaternary International* 239, 86–103.
- Conway, H., Hall, B.L., Denton, G.H., et al. 1999. Past and future grounding-line retreat of the West Antarctic Ice Sheet. *Science* 286, 280–283.
- Cook, E.R., Buckley, B.M., Palmer, J.G., et al. 2006. Millennia-long tree-ring records from Tasmania and New Zealand: a basis for modelling climate variability and forcing, past, present and future. *Journal of Quaternary Science* 21, 689–699.
- Coope, G.R. 1959. A late Pleistocene insect fauna from Chelford. *Proceedings of the Royal Society B* 151, 70–86.
- Coope, G.R. 1967. The value of Quaternary insect faunas in the interpretation of ancient ecology and climate. In *Quaternary Palaeoecology* (edited by E.J. Cushing, H.E. Wright Jr.). Yale University Press, New Haven, 359–380.
- Coope, G.R. 1977. Fossil coleopteran assemblages as sensitive indicators of climatic changes during the Devensian (last) cold stage. *Philosophical Transactions of the Royal Society of London B* 280, 313–340.
- Coope, G.R. 1987. The response of Late Quaternary insect communities to sudden climatic changes. In *Organization of Communities, Past and Present* (edited by J.H.R. Gee, P.S. Miller). Blackwell, Oxford and Boston, 421–438.
- Coope, G.R. 1990. The invasion of Northern Europe during the Pleistocene by Mediterranean species of Coleoptera. In *Biological Invasions in Europe and the Mediterranean Basin* (edited by F. di Castri, A. Hansen, M. Debussche). Kluwer, Dordrecht, 203–215.
- Coope, G.R. 2000. The climatic significance of coleopteran assemblages from the Eemian deposits in southern England. *Geologie en Mijnbouw (Netherlands Journal of Geosciences)* 79, 257–268.
- Coope, G.R. 2004. Several million years of stability among insect species because of, or in spite of, ice age climatic instability? *Philosophical Transactions of the Royal Society of London B* 359, 209–214.
- Coope, G.R. 2010. Coleopteran faunas as indicators of interglacial climates in central and southern England. *Quaternary Science Reviews* 29, 1507–1514.
- Coope, G.R., Brophy, J.A. 1972. Late Glacial environmental changes indicated by a coleopteran succession from North Wales. *Boreas* 1, 97–142.
- Coope, G.R., Lemdahl, G. 1995. Regional differences in the Lateglacial climate of northern Europe based on coleopteran analysis. *Journal of Quaternary Science* 10, 391–395.
- Coope, G.R., Lemdahl, G., Lowe, J.J., et al. 1998. Temperature gradients in Northern Europe during the Last Glacial–Interglacial Transition (14–9 ^{14}C ka BP) interpreted from coleopteran assemblages. *Journal of Quaternary Science* 13, 419–433.
- Corrège, T. 2006. Sea surface temperature and salinity reconstruction from coral geochemical tracers. *Palaeogeography, Palaeoclimatology, Palaeoecology* 232, 408–428.
- Cortijo, E., Labeyrie, L., Elliot, M., et al. 2000. Rapid climatic variability of the North Atlantic Ocean and global climate: a focus of the IMAGES program. *Quaternary Science Reviews* 19, 227–241.
- Covey, C., AchutaRao, K.M., Cubasch, U., et al. 2003. An overview of results from the Coupled Model Intercomparison Project. *Global and Planetary Change* 37, 103–133.
- Craddock, R.A., Hutchinson, M.F., Stein, J.A. 2010. Topographic data reveal a buried fluvial landscape in the Simpson Desert, Australia. *Australian Journal of Earth Sciences* 57, doi: 10.180/0812009 0903416278.
- Craw, D., Burridge, C., Anderson, L., et al. 2007. Late Quaternary river drainage and fish evolution, Southland, New Zealand. *Geomorphology* 84, 98–110.
- Craw, D., Burridge, C., Norris, R., et al. 2008. Genetic ages for Quaternary topographic evolution: a new dating tool. *Geology* 36, 19–22.
- Croitor, R., Brigal, J.-P. 2010. Ecological and evolutionary dynamics of the carnivore community in Europe during the last 3 million years. *Quaternary International* 212, 98–108.
- Cronin, T. 2009. *Paleoclimates: Understanding Climate Change Past and Present*. Columbia University Press, New York.
- Crowley T.J., Lowery, T.S. 2000. How warm was the Medieval Warm Period? *AMBIO: A Journal of the Human Environment* 29, 51–54.
- Crutzen, P.J. 2002. The geology of mankind. *Nature* 415, 23.
- Crutzen, P.J., Stoermer, E.F. 2000. The Anthropocene. *Global Change Newsletter* 41, 17–18.
- Cuenca-Bescós, G., Rofes, J., López-García, J.M., et al. 2010. Biochronology of Spanish Quaternary small vertebrate faunas. *Quaternary International* 212, 109–119.
- Cugny, C., Mazier, F., Galop, D. 2010. Modern and fossil non-pollen palynomorphs from the Basque mountains (western Pyrenees, France): the use of coprophilous fungi to reconstruct pastoral activity. *Vegetation History and Archaeobotany* 19, 391–408.

- Cullingford, R.A., Smith, D.E. 1966. Late-glacial shorelines in eastern Fife. *Transactions of the Institute of British Geographers* 39, 31–51.
- Cullingford, R.A., Caseldine, C.J., Gotts, P.E. 1980. Early Flandrian land and sea-level changes in Lower Strathearn. *Nature* 284, 159–161.
- Cummins, R.H. 1994. Taphonomic processes in modern freshwater molluscan death assemblages: implications for the freshwater fossil record. *Palaeogeography, Palaeoclimatology, Palaeoecology* 108, 55–73.
- Currrant, A.P., Jacobi, R. 2011. The mammal faunas of the British Late Pleistocene. In *The Ancient Human Occupation of Britain* (edited by N. Ashton, S.G. Lewis, C. Stringer). Elsevier, Amsterdam, 165–180.
- Curry, A.M., Cleasby, V., Zokowskyj, P. 2006. Paraglacial response of steep, sediment-mantled slopes to post-'Little Ice Age' glacier recession in the central Swiss Alps. *Journal of Quaternary Science* 21, 211–225.
- Curry, A.M., Porter, P.R., Irvine-Fynn, T.D.L., et al. 2009. Quantitative particle size, microtextural and outline shape analyses of glaciogenic sediment reworked by paraglacial debris flows. *Earth Surface Processes and Landforms* 34, 48–62.
- Curry, B.B., Baker, R.G. 2000. Palaeohydrology, vegetation, and climate since the late Illinois Episode (~130 ka) in south-central Illinois. *Palaeogeography, Palaeoclimatology, Palaeoecology* 155, 59–81.
- Curry, B.B., Grimley, D.A., McKay III, E.D. 2011. Quaternary glaciations in Illinois. In *Developments in Quaternary Science. Volume 15: Quaternary Glaciations – Extent and Chronology: A Closer Look* (edited by J. Ehlers, P.L. Gibbard, P.D. Hughes). Elsevier, Amsterdam, 467–488.
- Cushing, E.J. 1967. Late Wisconsin pollen stratigraphy and the glacial sequence in Minnesota. In *Quaternary Palaeoecology* (edited by E.J. Cushing, H.E. Wright Jr.). Yale University Press, New Haven, 59–88.
- Cutler, P.M., Mickelson, D.M., Colgan, P.M., et al. 2000. A numerical investigation of ice-lobe–permafrost interaction around the southern Laurentide ice sheet. *Journal of Glaciology* 46, 311–325.
- Cutler, P.M., MacAyeal, D.R., Mickelson, D.M., et al. 2001. Influence of the Great Lakes on the dynamics of the southern Laurentide ice sheet: numerical experiments. *Geology* 29, 1039–1042.
- Cuttelod, A., Seddon, M., Neubert, E. 2011. *European Red List of Non-marine Molluscs*. Publications Office of the European Union, Luxembourg.
- Dahl, S.O., Nesje, A. Lie , Ø., et al. 2002. Timing, equilibrium-line altitudes and climatic implications of two early-Holocene glacier advances during the Erdalen Event at Jostedalsbreen, western Norway. *The Holocene* 12, 17–25.
- Dahl-Jensen, D., Mosegaard, K., Gundestrup, N., et al. 1998. Past temperatures directly from the Greenland ice sheet. *Science* 282, 268–271.
- Dahl-Jensen, D., Gundestrup, N., Gogineni, S.P., et al. 2003. Basal melt at NorthGRIP modeled from borehole, ice-core and radio-echo sounder observations. *Annals of Glaciology* 37, 207–212.
- Dahms, D.E. 2002. Glacial stratigraphy of Stough Creek Basin, Wind River Range, Wyoming. *Geomorphology* 42, 59–83.
- Dahms, D., Favilli, F., Krebs, R., et al. 2012. Soil weathering and accumulation rates of oxalate-extractable phases derived from alpine chronosequences of up to 1 Ma in age. *Geomorphology* 151–152, 99–113.
- Dale, A.L., Dale, B. 2002a. Application of ecologically-based statistical treatments for micropalaeontology. In *Quaternary Environmental Micropalaeontology* (edited by S. Haslett). Arnold, London, 259–286.
- Dale, B., Dale, A.L. 2002b. Environmental applications of dinoflagellate cysts and Acritharchs. In *Quaternary Environmental Micropalaeontology* (edited by S. Haslett). Arnold, London, 207–240.
- Daley, T.J., Street-Perrott, F.A., Loader, N.J., et al. 2009. Terrestrial climate signal of the '8200 yr B.P. cold event' in the Labrador Sea region. *Geology* 37, 831–834.
- Daley, T.J., Barber, K.E. Street-Perrott, F.A., et al. 2010. Holocene climate variability revealed by oxygen isotope analysis of *Sphagnum* cellulose from Walton Moss, northern England. *Quaternary Science Reviews* 29, 1590–1601.
- Dalsgaard, K., Odgaard, B.V. 2001. Dating sequences of buried horizons of podzols developed in wind-blown sand at Ulfborg, western Jutland. *Quaternary International* 78, 53–60.
- Damon, P.E., Donahue, D.J., Gore, B.H., et al. 1989. Radiocarbon dating of the Shroud of Turin. *Nature* 337, 611–615.
- D'Anjou, R.M., Bradley, A.S., Balascio, N.L., et al. 2012. Climate impacts on human settlement and agricultural activities in northern Norway revealed through sediment biogeochemistry. *Proceedings of the National Academy of Sciences of the United States of America* 109, 20332–20337.
- Dansgaard, W., Johnsen, S.J., Møller, J., et al. 1969. One thousand centuries of climatic record from Camp Century on the Greenland ice sheet. *Science* 166, 499–502.
- Dansgaard, W., Clausen, H. B., Gundestrup, N., et al. 1982. A New Greenland Deep Ice Core. *Science* 218, 1273–1277.
- D'Argenio, A., Pescatore, T., Senatore, M.R. 2004. Sea-level change and volcano-tectonic interplay. The Gulf of Pozzuoli (Campi Flegrei, Eastern Tyrrhenian Sea) during the last 39 ka. *Journal of Volcanology and Geothermal Research* 133, 105–121.
- Davidson, D.A., Simpson, I.A. 2001. Archaeology and soil micromorphology. In *Handbook of Archaeological Sciences* (edited by D.R. Brothwell, A.M. Pollard). John Wiley, Chichester and New York, 166–177.
- Davidson, D.A., Grieve, I.C., Tyler, A.N., et al. 1998. Archaeological sites: assessment of erosion risk. *Journal of Archaeological Science* 25, 857–860.
- Davidson, D.A., Carter, S., Boag, B., et al. 1999. Analysis of pollen in soils: processes of incorporation and redistribution of pollen in five soil profile types. *Soil Biology and Biochemistry* 31, 643–653.
- Davidson, I. 2013. Peopling the last new worlds: the first colonisation of Sahul and the Americas. *Quaternary International* 285, 1–29.
- Davidson, T.A., Sayer, C.D., Bennion, H., et al. 2005. A 250 year comparison of historical, macrofossil and pollen records of aquatic plants in a shallow lake. *Freshwater Biology* 50, 1671–1686.
- Davies, P. 2008. *Snails: Archaeology and Landscape Change*. Oxbow Books, Oxford.

- Davies, P., Griffiths, H.I. 2005. Molluscan and ostracod biostratigraphy of Holocene tufa in the Test valley at Bossington, Hampshire, UK. *The Holocene* 15, 97–110.
- Davies, S.J., Metcalfe, S.E., Caballero, M.E., et al. 2002a. Developing diatom-based transfer functions for Central Mexican lakes. *Hydrobiologia* 467, 199–213.
- Davies, S.M., Branch, N.P., Lowe, J.J., et al. 2002b. Towards a European tephrochronological framework for Termination 1 and the Early Holocene. *Philosophical Transactions of the Royal Society of London A* 360, 767–802.
- Davies, S.M., Wastegård, S., Rasmussen, T.L., et al. 2008. Identification of the Fugloyarbarki tephra in the NGRIP ice core: a key tie point for marine and ice-core sequences during the last glacial period. *Journal of Quaternary Science* 23, 409–414.
- Davies, S.M., Larsen, G., Wastegård, S., et al. 2010. Widespread dispersal of Icelandic tephra: how does the Eyjafjöll eruption of 2010 compare to past Icelandic events? *Journal of Quaternary Science* 25, 605–611.
- Davis, S.R., Brown, A.G., Dinnin, M.H. 2007. Floodplain connectivity, disturbance and change: a palaeoentomological investigation of floodplain ecology from south-west England. *Journal of Animal Ecology* 76, 276–288.
- Dawson, S., Smith, D.E. 2000. The sedimentology of Middle Holocene tsunami facies in northern Sutherland, Scotland, UK. *Marine Geology* 170, 69–79.
- Dayan, T., Wool, D., Simberloff, D. 2002. Variation and co-variation of skulls and teeth: modern carnivores and the interpretation of fossil mammals. *Paleobiology* 28, 508–526.
- D'Costa, D.M., Palmer, J., Hogg, A., et al. 2009. Stratigraphy, pollen and ^{14}C dating of Johnston's Gum Hole, a late Quaternary fossil kauri (*Agathis australis*) site, Northland, New Zealand. *Journal of Quaternary Science* 24, 47–59.
- De Abreu, L., Shackleton, N.J., Schonfeld, J., et al. 2003. Millennial-scale oceanic climate variability off the western Iberian margin during the last two glacial periods. *Marine Geology* 196, 1–20.
- Dean, W.E. 1997. Rates, timing and cyclicity of Holocene eolian activity in north-central United States: evidence from varved lake sediments. *Geology* 25, 331–334.
- Dearing, J.A., Livingstone, I.P., Bateman, M.D., et al. 2001. Palaeoclimatic records from OIS 8.0–5.4 recorded in loess-palaeosol sequences on the Matmata Plateau, southern Tunisia, based on mineral magnetism and new luminescence dating. *Quaternary International* 76/77, 43–56.
- DeBusk Jr., G.H. 1997. The distribution of pollen in the surface sediments of Lake Malawi, Africa, and the transport of pollen in large lakes. *Review of Palaeobotany and Palynology* 97, 123–153.
- De Deckker, P. 2001. Late Quaternary cyclic aridity in tropical Australia. *Palaeogeography, Palaeoclimatology, Palaeoecology* 170, 1–9.
- De Deckker, P., Moros, M., Perner, K., et al. 2012. Influence of the tropics and southern westerlies on glacial inter-hemispheric asymmetry. *Nature Geoscience* 5, 266–269.
- Dee, M., Wengrow, D., Shortland, A., et al. 2013. An absolute chronology for early Egypt using radiocarbon dating and Bayesian statistical modelling. *Proceedings of the Royal Society A* 469(2159), 20130395.
- De Francesco, C.G., Hassan, G.S. 2008. Dominance of reworked fossil shells in modern estuarine environments: implications for paleoenvironmental reconstructions based on biological remains. *Palaios* 23, 14–23.
- De Geer, G. 1912. A geochronology of the last 12,000 years. *XIth International Geological Congress*, Stockholm, 1, 241–253.
- Degenhardt Jr., J.J. 2009. Development of tongue-shaped and multilobate rock glaciers in alpine environments – interpretations from ground penetrating radar surveys. *Geomorphology* 109, 94–107.
- Dehnert, A., Schlüchter, C. 2008. Sediment burial dating using terrestrial cosmogenic nuclides. *Eiszeitalter und Gegenwart (Quaternary Science Journal)* 57, 210–225.
- Dehnert, A., Kracht, O., Preusser, F., et al. 2011. Cosmogenic isotope burial dating of fluvial sediments from the Lower Rhine Embayment, Germany. *Quaternary Geochronology* 6, 313–325.
- De Jong, R., Kamenik, C. 2011. Validation of a chrysophyte stomatocyst-based cold-season climate reconstruction from high-Alpine Lake Silvaplana, Switzerland. *Journal of Quaternary Science* 26, 268–275.
- Delmonte, B., Andersson, P.S., Schöberg, H., et al. 2010. Geographic provenance of aeolian dust in East Antarctica during Pleistocene glaciations: preliminary results from Talos Dome and comparison with East Antarctic and new Andean ice core data. *Quaternary Science Reviews* 29, 256–264.
- Demarchi, B., Williams, M.G., Milner, N., et al. 2011. Amino acid racemization dating of marine shells: a mound of possibilities. *Quaternary International* 239, 114–124.
- Demetsopoulos, J.C., Burleigh, R., Oakley, K.P. 1983. Relative and absolute dating of the human skeleton from Galley Hill, Kent. *Journal of Archaeological Science* 10, 129–134.
- De Mulder, E., Geluk, M.C., Ritsma, I., et al. 2003. *De Ondergrond van Nederland*. Geologie van Nederland, deel 7. Nederlandse Organisatie voor toegepast-natuurwetenschappelijk onderzoek – TNO, Utrecht.
- Deng, W., Wei, G., Li, X., et al. 2009. Paleoprecipitation record from coral Sr/Ca and $\delta^{18}\text{O}$ during the mid Holocene in the northern South China Sea. *The Holocene* 19, 811–821.
- Denniston, R.F., Wyrwoll, K.-H., Asmerom, Y., et al. 2013. North Atlantic forcing of millennial-scale Indo-Australian monsoon dynamics during the Last Glacial period. *Quaternary Science Reviews* 72, 159–168.
- Denton, G. 2000. Does an asymmetric thermohaline–ice-sheet oscillator drive 100,000-yr glacial cycles? *Journal of Quaternary Science* 15, 301–318.
- Denton, G.H., Hughes, T.J. 2002. Reconstructing the Antarctic Ice Sheet at the Last Glacial Maximum. *Quaternary Science Reviews* 21, 193–202.
- Denton, G.H., Alley, R.B., Comer, G.C., et al. 2005. The role of seasonality in abrupt climate change. *Quaternary Science Reviews* 24, 1159–1182.
- Denton, G.H., Anderson, R.F., Toggweiler, J.R., et al. 2010. The last glacial termination. *Science* 328, 1652–1656.
- Derbyshire, E. (ed.). 2003. Loess and dust indicators and records of terrestrial and marine palaeoenvironments (DIRTMAP) database. *Quaternary Science Reviews* 22, 1813–2052.

- Derbyshire, E., Keen, D., Kemp, R.A., et al. 1995. Loess–palaeosol sequences as recorders of palaeoclimatic variations during the last glacial–interglacial cycle: some problems of correlation in North-Central China. *Quaternary Proceedings* 4, 7–18.
- Derbyshire, E., Meng, X.M., Dijkstra, T.A. (eds). 2000. *Landslides in Thick Loess Terrain of Northwest China*. John Wiley, Chichester and New York.
- Deschamps, P., Durand, N., Bard, E., et al. 2012. Ice-sheet collapse and sea-level rise at the Bølling warming 14,600 years ago. *Nature* 483, 559–563.
- Desmarchelier, J.M., Goede, A., Aycliffe, L.K., et al. 2000. Stable isotope record and its palaeoenvironmental interpretation for a late Middle Pleistocene speleothem from Victoria Fossil Cave, Naracoorte, South Australia. *Quaternary Science Reviews* 19, 763–774.
- Desprat, S., Sánchez-Góñi, M.F., Turon, J.-L., et al. 2006. Climatic variability of Marine Isotope Stage 7: direct land–sea–ice correlation from a multiproxy analysis of a north-western Iberian marine deep-sea core. *Quaternary Science Reviews* 25, 1010–1026.
- De Vernal, A., Henry, M., Bilodeau, G. 2010. Micropaleontological preparation techniques and analyses. *Les Cahiers du GEOTOP* 3, <http://www.geotop.ca/>.
- DeVogel, S.B., Magee, J.W., Manley, W.F., et al. 2004. A GIS-based reconstruction of late Quaternary paleohydrology: Lake Eyre, arid central Australia. *Palaeogeography, Palaeoclimatology, Palaeoecology* 204, 1–13.
- Dickinson, W.R. 2000. Hydro-isostatic and tectonic influences on emergent Holocene paleoshorelines in the Mariana Islands, western Pacific Ocean. *Journal of Coastal Research* 16, 735–746.
- Dickinson, W.R. 2004. Impacts of eustasy and hydro-isostasy on the evolution and landforms of Pacific atolls. *Palaeogeography, Palaeoclimatology, Palaeoecology* 213, 251–269.
- Dieffenbacher-Krall, A.C. 2007. Plant macrofossil methods and studies. Surface samples, taphonomy, representation. In *Encyclopedia of Quaternary Science* (edited by S.A. Elias). Elsevier, Amsterdam, 2367–2374.
- Dilcher, D.L., Kowalski, E.A., Wiemann, M.C., et al. 2009. A climatic and taxonomic comparison between leaf litter and standing vegetation from a Florida swamp woodland. *American Journal of Botany* 96, 1108–1115.
- Dillehay, T.D., Rossen, J., Andres, T.C., et al. 2007. Preceramic adoption of peanut, squash, and cotton in Northern Peru. *Science* 316, 1890–1893.
- Dillon, R.T. 2000. *The Ecology of Freshwater Molluscs*. Cambridge University Press, Cambridge.
- Ding, Z., Yu, Z., Rutter, N.W., et al. 1994. Towards an orbital time scale for Chinese loess deposits. *Quaternary Science Reviews* 13, 39–70.
- Ding, Z.L., Xiong, S.F., Sun, J.M., et al. 1999. Pedostratigraphy and palaeomagnetism of a similar to 7.0 Ma eolian loess–red clay sequence at Lingtai, Loess Plateau, north central China and the implications for paleomonsoon evolution. *Palaeogeography, Palaeoclimatology, Palaeoecology* 152, 49–66.
- Ding, Z.L., Ranov, V., Yang, S.L., et al. 2002a. The loess record in southern Tajikistan and correlation with Chinese loess. *Earth and Planetary Science Letters* 200, 387–4.
- Ding, Z.L., Derbyshire, E., Yang, S.L., et al. 2002b. Stacked 2.6–Ma grain size record from the Chinese loess based on five sections and correlated with the deep-sea $\delta^{18}\text{O}$ record. *Paleoceanography* 17, 1–21.
- Ding, Z.L., Derbyshire, E., Yang, S.L., et al. 2005. Stepwise expansion of desert environment across northern China in the past 3.5 Ma and implications for monsoon evolution. *Earth and Planetary Science Letters* 237, 45–55.
- Ditlevsen, P.D. 2009. Bifurcation structure and noise-assisted transitions in the Pleistocene glacial cycles. *Paleoceanography* 24, PA3204, doi: 10.1029/2008PA001673.
- Ditlevsen, P.D., Andersen, K.K., Svensson, A. 2007. The DO-climate events are probably noise induced: statistical investigation of the claimed 1470 years cycle. *Climate of the Past* 3, 129–134.
- Dixon, E.J. 2001. Human colonization of the Americas: timing, technology and process. *Quaternary Science Reviews* 20, 277–299.
- Dixon, J.C., McLaren, S.J. 2009. Duricrusts. In *Geomorphology of Desert Environments*, 2nd edn (edited by A.J. Parsons, A. Abraham). Springer, Dordrecht, 123–150.
- Dogan, U. 2010. Fluvial response to climate change during and after the Last Glacial Maximum in Central Anatolia, Turkey. *Quaternary International* 222, 221–229.
- Dokken, T.M., Nisancioglu, K.H. 2004. Palaeoclimatology: fresh angle on the polar seesaw. *Nature* 430, 842–843.
- Domack, E.W., Jacobson, E.A., Ship, S., et al. 1999. Late Pleistocene–Holocene retreat of the West Antarctic Ice-Sheet system in the Ross Sea: Part 2 – Sedimentologic and stratigraphic signature. *Geological Society of America Bulletin* 111, 1517–1536.
- Donahue, D.J., Olin, J.S., Harbottle, G. 2002. Determination of the radiocarbon age of the parchment of the Vinland Map. *Radiocarbon* 44, 45–52.
- Doney, S.C., Fabry, V.J., Feely, R.A., et al. 2009. Ocean acidification: the other CO_2 problem. *Annual Reviews of Marine Science* 1, 169–192.
- Dorale, J.A., Edwards, L., Alexander Jr., E.C., et al. 2007. Uranium series dating of speleothems: current techniques, limits and applications. In *Studies of Cave Sediments*, 2nd edn (edited by I.D. Sasowsky, J. Mylroie). Springer, Dordrecht, 177–197.
- Dorighel, O., Poupeau, G., Bellot-Gurlet, L., et al. 1998. Fission track dating and provenience of archaeological obsidian artefacts in Colombia and Ecuador. In *Advances in Fission-Track Geochronology* (edited by P. van den Haute, F. de Corte). Kluwer, Dordrecht, 313–324.
- Dortch, J.M., Owen, L.A., Cafee, M.W. (2013) Timing and climate drivers for glaciation across semi-arid western Himalayan–Tibetan orogen. *Quaternary Science Reviews* 78, 188–208.
- Dos Santos, R.A.L., Prange, M., Castañeda, I.S., et al. 2010. Glacial–interglacial variability in Atlantic meridional overturning circulation and thermocline adjustments in the tropical North Atlantic. *Earth and Planetary Science Letters* 300, 407–414.
- Douglas, M.E., Douglas, M.R., Schuett, G.W., et al. 2006. Evolution of rattlesnakes (Viperidae: *Crotalus*) in the warm deserts of western north America shaped by Neogene vicariance and Quaternary climate change. *Molecular Ecology* 15, 3353–3374.

- Douglass, D.C., Mickelson, D.M. 2007. Soil development and glacial history, West Fork of Beaver Creek, Uinta Mountains, Utah. *Arctic and Alpine Research* 39, 592–602.
- Dowdeswell, J.A., Elverhøi, A., Spielhagen, R. 1998. Glacimarine sedimentary processes and facies on the polar North Atlantic margins. *Quaternary Science Reviews* 17, 243–272.
- Dowdeswell, J.A., Elverhøi, A., Andrews, J.T., et al. 1999. Asynchronous deposition of ice-rafted layers in the Nordic seas and North Atlantic Ocean. *Nature* 400, 348–351.
- Dowdeswell, J.A., Ó Cofaigh, C., Pusey, C.J. 2004. Thickness and extent of the subglacial till layer beneath an Antarctic paleo-ice stream. *Geology* 32, 13–16.
- Dowdeswell, J.A., Hogan, K.A., Evans, J., et al. 2010. Past ice-sheet flow east of Svalbard inferred from streamlined subglacial landforms. *Geology* 38, 163–166.
- Drake, N., Bristow, C. 2006. Shorelines in the Sahara: geomorphological evidence for an enhanced monsoon from palaeolake Megachad. *The Holocene* 16, 901–911.
- Drake, N.A., Blench, R.M., Armitage, S.J., et al. 2010. Ancient watercourses and biogeography of the Sahara explain the peopling of the desert. *Proceedings of the National Academy of Sciences of the United States of America* 108, 458–462.
- Drysdale, R.N., Spötl, C., Hellstrom, J.C., et al. (eds). 2012. New advances in the dating of speleothem. *Quaternary Geochronology* 14, 1–114.
- Duller, G.A.T. 2004. Luminescence dating of Quaternary sediments: recent advances. *Journal of Quaternary Science* 19, 183–192.
- Duller, G.A.T., Wintle, A.G. 2012. A review of the thermally transferred optically stimulated luminescence signal from quartz for dating sediments. *Quaternary Geochronology* 7, 6–20.
- Dumitrica, P. 2013. *Clevieplexima* nov. gen., a new generic name for the radiolarian species *Rhizoplegma boreale* (Cleve, 1899). *Revue de Micropaléontologie* 56, 21–25.
- Dunai, T. 2010. *Cosmogenic Nuclides: Principles, Concepts, and Applications in the Earth Sciences*. Cambridge University Press, Cambridge.
- Dutta, K., Bushan, T., Somayajulu, B.L.K. 2001. Delta R correction values for the northern Indian Ocean. *Radiocarbon* 43, 483–488.
- Dwyer, G.S., Cronin, T.M., Baker, P.A., et al. 1993. North Atlantic deepwater temperature change during Late Pliocene and Late Quaternary climatic cycles. *Science* 270, 1347–1351.
- Dyke, A.S. 2004. An outline of North American deglaciation with emphasis on central and northern Canada. In *Developments in Quaternary Science. Volume 2: Quaternary Glaciations: Extent and Chronology* (edited by J. Ehlers, P.L. Gibbard). Elsevier, Amsterdam, 373–424.
- Dyke, A.S., Dale, J.E., McNeely, R.N. 1996. Marine mollusks as indicators of environmental change in glaciated North America and Greenland during the last 18 000 years. *Géographie physique et Quaternaire* 50, 125–184.
- Dyke, A.S., Andrews, J.T., Clark, P.U., et al. 2002. The Laurentide and Innuitian ice sheets during the Last Glacial Maximum. *Quaternary Science Reviews* 21, 9–31.
- Dynesius, M., Jansson, R. 2000. Evolutionary consequences of changes in species' geographical distributions driven by Milankovitch climate oscillations. *Proceedings of the National Academy of Sciences of the United States of America* 97, 9115–9120.
- Ebbesen, H., Hald, M. 2004. Unstable Younger Dryas climate in the northeast Atlantic. *Geology* 32, 673–676.
- Ebert, K., Willenbring, J., Norton, K.P., et al. 2012. Meteoric ^{10}Be concentrations from saprolite and till in northern Sweden: implications for glacial erosion and age. *Quaternary Geochronology* 12, 11–22.
- Eberwein, A., Mackensen, A. 2008. Last Glacial Maximum paleoproductivity and water masses off NW-Africa: evidence from benthic foraminifera and stable isotopes. *Marine Micropaleontology* 67, 87–103.
- Edwards, K.J., Rowntree, K.M. 1980. Radiocarbon and palaeoenvironmental evidence for changing rates of erosion at a Flandrian stage site in Scotland. In *Timescales in Geomorphology* (edited by R.A. Cullingford, D.A. Davidson, J. Lewin). John Wiley, Chichester and New York, 207–223.
- Edwards, K.J., Whittington, G. 2001. Lake sediments, erosion and landscape change during the Holocene in Britain. *Catena* 42, 143–173.
- Edwards, M.E., Brubaker, L.E., Lozhkin, A.V., et al. 2005. Structurally novel biomes: a response to past warming in Beringia. *Ecology* 86, 1696–1703.
- Edwards, R. 2007. Sea levels: resolution and uncertainty. *Progress in Physical Geography* 31, 621–632.
- Edwards, R., Horton, B.P. 2006. Developing detailed records of relative sea-level change using a foraminiferal transfer function: an example from North Norfolk, UK. *Philosophical Transactions of the Royal Society of London A* 364, 973–991.
- Edwards, R.L., Gallup, C.D., Cheng, H. 2003. Uranium-series dating of marine and lacustrine carbonates. In *Uranium Series Geochronology* (edited by B. Bourdon, G.M. Henderson, C.C. Lundstrom, et al.). *Reviews in Mineralogy and Geochemistry* 52, 363–405.
- Eerkens, J.W., Vaughn, K.J., Carpenter, T.R., et al. 2008. Obsidian hydration dating on the South Coast of Peru. *Journal of Archaeological Science* 35, 2231–2239.
- Eggermont, H., Martens, K. 2011. Preface: Cladocera crustaceans: sentinels of environmental change. *Hydrobiologia* 676, 1–7.
- Eggermont, H., Heiri, O. 2012. The chironomid–temperature relationship: expression in nature and palaeoenvironmental implications. *Biological Reviews* 87, 430–456.
- Egging, S.M., Grün, R., McCullough, M.T., et al. 2005. In situ U-series dating by laser-ablation multi-collector ICPMS: new prospects for Quaternary geochronology. *Quaternary Science Reviews* 24, 2523–2538.
- Eglinton, G., Calvin, M. 1967. Chemical fossils. *Scientific American* 216, 32–43.
- Ehlers, J., Gibbard, P.L. 2003. Extent and chronology of glaciations. *Quaternary Science Reviews* 15–17, 1561–1568.
- Ehlers, J., Gibbard, P.L. 2007. The extent and chronology of Cenozoic Global Glaciation. *Quaternary International* 164–165, 6–20.
- Ehlers, J., Gibbard, P.L., Hughes, P.D. (eds). 2011a. *Developments in Quaternary Science. Volume 15: Quaternary Glaciations – Extent and Chronology: A Closer Look*. Elsevier, Amsterdam.

- Ehlers, J., Grube, A., Stephan, H.-G., et al. 2011b. Pleistocene Glaciations of North Germany – new results. In *Developments in Quaternary Science. Volume 15: Quaternary Glaciations – Extent and Chronology: A Closer Look* (edited by J. Ehlers, P.L. Gibbard, P.D. Hughes). Elsevier, Amsterdam, 149–162.
- Ehrmann, W., Hillenbrand, C.-D., Smith, J.A., et al. 2011. Provenance changes between recent and glacial-time sediments in the Amundsen Sea embayment, West Antarctica: clay mineral assemblage evidence. *Antarctic Science* 23, 471–486.
- Eichler, A., Tinner, W., Brütsch, S., et al. 2011. An ice-core based history of Siberian forest fires since AD 1250. *Quaternary Science Reviews* 30, 1027–1034.
- Eide, W., Birks, H.H., Bigelow, N.H., et al. 2006. Holocene forest development along the Setesdal valley, southern Norway, reconstructed from macrofossil and pollen evidence. *Vegetation History and Archaeobotany* 15, 65–85.
- Eiríksson, J., Larsen, G., Knudsen, K.-L., et al. 2004. Marine reservoir age variability and water mass distribution in the Icelandic Sea. *Quaternary Science Reviews* 23, 2247–2268.
- Eitel, B., Blümel, W.D., Blümel, K., et al. 2001. Dust and loessic alluvial deposits in Northwestern Namibia (Damaraland, Kaokoveld): sedimentology and palaeoclimatic evidence based on luminescence dates. *Quaternary International* 76/77, 57–66.
- Ekdahl, E.J., Teranes, J.L., Guilderson, T.P., et al. 2004. Prehistorical record of cultural eutrophication from Crawford Lake, Canada. *Geology* 32, 745–748.
- Elderfield, H. (ed.). 2006. *The Oceans and Marine Geochemistry*. Elsevier, Oxford and Amsterdam.
- Elderfield, H., Rickaby, R.E.M. 2000. Oceanic Cd/P ratio and nutrient utilization in the glacial Southern Ocean. *Nature* 405, 305–310.
- Elderfield, H., Ferretti, P., Greaves, M., et al. 2012. Evolution of ocean temperature and ice volume through the Mid-Pleistocene Climate Transition. *Science* 337, 704–709.
- Elenga, H., de Namur, C., Vincens, A., et al. 2000. Use of plots to define pollen–vegetation relationships in densely forested ecosystems of Tropical Africa. *Review of Palaeobotany and Palynology* 112, 79–96.
- Elias, S.A. 1994. *Quaternary Insects and their Environments*. Smithsonian Institution Press, Washington, DC.
- Elias, S.A. 1997. The Mutual Climatic Range method of palaeoclimate reconstruction based on insect fossils: new applications and inter-hemispheric applications. *Quaternary Science Reviews* 16, 1217–1225.
- Elias, S.A. 2000. Late Pleistocene climates of Beringia, based on analysis of fossil beetles. *Quaternary Science Reviews* 53, 229–235.
- Elias, S.A. 2007a. Beetle records: overview. In *Encyclopedia of Quaternary Science* (edited by S.A. Elias). Elsevier, Amsterdam, 153–163.
- Elias, S.A. 2007b. Postglacial North America. In *Encyclopedia of Quaternary Science* (edited by S.A. Elias). Elsevier, Amsterdam, 275–286.
- Elias, S.A. 2010. *Developments in Quaternary Science. Volume 12: Advances in Quaternary Entomology*. Elsevier, Amsterdam.
- Elkibbi, M., Rial, J.A. 2001. An outsider's review of the astronomical theory of the climate: is the eccentricity-driven insolation the main driver of the ice ages? *Earth-Science Reviews* 56, 161–177.
- Elliott, S.M., Roe, H.M., Patterson, R.T. 2012. Testate amoebae as indicators of hydroseral change: an 8500 year record from Mer Bleue Bog, eastern Ontario, Canada. *Quaternary International* 268, 128–144.
- Ellis, B.S., Mark, D.F., Pritchard, C.J., et al. 2012. Temporal dissection of the Huckleberry Ridge Tuff using the $^{40}\text{Ar}/^{39}\text{Ar}$ dating technique. *Quaternary Geochronology* 9, 34–41.
- Ellis, C.J., Tallis, J.H., 2000. Climatic control of blanket mire development at Kentra Moss, north-west Scotland. *Journal of Ecology* 88, 869–889.
- Ellis, G.L., Goodfriend, G.A., Abbott, J.T., et al. 1996. Assessment of integrity and geochronology of archaeological sites using amino acid racemization in land snail shells: examples from Central Texas. *Geoarchaeology* 11, 189–213.
- Ellwood, B.B., Harrold, F.B., Benoist, S.L., et al. 2004. Magnetic susceptibility applied as an age-depth-climate relative dating technique using sediments from Scaldina Cave, a Late Pleistocene site in Belgium. *Journal of Archaeological Science* 31, 283–293.
- Elmore, A.C., Wright, J.D. 2011. North Atlantic deep water and climate variability during the Younger Dryas cold period. *Geology* 39, 107–110.
- Elsig, J., Schmitt, J., Leuenberger, D., et al. 2009. Stable isotope constraints on Holocene carbon cycle changes from an Antarctic ice core. *Nature* 461, 507–510.
- Emeis, K.C., Sakamoto, T., Wehausen, R., et al. 2000. The sapropel record of the eastern Mediterranean Sea – results of Ocean Drilling Program Leg 160. *Paleogeography, Palaeoclimatology, Palaeoecology* 158, 371–395.
- Enfield, D.B., Cid-Serrano, L. 2010. Secular and multi-decadal warmings in the North Atlantic and their relationships with major hurricane activity. *International Journal of Climatology* 30, 174–184.
- Engelhardt, H. 2004. Ice temperature and high geothermal flux at Siple Dome, West Antarctica, from borehole measurements. *Journal of Glaciology* 50, 251–256.
- Engelhart, S.E., Horton, B.P., Kemp, A.C. 2011. Holocene sea level changes along the United States' Atlantic coast. *Oceanography* 24, 70–79.
- Engels, S., van Geel, B. 2012. The effects of changing solar activity on climate: contributions from paleoclimatological studies. *Journal of Space Weather and Space Climate* 2, doi: org/10.1051/swsc/2012009.
- England, J. 1999. Coalescent Greenland and Innuitian ice during the Last Glacial Maximum: revising the Quaternary of the Canadian High Arctic. *Quaternary Science Reviews* 18, 421–456.
- England, J., Smith, I.R., Evans, D.J.A. 2000. The last glaciation of east-central Ellesmere Island, Nunavut: ice dynamics, deglacial chronology, and sea level change. *Canadian Journal of Earth Sciences* 37, 1355–1371.
- England, J., Atkinson, N., Bednarski, J., et al. 2006. The Innuitian Ice Sheet: configuration, dynamics and chronology. *Quaternary Science Reviews* 25, 689–703.
- English, P., Spooner, N.A., Chappell, J., et al. 2001. Lake Lewis basin, central Australia: environmental evolution and OSL chronology. *Quaternary International* 83–85, 81–102.

- EPICA Community Members. 2004. Eight glacial cycles from an Antarctic ice core. *Nature* 429, 823–828.
- EPICA Community Members. 2006. One-to-one coupling of glacial climate variability in Greenland and Antarctica. *Nature* 444, 195–198.
- Erdtman, G. 1969. *Handbook of Palynology*. Munksgaard, Copenhagen.
- Ericson, D.B., Wollin, G. 1968. Pleistocene climates and chronology in deep-sea sediments. *Science* 162, 1227–1234.
- Ericson, J.E., Dersch, O., Rauch, F. 2004. Quartz hydration dating. *Journal of Archaeological Science* 31, 883–902.
- Eronen, M., Zetterberg, P., Briffa, K.R., et al. 2002. The supra-long Scots pine tree-ring record for Finnish Lapland: Part 1, chronology construction and initial inferences. *The Holocene* 12, 673–680.
- Erthal, F., Kotzian, C.B., Simões, M.G. 2011. Fidelity of molluscan assemblages from the Touro Passo Formation (Pleistocene–Holocene), southern Brazil: taphonomy as a tool for discovering natural baselines for freshwater communities. *Palaios* 26, 433–446.
- Esat, T.M., McCulloch, M.T., Chappell, J., et al. 1999. Rapid fluctuations in sea level recorded at Huon Peninsula during the penultimate deglaciation. *Science* 283, 197–201.
- Esper, O., Zonneveld, K.A.F. 2007. The potential of organic-walled dinoflagellate cysts to reconstruct past sea-surface conditions in the Southern Ocean. *Marine Micropaleontology* 63, 185–212.
- Espizua, L.E., Bigazzi, G., Junes, P.J., et al. 2002. Fission-track dating of a tephra layer related to Poti-Malal and Seguro drifts in the Río Grande basin, Mendoza, Argentina. *Journal of Quaternary Science* 17, 781–788.
- Evans, D.J.A. 2003. Ice-marginal terrestrial landsystems: active temperate glacier margins. In *Glacial Landsystems* (edited by D.J.A. Evans). Arnold, London, 259–288.
- Evans, D.J.A. 2009. Controlled moraines: origins, characteristics and palaeoglaciological implications. *Quaternary Science Reviews* 28, 181–260.
- Evans, D.J.A., Twigg, D.R. 2002. The active temperate glacial landsystem: a model based on Breiðamerkurjökull and Fjallsjökull, Iceland. *Quaternary Science Reviews* 21, 2143–2177.
- Evans, D.J.A., Benn, D.I. 2004. *A Practical Guide to the Study of Glacial Sediments*. Arnold, London.
- Evans, D.J.A., Owen, L.A., Roberts, D. 1995. Stratigraphy and sedimentology of Devensian (Dimlington Stadial) deposits, east Yorkshire, England. *Journal of Quaternary Science* 10, 241–265.
- Evans, D.J.A., Archer, S., Wilson, D.J.H. 1999. A comparison of the lichenometric and Schmidt hammer dating techniques based on data from the proglacial areas of some Icelandic glaciers. *Quaternary Science Reviews* 18, 13–41.
- Evans, D.J.A., Clark, C.D., Mitchell, W.A. 2005. The last British Ice Sheet: a review of the evidence utilized in the compilation of the Glacial Map of Britain. *Earth-Science Reviews* 70, 253–312.
- Evans, D.J.A., Phillips, E.R., Hiemstra, J.F., et al. 2006. Subglacial till: formation, sedimentary characteristics and classification. *Earth-Science Reviews* 78, 115–176.
- Evans, D.J.A., Hiemstra, J.F., Boston, C.M., et al. 2012. Till stratigraphy and sedimentology at the margins of terrestrially terminating ice streams: case study of the western Canadian prairies and high plains. *Quaternary Science Reviews* 46, 80–125.
- Evans, M.E., Heller, F. 2003. *Environmental Magnetism: Principles and Applications of Enviromagnetics*. Academic Press, New York.
- Evans, M., Slaymaker, O. 2004. Spatial and temporal variability of sediment delivery from alpine lake basins, Cathedral Provincial Park, southern British Columbia. *Geomorphology* 61, 209–224.
- Evans, M., Warburton, J. 2007. *Geomorphology of Upland Peat: Erosion, Form and Landscape Change*. Blackwell, Malden, MA and Oxford.
- Everest, J., Bradwell, T., Fogwell, C.J., et al. 2006. Cosmogenic ^{10}Be age constraints for the Wester Ross Readvance Moraine: insights into British ice-sheet behaviour. *Geografiska Annaler. A. Physical Geography* 88, 9–17.
- Everest, T., Bradwell, T., Stoker, M., et al. 2013. New age constraints for the maximum extent of the last British–Irish Ice Sheet (NW sector). *Journal of Quaternary Science* 28, 2–7.
- Eyles, N., Lazorek, M. 2007. Glacial landforms, sediments. Glacigenic Lithofacies. In *Encyclopedia of Quaternary Science* (edited by S.A. Elias). Elsevier, Amsterdam, 920–932.
- Eyles, N., Boyce, J.I., Barendregt, R.W. 1999. Hummocky moraine: sedimentary record of stagnant Laurentide ice sheet lobes resting on soft beds. *Sedimentary Geology* 123, 163–174.
- Eyles, N., Doughty, M., Boyce, J.I., et al. 2003. Acoustic architecture of glaciolacustrine sediments deformed during zonal stagnation of the Laurentide Ice Sheet; Mazinaw Lake, Ontario, Canada. *Sedimentary Geology* 157, 133–151.
- Fabel, D., Ballantyne, C.K., Xu, S. 2012. Trimlines, blockfields, mountain-top erratics and the vertical dimensions of the last British–Irish ice sheet in NW Scotland. *Quaternary Science Review* 55, 91–102.
- Faegri, K., Iversen, J. 1989. *Textbook of Pollen Analysis*, 4th edn, with K. Krzywinski. John Wiley, Chichester and New York.
- Fagan, B. 2000. *The Little Ice Age*. Basic Books, New York.
- Fagel, N., Boës, X. 2008. Clay-mineral record in Lake Baikal sediments: the Holocene and Late Glacial transition. *Palaeogeography, Palaeoclimatology, Palaeoecology* 259, 230–243.
- Fairbanks, R.G., Mortlock, R.A., Chiu, T.-C., et al. 2005. Radiocarbon calibration curve spanning 0 to 50,000 years BP based on paired $^{238}\text{Th}/^{234}\text{U}/^{238}\text{U}$ and ^{14}C dates on pristine corals. *Quaternary Science Reviews* 24, 1781–1796.
- Fairchild, I.J. 2009. Trace elements in speleothems as recorders of environmental change. *Quaternary Science Reviews* 28, 449–468.
- Fairchild, I.J., McMillan, A. 2007. Speleothems as indicators of wet and dry periods. *International Journal of Speleology* 36, 69–74.
- Fairchild, I.J., Baker, A. 2012. *Speleothem Science. From Process to Past Environments*. Wiley Blackwell, Chichester.
- Faith, J.T., Surovell, T.A. 2009. Synchronous extinction of North America's Pleistocene mammals. *Proceedings of the National Academy of Sciences of the United States of America* 106, 20641–20645.
- Faith, J.T., Domínguez-Rodrigo, M., Gordon, A.D. 2009. Long-distance carcass transport at Olduvai Gorge? A quantitative examination of Bed I skeletal element abundances. *Journal of Human Evolution* 56, 247–256.

- Farmer, G.L., Licht, K., Swope, R.J., et al. 2006. Isotopic constraints on the provenance of fine-grained sediment in LGM tills from the Ross Embayment, Antarctica. *Earth Surface Processes and Landforms* 249, 90–107.
- Farmer, J.G., Anderson P., Cloy, J.M., et al. 2009. Historical accumulation rates of mercury in four Scottish ombrotrophic peat bogs over the past 2000 years. *Science of the Total Environment* 407, 5578–5588.
- Favilli, F., Egli, M., Brandová, D., et al. 2009. Combined use of relative and absolute dating techniques for detecting signals of Alpine landscape evolution during the late Pleistocene and early Holocene. *Geomorphology* 112, 48–66.
- Fedele, F.G., Giaccio, B., Isaia, R., et al. 2002. Ecosystem impact of the Campanian Ignimbrite eruption in Late Pleistocene Europe. *Quaternary Research* 57, 420–424.
- Fei, W., Hongchun, L., Rixiang, Z., et al. 2004. Late Quaternary downcutting rates of the Qianyou River from U/Th speleothem dates, Qinling Mountains, China. *Quaternary Research* 62, 194–200.
- Feng, Z.-D., Johnson, W.C., Sprowl, D.R., et al. 1994. Loess accumulation and soil formation in central Kansas, United States, during the past 400,000 years. *Earth Surface Processes and Landforms* 19, 55–67.
- Ferguson, C.W., Graybill, D.A. 1983. Dendrochronology of bristlecone pine; a progress report. *Radiocarbon* 25, 287–88.
- Fernández, E., Ortiz, J.E., Pérez-Pérez, A., et al. 2009. Aspartic acid racemization variability in ancient human remains: implications in the prediction of ancient DNA recovery. *Journal of Archaeological Science* 36, 965–972.
- Fernández, M.H. 2006. Rodent paleofaunas as indicators of climatic change in Europe during the last 125,000 years. *Quaternary Research* 65, 308–323.
- Fernández, M.H., Vrba, E.S. 2006. Plio–Pleistocene climatic change in the Turkana Basin (East Africa): evidence from large mammal faunas. *Journal of Human Evolution* 50, 595–626.
- Fiedel, S.J. 2005. Man's best friend – mammoth's worst enemy? A speculative essay on the role of dogs in Paleoindian colonization and megafaunal extinction. *World Archaeology* 37, 11–25.
- Field, J., Fillios, M., Wroe, S. 2008. Chronological overlap between humans and megafauna in Sahul (Pleistocene Australia–New Guinea): a review of the evidence. *Quaternary Science Reviews* 89, 97–115.
- Fifield, L.K., Morgenstern, U. 2009. Silicon-32 as a tool for dating the recent past. *Quaternary Geochronology* 4, 400–405.
- Finlayson, A., Merritt, J., Browne, M., et al. 2010. Ice sheet advance, dynamics, and decay configurations: evidence from west central Scotland. *Quaternary Science Reviews* 29, 969–988.
- Finsinger, W., Heiri, O., Valsecchi, V., et al. 2007. Modern pollen assemblages as climate indicators in southern Europe. *Global Ecology and Biogeography* 16, 567–582.
- Firestone, R.B., West, A., Kennett, J.P., et al. 2007. Evidence for an extra-terrestrial impact 12,900 years ago that contributed to the megafaunal extinctions and the Younger Dryas cooling. *Proceedings of the National Academy of Sciences of the United States of America* 104, 16016–16021.
- Firth, C.R., Smith, D.E., Cullingford, R.A. 1993. Late Devensian and Holocene glacio-isostatic uplift patterns in Scotland. In *Neotectonics: Recent Advances* (edited by L.A. Owen, I. Stewart, C. Vita-Finzi). *Quaternary Proceedings* 3, Quaternary Research Association, Cambridge, 1–13.
- Fischer, H., Traufetter, F., Oerter, H., et al. 2004. Prevalence of the Antarctic Circumpolar Wave over the last two millenia recorded in Dronning Maud Land ice. *Geophysical Research Letters* 31, doi: 10.1029/2003GL019186.
- Fischer, H., Siggaard-Andersen, M.-L., Ruth, U., et al. 2007. Glacial/interglacial changes in mineral dust and sea-salt records in polar ice cores: sources, transport, and deposition. *Reviews of Geophysics* 45, doi: 10.1029/2005RG000192.
- Fischer, H., Masson-Delmotte, V., Waelbroeck, C., et al. (eds). 2010a. Climate of the last million years: new insights from EPICA and other records. *Quaternary Science Reviews* 29, 1–365.
- Fischer, H., Schmitt, J., Lüthi, D., et al. 2010b. The role of Southern Ocean processes in orbital and millennial CO₂ variations – a synthesis. *Quaternary Science Reviews* 29, 193–205.
- Fisher, D., Osterberg, E., Dyke, A., et al. 2008. The Mt Logan Holocene–late Wisconsinan isotope record: tropical Pacific–Yukon connections. *The Holocene* 18, 1–11.
- Fisher, D.C., Tikhonov, A.N., Kosintsev, P.A., et al. 2012. Anatomy, death, and preservation of a woolly mammoth (*Mammuthus primigenius*) calf, Yamal Peninsula, northwest Siberia. *Quaternary International* 255, 94–105.
- Fitzsimmons, K.E., Magee, J.W., Amos, K.J. 2009. Characterisation of aeolian sediments from the Strzelecki and Tirari Deserts, Australia: implications for reconstructing palaeoenvironmental conditions. *Sedimentary Geology* 218, 61–73.
- Fitzsimmons, K.E., Marković, S.B., Hambech, U. 2012. Pleistocene environmental dynamics recorded in the loess of the middle and lower Danube basin. *Quaternary Science Reviews* 41, 104–128.
- Fjeldskaar, W., Lindholm, C., Dehls, J.F., et al. 2000. Postglacial uplift, neotectonics and seismicity in Fennoscandia. *Quaternary Science Reviews* 19, 1413–1422.
- Flato, G.M. 2011. Earth system models: an overview. *Wiley Interdisciplinary Reviews: Climate Change* 2, 783–800.
- Fleitmann, D., Burns, S.J., Neff, U., et al. 2004. Palaeoclimatic interpretation of high-resolution oxygen isotope profiles derived from annually laminated speleothems from southern Oman. *Quaternary Science Reviews* 23, 935–945.
- Fleming, K., Johnston, P., Zwart, D., et al. 1998. Refining the eustatic sea-level curve since the Last Glacial Maximum using far- and intermediate-field sites. *Earth and Planetary Science Letters* 163, 327–342.
- Flint, R.F. 1957. *Glacial and Pleistocene Geology*. John Wiley, New York.
- Flores, J.-A., Sierro, F.J. 2007. Coccoliths. In *Encyclopedia of Quaternary Science* (edited by S.A. Elias). Elsevier, Amsterdam, 1634–1646.
- Flores, J.-A., Colmenero-Hidalgo, E., Mejía-Melina, A.E., et al. 2010. Distribution of large *Emiliania huxleyi* in the Central and Northeast Atlantic as a tracer of surface ocean dynamics during the last 25,000 years. *Marine Micropaleontology* 76, 53–66.

- Flores, J.-A., Filippelli, G.M., Sierro, F.J., et al. 2012. The 'White Ocean' hypothesis: a late Pleistocene Southern Ocean governed by coccolithophores and driven by phosphorus. *Frontiers in Microbiology* 3, doi: 10.3389/fmicb.2012.00233.
- Florinski, V., Axford, W.I., Zank, G.P. 2004. The cosmic ray increases at 35 and 60 kyr BP. *Radiocarbon* 46, 683–690.
- Flower, B.P., Oppo, D.W., McManus, J.F., et al. 2000. North Atlantic intermediate to Deep Water circulation and chemical stratification during the past 1 Myr. *Paleoceanography* 15, 388–403.
- Flower, B.P., Hastings, D.W., Randle, N.J. 2009. Paired AMS ^{14}C dates on planktic foraminifera from a Gulf of Mexico sediment core: an assessment of stratigraphic continuity. *Radiocarbon* 53, 337–344.
- Flückiger, J., Knutti, R., White, J.W.C. 2006. Oceanic processes as potential trigger and amplifying mechanisms for Heinrich events. *Paleoceanography* 21, doi: 10.1029/2005PA001204.
- Ford, D. 2006. Karst geomorphology, caves and cave deposits: a review of North American contributions during the past half century. *Geological Society of America, Special Paper* 404, 1–13.
- Forester, R.M., Smith, A.J., Palmer, D.F., et al. 2005. North American Non-marine Ostracode Database 'NANODe' version 1, <http://www.kent.edu/NANODe>, Kent State University, Kent, OH.
- Forman, S.L., Marín, L., van der Veen, C., et al. 2007. Little Ice Age and neoglacial landforms at the Inland Ice margin, Isunguita Sernia, Kangerlussuaq, west Greenland. *Boreas* 36, 341–351.
- Forman, S.L., Marín, L., Gomez, G., et al. 2008. Late Quaternary eolian sand depositional record for southwestern Kansas: landscape sensitivity to droughts. *Palaeogeography, Palaeoclimatology, Palaeoecology* 265, 107–120.
- Fornós J.J., Gelabert B., Ginés A., et al. 2002. Phreatic overgrowths on speleothems: a useful tool in structural geology in littoral karstic landscapes. The example of eastern Mallorca (Balearic Islands). *Geodinamica Acta* 15, 113–125.
- Foss, P. 1987. The distribution and formation of Irish peatlands. In *The IPCC Guide to Irish Peatlands* (edited by C. O'Connell), Irish Peatland Conservation Council, Ireland, 5–12.
- Foulds, S.A., Macklin, M.G. 2006. Holocene land-use change and its impact on river basin dynamics in Great Britain and Ireland. *Progress in Physical Geography* 30, 589–604.
- Frauenfelder, R., Haeberli, W., Hoelzle, M., et al. 2001. Using relict rockglaciers in GIS-based modelling to reconstruct Younger Dryas permafrost distribution patterns in the Err-Julier area, Swiss Alps. *Norsk Geografisk Tidsskrift* 55, 195–205.
- Frechen, M., Vanneste, K., Veerbeeck, K., et al. 2001. The deposition history of the coversands along the Bree Fault escarpment, NE Belgium. *Geologie en Mijnbouw (Netherlands Journal of Geosciences)* 80, 171–185.
- Frechen, M., Serrialta, M., Oezen, D., et al. 2007. Uranium-series dating of peat from central and northern Europe. In *The Climate of Past Interglacials* (edited by F. Sirocko, M. Claussen, M.F. Sanchez-Góñi, et al.), Elsevier, Amsterdam, 93–118.
- French, C. 2003. *Geoarchaeology in Action*. Routledge, London.
- French, H.M. 2007. *The Periglacial Environment*, 3rd edn. John Wiley, Chichester and New York.
- French, H.M. 2008. Recent contributions to the study of past permafrost. *Permafrost and Periglacial Processes* 19, 179–194.
- French, H.M., Shur, Y. 2010. The principles of cryostratigraphy. *Earth-Science Reviews* 101, 190–206.
- Frenzel, P., Boomer, I. 2005. The use of ostracods from marginal marine, brackish waters as bioindicators of modern and Quaternary environmental change. *Palaeogeography, Palaeoclimatology, Palaeoecology* 225, 68–92.
- Fricke, H.C., O'Neill, J.R. 1999. The correlation between $^{18}\text{O}/^{16}\text{O}$ ratios of meteoric water and surface temperature: its use in investigating terrestrial climatic change over geologic time. *Earth and Planetary Science Letters* 170, 181–196.
- Friedman, I., Obradovich, J. 1981. Obsidian hydration dating of volcanic events. *Quaternary Research* 16, 37–47.
- Friedrich, M., Remmeli, S., Kromer, B., et al. 2004. The 12,460-year Hohenheim oak and pine tree-ring chronology from Central Europe – a unique annual record for radiocarbon calibration and paleoenvironment reconstructions. *Radiocarbon* 46, 1111–1122.
- Fritts, H.C. 2001. *Tree Rings and Climate*, 2nd edn. Blackburn Press, Caldwell, NJ.
- Fritz, S.C. 2008. Deciphering climatic history from lake sediments. *Journal of Paleolimnology* 39, 5–16.
- Fritz, S.C., Baker, P.A., Seltzer, G.O., et al. 2007. Quaternary glaciation and hydrologic variation in the South American tropics as reconstructed from the Lake Titicaca drilling project. *Quaternary Research* 68, 410–420.
- Fritz, S.C., Cumming, B.F., Gasse, F., et al. 2010a. Diatoms as indicators of hydrologic and climatic change in saline lakes. In *The Diatoms: Applications for the Environmental and Earth Sciences*, 2nd edn (edited by J.P. Smol, E.F. Stoermer). Cambridge University Press, Cambridge, 186–208.
- Fritz, S.C., Baker, P.A., Ekdahl, E., et al. 2010b. Millennial-scale climate variability during the Last Glacial period in the tropical Andes. *Quaternary Science Reviews* 29, 1017–1024.
- Froese, D.G., Lowe, D.J., Knott, J.R., et al. (eds). 2008. Global tephra studies: John Westgate and Andrei Sarna-Wojcicki commemorative volume. *Quaternary International* 178, 1–319.
- Froyd, C.A., Willis, K.J. 2008. Emerging issues in biodiversity & conservation management: the need for a palaeoecological perspective. *Quaternary Science Reviews* 17–18, 1723–1732.
- Frumkin, A., Ford, D.C., Schwarcz, H.P. 1999. Continental oxygen isotopic record of the last 170,000 years in Jerusalem. *Quaternary Research* 51, 317–327.
- Fuchs, M., Lang, A., Wagner, G.A. 2004. The history of Holocene soil erosion in the Phlious Basin, NE Peloponnese, Greece, based on optical dating. *The Holocene* 14, 334–345.
- Fuhrmann, A., Fischer, T., Lücke, A., et al. 2004. Late Quaternary environmental and climatic changes in central Europe as inferred from the composition of organic matter in annually laminated lake maar sediments. *Geochemistry, Geophysics, Geosystems (G3)*, 5, Q11015.
- Fujioka, T., Chappell, J., Fifield, L.K., et al. 2009. Australian desert dune fields initiated with Pliocene–Pleistocene global climatic shift. *Geology* 37, 51–54.
- Fuller, S., Murray, T. 2002. Sedimentological investigations in the forefield of an Icelandic surge-type glacier: implications for the surge mechanism. *Quaternary Science Reviews* 21, 1503–1520.

- Fullerton, D.S., Clayton, R.B. 1986. Stratigraphy and correlation of the glacial deposits on the Montana Plains. *Quaternary Science Reviews* 5, 161–169.
- Funder, S., Demidov, I., Yelovichcheva, Y. 2002. Hydrography and mollusc faunas of the Baltic and the White Sea–North Sea seaway in the Eemian. *Palaeogeography, Palaeoclimatology, Palaeoecology* 184, 275–304.
- Funnell, B.F. 1995. Global sea level and the (pen)insularity of late Cenozoic Britain. In *Island Britain: A Quaternary Perspective* (edited by R.C. Preece). Geological Society of London, Special Publication 96. Geological Society, London, 3–14.
- Gagan, M.K., Ayliffe, L.K., Beck, J.W., et al. 2000. New views of tropical paleoclimates from corals. *Quaternary Science Reviews* 19, 45–64.
- Gaiero, D.M. 2007. Dust provenance in Antarctic ice during glacial periods: from where in southern South America? *Geophysical Research Letters* 34, doi: 10.1029/2007GL030520.
- Gajewski, K. 2008. The Global Pollen Database in biogeographical and palaeoclimatic studies. *Progress in Physical Geography* 32, 379–402.
- Gale, S.J. 2009. Event chronostratigraphy: a high-resolution tool for dating the past. *Quaternary Geochronology* 4, 391–399.
- Gale, S.J., Hoare, P.J. 2011. *Quaternary Sediments: Petrographic Methods for the Study of Unlithified Rocks*, 2nd edn. Blackburn Press, Caldwell, NJ.
- Gale, S.J., Hoare, P.G. 2012. The stratigraphic status of the Anthropocene. *The Holocene* 23, 397–414.
- Galili, E., Zviely, D., Ronen, A., et al. 2007. Beach deposits of MIS 5e high sea stand as indicators for tectonic stability of the Carmel coastal plain, Israel. *Quaternary Science Reviews* 26, 2544–2557.
- Gallet, Y., Genevey, A., Courtillot, V. 2003. On the possible occurrence of ‘archaeomagnetic jerks’ in the geomagnetic field over the past three millennia. *Earth and Planetary Science Letters* 214, 237–242.
- Ganopolski, A., Calov, R. 2011. The role of orbital forcing, carbon dioxide and regolith in 100 kyr glacial cycles. *Climate of the Past* 7, 1415–1425.
- Gao, J., Liu, Y. 2001. Applications of remote sensing, GIS and GPS in glaciology: a review. *Progress in Physical Geography* 25, 520–540.
- Garcia, J.L., Kaplan, M.R., Hall, B.L. 2012. Glacier expansion in southern Patagonia throughout the Antarctic cold reversal. *Geology* 40, 859–862.
- Garcia, T., Féraud, G., Falguères C., et al. 2010. Earliest human remains in Eurasia: new $^{40}\text{Ar}/^{39}\text{Ar}$ dating of the Dmanisi hominid-bearing levels, Georgia. *Quaternary Geochronology* 5, 443–451.
- Garcin, Y., Junginger, A., Melnick, D., et al. 2009. Late Pleistocene–Holocene rise and collapse of Lake Suguta, northern Kenya Rift. *Quaternary Science Reviews* 28, 911–925.
- Gardner, T., Webb, J., Pezzia, C., et al. 2008. Episodic intraplate deformation of stable continental margins: evidence from Late Neogene and Quaternary marine terraces, Cape Liptrap, Southeastern Australia. *Quaternary Science Reviews* 28, 39–53.
- Garilli, V. 2011. Mediterranean Quaternary interglacial molluscan assemblages: Palaeobiogeographical and palaeoceanographical responses to climate change. *Palaeogeography, Palaeoclimatology, Palaeoecology* 312, 98–114.
- Garnett, E.R., Gilmour, M.A., Rowe, P.J., et al. 2004. $^{230}\text{Th}/^{234}\text{U}$ dating of Holocene tufas: possibilities and problems. *Quaternary Science Reviews* 23, 947–958.
- Gaschen, A.A.-M., Döbeli, M., Markwitz, A., et al. 2008. Restrictions on fluorine depth profiling for exposure age dating in archaeological bones. *Journal of Archaeological Science* 35, 535–552.
- Gauthier, E., Bichet, V., Petit, C., et al. 2010. Pollen and non-pollen palynomorph evidence of medieval farming activities in southwestern Greenland. *Vegetation History and Archaeobotany* 19, 427–438.
- Gavin, D.G., Hallett, D.J., Hu, F.S., et al. 2007. Forest fire and climate change in western North America: insights from sediment charcoal records. *Frontiers in Ecology and the Environment* 5, 499–506.
- Gearey, B.R., Caseldine, C.J. 2006. Archaeological applications of testate amoebae analyses: a case study from Derryville, Co. Tipperary, Ireland. *Journal of Archaeological Science* 33, 49–55.
- Gedye, S.J., Jones, R.T., Tinner, W., et al. 2000. The use of mineral magnetism in the reconstruction of fire history: a case study from Lago di Origlio, Swiss Alps. *Palaeogeography, Palaeoclimatology, Palaeoecology* 164, 101–111.
- Gehrels, R. 2010. Sea-level changes since the Last Glacial Maximum: an appraisal of the IPCC Fourth Assessment Report. *Journal of Quaternary Science* 25, 26–38.
- Gehrels, W.R., Milne, G.A., Kirby, J.R., et al. 2004. Late Holocene sea-level changes and isostatic crustal movements in Atlantic Canada. *Quaternary International*, 120, 79–89.
- Gehrels, W.R., Marshall, W.A., Gehrels, M.J., et al. 2006. Rapid sea-level rise in the North Atlantic Ocean since the first half of the 19th century. *The Holocene* 16, 948–964.
- Geiss, C.E., Umbanhowar, C.E., Camill, P., et al. 2003. Sediment magnetic properties reveal Holocene climate change along the Minnesota prairie–forest ecotone. *Journal of Paleolimnology* 30, 151–166.
- Genty, D., Blamart, D., Ouahdi, R., et al. 2003. Precise dating of Dansgaard–Oeschger climatic oscillations in western Europe from stalagmite data. *Nature* 421, 833–837.
- Georgetti, G., Talarico, F., Sandroni, S., et al. 2009. Provenance of Pleistocene sediments in the ANDRILL AND-1B drillcore: clay and heavy mineral data. *Global and Planetary Change* 69, 94–102.
- Gersonde, R., Zielinski, U. 2000. The reconstruction of late Quaternary Antarctic sea-ice distribution – the use of diatoms as a proxy for sea-ice. *Palaeogeography, Palaeoclimatology, Palaeoecology* 162, 263–286.
- Gersonde, R., Crosta, X., Abelmann, A., et al. 2005. Sea-surface temperature and sea ice distribution of the Southern Ocean at the EPILOG Last Glacial Maximum – a circum-Antarctic view based on siliceous microfossil records. *Quaternary Science Reviews* 24, 869–896.
- Gervais B.R., MacDonald G.M. 2001. Tree-ring and summer-temperature response to volcanic aerosol forcing at the northern tree-line, Kola Peninsula, Russia. *The Holocene* 11, 499–505.

470 REFERENCES

- Geyh, M., Schotterer, U., Grosjean, M. 1998. Temporal changes of the ^{14}C reservoir effect in lakes. *Radiocarbon* 40, 921–931.
- Gherardi, J.-M., Labeyrie, L., Nave, S., et al. 2009. Glacial–interglacial circulation changes inferred from $^{231}\text{Pa}/^{230}\text{Th}$ sedimentary record in the North Atlantic region. *Paleoceanography* 24, PA2204, doi: 10.1029/2008PA001696.
- Ghilani, C.D., Wolf, P.R. 2008. *Elementary Surveying: An Introduction to Geomatics*, 12th edn. Prentice Hall, Upper Saddle River, NJ.
- Ghoneim, E., El-Baz, F. 2007. The application of radar topographic data to mapping of a mega-paleodrainage in the Eastern Sahara. *Journal of Arid Environments* 69, 658–675.
- Giardino, J.R., Vitek, J.D. 1988. The significance of rock glaciers in the glacial–periglacial landscape continuum. *Journal of Quaternary Science* 3, 97–103.
- Gibbard, P.L. 1994. *Pleistocene History of the Lower Thames Valley*. Cambridge University Press, Cambridge.
- Gibbard, P.L., van Kolfschoten, Th. 2005. The Pleistocene and Holocene Series. In *A Geologic Timescale 2004* (edited by F. Gradstein, J. Ogg, A.G. Smith). Cambridge University Press, Cambridge, 441–452.
- Gibbard, P.L., Lewin, J. 2009. River incision and terrace formation in the Late Cenozoic of Europe. *Tectonophysics* 474, 41–55.
- Gibbard, P.L., Walker, M.J.C. 2013. The Term ‘Anthropocene’ in the Context of Formal Geological Classification. *Geological Society of London, Special Publication*, 395, doi: 10.1144/SP395.1.
- Gibbard, P.L., West, R.G., Zagwijn, W.H., et al. 1991. Early and Middle Pleistocene correlations in the Southern North Sea Basin. *Quaternary Science Reviews* 10, 23–52.
- Gibbard, P.L., Smith, A.G., Zalasiewicz, J., et al. 2005. What status for the Quaternary? *Boreas* 34, 1–6.
- Gibbard, P.L., Head, M.J., Walker, M.J.C., et al. 2010. Formal ratification of the Quaternary System/Period and the Pleistocene Series/Epoch with a base at 2.58 Ma. *Journal of Quaternary Science* 25, 96–102.
- Giesecke, T., Fontana, S.L. 2008. Revisiting pollen accumulation rates from Swedish lake sediments. *The Holocene* 18, 293–305.
- Gildor, H., Tziperman, E. 2001. A sea ice climate switch mechanism for the 100-kyr cycles. *Journal of Geophysical Research* 106, 9117–9133.
- Gildor, H., Tziperman, E., Toggweiler, J.R. 2002. Sea ice switch mechanism and glacial–interglacial CO_2 variations. *Global Biogeochemical Cycles* 16, 6–1 to 6–14.
- Gill, J.L., Williams, J.W., Jackson, S.T., et al. 2009. Pleistocene megafaunal collapse, novel plant communities, and enhanced fire regimes in North America. *Science* 326, 1100–1103.
- Gilligan, I. 2007. Neanderthal extinction and modern human behaviour: the role of climate change and clothing. *World Archaeology* 39, 499–514.
- Giraudeau, J., Grelaud, M., Solignac, S., et al. 2010. Millennial-scale variability in Atlantic water advection to the Nordic Seas derived from Holocene coccolith concentration records. *Quaternary Science Reviews* 29, 1276–1287.
- Gischler, E., Hudson, J.H., Storz, D. 2009. Growth of Pleistocene massive corals in south Florida: low skeletal extension-rates and possible ENSO, decadal, and multi-decadal cyclicity. *Coral Reefs* 28, 823–830.
- Gladstone, W. 2002. The potential value of indicator groups in the selection of marine reserves. *Biological Conservation* 104, 211–220.
- Glasser, N.F., Hambrey, M.J. 2001. Styles of sedimentation beneath Svalbard valley glaciers under changing dynamic and thermal regimes. *Journal of the Geological Society of London* 158, 697–707.
- Glasser, N.F., Bennett, M.R. 2004. Glacial erosional landforms: origins and significance for palaeoglaciology. *Progress in Physical Geography* 28, 43–75.
- Glasser, N., Harrison, S., Jansson, K.N. 2009. Topographic controls on glacier sediment–landform associations around the temperate North Patagonian Icefield. *Quaternary Science Reviews* 28, 2817–2832.
- Gob, F., Petit, F., Bravard J.-P., et al. 2003. Lichenometric application to historical and subrecent dynamics and sediment transport of a Corsican stream (Figarella River – France). *Quaternary Science Reviews* 22, 2111–2124.
- Goble, R.J., Mason, J.A., Loope, D.B., et al. 2004. Optical and radiocarbon ages of stacked paleosols and dune sands in the Nebraska Sand Hills, USA. *Quaternary Science Reviews* 23, 1173–1182.
- Godfrey-Smith, D.I., Casey, J.L. 2003. Direct thermoluminescence chronology for Early Iron Age smelting technology on the Gambaga Escarpment, northern Ghana. *Journal of Archaeological Science* 30, 1037–1050.
- Godsey, H.S., Currey, D.R., Chan, M.A. 2005. New evidence for an extended occupation of the Provo shoreline and implications for regional climate change, Pleistocene Lake Bonneville, Utah, USA. *Quaternary Research* 63, 212–223.
- Goehring, B.M., Lohne Ø.S., Mangerud, J., et al. 2012. Late Glacial and Holocene beryllium-10 production rates for western Norway. *Journal of Quaternary Science* 27, 89–96.
- Gögen K., Wagner, G.A. 2002. Alpha-recoil track dating of Quaternary volcanics. *Chemical Geology* 166, 127–137.
- Goldstein, S.J., Stirling, C.H. 2003. Techniques for measuring uranium-series nuclides: 1992–2002. In *Uranium Series Geochemistry* (edited by B. Bourdon, G.M. Henderson, C.C. Lundstrom, et al.). *Reviews in Mineralogy and Geochemistry* 52, 23–57.
- Golledge, N.R. 2010. Glaciation of Scotland during the Younger Dryas stadial: a review. *Journal of Quaternary Science* 25, 550–566.
- Goman, M. 2001. Statistical analysis of modern seed assemblages from the San Francisco Bay: applications for the reconstruction of paleo-salinity and paleo-tidal inundation. *Journal of Paleolimnology* 24, 393–409.
- Gomez, B., Carter, L., Trustrum, N.A., et al. 2004. El Niño–Southern Oscillation signal associated with middle Holocene climatic changes in intercorrelated terrestrial and marine sediment cores, New Zealand. *Geology* 32, 653–656.
- Gonzalez, L.M., Grimm, E.C. 2009. Synchronisation of late-glacial vegetation changes at Crystal Lake, Illinois, USA, with the North Atlantic Event Stratigraphy. *Quaternary Research* 72, 234–245.
- González-Sempériz, P., Valero-Garcés, Moreno, A., et al. 2006. Climate variability in the Spanish Pyrenees during the last

- 30,000 yr revealed by the El Portalet sequence. *Quaternary Research* 66, 38–52.
- Goodfellow, B.W. 2007. Relict non-glacial surfaces in formerly glaciated landscapes. *Earth-Science Reviews* 80, 47–73.
- Goodfriend, G.A., Mitterer, R.M. 1993. A 45,000 year record of a tropical lowland biota: the land snail fauna from cave sediments at Coco Ree, Jamaica. *Geological Society of America Bulletin* 105, 18–29.
- Goodfriend, G., Collins, M.J., Fogel, M.L., et al. (eds). 2000. *Perspectives in Amino Acid and Protein Geochemistry*. Oxford University Press, Oxford.
- Goodman, A.Y., Rodbell, D.T., Seltzer, G.O., et al. 2001. Subdivision of glacial deposits in southeastern Peru based on pedogenic development and radiometric ages. *Quaternary Research* 56, 31–50.
- Goodwin, D.H., Flessa, K.W., Schöne, B., et al. 2001. Cross-calibration of daily growth increments, stable isotope variation, and temperature in the Gulf of California bivalve mollusk *Chione coretzi*: implications for paleoenvironmental analysis. *Palaeo* 16, 387–398.
- Gordon, S.J., Dorn, R.I. 2005. *In situ* weathering rind erosion. *Geomorphology* 67, 97–113.
- Goslar, T., Arnold, M., Tisnerat-Laborde, N., et al. 2000. Variations of Younger Dryas atmospheric radiocarbon explicable without ocean circulation changes. *Nature* 403, 877–880.
- Gosling, W.D., Mayle, F.E., Killeen, T.J., et al. 2003. A simple and effective methodology for sampling modern pollen rain in tropical environments. *The Holocene* 13, 613–618.
- Gosse, J.C., Phillips, F.M. 2001. Terrestrial *in situ* cosmogenic nuclides: theory and applications. *Quaternary Science Reviews* 20, 1475–1560.
- Gosse, J.C., Evenson, E.B., Klein, J., et al. 1995. Precise cosmogenic ^{10}Be measurements in western North America: support for a global Younger Dryas cooling event. *Geology* 23, 877–880.
- Goudie, A.S. 2006. The Schmidt hammer in geomorphological research. *Progress in Physical Geography* 30, 703–718.
- Grab, S. 2005. Aspects of the geomorphology, genesis and environmental significance of earth hummocks (*thúfur, pounus*): miniature cryogenic mounds. *Progress in Physical Geography* 29, 139–155.
- Gradstein, F.M., Ogg, J.G., Smith, A.G., et al. 2005. *A Geological Time Scale 2004*. Cambridge University Press, Cambridge.
- Gradstein, F.M., Ogg, J.G., Ogg, G., et al. 2012. *A Geological Time Scale 2012*. Elsevier, Amsterdam.
- Graham, A.G.C., Lonergan, L., Stoker, M.S. 2007. Evidence for Late Pleistocene ice stream activity in the Witch Ground Basin, central North Sea, from 3D seismic reflection data. *Quaternary Science Reviews* 26, 627–643.
- Graham, I.J., Ditchburn, R.G., Whitehead, N.E. 2001. Be isotope analysis of a 0–500 ka loess–paleosol sequence from Rangitatau East, New Zealand. *Quaternary International* 76/77, 29–42.
- Graham R.W., Lundelius Jr., E.L., Graham, M.A., et al. 1996. Spatial response of mammals to Late Quaternary environmental fluctuations. *Science* 272, 1601–1606.
- Gray, J.M. 1984. The Quaternary geomorphology of Scotland: the research contribution of J.B. Sissons. *Quaternary Science Reviews* 3, 259–289.
- Green, D.G. 1995. Time and spatial analysis. In *Statistical Modelling and Quaternary Science Data* (edited by D. Maddy, J.S. Brew). Technical Guide 5. Quaternary Research Association, Cambridge, 65–105.
- Green, O.R. 2001. *A Manual of Practical Laboratory and Field Techniques in Palaeobiology*. Springer, Dordrecht.
- Greenwood, M.T., Agnew, M.D., Wood, P.J. 2003. The use of caddisfly fauna (Insecta: Trichoptera) to characterise the Late-glacial River Trent, England. *Journal of Quaternary Science* 18, 645–661.
- Greenwood, S.L., Clark, C.D. 2009. Reconstructing the last Irish Ice Sheet 1: changing flow geometries and ice flow dynamics deciphered from the glacial landform record. *Quaternary Science Reviews* 28, 3085–3100.
- Gregory, J.M., Lowe, J.A., Tett, S.F.B. 2006. Simulated global-mean sea level changes over the last half-millennium. *Journal of Climate* 19, 4576–4591.
- Griffiths, H.I. 2001. Ostracod evolution and extinction – its biostratigraphic value in the European Quaternary. *Quaternary Science Reviews* 20, 1743–1751.
- Griffiths, J.S. (ed.). 2002. *Mapping in Engineering Geology*. ('Key Issues in Earth Sciences' Series), Geological Society of London, London.
- Griffiths, J.S., Brunsden, D., Lee, E.M., et al. 1995. Geomorphological investigations of the Channel Tunnel Terminal and Portal. *The Geographical Journal* 161, 275–284.
- Griggs, C.B., Kromer, B. 2008. Wood macrofossils and dendrochronology of three mastodon sites in upstate New York. *Palaeontologica Americana* 61, 49–61.
- Grimley, D.A., Follmer, L.R., Hughes, R.E., et al. 2003. Modern Sangamon and Yarmouth soil development in loess of unglaciated southwestern Illinois. *Quaternary Science Reviews* 22, 225–244.
- Gröcke, D.R., Gilliken, D.P. 2008. Advances in mollusc sclerochronology and sclerochemistry: tools for understanding climate and environment. *Geo-Marine Letters* 28, 265–268.
- Gröcke, D.R., Schimmelman, A., Elias, S., et al. 2006. Stable hydrogen-isotope ratios in beetle chitin: preliminary European data and re-interpretation of North American data. *Quaternary Science Reviews* 25, 1850–1864.
- Gröcke, D.R., Van Hardenbroek, M., Sauer, P. E., et al. 2011. Hydrogen isotopes in beetle chitin. *Topics in Geobiology*, 34, 105–116.
- Groote, P.M. 1978. Carbon-14 timescale extended: comparison of chronologies. *Science* 200, 11–15.
- Gross, R.S., Fukumori, I., Menemenlis, D. 2005. Atmospheric and oceanic excitation of decadal-scale Earth orientation variations. *Journal of Geophysical Research* 110, doi: 10.1029/2004JB003565.
- Grosse, G., Jones, B.M. 2011. Spatial distribution of pingos in northern Asia. *The Cryosphere* 5, 13–33.
- Grosse, G., Schirrmeyer, L., Kunitsky, V.V., et al. 2005. The use of CORONA images in remote sensing of periglacial geomorphology: an illustration from the NE Siberian coast. *Permafrost and Periglacial Processes* 16, 163–172.
- Grottoli, A.G., Eakin, C.M. 2007. A review of modern coral $\delta^{18}\text{O}$ and $\Delta^{14}\text{C}$ proxy records. *Earth-Science Reviews* 81, 67–91.

- Grove, J.M. 1988. *The Little Ice Age*. Routledge, London.
- Grudn, H., Briffa, K.R., Karlén, W., et al. 2002. A 7400-year tree-ring chronology in northern Swedish Lapland: natural climatic variability expressed on annual to millennial timescales. *The Holocene* 12, 657–666.
- Grün, R. 2001. Trapped charge dating (ESR, TL, OSL). In *Handbook of Archaeological Science* (edited by D.E. Brothwell, A.M. Pollard). John Wiley, Chichester and New York, 47–62.
- Grün, R. (ed.). 2010. 12th International Conference on Luminescence and Electron Spin Resonance Dating (LED 2008). *Quaternary Geochronology* 5, 83–390.
- Grün, R., Schwarcz, H.P. 2000. Revised open-system U-series/ESR age calculations for teeth from Stratum C at the Hoxian Interglacial type locality, England. *Quaternary Science Reviews* 19, 1151–1154.
- Grün, R., Preusser, F. (eds). 2012. 13th International Conference on Luminescence and Electron Spin Resonance (LED 2011). *Quaternary Geochronology* 10, 1–442.
- Grün, R., Aubert, M., Hellstrom, J., et al. 2010. The challenge of direct dating of old human bones. *Quaternary International*, 223–224, 87–93.
- Gubbins, D. 2008. Earth science: Geomagnetic reversals. *Nature* 452, 165–167.
- Gunn, J. (ed.). 2003. *Encyclopedia of Caves and Karst Science*. Routledge, London.
- Gunnarsson, B.E., Linderholm, H.W. 2002. Low-frequency summer temperature variation in central Sweden since the tenth century inferred from tree rings. *The Holocene* 12, 667–672.
- Gunnell, Y., Jarman, D., Braucher, R., et al. 2013. The granite tors of Dartmoor, southwest England: rapid and recent emergence revealed by Late Pleistocene cosmogenic apparent exposure ages. *Quaternary Science Reviews* 61, 62–76.
- Günster, N., Eck, P., Skowronek, A., et al. 2001. Late Pleistocene loess and their paleosols in the Granada Basin, southern Spain. *Quaternary International* 76/77, 241–245.
- Gupta, A., Hock, L., Xiaojing, H., et al. 2002. Evaluation of part of the Mekong River using satellite imagery. *Geomorphology* 44, 221–239.
- Gupta, S., Collier, J.S., Palmer-Felgate, A., et al. 2007. Catastrophic flooding origin of shelf valley systems in the English Channel. *Nature* 448, 342–345.
- Gurney, S. 2003. Relict cryogenic mounds in the UK as evidence of climate change. In *Linking Climate Change to Land Surface Change* (edited by S.J. McLaren, D.R. Kniveton). Kluwer Academic Publishers, Dordrecht, 209–229.
- Guyard, H., Chapron, E., St-Onge, G., et al. 2007. High-altitude varve records of abrupt environmental change and mining activity over the last 4000 years in the western French Alps (Lake Bramant, Grandes Rousses Massif). *Quaternary Science Reviews* 26, 2644–2660.
- Haase, D., Fink, J., Haase G., et al. 2007. Loess in Europe – its spatial distribution based on a European Loess Map, scale 1:2,500,000. *Quaternary Science Reviews* 26, 1301–1312.
- Haeberli, W., Brandová, D., Burga, C., et al. 2003. Methods for absolute and relative age dating of rock-glacier surfaces in alpine permafrost. In *Permafrost: Proceedings of the 8th International Conference on Permafrost* (edited by M. Phillips, S.M. Springman, L.U. Arenson). Taylor & Francis Group, 343–348.
- Haesaerts, P., Mestdagh, H. 2000. Pedosedimentary evolution of the last interglacial and early glacial sequence in the European loess belt from Belgium to central Russia. *Geologie en Mijnbouw (Netherlands Journal of Geosciences)* 79, 313–324.
- Haflidason, H., Eiriksson, J., van Kreveld, S. 2000. The tephrochronology of Iceland and the North Atlantic region during the Middle and Late Quaternary: a review. *Journal of Quaternary Science* 15, 3–22.
- Hailer, F., Kutschera, V.E., Hallström, B.M., et al. 2012. Nuclear genomic sequences reveal that polar bears are an old and distinct bear lineage. *Science* 336, 344–347.
- Hajdas, I., Bonani, G., Moreno, P.I., et al. 2003. Precise radiocarbon dating of Late-Glacial cooling in mid-latitude South America. *Quaternary Research* 59, 70–78.
- Håkansson, L., Jansson, M. 1983. *Principles of Lake Sedimentology*. Springer, Berlin.
- Hall, A.R. 1996. A survey of palaeobotanical evidence for dyeing and mordanting from British archaeological excavations. *Quaternary Science Reviews* 15, 635–640.
- Hall, B.L., Denton, G.H., Fountain, A.G., et al. 2010. Antarctic lakes suggest millennial reorganizations of Southern Hemisphere atmospheric and oceanic circulation. *Proceedings of the National Academy of Sciences of the United States of America* 107, 21355–21359.
- Hall, R.D., Anderson, A.K. 2000. Comparative soil development of Quaternary paleosols of the central United States. *Palaeogeography, Palaeoclimatology, Palaeoecology* 158, 109–145.
- Hall, R.I., Smol, J.P. 2010. Diatoms as indicators of lake eutrophication. In *The Diatoms: Applications for the Environmental and Earth Sciences*, 2nd edn (edited by J.P. Smol, E.F. Stoermer). Cambridge University Press, Cambridge, 122–151.
- Hambley, G.W., Lamoureux, S.F. 2006. Recent summer climate recorded in complex varved sediments, Nicolay Lake, Cornwall Island, Nunavut, Canada. *Journal of Paleolimnology* 35, 629–640.
- Hambrey, M. 1994. *Glacial Environments*. UCL Press, London.
- Hambrey, M.J., Fitzsimons, S.J. 2010. Development of sediment–landform associations at cold glacier margins, Dry Valleys, Antarctica. *Sedimentology* 57, 857–882.
- Hambrey, M.J., Glasser, N. 2012. Discriminating glacier thermal and dynamic regimes in the sedimentary record. *Sedimentary Geology* 251–252, 1–33.
- Hambrey, M.J., Davies, J.R., Glasser, N.F., et al. 2001. Devensian glaciogenic sedimentation and landscape evolution in the Cardigan area of southwest Wales. *Journal of Quaternary Science* 16, 455–482.
- Hamilton, S.J., Whalley, W.B. 1995. Rock glacier nomenclature: a re-assessment. *Geomorphology* 14, 73–80.
- Hammarlund, D., Edwards, T.W.D., Björck, S., et al. 1999. Climate and environment during the Younger Dryas (GS-1) as reflected by composite stable isotope records of lacustrine carbonates at Torreberga, southern Sweden. *Journal of Quaternary Science* 14, 17–28.
- Hammarlund, D., Barnekow, L., Birks, H.J.B., et al. 2002. Holocene changes in atmospheric circulation recorded in the oxygen-

- isotope stratigraphy of lacustrine carbonates from southern Sweden. *The Holocene* 12, 339–351.
- Hammarlund, D., Björk, S., Buchardt, B., et al. 2003. Rapid hydrological changes during the Holocene revealed by stable isotope records of lacustrine carbonates from Lake Igelsjön, southern Sweden. *Quaternary Science Reviews* 22, 353–370.
- Hammer, C.U., Mayewski, P.A., Peel, D., et al. (eds). 1997. Greenland Summit Ice Cores. Greenland Ice Sheet Project 2/Greenland Ice Core Project. *Journal of Geophysical Research* 102, 26315–26886.
- Hancock, G.S., Anderson, R.S. 2002. Numerical modeling of fluvial strath-terrace formation in response to oscillating climate. *Geological Society of America Bulletin* 114, 1131–1142.
- Hansen, E.W.S. 2008. The application of lichenometry in dating of glacier deposits. *Danish Journal of Geography* 108, 143–151.
- Hansen, E.S. 2010. A review of lichen growth and applied lichenometry in southwest and southeast Greenland. *Geografiska Annaler* 92, 65–79.
- Hansen, J. 2001. Macroscopic plant remains from Mediterranean caves and rockshelters: avenues and interpretation. *Gearchaeology* 16, 401–432.
- Hanson, P.R., Arbogast, A.F., Johnson, W.C., et al. 2010. Megadroughts and late Holocene dune activation at the eastern margin of the Great Plains, north-central Kansas, USA. *Aeolian Research* 1, 101–110.
- Haq, B.U., Boersma, A. 1998. *Introduction to Marine Micropalaeontology*. Elsevier Science, Singapore.
- Harkness, D.D. 1975. The role of the archaeologist in C-14 measurement. In *Radiocarbon Calibration and Prehistory* (edited by T. Watkins). Edinburgh University Press, Edinburgh, 128–135.
- Harlan, T., Robertson, I. 2006. Confirmation of the extended Bristlecone pine chronology. *Quaternary Newsletter* 110, 37–39.
- Harland, E. 1988. Dinoflagellates, their cysts and Quaternary stratigraphy. *New Phytologist* 108, 111–120.
- Harland, R., FitzPatrick, M.E.J., Pudsey, C.J. 1999. Latest Quaternary dinoflagellate cyst climatostratigraphy for three cores from the Falkland Trough, Scotia and Weddell seas, Southern Ocean. *Review of Palaeobotany and Palynology* 107, 265–281.
- Harris, C., Kern-Luetschg, M., Smith, F., et al. 2008. Solifluction processes in an area of seasonal ground freezing, Dovrefjell, Norway. *Permafrost and Periglacial Processes* 19, 31–47.
- Harris, C., Arenson, L.U., Christiansen, H.H., et al. 2009. Permafrost and climate in Europe: monitoring and modelling thermal, geomorphological and geotechnical responses. *Earth-Science Reviews* 92, 117–171.
- Harrison, S.P., Dodson, J. 1993. Climates of Australia and New Guinea since 18,000 yr BP. In *Global Climates Since the Last Glacial Maximum* (edited by H.E. Wright Jr., J.E. Kutzbach, T. Webb III, et al.). University of Minnesota Press, Minneapolis and London, 265–292.
- Harrison, S.P., Prentice, C., Guiot, J. 1993. Climatic controls on Holocene lake-level changes in Europe. *Climate Dynamics* 8, 189–200.
- Harrison, S., Whalley, B., Anderson, E. 2008. Relict rock glaciers and protalus lobes in the British Isles: implications for Late Pleistocene mountain geomorphology and palaeoclimate. *Journal of Quaternary Science* 23, 287–304.
- Hart, J.K. 1994. Till fabric associated with deformable beds. *Earth Surface Processes and Landforms* 19, 15–32.
- Hart, J.K. 1997. The relationship between drumlins and other forms of subglacial glaciotectonic deformation. *Quaternary Science Reviews* 16, 93–107.
- Hart, J., Rose, J. 2001. Approaches to the study of glacier bed deformation. *Quaternary International* 86, 45–58.
- Hart, J.K., Rose, K.C., Martinez, K., et al. 2009. Subglacial clast behaviour and its implication for till fabric development: new results derived from wireless subglacial probe experiments. *Quaternary Science Reviews* 28, 597–607.
- Harvey, A., Foster, G., Hannam, J., et al. 2003. The Tabernas alluvial fan and lake system, southeast Spain: applications of mineral magnetic and pedogenic iron oxide analyses towards clarifying the Quaternary sediment sequences. *Geomorphology* 151–171.
- Haslett, S.K. (ed.). 2002. *Quaternary Environmental Micropalaeontology*. Arnold, London and New York.
- Haslett, S.K. 2004. Late Neogene–Quaternary radiolarian biostratigraphy: a brief review. *Journal of Micropalaeontology* 23, 39–47.
- Haslett, S.K., Smart, C.W. 2006. Late Quaternary upwelling off tropical NW Africa: new micropalaeontological evidence from ODP Hole 658C. *Journal of Quaternary Science* 21, 259–269.
- Hather, J.G. 2000. *The Identification of the Northern European Woods: A Guide for Archaeologists and Conservators*. Archetype, London.
- Hatzopoulos, J. 2008. *Topographic Mapping*. Universal Publishers, Boca Raton, FL.
- Haug, G.H., Günther, D., Peterson, L.C., et al. 2003. Climate and the collapse of the Maya civilization. *Science* 299, 1731–1735.
- Haug, G.H., Ganopolski, A., Sigman, D.M., et al. 2005. North Pacific seasonality and the glaciation of North America 2.7 million years ago. *Nature* 433, 821–825.
- Havinga, A.J. 1964. Investigation into the differential corrosion susceptibility of pollen and spores in various soil types. *Pollen et Spores* 4, 621–635.
- Hawkins, E., Jones, P.D. 2013. On increasing global temperatures: 75 years after Callendar. *Quarterly Journal of the Royal Meteorological Society*, doi: 10.1002/qj.2178.
- Hay, R.L., Kyser, T.K. 2001. Chemical sedimentology and palaeoenvironmental history of Lake Olduvai, a Pliocene lake in northern Tanzania. *Geological Society of America Bulletin* 113, 1505–1521.
- Hayes, A., Kucera, M., Kallel, N., et al. 2005. Glacial Mediterranean sea surface temperatures based on planktonic foraminiferal assemblages. *Quaternary Science Reviews* 24, 999–1016.
- Haynes, G. (ed.). 2009. *American Megafaunal Extinctions at the End of the Pleistocene*. Springer Science and Business Media, Dordrecht.
- Haynes, G. 2013. Extinctions in North America's Late Glacial landscapes. *Quaternary International* 285, 89–98.
- Hays, J.D., Imbrie, J., Shackleton, N.J. 1976. Variations in the earth's orbit: pacemaker of the Ice Ages. *Science* 194, 1121–1132.

474 REFERENCES

- Haywood, A.M., Valdes, P.J. 2004. Modelling Pliocene warmth: contribution of atmosphere, oceans and cryosphere. *Earth and Planetary Science Letters* 218, 363–377.
- He, F., Shakun, J.D., Clark, P.U., et al. 2013. Northern Hemisphere forcing of Southern Hemisphere climate during the last deglaciation. *Nature* 494, 81–85.
- Head, M.J., Gibbard, P.L., Salvador, A. 2008a. The Quaternary: its character and definition. *Episodes* 31, 234–238.
- Head, M.J., Gibbard, P.L., Salvador, A. 2008b. The Early–Middle Pleistocene Transition: characterisation and proposed guide for defining the boundary. *Episodes* 31, 255–259.
- Hearty, P.J. 2003. Stratigraphy and timing of aeolianite deposition on Rottnest Island, Western Australia. *Quaternary Research* 60, 211–222.
- Hearty, P.J., Kindler, P. 1995. Sea level highstand chronology from stable carbonate platforms (Bermuda and the Bahamas). *Journal of Coastal Research* 11, 675–689.
- Hearty, P.J., Kaufman, D.S. 2000. Whole-rock aminostratigraphy and Quaternary sea-level history of the Bahamas. *Quaternary Research* 54, 163–173.
- Hearty, P.J., O’Leary, M.J. 2007. Carbonate eolianites, quartz sands, and Quaternary sea-level cycles, Western Australia: a chronostratigraphic approach. *Quaternary Geochronology* 3, 26–55.
- Hearty, P.J., Olson, S.L., Kaufman, D.S., et al. 2004. Stratigraphy and geochronology of pitfall accumulations in caves and fissures, Bermuda. *Quaternary Science Reviews* 23, 1151–1171.
- Hebdon, N.J., Atkinson, T.C., Lawson T.J., et al. 1997. Rate of glacial valley deepening during the late Quaternary in Assynt, Scotland. *Earth Surface Processes and Landforms* 22, 307–315.
- Hedberg, H.D. (ed.). 1976. *International Stratigraphic Guide*. John Wiley, London and New York.
- Hedding, D.W., Sumner, P.D., Holness, S.D., et al. 2007. Formation of a pronyrampart on sub-Antarctic Marion Island. *Antarctic Science* 19, 443–450.
- Hedges, R.E.M. 2001. The future of the past. *Radiocarbon* 43, 141–148.
- Hegerl, G.C., Bindoff, N.L. 2005. Warming the world’s oceans. *Science* 309, 254–255.
- Heine, K., Reuther, A.U., Thieke, H.U., et al. 2009. Timing of Weichselian ice marginal positions in Brandenburg (northeastern Germany) using cosmogenic in situ ^{10}Be . *Zeitschrift für Geomorphologie* N.F., 53, 433–454.
- Heinemeier, J., Ringbom, Å., Lindroos, A., et al. 2010. Successful AMS ^{14}C dating of non-hydraulic lime mortars from the Medieval churches of the Åland Islands, Finland. *Radiocarbon* 52, 171–204.
- Heinrich, H. 1988. Origin and consequences of cyclic ice-rafting in the Northeast Atlantic Ocean during the past 130,000 years. *Quaternary Research* 29, 142–152.
- Heinrichs, M.L., Walker, I.R. 2006. Fossil midges and palaeosalinity: potential as indicators of hydrological balance and sea-level change. *Quaternary Science Reviews* 25, 1948–1965.
- Heiri, O., Lotter, A.F., Lemeke, G. 2001. Loss on ignition as a method for estimating organic and carbonate content in sediments: reproducibility and comparability of results. *Journal of Paleolimnology* 25, 101–110.
- Heiri, O., Brooks, S.J., Birks, H.J.B., et al. 2011. A 274-lake calibration data-set and inference model for chironomid-based summer air temperature reconstruction in Europe. *Quaternary Science Reviews* 30, 3445–3456.
- Helama, S., Lindholm, M., Timonen, M., et al. 2002. The supra-long Scots pine tree-ring record for Finnish Lapland: Part 2, interannual to centennial variability in summer temperatures for 7500 years. *The Holocene* 12, 681–687.
- Hellman, S., Bunting, M.J., Gaillard, M.-J. 2009. Relevant source area of pollen in patchy cultural landscapes and signals of anthropogenic landscape disturbance in the pollen record: a simulation approach. *Review of Palaeobotany and Palynology* 153, 245–258.
- Hemming, S.R. 2004. Heinrich events: massive Late Pleistocene detritus layers of the North Atlantic and their global climate imprint. *Review of Geophysics* 42, 1–43.
- Henderson, G.M. 2002. New oceanic proxies for paleoclimate. *Earth and Planetary Science Letters* 203, 1–13.
- Hendon, D., Charman, D. 2004. High-resolution peatland water-table changes for the past 200 years: the influence of climate and implications for management. *The Holocene* 14, 125–134.
- Hendon, D., Charman, D.J., Kent, M. 2001. Palaeohydrological records derived from testate amoebae analysis from peatlands in northern England: within-site variability, between-site comparability and palaeoclimatic implications. *The Holocene* 11, 127–148.
- Hendy, E.J., Gagan, M.K., Lough, J.M. 2003. Chronological control of coral records using luminescent lines and evidence for non-stationary ENSO teleconnections in northeastern Australia. *The Holocene* 13, 187–199.
- Herzschuh, U. 2006. Palaeo-moisture evolution in monsoonal Central Asia during the last 50,000 years. *Quaternary Science Reviews* 25, 163–178.
- Hess, D.P., Briner, J.P. 2009. Geospatial analysis of controls on subglacial bedform morphometry in the New York Drumlin Field – implications. *Earth Surface Processes and Landforms* 34, 1126–1135.
- Hesse, P.P., McTainsh, G.H. 2003. Australian dust deposits: modern processes and the Quaternary record. *Quaternary Science Reviews* 22, 2007–2035.
- Hesse, P.P., Magee, J.W., van der Kars, S. 2004. Late Quaternary climates of the Australian arid zone: a review. *Quaternary International* 118–119, 103–126.
- Hessler, I., Dupont, L., Bonnefille, R., et al. 2010. Millennial-scale changes in vegetation records from tropical Africa and South America during the last glacial. *Quaternary Science Reviews* 29, 2882–2899.
- Hetherington, A.M., Woodward, F.I. 2003. The role of stomata in sensing and driving environmental change. *Nature* 424, 901–908.
- Hetherington, R., Barrie, J.V. 2004. Interaction between local tectonics and glacial unloading on the Pacific margin of Canada. *Quaternary International* 120, 65–77.
- Hewitt, G.M. 2011. Quaternary phylogeography: the roots of hybrid zones. *Genetica* 139, 617–638.

- Hicks, S., Tinsley, H., Huusko, A., et al. 2001. Some comments on spatial variation in arboreal pollen deposition: first records from the Pollen Monitoring Programme (PMP). *Review of Palaeobotany and Palynology* 117, 183–194.
- Hicock, S.R., Goff, J.R., Lian, O.B., et al. 1996. On the interpretation of subglacial till fabric. *Journal of Sedimentary Research* 66, 928–934.
- Hiemstra, J.F., Evans, D.J., Scourse, J.D., et al. 2006. New evidence for a grounded Irish Sea glaciation of the Isles of Scilly. *Quaternary Science Reviews* 25, 299–309.
- Higham, T.F.G., Hedges, R.E.M., Andersen, A.J., et al. 2004. Problems associated with the AMS dating of small bone samples: the question of the arrival of Polynesian rats to New Zealand. *Radiocarbon* 46, 207–218.
- Higham, T.F.G., Jacobi, R.M., Bronk Ramsey, C., 2006. AMS radiocarbon dating of ancient bone using ultrafiltration. *Radiocarbon* 48, 179–195
- Hilgen, F., Brinkhuis, H., Zachariasse, W.-J. 2006. Unit stratotypes for global stages: the Neogene perspective. *Earth-Science Reviews* 74, 113–125.
- Hill, J.K., Griffiths, H.M., Thomas, C.D. 2011. Climate change and evolutionary adaptations at species' range margins. *Annual Review of Entomology* 56, 143–59.
- Hill, T.M., Kennett, J.P., Behl, R.J., et al. 2006. Pre-Bølling warming in Santa Barbara Basin, California: surface and intermediate water records of early deglacial warmth. *Quaternary Science Reviews* 25, 2835–2845.
- Hillaire-Marcel, C., Ochietti, S. 1980. Chronology, palaeogeography and palaeoclimatic significance of the late and post-glacial events in eastern Canada. *Zeitschrift für Geomorphologie* 24, 373–392.
- Hillaire-Marcel, C., De Vernal, A. (eds). 2007. *Proxies in Late Cenozoic Paleoceanography*. Elsevier, Amsterdam.
- Hillam, J., Groves, C.M., Brown, D.M., et al. 1990. Dendrochronology of the British Neolithic. *Antiquity* 64, 210–220.
- Hillebrand, C.-D., Moreton, S.G., Caburlotto, A., et al. 2008. Volcanic time-markers for Marine Isotope Stages 6 and 5 in the Southern Ocean sediments and Antarctic ice cores: Implications for correlations between palaeoclimatic records. *Quaternary Science Reviews* 27, 518–540.
- Hillebrand, C.-D., Ehrmann, W.U., Larter, R.D., et al. 2009. Clay mineral provenance of sediments in the southern Bellinghausen Sea reveals drainage changes of the West Antarctic Ice Sheet during the Late Quaternary. *Marine Geology* 265, 1–18.
- Hillman, G., Hedges, R., Moore, A., et al. 2001. New evidence of Lateglacial cereal cultivation at Abu Hureyra on the Euphrates. *The Holocene* 11, 383–393.
- Hinnov, L.A., Schulz, M., Yiou, P. 2002. Interhemispheric space-time attributes of the Dansgaard–Oeschger oscillations between 100 and 0 ka. *Quaternary Science Reviews* 21, 1213–1228.
- Hirmas, D.R., Allen, B.L. 2007. Degradation of pedogenic calcretes in West Texas. *Soil Science Society of America Journal* 71, 1878–1888.
- Hiscock, K., Southward, A., Tittley, I., et al. 2004. Effects of changing temperature on benthic marine life in Britain and Ireland. *Aquatic Conservation: Marine and Freshwater Ecosystems* 14, 333–362.
- Hocknull, S.A., Zhao, J.-X., Feng, Y.-X., et al. 2007. Responses of Quaternary rainforest vertebrates to climate change in Australia. *Earth and Planetary Science Letters* 264, 317–331.
- Hodder, K.R. 2009. Flocculation: a key process in the sediment flux of a large, glacier-fed lake. *Earth Surface Processes and Landforms* 34, 1151–1163.
- Hodgson, D.A., Convey, P. 2005. A 7000-year record of oribatid mite communities on a maritime-Antarctic island: responses to climate change. *Arctic, Antarctic, and Alpine Research* 37, 239–245.
- Hoek, W.Z. 1997. Late-glacial and Early Holocene climatic events and chronology of vegetation development in the Netherlands. *Vegetation History and Archaeobotany* 6, 197–213.
- Hoey, T.B., 2004. The size of sedimentary particles. In *A Practical Guide to the Study of Glacial Sediments* (edited by D.J.A. Evans, D.I. Benn). Edward Arnold, London, 52–77.
- Hof, C., Levinsky, I., Araújo, M.B., et al. 2011. Rethinking species' ability to cope with rapid climate change. *Global Change Biology* 17, 2987–2990.
- Hoffmann, T., Thorndycraft, V.R., Brown, A.G., et al. 2010. Human impact on fluvial regimes and sediment flux during the Holocene: review and future research agenda. *Global and Planetary Change* 72, 87–98.
- Hofreiter, M. 2008. Long DNA sequences and large data sets: investigating the Quaternary via ancient DNA. *Quaternary Science Reviews* 27, 2586–2592.
- Hofreiter, M., Stewart, J. 2009. Ecological change, range fluctuations and population dynamics during the Pleistocene (Review). *Current Biology* 19, R584–R594.
- Hofreiter, M., Barnes, I. 2010. Diversity lost: are all Holarctic large mammal species just relict populations? *BMC Biology* 8, 46.
- Hofreiter, M., Collins, M., Stewart, J.R. 2012. Ancient biomolecules in Quaternary palaeoecology. *Quaternary Science Reviews* 33, 1–13.
- Hogg, A.G., Higham, T.F.G., Lowe, D.J., et al. 2003. A wiggle-match date for Polynesian settlement of New Zealand. *Antiquity* 77, 116–125.
- Hogg, A.G., Fifeld, L.K., Turney, C.S.M., et al. 2006. Dating ancient wood by high-sensitivity liquid scintillation counting and accelerator mass spectrometry—pushing the boundaries. *Quaternary Geochronology* 1, 241–248.
- Holden, P.B., Mackay, A.W., Simpson, G.L. 2008. A Bayesian palaeoenvironmental transfer function model for acidified lake. *Journal of Paleolimnology* 39, 551–566.
- Höll, C., Karwath, B., Rühlemann, C., et al. 1999. Palaeoenvironmental information gained from calcareous dinoflagellates: the late Quaternary eastern and western tropical Atlantic Ocean in comparison. *Palaeogeography, Palaeoclimatology, Palaeoecology* 146, 147–164.
- Hollands, C.B., Nanson, G.C., Jones, B.G., et al. 2006. Aeolian–fluvial interaction: evidence for Late Quaternary channel change and wind-rift linear dune formation in the northwestern Simpson Desert, Australia. *Quaternary Science Reviews* 25, 142–162.
- Holliday, V.T. 2004. *Soils in Archaeological Research*. Cambridge University Press, Oxford and New York.

- Holmes, J.A. 2002. Ostracoda. In *Tracking Environmental Change Using Lake Sediments. Volume 4: Zoological Indicators* (edited by J.P. Smol, H.J.B. Birks, W.M. Last). Springer, Berlin, 125–151.
- Holmes, J.A., Chivas, A. 2002. *The Ostracoda: Applications in Quaternary Research*. Geophysical Monograph 131. American Geophysical Union, Washington, DC.
- Holmes, J.A., Atkinson, T., Darbyshire, D.B.F., et al. 2010. Middle Pleistocene climate and hydrological environment at the Boxgrove hominin site (West Sussex, UK) from ostracod records. *Quaternary Science Reviews* 29, 1515–1527.
- Holmgren, K., Tyson, P.D., Moberg, A., et al. 2001. A preliminary 3000-year regional temperature reconstruction for South Africa. *South African Journal of Science* 97, 49–51.
- Holmgren, K., Lee-Thorp, J.A., Cooper, G.R.J., et al. 2003. Persistent millennial-scale climatic variability over the past 25,000 years in Southern Africa. *Quaternary Science Reviews* 22, 2311–2326.
- Hölzel, N., Otte, A. 2004. Inter-annual variation in the soil seed bank of flood-meadows over two years with different flooding patterns. *Plant Ecology* 174, 279–291.
- Hölzer, A., Hölzer, A. 1998. Silicon and titanium in peat profiles as indicators of human impact. *The Holocene* 8, 685–696.
- Holzhauser, H., Magny, M., Zumbühl, H.J. 2005. Glacier and lake-level variations in west-central Europe over the last 3500 years. *The Holocene* 15, 789–801.
- Hongve, D. 2003. Chemical stratigraphy of recent sediments from a depth gradient in a meromictic lake, Nordbytjernet, SE Norway, in relation to variable external loading and sedimentary fluxes. *Journal of Paleolimnology* 30, 75–93.
- Hoogakker, B.A.A., McCave, I.N., Vautravers, M.J. 2007. Antarctic link to deep flow speed variation during Marine Isotope Stage 3 in the western North Atlantic. *Earth and Planetary Science Letters* 257, 463–473.
- Hooghiemstra, H., van Geel, B. 1998. World list of Quaternary pollen and spore atlases. *Review of Palaeobotany and Palynology* 104, 157–182.
- Hooghiemstra, H., van der Hammen, T. 2004. Quaternary ice-age dynamics in the Colombian Andes: developing an understanding of our legacy. *Philosophical Transactions of the Royal Society of London B* 359, 173–181.
- Hooke, J.M. 2006. Human impacts on fluvial systems in the Mediterranean region. *Geomorphology* 79, 311–335.
- Hooyer, T.S., Iverson, N.R. 2002. Flow mechanism of the Des Moines lobe of the Laurentide ice sheet. *Journal of Glaciology* 48, 575–586.
- Horne, D.J., Holmes, J.A., Rodriguez-Lazaro, J., et al. (eds). 2012. *Developments in Quaternary Science. Volume 17: Ostracoda as Proxies for Quaternary Climate Change*. Elsevier, Amsterdam.
- Horrocks, M., Jones, M., Scott, N., et al. 2002. Wetland microfossils in soil: implications for the study of land use on archaeological landscapes. *Environmental Archaeology* 7, 101–106.
- Horsák, M. 2005. Mollusc community patterns and species response curves along a mineral richness gradient: a case study in fens. *Journal of Biogeography* 33, 98–107.
- Horsák, M. 2011. Mollusc assemblages in palaeoecological reconstructions: an investigation of their predictive power using transfer function models. *Boreas* 40, 459–467.
- Horsák, M., Chitrý, M., Pokryszko, B.M., et al. 2010. Habitats of relict terrestrial snails in southern Siberia: lessons for the reconstruction of palaeoenvironments of full-glacial Europe. *Journal of Biogeography* 37, 1450–1462.
- Horton, B., Culver, S.J., Hardbattle, M.I.J., et al. 2007. Reconstructing Holocene sea-level change for the central Great Barrier Reef (Australia) using subtidal Foraminifera. *Journal of Foraminiferal Research* 37, 327–343.
- Houmark-Nielsen, M. 1989. The last interglacial–glacial cycle in Denmark. *Quaternary International* 3/4, 31–39.
- Howard, L.C., Wood, P.J., Greenwood, M., et al. 2010. Sub-fossil Chironomidae as indicators of palaeoflow regimes: integration into the PalaeoLIFE flow index. *Journal of Quaternary Science* 25, 1270–1283.
- Howarth, J.D., Fitzsimons, S.J., Jacobsen, G.E., et al. 2013. Identifying a reliable target fraction for radiocarbon dating sedimentary records from lakes. *Quaternary Geochronology* 17, 68–80.
- Howell, D., Siegert, M.J., Dowdeswell, J.A. 2000. Modelling the influence of glacial isostasy on Late Weichselian ice-sheet growth in the Barents Sea. *Journal of Quaternary Science* 15, 475–486.
- Hu, F.S., Kaufman, D., Yoneji, S., et al. 2003. Cyclic variation and solar forcing of Holocene climate in the Alaskan Subarctic. *Science* 301, 1890–1893.
- Hua, Q., Barbetti, M., Fink, D., et al. 2009. Atmospheric ^{14}C variations derived from tree rings during the early Younger Dryas. *Quaternary Science Reviews* 28, 2982–2990.
- Huang, C.C., Pang, J., Zhao, J. 2000. Chinese loess and the evolution of the east Asian monsoon. *Progress in Physical Geography* 24, 75–96.
- Huang, E., Tian, J. 2012. Sea-level rises at Heinrich stadials of early Marine Isotope Stage 3: evidence of terrigenous n-alkane input in the southern South China Sea. *Global and Planetary Change* 94–95, 1–12.
- Hubbard, B., Glasser, N. 2005. *Field Techniques in Glaciology and Glacial Geomorphology*. John Wiley, Chichester.
- Hubeny, J.B., King, J.W., Santos, A. 2006. Subdecadal to multidecadal cycles of Late Holocene North Atlantic climate variability preserved by estuarine fossil pigments. *Geology* 34, 569–572.
- Huggett, R.J. 1998. Soil chronosequences, soil development, and soil evolution: a critical review. *Catena* 32, 155–172.
- Hughen, K., Lehman, S., Suthon, J., et al. 2004a. ^{14}C activity and global carbon cycle changes over the past 50,000 years. *Science* 303, 202–207.
- Hughen, K.A., Eglinton, T.I., Xiu, L., et al. 2004b. Abrupt tropical vegetation response to rapid climatic changes. *Nature* 304, 1955–1959.
- Hughen, K., Suthon, J., Lehman, S., et al. 2006. Marine-derived C-14 calibration and activity record for the past 50,000 years updated from the Cariaco Basin. *Quaternary Science Reviews* 25, 3216–3227.
- Hughes, G.R., Kennedy, D.M. 2009. Late Pleistocene sea-level oscillations (MIS 10-2) recorded in shallow marine and coastal plain sediments of the southern Wanganui Basin, New Zealand. *Quaternary Research* 71, 477–489.
- Hughes, M.K., Swetnam, T.W., Diaz, H.F. (eds). 2011. *Dendroclimatology: Progress and Prospects*. Developments in Palaeo-environmental Research, 11. Springer, Berlin.

- Hughes, P.D. 2010. Geomorphology and Quaternary stratigraphy: the roles of morpho-, litho-, and allostratigraphy. *Geomorphology* 123, 189–199.
- Hughes, P.D.M., Mauquoy, D., Barber, K.E., et al. 2000. Mire development pathways and palaeoclimatic records from a full Holocene peat archive at Walton Moss, Cumbria, England. *The Holocene* 10, 465–479.
- Hughes, P.D., Gibbard, P.L., Woodward, J.C. 2003. Relict rock glaciers as indicators of Mediterranean palaeoclimate during the Last Glacial Maximum (Late Würmian) in northwest Greece. *Journal of Quaternary Science* 18, 431–440.
- Hughes, P.D., Gibbard, P.L., Ehlers, J. 2013. Timing of glaciation during the last glacial cycle: evaluating the concept of a global 'Last Glacial Maximum' (LGM). *Earth-Science Reviews* 125, 171–198.
- Huguet, C., Kim, J.-H., Damsté, J.S.S., et al. 2006. Reconstruction of sea surface temperature variations in the Arabian Sea over the last 23 kyr using organic proxies (TEX_{86} and U_{37}^{K}). *Paleoceanography* 21, doi: 10.1029/2005PA001215.
- Huijzer, A.S., Isarin, R.F.B. 1997. The reconstruction of past climates using multi-proxy evidence: an example of the Weichselian Pleniglacial in northwestern and central Europe. *Quaternary Science Reviews* 16, 513–533.
- Huijzer, B., Vandenberghe, J. 1998. Climatic reconstruction of the Weichselian Pleniglacial in northwestern and central Europe. *Journal of Quaternary Science* 13, 391–417.
- Hulbe, C.L., MacAyeal, D.R., Denton, G.H., et al. 2004. Catastrophic ice shelf breakup as the source of Heinrich event icebergs. *Paleoceanography* 19, PA1004, doi: 10.1029/2003PA000890.
- Hull, K.L. 2001. Reasserting the utility of obsidian hydration dating: a temperature-dependent empirical approach to practical temporal resolution with archaeological obsidians. *Journal of Archaeological Science* 28, 1025–1040.
- Hüls, C.M., Grootes, P.M., Nadeau, M.-J., et al. 2004. AMS radiocarbon dating of iron artefacts. *Nuclear Instruments and Methods in Physics Research B* 223–224, 709–715.
- Humlum, O., Christiansen, H.H. 2008. Lowland periglacial research: a review of published advances 2003–2007. *Permafrost and Periglacial Processes* 19, 211–235.
- Humlum, O., Christiansen, H.H., Juliussen, H. 2007. Avalanche-derived rock glaciers in Svalbard. *Permafrost and Periglacial Processes* 18, 75–88.
- Hüneke, H., Mulder, T. (eds). 2011. *Deep-Sea Sediments*. Elsevier, Amsterdam.
- Hunt, C.O. 1993. Mollusc taphonomy in caves: a conceptual model. *Cave Science* 20, 45–49.
- Hunt, C.O. 2005. Pollen taphonomy and airfall sedimentation in a tropical cave: the West Mouth of The Great Cave of Niah in Sarawak, Malaysian Borneo. *Journal of Archaeological Science* 32, 465–473.
- Huntley, B. 1992. Rates of change in the European palynological record of the last 13,000 years and their climatic interpretation. *Climate Dynamics* 6, 185–191.
- Huntley D.J., Lamothe, M. 2001. Ubiquity of anomalous fading in K-feldspars, and the measurement and correction for it in optical dating. *Canadian Journal of Earth Sciences* 38, 1093–1106.
- Hurford, A.J. 1991. Fission Track Dating. In *Quaternary Dating Methods – A User's Guide* (edited by P.L. Smart, P.D. Frances). Technical Guide 4. Quaternary Research Association, Cambridge, 84–107.
- Hurrell, J., Deser, C. 2009. North Atlantic climate variability: the role of the North Atlantic Oscillation. *Journal of Marine Science* 78, 28–41.
- Hutchinson, I., James, T.S., Clague, J.J., et al. 2004. Reconstruction of late Quaternary sea-level change in southwestern British Columbia from sediments in isolation basins. *Boreas* 33, 183–194.
- Hutri, K.-L., Kotilainen, A. 2007. An acoustic view into Holocene palaeoseismicity offshore southwestern Finland, Baltic Sea. *Marine Geology* 238, 45–59.
- Huybers, P. 2007. Glacial variability over the last two million years: an extended depth-derived age model, continuous obliquity pacing, and the Pleistocene progression. *Quaternary Science Reviews* 26, 37–55.
- Huybers, P. 2009. Pleistocene glacial variability as a chaotic response to obliquity forcing. *Climate of the Past* 5, 481–488.
- Huybers, P., Wunsch, C. 2005. Obliquity pacing of the late Pleistocene terminations. *Nature* 434, 491–494.
- Hubrechts, P. 2006. Numerical modeling of ice sheets through time. In *Glacier Science and Environmental Change* (edited by P.G. Knight). Blackwell Publishing, Oxford, 406–412.
- Ikehara, K., Itaki, T. 2007. Millennial-scale fluctuations in seasonal sea-ice and deep-water formation in the Japan Sea during the late Quaternary. *Palaeogeography, Palaeoclimatology, Palaeoecology* 247, 131–143.
- Ilyashuk, B., Gobet, E., Heiri, O., et al. 2009. Lateglacial environmental changes at the Maloja Pass, Central Swiss Alps, as recorded by chironomids and pollen. *Quaternary Science Reviews* 28, 1340–1353.
- Imbrie, J., Kipp, N.G. 1971. A new micropalaeontological method of quantitative palaeoclimatology: application to a Late Pleistocene Caribbean core. In *The Late Cenozoic Glacial Ages* (edited by K.K. Turekian). Yale University Press, New Haven, 71–181.
- Imbrie, J., Imbrie, K.P. 1979. *Ice Ages: Solving the Mystery*. Macmillan, London.
- Imbrie, J., Hays, J.D., Martinson, D.G., et al. 1984. The orbital theory of Pleistocene climate: support from a revised chronology of the marine $\delta^{18}\text{O}$ record. Terminations. In *Milanovitch and Climate* (edited by A. Berger, J. Imbrie, J. Hays, et al.). Reidel, Dordrecht, 269–306.
- Imbrie, J., Berger, A., Shackleton, N.J. 1993. Role of orbital forcing: a two-million year perspective. In *Global Changes in the Perspective of the Past* (edited by J.A. Eddy, H. Oeschger). John Wiley, Chichester and New York, 263–277.
- Ingólfsson, O. 2004. Quaternary glacial and climatic history of Antarctica. In *Developments in Quaternary Science. Volume 2: Quaternary Glaciations: Extent and Chronology* (edited by J. Ehlers, P.L. Gibbard). Elsevier, Amsterdam, 3–43.
- Ingólfsson, O., Landvik, J.Y. 2013. The Svalbard–Barents Sea ice sheet – historical, current and future perspectives. *Quaternary Science Reviews* 64, 33–60.
- Ingólfsson, O., Björck, S., Haflidason, H., et al. 1997. Glacial and climatic events in Iceland reflecting regional North Atlantic

- climatic shifts during the Pleistocene–Holocene transition. *Quaternary Science Reviews* 16, 1135–1144.
- Innes, J.L. 2006. Lichenometric dating of debris-flow deposits in the Scottish Highlands. *Earth Surface Processes and Landforms* 8, 579–588.
- Intergovernmental Panel on Climate Change. 2007. *Climate Change 2007: Synthesis Report*. Contribution of Working Groups I, II and III to the Fourth Assessment Report of the Intergovernmental Panel on Climate Change. IPCC, Geneva.
- Intergovernmental Panel on Climate Change. 2013. *Climate Change 2013: The Physical Science Basis*. Contribution of Working Group I to the Fifth Assessment Report of the Intergovernmental Panel on Climate Change (edited by T.F. Stocker, D. Qin, G.-K. Plattner, et al.). Cambridge University Press, Cambridge and New York.
- International Atomic Energy Agency. 2009. Reference Sheet for International Measurement Standards VSMOW2, SLAP2, Water, <http://nucleus.iaea.org/rpst/ReferenceProducts>.
- Isarin, R.F.B. 1997. Permafrost distribution and temperatures in Europe during the Younger Dryas. *Permafrost and Periglacial Processes* 8, 313–333.
- Isarin, R.F.B., Bohncke, S.J.P. 1999. Mean July temperatures during the Younger Dryas in Northwestern and Central Europe as inferred from climate indicator plant species. *Quaternary Research* 51, 158–173.
- Isarin, R.F.B., Renssen, H. 1999. Reconstructing and modelling Late Weichselian climates: the Younger Dryas in Europe as a case study. *Earth-Science Reviews* 48, 1–38.
- Isarin, R.F.B., Renssen, H., Koster, E.A. 1997. Surface wind climate during the Younger Dryas in Europe as inferred from aeolian records and model simulations. *Palaeogeography, Palaeoclimatology, Palaeoecology* 134, 127–148.
- Isarin, R.F.B., Renssen, H., Vandenberghe, J. 1998. The impact of the North Atlantic Ocean on the Younger Dryas climate in north western and central Europe. *Journal of Quaternary Science* 13, 447–453.
- Itaki, T., Komatsu, N., Motoyama, I. 2007. Orbital- and millennial-scale changes of radiolarian assemblages during the last 220 kyr in the Japan Sea. *Palaeogeography, Palaeoclimatology, Palaeoecology* 247, 115–130.
- Iturizaga, L. 2008. Paraglacial landform assemblages in the Hindu Kush and Karakoram Mountains. *Geomorphology* 95, 27–47.
- Ivanova, E.V., Beaufort, L., Vidal, L., et al. 2012. Precession forcing of productivity in the Eastern Equatorial Pacific during the last glacial cycle. *Quaternary Science Reviews* 40, 64–77.
- Ivanovich, M., Harmon, R.S. (eds). 1995. *Uranium-series Disequilibrium: Applications to Earth, Marine and Environmental Sciences*, 2nd edn. Clarendon Press, Oxford.
- Ivy-Ochs, S., Kober, F. 2008. Surface exposure dating with cosmogenic nuclides. *Eiszeitalter und Gegenwart (Quaternary Science Journal)* 57, 179–209.
- Ivy-Ochs, S., Poschinger, A.V., Syndal, H.-A., et al. 2009. Surface exposure dating of the Flims landslide, Grisons, Switzerland. *Geomorphology* 103, 104–112.
- Izett, G.A., Naeser, C.W. 1976. Age of the Bishop Tuff of eastern California as determined by the fission-track method. *Geology* 4, 587–590.
- Jackson, A., Jonkers, A.R.T., Walker, M.R. 2000. Four centuries of geomagnetic secular variation from historical records. *Philosophical Transactions of the Royal Society of London A* 358, 957–990.
- Jackson, L.E., Phillips, F.M., Shimamura, K., et al. 1997. Cosmogenic ^{36}Cl dating of the Foothills erratics train, Alberta, Canada. *Geology* 25, 195–198.
- Jackson, S.T., Williams, J.W. 2004. Modern analogs in Quaternary paleoecology: here today, gone yesterday, gone tomorrow? *Annual Review of Earth and Planetary Sciences* 32, 495–537.
- Jackson, S.T., Betancourt, J.L., Lyford, M.E., et al. 2005. A 40,000-year woodrat midden record of vegetational and biogeographical dynamics in north-eastern Utah, USA. *Journal of Biogeography* 32, 1085–1106.
- Jacob, D., Bähring, L., Christensen, O.B., et al. 2007. An inter-comparison of regional climate models for Europe: model performance in present-day climate. *Climatic Change* 81, 31–52.
- Jacobs, P.M., Mason, J.D. 2007. Late Quaternary climate change, loess sedimentation, and soil profile development in the central Great Plains: a pedosedimentary model. *Geological Society of America Bulletin* 119, 462–475.
- Jacobs, P.M., Konen, M.E., Curry, B.B. 2009. Pedogenesis of a catena of the Farmdale–Sangamon Geosol complex in the north central United States. *Palaeogeography, Palaeoclimatology, Palaeoecology* 282, 119–132.
- Jacomet, S. 2007. Plant macrofossil methods and studies: use in environmental archaeology. In *Encyclopedia of Quaternary Science* (edited by S.A. Elias). Elsevier, Amsterdam, 2384–2412.
- James, R.H., Austin, W.E.N. 2008. *Biogeochemical Controls on Palaeoceanographic Environmental Proxies: A Review*. Geological Society of London, Special Publication 303. Geological Society, London, 3–32.
- James, T.S., Clague, J.J., Wang, K., et al. 2000. Postglacial rebound at the northern Cascadia subduction zone. *Quaternary Science Reviews* 19, 1527–1541.
- Janke, J., Frauenfelder, R. 2008. The relationship between rock glacier and contributing area parameters in the Front Range of Colorado. *Journal of Quaternary Science* 23, 153–163.
- Jans, M.M.E., Kars, H., Nielsen-Marsh, C.M., et al. 2002. In situ preservation of archaeological bone: a histological study within a multidisciplinary approach. *Archaeometry* 44, 343–352.
- Jarman, D., Wilson, P., Harrison, S. 2013. Are there any relict rock glaciers in the British mountains? *Journal of Quaternary Science* 28, 131–143.
- Jass, C.N., George, C.O. 2010. An assessment of the contribution of fossil cave deposits to the Quaternary paleontological record. *Quaternary International* 217, 105–116.
- Jedoui, Y., Reyss, J.-L., Kallel, N., et al. 2003. U-series evidence for two high Late Interglacial sea levels in southeastern Tunisia. *Quaternary Science Reviews* 22, 343–351.
- Jellinek, A.M., Manga, M., Saar, M.O. 2004. Did melting glaciers cause volcanic eruptions in eastern California? Probing the mechanics

- of dike formation. *Journal of Geophysical Research* 109, B09206, doi: 10.1029/2004JB002978.
- Jenkins, D.L., Davis, L.G., Stafford Jr., T.W., et al. 2012. Clovis age western stemmed projectile points and human coprolites at the Paisley Caves. *Science* 337, 223–228.
- Jennings, A.E., Tedesco, K.A., Andrews, J.T., et al. 1996. *Shelf Erosion and Glacial Ice Proximity in the Labrador Sea During and After Heinrich Events (H-3 or 4 to H-0) as Shown by Foraminifera*. Geological Society of London, Special Publication 111. Blackwell Scientific Publications, Oxford, 29–49.
- Jennings, C. 2004. The status of glacial mapping in Minnesota. In *Developments in Quaternary Science. Volume 2: Quaternary Glaciations: Extent and Chronology* (edited by J. Ehlers, P.L. Gibbard). Elsevier, Amsterdam, 119–124.
- Jennings, C.E., Johnson, M.D. 2011. The Quaternary of Minnesota. In *Developments in Quaternary Science. Volume 15: Quaternary Glaciations – Extent and Chronology: A Closer Look* (edited by J. Ehlers, P.L. Gibbard, P.D. Hughes). Elsevier, Amsterdam, 499–511.
- Jensen, J.R. 2007. *Remote Sensing of the Environment: An Earth Resource Perspective*, 2nd edn. Prentice Hall, Upper Saddle River, NJ.
- Jewell, P.W. 2007. Morphology and paleoclimatic significance of Pleistocene Lake Bonneville spits. *Quaternary Research* 68, 421–430.
- Jex, C.N., Baker, A., Fairchild, I.J., et al. 2010. Calibration of speleothem $\delta^{18}\text{O}$ with instrumental climate records from Turkey. *Global and Planetary Change* 71, 207–217.
- Jex, C.N., Baker, A., Eden, J.M., et al. 2011. A 500 yr speleothem-derived reconstruction of late autumn–winter precipitation, northeast Turkey. *Quaternary Research* 75, 399–405.
- Jiménez-Espejo, F., Martínez-Ruiz, F., Finlayson, C., et al. 2007. Climate forcing and Neanderthal extinction in Southern Iberia: insights from a multi-proxy marine record. *Quaternary Science Reviews* 26, 836–852.
- Jin, Z., Bickle, M., Chapman, H., et al. 2006. An experimental evaluation of cleaning methods for fossil ostracod Mg/Ca and Sr/Ca determination. *Journal of Paleolimnology* 36, 211–218.
- Johnsen, S.J., Dahl-Jensen, D., Dansgaard, W., et al. 1995. Greenland palaeotemperatures derived from GRIP bore hole temperature and ice core isotope profiles. *Tellus* 47B, 624–629.
- Johnsen, S., Dahl-Jensen, D., Gundestrup, N., et al. 2001. Oxygen isotope and palaeotemperature records from six Greenland ice-core stations: Camp Century, Dye-3, GRIP, GISP2, Renland and NorthGRIP. *Journal of Quaternary Science* 16, 299–308.
- Johnson, A. 1999. *The Ancient Bristlecone Pine Forest*. Community Printing and Publishing, Bishop, CA.
- Johnson, M.D., Mickelson, D.M., Clayton, L., et al. 1995. Composition and genesis of glacial hummocks, western Wisconsin, USA. *Boreas* 24, 97–116.
- Johnson, M.D., Jennings, C., Hobbs, H. 2009. Lithostratigraphy for Quaternary glacial deposits: 'If it ain't broke, don't fix it'. *GSA Today* 19, 15–16.
- Johnson, M.R., Smith, A.M. 1997. Seabed topography under the southern and western Ronne Ice Shelf, derived from seismic surveys. *Antarctic Science* 9, 201–208.
- Johnsson, K. 1997. Chemical dating of bones based on diagenetic changes in bone apatite. *Journal of Archaeological Science* 24, 431–437.
- Johnston, P., Lambeck, K. 2002. Postglacial rebound and sea level contributions to changes in the geoid and the Earth's rotation axis. *Geophysical Journal International* 136, 537–555.
- Jones, A.P., Tucker, M.E., Hart, J.K. 1999. *The Description and Analysis of Quaternary Stratigraphic Field Sections*. Technical Guide 7. Quaternary Research Association, London.
- Jones, C. 2003. A Fast Ocean GCM without flux adjustments. *Journal of Atmospheric and Oceanic Technology* 20, 1857–1868.
- Jones, J., Tinsley, H., Brunning, R. 2007a. Methodologies for assessment of the state of preservation of pollen and plant macrofossil remains in waterlogged deposits. *Environmental Archaeology* 12, 71–86.
- Jones, M.D., Roberts, C.N., Leng, M.J., et al. 2006. A high-resolution late Holocene lake isotope record from Turkey and links to North Atlantic and monsoon climate. *Geology* 34, 361–364.
- Jones, M.D., Roberts, C.N., Leng, M.J. 2007b. Quantifying climatic change through the last glacial–interglacial transition based on lake isotope palaeohydrology from central Turkey. *Quaternary Science Reviews* 67, 463–473.
- Jones, P.D., Mann, M.E. 2004. Climate over past millennia. *Review of Geophysics* 42, doi: 10.129/2003RG000143.
- Jones, P.D., Briffa, K.R., Osborn, T.J., et al. 2009. High-resolution palaeoclimatology of the last millennium: a review of current status and future prospects. *The Holocene* 19, 3–49.
- Jones, P.D., Lister, D.H., Osborn, T.J., et al. 2012. Hemispheric and large-scale land-surface air temperature variations: an extensive revision and an update to 2010. *Journal of Geophysical Research* 117, D05127, doi: 10.1029/2011JD017139.
- Jones, R.T., Marshall, J.D., Crowley, S.F., et al. 2002. A high resolution multiproxy late-glacial record of climate change and intrasystem responses in NW England. *Journal of Quaternary Science* 17, 329–340.
- Jones, V. 2007. Diatom introduction. In *Encyclopedia of Quaternary Science* (edited by S.A. Elias). Elsevier, Amsterdam, 476–484.
- Joos, F., Gerber, S., Prentice, I.C., et al. 2004. Transient simulations of Holocene atmospheric carbon dioxide and terrestrial carbon since the Last Glacial Maximum. *Global Biogeochemical Cycles* 18, GB2002, doi: 10.1029/2003GB002156.
- Jordan, B.R., Sigurdsson, H., Carey, S.N., et al. 2006. Geochemical correlation of Caribbean Sea tephras with ignimbrites in central America. *Geological Society of America, Special Paper* 402, 175–208.
- Josephs, R.L. 2010. Micromorphology of an early Holocene loess–paleosol sequence, central Alaska, USA. *Arctic, Antarctic and Alpine Research* 42, 67–75.
- Jouzel, J., Alley, R.B., Cuffey, K.M., et al. 1997. Validity of the temperature reconstruction from water isotopes in ice cores. *Journal of Geophysical Research* 102, 26471–26487.
- Jouzel, J., Masson-Delmotte, V., Cattani, O., et al. 2007. Orbital and millennial Antarctic climate variability over the past 800,000 years. *Science* 317, 793–796.
- Juggins, S., Cameron, N.G. 2010. Diatoms and archaeology. In *The Diatoms: Applications for the Environmental and Earth Sciences*,

- 2nd edn (edited by J.P. Smol, E.F. Stoermer). Cambridge University Press, Cambridge, 514–522.
- Juyal, N., Chamyal, L.S., Bhandari, S., et al. 2006. Continental record of the southwest monsoon during the last 130 ka: evidence from the southern margin of the Thar Desert, India. *Quaternary Science Reviews* 25, 2632–2650.
- Kageyama, M., Paul, A., Roche, D.M., et al. 2010. Modelling glacial climatic millennial-scale variability related to changes in the Atlantic meridional overturning circulation: a review. *Quaternary Science Reviews* 29, 2931–2956.
- Kaiser, K., Hilgers, A., Schlaak, N., et al. 2009. Palaeopedological marker horizons in northern central Europe: characteristics of Lateglacial Usselo and Finow soils. *Boreas* 38, 591–609.
- Kaiser, K.F., Friedrich, M.N., Miramont, C., et al. 2012. Challenging process to make Lateglacial tree-ring chronologies from Europe absolute – an inventory. *Quaternary Science Reviews* 36, 78–90.
- Kale, V.S. 2007. Fluvio-sedimentary response of the monsoon-fed Indian rivers to Late Pleistocene–Holocene changes in monsoon strength: reconstruction based on existing ^{14}C dates. *Quaternary Science Reviews* 26, 1610–1620.
- Kalis, A.J., van der Knaap, W.O., Schweizer, A., et al. 2006. A three thousand year succession of plant communities on a valley bottom in the Vosges Mountains, NE France, reconstructed from fossil pollen, plant macrofossils, and modern phytosociological communities. *Vegetation History and Archaeobotany* 15, 377–390.
- Kamenik, C., Schmidt, R. 2005. Chrysophyte resting stages: a tool for reconstructing winter/spring climate from Alpine lake sediments. *Boreas* 34, 477–489.
- Kandiano, E.S., Bauch, H.A., Kirsten, F., et al. 2012. The meridional temperature gradient in the eastern North Atlantic during MIS 11 and its link to the ocean–atmosphere system. *Palaeogeography, Palaeoclimatology, Palaeoecology* 333/334, 24–39.
- Karali, L., Mavridis, F., Kjormazopoulou, L. 2005. Cultural landscapes during the Late and Final Neolithic of the Aegean. A case study from Leontari Cave, Mt Hymettos, Athens, Greece. *Antiquity* 79, 303.
- Karg, S., Märkle, T. 2002. Continuity and changes in plant resources during the Neolithic period in western Switzerland. *Vegetation History and Archaeobotany* 11, 169–176.
- Karner, D.B., Levine, J., Medeiros, B.P. 2002. Constructing a stacked benthic $\delta^{18}\text{O}$ record. *Paleoceanography* 17, 1030, doi: 10.1029/2001PA000667.
- Karney, G.B., Butler, P.G., Scourse, J.D., et al. 2011. Identification of growth increments in the shell of the bivalve mollusc *Arctica islandica* using backscattered electron imaging. *Journal of Microscopy* 241, 29–36.
- Kars, R.H., Wallinga, J., Cohen, K. 2008. A new approach towards anomalous fading correction for feldspar IRSL dating – tests on samples in field saturation. *Radiation Measurements* 43, 786–790.
- Karte, J. 1983. Periglacial phenomena and their significance as climatic and edaphic indicators. *GeoJournal* 7, 329–340.
- Kashiwaya, K., Ochiai, S., Sakai, H., et al. 2001. Orbit-related long-term climate cycles revealed in a 12-Myr continental record from Lake Baikal. *Nature* 410, 71–74.
- Kaspari, S.D.S., Schwikowski, M., Gysel, M., et al. 2011. Recent increases in black carbon concentrations from a Mt Everest ice core spanning 1860–2000 AD. *Geophysical Research Letters* 38, doi: 10.1029/2010GL046096.
- Kasse, C., Vandenberghe, J., De Corte, F., et al. 2007. Late Weichselian fluvio-aeolian sands and coversands of the type locality Grubbenvorst (southern Netherlands): sedimentary environments, climate record and age. *Journal of Quaternary Science* 22, 695–708.
- Kattel, G.R., Battarbee, R.W., Mackay, A.W., et al. 2008. Recent ecological change in a remote Scottish mountain loch: an evaluation of a Cladocera-based temperature transfer-function. *Palaeogeography, Palaeoclimatology, Palaeoecology* 259, 51–76.
- Katz, M.E., Cramer, B.S., Franzese, A., et al. 2010. Traditional and emerging geochemical proxies in Foraminifera. *Journal of Foraminiferal Research* 40, 165–192.
- Kaufman, D. 2003a. Dating deep-lake sediments by using amino acid racemization in fossil ostracodes. *Geology* 31, 1049–1052.
- Kaufman, D.S. 2003b. Amino acid paleothermometry of Quaternary ostracodes from the Bonneville Basin, Utah. *Quaternary Science Reviews* 22, 899–914.
- Kaufman, D.S., Manley, W.F. 1998. A new procedure for determining DL amino acid ratios in fossils using reverse phase liquid chromatography. *Quaternary Science Reviews* 17, 987–2000.
- Kaufman, D., Schneider, D., McKay, N., et al. 2009. Recent warming reverses long-term arctic cooling. *Science* 325, 1236–1239.
- Kaufmann, P., Fundel, F., Fischer, H., et al. 2010. Ammonium and non-sea salt sulfate in the EPICA ice cores as indicator of biological activity in the Southern Ocean. *Quaternary Science Reviews* 29, 313–323.
- Kawamura, K., Parrenin, F., Lisiecki, L., et al. 2007. Northern Hemisphere forcing of climatic cycles in Antarctica over the past 360,000 years. *Nature* 448, 912–916.
- Kearey, P., Brooks, M., Hill, I. 2002. *An Introduction to Geophysical Exploration*. Blackwell Publishing, Oxford.
- Kebede, S., Travi, Y., Alemayehu, T., et al. 2006. Water balance of Lake Tana and its sensitivity to fluctuations in rainfall, Blue Nile basin, Ethiopia. *Journal of Hydrology* 316, 233–247.
- Keen, D.H. 2001. Towards a late Middle Pleistocene non-marine molluscan biostratigraphy for the British Isles. *Quaternary Science Reviews* 20, 1657–1665.
- Kehl, M., Frechen, M., Skowronek, A. 2005. Paleosols derived from loess and loess-like sediments in the Basin of Persepolis, Southern Iran. *Quaternary International* 140/141, 135–149.
- Kehrwald, N.M., McCoy, W.D., Thiebault, J., et al. 2010. Paleoclimatic implications of the spatial patterns of modern and LGM European land-snail shell $\delta^{18}\text{O}$. *Quaternary Research* 74, 166–176.
- Kelley, S. 2002a. Excess argon in K–Ar and Ar–Ar geochronology. *Chemical Geology* 188, 1–22.
- Kelley, S. 2002b. K–Ar and Ar–Ar dating. *Reviews in Mineralogy and Geochemistry* 47, 785–818.
- Kellogg, T.B. 1976. Late Quaternary climatic changes: evidence from deep-sea cores of Norwegian and Greenland seas. In *Investigation of Late Quaternary Paleoceanography and Palaeoclimatology* (edited by R.M. Cline, J.D. Hays). Geological Society of America Memoir 145, 77–110.

- Kelly, M., Kubik, P.W., von Blanckenburg, F., et al. 2004. Surface exposure dating of the Great Aletsch Egesen moraine system, western Swiss Alps, using the cosmogenic nuclide ^{10}Be . *Journal of Quaternary Science* 19, 431–442.
- Kemp, A.C., Horton, B.P., Corbett, D.R., et al. 2009. The relative utility of foraminifera and diatoms for reconstructing late Holocene sea-level change in North Carolina, USA. *Quaternary Research* 71, 9–21.
- Kemp, A.C., Sommerfield, C.K., Vane, C.H., et al. 2012b. Use of lead isotopes for developing chronologies in recent salt-marsh sediments. *Quaternary Geochronology* 12, 40–49.
- Kemp, A.E.S. 2003. Evidence for abrupt climatic changes in annually laminated marine sediments. *Philosophical Transactions of the Royal Society of London, London A* 361, 1851–1870.
- Kemp, J., Radke, L.C., Olley, J., et al. 2012a. Holocene lake salinity changes in the Wimmera, southeastern Australia, provide evidence for millennial-scale climate variability. *Quaternary Research* 77, 65–76.
- Kemp, R.A. 1987. The interpretation and environmental significance of a buried Middle Pleistocene soil near Ipswich Airport, Suffolk, England. *Philosophical Transactions of the Royal Society of London B* 317, 365–391.
- Kemp, R.A. 1998. Role of micromorphology in paleopedological research. *Quaternary International* 51–52, 133–141.
- Kemp, R.A. 2001. Pedogenic modification of loess: significance for palaeoclimatic reconstructions. *Earth-Science Reviews* 54, 145–156.
- Kemp, R.A., Derbyshire, E. 1998. The loess soils of China as records of climate change. *European Journal of Soil Science* 49, 525–539.
- Kemp, R.A., Whiteman, C.A., Rose, J. 1993. Palaeoenvironmental and stratigraphic significance of the Valley Farm and Barham Soils in eastern England. *Quaternary Science Reviews* 12, 833–848.
- Kemp, R.A., Jerz, H., Grottenhaler, W., et al. 1994. Pedosedimentary fabrics of soils within loess and colluvium in southern England and southern Germany. In *Soil Micromorphology: Studies in Management and Genesis* (edited by A.J. Ringrose-Voase, G.S. Humphreys). Elsevier, Amsterdam, 207–219.
- Kemp, R.A., Derbyshire, E., Meng, X.M., et al. 1995. Pedosedimentary reconstruction of a thick loess–palaeosol sequence near Lanzhou in north-central China. *Quaternary Research* 43, 30–45.
- Kemp, R.A., Derbyshire, E., Meng, X. 2001. A high-resolution micromorphological record of changing landscapes and climates on the western Loess Plateau of China during oxygen isotope stage 5. *Palaeogeography, Palaeoclimatology, Palaeoecology* 170, 157–169.
- Kemp, R.A., Toms, P.S., Sayago, J.M., et al. 2003. Micromorphology and OSL dating of the basal part of the loess–palaeosol sequence at La Mesada in Tucumán province, Northwest Argentina. *Quaternary International* 106/107, 111–117.
- Kemp, R.A., King, M., Toms, P., et al. 2004. Pedosedimentary development of part of a Late Quaternary loess–palaeosol sequence in northwest Argentina. *Journal of Quaternary Science* 19, 567–576.
- Kemp, R.A., Zárate, M., Toms, P., et al. 2006. Late Quaternary paleosols, stratigraphy and landscape evolution in the Northern Pampa, Argentina. *Quaternary Research* 66, 119–132.
- Kenward, H., Carrott, J. 2006. Insect species associations characterise past occupation sites. *Journal of Archaeological Science* 33, 1452–1473.
- Kenward, H., Hall, A.R., Jones, A.K.G. 2012. Turf roofs and urban archaeological build-up. *Environmental Archaeology* 17, 66–79.
- Kerney, M. 1999. *Atlas of Land and Freshwater Molluscs of Britain and Ireland*. Harley Books, Colchester.
- Kerschner, H., Kaser, G., Sailer, R. 2000. Alpine Younger Dryas glaciers as palaeo-precipitation gauges. *Annals of Glaciology* 31, 80–84.
- Khan, K., Khan, S.A., Krusgaard, N.J., et al. 2012. Aerial photographs reveal late-20th century dynamic ice loss in northwestern Greenland. *Science* 337, 586–573.
- Khim, B.K., Ikehara, K., Irino, T. 2012. Orbital- and millennial-scale paleoceanographic changes in the north-eastern Japan basin, East Sea/Japan Sea during the late Quaternary. *Journal of Quaternary Science* 27, 328–335.
- Khursevich, G.K., Karabanov, E.B., Prokopenko, A.A., et al. 2001. Insolation regime in Siberia as a major factor controlling diatom production in Lake Baikal during the past 800,000 years. *Quaternary International* 80/81, 47–58.
- Kidwell, S.M. 2002. Mesh-size effects on the ecological fidelity of death assemblages: a meta-analysis of molluscan live–dead studies. *Geobios Memoire Special* 24, 107–119.
- Kilfeather, A.A., Ó Cofaigh, C., Dowdeswell, J.A., et al. 2010. Micromorphological characteristics of glacimarine deposits: implications for distinguishing genetic processes of massive diamicts. *Geo-marine Letters* 30, 77–97.
- Kim, J., Park, C., Kim, T.-H., et al. 2003. Effects of various pretreatments for enhanced anaerobic digestion with waste-activated sludge. *Journal of Bioscience and Bioengineering* 95, 271–275.
- Kim, J.-H., Schneider, R.R., Müller, P.J., et al. 2002. Interhemispheric comparison of deglacial sea-surface temperature patterns in Atlantic eastern boundary currents. *Earth and Planetary Science Letters* 194, 383–393.
- Kim, J.-H., Schouten, S., Hopmans, E.C., et al. 2008. Global sediment core-top calibration of the TEX_{86} paleo-thermometer in the ocean. *Geochimica et Cosmochimica Acta* 72, 1154–1173.
- Kindermann, K., Bubenzier, O., Nussbaum, S., et al. 2006. Palaeoenvironment and Holocene land use of Djara, Western Desert of Egypt. *Quaternary Science Reviews* 25, 1619–1637.
- Kindler, P., Hearty, P.J. 2000. Elevated marine terraces from Eleuthera (Bahamas) and Bermuda: sedimentological, petrographic and geochronological evidence for important deglaciation events during the middle Pleistocene. *Global and Planetary Change* 24, 41–58.
- King, E.C., Hindmarsh, R.C.A., Stokes, C.R. 2009a. Formation of mega-scale glacial lineations observed beneath a West Antarctic ice stream. *Nature Geoscience* 2, 585–588.
- King, G., Bailey, G. 2006. Tectonics and human evolution. *Antiquity* 80, 1–22.
- King, G.A. 2012. Isotopes as palaeoeconomic indicators: new applications in archaeoentomology. *Journal of Archaeological Science* 39, 511–520.

482 REFERENCES

- King, G.A., Gilbert, M.T.P., Willerslev, E., et al. 2009b. Recovery of DNA from archaeological insect remains: first results, problems and potential. *Journal of Archaeological Science* 36, 1179–1183.
- Kiss, L., Magnin, F., Torre, F. 2004. The role of landscape history and persistent biogeographical patterns in shaping the responses of Mediterranean land snail communities to recent fire disturbances. *Journal of Biogeography* 31, 145–157.
- Kjaer, K.H., Houmark-Nielsen, M., Richardt, N. 2003. Ice-flow patterns and dispersal of erratics at the southwestern margin of the last Scandinavian Ice Sheet: signature of palaeo-ice streams. *Boreas* 32, 130–148.
- Klassen, R.A. 2001. *A Quaternary Geological Perspective on Geochemical Exploration in Glaciated Terrain*. Geological Society of London, Special Publication 185. Blackwell Scientific Publications, Oxford, 1–17.
- Kleiven H.F., Jansen, E., Fronval, T., et al. 2002. Intensification of North Hemisphere glaciations in the circum Atlantic region (3.5–2.4 Ma) – ice rafted detritus evidence. *Palaeogeography, Palaeoclimatology* 184, 213–223.
- Kleiven, H.F., Kissel, C., Laj, C., et al. 2008. Reduced North Atlantic deep water coeval with the Glacial Lake Agassiz freshwater outburst. *Science* 319, 60–64.
- Kligrmann, D.M., Calderari, M. 2012. Diatoms and ceramic provenance: a cautionary tale. *Archaeometry* 54, 129–143.
- Klok, E.J., Oerlemans, J. 2004. Climate reconstructions derived from global glacier length records. *Arctic, Antarctic and Alpine Research* 36, 573–583.
- Klotz, S., Müller, U., Mosbrugger, V., et al. 2004. Eemian to early Würmian climate dynamics: history and pattern of changes in Central Europe. *Palaeogeography, Palaeoclimatology, Palaeoecology* 211, 107–126.
- Klütsch, C.F.C., Manseau, M., Wilson, P.J. 2012. Phylogeographical analysis of mtDNA data indicates Postglacial expansion from multiple glacial refugia in Woodland Caribou (*Rangifer tarandus caribou*). *PLoS ONE* 7(12): e52661, doi: 10.1371/journal.pone.0052661
- Kneisel, C. 2010. Frozen ground conditions in a subarctic mountain environment, Northern Sweden. *Geomorphology* 118, 80–92.
- Knight, J. 2012. Glaciectonic sedimentary and hydraulic processes at an oscillating ice margin. *Proceedings of the Geologists' Association* 123, 714–727.
- Knight, J., Harrison, S. (eds). 2009. *Periglacial and Paraglacial Processes and Environments*. Geological Society of London, Special Publication 320. Geological Society, London.
- Knight, P.J. 1999. *Glaciers*. Stanley Thores, Cheltenham.
- Knox, R.W.O'B., Pearson, P.N., Barry, T.L., et al. 2012. Examining the case for the use of the Tertiary as a formal period or informal unit. *Proceedings of the Geologists' Association* 123, 390–393.
- Knudsen, K.-L., Seidenkrantz, M.-S., Kristensen, P. 2002. Last interglacial and early glacial circulation in the northern North Atlantic Ocean. *Quaternary Research* 58, 22–26.
- Knudsen, K.L., Eiríksson, J., Bartels-Jónsdóttir, H.B. 2012. Oceanographic changes through the last millennium off North Iceland: temperature and salinity reconstructions based on foraminifera and stable isotopes. *Marine Micropaleontology* 84–85, 54–73.
- Knudsen, M.F., Riisager, P., Jacobsen, B.H., et al. 2009. Taking the pulse of the sun during the Holocene by joint analysis of ^{14}C and ^{10}Be . *Geophysical Research Letters* 36, doi: 10.1029/2009GL039439
- Knutti, R., Flückiger, J., Stocker, T.F., et al. 2004. Strong hemispheric coupling of glacial climate through freshwater discharge and ocean circulation. *Nature* 430, 851–856.
- Kober, B., Schwalb, A., Schettler, G., et al. 2007. Constraints on paleowater dissolved loads and on catchment weathering over the past 16 ka from $^{87}\text{Sr}/^{86}\text{Sr}$ ratios and Ca/Mg/Sr chemistry of freshwater ostracode tests in sediments of Lake Constance, Central Europe. *Chemical Geology* 240, 361–376.
- Koç, N. 2007. Diatom records – North Atlantic and Arctic. In *Encyclopedia of Quaternary Science* (edited by S.A. Elias). Elsevier, Amsterdam, 567–576.
- Koch, P.L., Barnosky, A.D. 2006. Late Quaternary extinctions: state of the debate. *Annual Review of Ecology, Evolution, and Systematics* 37, 215–250.
- Kohfeld, K.E., Harrison, S.P. 2000. How well can we simulate past climates? Evaluating the models using global palaeoenvironmental datasets. *Quaternary Science Reviews* 19, 321–346.
- Kohfeld, K.E., Harrison, K.E. 2003. Glacial-interglacial changes in dust deposition on the Chinese Loess Plateau. *Quaternary Science Reviews* 22, 1859–1878.
- Kohn, M.J., McKay, M.P. 2012. Paleoecology of late Pleistocene–Holocene faunas of eastern and central Wyoming, USA, with implications for LGM climate models. *Palaeogeography, Palaeoclimatology, Palaeoecology* 326–328.
- Kolstrup, E. 1993. Complex frost wedge casts as indicators of ice age environmental change. *Würzburger Geographische Arbeiten* 87, 269–282.
- Kolstrup, E. 2004. Stratigraphic and environmental implications of a large ice-wedge cast at Tjæreborg, Denmark. *Permafrost and Periglacial Processes* 15, 31–40.
- Konopinski, D.I., Hudziak, S., Morgan, R., et al. 2012. Investigation of quartz surface textures by atomic force microscopy for forensic science. *Forensic Science International* 223, 245–255.
- Korholka, A. 2007. Diatom methods: data interpretation. In *Encyclopedia of Quaternary Science* (edited by S.A. Elias). Elsevier, Amsterdam, 494–507.
- Korsun, S., Hald, M. 1998. Modern benthic Foraminifera off Novaya Zemlya tidewater glaciers, Russian Arctic. *Arctic and Alpine Research* 30, 61–77.
- Kos, A.M. 2003. Characterisation of post-depositional taphonomic processes in the accumulation of mammals in a pitfall cave deposit in southeastern Australia. *Journal of Archaeological Science* 30, 781–796.
- Kosnik, M.A., Kaufman, D.S., Hua, Q. 2008. Identifying outliers and assessing the accuracy of amino acid racemization measurements for geochronology: I. Age calibration curves. *Quaternary Geochronology* 3, 308–327.
- Kossler, A., Tarasov, P., Schlögl, G., et al. 2011. Onset and termination of the late-glacial climate reversal in the high-resolution diatom and sedimentary records from the annually laminated SG06 core from Lake Suigetsu, Japan. *Palaeogeography, Palaeoclimatology, Palaeoecology* 306, 103–115.

- Kovanen, D.J., Easterbrook, D.J. 2002. Timing and extent of Allerød and Younger Dryas Age (ca. 12,500–10,000 ^{14}C yr B.P.) oscillations of the Cordilleran Ice Sheet in the Fraser Lowland, Western North America. *Quaternary Research* 57, 208–224.
- Kovanen, D.J., Slaymaker, O. 2004. Relict shorelines and ice flow patterns of the Northern Puget Lowland from lidar data and digital terrain modelling. *Geografiska Annaler A* 86, 385–400.
- Krachler, M., Zheng, J., Fisher, D., et al. 2009. Global atmospheric As and Bi contamination preserved in 3000 year old Arctic ice. *Global Biogeochemical Cycles* 23, doi: 10.1029/209/GB003471.
- Kramer, A., Herzschuh, U., Mischke, S., et al. 2010. Late Quaternary environmental history of the south-eastern Tibetan Plateau inferred from the Lake Naleng non-pollen palynomorph record. *Vegetation History and Archaeobotany* 19, 453–468.
- Krasilnikov, P., García-Calderón, N.E. 2006. A WRB-based buried paleosol classification. *Quaternary International* 156–157, 176–188.
- Kravchinsky, V.A., Langereis, C.G., Walker, S.D., et al. 2013. Discovery of Holocene millennial climate cycles in the Asian continental interior: has the sun been governing the continental climate? *Global and Planetary Change* doi: 10.1016/j.gloplacha2013.02.011.
- Krishnan, R., Sugi, M. 2003. Pacific decadal oscillation and variability of the Indian summer monsoon rainfall. *Climate Dynamics* 21, 233–242.
- Kromer, B. 2009. Radiocarbon and dendrochronology. *Dendrochronologia* 27, 15–19.
- Kubala-Kukus, A., Ludwikowska-Kedzia, M., Banas, D., et al. 2013. Application of the X-ray fluorescence analysis and X-ray diffraction in geochemical studies of the Pleistocene tills from Holy Cross Mountains. *Radiation Physics and Chemistry* 93, 92–98.
- Kubiak-Martens, L. 1999. The plant food component of the diet at the late Mesolithic (Ertebolle) settlement at Tybrind Vig, Denmark. *Vegetation History and Archaeobotany* 8, 117–127.
- Kucera, M. 2007. Planktonic Foraminifera as tracers of past oceanic environments. In *Developments in Marine Geology, Volume 1: Proxies in Late Cenozoic Paleoceanography* (edited by C. Hillaire-Marcel, A. De Vernal). Elsevier, Amsterdam, 213–262.
- Kucera, M., Rosell-Melé, A., Schneider, R., et al. 2005a. Multiproxy approach for the reconstruction of the glacial ocean surface (MARGO). *Quaternary Science Reviews* 24, 813–819.
- Kucera, M., Schneider, R., Weinelt, M. (eds). 2005b. MARGO: Multiproxy approach for the reconstruction of the glacial ocean surface. *Quaternary Science Reviews* 24, 813–1107.
- Kuehn, S.C., Froese, D.G., Carrara, P.E., et al. 2009. Major- and trace-element characterization, expanded distribution, and a new chronology for the latest Pleistocene Glacier Peak tephras in western North America. *Quaternary Research* 71, 201–216.
- Kühl, N., Gebhardt, C., Litt, T., et al. 2002. Probability density functions as botanical-climatological transfer functions for climate reconstruction. *Quaternary Research* 58, 381–392.
- Kuhlmann, G., Langereis, C.G., Munsterman, D., et al. 2006. Integrated chronostratigraphy of the Pliocene–Pleistocene interval and its relation to the regional stratigraphical stages in the southern North Sea region. *Geologie en Mijnbouw (Netherlands Journal of Geosciences)* 85, 19–35.
- Kuhn, B.F., Berger, L.R., Skinner, J.D. 2010. Examining criteria for identifying and differentiating fossil faunal assemblages accumulated by hyenas and hominins using extant hyenid accumulations. *International Journal of Osteoarchaeology* 20, 15–35.
- Kühn, P., Terhorst, B., Ottner, F. 2006. Micromorphology of middle Pleistocene paleosols in northern Italy. *Quaternary International* 156/157, 156–166.
- Kukla, G.J. 1977. Pleistocene land–sea correlations – 1. Europe. *Earth-Science Reviews* 13, 307–374.
- Kumambala, P.G., Ervine, A. 2010. Water balance model of Lake Malawi and its sensitivity to climate change. *The Open Hydrology Journal* 4, 152–162.
- Kumar, S. 2005. Molecular clocks: four decades of evolution. *Nature Reviews Genetics* 6, 654–662.
- Kurtén, B. 2009. *Pleistocene Mammals of Europe*, 2nd edn. Transaction Publishers, New Brunswick, NJ.
- Kurth, G., Phillips, F.M., Rehels, M., et al. 2010. Cosmogenic nuclide and uranium-series dating of old, high shorelines in the western Great Basin, USA. *Geological Society of America Bulletin* 123, 744–768.
- Kutzbach, J.E., Guetter, P.J. 1986. The influence of changing orbital parameters and surface boundary conditions on climate simulations for the past 18,000 years. *Journal of Atmospheric Sciences* 43, 1726–1759.
- Kutzbach, J.E., Webb III, T. 1993. Conceptual basis for understanding Late Quaternary climates. In *Global Climates Since the Last Glacial Maximum* (edited by H.E. Wright Jr., J.E. Kutzbach, T. Webb III, et al.). University of Minnesota Press, Minneapolis and London, 1–5.
- Kutzbach, J.E., Guetter, P.J., Behling, P.J., et al. 1993. Simulated climatic changes: results of the COHMAP climate-model experiments. In *Global Climates Since the Last Glacial Maximum* (edited by H.E. Wright Jr., J.E. Kutzbach, T. Webb III, et al.). University of Minnesota Press, Minneapolis and London, 24–93.
- Kuzmin, Y.V., Burr, G.S., Jull, A.H.T. 2001. Radiocarbon reservoir correction ages in the Peter the Great Gulf, Sea of Japan, and eastern coast of the Kunashir, southern Kuriles (northwestern Pacific). *Radiocarbon* 43, 477–481.
- Kuzmina, S.A., Sher, A.V., Edwards, M.E., et al. 2011. The late Pleistocene environment of the Eastern West Beringia based on the principal section at the Main River, Chukotka. *Quaternary Science Reviews* 30, 2091–2106.
- Kwiecien, O., Arz, H.W., Lamy, F., et al. 2008. Estimated reservoir ages of the Black Sea since the Last Glacial. *Radiocarbon* 50, 99–118.
- Lachniet, M.S., Vazquez-Selmi, L. 2005. Last Glacial Maximum equilibrium line altitudes in the circum-Caribbean (Mexico, Guatemala, Costa Rica, Colombia, and Venezuela). *Quaternary International* 138/139, 129–144.
- Laepple, T., Werner, M., Lohmann, G. 2011. Synchronicity of Antarctic temperatures and local solar insolation on orbital timescales. *Nature* 471, 91–94.

- Lagerlund, E., Houmark-Nielsen, M. 2008. Timing and pattern of the last deglaciation in the Kattegat region, southwest Scandinavia. *Boreas* 22, 337–347.
- Lagoe, M.B., Eyles, C.H., Eyles, N., et al. 1993. Timing of Late Cenozoic tidewater glaciation in the far North Pacific. *Geological Society of America Bulletin* 105, 1542–1560.
- Laird, K.R., Michels, A., Stuart, C.T.L., et al. 2007. Examination of diatom-based changes from a climatically sensitive prairie lake (Saskatchewan, Canada) at different temporal perspectives. *Quaternary Science Reviews* 26, 3328–3343.
- Laj, C., Kissel, C., Mazaud, A., Michel, E., et al. 2002. Geomagnetic field intensity, North Atlantic Deep Water circulation and atmospheric $\Delta^{14}\text{C}$ during the last 50 k yr. *Earth and Planetary Science Letters* 200, 177–190.
- Lakeman, T.R., Clague, J.J., Menonous, B. 2008. Advance of alpine glaciers during final retreat of the Cordilleran ice sheet in the Finlay River area, northern British Columbia, Canada. *Quaternary Research* 69, 188–200.
- Lambeck, K., Chappell, J. 2001. Sea level change through the last glacial cycle. *Science* 292, 679–686.
- Lambeck, K., Purcell, A., Johnston, P., et al. 2003. Water-load definition in the glacio-hydro-isostatic sea-level equation. *Quaternary Science Reviews* 22, 309–318.
- Lambert, D.M., Ritchie, P.A., Millar, C.D., et al. 2002. Rates of evolution in ancient DNA from Adélie penguins. *Science* 295, 2270–2273.
- Lambert, F., Delmonte B., Petit, J.R., et al. 2008. Dust record from the EPICA Dome C ice core, Antarctica, covering 0 to 800 kyr BP. *Nature* 452, 616–619.
- Lamoureux, S.F., England, J.H., Sharp, M.J., et al. 2001. A varve record of increased ‘Little Ice Age’ rainfall associated with volcanic activity, Arctic Archipelago, Canada. *The Holocene* 11, 243–249.
- Lamy, F., Kaiser, J., Ninnemann, U., et al. 2004. Antarctic timing of surface water changes off Chile and Patagonian ice sheet response. *Science* 304, 1959–1962.
- Lancaster, N. 2000. How dry was dry? Late Pleistocene palaeoclimates in the Namib Desert. *Quaternary Science Reviews* 21, 769–782.
- Lancaster, N. 2008. Desert dune dynamics and development: insights from luminescence dating. *Boreas* 37, 559–573.
- Lancaster, N., Kocurek, G., Singhvi, A., et al. 2002. Late Pleistocene and Holocene dune activity and wind regimes in the western Sahara Desert of Mauritania. *Geology* 30, 991–994.
- Lane, C.S., Blockley S.P.E., Lotter, A.F., et al. 2010. A regional tephrostratigraphical framework for central and southern European climate archives during the Last Glacial to Interglacial transition: comparisons north and south of the Alps. *Quaternary Science Reviews* 36, 50–58.
- Lane, C.S., Andric, M., Cullen, V.L., et al. 2011. The occurrence of distal Icelandic and Italian tephra in the Lateglacial of Lake Bled, Slovenia. *Quaternary Science Reviews* 30, 1013–1018.
- Lane, C.S., Blockley, S.P.E., Mangerud, J., et al. 2012. Was the 12.1 ka Icelandic Vedde Ash one of a kind? *Quaternary Science Reviews* 33, 87–99.
- Lane, C.S., Brauer, A.C., Blockley, S.P.E., et al. 2013. Volcanic ash reveals a time-transgressive abrupt climate change during the Younger Dryas. *Geology* 41, 1251–1254.
- Lane, S.N., Chandler, J.H. 2003. The generation of high quality topographic data for hydrology and geomorphology: new data sources, new applications and new problems. *Earth Surface Processes and Landforms* 28, 229–230.
- Lang, B., Bedford, A.P., Richardson, N., et al. 2003. The use of ultrasound in the preparation of carbonate and clay sediments for chironomid analysis. *Journal of Paleolimnology* 30, 451–460.
- Lang, N., Wolff, E.W. 2011. Interglacial and glacial variability from the last 800 ka in marine, ice and terrestrial archives. *Climate of the Past* 7, 361–380.
- Langdon, P.G., Barber, K.E. 2004. Snapshots in time: precise correlations of peat based proxy climate records in Scotland using mid-Holocene tephras. *The Holocene* 14, 21–33.
- Langdon, P.G., Barber, K.E. 2005. The climate of Scotland over the last 5000 years inferred from multiproxy peatland records: inter-site correlations and regional variability. *Journal of Quaternary Science* 20, 549–566.
- Langdon, P.G., Barber, K.E., Hughes, P.D.M. 2003. A 7500-year peat-based palaeoclimatic reconstruction and evidence for an 1100-year cyclicity in bog surface wetness from Temple Hill Moss, Pentland Hills, southeast Scotland. *Quaternary Science Reviews* 22, 259–274.
- Lanphere, M.A. 2000. Comparison of conventional K–Ar and $^{40}\text{Ar}/^{39}\text{Ar}$ dating of young mafic volcanic rocks. *Quaternary Research* 53, 294–301.
- Larkin, N.R. 2010. Literally a ‘mammoth task’: the conservation, preparation and curation of the West Runton Mammoth skeleton. *Quaternary International* 228, 233–240.
- Larocque, I., Hall, R.I. 2003. Chironomids as quantitative indicators of mean July air temperature: validation by comparison with century-long meteorological records from northern Sweden. *Journal of Paleolimnology* 29, 475–493.
- Larocque, S.J., Smith, D.J. 2003. Little Ice Age glacial activity in the Mt. Waddington area, British Columbia Coast Mountains, Canada. *Canadian Journal of Earth Science* 40, 1413–1436.
- Larsen, N.K., Piotrowski, J.A. 2003. Fabric pattern in a basal till succession and its significance for reconstructing subglacial processes. *Journal of Sedimentary Research* 73, 725–734.
- Larson, G.J. 2011. Ice-margin fluctuations at the end of the Wisconsin episode, Michigan, USA. In *Developments in Quaternary Science. Volume 15: Quaternary Glaciations – Extent and Chronology: A Closer Look* (edited by J. Ehlers, P.L. Gibbard, P.D. Hughes). Elsevier, Amsterdam, 489–497.
- Last, W.M., Smol, J.P. (eds). 2001. *Tracking Environmental Change Using Lake Sediments. Volume 1: Basin Analysis, Coring, and Chronological Techniques*. Kluwer, Dordrecht.
- Latalowa, M., Van der Knaap, W.O. 2006. Late Quaternary expansion of Norway spruce *Picea abies* (L.) Karst. in Europe according to pollen data. *Quaternary Science Reviews* 25, 2780–2805.
- Latham, A.G. 2001. Uranium-series dating. In *Handbook of Archaeological Sciences* (edited by D.E. Brothwell, A.M. Pollard). John Wiley, Chichester and New York, 63–72.

- Latrubesse, E.M., Nelson, B.W. 2001. Evidence for Late Quaternary aeolian activity in the Roraima–Guyana Region. *Catena* 43, 63–80.
- Lauritzen, S.-E. 1993. Natural environmental change in karst: the Quaternary record. In *Karst Terrains: Environmental Changes and Human Impact* (edited by P.W. Williams). *Catena Supplement* 25, Catena, Cremlingen-Destedt, 21–40.
- Lauritzen, S.-E., Lundberg, J. (eds). 1999. Speleothems as high-resolution palaeoclimatic archives. *The Holocene* 9, 643–726.
- Lawson, I., Frogley, M., Bryant, C., et al. 2004. The Lateglacial and Holocene environmental history of the Ioannina basin, north-west Greece. *Quaternary Science Reviews* 23, 1599–1625.
- Laxon, S.W., Giles, K.A., Ridout, A.L., et al. 2013. CryoSat-2 estimates of Arctic sea ice thickness and volume. *Geophysical Research Letters* doi: 10.1002/grl.50193.
- Lea, D.A., Martin, P.A., Pak, D.K., et al. 2002. Reconstructing a 350 ky history of sea level using planktonic Mg/Ca and oxygen isotope records from a Cocos Ridge core. *Quaternary Science Reviews* 21, 283–293.
- Lea, D.W., Mashotta, T.A., Spero, H.J. 1999. Controls on magnesium and strontium uptake in planktonic foraminifera determined by live culturing. *Geochimica et Cosmochimica Acta* 63, 2369–2379.
- Lea, D.W., Pak, D.K., Peterson, L.C., et al. 2003. Synchronicity of tropical and high-latitude Atlantic temperatures over the Last Glacial Termination. *Science* 301, 1361–1364.
- Lean, J. 2009. Cycles and trends in solar irradiance and climate. *Climate Change* 1, 111–122.
- Leblanc, M.J., Leduc, C., Stagnitti, F., et al. 2006. Evidence for Megalake Chad, north-central Africa, during the late Quaternary from satellite data. *Palaeogeography, Palaeoclimatology, Palaeoecology* 230, 230–242.
- Lécuyer, C., Daux, V., Moisette, P., et al. 2012. Stable carbon and oxygen isotope compositions of invertebrate carbonate shells and the reconstruction of paleotemperatures and paleosalinities – A case study of the early Pleistocene of Rhodes, Greece. *Palaeogeography, Palaeoclimatology, Palaeoecology* 350–352, 39–48.
- Lee, J.R., Phillips, E.R. 2008. Progressive soft sediment deformation within a subglacial shear zone – a hybrid mosaic-pervasive deformation model for Middle Pleistocene glaciectonised sediments from eastern England. *Quaternary Science Reviews* 27, 1350–1362.
- Lee, J., Rose, J., Hamblin, R.J.O., et al. 2004. Dating the earliest lowland glaciation of eastern England: a pre-MIS 12 early Middle Pleistocene Happisburgh glaciation. *Quaternary Science Reviews* 23, 1551–1566.
- Lee, J.R., Rose, J., Hamblin, R.J.O., et al. 2011. The glacial history of the British Isles during the Early and Middle Pleistocene: implications for the long-term development of the British Ice Sheet. In *Developments in Quaternary Science. Volume 15: Quaternary Glaciations – Extent and Chronology: A Closer Look* (edited by J. Ehlers, P.L. Gibbard, P.D. Hughes). Elsevier, Amsterdam, 59–74.
- Lehmann, G., Röttger, R. 1997. Techniques for the concentration of foraminifera from coastal salt meadow sediments. *Journal of Micropalaeontology* 16, 144.
- Lehtonen, M.L., Marmo, J.S., Nissinen, A.J., et al. 2005. Glacial dispersal studies using indicator minerals and till geochemistry around two eastern Finland kimberlites. *Journal of Geochemical Exploration* 87, 19–43.
- Leier, A.L., DeCelles, P.G., Pelletier, J.D. 2005. Mountains, monsoons, and megafans. *Geology* 33, 289–292.
- Lekens, W.A.H., Sejrup, H.P., Haflidason, H., et al. 2005. Laminated sediments preceding Heinrich Event 1 in the northern North Sea and southern Norwegian Sea: origin, processes and regional linkage. *Marine Geology* 216, 27–50.
- Lemieux-Dudon, B., Blayo, E., Petit, J.-R., et al. 2010. Consistent dating for Antarctic and Greenland ice cores. *Quaternary Science Reviews* 29, 8–20.
- Leng, M.J. (ed.). 2004. Isotopes in Quaternary palaeoenvironmental reconstruction (ISOPAL). *Quaternary Science Reviews* 23, 739–991.
- Leng, M.J., Marshall, J.D. 2004. Palaeoclimatic interpretation of stable isotope data from lake sediment archives. *Quaternary Science Reviews* 23, 811–831.
- Leng, M.J., Heaton, T.H.E., Lamb, H.F., et al. 1998. Carbon and oxygen isotope variations within the shell of an African land snail (*Limicolaria kambeul chudeaui* Germain): a high-resolution record of climate seasonality? *The Holocene* 8, 407–412.
- Leng, M.J., Barker, P.A., Schwalb, A. 2013. Isotopes and lakes. *Quaternary Science Reviews* 66, 1–36.
- Lenton, T.M., Myerscough, R.J., Marsh, R., et al. 2009. Using GENIE to study a tipping point in the climate system. *Philosophical Transactions of the Royal Society of London A* 367, 871–884.
- Leroy, S., Dupont, L. 1994. Development of vegetation and continental aridity in northwestern Africa during the Late Pliocene: the pollen record of ODP Site 658. *Palaeogeography, Palaeoclimatology, Palaeoecology* 109, 295–316.
- Leverington, D.W., Mann, J.D., Teller, J.T. 2002. Changes in the bathymetry and volume of glacial Lake Agassiz between 9200 and 7700 ^{14}C yr BP. *Quaternary Research* 57, 244–252.
- Lewis, S.E., Sloss, C.R., Murray-Wallace, C.V., et al. 2012. Post-glacial sea-level changes around the Australian margin: a review. *Quaternary Science Reviews* 74, 115–138.
- Lewis, S.G., Maddy, D., Buckingham, C., et al. 2006. Pleistocene fluvial sediments, palaeontology and archaeology of the upper River Thames at Latton, Wiltshire, England. *Journal of Quaternary Science* 21, 181–205.
- Li, Y., Morrill, C. 2010. Multiple factors causing Holocene lake-level change in monsoonal and arid central Asia as identified by model experiments. *Climate Dynamics* 35, 1119–1132.
- Lian, O., Huntley, D.J. 2001. Luminescence dating. In *Tracking Environmental Change Using Lake Sediments. Volume 1: Basin Analysis, Coring and Chronological Techniques* (edited by W.M. Last, J.P. Smol). Kluwer, Dordrecht, 261–282.
- Libby, W.F. 1955. *Radiocarbon Dating*, 2nd edn. University of Chicago Press, Chicago.
- Licciardi, J.M. 2001. Chronology of latest Pleistocene lake-level fluctuations in the pluvial Lake Chewaucan basin, Oregon, USA. *Journal of Quaternary Science* 16, 545–553.
- Lillesand, T.M., Kiefer, R.W., Chipman, J. 2004. *Remote Sensing and Image Interpretation*, 5th edn. John Wiley, Chichester and Hoboken, NJ.

- Lima, F.P., Ribeiro, P.A., Queiroz, N., et al. 2007. Modelling past and present geographical distribution of the marine gastropod *Patella rustica* as a tool for exploring responses to environmental change. *Global Change Biology* 13, 2065–2077.
- Limondin-Lozouet, N., Antoine, P. 2006. A new *Lyrodiscus* (Mollusca, Gastropoda) assemblage from Saint-Acheul (Somme Valley): a reappraisal of MIS 11 malacofaunas from northern France. *Boreas* 35, 622–633.
- Linderholm, H.W., Bjorklund, J.A., Seftigen, K., et al. 2010. Dendroclimatology in Fennoscandia – from past accomplishments to future potential. *Climate of the Past* 6, 93–114.
- Lindqvist, C., Schuster, S.C., Sun, Y., et al. 2010. Complete mitochondrial genome of a Pleistocene jawbone unveils the origin of polar bear. *Proceedings of the National Academy of Sciences of the United States of America* 107, 5053–5057.
- Linge, H., Lauritzen, S.-E., Lundberg, J. 2001. Stable isotope stratigraphy of a late last interglacial speleothem from Rana, northern Norway. *Quaternary Research* 56, 155–164.
- Lingle, C.S., Fatland, D.R. 2003. Does englacial water storage drive temperate glacier surges? *Annals of Glaciology* 36, 14–20.
- Liritzis, I. 2006. SIMS-SS, a new obsidian hydration dating method: analysis and theoretical principles. *Archaeometry* 48, 533–547.
- Lisé-Pronovost, A., St-Onge, G., Gogorza, C., et al. 2013. High-resolution paleomagnetic secular variations and relative paleointensity since the Late Pleistocene in southern South America. *Quaternary Science Reviews* 71, 91–108.
- Lisiecki, L.E., Raymo, M.E. 2005. A Pliocene–Pleistocene stack of 57 globally distributed benthic $\delta^{18}\text{O}$ records. *Paleoceanography* 20, PA1003, doi: 10.1029/2004PA001071.
- Lisiecki, L.E., Raymo, M.E. 2007. Plio–Pleistocene climate evolution: trends and transitions in glacial cycle dynamics. *Quaternary Science Reviews* 26, 56–69.
- Lisker, S., Vaks, A., Bar-Matthews, M., et al. 2009. Stromatolites in caves of the Dead Sea Fault Escarpment: implications to latest Pleistocene lake levels and tectonic subsidence. *Quaternary Science Reviews* 28, 80–92.
- Lister, A.M. 2004. The impact of Quaternary ice ages on mammalian evolution. *Philosophical Transaction of the Royal Society of London B* 359, 221–241.
- Lister, A.M. 2009. Late-glacial mammoth skeletons (*Mammuthus primigenius*) from Condover (Shropshire, UK): anatomy, pathology, taphonomy and chronological significance. *Geological Journal* 44, 447–479.
- Lister, A.M., Bahn, P. 2009. *Mammoths: Giants of the Ice Age*. University of California Press, Berkeley.
- Litt, T., Gibbard, P.L. 2008. A proposed Global Stratotype Section and Points (GSSP for the base of the Upper (Late) Pleistocene Subseries (Quaternary System/Period). *Episodes* 31, 260–263.
- Litt, T., Brauer, A., Goslar, T., et al. 2001. Correlation and synchronisation of Lateglacial continental sequences in northern Central Europe based on annually laminated lacustrine sediments. *Quaternary Science Reviews* 20, 1233–1249.
- Liu, K.-b., Yao, Z., Thompson, L.G. 1998. A pollen record of Holocene climatic changes from the Dunde ice cap, Qinghai-Tibetan Plateau. *Geology* 26, 135–138.
- Liu, T. 2003. Blind testing of rock varnish microstratigraphy as a chronometric indicator: results on late Quaternary lava flows in the Mojave Desert, California. *Geomorphology* 53, 209–234.
- Liu, T., Ding, Z. 1998. Chinese loess and the paleomonsoon. *Annual Reviews of Earth and Planetary Sciences* 26, 111–145.
- Liu, T., Broecker, W.S. 2008. Rock varnish microlamination dating of late Quaternary geomorphic features in the drylands of western USA. *Geomorphology* 93, 501–523.
- Liu X.-J., Lai Z.-P. 2013. Optical dating of sand wedges and ice-wedge casts from Qinghai Lake area on the northeastern Qinghai-Tibetan Plateau and its palaeoenvironmental implications. *Boreas* 42, 333–341.
- Liu, Z., Alexander, M. 2007. Atmospheric bridge, oceanic tunnel, and global climatic teleconnections. *Reviews of Geophysics* 45, doi: 2005RG000172.
- Livingstone, S.J., Evans, D.J.A., Ó Cofaigh, C. 2010. Re-advance of Scottish ice into the Solway Lowlands (Cumbria, UK), during the Main Late Devensian deglaciation. *Quaternary Science Reviews* 29, 2544–2570.
- Lloyd, G.T., Pearson, P.N., Young, J.R., et al. 2012. Sampling bias and the fossil record of planktonic foraminifera on land and in the deep sea. *Paleobiology* 38, 569–584.
- Loader, N.J., McCarroll, D., van der Knaap, W.O., et al. 2007. Characterising carbon isotopic variability in *Sphagnum*. *The Holocene* 17, 403–410.
- Loader, N.J., Young, G.H.F., Grudd, H., et al. 2013. Stable carbon isotopes from Torneträsk, northern Sweden provide a millennial length reconstruction of summer sunshine and its relationship to Arctic circulation. *Quaternary Science Reviews* 62, 97–113.
- Lohne, Ø.S., Bondevik, S., Mangerud, J., et al. 2007. Sea-level fluctuations imply that the Younger Dryas ice-sheet expansion in western Norway commenced during the Allerød. *Quaternary Science Reviews* 26, 2128–2151.
- Lohne, Ø.S., Mangerud, J., Birks, H.H. 2013. Precise ^{14}C ages of the Vedde and Saksunarvatn ashes and the Younger Dryas boundaries from western Norway and their comparison with the Greenland Ice Core (GICC05) chronology. *Journal of Quaternary Science* 28, 490–500.
- Lomas-Clarke, S.H., Barber, K.E. 2006. Human impact signals from peat bogs: a combined palynological and geochemical approach. *Vegetation History and Archaeobotany* 16, 419–429.
- Long, A.J., Roberts, D.H., Simpson, M.J.R., et al. 2008. Late Weichselian relative sea-level changes and ice sheet history in southeast Greenland. *Earth and Planetary Science Letters* 272, 8–18.
- Long, A.J., Woodroffe, S., Dawson, S., et al. 2009. Late Holocene relative sea level rise and the Neoglacial history of the Greenland Ice Sheet. *Journal of Quaternary Science* 24, 345–359.
- Lord, A., Cabral, M.C., Dambeck, R., et al. 2011. Ostracod evidence for the Neolithic environment of Rio Sizandro, Portugal. *Palaeobiodiversity and Palaeoenvironments* 91, 215–228.
- Lord, A.R., Boomer, I., Brouwers, E., et al. 2012. Ostracod taxa as palaeoclimatic indicators in the Quaternary. In *Developments in Quaternary Science. Volume 17: Ostracoda as Proxies for Quaternary Climate Change* (edited by D.J. Horne, J.A. Holmes, J. Rodriguez-Lazaro, et al.). Elsevier, Amsterdam, 37–46.

- Loso, M.G., Doak, D.F. 2006. The biology behind lichenometric dating curves. *Oecologia* 147, 223–229.
- Lotter, A.F., Heiri, O., Brooks, S., et al. 2012. Rapid summer temperature changes during Termination 1a: high-resolution multi-proxy climate reconstructions from Gerzensee (Switzerland). *Quaternary Science Reviews* 36, 103–113.
- Loubere, P., Creamer, W., Haas, J. 2013. Evolution of the El Niño–Southern Oscillation in the late Holocene and insolation driven change in the tropical annual SST cycle. *Global and Planetary Change* doi: 10.1016/j.glochaha.2012.10.007.
- Louchart, A., Wesselmann, H., Blumenshine, R.J., et al. 2009. Taphonomic, avian, and small-vertebrate indicators of *Ardipithecus ramidus* habitat. *Science* 326, 66 (66e1–66e4).
- Lough, J.M., Cooper, T.F. 2011. New insights from coral growth band studies in an era of rapid environmental change. *Earth-Science Reviews* 108, 170–184.
- Loulerge, L., Parrein, F., Blnier, T., et al. 2007. New constraints on the gas age–ice age difference along the EPICA ice cores, 0–50 kyr. *Climate of the Past* 3, 527–540.
- Loulerge, L., Schilt, A., Spahni, R., et al. 2008. Orbital and millennial-scale features of atmospheric CH₄ over the past 800,000 years. *Nature* 453, 383–386.
- Lourens, L. 2004. Revised tuning of Ocean Drilling Program Site 964 and KC01B (Mediterranean) and implications for the δ¹⁸O, tephra, calcareous nannofossil, and geomagnetic reversal chronologies of the past 1.1 Myr. *Paleoceanography* 19, doi: 10.1029/2003PA000997.
- Lourens, L.J. 2008. On the Neogene–Quaternary debate. *Episodes* 31, 239–242.
- Lourens, L.J., Hilgen, F.J. 1997. Long-period variations in the Earth's obliquity and their relation to third-order eustatic cycles and late Neogene glaciations. *Quaternary International* 40, 43–52.
- Lourens L., Hilgen, F., Shackleton, N.J., et al. 2005. The Neogene Period. In *A Geologic Time Scale 2004* (edited by F. Gradstein, L.G. Ogg, A.G. Smith). Cambridge University Press, Cambridge, 409–440.
- Lowe, D.J. 2011. Tephrochronology and its applications. *Quaternary Geochronology* 6, 107–153.
- Lowe, D.J., Shane, P.A.R., Alloway, B.V., et al. 2008a. Fingerprints and age models for widespread New Zealand tephra marker beds erupted since 30,000 years ago: a framework for NZ-INTIMATE. *Quaternary Science Reviews* 27, 95–126.
- Lowe, J.J., Lowe, S., Fowler, A.J., et al. 1988. Comparison of accelerator and radiometric age measurements obtained from Late Devensian Lateglacial lake deposits from Llyn Gwernan, North Wales. *Boreas* 17, 355–369.
- Lowe, J.J., Hoek, W., INTIMATE Group. 2001. Inter-regional correlation of palaeoclimatic records for the Last Glacial–Interglacial Transition: a protocol for improved precision recommended by the INTIMATE project group. *Quaternary Science Reviews* 20, 1175–1187.
- Lowe, J.J., Blockley, S., Trincardi, F., et al. 2007. Age modelling of late Quaternary marine sequences in the Adriatic: towards improved precision and accuracy using volcanic event stratigraphy. *Continental Shelf Research* 27, 560–582.
- Lowe, J.J., Rasmussen, S.O., Björck, S., et al. 2008b. Synchronisation of palaeoenvironmental events in the North Atlantic region during the Last Termination: a revised protocol recommended by the INTIMATE group. *Quaternary Science Reviews* 27, 6–17.
- Lowe, J., Barton, N., Blockley, S., et al. 2012. Volcanic ash layers illuminate the resilience of Neanderthals and early modern humans to natural hazards. *Proceedings of the National Academy of Sciences of the United States of America* 109, 13532–13537.
- Lowell, T.V., Hayward, R.K., Denton, G.H. 1999. Role of climate oscillations in determining ice-margin position: hypothesis, example and implication. *Geological Society of America, Special Paper* 337, 192–203.
- Lozier, M.S. 2010. Deconstructing the conveyor belt. *Science* 328, 1507–1511.
- Lücke, A., Schleser, G.H., Zolitschka, B., et al. 2003. A Lateglacial and Holocene organic carbon isotope record of lacustrine palaeoproductivity and climate change derived from varved lake sediments of Lake Holzmaar, Germany. *Quaternary Science Reviews* 22, 569–580.
- Luckman, B.H. 2000. The Little Ice Age in the Canadian Rockies. *Geomorphology* 32, 357–384.
- Luckman, B.H., Holdsworth, G., Osborn G.D. 1993. Neoglacial glacier fluctuations in the Canadian Rockies. *Quaternary Research* 39, 144–153.
- Lüter, V., Hollis, C.J., Willems, H. 2008. Late Quaternary radiolarian assemblages as indicators of paleoceanographic changes north of the subtropical front, offshore eastern New Zealand, southwest Pacific. *Micropaleontology* 54, 49–69.
- Lukas, S. 2006. Morphostratigraphic principles in glacier reconstruction – a perspective from the British Younger Dryas. *Progress in Physical Geography* 30, 719–736.
- Lukas, S., Benn, D.I. 2006. Retreat dynamics of Younger Dryas glaciers in the far NW Scottish Highlands reconstructed from moraine sequences. *Scottish Geographical Journal* 122, 308–325.
- Lukas, S., Nicholson, L.I., Ross, F.H., et al. 2005. Formation, melt-out processes and landscape alteration of high-Arctic ice-cored moraines – examples from Nordenskiöld Land, Central Spitsbergen. *Polar Geography* 29, 157–187.
- Lukas, S., Spencer, J.Q.G., Robinson, R.A.J., et al. 2007. Problems associated with luminescence dating of Late Quaternary glacial sediments in the NW Scottish Highlands. *Quaternary Geochronology* 2, 243–248.
- Lundqvist, J. 1986. Late Weichselian glaciation and deglaciation in Scandinavia. *Quaternary Science Reviews* 5, 269–292.
- Lundqvist, J., Wohlfarth, B. 2001. Timing and east–west correlation of south Swedish ice marginal lines during the Late Weichselian. *Quaternary Science Reviews* 20, 1127–1148.
- Lunt, D.J., Williamson, M.S., Valdes, P.J.I. 2006. Comparing transient, accelerated, and equilibrium simulations of the last 30000 years with the GENIE-1 model. *Climate of the Past* 2, 221–235.
- Luoto, M., Seppälä, M. 2003. Thermokarst ponds as indicators of the former distribution of palsas in Finnish Lapland. *Permafrost and Periglacial Processes* 14, 19–27.

- Luoto, M., Fonzek, S., Zuidhoff, F.S. 2004. Spatial modelling of palsas in relation to climate in northern Europe. *Earth Surface Processes and Landforms* 29, 1373–1387.
- Lusch, D.P., Stanley, K.E., Schaetzl, R.J., et al. 2009. Characterization and mapping of patterned ground in the Saginaw Lowlands, Michigan: possible evidence for Late-Wisconsin permafrost. *Annals of the Association of American Geographers* 99, 445–466.
- Lydeard, C., Cowie, R.H., Ponder, W.F., et al. 2004. The global decline of nonmarine mollusks. *BioScience* 54, 321–330.
- Lykke-Andersen, H. 1998. Neogene–Quaternary depositional history of the East Greenland shelf in the vicinity of Leg 152 shelf sites. *Proceedings of the Ocean Drilling Program, Scientific Results* 152, 29–38.
- Lyman, R.L., Rosania, C.N., Boulanger, M.T. 2012. Comparison of fluoride and direct AMS radiocarbon dating of black bear bone from Lawson Cave, Missouri. *Journal of Field Archaeology* 37, 226–237.
- Lynch-Stieglitz, J., Adkins, J.F., Curry, W.B., et al. 2007. Atlantic meridional overturning circulation during the Last Glacial Maximum. *Science* 316, 66–69.
- Lyons, S.K. 2005. A quantitative model for assessing community dynamics of Pleistocene mammals. *The American Naturalist* 165, E168–E185.
- Lyons, S.K., Wagner, P.J., Dzikiewicz, K. 2010. Ecological correlates of range shifts of Late Pleistocene mammals. *Philosophical Transactions of the Royal Society of London B* 365, 3681–3693.
- Ma, Z., Wang, Z., Liu, J., et al. 2004. U-series chronology of sediments associated with Late Quaternary fluctuations, Balikun Lake, northwestern China. *Quaternary International* 121, 89–98.
- Maat, P.B., Johnson, W.C. 1996. Thermoluminescence and new ^{14}C age estimates for the late Quaternary loesses in southwestern Nebraska. *Geomorphology* 17, 115–128.
- McAndrews, J.H., Turton, C.L. 2010. Fungal spores record Iroquoian and Canadian agriculture in 2nd millennium AD sediment of Crawford Lake, Ontario, Canada. *Vegetation History and Archaeobotany* 19, 495–501.
- MacAyeal, D.R. 1992. Irregular oscillations of the West Antarctic ice sheet. *Nature* 359, 29–32.
- McCabe, G.J., Palecki, M.A., Betancourt, J.L., 2004. Pacific and Atlantic Ocean influences on multidecadal drought frequency in the United States. *Proceedings of the National Academy of Sciences of the United States of America* 101, 4136–4141.
- McCabe, M., Clark, P.U., Clark, J., et al. 2007. Radiocarbon constraints on readvances of the British–Irish Ice Sheet in the northern Irish Sea Basin during the last deglaciation. *Quaternary Science Reviews* 26, 1204–1211.
- McCarroll, D. 2002. Amino-acid geochronology and the British Pleistocene: secure stratigraphical framework or a case of circular reasoning? *Journal of Quaternary Science* 17, 647–651.
- McCarroll, D.M., Harris, C. 1992. The glaciogenic deposits of western Lleyn, north Wales. *Journal of Quaternary Science* 7, 19–30.
- McCarroll, D.M., Ballantyne, C.K. 2000. The last ice sheet in Snowdonia. *Journal of Quaternary Science* 15, 765–778.
- McCarroll, D., Rijsdijk, K. 2003. Deformation styles as a key for interpreting glacial depositional sequences. *Journal of Quaternary Science* 18, 473–489.
- McCarroll, D., Shakesby, R.A., Matthews, J.A. 1998. Spatial and temporal patterns of Late Holocene rockfall activity on a Norwegian talus slope: a lichenometric and simulation-modelling approach. *Arctic and Alpine Research* 30, 51–60.
- McCarroll, D., Knight, J., Rijsdijk, K. (eds). 2001. The glaciation of the Irish Sea Basin. *Journal of Quaternary Science* 16, 391–506.
- McCarroll, D., Jalkanen, R., Hicks, S., et al. 2003. Multiproxy dendroclimatology: a pilot study in northern Finland. *The Holocene* 13, 829–838.
- McCarthy, L., Head, L. 2001. Holocene variability in semi-arid vegetation: new evidence from *Leporillus* middens from the Flinders Ranges, South Australia. *The Holocene* 11, 681–689.
- McCave, I.N., Hall, I.R., Bianchi, G.G. 2006. Laser vs. settling velocity differences in silt grainsize measurements: estimation of palaeocurrent vigour. *Sedimentology* 53, 919–928.
- McClmont, E.L., Rosell-Melé, A. 2005. Links between the onset of modern Walker circulation and the mid-Pleistocene climate transition. *Geology* 33, 389–392.
- McClmont, E.L., Sosdian, S.M., Rosell-Melé, A., et al. 2013. Pleistocene sea-surface temperature evolution: early cooling, delayed glacial intensification, and implications for the mid-Pleistocene climate transition. *Earth-Science Reviews* doi: 10.1016/j.earscirev.2013.04.006.
- McCoy, W.D. 1987. The precision of amino acid geochronology and palaeothermometry. *Quaternary Science Reviews* 6, 43–54.
- McCullagh, J.S.O., Marom, A., Hedges, R.E. 2010. Radiocarbon dating of individual amino acids from archaeological bone collagen. *Radiocarbon* 52, 620–634.
- McCullough, M.T., Esat, T. 2000. The coral record of last interglacial sea levels and sea surface temperatures. *Chemical Geology* 169, 107–129.
- McDermott, F. 2004. Palaeo-climate reconstruction from stable isotope variations in speleothems: a review. *Quaternary Science Reviews* 23, 901–918.
- McDermott, F., Frisia, S., Huang, Y., et al. 1999. Holocene climatic variability in Europe: evidence from $\delta^{18}\text{O}$ and textural variations in speleothems. *Quaternary Science Reviews* 18, 1021–1038.
- MacDonald, G.M., Case, R.A. 2005. Variations in the Pacific Decadal Oscillation over the past millennium. *Geophysical Research Letters* 32.
- MacDonald, G.M., Bennett, K.D., Jackson, S.T., et al. 2008. Impacts of climate change on species, populations and communities: palaeobiogeographical insights and frontiers. *Progress in Physical Geography* 32, 139–72.
- Macdougall, D. 2008. *Nature's Clocks: How Scientists Measure the Age of Almost Everything*. University of California Press, Berkeley, Los Angeles and London.
- Macdougall, I., Harrison, T.M. 1999. *Geochronology and Thermo-chronology by the 40Ar/39Ar Method*, 2nd edn. Oxford University Press, Oxford.
- Macdougall, I., Brown, F.H., Fleagle, J.G. 2005. Stratigraphic placement and age of modern humans from Kibish, Africa. *Nature* 433, 733–735.
- Mcelwain, J.C., Mayle, F.E., Beerling, D.J. 2002. Stomatal evidence for a decline in atmospheric CO_2 concentration during the

- Younger Dryas stadial: a comparison with Antarctic ice core records. *Journal of Quaternary Science* 17, 21–29.
- McElwain, M.W., McFadden, P.L. 2000. *Palaeomagnetism: Continents and Oceans*. Academic Press, London and San Diego.
- McFarlane, D.A., Blake, J. 2005. The late Pleistocene hutlas (*Geocapromys brownii*) of Red Hills Fissure, Jamaica. *Geological Journal* 40, 3899–404.
- McGarry, S., Baker, A. 2000. Organic acid fluorescence: applications to speleothem palaeoenvironmental reconstruction. *Quaternary Science Reviews* 19, 1087–1101.
- McGarry, S.F., Caseldine, C.J. 2004. Speleothem palynology: an undervalued tool in Quaternary studies. *Quaternary Science Reviews* 23, 2389–2404.
- McGarry, S., Bar-Matthews, M., Matthews, A., et al. 2004. Constraints on hydrological and paleotemperature variations in the Eastern Mediterranean region in the last 140 ka given by the δD values of speleothem fluid inclusions. *Quaternary Science Reviews* 23, 919–934.
- McGee, D., Broecker, W.S., Winckler, G. 2010. Gustiness: The driver of glacial dustiness? *Quaternary Science Reviews* 29, 2340–2350.
- McGlone, M.S., Wilmshurst, J.M. 1999. A Holocene record of climate, vegetation change and peat bog development, east Otago, South Island, New Zealand. *Journal of Quaternary Science* 14, 239–254.
- McGuffie, K., Henderson-Sellars, A. 2005. *A Climate Modelling Primer*, 3rd edn. John Wiley, Chichester and New York.
- McGuire, W.J., Howarth, R.J., Firth, C.R., et al. 1997. Correlation between rate of sea-level change and frequency of explosive volcanism in the Mediterranean. *Nature* 389, 473–476.
- Machette, M.N., Slate, J.L., Phillips, F.M. 2008. Terrestrial cosmogenic-nuclide dating of alluvial fans in Death Valley, California, USA. *U.S. Geological Survey Professional Paper* 1745, 1–45.
- Machida, H. 1999. The stratigraphy, chronology and distribution of distal marker-tephras in and around Japan. *Global and Planetary Change* 21, 71–94.
- McIntyre, A., Ruddiman, W.F. 1972. North-east Atlantic post-Eemian paleceanography: a predictive analog for the future. *Quaternary Research* 2, 350–354.
- McIntyre, A., Ruddiman, W.F., Jantzen, R. 1972. Southward penetration of the North Atlantic Polar Front and faunal and floral evidence of large scale surface water mass movements over the past 225,000 years. *Deep Sea Research* 19, 61–77.
- Mackay, A.W. 2007. The palaeoclimatology of Lake Baikal: a diatom synthesis and prospectus. *Earth-Science Reviews* 82, 181–215.
- Mackay, A., Battarbee, R.W., Birks, J., et al. (eds). 2003. *Global Change in the Holocene*. Arnold, London.
- Mackay, J.R., Burns, C.R. 2002. The first 20 years (1978–1979 to 1998–1999) of ice-wedge growth at the Illisarvik experimental drained lake site, western Arctic coast, Canada. *Canadian Journal of Earth Sciences* 39, 95–111.
- Mackereth, F.J.H. 1965. Chemical investigations of lake sediments and their interpretation. *Proceedings of the Royal Society B* 161, 295–3090.
- Mackintosh, A.N., Barrows, T.T., Colhoun, E.A., et al. 2006. Exposure dating and glacial reconstruction at Mt. Field, Tasmania, Australia, identifies MIS 3 and MIS 2 glacial advances and climatic variability. *Journal of Quaternary Science* 21, 363–376.
- McLaren, S.J., Rowe, P.J. 1996. The reliability of uranium-series mollusc dates from the western Mediterranean basin. *Quaternary Science Reviews* 15, 709–717.
- MacLeod, A., Palmer, A., Lowe, J., Rose, J., Bryant, C., Merritt, J. 2011. Timing of glacier response to Younger Dryas climatic cooling in Scotland. *Global and Planetary Change* 79, 264–274.
- MacLeod, D.M., Osborn, G., Spooner, I. 2006. A record of post-glacial moraine deposition and tephra stratigraphy from Otokomi Lake, Rose Basin, Glacier National Park, Montana. *Canadian Journal of Earth Sciences* 43, 447–460.
- Macklin, M., Lewin, J. 2008. Alluvial responses to the changing Earth system. *Earth Surface Processes and Landforms* 33, 1374–1395.
- Macklin, M., Woodward, J. 2009. River systems and environmental change. In *The Physical Geography of the Mediterranean* (edited by J. Woodward). Oxford University Press, Oxford, 320–351.
- McMartin, I., Henderson, P.J. 2004. Evidence from Keewatin (central Nunavut) for paleo-ice divide migration. *Géographie physique et Quaternaire* 58, 163–186.
- McMillan, A.A. 2005. A provisional Quaternary and Neogene lithostratigraphical framework for Great Britain. *Geologie en Mijnbouw (Netherlands Journal of Geosciences)* 84, 87–107.
- McMillan, E.A., Fairchild, I.J., Frisia, S., et al. 2005. Annual trace element cycles in calcite–aragonite speleothems: evidence of drought in the western Mediterranean 1200–1100 yr BP. *Journal of Quaternary Science* 20, 423–433.
- Maddy, D. 1997. Uplift-driven valley incision and river terrace formation in southern England. *Journal of Quaternary Science* 12, 539–545.
- Maddy, D., Demir, T., Bridgland, D.R., et al. 2005. An obliquity-controlled Early Pleistocene river terrace record from Western Turkey? *Quaternary Research* 63, 339–346.
- Magnani, G., Bartolomei, P., Cavalli, F., et al. 2007. U-series and radiocarbon dates on mollusc shells from the uppermost layer of the archaeological site of KHB-1, Ra's al Khabbah, Oman. *Journal of Archaeological Science* 34, 749–755.
- Magny, B. 2007. Lake level studies: west-central Europe. In *Encyclopedia of Quaternary Science* (edited by S.A. Elias). Elsevier, Amsterdam, 1389–1399.
- Magny, M. 2001. Palaeohydrological changes as reflected by lake-level fluctuations in the Swiss Plateau, the Jura Mountains and the northern French Pre-Alps during the Last Glacial–Holocene transition: a regional synthesis. *Global and Planetary Change* 30, 85–101.
- Magny, M. 2004. Holocene climate variability as reflected by mid-European lake-level fluctuations and its probable impact on prehistoric human settlement. *Quaternary International* 113, 65–79.
- Magny, M., Bégeot, C., Guiot, J., et al. 2003. Reconstruction and palaeoclimatic interpretation of mid-Holocene vegetation and lake-level changes at Saint-Jorioz, Lake Annecy, French Pre-Alps. *The Holocene* 13, 265–275.
- Magri, D. 2010. Persistence of tree taxa in Europe and Quaternary climate changes. *Quaternary International* 219, 145–151.

- Mahaney, W.C., Kalm, V., Kapran, B., et al. 2009. A soil chrono-sequence in Late Glacial and Neoglacial moraines, Humboldt Glacier, northwestern Venezuelan Andes. *Geomorphology* 109, 236–245.
- Maher, B. 2007. Environmental magnetism and climate change. *Contemporary Physics* 48, 247–274.
- Maher, B.A., Thompson, R. (eds). 1999. *Quaternary Climates, Environments and Magnetism*. Cambridge University Press, Cambridge.
- Maher, B.A., Hallam, D.F. 2005. Palaeomagnetic correlation and dating of Plio/Pleistocene sediments at the southern margins of the North Sea Basin. *Journal of Quaternary Science* 20, 67–77.
- Maher, B.A., Prospero, J.M., Mackie, D., et al. 2010. Global connections between aeolian dust, climate and ocean biogeochemistry at the present day and at the last glacial maximum. *Earth-Science Reviews* 99, 61–97.
- Major, C.O., Goldstein, S.L., Ryan, W.B.F., et al. 2006. The co-evolution of Black Sea level and composition through the last deglaciation and its paleoclimatic significance. *Quaternary Science Reviews* 25, 2031–2047.
- Maldonado, A., Betancourt, J.L., Latorre, C., et al. 2005. Pollen analyses from a 50,000-yr rodent midden series in the southern Atacama Desert (25°30'S). *Journal of Quaternary Science* 20, 493–507.
- Mallick, R., Frank, N. 2002. A new technique for precise uranium-series dating of travertine micro-samples, *Geochimica et Cosmochimica Acta* 66, 4261–4272.
- Mallol, C., Cabanes, D., Baene, J. 2010. Microstratigraphy and diagenesis at the upper Pleistocene site of Esquilleu Cave (Cantabria, Spain). *Quaternary International* 214, 70–81.
- Manabe, S., Stouffer, R.J. 1997. Coupled ocean–atmosphere model response to freshwater input: comparison to Younger Dryas Event. *Paleoceanography* 12, 321–336.
- Mangerud, J. 1977. Late Weichselian marine sediments containing shells, Foraminifera and pollen at Agotnes, western Norway. *Norsk Geologiske Tidsskrift* 57, 23–54.
- Mangerud, J., Andersen, S.T., Berglund, B.E., et al. 1974. Quaternary stratigraphy of Norden, a proposal for terminology and classification. *Boreas* 3, 109–128.
- Mangerud, J., Jakobsson, M., Alexanderson, H., et al. 2004. Icedammed lakes and rerouting of the drainage of northern Eurasia during the Last Glaciation. *Quaternary Science Reviews* 23, 1313–1332.
- Mangini, A., Spötl, C., Verdes, P. 2005. Reconstruction of temperature in the Central Alps during the past 2000 yr from a $\delta^{18}\text{O}$ stalagmite record. *Earth and Planetary Science Letters* 235, 741–751.
- Mann, M.E., Bradley, R.S., Hughes, M.K. 1998. Global-scale temperature patterns and climate forcing over the past six centuries. *Nature* 392, 779–787.
- Mannes, D., Lehmann, E., Cheubini, P., et al. 2007. Neutron imaging versus standard X-ray densitometry as method to measure tree-ring wood density. *Trees – Structure and Function* 21, 605–612.
- Manning, A., Birley, R., Tipping, R. 2007. Roman impact on the environment at Hadrian's Wall: precisely dated pollen analysis from Vindolanda, northern England. *The Holocene* 17, 527–538.
- Mantua, N., Hare, S.R. 2002. The Pacific Decadal Oscillation. *Journal of Oceanography* 58, 35–44.
- Marchant, D.R., Lewis, D.R., Phillips, W.M., et al. 2002. Formation of patterned ground and sublimation till over Miocene glacier ice in Beacon Valley, southern Victoria Land, Antarctica. *Geological Society of America Bulletin* 114, 718–730.
- Marchetti, M. 2002. Environmental changes in the central Po Plain (northern Italy) due to fluvial modifications and anthropogenic activities. *Geomorphology* 44, 361–373.
- Marcolini, F., Bigazzi, G., Bonadonna, F.P., et al. 2003. Tephrochronology and tephrostratigraphy of two Pleistocene continental fossiliferous successions from central Italy. *Journal of Quaternary Science* 18, 545–556.
- Marcott, S.A., Clark, P.U., Padman, L., et al. 2011. Ice-shelf collapse from subsurface warming as a trigger for Heinrich events. *Proceedings of the National Academy of Sciences of the United States of America* 108, 13415–13419.
- Marcott, S.A., Shakun, J.D., Clark, P.U., et al. 2013. A reconstruction of regional and global temperature for the past 11,300 years. *Science* 339, 1198–1201.
- Margari, V., Skinner, L.C., Tzedakis, P.C., et al. 2010. The nature of millennial-scale climate variability during the past two glacial periods. *Nature Geoscience* 3, 127–131.
- MARGO Project Members. 2009. Constraints on the magnitude and patterns of ocean cooling at the Last Glacial Maximum. *Nature Geoscience* 2, 127–132.
- Marín-Arroyo, A.B., Fosse, P., Vigne, J.-D. 2009. Probable evidence of bone accumulation by Pleistocene bearded vulture at the archaeological site of El Mirón Cave, Spain. *Journal of Archaeological Science* 36, 284–296.
- Mark, B.G., Seltzer, G.O., Rodbell, D.T. 2004. Late Quaternary glaciations of Ecuador, Peru and Bolivia. In *Developments in Quaternary Science. Volume 2: Quaternary Glaciations: Extent and Chronology* (edited by J. Ehlers, P.L. Gibbard). Elsevier, Amsterdam, 151–163.
- Mark, D.F., Petraglia, M., Smith, V.C. 2013. A high-precision $^{40}\text{Ar}/^{39}\text{Ar}$ age of the Young Toban Tuff and dating of ultradistal tephra: forcing of Quaternary climate and implications for hominin occupation of India. *Quaternary Geochronology* doi: 10.1016/j.quageo.2012.12.004.
- Markova, A.K. 2005. Eastern European rodent (Rodentia, mammalia) faunas from the Early–Middle Pleistocene transition. *Quaternary International* 131, 71–77.
- Marković, S.B., Bokhorst, M.P., et al. 2007. Late Pleistocene loess-palaeosol sequences in the Vojvodina region, north Serbia. *Journal of Quaternary Science* 23, 73–84.
- Marks, L. 2012. Timing of the Late Vistulan (Weichselian) glacial phases in Poland. *Quaternary Science Reviews* 44, 81–88.
- Marotzke, J. 2000. Abrupt climate change and thermohaline circulation: mechanisms and predictability. *Proceedings of the National Academy of Sciences of the United States of America* 97, 1347–1350.
- Marquardt, C., Lavenu, A., Ortlieb, L., et al. 2004. Coastal neotectonics in Southern Central Andes: uplift and deformation of marine terraces in Northern Chile (27°S). *Tectonophysics* 394, 193–219.

- Marquez-Grant, N., Fibiger, L. (eds). 2011. *The Routledge Handbook of Archaeological Human Remains and Legislation. An international guide to laws and practice in the excavation and treatment of archaeological human remains*. Routledge, London.
- Marra, F., Karner, D.B., Freda, C., et al. 2009. Large mafic eruptions at Alban Hills Volcanic District (Central Italy): chronostratigraphy, petrography and eruptive behaviour. *Journal of Volcanology and Geothermal Research* 179, 217–232.
- Marra, M.J., Leschen, R.A.B. 2011. Persistence of New Zealand Quaternary beetles. *New Zealand Journal of Geology and Geophysics* 54, 403–413.
- Marret, F., Scourse, J. 2002. Control of modern dinoflagellate cyst distribution in the Irish and Celtic seas by seasonal stratification dynamics. *Marine Micropaleontology* 47, 101–116.
- Marret, F., Zonneveld, K.A.F. 2003. Atlas of modern organic-walled dinoflagellate cyst distribution. *Review of Palaeobotany and Palynology* 125, 1–200.
- Marshall, S.J. 2005. Recent advances in understanding ice sheet dynamics. *Earth and Planetary Science Letters* 240, 191–204.
- Marshall, S.J., James, T.S., Clarke, G.K.C. 2002. North American Ice Sheet reconstructions at the Last Glacial Maximum. *Quaternary Science Reviews* 21, 175–192.
- Marshall, W.A., Chalmers, M.O. 1997. Airborne dispersal of Antarctic terrestrial algae and cyanobacteria. *Ecography* 20, 585–594.
- Martens, K., Schön, I., Meisch, C., et al. 2008. Global diversity of ostracods (Ostracoda, Crustacea) in freshwater. *Hydrobiologia* 595, 185–193.
- Martin, P., Archer, D., Lea, D.W. 2005. Role of deep sea temperature in the carbon cycle during the last glacial. *Paleoceanography* 20, PA2015, doi: 10.1029/2003PA000914.
- Martínez-Cortizas, A., Mighall, T., Pontevedra-Pombal, X., et al. 2005. Linking changes in atmospheric dust deposition, vegetation change and human activities in northwest Spain during the last 5300 years. *The Holocene* 15, 698–706.
- Martínez-Cortizas, A., Pontevedra-Pombal, X., Nóvoa Muñoz, J.C. et al. 1997. Four thousand years of atmospheric Pb, Cd, and Zn deposition recorded by the ombrotrophic peat bog of Penido Vello (Northwestern Spain). *Water, Air & Soil Pollution* 100, 387–403.
- Martinez-Garcia, A., Rosell-Mele, A., Jaccard, S.L., et al. 2011. Southern Ocean dust–climate coupling over the past four million years. *Nature* 476, 312–315.
- Martini, I.P., French, H.M., Alberti, A.P. (eds). 2011. *Ice-Marginal and Periglacial Processes and Sediments*. Geological Society of London, Special Publication 354. Geological Society, London.
- Martinson, D.G., Pisias, N.G., Hays, J.D., et al. 1987. Age dating and the orbital theory of ice ages: development of a high-resolution 0–300 000 year chronostratigraphy. *Quaternary Research* 27, 1–29.
- Maslin, M.A., Ridgwell, A.J. 2005. Mid-Pleistocene Revolution and the ‘eccentricity myth’. In *Early–Middle Pleistocene Transitions: The Land–Ocean Evidence* (edited by M.J. Head, P.L. Gibbard). Geological Society of London, Special Publication 247. Geological Society, Bath, 19–34.
- Maslin, M.A., Li, X.S., Loutre, M.F., et al. 1998. The contribution of orbital forcing to the progressive intensification of Northern Hemisphere glaciation. *Quaternary Science Reviews* 17, 411–426.
- Maslin, M., Seidov, D., Lowe, J.J. 2001. Synthesis of the nature and causes of rapid climate transitions during the Quaternary. In *The Oceans and Rapid Climatic Change: Past, Present and Future* (edited by D. Seidov, M. Maslin, B.J. Haupt). American Geophysical Union, Geophysical Monograph 126, 9–52.
- Mason, B.G., Pyle, D.M., Oppenheimer, C. 2004. The size and frequency of the largest explosive eruptions on Earth. *Bulletin of Vulcanology* 66, 735–478.
- Mason, J.A. 2001. Transport direction of Peoria loess in Nebraska and implications for loess sources on the central Great Plains. *Quaternary Research* 56, 79–86.
- Massari, F., Rio, D., Serandrei Barbero, R., et al. 2004. The environment of Venice area in the past two million years. *Palaeogeography, Palaeoclimatology, Palaeoecology* 202, 273–308.
- Masson-Delmotte, V., Stenni, B., Jouzel, J. 2004. Common millennial-scale variability of Antarctic and Southern Ocean temperatures during the past 5000 years reconstructed from the EPICA Dome C ice core. *The Holocene* 14, 145–151.
- Masson-Delmotte, V., Jouzel, J., Landais, A., et al. 2005. GRIP deuterium excess reveals rapid and orbital-scale changes in Greenland moisture origin. *Science* 209, 118–121.
- Masson-Delmotte, V., Stenni, B., Pol, K., et al. 2010. Epica Dome C record of glacial and interglacial intensities. *Quaternary Science Reviews* 29, 113–128.
- Mastronuzzi, G., Sanso, P., Murray-Wallace, C.V., et al. 2005. Quaternary coastal morphology and sea-level changes – an introduction. *Quaternary Science Reviews* 24, 1963–1968.
- Matsuoka, N. 2011. Climate and material controls on periglacial soil processes: toward improving periglacial climate indicators. *Quaternary Research* 75, 356–365.
- Matthews, J.A. 1992. *The Ecology of Recently Deglaciated Terrain*. Cambridge University Press, Cambridge.
- Matthews, J.A. 2005. ‘Little Ice Age’ glacier variations in Jotunheimen, southern Norway: a study in regionally controlled lichenometric dating of recessional moraines with implications for climate and lichen growth. *The Holocene* 15, 1–29.
- Matthews, J.A., Dresser, P.Q. 2008. Holocene glacier variation chronology of the Smørstabbtindan massif, Jotunheimen, southern Norway, and the recognition of century- to millennial-scale European Neoglacial Events. *The Holocene* 18, 181–201.
- Matthiessen, J., Knies, J., Nowaczyk, N.R., et al. 2001. Late Quaternary dinoflagellate cyst stratigraphy at the Eurasian continental margin, Arctic Ocean: indications for Atlantic water inflow in the past 150,000 years. *Global and Planetary Change* 31, 65–86.
- Maul, L.C., Parfitt, S.A. 2010. Micromammals from the 1995 Mammoth Excavation at West Runton, Norfolk, UK: morphometric data, biostratigraphy and taxonomic reappraisal. *Quaternary International* 228, 91–115.
- Mauquoy, D., Barber, K.E., 1999a. A replicated 3000 year proxy-record from Coom Rigg Moss and Felecia Moss, the Border Mires, northern England. *Journal of Quaternary Science* 14, 263–275.
- Mauquoy, D., van Geel, B., Blaauw, M., et al. 2004. Changes in solar activity and Holocene climatic shifts derived from ^{14}C wiggle-match dated peat deposits. *The Holocene* 14, 45–52.

- Mauquoy, D., Hughes, P.D.M., van Geel, B. 2010. A protocol for plant macrofossil analysis of peat deposits. *Mires and Peat* 7 (art. 6), 1–5.
- Mauz, B., Felix-Henningsen, P. 2005. Palaeosols in Saharan and Sahelian dunes of Chad: archives of Holocene and North African climate changes. *The Holocene* 15, 453–458.
- Maxwell, T.A., Issawi, B., Haynes Jr., C.V. 2010. Evidence for Pleistocene lakes in the Tushka region, south Egypt. *Geology* 38, 1135–1138.
- Mayewski, P.A., Rohling, E.E., Stager, J.C., et al. 2004. Holocene climate variability. *Quaternary Research* 62, 243–255.
- Meese, D.A., Gow, A.J., Alley, R.B., et al. 1997. The Greenland Ice Sheet Project 2 depth-age scale: methods and results. *Journal of Geophysical Research* 102, 26411–26423.
- Megaloudi, F. 2005. Burnt sacrificial plant offerings in Hellenistic times: an archaeobotanical case study from Messene, Peloponnes, Greece. *Vegetation History and Archaeobotany* 14, 329–340.
- Meijer, T., Preece, R.C. 1995. Malacological evidence relating to the insularity of the British Isles during the Quaternary. In *Island Britain: A Quaternary Perspective* (edited by R.C. Preece). Geological Society of London, Special Publication 96. Geological Society, London, 89–110.
- Meissner, K.J., Eby, M., Weaver, A.J., et al. 2007. CO₂ threshold for millennial-scale oscillations in the climate system: implications for global warming scenarios. *Climate Dynamics* 30, 161–174.
- Meland, M.Y., Jansen, E., Elderfield, H. 2005. Constraints on SST estimates for the northern North Atlantic/Nordic Seas during the LGM. *Quaternary Science Reviews* 24, 835–852.
- Menounos, B., Clague, J.J., Osborn, G., et al. 2008. Western Canadian glaciers advance in concert with climate change circa 4.2 ka. *Geophysical Research Letters* 35, doi: 10.1029/2008GL033172.
- Menzies, J., Zaniewski, K. 2003. Microstructures within a modern debris flow deposit derived from Quaternary glacial diamicton – a comparative micromorphological study. *Sedimentary Geology* 157, 31–48.
- Menzies, J., van der Meer, J.J.M., Rose, J. 2006. Till – as a glacial ‘tectomict’, its internal architecture, and the development of a ‘typing’ method for till differentiation. *Geomorphology* 75, 172–200.
- Merritt, D. 2007. Fluvial environments: terrace sequences. In *Encyclopedia of Quaternary Science* (edited by S.A. Elias). Elsevier, Amsterdam, 694–704.
- Mertens, K.N.J.M., Lynn, M., Aycard, M., et al. 2009. Coccolithophores as palaeoecological indicators for shifts of the ITCZ in the Cariaco Basin during the late Quaternary. *Journal of Quaternary Science* 24, 159–174.
- Mesolella, K.J., Matthews, R.K., Broecker, W.S., et al. 1969. The astronomical theory of climatic change: Barbados data. *Journal of Geology* 77, 250–277.
- Mesquita, F., Roca, J.R., Reed, J.M., et al. 2005. Quantifying species–environment relationships in non-marine Ostracoda for ecological and palaeoecological studies: examples using Iberian data. *Palaeogeography, Palaeoclimatology, Palaeoecology* 225, 93–117.
- Mesquita-Joanes, F., Smith, A.J., Viehberg, F.A. 2012. The ecology of Ostracoda across levels of biological organization from individual to ecosystem: a review of recent developments and future potential. In *Developments in Quaternary Science. Volume 17: Ostracoda as Proxies for Quaternary Climate Change* (edited by D.J. Horne, J.A. Holmes, J. Rodriguez-Lazaro, et al.). Elsevier, Amsterdam, 15–35.
- Meyer, E., Sarna-Wojcicki, A.M., Hillhouse, J.W., et al. 1991. Fission-track age (400,000 yr) of the Rockland tephra, based on inclusions of zircon grains lacking fossil fission tracks. *Quaternary Research* 39, 54–162.
- Meyer, M.C., Spötl, C., Mangini, A. 2008. The demise of the Last Interglacial recorded in isotopically dated speleothems from the Alps. *Quaternary Science Reviews* 27, 476–496.
- Meyers, P.A. 2006. Paleoceanographic and paleoclimatic similarities between Mediterranean sapropels and Cretaceous black shales. *Palaeogeography, Palaeoclimatology, Palaeoecology* 235, 305–320.
- Meyers, P.A., Teranes, J.J. 2001. Sediment organic matter. In *Tracking Environmental Changes Using Lake Sediments. Volume II: Physical and Chemical Techniques* (edited by W.M. Last, J.P. Smol). Kluwer, Dordrecht, 239–269.
- Meyers, S.R., Sageman, B.B., Pagani, M. 2008. Resolving Milankovitch: consideration of signal and noise. *American Journal of Science* 308, 770–786.
- Meyrick, R. 2003. Holocene Molluscan faunal history and environmental change at Kloster Mühle, Rheinland-Pfalz, western Germany. *Journal of Quaternary Science* 18, 121–132.
- Meyrick, R.A., Karrow, P.F. 2007. Three detailed, radiocarbon-dated, Holocene tufa and alluvial fan mollusc successions from southern Ontario: the first in north-eastern North America. *Palaeogeography, Palaeoclimatology, Palaeoecology* 243, 250–271.
- Meyrick, R.A., Preece, R.C. 2001. Molluscan successions from two Holocene tufas near Northampton, English Midlands. *Boreas* 28, 77–93.
- Miall, A.D. 2000. *Principles of Sedimentary Basin Analysis*, 3rd edn. Springer, Berlin.
- Miallier, D., Condomines, M., Pilleyre, T., et al. 2004. Concordant thermoluminescence and ²³⁸U–²³⁰Th ages for a trachytic dome (Grand Sarcouï) from the Chaîne des Puys (French Massif Central). *Quaternary Science Reviews* 23, 709–715.
- Mighall, T.M., Timberlake, S., Clark, S.H.E., et al. 2002. A palaeoenvironmental investigation of sediments from the prehistoric mine of Copa Hill, Cwmystwyth, mid-Wales. *Journal of Archaeological Science* 29, 1161–1188.
- Migowski, C., Agnon, A., Bookman, R., et al. 2004. Recurrence pattern of Holocene earthquakes along the Dead Sea transform revealed by varve counting and radiocarbon dating of lacustrine sediments. *Earth and Planetary Science Letters* 222, 301–314.
- Milker, Y., Schmiedl, G., Betzler, C. 2011. Paleobathymetric history of the Western Mediterranean Sea shelf during the latest glacial period and the Holocene: quantitative reconstructions based on foraminiferal transfer functions. *Palaeogeography, Palaeoclimatology, Palaeoecology* 307, 324–338.
- Millard, A.R. 2006. Bayesian analysis of Pleistocene chronometric methods. *Archaeometry* 48, 359–375.

- Millard, A.R., Hedges, R.E.M. 1996. A diffusion–adsorption model of uranium uptake by archaeological bone. *Geochimica et Cosmochimica Acta* 60, 2139–2152.
- Miller, B.B., Tevesz, M.J.S. 2001. Freshwater molluscs. In *Tracking Environmental Change Using Lake Sediments. Volume 4: Zoological Indicators* (edited by J.P. Smol, H.J.B. Birks, W.M. Last). Kluwer, Dordrecht, 153–171.
- Miller, G.H., Clarke, S.J. 2007. Amino-acid dating. In *Encyclopedia of Quaternary Science* (edited by S.A. Elias). Elsevier, Amsterdam, 41–52.
- Miller, G.H., Beaumont, P.B., Jull, A.J.T., et al. 1992. Pleistocene geochronology and palaeothermometry from protein diagenesis in ostrich eggshells: implications for the evolution of modern humans. *Philosophical Transactions of the Royal Society of London B* 337, 149–157.
- Miller, G.H., Magee, J.W., Jull, A.J.T. 1997. Low-latitude glacial cooling in the Southern Hemisphere from amino acids in emu eggshells. *Nature* 385, 241–244.
- Miller, G.H., Beaumont, P.B., Deacon, H.J., et al. 1999a. Earliest modern humans in southern Africa dated by isoleucine epimerization in ostrich eggshell. *Quaternary Science Reviews* 18, 1537–1548.
- Miller, G.H., Magee, J.W., Johnson, B.J., et al. 1999b. Pleistocene extinction of *Gonyornis newtoni*: human impact on Australian megafauna. *Science* 283, 205–208.
- Miller, G.H., Fogel, M.L., Magee, J.W., et al. 2005. Ecosystem collapse in Pleistocene Australia and a human role in megafaunal extinction. *Geology* 309, 287–290.
- Miller, G.H., Geirdsdottir, A., Zhong, Y., et al. 2012. Abrupt onset of the Little Ice Age triggered by volcanism and sustained by sea-ice/ocean feedbacks. *Geophysical Research Letters* 39, doi: 10.1029/2011/GL050168.
- Miller, K.G., Kominz, M.A., Browning, J.V., et al. 2005. The Phanerozoic record of global sea-level change. *Science* 310, 1293–1298.
- Miller, K.G., Mountain, G.S., Wright, J.D., et al. 2011. A 180-million-year record of sea level and ice volume variations from continental margins and deep-sea isotopic records. *Oceanography* 24, 40–53.
- Miller, R.F., Elias, S.A. 2000. Late-glacial climate in the Maritimes Region, Canada, reconstructed from mutual climatic range analysis of fossil Coleoptera. *Boreas* 29, 79–88.
- Miller, W., Schuster, S.C., Welch, A.J., et al. 2013. Polar and brown bear genomes reveal ancient admixture and demographic footprints of past climate change. *Proceedings of the National Academy of Sciences of the United States of America*, doi: 101073/pnas.1210506109.
- Millien, V., Lyons, S.K., Olson, L., et al. 2006. Ecotypic variation in the context of global climate change: revisiting the rules. *Ecology Letters* 9, 853–869.
- Millière, L., Spangenberg, J.E., Bindschedler, S., et al. 2011. Reliability of stable carbon and oxygen isotope compositions of pedogenic needle fibre calcite as environmental indicators: examples from Western Europe. *Isotopes and Environmental Health Studies* 47, 341–358.
- Mills, H.H. 2005. Relative-age dating of transported regolith and application to study of landform evolution in the Appalachians. *Geomorphology* 67, 63–96.
- Milne, G.A., Mitrovica, J.X. 2008. Searching for eustasy in deglacial sea-level histories. *Quaternary Science Reviews* 27, 2292–2302.
- Milne, G.A., Gehrels, W.R., Hughes, C.W., et al. 2009. Identifying the causes of sea-level change. *Nature Geoscience* 2, 471–478.
- Milner, N., Conneller, C., Elliott, B., et al. 2011. From riches to rags: organic deterioration at Star Carr. *Journal of Archaeological Science* 38, 2818–2832.
- Mishra, S., White, M.J., Beaumont, P., et al. 2007. Fluvial deposits as an archive of early human activity. *Quaternary Science Reviews* 26, 2996–3016.
- Mithen, S., Reed, M. 2002. Stepping out: a computer simulation of hominid dispersal from Africa. *Journal of Human Evolution* 43, 433–462.
- Mitrovica, J.X. 2003. Recent controversies in predicting post-glacial sea-level change. *Quaternary Science Reviews* 22, 127–133.
- Mitrovica, J.X., Peltier, W.R. 1991. On postglacial geoid subsidence over the equatorial oceans. *Journal of Geophysical Research*, 96, 20053–20071.
- Miura, O. 1987. Vertical migration of pollen in soils. *Ecological Review* 21, 125–132.
- Mix, A.C., Bard, E., Schneider, R. 2001. Environmental processes of the ice age: land, oceans, glaciers (EPILOG). *Quaternary Science Reviews* 20, 627–657.
- Miyahara, H., Masuda, K., Nagaya, K., et al. 2007. Variation of solar activity from the Spoerer to the Maunder minima indicated by radiocarbon content in tree-rings. *Advances in Space Research* 40, 1060–1063.
- Miyoshi, N., Fujiki, T., Morita, Y. 1999. Palynology of a 250-m core from Lake Biwa: a 430,000-year record of glacial–interglacial vegetation change in Japan. *Review of Palaeobotany and Palynology* 104, 267–283.
- Moine, O., Rousseau, D.-D., Jolly, D., et al. 2002. Paleoclimatic reconstruction using Mutual Climatic Range on terrestrial mollusks. *Quaternary Research* 57, 162–172.
- Molinaroli, E., De Falco, G., Rabitti, S., et al. 2000. Stream-scanning laser system, electric sensing counter and settling grain size analysis: a comparison using reference materials and marine sediments. *Sedimentary Geology* 130, 269–281.
- Millard, J.D. 2000. Ice-shaped ring-forms in Western Canada: their airphoto expressions and manifold polygenetic origins. *Quaternary International* 68–71, 187–198.
- Molloy, K., O'Connell, M. 2004. Holocene vegetation and land-use dynamics in the karstic environment of Inis Oirr, Aran Islands, western Ireland: pollen analytical evidence evaluated in light of the archaeological record. *Quaternary International* 113, 41–64.
- Montaggioni, L.F., Braithwaite, C.J.R. 2009. *Developments in Marine Geology. Volume 5: Quaternary Coral Reef Systems: History, Development Processes and Controlling Factors*. Elsevier Science, Burlington, MA.
- Mooers, H.D. 1989. Drumlin formation: a time-transgressive model. *Boreas* 18, 99–107.

- Mooney, S.D., Harrison, S.P., Bartlein, P.J., *et al.* 2011. Late Quaternary fire regimes of Australasia. *Quaternary Science Reviews* 30, 28–46.
- Moore, A.E., Cotterill, F.P.D. (Woody), Eckartd, F.D. 2012. The evolution and ages of Makgadikgadi Palaeo-lakes: consilient evidence from Kalahari drainage evolution South-central Africa. *South African Journal of Geology* 1156, 385–423.
- Moore, P.D., Webb, J.A., Collinson, M.D. 1991. *Pollen Analysis*. Blackwell, Oxford.
- Moos, M.T., Laird, K.R., Cumming, B.F. 2009. Climate-related eutrophication of a small boreal lake in northwestern Ontario: a palaeolimnological perspective. *The Holocene* 19, 359–367.
- Moreno, A., Cacho, I., Canals, M., *et al.* 2005. Links between marine and atmospheric processes oscillating on a millennial timescale. A multi-proxy study of the last 50,000 yr from the Alboran Sea (western Mediterranean Sea). *Quaternary Science Reviews* 24, 1623–1636.
- Morgenstern, U., Fifield, L.K., Zondervan, A. 2000. New frontiers in glacial ice dating: measurement of natural ^{32}Si by AMS. *Nuclear Instruments and Methods B* 172, 605–609.
- Morgenstern, U., Geyh, M.A., Kudrass, H.R., *et al.* 2001. ^{32}Si dating of marine sediments from Bangladesh. *Radiocarbon* 43, 909–916.
- Mörner, N.-A. 1980. Eustasy and geoid changes as a function of core/mantle changes. In *Earth Rheology, Isostasy and Eustasy* (edited by N.-A. Mörner). John Wiley, Chichester and New York, 535–553.
- Moros, M., De Dekker, P., Jansen, E., *et al.* 2009. Holocene climatic variability in the Southern Ocean recorded in a deep-sea sediment core off South Australia. *Quaternary Science Reviews* 28, 1932–1940.
- Morrill, C., Overpeck, J.T., Cole, J.E., *et al.* 2006. Holocene variations in the Asian monsoon inferred from the geochemistry of lake sediments in central Tibet. *Quaternary Research* 65, 232–243.
- Mortensen, A.K., Bigler, M., Grönvold, K., *et al.* 2005. Volcanic ash layers from the Last Glacial termination in the NGRIP ice core. *Journal of Quaternary Science* 20, 209–219.
- Morwood, M.J., O'Sullivan, P.B., Aziz, E., *et al.* 1998. Fission-track ages of stone tools and fossils on the east Indonesian island of Flores. *Nature* 392, 173–176.
- Moucha, R., Forte, A.M., Mitrovica, J.X., *et al.* 2008. Dynamic topography and long-term sea-level variations: There may be no such thing as a stable continental platform. *Earth and Planetary Science Letters* 271, 101–108.
- Mroczeck, P. 2013. Recycled loess – a micromorphological approach to the determination of local source areas of loess. *Quaternary International* 296, 241–250.
- Mudelsee, M., Schultz, M. 1997. The Mid-Pleistocene climate transition: onset of the 100 ka cycle lags ice volume build-up by 280 ka. *Earth and Planetary Science Letters* 151, 117–123.
- Mudelsee, M., Raymo, M.E. 2005. Slow dynamics of the Northern Hemisphere glaciation. *Paleoceanography* 20, PA4022, doi: 10.1029/2005PA001153.
- Mudie, P.J., Aksu, A.E., Yasar, D. 2001. Late Quaternary dinoflagellate cysts from the Black, Marmara and Aegean seas: variations in assemblages, morphology and paleosalinity. *Marine Micropaleontology* 43, 155–178.
- Muhs, D.R. 2013. The geologic records of dust in the Quaternary. *Aeolian Research* 9, 3–48.
- Muhs, D.R., Bettis III, E.A. 2000. Geochemical variations in Peoria Loess of western Iowa indicate Last Glacial paleowinds of mid-continent North America. *Quaternary Research* 53, 49–61.
- Muhs, D.R., Roskin, J., Tsoar, H., *et al.* 2013. Origin of the Sinai–Negev erg, Egypt and Israel: mineralogical and geochemical evidence for the importance of the Nile and sea level history. *Quaternary Science Reviews* 69, 28–48.
- Muller, R.A., MacDonald, G.J. 1997. Glacial cycles and astronomical forcing. *Science* 277, 215–218.
- Müller, R.D., Sdrolius, M., Gaina, C., *et al.* 2008. Long-term sea-level fluctuations driven by ocean basin dynamics. *Science* 319, 1357–1362.
- Müller, U.C., Klotz, S., Geyh, M.A., *et al.* 2005. Cyclic climate fluctuations during the last interglacial in central Europe. *Geology* 33, 449–452.
- Munroe, J.S., Mickelson, D.M. 2002. Last Glacial Maximum equilibrium-line altitudes and paleoclimate, northern Uinta Mountains, Utah, USA. *Journal of Glaciology* 48, 257–266.
- Murray, J.W. 2006. *Ecology and Applications of Benthic Foraminifera*. Cambridge University Press, Cambridge.
- Murray, J.W., Alve, E. 1999. Natural dissolution of modern shallow water benthic foraminifera: taphonomic effects on the palaeoecological record. *Palaeogeography, Palaeoclimatology, Palaeoecology* 146, 195–209.
- Murray-Wallace, C.V. 2002. Pleistocene coastal stratigraphy, sea-level highstands and neotectonism of the southern Australian passive continental margin – a review. *Journal of Quaternary Science* 17, 469–489.
- Murray-Wallace, C.V., Bouman, R.P., Prescott, J.R., *et al.* 2010. Aminostratigraphy and thermoluminescence dating of coastal aeolianites and the later Quaternary history of a failed delta: the River Murray mouth region, South Australia. *Quaternary Geochronology* 5, 28–49.
- Murray-Wallace, C.V., Woodroffe, C.D. 2014. *Quaternary Sea-Level Changes: A Global Perspective*. Cambridge University Press, Cambridge.
- Murton, J.B., Worsley, P., Gozdzik, J. 2000. Sand veins and wedges in cold aeolian environments. *Quaternary Science Reviews* 19, 899–922.
- Muscheler, R., Beer, J., Qwagner, G., *et al.* 2004. Changes in the carbon cycle during the last deglaciation as indicated by the comparison of Be-10 and C-14 records. *Earth and Planetary Science Letters* 219, 325–340.
- Muscheler, R., Beer, J., Kubik, P.W., *et al.* 2005. Geomagnetic field intensity during the last 60,000 years based on ^{10}Be and ^{36}Cl from the Summit ice cores and ^{14}C . *Quaternary Science Reviews* 24, 1849–1860.
- Nádor, A., Lantos, M., Tóth-Makk, Á., *et al.* 2003. Milankovitch-scale multi-proxy records from fluvial sediments of the last 2.6 Ma, Pannonian Basin, Hungary. *Quaternary Science Reviews* 22, 2157–2175.

- Naegler, T., Levin, I. 2006. Closing the global radiocarbon budget 1945–2005. *Journal of Geophysical Research* 111, D12311.
- Naidu, P.D., Govil, P. 2010. New evidence on the sequence of deglacial warming in the tropical Indian Ocean. *Journal of Quaternary Science* 25, 1138–1143.
- Nakagawa, T., Kitagawa, H., Yasuda, Y., et al. 2005. Pollen/event stratigraphy of the varved sediment of Lake Suigetsu, central Japan from 15,701 to 10,217 SG vyr (Suigetsu varve years before present): description, interpretation and correlation with other regions. *Quaternary Science Reviews* 24, 1691–1701.
- Nakagawa, T., Nakagawa, T., Gotanda, K., et al. 2012. SG06, a fully continuous and varved sediment core from Lake Suigetsu, Japan: stratigraphy and potential for improving the radiocarbon calibration model and understanding late Quaternary climate changes. *Quaternary Science Reviews* 36, 164–176.
- Namiotko, T., Danielopol, D.L., Baltanás, A. 2011. Soft body morphology: dissection and slide preparation of Ostracoda: a primer. *Joannea-Geologie und Paläontologie* 11, 327–343.
- Nanson, G.C., Jones, B.J., Price, D.M., et al. 2005. Rivers turned to rock: Late Quaternary alluvial induration influencing the behaviour and morphology of an anabranching river in the Australian monsoon tropics. *Geomorphology* 70, 398–420.
- Nanson, G.C., Price, D.M., Jones, B.G., et al. 2008. Alluvial evidence for major climate and flow regime changes during the middle and late Quaternary in eastern central Australia. *Geomorphology* 101, 109–129.
- Narcisi, B., Petit, J.R., Delmonte, B., et al. 2005. Characteristics and sources of tephra layers in the EPICA-Dome C ice record (East Antarctica): implications for past atmospheric circulation and ice core stratigraphic correlations. *Earth and Planetary Science Letters* 239, 253–265.
- Narcisi, B., Petit, J.R., Delmonte, B. 2010. Extended East Antarctic ice-core tephrostratigraphy. *Quaternary Science Reviews* 29, 21–27.
- Nash, D.J., Thomas, D.S.G., Shaw, P.A. 1994. Silicious duricrusts as palaeoclimatic indicators: evidence from the Kalahari desert of Botswana. *Palaeogeography, Palaeoclimatology, Palaeoecology* 112, 279–295.
- Nathan, R., Casagrandi, R. 2004. A simple mechanistic model of seed dispersal, predation and plant establishment: Janzen-Connell and beyond. *Journal of Ecology* 92, 733–746.
- Navarro, C., Carrión, J.S., Navarro, J., et al. 2000. An experimental approach to the palynology of cave deposits. *Journal of Quaternary Science*, 15, 603–619.
- Nayling, N., McGrail, S. 2004. *The Barland's Farm Romano-Celtic Boat*. CBA Research Report 138, Council for British Archaeology, York.
- Naysmith, P., Cook, G.T., Phillips, M., et al. 2004. Preliminary results for the extraction and measurement of in situ ^{14}C from quartz. *Radiocarbon* 46, 210–208.
- Neal, A. 2004. Ground-penetrating radar and its use in sedimentology: principles, problems and progress. *Earth-Science Reviews* 66, 261–330.
- Nederbragt, A.J., Thurrow, J. 2005. Geographic coherence of millennial-scale climatic cycles during the Holocene. *Palaeogeography, Palaeoclimatology, Palaeoecology* 221, 313–324.
- NEEM Community Members. 2013. Eemian interglacial reconstructed from a Greenland folded ice core. *Nature* 493, 489–494.
- Nelson, K.J.P., Nelson, F.E., Walegur, M.T. 2007. Periglacial Appalachia: paleoclimatic significance of blockfield elevation gradients, eastern USA. *Permafrost and Periglacial Processes* 18, 61–73.
- Nelson, S.T., Wood, M.J., Mayo, A.L., et al. 2005. Shoreline tufa and tufaglomerate from Pleistocene Lake Bonneville, Utah, USA: stable isotopic and mineralogical records of lake conditions, processes, and climate. *Journal of Quaternary Science* 20, 3–19.
- Nesje, A., Sejrup, H.-P. 1988. Late Weichselian/Devensian ice sheets in the North Sea and adjacent land areas. *Boreas* 17, 371–384.
- Nesje, A., Dahl, S.O. 2003. The ‘Little Ice Age – only temperature? *The Holocene* 13, 39–145.
- Nesje, A., Dahl, S.O., Andersson, C., et al. 2000. The lacustrine sedimentary sequence in Sygneksardvatnet, western Norway: a continuous high-resolution record of the Jostedalsbreen ice cap during the Holocene. *Quaternary Science Reviews* 19, 1047–1065.
- Nesje, A., Matthews, J.A., Dahl, S.O., et al. 2001. Holocene glacier fluctuations of Flatebreen and winter-precipitation changes in the Jostedalsbreen region, western Norway, based on glacio-lacustrine sediment records. *The Holocene* 11, 267–280.
- Nesje, A., Bakke, J., Dahl, S.O., et al. 2008. Norwegian mountain glaciers in the past, present and future. *Global and Planetary Change* 60, 10–27.
- Nevalainen, L., Sarmaja-Korjonen, K., Luoto, T.P. 2011. Sedimentary Cladocera as indicators of past water-level changes in shallow northern lakes. *Quaternary Research* 75, 430–437.
- Newman, M., Compo, G.P., Alexander, M. 2003. ENSO-forced variability of the Pacific Decadal oscillation. *Journal of Climate* 16, 3853–3857.
- Newnham, R.M., Eden, D.N., Lowe, D.J., et al. 2003. Rerewhakaaitu Tephra, a land-sea marker for the last termination in New Zealand, with implications for global climate change. *Quaternary Science Reviews* 22, 289–308.
- Ng, F.S.L., Barr, I.D., Clark, C.D. 2010. Using the surface profiles of modern ice masses to inform palaeo-glacier reconstructions. *Quaternary Science Reviews* 29, 3240–3255.
- Nichols, J.E., Booth, R.K., Jackson, S.T., et al. 2006. Paleohydrologic reconstruction based on n-alkane distributions in ombrotrophic peat. *Organic Geochemistry* 37, 1505–1513.
- Nichols, J.E., Booth, R.K., Jackson, S.T., et al. 2010. Differential hydrogen isotopic ratios of *Sphagnum* and vascular plant biomarkers in ombrotrophic peatlands as a quantitative proxy for precipitation–evaporation balance. *Geochimica et Cosmochimica Acta* 74, 1407–1416.
- Nicoll, K. 2001. Radiocarbon chronologies for prehistoric human occupation and hydroclimatic change in Egypt and Northern Sudan. *Geoarchaeology* 16, 47–64.
- Nicoll, K. 2004. Recent environmental change and prehistoric human activity in Egypt and Northern Sudan. *Quaternary Science Reviews* 23, 561–580.
- Nielsen, A.B., Odgaard, B.V. 2004. The use of historical analogues for interpreting fossil pollen records. *Vegetation History and Archaeobotany*, 13, 33–43.

- Nielsen-Marsh, C., Hedges, R.E.M. 2000. Patterns of diagenesis in bone 1: the effects of site environments. *Journal of Archaeological Science* 27, 1139–1150.
- Nijampurkar, V.N., Rao, D.K., Oldfield, F., et al. 1998. The half-life of ^{32}Si : a new estimate based on varved lake sediments. *Earth and Planetary Science Letters* 163, 191–196.
- Nivière, B., Bruestle, A., Bertrand, G., et al. 2008. Active tectonics of the southeastern Upper Rhine Graben, Freiburg area (Germany). *Quaternary Science Reviews* 27, 541–555.
- North American Commission on Stratigraphic Nomenclature. 1983. North American Stratigraphic Code. *American Association of Petroleum Geologists Bulletin* 67, 841–875.
- North American Commission on Stratigraphic Nomenclature. 2005. North American Stratigraphic Code. *American Association of Petroleum Geologists Bulletin* 89, 1547–1591.
- North Greenland Ice Core Project Members. 2004. High-resolution record of Northern Hemisphere climate extending into the last interglacial period. *Nature* 431, 147–151.
- Notebaert, B., Verstraeten, G. 2010. Sensitivity of West and Central European river systems to environmental changes during the Holocene: a review. *Earth-Science Reviews* 103, 163–182.
- O'Brien, C., Selby, K., Ruiz, Z., et al. 2005. A sediment-based multiproxy palaeoecological approach to the environmental archaeology of lake dwellings (crannogs), central Ireland. *The Holocene* 15, 707–719.
- Obrochta, S.P., Miyahara, H., Yokoyama, Y., et al. 2012. A re-examination of evidence for the North Atlantic '1500-year cycle' at Site 609. *Quaternary Science Reviews* 55, 23–33.
- Occhietti, S. 2007. The Saint-Narcisse morainic complex and early Younger Dryas events on the southeastern margin of the Laurentide Ice Sheet. *Géographie physique et Quaternaire* 61, 89–117.
- Oches, E.A., McCoy, W.D. 1995. Aminostratigraphic evaluation of conflicting age estimates for the 'Younger Loess' of Hungary. *Quaternary Research* 44, 160–170.
- Oches, E.A., McCoy, W. 2001. Historical developments and recent advances in amino acid geochronology applied to loess research: examples from North America, Europe and China. *Earth-Science Reviews* 54, 173–192.
- Oches, E.A., McCoy, W.D., Clark, P.U. 1996. Amino acid estimates of latitudinal temperature gradients and geochronology of loess deposition during the last glaciation, Mississippi Valley, United States. *Geological Society of America Bulletin* 108, 892–903.
- Oches, E.A., McCoy, W.D., Grieser, D. 2000. Aminostratigraphic correlations of loess–paleosol sequences across Europe. In *Perspectives in Amino Acid and Protein Geochemistry* (edited by G.A. Goodfriend, M.J. Collins, M.L. Fogel, et al.). Oxford University Press, New York, 331–348.
- Ó Cofaigh, C. 2007. Glacimarine sediments and ice rafted debris. In *Encyclopedia of Quaternary Science* (edited by S.A. Elias). Elsevier, Amsterdam, 932–945.
- Ó Cofaigh, C. 2013. Glacimarine sediments and ice rafted debris. In *Encyclopedia of Quaternary Science*, volume 2, 2nd edn (edited by S.A. Elias). Elsevier, Amsterdam, 30–42.
- Ó Cofaigh, C., Dowdeswell, J.A. 2001. Laminated sediments in glacimarine environments: diagnostic criteria for their interpretation. *Quaternary Science Reviews* 20, 1411–1436.
- Ó Cofaigh, C., Evans, D.J.A. 2007. Radiocarbon constraints on the age of the maximum advance of the British–Irish Ice Sheet in the Celtic Sea. *Quaternary Science Reviews* 26, 1197–1203.
- Ó Cofaigh, C., Evans, D.J.A., Smith, I.R. 2009. Large-scale reorganisation and sedimentation of terrestrial ice streams during late Wisconsinan Laurentide Ice Sheet deglaciation. *Geological Society of America Bulletin* 122, 743–756.
- Ó Cofaigh, C., Telfer, M.W., Bailey, R.M., et al. 2012a. Late Pleistocene chronostratigraphy and ice sheet limits, southern Ireland. *Quaternary Science Reviews* 44, 160–179.
- Ó Cofaigh, C., Dowdeswell, J.A., Jennings, A.E., et al. 2012b. An extensive and dynamic ice sheet on the West Greenland shelf during the last glacial cycle. *Geology* 41, 219–222.
- O'Connor, T.P. (ed.). 2005. *Biosphere to Lithosphere – New Studies in Vertebrate Taphonomy*. Oxbow Books, Oxford.
- Odgaard, B.V. 1999. Fossil pollen as a record of past biodiversity. *Journal of Biogeography* 26, 7–17.
- O'Donnell, T.H., Macko, S.A., Wehmiller, J.F. 2006. Stable carbon isotope composition of amino acids in modern and fossil *Mercenaria*. *Organic Geochemistry* 38, 485–498.
- Orlemans, J. 2001. *Glaciers and Climate Change*. Balkema, Lisse.
- Ó Foighil, D., Lee, T., Slapcinsky, J. 2011. Prehistoric anthropogenic introduction of partulid tree snails in Papua New Guinean archipelagos. *Journal of Biogeography* 38, 1625–1632.
- Ohmura, A., Kasser, P., Funk, M. 1992. Climate at the equilibrium line of glaciers. *Journal of Glaciology* 38, 397–411.
- Ojala, A.E.K., Tiljander, M. 2003. Testing the fidelity of sediment chronology: comparison of varve and palaeomagnetic results from Holocene lake sediments from central Finland. *Quaternary Science Reviews* 22, 1787–1803.
- Ojala, A.E.K., Alenius, T. 2005. 10 000 years of interannual sedimentation recorded in the Lake Nautajärvi (Finland) clastic-organic varves. *Palaeogeography, Palaeoclimatology, Palaeoecology* 219, 285–302.
- Ojala, A.E.K., Kubischa, F., Kaakinen, A., et al. 2011a. Characterization of diamictites on the basis of their mineral magnetic properties in Murchisonfjorden, Nordaustlandet, Svalbard. *Sedimentary Geology* 233, 150–158.
- Ojala, A.E.K., Francus, P., Zolitschka, B., et al. 2011b. Characteristics of sedimentary varve chronologies—a review. *Quaternary Science Reviews* 43, 45–60.
- Okazaki, Y., Timmermann, A., Menzel, L., et al. 2010. Deepwater formation in the North Pacific during the Last Glacial Termination. *Science* 329, 200–204.
- Oldfield, F., Richardson, N., Appleby, P.G. 1995. Radiometric dating (^{210}Pb , ^{137}Cs , ^{241}Am) of recent ombrotrophic peat accumulation and evidence for changes in mass balance. *The Holocene* 5, 141–148.
- Oldfield, F., Wake, R., Boyle, J., et al. 2003. The late-Holocene history of Gormire Lake (NE England) and its catchment: a multiproxy reconstruction of past human impact. *The Holocene* 13, 677–690.

- Oliver, K.I.C., Hoogakker, B.A.A., Crowhurst, S., et al. 2009. A synthesis of marine sediment core $\delta^{13}\text{C}$ data over the last 150 000 years. *Climate of the Past Discussions* 5, 2497–2554.
- Ollier, C., Sheth, H.C. 2008. The High Deccan duricrusts of India and their significance for the ‘laterite’ issue. *Journal of Earth System Science* 117, 537–551.
- Olson, C.G., Nettleton, W.D. 1998. Paleosols and the effects of alteration. *Quaternary International* 51/52, 185–194.
- Olsson, F., Lemdahl, G. 2009. A continuous Holocene beetle record from the site Stavsvåkra, southern Sweden: implications for the last 10 600 years of forest and land use history. *Journal of Quaternary Science* 24, 612–626.
- Onac, B., Constantin, S., Lundberg, J., et al. 2002. Isotopic climate record in a Holocene stalagmite from Usilor Cave (Romania). *Journal of Quaternary Science* 17, 319–327.
- O’Neal, M.A., Schoenenberger, K.R. 2003. A *Rhizocarpon geographicum* growth curve for the Cascade Range of Washington and northern Oregon, USA. *Quaternary Research* 60, 233–241.
- Opgenoorth, L., Vendramin, G.C., Mao, K., et al. 2010. Tree endurance on the Tibetan Plateau marks the world’s highest known tree line of the Last Glacial Maximum. *New Phytologist* 185, 332–342.
- Oppenheimer, C. 2011. *Eruptions that Shook the World*. Cambridge University Press, Cambridge.
- Ori, G.G., Diachille, G., Komatsu, G., et al. 2009. River morphologies and palaeodrainages of Western Africa (Sahara and Sahel) during humid climatic conditions. In *Sedimentary Processes, Environments and Basins: A Tribute to Peter Friend* (edited by G. Nichols, E. Williams, C. Paola). Blackwell Publishing, Oxford, 519–534.
- Orme, A.R. 2008. *Pleistocene Pluvial Lakes of the American West: A Short History of Research*. Geological Society of London, Special Publication 301. Blackwell Scientific Publications, Oxford, 51–78.
- Orme, A.R., Orme, A.J., 2008. Late Pleistocene shorelines of Owens Lake, California, and their hydroclimatic and tectonic implications. In *Late Cenozoic Drainage History of the Southwestern Great Basin and Lower Colorado River Region: Geologic and Biotic Perspectives* (edited by M.C. Reheis, R. Hershler, D.M. Miller). Geological Society of America, Special Paper 439, 207–225.
- Ortiz, J.E., Torres, T., Julia, R., et al. 2004. Numerical dating algorithms of amino acid racemization ratios from continental ostracodes. Application to the Guadix-Baza Basin (southern Spain). *Quaternary Science Reviews* 23, 717–730.
- Osborn, G., Bevis, K. 2001. Glaciation in the Great Basin of the Western United States. *Quaternary Science Reviews* 20, 1377–1410.
- Osborn, G., Menounos, B., Koch, J., et al. 2007. Multi-proxy record of Holocene glacial history of the Spearhead and Fitzsimmons ranges, southern British Columbia. *Quaternary Science Reviews* 26, 479–493.
- Oschmann, W. 2009. Editorial (special issue on sclerochronology). *International Journal of Earth Sciences (Geologische Rundschau)* 98, 1–2.
- Osipov, E.U. 2004. Equilibrium-line altitudes on reconstructed LGM glaciers of the northwest Barguzinsky Ridge, Northern Baikal, Russia. *Quaternary International* 209, 219–226.
- Osterberg, E., Mayewski, P.A., Kreutz, K.J., et al. 2008. Ice core record of rising lead pollution in the North Pacific Atmosphere. *Geophysical Research Letters* 35, doi: 10.1029/2007GL032680.
- O’Sullivan, P.B., Morwood, M., Hobbs, D., et al. 2001. Archaeological implications of the geology and chronology of the Soa basin, Flores, Indonesia. *Geology* 29, 607–610.
- Ota, Y., Yamaguchi, M. 2004. Holocene coastal uplift in the western Pacific Rim in the context of late Quaternary uplift. *Quaternary International* 120, 105–117.
- Otto-Bliesner, B.L., Brady, E.C. 2010. The sensitivity of the climate response to the magnitude and location of freshwater forcing: last glacial maximum experiments. *Quaternary Science Reviews* 29, 56–73.
- Otvos, E.G. 2004. Prospects for interregional correlations using Wisconsin and Holocene aridity episodes, northern Gulf of Mexico coastal plain. *Quaternary Research* 61, 105–118.
- Overpeck, J.T., Webb, R.S. 1992. Mapping eastern North American vegetation change of the past 18 ka: no-analogs and the future. *Geology* 20, 1071–1074.
- Overpeck, J.T., Otto-Bliesner, B., Miller, G.H., et al. 2006. Paleoclimatic evidence for future ice-sheet instability and rapid sea-level rise. *Science* 311, 1747–1750.
- Oviatt, C.G. 1997. Lake Bonneville fluctuations and global climate change. *Geology* 25, 155–158.
- Oviatt, C.G., Thompson, R.S., Kaufman, D.S., et al. 1999. Reinterpretation of the Burnester Core, Bonneville Basin, Utah. *Quaternary Research* 52, 180–184.
- Owen, L.A., Richards, B., Rhodes, E.J., et al. 1998. Relic permafrost structures in the Gobi of Mongolia: age and significance. *Journal of Quaternary Science* 13, 539–547.
- Owen, L.A., Finkel, R.C., Minnich, R.A., et al. 2003. Extreme southwestern margin of late Quaternary glaciation in North America: timing and controls. *Geology* 31, 729–732.
- Owen, L.A., Caffee, M.W., Bovard, K.R., et al. 2006. Terrestrial cosmogenic nuclide surface exposure dating of the oldest glacial succession in the Himalayan orogen: Ladakh Range, northern India. *Geological Society of America Bulletin* 118, 383–392.
- Owen, L.A., Bright, J., Finkel, R.C., et al. 2007. Numerical dating of a Late Quaternary spit-shoreline complex at the northern end of Silver Lake playa, Mojave Desert, California: a comparison of the applicability of radiocarbon, luminescence, terrestrial cosmogenic nuclide, electron spin resonance, U-series and amino acid racemization methods. *Quaternary International* 166, 87–110.
- Owen, L.A., Thackray, G., Anderson, R.S., et al. 2009. Integrated research on mountain glaciers: current status, priorities and future prospects. *Geomorphology* 103, 158–171.
- Paillard, D. 2001. Glacial cycles: toward a new paradigm. *Reviews of Geophysics* 39, 325–346.
- Paillard, D., Parrenin, F. 2004. The Antarctic ice sheet and the triggering of deglaciations. *Earth and Planetary Science Letters* 227, 263–271.
- Palmer, A.P., Rose J., Lowe, J.J., et al. 2010. Annually-resolved dating of Younger Dryas glaciation and proglacial lake duration in Glen Roy and Glen Spean, western Scottish Highlands. *Journal of Quaternary Science* 25, 581–596.

- Palmer, A.P., Rose, J., Rasmussen, S.O. 2012. Evidence for phase-locked changes in climate between Scotland and Greenland during GS-1 (Younger Dryas) using micromorphology of glaciolacustrine varves in Glen Roy. *Quaternary Science Reviews* 36, 114–123.
- Palmer, J., Lorrey, A., Turney, C.S.M., et al. 2006. Extension of New Zealand kauri (*Agathis australis*) tree-ring chronologies into Oxygen Isotope Stage (OIS) 3. *Journal of Quaternary Science* 21, 779–787.
- PALSEA (PALEo SEA Level Working Group). 2010. The sea-level conundrum: case studies from palaeo-archives. *Journal of Quaternary Science* 25, 19–25.
- Pan, B., Burbank, D., Wang, Y., et al. 2003. A 900 k.y. record of strath terrace formation during glacial–interglacial transitions in northwest China. *Geology* 31, 957–960.
- Panagiotakopulu, E., Greenwood, M.T., Buckland, P.C. 2012. Insect fossils and irrigation in medieval Greenland. *Geografiska Annaler Series A, Physical Geography* 94, 531–548.
- Pancost, R.D., McClymont, L., Bingham, E.M., et al. 2011. Archaeol as a methanogen biomarker in ombrotrophic bogs. *Organic Geochemistry* 42, 1279–1287.
- Panieri, G., Camerlenghi, A., Cacho, I., et al. 2012. Tracing seafloor methane emissions with benthic foraminifera: results from the Ana submarine landslide (Eivissa Channel, Western Mediterranean Sea). *Marine Geology* 291/294, 97–112.
- Panyushkina, I., Sljusarenko, I., Bikov, N., et al. 2007. Floating larch tree-ring chronologies from archaeological timbers in the Russian Altai between about 800 BC and AD 800. *Radiocarbon* 49, 693–702.
- Parfitt, S.A., Barendregt, R.W., Breda, M., et al. 2005. The earliest record of human activity in northern Europe. *Nature* 438, 1008–1012.
- Parham, P.R., Riggs, S.R., Culver, S.J., et al. 2007. Quaternary depositional patterns and sea-level fluctuations, northeastern North Carolina. *Quaternary Research* 67, 83–99.
- Parker, A.G., Goudie, A.S., Anderson, D.E., et al. 2002. A review of the mid-Holocene elm decline in the British Isles. *Progress in Physical Geography* 26, 1–45.
- Parmalee, P.W. 2005. Ice Age cave faunas of North America. *Gearchaeology* 20, 331–334.
- Parmesan, C. 1999. Coping with modern times? Insect movement and climate change. In *Insect Movement: Mechanisms and Consequences* (edited by I.P. Woiwod, D.R. Reynolds, C.D. Thomas). CABI Publishing, Oxford and New York, 387–414.
- Parrenin, F., Barnola, J.M., Beer, J., et al. 2007. The ED3 chronology for the EPICA Dome C ice core. *Climate of the Past* 3, 485–497.
- Parrenin F., Petit J.-R., Masson-Delmotte V., et al. 2012. Volcanic synchronisation between the EPICA Dome C and Vostok ice cores (Antarctica) 0–145 kyr BP. *Climate of the Past* 8, 1031–1045.
- Paterson, W.S.B. 1994. *The Physics of Glaciers*, 3rd edn. Elsevier, Amsterdam.
- Patterson, R.T., Kumar, A. 2002. A review of current testate rhizopod (thecamoebian) research in Canada. *Palaeogeography, Palaeoclimatology, Palaeoecology* 180, 225–251.
- Patterson, W.P., Dietrich, K.A., Holmden, C., et al. 2010. Two millennia of North Atlantic seasonality and implications for Norse colonies. *Proceedings of the National Academy of Sciences of the United States of America* 107, 5306–5310.
- Pauslen, D.E., Li, H.-C., Ku, T.-L. 2003. Climate variability in central China over the last 1270 years revealed by high-resolution stalagmite records. *Quaternary Science Reviews* 22, 691–701.
- Pawley, S.M., Rose, J., Lee, J.R., et al. 2004. Middle Pleistocene sedimentology and lithostratigraphy of Weybourne, northeast Norfolk, England. *Proceedings of the Geologists' Association* 115, 25–42.
- Pawley, S.M., Toms, P., Armitage, S.J., et al. 2010. Quartz luminescence dating of Anglian Stage (MIS12) fluvial sediments: comparison of SAR age estimates to the terrace chronology of the Middle Thames Valley, UK. *Quaternary Geochronology* 5, 569–582.
- Payne, A.J. 1999. A thermomechanical model of ice flow in West Antarctica. *Climate Dynamics* 15, 115–125.
- Payne, R.J., Blackford, J.J. 2008. Peat humification and climate change: a multi-site comparison from mires in south-east Alaska. *Mires and Peat* 3(art. 9), 1–11.
- Pazzaglia, F.J., Brandon, M.T. 2001. A fluvial record of long-term steady-state uplift and erosion across the Cascadia Forearc High, Western Washington State. *American Journal of Science* 301, 385–431.
- Peacock, J.D. 1993. Late Quaternary marine mollusca as palaeoenvironmental proxies: a compilation and assessment of basic numerical data for NE Atlantic species found in shallow water. *Quaternary Science Reviews* 12, 263–275.
- Pearce, N.J.G., Westgate, J.A., Preece, S.J., et al. 2004. Identification of Aniakchak (Alaska) tephra in Greenland ice core challenges the 1645 BC date for Minoan eruption of Santorini. *Geochemistry, Geophysics, Geosystems* 5, doi: 10.1029/2003GC000672.
- Pearson, P.N. 2012. Oxygen isotopes in Foraminifera: overview and historical review. In *Reconstructing Earth's Deep-Time Climate – The State of the Art in 2012* (edited by L.C. Ivany, B.T. Huber). The Palaeontological Society Special Papers 18. The Paleontological Society, London, 1–38.
- Pedoja, K., Regard, V., Husson, L., et al. 2011. Uplift of Quaternary shorelines in eastern Patagonia: Darwin revisited. *Geomorphology* 127, 121–142.
- Pedro, J.B., van Ommen, T.D., Rasmussen, S.O., et al. 2011. The last deglaciation: timing the bipolar seesaw. *Climate of the Past* 7, 671–683.
- Peeters, F.J.C., Acheson, R., Brummer, G.-J.A., et al. 2004. Vigorous exchange between the Indian and Atlantic oceans at the end of the past five glacial periods. *Nature* 430, 661–665.
- Peglar, S.M. 1993. The mid-Holocene *Ulmus* decline at Diss, Norfolk, UK: a year-by-year pollen stratigraphy from annual laminations. *The Holocene* 3, 1–13.
- Peglar, S.M., Birks, H.J.B. 1993. The mid-Holocene *Ulmus* fall at Diss Mere, south-east England – disease and human impact? *Vegetational History and Archaeobotany* 2, 61–68.
- Peltier, W.R. 2002. Global glacial isostatic adjustment: palaeogeodetic and space-geodetic tests of the ICE-4G (VM2) model. *Journal of Quaternary Science* 17, 491–510.

- Peltier, W.R. 2005. On the hemispheric origins of meltwater pulse 1a. *Quaternary Science Reviews* 24, 1655–1671.
- Peltier, W.R., Fairbanks, R.G. 2006. Global glacial ice volume and Last Glacial Maximum duration from an extended Barbados sea level record. *Quaternary Science Reviews* 25, 3322–3337.
- Pelto, M.S., Hedlund, C. 2001. Terminus behavior and response time of North Cascade glaciers, Washington, USA. *Journal of Glaciology* 47, 497–506.
- Peña-Chocarro, L., Zopata, L., Iriarte, M.J., et al. 2005. The oldest agriculture in northern Atlantic Spain: new evidence from El Mirón Cave (Ramales de la Victoria, Cantabria). *Journal of Archaeological Science* 32, 579–587.
- Penkman, K.E.H. 2010. Amino acid geochronology: its impact on our understanding of the Quaternary stratigraphy of the British Isles. *Journal of Quaternary Science* 25, 501–514.
- Penkman, K.E.H., Preece, R.C., Keen, D.H. et al. 2007. Testing the aminostratigraphy of fluvial archives: the evidence from intra-crystalline proteins within freshwater shells. *Quaternary Science Reviews* 26, 2958–2969.
- Penkman, K.E.H., Kaufman, D.S., Maddy, D., et al. 2008. Closed-system behaviour of the intra-crystalline fraction of amino acids in mollusc shells. *Quaternary Geochronology* 3, 2–25.
- Penkman, K.E.H., Preece, R.C., Bridgland, D.R., et al. 2013. An aminostratigraphy for the British Quaternary based on *Bithynia opercula*. *Quaternary Science Reviews* 61, 111–134.
- Pennington, W., Haworth, E.Y., Bonny, A.P., et al. 1972. Lake sediments in northern Scotland. *Philosophical Transactions of the Royal Society of London B* 264, 191–294.
- Pentecost A. 2005. *Travertine*. Springer, Berlin.
- Perez, K.E., Cordeiro, J.R., Coppolino, L. 2008. *A Guide for Terrestrial Gastropod Identification*. American Malacological Society, Carnondale, IL.
- Perner, K., Moros, M., Lloyd, J.M., et al. 2011. Centennial scale benthic foraminiferal record of late Holocene oceanographic variability in Disko Bugt, West Greenland. *Quaternary Science Reviews* 30, 2815–2826.
- Pessenda, L.R.C., Gouveia, S.E.M., Aravena, R. 2001. Radiocarbon dating of total soil organic matter and humin fractions and its comparison with ^{14}C ages of fossil charcoal. *Radiocarbon* 43, 595–601.
- Peteet, D. 1995. A global Younger Dryas? *Quaternary International* 28, 93–104.
- Peterson, L.C., Haug, G.H., Hughen, K.A., et al. 2000. Rapid changes in the hydrologic cycle of the Tropical Atlantic during the Last Glacial. *Science* 290, 1947–1951.
- Petit, J.R., Jouzel, J., Raynaud, D., et al. 1999. 420,000 years of climate and atmospheric history revealed by the Vostok deep Antarctic ice core. *Nature* 399, 429–436.
- Petoukhov, V., Claussen, M., Berger, A., et al. 2005. EMIC Inter-comparison Project (EMIP-CO₂): comparative analysis of EMIC simulations of climate, and of equilibrium and transient responses to atmospheric CO₂ doubling. *Climate Dynamics* 25, 363–385.
- Petruglia, M., Korisettar, R., Boivin, N., et al. 2007. Middle Palaeolithic assemblages from the Indian subcontinent before and after the Toba super-eruption. *Science* 317, 114–116.
- Petsko, G.A., Ringe, D. 2004. *Protein Structure and Function*. New Science Press, London.
- Pettersson, G. 1996. Varved sediments in Sweden: a brief review. In *Palaeoclimatology and Palaeoceanography from Laminated Sediments* (edited by A.E.S. Kemp). Geological Society, London, 73–77.
- Péwé, T.L. 1966. Palaeoclimatic significance of fossil ice wedges. *Bulletyn Peryglacjalny* 15, 65–73.
- Pflaumann, U., Duprat, J., Pujol, C., et al. 1996. SIMMAX: A modern analog technique to deduce Atlantic sea surface temperatures from planktonic foraminifera in deep-sea sediments. *Paleoceanography* 11, 15–35.
- Phillips, E., Lee, J.R., Burke, H. 2008a. Progressive proglacial to sub-glacial deformation and syntectonic sedimentation at the margins of the Mid-Pleistocene British Ice Sheet: evidence from north Norfolk, UK. *Quaternary Science Reviews* 27, 1848–1871.
- Phillips, T.J., Potter, G.L., Williamson, D.L., et al. 2004. Evaluating parameterizations in General Circulation Models: climate simulation meets weather prediction. *Bulletin of the American Meteorological Society* 85, 1903–1915.
- Phillips, W.M., Hall, A.R., Mottram, R., et al. 2006. Cosmogenic ^{10}Be and ^{26}Al exposure ages of tors and erratics, Cairngorm Mountains, Scotland: timescales for the development of a classic landscape of selective glacial erosion. *Geomorphology* 73, 222–245.
- Phillips, W.M., Hall, A.M., Ballantyne, C.K., et al. 2008b. Extent of the last ice sheet in northern Scotland tested with cosmogenic ^{10}Be exposure ages. *Journal of Quaternary Science* 23, 101–108.
- Pickering, R., Jacobs, Z., Herries, A.I.R., et al. 2013. Palaeo-anthropologically significant South African sea caves dated to 1.1–1.0 million years using a combination of U–Pb, TT-OLS and palaeomagnetism. *Quaternary Science Reviews* 65, 39–52.
- Pierce, K.L. 2003. Pleistocene glaciations of the Rocky Mountains. In *Developments in Quaternary Science. Volume 1: The Quaternary Period in the United States* (edited by A.R. Gillespie, S.C. Porter, B.F. Atwater). Elsevier, Amsterdam, 63–76.
- Pierce, K.L., Obradovich, J.D., Friedman, I. 1976. Obsidian hydration dating and correlation of Bull Lake and Pinedale Glaciations near west Yellowstone, Montana. *Geological Society of America Bulletin* 87, 703–710.
- Pike A.W.G., Pettitt, P.B. 2003. U-series dating and human evolution. In *Uranium Series Geochemistry* (edited by B. Bourdon, G.M. Henderson, C.C. Lundstrom, et al.). *Reviews in Mineralogy and Geochemistry* 52, 607–630.
- Pike, A.W.G., Hedges, R.E.M., van Calsteren, P. 2002. U-series dating of bone using the diffusion-absorption model. *Geochimica et Cosmochimica Acta* 66, 4273–4286.
- Pike, A.W.G., Hoffmann, D.L., García-Diez, M., et al. 2012. U-series dating of Palaeolithic art in 11 caves in Spain. *Science* 336, 1409–1413.
- Pike, J., Stickley, C.E. 2007. Diatom records: marine laminated sediments. In *Encyclopedia of Quaternary Science* (edited by S.A. Elias). Elsevier, Amsterdam, 557–566.
- Pike, R.J. 2000. Geomorphometry – diversity in quantitative surface analysis. *Progress in Physical Geography* 24, 1–20.
- Pillans, B. 2004. Defining the Quaternary. *Quaternary Science Reviews* 23, 2271–2282.

500 REFERENCES

- Pillans, B., Gibbard, P.L. 2012. The Quaternary Period. In *The Geologic Time Scale 2012* (edited by F. Gradstein, J. Ogg, M. Schmitz, et al.). Elsevier, Amsterdam, 980–1009.
- Pillans, B.J., Alloway, B.V., Naish, T.R., et al. 2005. Silicic tephras in Pleistocene sediments of Wanganui Basin, New Zealand. *Journal of the Royal Society of New Zealand* 35, 43–90.
- Pint, A., Frenzel, P., Fuhrmann, R., et al. 2012. Distribution of *Cyprideis torosa* (Ostracoda) in Quaternary athalassic sediments in Germany and its application for palaeoecological reconstructions. *International Review of Hydrobiolgy* 97, 330–355.
- Pinter, N., Scott, A.C., Daulton, T.L. et al. 2011. The Younger Dryas impact hypothesis: a requiem. *Earth-Science Reviews* 106, 247–264.
- Piotrowski, J.A., Larsen, N.K., Junge, F.W. 2004. Reflections on soft subglacial beds as a mosaic of deforming and stable spots. *Quaternary Science Reviews* 23, 993–1000.
- Piro, S., Campana, S. 2012. GPR investigations in different archaeological sites in Tuscany (Italy). Analysis and comparison of the obtained results. *Near Surface Geophysics* 10, 47–56.
- Pisaric, M.F.J. 2002. Long-distance transport of terrestrial plant material by convection resulting from forest fires. *Journal of Paleolimnology* 28, 349–354.
- Pissart, A. 2001. Remnants of lithalsas of the Hautes Fagnes, Belgium: a summary of present-day knowledge. *Permafrost and Periglacial Processes* 11, 327–355.
- Pissart, A. 2002. Palsas, lithalsas and remnants of these periglacial mounds: a progress report. *Progress in Physical Geography* 26, 605–621.
- Pla, S., Anderson, N.J. 2005. Environmental factors correlated with chrysophyte cyst assemblages in low Arctic lakes of Southwest Greenland. *Journal of Phycology* 41, 957–974.
- Pla-Rabes, S., Catalan, J. 2011. Deciphering chrysophyte responses to climate seasonality. *Journal of Paleolimnology* 46, 139–150.
- Plag, H.-P., Engen, B., Clark, T.A., et al. 1998. Post-glacial rebound and present-day three-dimensional deformations. *Journal of Geodynamics* 25, 263–301.
- Plagnes, V., Causse, C., Genty, D., et al. 2002. A discontinuous climatic record from 187 to 74 ka from a speleothem of the Clamouse Cave (south of France). *Earth and Planetary Science Letters* 201, 87–103.
- Plug L.J., Twerner B.P. 2008. Modelling ice-wedge networks. *Permafrost and Periglacial Processes* 19, 63–69.
- Plunkett, G.M., Whitehouse, N.J., Hall, V.A., et al. 2004. A precisely-dated lake-level rise marked by diatomite formation in northeastern Ireland. *Journal of Quaternary Science* 19, 3–7.
- Poli, M.S., Thunnell, R.C., Rio, D. 2000. Millennial-scale changes in North Atlantic Deep Water circulation during marine isotope stages 11 and 12: linkage to Antarctic climate. *Geology* 28, 807–810.
- Pollack, H.N., Huang, S., Smerdon, J.E. 2006. Five centuries of climate change in Australia: the view from underground. *Journal of Quaternary Science* 21, 701–706.
- Pollard, A.M., Heron, C. 1996. *Archaeological Chemistry*. Royal Society of Chemistry, Cambridge.
- Pollard, A.M., Blockley, S.P.E., Ward, K.R. 2003. Chemical alteration of tephra in the depositional environment: theoretical stability modelling. *Journal of Quaternary Science* 18, 385–394.
- Pollard, A.M., Blockley, S.P.E., Lane, C.S. 2006. Some numerical considerations in the geochemical analysis of distal microtephra. *Applied Geochemistry* 21, 1692–1714.
- Pollard, D., DeConto, R.M. 2009. Modelling West Antarctic ice sheet growth and collapse through the past five million years. *Nature* 458, 329–332.
- Polly, P.D., Eronen, J.T. 2011. Mammal associations in the Pleistocene of Britain: implications of Ecological Niche Modelling and a method for reconstructing palaeoclimate. In *The Ancient Human Occupation of Britain* (edited by N. Ashton, S.G. Lewis, C. Stringer). Elsevier, Amsterdam, 279–304.
- Posel, P., Coope, G.R., Antoine, P., et al. 2005. Lateglacial palaeoenvironments and palaeoclimates from Cont and Houdancourt, northern France, reconstructed from beetle remains. *Quaternary Science Reviews* 24, 2449–2465.
- Poole, G.C., Stanford, J.A., Frissell, C.A., et al. 2002. Three-dimensional mapping of geomorphological controls on floodplain hydrology and connectivity from aerial photos. *Geomorphology* 48, 329–347.
- Popov, D., Vandenberghe, D.A., Marković, V.C. 2012. Luminescence dating of fluvial deposits in Vojvodina, N. Serbia: first results. *Quaternary Geochronology* 13, 42–51.
- Porch, N. 2010. Climate space, bioclimatic envelopes and coexistence methods for the reconstruction of past climates: a method using Australian beetles and significance for Quaternary reconstruction. *Quaternary Science Reviews* 29, 633–647.
- Porinchu, D.F., MacDonald, G.M. 2003. The use and application of freshwater midges (Chironomidae: Insecta: Diptera) in geographical research. *Progress in Physical Geography* 27, 378–422.
- Porinchu, D.F., Rolland, N., Moser, K. 2009. Development of a chironomid-based air temperature inference model for the central Canadian Arctic. *Journal of Paleolimnology* 41, 349–368.
- Porter, S.C. 2000. Snowline depression in the tropics during the Last Glaciation. *Quaternary Science Reviews* 20, 1067–1091.
- Porter, S.C. 2001. Chinese loess record of monsoon climate during the last glacial–interglacial cycle. *Earth-Science Reviews* 54, 115–128.
- Porter, S.C., Singhvi, A., Zhishng, A., et al. 2001. Luminescence age and palaeoenvironmental implications of a late Pleistocene ground wedge on the Northeastern Tibetan Plateau. *Permafrost and Periglacial Processes* 12, 203–210.
- Potter, E.-K., Lambeck, K. 2003. Reconciliation of sea-level observations in the Western North Atlantic during the last glacial cycle. *Earth and Planetary Science Letters* 217, 171–181.
- Povinec, P.P., Litherland, A.E., von Reden, K.F. 2009. Developments in radiocarbon technologies: from the Libby Counter to compound-specific AMS analyses. *Radiocarbon* 51, 45–78.
- Powell, E.N., Staff, G.M., Callender, W.R., et al. 2011. The influence of molluscan taxon on taphofacies development over a broad range of environments of preservation: the SSETI experience. *Palaeogeography, Palaeoclimatology, Palaeoecology* 312, 233–264.
- Power, S., Delage, F., Chung, C., et al. 2013. Robust twenty-first century projections of El Niño and related precipitation variability. *Nature* doi: org/10.1038/nature12580.

- Praetorius, S.K., McManus, J.F., Oppo, D.W., *et al.* 2008. Episodic reductions in bottom-water currents since the last ice age. *Nature Geoscience* 1, 449–452.
- Prasad, S., Negendank, J.F.W., Stein, M. 2009. Varve counting reveals high resolution radiocarbon reservoir variations in palaeolake Lisan. *Journal of Quaternary Science* 24, 690–696.
- Preece, R.C. 2001. Molluscan evidence for differentiation of interglacials within the ‘Cromerian Complex’. *Quaternary Science Reviews* 20, 1643–1656.
- Preece, R.C., Bridgland, D.R. 1999. Holywell Coombe, Folkestone: a 13,000 year history of an English chalkland valley. *Quaternary Science Reviews* 18, 1075–1125.
- Preece, R.C., Parfitt, S.A. 2012. The Early and middle Pleistocene context of human occupation and lowland glaciation in Britain and northern Europe. *Quaternary International* 271, 6–28.
- Preece, R.C., Gowlett, J.A.J., Parfitt, S.A., *et al.* 2006. Humans in the Hoxnian: habitat, context and fire use at Beeches Pit, West Stow, Suffolk, UK. *Journal of Quaternary Science* 21, 485–496.
- Preece, R.C., Parfitt, S.A., Coope, G.R., *et al.* 2009. Biostratigraphic and aminostratigraphic constraints on the age of the Middle Pleistocene glacial succession in north Norfolk, UK. *Journal of Quaternary Science* 24, 557–580.
- Prentice, I.C., Farquhar, G.D., Fasham, M.J.R., *et al.* 2001. The carbon cycle and atmospheric carbon dioxide. In *Climate Change 2001: The Scientific Basis* (edited by J.T. Houghton, Y. Ding, D.J. Griggs, *et al.*). Cambridge University Press, Cambridge, 185–235.
- Previsic, A., Walton, C., Kucinic, M., *et al.* 2009. Pleistocene divergence of Dinaric *Drusus* endemics (Tricoptera, Limnephilidae) in multiple microrefugia within the Balkan Peninsula. *Molecular Ecology* 18, 634–647.
- Prevosti, F.J., Tonni, E.P., Bidegain, J.C. 2009. Stratigraphic range of the large canids (Carnivora, Canidae) in South America and its relevance to quaternary biostratigraphy. *Quaternary International* 210, 76–81.
- Price, G.J., Webb, G.E. 2006. Late Pleistocene sedimentology, taphonomy and megafauna extinction on the Darling Downs, southeastern Queensland. *Australian Journal of Earth Sciences* 53, 947–970.
- Prichard, S.J., Gedalof, Z., Oswald, W.W., *et al.* 2009. Holocene fire and vegetation dynamics in a montane forest, North Cascade Range, Washington, USA. *Quaternary Research* 72, 57–67.
- Prinn, R.G. 2011. Development and application of earth system models. *Proceedings of the National Academy of Sciences of the United States of America* 110, 3673–3680.
- Prinn, R., Paltsev, S., Sokolov, A., *et al.* 2011. Scenarios with MIT integrated global systems model: significant global warming regardless of different approaches. *Climatic Change* 104, 515–537.
- Prokopenko, A.A., Hinnov, L.A., Williams, D.F., *et al.* 2006. Orbital forcing of continental climate during the Pleistocene: a complete astronomically tuned climatic record from Lake Baikal, SE Siberia. *Quaternary Science Reviews* 25, 3431–3457.
- Pross, J., Klotz, S., Mosbrugger, V. 2000. Reconstructing palaeotemperatures for the Early and Middle Pleistocene using the mutual climatic range method based on plant fossils. *Quaternary Science Reviews* 19, 1785–1799.
- Pruher, L.M., Rea, D.K. 1998. Rapid onset of glacial conditions in the subarctic North Pacific region at 2.67 Ma: clues to causality. *Geology* 26, 1027–1030.
- Pudsey, C.J., Murray, J.W., Appleby, P., *et al.* 2006. Ice shelf history from petrographic and foraminiferal evidence, Northeast Antarctic Peninsula. *Quaternary Science Reviews* 25, 2357–2379.
- Pugh, R.S., McCave, I.N., Hillebrand, C.-D., *et al.* 2009. Circum-Antarctic age modelling of Quaternary marine cores under the Antarctic Circumpolar Current: ice-core dust–magnetic correlation. *Earth and Planetary Science Letters* 284, 113–123.
- Punt, W., Blackmore, S., Hoen, P.P., *et al.* 2009. *The Northwest European Pollen Flora IX*. Elsevier, Amsterdam.
- Puthusserry, J.T., Murray, A.S., Kjaer, K.H., *et al.* 2008. Optically stimulated luminescence (OSL) dating of glacial sediments from Arctic Russia – depositional bleaching and methodological aspects. *Boreas* 35, 587–599.
- Putkonen, J., Swanson, T. 2003. Accuracy of cosmogenic ages for moraines. *Quaternary Research* 59, 255–261.
- Putnam, A.E., Denton, G.H., Schaefer, J.M., *et al.* 2010. Glacier advance in southern middle-latitudes during the Antarctic Cold Reversal. *Nature Geoscience* 3, 700–704.
- Pyle, D.M., Ricett, G.M., Margari, V., *et al.* 2006. Wide dispersal and deposition of distal tephra during the Pleistocene ‘Campanian Ignimbrite/Y5’ eruption, Italy. *Quaternary Science Reviews* 25, 2713–2728.
- Qin, B., Harrison, S.P., Kutzbach, J.E. 1998. Evaluation of modelled regional water balance using lake status data: a comparison of 6 ka simulations with the NCAR CCM. *Quaternary Science Reviews* 17, 659–668.
- Quigley, M.C., Horton, T., Helstrom, J.C., *et al.* 2010. Holocene climate change in arid Australia from speleothem and alluvial records. *The Holocene* 20, 1093–1104.
- Rabassa, J., Ponce, J.F. 2013. The Heinrich and Dansgaard–Oeschger climatic events during Marine Isotope Stage 3: searching for appropriate times for human colonisation of the Americas. *Quaternary International* 299, 94–105.
- Radtke, U., Schellman, G., Scheffers, A., *et al.* 2003. Electron spin resonance and radiocarbon dating of coral deposited by Holocene tsunami events on Curaçao, Bonaire and Aruba (Netherlands Antilles). *Quaternary Science Reviews* 22, 1309–1315.
- Rahmstorf, S. 1996. On the freshwater forcing and transport of the Atlantic thermohaline circulation. *Climate Dynamics* 12, 799–811.
- Rahmstorf, S. 2002. Ocean circulation and climate during the past 120,000 years. *Nature* 419, 207–214.
- Rahmstorf, S. 2003. Timing of abrupt climate change: a precise clock. *Geophysical Research Letters* 30, 1510, doi: 10.1029/2003GL017115.
- Rahmstorf, S., Crisifix, M., Ganopolski, A., *et al.* 2005. Thermohaline circulation hysteresis: A model intercomparison. *Geophysical Research Letters* 32, L23605, doi: 10.1029/2005GL023655.
- Raia, P., Meiri, S. 2006. The Island Rule in large mammals: paleontology meets ecology. *Evolution* 60, 1731–1742.
- Rainio, H., Saarnisto, M., Ekman, I. 1995. Younger Dryas end moraines in Finland and NW Russia. *Quaternary International* 28, 179–192.

502 REFERENCES

- Raisbeck, G.M., Yiou, F., Jouzel, J., et al. 2007. Direct North–South synchronisation of abrupt climate change record in ice cores using beryllium 10. *Climate of the Past Discussions* 3, 541–547.
- Ram, M., Donarummo, J., Stoltz, M.R., et al. 2012. Calibration of laser-light scattering measurements of dust concentration for Wisconsinan GISP2 ice using instrumental neutron activation analysis of aluminium: results and discussions. *Journal of Geophysical Research Atmospheres* 105, 24731–24738.
- Ramillien, G., Lombard, A., Cazenave, A., et al. 2006. Interannual variations of the mass balance of the Antarctica and Greenland ice sheets from GRACE. *Global and Planetary Change* 53, 198–208.
- Rampino, M.R., Self, S., Fairbridge, R.W. 1979. Can rapid climate change cause volcanic eruptions? *Science* 206, 826–829.
- Ran, Y., Li, X., Cheng, G., et al. 2012. Distribution of permafrost in China: an overview of existing permafrost maps. *Permafrost and Periglacial Processes* 23, 322–333.
- Randall, D.A., Wood, R.A., Bony, S., et al. 2007. Climate models and their evaluation. In *Climate Change 2007: Working Group I: The Physical Science Basis* (edited by S. Solomon, D. Qin, M. Manning, et al.). Cambridge University Press, Cambridge, 591–662.
- Rankin, A.M., Wolff, E.W., Mulvaney, R. 2004. A reinterpretation of sea-salt records in Greenland and Antarctic ice cores. *Annals of Glaciology* 39, 276–282.
- Räsenen, M.E., Auri, J.M., Huiti, J.V., et al. 2009. A shift from lithostratigraphic to allostratigraphic classification of Quaternary glacial deposits. *GSA Today* 19, 4–11.
- Rasmussen, S.O., Andersen, K.K., Johnsen, S.J., et al. 2005. Deconvolution-based resolution enhancement of chemical ice core records obtained by continuous flow analysis. *Journal of Geophysical Research* doi: 10.1029/2004JD005717.
- Rasmussen S.O., Andersen K.K., Svensson A.M., et al. 2006. A new Greenland ice core chronology for the last glacial termination. *Journal of Geophysical Research*, 111:D06102, doi: 10.1029/2005JD006079.
- Rasmussen, S.O., Vinther, B., Clausen, H.B., et al. 2007. Early Holocene climate oscillations recorded in three Greenland ice cores. *Quaternary Science Reviews* 26, 1907–1914.
- Rasmussen, S.O., Seierstad, I.K., Andersen, K.K., et al. 2008. Synchronisation of the NGRIP, GRIP and GISP2 ice cores across MIS 2 and palaeoclimatic implications. *Quaternary Science Reviews* 27, 18–28.
- Rasmussen, T.L., Thomsen, E. 2004. The role of the North Atlantic Drift in the millennial timescale glacial climate fluctuations. *Palaeogeography, Palaeoclimatology, Palaeoecology* 210, 101–116.
- Rathore, V.S., Nathawat, M.S., Champatiray, P.K. 2010. Palaeochannel detection and aquifer performance assessment in Menda River catchment, Western India. *Journal of Hydrology* 395, 216–225.
- Rawson, P.F., Allen, P.M., Brenchley, P.J., et al. 2002. *Stratigraphical Procedure* ('Professional Handbook' Series). Geological Society, Bath.
- Rayburn, J.A., Cronin, T.M., Franz, D.A., et al. 2011. Timing and duration of North American glacial lake discharges and the Younger Dryas climate reversal. *Quaternary Research* 75, 541–551.
- Raymo, M.E. 1997. The timing of major climatic terminations. *Paleoceanography* 12, 577–585.
- Raymo, M.E., Ruddiman, W.F. 1992. Tectonic forcing of late Cenozoic climate. *Nature* 359, 117–122.
- Raymo, M., Nisancioğlu, K. 2003. The 41 kyr world: Milankovitch's other unsolved mystery. *Paleoceanography* 18, doi: 10.1029/2002PA000791.
- Raymo, M., Ruddiman, Froelich, P.M. 1992. Influence of late Cenozoic mountain building on ocean geochemical cycles. *Geology* 16, 649–653.
- Raymo, M.E., Mitrovica, J.X., O'Leary, R.M., et al. 2011. Departures from eustasy in Pliocene sea-level records. *Nature Geoscience* 4, 328–332.
- Rayner, D., Hirschi, J.J.-M., Kanzow, T., et al. 2011. Monitoring the Atlantic meridional overturning circulation. *Deep-Sea Research II* 58, 1744–1753.
- Rea, B.R. 2009. Defining modern day Area-Altitude Balance ratios (AABRs) and their use in glacier-climate reconstructions. *Quaternary Science Reviews* 28, 237–248.
- Rea, D.K., Snoek, H., Joseph, L.H. 1998. Late Cenozoic eolian deposition in the North Pacific: Asian drying, Tibetan uplift, and cooling of the Northern Hemisphere. *Paleoceanography* 13, 215–224.
- Reeves, J.M., Chivas, A.R., Garcia, A., et al. 2007. Palaeoenvironmental change in the Gulf of Carpentaria (Australia) since the last interglacial based on Ostracoda. *Palaeogeography, Palaeoclimatology, Palaeoecology* 246, 163–187.
- Refsnider, K.A., Brugger, K.A. 2007. Rock glaciers in Central Colorado, U.S.A., as indicators of Holocene climate change. *Arctic, Antarctic, and Alpine Research* 39, 127–136.
- Refsnider, K.A., Laabs, B.J.C., Plummer, M.A., et al. 2008. Last glacial maximum climate inferences from cosmogenic dating and glacier modeling of the western Uinta ice field, Uinta Mountains, Utah. *Quaternary Research* 69, 130–144.
- Refsnider, K.A., Brugger, K.A., Leonard, E.M., et al. 2009. Last Glacial Maximum equilibrium-line altitude trends and precipitation patterns in the Sangre de Cristo Mountains, southern Colorado, USA. *Boreas* 38, 663–678.
- Reichert, K.L., Licciardi, J.M., Kaudfman, D.S. 2011. Amino acid racemization in lacustrine ostracodes, Part II: paleothermometry in Pleistocene sediments at Summer Lake, Oregon. *Quaternary Geochronology* 6, 174–185.
- Reille, M. 1995. *Pollen et Spores d'Europe et d'Afrique du Nord*. Supplement 1. Laboratoire de Botanique Historique et de Palynologie, Université d'Aix-Marseille.
- Reille, M., de Beaulieu, J.-L., Svobodova, H., et al. 2000. Pollen analytical biostratigraphy of the last five climatic cycles from a long continental sequence from the Velay region (Massif Central, France). *Journal of Quaternary Science* 15, 665–685.
- Reimer, P.J., Reimer, R.W. 2001. A marine reservoir correction database and on-line interface. *Radiocarbon* 43, 461–463.
- Reimer, P.J., Bard, E., Bayliss, A., et al. 2013. IntCal13 and Marine13 radiocarbon age calibration curves 0–50,000 years cal BP. *Radiocarbon* 55, 1869–1887.
- Reiss, R.A. 2006. Ancient DNA from ice age insects: proceed with caution. *Quaternary Science Reviews* 25, 1877–1893.

- Rember, W.C., Erdman, T.W., Hoffman, M.L., et al. 1993. Dating of mine waste in lacustrine sediments using cesium-137. *Environmental Earth Sciences* 22, 242–245.
- Rémy, F., Parouty, S. 2009. Antarctic ice sheet and radar altimetry: a review. *Remote Sensing* 1, 1212–1239.
- Renberg, I., Braånvall, M.-L., Bindler, R., et al. 2002. Stable lead isotopes and lake sediments – a useful combination for the study of atmospheric lead pollution history. *The Science of the Total Environment* 292, 45–54.
- Renberg, I., Bigler, C., Bindler, R., et al. 2009. Environmental history: a piece in the puzzle for establishing plans for environmental management. *Journal of Environmental Management* 90, 2794–2800.
- Renfrew, C. 1973. *Before Civilisation: The Radiocarbon Revolution and Prehistoric Europe*. Jonathan Cape, London.
- Renne, P.R., Sharp, W.D., Deino, A.L., et al. 1997. $^{40}\text{Ar}/^{39}\text{Ar}$ dating into the historical realm: calibration against Pliny the Younger. *Science* 277, 1279–1280.
- Renssen, H., Vandenberghe, J. 2003. Investigation of the relationship between permafrost distribution in NW Europe and extensive winter sea-ice cover in the North Atlantic Ocean during the cold phases of the Last Glaciation. *Quaternary Science Reviews* 22, 209–223.
- Renssen, H., Isarin, R.F.B., Vandenberghe, J. 2002. Thermal gradients in Europe during the last glacial-interglacial transition. *Geologie en Mijnbouw (Netherlands Journal of Geosciences)* 81, 113–122.
- Renssen, H., Goosse, H., Fichefet, T., et al. 2005. Holocene climate evolution in the high-latitude Southern Hemisphere simulated by a coupled atmosphere–sea ice–ocean–vegetation model. *The Holocene* 15, 951–964.
- Renssen, H., Kasse, K., Vandenbergh, J., et al. 2007a. Weichselian Late Pleniglacial surface winds over northwest and central Europe: a model-data comparison. *Journal of Quaternary Science* 22, 281–293.
- Renssen, H., Goose, H., Fichefet, T. 2007b. Simulation of Holocene cooling events in a coupled climate model. *Quaternary Science Reviews* 26, 2019–2029.
- Retallack, G.J. 2001. *Soils of the Past*, 2nd edn. Blackwell, New York.
- Reuther, A.U., Urdea, P., Geoger, C., et al. 2007. Late Pleistocene glacial chronology of the Pietrele Valley, Retezat Mountains, southern Carpathians, constrained by ^{10}Be exposure dating and pedological investigations. *Quaternary International* 164/165, 151–169.
- Reyes, A.V., Wiles, G.C., Smith, D.J., et al. 2006. Expansion of alpine glaciers in Pacific North America in the first millennium AD. *Geology* 34, 57–60.
- Rhodes, R.H., Bertler, N.A.N., Baker, J.A., et al. 2012. Little Ice Age climate and oceanic conditions of the Ross Sea, Antarctica from a coastal ice core record. *Climate of the Past* 8, 1223–1238.
- Rial, J.A. 2012. Synchronization of polar climate variability over the last ice age: in search of simple rules at the heart of climate's complexity. *American Journal of Science* 312, 417–448.
- Rial, J.A., Anacleto, C.A. 2000. Understanding non-linear response of the climate system to orbital forcing. *Quaternary Science Reviews* 19, 1709–172.
- Rial, J.A., Oh, J., Reischmann, E. 2013. Synchronization of the climate system to eccentricity forcing and the 100,000-year problem. *Nature Geoscience* 6, 289–293.
- Ribera, I., Vogler, A.P. 2004. Speciation of Iberian diving beetles in Pleistocene refugia (Coleoptera, Dytiscidae). *Molecular Ecology* 13, 179–193.
- Richards, D.A., Smart, P.L. 1991. Potassium–argon and argon–argon dating. In *Quaternary Dating Methods – A User's Guide* (edited by P.L. Smart, P.D. Frances). Technical Guide 4. Quaternary Research Association, Cambridge, 37–44.
- Richards, D.A., Dorale, J.A. 2003. U-series chronology and environmental applications of speleothems. In *Uranium Series Geochemistry* (edited by B. Bourdon, G.M. Henderson, C.C. Lundstrom, et al.). *Reviews in Mineralogy and Geochemistry* 52, 407–460.
- Richter, D. 2007. Advantages and limitations of thermoluminescence dating of heated flint from Palaeolithic sites. *Geoarchaeology* 22, 671–683.
- Rickaby, R.E.M., Elderfield, H. 2005. Evidence from the high-latitude North Atlantic for variations in Antarctic Intermediate water flow during the last deglaciation. *Geochemistry, Geophysics, Geosystems* 6, Q05001, doi: 10.1029/2004GC000858.
- Ridefelt, H., Boelhouwers, J., Eiken, T. 2009. Measurement of solifluction rates using multi-temporal aerial photography. *Earth Surface Processes and Landforms* 34, 725–737.
- Ridente, D., Trincardi, F. 2002. Eustatic and tectonic control on deposition and lateral variability of Quaternary regressive sequences in the Adriatic basin (Italy). *Marine Geology* 184, 273–293.
- Ridge, J.C., Balco, G., Bayless, R.L. 2012. The new North American Varve Chronology: a precise record of southeastern Laurentide Ice Sheet deglaciation and climate, 18.2–12.5 kyr BP, and correlations with Greenland ice core records. *American Journal of Science* 312, 685–722.
- Ridgwell, A.J. 2002. Dust in the Earth system: the biogeochemical linking of land, air and sea. *Philosophical Transactions of the Royal Society of London A* 360, 2905–2924.
- Ridings, R. 1996. Where in the world does obsidian hydration work? *Antiquity* 61, 136–148.
- Riera, S., López-Sáez, J.A., Julià, R. 2006. Lake responses to historical land use changes in northern Spain: the contribution of non-pollen palynomorphs in a multiproxy study. *Review of Palaeobotany and Palynology* 141, 127–137.
- Rignot, E., Hallet, B., Fountain, A. 2002. Rock glacier surface motion in Beacon Valley, Antarctica, from synthetic-aperture radar interferometry. *Geophysical Research Letters* 29, 1607, doi: 10.1029/2001GL013494.
- Rind, D., Peteet, D., Broecker, W.S., et al. 1986. The impact of cold North Atlantic sea surface temperatures on climate. Implications for the Younger Dryas cooling. *Climate Dynamics* 1, 3–33.
- Ringrose, S., Harris, C., Huntsman-Mapila, P., et al. 2009. Origins of strandline duricrusts around the Makgadikgadi Pans (Botswana Kalahari) as deduced from their chemical and isotope composition. *Sedimentary Geology* 219, 262–279.
- Rink, W.J. 1997. Electron spin resonance (ESR) dating and ESR applications in Quaternary science and archaeometry *Radiation Measurements* 27, 975–1025.

504 REFERENCES

- Rinterknecht, V., Clark, P.U., Raisbeck, G.M., *et al.* 2004. Cosmogenic ^{10}Be dating of the Salpausselkä I Moraine in southwestern Finland. *Quaternary Science Reviews* 23, 2283–2289.
- Rinterknecht, V.R., Marks, L., Piotrowski, J.A., *et al.* 2005. Cosmogenic ^{10}Be ages on the Pomeranian Moraine, Poland. *Boreas* 34, 186–191.
- Rinterknecht, V.R., Clark, P.U., Raisbeck, G.M., *et al.* 2006. The last deglaciation of the southeastern sector of the Scandinavian Ice Sheet. *Science* 311, 1449–1452.
- Rinterknecht, V.R., Pavlovskaya, I.E., Clark, P.U. 2007. Timing of the last deglaciation in Belarus. *Boreas* 36, 307–313.
- Rinterknecht, V., Braucher, R., Böse, M., *et al.* 2012. Late Quaternary ice sheet extents in northeastern Germany inferred from surface exposure dating. *Quaternary Science Reviews* 44, 89–95.
- Rio, D., Sprovieri, R., Castradori, D., *et al.* 1998. The Gelasian Stage (Upper Pliocene): a new unit of the global standard chronostratigraphic scale. *Episodes* 21, 82–87.
- Ritchie, J.C., Cwynar, L.C., Spear, R.W. 1983. Evidence from northwest Canada for an early Holocene Milankovitch thermal maximum. *Nature* 305, 126–228.
- Rixhon, G., Braucher, R., Bourlès, D., *et al.* 2011. Quaternary river incision in NE Ardennes (Belgium) – insights from $^{10}\text{Be}/^{26}\text{Al}$ dating of river terraces. *Quaternary Geochronology* 6, 273–284.
- Robert, C.M. 2009. *Developments in Marine Geology. Volume 3: Global Sedimentology of the Ocean: An Interplay Between Geodynamics and Paleoenvironment*. Elsevier, Oxford.
- Roberts, A.P., Tauxe, L., Heslop D. 2013. Magnetic paleointensity stratigraphy and high-resolution Quaternary geochronology: successes and future challenges. *Quaternary Science Reviews* 61, 1–16.
- Roberts, D.H., Hart, J.K. 2005. The deforming bed characteristics of a stratified till assemblage in north East Anglia, UK: investigating controls on sediment rheology and strain signatures. *Quaternary Science Reviews* 24, 123–140.
- Roberts, H.M., Plater A.J. 2007. Reconstruction of Holocene foreland progradation using optically stimulated luminescence (OSL) dating: an example from Dungeness, UK. *The Holocene* 17, 495–505.
- Roberts, H.M., Muhs, D.R., Wintle, A.G., *et al.* 2003. Unprecedented last-glacial mass accumulation rates determined by luminescence dating of loess from western Nebraska. *Quaternary Research* 59, 411–419.
- Roberts, N., Jones, M.D., Benkaddour, A., *et al.* 2008. Stable isotope records of Late Quaternary climate and hydrology from Mediterranean lakes: the ISOMED synthesis. *Quaternary Science Reviews* 27, 2426–2441.
- Roberts, N.L., Piotrowski, A.M., McManus, J.F., *et al.* 2010. Synchronous deglacial overturning and water mass source changes. *Science* 327, 75–78.
- Robinson C., El-Baz, F., Ozdogan, M., *et al.* 2000. Use of radar data to delineate palaeodrainage flow directions in the Selima Sand Sheet, Eastern Sahara. *Photogrammetric Engineering and Remote Sensing* 66, 645–753.
- Robinson, C.A., El-Baz, F., Al-Saud, T.S.M., *et al.* 2006. Use of radar data to delineate palaeodrainage leading to the Kufra Oasis in the eastern Sahara. *Journal of African Earth Sciences* 44, 229–240.
- Robinson, S.G., Maslin, M.A., McCave, I.N. 1995. Magnetic susceptibility variations in Upper Pleistocene deep-sea sediments on the NE Atlantic: implications for ice-rafting and palaeocirculation at the last glacial maximum. *Paleoceanography* 10, 221–250.
- Robinson, S., Beaudoin, A.B., Froese, D.G., *et al.* 2007. Plant macrofossils associated with an early Holocene beaver dam in interior Alaska. *Arctic* 60, 430–438.
- Robson, J., Sutton, R., Lohmann, K., *et al.* 2012. Causes of the rapid warming of the North Atlantic Ocean in the mid-1990s. *Journal of Climate* 25, 4116–4134.
- Rodbell, D.T. 1990. Soil-age relationships on Late Quaternary moraines, Arrowsmith Range, Southern Alps, New Zealand. *Arctic & Alpine Research* 22, 355–365.
- Rodríguez-Lázaro, J., Ruiz-Muñoz, F. 2012. A general introduction to ostracods: morphology, distribution, fossil record and applications. In *Developments in Quaternary Science. Volume 17: Ostracoda as Proxies for Quaternary Climate Change* (edited by D.J. Horne, J.A. Holmes, J. Rodríguez-Lázaro, *et al.*). Elsevier, Amsterdam, 1–14.
- Roe, G. 2006. In defense of Milankovitch. *Geophysical Research Letters* 33, L24703, doi: 10.1029/2006GL027817.
- Roe, H., van de Plassche, O. 2005. Modern pollen distribution in a Connecticut saltmarsh: implications for studies of sea-level change. *Quaternary Science Reviews* 24, 2030–2049.
- Roe, H.M., Coope, G.R., Devoy, R.J.N., *et al.* 2009. Differentiation of MIS 9 and MIS 11 in the continental record: vegetational, faunal, aminostratigraphic and sea-level evidence from coastal sites in Essex, UK. *Quaternary Science Reviews* 28, 2342–2373.
- Rogalla, U., Andrleit, H. 2005. Precessional forcing of coccolithophore assemblages in the northern Arabian Sea: implications for monsoonal dynamics during the last 200,000 years. *Marine Geology* 217, 31–48.
- Rogers, A.K. 2007. Effective hydration temperature of obsidian: a diffusion theory analysis of time-dependant hydration rates. *Journal of Archaeological Science* 34, 656–665.
- Rogers, R.R., Eberth, D.A., Fiorillo, R. (eds). 2007. *Bonebeds: Genesis, Analysis and Paleobiological Significance*. University of Chicago Press, Chicago.
- Rogerson, M., Bigg, G.R., Rohling, E.J. 2011. Vertical density gradient in the eastern North Atlantic during the last 30,000 years. *Climate Dynamics* 39, 589–598.
- Rogerson, M., Rohling, E.J., Bigg, G.R., *et al.* 2012. Paleoceanography of the Atlantic–Mediterranean exchange: overview and first quantitative assessment of climatic forcing. *Reviews of Geophysics* 50, RG2003, doi: 10.1029/2011RG000376.
- Rohling, E., Pálike, H. 2005. Centennial-scale climate cooling with a sudden cold event around 8,200 years ago. *Nature* 434, 975–979.
- Rohling, E., Marsh, R., Wells, N.C., *et al.* 2004. Similar meltwater contributions to glacial sea level changes from Antarctic and northern ice sheets. *Nature* 430, 1016–1021.
- Rohling, E.J., Grant, K., Hemleben, C., *et al.* 2008. New constraints on the timing of sea-level fluctuations during early to middle

- marine isotope stage 3. *Paleoceanography* 23, PA3219, doi: 10.1029/2008PA001617.
- Rolland, N., Larocque, I. 2007. The efficiency of kerosene flotation for extraction of chironomid head capsules from lake sediments samples. *Journal of Paleolimnology* 37, 565–572.
- Romero, O., Schmieder, F. 2006. Occurrence of thick *Ethmodiscus* oozes associated with a terminal Mid-Pleistocene Transition event in the oligotrophic subtropical South Atlantic. *Palaeogeography, Palaeoclimatology, Palaeoecology* 235, 321–329.
- Romero, O.E., Dupont, L., Wyputta, U., et al. 2003. Temporal variability of fluxes of eolian-transported freshwater diatoms, phytoliths and pollen grains off Cape Blanc as reflection of land–atmosphere–ocean interactions in northwest Africa. *Journal of Geophysical Research* 108, doi: 10.1029/2000JC000375.
- Romero-Viana, L., Kienel, U., Sachse, D. 2012. Lipid biomarker signatures in a hypersaline lake on Isabel Island (Eastern Pacific) as a proxy for past rainfall anomaly (1942–2006 AD). *Palaeogeography, Palaeoclimatology, Palaeoecology* 350–352, 49–61.
- Roos-Barracough, F., van der Knaap, W.O., van Leeuwen, J.F.N., et al. 2004. A Late-glacial and Holocene record of climatic change from a Swiss peat humification profile. *The Holocene* 14, 21–34.
- Rose, J. 1985. The Dimlington Stadial/Dimlington Chronozone: a proposal for naming the main glacial episode of the Late Devensian in Britain. *Boreas* 14, 225–230.
- Rose, J., Boardman, J., Kemp, R.A., et al. 1985. Palaeosols and the interpretation of the British Quaternary stratigraphy. In *Geomorphology and Soils* (edited by K.S. Richards, R.R. Arnett, S. Ellis). George Allen and Unwin, London, 348–375.
- Rose, J., Whiteman, C.A., Allen, P., et al. 1999. The Kesgrave Sands and Gravels: 'preglacial' Quaternary deposits of the River Thames in East Anglia and the Thames valley. *Proceedings of the Geologists' Association* 110, 93–116.
- Rose, J., Lee, J.A., Kemp, R.A., et al. 2000. Palaeoclimate, sedimentation and soil development during the Last Glacial Stage (Devensian), Heathrow Airport, London, UK. *Quaternary Science Reviews* 19, 827–847.
- Rose, J., Moorlock, B.S.P., Hamblin, R.J.O. 2001. Pre-Anglian fluvial and coastal deposits in eastern England: lithostratigraphy and palaeoenvironments. *Quaternary International* 79, 5–22.
- Rose, K.A., Sikes, E.L., Guilderson, T., et al. 2010. Upper-ocean-to-atmosphere radiocarbon offsets imply fast deglacial carbon dioxide release. *Nature* 466, 1093–1097.
- Rosell-Melé, A., McClymont, E.L. 2007. Biomarkers as paleoceanographic proxies. In *Developments in Marine Geology. Volume 1: Proxies in Late Cenozoic Paleoceanography* (edited by C. Hillaire-Marcel, A. de Vernal). Elsevier, Amsterdam, 441–509.
- Rosen, D., Dumayne-Peaty, L. 2001. Human impact on the vegetation of South Wales during late historical times: palynological; and palaeoenvironmental results from Crymlyn Bog NNR, West Glamorgan, Wales, UK. *The Holocene* 11, 11–23.
- Rosendahl, D., Ulm, S., Weisler, M.I. 2007. Using foraminifera to distinguish between natural and cultural shell deposits in coastal eastern Australia. *Journal of Archaeological Science* 34, 1584–1593.
- Ross, M., Campbell, J.E., Parent, M., et al. 2009. Palaeo-ice streams and the subglacial landscape mosaic of the North American mid-continent prairies. *Boreas* 38, 421–439.
- Ross, N., Harris, C., Christiansen, H.H., Brabham, P.J. 2005. Ground penetrating radar investigations of open system pingos, Adventdalen, Svalbard. *Norsk Geografisk Tidsskrift* 59, 129–138.
- Rossignol, J., Moine, O., Rousseau, D.-D. 2004. The Buzzard's Roost and Eustis mollusc sequences: comparison between the paleo-environments of two sites in the Wisconsinan loess of Nebraska, USA. *Boreas* 33, 145–154.
- Rothwell, R.G. 2006. *New Techniques in Sediment Core Analysis*. Geological Society of London, Special Publication 267. Geological Society, London.
- Roucoux, K.H., de Abreu, L., Shackleton, N.J., et al. 2005. The response of NW Iberian vegetation to North Atlantic climate oscillations during the last 65 kyr. *Quaternary Science Reviews* 24, 1637–1653.
- Round, F. E., Crawford, R.M., Mann, D.G. 1990. *The Diatoms: Biology and Morphology of the Genera*. Cambridge University Press, Cambridge.
- Rousseau, D.-D. 2001. Loess biostratigraphy: new advances and approaches in mollusk studies. *Earth-Science Reviews* 54, 157–171.
- Rousseau, D.-D., Limondin, N., Puissegur, J.-J. 1993. Holocene environmental signals from mollusc assemblages in Burgundy (France). *Quaternary Research* 40, 237–253.
- Rousseau, D.-D., Limondin, N., Magnin, F., et al. 1994. Temperature oscillations over the last 10,000 years in western Europe estimated from terrestrial mollusc assemblages. *Boreas* 23, 66–73.
- Rousseau, D.-D., Schevin, P., Duzer, D., et al. 2006. New evidence of long distance pollen transport to southern Greenland in late spring. *Review of Palaeobotany and Palynology* 141, 277–286.
- Rowe, P.J., Maher, B.A. 2000. 'Cold' stage formation of calcrite nodules in the Chinese Loess Plateau: evidence from U-series dating and stable isotope analysis. *Palaeogeography, Palaeoclimatology, Palaeoecology* 157, 109–125.
- Roy, K., Jablonsk, D., Valentine, J.W. 1995. Thermally anomalous assemblages revisited: patterns in the extraprovincial latitudinal range shifts of Pleistocene marine mollusks. *Geology* 23, 1071–1074.
- Roy, M., Clark, P.U., Duncan, R.A., et al. 2007. Insights into the late Cenozoic configuration of the Laurentide Ice Sheet from $^{40}\text{Ar}/^{39}\text{Ar}$ dating of glacially transported minerals in midcontinent tills. *Geochemistry, Geophysics, Geosystems* 8, doi: 10.1029/2006GC001572.
- Ruddiman, W.F. 2003a. Orbital insolation, ice volume and greenhouse gases. *Quaternary Science Reviews* 22, 1597–1629.
- Ruddiman, W.F. 2003b. The anthropogenic greenhouse era began thousands of years ago. *Climate Change* 61, 261–293.
- Ruddiman, W.F. 2005a. *Plows, Plagues and Petroleum*. Princeton University Press, Princeton, NJ.
- Ruddiman, W.F. 2005b. The early anthropogenic hypothesis a year later. *Climatic Change* 69, 427–434.
- Ruddiman, W.F. 2006. Ice-driven CO_2 feedback on ice volume. *Climate of the Past* 2, 43–55.

- Ruddiman, W.F. 2013. The Anthropocene. *Annual Review of Earth and Planetary Sciences* 41, 1–24.
- Ruddiman, W.F., McIntyre, A. 1976. Northeast Atlantic palaeoclimatic changes over the past 600,000 years. *Geological Society of America Memoir* 145, 111–146.
- Ruddiman, W.F., Kutzbach, J.E. 1990. Late Cenozoic plateau uplift and climate change. *Transactions of the Royal Society of Edinburgh: Earth Sciences* 81, 301–314.
- Ruddiman, W.F., Thomson, J.F. 2001. The case for human causes of increased CH₄ over the last 5000 years. *Quaternary Science Reviews* 20, 1769–1777.
- Ruddiman, W.F., Raymo, M.E. 2003. A methane-based time scale for Vostok ice. *Quaternary Science Reviews* 22, 141–155.
- Ruddiman, W.F., Ellis, E.C. 2009. Effect of per-capita land use changes on Holocene forest clearance. *Quaternary Science Reviews* 27/28, 3011–3015.
- Ruddiman, W.F., Vavrus, S.J., Kutzbach, J.E. 2005. A test of the overdue-glaciation hypothesis. *Quaternary Science Reviews* 24, 1–10.
- Ruddiman, W.F., Kutzbach, J.E., Vavrus, S.J. 2011. Can natural or anthropogenic explanations of Late Holocene CO₂ and CH₄ increases be falsified? *The Holocene* 21, 865–879.
- Ruiz, F., Abad, M., Cáceres, L.M., et al. 2010. Ostracods as tsunami tracers in Holocene sequences. *Quaternary Research* 73, 130–135.
- Ruiz, Z., Brown, A.G., Langdon, P.G. 2006. The potential of chironomid (Insecta: Diptera) larvae in archaeological investigations of floodplain and lake settlements. *Journal of Archaeological Science* 33, 14–33.
- Rundgren, M., Björck, S. 2003. Late-glacial and early Holocene variations in atmospheric CO₂ concentration indicated by high-resolution stomatal index data. *Earth and Planetary Science Letters* 213, 191–204.
- Ruszkiczay-Rüdiger, Z., Fodor, L., Bada, G., et al. 2005. Quantification of Quaternary vertical movements in the central Pannonian Basin: A review of chronologic data along the Danube River, Hungary. *Tectonophysics* 410, 157–172.
- Rutherford, S., D'Hoydt, S. 2000. Early onset and tropical forcing of 100,000-year Pleistocene glacial cycles. *Nature* 408, 72–75.
- Rutter, N.W., Ding, Z. 1993. Palaeoclimates and monsoon variations interpreted from micromorphogenic features of the Baoji palaeosols, China. *Quaternary Science Reviews* 12, 853–862.
- Rutter, N.W., Ding, Z., Liu, T. 1996. Long paleoclimate records from China. *Geophysica* 32, 7–34.
- Rutter, N.W., Velichko, A.A., Dlussky, K.G., et al. 2006. New insights on the loess/paleosol Quaternary stratigraphy from key sections in the US Midwest. *Catena* 67, 15–34.
- Ryder, J.M. 1971. The stratigraphy and morphology of paraglacial alluvial fans in south-central British Columbia. *Canadian Journal of Earth Sciences* 8, 1252–1264.
- Ryves, D.B., Jewson, D.H., Sturm, M., et al. 2003. Quantitative and qualitative relationships between planktonic diatom communities and diatom assemblages in sedimenting material and surface sediments in Lake Baikal, Siberia. *Limnology and Oceanography* 48, 1643–1661.
- Saarinen, T. 1999. Palaeomagnetic dating of Late Holocene sediments in Fennoscandia. *Quaternary Science Reviews* 18, 889–897.
- Sacchetti, F., Benetti, S., Quinn, R., et al. 2013. Glacial and post-glacial sedimentary processes in the Irish Rockall Trough from an integrated acoustic analysis of near-seabed sediments. *Geo-Marine Letters* 33, 49–66.
- Sachs, J.P., Anderson, R.F. 2005. Increased productivity in the subantarctic ocean during Heinrich events. *Nature* 434, 1118–1121.
- Sack, D. 2009. Evidence for climate change from desert basin palaeolakes. In *Geomorphology of Desert Environments*, 2nd edn (edited by A.J. Parsons, A. Abrahams). Springer, Dordrecht, 743–756.
- Saher, M., Kristensen, D.K., Hald, M., et al. 2012. Changes in distribution of calcareous benthic foraminifera in the central Barents Sea between the periods 1965–1992 and 2005–2006. *Global and Planetary Change* 98–99, 81–96.
- Saikku, R., Stott, L., Thunell, R. 2009. A bi-polar signal recorded in the western tropical Pacific: Northern and Southern Hemisphere climate records from the Pacific warm pool during the last Ice Age. *Quaternary Science Reviews* 28, 2374–2385.
- St. Jacques, J.-M., Cumming, B.F., Smol, J.P. 2008. A pre-European settlement pollen-climate calibration set for Minnesota, USA: developing tools for palaeoclimatic reconstructions. *Journal of Biogeography* 35, 306–324.
- St. Jacques, J.-M., Cumming, B.F., Smol, J.P. 2009. A 900-yr diatom and chrysophyte record of spring mixing and summer stratification from varved Lake Mina, west-central Minnesota, USA. *The Holocene* 19, 537–547.
- Salvador, A. (ed.). 1994. *International Stratigraphic Guide: A Guide to Stratigraphic Classification, Terminology and Procedure*, 2nd edn. International Commission on Stratigraphy, Geological Society of America, Boulder, CO.
- Salvigsen, O., Forman, S.L., Miller, G.H. 1992. Thermophilous molluscs on Svalbard during the Holocene and their paleoclimatic implications. *Polar Research* 11, 1–10.
- Sambridge, M., Grün, R., Eggins, S. 2012. U-series dating of bone in an open system: the diffusion-adsorption-decay model. *Quaternary Geochronology* 9, 42–53.
- Sampson, K.M., Smith, L.C. 2006. Relative ages of Pleistocene moraines discerned from pebble counts: Eastern Sierra Nevada, California. *Physical Geography* 27, 223–235.
- Sánchez Goñi, M.F., Landais, A., et al. 2008. Contrasting impacts of Dansgaard–Oeschger events over a western European latitudinal transect modulated by orbital parameters. *Quaternary Science Reviews* 27, 1136–1151.
- Santacreu, D.A., Vicens, G.M. 2012. Raw materials and pottery production at the Late Bronze and Iron Age Site of Puig de Sa Morisca, Mallorca, Spain. *Geoarchaeology* 27, 285–299.
- Sapart, C.J., Montiel, G., Prokopioiu, M., et al. 2012. Natural and anthropogenic variations in methane sources during the past two millennia. *Nature* 490, 85–88.
- Sarala, P., Peuraniemi, V. 2007. Exploration using till geochemistry and heavy minerals in the ribbed moraine area of southern Finnish Lapland. *Geochemistry: Exploration, Environment, Analysis* 7, 195–205.
- Sarnthein, M., Kiefer, T., Grootes, P.M., et al. 2006. Warmings in the far northwestern Pacific promoted pre-Clovis immigration to America during Heinrich event 1. *Geology* 34, 141–144.

- Sawada, M., Viau, A.E., Vettoretti, G., et al. 2004. Comparison of North-American pollen-based temperature and global lake-status with CCCma AGCM2 output at 6 ka. *Quaternary Science Reviews* 23, 225–244.
- Saxena, A. 2005. *Text Book of Mollusca*. Discovery Publishing House, New Delhi.
- Scarciglia, F., Pulice, I., Robustelli, G., et al. 2006. Soil chrono-sequences on Quaternary marine terraces along the north-western coast of Calabria (southern Italy). *Quaternary International* 156/157, 133–155.
- Schaefer, J.M., Denton, G.H., Barrell, D.J.A., et al. 2006. Near-synchronous interhemispheric termination of the Last Glacial Maximum in mid-latitudes. *Science* 312, 1510–1513.
- Scharpenseel, H.W., Becker-Heidemann, P. 1992. Twenty-five years of radiocarbon dating soils: paradigm erring and learning. *Radiocarbon* 34, 541–549.
- Schellenberger, A., Heller, F., Veit, H. 2003. Magnetostratigraphy and magnetic susceptibility of the Las Carreras loess–paleosol sequence in Valle de Tafí, Tucumán, NW-Argentina. *Quaternary International* 106/107, 159–167.
- Schellmann, G., Radtke, U. 2004. A revised morpho- and chronostratigraphy of the Late and Middle Pleistocene coral reef terraces on Southern Barbados (West Indies). *Earth-Science Reviews* 64, 157–187.
- Schellmann, G., Beerten, K., Radtke, U. 2008. Electron spin resonance (ESR) dating of Quaternary materials. *Eiszeitalter und Gegenwart (Quaternary Science Journal)* 57, 150–178.
- Schellnhuber, H.J. 1999. ‘Earth System’ analysis and the second Copernican revolution. *Nature* 402 (Suppl.), C19–C23.
- Schettler, G., Liu, Q., Mingram, J., et al. 2006. Palaeovariations in the East-Asian monsoon regime geochemically recorded in varved sediments of Lake Sihailongwan (Northeast China, Jilin Province). Part 1. Hydrological conditions and dust flux. *Journal of Paleolimnology* 35, 239–270.
- Schlitzer, R. 2003. *eWoce – Electronic Atlas of WOCE Hydrographic and Tracer Data*. Alfred Wegener Institute for Polar and Marine Research, Bremerhaven, <http://www.ewoce.org>.
- Schmidt, G.A. 2010. Enhancing the relevance of palaeoclimate model/data comparisons for assessments of future climate change. *Journal of Quaternary Science* 25, 79–87.
- Schmieder, J., Fritz, S.C., Swinehart, J.B., et al. 2011. A regional-scale climate reconstruction of the last 4000 years from lakes in the Nebraska Sand Hills, USA. *Quaternary Science Reviews* 30, 1797–1812.
- Schmittner, A., Saenko, O.A., Weaver, A.J. 2003. Coupling of the hemispheres in observations and simulations of glacial climate change. *Quaternary Science Reviews* 22, 659–671.
- Schneider, B., Schmittner, A. 2006. Simulating the impact of the Panamanian seaway closure on ocean circulation, marine productivity and nutrient cycling. *Earth and Planetary Science Letters* 246, 367–380.
- Schnurrenberger, D., Russell, J., Kelts, K. 2003. Classification of lacustrine sediments based on sedimentary components. *Journal of Paleolimnology* 29, 141–154.
- Scholz, D., Magini, A., Felis, T. 2004. U-series dating of diagenetically altered fossil reef corals. *Earth and Planetary Science Letters* 218, 163–178.
- Scholz, D., Hoffman, D.L., Hellstrom, J., et al. 2012. A comparison of different methods for speleothem age modelling. *Quaternary Geochronology* 14, 94–104.
- Schöne, B.R. 2003. A ‘clam-ring’ master-chronology constructed from a short-lived bivalve mollusc from the northern Gulf of California, USA. *The Holocene* 13, 39–50.
- Schöne, B.R., Feibig, J. 2009. Seasonality in the North Sea during the Allerød and Late Medieval Climate Optimum using bivalve sclerochronology. *International Journal of Earth Science (Geologische Rundschau)* 98, 83–98.
- Schöne, B.R., Oschmann, W., Rössler, J., et al. 2003. North Atlantic Oscillation dynamics recorded in shells of a long-lived bivalve mollusk. *Geology* 31, 1037–1040.
- Schöne, B.R., Dunca, E., Mutvei, H., et al. 2004. A 217-year record of summer air temperature reconstructed from freshwater pearl mussels (*M. margarifera*, Sweden). *Quaternary Science Reviews* 23, 1803–1816.
- Schönfeld, J. 2012. History and development of methods in Recent benthic foraminiferal studies. *Journal of Micropalaeontology* 31, 53–72.
- Schrag, D.P., Hampt, G., Murray, D.W. 1996. Pore fluid constraints on the temperature and oxygen isotopic composition of the glacial ocean. *Science* 272, 1930–1932.
- Schramm, A., Stein, M., Goldstein, S.L. 2000. Calibration of the ^{14}C timescale to >40 ka by ^{234}U - ^{230}Th dating of Lake Lisan sediments (last glacial Dead Sea). *Earth and Planetary Science Letters* 175, 27–40.
- Schreve, D. 2007. Vertebrate overview. In *Encyclopedia of Quaternary Science* (edited by S.A. Elias). Elsevier, Amsterdam, 3123–3132.
- Schreve, D.C., Thomas, G.N. (eds). 2001. European Quaternary biostratigraphy. *Quaternary Science Reviews* 20, 1577–1764.
- Schreve, D., Candy, I. 2010. Interglacial climates: advances in our understanding of warm climate episodes. *Progress in Physical Geography* 34, 845–856.
- Schreve, D.C., Keen, D.H., Limondon-Lozouet, N., et al. 2007. Progress in faunal biostratigraphy of Late Cenozoic fluvial sequences during IGCP 449. *Quaternary Science Reviews* 26, 2970–2995.
- Schulz, K.G., Zeebe, R.E. 2006. Pleistocene glacial terminations triggered by synchronous changes in Southern and Northern Hemisphere insolation: the insolation canon hypothesis. *Earth and Planetary Science Letters* 249, 326–336.
- Schulz, M. 2002. On the 1470-year pacing of Dansgaard–Oeschger warm events. *Paleoceanography* 17, doi: 10.1029/2000PA000571.
- Schurr, M.R., Gregory, D.A. 2002. Fluoride dating of faunal materials by ion-selective electrode: high resolution relative dating at an early agricultural period site in the Tucson basin. *American Antiquity* 67, 281–299.
- Schuster, M., Roquin, C., Düringer, P., et al. 2005. Holocene Lake Mega-Chad palaeoshorelines from space. *Quaternary Science Reviews* 24, 1821–1827.
- Schüttenhelm, R.T.E., Laban, C. 2005. Heavy minerals, provenance and large scale dynamics of seabed sands in the Southern North Sea: Baak’s (1936) heavy mineral study revisited. *Quaternary International* 133/134, 170–193.
- Schweingruber, F.H. 1996. *Tree Rings and Environment: Dendroecology*. Paul Haupt, Bern.

- Scott, D.B., Collins, E.S., Gayes, P.T., et al. 2003. Records of prehistoric hurricanes on the South Carolina coast records. *Geological Society of America Bulletin* 115, 1027–1039.
- Scott, D.B., Schell, T., Rochon, A., et al. 2008. Benthic foraminifera in the surface sediments of the Beaufort Shelf and slope, Beaufort Sea, Canada: applications and implications for past sea-ice conditions. *Journal of Marine Systems* 74, 840–863.
- Scott, E.M., Cook, G.T., Naysmith, P. 2010a. A Report on Phase 2 of the Fifth International Radiocarbon Intercomparison (VIRI). *Radiocarbon* 52, 846–858.
- Scott, E.M., Cook, G.T., Naysmith, P. 2010b. The Fifth International Radiocarbon Intercomparison (VIRI): an assessment of laboratory performance in Stage 3. *Radiocarbon* 52, 859–865.
- Scourse, J., Richardson, C., Forsythe, G., et al. 2006. First cross-matched floating chronology from the marine fossil record: data from growth lines of the long-lived bivalve mollusc *Arctica islandica*. *The Holocene* 16, 967–974.
- Scourse, J.D., Haapaniemi, A.I., Colmenero-Hidalgo, E., et al. 2009. Growth, dynamics and deglaciation of the last British–Irish ice sheet: the deep-sea ice rafted detritus record. *Quaternary Science Reviews* 28, 3066–3084.
- Scrivner, A.E., Vance, D., Rohling, E.J. 2004. New neodymium isotope data quantify Nile involvement in Mediterranean anoxic episodes. *Geology* 32, 565–568.
- Sedov, S., Sycheva, S., Targulian, V., et al. 2013. Last Interglacial paleosols with Argic horizons in Upper Austria and Central Russia – pedogenetic and palaeoenvironmental inferences from comparison with the Holocene analogues. *Eiszeitalter und Gegenwart (Quaternary Science Journal)* 62, 44–58.
- Seidov, D., Maslin, M. 2001. Atlantic Ocean heat piracy and the bipolar climate see-saw during Heinrich and Dansgaard–Oeschger events. *Journal of Quaternary Science* 16, 321–328.
- Seidov, D., Haupt, B.J., Barron, E.J., et al. 2001. Ocean bi-polar seesaw: southern versus northern meltwater impacts. In *The Oceans and Rapid Climate Change: Past, Present & Future* (edited by D. Seidov, B.J. Haupt, M. Maslin). American Geophysical Union, Washington DC, 169–197.
- Seidov, D., Stouffer, R.J., Haupt, B.J. 2005. Is there a simple bi-polar ocean seesaw? *Global and Planetary Change* 49, 19–27.
- Sejrup, H.P., Hjelstuen, B.O., Dahlgren, K.I.T., et al. 2005. Pleistocene glacial history of the NW European continental margin. *Marine and Petroleum Geology* 22, 1111–1129.
- Sejrup, H.P., Nygård, A., Hall, A.M., et al. 2009. Middle and Late Weichselian (Devensian) glaciation history of south-western Norway, North Sea and eastern UK. *Quaternary Science Reviews* 28, 370–380.
- Selby, K., Smith, D.E. 2007. Late Devensian and Holocene relative sea-level changes on the Isle of Skye, Scotland, UK. *Journal of Quaternary Science* 22, 119–139.
- Sella, G.F., Stein, S., Dixon, T.H., et al. 2007. Observation of glacial isostatic adjustment in ‘stable’ North America with GPS. *Geophysical Research Letters* 34, doi: 10.1029/2006GL027081.
- Sémah, F., Saleki, H., Falguères, C. 2000. Did early man reach Java during the Late Pliocene? *Journal of Archaeological Science* 27, 763–769.
- Sen Gupta, B.K. (ed.) 2002. *Modern Foraminifera*. Kluwer Academic Publishers, Dordrecht.
- Seong, Y.B., Owen, L.A., Yi, C., et al. 2009. Geomorphology of anomalously high glaciated mountains at the northwestern end of Tibet: Muztag Ata and Kongur Shan. *Geomorphology* 103, 227–250.
- Seppä, H., Bennett, K.D. 2003. Quaternary pollen analysis: recent progress in palaeoecology and palaeoclimatology. *Progress in Physical Geography* 27, 548–579.
- Seppä, H., Birks, H.J.B., Odland, A., et al. 2004. A modern pollen–climate calibration set from northern Europe: developing and testing a tool for palaeoclimatological reconstructions. *Journal of Biogeography* 31, 251–267.
- Serefiddin, F., Schwarcz, H.P., Ford, D.C., et al. 2004. Late Pleistocene paleoclimate in the Black Hills of South Dakota from isotope records in speleothems. *Paleogeography, Palaeoclimatology, Palaeoecology* 203, 1–17.
- Serieyssol, K., Chatelard, S., Cubizolle, H. 2011. Diatom fossils in mires: a protocol for extraction, preparation and analysis in palaeoenvironmental studies. *Mires and Peat* 7(art. 12), 1–11, <http://www.mires-and-peat.net/>.
- Severinghaus, J.P. 2009. Southern see-saw seen. *Nature* 457, 1093–1094.
- Shackleton, N.J. 1987. Oxygen isotopes, ice volume and sea level. *Quaternary Science Reviews* 6, 183–190.
- Shackleton, N.J. 2000. The 100,000-year ice-age cycle identified and found to lag temperature, carbon dioxide and orbital eccentricity. *Science* 289, 1897–1902.
- Shackleton, N.J. 2006. Formal Quaternary stratigraphy – what do we expect and need? *Quaternary Science Reviews* 25, 3458–3462.
- Shackleton, N.J., Opdyke, N.D. 1973. Oxygen isotope and palaeomagnetic stratigraphy of equatorial Pacific core V28-238: oxygen isotope temperatures and ice volume on a 10^5 and 10^6 year scale. *Quaternary Research* 3, 39–55.
- Shackleton, N.J., Berger, A., Peltier, W.R. 1990. An alternative astronomical calibration of the lower Pleistocene timescale based on ODP Site 677. *Transactions of the Royal Society of Edinburgh: Earth Science* 81, 251–261.
- Shackleton, N.J., Fairbanks, R.G., Chiu, T.-C., et al. 2004. Absolute calibration of the Greenland time scale: implications for Antarctic time scales and for $\Delta^{14}\text{C}$. *Quaternary Science Reviews* 23, 1513–1522.
- Shakesby, R.A. 1997. Pronival (protalus) ramparts: a review of forms, processes, diagnostic criteria and palaeoenvironmental implications. *Progress in Physical Geography* 21, 394–418.
- Shakesby, R.A., Matthews, J.A., Winkler, S. 2004. Glacier variations in Breihemen, southern Norway: relative-age dating of Holocene moraine complexes at six high-altitude glaciers. *The Holocene* 14, 899–910.
- Shakesby, R.A., Matthews, J.A., Owen, G. 2006. The Schmidt hammer as a relative-age tool and its potential for calibrated-age dating in Holocene glaciated environments. *Quaternary Science Reviews* 25, 2846–2867.
- Shakun, J.D., Clark, P.U., Feng, H., et al. 2012. Global warming preceded by increasing carbon dioxide concentrations during the last deglaciation. *Nature* 484, 49–55.
- Shanahan, T.M., Overpeck, J.T., Anchukaitis, K.J., et al. 2009. Atlantic forcing of persistent drought in West Africa. *Science* 324, 377–380.

- Shane, P. 2005. Towards a comprehensive distal andesitic tephrostratigraphic framework for New Zealand based on eruptions from Egmont volcano. *Journal of Quaternary Science* 20, 45–57.
- Shane, P.A., Narin, I.A., Martin, S.B., et al. 2008. Compositional heterogeneity in tephra deposits resulting from the eruption of multiple magma bodies: implications for tephrochronology. *Quaternary International* 178, 44–53.
- Sharp, M., Dowdeswell, J.A., Gemmell, J.C. 1989. Reconstructing past glacier dynamics and erosion from glacial geomorphic evidence: Snowdon, North Wales. *Journal of Quaternary Science* 4, 115–130.
- Sharp, W.D., Ludwig, K.R., Chadwick, O.A., et al. 2003. Dating fluvial terraces by $^{230}\text{Th}/\text{U}$ on pedogenic carbonate, Wind River Basin, Wyoming. *Quaternary Research* 59, 139–150.
- Shaw, J., Gareau, P., Courtney, R.C. 2002. Paleogeography of Atlantic Canada 13–0 kyr. *Quaternary Science Reviews* 21, 1861–1878.
- Shennan, I., Horton, B. 2002. Holocene land- and sea-level changes in Great Britain. *Journal of Quaternary Science* 17, 511–526.
- Shennan, I., Innes, J., Long, A.J., et al. 1994. Late Devensian and Holocene sea-level changes at Loch an Eala near Arisaig, northwest Scotland. *Journal of Quaternary Science* 9, 261–284.
- Shennan, I., Bradley, S., Milne, G., et al. 2006a. Relative sea-level changes, glacial isostatic modelling and ice-sheet reconstructions from the British Isles since the Last Glacial Maximum. *Journal of Quaternary Science* 21, 585–599.
- Shennan, I., Hamilton, S., Hiller, C., et al. 2006b. Relative sea-level observations in western Scotland since the Last Glacial maximum for testing models of glacial isostatic land movements and ice-sheet reconstructions. *Journal of Quaternary Science* 21, 601–613.
- Sherwood, S.C., Huber, M. 2010. An adaptability limit to climate change due to heat stress. *Proceedings of the National Academy of Sciences of the United States of America* 107, 9552–9555.
- Shi, C., Zhu, R., Glas, B.P., et al. 2003. Climate variations since the last interglacial recorded in Czech loess. *Geophysical Research Letters* 30, doi: 10.1029/2003GL017251.
- Shimada, C., Sato, T., Toyoshima, S., et al. 2008. Paleoecological significance of laminated diatomaceous oozes during the middle-to-late Pleistocene, North Atlantic Ocean (IODP Site U1304). *Marine Micropaleontology* 69, 139–150.
- Shindell, D.T., Schmidt, G.A., Miller, R.L., et al. 2003. Volcanic and solar forcing of climate change during the Preindustrial Era. *Journal of Climate* 16, 4094–4107.
- Shuman, B., Newby, P., Huang, Y., et al. 2004. Evidence for the close climatic control of New England vegetation history. *Ecology* 85, 1297–1310.
- Siddall, M., Rohling, E.J., Almogi-Labin, A., et al. 2003. Sea-level fluctuations during the last glacial cycle. *Nature* 423, 853–858.
- Siddall, M., Rohling, E.J., Thompson, W.G., et al. 2008. Marine isotope stage 3 sea level fluctuations: data synthesis and new outlook. *Review of Geophysics* 46, RG4003, doi: 10.1029/2007RG000226.
- Siddall, M., Höönsch, B., Waelbroeck, C., et al. 2010a. Changes in deep Pacific temperature during the mid-Pleistocene Transition and Quaternary. *Quaternary Science Reviews* 29, 170–181.
- Siddall, M., Kaplan, M.R., Schaefer, J.M., et al. 2010b. Changing influence of Antarctic and Greenlandic temperature records on sea-level over the last glacial cycle. *Quaternary Science Reviews* 29, 410–423.
- Siegert, M.J. 2001. *Ice Sheets and Late Quaternary Environmental Change*. John Wiley, Chichester and New York.
- Siegert, M.J. 2005. Lakes beneath the ice sheet: the occurrence, analysis, and future exploration of Lake Vostok and other Antarctic subglacial lakes. *Annual Review of Earth and Planetary Sciences* 33, 215–245.
- Siegert, M.J., Dowdeswell, J.A. 2004. Numerical reconstructions of the Eurasian Ice Sheet and climate during the Late Weichselian. *Quaternary Science Reviews* 23, 1273–1284.
- Sierro, F.J., Andersen, N., Bassetti, M.A., et al. 2009. Phase relationship between sea level and abrupt climate change. *Quaternary Science Reviews* 28, 2867–2881.
- Sigman, D.M., Boyle, E.A. 2000. Glacial/interglacial variations in atmospheric carbon dioxide. *Nature* 407, 859–869.
- Sigman, D.M., Hain, M.P., Haug, G.H. 2010. The polar and glacial cycles in atmospheric CO_2 concentration. *Nature* 466, 47–55.
- Sime, L.C., Ferguson, R.I. 2003. Information on grain sizes in gravel-bed rivers by automated image analysis. *Journal of Sedimentary Research, Section B: Stratigraphy and Global Studies* 73, 630–636.
- Sime, L.C., Wolff, E.W., Oliver, K.I.C., et al. 2009. Evidence for warmer interglacials in East Antarctic ice cores. *Nature* 462, 342–346.
- Simms, A.R., Lambbeck, K., Purcell, A., et al. 2007. Sea-level history of the Gulf of Mexico since the Last Glacial Maximum with implications for the melting history of the Laurentide Ice Sheet. *Quaternary Science Reviews* 26, 920–940.
- Simpson, G.L., Shilland, E.M., Winterbottom, J.M., et al. 2005. Defining reference conditions for acidified waters using a modern analogue approach. *Environmental Pollution* 137, 119–133.
- Simpson, M.J.R., Milne, G.A., Huybrechts, P., et al. 2009. Calibrating a glaciological model of the Greenland ice sheet from the Last Glacial Maximum to present-day using field observations of relative sea level and ice extent. *Quaternary Science Reviews* 28, 1631–1657.
- Singer, B.S., Ackert, R.P., Guillou, H. 2004. $^{40}\text{Ar}/^{39}\text{Ar}$ and K–Ar chronology of Pleistocene glaciations in Patagonia. *Geological Society of America Bulletin*, 434–450.
- Singhvi, A.K., Porat, N. 2008. Impact of luminescence dating on geomorphological and palaeoclimate research in drylands. *Boreas* 37, 536–558.
- Singhvi, A.K., Williams, M.A.J., Rajaguru, S.N., et al. 2010. A c. 200 ka record of climatic change and dune activity in the Thar Desert, India. *Quaternary Science Reviews* 29, 3095–3105.
- Sinka, H.J., Atkinson, T.C. 1999. A mutual climatic range method for reconstructing palaeoclimate from plant remains. *Journal of the Geological Society of London* 156, 381–396.
- Sissons, J.B. 1967. *The Evolution of Scotland's Scenery*. Oliver and Boyd, Edinburgh.
- Sissons, J.B. 1974. A Late-glacial ice cap on the central Grampians, Scotland. *Transactions of the Institute of British Geographers* 62, 95–114.
- Sissons, J.B. 1979. The Loch Lomond Stadial in the British Isles. *Nature* 280, 1990–202.
- Sissons, J.B. 1980. Palaeoclimatic inferences from Loch Lomond Advance glaciers. In *Studies in the Lateglacial of North-West Europe* (edited by J.J. Lowe, J.M. Gray, J.E. Robinson). Pergamon Press, Oxford, 31–44.

510 REFERENCES

- Sivakumar, B. 2004. Chaos theory in geophysics: past, present and future. *Chaos, Solitons & Fractals* 19, 441–462.
- Sjunneskog, C., Scherer, R.P. 2005. Mixed diatom assemblages in glaciogenic sediment from the central Ross Sea, Antarctica. *Palaeogeography, Palaeoclimatology, Palaeoecology* 218, 287–300.
- Skinner, L.C., Fallon, S., Waelbroeck, C., et al. 2010. Ventilation of the deep Southern Ocean and deglacial CO₂ rise. *Science* 328, 1147–1151.
- Smart, D. 2003. Sub-sea level speleothems from the Andaman coast of southern Thailand, and sea-level change in Southeast Asia. *Cave and Karst Science* 30, 39–42.
- Smart, P.L. 1991a. Uranium series dating. In *Quaternary Dating Methods – A User's Guide* (edited by P.L. Smart, P.D. Frances). Technical Guide 4. Quaternary Research Association, Cambridge, 45–83.
- Smart, P.L. 1991b. Electron Spin Resonance (ESR) dating. In *Quaternary Dating Methods – A User's Guide* (edited by P.L. Smart, P.D. Frances). Technical Guide 4. Quaternary Research Association, Cambridge, 128–160.
- Smith, A.M., Murray, T., Nicholls, K.W., et al. 2007. Rapid erosion, drumlin formation, and changing hydrology beneath an Antarctic ice stream. *Geology* 35, 127–130.
- Smith, C.W. 2003. *Archaeological Conservation Using Polymers*. Texas A & M University, Anthropology Series 6. Texas A & M University Press, College Station.
- Smith, D., Kenward, H. 2011. Roman grain pests in Britain: implications for grain supply and agricultural production. *Britannia* 42, 243–262.
- Smith, D.E., Shi, S., Cullingford, R.A., et al. 2004. The Holocene Storegga Slide tsunami in the United Kingdom. *Quaternary Science Reviews* 23, 2291–2321.
- Smith, D.E., Fretwell, P.T., Cullingford, R.A., et al. 2006. Towards improved empirical isobase models of Holocene land uplift for mainland Scotland, UK. *Philosophical Transactions of the Royal Society of London A* 364, 949–972.
- Smith, D.E., Davies, M.H., Brooks, C.L., et al. 2010. Holocene relative sea levels and related prehistoric activity in the Forth lowland, Scotland, United Kingdom. *Quaternary Science Reviews* 29, 2382–2410.
- Smith, D.E., Hunt, N., Firth, C.R., et al. 2012. Patterns of Holocene relative sea level change in the north of Britain and Ireland. *Quaternary Science Reviews* 54, 58–76.
- Smith, G.I. 2009. Late Cenozoic geology and lacustrine history of Searles Valley, Inyo and San Bernardino Counties, California. *US Geological Survey Professional Paper* 1727.
- Smith, G.I., Street-Perrott, A.F. 1983. Pluvial lakes of the western United States. In *Late Quaternary Environments of the United States. 1. The Late Pleistocene* (edited by S.C. Porter). Longman, London, 190–212.
- Smith, M.A., Watchman, A., Ross, J. 2009. Direct dating indicates a Mid Holocene age for archaic rock engravings in arid Central Australia. *Geoarchaeology* 24, 191–203.
- Smith, M.W., Riseborough, D.W. 2002. Climate and the limits of permafrost: a zonal analysis. *Permafrost and Periglacial Processes* 13, 1–15.
- Smol, J.P., Stoermer, E.F. (eds). 2010. *The Diatoms: Applications for the Environmental and Earth Sciences*, 2nd edn. Cambridge University Press, Cambridge.
- Snowball, I., Sandgren, P. 2002. Geomagnetic field variations in northern Sweden during the Holocene quantified from varved lake sediments and their implications for cosmogenic nuclide production rates. *The Holocene* 12, 517–530.
- Snowball, I., Zillen, L., Ojala, A., Saarinen, T., et al. 2007. FENNO-STACK and FENNORPIS: varve dated Holocene palaeomagnetic secular variation and relative palaeointensity stacks for Fennoscandia. *Earth and Planetary Science Letters* 255, 106–115.
- Snowball, T., Thompson, R. 1992. a mineral magnetic study of Holocene sediment yields and deposition patterns in the Llyn Geirionydd catchment, north Wales. *The Holocene* 2, 238–248.
- Solomina, O., Haeberli, W., Kull, C., et al. 2008. Historical and Holocene glacier-climate variations: general concepts and overview. *Global and Planetary Change* 60, 1–9.
- Solomon, S., Qin, D., Manning, M. et al. (eds). 2007. *Climate Change 2007: The Physical Science Basis*. Contribution of Working Group I to the Fourth Assessment Report of the Intergovernmental Panel on Climate Change. Cambridge University Press, Cambridge.
- Sonnent, C.P., Finney, S.A. 1990. The spectrum of radiocarbon. *Philosophical Transactions of the Royal Society, London A* 330, 238–248.
- Spalding, M.D., Fox, H.E., Allen, G.R., et al. 2007. Marine ecoregions of the world: a bioregionalization of coastal and shelf areas. *BioScience* 57, 573–583.
- Speer, J.H. 2010. *Fundamentals of Tree Ring Research*. University of Arizona Press, Tucson.
- Speirs, J.C., McGowan, H.A., Neil, D.T. 2008. Meteorological controls on sand transport and dune morphology in a polar-desert: Victoria Valley, Antarctica. *Earth Surface Processes and Landforms* 33, 1875–1891.
- Spencer, J., Frizzelle, B.G., Page, P.H., et al. 2003a. *Global Positioning System: A Field Guide for the Social Sciences*. Blackwell, Malden, MA and Oxford.
- Spencer, L.M., Van Valkenburgh, B., Harris, J.M. 2003b. Taphonomic analysis of large mammals recovered from the Pleistocene Rancho La Brea tar seeps. *Paleobiology* 29, 561–575.
- Speranza, A., van Geel, B., van der Plicht, J. 2002. Evidence for solar forcing of climate change at ca. 850 cal. BC from a Czech peat sequence. *Global and Planetary Change* 35, 51–65.
- Spötl, C., Mangini, A. 2002. Stalagmite from the Austrian Alps reveals Dansgaard-Oeschger events during isotope stage 3: implications for the absolute chronology of Greenland ice cores. *Earth and Planetary Sciences Letters* 203, 507–518.
- Spötl, C., Magnini, A. 2007. Speleothems and palaeoglaciers. *Earth and Planetary Science Letters* 254, 323–331.
- Spötl, C., Scholz, D., Mangini, A. 2008. A terrestrial U/Th-dated stable isotope record of the Penultimate Interglacial. *Earth And Planetary Science Letters* 276, 283–292.
- Staff, R.A., Ramsey, C.B., Bryant, C.L., et al. 2011. New ¹⁴C determinations from Lake Suigetsu, Japan: 12,000 to 0 cal BP. *Radiocarbon* 53, 3, 511–528.

- Stager, J.C., Ruzmaikin, A., Conway, D., et al. 2007. Sunspots, El Niño, and the levels of Lake Victoria, East Africa. *Journal of Geophysical Research* 112, D15, 16; doi: 10.1029/2006JD008362.
- Stahl, P.W. 1996. The recovery and interpretation of microvertebrate bone assemblages from archaeological contexts. *Journal of Archaeological Method and Theory* 3, 31–75.
- Stahle, D.W., Fyfe, F.K., Cook, E.R., et al. 2007. Tree-ring reconstructed megadroughts over North America since AD 1300. *Climate Change* 8, 133–149.
- Staiger, J.W., Gosse, J., Little, E.C., et al. 2006. Glacial erosion and sediment dispersion from detrital cosmogenic nuclide analyses of till. *Quaternary Geochronology* 1, 29–42.
- Stambaugh, M.C., Guyette, R.P. 2009. Progress in constructing a long oak chronology from the central United States. *Tree-Ring Research* 65, 147–156.
- Stanford, J.D., Rohling, E.J., Bacon, S., et al. 2011. A new concept for the paleoceanographic evolution of Heinrich event 1 in the North Atlantic. *Quaternary Science Reviews* 30, 1047–1066.
- Stanton, T., Snowball, I., Zillén, L., et al. 2010. Validating a Swedish varve chronology using radiocarbon, palaeomagnetic secular variation, lead pollution history and statistical correlation. *Quaternary Geochronology* 5, 611–624.
- Starkey, L. 2003. Climatically controlled terraces in uplifting mountain areas. *Quaternary Science Reviews* 22, 2189–2198.
- Steadman, D.W., Franz, R.S., Morgan, G.S., et al. 2007. Exceptionally well preserved late Quaternary plant and vertebrate fossils from a blue hole on Abaco, The Bahamas. *Proceedings of the National Academy of Sciences of the United States of America* 104, 19897–19902.
- Stearta, D.C., Greenwood, D.R., Boon, P.I. 2009. The chemical constraints upon leaf decay rates: taphonomic implications among leaf species in Australian terrestrial and aquatic environments. *Review of Palaeobotany and Palynology* 157, 358–374.
- Steffen, W., Grinevald, J., Crutzen, P.J., et al. 2011. The Anthropocene: conceptual and historical perspectives. *Philosophical Transactions of the Royal Society of London A* 369, 842–867.
- Steffensen, J.P., Andersen, K.K., Bigler, M., et al. 2008. High-resolution Greenland ice core data show abrupt climate change happens in few years. *Science* 321, 680–684.
- Stein, J.K., Deo, J.N. 2003. Big sites – short time. Accumulation rates in archaeological sites. *Journal of Archaeological Science* 30, 297–316.
- Stein, M. 2001. The sedimentary and geochemical record of Neogene–Quaternary water bodies in the Dead Sea Basin: inferences for the regional paleoclimatic history. *Journal of Paleolimnology* 26, 271–282.
- Stein, R., Fahl, K. 2013. Biomarker proxy shows potential for studying the entire Quaternary Arctic sea ice history. *Organic Geochemistry* 55, 98–102.
- Steinhilber, F., Abreu, J.A., Beer, J., et al. 2012. 9,400 years of cosmic radiation and solar activity from ice cores and tree rings. *Proceedings of the National Academy of Sciences of the United States of America*, doi: 10.1073/pnas.1118965109.
- Stenni, B., Buiron, D., Frezzotti, M., et al. 2011. Expression of the bipolar see-saw in Antarctic climate records during the last deglaciation. *Nature Geoscience* 4, 46–49.
- Sternberg, R.S. 2001. Magnetic properties and archaeomagnetism. In *Handbook of Archaeological Sciences* (edited by D.R. Brothwell, A.M. Pollard). John Wiley, Chichester and New York, 73–79.
- Stevens, R.E., Metcalfe, S.E., Leng, M.J., et al. 2012. Reconstruction of late Pleistocene climate in the Valsequillo Basin (Central Mexico) through isotopic analysis of terrestrial and freshwater snails. *Palaeogeography, Palaeoclimatology, Palaeoecology* 319–320, 16–27.
- Stewart, J.R. 2009. The evolutionary consequence of the individualistic response to climate change. *Journal of Evolutionary Biology* 22, 2363–2375.
- Stewart, J.R., Lister, A.M., Barnes, I., et al. 2010. Refugia revisited: individualistic responses of species in space and time. *Proceedings of the Royal Society B* 277, 661–671.
- Stewart, T.G. 1991. Glacial marine sedimentation from tidewater glaciers in the Canadian High Arctic. In *Glacial Marine Sedimentation; Paleoclimatic Significance* (edited by J.B. Anderson, G.M. Ashley), *Geological Society of America, Special Paper* 261, 95–105.
- Stickley, C.E., Pike, J., Leventer, A., et al. 2005. Deglacial ocean and climate seasonality in laminated diatom sediments, MacRobertson Shelf, Antarctica. *Paleogeography, Paleoceanography, Palaeoecology* 227, 290–310.
- Stiner, M.C. 1999. Palaeolithic mollusc exploitation at Riparo Mochi (Balzi Rossi, Italy): food and ornaments from the Aurignacian through Epigravettian. *Antiquity* 73, 735–754.
- Stirling, C.H., Andersen, M.B. 2009. Uranium series dating of fossil coral reefs: extending the sea-level record beyond the last glacial cycle. *Earth and Planetary Science Letters* 284, 269–283.
- Stocchi, P., Spada, G. 2007. Glacio and hydro-isostasy in the Mediterranean Sea: Clark's zones and role of remote ice sheets. *Annals of Geophysics* 50, 741–761.
- Stocker, T.F. 1998. The see-saw effect. *Science* 282, 61–62.
- Stocker, T.F., Johnsen, S.J. 2003. A minimum thermodynamic model for the bipolar seesaw. *Paleoceanography* 18, doi: 10.1029/2003PA000920.
- Stoddard, J.L., Jeffries, D.S., Lükewille, A., et al. 1999. Regional trends in aquatic recovery from acidification in North America and Europe. *Nature* 401, 575–578.
- Stoermer, E.F. 2001. Diatom taxonomy for paleolimnologists. *Journal of Paleolimnology* 25, 393–398.
- Stokes, C.R., Tarasov, L. 2010. Ice streaming in the Laurentide Ice Sheet: a first comparison between data-calibrated numerical model output and geological evidence. *Geophysical Research Letters* 37, doi: 10.1029/2009GL040990.
- Stokes, C.R., Clark, C.D., Darby, D.A., et al. 2005. Late Pleistocene ice export events into the Arctic Ocean from the M'Clure Strait Ice Stream, Canadian Arctic Archipelago. *Global and Planetary Change* 49, 139–162.
- Stokes, C.R., Tarasov, L., Dyke, A.S. 2012. Dynamics of the North American Ice Sheet Complex during its inception and build-up to the Last Glacial Maximum. *Quaternary Science Reviews* 50, 86–104.
- Stone, E.J., Lunt, D.J., Annan, J.D. 2013. Quantification of the Greenland ice sheet contribution to Last Interglacial sea level rise. *Climate of the Past Discussions* 9, 621–639.

512 REFERENCES

- Stone, J.O. 2000. Air pressure and cosmogenic isotope production. *Journal of Geophysical Research* 105, 23753–23759.
- Stoops, G. (ed.). 2003. Achievements in micromorphology. *Catena* 54, 317–678.
- Stott, A.W., Berstan, R., Evershed, P., et al. 2001. Radiocarbon dating of single compounds isolated from pottery cooking vessel residues. *Radiocarbon* 43, 191–197.
- Stott, K.J., Austin, W.E.N., Sayer, M.D.J., et al. 2010. The potential of *Arctica islandica* growth records to reconstruct coastal climate in north west Scotland, UK. *Quaternary Science Reviews* 29, 1602–1633.
- Stott, L., Timmermann, A., Thunell, R. 2007. Southern hemisphere and deep-sea warming led deglacial atmospheric CO₂ rise and tropical warming. *Science* 318, 435–438.
- Street, F.A., Grove, A.T. 1979. Global maps of lake-level fluctuations in Africa. *Quaternary Research* 12, 83–118.
- Street-Perrott, F.A., Holmes, J.A., Waller, M.P., et al. 2000. Drought and dust deposition in the West African Sahel: a 5500-year record from Kajemarun Oasis, northeastern Nigeria. *The Holocene* 10, 293–302.
- Stuart, A.J. 1979. Pleistocene occurrences of the European pond tortoise (*Emys orbicularis* L.) in Britain. *Boreas* 8, 359–371.
- Stuart, A.J. 2005. The extinction of woolly mammoth (*Mammuthus primigenius*) and straight-tusked elephant (*Palaeoloxodon antiquus*) in Europe. *Quaternary International* 126–12, 171–177.
- Stuart, A.J., Lister, A.M. 2001. The mammalian faunas of Pakefield/ Kessingland and Corton, Suffolk, UK: evidence for a new temperate episode in the British Middle Pleistocene. *Quaternary Science Reviews* 20, 1677–1692.
- Stuart, A.J., Lister, A.M. 2011. Extinction chronology of the cave lion *Panthera spelaea*. *Quaternary Science Reviews* 30, 2329–2340.
- Stuart, A.J., Lister, A.M. 2012. Extinction chronology of the woolly rhinoceros *Coelodonta antiquitatis* in the context of late Quaternary megafaunal extinctions in northern Eurasia. *Quaternary Science Reviews* 30, 2329–2340.
- Stuiver, M., Braziunas, T.F., Becker, B., et al. 1991. Climatic solar, oceanic and geomagnetic influences on Late-Glacial and Holocene atmospheric ¹⁴C/¹²C change. *Quaternary Research* 35, 1–24.
- Stuiver, M., Reimer, P.J., Bard, E., et al. 1998. INTCAL98 radiocarbon age calibration, 24,000–0 cal BP. *Radiocarbon* 40, 1041–1084.
- Stuiver, M., Reimer, P.J., Reimer, R. 2013. CALIB Radiocarbon Calibration Version 7.0, <http://calib.qub.ac.uk/calib/>.
- Sturm, C.F., Pearce, T.A., Valdés, A. 2006. *The Mollusks: A Guide to their Study, Collection and Preservation*. American Malacological Society, Pittsburgh, PA.
- Sturm, M., Lotter A. 1995. Lake sediments as environmental archives. *EAWAG News* 38E, 6–9.
- Suckow, A., Morgenstern, U., Kudrass, H.-R. 2001. Absolute dating of recent sediments in the cyclone-influenced shelf area off Bangladesh: comparison of gamma spectrometric (¹³⁷Cs, ²¹⁰Pb, ²²⁸Ra), radiocarbon and ³²Si ages. *Radiocarbon* 43, 917–927.
- Sucré, E.B., Tuttle, J.W., Fox, T.R. 2011. The use of ground-penetrating radar to accurately estimate soil depth in rocky forest soils. *Forest Science* 57, 59–66.
- Sugden, D.E., McCulloch, R.D., Bory, A.J.-M., et al. 2009. Influence of Patagonian glaciers on Antarctic dust deposition during the Last glacial period. *Nature Geoscience* 2, 281–285.
- Sugita, S. 1994. Pollen representation of vegetation in Quaternary sediments: theory and method in patchy vegetation. *Journal of Ecology* 82, 881–897.
- Sugita, S. 2007. Theory of quantitative reconstruction of vegetation I: pollen from large sites REVEALS regional vegetation composition. *The Holocene* 17, 229–241.
- Sulpizio, R., Giaccio, B., Isaia, R., et al. (eds). 2008. Explosive volcanism in the central Mediterranean area during the late Quaternary – linking sources and distal archives. *Journal of Volcanology and Geothermal Research* 177, 1–300.
- Summerhayes, C.P., Thorpe, S.A. 2002. *Oceanography: An Illustrated Guide*, 3rd impr. Manson Publishing, London.
- Sun, D., Gagan, M.K., Cheng, H., et al. 2005. Seasonal and interannual variability of the Mid-Holocene East Asian monsoon in coral δ¹⁸O records from the South China Sea. *Earth and Planetary Science Letters* 237, 69–84.
- Sun, J., Huang, X. 2006. Half-precessional cycles recorded in Chinese loess: response to low-latitude insolation forcing during the Last Interglaciation. *Quaternary Science Reviews* 25, 1065–1072.
- Sun, Q., Chu, G., Liu, J., et al. 2006a. A 150-year record of heavy metals in the varved sediments of Lake Bolterskardet, Svalbard. *Arctic and Alpine Research* 38, 436–445.
- Sun, Y., Clemens, S.C., An, Z., et al. 2006b. Astronomical timescale and palaeoclimatic implication of stacked 3.6-Myr monsoon records from the Chinese Loess Plateau. *Quaternary Science Reviews* 25, 33–48.
- Sun, Y.J., Lai, Z.P., Madsen D., et al. 2012. Luminescence dating of a hearth from the archaeological site of Jiangxigou in the Qinghai Lake area of northeastern Qinghai-Tibetan Plateau. *Quaternary Geochronology* 12, 107–110.
- Surić, M., Richards, D., Hoffman, D.L., et al. 2009. Sea-level change during MIS 5e based on submerged speleothems from eastern Adriatic Sea (Croatia). *Marine Geology* 262, 62–67.
- Sutherland, D.G. 1984. Modern glacier characteristics as a basis for inferring former climates, with particular reference to the Loch Lomond Stadial. *Quaternary Science Reviews* 3, 291–309.
- Svendsen, J.I., Alexanderson, H., Astakhov, V.I., et al. 2004. Late Quaternary ice sheet history of northern Eurasia. *Quaternary Science Reviews* 23, 1229–1271.
- Svensson, A., Nielsen, S.W., Kipfstuhl, S., et al. 2005. Visual stratigraphy of the NorthGRIP ice core during the last glacial period. *Journal of Geophysical Research* 110, D02108, doi: 10.1029/2004JD005134.
- Svensson, A., Andersen, K.K., Bigler, M., et al. 2008. A 60 000 year Greenland stratigraphic ice core chronology. *Climate of the Past* 4, 47–57.
- Svensson, A., Bigler, M., Blunier, T., et al. 2012. Direct linking of Greenland and Antarctic ice cores at the Toba eruption (74 kyr BP). *Climate of the Past* 8, 5389–5427.
- Svensson, H. 2005. From relict polygon patterns in South Scandinavia to active ice wedge polygons in Svalbard: A review of former studies. *Norsk Geografisk Tidsskrift* 59, 164–170.

- Sverdrup, K.A., Kudela, R.M. 2011. *Investigating Oceanography*. McGraw-Hill Companies, Higher Education e-book.
- Sweetman, J.N., LaFace, E., Rühland, K.M., et al. 2008. Evaluating the response of Cladocera to recent environmental changes in lakes from the central Canadian Arctic treeline region. *Arctic, Antarctic, and Alpine Research* 40, 584–591.
- Swindles, G.T., Plunkett, G., Roe, H. 2007. A delayed climatic response to solar forcing at 2800 cal. BP: multiproxy evidence from three Irish peatlands. *The Holocene* 17, 177–182.
- Swingedouw, D., Fichefet, T., Goosse, H., et al. 2009. Impact of transient freshwater releases in the Southern Ocean on the AMOC and climate. *Climate Dynamics* 33, 365–381.
- Sykes, G. 1991. Amino-acid dating. In *Quaternary Dating Methods: A User's Guide* (edited by P.L. Smart, P.D. Francis). Technical Guide 4. Quaternary Research Association, Cambridge, 161–176.
- Sykes, G.A., Collins, M.J., Walton, D.I. 1995. The significance of a geochemically isolated intra-crystalline organic fraction within biominerals. *Organic Geochemistry* 23, 1059–1065.
- Syvitski, J.P.M. 2002. Sediment discharge variability in Arctic rivers: implications for a warmer future. *Polar Research* 21, 323–330.
- Syvitski, J.P.M., Vörösmarty, C.J., Kettner, A.J., et al. 2005. Impact of humans on the flux of terrestrial sediment to the global coastal ocean. *Science* 308, 376–380.
- Szabo, B.J. 1990. Ages of travertine deposits in eastern Grand Canyon National Park, Arizona. *Quaternary Research* 34, 24–32.
- Szostek, K. 2009. Chemical signals and reconstruction of life strategies from ancient human bones and teeth – problems and perspectives. *Anthropological Review* 72, 3–30.
- Takano, Y., Kobayashi, K., Ishikawa, Y., et al. 2005. Emergence of the inflection point on racemization rate constants for d- and l-amino acids in the early stages of terrestrial diagenesis. *Organic Geochemistry* 37, 334–341.
- Támas, T., Onac, B., Bojar, A.-V. 2005. Lateglacial–Middle Holocene stable isotope records in two coeval stalagmites from the Bihor Mountains, NW Romania. *Geological Quarterly* 49, 185–194.
- Tanabe, S., Tateishi, M., Shibata, Y. 2009. The sea-level record of the last deglacial in the Shinano River incised-valley fill, Echigo Plain, central Japan. *Marine Geology* 266, 223–231.
- Tang, K., Feng, X., Ettl, G.J. 2000. The variations in δD of tree-rings and the implications for climatic reconstructions. *Geochimica et Cosmochimica Acta* 64, 1663–1673.
- Tankersley, K.B., Schlecht, K.D., Laub, R.S. 1998. Fluoride dating of mastodon bone from an early palaeoindian spring site. *Journal of Archaeological Science* 25, 805–811.
- Tapley, B.D., Bettadpur, S., Ries, J.C., et al. 2004. GRACE measurements of mass variability in the earth system. *Science* 305, 503–505.
- Tarasov, L., Peltier, W.R. 2004. A geophysically constrained large ensemble analysis of the deglacial history of the North American ice-sheet complex. *Quaternary Science Reviews* 23, 359–388.
- Tattersfield, P., Warui, C.M., Seddon, M.B., et al. 2001. Land-snail faunas of afro-montane forests of Mount Kenya, Kenya: ecology, diversity and distribution patterns. *Journal of Biogeography* 28, 843–861.
- Tauber, H. 1965. Differential pollen dispersal and the interpretation of pollen diagrams. *Danmarks Geologiske Undersøgelse* II, 89, 1–69.
- Taylor, K.C., Alley, R.B.V., Lamorey, G.W., et al. 1997. Electrical measurements on the Greenland Ice Sheet Project 2 core. *Journal of Geophysical Research* 102, 26511–26517.
- Taylor, K.C., Alley, R.B., Meese, D.A., et al. 2004. Dating the Siple Dome (Antarctica) ice core by manual and computer interpretation of annual layering. *Journal of Glaciology* 50, 453–461.
- Tchakerian, V.P. 2009. Palaeoclimatic interpretations from desert dunes and sediments. In *Geomorphology of Desert Environments*, 2nd edn (edited by A.J. Parsons, A. Abrahams). Springer, Dordrecht, 757–772.
- Teixell, A., Bertotti, G., de Lamotte, D.F., et al. 2009. The geology of vertical movements of the lithosphere: an overview. *Tectonophysics* 475, 1–8.
- Telford, R.J. 2006. Limitations of dinoflagellate cyst transfer functions. *Quaternary Science Reviews* 25, 1375–1382.
- Telford, R.J., Heegaard, E., Birks, H.J.B. 2004. All age-depth models are wrong: but how badly? *Quaternary Science Reviews* 23, 1–5.
- Thomas, G.N. 2001. Late Middle Pleistocene pollen bisotratigraphy in Britain: pitfalls and possibilities in the separation of interglacial sequences. *Quaternary Science Reviews* 20, 1621–1630.
- Thomas, G.S.P., Chiverrell, R.C. 2007. Structural and depositional evidence for repeated ice-marginal oscillation along the eastern margin of the Late Devensian Irish Sea Ice Stream. *Quaternary Science Reviews* 26, 2375–2405.
- Thomas, G.S.P., Chiverrell, R.C., Huddart, D. 2004. Ice-marginal depositional responses to readvance episodes in the Late Devensian deglaciation of the Isle of Man. *Quaternary Science Reviews* 23, 85–106.
- Thomas, P.A., Easterbrook, D.J., Clark, P.U. 2000. Early Holocene glaciation on Mount Baker, Washington State, USA. *Quaternary Science Reviews* 19, 1043–1046.
- Thomas, P.J. 2009. Luminescence dating of beachrock in the southeast coast of India – potential for Holocene shoreline reconstruction. *Journal of Coastal Research* 25, 1–7.
- Thompson, D.W.J., Lee, S., Baldwin, M.P. 2003. Atmospheric processes governing the Northern Hemisphere annular mode/North Atlantic Oscillation. In *The North Atlantic Oscillation: Climatic Significance and Environmental Impact* (edited by J. Hurrell, Y. Kushnir, G. Ottersen, et al.). Geophysical Monograph 134. American Geophysical Union, Washington DC, 81–112.
- Thompson, L.G. 2000. Ice core evidence for climate change in the Tropics: implications for our future. *Quaternary Science Reviews* 19, 19–35.
- Thompson, L.G., Yao, T., Davis, M.E., et al. 1997. Tropical climate instability: the last glacial cycle from a Qinghai-Tibetan ice core. *Science* 276, 1821–1825.
- Thompson, L.G., Mosley-Thompson, E., Davis, M.E., et al. 2013. Annually-resolved ice core records of tropical climate variability over the past ~1800 years. *Science* 340, 945–950.
- Thompson, R., Oldfield, F. 1986. *Environmental Magnetism*. Allen and Unwin, London.
- Thompson, R., Price, D., Cameron, N., et al. 2005. Quantitative calibration of remote mountain-lake sediments as climatic recorders of air temperature and ice-cover duration. *Arctic, Antarctic and Alpine Research* 37, 626–635.

514 REFERENCES

- Thompson, W.G., Goldstein, S.L. 2005. Open-system coral ages reveal persistent suborbital sea-level cycles. *Science* 308, 401–404.
- Thompson, W.G., Goldstein, S.L. 2006. A radiometric calibration of the SPECMAP timescale. *Quaternary Science Reviews* 25, 3207–3215.
- Thompson, W.G., Cirri, H.A., Wilson, M.A., et al. 2011. Sea-level oscillations during the last interglacial highstand recorded by Bahamas corals. *Nature Geoscience* 4, 684–687.
- Thompson Davis, P., Menounos, B., Osborn, G. 2009. Holocene and latest Pleistocene alpine glacier fluctuations: a global perspective. *Quaternary Science Reviews* 28, 2021–2033.
- Thorn, C.E., Hall, K. 2002. Nivation and cryoplanation: the case for scrutiny and integration. *Progress in Physical Geography* 26, 533–550.
- Thornalley, D.J.R., Elderfield, H., McCave, I.N. 2010. Intermediate and deep water paleoceanography of the northern North Atlantic over the past 21,000 years. *Paleoceanography* 25, doi: 10.1029/2009PA001833.
- Thornalley, D.J.R., McCave, I.N., Elderfield, H. 2011. Tephra in deglacial ocean sediments south of Iceland: stratigraphy, geochemistry and oceanic reservoir ages. *Journal of Quaternary Science* 26, 190–198.
- Thorne, P.D., Hanes, D.M. 2002. A review of acoustic measurement of small-scale sediment processes. *Continental Shelf Research* 22, 603–632.
- Thorpe, P.W. 1981. A trimline method for defining the upper limit of Loch Lomond Advance glaciers: examples from the Loch Leven and Glen Coe areas. *Scottish Journal of Geology* 17, 49–64.
- Thorson, R.M. 2000. Glacial tectonics: a deeper perspective. *Quaternary Science Reviews* 14–15, 1391–1398.
- Thunell, R.C., Varela, R., Llano, M., et al. 2000. Organic carbon fluxes, degradation, and accumulation in an anoxic basin: sediment trap results from the Cariaco Basin. *Limnology and Oceanography* 45, 300–308.
- Tietze, E., De Francesco, C.G. 2012. Compositional fidelity of subfossil mollusk assemblages in streams and lakes of the south-eastern Pampas, Argentina. *Palaios* 27, 401–413.
- Timm, O., Timmermann, A. 2007. Simulation of the last 21 000 years using accelerated transient boundary conditions. *Journal of Climate* 20, 4377–4401.
- Timmermann, A., An, S.-I., Krebs, U., et al. 2005. ENSO Suppression due to weakening of the North Atlantic Thermohaline Circulation. *Journal of Climate* 18, 3122–3139.
- Timmermann, A., Timm, O., Stott, L., et al. 2009. The roles of CO₂ and orbital forcing in driving Southern Hemispheric temperature variations during the last 21 000 yr. *Journal of Climate* 22, 1626–1640.
- Tinner, W., Hubschmid, P., Wehrli, M., et al. 1999. Long-term forest fire ecology and dynamics in southern Switzerland. *Journal of Ecology* 87, 273–289.
- Tobolski, K., Ammann, B. 2000. Macrofossils as records of plant responses to rapid Late Glacial climatic changes at three sites in the Swiss Alps. *Palaeogeography, Palaeoclimatology, Palaeoecology* 159, 251–259.
- Tomescu, A.M.F. 2000. Evaluation of Holocene pollen records from the Romanian Plain. *Review of Palaeobotany and Palynology* 109, 219–233.
- Tonni, E.P., Cione, A.L., Figini, A.J. 1999. Predominance of arid climates indicated by mammals in the pampas of Argentina during the Late Pleistocene and Holocene. *Palaeogeography, Palaeoclimatology, Palaeoecology* 147, 257–281.
- Tooth, S. 2000. Process, form and change in dryland rivers: a review of recent research. *Earth-Science Reviews* 51, 67–107.
- Torfstein, A., Haase-Schramm, A., Waldmann, N., et al. 2009. U-series and oxygen isotope chronology of the mid-Pleistocene Lake Amora (Dead Sea basin). *Geochimica et Cosmochimica Acta* 73, 2603–2630.
- Torfstein, A., Goldstein, S.L., Stein, M.I. 2013. Impacts of abrupt climate changes in the Levant from Last Glacial Dead Sea levels. *Quaternary Science Reviews* 69, 1–7.
- Törnqvist, T.E. 2007. Fluvial environments: responses to rapid environmental change. In *Encyclopedia of Quaternary Science* (edited by S.A. Elias). Elsevier, Amsterdam, 686–694.
- Törnqvist, T.E., González, J.L., Newsom, L.A., et al. 2004. Deciphering Holocene sea-level history on the US Gulf Coast: a high-resolution record from the Mississippi Delta. *Geological Society of America Bulletin* 116, 1026–1039.
- Torres, V., Hooghiemstra, H., Lourens, L., et al. 2013. Astronomical tuning of long pollen records reveals the dynamic history of montane biomes and lake levels in the tropical high Andes during the Quaternary. *Quaternary Science Reviews* 63, 59–72.
- Toyoda, S., Tsukamoto, S., Hameau, S., et al. 2006. Dating of Japanese tephras by ESR and luminescence methods. *Quaternary Geochronology* 1, 320–326.
- Trauth, M.H., Deino, A., Strecker, M.R. 2001. Response of the East African climate to orbital forcing during the last interglacial (130–117 ka) and the early last glacial (117–60 ka). *Geology* 29, 499–503.
- Trauth, M.H., Maslin, M.A., Deino, A., et al. 2005. Late Cenozoic moisture history of East Africa. *Science* 23, 2051–2053.
- Trimble Navigation. GPS Tutorial, http://www.trimble.com/gps_tutorial/.
- Tripaldi, A., Forman, S.L. 2007. Geomorphology and chronology of Late Quaternary dune fields of western Argentina. *Palaeogeography, Palaeoclimatology, Palaeoecology* 251, 300–320.
- Tripevich, N., Eerkens, J.W., Carpenter, T.R. 2012. Obsidian hydration at high elevation: archaic quarrying at the Chivay source, southern Peru. *Journal of Archaeological Science* 39, 1360–1367.
- Tröftén, P.-E. 2000. The use of varved clay chronology for dating palaeoseismic events: the Erstavik record in the Stockholm area, south Sweden. *Sedimentary Geology* 130, 167–181.
- Tsai, H., Hsue, Z.-Y., Huang, W.-S., et al. 2007. Pedogenic approach to resolving the geomorphic evolution of the Pakua river terraces in central Taiwan. *Geomorphology* 83, 14–28.
- Tsatskin, A., Ronen, A. 1999. Micromorphology of a Mousterian paleosol in aeolianites at the site Habonim, Israel. *Catena* 34, 365–384.
- Tschumi, T., Joos, F., Gehlen, M., et al. 2010. Deep ocean ventilation, carbon isotopes, marine sedimentation and the deglacial CO₂ rise. *Climate of the Past* 7, 771–800.
- Tudhope, A.W., Chilcott, C.P., McCulloch, M.T., et al. 2001. Variability in the El Niño–Southern Oscillation through a glacial–interglacial cycle. *Science* 291, 1511–1517.

- Tuovinen, N., Virtasalo, J.J., Kotilainen, A.T. 2008. Holocene diatom stratigraphy in the Archipelago Sea, northern Baltic Sea. *Journal of Paleolimnology* 40, 793–807.
- Turner, M.B., Cronin, S.J., Bebbington, M.S., et al. 2008. Developing probabilistic eruption forecasts for dormant volcanoes: a case study from Mt Taranaki, New Zealand. *Bulletin of Volcanology* 70, 507–515.
- Turner-Walker, G. 2008. The chemical and microbial degradation of bones and teeth. In *Advances in Human Palaeopathology* (edited by R. Pinhasi, S. Mays). John Wiley, Chichester and New York, 3–30.
- Turner, C.S.M., Lowe, J.J. 2001. Tephrochronology. In *Tracking Environmental Change Using Lake Sediments. Volume 1: Basin Analysis, Coring and Chronological Techniques* (edited by J.P. Last, W.M. Smol). Kluwer, Dordrecht, 451–471.
- Turner, C.S.M., Brown, H. 2007. Catastrophic early Holocene sea level rise, human migration and the Neolithic transition in Europe. *Quaternary Science Reviews* 26, 2036–2041.
- Turner, C.S.M., Coopé, G.R., Harkness, D.D., et al. 2000. Implications for the dating of Wisconsinan (Weichselian) Lateglacial events of radiocarbon age differences between terrestrial macrofossils from a site in SW Ireland. *Quaternary Research* 53, 114–121.
- Tweddle, J.C., Edwards, K.J. 2010. Pollen preservation zones as an interpretative tool in Holocene palynology. *Review of Palaeobotany and Palynology* 161, 59–76.
- Twiddale, C.L., Bunting, M.J. 2010. Experimental investigations into the preservation of pollen grains: a pilot study of four pollen types. *Review of Palaeobotany and Palynology* 162, 621–630.
- Tyrácek, J., Havlíček, P. 2009. The fluvial record in the Czech Republic: a review in the context of IGCP 518. *Global and Planetary Change* 68, 311–325.
- Tzedakis, P.C., McManus, J.F., Hooghiemstra, H., et al. 2003. Comparison of changes in vegetation in northeast Greece with records of climatic variability on orbital and suborbital frequencies over the last 450,000 years. *Earth and Planetary Science Letters* 212, 197–212.
- Tzedakis, P.C., Roucoux, K.H., de Abreu, L., et al. 2004. The duration of forest stages in Southern Europe and interglacial climate variability. *Science* 306, 2231–2235.
- Tzedakis, P.C., Channell, J.E.T., Hodell, D.A., et al. 2012. Determining the natural length of the current interglacial. *Nature Geoscience* 5, 138–141.
- Tziperman, E., Gildor, H. 2003. On the mid-Pleistocene transition to 100-kyr glacial cycles and the asymmetry between glaciation and deglaciation times. *Paleoceanography* 18, doi: 10.1029/2001PA000627.
- Ubelaker, D.H., Zarenko, K.M. 2011. Adipocere: what is known after over two centuries of research? *Forensic Science International* 208, 167–172.
- Valentine, K.W.G., Dalrymple, J.B. 1975. The identification, lateral variation and chronology of two buried palaeocatenas at Woodhall Spa and West Runton, England. *Quaternary Research* 4, 551–590.
- Valero-Garcés, B.L., Arenas, C., Delgada-Huertas, A. 2001. Depositional environments of Quaternary lacustrine travertine and stromatolites from high-altitude Andean lakes, northwestern Argentina. *Canadian Journal of Earth Sciences* 38, 1263–1283.
- Van Calsteren, P., Thomas, L. 2006. Uranium-series dating applications in natural environmental science. *Earth-Science Reviews* 75, 155–175.
- Van den Bergh, G.D., Meijer, H.J.M., Awe, R.D., et al. 2009. The Liang Bua faunal remains: a 95 k.yr. sequence from Flores, East Indonesia. *Journal of Human Evolution* 57, 527–537.
- Vandenberge, J. 1988. Cryoturbations. In *Advances in Periglacial Geomorphology* (edited by M.J. Clark). John Wiley, Chichester and New York, 179–198.
- Vandenberge, J. 2003. Climate forcing of fluvial system development: an evolution of ideas. *Quaternary Science Reviews* 22, 2053–2060.
- Vandenberge, J., Woo, M. 2002. Modern and ancient periglacial river types. *Progress in Physical Geography* 26, 479–506.
- Vandenberge, J., Zhijiu, C., Liang, Z., et al. 2004. Thermal-contraction-crack networks as evidence for late-Pleistocene permafrost in Inner Mongolia, China. *Permafrost and Periglacial Processes* 15, 21–29.
- Van den Bogard, P. 1995. $^{40}\text{Ar}/^{39}\text{Ar}$ ages of sanidine phenocrysts from Laacher See Tephra (12,900 yrs BP): chronostratigraphic and petrologic significance. *Earth and Planetary Science Letters* 133, 163–174.
- Van den Haute, P., Corte, F. (eds). 1998. *Advances in Fission Track Geochronology*. Kluwer, Dordrecht.
- Van der Geer, A., Lyras, G., de Vos, J., et al. 2010. *Evolution of Island Mammals: Adaptation and Extinction of Placental Mammals on Islands*. Wiley-Blackwell, Hoboken, NJ.
- Vandergoes, M.C., Dieffenbacher-Krall, A.C., Newham, R.M., et al. 2008. Cooling and changing seasonality in the Southern Alps, New Zealand during the Antarctic Cold Reversal. *Quaternary Science Reviews* 27, 589–601.
- Vandergroes, M.J., Prior, C.A. 2003. The AMS dating of pollen concentrates: a methodological study of Late Quaternary sediments from South Westland, New Zealand. *Radiocarbon* 45, 479–491.
- Van der Knaap, W.O., Lamentowicz, M., van Leeuwen, J.F.N., et al. 2011. A multi-proxy, high-resolution record of peatland development and its drivers during the last millennium from the subalpine Swiss Alps. *Quaternary Science Reviews* 30, 3467–3480.
- Van der Knaap, W.O., van Leeuwen, F.F.N., Finsinger, W., et al. 2005. Migration and population expansion of *Abies*, *Fagus*, *Picea* and *Quercus* since 15000 years in and across the Alps, based on pollen-percentage threshold values. *Quaternary Science Reviews* 24, 645–680.
- Van der Meer, J.J.M., Menzies, J., Rose, J. 2003. Subglacial till: the deforming glacier bed. *Quaternary Science Reviews* 22, 1659–1685.
- Van der Plicht, J., van der Sanden, W.A.B., Aerts, A.T., et al. 2004. Dating of bog bodies by means of ^{14}C -AMS. *Journal of Archaeological Science* 31, 471–491.
- Van der Veen, M. 2007. Formation processes of desiccated and carbonized plant remains—the identification of routine practice. *Journal of Archaeological Science* 34, 968–990.

516 REFERENCES

- Van der Zwaan, G.J., Duijnstee, I.A.P., den Dilk, M., *et al.* 1999. Benthic foraminifers: proxies or problems? A review of paleoecological concepts. *Earth-Science Reviews* 46, 213–236.
- Van Geel, B., Aptroot, A. 2006. Fossil ascomycetes in Quaternary deposits. *Nova Hedwigia* 82, 313–329.
- Van Geel, B., Coope, G.R., van der Hammen, T. 1989. Palaeoecology and stratigraphy of the Lateglacial type section at Usselo (the Netherlands). *Review of Palaeobotany and Palynology* 60, 25–129.
- Van Geel, B., Buurman, J., Waterbolk, H.T. 1996. Archaeological and palaeoecological indications for an abrupt climate change in the Netherlands and evidence for climatological teleconnections around 2650 BP. *Journal of Quaternary Science* 11, 451–460.
- Van Geel, B., van der Plicht, J., Renssen, H. 2003. Major $\Delta^{14}\text{C}$ excursions during the late glacial and early Holocene: changes in ocean ventilation or solar forcing of climate change. *Quaternary International* 105, 71–76.
- Van Geel, B., Bokovenko, N.A., Burova, N.D., *et al.* 2004. Climate change and the expansion of the Scythian culture after 850 BC, a hypothesis. *Journal of Archaeological Science* 31, 1735–1742.
- Van Geel, B., Zazula, G.D., Schweger, C.E. 2007. Spores of coprophilous fungi from under the Dawson tephra (25,300 ^{14}C years BP), Yukon Territory, northwestern Canada. *Palaeogeography, Palaeoclimatology, Palaeoecology* 252, 481–485.
- Van Geel, B., Aptroot, A., Baittinger, C., *et al.* 2008. The ecological implications of a Yakutian mammoth's last meal. *Quaternary Research* 69, 361–376.
- Van Huissteden, K., Vandenberghe, J., Pollard, D. 2003. Palaeotemperature reconstructions of the European permafrost zone during marine oxygen isotope stage 3 compared with climate model results. *Journal of Quaternary Science* 18, 453–464.
- Van Koenigswald, W., van Kolfschoten, T. 1996. The *Mimomys-Arvicola* boundary and the enamel thickness quotient (SDQ) of Arvicola as stratigraphic markers in the Middle Pleistocene. In *The Early–Middle Pleistocene in Europe* (edited by C. Turner). Balkema, Rotterdam, 211–226.
- Van Leeuwen, R.J.W., Beets, D.J., *et al.* 2000. Stratigraphy and integrated facies analysis of the Saalian and Eemian sediments in the Amsterdam-Terminal borehole. *Geologie en Mijnbouw (Netherlands Journal of Geosciences)* 79, 161–196.
- Van Raden, U.J., Colombaroli, D., Gilli, A., *et al.* 2013. High-resolution late-glacial chronology for the Gerzensee lake record (Switzerland): $\delta^{18}\text{O}$ correlation between a Gerzensee-stack and NGRIP. *Palaeogeography, Palaeoclimatology, Palaeoecology* 391, 13–24.
- Vardy, M.E., Pinson, J.J.W., Bull, J.M., *et al.* 2010. 3D seismic imaging of buried Younger Dryas mass movement flows: Lake Windermere, UK. *Geomorphology* 118, 176–187.
- Varela, S., Lobo, J.M., Rodriguez, J., *et al.* 2010. Were the Late Pleistocene climatic changes responsible for the disappearance of the European spotted hyena populations? Hindcasting a species geographic distribution across time. *Quaternary Science Reviews* 29, 2027–2035.
- Vaughan, A.P.M., Dowling, L.A., Mitchell, F.J., *et al.* 2004. Depositional and post-depositional history of warm stage deposits at Knocknacran, Co. Monaghan, Ireland: implications for preservation of Irish last interglacial deposits. *Journal of Quaternary Science* 19, 577–590.
- Velichkevich, F.Y., Zastawniak, E. 2008. *Atlas of the Pleistocene Vascular Plant Macrofossils of Central and Eastern Europe – Part 2: Herbaceous Dicotyledones*. Polish Academy of Sciences, W. Szafer Institute of Botany, Krakow.
- Veres, D., Bazin, L., Landais, A., *et al.* 2012. The Antarctic ice core chronology (AICC2012): an optimised multi-parameter and multi-site dating approach for the last 120 thousand years. *Climate of the Past Discussions* 8, 6011–1049.
- Verleye, T.J., Louwye, S. 2010. Late Quaternary environmental changes and latitudinal shifts of the Antarctic Circumpolar Current as recorded by dinoflagellate cysts from offshore Chile (40°S). *Quaternary Science Reviews* 29, 1025–1039.
- Verschuren, D., Eggermont, H. 2006. Quaternary paleoecology of aquatic Diptera in tropical and Southern Hemisphere regions, with special reference to the Chironomidae. *Quaternary Science Reviews* 25, 1926–1947.
- Veski, S., Heinsalu, A., Klassen, V., *et al.* 2005a. Early Holocene coastal sediments and palaeoenvironment on the shore of the Baltic Sea at Pärnu, southwestern Estonia. *Quaternary International* 130, 75–85.
- Veski, S., Koppel, K., Poska, A. 2005b. Integrated palaeoecological and historical data in the service of fine-resolution land use and ecological change assessment during the last 1000 years in Rõuge, southern Estonia. *Journal of Biogeography* 32, 1473–1488.
- Veski, S., Amon, L., Heinsalu, A., *et al.* 2012. Lateglacial vegetation dynamics in the eastern Baltic region between 14,500 and 11,400 cal yr BP: a complete record since the Bølling (GI-1e) to the Holocene. *Quaternary Science Reviews* 40, 39–53.
- Viau, A.E., Gajewski, K. 2001. Holocene variations in the global hydrological cycle quantified by objective gridding of lake level databases. *Journal of Geophysical Research* 106, 31703–31716.
- Viehberg, F.A., Mesquita-Joanes, F. 2012. Quantitative transfer function approaches in palaeoclimatic reconstruction using Quaternary ostracods. In *Developments in Quaternary Science. Volume 17: Ostracoda as Proxies for Quaternary Climate Change* (edited by D.J. Horne, J.A. Holmes, J. Rodriguez-Lazaro, *et al.*). Elsevier, Amsterdam, 47–64.
- Viklund, K. 2011. Flax in Sweden: the archaeobotanical, archaeological and historical evidence. *Vegetation History and Archaeobotany* 20, 509–515.
- Viles, H., Goudie, A., Grab, S., *et al.* 2011. The use of the Schmidt hammer and Equotip for rock hardness assessment in geomorphology and heritage science: a comparative analysis. *Earth and Planetary Science Letters* 36, 320–333.
- Vimeux, F., Ginot, P., Schwikowski, M., *et al.* 2009. Climate variability during the last 1000 years inferred from Andean ice core: a review of methodology and recent results. *Palaeogeography, Palaeoclimatology, Palaeoecology* 281, 229–241.
- Vink, A., Steffen, H., Reinhardt, L., *et al.* 2007. Holocene relative sea-level change, isostatic subsidence and the radial viscosity structure of the mantle of northwest Europe (Belgium, the Netherlands, Germany, southern North Sea). *Quaternary Science Reviews* 26, 3249–3275.

- Vinther, B.M., Clausen, H.B., Johnsen, S.J., et al. 2006. A synchronised dating of three Greenland ice cores throughout the Holocene. *Journal of Geophysical Research* 111, D13201, doi: 10.1029/2005JD006921.
- Voelker, A.H.L. 2002. Global distribution of centennial-scale records for marine isotope stage (MIS)3: a database. *Quaternary Science Reviews* 21, 1185–1212.
- Voelker, A.H.L., Grootes, P.M., Nadeau, M.-J., et al. 2000. Radiocarbon levels in the Iceland Sea from 25–53 kyr and their link to the earth's magnetic field. *Radiocarbon* 42, 437–452.
- Voinchet, P., Despriée, J., Tissoux, H., et al. 2010. ESR chronology of alluvial deposits and first human settlement of the Middle Loire Basin (Region Centre, France). *Quaternary Geochronology* 5, 381–384.
- Völk, J., Grunert, J. 1990. To the problem of dune formation and dune weathering during the Late Pleistocene and Holocene in the southern Sahara and the Sahel. *Zeitschrift für Geomorphologie* 34, 1–17.
- Vonmoos, M., Beer, J., Muscheler, R. 2006. Large variations in Holocene solar activity: constraints from ^{10}Be in the Greenland Ice Core project ice core. *Journal of Geophysical Research* 111, A10105, doi: 10.1029/2005JA011500.
- Vork, K.A., Thomsen, E. 1996. Lusitanian/Mediterranean ostracods in the Holocene of Denmark: implications for the interpretation of winter temperatures during the postglacial temperature maximum. *The Holocene* 6, 423–432.
- Vorren T.O., Plassen, L. 2008. Deglaciation and palaeoclimate of the Andfjord Vågsfjord area, North Norway. *Boreas* 31, 97–125.
- Vött, A. 2007. Relative sea level changes and regional tectonic evolution of seven coastal areas in NW Greece since the mid-Holocene. *Quaternary Science Reviews* 26, 894–919.
- Waelbroeck, C., Labeyrie L., Michel E., et al. 2002. Sea-level and deepwater temperature changes derived from benthic foraminifera isotopic records. *Quaternary Science Reviews* 21, 295–305.
- Waelbroeck, C., Mulitza, S., Spero, H., et al. 2005. A global compilation of late Holocene planktonic foraminiferal $\delta^{18}\text{O}$: relationship between surface water temperature and $\delta^{18}\text{O}$. *Quaternary Science Reviews* 24, 853–868.
- Wagner, G.A. 1998. *Age Determination of Young Rocks and Artefacts*. Springer, Heidelberg, Berlin and New York.
- Wagner, G.A., van den Haute, P. 1992. *Fission Track Dating*. Kluwer, Dordrecht.
- Wagner, G., Masarik, J., Beer, J., et al. 2000. Reconstruction of the geomagnetic field between 20 and 60 kyr BP from cosmogenic radionuclides in the GRIP ice core. *Nuclear Instruments and Methods in Physics Research Section B: Beam Interactions with Materials and Atoms* 172, 597–604.
- Walden, J., Oldfield, F., Smith, J. (eds). 1999. *Environmental Magnetism: a Practical Guide*. Technical Guide 6. Quaternary Research Association, London.
- Walker, M.J.C. 1995. Climatic changes in Europe during the Last Glacial/Interglacial Transition. *Quaternary International* 28, 63–76.
- Walker, M.J.C. 2001. Rapid climate change during the last glacial–interglacial transition; implications for stratigraphic subdivision, correlation and dating. *Global and Planetary Change* 30, 59–72.
- Walker, M. 2005. *Quaternary Dating Methods*. John Wiley, Chichester and New York.
- Walker, M.J.C., Lowe, J.J. 1990. Reconstructing the environmental history of the last glacial–interglacial transition: evidence from the Isle of Skye, Inner Hebrides, Scotland. *Quaternary Science Reviews* 9, 15–49.
- Walker, M.J.C., Merritt, J.W., Auton, C.A., et al. 1992. Allt Odhar and Dalcharrn: two pre-Late Devensian sites in northern Scotland. *Journal of Quaternary Science* 7, 69–86.
- Walker, M.J.C., Coope, G.R., Lowe, J.J. 1993. The Devensian (Weichselian) Lateglacial palaeoenvironmental record from Gransmoor, East Yorkshire, England. *Quaternary Science Reviews* 12, 659–680.
- Walker, M.J.C., Björck, S., Lowe, J.J., et al. 1999. Isotopic ‘events’ in the GRIP ice core: a stratotype for the Late Pleistocene. *Quaternary Science Reviews* 18, 1143–1151.
- Walker, M.J.C., Bryant, C., Coope, G.R., et al. 2001. Towards a radiocarbon chronology for the Lateglacial: sample selection strategies. *Radiocarbon* 43, 1007–1020.
- Walker, M.J.C., Coope, G.R., Sheldrick, C., et al. 2003. Devensian Lateglacial environmental changes in Britain: a multi-proxy environmental record from Llanilid, South Wales, UK. *Quaternary Science Reviews* 22, 475–520.
- Walker, M., Johnson S., Rasmussen S.O., et al. 2009. Formal definition and dating of the GSSP (Global Stratotype Section and Point) for the base of the Holocene using the Greenland NGRIP ice core, and selected auxiliary records. *Journal of Quaternary Science* 24, 3–17.
- Walker, M.J.C., Berkhalmer, M., Björck, S., et al. 2012. Formal subdivision of the Holocene Series/Epoch: a Discussion Paper by a Working Group of INTIMATE (Integration of ice-core, marine and terrestrial records) and the Subcommission on Quaternary Stratigraphy (International Commission on Stratigraphy). *Journal of Quaternary Science* 27, 649–659.
- Walker, S.E., Goldstein, S.T. 1999. Taphonomic tiering: experimental field taphonomy of molluscs and foraminifera above and below the sediment–water interface. *Palaeogeography, Palaeoclimatology, Palaeoecology* 149, 227–244.
- Walkington, H. 2010. Soil science applications in archaeological contexts: a review of key challenges. *Earth-Science Reviews* 103, 122–134.
- Wallin, J.-E. 1996. History of sedentary farming in Ångermanland, northern Sweden, during the Iron Age and Medieval period based on pollen analytical investigations. *Vegetation History and Archaeobotany* 5, 301–312.
- Wallis, L.A. 2001. Environmental history of northwest Australia based on phytolith analysis at Carpenter's Gap 1. *Quaternary International* 83–85, 103–117.
- Walsh, S. 2005. The role of stratotypes in stratigraphy. Part 1. Stratotype functions. *Earth-Science Reviews* 69, 307–332.
- Walsh, S.J., Butler, D.R., Malanson, J.P., et al. 2003. Mapping, modeling, and visualization of the influences of geomorphic processes on the alpine treeline ecotone, Glacier National Park, MT, USA. *Geomorphology* 53, 129–145.
- Wanamaker Jr., A.D., Hetzinger, S., Halfar, J. 2011. Reconstructing mid- to high-latitude marine climate and ocean variability using

- bivalves, coralline algae, and marine sediment cores from the Northern Hemisphere. *Palaeogeography, Palaeoclimatology, Palaeoecology* 302, 1–9.
- Wang, H., Hughes, R.E., Steele, J.D., et al. 2003. Correlation of climatic cycles in middle Mississippi Valley loess and Greenland ice. *Geology* 31, 179–182.
- Wang, L., Sarnthein, M., Grootes, P.M., et al. 1999. Millennial reoccurrence of century-scale abrupt events of East Asian monsoon: a possible heat conveyor for the global deglaciation. *Paleoceanography* 14, 725–731.
- Wang, L., Duan, J., Chen, J., et al. 2010. Temperature reconstruction from tree-ring maximum density of Balfour spruce in eastern Tibet, China. *International Journal of Climatology* 30, 972–979.
- Wang, X., Dong, Z., Zhang, J., et al. 2004. Formation of the complex linear dunes in the central Taklimakan Sand Sea, China. *Earth Surface Processes and Landforms* 29, 677–686.
- Wang, X., Auler, A.S., Edwards, R.L., et al. 2006. Interhemispheric anti-phasing of rainfall during the last glacial period. *Quaternary Science Reviews* 25, 3391–3403.
- Wang, Y., Amundson, R., Trumbore, S. 1996. Radiocarbon dating of soil organic matter. *Quaternary Research* 45, 282–288.
- Wang, Y.J., Cheng, H., Edwards, R.L., et al. 2001. A high-resolution absolute-dated Late Pleistocene monsoon record from Hulu Cave, China. *Science* 294, 2345–2348.
- Wang, Y., Cheng, H., Edwards, R.L., et al. 2008. Millennial- and orbital-scale changes in the East Asian monsoon over the past 224,000 years. *Nature* 451, 1090–1093.
- Wanner, H., Solomina, O., Grosjean, M., et al. 2011. Structure and origin of Holocene cold events. *Quaternary Science Reviews* 30, 3109–3123.
- Washburn A.L. 1980. Permafrost features as evidence of climatic change. *Earth-Science Reviews* 15, 327–402.
- Wastegård, S., Rasmussen, T. 2001. New tephra horizons from Oxygen Isotope Stage 5 in the North Atlantic: correlation potential for terrestrial, marine and ice-core archives. *Quaternary Science Reviews* 20, 1587–1593.
- Watanabe, O., Jouzel, J., Johnsen, S., et al. 2003b. Homogeneous climate variability across East Antarctica over the past three glacial cycles. *Nature* 422, 509–512.
- Watanabe, S., Ayta, W.E.F., Hamaguci, H., et al. 2003a. Some evidence of a date of first humans to arrive in Brazil. *Journal of Archaeological Science* 30, 351–354.
- Watanabe, T., Nakamura, T., Watanabe Nara, F., et al. 2009. High-time resolution AMS ^{14}C data sets for Lake Baikal and Lake Hovsgol sediment cores: changes in radiocarbon age and sedimentation rates during the transition from the last glacial to the Holocene. *Quaternary International* 205, 12–20.
- Watchman, A. 2000. A review of the history of dating rock varnishes. *Earth-Science Reviews* 49, 261–277.
- Watson, A.J., Bakker, D.C.E., Ridgwell, A.J., et al. 2000. Effect of iron supply on Southern Ocean CO_2 uptake and implications for atmospheric CO_2 . *Nature* 407, 730–733.
- Watson, E., Luckman, B.H. 2001. Dendroclimatic reconstruction of precipitation for sites in the southern Canadian Rockies. *The Holocene* 11, 203–213.
- Webb, S.D., Graham, R.W., Barnosky, A.D., et al. 2003b. Vertebrate paleontology. In *Developments in Quaternary Science. Volume 1: The Quaternary Period in the United States* (edited by A.R. Gillespie, S.C. Porter, B.F. Atwater). Elsevier, Amsterdam, 519–538.
- Webb III, T., Ruddiman, W.F., Street-Perrott, F.A., et al. 1993. Climatic changes during the past 18,000 years: regional syntheses, mechanisms and causes. In *Global Climates Since the Last Glacial Maximum* (edited by H.E. Wright Jr., J.E. Kutzbach, T. Webb III, et al.). University of Minnesota Press, Minneapolis and London, 514–535.
- Webb III, T., Shuman, B., Williams, J.W. 2003a. Climatically forced vegetation dynamics in eastern North America during the Late Quaternary Period. In *Developments in Quaternary Science. Volume 1: The Quaternary Period in the United States* (edited by A.R. Gillespie, S.C. Porter, B.F. Atwater). Elsevier, Amsterdam, 459–478.
- Weber, S.L. 2010. The utility of Earth system Models of Intermediate Complexity (EMICs). *Wiley Interdisciplinary Reviews: Climate Change* 1, 243–252.
- Weber, S.L., Drijfhout, S.S., Abe-Ouchi, A., et al. 2007. The modern and glacial overturning circulation in the Atlantic ocean in PMIP coupled model simulations. *Climate of the Past* 3, 51–64.
- Webster, R., Oliver, M.A. 2000. *Geostatistics for Environmental Scientists*. Wiley, Chichester.
- Wehmiller, J.F., Miller, G.H. 2000. Aminostratigraphic dating methods in Quaternary geology. In *Quaternary Geochronology, Methods and Applications* (edited by J.S. Noller, J.M. Sowers, W.R. Letts). American Geophysical Union, Washington, DC, 187–222.
- Weidman, C.R., Jones, G.A., Lohmann, K.C. 1994. The long-lived mollusc *Arctica islandica*: a new paleoceanographic tool for the reconstruction of bottom temperatures for the continental shelves of the northern North Atlantic Ocean. *Journal of Geophysical Research* 99, 18305–18314.
- Weiss, D., Shotyk, W., Kempf, O. 1999. Archives of atmospheric lead pollution. *Naturwissenschaften* 86, 262–275.
- Weldeab, S. 2012. Bipolar modulation of millennial-scale West African monsoon variability during the last glacial (75,000–25,000 years ago). *Quaternary Science Reviews* 40, 21–29.
- Weng, C., Hooghiemstra, H. and Duivenvoorden, J.F. 2006. Challenges in estimating past plant diversity from fossil pollen data: statistical assessment, problems and possible solutions. *Biodiversity and Distributions* 12, 310–318.
- Weninger, B., Jöris, O. 2008. A ^{14}C age calibration curve for the last 60 ka: the Greenland-Hulu U/Th timescale and its impact on understanding the Middle to Upper Paleolithic transition in Western Eurasia. *Journal of Human Evolution* 55, 772–781.
- Werdelin, L., Lewis, M.E. 2005. Plio–Pleistocene Carnivora of eastern Africa: species richness and turnover patterns. *Zoological Journal of the Linnean Society* 144, 121–144.
- Werner, C.M., Mason, J.A., Hanson, P.R. 2011. Non-linear connections between dune activity and climate in the High Plains, Kansas and Oklahoma, USA. *Quaternary Research* 75, 267–277.

- Werner, M., Mikolajewicz, U., Heimann, M., et al. 2000. Borehole versus isotope temperatures on Greenland: seasonality does matter. *Geophysical Research Letters* 27:723–7726.
- West, R.G. 1977. *Pleistocene Geology and Biology*, 2nd edn. Longman, London.
- West, R.G. 2000. *Plant Life of the Quaternary Cold Stages*. Cambridge University Press, Cambridge.
- Westaway, R. 2002. Geomorphological consequences of weak lower continental crust, and its significance for studies of uplift, landscape evolution, and the interpretation of river terrace sequences. *Geologie en Mijnbouw (Netherlands Journal of Geosciences)* 81, 283–303.
- Westaway, R. 2009. Calibration of decomposition of serine to alanine in *Bithynia opercula* as a quantitative dating technique for Middle and Late Pleistocene sites in Britain. *Quaternary Geochronology* 4, 241–259.
- Westaway, R., Bridgland, D.R., Sinha, R., Demir, T. 2009. Fluvial sequences as evidence for landscape and climatic evolution in the Late Cenozoic: a synthesis of data from IGCP 518. *Global and Planetary Change* 68, 237–253.
- Westgate, J. 1989. Isothermal plateau fission track ages of hydrated glass shards from silicic tephra beds. *Earth and Planetary Science Letters* 95, 226–234.
- Westgate, J.A., Preece, S.J., Froese, D.G., et al. 2001. Dating Early and Middle (Reid) Pleistocene glaciations in central Yukon by tephrochronology. *Quaternary Research* 56, 335–348.
- White, W.B. 2007. Cave sediments and paleoclimate. *Journal of Cave and Karst Studies* 69, 76–93.
- Whitehouse, N.J. 2006. The Holocene British and Irish ancient forest fossil beetle fauna: implications for forest history, biodiversity and faunal colonisation. *Quaternary Science Reviews* 25, 1755–1789.
- Whitehouse, N.J., Smith, D. 2010. How fragmented was the British Holocene wildwood? Perspectives on the 'Vera' grazing debate from the fossil beetle record. *Quaternary Science Reviews* 29, 539–553.
- Whiteman, C.A., Kemp, R.A. 1990. Pleistocene sediments, soils and landscape evolution at Stebbing, Essex. *Journal of Quaternary Science* 5, 145–161.
- Whitlock, C., Bianchi, M.M., Bartlein, P.J., et al. 2006. Postglacial vegetation, climate, and fire history along the east side of the Andes (lat 41–42.5°S), Argentina. *Quaternary Research* 66, 187–201.
- Whitmore, J., Gajewski, K., Sawada, M., et al. 2005. Modern pollen data from North America and Greenland for multi-scale paleoenvironmental applications. *Quaternary Science Reviews* 24, 1828–1848.
- Widdowson, M. 2007. Laterite and Ferricrete. In *Geochemical Sediments and Landscapes* (edited by D.J. Nash, S.J. McLaren). Blackwell, Oxford.
- Wiersma, A.P., Riche, D.M., Renssen, H. 2011. Fingerprinting the 8.2 ka event climate response in a coupled climate model. *Journal of Quaternary Science* 26, 118–127.
- Wild, M.T., Tabner, B.J., Macdonald, R. 1999. ESR dating of quartz phenocrysts in some rhyolitic extrusive rocks using Ti and Al impurity centres. *Quaternary Science Reviews* 18, 1507–1514.
- Wiles, G.C., Barclay, D.J., Young, N.E. 2010. A review of lichenometric dating of glacial moraines in Alaska. *Geografiska Annaler* 92, 101–109.
- Wilkins, D., De Deckker, P., Fifield, L.K., et al. 2012. Comparative optical and radiocarbon dating of laminated Holocene sediments in two maar lakes: Lake Kellambete and Lake Gnotuk, south-western Victoria, Australia. *Quaternary Geochronology* 9, 3–15.
- Willerslev, E., Cooper, A. 2005. Ancient DNA. *Proceedings of the Royal Society of London B* 272, 3–16.
- Willerslev, E., Cappellini, E., Boomsma, W., et al. 2007. Ancient biomolecules from deep ice cores reveal a forested southern Greenland. *Science* 317, 111–114.
- Williams, D.F., Kuzmin, M.I., Prokopenko, A.A., et al. 2001. The Lake Baikal drilling project in the context of a global drilling initiative. *Quaternary International* 80–81, 3–18.
- Williams, J.W. 2002. Variations in tree cover in North America since the last glacial maximum. *Global and Planetary Change* 35, 1–23.
- Williams, J.W., Shuman, B.N., Webb III, T., et al. 2004b. Late Quaternary vegetation dynamics in North America: scaling from taxa to biomes. *Ecological Monographs* 74, 309–334.
- Williams, M. 2012. The ~73 ka Toba super-eruption and its impact: history of a debate. *Quaternary International* 258, 19–29.
- Williams, M.A.J., Dunkerley, D.L., De Deckker, P., et al. 1998. *Quaternary Environments*, 2nd edn. Edward Arnold, London.
- Williams, M.A.J., Ambrose, S.H., van der Kaars, S., et al. 2009. Environmental impact of the 73 ka Toba super-eruption in South Asia. *Palaeogeography, Palaeoclimatology, Palaeoecology* 284, 295–314.
- Williams, P.W., King, D.N.T., Zhao, J.-X., et al. 2004a. Speleothem master chronologies: combined Holocene ^{18}O and ^{13}C records from the North Island of New Zealand and their palaeoenvironmental implications. *The Holocene* 14, 194–208.
- Williams, P.W., Neil, H.L., Zhao, J.-X. 2010. Age frequency distribution and revised stable isotope curves for New Zealand speleothems: palaeoclimatic implications. *International Journal of Speleology* 39, 99–112.
- Willis, K.J., van Andel, T.H. 2004. Trees or no trees? The environments of central and eastern Europe during the Last Glaciation. *Quaternary Science Reviews* 23, 2369–2387.
- Willis, K.J., Araújo, M.B., Bennett, K.D., et al. 2007. How can a knowledge of the past help to conserve the future? Biodiversity conservation and the relevance of long-term ecological studies. *Philosophical Transactions of the Royal Society of London B* 362, 175–187.
- Willman, H.B., Frye, J.C. 1970. Pleistocene stratigraphy of Illinois. *Illinois Geological Survey Bulletin* 94.
- Wilmshurst, J.M., McGlone, M.S. 2005. Corroded pollen and spores as indicators of changing lake sediment sources and catchment disturbance. *Journal of Paleolimnology* 34, 503–517.
- Wilmshurst, J.M., Higham, T.F.G., Allen, H., et al. 2004. Early Maori settlement impacts in northern coastal Taranaki, New Zealand. *New Zealand Journal of Ecology* 28, 167–179.
- Wilson, R.S.J., Luckman, B.H. 2003. Dendroclimatic reconstruction of maximum summer temperatures from upper treeline sites in Interior British Columbia. *The Holocene* 3, 851–861.

- Winchester, V., Harrison S. 2000. Dendrochronology and lichenometry: colonisation, growth rates and dating of geomorphological events on the east side of the North Patagonian Icefield, Chile. *Geomorphology* 34, 181–194.
- Winkler, S. 2000. The ‘Little Ice Age’ maximum in the Southern Alps, New Zealand: preliminary results at Mueller Glacier. *The Holocene* 10, 643–647.
- Winkler, S. 2004. Lichenometric dating of the ‘Little Ice Age’ maximum in Mt Cook National Park, Southern Alps, New Zealand. *The Holocene* 14, 911–920.
- Winkler, S., Matthews, J.A., Shakesby, R.A., et al. 2003. Glacier variations in Breheimen, southern Norway: dating Little Ice Age moraine sequences at seven low-altitude glaciers. *Journal of Quaternary Science* 18, 395–413.
- Winsborrow, M.C.M., Clark, C.D., Stokes, C.R. 2010. What controls the location of ice streams? *Earth-Science Reviews* 103, 45–59.
- Winsemann, J., Asprion, U., Meyer, T., et al. 2007. Facies characteristics of Middle Pleistocene (Saalian) ice-margin subaqueous fan and delta deposits, glacial Lake Leine, NW Germany. *Sedimentary Geology* 193, 105–129.
- Wintle, A.G. 1996. Archaeologically-relevant dating techniques for the next century. *Journal of Archaeological Science* 23, 395–413.
- Wintle, A.G. 2008. Luminescence dating: where it has been and where it is going. *Boreas* 37, 471–482.
- Wintle, A.G. 2010. Future directions of luminescence dating of quartz. *Geochronometria* 37, 1–7.
- Wintle, A.G., Murray, A.S. 2000. Quartz OSL: effects of thermal treatment and their relevance to laboratory dating procedures. *Radiation Measurements* 32, 387–400.
- Wiseman, J., El-Baz, F. 2007. *Remote Sensing in Archaeology*. Springer, Heidelberg and New York.
- Wittkop, C.A., Teranes, J.L., Dean, W.E., et al. 2009. A lacustrine carbonate record of Holocene seasonality and climate. *Geology* 37, 695–698.
- Wohlfarth, B., Possnert, G. 2000. AMS radiocarbon measurements from the Swedish varved clays. *Radiocarbon* 42, 323–333.
- Wohlfarth, B., Blaauw, M., Davies, S.M., et al. 2006. Constraining the age of Lateglacial and early Holocene pollen zones and tephra horizons in southern Sweden with Bayesian probability methods. *Journal of Quaternary Science* 21, 321–334.
- Woillard, G.M., Mook, W.G. 1982. Carbon-14 dates at Grande Pile: correlation of land and sea chronologies. *Science* 215, 159–161.
- Wolfe, A.P. 1997. On diatom concentrations in lake sediments: results from an inter-laboratory comparison and other tests performed on a uniform sample. *Journal of Paleolimnology* 18, 261–268.
- Wolfe, A.P. 2002. Climate modulates the acidity of Arctic lakes on millennial time scales. *Geology* 30, 215–218.
- Wolff, E.W., Fischer, H., Röthlisberger, R. 2009. Glacial terminations as southern warmings without northern control. *Nature Geoscience* 2, 206–209.
- Wolff, E., Barbante, C., Becagli, S., et al. 2010. Changes in environment over the last 800,000 years from chemical analysis of the EPICA Dome C ice core. *Quaternary Science Reviews* 29, 285–295.
- Wolin, J.A., Stone, J.R. 2010. Diatoms as indicators of water-level change in freshwater lakes. In *The Diatoms: Applications for the Environmental and Earth Sciences*, 2nd edn (edited by J.P. Smol, E.F. Stoermer). Cambridge University Press, Cambridge, 174–185.
- Woodhead, J., Hellstrom, J., Maas, R., et al. 2006. U-Pb geochronology of speleothems by MC-ICPMS. *Quaternary Geochronology* 1, 208–221.
- Woodroffe, C.D., Murray-Wallace, C.V. 2012. Sea-level; rise and coastal change: the past as a guide to the future. *Quaternary Science Reviews* 54, 4–11.
- Woodroffe, S.A. 2009. Recognising subtidal foraminiferal assemblages: implications for quantitative sea-level reconstructions using a foraminifera-based transfer function. *Journal of Quaternary Science* 24, 215–223.
- Woodroffe, S.A., Horton, B.P., Larcombe, P., et al. 2005. Contemporary intertidal foraminifera distributions of mangrove environments from the central Great Barrier Reef shelf, Australia: implications for sea-level reconstructions. *Journal of Foraminiferal Research* 35, 259–270.
- Woodward, J.C. 2014. *The Ice Age: A Very Short Introduction*. Oxford University Press, Oxford.
- Woodward, J.C., Goldberg, P. 2001. The sedimentary record in Mediterranean rockshelters and caves: archives of environmental change. *Geoarchaeology* 16, 327–354.
- Wooldridge, S.W., Linton, D.L. 1955. *Structure, Surface and Drainage in South-east England*. George Philip, London.
- Wolfenden, W.B. 2003. A 180,000-year pollen record from Owens Lake, CA: terrestrial vegetation change on orbital scales. *Quaternary Research* 59, 430–444.
- Wooller, M.J., Francis, D., Fogel, M.L., et al. 2004. Quantitative paleotemperature estimates from $\delta^{18}\text{O}$ of chironomid head capsules preserved in arctic lake sediments. *Journal of Paleolimnology* 31, 267–274.
- Worni, R., Stioffel, M., Huggel, C., et al. 2012. Analysis and dynamic modelling of a moraine failure and glacier lake outburst flood at Ventisquero Negro, Patagonian Andes (Argentina). *Journal of Hydrology* 444/445, 134–145.
- Wright Jr., H.E., Kutzbach, J.E., Webb III, T., et al. (eds). 1993. *Global Climates Since the Last Glacial Maximum*. University of Minneapolis Press, Minnesota.
- Wright Jr., H.E., Stefanova, I., Tian, J., et al. 2004. A chronological framework for the Holocene vegetational history of central Minnesota: the Steel Lake pollen record. *Quaternary Science Reviews* 23, 611–626.
- Wright, J.S. 2001. ‘Desert’ loess versus ‘glacial’ loess: quartz silt formation, source areas and sediment pathways in the formation of loess deposits. *Geomorphology* 36, 231–256.
- Wroe, S., Field, J. 2006. A review of the evidence for a human role in the extinction of Australian megafauna and an alternative interpretation. *Quaternary Science Reviews* 25, 2692–2703.
- Wu, H., Guiot, J., Brewer, S., et al. 2007. Climate changes in Eurasia and Africa at the last glacial maximum and mid-Holocene: reconstruction from pollen data using inverse vegetation modelling. *Climate Dynamics* 29, 211–229.

- Wu, N., Liu, T., Liu, X.P., et al. 2002. Mollusk record of millennial climate variability in the Loess Plateau during the Last Glacial Maximum. *Boreas* 31, 20–27.
- Wu, Y., Shijie, L., Lücke, A., et al. 2010. Lacustrine radiocarbon reservoir ages in Co Ngin and Zigé Tangco, central Tibetan Plateau. *Quaternary International* 212, 21–25.
- Wulf, S., Kraml, M., Brauer, A., et al. 2004. Tephrochronology of the last 100 ka lacustrine sediment record of Lago Grande di Monticchio (southern Italy). *Quaternary International* 122, 7–30.
- Wünnemann, B., Hartmann, K., Janssen, M., et al. 2007. Responses of Chinese desert lakes to climate instability during the past 45,000 years. In *Developments in Quaternary Sciences, Volume 9: Late Quaternary Climate Change and Human Adaptation in Arid China* (edited by D.B. Madsen, F.H. Chen, X. Gao). Elsevier, Amsterdam, 11–24.
- Wunsch, C. 2004. Quantitative estimate of the Milankovitch-forced contribution to observed Quaternary climate change. *Quaternary Science Reviews* 23, 1001–1012.
- Wunsch, C. 2010. Towards understanding the Paleocean. *Quaternary Science Reviews* 29, 1960–1967.
- Wurth, G., Niggemann, S., Richter, D.K., et al. 2004. The Younger Dryas and Holocene climate record of a stalagmite from Höllloch Cave (Bavarian Alps, Germany). *Journal of Quaternary Science* 19, 291–298.
- Wyrwoll, K.-H., Miller, G.H. 2001. Initiation of the Australian summer monsoon, 14,000 years ago. *Quaternary International* 83–85, 119–128.
- Xiong, S., Ding, Z., Liu, T. 2001. Climatic implications of loess deposits from the Beijing area. *Journal of Quaternary Science* 16, 575–582.
- Yadava, M.G., Ramesh, R. 2005. Monsoon reconstruction from radiocarbon dated tropical Indian speleothems. *The Holocene* 15, 48–59.
- Yamazaki, T., Oda, H. 2002. Orbital influence on Earth's magnetic field: 100,000-year periodicity in inclination. *Science* 295, 2435–2438.
- Yanes, Y., Aguirre, J., Alonso, M.R., et al. 2011. Ecological fidelity of Pleistocene–Holocene land snail shell assemblages preserved in carbonate-rich paleosols. *Palaeos* 26, 406–419.
- Yang, G., Zhang, X., Tian, M., et al. 2011. Alluvial terrace systems in Zhangjiajie of northwest Hunan, China: Implications for climatic change, tectonic uplift and geomorphic evolution. *Quaternary International* 233, 27–39.
- Yang, J.-D., Chen, J., Zhang, J.-X. 2005. Variations in $^{87}\text{Sr}/^{86}\text{Sr}$ of the Huanxian profile, Loess Plateau of China from 40 ka B.P. to 10 ka B.P. and Heinrich events. *Geochemical Journal* 39, 165–171.
- Yang, X., Rost, K.T., Lehmkuhl, F., et al. 2004. The evolution of dry lands in northern China and in the Republic of Mongolia since the Last Glacial Maximum. *Quaternary International* 118–119, 69–85.
- Yasuhara, M., Yamazaki, H., Irizuki, T., et al. 2003. Temporal changes of ostracode assemblages and anthropogenic pollution during the last 100 years, in sediment cores from Hiroshima Bay, Japan. *The Holocene* 13, 527–536.
- Yasuhara, M., Hunt, G., Cronin, T.M., et al. 2012. Climatic forcing of Quaternary deep-sea benthic communities in the North Pacific Ocean. *Paleobiology* 38, 162–179.
- Yeloff, D., Charman, D., van Geel, B., et al. 2007. Reconstruction of hydrology, vegetation and past climate change in bogs using fungal microfossils. *Review of Palaeobotany and Palynology* 146, 102–145.
- Yokoyama, Y., Lambeck, K., De Deckker, P., et al. 2000. Timing of the Last Glacial Maximum from observed sea-level data. *Nature* 406, 713–716.
- Young, G.H.F., Bale, R.J., Loader, N.J., et al. 2012. Central England temperature since AD 1850: the potential of stable carbon isotopes in British oak trees to reconstruct past summer temperatures. *Journal of Quaternary Science* 27, 606–614.
- Young, N.E., Schaeffer, J.M., Briner, J.P., et al. 2013. A ^{10}Be production-rate calibration for the Arctic. *Journal of Quaternary Science* 28, 515–526.
- Yu, G., Harrison, S.P. 1995. Holocene changes in atmospheric circulation patterns as shown by lake status change in northern Europe. *Boreas* 24, 260–268.
- Yu, Z., Wright Jr, H.E. 2001. Response of interior North America to abrupt climate oscillations in the North Atlantic region during the last deglaciation. *Earth-Science Reviews* 52, 333–369.
- Zachos, J.C., Pagani, M., Sloan, L., et al. 2001. Trends, rhythms and aberrations in global climate 65 Ma to present. *Science* 292, 686–693.
- Zagwijn, W.H. 1994. Reconstruction of climate change during the Holocene in western and central Europe based on pollen records of indicator species. *Vegetation History and Archaeobotany* 3, 65–88.
- Zalasiewicz, J., Smith, A., Brenchley, P., et al. 2004. Simplifying the stratigraphy of time. *Geology* 32, 1–4.
- Zalasiewicz, J., Smith, A., Barry, T.L. 2008. Are we now living in the Anthropocene? *GSA Today* 18, 4–8.
- Zalasiewicz, J., Williams, M., Haywood, A., et al. 2011. The Anthropocene: a new epoch of geological time. *Philosophical Transactions of the Royal Society of London A* 369, 1036–1055.
- Zárate, M.A. 2003. Loess of southern South America. *Quaternary Science Reviews* 22, 1987–2006.
- Zazo, C., Goy, J.L., Dabrio, C.J., et al. 2003. Pleistocene raised marine terraces of the Spanish Mediterranean and Atlantic coasts: records of coastal uplift, sea-level highstands and climate changes. *Marine Geology* 194, 103–133.
- Zazula, G.D., Telka, A.M., Harrington, C.R., et al. 2006. Macrofossils from Yukon Territory: implications for Late Pleistocene refugia in Eastern Beringia. *Arctic* 59, 391–400.
- Zech, W., Glaser, B., Abramowski, U., et al. 2003. Reconstruction of the Late Quaternary glaciation of the Macha Khola Valley (Gorkha Himal, Nepal) using relative and absolute (^{14}C , ^{10}Be , dendrochronology) dating techniques. *Quaternary Science Reviews* 22, 2253–2265.
- Zeeb, B.A., Smol, J.P. 2001. Chrysophyte scales and cysts. In *Tracking Environmental Change Using Lake Sediments. Volume 3: Terrestrial, Algal and Siliceous Indicators* (edited by J.P. Smol, H.J.B. Birks, W.M. Last). Kluwer, Dordrecht, 203–223.

522 REFERENCES

- Zerboni, A. 2008. Holocene rock varnish on the Messak plateau (Libyan Sahara): chronology of weathering processes. *Geomorphology* 102, 640–651.
- Zhai, D., Xiao, J., Zhou, L., et al. 2011. Holocene East Asian monsoon variation inferred from species assemblage and shell chemistry of the ostracodes from Hulun Lake, Inner Mongolia. *Quaternary Research* 75, 512–522.
- Zhang, M., DaoXian, Y., Lin, Y., et al. 2004. A 6000-year high-resolution stalagmite in Xiangshui Cave, Guinin, China. *The Holocene* 14, 697–702.
- Zhang, J., Chen, F., Holmes, J.A., et al. 2011. Holocene monsoon climate documented by oxygen and carbon isotopes from lake sediments and peat bogs in China: a review and synthesis. *Quaternary Science Reviews* 30, 1973–1987.
- Zhang, R., Delworth, T.L. 2006. Impact of Atlantic Multidecadal Oscillations on India/Sahel rainfall and Atlantic hurricanes. *Geophysical Research Letters* 33, L17712, doi: 10.1029/2006GL026267.
- Zhang, Y., Fountain, D.W., Hodgson, R.M., et al. 2004a. Towards automation of palynology 3: pollen pattern recognition using Gabor transforms and digital moments. *Journal of Quaternary Science* 19, 763–768.
- Zhang, Z., Mann, M.E., Cook, E.R. 2004b. Alternative methods of proxy-based climate field reconstruction: applications to summer drought over the coterminous United States back to AD 1700 from tree-ring data. *The Holocene* 14, 502–516.
- Zhao, J., Xia, Q., Collerson, K. 2001. Timing and duration of the last interglacial inferred from high resolution U-series chronology of stalagmite growth in Southern Hemisphere. *Earth and Planetary Science Letters* 184, 635–644.
- Zhao, Y., Sayer, C. D., Birks, H. H., et al. 2006. Spatial representation of aquatic vegetation by macrofossils and pollen in a small and shallow lake. *Journal of Paleolimnology* 35, 335–350.
- Zhou, C., Liu, Z., Wang, Y., et al. 2001. Climatic cycles investigated by sediment analysis in Peking Man's Cave, Zhoukoudian, China. *Journal of Archaeological Science* 27, 101–109.
- Zhou, E.W., Zheng, Y., Meyers, P.A., et al. 2010. Postglacial climate-change record in biomarker lipid compositions of the Hani peat sequence, Northeastern China. *Earth and Planetary Science Letters* 294, 37–46.
- Zhou, S., Li, J., Zhang, S. 2002. Quaternary glaciation of the Bailang River Valley, Qilian Shan. *Quaternary International* 97–98, 103–110.
- Zic, M., Negrini, R.M., Wigand, P.E. 2002. Evidence of synchronous climatic change across the Northern Hemisphere between the North Atlantic and the northwestern Great Basin, United States. *Geology* 30, 635–638.
- Zillén, L., Lenz, C., Julbert, T. 2012. Stable lead (Pb) isotopes and concentrations – a useful independent dating tool for Baltic Sea sediments. *Quaternary Geochronology* 9, 41–45.
- Zink, A.J.C., Susino, G.J., Porto, E., et al. 2012. Direct OSL dating of Iron Age pottery from South Africa – preliminary dosimetry investigations. *Quaternary Geochronology* 8, 1–9.
- Zinovjev, E.V. 2006. Problems of ecological interpretation of Quaternary insect faunas from the central part of Northern Eurasia. *Quaternary Science Reviews* 25, 1821–1840.
- Zolitschka, B. 2007. Varved lake sediments. In *Encyclopedia of Quaternary Science* (edited by S.A. Elias). Elsevier, Amsterdam, 3105–3114.
- Zolitschka, B., Brauer, A., Negendank, J.F.W., et al. 2000. Annually dated late Weichselian continental paleoclimate record from the Eifel, Germany. *Geology* 28, 783–786.
- Zolitschka, B., Behre, K.-E., Schneider, J. 2003. Human and climatic impact on the environment as derived from colluvial, fluvial and lacustrine archives – examples from the Bronze Age to the Migration period, Germany. *Quaternary Science Reviews* 22, 81–100.
- Zwally, H.J., Giovinetto, M.B., Li, J., et al. 2005. Mass changes of the Greenland and Antarctic ice sheets and shelves and contributions to sea-level rise: 1992–2002. *Journal of Glaciology* 51, 509–527.

Index

Page numbers in **bold** refer to figures, page numbers in *italic* refer to tables, n refers to notes

2.6 Ma event 5
2.8 ka event 433
4.2 ka event 431, **432, 433**
8.2 ka event 429, **430, 431**

AABR (area-altitude balance ratio) 49
AAR (accumulation area ratio) 48–50
AAR chronology 334, **335**
ablation area (glacier) 48
accumulation area (glacier) 48
abandoned lake shorelines 83–5, 83
absolute dating 343
absolute sea-level change 59
accelerator mass spectrometry 271, 272–5, **273, 274, 278–9**
accretionary soils 123
acidity profiles 178
acoustic profiling 24
aerial photography 20, 22
Africa: dunefields 87; early hominid sites 285; ice-core stratigraphy 172; lake-levels 135, 137, 138; pluvial lake sequences 133; pollen analysis 192; Quaternary environments 260; vertebrate remains 260
African Humid Period 137
Agassiz, Louis 6
age estimate techniques 267
age modelling: Lateglacial 420–1; radiocarbon dating 282–3, 283
age-equivalence techniques 267
age-equivalent stratigraphic markers 319; biostratigraphy 319; oxygen isotope chronostratigraphy 319; palaeomagnetism 319, 319–24, 321, 322, 323, 324, 325; tephrochronology 319, 325–31, 326, 328, 329, 331
agriculture, human impacts 437

airborne laser swath mapping (ALSM) 26
Alaska, United States of America 214
algal blooms 246
Allerød Interstadial 12, 413
allostratigraphy 352
alpha-recoil track (ART) dating 290
altiplanation 54
American Bureau of Standards 272
American Stratigraphic Commissions 359
amino-acid geochronology 332; AAR chronology 334, 335; aminostratigraphy 334; applications 336, 337, 338–9; diagenesis 334, 336; epimerization 334; fossils 339; intra-crystalline fraction 335, 336; isomeric forms 333; molluscan remains 336, 338, **338, 339**; palaeothermometry 339; problems 334, 336; protein chemistry 332–3, 333; protein degradation 336; racemization 334, 336, 339; recent developments 336; sequence correlation 335, 336, 337, 338; source material 334
amino-acid ratios 334
aminostratigraphy 334
aminozones 336
Anglian Glacial Stage 351
Annual Greenhouse Gas Index 396
annual ice increments 173–5, 174
Antarctic Bottom Water current 404
Antarctic Circumpolar Current 246
Antarctic Ice Core Chronology 315
Antarctica: 4.2 ka event 431; annual layers 312, 313, 315; anti-phase behaviour 406–7; correlation 377; deglaciation 404; dust record 132; glacial–interglacial cycles 394–5; glaciation, 35 Ma 5; ice streams 105; ice volume 170, 392; ice-accumulation years 174; ice-core stratigraphy 8, 172, 173, 177–8, 394–5, 395, 396, 397, 397, 399, 405–6, 405; ice-sheet modelling 46–7; isotope ratios 411, 411; Last Termination 414, 414, 415; Lateglacial climate change 422–3; methane signal 406, 406; Milankovitch cycle correlation 371; teleconnection 405–7, **405, 406**; tephra marker horizons 329
Antevs, Ernst 307
Anthropocene, the 439–40
anthropogenic signature 196, **197, 427, 436–40, 437, 438**
anthropogenic warming 437–9, 437, **438**
Aqua (EOS PM-1) 23
Arabian Sea 246
Aral Sea 83–4
Aran Islands 196, **197**
archaeobotanical evidence 215
archaeoentomology 225
archaeology 24, 205–6, 225, 234–5, 241, 243, 265, 293, 339, 340, 342
archaeomagnetic measurements 320
Arduino, Giovanni 5
argon–argon dating 285
argon-isotope dating 284–5, **284, 322–3, 325, 327**
Arrhenius, Svante 437
assemblage biozones 353, 354
astronomical forcing 4, 390–2, 393
astronomical parameters 4
Astronomical Theory 13–15, **14, 389, 389–90, 390–2, 398**
Atlantic Bottom Water (ABW) current 401, **402, 403, 408, 408**
Atlantic Cold Reversal (ACR), the 414

- Atlantic Meridional Overturning
Circulation (AMOC) 401, 402, 403–4, 403, 406–7, 408, 408, 417, 422, 424
- Atlantic Multidecadal Oscillation (AMO)
436
- atmospheric circulation 140; general
circulation models 8–9; and lake-level
changes 137, 160
- atmospheric forcing 395–7, 395, 396, 397
- atmospheric variations, CO₂ 172
- atomic absorption spectrophotometer
(AAS) 98
- atomic force microscopy (AFM) 97
- atomic numbers 269
- Aura (EOS CH-1) 23
- Australia 66, 69, 73; amino-acid
geochronology 336, 337;
dendrochronology 302; dunefields 86,
87, 87–8, 87, 88; dust circulation 88, 89;
fire histories 214–15; fluvial landforms
89; lake-level changes 137; Little Ice Age
434; mass extinctions 261–2; mutual
climatic range (MCR) 224; ostracod
analysis 240; plant macrofossils 212;
Quaternary environments 260; sand seas
131; sea-level change 169; speleothem
growth and climatic change 145;
vertebrate remains 260
- Austria 143
- autochthonous sediments 142
- Baffin Island 115
- bald-earth elevation mapping 25
- Baltic Sea 160
- Barbados, oxygen isotope record 61
- bathymetry 24, 25, 33
- Bayesian-based statistical modelling 282–3,
282; *see also* radiocarbon dating
- Beaver Lake, United States of America 201
- Belgium 56, 119, 120
- benthic foraminifera 169, 170, 171, 172
- Berger–Parker index (BPI) 233
- Bering Sea 221
- Bering Strait 73
- Bermuda 62
- Bernhardi, Albrecht 5
- Beschel, Roland 315
- beta decay 271–2
- Bhutan-Himalaya 28
- binge-purge episodes 404, 405
- biogenic sediments 93
- biogeochemical cycle 384
- biological evidence 181, 266
- biomarkers 253, 265
- biomass 195
- BIOME-6000 388
- biomolecular products 181
- biostratigraphic correlation 233, 237, 259
- biostratigraphy 181, 319, 331–2, 348,
353–4, 353, 363
- biozones 348, 353–4, 353; boundaries 354,
419
- bipolar seesaw 406–7, 409, 411, 412, 418,
421–2, 440
- Black Sea 237, 240
- block-fields 54, 54, 58
- Blytt–Sernander climatic scheme 161
- bogs: *see* lake, mire and bog sediments
- Bölling 12
- Bond, Gerard 400
- Bond cycles 400, 401, 404
- bone, vertebrate 254, 255, 256; amino-acid
geochronology 334; dating 258, 278,
289; excavation 257; fluorine content
339–40; fossilization 256; identification
257; micro-vertebrates 257; uranium
content 339–40
- borehole records 94–5
- borehole thermometry 177
- boundary conditions 251, 266n9
- boundary stratotypes 3, 4–5, 4, 349
- box models 380–1, 381, 393
- Braldu Valley, Pakistan 108
- Brandenburg moraines 30–1
- Brazil 62, 150, 150
- brickearths 128
- Britain and Ireland: biostratigraphy 354;
Coleoptera 218, 219, 220, 220, 222, 224,
224; deglaciation 34–5, 307; episodes of
climatic deterioration 213, 213; eustatic
sea-level change 64–5, 65, 66; extent of
ice cover 32, 33–5, 34; fire histories 214;
Foraminifera 242; ice-sheet modelling
45, 46; indicator erratics 113; lake
sedimentation rates 157–8, 158; mean
annual air temperature (MAAT)
119–20, 121; molluscan remains 228,
231, 232, 233, 234, 336, 338, 338; North
Atlantic Oscillation (NAO) 436;
ostracod analysis 239; pingos 56; plant
macrofossils 207, 213; pollen assemblage
zones 332; Quaternary environments
261; readvances 34–5, 47; soil
stratigraphy 355; surface wetness change
163, 164; vertebrate biostratigraphy 259;
vertebrate remains 261
- BRITICE project 33, 91n6
- Broecker, Wally 403
- Brückner, Eduard 6, 13, 33
- Buckland, William 7
- Bugs-CEP website 218
- buried palaeosols 122, 126
- Cader Idris, Wales 57
- caesium-137 296, 297–8
- Cairngorm Mountains, Scotland 54
- calcareous nannoplankton 245
- calcrete 91
- CALIB 280–1
- California, Gulf of 306
- Callendar, Guy 437
- Canada 68, 68; isobase patterns 71;
Keewatin 41; lake sedimentation rates
158; sea-level change 72
- carbon: global reservoirs 270, 276; isotopic
fractionation 276, 277; marine
circulation 276–7
- carbon cycle 195
- carbon dioxide 15, 15, 16, 270–1;
atmospheric variations 172; exchange
408–9; greenhouse effect 437–8; human
impacts 437–9, 438, 442
- carbon isotopes: deep-sea sediment 171–2;
molluscan remains, non-marine 234
- carbonate modelling 284
- carbon sinks 384
- carbon storage and release 195, 407–9, 408,
416–17
- carbonate cave deposits 149–50, 150, 289;
see also speleothem
- carbonate dissolution, deep-sea sediment
171
- carbonate lake deposits 138, 140
- carbonate production 91
- carbonate varves 306
- Cariaco Basin, Venezuela 280, 306, 309,
373, 373, 423
- Caspian Sea 83–4
- Catastrophist philosophy 5
- cation-ratio dating 341
- causality 380
- cave sediments 140–1; autochthonous 142;
carbonate 149–50, 150; cave earth 142;
dating 141; detrital 141–3; detritus types
140–1, 141; dripstone 141, 143;
flowstone 141, 143; fossil content 142;
human coprolites 143; molluscan
remains 231–2; organic components
142; plant macroremains 142; pollen
142, 193; sedimentation 142; sequences
142–3; speleothem 141, 143, 149, 334,
371; speleothem formation and sea-level
change 149; speleothem formation and
tectonic activity 149; speleothem growth
and climatic change 143–4, 144;
speleothem isotope ratios 145–8, 147,
148; vertebrate remains 257–8; water-
filled passages 179n7
- cave sequences 126–7

- Cenozoic era 1, 2, 3, 3
Challenger, HMS 8, 241
 Chapman Glacier, Canada 49
 Chappell, J. 62
 charcoal 127, 142, 196, 196, 210, 214–15
 chemical alteration processes chronology 332; amino-acid geochronology 332–9, 333, 335, 337, 338; bone fluorine content 339–40; bone uranium content 339–40; obsidian hydration dating (OHD) 340; pedogenesis 342–3; rock weathering 340–2, 341
 chemical fossils 265
 chemical remanent magnetism (CRM) 320
 chemical stratigraphy 348
 chemical tracers 254
 chemical varves 152, 304, 306
 China: 4.2 ka event 431; biomarkers 265; dust flux 309; Loess Plateau 127, 128, 128, 129, 131–2, 132, 234, 325, 355, 364, 370, 371, 374; molluscan remains 234; pollen analysis 192; sand seas 131
 Chironomidae 225–8, 226, 227
 chronohorizons 361–2
 chronostratigraphic units 2, 361–2, 362
 chronostratigraphy 348, 361–2, 362, 378
 chronozones 362
 chronos 2
 Chrysophytes 263
 Cladocera 263
 clastic varves 304, 304–5, 305
 clasts 93
 clay mineral ratios 115
 clay mineralogy 98
 CLIMAP (Climate/Long Range Investigation Mapping and Prediction) 9, 250–1, 265–6, 379
 climate change 309; anthropogenically induced 388–9; Astronomical Theory 13–15, 14; astronomically driven 389; atmospheric influences 15–16, 15; boundaries 358–60, 359, 360; causes 13–16, 14, 15; and coccolith productivity 246; dendroclimatology records 303; feedback loops 15–16; geologic-climatic units 358–61; and lake sediments 155–61, 156, 157, 158, 159; lake-level changes and 135, 159–60, 159; Lateglacial 421–6, 423, 424, 425, 426; Milankovitch cycles 389–99, 390, 391, 394, 395, 396, 397, 398; the Milankovitch hypothesis 14–15; and river terraces 76–7, 81–2; and speleothem growth 143–4, 144; sub-Milankovitch events 16; time-transgression 367; and volcanic activity 330
 climate GCMs 383
 climate rhythms 4–5
 Climate/Long Range Investigation Mapping and Prediction (CLIMAP) 9, 250–1, 265–6, 379
 climatic events, synchronization 420, 421
 climatic signal, isotopic ratios 145
 climatic terraces 77
 climatostratigraphy 9, 348, 358–61, 359, 360, 361, 378
 Clogher Head Readvance, Ireland 35
 closed basin (endoreic) lakes 133–4, 203
 Coccolithophores 245–6, 245, 246, 248, 250
 Cockburn Event, the 38
 coercivity curves 324
 COHMAP (Co-operative Holocene Mapping Project) 9, 251, 379, 384, 384
 cold stage 9
 Coleoptera 119, 215, 215–16, 216, 217; analysis 218–25, 220, 221, 223, 224; archaeoentomology 225; climate change boundaries 360; distribution 221–2, 221; evolutionary stasis 218–19; habitat preferences 219–21, 220; human impacts 225; identification 216; isotope ratios 224; palaeoenvironmental reconstruction 221–4, 221, 223, 224; record 216, 218; sensitivity to temperature variations 222; speciation 219
 computer-based models 8–9
 continental levering 69
 continuous flow analysis (CFA) 175
 Coope, Russell 215, 218–19, 222
 Co-operative Holocene Mapping Project (COHMAP) 9, 251, 379, 384, 384
 coral polyps 263–4
 coral reef terraces 67, 67
 coral reefs 61–2, 263–4, 331; dating 288–9, 294
 coral stratigraphy 264, 316, 317, 317, 318, 319
 Cordilleran ice sheet, North America 35, 36, 38–9, 68, 73
 coring 94–6, 95, 151; *see also* ice-core stratigraphy
 coring equipment 94, 95, 172
 correlation 2; definition 363; difficulties 359, 363; event stratigraphy 365; homotaxial errors 363; ice-core stratigraphy 366–7; land-sea 366–7, 371, 373, 377–8, 377; Lateglacial 420–1, 421; marine oxygen isotope record 366, 399; Milankovitch cycles 367–9, 368, 369, 370, 371, 378; oxygen isotope ratios 399; palaeosols 364; pollen and pollen analysis 368; principles 362–3; radiometric dating 365; record synchronization 374–8, 375, 376, 377; sea-level change 365; shoreline 364–5; sub-Milankovitch timescales 371, 371, 372, 373–4, 373, 374; tephra 364
 cosmic ray flux 433
 cosmogenic nuclides 115, 294, 295, 295
 cosmogenic radionuclide (CRN) dating 294–6, 295, 297
 coversand 127, 130, 130
 Crawford Lake, Canada 158
 crag-and-tail features 41
 crescentic fractures 40, 42
 crescentic gouges 40
 Croatia 149
 Croll, James 13
 crossing striations 40, 41
 crustal flexuring 68, 68; isostatic recovery 69, 69
 crustal warping 6
 cryoplanation terraces 54
 cryostatic facies 121
 cryostructures 117
 cryoturbation structures 117–18, 117, 118, 119
 cultural eutrophication 205
 cultural landscape 196
 cumulative soils 123
 Dansgaard–Oeschger (DO) events 78, 176, 243, 261, 371, 399, 400, 400, 401, 403–5, 440
 Danube, River 75, 77, 78, 128, 338
 dating 2, 7–8, 33; accuracy 267, 269, 345; bias 267; carbonate cave deposits 289; cave sediments 141; corals 288–9, 294; deep-sea sediment 287; dunefields 87, 88; early hominid sites 285; glacial sediments 292, 294; glacier ice 298, 311–12; Greenland ice sheet 268; Heinrich events 373; ice-core stratigraphy 175, 297, 313; lake sediment 278, 279, 287, 297; lake-level changes 135; Lateglacial 419–20; marine oxygen isotope record 268; molluscan remains 235, 277, 278, 289, 294, 339; moraines 296, 297, 316, 342; palaeosols 126; peat deposits 161–2, 289; periglacial structures 122; plant macrofossils 210; polarity events 322–3; pollen 189, 362; precision 267, 269, 274–5, 345, 426, 440; Quaternary events 308–9; ratite eggshell 338; reliability 267; river terraces 77;

- sea-level change 59, 61–2; sea-waters 276–7; soils 279; speleothem 143, 144, 149, 286–7, 288, 293, 298, 316–17; stratigraphic resolution 343–4, 344; temporal resolution 343–4, 344; tephra 325, 327; trapped gas 312; uncertainty 267, 272, 362; vertebrate remains 258, 278, 289, 294; volcanic rocks 284–5, 289; weathering 294
- dating methods 267, 268, 344–5; *see also* individual methods
- daughter deficient (DD) U-series dating 287
- daughter excess (DE) U-series dating 287
- debris flow deposit 102, 103
- deep-sea sediment 2, 8; accumulation 165; carbon isotopes 171–2; carbonate compensation depth (CCD) 171; carbonate dissolution 171; correlation 365, 366, 366–7, 377–8, 377; dating 287; event stratigraphy 365; fossil record 166; Heinrich layers 166, 166; ice-raftered debris (IRD) 165–6; isotopic equilibrium 171; magnetostratigraphy 323–4; micropalaeontology 243–8, 245, 247, 249, 250–4, 250, 251, 252, 253; mixing 171; nature of 165–6, 166; oxygen isotope ratios 166–71, 168, 169, 390, 390; oxygen isotope record 9; sedimentation rates 170–1; stratigraphic resolution 170–1
- deep-sea temperature 169
- deformation 179n3
- deformation tills 102–5, 104, 105, 106
- deforming bed 103, 104–5
- deglaciation 393; Antarctica 404; Britain and Ireland 34–5; freshwater release 404; Last Termination 418; North America 37, 39, 404; Northern Europe 32; paraglacial deposits 105–7, 108; varve chronology 307, 308
- dendrochronology 7, 298; 2.8 ka event 433; Australia 302; cross-dating 299–300, 300; dendroclimatology 299, 302–4; Europe 301–2, 302, 303; general principles 298, 299; Hohenheim master chronology 301–2, 302; isotope dendroclimatology 303–4; Lateglacial 420; Little Ice Age 434; markers 299; master chronology 299, 300; New Zealand 302; North America 301, 301; Pacific Decadal Oscillation (PDO) 436; and radiocarbon dating calibration 279, 280, 283; records 300; ring measurement 298–9; ring-width indices 299, 301; tree-ring width 299; United States of America 301, 301; wood density 303
- dendroclimatology 299, 302–4
- denivation features 130
- Denmark 32, 157–8, 207, 293
- depositional landforms 42–3
- Desnoyers, Jules 5
- detrital remanent magnetism (DRM) 320
- Devensian Lateglacial 10, 12, 33–5, 34, 44–5, 45
- diagenesis 123–4, 179n5
- diamicton 99, 179n2
- diatom analysis 197–8, 246, 306; applications 202–3, 204, 205–6, 205, 206; concentrations 200, 201; diatom range 199; diatom types 198–200, 199; halobian system 202–3; human impacts 205–6; identification 200; interpretation 202; and lake-level changes 203; and pH 203, 205, 206; procedures 198, 200, 201, 202; salinity indicators 202–3, 205; samples 200; and sea-level change 202–3, 202, 204; species distribution 200
- diatom mats 248
- diatom stratigraphy 206
- differential frost heave 118
- differential global positioning system (DGPS) 91n2
- differential receivers 22
- digital elevation models (DEM) 25–6, 26
- digital images 23
- digital surface models (DSM) 26
- digital terrain models (DTM) 25–6, 26
- diluvium 99
- Dimlington Stadial 33
- Dinoflagellates (dinocysts) 246, 247, 248
- DIRTMAP 387–8
- DiTe index 265
- DNA analysis 8, 262, 265, 332
- drift 6
- drumlins 40, 42–3, 42
- dump moraines 27, 28
- Dundalk Bay 35
- dune patterns 88–9
- dunefields 86–9, 87, 88
- duricrusts 90–1
- dust: air-transported 127, 130; annual cycles 175; circulation 410–11, 410; and global cooling 410–11; ice-core stratigraphy 175, 178; Last Glacial Maximum (LGM) 131; Pleistocene–Holocene transition 428; role of 412–13, 412; and sea-level change 411, 411; transport fluxes 132; varve chronology 309
- dust bowl events 309
- earth hummocks 58
- Earth Observing System (EOS) 23
- Earth Resource Technology Satellites (ERTS) 22–3
- earth system models of intermediate complexity (EMICs) 383–4, 384, 385, 386, 386, 393
- East African Rift Valley 330, 369
- East Asian monsoon system 131–2, 240, 245, 309, 371, 374, 409
- East Jutland Line 31
- echo sounders 23–4
- ecological changes, early evidence 7
- ecological niche models 261
- ecosystems 182
- Eemian 10, 126, 307–8
- eggshell, ratite, dating 338
- Egypt 88, 89, 131, 133
- eigenvalues 114
- El Niño–Southern Oscillation (ENSO) 214, 431, 435, 440
- electrical conductivity measurements (ECM) 175, 348
- electron paramagnetic resonance 293
- electron probe micro-analysis (EPMA) 325
- electron spin resonance (ESR) 293–4
- electron traps 291, 294
- electronic distance measures (EDMs) 20
- Ellesmere Island 39
- Emiliani, Cesare 170
- Emiliani chron 391, 391
- end moraines 27, 29, 29–30
- englacial subenvironments 100, 100
- ENSO (El Niño–Southern Oscillation) 214, 431, 435, 440
- environmental change: record synchronization 374–8, 375, 376, 377; time-stratigraphic framework 347; *see also* global environmental change
- environmental simulation models (ESMs) 380; box models 380–1, 381, 393; earth system models of intermediate complexity (EMICs) 383–4, 384, 385, 386–6, 386, 393; general circulation models (GCMs) 381–3, 382, 383; hindcasting 388; importance of 388–9; Integrated Global System Model 386, 386; limitations of 388; Milankovitch cycles 393; oversimplification 388; palaeodata-model comparisons 387–8; testing 387; transient simulations 386–7
- Envisat 23
- EPICA (European Project for Ice Coring in Antarctica) 8, 172, 177–8
- epochs 2

- equifinality 126
 equilibrium line altitude (ELA) 48–50, 57;
 palaeoclimatic inferences 50–3, 51, 52
 eras 1, 2
 erathem 2
 Erdalen Event, the 32–3
 erosion rates 294
 erratics 111, 113, 113
 Esmark, Jens 5
 estuarine sediments, and sea-level change
 63–4, 64
 Ethiopia 234
 Europe: 2.8 ka event 433; amino-acid
 geochronology 338; Coleoptera 221,
 221; coversand 130, 130; deglaciation
 404; dendrochronology 301–2, 303;
 dendroclimatology 299; human
 evolution 330; Little Ice Age 433–4; loess
 deposits 128, 131; molluscan remains
 233; phyleogeography 262; textural B
 horizon 126; *Ulmus* (elm) decline 194;
 vertebrate biostratigraphy 259; wind
 directions 131; Younger Dryas Stadial
 424
 European Greenland Ice-core Project 8
 European North Greenland Eemian Project
 8
 European Project for Ice Coring in
 Antarctica (EPICA) 8, 172, 177–8
 European Space Agency (ESA) 23
 eustatic sea-level change 59, 59–60, 60–7,
 60, 61, 62, 63, 64, 65, 66, 76
 evaporitic varves 306
 event alignment 367
 event stratigraphy 348, 365
 exemplary stratotypes 349
 exhumed palaeosols 123
 Eyjafjallajökull 327
- facies 100, 102, 109–11, 111, 112, 351
 facies logs 109–10, 111, 112
 far field locations 62–3
 faunal evidence 5
 feedback loops: climate change 15–16;
 global environmental change 381, 384,
 392, 395–6, 395, 396, 396–7, 396, 404;
 Holocene 435; interdependency 412–13,
 413; Last Termination 417–18;
 teleconnection 407, 409, 410–11
 fidelity 232
 field mapping 19–20, 21, 40
 Finland 32, 307, 322
 Finse Event, the 32–3
 fire histories 214–15
 fission track dating 289–91, 325, 327
 flame photometer 98
- Flandrian 11
 Flint, Richard Foster 14
 flint artefacts 151
 floating chronologies 304, 307, 308, 317,
 319, 420
 Florida, United States of America 212
 flow till 102, 103, 103
 fluted moraines 40, 42
 fluvial landforms, low latitude 89–90, 90
 Foraminifera 241–4, 241, 243, 246, 248,
 249, 250, 309
 Forbes, Sir Edward 1, 7
 forcing factors 379
 forest history 214
 fossils and the fossil record: amino-acid
 geochronology 339; analysis 181;
 biomolecular products 181;
 biostratigraphy 348; deep-sea sediment
 166; formation 182; identification 182;
 indices of environmental change 8;
 interpretation 182–3; lake sediment 155,
 305–6; macrofossils 181; microfossils
 181; modern analogue approach 182,
 183; molecular clock analysis 332;
 palaeobiological context 182;
 preservation 182; process 256; proxy
 records 182; range 181; screening 339; in
 situ fossils 182; stromatolites 150;
 taphonomy 182
 France: amino-acid geochronology 338;
 Coleoptera 224, 224; Grotte de
 Clamouse 145, 148; Lac d'Annecy 306;
 molluscan remains 233; permafrost
 boundary 119; Sevrier-Les-Charretières
 159; Vosges Mountains 212
 freeze-thaw activity 115, 121
 freshwater hosing experiments 380, 424
 freshwater release 404, 422, 423–4, 431
 friction cracks 40
 frost action 27, 29
 frost-shattering 54
 fungal remains 264
- gas, trapped 312
 GCMs (general circulation models) 8–9,
 381–3, 382, 383
 Geer, Gerard de 7, 304–5, 307
 Geikie, Archibald 99
 Geikie, James 6, 27
 Gelasian 5
 gelification 54, 115
 general circulation models (GCMs) 8–9,
 381–3, 382, 383
 genetic facies 102
 genetic modification 262
 GENIE initiative 386
- geochemical fingerprinting 325
 geochronological potential 343
 geochronological resolution 343, 344
 geochronological units 2, 348, 361–2,
 362
 geochronology 361–2, 362
 geodetic datum 20
 geoidal eustasy 66–7
 geological ages, abbreviating conventions
 17n1
 geological timescale 1, 2–3
 geologic-climatic units 358–61, 363, 366,
 378
 geomagnetic field: components 320;
 polarity changes 319–20, 321–4, 322,
 323, 324; polarity epochs 321–3, 323;
 secular variations 320–1, 321
 geomorphological evidence 19, 91;
 direction of ice movement 39–43, 41,
 42, 43; extent of ice cover 27–30, 28, 29;
 extent of ice cover, Britain and Ireland
 32, 33–5, 34; extent of ice cover, North
 America 35, 36, 37–9, 37, 39; extent of
 ice cover, Northern Europe 30–3, 30, 31;
 field methods 19–26, 21, 25, 26; low
 latitude landforms 82–91, 83, 84, 85, 86,
 87, 88, 89, 90; river terraces 73–82, 74,
 75, 76, 78, 79, 80; sea-level change
 58–73; *see also* glacial landforms
 geomorphological mapping 20, 21
 geophones 24
 GEOSAT 23
 geosols 355
 Germany 32, 56, 68, 119, 120, 161, 190,
 207, 212–13, 285, 301, 302, 309, 376,
 424, 433
 GICC05 *see* Greenland Ice-core
 Chronology
 Gilbert, Grove Karl 6–7
 GISP2 *see* Greenland Ice Sheet Project
 Glacial Epoch 1
 glacial ice storage, and marine oxygen
 isotope ratios 167–9, 168
 glacial landforms: distribution 27; and
 extent of ice cover 27, 28, 29;
 geomorphological evidence 26–7;
 modification 27, 29; preservation 27
 Glacial North Atlantic Intermediate Water
 (GNAIW) 409
 glacial sediments 99; dating 292, 294;
 deformation 102; deformation tills
 102–5, 104, 105, 106; erratics 111, 113,
 113; extent 99; facies 100, 102, 109–11,
 111, 112, 351; factors affecting 100, 100,
 102; flow till 102, 103, 103; glaciofluvial
 99–100; glaciolacustrine deposits 100;

and ice thermal regime 107–9; ice-contact deposits 99; ice-directional indicators 111, 113–15, 113, 114; lithofacies interpretations 109–11, 111; lodgement till 102, 103, 104; luminescence dating 292; melt-out till 102, 103, 104; micromorphology 103–4; modes of deposition 101, 102; nomenclature 99; outwash deposits 99–100; paraglacial deposits 105–7, 108; particle size and shape analysis 109, 110, 112; plastering on process 103; proglacial 99–100; sequence analysis 109–11, 110, 111; stratified 99; subglacial traction till 104; sublimation till 102, 103; till classifications 102–7, 103, 104, 105, 106, 107; till fabric 113–15, 114; till matrix properties 115; till provenance 113; till sequences 109; unstratified 99
glacial stages 1, 9, 10
Glacial Theory 5–6, 26
glacial troughs 41–2
glacial–interglacial cycles 2, 359–60, 360; last 800 ka 394–7, 395, 396, 397, 398, 399
glacially moulded/sculpted terrain 41, 42
glaciations: correlation 359, 363; early mapping 6; maximum extent 6; outwash terraces 77; and river terraces 77
glacier ice: annual layers 298, 310–13, 313, 314, 314, 315; dating 298, 311–12; thermal regime 107–9
glaciers 48; ablation area 48; accumulation area 48; accumulation area ratio (AAR) 48–50; cirque floor altitude (CFA) 49, 50; equilibrium line 48, 48–50, 57; firn lines 48, 48–50, 49; ice surface contours 47–8, 48; lapse-rate calculations 50; palaeoclimatic inferences from ELA 50–3, 51, 52; as palaeoenvironmental archives 173; readvance 30; reconstruction 47–50, 49; retreat, rate of 27; surges 30, 91n5; toe-to-headwall (THAR) 50; transition zones 92n9
glaciogenic sequences 100, 109–11, 110, 111
glaciogenic varves 304, 304–5
glacimarine deposits 100
Glacio-eustatic Theory 6
glacio-eustatic sea-level change 60–1
glacio-isostasy 6, 68–9, 69–73, 70, 71, 72
glacitectonite 104
Glen Roy, Scotland 75
Global Boundary Stratotype Sections and Points (GSSPs) 4, 349
global carbon reservoirs 270, 276

global circulation models 251
global circulation processes 385
global conveyor 401, 402
global environmental change 379–80, 408, 440, 441, 442–3, 442; amplification agents 392–4; the Anthropocene 439–40; anthropogenic signature 436–40, 437, 438; astronomically driven 389; bipolar teleconnection 405–7, 405, 406; boundary conditions 381–2, 383–4, 384, 387; cause-and-effect pathways involved 388; complexity 384; dynamic conditions 382; environmental simulation models (ESMs) 380–9; feedback loops 381, 384, 392, 395–6, 395, 396, 396–7, 396, 397–8, 404; glacial–interglacial cycles of the last 800 ka 394–7, 395, 396, 397, 398, 399; global teleconnections 407–13, 408, 410, 411, 412; the Great Acceleration 440; greenhouse effect 437–8, 437, 438; Holocene. *see* Holocene; human impacts 436–40, 437, 438, 442–3; interdependency 412–13, 412; lags 380; Last Termination 380, 413–19, 414, 415, 416, 417; Lateglacial 419–26, 421, 423, 424, 425, 426; leads 380; Middle Pleistocene Transition (MPT) 389, 390–4, 390, 391, 394, 398–9; Milankovitch cycles 380, 389–99, 390, 391, 394, 395, 396, 397, 398; ocean–ice interactions, North Atlantic 400–1, 401, 402, 403–5, 403; proxy records 379–80; sub-Milankovitch timescales 380; sub-orbital (millennial) timescales 399–413, 400, 401, 402, 403, 405, 406, 408, 410, 411, 412; timescale 440; tipping points 386, 404, 438, 440; transitions 387; variability 440, 441, 442
Global Lake Status Data Base 135, 136, 388
Global Positioning System (GPS). 20, 22
global stratotypes 349
global tephra database 327
Grand Canyon, Arizona 149
Gravity Recovery and Climate Experiment (GRACE) satellite 47
Great Acceleration, the 440
Great Barrier Reef 242
Great Ice Age 27
Greatlakean Advance 35, 37
greenhouse effect 397, 437–8, 437, 438
greenhouse gases 16, 73, 395–6, 409, 437–8, 438, 442
Greenland: lichen growth curve 315, 315; ostracod analysis 240

Greenland Ice-Core Chronology (GICC05) 312–13, 313, 314, 355, 326, 375, 406, 419, 420, 421, 423
Greenland ice sheet 73, 160; 8.2 ka event 429; annual layers 312; anti-phase behaviour 406–7; Chironomidae 227, 228; coring 8; correlation 371, 371, 372, 373–4, 373, 374, 377; crustal flexuring 68; dating 268; dust record 132, 410, 410; ice core chronology 312–13, 313, 314; ice-accumulation years 174; ice-core stratigraphy 172, 173, 176–7, 176, 178, 399, 405–6, 405, 419–20, 422; ice-sheet modelling 45–6, 46–7; isotope ratios 176, 176; Last Termination 414, 415–16; Lateglacial 419–20; Lateglacial climate change 422, 423–4; methane signal 406, 406; oxygen isotope ratios 427; Pleistocene–Holocene transition 428; principal sites 172, 173; retreat 39, 203, 204; teleconnection 405, 405–7, 406; temperature change 177
Greenland Ice-core Project (GRIP) 8, 12, 12, 172, 176–7, 176, 312–13, 314, 349, 371, 371, 375, 377, 401, 415, 423, 433
Greenland Ice Sheet Project (GISP2) 8, 146, 148, 172, 177, 309, 312, 373, 373, 374, 411, 411
Greenland Interstadials (GI) 12, 12, 371
Grimsel Pass, Switzerland 29
GRIP *see* Greenland Ice-core Project
Gros Morne Mountain, Newfoundland 54, 55
Grotte de Clamouse, France 145, 148
ground ice 54
ground moraine 99
ground penetrating radar (GPR) 24
ground wedges 117
grounding lines 47
Gulf Stream 403, 406–7
gypcrete 91
hard-water error 277–8
heat piracy 407
heavy mineral assemblages 98
Heer, Oswald 7
Heinrich events 62, 105, 138, 246, 365, 371, 371, 401, 436; dating 373; deep-sea sediment 166, 166; Lateglacial 423; North Atlantic 372, 373, 374, 404, 411; proxy records 373
Heinrich layers 166, 166
Hölloch Cave, Bavarian Alps 146, 147
Holocene 2–3, 10, 32, 33, 39, 413, 427; 2.8 ka event 433; 4.2 ka event 431, 432, 433; 8.2 ka event 429, 430, 431;

- anthropogenic signature 427; Atlantic Multidecadal Oscillation (AMO) 436; atmospheric circulation regime 428; climate change episodes 427; climate trends 427, 427; climatic cycles 434–6; definition 427; dunefields 87; El Niño–Southern Oscillation (ENSO) 431, 435; eustatic sea-level change 65–6; feedback loops 435; global environmental change 380; human impacts 436–40, 437, 438; ice-accumulation years 174; lake-level changes 138, 160; Little Ice Age 433–4, 433; methane levels 431; North Atlantic Oscillation (NAO) 435–6; onset 413, 414; Pacific Decadal Oscillation (PDO) 436; Pleistocene–Holocene transition 428–9, 428, 429; proxy records 427; sea-level change 66, 69; solar output variations 431, 433, 433, 434, 434–5; speleothem growth 146; sub-epochs 431; temperature anomaly record 398; temperatures 427, 427, 434
- Holocene Thermal Maximum 427
- homotaxial errors 363
- Hudson Bay, Canada 63
- Hulu Cave, China 146, 148
- human evolution, and volcanic activity 330
- human impacts: agriculture 437; the Anthropocene 439–40; anthropogenic indicators 196, 197; anthropogenic warming 437–9, 437, 438; Coleoptera 225; diatom analysis 205–6; fire histories 214; global environmental change 442–3; the Great Acceleration 440; Holocene 427, 436–40, 437, 438; ice-core stratigraphy 178; industrial activity 178; lake sediment 158–9; molluscan remains, non-marine 234–5; on peat deposits 165; plant macrofossils 212, 215; and pollen analysis 183, 195–6, 196, 197; and population numbers 442, 442; on radiocarbon dating 276; and river terraces 77–8, 78; synanthropic species 225; temperatures 442; time-transgression 440; tipping point 438, 440; varve chronology 309; vertebrate remains 261–2
- human occupation sites 258
- human population numbers 442, 442
- human skeletal remains 256–7
- hummocky moraines 27, 28
- Huon Peninsula, Papua New Guinea 67, 67
- Hutton, James 5
- hydraulic sorting 258
- hydrographs 84, 86
- hydro-isostasy 60, 68, 69
- hydrophones 24
- hydroseral successions 153, 154, 155
- Iberian Peninsula 219
- ice, dielectrical properties (DEP) 175
- ice cover, extent of 27–30, 28, 29, 342; Britain and Ireland 32, 33–5, 34; Foraminifera and 243; Last Glacial Maximum (LGM) 33; North America 35, 36, 37–9, 37, 39; Northern Europe 30–3, 30, 31; readvances, Britain and Ireland 35; readvances, North America 35, 37, 38, 38–9
- ice divides 46
- ice lobes 37, 44, 45, 46
- ice masses, as palaeoenvironmental archives 173
- ice masses, reconstruction: flowlines 43, 43; glaciers 47–50, 49; ice caps 47, 48; ice-sheet modelling 43–7, 44, 45, 46, 47; palaeoclimatic inferences 50–3, 51, 52; parameters 43; steady-state models 44
- ice movement, direction 39–40; crescentic fractures 42; crossing striations 40; flowlines 43; friction cracks 40; glacial sediments and 113–15, 113, 114; ice streams 40, 41; ice-moulded (streamlined) bedrock 40–2, 42; macro-scale patterns 43, 43; streamlined glacial deposits 42–3; striations 40, 41, 42
- ice sheets 47; annual ice increments 173–5, 174; annual layering 311; collapse 404, 422; freshwater release 404, 422, 423–4, 431; steady-state 29, 44, 49, 91n4
- ice streams 40, 44, 46
- ice volume 27; environmental simulation models (ESMs) 393; global 26–7; last cold stage 9; Middle Pleistocene Transition (MPT) 392; and oxygen isotope ratios 169; Pleistocene–Holocene transition 429; and sea-level change 169–70
- ice-accumulation years 174
- ice-contact deposits 99
- ice-core stratigraphy 8, 172–3; 4.2 ka event 431; 8.2 ka event 431; acidity profiles 178; analysis 173–5, 174; annual increments 173–5, 174; Antarctica 8, 172, 173, 177–8, 394–5, 395, 396, 397, 399, 405–6, 405; borehole thermometry 177; chemical content 175; chronology errors 312; correlation 366–7, 377; dating 175, 297, 313; dust content 175, 178; glacier ice annual layers 311, 311; Greenland ice sheet 172, 173, 176–7, 176, 178, 399, 405–6, 405, 419–20, 422; human impacts 178; isotope ratios 175, 175–6, 176; Lateglacial 419; the palaeoenvironmental archive 173; palaeoenvironmental reconstruction 175–8, 176; proxy records 176; statistical uncertainties 177; and temperature change 177; tephra 327; trace substances 175, 178; upper levels 8
- Iceland 326, 327, 329
- Icelandic Sea 277, 330
- ice-moulded (streamlined) bedrock 40–2, 42
- ice rafted debris (IRD) 165–6, 327, 373, 404
- ICESat 23
- ice-sheet modelling: and ice divides 46; inverse models 44–5, 45; numerical simulations 44–7, 44; parameters 43–4, 44; present Antarctic and Greenland ice sheets 46–7; steady-state models 44; and wind patterns 45–6
- ice-wedges 116–17, 116, 118–19, 122
- illuviation 109
- imaging radar 24
- incremental dating methods 267; biostratigraphy 331–2; dendrochronology 298, 298–304, 299, 300, 301, 302, 303; glacier ice annual layers 298, 310–13, 313, 314, 314, 315; lichenometry 298, 315–16, 315; molecular clock analysis 332, 345; oxygen isotope chronology 330–1, 331; sclerochronology 298, 316, 317, 318, 319; speleothem 298, 316–17; *see also* varve chronology
- India 62, 89, 90
- indicator erratics 111
- Indonesian Islands 73
- inductively coupled plasma atomic emission spectrometry (ICP-AES) 98
- industrial activity 8, 178, 437, 437–8, 438
- Industrial Revolution 438, 439
- infrared stimulated luminescence 292
- Innuitian ice sheet, North America 35, 36, 39
- inorganic deposits 93
- insect remains, fossil 215; analysis 218–25, 220, 221, 223, 224; archaeoentomology 225; Chironomidae 215, 225–8, 226, 227; Coleoptera 215, 215–16, 216, 217, 218–25, 218, 220, 221, 223, 224; distribution 221–2, 221; evolutionary stasis 218–19; human impacts 225; identification 216; isotope ratios 224;

laboratory methods 216, 218, 218; palaeoenvironmental reconstruction and 221–4, 221, 223, 224; types 215
 instrumental levelling 20, 22
 Inter-Allerød Cold Phase: IACP 413, 422
 interdisciplinary approach 2, 9
 interferometric synthetic aperture radar (IFSAR) 25
 interglacials 1; definition 9; duration 307–8; number 10
 Intergovernmental Panel on Climate Change (IPCC) 388, 437, 443
 International Atomic Energy Authority (IAEA) 167, 272
 International Geological Congress: 1885 3; 1948 4
 International Union of Geological Sciences (IUGS) 3, 17n3
 International Union of Quaternary Research (INQUA) 3, 17n4; Congress, 1982 4
 interpluvial episodes 6–7, 82
 interstadial episodes, definition 9
 Inter-Tropical Convergence Zone (ITCZ) 246, 407, 409–10, 418, 431
 INTIMATE (INTegration of Ice-core, MARine and TERrestrial records) 375–6, 419, 421
 involution structures 117–18, 117, 118
 ionization 269
 IP25 index 265
 Ipswichian 10
 Ireland 33, 35, 43, 72–3
 Irish Sea 33, 34, 35; ice wastage record 110–11
 island rule, the 260
 Islay, Hebrides 58
 isobases 71, 71
 isolation basins 64, 65
 isopollen maps 195, 195, 332
 isostatic equilibrium 59
 isostatic movements 59
 isostatic recovery 69, 69, 71, 72–3
 isostatic sea-level change 66, 68–73, 68, 69, 70, 71, 72
 isothermal plateau fission track technique (ITPFT) 290
 isothermal remanent magnetization (IRM) 324
 isotope dendroclimatology 303–4
 isotope ratio mass spectrometry 273–4
 isotope ratios 98–9; Antarctica 411, 411; climatic signal 145; Coleoptera 224; deep-sea sediment 166–72, 168, 169; dendrochronology 303–4; ice-core stratigraphy 175, 175–6, 176; lake

sediment 160–1; micropalaeontology, deep-sea sediment 253–4; molluscan remains 234, 237; peat deposits 163, 165; speleothem 145–8, 147, 148
 isotopes 17n5, 269
 isotopic enrichment 271–2
 isotopic equilibrium 145, 171
 isotopic fractionation 145, 167, 179n9, 271–2, 276, 277
 isotopic records 8
 isotopic signals, oxygen isotope record 9, 10
 isotopic stages 9–10, 10, 169, 330, 358
 Israel 67, 131
 Italy 78, 149, 326, 327
 James Ross Island, Antarctica 28
 Jamieson, Thomas 6
 Japan 283, 309–10, 310, 365, 422, 423
 Jason-1 23
 jet stream 137
 jökulhlaups 77
 Jutland 31, 31
 kame terraces 27
 Keewatin, Canada 41
 Kennard, Alfred 7, 228
 Kenya 133
 Killard Point Readvance, Ireland 35
 Kråkenes Lake, Norway 424–6, 425, 426
 Kullenberg, Börje 8
 laboratory methods 96–9
 Lac d'Annecy, France 306
 lake, mire and bog sediments:
 accumulation 151; allochthonous 151;
 autochthonous 151; biogeochemistry 279; bog formation 155; bog types 154; chemical composition 155–7, 157; and climatic change 155–61, 156, 157, 158, 159; coring 151; dating 287, 297; density/thermal stratification 152; deposits 151–2; eutrophic 151; fossil record 155, 305–6; human impacts 158–9; importance 150–1; insect remains 215; isotope ratios 160–1; lake age 150–1; and lake chemistry 152; lake classification 150, 150; Lateglacial 425, 425; limnic accumulation 151, 151; magnetic data 158–9; Milankovitch cycle correlation 368–9, 369, 370, 371; mire formation 153, 155; mire types 154; molluscan remains 232; nature of 151–4, 154; oligotrophic 151; organic varves 305–6; and oxygenation of lake waters 152; palaeoenvironmental

evidence from lake sediments 154–61, 156, 157, 158, 159; palaeoenvironmental evidence from mire and bog sediments 161–5, 162, 163, 164; palaeolimnology 155; and palaeotemperatures 160–1; peat formation 153–4; plant macrofossils 210, 211; pollen content 155, 157, 192; pollen diagrams 185, 186, 188–9, 188; radiocarbon dating 278, 279; sedimentation patterns 154–5; sedimentation rates 157–8, 158; sequences 151, 151, 155, 155–6, 157, 159; shoreline correlation 365; shoreline features 150; stratification 152; vegetation patterns 158–9; vertebrate remains 258; *see also* pluvial lakes
 Lake Baikal 369, 369
 Lake Bonneville 82, 83–6, 84, 86, 133, 339
 Lake Chad 82, 85, 89
 Lake Kinneret 133
 Lake Lahontan 82, 83, 84
 Lake Lisan 133
 Lake Malawi 135
 Lake Neuchatel 215
 Lake Tana 135
 Lake Torreberga 160
 lake-level changes 132–3, 154–5, 409; and atmospheric circulation patterns 160; causes 134–5, 137–8, 140; Chironomidae 227; and climatic change 135, 159–60, 159; dating 135; diatoms and 203; geochemical variations 134, 134, 135; Global Lake Status Data Base 135, 136; hydrological balance 134; isotope variations 138, 140; Last Glacial Maximum (LGM) 135, 137; ostracod analysis 240; palaeoclimatic reconstruction 135, 137–9, 140; plant macrofossils and 211; pluvial lake sequences 133–5, 133, 134; proxy records 138, 139; reconstruction data 159–60; sedimentary sequences 133–4; status data 136; and the sunspot cycle 138; water balance models 135
 lakes: age 150–1; catchment histories 155–6; classification 150; closed-basin 203; density structure 152; high-altitude 152; pH 205; thermocline 152; trophic status 153, 205; water temperature 152; *see also* lake, mire and bog sediments; lake-level changes; pluvial lakes
 land bridges 73
 Landsat 22–3
 land-use changes 309
 Lapland 300, 302, 303

- laser altimetry 26
 laser diffraction 96–7
 laser technology 22
 Last Glacial Maximum (LGM) 33, 36, 260, 383–4, 413; dust flux 131; forest refugia 214; and ice volume 169; ice-sheet modelling 45–6, 47; lake-levels 135, 137; marine oxygen isotope ratios 167–8; megadroughts 86; multi-proxy investigation 266; onset 415; River Thames 81; sea-level change 62–3; sea-surface temperatures (SSTs) 251, 252; temperatures 148, 339
 Last Glacial–Interglacial Transition 413
 Last Termination 413; bipolar seesaw 418–19; carbon storage and release 416–17; definition 413–15, 414, 415; feedback loops 417–18; global environmental change 380; global temperature records 417–18, 417; isotope records 414–15, 415; onset 415–18, 416, 417, 418; record synchronization 375; sea-surface temperatures (SSTs) 415, 416; sequence 417–18, 418; teleconnections 418–19; terminology 413–14; trigger 415–17
 Late Weichselian ice sheet 30–1, 30–3, 30, 31, 73, 117
 Late Wisconsinan events, correlation 364
 Lateglacial Interstadial 12, 413, 419–26, 421, 422, 423, 423, 424, 425, 426
 laterites 90–1
 Latvia 209
 Laurentide ice sheet, North America 35, 36, 37–8, 37, 137, 384, 385; 8.2 ka event 431; collapse 404; discharges 105; ice-sheet modelling 44, 44, 45, 46; retreat 243
 lead-210 296, 297
 Leszno moraine 31
 Levene Moraine 32
 Libby, Willard 7, 270
 lichen growth curve 315, 315
 lichenometry 298, 315–16, 315
 light detection and ranging (LIDAR) 26
 lithalsas 56
 lithofacies 102, 112
 lithological changes 93
 lithostratigraphy 348, 349–53, 350, 351, 352, 378
 Little Ice Age 33, 39, 78, 243, 309, 433–4, 433
 load structures 117–18, 117, 118, 179n4
 local vegetation reconstructions 194
 locations, pinpointing 20, 22
 Loch Lomond Readvance 35, 47
 Loch Lomond Stadial 12, 35, 40, 155, 156; ELAs 52, 52; palaeoclimatic inferences 51–2, 51, 52; prinal (protalus) ramparts 57, 57; reconstruction 47–8, 48, 50
 lodgement till 102, 103, 104
 loess: cooling onset evidence 5; correlation 374; extent 127; fabric 127; magnetic susceptibility 325; Milankovitch cycle correlation 369, 370; particle size 127, 131–2, 132; sequences 122, 127, 128, 129; sources 128; stratigraphy 127–8, 128, 129, 130, 130, 355; thickness 127
 low latitude landforms 82; dunefields 86–9, 87, 88; fluvial landforms 89–90, 90; pluvial lakes 82–6, 83, 84, 85, 86; weathering crusts 90–1
 Lozinski, Walery von 7, 55
 luminescence dating 61–2, 291–3, 291, 327
 Lyell, Charles 5, 6, 99
 Lytton, British Columbia 56
 Mackereth, F.J.H. 155, 156–7
 MacLaren, Charles 6
 McMurdo Ice Shelf 115
 macrofossils 181
 magnetic field variation 283
 magnetic susceptibility 324, 325
 magnetostratigraphy 320–4, 321, 322, 324, 325, 348, 363–4
 magnetozones 363–4
 Main Stationary Line 31
 mammoths 254, 255, 258, 260, 260
 MARGO 253, 388
 marine carbon circulation 276–7
 marine deposits: dust record 132; and sea-level change 58
 marine molluscan remains 235–8, 235, 236, 237
 marine oozes 166, 248
 marine oxygen isotope record 4, 355–7, 357, 358, 400; boundaries 356; correlation 366, 399; dating 268; deep-sea sediment 166–71, 168, 169; and glacial ice storage 167–9, 168; isotopic stages 356–7, 357; Last Glacial Maximum (LGM) 167–8; marker horizons 366; Middle Pleistocene Transition (MPT) 390, 390, 391; Milankovitch cycles 367–8, 368, 369, 369, 389; and sea-level change 169–70, 169; and sea-surface temperatures 170; signal noise 366; stage boundaries 366; terminations 357, 358, 366, 413; time-transgression 366; tuning 367; warm phases 356, 357
 marine palaeoclimatology 248, 249, 250–3, 250, 251, 252, 253
 marine palaeoproductivity 253–4
 marine regressions 64, 64
 marine reservoir age 276–7
 marine reservoir errors 276, 329–30
 marine snow 248
Marine Species Identification Portal 242
 marine terraces 62
 Marquette Advance, North America 37
 mass balance 43–4
 mass extinctions 261–2
 mass flow diamicton 102, 103
 mass flow tills 114–15
 mass spectrometric analyses 167
 Massachusetts Institute of Technology 386, 386
 maximum counting error (MCE) 312
 mean annual air temperature (MAAT) 53, 118–19, 119, 121, 121, 122
 mean annual ground temperature (MAGT) 122
 Mediterranean 62, 69, 77–8, 138, 149, 237, 240, 242, 243, 277, 411
 Mediterranean precession-related sapropels 377–8
 megadroughts 86
 megafaunal extinctions 261–2
 mega-grooved terrain 41, 42
 melt-out till 102, 103, 104
 metallic ions, sediments 98
 methane 15, 15, 405–6, 406, 431
 Methuselah Tree 301, 301
 Mexico, Gulf of 68, 69
 Micromorphological analysis 97
 microfloral assemblages, deep-sea sediment: chemical tracers 254; Coccolithophores 244, 245, 246, 248, 250; Dinoflagellates (dinocysts) 246, 247, 248; exhumation and reburial 248; Foraminifera 246, 248, 249, 250; identifications 248; isotope ratios 253–4; laboratory methods 248; and marine palaeoclimatology 248, 249, 250–3, 250, 251, 252, 253; planktonic foram tests 252–3, 253; Radiolaria 244, 244–5, 245, 248
 micromorphology 97, 103–4, 105, 106
 micropalaeontology, deep-sea sediment 244; chemical tracers 254; Coccolithophores 245–6, 245, 246, 248, 250; Dinoflagellates (dinocysts) 246, 247, 248; Foraminifera 246, 248, 249, 249, 250; identifications 248; isotope ratios 253–4; laboratory methods 248; and marine palaeoclimatology 248, 249,

- 250–3, 250, 251, 252, 253; planktonic foram tests 252–3, 253; Radiolaria 244–5, 245, 248
 microscopy 248
 micro-vertebrates 257
 Middle Pleistocene Transition (MPT) 15, 389, 390–4, 390, 391, 394, 398–9
 Mid-Pleistocene Revolution 15, 390
 Milankovitch chron, the 390–1, 393
 Milankovitch cycles 15, 78, 81, 167, 169, 262–3, 330, 367, 379, 440; the 100 kyr problem 389, 392, 393, 394, 398–9; astronomical forcing 390–2, 393; astronomically driven 389, 398; climate change over 389–99, 390, 391, 394, 395, 396, 397, 398; correlation 367–9, 368, 369, 370, 371, 378; deaf zones 390–2; environmental simulation models (ESMs) 393; glacial–interglacial cycles of the last 800 ka 394–7, 395, 396, 397, 398, 399; marine oxygen isotope record 389; Middle Pleistocene Transition (MPT) 389, 390–4, 390, 391, 394, 398–9; precessional cycles 393; rhythms 389, 392–3; signal clarity 389
 Milankovitch hypothesis, the 14–15, 178
 mineral carbon error 277–8
 mineral magnetic analysis 98, 125, 126
 mineral magnetic susceptibility 324, 325
 mineral palsas 56
 mires: *see* lake, mire and bog sediments
 MIS (marine isotope stage) 9–10, 11
 molecular clock analysis 8, 332, 345
 molluscan remains: absolute abundance 231, 231; amino-acid geochronology 336, 338, 338, 339; archaeological relevance 234–5; assemblage zones 230, 231; and biostratigraphic correlation 233, 237; climate change boundaries 360, 361; dating 277, 278, 289, 294, 339; distribution 229, 234, 235; fidelity 232; field work 229; growth banding 319; habitat groups, non-marine 232–3, 232; identification 230–1; isotope ratios 234, 237; laboratory methods 229–31; marine 235–8, 235, 236, 237, 319; marker bands 319; mutual climatic range (MCR) 234; nature of 229; non-marine 227–35, 228, 230, 231, 232; palaeoenvironmental reconstruction 234, 236–7, 237; in palaeosols 122; relative abundance 230, 231; species bias 231–2; species diversity, non-marine 233; taphonomy, marine 236; taphonomy, non-marine 231–2; types 229
 Mono Lake, United States of America 150
 monolith tins 94, 94
 monsoon belts 409–10
 monsoonal circulation 15–16
 Monte San Nicola section 4, 5, 10
 moraines 27, 28, 29, 29–30, 40, 42, 99; dating 296, 297, 316, 342; Late Weichselian ice sheet 30–1, 31; morphostratigraphy 354–5, 354
 morainic rock glaciers 55
 morphological mapping 19–20
 morphostratigraphic units 354
 morphostratigraphy 348, 354–5, 354, 378
 Mt Edziza, British Columbia 55
 Mt St Helens, United States of America 327, 328
 multidisciplinary approach 2, 9
 multi-parameter approach 174, 311
 multi-proxy palaeoecological studies 265–6
 multispectral (multi-wavelength) scanning systems 22, 23
 Munsell colour charts 93
 mutual climatic range (MCR) 212–13, 222–4, 223, 224, 234, 261
 mutual temperature range 240
 National Aeronautics and Space Administration (NASA) 22–3
 National Climatic Data Center 438
 National Oceanic and Atmospheric Administration 22
 natural luminescence signal 291
 natural remanent magnetism (NRM) 320
 NEEM ice core 172, 313
 negative sea-level tendency 64, 64
 Neogene 1, 3
 Neoglacial period 33
 Neolithic 73
 Netherlands 56, 119, 160, 368, 368
 New England Varve Chronology (NEVC) 307
 New Guinea 61, 73, 169, 169, 240
 New Zealand 77, 145, 237, 283, 302, 329, 375–6, 434
 NEXTMap 25–6, 26
 NGRIP ice core *see* North Greenland Ice Core Project
 nivation ridges 57
 niveo-aeolian deposition 130
 nominal stratotypes 349
 non-marine molluscan remains 227–35, 228, 230, 231, 232, 232, 234
 Norden Model 419
 Nordic Sea 251–2, 251
 North America: 2.8 ka event 433; 4.2 ka event 431; arrivals of humans in 436; the Cockburn Event 38; Coleoptera 219, 220, 223; Cordilleran ice sheet 35, 36, 38–9, 68, 73; coversand 130; deglaciation 37, 39, 307, 404; dendrochronology 301, 301; dunefields 87; ELAs 52; extent of ice cover 35, 36, 37–9, 37, 39; fission track dating 290–1; Foothills Erratics Train 113; fungal remains 264; Greatlakean Advance 35, 37; ice-sheet modelling 45; Innuittian ice sheet 35, 36, 39; lake sedimentation rates 158; lake-level changes 135, 137; Last Glacial Maximum (LGM) 36; Lateglacial climate change 422; Little Ice Age 434; loess deposits 128, 130; Marquette Advance 37; mass extinctions 261; molluscan remains 233, 234; ostracod analysis 240; palaeoclimatic inferences 52; palaeosol correlation 364; palaeovegetation maps 195, 195; permafrost 118; phylogeography 262; pluvial lakes 82, 83–6, 83, 84, 86, 133; Port Huron Advance 35; readvances 35, 37, 38, 38–9; record synchronization 375; retreat pattern 37; soil stratigraphy 355; Tahoe Moraines 38, 39; Tiedemann–Peyto Advance 39; *Tsuga* (hemlock) decline 194; vertebrate biostratigraphy 259; vertebrate remains 261; Younger Dryas Stadial 424; *see also* Laurentide ice sheet, North America
 North Atlantic 250, 379; 2.8 ka event 433; 8.2 ka event 431; circulation system 400–1, 402, 403–4, 403, 406–7, 408–9, 417, 431; CO₂ content 408–9, 408; and freshwater release 404, 422, 423–4, 431; Heinrich events 372, 373, 374, 404, 411; ice-raftered debris (IRD) 404; Last Termination 417; Lateglacial 422; Little Ice Age 434; magnetostratigraphy 323; marine molluscs 235, 236, 236, 319; ocean–ice interactions 400–1, 401, 402, 403–5, 403; sea-surface temperatures (SSTs) 251–2, 252; tephra marker horizons 329; thermal stratification 401, 402, 403; thermohaline circulation: THC 401, 402, 436
 North Atlantic Ash Zone 326
 North Atlantic Deep Water (NADW) current 401, 402, 403, 404, 408–9, 408, 422, 424, 431, 434
 North Atlantic Event Stratigraphy 375
 North Atlantic Oscillation (NAO) 303, 309, 404, 435–6
 North Atlantic Polar Front 236, 243, 250, 266n6

- North Cascade Range, United States of America 210, 214
- North Greenland Ice Core Project (NGRIP) 8, 172, 174, 176, 176, 177, 227, 311, 312–14, 313, 314, 315, 326, 349, 375, 377, 399, 405, 406, 413–15, 415, 421, 425, 426, 428, 428, 429, 429, 430, 442
- North Icelandic Shelf 243
- North Sea 33, 319
- Northern Europe: deglaciation 32–3; extent of ice cover 30–3, 30, 31; ice-sheet modelling 44–5, 45; indicator erratics 113; mean annual temperatures 119–20, 120; permafrost limits 119, 121, 121
- Norway 32, 51, 52, 73, 118, 143, 145, 224, 224, 236–7, 315, 424–6, 425, 426, 436
- Norwegian Sea 277
- Nova Scotia 165
- nuclear bomb testing 440
- obsidian diffusion dating 340
- obsidian hydration dating (OHD) 340
- ocean circulation 254, 401, 402
- ocean siphoning 69
- ocean–ice interactions, North Atlantic 400–1, 401, 402, 403–5, 403
- oceans, salt-density variations 16
- Okotoks erratic, The Big Rock 111, 113, 113
- Older Dryas (OD) cold oscillation 413, 422
- optically stimulated luminescence 291
- orbital forcing 15, 138, 390–2
- orbital tuning 4, 330–1, 331, 366
- Ordnance Survey Bench Marks 20
- organic varves 152, 304, 305–6, 305
- Orkney Islands 33
- Oro Lake, Canada 203, 205
- orthorectification 26
- ostracod analysis 238–41, 239
- outwash terraces 77
- overkill hypothesis, the 262
- Owen, Richard 7
- OxCal 281, 282
- oxygen isotope chronology 330–1, 331
- oxygen isotope chronostratigraphy 319
- oxygen isotope ratios: and cave sediments 142; climate change boundaries 360; correlation 366, 399; dating 268; deep-sea sediment 166–71, 168, 169, 390; and fractionation 167; and glacial ice storage 167–9, 168; Holocene 427; and ice volume 169; ice-core stratigraphy 175; isotopic forms 167; isotopic stages 9–10, 10, 169, 330, 358; limitations 170–1; mass spectrometric analyses 167; micropalaeontology, deep-sea sediment 253–4; Middle Pleistocene Transition (MPT) 390, 390, 391; the Milankovitch hypothesis 15; profiles 168–9, 168; sea-level change 60–1, 61; and sea-level change 169–70, 169; seasonal variations 174; and sea-surface temperatures 170; signal 9, 10; speleothem 373–4; standards 167, 179n10; stratigraphic application 170; terminations 357, 358; trace timescale 1; tuning 367
- oxygen isotope stratigraphy 170, 348, 355–7, 357, 358
- Pacific Decadal Oscillation (PDO) 303, 436
- Pakefield, Suffolk 151
- palaeocatenas 124
- palaeooceanography 265
- palaeoclimatic reconstruction 358–9, 360; and ELA 50–3, 51, 52; lake-level changes 135, 137–9, 140
- palaeodata-model comparisons 387–8
- palaeo-drainage channels 90, 90, 131
- palaeoecology 7, 181, 265–6
- palaeoenvironmental reconstruction 360–1, 361; Coleoptera and 221–4, 221, 223, 224; dendroclimatology 299, 302–4; Foraminifera 241, 242; glaciers and 50–3, 51, 52; ice-core stratigraphy 175–8, 176; and lake sediments 154–61, 156, 157, 158, 159; marine 248, 249, 250–3, 250, 251, 252, 253; and mire and bog sediments 161–5, 162, 163, 164; molluscan remains, marine 236–7, 237; mutual climatic range (MCR) method 222–4, 223, 224; ostracod analysis 240; palaeosols and 125–7; periglacial structures and 55–8, 56, 57, 58, 118–22, 119, 120, 121; plant macrofossils 212–14, 213; pollen data 197, 212; range overlap method 222; wind-blown sediments and 131–2, 132
- palaeoenvironmental synthesis 2
- Palaeogene 1, 3
- palaeo-ice streams 41
- palaeolimnology 155
- palaeomagnetic correlation 363–4
- palaeomagnetism 4, 7, 319, 319–24, 321, 322, 323, 324, 325
- palaeoseismicity 309
- palaeosols 122–7, 123, 125, 127, 128, 355, 364
- palaeotemperatures, and lake sediments 160–1
- palaeothermometry 339
- palaeovegetation maps 195
- palsas 56–7
- palynology 183
- paraglacial deposits 105–7, 108
- paraglacial landscape 106, 108
- paraglacial period 106–7, 116
- particle settling velocities 97
- particle shape: glacial sediments 109; sediments 97
- particle size: distribution 96–7, 97; glacial sediments 109, 110, 112; loess 127; wind-blown sediments 131–2, 132
- peat deposits 151; 2.8 ka event 433; biomarkers 265; chronologies 161; dating 161–2, 289; down-profile variations 162; formation 153–4; formation rates 161; human impacts on 165; isotope ratios 163, 165; palaeoenvironmental evidence from mire and bog sediments 161, 161–3, 162, 163; plant macrofossils 162, 213; pollen content 161, 165; profiles 162; radiocarbon dating 161–2; radiocarbon wiggle-matching 282, 283; recurrence surfaces 161; *Sphagnum* 161, 162; tephra 327; testate amoebae analysis 162–3
- pedogenesis 342–3, 355
- pedogenic carbonate 150
- Penck, Albrecht 6, 13
- Pennington, Winifred 155
- periglacial domain, the 53–4
- periglacial landforms 53–4, 53; air temperature thresholds 119; features 54, 55; palaeoclimatic inferences 55–8, 56, 57, 58; patterned ground 54–5, 55
- periglacial loading 117–18
- periglacial sediments 115–22, 116, 117, 118, 119, 120, 121
- perlite 340
- permafrost 53, 53, 56; climate 118–21; continuous 116, 119; discontinuous 116, 119–20, 121; extent 118, 119, 121, 121; and MAAT 118–19, 121, 121; palaeoclimatic inferences 118–22, 119, 120, 121; periglacial sediments 115–22, 116, 117, 118, 119, 120, 121; structures 116–18, 116, 117, 118
- pH, diatoms and 203, 205, 206
- Phanerozoic 59, 92n10
- phenotypic plasticity 262
- photography 20, 22
- photo-imaging 95
- phreatic conditions 143
- phylogeography 262
- phytoliths 142, 179n6

pingos 56–7
 pixels 23
 planetary harmonics 389
 plankton blooms 304
 planktonic assemblage zones 332
 planktonic foram tests 252–3, 253
 plant function types (PFTs) 266n2
 plant macrofossils 142, 162, 207–15, 207, 209, 210, 211, 213, 332
 plant refugia 195
 plasma 103
 plateau correction procedure 290
 Playfair, John 5, 6
 Pleistocene 2, 5, 104, 126
 Pleistocene–Holocene transition 428–9, 428, 429
 Pliocene 4, 5, 61
 pluvial episodes 6–7, 82
 pluvial lakes 82, 82–6, 84, 85, 86, 140
 PMIP (the Paleoclimate Model Intercomparison Project) 388
 Poland 31, 32, 56, 77, 119, 120, 224, 224
 polar bears 262
 polar deserts 55
 pollen and pollen analysis 183, 209, 214, 266n1, 308; anthropogenic indicators 196, 197; applications 194–7, 194, 195, 196, 197; assemblage zones 331–2; calibration 197; cave sediments 142, 193; climate change boundaries 360; compositional variation 192; concentrations 188–9; cooling onset evidence 5; correlation 368; corrosion 193, 193; dating 189, 362; deposition 192; deterioration 193, 193; dispersal 191–2; dissemination 183–4; exotic 188; field work 184–5; human impacts 165, 183, 195–6, 196, 197; identification 185, 194; indicator species 197; laboratory methods 185; lake, mire and bog sediments 155, 157, 185, 186, 188–9, 188, 192; local vegetation reconstructions 194; mixing 192–3; nature of 183–4, 184; oxidation 193, 193; palaeoenvironmental reconstruction 197, 212; peat deposits 161, 165; pollen assemblage 185; pollen diagrams 185, 186, 187–9, 187, 188, 189, 197; pollen diagrams, interpretation 190–4, 190, 191, 193; pollen grains 183, 184; pollen influx 189, 192; pollen sources 191–2; pollen spectrum 185; pollen structure 183; the pollen sum 185, 187; pollen zones 189; preservation 184; production 190–1, 191; redeposited pollen 193; regional pollen databases

194; regional vegetation reconstructions 194; R-values 190–1; sample sources 184–5; space–time reconstructions 195, 195; taphonomy 197; transport mechanisms 191; *Tsuga* (hemlock) decline 194; *Ulmus* (elm) decline 194; zone boundaries 376, 419
 pollen diagrams 185, 186, 187–9, 187, 188, 189, 197; interpretation 190–4, 190, 191, 193
 pollen response functions 197
 pollen stratigraphy, applications 194–7, 194, 195, 196, 197
 pollen zones 189
 pollution levels 243, 297, 307, 309, 376, 419
 Port Huron Advance 35
 Post, Lennart von 7
 postglacial erosion 29
 postglacial rebound 69
 potassium–argon dating 284–5, 284
 Poznan moraine 31
 precipitation 120, 140; and ELA 50, 52; isotope dendroclimatology 304; monsoonal circulation 15–16; and peat deposits 162, 163; Pleistocene–Holocene transition 429; and river landforms 74
 pronival (protalus) ramparts 57–8, 57
 protalus lobes 56
 protalus rock glaciers 56
 protein chemistry 332, 333, 334, 336
 proxy records 2, 379; 2.8 ka event 433; 8.2 ka event 430, 431; databases 387–8; definition 17n2; dendroclimatology 302; fossils and the fossil record 182; global environmental change 379–80; Heinrich events 373; Holocene 427; ice-core stratigraphy 176; lake-level changes 138; multi 182, 265–6, 304; North Atlantic Oscillation (NAO) 436; palaeodata-model comparisons 387–8; Pleistocene–Holocene transition 428, 429; quality and quality control 380, 387–8; record synchronization 375; single 182; surface wetness change 162–3, 164; tuning 312
 pseudosozils 124
 pulse counters 96
 Pyramid Lake, United States of America 228
 quartz particles 97
 Quaternary: character 1–2; definition 1, 5; duration 3–5; event dating 308–9; framework 9–10, 10, 11, 12–13, 12; first use of term 5; geochronological status 2–3; geological timescale 1, 2–3; glacial stages 1, 9; interglacial stages 9; interstadial episodes 9; onset 3; sequence correlation 336, 337, 338; stadial episodes 9; system 2; time intervals 307–8
 Quaternary studies 5–9
 Queen Charlotte Island 68
 Queen Maud Mountains, Antarctica 29
 Quelcaya ice cap, Peru 174
 radar sensing 22, 23–4, 90, 90
 radiative forcing 395–6, 396
 radioactive decay 268, 269–70, 286, 286
 radioactive nuclides 269, 440
 radioactivity 268–70
Radiocarbon (journal) 270
 radiocarbon dating 7; accelerator mass spectrometry 271, 272–5, 273, 274, 278–9; age estimates 271; age modelling 282–3, 283; applicability 268, 270, 274; Bayesian-based statistical modelling 282–3, 282; beta decay 271; bone 278; calendar years 275, 275, 279; CALIB 280–1; calibration 279–84, 280, 281, 282, 283, 309–10; calibration curve 280–1, 281, 282, 283–4; CalPal 281; chronological order reversals 281; contamination 277–9, 278; counting statistics 274–5; date calculation 272; decay curve 270–1, 271, 271; Fairbanks calibration model 281; fluctuations 280; gas proportional counting 271; Gaussian errors 281, 282; general principles 270–1; hard-water error 277–8; human impacts on 276; IntCal model 280, 281, 281; isotopic enrichment 271–2; isotopic fractionation 276, 277; lake sediment 278, 279; lake-level changes 135; Late Weichselian ice sheet 30–1; liquid scintillation counting 271; marine carbon circulation 276–7; marine reservoir errors 276, 329–30; measurement of ^{14}C 271–5, 273, 274; mineral carbon error 277–8; modern reference standard 272; molluscan remains 277, 278; OxCal 281, 282; palaeoenvironmental applications 283–4; peat deposits 161–2; plant macrofossils 210; pollen 189; precision 274–5; quality assurance 275; radiocarbon wiggle-matching 280, 282, 283; radiocarbon years 275, 275; radiometric dating 271, 271–2; reference year 271; sea-waters 276–7; sediments 282; soils 279; standards 272; temporal

- variations, ^{14}C production 275–6, 275; timescale calibration 275; uncertainty 272, 274–5
 radiocarbon wiggle-matching 280, 282, 283
Radiolaria 248
radiometric clocks 270
radiometric dating 267, 268–70; alpha-recoil track (ART) dating 290; argon-isotope dating 284–5, 284; correlation 365; cosmogenic radionuclide (CRN) dating 294–6, 295, 297; electron spin resonance (ESR) 293–4; fission track dating 289–91; luminescence dating 291–3, 291; short-lived radioactive isotopes 296–8; uranium-series (U-series) dating 286–9, 286, 288;
see also radiocarbon dating
 raised shorelines 70, 71, 72–3
 range charts 242
 range fossils 233
 range overlap method 222
 ratite eggshell, dating 338
 Rayleigh test 443n1
 Reboul, Henri 5
 recessional stages 27
 record synchronization 374–8, 375, 376, 377
 recurrence surfaces 161
 Red Sea 61, 411, 411
 regional pollen databases 194
 regional stratotypes 349
 regional vegetation reconstructions 194
 Reid, Clement, *The Origin of the British Flora* 207
 relative age methods 267
 relict palaeosols 122
 remanent magnetism 320
 remote sensing 7, 22–6, 25, 26, 31–2, 40, 95
 reservoir effect, the 278
 residual rebound 69
 restrained rebound 69
 Rhine, River 75, 76, 77
 Rhine–Meuse system 77
 Rhône, River 212
 rice farming 438
 Riss–Würmian 10
 river sediments, vertebrate remains 258
 river terraces 74–5, 75; aggradation 76, 76–7; alluviation 78, 78; backswamp deposits 78; climatic 76–7; and climatic change 76–7, 81–2; cut and fill 75, 76; dating 77; evolution 78–82; and glaciation 77; gradients 77; and human activity 77–8, 78; origins 76–8, 78;
 outwash 77; paired 75; and palaeoenvironmental reconstruction 78; preservation 74–5; River Thames 78–82, 79, 80; and sea-level change 76, 81; sequences 75–6, 77, 78, 81; staircases 74–5, 76, 79, 82; strath 75, 76; tectonic influences 77; thalassostatic 76; unpaired 75
roches moutonnées 40, 92n8
 rock glaciers 55–6, 56
 rock platforms 58, 58
 rock-hardness 341
 rock-weathering 340–2, 341
 Roman period 78
 Russell, Israel 6–7
 Russia 31, 259, 304
 Sahara, the 86
 salinity indicators: Cocco lithophores 246; diatoms as 202–3, 205; Foraminifera 241, 243; ostracod analysis 240
 Salpausselkä Moraines 32
 salt lakes 134, 203
 salt oscillator hypothesis 403–4
 salt-density variations 16
 San Francisco Bay 212
 sand seas 127, 131
 sand wedges 116–17, 116, 119
 Sandar 91n3
 Sangamonian 10
 sapropels 17n6, 377–8, 377
 satellite images 20, 22–3, 33
 Saussure, Horace-Bénédict de 111
 Scandinavia 71, 307, 308, 433
 scanning electron microscopy (SEM) 97, 107, 127, 179n1, 207, 208
 Schmidt hammer 341, 341–2
 Schott, Wolfgang 8
 Scilly Isles 33
 sclerochronology 298, 316, 317, 318, 319
 Scotland 33, 35; equilibrium line altitude (ELA) 57, 57; isobase patterns 71; marine molluscs 319; palaeoclimatic inferences 51–2, 51, 52; sea-level change 70
 seabed, hydro-isostatic load 60
 sea-floor spreading, and sea-level change 60
 sea-ice formation 178
 sea-level change 19; absolute 59; cause differentiation 66; chronologies 61–2; and coral 319; and coral polyps 263–4; correlation 365; cycles 62, 62; dating 59, 61–2; diatoms and 203, 204; and dust 411, 411; and estuarine sediments 63–4, 64; eustatic 59–77, 60, 61, 62, 63, 64, 65, 66, 76; Foraminifera and 242, 243; geoidal irregularity 66–7; geomorphological evidence 58–73; geomorphological features 58, 58, 62; Glacio-eustatic Theory 6; glacio-eustasy 60–1; glacio-isostasy 68–9, 68, 69–73, 70, 71, 72; Holocene 65–6, 66, 69; hydro-isostasy 68, 69; and ice volume 169–70; isostatic 59, 66, 68–73, 68, 69, 70, 71, 72; isostatic recovery 69, 71, 72–3; Last Glacial Maximum (LGM) 62–3; Lateglacial 422; and marine deposits 58; and marine oxygen isotope record 169–70, 169; marine regressions 64, 64; meltwater pulse (MWP) 1a 63; Middle Pleistocene Transition (MPT) 390; the Milankovitch hypothesis 14–15; modelling 66; negative sea-level tendency 64, 64, 202, 203; ocean siphoning 69; ostracod analysis 240; oxygen isotope record 60–1, 61; palaeoenvironmental significance of 73; Pliocene 60; positive sea-level tendency 64, 64, 202, 203; Pre-Quaternary eustatic 59–60; reconstruction 59; relative curves 243; and river terraces 76, 81; and sea-floor spreading 60; and speleothem formation 149; tectonic influences 67–8, 67; teleconnection 411, 411; worldwide 59, 60
 sea-level index point 63, 64
 Searles Lake basin, United States of America 133
 sea-surface temperatures (SSTs) 16, 373; cooling trend 394; and coral 319; Dinoflagellates (dinocysts) and 246; Last Termination 415, 416; and marine oxygen isotope record 170; micropalaeontology, deep-sea sediment 249, 250–1, 250, 251, 252; Middle Pleistocene Transition (MPT) 390; molluscan remains and 237; ocean–ice interactions, North Atlantic 400; ostracod analysis 240; Pleistocene–Holocene transition 429; Radiolaria and 245
 sea-waters, age estimates 276–7
 secular magnetic database 345n2
 secular magnetic variations 320–1, 321, 363–4
 sedigraph 97
 sedimentary record 93
 sedimentary sequences 93, 94–5
 sedimentation rates: deep-sea sediment 170–1; lakes 157–8, 158
 sedimentological analysis 7

- sediments 97–8, 178–9; beds 349; clay mineralogy 98; dating 282, 292; deep-sea 165–71, 166, 168, 169; deformation 352, 353; fabrics 93; Foraminifera 241, 242; heavy mineral assemblages 98; insect remains 215, 226; lake-level records 132–6, 133, 134, 136, 137–8, 137, 139, 140–1, 140; lithostratigraphic units 349–51, 350, 351; luminescence dating 292; metallic ions 98; Milankovitch cycle correlation 368–9, 369, 370, 371; mineral magnetic analysis 98; molluscan remains 231–2; palaeosols 122–7, 123, 125; particle shape 97; particle size distribution 96–7, 97; periglacial 115–22, 116, 117, 118, 119, 120, 121; plant macrofossils 207, 209, 210, 211; radiocarbon dating 282; sections 93–4, 94; sequence stratigraphy 352, 352; shelf seas 242; stable isotope analysis 98–9; thin sections 97, 106; types 93; varved 304; vertebrate remains 257–8; wind-blown 127–8, 128, 129, 130–2, 130, 132; *see also* cave sediments; glacial sediments; lake, mire and bog sediments
- seismic events 309
- seismic sensing 24
- seismic stratigraphy 348
- seismic surveys 24
- sequence stratigraphy 351–2, 352
- series 2
- Sernander, Rutger 7
- Sevrier-Les-Charretières, France 159
- shallow marine water mass, temperature change 243–4
- Shannon diversity index (SDI) 233
- Shetland Isles 33
- shoreline correlation 364–5
- shoreline displacement 67–8, 67
- side-looking airborne radar (SLAR) 24
- silcrete 91
- silicon-32 297, 298
- SIMMAX 251–2
- single aliquot regeneration method (SAR) 292
- single laser crystal fusion (SLCF) $^{40}\text{Ar}/^{39}\text{Ar}$ dating 285
- skeleton grains 103
- Skye, Isle of 157
- S-matrix structures 104
- smear slides 248
- Smith, James 7
- snow shadow 45–6
- Snowdonia, Wales 40
- soil catena chronosequences 343
- soil wedges 117, 119
- soils: dating 126, 279; diagenesis 123–4; fabric 124–5; formation 122–3, 355; horizon boundaries 124; mean residence time 279; micromorphology 124–5, 125; mineral magnetic analysis 125, 126; plant macrofossils 207; profiles 123, 124; properties 124; radiocarbon dating 279; relict features 122, 123; stratigraphy 355; *see also* palaeosols
- solar output variations 16, 160, 275–6, 283, 296, 404, 415, 431, 433, 433, 434, 434–5, 438, 440
- Somme, River 75, 76, 77
- sonar signals 22, 24, 25, 95
- Soreq Cave, Israel 146, 148
- South America 128; Quaternary environments 260; sand seas 131; vertebrate biostratigraphy 259; vertebrate remains 260
- Southern Oscillation 435
- Space Imaging, Inc 22
- Spain 91, 240, 259
- spallation 294
- species diversity 233
- species richness 233
- SPECMAP timescale 330–1, 331, 356
- spectral analysis 15, 17n7, 393
- speleothem 141, 409; amino-acid geochemistry 334; dating 143, 144, 149, 286–7, 288, 293, 298, 316–17; formation 141, 141, 143; formation and sea-level change 149; formation and tectonic activity 149; growth and climatic change 143–4, 144; growth layers 143, 144, 316–17, 371; isotope ratios 145–8, 147, 148; Milankovitch cycle correlation 371; oxygen isotope ratios 373–4; trace elements 148
- Sphagnum* mosses 154, 155, 210, 213
- Spitsbergen 102
- spontaneous fission 289, 290
- spores: *see* pollen and pollen analysis
- SPOT 23
- stable isotope analysis 98–9
- stadial episodes, definition 9
- stages 2
- Steel Lake, United States of America 188
- stereonets 114, 114
- stochastic resonance 413, 443n2
- Stockholm 305
- stoss-and-levee landforms 40
- stratigraphic boundaries 349, 349
- stratigraphic markers 127, 267
- stratigraphic resolution 343–4, 344
- stratigraphy 264, 347; age modelling 420–1; allostratigraphy 352; the Anthropocene 439; approaches 348; beds 350, 351; biostratigraphy 348, 353–4, 353, 363; biozone correlation 353–4; chemical 348; chronostratigraphy 348, 361–2, 362, 378; climatostratigraphy 348, 358–61, 359, 360, 361, 378; codes of practice 348; correlation 347, 359, 362–3; definition 347; diatom 206; electrical conductivity measurements 348; equifinality 352–3; event 348, 365; geochronological units 348; geochronology 361–2, 362; Lateglacial synchronization 419–20; lateral 363; lithostratigraphy 348, 349–53, 350, 351, 352, 378; loess 127–8, 128, 129, 130, 130; magnetostratigraphy 348; morphostratigraphy 348, 354–5, 354, 378; oxygen isotope 348, 355–7, 357, 358; palaeomagnetic correlation 363–4; palaeosol correlation 364; pollen 194–7, 194, 195, 196, 197; principles 347–8, 349; record synchronization 374–8, 375, 376, 377; seismic 348; sequence 351–2, 352; shoreline correlation 364–5; soil stratigraphy 355; stages 362, 378; stratotypes 349; synchronization 367; tephra correlation 364; time-rock units 362; time-stratigraphic markers 362; time-transgression 348, 349, 362, 363; units 348, 349; vertebrate 259; *see also* ice-core stratigraphy
- stratotypes 4
- streamlined glacial deposits 42–3
- striations 40, 41, 42
- stromatolites 134, 150
- Subcommission on Quaternary Stratigraphy (SQS) 3, 17n3, 349
- subenvironments 100, 100, 101, 102
- subglacial deformation 102–3
- subglacial subenvironments 100, 100
- subglacial traction till 104
- sublimation 102
- sublimation till 102, 103
- submarine landforms 33
- sub-Milankovitch timescales 16, 367, 371, 371, 372–4, 372, 373, 374, 378, 379
- Sudan 90, 234
- Sumatra 327
- sunspot cycle 138, 434
- superposition, 267, 336, 351, 361, 363, 365, 375; principle of 345n1
- supraglacial subenvironments 100, 100
- surface exposure dating 294
- surface wetness change: and peat deposits 162, 163; and plant macrofossils 162; proxy records 162–3, 163, 164

- surging 30, 37
 Svalbard-Barents Sea 31
 swathe bathymetry 24
 Sweden 63, 161, 224, 224, 305, 307, 309
 Switzerland 42, 160, 196, 196
 syngenetic ice wedges 116
 synthetic aperture radar (SAR) 24, 90, 90
- Tahoe Moraines, North America 38, 39
 Tajikistan 128
 TALDICE consortium 172
 technological advances 7
 tectomicts 104
 tectonic basins 368
 tectonic influences 15; Middle Pleistocene Transition (MPT) 392; river terraces 77; sea-level change 67–8, 67; speleothem formation 149; uplift 77
 teeth, vertebrate 254, 255, 256, 294
 teleconnection 399–400; anti-phase behaviour 406–7; bipolar 405–7, 405, 406; bipolar seesaw 406–7, 409, 411, 412, 418, 440; dust circulation 410–11, 410, 412; feedback loops 407, 409, 410–11; global mechanisms 407–13, 408, 410, 411, 412; heat piracy 407; interdependency 412–13, 412; Last Termination 418–19; ocean–ice interactions, North Atlantic 400, 400–1, 401, 402, 403–5, 403; problems 412–13; sea-level change 411, 411; tunnel linking 400
 temperate stage 9
 temperatures 1–2; anthropogenic warming 437–9, 437, 438; bipolar seesaw 406–7; Chironomidae 227–8, 227; deep-sea 169; and ELA 50, 51; environmental simulation models (ESMs) 393, 394; GCMs 382, 383; glacial–interglacial cycles of the last 800 ka 398, 399; greenhouse effect 437–8, 437, 438; Holocene 427, 427, 434; human impacts 436, 437–8, 437, 438, 442; ice-core stratigraphy 177; Last Glacial Maximum (LGM) 148, 339; Last Termination 417–18, 417; Little Ice Age 434; mean annual temperatures 119–20; mean global 417; palaeothermometry 339; periglacial landforms and 56; shallow marine water mass 243–4; surface water 227–8, 227; summer 51–2; *see also* sea-surface temperatures (SSTs)
 temporal resolution 343–4, 344
 tephra 364, 375; correlation 420; marker horizons 329, 329
- tephrochronology 319, 325–31, 326, 328, 329, 331, 364, 420
 tephrostratigraphy 325
 terminations 246, 357, 358, 365, 366, 367, 396, 413
 terminology (stratigraphic) 9
 Terra (EOS AM-1) 23
 TerraSAR-X satellite 24
 terrestrial *in situ* cosmogenic nuclide (TCN) dating 294
 Tertiary 3
 testate amoebae analysis 162–3, 264–5
 TEX86 index 265
 textural B horizon, Europe 126
 thalassostatic terraces 76
 Thames, River 1; amino-acid geochronology 336, 338, 338; drainage system 80, 81; Last Glacial Maximum (LGM) 81; luminescence dating 293; river terrace sequences 78–82, 79, 80; vertebrate biostratigraphy 259
 thermal ionization mass spectrometry 287
 thermally transferred optically stimulated luminescence 292–3
 thermistors 177, 179n111
 thermoclastic scree 142
 thermohaline circulation 16, 401, 402
 thermokarst 55
 thermoluminescence 291
 thermoremanent magnetization (TRM) 320
 thin sections 97, 106
 thifur 58
 Tibet 134, 138, 172
 Tiedemann–Peyto Advance, North America 39
 tills 99; classification of 102–7, 103, 104, 105, 106, 107; clay mineral ratios 115; cosmogenic nuclides 115; fabric 113–15, 114; indicator minerals 115; matrix properties 115; provenance 113
 time-rock units 362
 time-stratigraphic correlation 374–8, 375, 376, 377
 time-stratigraphic markers 362
 time-transgression 354; climate change 367; human impacts 440; marine oxygen isotope record 366; stratigraphy 348, 349, 362, 363
 tipping points 386, 404, 438, 440
 TOPEX/Poseidon satellite 23
 toposequences 124
 tors 54, 54
 total stations 20
 transfer functions 192, 205, 212, 234, 240, 242, 243, 246, 250–1, 263–4, 266n4
- transient accelerated palaeo-simulations 387
 transient simulations 386–7
 travertine 149–50, 150
 tree rings: *see* dendrochronology
 trimlines 27, 28, 29, 33
 trophic status 153, 205
 tsunami deposits 240, 364–5
 tufa 150, 150
 tunnel valleys 33, 91n7
 Turkey 78, 78
 turnover rate 262
 Tuscany, Italy 233
 Tyndall, John 437
 type sites 349
- uniformitarian principle, the 125–6, 181, 182
 Uniformitarianism 5
 United States of America: Alaska 214; Beaver Lake 201; Bishop Tuff 290–1; dendrochronology 301, 301; dust flux 309; Florida 212; Lake Bonneville 82, 83–6, 84, 86, 133, 339; Lake Lahontan 82, 83, 84; Mono Lake 150; Mt St Helens 327, 328; North Cascade Range 210, 214; Pyramid Lake 228; record synchronization 375; Searles Lake basin 133; soil stratigraphy 355; Steel Lake 188; tephra 327, 328; Yellowstone 285, 327; *see also* North America
 uranium-series (U-series) dating 286–9, 286, 288
 uranium-series disequilibrium dating method 286–7
 urbanization 437
 Urströmtaler 30
 U.S. Geological Survey (USGS) 22, 200
 Ussher, James, Archbishop of Armagh 5
- vadose 143
 varnish micro-lamination (VML) dating 341
 varves and varve chronology 100, 298, 304; applications 307–10, 308, 310; chemical 306; chronological errors 306; clastic 304, 304–5, 305; complex 306; counting error sources 306–7; cross dating 306; glacigenic 304, 304–5; human impacts 309; Lateglacial 420; nature of 304; organic 304, 305–6, 305; radiocarbon dating calibration 309–10; sublaminations 306; Swedish Timescale (STS) 307; year zero 307

vegetation reconstructions 194, 195, 195
 vegetational change, early evidence 7
 vegetational productivity 211
 vegetational signatures 9
 Venetz, Ignaz 5
 vertebrate biogeography 259–60, 259,
 260
 vertebrate biostratigraphy 259
 vertebrate remains 254; bioclimatic limits
 261; biogeography 259–60, 259, 260;
 bone 254, 255, 289, 334; bone structure
 256; burial effects 256; cave and fissure
 deposits 257–8; changes in animal
 morphology 260, 260; dating 258, 278,
 289, 294; decalcification 256; DNA
 analysis 262; ecological niche models
 261; excavation 257; and faunal
 evolution 262–3; field methods 256–7;
 fluorine content 339–40; fluvial
 sediments 258; fossilization process
 256; human impacts 261–2; hydraulic
 sorting 258; identification 257; indicator
 species 260–1; lacustrine sediments
 258; micro-vertebrates 257; molecular
 clock analysis 332; phylogeography 262;
 and Quaternary environments 260–2;
 range 254, 259–60, 259; records 258–63,
 259, 260; recovery sites 256;
 stratigraphic ranges 259; taphonomy
 257–8; teeth 254, 255, 256, 294;
 turnover rate 262; uranium content
 339–40; weathering 256

volcanic activity: and climate change 330;
 and human evolution 330; record
 synchronization 377
 volcanic ash: *see* tephrochronology
 volcanic histories 330
 volcanic rocks: dating 284–5, 289;
 luminescence dating 291;
 recrystallization 285
 Vosges Mountains, France 212
 Vostok core, the 8
 Vrica section, Calabria 4
 Wales 33, 40, 107, 111, 218
 Walton Moss 163, 163
 water volume 59–60
 weathering: crusts 90–1; dating 294;
 profiles 124; rinds 341, 341; rocks
 340–2, 341
 Weichselian Lateglacial 10, 12
 welded soils 122
 West Runton, Norfolk 104
 whalebacks 40
 wiggle matching 280, 282, 283, 367
 wind erosion 54
 wind patterns: 2.8 ka event 433; and ice-
 sheet modelling 45–6; reconstruction
 131
 wind-blown sediments 127–8, 128, 129,
 130–2, 130, 132
 Windermere Interstadial 12
 Wisconsinan 10, 35, 36, 39
 Woodward, Bernard 7, 228

Working Group of the Subcommission
 on Quaternary Stratigraphy 439
World Modern Foraminifera Database
 242
 Würmian 10

X-radiography 95, 96, 96
 X-ray densitometry 299
 X-ray diffraction (XRD) 98
 X-ray fluorescence (XRF), 95–6

Yellowstone, United States of America
 285, 327
 Younger Dryas Stadial 12, 52, 56, 138, 155,
 277, 413, 414, 419; dendrochronology
 301–2; duration of 308; lake-level
 changes 160; mean annual air
 temperature (MAAT) 121, 121;
 molluscan remains 237; moraines 32;
 mutual climatic range (MCR) 224;
 onset 423–5, 424, 425; permafrost
 limits 121, 121; plant macrofossils 212;
 Polar Front position 424–5, 424, 426;
 speleothem growth 146; transitions 426,
 426

Yukon Territory, Canada 214

Zeuner, Frederick 261
 zonal soils 122
 zoogeographical provinces: marine fauna
 236, 236